Claudio Margottini
Paolo Canuti · Kyoji Sassa
Editors

Landslide Science and Practice

Volume 1
Landslide Inventory and Susceptibility and Hazard Zoning

Springer

Claudio Margottini • Paolo Canuti • Kyoji Sassa
Editors

Landslide Science and Practice

Volume 1: Landslide Inventory and Susceptibility and Hazard Zoning

Springer

Editors
Claudio Margottini
ISPRA - Italian Institute for
Environmental Protection and Research
Geological Survey of Italy
Rome, Italy

Paolo Canuti
ICL - International Consortium on Landslides
Florence, Italy

Kyoji Sassa
UNITWIN Headquarters Building
Kyoto University Uji Campus
Uji, Kyoto, Japan

Associate Editors
Filippo Catani
Department of Earth Sciences
University of Florence
Firenze, Italy

Alessandro Trigila
ISPRA - Italian Institute for
Environmental Protection and Research
Geological Survey of Italy
Rome, Italy

Additional material to Volume 1 can be downloaded from http://extras.springer.com

ISBN 978-3-642-31324-0 ISBN 978-3-642-31325-7 (eBook)
DOI 10.1007/978-3-642-31325-7
Springer Heidelberg New York Dordrecht London

Library of Congress Control Number: 2013932640

Printed on acid-free paper

Springer is part of Springer Science+Business Media (www.springer.com)

Preface

Landslide Science and Practice

Proceedings of the Second World Landslide Forum

The Second World Landslide Forum (**WLF**) was organized at the headquarters of the Food and Agriculture Organization of the United Nations (FAO), Rome, Italy, on 3–9 October 2011. WLF is a triennial mainstream conference of the International Programme on Landslides (**IPL**) which is jointly managed by the IPL Global Promotion Committee consisting of the International Consortium on Landslides (**ICL**), the United Nations Educational, Scientific and Cultural Organization (UNESCO), the World Meteorological Organization (WMO), the Food and Agriculture Organization of the United Nations (FAO), the United Nations International Strategy for Disaster Risk Reduction (UNISDR), the United Nations University (UNU), the International Council for Science (ICSU), and the World Federation of Engineering Organizations (WFEO).

Background to the World Landslide Forums

The International Consortium on Landslides (ICL) was established by the 2002 Kyoto Declaration "Establishment of an International Consortium on Landslides," with the Statutes adopted in January 2002. The Statutes defined the **General Assembly** of ICL: In order to report and disseminate the activities and achievements of the consortium, a General Assembly shall be convened every 3 years by inviting Members of the International Consortium on Landslides, individual members within those organizations, and all levels of cooperating organizations and individual researchers, engineers, and administrators. The General Assembly will receive reports on Consortium activities and provide a forum for open discussion and new initiatives from all participants.

The First General Assembly 2005 to the First World Landslide Forum 2008

The First General Assembly was organized at the Keck Center of the National Academy of Sciences in Washington D.C., USA, on 12–14 October 2005. At this Assembly, the first full-color book reporting consortium activities for the initial 3 years, 2002–2005, was published as "Landslides-Risk analysis and sustainable disaster management" through Springer. The 2006 Tokyo Round-Table Discussion – "Strengthening Research and Learning on Earth System Risk Analysis and Sustainable Disaster Management within UN-ISDR as Regards Landslides" – toward a dynamic global network of the International Programme on Landslides (IPL) was held at the United Nations University, Tokyo, on 18–20 January 2006. **The 2006 Tokyo**

Action Plan – *Strengthening research and learning on landslides and related earth system disasters for global risk preparedness* – was adopted. The Tokyo Action Plan established a new global International Programme on Landslides (IPL) including holding World Landslide Forums. Accordingly, the Second General Assembly 2008 was replaced by the **First World Landslide Forum** and held at the United Nations University, Tokyo, Japan, on 18–21 November 2008.

Report of the Second World Landslide Forum

The Second World Landslide Forum – *Putting Science into Practice* – was organized at the Headquarters of the Food and Agriculture Organization of the United Nations (FAO) on 3–9 October 2011. It was jointly organized by the IPL Global Promotion Committee (ICL, UNESCO, WMO, FAO, UNISDR, UNU, ICSU, WFEO) and two ICL members in Italy: the Italian Institute for Environmental Protection and Research (ISPRA) and the Earth Science Department of the University of Florence with support from the Government of Italy and many Italian landslide-related organizations.

- 864 people from 63 countries participated. Attendance was larger than expected, and twice the attendance at the First World Landslide Forum 2008 in Tokyo (430 participants: 175 from Japan and 255 from abroad).
- 25 technical sessions were held, and 465 full papers were submitted. All accepted papers were edited in 7 volumes including this volume:
  1. **Landslide Inventory and Susceptibility and Hazard Zoning – this volume**
  2. Early Warning, Instrumentation and Monitoring
  3. Spatial Analysis and Modeling
  4. Global Environmental Change
  5. Complex Environment
  6. Risk Assessment, Management and Mitigation
  7. Social and Economic Impact and Policies

Requests of Cooperation for Further Development of ICL and IPL

ICL and IPL are global multidisciplinary and cross-sectoral initiatives to promote landslide science and capacity-development to reduce landslide disasters. The core activities of ICL and IPL are ***Landslides:*** Journal of International Consortium on Landslides, World Landslide Forum, and IPL projects. Thanks to worldwide support of the journal, the Impact Factor of ***Landslides*** was 2.216 for 2011 which is the highest within 30 ISI journals in category of Engineering, Geological. The journal will develop from a quarterly journal to a bimonthly journal from Vol. 10 in 2013. The Third World Landslide Forum – Landslide risk mitigation toward a safer geo-environment – at the China National Convention Center, Beijing, China, on 2–6 June (conference) and 7–11 June (Field Trip) 2014. The ICL entered into the second decade of its activities and organized a 10th anniversary Conference on 17–20 January 2012, in Kyoto, Japan. ICL adopted the ICL Strategic Plan 2012–2021, *To create a safer geo-environment*- as an outcome of this conference.

ICL is an international nongovernmental and nonprofit scientific organization promoting landslide research and capacity-building for the benefit of society and the environment, and is

the thematic landslides platform in the UNISDR Global Platform for Disaster Risk Reduction. ICL activities are supported by voluntary efforts of ICL members and supporting organizations. All people involving in landslide research and landslide disaster mitigation activities are requested to cooperate for the development of this initiative through its second decade 2012–2021. (http://www.iplhq.org/ *and* http://icl.iplhq.org/).

We are deeply appreciative of all e Second World Landslide Forum participants and of the contributions from our UNESCO, WMO, FAO, UNISDR, UNU, ICSU, WFEO partners and all of our colleagues in ICL for the development of IPL up to now. Finally we address our sincere thanks to Filippo Catani and Alessandro Trigila (the associate editors) for their extensive efforts covering the technical sessions, and reviewing and editing the papers.

Claudio Margottini
Forum Chair

Paolo Canuti
President of ICL

Kyoji Sassa
Executive Director of ICL

ICL and IPL Secretariat

IPL office: UNITWIN headquarters Buildings, Kyoto University Uji Campus,
Uji, Kyoto 611-0011, Japan
ICL office: The Association for Diaster Prevention Research,
138-1 Tanaka Asukai-cho, Sakyo-ku, Kyoto 606-8226, Japan
Email: secretariat@iclhq.org
URL: http://www.iplhq.org/ and http://icl.iplhq.org/

Organizational Structure of the Second World Landslide Forum

Organizers

IPL Global Promotion Committee including:
- International Consortium on Landslides (ICL) *
- United Nations Educational, Scientific and Cultural Organization (UNESCO)
- World Meteorological Organization (WMO)
- Food and Agriculture Organization of the United Nations (FAO)
- United Nations International Strategy for Disaster Risk Reduction (UNISDR)
- United Nations University (UNU)
- International Council for Science (ICSU)
- World Federation of Engineering Organizations (WFEO)
- Italian Institute for Environmental Protection and Research (ISPRA)

(* Members are listed in the last page of this book)

Co-sponsors

- International Union of Geological Sciences (IUGS)
- International Union of Geodesy and Geophysics (IUGG)
- International Geographical Union (IGU)
- International Flood Initiative (IFI)

Under the Auspices of

- International Association for Engineering Geology and the Environment, Italian Section (IAEG)
- Italian Association of Engineering Geologists (AIGA)
- Italian Association of Geotechnique (AGI)
- Italian Association for Mining Engineers, Environment and Territory (ANIM)
- Italian Georesources and Environment Association (GEAM)

International Organizing Board

Honorary Chairpersons

- Irina BOKOVA (UNESCO Director-General)
- Catherine BRECHIGNAC (ICSU President)
- Jacques DIOUF (FAO Director-General)

- Michel JARRAUD (WMO Secretary-General)
- Maria P. LAFFARGUE (WFEO President)
- Konrad OSTERWALDER (UNU Rector)
- Bernardo DE BERNARDINIS (ISPRA President)
- UNISDR Director

Chairpersons

- Claudio MARGOTTINI (ISPRA, Forum Chair)
- Paolo CANUTI (ICL President)
- Kyoji SASSA (ICL Executive-Director)

Deputy Chairpersons

- Peter BOBROWSKY (IUGS Secretary General)
- Deliang CHEN (ICSU Executive Director)
- Peter LYTTLE (ICL Vice President, US Geological Survey)
- Eduardo ROJAS-BRIALES (Assistant Director General of FAO)
- Badaoui ROUHBAN (Director of UNESCO's Section for Disaster Reduction)
- Yueping YIN (ICL Vice President, China Geological Survey)

Scientific Advisory Board

Representing Organisation

- Irasema ALCANTARA-AYALA (Vice President of International Geographical Union - IGU)
- Walter AMMAN (President Davos Forum)
- Michael CROZIER (President of International Association of Geomorphologists - IAG)
- Carlos DELGADO (President of International Association of Engineering Geology - IAEG)
- Luca DEMICHELI (Secretary General of EuroGeoSurveys)
- John HARDING (United Nations Secretariat to International Strategy for Disaster Reduction - UNISDR)
- Srikantha HERATH (Senior Academic Programme Officer of the United Nations University - UNU)
- Thomas HOFER (Forestry officer, Food and Agriculture Organization of the United Nations - FAO)
- Yumio ISHII (Chair of the Committee on Disaster Risk Management of The World Federation of Engineering Organizations WFEO)
- Derek MARTIN (Vice President for North America of International Society for Rock Mechanics - ISRM)
- Howard MOORE (Senior Advisor, International Council for Science - ICSU)
- Pedro SECO E PINTO (Past President of International Society for Soil Mechanics and Geotechnical Engineering - ISSMGE)
- Luciano PICARELLI (Chairperson of the Joint Technical Committee on Landslides and Engineered slopes - JTC1 of ISSMGE, ISRM, IAEG)
- Kaoru TAKARA (Vice chairperson of the Intergovernmental Council of the International Hydrological Programme of UNESCO - IHP)
- Kuniyoshi TAKEUCHI (President of GeoRisk Commission of International Union of Geodesy and Geophysics - IUGG)

Landslide Experts

- Giovanni BARLA (Politecnico di Torino, Italy)
- R.K. BHANDARI (Consultant, India)
- Christophe BONNARD (Swiss Federal Institute of Technology, Lausanne, Switzerland)
- Nicola CASAGLI (University of Florence, Italy)
- Leonardo CASCINI (University of Salerno, Italy)
- Giovanni CROSTA (University of Milano Bicocca, Milano, Italy)
- Jordi COROMINAS (Technical University of Catalonia, Barcelona, Spain)
- Dave CRUDEN (University of Alberta, Edmonton, Alberta, Canada)
- Thomas GLADE (University of Vienna, Austria)
- Jerome DE GRAFF (United States Department of Agriculture , Fresno - Ca - USA)
- Michel HERMELIN (Universidad EAFIT, Medellin, Colombia)
- Ken HO (Hong Kong Geotechnical office, Hong Kong, China)
- Jurgen KROPP (Potsdam Institute for Climate Change - PIK, Potsdam, Germany)
- Richard M. IVERSON (United States Geological Survey - Vancouver, WA , USA)
- C. F. LEE (Hong Kong University, China)
- Jacques LOCAT (University of Laval, Canada)
- Paul MARINOS (University of Athens, Greece)
- Hideaki MARUI (Niigata University, Japan)
- Hormoz MODARESSI (BRGM, Orléans, France)
- Farrouk NADIM (Norwegian Geothecnical Institute - NGI, Oslo, Norway)
- Gabriele SCARASCIA MUGNOZZA (University of Rome, Italy)
- Wang SIJING (Tsinghua University, China)
- Vern SINGHROY (Canada Centre for Remote Sensing, Ottawa, Canada)
- Alexander STROM (Institute of Geospheres Dynamics, RAS, Moscow, Russia)
- Ikuo TOWHATA (University of Tokyo, Japan)
- Keith TURNER (Emeritus Professor, Colorado School of Mines, Denver, Colorado USA)
- Keizo UGAI (Gunma University, Kiryu,Gunma, Japan)
- Roger URGELES (Institut de Ciències del Mar - CSIC, Barcelona, Spain
- Yasser el SHAYEB (Cairo University, Egypt)
- Sergio SEPULVEDA (University of Chile, Santiago)
- Mauro SOLDATI (University of Modena and Reggio Emilia, Italy)
- Pasquale VERSACE (Calabria University, Cosenza, Italy)
- Cees van WESTEN (ITC, Enschede, Netherlands)
- Kifle WOLDEAREGAY (University of Mekelle, Ethiopia)

Local Organizing Board

Forum Chairs

- Paolo CANUTI (ICL President - WLF2 Chairperson)
- Claudio MARGOTTINI (ISPRA - WLF2 Chairperson)
- Kyoji SASSA (ICL Secretary General - WLF2 Chairperson)

Scientific Programme Committee

- Luciano PICARELLI (Second University of Napoli)
- Marco AMANTI (ISPRA)
- Filippo CATANI (University of Firenze)
- Fausto GUZZETTI (CNR-IRPI)
- Javier HERVAS (JRC)

- Thomas HOFER (FAO)
- Carla IADANZA (ISPRA)
- Claudio MARGOTTINI (ISPRA - WLF2 Chairperson)
- Paolo TOMMASI (CNR-IGAG)
- Alessandro TRIGILA (ISPRA)

Editorial Committee

- Filippo CATANI (University of Firenze)
- Riccardo FANTI (University of Firenze)
- Fausto GUZZETTI (CNR-IRPI)
- Javier HERVAS (JRC)
- Irene RISCHIA (ISPRA)
- Gabriele SCARASCIA MUGNOZZA (Università di Roma "La Sapienza")
- Alessandro TRIGILA (ISPRA)

Logistic Committee

- Thomas HOFER (FAO)
- Claudio MARGOTTINI (ISPRA - WLF2 Chairperson)
- Orlando PANDOLFI (ECN)
- Luna GUBINELLI

Field Trips

- Gabriele SCARASCIA MUGNOZZA (University of Roma "La Sapienza")
- Giuseppe DELMONACO (ISPRA)
- Riccardo FANTI (University of Firenze)
- Irene RISCHIA (ISPRA)
- Daniele SPIZZICHINO (ISPRA)
- Paolo TOMMASI (CNR-IGAG)

Fund Raising and Exhibition

- Claudio MARGOTTINI (ISPRA - WLF2 Chairperson)
- Paolo FARINA (IDS SpA)
- Giorgio LOLLINO (CNR-IRPI)

Secretariat

ISPRA, Italian Institute for Environmental Protection and Research
Dept. Geological Survey of Italy, Via Vitaliano Brancati, 48-00144 Rome, Italy.

Logistics and Administration

Orlando PANDOLFI - ECN yourLIFE Foundation

Contents

Part I

Landslide Inventory and Susceptibility and Hazard Zoning

Introduction by Javier Hervás[1], Miet Van Den Eeckhaut[1], Gabriel Legorreta[2], and Alessandro Trigila[3],

1) Institute for Environment and Sustainability, Joint Research Centre (JRC), European Commission, Ispra (VA), Italy
2) Instituto de Geografía, Universidad Nacional Autónoma de México, Coyoacán, Mexico, DF, Mexico
3) Dipartimento Difesa del Suolo - Servizio Geologico d'Italia, Istituto Superiore per la Protezione e la Ricerca Ambientale (ISPRA), Rome, Italy

Landslide inventories and susceptibility and hazard maps are key tools for land use planning and management, civil protection plans, civil engineering works, and risk reduction programmes. Their importance helps understanding why approximately one sixth of all contributions to the Second World Landslide Forum were related to recent advances in these topics.

This volume presents the state of the art on landslide inventory and susceptibility and hazard zoning. It contains experiences, methods and techniques applied in different physiographic, geological and climate settings of the world and for different types of landslides, from site-specific investigations to global scale analysis. 65 % of the submitted papers describe studies carried out in Europe, 25 % in Asia, and 8 % in South America, while contributions from North America and Africa are highly underrepresented in this session. Since the number of contributions to session L04 was fairly large, with 57 oral presentations, 24 poster presentations and 78 papers accepted for publication, this preface will not make specific references to the papers included in this volume.

A landslide inventory is the most important information source for quantitative zoning of landslide susceptibility, hazard and risk. It should give insight into the location, date, type, size, activity and causal factors of landslides as well as resultant damage. Therefore, many countries have created or are creating national and/or regional landslide databases, and several of these databases are presented in this volume (e.g. the national inventories of Poland, Slovakia, Sri Lanka, and UK). An overview of national landslide databases in Europe shows, among other things, that data collection methods used for compiling national databases are generally still rather traditional (field surveys, analysis of historical documents, including scientific literature and technical reports, and aerial-photo interpretation).

In contrast with the traditional landslide identification methods generally used for national inventories, the session showed how modern remote sensing techniques can be useful in identifying landslides and their features and activity. Important progress has been made towards pixel- and object-based automatic extraction of landslides using either passive or active optical imagery. LiDAR derivatives have become well-accepted for creation and updating of landslide inventories. For the same purposes significant progress was also achieved with satellite SAR interferometry techniques, including new data processing algorithms. Another interesting trend for updating landslide inventories is the integration of remote sensing data and conventional monitoring.

This volume contains additionally numerous studies on local (from landslide site or single slope) to national (e.g. El Salvador, France, Greece, Italy, Norway) and even continental (e.g. Europe) landslide susceptibility assessment. At very local scale, some contributions show landslide characterisation, including geotechnical investigations of landslide mechanisms and runout modelling, to determine susceptibility or hazard to specific landslide types using mainly deterministic models. For other scales, a limited set of studies used heuristic models (e.g. spatial multicriteria evaluation) while well-known and more innovative statistical models (e.g. logistic regression, artificial neural networks, fuzzy emerging patterns) remain most popular. In this context, comparison of different models, a trend that started a few years ago, continues. However, rather than focussing on the comparison of different statistical models, more attention should be paid to improving the selection and pre-processing of the input variables because this has probably much more effect on the model results than the statistical model used. Standard evaluation techniques, such as ROC curves and success rate curves, are generally accepted by now. Increasing attention is also paid to representation of the classified landslide susceptibility maps. This is very important when these maps are used for spatial planning.

Compared to the relatively high number of contributions on landslide susceptibility modelling, the number of works dealing with hazard assessment is still relatively low. Inclusion of information on the landslide frequency seems to remain difficult, although several studies prove that multitemporal remote sensing analysis, rainfall data analysis, and dendrochronology contribute here. Yet, landslide hazard studies are important for landslide risk assessment.

Although not specifically envisaged in the session, a limited number of contributions deal with local scale risk assessment. Moreover, the invited keynote lecture presents a methodological approach for landslide risk assessment starting from multitemporal landslide inventory maps and susceptibility and hazard models.

As conveners of this session, we thank all the authors for their contributions to this volume. We also thank the International Consortium on Landslides (ICL), the UN Secretariat, and various UN agencies which, through the International Programme on Landslides (IPL), provided the opportunity to organise this session from which this volume was produced.

From Landslide Inventories to Landslide Risk Assessment; An Attempt to Support Methodological Development in India

Cees J. van Westen, Saibal Ghosh, Pankaj Jaiswal, Tapas Ranjan Martha, and Sekhar Lukose Kuriakose

Abstract

India is now housing 17 % of the world's population. Landslides are an increasing concern in India due to the rapid population expansion in hilly and mountainous terrain. Landslides affect vast areas within India, in particular in the Himalayan chain in the North and Eastern part of the country and the Western Ghats in the Southwest. The Geological Survey of India (GSI) has been designated as agency responsible for landslide inventory, susceptibility and hazard assessment. Until recently their landslide susceptibility assessment was based on a heuristic approach using fixed weights or ranking of geofactors, following guidelines of the Bureau of Indian Standards (BIS). However, this method is disputed as it doesn't provide accurate results.

This paper gives an overview of recent research on how the existing methods for landslide inventory, susceptibility and hazard assessment in India could be improved, and how these could be used in (semi)quantitative risk assessment. Due to the unavailability of airphotos in large parts of India, satellite remote sensing data has become the standard data input for landslide inventory mapping. The National Remote Sensing Center (NRSC) has developed an approach using semi-automatic image analysis algorithms that combine spectral, shape, texture, morphometric and contextual information derived from high resolution satellite data and DTMs for the preparation of new as well as historical landslide inventories. Also the use of existing information in the form of maintenance records, and other information to generate event-based landslide inventories is presented. Event-based landslide inventories are used to estimate the temporal probability, landslide density and landslide size distribution.

Landslide susceptibility methods can be subdivided in heuristic, statistical and deterministic methods. Examples are given on the use of these methods for different scales of analysis. For medium scales a method is presented to analyze the spatial association between landslides and causal factors, including those related to structural geology, to select the most appropriate spatial factors for different landslide types, and integrate them using a combination of heuristic and multivariate methods. For transportation corridors a method is

C.J. van Westen (✉)
Faculty of Geo-Information Science and Earth Observation (ITC),
University of Twente, 7500 AE, Enschede, P.O. Box 217,
The Netherlands
e-mail: c.j.vanwesten@utwente.nl

S. Ghosh • P. Jaiswal
Geological Survey of India, Kolkata, India

T.R. Martha
National Remote Sensing Center, Hyderabad, India

S.L. Kuriakose
Centre for Earth Science Studies, Trivandrum, India

C. Margottini et al. (eds.), *Landslide Science and Practice*, Vol. 1,
DOI 10.1007/978-3-642-31325-7_1,

presented for quantitative hazard and risk assessment based on a nearly complete landslide database. Deterministic methods using several dynamic slope-hydrology and slope stability models have been applied to evaluate the relation between landuse changes and slope stability.

The susceptibility maps can be combined with the landslide databases to convert them into hazard maps which are subsequently used in (semi) quantitative risk assessment at different scales of analysis.

Keywords
Landslides • India • Landslide inventory • Susceptibility • Hazard • Risk assessment

Introduction

Landslides are significant hazards that can be disastrous to human life and property. Recent global landslide assessment studies (Petley et al. 2005; Nadim and Kjekstad 2009; OFDA/CRED 2010) reveal that the countries with the highest risk to landslides are mostly in the developing world.

About 15 % of India (~0.49 million km^2) including the mountain areas of the Himalayas, the Meghalaya plateau, and the Western Ghats are landslide-prone (NDMA 2009). During the monsoon, those areas witness frequent landslide events triggered by rainfall. Many landslide-prone areas also belong to the maximum earthquake-prone areas in India (BIS 1998), where earthquakes of Modified Mercalli intensity VIII to IX can occur, and thus, are also susceptible to earthquake-triggered landslides as well.

To mitigate the effects of such disasters, the Government of India has enacted the National Disaster Management Act in 2005. This act aims at adopting proactive and multidisciplinary approaches towards achieving disaster awareness and mitigation. The policy stresses that investments in disaster-preparedness and mitigation are much more cost-effective than expenditures on relief and rehabilitation (NDMA 2009). In this regard, predictive maps of landslide hazard, preferably at medium scales (1:25,000 to 1:50,000) are vital geo-information products that administrators/planners can use in formulating regional mitigation plans for landslide disasters. The aim of using medium-scale landslide hazard maps is to draft proper land-use zoning regulations in landslide-prone areas to alleviate, if not prevent potential loss of human life and damage to property.

Landslide research in India has always been hampered by the lack of data. In the border zones of the country, including the entire Himalayan range the use of topographical maps and airphotos has been restricted for security purposes. Thus the generation of landslide inventory maps has always been a major problem. However, due to the availability of India's own system of Earth Observation satellites, high-resolution remote sensing data (e.g. Cartosat) has become the standard input data for landslide inventory mapping, and for the generation of Digital Elevation Models used in landslide studies.

Up to now there are very few examples in India of landslide hazard maps (Sarkar and Kanungo 2005; Bhandari 2006; Sharda 2008), although a substantial part of the country's most landslide-prone area is now covered by medium-scale qualitative landslide susceptibility maps (BMTPC 2003). The Bureau of Indian Standards has formulated guidelines, among others, for landslide susceptibility zonation on a medium scale (1:50,000) (BIS 1998), using an expert-based indirect weighting approach (Anbalagan 1992). The method uses fixed weights or ranking of geofactors without directly or indirectly considering the landslide inventory data. There have been discussions on the improvement of this method, and the inclusion of landslide inventories combined with GIS-based statistical analysis as an alternative for medium scale susceptibility assessment (Sharda 2008; NDMA 2009).

In 2006 a joint research agreement was made between the Geological Survey of India (GSI), the National Remote Sensing Centre (NRSC; Department of Space, Government of India) and the Faculty of Geo-Information Science and Earth Observation (ITC), University of Twente, The Netherlands. The agreement focused on the development of training courses and the implementation of joint research projects. The Geological Survey of India (GSI) has been designated as the nodal agency for landslides by the Indian government. The National Remote Sensing Center (NRSC) under the Indian Space Research Organisation (ISRO) is in charge of rapid damage assessment using the suite of India's own satellites, and in the use of satellite data for inventory mapping and susceptibility assessment. The research collaboration included two Ph.D. researchers from GSI and one from NRSC. Later also other organizations were involved in the research. Another Ph.D. researcher from the Centre for Earth Science Studies (CESS), in Thiruvananthapuram, Kerala, was integrated in the project, as well as one from the Indian Institute of Remote Sensing (IIRS), which is the training center of the Indian Space Organization. The research collaboration also involved a number of European institutions, such as the Faculty of Geosciences of Utrecht University (The Netherlands), the National Research Council of Italy (CNR-IRPI, Perugia), the University of Vienna, and the German Geological Survey (BGR, Hannover).

The main objective of the research project was to develop and test methods for landslide inventory mapping, susceptibility-, hazard and risk assessment that are applicable in India, considering the variability and complexities of the landslide-prone terrains, and considering the data availability. Methods were developed for different scales of analysis. The methods focused on techniques for generating landslide inventories, the application of appropriate susceptibility models (heuristic, statistical, physically based), the characterization of landslide hazard in terms of temporal, spatial and size probability, and the use of this information in landslide risk analysis.

Study Areas

It was decided to develop and test the methodology in four different areas in India, each one linked with a Ph.D. research. Figure 1 shows the location of the four study areas.

Each of the four studies had its own main research focus, as can be seen from Table 1.

In the following sections the main results from these four studies will be presented.

Case Study A: Landslide Inventory Using Object Oriented Image Analysis

Landslide inventories that span a substantial period of time are one of the key requirements for landslide studies (Van Westen et al. 2008). Image interpretation still is the main method for generating these. Several research attempts have been made to automate and speed up the process of landslide interpretation as major trigering events might cause hundreds or even thousands of landslides. Since pixel-based methods have not produced sufficiently accurate results for detection and classification of landslides, object-oriented analysis (OOA) which imitates the human interpretation process in identification of landslides, has emerged as a good alternative due to its inherent ability to incorporate additional information layers such as digital terrain models (DTMs) and thematic maps in the analysis. Furthermore, as landslides are geomorphic processes, their characterisation in different types mostly relies on contextual criteria, which can best be described by objects obtained from segmenting the digital image into spatially cohesive regions/objects rather than pixel values. Martha et al. (2011b) developed semi-automatic image analysis algorithms that combine spectral, shape, texture, morphometric and contextual information derived from high resolution satellite data and DTMs for the preparation of landslide inventories. The main innovative aspect of the research lies in the selection of landslide diagnostic parameters and their use in the comprehensive characterisation of different types of landslides, a concept which is addressed for the first time for detection of landslides in an object-based environment.

DTM accuracy is an important factor since its morphometric derivatives, such as terrain curvature, slope, and flow direction, contribute to the successful detection and classification of landslides. Cartosat-1 along-track stereoscopic data, which are provided with RPCs for block triangulation, were used to create a DTM with 10 m grid size (Martha et al. 2010a). Conversion of a DSM to a DTM was carried out for calculating landslide volume and terrain morphometric parameters, by subtracting vegetation height from the DSM. The landslide volume extracted from pre- and post-landslide DTMs (Fig. 2) without control points matched well with volume extracted from the DTMs with control points, indicating that a field survey for control points is not a strict requirement (Martha et al. 2010b). It also showed that landslide volume information can be derived only with RPCs, if both pre- and post-image pairs can be brought into the same relative reference framework.

A set of approaches was developed that exploit the object properties extracted using a region-growing segmentation of multispectral Resourcesat-1 LISS-IV Mx (5.8 m) image (Martha et al. 2010c). The method was tested in the Okhimath area, in Uttarakandh. An algorithm comprising 45 individual routines, such as controlled segmentation, merging and classification was developed using eCognition software, which detected 42 major and minor landslides in an 80 km^2 area. The algorithm, initially extracts landslide candidates using an NDVI threshold, and subsequently false positives were eliminated from the landslide candidates using spectral, texture, shape and contextual criteria (Fig. 3). Landslide classification was done using terrain curvature and contextual criteria, and five different types of landslides were identified. The object-based classification, when compared with a landslide inventory map prepared by stereoscopic photo-interpretation and detailed field check, resulted in a detection accuracy of 76.4 %, while 69.1 % of the landslides were correctly classified in different landslide types. The results are considered to be good, since landslides are detected in an area dominated by false positives such as rocky barren land, uncultivated agricultural terraces and river sands. The minimum landslide size detected by the method was 700 m^2.

The algorithm developed required user-defined segmentation criteria to control the object size, which was considered a drawback in applying a fast and generic method for landslide detection and classification. Therefore, an objective method to optimise segments was developed subsequently (Martha et al. 2011a). Using spatial autocorrelation and intrasegment variance, a new plateau objective function (POF) was developed, which was used to determine the segmentation criteria for multi-scale analysis, essential for the detection of landslides and elimination of false positives. Another drawback of the originally developed algorithm was the use

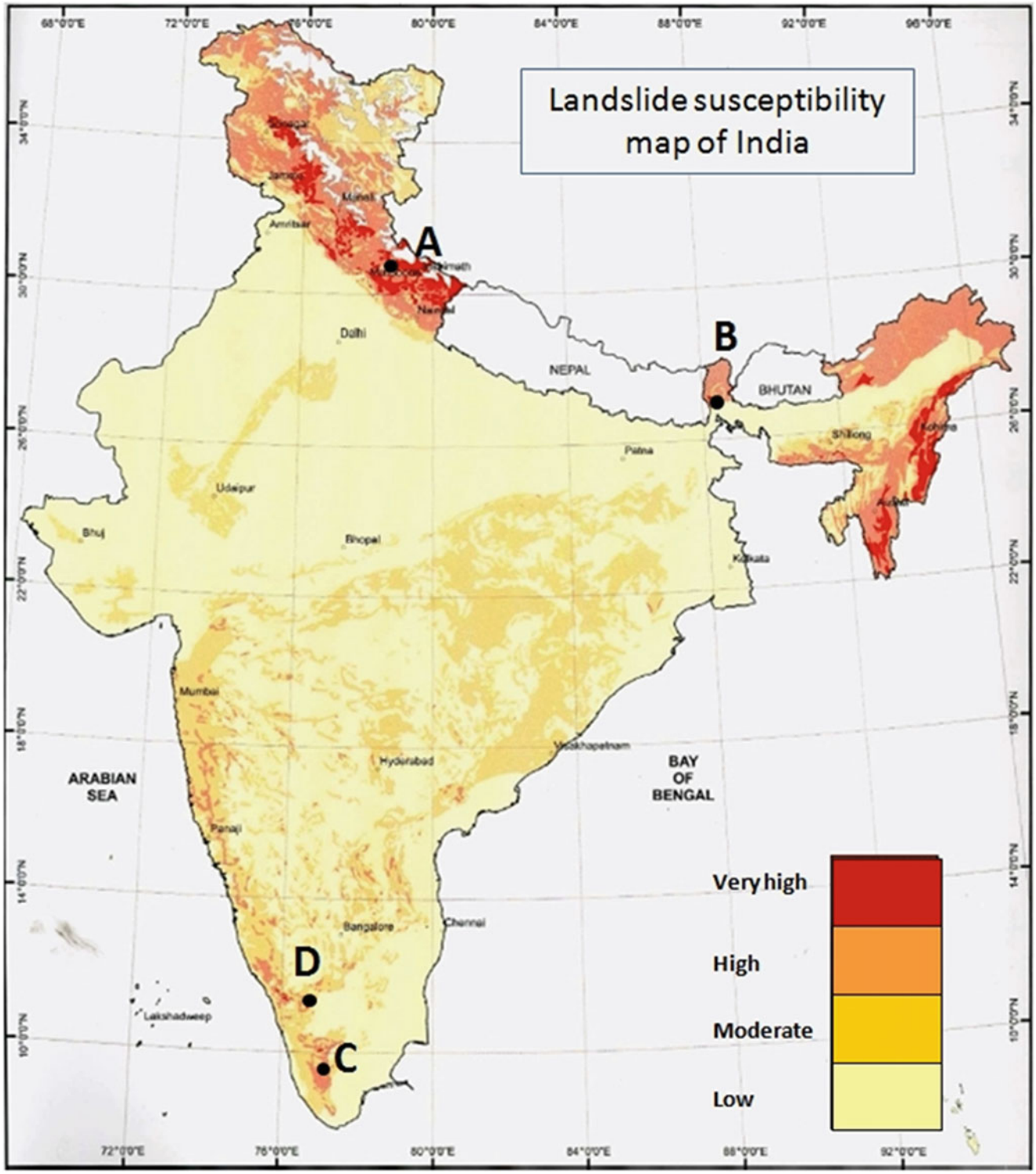

Fig. 1 National landslide susceptibility map (Rajarathnam and Ganapathy 2006) with the location of the test sites. A: Okhimath (Uttarakhand state), B: Kurseong (Darjeeling state); C: Tikovil (Kerala state), D: Nilgiri (Tamilnadu state)

of manual thresholds for the elimination of false positives from landslide candidates. This was adjusted using a K-means clustering method. The improved algorithm, comprising of four sub-modules, resulted in a detection accuracy of 76.9 % for the training area and 77.7 % accuracy for a geomorphologically distinct validation area (Fig. 4). It not only increased the accuracy of detection but also reduced the overall error of commission.

Another algorithm was used for landslide detection from archived high resolution panchromatic images, which is a

Table 1 Main research themes in the four case study areas, indicated in Fig. 1

Area	Research focus
A: Okhimath & Uttarkashi (Uttarakhand)	**Detection of landslides by object – oriented image analysis.** Generation of Digital Surface Models from Cartosat satellite images; application of NDVI-based thresholds for landslide detection; development of a rule set for removal of false polygons; semi-automatic classification of landslide types; development of a method for landslide detection from multi-temporal panchromatic images; bivariate statistical analysis; and semi-qualitative risk analysis (Martha et al. 2011b; Das et al. 2010, 2011)
D: Kurseong (Darjeeling)	**Knowledge guided empirical prediction of landslide hazard**. Landslide inventory made through multi-temporal image interpretation; event-based landslide inventories; relation with triggering rainfall; analysis of the structural control of discontinuities on rock slides; combination of heuristic and statistical methods for susceptibility assessment; temporal- spatial- and size frequency analysis; semi-quantitative risk analysis (Ghosh et al. 2011b)
C: Tikovil (Kerala)	**Physically-based dynamic modelling of the effect of land use changes on shallow landslide initiation.** Inventory made with community-based mapping; detailed soil thickness modelling; geotechnical and hydrological characterization; ground water modelling; slope stability analysis; failure probability analysis; runout modelling; prediction of future slope stability scenarios (Kuriakose et al. 2010)
D: Nilgiri (Tamilnadu)	**Landslide risk quantification along transportation corridors based on historical information.** Landslide inventory made from maintenance records for road and railroad; rainfall threshold analysis; frequency-size analysis; hazard analysis; quantitative direct and indirect risk analysis; use of risk information for disaster risk reduction (Jaiswal et al. 2011c)

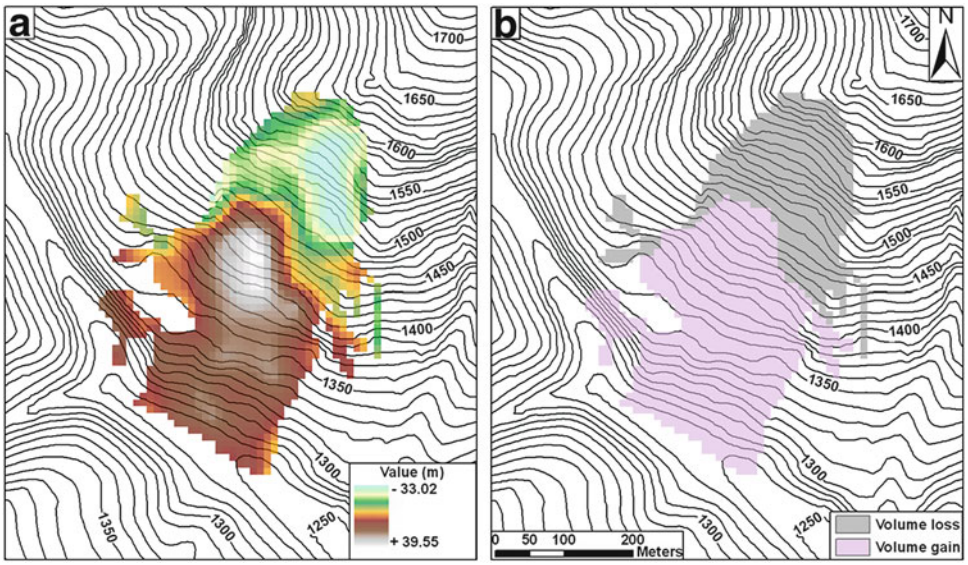

Fig. 2 Volumetric analysis of the Salna landslide based on satellite derived DTMs. (**a**) Elevation difference due to the landslide with negative values showing lowering of surface and positive values showing rising of the surface after the event, and (b) extent of the volume loss and volume gain, which corresponds to the zones of depletion and accumulation, respectively (Martha et al. 2010b)

modified version of the second one. It uses a brightness threshold instead of NDVI to extract landslide candidates (Martha et al. 2012). Local thresholds using contextual criteria showed better results than global thresholds, and allowed to identify small translational landslides within barren rocky land that are generally bright. To eliminate false positives, more texture measures, such as GLCM homogeneity and standard deviation, were used along with shape and contextual criteria. Finally, a multi-temporal annual landslide inventory for 13 years was prepared and used for the generation of a landslide susceptibility map with the help of a bivariate model (Martha et al. 2013).

The final algorithm for the detection of landslides, developed by Martha et al. (2011b) is generic and requires two primary inputs (a satellite image and a DTM), and doesn't require information that should be collected in the field. The semi-automatic approach is flexible enough to address the spatial and spectral variability of landslides and false positives. The knowledge-based method shows considerable improvement over previous pixel- and object-based methods of landslide detection in terms of the location, size and type of landslide. The method has increased the potential to rapidly generate event-based landslide inventories after major triggering events, within a short

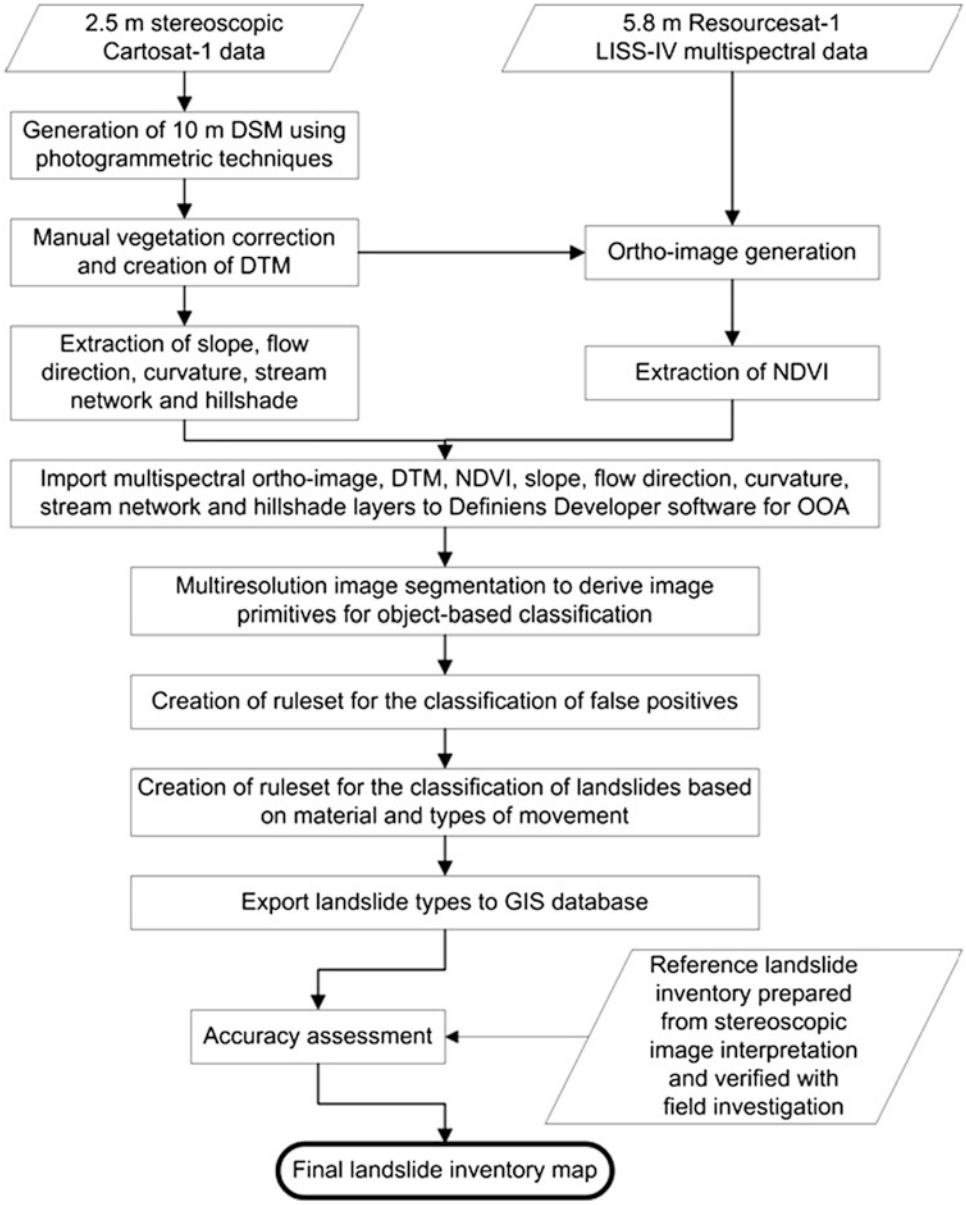

Fig. 3 Generalised methodology flowchart for semi-automatic detection of landslides using object-based methods (Martha et al. 2010c)

period of time. The method developed in this research has proven its value in several areas in the Indian Himalayas and could potentially contribute to the rapid detection of landslides in other susceptible areas.

Case Study B: Knowledge-Guided Empirical Prediction of Landslide Hazard at the Medium Scale

Estimating and mapping variations in the spatial likelihood of occurrence of landslides (susceptibility assessment) is a fundamental step towards landslide hazard prediction. Landslide susceptibility aims to identify where future landslides are likely to occur, based on the fundamental assumption that spatial factors that caused present and past landslides are likely to cause similar landslides in the future.

In Indian, the BIS guidelines (BIS 1998) recommended an indirect approach to landslide susceptibility mapping and provides a generalized heuristic system of fixed weighting or ranking of geofactors called landslide hazard evaluation factor (LHEF) rating. These LHEF ratings are applied irrespective of various terrain conditions and were determined by an expert group without directly considering the landslide inventory data. Since the spatial extents of landslide geofactors and their respective causal association with different types of landslides and failure mechanisms are variable, the fixed LHEF ratings assigned to geofactors

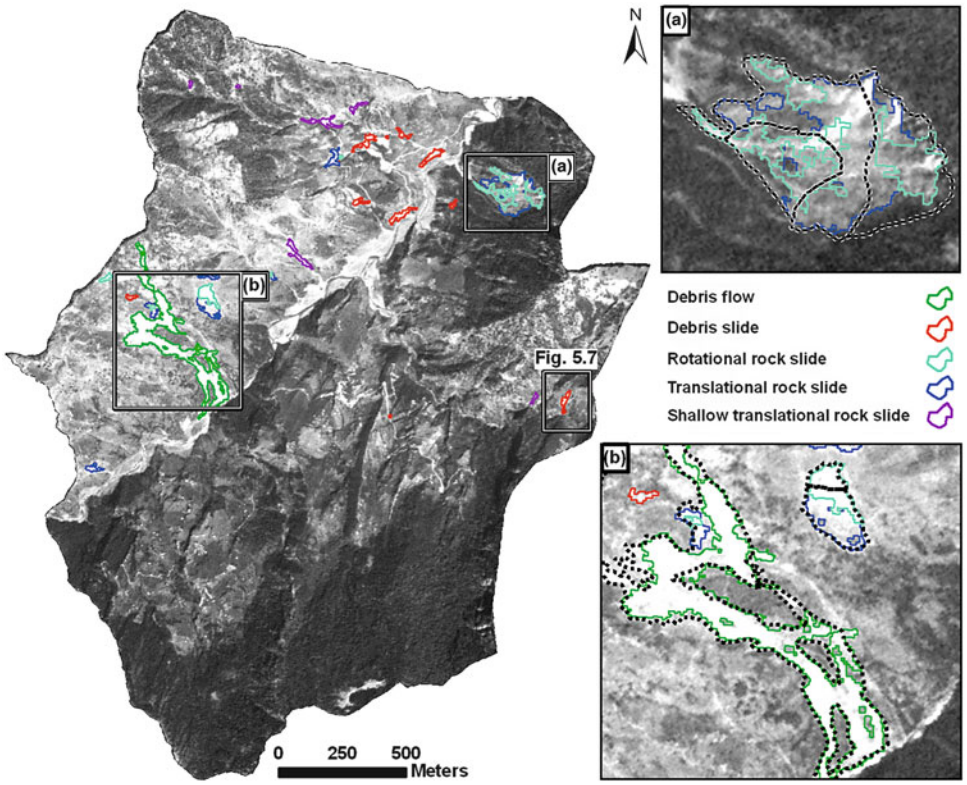

Fig. 4 Landslide types recognised using OOA in the Okhimath area. The *dotted lines* in insets (*a*) and (*b*) show the reference landslide inventory (Martha et al. 2011a)

can be inappropriate and lead to less accurate landslide prediction rates when applied to different areas. The aim of this research was to propose an effective method for medium scale landslide hazard and risk analysis suitable for the Indian geo-environment which can be readily used by the public research Institutes/Organisations engaged in landslide research in India. The proposed method considered the variability and complexities of the one of the predominant landslide-prone terrains (e.g., the Darjeeling Himalayas) and the landsliding processes prevalent there, so that the aspects of variable controls of landsliding factors can be better understood (Ghosh et al. 2009a, 2011b). This was done through:

- Generation of landslide inventory maps for different triggering events, based on the available information in the forms of landslide maps, images and archives. These maps should portray the landslide patterns and types of triggering events with a range of return periods, which can be used to analyse the temporal and magnitude probabilities (Ghosh et al. 2009b, 2012a);
- Development of an exploratory analytical technique for understanding the mutual/exclusive spatial relation between regional structures (e.g., faults/fractures) and slope aspects with rockslides of a certain type (Ghosh and Carranza 2010);
- Develop a specific method for analyzing different rock slope failure modes, by spatially incorporating the 3-D structural orientation data (Ghosh et al. 2010);
- Analyze the spatial associations between landslides of specific types and a set of causal factors, using bivariate statistical methods for selecting and weighting the appropriate spatial factors and integrate the right and weighted spatial factors into landslide susceptibility maps for each type of landslide (Ghosh et al. 2011a);
- Integrate the spatial, temporal and size probabilities of landslide events and convert the susceptibility maps into hazard maps (Ghosh et al. 2012a);

Generating Inventory Maps

The source data sets that were used in this study for landslide inventory mapping consisted of high-resolution satellite images, aerial photographs, topographic maps, old landslide inventory maps and reports of field investigations which were available for the study area in Darjeeling. The oldest data set consists of topographic maps prepared by the Survey of India (SOI) in 1969, which included the locations of prominent and active landslides of a major triggering event in 1968. The next data set consists of 1:50,000 and 1:10,000 scale black-and-white stereo-air photos from 1980, which

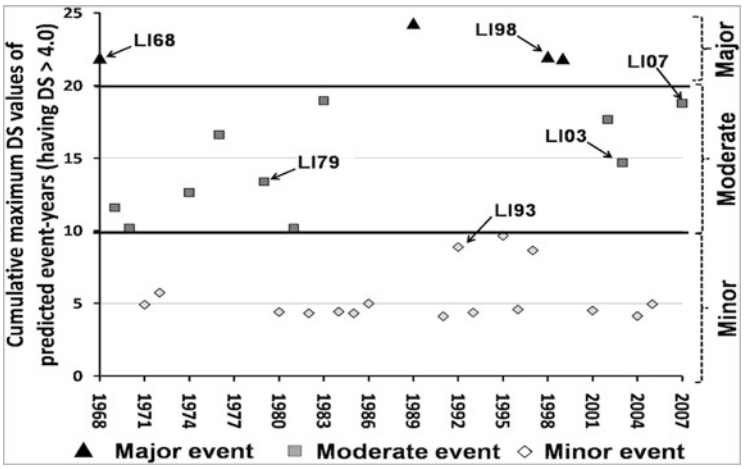

Fig. 5 Threshold cumulative discriminant scores (DS) for predicted "*minor*", "*moderate*" and "*major*" landslide events. The available six events are shown and associated with corresponding inventory numbers to depict validity of model-derived severity classifications of known landslide events

were interpreted using stereo-image interpretation. The third and fourth data sets are field-based landslide inventory map from 1993 and 1998 prepared by GSI soon after major triggering events. For the period 2002–2006, three high-resolution Indian satellite images were used as source data. The most recent data set is a detailed landslide inventory map prepared during this research through field surveys soon after a recent landslide event in 2007. For each period a landslide inventory was made, and landslides were mapped as polygons, resulting in a total of six event-based landslide inventories, which were compared to examine variations in landslide characteristics (frequency, area, density, type and activity). Unfortunately the available data was not covering all landslide triggering events in the last 50 years.

Therefore a multivariate classification technique (discriminant analysis) was used to define an empirical relationship between days with and without landslide events as response variable and daily variation in rainfall amounts as predictor variables. The frequencies of landslide events predicted via DA that were linked to triggering rainfalls were then used in a Poisson distribution model to calculate the temporal probability of similar landslide events in the future, which were classified in major, moderate and minor events (Fig. 5).

Rock Failure Type Modelling

Many of the landslides in the Himalayas are rock slides, or are in weathering soil with a clear structural control. For rock slides, since failure propagates along a near-planar surface (planar) or triggered along the intersection of two planes (wedge), the presence/absence of any planar discontinuity, its nature, extent, orientation and frequency of occurrence in relation to topography are crucial deciding geofactors. The geometric or kinematic interrelationships between the attitudes of bedding/foliation/joint planes and topography are important in deciding the mode of movement of rock slides. To determine kinematically the unfavourable discontinuity-topography/structure domains, different topographic segments were identified after establishing the geometric interrelationships of the orientations between topography and prominent discontinuity surfaces (Ghosh et al. 2010). For the calculation of the angular interrelationship, raster maps of topographic slope, topographic aspect, discontinuity dip and discontinuity dip direction were used. Dip and dip direction raster maps of prominent discontinuities were generated through interpolation of discrete dip/dip direction values of foliation planes, measured at different point locations. After this structural domains were derived by combining the above four raster maps and calculating their angular relationships. Different rock slide failure mechanisms were successfully identified spatially by studying the kinematic interrelationships between the attitudes of distributed bedding/foliation/joint planes and topography through spatial correlation. A GIS-based application was used for the spatial analysis with distributed rock structure data (Günther 2003) and areas susceptible to wedge, planar and toppling failure modes were delineated (Fig. 6). The best approach would be to parameterize all these structure domains per failure mechanism spatially and utilise them for a detailed quantitative rock slope susceptibility analysis.

Combining Heuristic and Statistical Methods

Heuristic methods for spatial prediction of landslide occurrence can either be direct or indirect. In indirect heuristic methods, individual factors are assigned specified weight values or ratings that are based on subjective criteria. The main limitations/problems of heuristic methods are related to the subjectivity involved. Although the same subjectivity could be present in selecting and mapping of the factors for data-driven methods, but the relative importance of

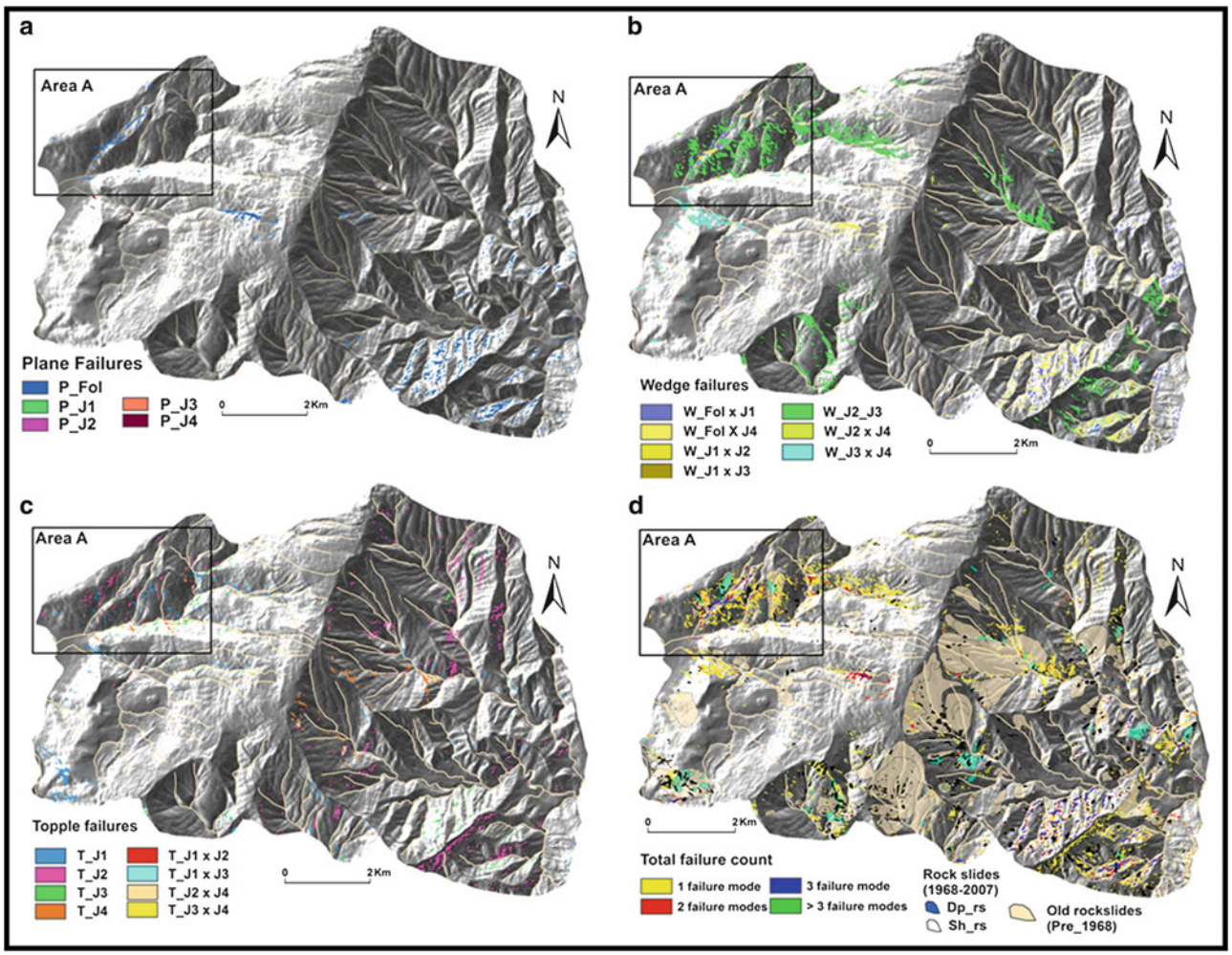

Fig. 6 Modelled unstable slopes for different types of rock slope failure (**a**) plane failure (**b**) wedge failure (**c**) topple failure (**d**) slopes where at least one failure mode is kinematically possible

the factors is determined by more objective techniques. One of the main advantages of heuristic methods is that they can allow site specific and landslide type specific evaluations of the causal factors, and avoid the generalization that is often used in data-driven ones.

Landslide susceptibility is a function of two types of spatial associations: (1) spatial associations of individual spatial factors with known landslides of a certain type; and (2) relative importance of individual spatial factors with respect to one another in relation to those known landslide occurrences. Methods of bivariate empirical analysis can model only the first type of spatial association. In contrast, multivariate methods can model those two types of spatial associations simultaneously, but often include spatial factors that do not seem to have a direct relation with the landslide process and generally do not include expert opinion. Therefore an empirical method was developed for the analysis of spatial association at a medium-scale. The data used are presented in Table 2.

For each class of a categorical factor, the Yule's coefficient was used to quantify its spatial association with known occurrence of shallow landslides. Based on calculated values of Yc for every factor, a Landslide Occurrence Favourability Score (LOFS) was calculated per factor class. Distance distribution analysis (DDA) was used for measuring the spatial association of continous variables.

For the analysis of inter-predictor weights the analytical hierarchy process (AHP) was applied. Based on the spatial association analyses and the predictor weights derived via AHP, 14 out of 21 identified spatial factors for shallow translational rockslides were used and 12 out 22 spatial factors for shallow translational debris slides. To integrate the selected predictors of each type of shallow landsliding, the weighted multi-class index overlay method was applied (Fig. 7).

The results were compared with a backward stepwise Logistic Regression analysis, which starts with all input predictors and ends with only statistically significant predictors that contribute to the prediction or classification.

Table 2 Data source, methods of preparation/mapping of spatial factors of shallow landslides. Sh_rs = shallow translational rockslides. Db_rs = shallow translational debris slides

Generic factor theme	Specific factor	Source data, scale or spatial resolution and method of mapping of factor	Landslide type	
			Directly related	Indirectly related
Topography/ morphometry	Slope aspect curvature	DEM of 10m × 10m pixel resolution; automated mapping in GIS	Sh_rs, Db_rs	–
Lithology or slope material	Rock and soil type	Field data, information from existing geological maps (1:10,000–1:50,000 scales)	Sh_rs, Db_rs	–
Depth to bedrock	Soil/overburden thickness	Estimated using field data from 400 sites and linked to lithology map	Db_rs	–
Structure	Distance to major thrusts	Compiled from 1:50,000 and 1:25,000 geological maps; interpreted from high spatial resolution satellite imagery and stereo air-photos (1:50,000 and 1:10,000); ground-truthing in the field.	Sh_rs,	Db_rs
	Distance to faults/ fractures	Interpreted from stereo-pairs of 1:10,000 and 50,000 B × W air-photos with limited ground-truthing in the field.	Sh_rs,	Db_rs
	Distance to kinematically unstable slopes	Determined using field data of rock discontinuity orientations and DEM-derived slope and aspect maps (Ghosh et al. 2012b)	Sh_rs,	Db_rs
Land-use/ land-cover	Land-use/land-cover	Interpreted from 1:10,000 and 1:50,000 B×W air-photos and multispectral IRS LISS 4 MX imagery (5.8 m spatial resolution) with limited ground-truthing in the field	Sh_rs, Db_rs	–
Old rockslides	Distance to old rockslides (pre-1968)	Mapped from stereo interpretation of 1:10,000 scale B × W stereo air-photos of 1980	Sh_rs, Db_rs	–
Hydrology	Contributing area upslope	DEM of 10 × 10m pixel resolution	Sh_rs, Db_rs	–
	Wetness index	DEM of 10 × 10m pixel resolution		
	Drainage density	DEM of 10 × 10m pixel resolution; digitized streams from 1:25,000 topographic maps		
	Distance to streams	DEM of 10 × 10m pixel resolution; digitized streams from 1:25,000 topographic maps		

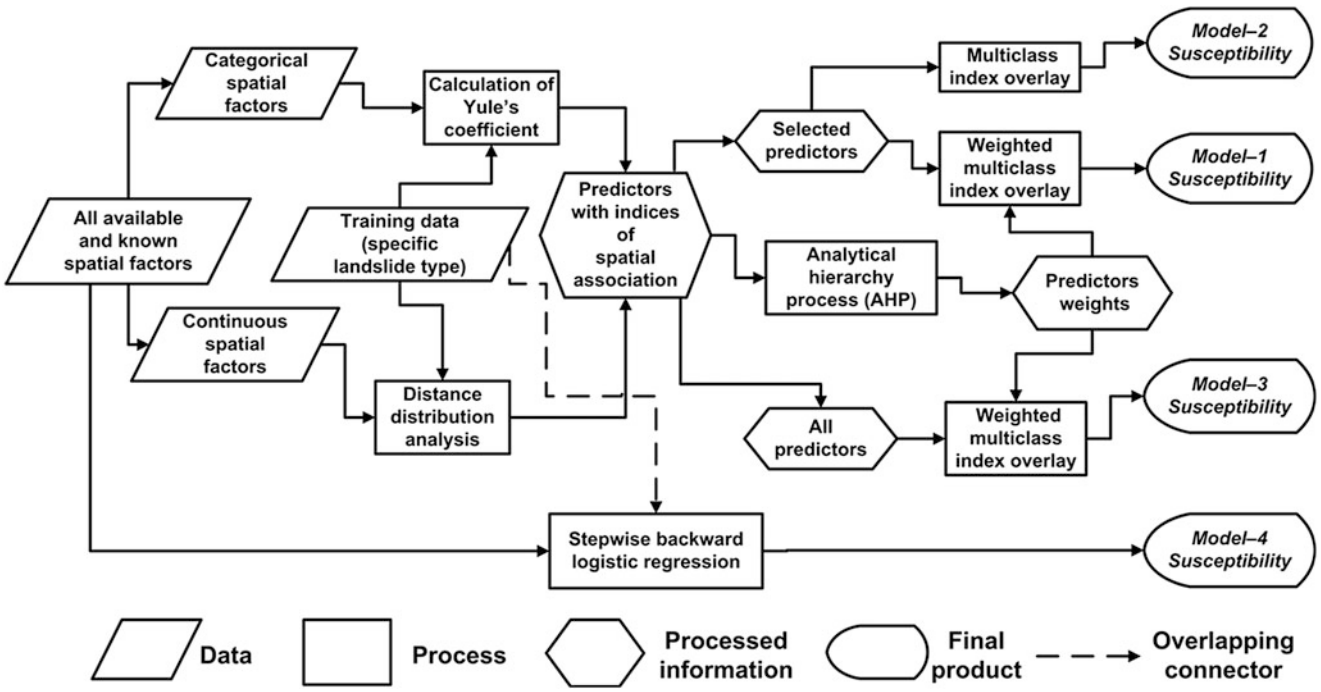

Fig. 7 Schematic flow diagram showing data, processes and steps for developing four different models of susceptibility to shallow landsliding

The resulting susceptibility map was combined with the landslide inventories for different types of triggering events (major, moderate and minor), which were used to estimate temporal and spatial probability and to convert them into a hazard map, which was subsequently used in a semi-quantitative risk assessment (Ghosh et al. 2012a).

Case Study C: Physically Based Landslide Hazard Assessment

The third case study focused on the application of deterministic modelling at local scale, and to use it to evaluate the effect of environmental changes on landslide activity. The case study area is in the highland region forming the western slopes of the Western Ghats of Kerala state, which is increasingly affected by shallow landslides and debris flows. High intensity rainfall, and the presence of perched water tables resulting in high pore-water pressure conditions are considered as the principal trigger of these landslides. The spatio-temporal probabilities of shallow landslide initiation in this area are dependent on the land use which in turn determines the mechanical and hydrological effects of vegetation on slope stability. The application of physically-based spatially distributed modelling was the most suitable approach to verify this hypothesis as it has the capability to not only estimate the spatio-temporal probabilities of shallow landslide initiation, but also quantitatively assess the influence of changes in environmental conditions on slope stability, for example those of land use changes.

Four shallow landslide initiation models were applied, namely SHALSTAB, SINMAP, TRIGRS and STARWARS + PROBSTAB (Kuriakose et al. 2010). The STARWARS (Storage and Redistribution of Water on Agricultural and Revegetated Slopes) + PROBSTAB (Probability of Stability) model, which is a coupled hydrology and stability model that uses a first order second moment approach for quantifying the probability of failure, was identified as the most suitable for this research. A pilot study conducted in the upper Tikoy river basin (55 km^2) revealed that it was necessary to accurately measure and spatially parameterize root reinforcement, soil depth, soil hydraulic conductivity and soil strength properties to derive reliable results from the model (Kuriakose et al. 2008). It was also evident that a detailed characterization of rainfall patterns and corresponding slope hydrological responses such as transient ground water level and discharge was necessary to calibrate and validate the STARWARS (the hydrology model) while a detailed landslide inventory was needed for the calibration and validation of PROBSTAB (the slope stability model).

To acquire hydrological data with a high temporal resolution, 13 automated open stand pipe piezometers, one discharge station (stage gauge) and one weather station were deployed in the Aruvikkal catchment from May 2007 onwards. A partially complete landslide inventory was prepared based on governmental reports, news paper clips, field work and community-based approaches. Time series analysis conducted on the rainfall and the corresponding hydrological responses revealed that the slope hydrology of the catchment exhibits very rapid response to rainfall; the discharge of the catchment will respond within 1 h. The average time necessary for a significant response of the perched water level to rainfall was 6 h while during the peak rainy season this lag may reduce to less than 1 h. It was also observed that continuous and high intensity rainfall of about 4 h may cause a steep rise in the perched water table up to critical levels in regolith filled bed rock depressions and the persistence of this level for ~10 h may lead to shallow landslides in the catchment. Thus to capture the hydrological responses that lead to shallow landslide initiation in the catchment, the hydrology model should be able to predict these responses with a temporal accuracy of at least 6 h which necessitates the model time step to be of at least 1 h in resolution.

All soil mechanical properties necessary was measured and spatially parameterized. Block regression kriging with altitude, aspect, slope, distance from streams, compound terrain index, curvature and land use as predictors was identified as the 'best' predictor of soil depth in such anthropogenic landscapes (Kuriakose et al. 2009b). Depending on the dominant plant species in each land use unit and the soil depth the corresponding root reinforcement applicable was derived from measured root tensile strength, pull out strength, root diameter and root density data. Nine species of plants were tested of which Teak (Tectona grandis) trees offered the highest amounts of net root reinforcement (Kuriakose and Van Beek 2011). The STARWARS model was calibrated and validated against the observational data of 2007–2008 period. The PROBSTAB was calibrated and validated against the landslide inventory of 2001 and 1993 respectively, for which the corresponding daily rainfall data available from a nearby tea estate was disaggregated to hourly using stochastic methods (Kuriakose et al. 2009a).

In order to evaluate the effects of long term and short term land use changes on slope stability in the region, historic (1913–2008) land use maps, soil depth maps and root reinforcement maps were derived. In addition the land use maps and corresponding root reinforcement maps of two future scenarios (2016 and 2058) were also derived. Although, these future land use scenarios represent only one of the many possible realizations, the interest in them lies in the fact that they show a possible scenario of reforestation, and hence conservation of the area. These data sets were used to simulate the corresponding slope stability and probability of failure conditions based on the 1985 rainfall time series (disaggregated to hourly) which included the most extreme

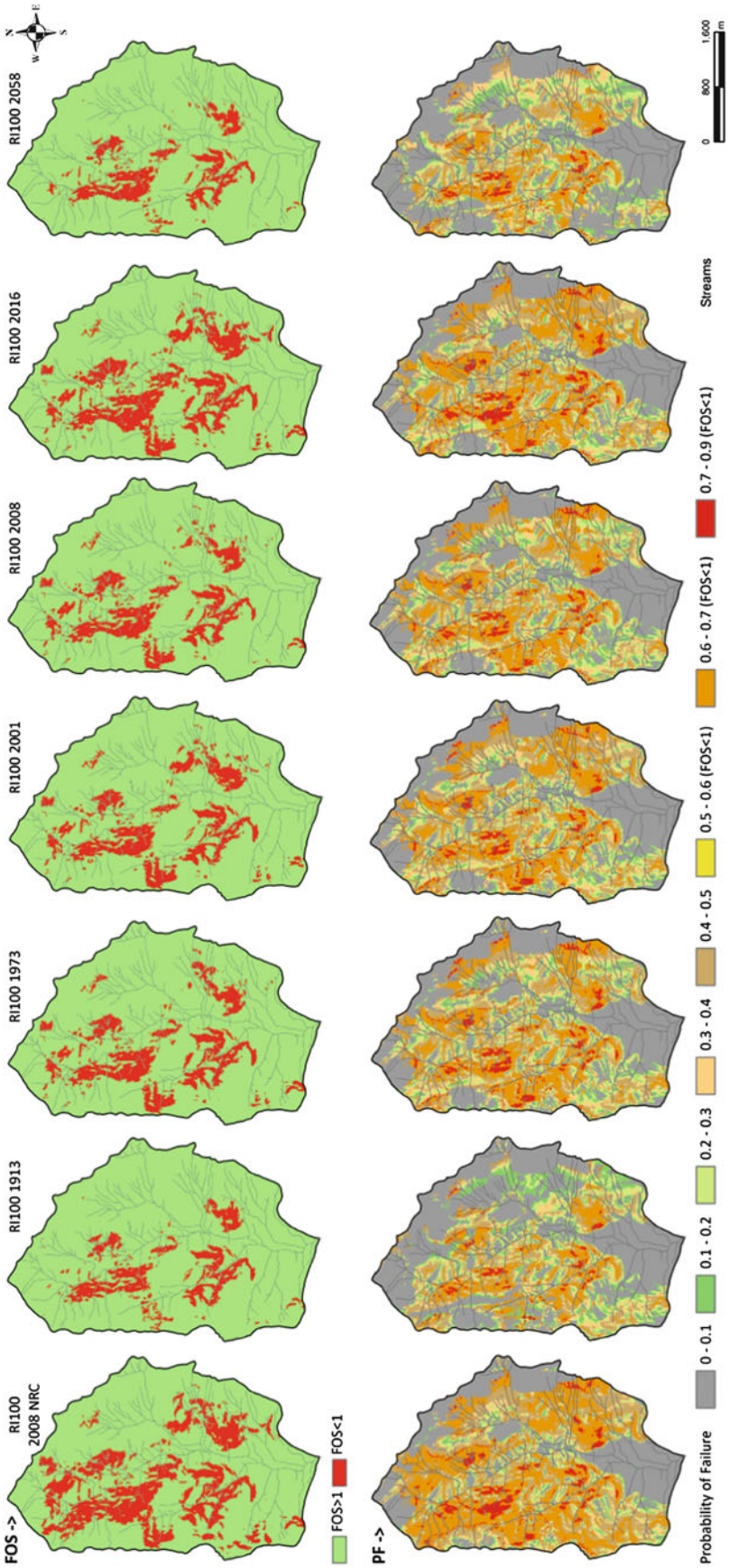

Fig. 8 Area with FOS < 1 and the probability of failure corresponding to the land use scenarios of 1913, 1973, 2001, 2008, 2016, 2058 and the no-root cohesion condition (Kuriakose et al. 2010)

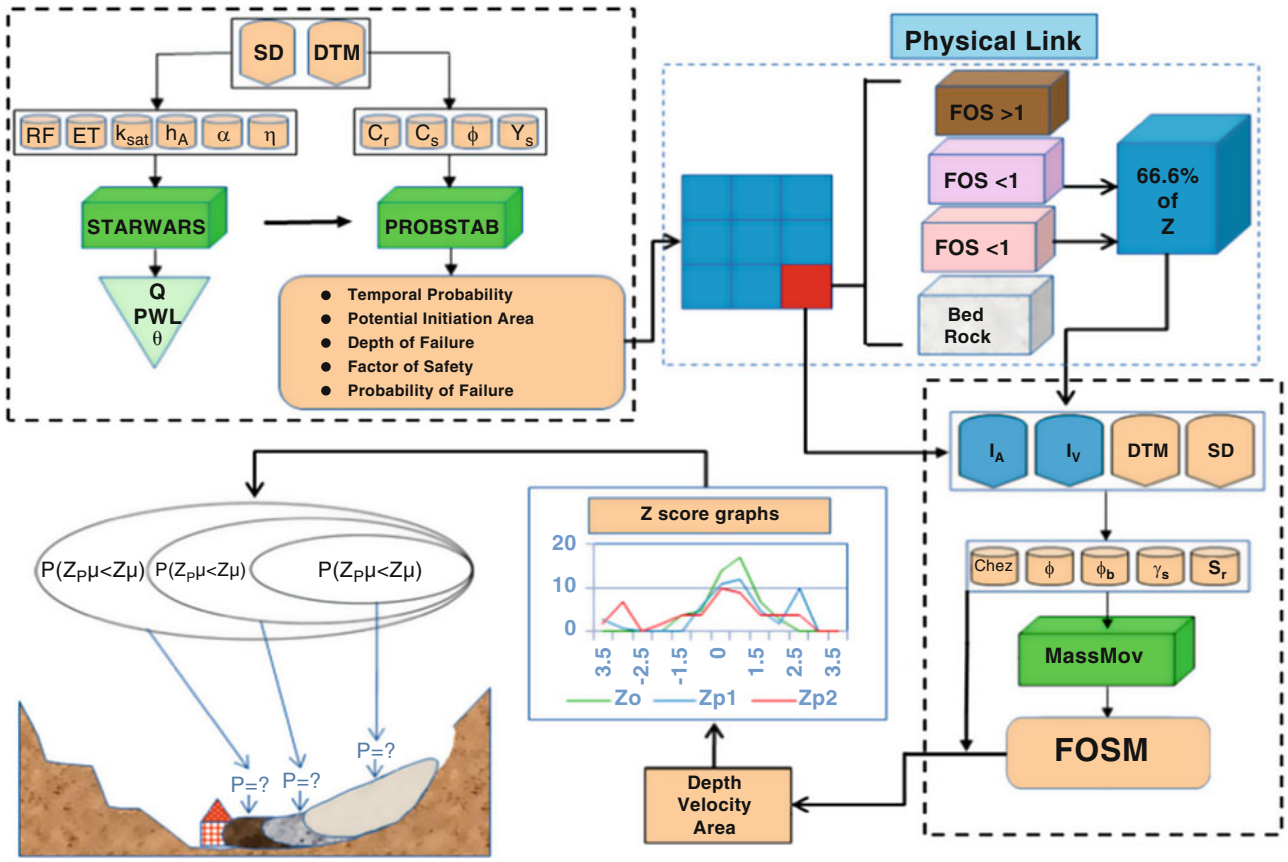

Fig. 9 Scheme for coupling the results of STARWARS + PROBSTAB with the runout model MassMov2D

daily rainfall that has caused at least one shallow landslide in the study area in the past 57 years (Fig. 8).

The land use changes from the pre-plantation (1913) scenario to present (2008) have resulted in an average increase in the potential area of failure by 43 % and the spatio-temporal probability of failure by 49 %. Despite setting up an idealistic land use scenario for the distant future (2058), the overall slope stability did not revitalize to the pre-plantation period (1913) because the root reinforcement available was relatively lower as compared to the pre-plantation period.

The simulation may imply that a policy of reforesting to promote conservation (stability) in the area might not have the intended results.

The research showed that in the study area, the transition probability of land use change (and consequently the changes in soil depth and root cohesion) outweighs the rainfall quantity in determining the spatio-temporal probability of shallow landslide occurrence. This is in contradiction with the commonly held belief that the temporal probability of shallow landslides can be quantified with only the return probability of landslide-causing extreme rainfall events. Hence, transition probabilities of land use should be assessed and incorporated in regional scale landslide hazard assessments that utilize heuristic and stochastic techniques, especially in such anthropogenically modified terrains.

The study also analyzed the coupling of the initiation model with a runout model. A tentative scheme for coupling the results of STARWARS + PROBSTAB with a runout model named MassMov 2D (Begueria et al. 2009) is presented in Fig. 9. By systematically varying the input variables based on a first order second moment approach (FOSM), one can derive the maximum, average and minimum extent of runout possible, given a certain initiation area and volume of material. Depending on the number of times that a given pixel gets affected by a debris flow, one can derive the spatial probability of being affected by a certain magnitude (depth, area or velocity) of debris flow, while the initiation model can provide the temporal probability of initiation of such a debris flow.

Case Study D: Landslide Risk Assessment Along Transportation Corridors

The fourth case study focused on quantitative landslide risk assessment along transportation corridors (a road and a railroad) in the Nilgiri area (Tamilnadu), making use of a nearly

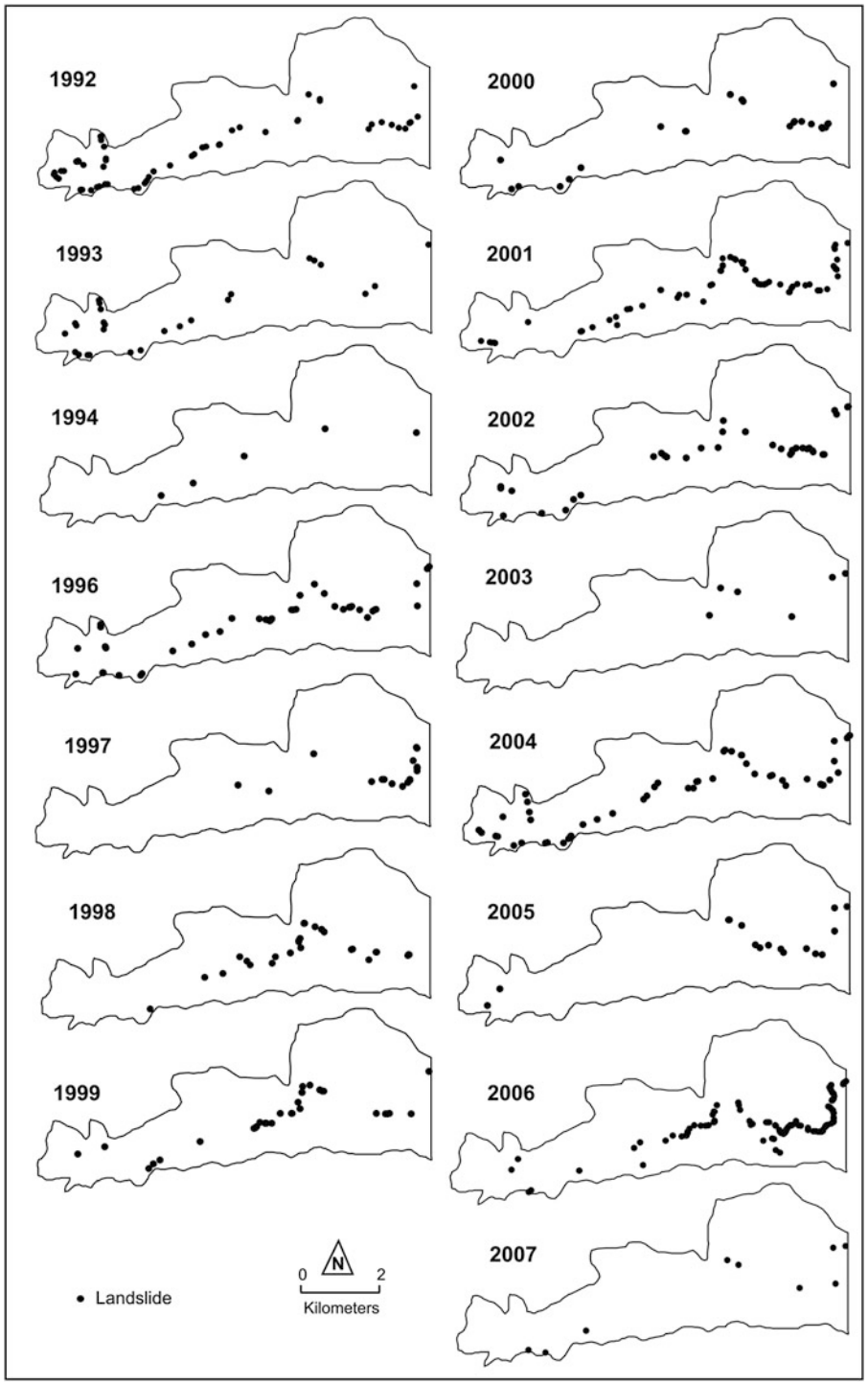

Fig. 10 Spatial distribution of landslides in different years along the railroad. Landslides are shown as *points* irrespective of their size

complete historical database of landslide occurrences over the past 24 years (Jaiswal et al. 2011c).

Generation of Landslide Inventory from Archives

In the Nilgiri area it was possible to generate a very detailed landslide inventory based on historical data. The records include railroad and road maintenance registers, and technical reports. From 1987 maintenance data were present in an analog form recorded in a register. This register is updated soon after the occurrence of a landslide triggering event and is used for tendering contracts for (rail)road clearance. The technical reports include published and unpublished technical

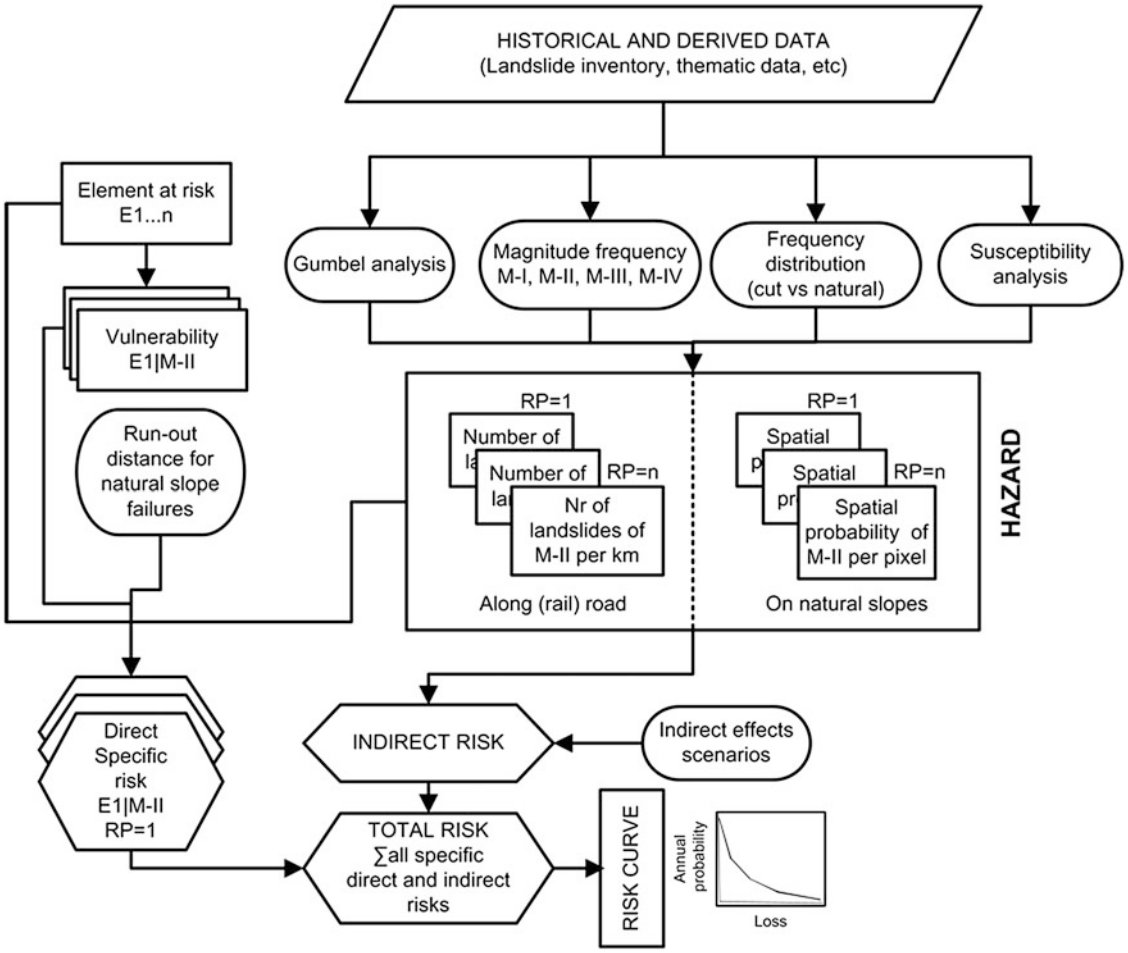

Fig. 11 Flow diagram showing the process adopted for landslide risk analysis (Jaiswal et al. 2010b)

documents of landslide investigations. The data were used to reconstruct the landslide occurrences along the road and railroad over several decades. Data on 901 landslides were compiled from the historical records covering a 21 years period from 1987 to 2007. Figure 10 displays annual landslide maps from 1992 to 2007 (Jaiswal).

The landslide dataset was used to analyze the landslide intensity for different years, by calculating the recurrence interval of the percentage of unit lengths of the road and railroad that would be interrupted during triggering events (Jaiswal and Van Westen 2009).

To quantify landslide hazard using such a complete inventory, as was the case for the Nilgiri case, two essential parameters were assessed: the probability that landslides affecting the infrastructure are of a given magnitude, and total number of landslides per kilometer affecting the infrastructure in a given return period. The landslides in the study area were grouped in five magnitude classes ranging from I (less severe) to V (catastrophic). The classification is essentially based on landslide type and volume but it also gives other characteristics such as the location of the source, damage potential and human perception about the risk

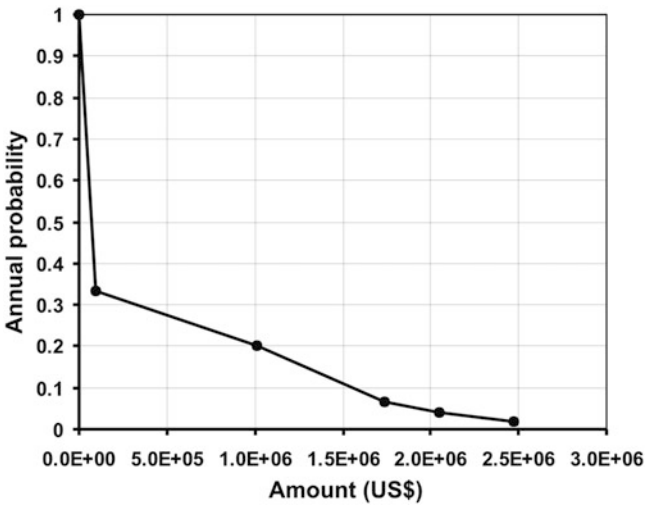

Fig. 12 Risk curve for total landslide losses in the study area (maximum risk) expressed in monetary value (US$) (Jaiswal et al. 2011a)

related to landslides. The probability that a landslide affecting the infrastructure is of a given magnitude class was estimated using magnitude-frequency relationships. Annual

Fig. 13 Participants of the symposium on landslide hazard and risk assessment in India, held in ITC on 4 and 5 July 2011

probability of landslide occurrence was estimated from the observation of the frequency of past landslide events, by determining the annual exceedance probability (AEP), using Poisson and Binomial distribution models. The estimation of landslide risk, particularly indirect risk resulting from the blockage of transportation line, requires estimation of the number of landslides reaching the infrastructure per year. The number of landslides is required to calculate the blockage period based on clearance time needed per cubic meter of debris. The relation between the annual probability of occurrence of landslides (or return period) and the number of landslides of a magnitude class per kilometer was established using a Gumbel extreme value distribution (Jaiswal et al. 2010a).

Logistic regression analysis was carried out to model the susceptible areas to landslides on natural slopes. Rainfall threshold analysis was used to estimate the temporal probability of landslides, and magnitude-frequency analysis to obtain the probability of landslide size. These data were combined in an analysis of landslide initiation hazard on cut and natural slopes (Jaiswal et al. 2010a). Landslide run-out analysis was carried for landslides on natural slopes. Landslide vulnerability was established for landslides with different magnitudes and for different elements at risk. Landslide hazard and risk estimation was done using landslide events that occurred between 1987 and 2007 and the results were validated using landslides that occurred in 2008 and 2009. As a final output direct risk was quantified for properties (alignments, vehicles, buildings, and plantations) and people (commuters and residents) and indirect risks due to the traffic interruption (Jaiswal et al. 2010b, 2011a, b) (See Fig. 11).

The results provided a quantitative estimate of total annual landslide losses, expressed in monetary value (US$) for properties (Fig. 12) and in annual probability of death for people. An F-N curve was used to express the societal risks. The results are of important societal value and will provide inputs for planning risk reduction strategies, for developing risk acceptance criteria and for financial analysis for possible damage in the study area. The methodology provides a cost-effective approach to estimate direct and indirect landslide risks. The methods can be applied elsewhere if a similar historical landslide data is made available.

The research also presented the perception of Nilgiri people to landslide risk and the use of the obtained hazard and risk information in reducing landslide risk to the society.

Conclusions

The joint research programme between GSI, NRSC and ITC, in which also other Indian organizations were involved (IIRS and CESS) resulted in five Ph.D. thesises (Kuriakose et al. 2010; Ghosh et al. 2011b; Jaiswal et al. 2011c; Martha et al. 2011b; Das et al. 2011) and over 20 publications in scientific journals. The defence of four of the researchers was integrated with a symposium on landslide hazard and risk assessment in India, which was held on 4 and 5 July 2011 (See Fig. 13) in ITC, The Netherlands. The results will also be presented in a workshop in November 2011 in Hyderabad, India, during which further steps towards the development of improved guidelines for hazard and risk assessment in India will be discussed.

Acknowledgments This research was carried out under the collaboration agreement between the Geological Survey of India (GSI), the

National Remote Sensing Center (Indian Space Research Organisation) and the United Nations University – ITC School for Disaster Geo-Information Management, University of Twente, the Netherlands.

We acknowledge the contribution of the following researchers, who collaborated in some way to the project (e.g. through joint field campaigns, training courses, image interpretation, modelling and discussions): Mauro Cardinali, Paola Reichenbach, Mauro Rossi and Fausto Guzzetti (CNR-IRPI); Andreas Günther (BGR); John Carranza, Norman Kerle, Victor Jetten and Alfred Stein (ITC); Steven de Jong, Theo van Asch and Rens van Beek (Utrecht University); Santiago Begueria (University of Zaragoza, Spain); Thomas Glade (University of Vienna); Jean-Philippe Malet (CNRS, Strasbourg); Dr. Sankar (CESS); P.K. Champati Ray and R.C. Lakhera (IIRS); Vinod Kumar (NRSC). The project was possible due to the efforts made by Dr. Rajendran of GSI. The research was also a contribution to the EU FP7 SafeLand project (www.safeland-fp7.eu) in which India is one of the two countries selected outside of Europe.

References

Anbalagan R (1992) Landslide hazard evaluation and zonation mapping in mountainous terrain. Eng Geol 32(4):269–277

Begueria S, van Asch TWJ, Malet JP, Grondahl S (2009) A GIS-based numerical model for simulating the kinematics of mud and debris flows over complex terrain. Nat Hazards Earth Syst Sci 9 (6):1897–1909

Bhandari RK (2006) The Indian landslide scenario, strategic issues and action points, a key note address – technical session on landslides. First India disaster management congress, New Delhi, 29–30 Nov 2006

BIS (1998) Preparation of landslide hazard zonation maps in mountainous terrains, IS 14496 (Part - 2) – Guidelines, Bureau of Indian Standards, Government of India, New Delhi

BMTPC (2003) Landslide hazard zonation atlas of India. Published by Building Materials and technology Promotion Council, Government of India and Anna University, Chennai

Das IC, Sahoo S, Van Westen CJ, Stein A, Hack R (2010) Landslide susceptibility assessment using logistic regression and its comparison with a rock mass classification system, along a road section in the northern Himalayas (India). Geomorphology 114(4):627–637

Das I, Stein A (Promotor), Kerle N (assistant promotor) (2011) Spatial statistical modelling for assessing landslide hazard and vulnerability. Ph.D thesis, University of Twente; summaries in Dutch and English. ITC Dissertation 192, ISBN: 978-90-6164-312-8

Ghosh S, van Westen CJ, Carranza EJM, Ghoshal T, Sarkar N, Surendranath M (2009a) A quantitative approach for improving the BIS (Indian) method of medium-scale landslide susceptibility. J Geol Soc India 74:625–638

Ghosh S, van Westen CJ, Carranza EJM, Jetten VG (2009b) Generation of event – based landslide inventory maps in a data – scarce environment: case study around Kurseong, Darjeeling district, West Bengal, India. In: Malet JP, Remaitre A, Bogaard T (eds) Landslide processes: from geomorphologic mapping to dynamic modeling: proceedings of the landslide processes, European Centre on Geomorphological Hazards (CERG), Strasbourg, pp 37–44

Ghosh S, Carranza EJM (2010) Spatial analysis of mutual fault/fracture and slope controls on rocksliding in Darjeeling Himalaya, India. Geomorphology 122:1–24

Ghosh S, Günther A, Carranza EJM, van Westen CJ, Jetten VG (2010) Rock slope instability assessment using spatially distributed structural orientation data in Darjeeling Himalaya (India). Earth Surf Proc Landf 35:1773–1792

Ghosh S, Carranza EJM, van Westen CJ, Jetten VG, Bhattacharya DN (2011a) Selecting and weighting of spatial predictors for empirical modeling of landslide susceptibility in Darjeeling Himalaya (India). Geomorphology 131(1–2):35–56

Ghosh S, Jetten VG (Promotor), van Westen CJ (assistant promotor), Carranza EJM (assistant promotor) (2011b) Knowledge guided empirical prediction of landslide hazard (e-book). University of Twente Faculty of Geo-Information and Earth Observation ITC, Enschede. ITC Dissertation 190, ISBN: 978-90-6164-310-4

Ghosh S, van Westen CJ, Carranza EJM, Jetten VG (2012a) Integrating spatial, temporal and magnitude probability for medium scale landslide hazard and risk analysis in Darjeeling Himalayas (India). Landslides: J Int Consortium Landslides, 9(3):371–384

Ghosh S, van Westen CJ, Carranza EJM, Jetten VG, Cardinali M, Rossi M, Guzzetti F, (2012b) Generating event-based landslide maps in a data-scarce Himalayan environment for estimating temporal and magnitude probability. Eng Geol 128:49–62

Günther A (2003) SLOPEMAP: programs for automated mapping of geometrical and kinematical properties of hard rock hill slopes. Comput Geosci 29:865–875

Jaiswal P, van Westen CJ (2009) Estimating temporal probability for landslide initiation along transportation routes based on rainfall threshold. Geomorphology 112:96–105

Jaiswal P, van Westen CJ, Jetten V (2010a) Quantitative landslide hazard assessment along a transportation corridor in southern India. Eng Geol 116:236–250

Jaiswal P, van Westen CJ, Jetten V (2010b) Quantitative assessment of direct and indirect landslide risk along transportation lines in southern India. Nat Hazards Earth Syst Sci 10:1253–1267

Jaiswal P, van Westen CJ, Jetten VG (2011a) Quantitative assessment of landslide hazard along transportation lines using historical records. In: Landslides: J Int Consortium Landslides 8(3):279–291

Jaiswal P, van Westen CJ, Jetten V (2011b) Quantitative assessment of landslide hazard along transportation lines using historical records. Landslides. doi:10.1007/s10346-011-0252-1

Jaiswal P, Jetten VG (Promotor), van Westen CJ (assistant promotor), Ayyasami K (assistant promotor) (2011c) Landslide risk quantification along transportation corridors based on historical information (e-book). University of Twente Faculty of Geo-Information and Earth Observation ITC, Enschede. ITC Dissertation 191, ISBN: 978-90-6164-311-1

Kuriakose SL, Jetten VG, van Westen CJ, Sankar G, van Beek LPH (2008) Pore water pressure as a trigger of shallow landslides in the western Ghats of Kerala, India: some preliminary observations from an experimental catchment. Phys Geogr 29(4):374–386

Kuriakose SL, van Beek LPH, van Westen CJ (2009a) Parameterizing a physically based shallow landslide model in a data poor region. Earth surf proc landf 34(6):867–881

Kuriakose SL, Sanjaya Devkota DG, Rossiter VGJ (2009b) Prediction of soil depth using environmental variables in an anthropogenic landscape, a case study in the Western Ghats of Kerala, India. Catena 79(1):27–38

Kuriakose SL, Jetten VG (Promotor), de Jong SM (Promotor), van Westen CJ (co-promotor), van Beek LPH (co-promotor) (2010) Physically-based dynamic modelling of the effect of land use changes on shallow landslide initiation in the Western Ghats of Kerala, India + CD-ROM with appendices. University of Twente Faculty of Geo-Information and Earth Observation ITC, Enschede. ITC Dissertation 178, ISBN: 978-90-6164-298-5

Kuriakose SL, van Beek LPH (2011) Plant root strength and slope stability. In: Glinski J, Horabik J, Lipiec J (eds) Encyclopaedia of agrophysics, Encyclopaedia of earth sciences series. Springer, Dordrecht. doi:10.1007/978-90-481-3585-1

Martha TR, Kerle N, van Westen CJ, Jetten V, Vinod Kumar K (2010a) Effect of sun elevation angle on DSMs derived from Cartosat - 1 data. Photogramm Eng Remote Sens 76(4):429–438

Martha TR, Kerle N, van Westen CJ, Jetten V, Vinod Kumar K (2010b) Landslide volumetric analysis using Cartosat - 1 derived DEMs. IEEE Geosci Remote Sens Lett 7(3):582–586

Martha TR, Kerle N, van Westen CJ, Jetten V, Vinod Kumar K (2010c) Characterising spectral, spatial and morphometric properties of landslides for semi – automatic detection using object – oriented methods. Geomorphology 116(1–2):24–36

Martha TR, Kerle N, van Westen CJ, Jetten V, Vinod Kumar K (2011a) Segment optimisation and data-driven thresholding for knowledge-based landslide detection by object-based image analysis. IEEE Trans Geosci Remote Sens 49(12):4928–4943

Martha TR, Jetten VG (Promotor), van Westen CJ (assistant promotor), Kerle N (assistant promotor) (2011b) Detection of landslides by object – oriented image analysis (e-book). University of Twente Faculty of Geo-Information and Earth Observation ITC, Enschede. ITC Dissertation 189, ISBN: 978-90-6164-309-8

Martha TR, Kerle N, van Westen CJ, Jetten V, Vinod Kumar K (2012) Object-oriented analysis of multi-temporal panchromatic images for creation of historical landslide inventories. ISPRS J Photogramm Remote Sens 67:105–119

Martha TR, Kerle N, van Westen CJ, Jetten V, Vinod Kumar K (2013) Landslide hazard and risk assessment using landslide inventories created semi-automatically by object-oriented analysis. Geomorphology 184(February):139–150

Nadim F, Kjekstad O (2009) Assessment of global high-risk landslide disaster hotspots. In: Sassa K, Canuti P (eds) Landslides – Diaster risk reduction. Springer, Berlin, pp 213–221

NDMA (2009) Management of landslides and snow avalanches, 2009. National Disaster Management Authority (NDMA), Government of India, New Delhi, pp 144pp

OFDA/CRED (2010) EM-DAT International Disaster Database. www.em-dat.net. Université Catholique de Louvain, Brussels, Belgium

Petley DN, Dunning SA, Rosser NJ (2005) The analysis of global landslide risk through the creation of a database of worldwide landslide fatalities. In: Hungr O, Fell R, Couture R, Eberhardt E (eds) Landslide risk management. Taylor & Francis, London, pp 367–373

Rajarathnam S, Ganapathy GP (2006) Landslide hazard zonation of India using GIS techniques. Thematic session – landslide, avalanche and other mass movements. First Indian disaster management congress, New Delhi, India, 29–30 Nov 2006

Sarkar S, Kanungo DP (2005) Landslide hazard zonation in India: a review. In: Proceedings of the international conference on geotechnical engineering for disaster management & rehabilitation, Kyoto University, Japan

Sharda YP (2008) Landslide studies in India, glimpses of geoscience research in India. The Indian report to IUGS 20042008, Indian National Science Academy, Silver Jubilee Volume, pp 98–101

van Westen CJ, Castellanos E, Kuriakose SL (2008) Spatial data for landslide susceptibility, hazard, and vulnerability assessment: an overview. Eng Geol 102:112–131

Mapping a Nation's Landslides: A Novel Multi-Stage Methodology

Hannah Evans, Catherine Pennington, Colm Jordan, and Claire Foster

Abstract

Through combining new technologies and traditional mapping techniques, the British Geological Survey (BGS) has developed a novel, multi-stage methodology for landslide mapping. 3-D aerial photograph interpretation, variable-perspective 3-D topographic visualisation and field mapping with digital data capture are being used to map the UK's landslides. The resulting ESRI ArcGIS polygons are published on BGS 1:50,000 geological maps and as digital data products. Data collected during mapping are also uploaded directly into the National Landslides Database maintaining a systematic, nationally-uniform landslide inventory. Repeat monitoring of selected landslides using terrestrial LIDAR and dGPS allows the database to be frequently updated and the proactive Landslide Response Team means that new landslide events can be mapped within days, if not hours, of their occurrence. The long-term aim is to apply this methodology throughout the UK, providing a wealth of data for scientific research and hazard assessment. This methodology is also suitable for application in an international context.

Keywords

Landslide mapping • Hazard assessment • 3-D visualisation • Digital data capture

Introduction

When examining the pre-conditioning and triggering factors required to generate a landslide (Fig. 1), the UK at first appears to be at a relatively low risk of landslide events. The country is largely unaffected by the extreme climatic and tectonic events experienced elsewhere in the world and the role of such major landslide-inducing factors as earthquakes, rainfall and changes in water level is less extreme than in the global context. However, the densely populated nature of the country combined with an abundance of relict landslides means that landslide research in the UK is paramount. Furthermore, heightened anthropogenic activity witnessed in the UK over the last few decades has added a new dimension to the landslide pre-conditioning and triggering factors, increasing the likelihood of landslide events, both through new failures and the reactivation of existing features.

Since the 1930s the British Geological Survey (BGS) has been engaged in the mapping and inventory of landslides across the UK. The BGS uses a modified version of the landslide classification schemes detailed in Varnes (1978), Flageollet (1993) and WP/WLI (1990). Five main landslide types are recognised (falls, flows, topples, slides and spreads) occurring as single, multiple, complex or composite events. Landslides with a discernable back scar and a zone of deposition are considered as mappable units. As defined by McMillan and Powell (1999) there are four types of mass movement deposit: landslide, talus, head and dry valley deposits. Mass movement deposits where the origin of the feature cannot be reliably attributed to landslide processes are not mapped in the landslide surveys.

H. Evans (✉) • C. Pennington • C. Jordan • C. Foster
British Geological Survey, Keyworth, Nottingham NG12 5GG, UK
e-mail: hann@bgs.ac.uk

C. Margottini et al. (eds.), *Landslide Science and Practice*, Vol. 1,
DOI 10.1007/978-3-642-31325-7_2,

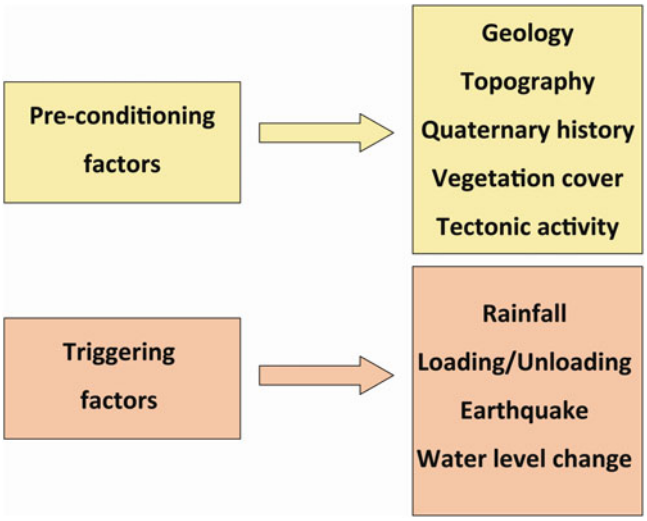

Fig. 1 Selected landslide pre-conditioning and triggering factors

Recent technological developments have been combined with traditional mapping techniques to develop the novel multi-stage methodology described in this paper. This methodology is applied through the combination of strategic, repeat and responsive landslide surveys carried out by the BGS. The long-term aim of this research is to allow the BGS to better characterise and understand the country's landslides by investigating the links between geology, geomorphology and palaeoenvironmental evolution. This will facilitate hazard assessment and infrastructure planning as well as informing the UK's landslide susceptibility model. Sections of the methodology have also been applied further afield in an international context.

The BGS's Landslide Mapping Methodology

A range of complementary techniques is employed by the BGS to map the UK's landslides. Prior to commencing a strategic field survey a desk-based interpretation is made using visualisation and photogrammatic software. In the field digital data capture is used to aid mapping speed and accuracy, whilst the existence of the BGS Landslide Response Team allows rapid mobilisation to record new events. Repeat surveys of selected active landslides are also undertaken in order to provide data in 4-D. The data captured is then stored in a range of formats: as attributed georeferenced ESRI ArcGIS polygons published on BGS 1:50,000 and 1:10,000 scale geological map sheets and as BGS DiGMap50 and DiGMap10 digital data products as well as attributed point data in the BGS National Landslide Database (NLD). The individual mapping techniques and data storage mechanisms are detailed below:

3-D Aerial Photograph Interpretation

The distinct morphology created by landslides, such as hummocky terrain, arcuate scarps and tension cracks, can often be readily identifiable from aerial photographs (Mantovani et al. 1996; Mason and Rosenbaum 2002). At a scale of 1:50,000 aerial photographs allow detection of objects as small as 7.5 × 7.5 m and the minimum detectable size decreases with increased photograph resolution (Tribe and Leir 2004). Prior to commencing a strategic landslide field survey the BGS uses SOCET for ArcGIS software for 3-D visualisation of georeferenced colour vertical aerial photographs of the area concerned. Draft georeferenced ESRI ArcGIS polygons are derived by digitising around the landslide deposits identified in a linked digital stereoscope and ESRI ArcGIS environment. These polygons are assigned X, Y and Z dimensions by combining the horizontal georeferencing information with Z values assigned from an underlying digital elevation model.

Variable-Perspective 3-D Visualisation of Topographic Features

Developed jointly by the BGS and Virtalis Ltd., Geovisionary™ visualisation and photogrammetric software provides seamless streaming of aerial photographs, topographic maps, geological models and other GIS data into a 3D terrain which can be viewed in stereo. In addition, Geovisionary™ allows the user to fly through a 3D photo-realistic rendered view of the data and is often used to provide an additional perspective not available through the use of SOCET for ArcGIS software. When used in landslide mapping campaigns, this allows a range of resources to be interrogated and landslide deposits to be digitised as georeferenced ESRI ArcGIS polygons prior to the field survey. BGS geological maps, historical topographic maps, and existing literature are also consulted to augment data gathered during the 3-D visualisation stages.

Field Mapping with Digital Data Capture

BGS•SIGMAmobile was developed by the BGS to provide an integrated field mapping software system with graphical map interface tools, free text and structured input using drop-down menus (downloadable for free from

Fig. 2 BGS landslide survey using a ruggedised tablet PC with BGS•SIGMAmobile

Fig. 3 The BGS Riegl LPM-i800HA laser scanner which can achieve an accuracy of ±15 mm

www.bgs.ac.uk/research/technologies_epo.html). Ruggedised tablet PCs carrying BGS•SIGMAmobile allow the ESRI ArcGIS polygons digitised during the desk-based interpretation to be taken into the field along with the full suite of pre-existing data (Fig. 2). Any modifications to the landslide deposit polygons required following field validation can, therefore, be performed at the landslide site. A bespoke digital landslide proforma has also been incorporated into the system in order to aid the systematic and comprehensive recording of attributed point data for input into the NLD. In addition to this, ancillary data such as digital photographs can be spatially linked to the landslide data and annotated as required.

Repeat Terrestrial LIDAR and dGPS Surveys

In addition to strategic field surveys, the BGS has performed repeated monitoring of selected landslides using terrestrial laser scanning (LIDAR) for the last 9 years (Fig. 3). Terrestrial LIDAR works by measuring the relative distance, elevation and azimuthal angles between the laser scanner and landslide and, when georeferenced with differential GPS (dGPS), a 3-D surface model can be generated (Hobbs et al. 2002; Rowlands et al. 2003). Analysis of repeated scans over regular time intervals can accurately determine, for example, the nature of the landslide processes (Hobbs et al. 2010). A high resolution digital camera mounted onto the scanner enables coloured point-clouds, textured triangulated surfaces or orthophotos with depth information to be captured. Landslides routinely visited by the BGS include the Hollin Hill Landslide Observatory, Terrington, North Yorkshire (Chambers et al. 2011) and that at Happisburgh, Norfolk. Insights into landslide processes gained from these repeat surveys are used to supplement those at the national scale derived from BGS strategic surveys.

Landslide Response

The BGS has established a 24-h on-call Landslide Response Team that can respond quickly to new landslide events, allowing them to be mapped within days, if not hours, of their occurrence. This is vital given the relatively low preservation potential of landslide deposits in areas with increased anthropogenic activity. Responsive landslide surveys are triggered through daily email alters from online news searching services, media reports and public enquiries. On mobilisation to the landslide site the team gathers geomorphological and process information about the new landslide to update the BGS geological maps and digital data products; enter data into the NLD and to provide, where possible, an immediate impartial assessment of the cause, state and potential for further landslide movement. Terrestrial LIDAR scanning and dGPS surveys can also be employed in these responsive situations. To-date the BGS has visited landslides throughout the UK, including the Rest and Be Thankful Landslide, Argyll, Scotland; Black Ven Landslide, Dorset, England and; Oxwich Bay Landslide, Swansea, Wales (www.bgs.ac.uk/landslides/casestudies.html).

National Landslide Database

The BGS runs the definitive source of information on British landslides: the NLD. The database currently holds over 15,000 records and provides a systematic, nationally-uniform inventory of the UK's landslides. Each record can hold information on over 35 attributes including location, dimensions, failure type, causal mechanisms, damage, geology, hydrogeology and a full bibliographic reference. The database is linked to a GIS which displays the landslide events as point data. Data come from a variety of sources including published BGS geological maps; BGS strategic,

repeat and responsive surveys; existing literature and media reports. The database is dynamic and new records are continuously added. Selected information from the NLD is now freely available through the BGS's online GIS – GeoIndex (www.bgs.ac.uk/geoindex/).

BGS Strategic, Repeat, Responsive and International Landslide Surveys

To-date the novel landslide mapping methodology developed by the BGS has been applied to several UK locations. The on-going aim is to extend this methodology throughout the nation in order to provide a definitive survey and inventory of UK landslides. The methodology described herein has also been trialled in selected international contexts. Detailed examples of the application of this methodology are given below:

Strategic Landslide Survey

Continuing a series of strategic landslide mapping programmes, the BGS is currently mapping landslides in the North York Moors, Yorkshire. 3-D aerial photograph interpretation was used to derive georeferenced ESRI ArcGIS polygons for validation in the field. A total of 302 potential landslide polygons were to be investigated across the area covered by the Egton and Guisborough BGS 1:50,000 map sheets. Preliminary results show two main types of failure in the area: large-scale, deep-seated multiple rotational or translational failures and smaller-scale, shallow earth flows or translational slides. The degree of degradation and geomorphology of the large-scale, deep-seated features suggest development under periglacial conditions, last experienced in the area during the Pleistocene, whilst the smaller-scale features and impact on archaeology implies a maximum age of approximately 200–500 years for the small-scale earth flows and translational slides. Examination of the relationship between landslide location, geology and slope angle demonstrates a clustering of landslide around structurally weaker geological units such as the Jurassic Whitby Mudstone Formation (Lias Group) and higher slope angles (Fig. 4).

Repeat Landslide Survey

Since 2006 the BGS has undertaken annual terrestrial LIDAR and dGPS surveys at the Hollin Hill Landslide Observatory, Terrington, North Yorkshire. This active inland landslide displays multiple headscarps, flows and toe lobes across a series of geological benches within an area of approximately 300 × 250 m. Elevation change models derived from re-occupation of identical scan positions year on year reveal zones of depletion and accumulation. Changes in the range of ±2 m are not uncommon throughout the downslope portion of the landslide (Fig. 5).

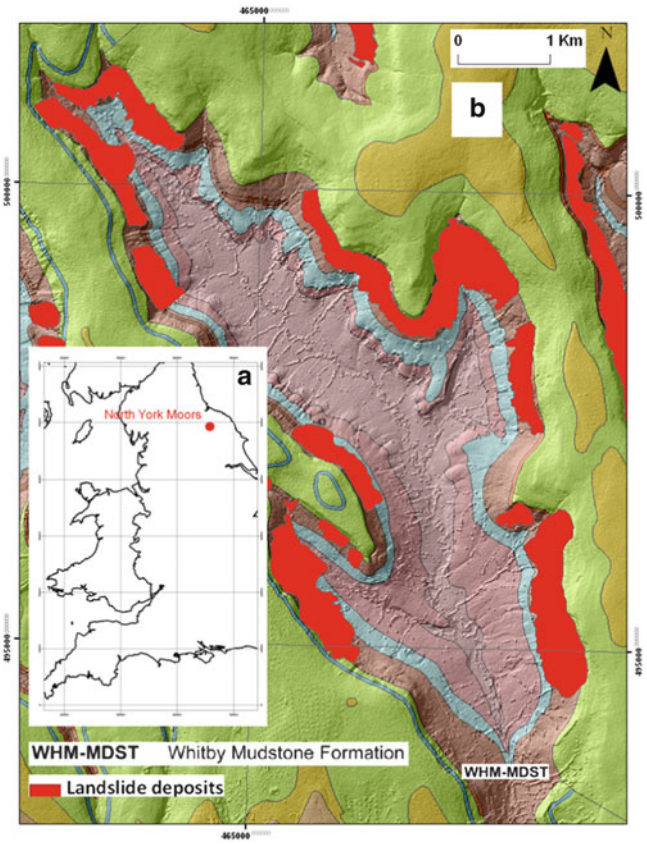

Fig. 4 BGS strategic landslide survey of the North York Moors, UK: (**a**) location of the study area, (**b**) clustering of landslides in areas of increased slope angle and weaker lithologies, Farndale, North York Moors, UK (NEXTMap Britain elevation data from Intermap Technologies)

Responsive Landslide Survey

In May 2008 the BGS Landslide Response Team was alerted to the reactivation of a portion of the Black Ven Landslide, Lyme Regis, Dorset (Fig. 6). This landslide is one of the largest and most studied in the UK but the mechanisms of failure are so complex that debate continues as to the exact causal processes. The reactivation was widely reported in the national media amid fears that a triggering of the whole complex would follow. The BGS undertook a field survey with digital data collection using BGS•SIGMAmobile software. Data was gathered in order to update the BGS 1:50,000 and 1:10,000 scale geological

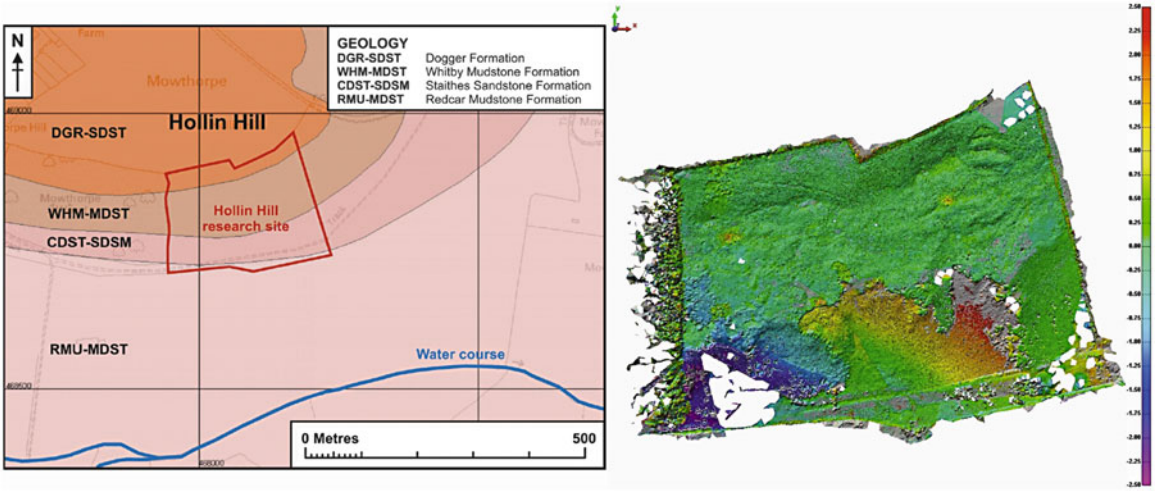

Fig. 5 BGS repeat landslide survey of the Hollin Hill Landslide, Yorkshire: (*left*) geological conditions at the study site after Chambers et al. (2011), (*right*) terrestrial LIDAR elevation change model for 2006–2007

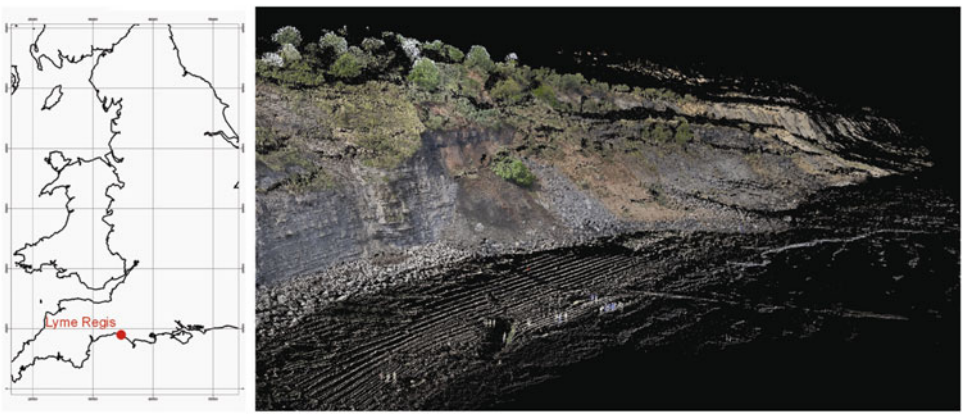

Fig. 6 BGS responsive survey of the May 2008 reactivation at the Black Ven Landslide Complex, Lyme Regis, Dorset, UK: (*left*) location of the Black Ven Landslide, (*right*) terrestrial LIDAR point cloud of the May 2008 reactivation zone

maps, DiGMap50 and DiGMap10 digital data products and the NLD. In addition a terrestrial LIDAR and dGPS survey was conducted and digital terrain model of the failure developed.

International Survey

In February 2005 the BGS was funded by the World Bank to undertake a 3 year geological and geomorphological mapping project in Madagascar. A major constituent of the commissioned geomorphological maps, which covered an area of 250,000 km^2 at a scale of 1:500,000, was delineation of the recent and extensive landsliding, known as lavaka. With such a short time scale available to map a large area with a poor road network, a combination of efficient image interpretation and focussed field mapping was called for. SOCET for ArcGIS and Geovisionary™ allowed rapid landform mapping, whilst the imagery and resulting linework taken to Madagascar on BGS•SIGMAmobile enabled focussed field research.

Further afield, BGS undertook a pilot geological mapping project, funded by the European Space Agency, demonstrating how modern digital workflows can be applied to the geological and geomorphological mapping of Mars. With collaborators in the Netherlands Organisation for Applied Scientific Research/ Deltares, Geological Survey of the Netherlands and University College London, the team used SOCET for ArcGIS and Geovisionary™ software to successfully interpret a range of remotely sensed imagery. The landscape on Mars contains landforms that are significantly larger than those found on Earth, with landslide dimensions of, for example, 5 × 70 km (Fig. 7). The use of systems like Geovisionary™ to quickly and efficiently analyse vast landscapes is a major benefit, especially when fieldwork is impractical.

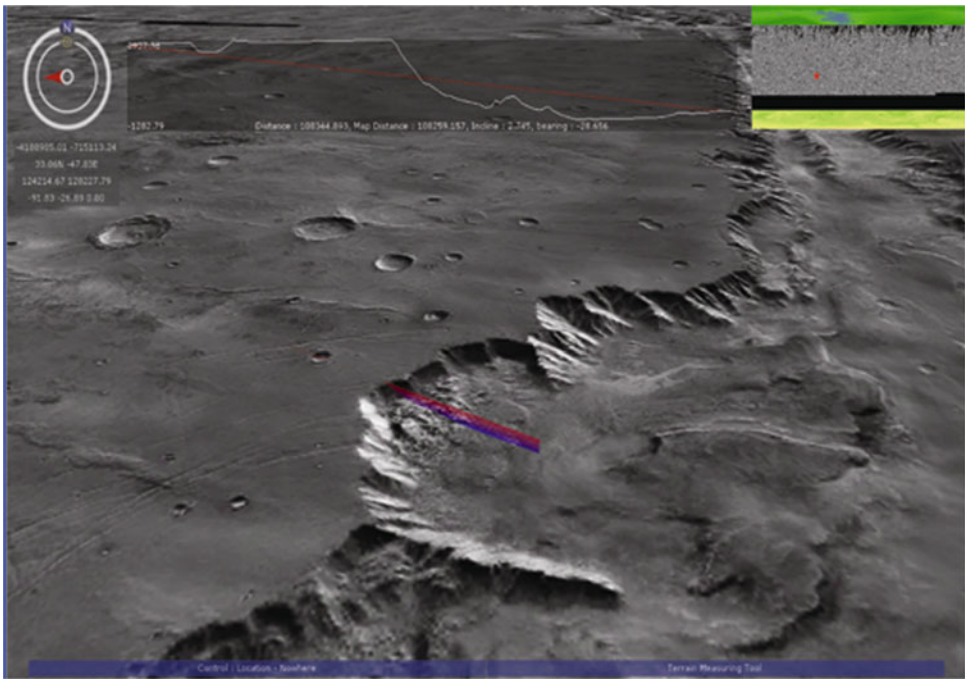

Fig. 7 Geovisionary™ visualisation of a landslide on Mars looking west along the Valles Marineris to Melas Chasmas using MOLA and THEMIS data (Raw imagery from NASA)

Conclusions

The BGS has developed a novel, multi-stage methodology for landslide mapping and inventory within the UK. This methodology blends new technologies and traditional mapping practices to include six complementary mapping techniques and three data storage and presentation mechanisms. BGS is unique in the UK in that it possess the capability to study landslides at the national and regional scales and its long-term aim is to apply this methodology throughout the UK in order to better understand and characterise the nation's landslides. This will provide a wealth of data for scientific research, hazard assessment and infrastructure planning as well as informing a landslide susceptibility model of the UK. To-date the methodology has been rolled out across a number of BGS 1:50,000 map sheets through strategic field surveys and applied to numerous individual inland and coastal landslides through repeat and responsive field surveys. The methodology is also suitable for application in an international context and aspects of the process have already been trialled in Madagascar and applied to Martian landslides. Development of the BGS landslide mapping methodology is an on-going process and continued technological developments for example, advances in remote sensing, digital data capture and data visualisation technologies, will be incorporated where possible.

Acknowledgements The authors publish with the permission of the Executive Director of the British Geological Survey (Natural Environment Research Council). The National Grid and other Ordnance Survey data are used with the permission of the Controller of Her Majesty's Stationery Office. Licence No: 100017897/2010. Mars data acquired by D. Tragheim (BGS).

References

Chambers JE, Wilkinson PB, Kuras O, Ford JR, Gunn DA, Meldrum PI, Pennington CVL, Weller AL, Hobbs PRN, Ogilvy RD (2011) Three-dimensional geophysical anatomy of an active landslide in Lias Group mudrocks, Cleveland Basin, UK. Geomorphology 125 (4):472–484

Flageollet JC (ed) (1993) Temporal occurrence and forecasting of landslides in the European Community. EPOCH (European Community Programme). 3 volumes, Contract number 90 0025

Hobbs P, Humphreys B, Rees J, Tragheim D, Jones L, Gibson A, Rowlands K, Hunter G, Airey R (2002) Monitoring the role of landslides in 'soft cliff' coastal recession. In: Jakeways J, McInnes RG (eds) Instability planning and management. Thomas Telford, Isle of Wight, pp 589–600

Hobbs PRN, Gibson AD, Jones L, Pennington CVL, Jenkins G, Pearson SG, Freeborough KA (2010) Monitoring coastal change using terrestrial LiDAR. In: Fleming C, Marsh SH, Giles JRA (eds) Elevation models for geoscience. Geological Society, London, pp 117–127, Special publications 345

Mantovani F, Soeters R, Van Westen CJ (1996) Remote sensing techniques for landslide studies and hazard zonation in Europe. Geomorphology 15:213–225

Mason P, Rosenbaum MS (2002) Geohazard mapping for predicting landslides: the Langhe Hills in Piemonte, NW Italy. Q J Eng Geol Hydrol 35(4):317–326

McMillan AA, Powell JP (1999) BGS rock classification scheme, vol 4. Classification of artificial (man made) ground and natural superficial deposits – applications to geological maps and datasets in the UK. British Geological Survey Research Report RR 99-04, HMSO, London, 66p

Rowlands K, Jones L, Whitworth M (2003) Photographic feature: landslide laser scanning: a new look at an old problem. Q J Eng Geol 36(2):155–158

Tribe S, Leir M (2004) The role of aerial photograph interpretation in natural hazard and risk assessment. In: Proceedings of the international pipeline conference, Calgary, Oct 2004, 6p

Varnes DJ (1978) Slope movements types and processes. In: Schuster RL, Krizek RJ (eds) Landslides: analysis and control, Transportation Research Board, National Academy of Sciences, Washington, DC, Special Report, No. 176. pp 11–33

WP/WLI (1990) International Geotechnical Societies' UNESCO Working Party on World Landslide Inventory: a suggested method for reporting a landslide. Bull Int Assoc Eng Geol 41:5–12

Systematic Mapping of Large Unstable Rock Slopes in Norway

Reginald L. Hermanns, Lars H. Blikra, Einar Anda, Aline Saintot, Halgeir Dahle, Thierry Oppikofer, Luzia Fischer, Halvor Bunkholt, Martina Böhme, John F. Dehls, Tom R. Lauknes, Thomas F Redfield, Per T. Osmundsen, and Trond Eiken

Abstract

Historically, large rock slope failures impacting into a fjord and causing a several tens of metre high displacement wave have been one of the natural hazards in Norway claiming most lives. In the last 7 years, the Geological Survey of Norway has implemented a systematic mapping approach to characterize unstable rock slopes prone to catastrophic failures, so that future events can be recognized beforehand and society can adapt to the hazard. Systematic mapping has been carried out in three countries and more than 285 unstable slopes have been found. Of these sites, 62 are monitored periodically and 4 have been characterized as high risk objects with continuous monitoring systems installed. In order to classify the likelihood of a future event, rock slope mapping of each object includes the analyses of slide kinematic, velocity of the slide accompanied with other indicators of slide activity and an analysis of recurrence of previous events along the slope.

Keywords

Displacement wave • Likelihood estimation • Monitoring • Norwegian Fjordland • Rock avalanches • Rock slope failure

Introduction

In the twentieth century, three rock avalanches occurred in Norway, all of them impacting into a lake or a fjord causing displacement waves with run up heights of several tens of metres (Blikra et al. 2005; Hermanns et al. 2006). These events caused a total of 175 casualties. Historic documents indicate that this number was similar also in previous centuries (Furseth 2006). This makes rock avalanches the natural hazard which claimed the second largest number of lives in Norway, topped only by snow avalanches (Hermanns et al. 2012a). However, in contrast to snow avalanches, which in the last decades claimed most victims in open mountain terrain during recreational time, all victims caused by rock avalanches were caused in settlements. Therefore in contrast to snow avalanches, where potential victims voluntarily move into the hazard zone, victims of rock avalanches live within the hazard zone. The unique exposure of the Norwegian society to rockslides and its secondary effects, such as the rockslide impact into a water body or valley damming, has also been showcased in a recent report based upon a colaborative analyses guided by the Norwegian Civil Defense (Direktoratet for samfunns-sikkerhet og beredskap DSB 2011). Base of this analyses was the assessment of the Norwegian Civil Defense in 2010

R.L. Hermanns (✉) • A. Saintot • H. Dahle • T. Oppikofer • L. Fischer • H. Bunkholt • M. Böhme • J.F. Dehls • T.F. Redfield • P.T. Osmundsen
Landslide Department, Geological Survey of Norway, Leiv Eirikssons vei 39, Trondheim, Norway
e-mail: Reginald.Hermanns@ngu.no

L.H. Blikra
Åknes/Tafjord Beredskap IKS, Stranda, Norway

E. Anda
Council of Møre og Romsdal, Molde, Norway

T.R. Lauknes
Northern research Institute, Troms, Norway

T. Eiken
University of Oslo, Institute for geofag, Oslo, Norway

C. Margottini et al. (eds.), *Landslide Science and Practice*, Vol. 1,
DOI 10.1007/978-3-642-31325-7_3,

Fig. 1 Comparison of the ten most important threats to Norwegian society (After DSB 2011)

that war, pandemic, nuclear crises, storm, energy crises, rock avalanche, ship collision, cyber attack, terror attack, and gas spill represent the ten largest individual threats to society in Norway. A rock avalanche is ranked as the fourth most likely and the fifth most severe of all these hazards (Fig. 1).

A systematic mapping approach focussing on characterizing unstable slopes prone to fail catastrophically in future has therefore a high potential to reduce the threat and number of victims during future natural disasters if monitoring systems coupled with early-warning systems are installed, and the population are warned and evacuated from the hazard area. This paper focuses on the systematic mapping approach which is carried out by the Norwegian Geological Survey (NGU) under the supervision and financed by the Norwegian Water Resources and Energy Directorate (Norges vassdrags- og energidirektorat = NVE) which has the responible in Norway to assist municipalities with flood and landslide controle. A unified mapping methodology is under discussion with multiple national and international experts named within the acknowledgements and will be published once finalized. Scientific and technical challenges on the early-warning systems have been discussed in a previous paper (Blikra 2008).

Geological Setting

Large regions of the landscape of Norway are characterised by an extreme alpine relief with steep slopes, heavily oversteepened U-shaped glacial valleys reaching below sea level and forming a several tens of thousands kilometre long coast line with strongly ramified fjords intruding into the continent for up to 200 km. Those regions are most prone for large rock slope failures although deposits of prehistoric rock slope failures also exist in more subdued valleys. The bedrock comprises mainly metamorphic rocks of Precambrian to Palaeozoic age. The bedrock is highly tectonized due to protracted intense ductile and brittle tectonics acting since Precambrian times over the entire region. In the Quaternary, multiple glacial cycles covered the landscape with kilometre thick ice caps and eroded into the valleys causing loading and subsequent isostatic rebound. The high concentration of structures due to tectonics and glacial unloading in the bedrock and the steepness of the rock slopes would be the two main parameters that render the slope susceptible to development of large gravitational rock-slope deformation (e.g. Braathen et al. 2004; Saintot et al. 2011; Böhme et al. 2011; Henderson and Saintot 2011).

Methodology

Assumptions for Mapping Approach

Two principal assumptions are the base of our mapping and monitoring approach: (1) that large rock slope deformation occurs prior to catastrophic failure and (2) that there is an acceleration phase prior to collapse. In contrast to other seismically more active geological settings in the world such as the fjordland in Chilean Patagonia (e.g. Sepulveda et al. 2010), the development of historic catastrophic events in Norway (Hermanns et al. 2006) support that these

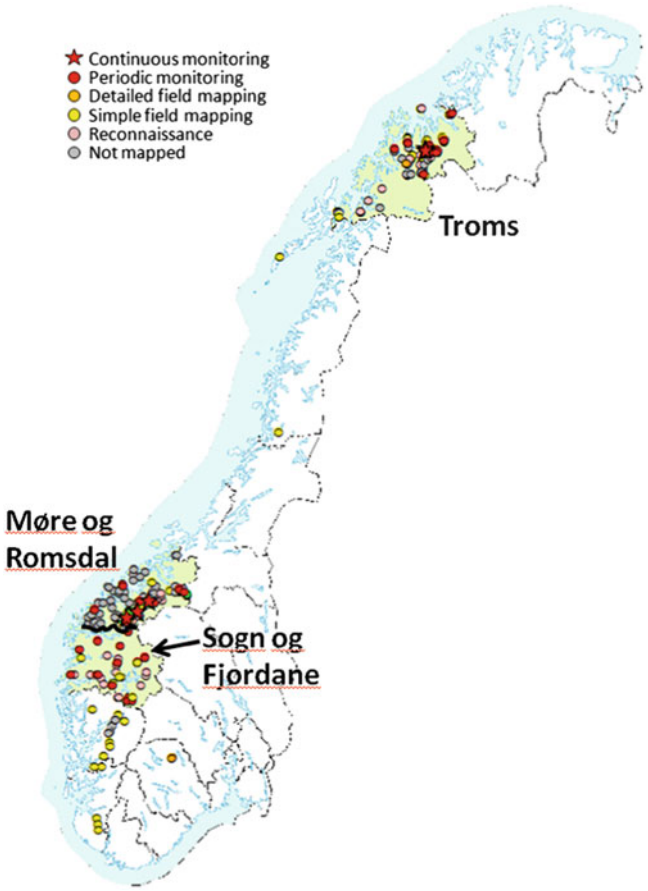

Fig. 2 Overview map showing the position of known unstable slopes and giving the detail of mapping effort carried out until today. Note that mapping effort does not in all cases indicate a classification of hazard and risk level. Only sites marked with a *star* are classified as high risk objects

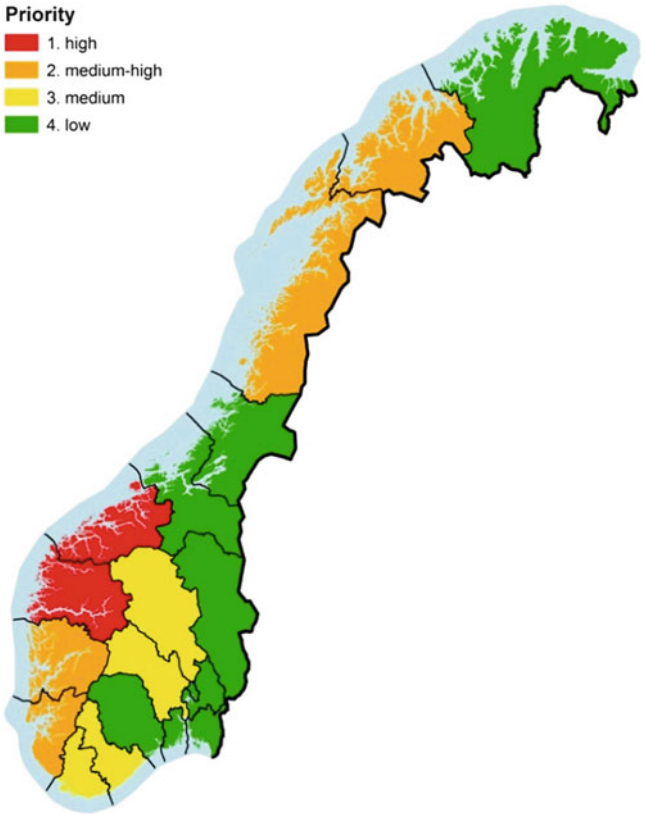

Fig. 3 Priority map for mapping and investigating of rock slope instabilities in Norway based upon historic analyses summarized in Table 1

assumptions are realistic, especially for the tectonic setting of Norway along a passive continental margin where high magnitude earthquakes have been absent in the historic past. However, the effect of low frequency medium magnitude events is still poorly understood and discussed. In addition these observations also fit with the development of large rock slope failures in other mountain areas in the world with low seismicity (Eisbacher and Clague 1984 and references therein).

Regional Mapping

Due to the large extent of the mountainous area in Norway, systematic mapping has up to now concentrated on three counties only: Møre og Romsdal, Sogn og Fjordane, and Troms (Fig. 2) (Dahle et al. 2011; Saintot et al. 2011; Böhme et al. 2011; Henderson et al. 2011; Bunkholt et al. 2011). In other counties, unstable rock slopes are only known for sites which have been reported to the mapping program by any other means. The systematically mapped provinces are also those with most historic large rock slope failures and most victims in the past centuries (Fig. 3, Table 1).

In a first approach, unstable rock slopes are identified using differential interferometric synthetic aperture radar (DInSAR), predominantly using the European Space Agency's archive of ERS-1 and ERS-2 images (Lauknes et al. 2010; Henderson et al. 2011). This method works best in northern Norway where vegetation cover only exists on the lower slopes below 400 m a.s.l. All slopes above the tree line are systematically mapped by air photos and helicopter reconnaissance. Further sources of information are the local citizens who report opening of cracks to the county geologist or directly to the geological survey.

Mapping on Slope Scale

In a second step all sites which might present a threat to any settlement or life line are visited in the field to assess the state of activity (opening of cracks, rock deformation controlled disturbance of soil cover and vegetation, rock fall activity), and all of those sites which have indications of being active get followed up with detailed analyses. This includes

Table 1 Overview of historic rock avalanches and large rock fall events organized by county

County	Rock avalanche		Large rock fall[a]	
	Total	Certain	Total	With casualties
Møre og Romsdal	9	4	114	35
Sogn og Fjordane	5	2	113	48
Hordaland	0	0	71	17
Troms	1	1	10	2
Rogaland	1	1	27	7
Nordland	0	0	31	8
Oppland	0	0	14	6
Buskerud	1	1	3	0
Vest-Agder	0	0	8	4
Aust-Agder	0	0	9	2
Finnmark	0	0	8	0
Telemark	0	0	4	2
Nord-Trøndelag	0	0	6	2
Vestfold	0	0	6	0
Sør-Trøndelag	0	0	4	1
Akerhus	0	0	2	0
Hedmark	0	0	1	0
Oslo	0	0	0	0
Østfold	0	0	0	0
Total	17	9	431	134

[a]With a volume large enough to cause severe damage in the run out area and possibly also displacement waves when impacting a water body, ca. 30,000 m^3

(1) structural mapping to assess the kinematic mode and development of deformation, (2) determination of slide velocity and (3) the analyses of historical and pre-historical rockslide and rock fall events on the slope and in the surroundings. (1) Structural mapping is based on field measurements (Oppikofer and Jaboyedoff 2008; Osmundsen et al. 2009; Redfield and Osmundsen 2009; Henderson and Saintot 2011; Hermanns et al. 2011), and also, in steep terrain areas, on remote techniques generating high resolution digital elevation models (DEMs) such as terrestrial or airborne laser scanning (Oppikofer et al. 2009, 2011). (2) The velocity of the rockslides is mainly determined by high accuracy differential GPS measurements using yearly or multi-yearly intervals (e.g. Henderson and Blikra 2008; Bunkholt et al. 2011a; Hermanns et al. 2011a). Repeated terrestrial laser scanning measurements and ground-based RADAR (GBInSAR) measurements on selected sites are used for periodic monitoring of slope movements and to verify the kinematic model (Oppikofer et al. 2009). (3) The historical activity of rock avalanches and large rock falls has been collected out from historical archives (Furseth 2006), and modern rock fall activity is registered in databases maintained by the Geological Survey of Norway and published on the web (http://www.skrednett.no/). A new database on unstable rock slopes, which will become publicly available on skrednett, is under construction (Bunkholt et al. 2013, this volume). The age and regional recurrence of pre-historic failures is dated using multiple dating techniques (e.g. Aa et al. 2007; Fenton et al. 2011).

Hazard and Risk Classification of Unstable Slopes

Due to the expected large number of unstable rock slopes prone to fail catastrophically in Norway, a hazard and risk classification system for objectively ranking the sites for importance for follow-up is required (Hermanns et al. 2010; Hermanns et al. 2012b). The classification system was constructed in collaboration with an expert group formed of national and international experts in the field. Except the four high risk objects (Åknes, Mannen, Nordness, Hegguraksla) which have been classified in the past years (see Fig. 2), a preliminary classification has been completed for singular sites and sites in the Møre og Romsdal county (Hermanns et al. 2011; Dahle et al. 2011). These classifications were based upon principles agreed upon by the expert group and the final system is based upon the combination of the following data:

The hazard area is defined as the area affected by the primary rockslide event and secondary effects. This includes defining the magnitude as well as multiple scenarios of catastrophic collapse as slope deformation in general varies significantly over the entire unstable rock slope making widely-differing critical volumes and run-out distances possible. To each of these scenarios the secondary effects are evaluated, such as the displacement wave in cases where the rockslide hits a water body or the up-damming of the valley with upstream and potential downstream flooding (Hermanns et al. 2013, this volume). Most difficult to define is the likelihood of the event happening in the future as globally only very limited instrumental data exists on catastrophic rock slope collapses impeding temporal prediction. We base our evaluation on a combination of observations from our detailed mapping: (1) the state of activity (rockslide velocity in the deforming slope, rock fall activity), (2) a structural and kinematic slide analysis including an analysis of where and how much deformation has occurred in the past and (3) a regional analyses of frequency of failures on geologically and morphological similar slopes. Based upon these observations the likelihood is defined as very high, high, medium, low, or very low (Hermanns et al. 2012b). The risk estimation finally is a combination of the estimation of likelihood of a future event with a rough estimation of the potential loss of life in the hazard area in the case that no mitigation measures are taken. All sites will be grouped in three classes as: (1) no mitigation measures are necessary, (2) periodic monitoring required, and (3) continuous monitoring in combination with mitigation is necessary.

Results and Conclusions

In Norway, unstable rock slopes are mapped systematically. The approach is risk based starting with mapping activities in those provinces with the highest number of historic incidents and focusing on those slopes in areas with settlement or important infrastructure. So far systematic mapping has been carried out in three provinces resulting in more than 285 sites being characterized as unstable slopes. Of those, a total of 62 sites are monitored at present (Fig. 2). Slide velocities at those sites range between under detection limits over a 3 years period up to ~10 cm/year.

A classification system to objectively evaluate the hazard and risk level was established (Hermanns et al. 2012b) is under construction and will finally give direction on how intensely each object will be followed up in future.

Four sites with high movement velocities, slide kinematics favoring failure, and an intense slope deformation indicating a possible failure in close future are classified as high risk objects at present. At those sites consequences are high, either due to severe secondary rockslide effects, such as the impact of the rockslide in a water body leading to displacement waves, or due to likely valley impoundment with related upstream and potential downstream flooding. These sites are continuously monitored and an early warning system in combination with an evacuation plan is in place or under construction.

Acknowledgments We want to acknowledge the financial support of this mapping program by the Norwegian Water and Energy Directorate (NVE) and namely Graziella Devoli and Olianne Eikenæs for fruitful discussions throughout the years. We also want to acknowledge the fruitful discussion of the expert group working on the final document on the classification system namely: Jodi Corominas, Giovanni Crosta, Corey Froese, Sylfest Glimsdal, Carl Harbitz, Michel Jaboyedoff, and Simon Löw.

References

Aa AR, Sjåstad J, Sønstegaard E, Blikra LH (2007) Chronology of holocene rock-avalanche deposits based on schmidt-hammer relative dating and dust stratigraphy in nearby bog deposits, Vora, inner Nordfjord, Norway. Holocene 17(7):955–964

Blikra LH (2008) The Åknes rockslide; monitoring, threshold values and early-warning. Landslides and engineered slopes. From the past to the future. In: Zuyu C, Jian-Min Z, Ken H, Fa-Quan W, Zhong-Kui L (eds) Proceedings of the 10th international symposium on landslides and engineered slopes, Taylor and Francis, Xi'an, 30 June–4 July 2008, 1850pp, ISBN 9780415411967

Blikra LH, Longva O, Harbitz C, Løvholt F (2005) Quantification of rock-avalanche and tsunami hazard in Storfjorden, Western Norway. In: Senneset K, Flaate K, Larsen JO (eds) Landslides and avalanches: ICFL 2005 Norway. Taylor & Francis, London, pp 57–64

Böhme M, Henderson I, Saintot A, Hermanns RL, Henriksen H (2011) Rock-slope instability investigations in Sogn & Fjordane County, Norway: a detailed structural and geomorphological analysis. In: Jaboyedoff M (ed) Slope tectonics. Geological Society, London, pp 97–112, Special Publication, 351. ISBN 978-1-86239-324-0

Braathen A, Blikra LH, Berg SS, Karlsen F (2004) Rock-slope failures in Norway; type, geometry, deformation mechanisms and stability. Norw J Geol 84:67–88

Bunkholt H, Osmundsen PT, Redfield T, Oppikofer T, Eiken T, L'Hereux J-S, Hermanns RL, Laukens TR (2011) ROS Fjellskred i Troms: status og analyser etter feltarbeid 2010. NGU rapport 2011.031, ISSN 0800-3416, 135p

Bunkholt H, Nordahl B, Hermanns RL, Oppikofer T, Fischer L, Blikra LH, Anda E, Dahle H, Sætre S (2013) Database of unstable rock slopes in Norway. In: Margottini et al. (eds) Landslide science and practice, Springer, (in press)

Dahle H, Anda E, Sætre S, Saintot A, Böhme M, Hermanns RL, Oppikofer T, Dalsegg E, Rønning JS, Derron MH (2011) Risiko og sårbarheitsanalyse for fjellskred i Møre og Romsdal, 105p

Direktoratet for samfunnssikkerhet og beredskap (2011) Nasjonal sårbarhets- og beredskapsrapport 2011, ISBN 978-82-7768-246-4, 80p

Eisbacher GH, Clague JJ (1984) Destructive mass movements in high mountains: hazard and management. Geological Survey of Canada, Paper 84-16 (0-660-11729-0), 230p

Fenton CR, Hermanns RL, Blikra LH, Kubik PW, Bryant C, Niedermann S, Meixner A, Groethals MM (2011) Regional ^{10}Be production rate calibration for the past 12 ka deduced from the radiocarbon-dated Grøtlandsura and Russenes rock avalanches at 69° N, Norway. Quat Geochronol 6(5):437–452 doi:10.1016/j.quageo.2011.04.005

Furseth A (2006) Skredulykker i Norge. Tun Forlag, Oslo, p 207p

Henderson IHC, Blikra LH (2008) Ustabile fjellparti i fyllittområde i Flåm – Aurland. NGU rapport 2008.033, ISSN 0800-3416, 16p

Henderson IHC, Saintot A (2011) Regional spatial variations in rockslide distribution from structural geology ranking: an example from Storfjorden, Western Norway. In: Jaboyedoff M (ed) Slope tectonics. Geological Society, London, pp 79–96, Special Publication, 351. ISBN 978-1-86239-324-0

Henderson IHC, Laukens TR, Osmundsen PT, Dehls JF, Larsen Y, Redfield TF (2011) A structural, geomorphological and InSAR study of fractures in the development of rock slope failures. In: Jaboyedoff M (ed) Slope tectonics. Geological Society, London, pp 185–201, Special Publication, 351. ISBN 978-1-86239-324-0

Hermanns RL, Blikra LH, Naumann M, Nilsen B, Panthi KK, Stromeyer D, Longva O (2006) Examples of multiple rock-slope collapses from Köfels (Ötz valley, Austria) and Western Norway. Eng Geol 83:94–108

Hermanns RL, Anda E, Henderson I, Dahle H, Saintot A, Blikra LH, Bøhme M, Dehls J, Redfield TF, Eiken T (2010) Towards a hazard classification system for large rock slope failures in Norway, European Geosciences Union, Vienna, 2–7 Mai 2010, Geophysical Research Abstracts. 12: EGU2010-13657

Hermanns RL, Bunkholt H, Böhme M, Fischer L, Oppikfer T, Rønning JS, Eiken T (2011) Foreløpig fare- og risikovudering av ustabile fjellparti ved Joasete-Furenkamben-Ramnanosi, Aurland commune. NGU rapport 2011.025, ISSN 0800-3416, 47p

Hermanns RL, Dahle H, Bjerke PL, Crosta G, Anda E, Blikra LH, Saintot A, Longva O, Eiken T (2013) Rock slide dams in Møre og Romsdal county, Norway: examples for the hazard and potential of rockslide dams. In: Margottini et al. (eds) Landslide science and practice, Springer, in press

Hermanns RL, Hansen L, Sletten K, Böhme M, Bunkholt H, Dehls JF, Eilertsen R, Fischer L, L'Heureux J-S, Høgaas F, Nordahl B, Oppikofer T, Rubensdotter L, Solberg I-L, Stalsberg K, Yugsi

Molina FX (2012a) Systematic geological mapping for landslide understanding in the Norwegian context. In: Eberhardt E, Froese C, Turner AK, Leroueil S (eds) Landslide and engineered slopes: protecting society through improved understanding. Taylor & Francis Group, London, pp 265–271

Hermanns RL, Oppikofer T, Anda E, Blikra LH, Böhme M, Bunkholt H, Crosta GB, Dahle H, Fischer L, Jaboyedoff M, Loew S, Yugsi Molina F (2012b) Recommended hazard and risk classification for large unstable rock slopes in Norway. NGU rapport 2012.029, ISSN 0800–3416 53p

Lauknes TR, Piyush Shanker A, Dehls JF, Zebker HA, Henderson IHC, Larsen Y (2010) Detailed rockslide mapping in northern Norway with small baseline and persistent scatter interferometric SAR time series methods. Remote Sens Environ 114(9):2097–2109

Oppikofer T, Jaboyedoff M (2008) Åknes/Tafjord project: analysis of ancient rockslide scars and potential instabilities in the Tafjord area & Laser scanner monitoring of instabilities at Hegguraksla. IGAR report IGAR-TO-009, Institute of Geomatics and Analysis of Risk, University of Lausanne, Lausanne

Oppikofer T, Jaboyedoff M, Blikra LH, Derron M-H (2009) Characterization and monitoring of the Åknes rockslide using terrestrial laser scanning. Nat Hazard Earth Syst Sci 9:1003–1019

Oppikofer T, Jaboyedoff M, Pedrazzini A, Derron M-H, Blikra LH (2011) Detailed DEM analysis of a rockslide scar to improve the basal failure surface model of active rockslides. J Geophys Res 116: F02016. doi:10.1029/2010JF001807

Osmundsen PT, Henderson I, Lauknes TR, Larsen Y, Redfield TF, Dehls JF (2009) Active normal fault control on landscape and rock-slope failure in northern Norway. Geology 37(2):135–138. doi:10.1130/G25208A.1

Redfield TF, Osmundsen PT (2009) The Tjellefonna fault system of Western Norway; linking late-Caledonian extension, post-caledonian normal faulting, and tertiary rock column uplift with the landslide-generated tsunami event of 1756. Tectonophysics 474:106–123

Saintot A, Henderson IHC, Derron M-H (2011) Inheritance of ductile and brittle structures in the development of large rock slope instabilities: examples from Western Norway. In: Jaboyedoff M (ed) Slope tectonics. Geological Society, London, pp 27–78, Special Publication, 351. ISBN 978-1-86239-324-0

Sepulveda S, Serey A, Lara M, Pavez A, Rebolledo S (2010) Landslides induced by the April 2007 Aysén fjord earthquake, Chilean Patagonia. Landslides 7(4):483–492

Landslide Databases in Europe: Analysis and Recommendations for Interoperability and Harmonisation

Miet Van Den Eeckhaut, Javier Hervás, and Luca Montanarella

Abstract

Landslide inventories, usually including digital inventory maps and linked alphanumeric attributes, are the most important input for further landslide zoning. However, to allow landslide susceptibility, hazard and risk assessment the inventory databases should contain information on the location of landslide phenomena, types, history, state of activity, magnitude or size, causal factors and the damage caused. Yet, in Europe it is not known which national (or regional) landslide databases contain all this information, and thus allow landslide risk assessment. Therefore this study presents a review of existing national landslide databases in Europe together with a number of regional databases, and proposes improvements in agreement with the EU Soil Thematic Strategy, and with INSPIRE Directive.

Replies received to a detailed questionnaire learned that currently 22 out of 37 contacted European countries have a national landslide database. Six other countries only have regional databases. In total the databases contain so far more than 642,000 landslides. About half of the databases contain less than 50 % of all landslides in the country and also information on landslide history, triggering factor and consequences is generally only available for less than 25 % of the landslides in the databases. A positive observation is that 60 % of the databases are updated at least once a year or after a major event. The spatial data are almost always collected with traditional methods such as field surveys, and analysis of aerial photographs and historical records. 67 % of the databases use a classification system adapted from Cruden and Varnes (Cruden DM, Varnes DJ (1996) Landslide types and processes. In: Turner AK, Schuster RL (eds) Landslides, investigation and mitigation, Special Report 247: Transportation Research Board. National Research Council, National Academy Press, Washington, DC, pp 36–71), so it should be possible to define a limited number of major landslide types and activity classes to be used in all databases. Other problems with regard to interoperability and harmonisation are due to differences in language, the absence of a digital database where spatial and alphanumeric information is linked (the case for 58 % of the databases), and the restricted accessibility.

Keywords

Landslide inventory • National database • Completeness • Europe • EU soil thematic strategy • INSPIRE

M. Van Den Eeckhaut (✉) • J. Hervás • L. Montanarella
Institute for Environment and Sustainability, Joint Research Centre (JRC), European Commission, 21027 Ispra, Italy
e-mail: miet.van-den-eeckhaut@jrc.ec.europa.eu

C. Margottini et al. (eds.), *Landslide Science and Practice*, Vol. 1,
DOI 10.1007/978-3-642-31325-7_4,

Introduction

For landslide susceptibility, hazard and risk assessment four types of data layers are required: landslide inventory data, conditioning and triggering factors, and elements at risk. The landslide database (LDB) is the most important. With regard to its content, Hervás (2012) distinguishes between core attributes, additional information and complementary data. Core attributes of a LDB are a unique identification code, location (geographical coordinates, landslide site name, municipality, province or county, region or state), type of landslide, date of occurrence or last reactivation, state of activity and volume or surface extent. Additional information may include landslide geometry (surface dimensions, depth of failure surface), geology (lithology, structure, material properties), hydrogeology, land cover or use, slope geometry, triggering factor, impact (casualties, damage), remedial measures, surveying methods and date, surveyor's name and bibliographical references. Finally, complementary data can be illustrations (ground or aerial photographs) and monitoring data.

In Europe, many countries have or are creating national and/or regional LDB. Yet, little is known on their content, completeness, format, structure, language and accessibility, and hence on their suitability to perform national or even transnational (e.g. major river catchment or continent-wide) susceptibility, hazard or risk assessment. Therefore the objectives of this study are to make a detailed review of existing national LDB in Europe and to propose improvements for delineating areas at risk in agreement with the EU Soil Thematic Strategy and its associated Proposal for a Soil Framework Directive (EC 2006a, b), and for achieving interoperability and harmonisation in agreement with the INSPIRE Directive (EC 2007). To meet these objectives a detailed questionnaire was created and sent out to the competent persons in each European country, and a review of literature, websites and main European legislation on the subject was carried out.

Materials and Methods

For analysing national and regional LDB in Europe, a comprehensive questionnaire was created. Inspiration was taken from published questionnaires on landslide inventories (Dikau et al. 1996; Di Mauro et al. 2003; RAMSOIL 2007–2008; Schweigl and Hervás 2009). We also checked the content of some publically available LDB both in Europe and outside Europe to make our enquiry as complete as possible. Before sending out the questionnaire, it was reviewed for completeness and clearness by two external evaluators. The questionnaire consists of the following sections: (0) introduction to the questionnaire; (1) contact information; (2) database availability; (3) general information of LDB; (4) content of LDB; (5) format of LDB; (6) conditions to access and use of LDB; (7) information related to INSPIRE; and (8) availability of complementary data for landslide hazard and risk assessment (e.g. digital elevation model, geology, meteorology and seismicity, elements at risk). A list of definitions of terminology used throughout the questionnaire was provided and contact persons were invited to provide us additional information.

The questionnaire was sent to competent persons in geological surveys, research institutes and universities in the first half of 2010.

Results

Response

Thirty-three out of thirty-seven EU member states, EU official candidate and potential candidate countries, and EFTA countries contacted responded to our request. More specifically, 22 countries have a national LDB, 6 other countries only have one or more regional LDB (i.e. Belgium, Croatia, Estonia, Germany, Romania, Serbia) and 5 do not have a LDB (Figs. 1 and 2; Table 1). Information on both national and regional LDB was collected for Austria, Italy, Portugal and Spain. In total, information on 22 regional LDB was collected.

National Databases

In this section the national LDB are discussed. The graphs shown also include the main results obtained for the regional LDB. This is done for comparison, but the results of the regional databases will not be discussed in detail. As for Italy (IFFI and AVI) and Sweden (MSB and SGI), two different national LDB exist, this overview contains 24 national databases of 22 different European countries. Twenty-one LDB are created in the official language of the country only, while the remaining three (i.e. Greece, Italy – IFFI and Sweden – MSB) also provide the information in English. About 58 % of the databases contain also other natural hazards (e.g. floods, sinkholes). In total, the databases contain more than 642,000 landslides, of which about 75 % are located in Italy. Austria, Czech Republic, France, Norway, Poland, Slovakia and UK, all having more than 10,000 landslides, account for 18 % of the recorded landslides (Table 1). Yet, it is important to note that not all countries have decided to create a LDB that includes as many landslide locations as possible. The database of Switzerland, for example, contains only the 317 most relevant landslide

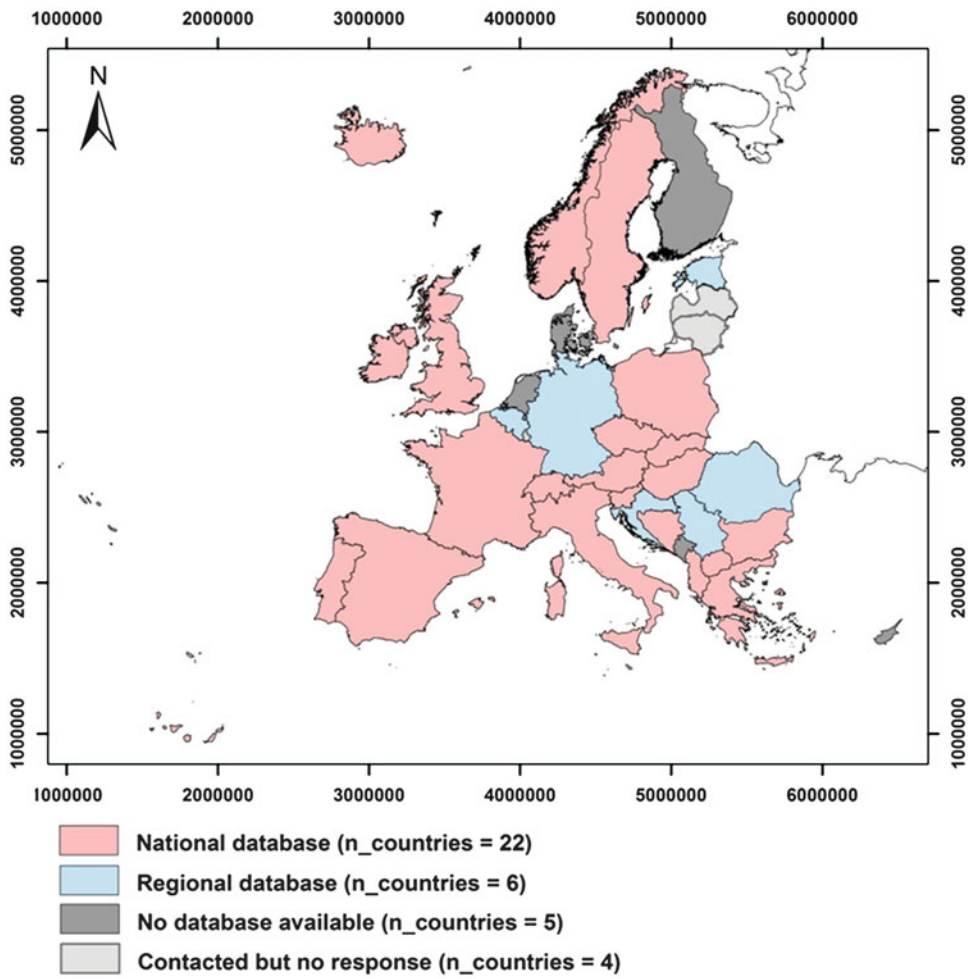

Fig. 1 Distribution of national landslide databases in EU member states, EU official candidate and potential candidate countries and EFTA countries, and regional databases in countries where no national database exists. We refer to Fig. 2 for a detailed location of the regional databases

events, and the Swedish Natural Hazards Information System (MSB) contains only detailed information of the 17 most severe landslides, because it focuses on those events of which lessons can be learnt with regard to management. However, although almost all other countries try to include as many landslides as possible, the completeness of most databases is estimated lower than 50 % of all landslides that have ever occurred in the country (Fig. 3). Databases of France, Italy (IFFI) and Czech Republic are estimated to be most complete. The completeness of a database is related to the abovementioned difference in objective of the LDB, to the methodology (see further) and resources employed and to the time span of landslide events covered. The latter is highly variable and ranging from countries with LDB including landslides with pre-Holocene origin to LDB including only the landslides that occurred after 2000.

More important than the creation date is the updating of the LDB. For only 4 out of 24 national LDB no updating of the database is foreseen. However, for some of these countries this might change if updating appears to be necessary. The other databases are generally updated at least once a year or after a major event.

Landslide inventory maps were created at a scale between 1:10,000 and 1:1,000,000 with a maximum number of maps having a scale of 1:10,000. With regard to the reference coordinate system used, generally a local coordinate system was used. Landslides are either represented as points (52 %) or as a combination of points, lines and polygons (48 %). Only for six landslide inventory maps information on the spatial accuracy is included.

Landslide locations are generally obtained through a combination of different techniques (Fig. 4). Most commonly used are field surveys (67 %, or 16 of the databases), historical documents (75 %, or 18 of the databases) and aerial photograph analysis (38 %, or 9 of the databases). Alternative methods for obtaining landslide locations are collecting local and regional inventories (Italy and Austria), or observations by road authorities and railroad companies (Norway).

In 21 out of the 24 LDB landslides are further classified according to e.g. type of movement, type of material, size or velocity. Exceptions are the Portuguese database and the two databases of Sweden. With regard to the classification system used, 16 LDB use a system that is derived from the

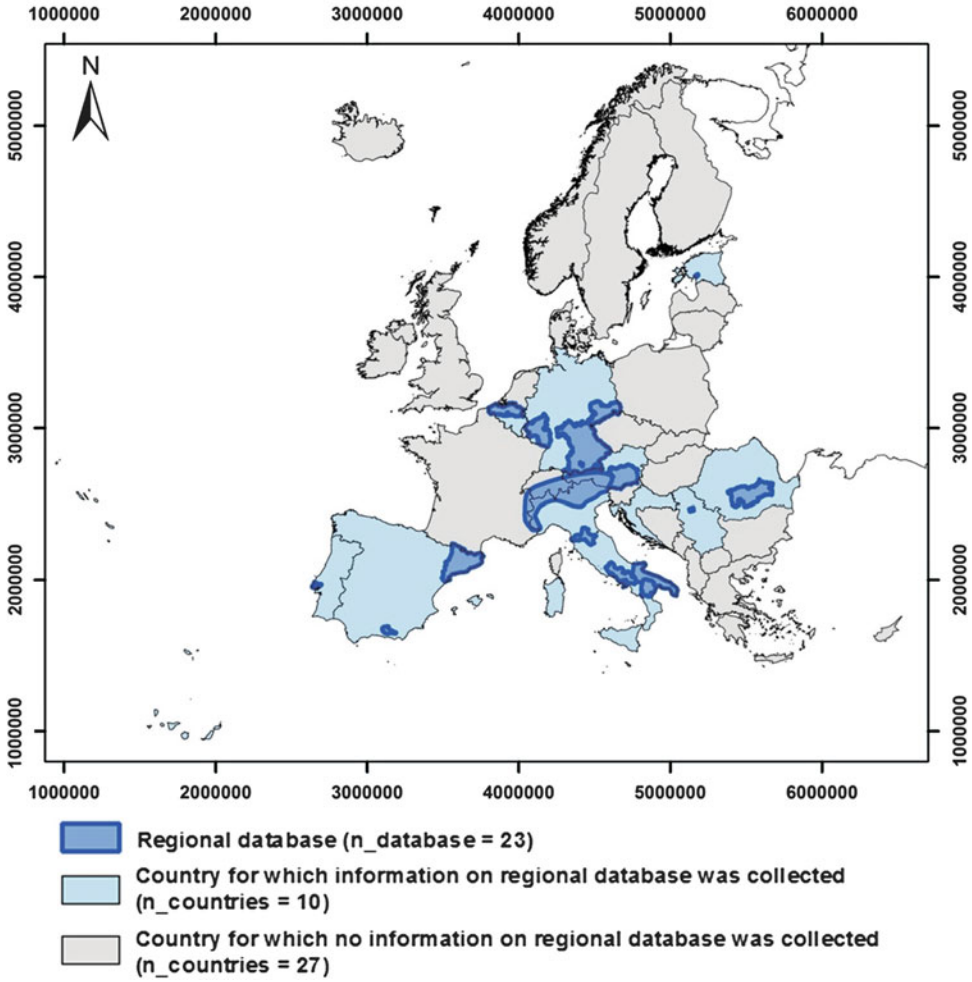

Fig. 2 Distribution of regional landslide databases in Europe analysed in this study

one suggested by Cruden and Varnes (1996), while the five other databases use a local classification system. The number of classes generally ranges from three to six classes. Exceptions are Italy (IFFI; n = 12), Slovenia (n = 15) and Greece (n = 24).

Figure 5 displaying the landslide size characteristics stored in the database shows that almost all LDB contain information on the landslide length and width (i.e. 21) and on the area affected by the landslide (i.e. 18). As landslide volume is more difficult to assess than the affected area, the number of databases containing this information is somewhat lower (i.e. 16). Most LDB also contain additional information on the geo-environmental characteristics at the landslide site, especially on lithology or structure, hydrogeology and slope gradient. About half of the databases additionally provide information on the orientation and form of the slope (slope curvature).

Information on landslide history and activity, triggering factors and consequences is low in most of the databases (i.e. completeness generally less than 25 %), which is problematic for nationwide landslide hazard and risk studies.

With regard to the accessibility, 12 LDB allow the general public access to the data. However, public access is restricted to consultation for nine of these LDB. In the absence of a web GIS interface a few of these databases can only be consulted in the database holder's office. Those countries providing a web GIS interface (Van Den Eeckhaut and Hervás 2012) generally have it in the local language only, hampering consultation to most foreigners. Four databases allow free use of the data. These are Andorra, Ireland, Slovakia and Sweden (MSB). Other countries eventually provide the data, but under special conditions.

Policy-Related Suggestions for Harmonisation and Interoperability

EU Soil Thematic Strategy and Framework Directive

Landslides constitute one of the eight soil threats considered in the EU Thematic Strategy for Soil Protection (EC 2006a). However, up to date this Strategy does not have legally binding regulations for LDB, because its associated legislative proposal for a Soil Framework Directive (EC 2006b) is still not approved. According to the current proposal,

Table 1 Overview of the national landslide databases in Europe (EU member states, EU official candidate and potential candidate countries, and EFTA countries). We refer to Van Den Eeckhaut and Hervás (2012) for more detailed information

Country	No of landslides	Name
Albania	210	Landslide database
Andorra[a]	274	Natural hazard database of Andorra
Andorra	160	Terrain zonation according to geological – geotechnical problems
Austria	25,000	GEORIOS
Bosnia and Herzegovina	1,500	The engineering-geology map Federation of Bosnia and Herzegovina
Bulgaria	1,107	Map of landslides
Czech Republic	14,178	National landslide register
France	10,000	National database of ground movements (BDMvT)
Greece	2,200	Geodatabase I.G.M.E./eng_geol/ground_failures
Hungary	400	National landslides cadastre
Iceland	5,000	OLI
Ireland	422	National landslide database
Italy	485,004	IFFI project
Italy	21,159	AVI project
Macedonia	150	Landslide cadastre
Norway	31,500	National landslide database
Poland	12,150	SOPO
Portugal	163	Disaster database
Slovakia	21,190	Landslide register
Slovenia	6,602	GIS_UJME (part of larger database)
Spain	569	Spanish database of geological hazards
Sweden	17	Swedish natural hazards information system (MSB)
	550	SGI landslide database
Switzerland	317	InfoSlide
United Kingdom	15,210	National landslide database

[a]Not included in data set of a LDB as it is rather a landslide hazard map with a limited number of recorded landslides

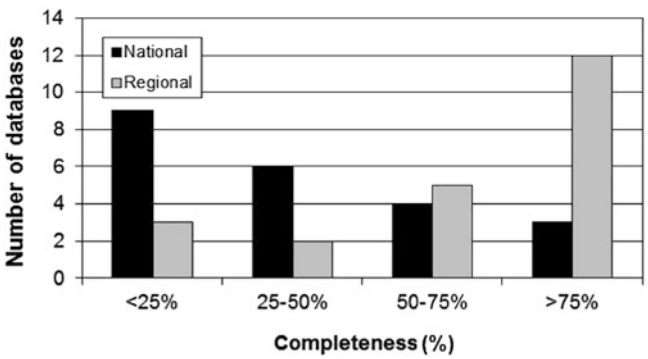

Fig. 3 Estimated completeness of the national and regional landslide databases

identification of risk zones will be required. Landslide information from the EU member states will be necessary, because a set of "common criteria" including besides a selection of conditioning and triggering factors also the occurrence/density of existing landslides was selected by the Soil Information Working Group (SIWG) of the European Soil Bureau Network (ESBN) (Eckelmann et al. 2006). The SIWG further suggested using a nested geographical approach based on "Tiers". As currently no harmonised LDB are available throughout Europe, the European Landslide Expert Group recommended carrying out a pan-European landslide inventory by reviewing (collecting) the data already available and including at least information on the location and type of historical landslides, but if possible also on date of occurrence, surface extent and direct impact (Hervás et al. 2007). The minimum suggested information would then allow creation of a European landslide susceptibility map (see also Günther et al. this volume).

INSPIRE

INSPIRE is a Directive adopted by the European Parliament and the Council of the European Union, setting the legal framework for the establishment of the Infrastructure for Spatial Information in the European Community, for the purposes of Community environmental policies and policies or activities which may have an impact on the environment (EC 2007; http://inspire.jrc.ec.europa.eu/documents/Data_Specifications/D2.5_v3.2.pdf).

With regard to LDB, INSPIRE might help in overcoming the problem of variability in language, coordinate system, format, structure and accessibility in the near future. The definition of INSPIRE regulation including data

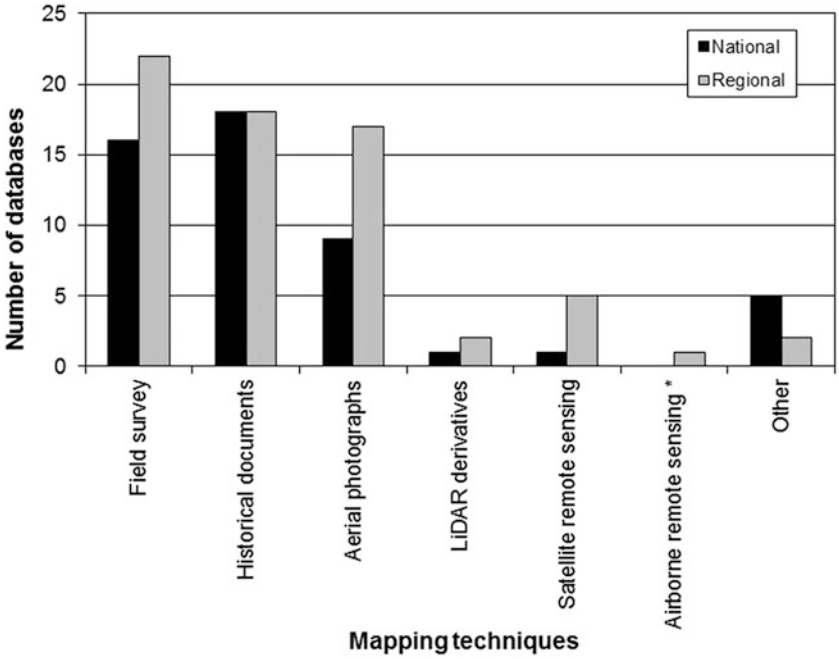

Fig. 4 Techniques used to collect landslide locations (*Other than aerial photographs and LiDAR)

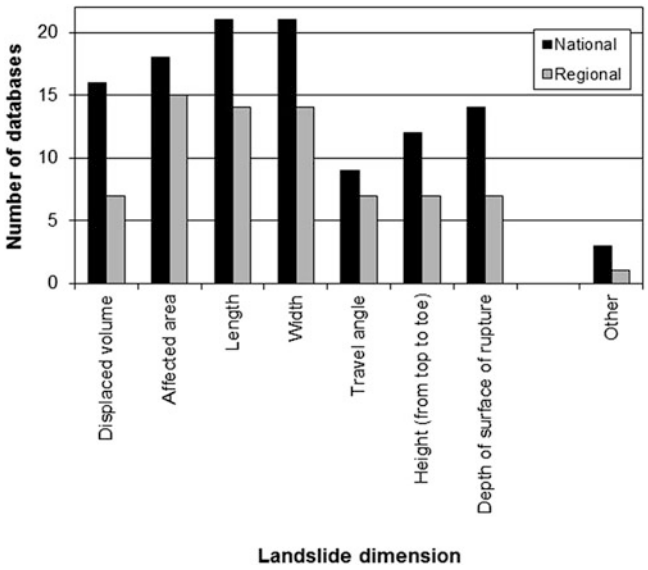

Fig. 5 Landslide size characteristics reported in national and regional landslide databases

specifications of Natural Risk Zones such as landslides (INSPIRE Thematic Working Group Natural Risk Zones 2011) is an on-going process. After launching the Call for Expression of Interest for participation in development of INSPIRE data specifications in November 2009, the Thematic Working Group produced the first version of the data specifications in September 2010. In June 2011 version 2.0 was made publically available on the INSPIRE webpage (http://inspire.jrc.ec.europa.eu/index.cfm/pageid/2/list/1) Until October 2011 there is time for an external quality check and by March 2012 the third and final version should be published.

Since physical combination of all landslides in one harmonised European database is currently impossible, and probably not recommended, the procedure followed by the INSPIRE regulation seems feasible. INSPIRE focuses on designing a framework or infrastructure to ensure that spatial data are stored, made available and maintained at the most appropriate level; that it is possible to combine spatial data and services from different sources across the Community in a consistent way and share them between several users and applications; that spatial data and services are made available under conditions that do not restrict their extensive use; and that it is easy to discover available spatial data, to evaluate their fitness for purpose and to know the conditions applicable to their use.

Each EU member state transposing the directive should create and maintain this infrastructure, including general schemes on natural risk zones such as landslides (see http://inspire.jrc.ec.europa.eu/index.cfm/pageid/2/list/1 for a detailed description of the Natural Risk Zones application scheme), and share this information with other public authorities in EU member states. This should increase interoperability and accessibility of spatial landslide information, including a limited set of features (i.e. mandatory are a digital landslide inventory map, a landslide INSPIRE identifier and the hazard type, while landslide history can be included if available) among member states. The general scheme itself will be in English, but feature catalogues are

envisaged to be multilingual, so it should be possible to translate the limited set of features in a national LDB from one language into another.

The limited information to be included in the general model as defined by INSPIRE regulation will normally allow quantitative landslide susceptibility modelling at a national or European scale. For landslide hazard and risk modelling, however, more datasets regarding landslides are needed.

As mentioned before in our questionnaire, a limited section focussed on INSPIRE regulations that are already approved. These regulations mainly deal with metadata (http://inspire.jrc.ec.europa.eu/index.cfm/pageid/101) and network services (http://inspire.jrc.ec.europa.eu/index.cfm/pageid/5). The results showed that currently only five national LDB have metadata complying with INSPIRE regulations while in only three LDB the landslide data are implemented in a network service meeting the INSPIRE specifications. More important is that the persons responsible for the database did not seem to be well-informed about these INSPIRE regulations. So in the future it is suggested to pay more attention to the correct distribution of information on INSPIRE to competent persons in member states.

Conclusions

Landslide databases provide information on the location, timing, type, size and activity of landslide phenomena, the controlling and triggering factors, and the damage caused for scientific, planning, decision-making and other purposes. We provided a detailed overview and analysis of 24 national and a limited set of 22 regional LDB in Europe to provide insight in their content, completeness, format, structure, language and accessibility, and hence in their suitability to perform national or continental landslide zoning.

In Europe currently 22 out of 37 contacted countries have a national database, and six other countries only have regional databases. In total the national databases contain more than 642,000 landslides, of which about 75 % are located in Italy, but also for Austria, Czech Republic, France, Norway, Poland, Slovakia and UK more than 10,000 landslides are recorded.

National LDB are generally created in the official language of the country and 58 % of the databases contain other natural hazards (e.g. floods, sinkholes). With regard to the completeness of LDB about 68 % of the 24 databases contain less than 50 % of all landslides in the country. This is related to the fact that landslides are local phenomena, with sometimes small dimensions and short preservation times. Yet, a positive observation is that more than 60 % of the databases are updated at least once a year or after a major event. The spatial data are almost always collected with traditional methods using map scales varying between 1:10,000 and 1:1,000,000.

The preliminary conceptual model for Natural Risk Zones (INSPIRE) and the recommendations proposed by the European Landslide Expert Group for interoperability and harmonisation are more or less in agreement. Both define a limited mandatory set of information to be included in the database, while other information can be provided too. The minimum set of information allows assessment of landslide susceptibility, and includes a unique European identification code, location (geographical coordinates), and type of landslide (using classification of Cruden and Varnes 1996). Additional information such as date of occurrence and/or last reactivation (if known), volume, triggering factor, and consequences (e.g. casualties, damage; if known) would allow further hazard and risk zoning. For quality control, it is recommended to also include some meta-data.

A more detailed description of the results obtained from this enquiry can be found in Van Den Eeckhaut and Hervás (2012).

Acknowledgments Special thanks go to all the contact persons and organizations that took the effort to complete the questionnaire. This study has been carried out in the framework of the EU-FP7 project SafeLand: Living with landslide risk in Europe: Assessment, effects of global change, and risk management strategies (Grant Agreement 226479; http://www.safeland-fp7.eu/). The authors thank all the project partners that have contributed to the distribution of the questionnaire to the responsible organizations in their country. Special thanks go to Dr. J.P. Malet and Prof. J. Corominas for reviewing the questionnaire, and to R. Tomas, V. Lima and M. Van Liedekerke (JRC) for providing information on the INSPIRE regulation status.

References

Cruden DM, Varnes DJ (1996) Landslide types and processes. In: Turner AK, Schuster RL (eds) Landslides, investigation and mitigation. National Academy, Washington, DC, pp 36–71, Special Report 247: Transportation Research Board. National Research Council

Dikau R, Cavallin A, Jager S (1996) Databases and GIS for landslide research in Europe. Geomorphology 15:227–239

Di Mauro C, Vetere Arellano AL, Ranguelov B, Hervás J, Peckham R, Christou MD, Duffield JS, Wood M, Nordvik JP, Lucia AC (2003) Questionnaire: risk mapping – natural and technological risk and contaminated lands. Special Publication No. I.03.222, JRC, Ispra, 108p

EC (2006a) Thematic strategy for soil protection. COM(2006)231 final, Brussels, 12p

EC (2006b) Proposal for a directive of the European Parliament and of the Council establishing a framework for the protection of soil and amending directive 2004/35/EC. COM(2006)232 final, Brussels, 30p

EC (2007) Directive 200/7/2/EC of the European Parliament and the Council of 14 March 2007 establishing an Infrastructure for Spatial Information in the European Community (INSPIRE). Official

Journal of the European Union, L108/1-14, Luxembourg, 14p. http://inspire.jrc.ec.europa.eu

Eckelmann W, Baritz R, Bialousz S, Bielek P, Carre F, Houskova B, Jones RJA, Kibblewhite MG, Kozak J, Le Bas C, Toth G, Varallyay G, Yli Halla M, Zupan M (2006) Common criteria for risk area identification ac-cording to soil threats. European Soil Bureau Research Report n. 20, EUR 22185 EN, Office for Official Publications of the European Communities, Luxembourg, 94p

Günther A, Van Den Eeckhaut M, Reichenbach P, Hervás J, Malet JP, Foster C, Guzzetti F (2011) New developments in harmonized landslide susceptibility mapping over Europe in the framework of the European soil thematic strategy. In: Proceedings of the 2nd world landslide forum, Rome, this volume, 3–9 Oct 2011

Hervás J (2012) Landslide inventory. In: Bobrowky PT (ed) Encyclopedia of natural hazards. Springer, Heidelberg (ISBN 978-90-481-8699-0) (in press)

Hervás J, Günther A, Reichenbach P, Chacón J, Pasuto A, Malet J-P, Trigila A, Hobbs P, Maquaire O, Tagliavini F, Poyiadji E, Guerrieri L, Montanarella L (2007) Recommendations on a common approach for mapping areas at risk of landslides in Europe. In: Hervás J (ed) Guidelines for mapping areas at risk of landslides in Europe. Proceedings experts meeting, Ispra. JRC Report EUR 23093 EN, Office for Official Publications of the European Communities, Luxembourg, pp 45–49, 23–24 Oct 2007

INSPIRE Thematic Working Group Natural Risk Zones (2011) D2.8. III.12 Data specification on natural risk zones – draft guidelines, version 2.0 (22/06/2011). INSPIRE Thematic Working Group Natural Risk Zones, 175p. http://inspire.jrc.ec.europa.eu/index.cfm/pageid/2/list/1

RAMSOIL (2007–2008) RAMSOIL: risk assessment methodologies for SOIL threats. http://eusoils.jrc.ec.europa.eu/projects/Ramsoil/data.html

Schweigl J, Hervás J (2009) Landslide mapping in Austria. JRC Report EUR 23785 EN, Office for Official Publications of the European Communities, Luxembourg, 61p

Van Den Eeckhaut M, Hervás J (2012) State of the art of national landslide databases in Europe and their potential for hazard and risk assessment. Geomorphology 139–140:545–558

Working with Landslide Inventories and Susceptibility Maps in Lower Austria

Joachim Schweigl and Wolfgang Straka

Abstract

The landslide inventory is an essential tool for working with landslides and related preventive and remedial measures in practice, and for the development of landslide susceptibility, hazard or risk maps. In Lower Austria, the regional Geological Survey has been developing its landslide inventory since 1953. In 2000 a digital version replaced the paper archive. For every geological or geotechnical report issued by the Survey the inventory is consulted. In 2007–2008 a pilot project was set up to produce the first landslide susceptibility maps. Three contracted organizations presented their proposals for the map design, using a heuristic approach, on the example of 12 selected municipalities. The results and the advantages as well as drawbacks of the method are discussed.

Keywords

Landslide inventory • Landslide susceptibility map • Heuristic method • Building ground register • Airborne laser scan

Introduction

Public landslide inventories are an essential tool for efficiently dealing with problems related to or caused by natural hazards. This is no less true for landslide susceptibility, hazard, or risk maps that are derived from such inventories. However, only a few complete as well as consistent landslide inventories covering areas >1,000 km^2 are available, even in industrialized countries.

J. Schweigl (✉)
Federal State of Lower Austria, BD1 – Geological Survey, Landhausplatz 1, St. Pölten, Austria
e-mail: joachim.schweigl@noel.gv.at

W. Straka
Department of Civil Engineering and Natural Hazards, University of Natural Resources and Life Sciences, Vienna, Austria

Landslide Inventories

In Austria, the Geological Survey of Austria and the Forest Engineering Service in Torrent and Avalanche Control, both in Vienna, are collecting landslide information on a nationwide scale (Schweigl and Hervas 2009). In each case, the information is held in a GIS database containing polygons representing areas prone to or affected by landslides, and is based on data collected during field mapping or work on events that have caused actual damage. In addition, it may contain the time of events, but hardly any further information.

In the Federal State of Lower Austria, more specific information on landslides causing human and economic loss is collected by the Geological Survey of the regional government, and added to their GIS on a regular basis. The largest and best inventory of this information (and further geological, geotechnical and mining data) for Lower Austria is contained in the building ground register *(Baugrundkataster)* of the Geological Survey of Lower Austria (Schwenk 1992). Second in importance and frequency of use for Lower Austria is the GEORIOS database, maintained by the Geological Survey of Austria in Vienna.

C. Margottini et al. (eds.), *Landslide Science and Practice*, Vol. 1,
DOI 10.1007/978-3-642-31325-7_5,

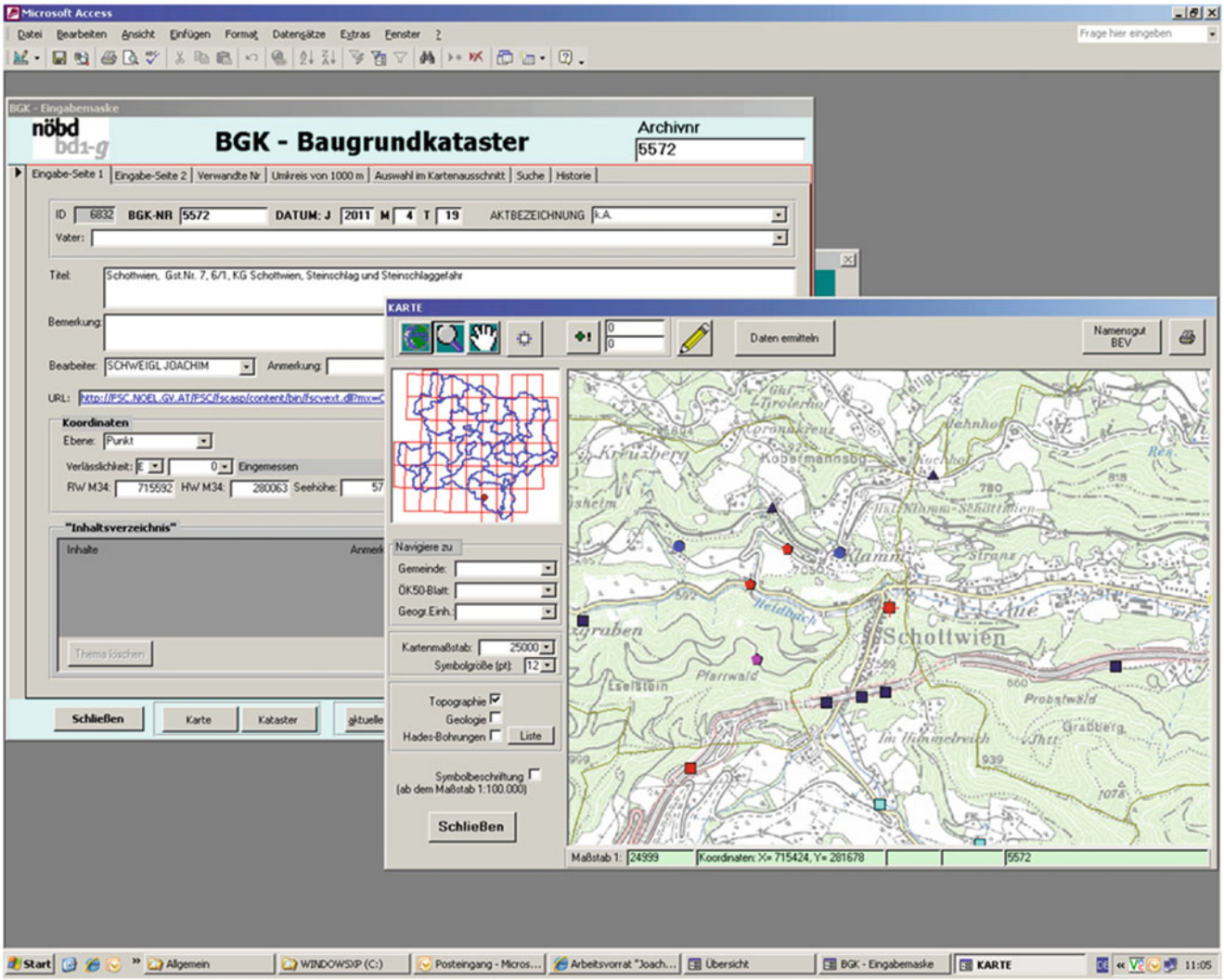

Fig. 1 Screenshot of the digital building ground register of Lower Austria, with data input form (*upper left*) and map objects tool (*lower right*). The added location is indicated by the *red center point* of the topographic map (scale 1:50,000)

Landslides reported in the building ground register of Lower Austria have all been recorded by experts on the basis of field surveys. The inventory was set up after 1953, and replaced by a digital database (MS Access) and GIS (IMAP, based on ESRI software) in 2000. Since, all data from 1990 onward have been added in digital form, whereas all data up to 1990 were converted to image and portable document format and linked to point data in the database. The database contains a map objects tool for input and graphic display of the landslide location (Fig. 1) as well as a web GIS application (Fig. 2). Each landslide is represented as point data only, because most landslides are <100 m maximum dimension.

This digital inventory of past events has been finalized in 2010. At present, a total of 2,000 landslides having caused damage to infrastructure, buildings or persons are reported. Other landslides, including those having effected economic loss in the order of less than 1,000 Euro, are not included. It is clear that the landslides not included outnumber the reported ones. The ongoing interpretation of the new digital terrain model (based on airborne laser scan data), as well as field trips to selected locations and comparisons with data of the Geological Survey of Austria all demonstrate this. Most events occur, often unrecognized, in forests, grass land, and mountain areas.

For all events reported, the landslide inventory takes account of the following information: Type of landslide, type of process, date of (main) event, date of report, reporter; municipality, cadastral municipality and plot number; land use, geological unit, soil/rock description, slope aspect and inclination, maximum width and length of the landslide, estimated depth and volume, history, likely trigger, typical features (e.g. tension cracks), pictures, description of damage, and urgent protection or stabilization works. In some

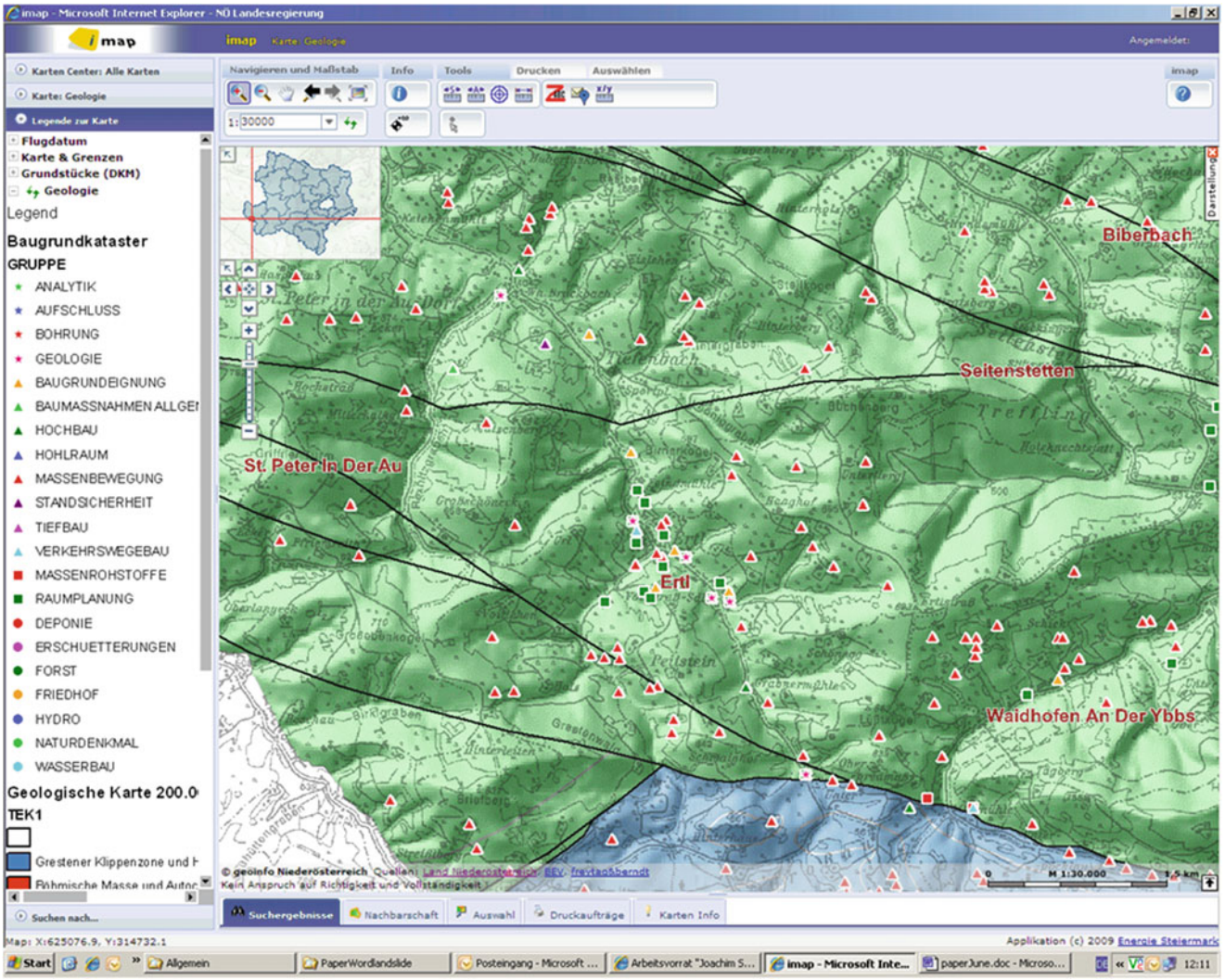

Fig. 2 Screenshot of the web GIS application of the building ground register, displaying various geohazard locations, most of them landslides (*red triangles*), on *top* of the geological map (*green* = Flysch zone, *blue* = Helvetic zone)

cases a history of a complex landslide is included. The inventory is mainly used to inform planning of and reporting on construction and spatial zoning. In case of emergencies, while early decisions naturally have to be based on field work, another purpose of consulting the inventory is to evaluate the larger situation and later to help in planning for long-term security.

A Pilot Project for Lower Austria

In 2007, a pilot project was set up in order to create the first landslide susceptibility maps (scale 1:25,000) for selected areas of Lower Austria, and two engineering consulting companies as well as the University of Natural Resources and Life Sciences, Vienna, were contracted to independently produce the maps and guidelines for respective procedure. A total of 12 municipalities, located in various geological units, were covered by this study, some of them by all three contractors, for the purpose of comparing their approaches. In addition to the data mentioned above, archived information and personal knowledge of other institutions (primarily municipal offices) as well as airborne photographs and 3D laser scan data were used. The susceptibility was evaluated on infrastructure and urban settlement zones only, by means of a heuristic (as opposed to a statistical) approach.

In the following sections, three different types of landslide susceptibility maps, which resulted from the pilot project, will be presented, and guidelines for the production of such maps will be discussed, with emphasis on the advantages and handicaps in practice.

Base Data for the Pilot Project

Much relevant information is in fact available, not formalized in maps and digital databases but as "expert knowledge" of experienced investigators. To illustrate this, let's undertake the following geological overview.

When crossing Lower Austria from north to south, the following geological units are encountered: (1) Bohemian Massif: mostly crystalline rocks; rockfalls occur where rivers have formed steep-sided valleys. (2) Molasse Zone: soft sedimentary rocks, many prone to subsidence, some well-known for sliding even at slope angles of just a few degrees. The same applies to some intramontane basins, including the large Vienna Basin. (3) Flysch Zone: in eastern Austria often sandstone-dominated; weathering crust in creeping movement everywhere, otherwise a fair number of slides, but not as many as might be expected. (4) Helvetic Klippen Belt: dominated by variegated shales and clay-marlstones; many active slides and earthflows, the inactive ones easily reactivated. (5) Northern Calcareous Alps: slumps and earthfalls mainly in Permotriassic rocks with evaporitic members, otherwise many rockfalls and occasional rockslides and rock avalanches. (6) Greywacke Zone and Lower Austroalpine: shales, phyllites and mica schists; many slopes in deep-reaching creep. (7) Quaternary cover sediments: subsidence and earthfalls tend to occur in loess, whereas rockfalls as well as earthfalls are observed in conglomerated fluvial terraces. Soil liquefaction has occurred in some fine-grained periglacial valley fills.

The landslide inventory is based on field work by experts and, where it is sufficiently comprehensive, is a big help in objectifying experience such as illustrated above. In our view, it offers the best way of producing landslide susceptibility, hazard, or risk maps, if detailed assessment can be made of events representative of various geological and practical conditions, after initial reporting. Unfortunately, this kind of work is time-consuming and hence expensive, as it has to be mostly done by contracted experts.

From 2007 to 2010, a new high resolution (1 × 1 m) digital terrain model (DTM), based on airborne laser scan data, has been created for the whole of Lower Austria (approx. 70 % of Austria has been covered so far). This comes in handy as a perfect means of controlling location and area of reported objects in the existing landslide inventory (Fig. 3). However, we should say that such data, like aerial photographs and satellite images, are not that trustworthy as a basis of an inventory, compared to field assessment. Control surveys by the authors have uncovered some slides indicated by airborne data, which turned out to be non-existent.

It is well established practice to check on an initial ("unsupervised") interpretation of satellite imagery at selected locations, in order to develop a more reliable ("supervised") interpretation backed by empirical evidence.

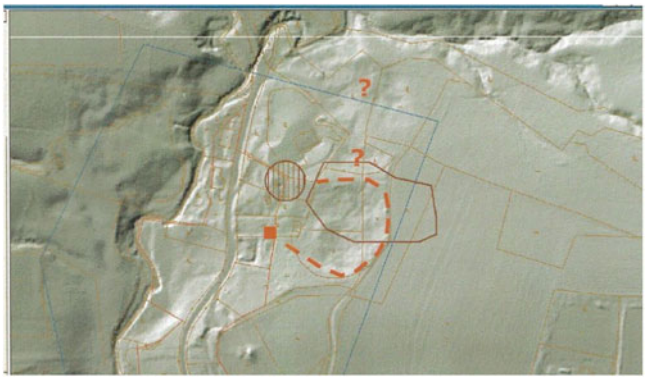

Fig. 3 Example of a sliding area as indicated by different landslide inventories, as well as the digital terrain model (DTM) based on airborne laser scan data. *Red square*: point data in the public building ground register; *brown polygon* and *hatched circular area*: representations on two different layers in the database of the Geological Survey of Austria; *red stitched line*: scarp as interpreted from the DTM. There seem to be one or two other similar slides immediately to the north (*red question marks*). The ambiguity inherent in the existing inventories, as well as the value of the DTM in clarifying the extent of the problem, is obvious. Nonetheless a detailed assessment (1, 2 or 3 landslides; indications for activity) certainly requires field work

We are well aware that this should likewise be taken into account when theorizing or working on susceptibility maps. If our pilot study could not quite live up to this principle, it has been for one reason: The main purpose of the project was to work out proposals for the map design and guidelines for the work flow, and for that purpose, the budget could not be extended to include more than occasional field work.

One other existing inventory to be used was the GEORIOS database and GIS of the Geological Survey of Austria (Kociu et al. 2007). Its background is completely different from the building ground register of Lower Austria. Information on landslides was created by the geologists who did field work on the Geological Map of Austria (scale of field maps 1:10,000, published maps 1:50,000). More often than not there is no information about age, dimension of, or damage by the landslide. Only type, location or the area covered by the landslide is recorded. Often there are quite large areas (polygons) containing many comparatively small objects, or small circles really meaning points, with the type or character of the individual objects not clearly indicated. The main reason for this is the fact that the original information is of an extremely heterogeneous and often haphazard nature (by-product of scientific mapping). Similar issues apply to the landslide information ("brown zones") included in the flooding hazard zonation of the Forest Engineering Service in Torrent and Avalanche Control *(Wild Bach- und Lawinenverbauung)*.

In addition to the geohazard-related databases just described, there are some man-made hazards to be taken into account, be it as triggers of landslides or aggravating

factors. Those related to mining and mine tailings can be pinpointed with the help of the mining register (BergGIS database), others related to waste deposits and contaminated soil are pointed to by a similar database. Both are available for the whole of Austria and held by the Ministry of Economic Affairs and the Federal Agency for the Environment *(Umweltbundesamt)*, respectively. They contain GIS polygons defining areas to which rights to mining exploration and production or waste deposition are assigned, but also areas suspected of having served as deposits in the past or being capable to be used that way in the future (mostly sand and gravel pits). The limits of all those areas follow cadastral plot boundaries.

Contrary to the data so far described, some others were deliberately not included. This applies, on the one hand, to radon emissions: there are too few measurement sites for the purpose, and the results are presented nation-wide on the scale of whole municipalities. On the other hand, the flooding protection zones ("yellow" and "red zones") defined by the Forest Engineering Service in Torrent and Avalanche Control should not be included: this is to prevent any mingling of an inventory, which merely indicates any actual or potential problems, with a zoning map, which constitutes a binding legal document.

Base maps on which to work include the following: the Austrian Topographic Map 1:50,000, ortho-corrected aerial photo mosaic, DTM based on airborne laser scan, digital ground register, and the building ground register. The latter includes the boundaries of the approved building land, on which the landslide susceptibility had to be evaluated in course of the pilot project. The scale of the final susceptibility map to be presented to interested clients in printed form was set to 1:25,000.

Results of the Pilot Project

We skip the technical details of the production of the maps, which has been assisted by standard software, and go right to the experience gained and problems encountered by the contracted investigators while working on the available data. This experience was shared by all investigators, and is therefore presented in unified form as follows:

Most of the archived spatial data are available in digital form (point data and attributes in the building ground register, shape-files containing the mining areas, etc.), so adding this to the map, on the one hand, is the easy part. Classifying the information or consolidating it on a map of "landslide susceptibility", even for a frequent type of landslide, on the other hand, turned out to be tricky. One has to rely on additional information, which is of a quite haphazard nature, for two reasons:

Information created as a by-product of scientific mapping (by the Geological Survey of Austria) hardly contains any specifics of individual objects, and more often than not just summarizes the impression by the field geologist that the landscape seemed to be unstable in certain areas. These generalized areas show up in the GEORIOS database and come with a classification into "creep", "area with small slumps", "slide/slump", and "landslide". Most other relevant parameters are seldom specified, mainly for well-known cases.

Information created by experts in the public service most often (not always) does contain specific information on individual objects, because their occurrence was the reason for investigating in the first place, but the official documents tend to have little information on the wider geological context because there was no time to collect it. Therefore it is difficult to establish (not only assume via "expert knowledge") a relation of the occurrence and the geological, e.g. structural, conditions like bedding or the fault system.

For these reasons, on the one hand, it is hardly anywhere feasible to derive areal information from the point data in the building ground register (our most reliable source). This is all the more critical because of the requirement that areas derived from the data should not just encompass, or circumscribe a cluster of, actual slides, but also define areas of future slope failure, where nothing has happened yet. This, in turn, requires criteria which should be extracted from existing data valid for the area of interest (they need not be valid in other regions).

The areal information of the other databases, on the other hand, is hard to harmonize with the point data in the building ground register, let alone to rationally evaluate one by the other. Sometimes, the information is decidedly incorrect. Correction, being an obvious option in some cases (cf. Figs. 4 and 5), nonetheless involves judgement by a person without any knowledge of the circumstances of production of the data, as well as working on assumptions and with incomplete evidence. In any case, the original input by a certain (corporative) author should be preserved in the database, and layers further interpreted by the map creators must be labelled as such, so as not to confuse authorship of critical information.

Then, what about statistical methods and the DTM based on airborne laser scan data? For one thing, information is very unevenly distributed, and significant statistical results can be achieved only for areas densely populated by reported sites. In such cases, which are relatively few, the susceptibility of the enveloping area is nearly always obvious, and information is often sufficient to draw conclusions about critical geological factors, and statistics may seem superfluous. Furthermore, the various factors of influence will have to be weighted differently. In view of the complexity of the

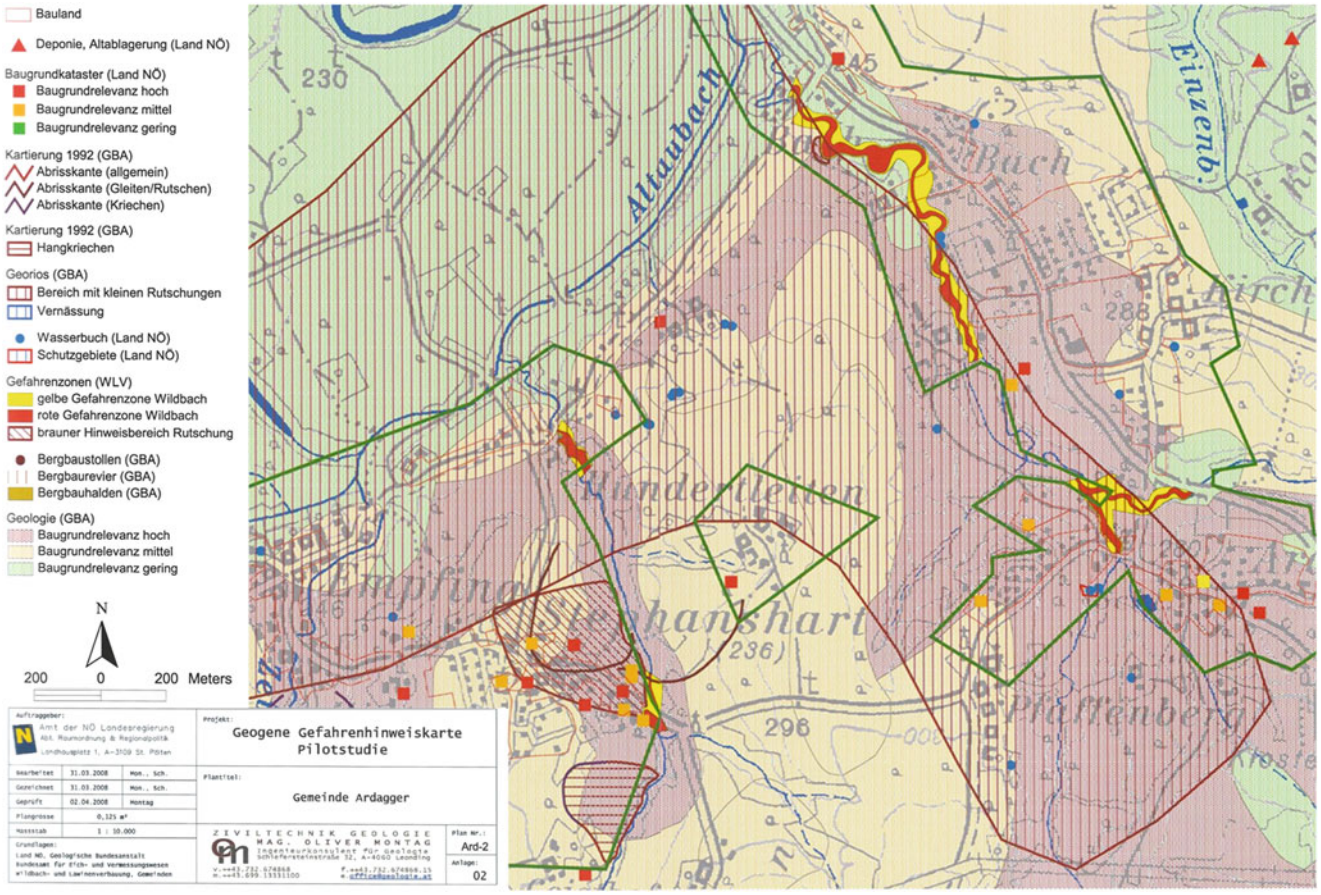

Fig. 4 Sample map of landslide susceptibility in *Stephanshart* municipality, Lower Austria. Original scale 1:10,000. This map seeks to classify the whole area according to "building ground relevance" (i.e. intensity of response to human interaction), based on geological units. Problems documented in the building ground register are indicated by *squares*, color-coded according to the same kind of classification: *purple area/red square* = high "building ground relevance", *beige area/brown square* = medium, *green area/yellow square* = low relevance. *Purple areas* coincide with the distribution of a certain sensitive formation *(Älterer Schlier)*. *Vertical hatches* = area of small slumps, *horizontal hatches* = area creeping slopes, *brown line* = scarp, according to the GEORIOS database of the Geological Survey of Austria. The extension of the large hatched area into the virtually flat flood plain of the Danube to the north is obviously incorrect information in the original database! But, for the problems of correction see text. *Dark red, dark yellow* and *cross-hatched areas* are the *"red", "yellow"* and *"brown zones"* taken from the flooding protection zonation of the Forest Engineering Service in Torrent and Avalanche Control (they were not required by contract). *Green line*: boundary of designated building land

matter and the relative scarcity of detailed information it is not possible in most areas to do this in a rational way. Therefore geostatistics may seem rational, but actually involves a fair share of subjective judgement.

The new DTM, for sure, is excellent data, especially when it comes to control and correct multiple but slightly differing indications for a single site. Also, additional indications may be derived, even by means of numerical extraction methods. However, in our experience, there is hardly any method capable of finally deciding what to make of it, except for a ground check (think of a soft indentation of a slope in the Molasse Zone: could as well be an overgrown former marl pit, of which there were many in the past; cf. again Fig. 3). By comparison, aerial photographs could not improve in any way on the information derived from the DTM.

As a result of all of this, it was decided not to correct any of the given information, not to use any statistical approach, but leave the spatial information extracted from pre-existing sources as it is, and rather overlay this data by three kinds of independent interpretation, namely: (1) a simple classification according to relevance for building or intensity of potential problems indicated by the data; (2) another classification, of the geological formations delineated in published geological maps, according to their natural tendency to slide, possibly because of human interference, as far as known from past experience; (3) addition of spatial information based on a DTM survey, where it helped to clarify the areal extent of indicated phenomena.

Concerning the abovementioned point (2), another big problem is seen in the fact that detailed published geological maps (scale 1:50,000), while excellent where they exist,

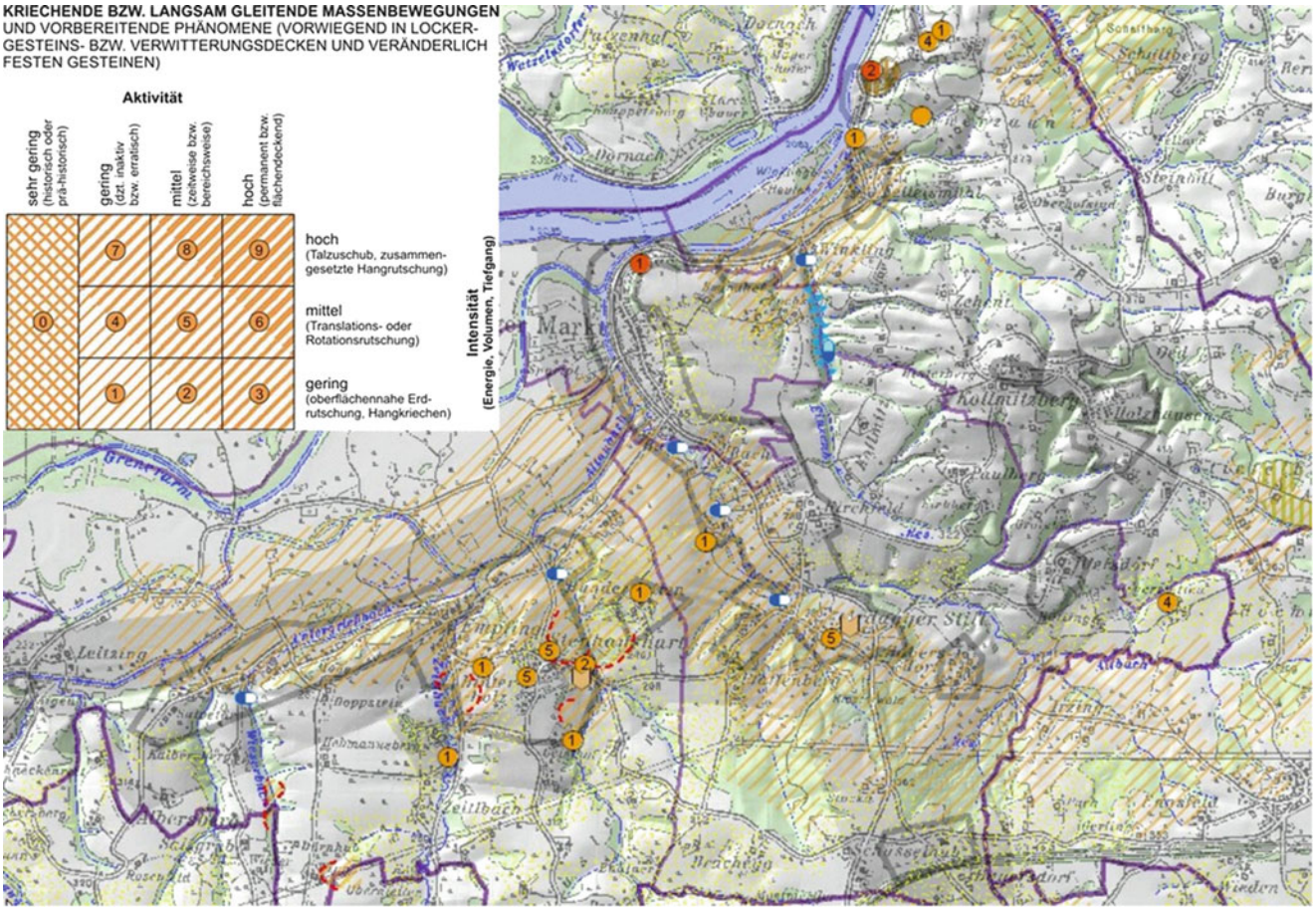

Fig. 5 Another sample susceptibility map, centred on the same municipality as in Fig. 3, created by another contractor in the pilot project. Original scale 1:25,000 (the one required for the printed version of the map). The point information in this case includes a threefold classification: (*1*) form of symbol refers to type of problem reported (*circle* = mass movement, *arrow* = subsidence, *blue/white horizontal* = slumping, and *dark/light blue vertical* = strong valley deepening, both due to fluvial erosion), (*2*) colour of circular sign refers to type of mass movement (*red* = fall, *brown* = slide), (*3*) number in circular sign refers to the classification diagram for mass movements (insert to the upper left). This classification combines qualitative information on activity (*left to right*, *far left* = historic or prehistoric) and intensity, i.e. size of the problem, according to volume or areal or vertical extension (increasing upwards). The brown hatching also refers to this classification. This is a layer consolidated from areal information in the GEORIOS database and a classification of landslide sensitivity similar to the one presented in Fig. 3. *Green vertical hatching*: mining area; *thick dark grey line*: boundary of designated building land; *dark purple line*: municipal boundary

are still missing for approximately half the country. Therefore, and because the evaluated municipalities had been chosen for availability of the DTM rather than the geological map, we had to rely for the most part on the Geological Map of Lower Austria with a scale of 1:200,000.

The results arrived at by the three investigators differed in detail, but otherwise suggested very similar conclusions. The way of presenting the results naturally differed also, and two examples by different investigators are shown in Figs. 4 and 5 (the maps produced by the third investigator looked similar to the first one). Both maps represent a part of the same municipality, centred on the same village, which is well known for extensive damage caused by a very slow but consistent slope movement in soft marly clay-siltstones with a high content of active clay minerals.

Use of the Susceptibility Map

Most of the time, there are two ways by which landslides come to the attention of an expert, in the public as well as in the private sector. First, a landslide occurs as a sudden natural event and endangers lives or buildings or infrastructure, and measures are called for immediately. Second, while planning for new buildings or infrastructure one finds active or potential landslides in the study area.

In the first case, at first there will be hardly any time to look for documents that are not organized already, at least according to geographical location, which is the main advantage of a GIS inventory. Of course, when planning field investigations and laboratory work ahead of a construction

project, which is the second case, the knowledge of past landslides in the study area, and easy access to detailed documents pertaining to the events, is even more useful. The inventory, in that case, functions as a perfect witness of an unstable landscape. That means, it can be used as an, albeit simplified, landslide susceptibility map. Both can be understood as a kind of warning system, supplying stakeholders in land development and building with hints to possible or likely problems in advance, without any legally binding consequences.

All this should be of interest to planners, engineers, geologists, and officials, who will be expected to consult the digital inventory as well as the landslide susceptibility map, both integrated with the building ground register, for potential geological hazards to their projects. This consulting will be free of charge, but the planners are expected to leave digital copies of reports based on the retrieved data to the geological survey, to put it in the database. In this way the database shall continuously grow by way of new entries of actual events as well as feedback of conclusions from its data.

Discussion and Conclusions

One evident advantage of a digital landslide database is that it is faster to consult and needs less space than a paper archive. It is much more expensive to maintain, but the additional costs outweigh by far the economic loss that may result from landslides that could otherwise have been prevented by effective information on the hazard.

The main challenges of working with the existing inventory have been (1) inconsistent reporting by various investigators, especially concerning reports before 1990; (2) incomplete reporting by involved parties: sometimes even remediation or stabilization work is done, but no one tells the geological survey; (3) missing parameters: most often the case with land use and its history, and on the geological side especially with structural information; and (4) incomplete information on the location and/or extent of a landslide.

These problems can be solved by the creation of susceptibility maps which consist of an interpretation of the events that is cast into a simple classification scheme. The susceptibility maps are provided with a well described classification scheme and allow an easier interpretation of the events by users with less experience.

The main advantage of the susceptibility map must be seen in the fact that it can be interpreted by the non-expert, which is hardly possible with the inventory. Thereby, planners and decision makers are presented with the possibility to make sure to circumvent indicated geohazards, or take preventive measures, in due time. This is most urgent in land and urban planning, where plots endangered by actual or potential mass movements have repeatedly been designated as building ground without consulting a geologist (or finally not designated after a belated consultation).

Given all the handicaps inherent in the existing data as described in this paper, a feasible approach toward a susceptibility map for Lower Austria had to be a simplified one. It is not really difficult and therefore cost effective to produce a simplified susceptibility map from the following data: the landslide inventories created by national and regional geological surveys, geological maps, high-resolution topographic (airborne laser scan) data, and simple classifications of (a) past events according to activity and size, and of (b) geological units, as defined in published maps, according to their natural tendency to landsliding and likely reaction to human activities.

The new high-resolution DTM (1×1 m digital terrain model) created from airborne laser scan data proved invaluable in complementing the field mapping, and a big help in resolving unclear situations while creating the susceptibility map. This should apply especially to the many cases where vegetation impedes the mapping of a landslide in the field as well as from aerial images.

There are two major weaknesses in the presented approach: (1) Conditions like slope angle/aspect or land use (history), etc. are not and often cannot be properly accounted for. (2) As a result, the method is highly dependent on expert knowledge of the study area. Therefore, and despite the misgivings of the authors about statistical methods, given the character of the available data, another study group has been contracted to work on the DTM by means of a complex statistical model integrating several parameters missing from the present study.

References

Kociu A, Kautz H, Tilch N, Grösel K, Heger H, Reischer J (2007) Massenbewegungen in Österreich. Jahrbuch der Geologischen Bundesanstalt, Wien 147(1, 2):215–220

Schweigl J, Hervas J (2009) Landslide mapping in Austria. JRC scientific and technical report, Office for Official Publications of the European Communities, Luxembourg (ISBN 978-92-79-11776-3), 61p

Schwenk H (1992) Massenbewegungen in Niederösterreich 1953–1990. Jahrbuch der Geologischen Bundesanstalt, Geologische Bundesanstalt. Wien 135(2):597–660

Landslide Inventory at 1:10,000 Scale in Poland: Benefits and Dilemmas of a National Project

Teresa Mrozek, Antoni Wójcik, Ziemowit Zimnal, and Dariusz Grabowski

Abstract

Damages related to landslides triggered by extreme rainfall in southern Poland in 1997 pointed to a vital need for an improved system of data acquisition, natural hazard awareness building and developing mitigation measures. After several years of struggle and compelled changes in legislative acts, a national landslide inventory project was launched in 2008. This project, known as the Landslide Counteracting System (SOPO in Polish) is meant to provide support in the field of environmental protection and public safety as well as mass movement mitigation. The end-users of the project are administrative bodies, environmental protection inspectorates as well as non-governmental organizations acting in the area of constructing works, transportation, estate and property trade and education-research activities. The first stages of the project implementation involved pilot surveying and database testing and were followed by a systematic landslide inventory, starting from the most threatened municipalities in the Polish flysch Carpathians. Over 12,000 landslide bodies have been already recorded in the Polish Carpathians. The updated landslide prone areas in examined municipalities are unquestionable advantages of the project but this outcome was not appreciated by local communities, property owners or policy makers.

Keywords

Landslide inventory • SOPO project • SOPO database

Introduction

Although the exposure of the Polish territory to natural hazards is moderate, yet landslides belong to the most important dangers which for a long time were underrated. It was probably attributed to a fact that the number of landslide-related fatalities is rather low. Nevertheless, landsliding is a widespread phenomenon resulting in considerable damages to buildings, infrastructure and environmental and cultural assets, so real losses are often as high as or higher than those generated by floods.

Certain regions of Poland are prone to mass movements (Fig. 1), however, landsliding in Poland is predominantly concentrated in the southern part of the country in the region of the Polish Flysch Carpathians.

More than 90 % of all landslides in the country occur within this area, which amounts to approximately 22,000 km^2 and represents only 6 % of the Polish territory (Mrozek et al. 2000; Poprawa and Rączkowski 2003; Wójcik et al. 2006). This region is known to be highly susceptible to mass movements due to lithological heterogeneity and tectonic anisotropy of the flysch rocks (Nemčok 1982; Margielewski 2006).

The last years of the twentieth century and the beginning of the twenty-first century manifested themselves as a period of an extraordinary intensification of catastrophic events. Due

T. Mrozek (✉) • A. Wójcik • Z. Zimnal
Carpathian Branch, Polish Geological Institute – National Research Institute, Skrzatow 1, 31-560, Cracow, Poland
e-mail: teresa.mrozek@pgi.gov.pl

D. Grabowski
Polish Geological Institute – National Research Institute, Rakowiecka 4, 00-975, Warszawa, Poland

C. Margottini et al. (eds.), *Landslide Science and Practice*, Vol. 1,
DOI 10.1007/978-3-642-31325-7_6,

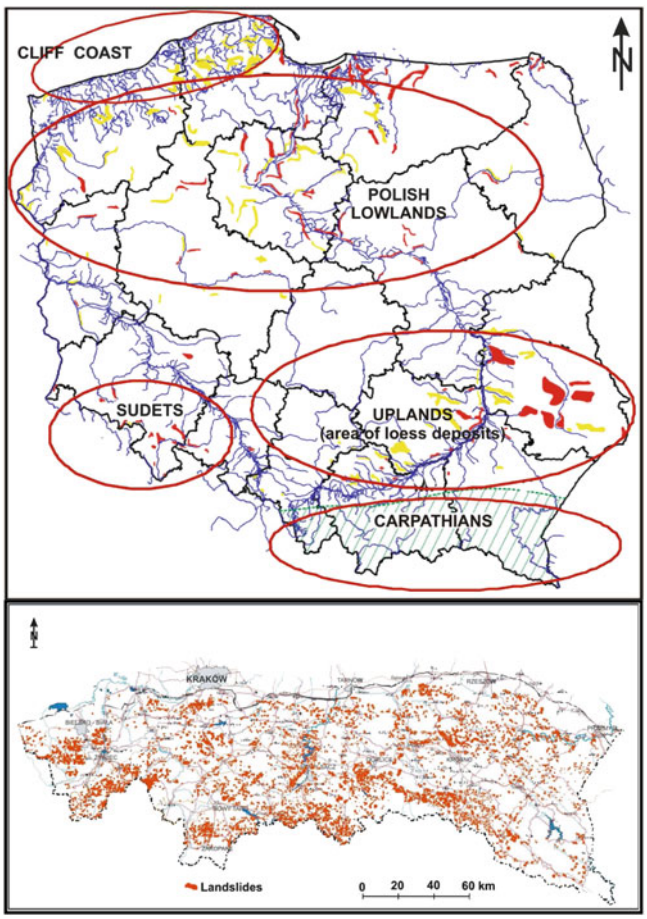

Fig. 1 Landslide-prone regions in Poland and landslides in the Polish Flysch Carpathians (As compiled from published documents and maps by Rączkowski, 2007)

to combined effects of causative triggers (in form of extreme rainfalls) and spontaneous urbanization, many households, transportation routes and lifelines were damaged. Especially, the damages related to landslides, set off by heavy rainfalls in southern Poland in 1997, pointed to a crucial need for an improved system of data acquisition, natural hazard awareness building and developing mitigation measures. After several years of struggle and compelled changes in legislative acts, a national landslide inventory project was launched. This project, known as the Landslide Counteracting System (with SOPO acronym derived from the Polish title) is meant to identify and map landslides over the entire territory of Poland on the basis of standardized criteria, as well as to provide support in the field of mass movement mitigation, public safety and environmental protection.

The intent of this contribution is to show benefits of the inventory project achieved to date and to indicate implications for the end-users, bearing in mind that the inventory is a crucial step in assessment of landslide susceptibility and risk on a national level and in developing sustainable strategies for mitigation tasks.

The Polish Landslide Inventory

Historical Background and Project Genesis

The first scientific description of landslide events in Poland and their devastating effects on properties was published at the beginning of the twentieth century (Zuber and Blauth 1907). Although the paper pointed out a complexity of mass movement problems and even signalled cost-benefit aspects, still for a long time landslides were treated marginally as local matters, so they were subject of interest merely to geologists or geotechnicians. Within a framework of geological surveying, being performed since the 1950s, landslides were progressively mapped on sheets of the Detail Geologic Map of Poland at scale of 1:50,000. The outcomes were just locations of larger landslide bodies and their head scarps. A special endeavour was a quite "systematic" registration of landslides over entire Poland performed in 1968–1970. Although the registration was incomplete and focused mainly on landslides threatening transportation tracks, the information about landslides, their typology and damages, was consistently filled in data sheets. The outcomes were put together in so called "*Landslide Catalogues*" for particular provinces and accompanied by corresponding maps at 1:100,000 scale compiled in 1970–1975. The collective issue was a "*Landslide register in Poland*" of 1971 with the enclosed maps: at scale 1:200,000 for the Carpathian region and at scale of 1:500,000 for the rest of the Polish territory. Practically it was the only inventory conducted in the entire country. Later undertakings were in principle case studies performed to satisfy individual research interests or needs of particular investments tasks (mainly dam and road building). An exception is a study by Bober (1984) who examined links between landslide distribution and geologic settings, and signalled a scale of the problem at least in the southern Poland. Afterwards, interests in landslide recognition declined again. It coincided with a period of lower precipitation in the mid-1980s, so the rainfall, usually the primary triggering factor here, was of minor importance. In addition, the investment pressure on unstable land was fairly low because of economic breakdown, so the human impact was also a limited trigger. What is more, many of the Polish landslides are slow-moving and the associated indicators of instability are not easily perceived, thus a potential danger either was not noticed or neglected. Due to all the above, landslides were not treated as dangerous as floods.

A turning point was the year of 1997. Then, the combined effect of long-lasting rainfalls followed by heavy downpours resulted in activating numerous landslides in the Carpathian region. By that time, the built-up areas with related infrastructure had spread and invaded onto the slopes which were ignored as prone to sliding, thus the damages were extraordinarily high.

Destruction related to the landslides triggered in 1997 prompted to a vital need for a natural hazard awareness building and developing mitigation measures. Yet it was not earlier than 2002 when significant changes were introduced to Polish legislative acts dealing with nature protection and environmental management. The inspiration for these changes was the catastrophic events of 1997 (floods and mass movements) and subsequent ones that occurred also in 2000, 2001. At that period landslides acquired a legal status of a natural cataclysm. The modified legislation system imposed new tasks on authorities both on a state and regional level. With these new legislative rules, *starostowie* (i.e. mayors of second-level administrative units) are in charge of keeping registers of terrains prone to mass movements. The scope and methods of recording and observing mass movements in the affected terrains were specified in the *Regulation of 20 June 2007 of Minister of Environment on information about mass movements*. This gave a background for starting a project dedicated to landslide damage recovery and to improve landslide management. Initially, the project was subdivided into two components:

- Component A focused on ensuring funds for reconstructing or relocating failed infrastructures which were under supervision of regional authorities;
- Component B was meant to provide landslide inventory maps and to start monitoring in selected sites with a purpose of improved hazard warning and management.

With time the project split into separate parts. Component A, run with a financial support from European Investment Bank loan, concentrated only on recovery tasks associated with implementation of effective structural measures. Component B gave rise to independent project known now as Landslide Counteracting System – SOPO. It is commissioned by the Polish Ministry of Environment and financially supported by the National Fund for Environmental Protection and Water Management.

The Polish Geological Institute – *Geological Survey of Poland* has the task of organizing and coordinating activities under this project in order to collect and to integrate landslide data as well as to set-off administrative bodies for making their registers running.

SOPO Objectives and Strategies

The SOPO project objectives concentrate on:

- Identifying and mapping landslides over the territory of Poland based on standardized criteria in order to workout landslide inventory maps in scale 1:10,000 for particular administrative units of Poland;
- Indicating landslides for instrumental monitoring;
- Building up a national landslide database using Geographic Information System capacities;
- Providing support for hazard and risk assessment and sustainable land use management.

The end-users of the project are administrative bodies of municipalities, regions and provinces, environmental protection inspectorates as well as non-governmental organizations acting in areas of constructing works, transportation, estate and property trade, insurance providing and education-research activities. The Ministry of Environment as a commissioning body is the interested party as are other governmental institutions which by their status deal with territorial management.

SOPO Project Logistics and Setup

Data Collection and Representation

The SOPO project combines both geomorphologic (historical) inventories, being the sum of a number of landslide events over time in a given region, with landslide events that are associated with a particular trigger (Malamud et al. 2004). Large-scale inventory (1:10,000) is carried out using both interpretation of aerial photographs and extensive field investigations that use an array of techniques and tools pertaining to geologic and geomorphologic mapping supported by engineering geology and/or geotechnical engineering. Thus, the project logistics involves a stage-by-stage field surveying and mapping of landslides and landslide-prone terrains, according to a standardized methodology described in project guidebooks. Rather than working in natural boundaries of drainage basins, the inventory is carried out with partitioning into administrative units because the key end-user are municipalities which are obliged to utilize the inventory outcomes in their territorial management planning.

To achieve the most reliable results the project is divided in three stages:

- Stage 1 – pilot mapping of landslides and identification of landslide prone areas in selected municipalities with the purpose of testing the adopted methodology and possibility of making adjustments to the guidelines (already completed);
- Stage 2 – mapping of landslides and prone terrains in the Polish Carpathians (75 % of the area) as well as instrumental monitoring of selected sites in the Carpathians (in progress);
- Stage 3 – continued mapping of landslides in the Carpathians and mapping in the out-of-Carpathian parts of Poland as well as instrumental monitoring of selected sites in any part of the country (to be started in 2015).

The SOPO project database handles attribute, descriptive data referring to each landslide and graphic documents (photos, sketches etc.), and cartographic representations.

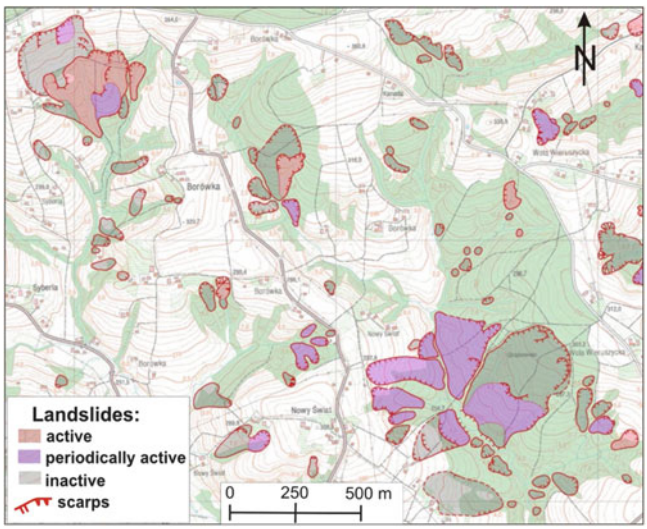

Fig. 2 Example of landslides mapped in scale 1:10,000 in the municipality of Łapanów, the Carpathians

The classification of the landslides is in principle based on schemes by Varnes (1978), Cruden and Varnes (1996) and recommendations by the International Geotechnical Societies' UNESCO Working Party on World Landslide Inventory (1990, 1993). These global landslide classifications are also coupled with terminology traditionally used in Poland (Margielewski 2004, 2009) in order to facilitate referencing with older landslides mapping or historical documents.

The information related to each landslide is collected using a landslide data form – KDO. The data comprise 21 items and refer to such fundamental aspects as: (1) landslide unique id number, basic data on landslide location with reference to a drainage basin, type of movement and state of activity, and a descriptive précis; (2) morphometric parameters of a landslide, geologic units, lithology, bedding attitude, hydrogeologic aspects, age, date of occurrence and causes, land use; (3) information on damages, expected hazard, mitigation measures, related documents and investigations, monitoring status; (4) illustrative materials comprising sketch or map of the landslide, geologic profile, photos and extra comments on potential stabilising measures and (5) identification data of the person who inventories the landslide.

Landslides are presented on topographic maps in scale 1:10,000 (Fig. 2) and are represented by a polygon if the landslide area is larger than 500 m^2 and by a dot if the landslides are smaller or equal to that. For each landslide a centroid is a georeferenced point.

The inventory is carried out by various geologic bodies, including commercial geo-engineering companies, yet within the framework of standardized methodology. For purpose the Polish Geological Institute developed the guidebooks which outline the principles of inventory, mapping schemes and convention of completing the landslide data forms (Grabowski et al. 2008). In order to avoid misunderstandings in terminology used and to minimize biased assessment the keys, codes and glossaries supplement the guidebooks.

Web Services for Data Management and Information Dissemination

The SOPO inventory is available via Web services (http://www.osuwiska.pgi.gov.pl) and progressively updated as mapping progresses. The services manage large amounts of spatial data (including vector and raster data sets), served by ArcSDE and ArcIMS Server (ESRI) and Oracle DB. The service architecture for the SOPO clients was designed by GIS Partner Co. of Wrocław, Poland. Each user can view, display and search attributive and spatial data, and this way has access to landslide data sheets and maps, which can be printed in the basic scale or smaller. With this facility inventory data are available to all individuals interested in landslide affected terrains. On the other hand, only the advanced users may edit and verify input data. Here is also room for updating data, in compliance with obligation imposed by legislation acts.

Inventory Results, Benefits and Dilemmas

The SOPO project was started with the aim of mapping landslides in 253 municipalities in the Carpathians (ca. 22,500 km^2) and in 271 *powiats* (second-level administrative units) in the remaining parts of the country. The project assumed also monitoring of ca. a hundred landslides threatening crucial assets (e.g. important transportation routes). The initial stages of the project implementation involved pilot surveying and database testing, and were followed by the systematic landslide inventory starting from the most threatened municipalities in the Polish Flysch Carpathians. The landslide inventory progresses successively (Fig. 3).

By the end of 2010, the tasks of mapping landslides were completed in 71 municipalities of southern Poland (41 in the province of Little Poland, 29 in the Silesian province and 1 in the Subcarpathian province) and 45 landslides are inclinometer monitored. The data base handles now about 12,150 landslides being equivalent of 4,750 km^2 (21 % of the Carpathian area). This number is much larger than that summarized by Rączkowski (2007) for the same area based on the inventory of 1970s. It also allows to expect that the landslide total in the Carpathians might significantly exceed 25,000, the number compiled only from published sources and documentaries (Poprawa and Rączkowski 2003). Being aware of the differences in methodologies applied in particular surveys, the results obtained in the current inventory emphasise how large is the scale of landslide hazard.

Another benefit of the SOPO project is the integrating and harmonizing aerial photos, historical documentaries and field surveying. The applied approach to data collection allows for improving quality of the landslide information

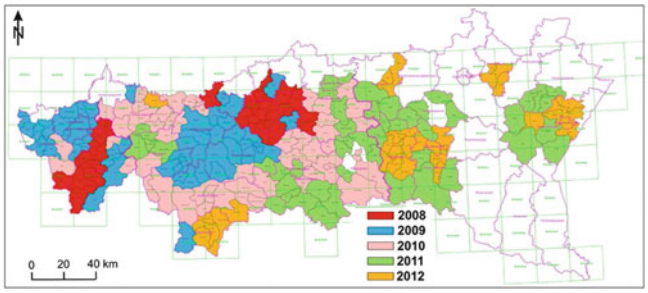

Fig. 3 Municipalities of the Polish Flysch Carpathians where landslides have been inventoried in given years

input to the inventory database. The use merely of aerial photos, especially in the Carpathian region, is inefficient in many cases. Hills and ridges in this region are often covered by thick vegetation (shrubs, forests etc.) or remodelled by farming activities, so identification of landslides is very difficult or even often impossible. Therefore field validation and geomorphologic analysis are very crucial to project.

Unfortunately, the extreme weather conditions in May and June 2010 (exceeding 200 mm of rain in 24 h) gave rise to reactivation and mobilization of both existing and new landslides and had many-fold consequences. First, the regular mapping tasks scheduled for particular municipalities had to be modified, as new sites were to be surveyed on emergency basis. In the frame of such additional challenges over 400 sites were visited and landslide documentary forms were completed for them. The ad-hoc inventoried cases contribute to landslide-frequency datasets. The mass movements generated huge losses in terms of hundreds of houses destroyed and numerous damaged roads. In the most affected areas, modern remote sensing techniques (e.g. airborne and terrestrial laser scanning) were used to register and trace the dynamics of landslide processes.

The adverse effects of the extreme events woke again a general demand for a better recognition of potentially threatened areas. In this respect the inventory is perceived as a very useful. Yet it is also the source of many dilemmas. The municipality authorities are willing to have landslides inventoried as soon as possible, yet they are not particularly pleased with the extent of the landslide affected areas. Because of that changes in regional policy and land use planning are compelled. Local communities and property owners do not really appreciate the inventory outcomes as well. Investment restrictions related to landslide prone terrains cause many lots to lose their value, so the owners often express their doubts as to the extent of landslides limits and buffering zones depicted on the maps. On the other hands, those who suffered from mass movements expect a support from governmental institutions and claim them guilty for not warning about mass movement hazard.

Another controversial issue is related to insurance policy in landslide prone regions. The catastrophic losses cumulated in one season showed that the system of compensation payments has to be improved.

Conclusions

Due to the adopted scheme of data acquisition the ongoing Polish inventory is similar to other inventory challenges undertaken in European countries (e.g. Trigila et al. 2010). It also provides a good background for landslide susceptibility assessment and is a starting point for working out an improved landslide warning system in Poland.

References

Bober L (1984) Rejony osuwiskowe w polskich Karpatach fliszowych i ich związek z budową geologiczną regionu. Biul Inst Geol 340:115–162

Cruden DM, Varnes DJ (1996) Landslides types and processes. In: Turner AK, Schuster RL (eds) Landslides investigation and mitigation (Special Report 247). Transportation Research Board, National Academy Press, Washington, DC, pp 36–75

Grabowski D, Marciniec P, Mrozek T, Nescieruk P, Rączkowski W, Wójcik A, Zimnal Z (2008) Instrukcja opracowania Mapy osuwisk i terenów zagrożonych ruchami masowymi w skali 1:10 000. Państwowy Instytut Geologiczny, Warszawa

Malamud BD, Turcotte DL, Guzzetti F, Reichenbach P (2004) Landslide inventories and their statistical properties. Earth Surf Proc Landf 29:687–711

Margielewski W (2004) Typy przemieszczń grawitacyjnych mas skalnych w obrębie form osuwiskowych w polskich Karpatach fliszowych. Przegląd Geologiczny 52:603–614

Margielewski W (2006) Structural control and types of movements of rock mass in anisotropic rocks: case studies in the Polish Flysch Carpathians. Geomorphology 77:47–68

Margielewski W (2009) Problematyka osuwisk strukturalnych w Karpatach fliszowych w świetle zunifikownaych kryteriów klasyfikacji ruchów masowych – przegląd krytyczny. Przegląd Geologiczny 57:905–917

Mrozek T, Rączkowski W, Limanówka D (2000) Recent landslides and triggering climatic factors in Laskowa and Pleśna regions, Polish Carpathians. Stud Geomorph Carpatho-Balcan 34:89–112

Nemčok A (1982) Zosuvy v Slovenskych Karpatach, Veda. Bratislava 1–319

Poprawa D, Rączkowski W (2003) Osuwiska Karpat. Przegląd Geologiczny 51:685–692

Rączkowski W (2007) Landslide hazard in the Polish Flysch Carpathians. Stud Geomorph Carpatho-Balcan 41:61–75

Trigila A, Iadanza C, Spizzichino D (2010) Quality assessment of the Italian Landslide Inventory using GIS processing. Landslides 7:455–470

Varnes DJ (1978) Slope movements types and processes. In: Schuster RL, Krizek RJ (eds) Landslides: analysis and control (Special Report 176). Transportation Research Board, National Academy of Sciences, Washington, pp 11–33

Wójcik A, Mrozek T, Granoszewski W (2006) Lithological conditioning of landslides and climatic changes with examples from the Beskidy Mts., Western Carpathians, Poland. Geografia Fisica e Dinamica Quaternaria 29:197–209

WP/WLI (International Gotechnical Societies' UNESCO Working Party on World Landslide Inventory) (1990) A suggested method for reporting a landslide. Bull Int Assoc Eng Geol 41:5–12.

WP/WLI (International Geotechnical Societies' UNESCO Working Party on World Landslide Inventory) (1993) A suggested method for describing the activity of a landslide. Bull Int Assoc Eng Geol 47:53–57.

Zuber R, Blauth J (1907) Katastrofa w Duszatynie. Czasopismo Techniczne 25:218–221

Landslides Along the North-West Coast of the Island of Malta

Stefano Devoto, Sara Biolchi, Viola Maria Bruschi, Alberto González Díez, Matteo Mantovani, Alessandro Pasuto, Daniela Piacentini, John A. Schembri, and Mauro Soldati

Abstract

The paper shows the results of geomorphological and engineering-geological investigations carried out along the north-western coast of the Island of Malta, with special emphasis on landslides. Field surveys and aerial-photo interpretation allowed the recognition, identification and mapping of a series of landslides of different type and size, some of which showing evidence of activity. Coastal instability in the studied area is deeply controlled by structural factors, such as tectonic and stratigraphic ones. The research envisaged a multidisciplinary approach, which also included landslide monitoring in specific sites which were selected for detailed investigations, owing to the peculiarity of the instability processes occurring and for the related hazard and risk conditions. The paper outlines the research phases and the results achieved which proved to be fruitful thanks to the application of different methodologies for the study of coastal landslides. Particular attention has been paid to rock spreading phenomena, which are widespread along the north-western coast of Malta due to the superimposition of limestones over clayey terrains.

Keywords

Coastal geomorphology • Landslides • Rock spreading • Malta

Introduction

This paper presents the outputs of field surveys and aerial-photo interpretation carried out along the north-western coast of the Island of Malta, which is located in the central Mediterranean Sea between Africa and Sicily. The investigations were focused on landslides along a coastal stretch of 15 km^2 comprised between Marfa Ridge to the north and Il-Pelegrin promontory to the south (Fig. 1).

Previous literature describes in detail the geological features and evolution of the Island of Malta (cf. Pedley et al. 1978; Illies 1981; Pedley et al. 2002), whereas geomorphological features have only rarely been investigated (Alexander 1988). However, a series of papers has recently highlighted the most interesting geomorphological features of the north-western coast of the Island of Malta, with particular reference to mass movements (Dykes 2002; Farrugia 2008; Magri et al. 2007, 2008; Magri 2009; Soldati et al. 2010; Coratza et al. 2011).

S. Devoto (✉) • S. Biolchi • D. Piacentini • M. Soldati
Dipartimento di Scienze della Terra, Università di Modena e Reggio Emilia, Largo S. Eufemia 19, 41121 Modena, Italy
e-mail: stefano.devoto@unimore.it

V.M. Bruschi • A.G. Díez
Departamento de Ciencias de la Tierra y Física de la Materia Condensada, Universidad de Cantabria, Avenida Los Castros s/n, 39005 Santander, Spain

M. Mantovani • A. Pasuto
Consiglio Nazionale delle Ricerche, Istituto di Ricerca per la Protezione Idrogeologica (IRPI), Corso Stati Uniti 4, 35127 Padova, Italy

J.A. Schembri
Geography Division, University of Malta, Mediterranean Institute, MSD2080 Msida, Malta

C. Margottini et al. (eds.), *Landslide Science and Practice*, Vol. 1,
DOI 10.1007/978-3-642-31325-7_7,

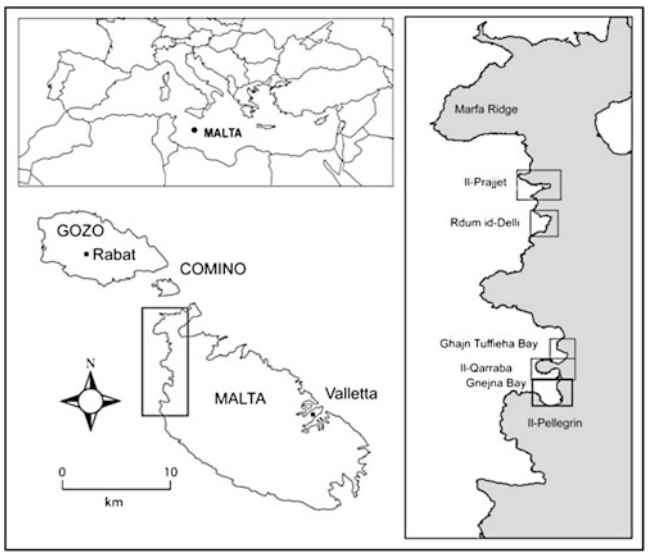

Fig. 1 Location of the study area

The research has included the recognition, identification, mapping and monitoring of different types of landslides occurring in the study area. Among these, worthy of note are extensive lateral spreading phenomena which are favoured by the different mechanical properties of the two main rock types outcropping in the area, such as those belonging to the Upper Coralline Limestone and the Blue Clay formations (cf. Oil Exploration Directorate 1993).

The research has been carried out in the frame of a project entitled "*Coastline at risk: methods for multi-hazard assessment*", funded by the EUR-OPA Major Hazards Agreement of the Council of Europe during the period 2009–2011. The project is managed by the European Centre on Geomorphological Hazards (CERG) and deals with the study of slope instability in critical coastal areas of Malta, France (Normandy) and Central Portugal. The study has been co-funded by the project "*Multidisciplinary research in the open-air laboratory of the island of Malta: an international network for landslide hazard assessment in coastal areas*", co-ordinated by the University of Modena and Reggio Emilia and supported by the Fondazione Cassa di Risparmio di Modena. The aims of the above mentioned projects have been pursued through multidisciplinary investigations integrating geomorphological and engineering-geological approaches. Avant-garde research techniques, both traditional and innovative, have been applied with special reference to mapping and monitoring of coastal instability phenomena. The results achieved make up a significant step toward the final objective of the CERG project which is to propose a method for coastal multi-hazard assessment that can be used to face and manage coastline hazards in Europe.

The Study Area

The study area is located in the Island of Malta, in particular on its north-west coast.

The Maltese archipelago lies approximately 96 km south of Sicily and 290 km north of Africa. From north to south, Malta consists of three main islands: Gozo, Comino and Malta, the latter being the largest, with an area of 246 km^2 (Fig. 1).

From a geodynamical point of view, the Maltese Islands lie in the Sicily Channel, which has been affected during Neogene-Quaternary (Finetti 1984) by continental rifting which produced extensive structures, such as the Pantelleria, Malta and Linosa tectonic depressions controlled by the NW-SE-trending Pantelleria Rift (Argnani 1990; Civile et al. 2010). The Maltese tectonic setting is characterised by two intersecting fault trends: the NW-SE-trending Pantelleria Rift and the ENE-WSW graben system, dominated by the Victoria Lines fault, which makes up the main tectonic discontinuity of Malta. From a structural viewpoint, the Island of Malta is actually divided into two regions by the Victoria Lines fault. A series of pronounced horst and graben features, oriented ENE-WSW, occurs north of the fault and deeply influences the morphology of the northern stretch of the island, which is thus characterised by prominent ridges and well-shaped-valleys.

The Maltese archipelago is characterised by a warm climate with prolonged summers and mild winters. As in typical Mediterranean climate conditions, precipitation is concentrated in the cold season. The mean annual value of precipitation in the Island of Malta is of 550 mm (period 1922–2007). The relatively flat topography does not influence the distribution of rainfall on the island.

Geological and Geomorphological Settings

The Maltese archipelago is composed of Tertiary limestones, clays and marls capped by thin superficial deposits, such as red soils or alluvial/colluvial sediments.

The bedrock consists of sedimentary rocks, deposited in a period of time comprised between Miocene and Upper Oligocene, that is from about 30 million to about 5 million years ago (Pedley et al. 1978, 2002).

The *Lower Coralline Limestone Formation* (Upper Oligocene) is the oldest unit of the stratigraphic sequence. It is characterised by hard, pale grey limestones made by

reef-building organisms and reef-related sediments. It outcrops mainly in Gozo and southern Malta where it is responsible for forming spectacular cliffs, some reaching 140 m in height.

The *Globigerina Limestone Formation* (Lower-Middle Miocene) lies above the Lower Coralline Limestone Formation and widely outcrops at the sea level in the study area. The Formation is made up of fine-grained and lightly-cemented limestones, which vary in thickness from 20 to over 200 m. The fair qualities of the Globigerina limestone and the exposition to wave action are the causes of extensive rock falling.

The stratigraphic sequence continues with the *Blue Clay Formation* (Middle Miocene) which can reach a thickness of 65 m and is composed by silty sand, marls or clays. The poor geotechnical quality of sediments has favoured the shaping of gentle slopes which are sometimes used by locals for agricultural purposes, such as at the Marfa Ridge or along the slopes of Gnejna Bay.

The stratigraphic sequence ends up with the *Upper Coralline Limestone Formation* (Upper Miocene) which is mainly composed by shallow marine sediments, the youngest outcropping in the Maltese archipelago. The Formation is affected by a dense network of tectonic discontinuities which provide the rock masses with a brittle behaviour. The limestones often show karst features such as sinkholes and caves. Karst is also the cause of barren grey pavements inland. The presence of the Upper Coralline Limestone Formation gives rise to vertical cliffs of varying heights along the coastline, which range from a few metres to over 30 m.

The different mechanical behaviour of the Blue Clay and the Upper Coralline Limestone formations favours the development of a series of landslides of different type and size which widely affect the north-western coastline of Malta (Fig. 2). Landslides are locally favoured by coastal erosion, which induces hazardous situations that urge to be investigated in order to prevent risk for population, buildings and infrastructures. However, it should be emphasised that locally rock blocks deposited at the sea level protect the shoreline from marine erosion.

Rock spreading phenomena are clearly favoured by the above mentioned stratigraphic setting. Evidence of rock spreading is widespread all along the edges of the Upper Coralline Limestone plateaus. Outstanding examples have been recognised at Il-Qarraba (Ghajn Tuffieha Bay) (Fig. 3), Il-Prajjet (Anchor Bay) and along the western sector of Marfa Ridge. The lateral extension of rock masses tend to evolve into *block sliding* whose onset is extensively witnessed by scattered blocks of variable size lying on the clayey slopes which gently degrade toward the sea.

Rock falls and *topples* are abundant along the coastline and mainly affect the Upper Coralline Limestones Formation which is characterised by persistent fissures and cracks of tectonic origin, locally widened by lateral spreading

Fig. 2 The superimposition of the Upper Coralline Limestone Formation on the Blue Clay Formation is a predisposing cause of landslide occurrence along the north-west coast of Malta (Courtesy of Ten. Col. M. Marchetti)

(Fig. 4). The Lower Coralline Limestone and the Globigerina Limestone formations are also affected by these types of movement.

Earth flows and *earth slides* occur along clayey slopes and are triggered by rainfall during the autumn and winter months, when the clay material becomes wet, also due to the infiltration of water coming from the overlying limestones (Mangion 1991). After dry summer periods, deep desiccation cracks develop in the Blue Clay terrains which are able to convey a significant amount of water inside the slopes during the following wet season, increasing pore pressure and favouring the occurrence of mass movements (Dykes 2002; Magri et al. 2008). The latter occur especially where the vegetation cover is scarce or missing, such as at Rdum-id-Delli and Ghajn Tuffieha Bay.

Methods and Results

The investigations on landslides along the north-western coast of the Island of Malta have been developed through a multidisciplinary approach which envisaged the following research phases:

Fig. 3 Il-Qarraba promontory at Ghajn Tuffieha Bay. The superimposition of limestones on clayey terrains favours the onset of rock spreading phenomena and of associated landslides which occur at the edges of the plateaux

Fig. 4 Evidence of rock falls occurring along the north-western coast of Malta (Courtesy of Ten. Col. M. Marchetti)

- Retrospective analysis of landslide occurrence;
- Analysis of climatic data;
- Interpretation of multi-temporal aerial photographs;
- Geomorphological survey and mapping;
- Landslide monitoring.

The study area can actually be considered as a natural laboratory for the study of landslide phenomena and their geomorphological hazard and risk implications and for the peculiar geological and geomorphological conditions.

As a consequence, the application of integrated research methods and techniques, with special reference to mapping and monitoring of coastal instability, proved to be particularly fruitful in terms of testing methodologies and achievement of significant results.

Retrospective Study on Landslide Occurrence

The first phase of the research has consisted of a retrospective study on landslide events that took place within the research area during historic times. Bibliographic and archival research has been carried out at public and private institutions and on newspapers. The aim was to obtain a comprehensive picture on slope instability and define the spatio-temporal distribution of past landslide events, whilst at the same time identifying useful elements for typological definitions. However, the information available has given quite a scattered picture of the temporal occurrence of landslides in the study area (Magri 2009). Information was available only for those cases in which significant damage was caused.

Analysis of Climatic Data

Climatic data have been obtained from the Luqa meteorological station (located at the centre of the Island of Malta), monitored since 1920, to determine the relationship between the identified landslide events and particular meteorological conditions. Data regarding the total annual amounts of rainfall for the period 1929–2007, the average monthly precipitation for the period 1922–2007 and the maximum monthly precipitation for the period 1922–2007 have been collected and analysed.

In particular, the annual average precipitation during the above mentioned period is of 550 mm. However, it should be noticed that annual average precipitation has varied significantly throughout that period, ranging from about 400 to 1,000 mm per year. During the last decade, notable variations have also been recorded, being the year 2003 the rainiest with an average of 837 mm and 2004 the driest with 455 mm. These rainfall variations have to be properly taken into account to define the role of precipitation on landslide occurrence.

Interpretation of Multi-temporal Aerial Photographs

A multi-temporal analysis of aerial photographs has been completed with special attention given to landslide phenomena. To achieve this aim both traditional stereoscopic techniques and digital photogrammetry techniques have

been used. The study of landforms represented in a sequence of images corresponding to different years enabled to reconstruct the evolution of the coastal stretch under study. Aerial photographs available for the north-western coast of the Island of Malta have been selected and analysed. Particular attention has been given to the first and last series of aerial photographs available (1957 and 2008).

Geomorphological Survey and Mapping

A geomorphological survey has been carried out at a scale of 1:5,000 for the entire north-western coastal stretch of the Island of Malta. This phase of the research has also included a check and update of the existing geological map (Oil Exploration Directorate 1993) as well as investigations aiming at the recognition of ductile and fragile deformation features, which are of topical importance for the assessment of slope stability. This phase has finally led to the production of a detailed geomorphological map that covers the coast between Marfa Ridge to the north and Victoria Lines fault to the south. Mapping has been conducted following the guidelines of the Italian Geological Survey (Gruppo di Lavoro per la Cartografia Geomorfologica 1994), which foresee the representation of landforms according to their genesis with indication of their state of activity by means of colours, symbols and retina.

Particular attention has been paid to the mapping of landslides which make up a predominant feature along the investigated coastline. Landslides have been distinguished according to the following types of movement and their areal distribution was calculated: (1) rock falls, including topples (18%); (2) earth flows and earth slides (3%); (3) rock spreads (14 %) and (4) block slides (65 %) (Fig. 5).

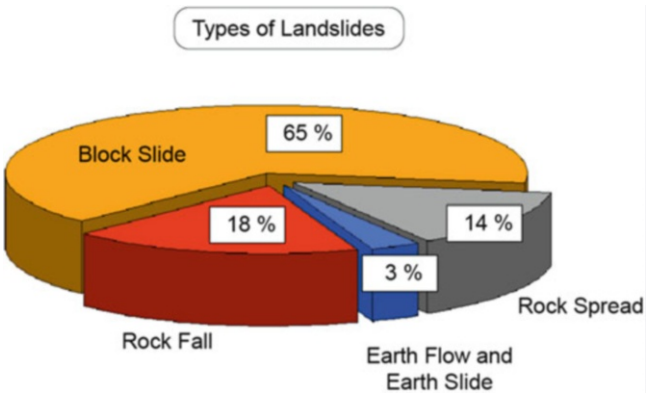

Fig. 5 Areal distribution of landslide types along the north-west coast of Malta with respect to the total area affected by landslides

Fig. 6 Evidence of large block sliding occurring at Il-Prajjet (Anchor Bay) as a consequence of rock spreading phenomena affecting the Upper Coralline Limestone Formation

Landslide Monitoring

In-depth investigations have been focused on two sites where exemplary cases of rock spreading and associated movements, which induce hazard and risk situations, were identified. This is the case of Il-Qarraba at Ghajn Tuffieha Bay (Fig. 3) and Il-Prajjet at Anchor Bay (Fig. 6). These sites have been monitored to determine whether rock spreading phenomena, and associated block slides, were active and, in case, which was the rate of movement. This was considered as crucial for hazard assessment at the two sites.

Actually, landslide monitoring had already started in 2005 at these two sites, with the onset of two GPS monitoring networks on rock plateaus. The networks consist of 2 reference stations and 17 benchmarks spread all over the unstable areas. The first measures already showed that the identified and monitored rock spreading phenomena were active (Magri et al. 2007, 2008) and worth of being monitored for longer periods, in order to define their rate of movement and possible relationships with precipitation patterns.

Therefore field-monitoring campaigns have been continued, and further instrumentation used, in the frame of the research project here described. This has happened approximately every 6 months, in April and October/November, corresponding to the end of the wet and dry seasons. These periods have been chosen in order to define the role of rainfall in the deformation processes.

The results of the GPS technique on the investigated rock spreading phenomena have shown vertical displacements that exceed 10 cm in the last 4 years and horizontal ones almost reaching 3 cm, namely at Il-Prajjet (Anchor Bay). In order to continuously monitor the displacements along the more active fractures, extensometers were installed in 2010 along some cracks at Il-Prajjet (Anchor Bay).

Fig. 7 Hazardous situation south of Il-Qarraba promontory due to the presence of limestone blocks in critical stability conditions. It should be noted that the blocks are overhanging footpaths and beach areas

The trend of movement seems to be sensitive to seasonality, in relation to rainfall distribution, but further data are needed to properly define this issue.

Discussion and Conclusions

The north-western coast of the Island of Malta displays a wide variety of landslides of different type, size, state and rate of activity. Coastal instability processes are strictly linked to the structural setting of the area which is characterised by the superimposition of deeply-jointed limestones on clayey materials.

The integration of geomorphological survey, aerial-photo interpretation and landslide monitoring enabled the definition of the state of activity and rate of movement of the rock spreading phenomena which affect two specific sites within the study area. This is of fundamental importance as far as landslide hazard is concerned, since lateral spreading phenomena may favour the occurrence of collateral movements (cf. Pasuto and Soldati 1996), such as block slides, rock falls and topples as well as earth slides and flows, which may induce sudden risk situations (Fig. 7).

The results of this research are aiming at providing local authorities with a sound knowledge of the causes of coastal instability phenomena and means to face related risks. Actually, the north-western coast of Malta is one most aesthetically pleasant areas in the island and therefore it attracts tourists and locals in all seasons. Moreover, since this area perfectly integrates natural and cultural heritage (Coratza et al. 2011), it is likely that the number of visitors will increase in the near future, since these aspects are likely to be further exploited and promoted within the sphere of tourism, where a different niche can be created. Therefore, the need to provide safe conditions for visitors – preserving at the same time this valuable strecht of coast – is clear (May 2008; Panizza and Piacente 2008; Soldati et al. 2008a).

The research team has tried to identify strategies to involve and sensitize technical and administrative staff from public institutions responsible for the protection of the environment, as well as academic staff, towards aspects of landslide hazard and risk assessment and mitigation. This has also included scientific workshops and meetings (Soldati et al. 2008b) and the use of the study area as a teaching/demonstration medium for Maltese and foreign stakeholders, as well as students and young researchers (Soldati et al. 2010).

Acknowledgments The research activities were funded by (1) the EUR-OPA Major Hazards Agreement of the Council of Europe through the European Centre on Geomorphological Hazards (CERG) in the frame of the project "*Coastline at risk: methods for multi-hazard assessment*" (Co-ordinator M. Soldati) and (2) the Fondazione Cassa di Risparmio di Modena within the project "*Multidisciplinary research in the open-air laboratory of the island of Malta: an international network for landslide hazard assessment in coastal areas*" (Co-ordinator M. Soldati).

The Authors are grateful to Dr. Simon Mercieca, Director of the Mediterranean Institute of the University of Malta, for the continuous support offered.

References

Alexander D (1988) A review of the physical geography of Malta and its significance for the tectonic geomorphology. Quaternary Sci Rev 7:41–53

Argnani A (1990) The Strait of Sicily rift zone: foreland deformation related to the evolution of a back-arc basin. J Geodyn 12:311–331

Civile D, Lodolo E, Accettella D, Geletti R, Ben-Avraham Z, Deponte M (2010) The Pantelleria graben (Sicily Channel, Central Mediterranean): an example of intraplate "passive" rift. Tectonophysics 490 (3–4):173–183

Coratza P, Bruschi VM, Piacentini D, Saliba D, Soldati M (2011) Recognition and assessment of geomorphosites in Malta at the Il-Majjistral nature and history park. Geoheritage 3(3):175–185

Dykes AP (2002) Mass movements and conservation management in Malta. J Environ Manage 66:77–89

Farrugia MT (2008) Coastal erosion along Northern Malta. Geografia Fisica e Dinamica Quaternaria 31(2):149–160

Finetti IR (1984) Geophysical study of the Sicily Channel Rift Zone. Boll Geofis Teor Appl 26:3–28

Gruppo di Lavoro per la Cartografia Geomorfologica (1994) Carta geomorfologica d'Italia – 1:50.000 – Guida al rilevamento. Servizio Geologico Nazionale, Quaderni serie III, vol 4, 42p

Illies JH (1981) Graben formation – the Maltese Islands – a case history. Tectonophysics 73:151–168

Magri O (2009) Investigation of landslides along the North-West coast of Malta and related hazard issues. Ph.D. thesis, University of Modena and Reggio Emilia, Modena

Magri O, Mantovani M, Pasuto A, Soldati M (2007) Monitoring the state of activity of lateral spreading phenomena along the north-west coast of Malta using the GPS technique. Analele Universitatii Din Oradea 17:5–10

Magri O, Mantovani M, Pasuto A, Soldati M (2008) Geomorphological investigation and monitoring of lateral spreading phenomena along the north-west coast of Malta. Geografia Fisica e Dinamica Quaternaria 31(2):171–180

Mangion M (1991) Impact of geological structural features on the hydrology and hydrogeology of Malta. Bachelor thesis, University of Malta, Msida, Malta

May V (2008) Integrating the geomorphological environment, cultural heritage, tourism and coastal hazards in practice. Geografia Fisica e Dinamica Quaternaria 31(2):187–194

Oil Exploration Directorate (1993) Geological map of the Maltese Islands. Office of the Prime Minister, Valletta

Panizza M, Piacente S (2008) Geomorphology and cultural heritage in coastal environments. Geografia Fisica e Dinamica Quaternaria 31(2):205–210

Pasuto A, Soldati M (1996) Rock spreading. In: Dikau R, Brunsden D, Schrott L, Ibsen M-L (eds) Landslide recognition: identification, movement and causes. Wiley, Chichester, pp 122–136

Pedley HM, House MR, Waugh B (1978) The geology of the Pelagian block: the Maltese Islands. In: Nairn AEM, Kanes WH, Steheli FG (eds) The ocean basins and margins. vol. 4B: the Western Mediterranean. Plenum Press, London, pp 417–433

Pedley M, Hughes Clarke M, Galea P (2002) Limestone Isles in a Crystal Sea: the geology of the Maltese Islands. PEG, Malta, p 109p

Soldati M, Buhagiar S, Coratza P, Magri O, Pasuto A, Schembri JA (2008a) Integration of geomorphology and cultural heritage: a key issue for present and future times. Geografia Fisica e Dinamica Quaternaria 31(2):95–96

Soldati M, Buhagiar S, Coratza P, Pasuto A, Schembri JA (2008b) Integration of the geomorphological environment and cultural heritage for tourism promotion and hazard prevention – Malta, 24–27 April 2007. Geografia Fisica e Dinamica Quaternaria 31 (2):93–249

Soldati M, Barbieri M, Biolchi S, Buldrini F, Devoto S, Forte E, Furlani S, Gualtieri A, Lugli S, Mantovani M, Mocnik A, Padovani V, Pasuto A, Piacentini D, Prampolini M, Remitti F, Schembri JA, Tonelli C, Vescogni A (2010) Multidisciplinary geological excursion in the open-air laboratory of the Island of Malta. Field-Trip Guide, Dipartimento di Scienze della Terra, Università di Modena e Reggio Emilia, Modena, 11–18 Nov 2010, 41p

Developments in Landslides Inventory and Registry in Slovakia

Pavel Liščák and Štefan Káčer

Abstract

Slope deformations represent the most dangerous exogenous geodynamic phenomenon in the Slovak Western Carpathians. Over about five decades of systematic inventory of slope deformations almost 22,000 slope deformations covering an area of 2,575,912 km^2 were registered; they pose either damage or threat for 5.25 % of the area of the Slovak Republic. In the year 2010 we evidenced numerous new or reactivated landslides throughout Slovakia, generated by excessive precipitation in the late spring. This situation led to a number of emergency situations in the municipalities and the geologists from the State Geological Institute of Dionýz Štúr (SGIDŠ) carried out inventory and assessment of extent and magnitude of evolved slope deformations. For the first time in the history of systematic inventory of geological phenomena in Slovakia we made use of very precise, "scaleless" levelling of the slope deformations in the territory morphology based on GNSS technology.

Keywords

Slope deformation inventory • GNSS – Global Navigation Satellite System • GIS – Geographic Information Systems • Map server • Socio-economic relevance

Introduction

In 2010 due to extremely abundant rainfall in May and June and the flood situation a great number of new or reactivated landslides were generated mainly in eastern Slovakia, in the region of Carpathian Flysch and Klippen Belt. The number of registered slope deformations in Slovakia was increased on more than 550 new landslides. From these, over 60 slope deformations endangered lives and property. The most affected villages were Nižná Myšľa, Kapušany, Prešov, Varhaňovce, Chmiňany, Vyšný Čaj, Ďačov, Košice, Nižná Hutka, Žipov and Ondrašovce. Severe damage to buildings and infrastructure occurred, including destruction of the environment. 136 houses were heavily damaged, among which 38 had to be demolished and 11 forcibly abandoned, 4,232 m of road sections were violated. About 400 housing estates, 17,846 m sections of roads and 364 m sections of railroads are now in a permanent state of threat. In these municipalities, public authorities had to declare emergencies. Based upon the inventory carried out by SGIDŠ, with a purpose-made database, the Ministry of the Environment of the Slovak Republic ordered exploration works on 37 emergency sites; several of them have been selected for further remedial measures with estimated costs exceeding 24 million EURO.

P. Liščák (✉) • Š. Káčer
State Geological Institute of Dionýz Štúr, Mlynská dolina,
817 04 Bratislava, Slovakia
e-mail: pavel.liscak@geology.sk

Overview of up to Now Slope Deformation Inventory

Inventory

The momentum for systematic research in slope deformations in the former Czechoslovakia was reached by activation of a catastrophic landslide in the town of Handlová, which in 1960/1961 destroyed 150 housing units, water pipeline,

C. Margottini et al. (eds.), *Landslide Science and Practice*, Vol. 1,
DOI 10.1007/978-3-642-31325-7_8,

state road, and electric line. The sliding volumes equalled to 20 million m^3 (Záruba and Mencl 1969).

The cases of the Handlová landslide and several others have shown that stabilization of active slope deformations is far more expensive than preventive measures. Another important finding has been the fact that the slope movements are recurrent in the areas of old landslides, mainly.

In the light of the above the next logical step in the research into slope deformations was their inventory; this effort has contributed to the development of a prominent school of Czechoslovak engineering geologists dealing with landslides around Nemčok and co. (for instance, Nemčok 1982).

The first registration of slope movements on the territory of Slovakia was made between 1962 and 1964 by the SGIDŠ, the Department of Geotechnics of Technical University (TU) in Bratislava, Department of Engineering Geology of the Faculty of Natural Sciences, Comenius University (CU), Bratislava and the Central Geological Institute in Prague. Slope movements were registered mainly in investment-relevant areas, especially around roads, rivers, towns and villages. The records on occurrence were mostly done on punch cards and drawn on maps at 1:25,000 scale. The results of this phase of registration are archived in Geofond.

The second stage of inventory of slope deformations was conducted in 1974–1978 by the Department of Geotechnics of the TU in Bratislava. On the basis of new knowledge about conditions for the occurrence of landslides in mountainous areas, slope failures were registered in the Nízke Tatry, Liptovské Tatry, Vysoké Tatry, Malá and Vel'ká Fatra Mts., etc., as well as in some lower mountain ranges and basins. Their findings were very valuable for understanding patterns and conditions of the emergence and development of slope deformations in Slovakia.

In 1981, the staff of SGIDŠ Department of Engineering Geology began the third stage of registration of slope deformations in Slovakia. The aim was to create a new register of slope deformations in accordance with national Guidelines for the registration of landslides and other dangerous slope deformations. They registered slope deformations of the Flysch Region, mainly, covering also the flysch areas of Eastern Slovakia (along with Eastern Slovakia neovolcanites and neotectonic depressions).

The output maps were at a scale of 1: 10,000 containing slope deformations and their documentation in the form of the record sheets for computer processing.

Landslide Atlas

A synthesis summarizing nearly 50-year regional research in the field of slope deformations is provided by Atlas of slope stability maps in SR at scale 1:50,000 (Landslide Atlas, Martinčeková et al. 2007). Within this project there have been reviewed results of registration of slope deformations, the final reports of landslide site surveys and scientific and professional publications. In the scope of the project also field work was conducted, which consisted of (Kopecký et al. 2008):

- Harmonization of the evaluation of damaged areas;
- Verification of unsatisfactory, or contradictory data on slope movements, retrieved from archival materials;
- Reconnaissance in unmapped territories in order to detect dangerous slope deformations, especially those that already threatened the constructions.

A total of 21,190 slope deformations were registered, which cover 5.25 % of the area of Slovakia. We have to note that in the Atlas database only so-called large scale failures are included, reaching a number of 16,212 and an area of 24,777,846 km^2. The rest of 4,978 so-called small-scale failures are not included in the database; they cover an area of 981,274 km^2.

The former attributes table of the Atlas distinguished 22 types and combinations of slope failures; Bednarik and Liščák (2010) reclassified them into five categories (Fig. 1).

Landslides Database as a Component of GeoIS

Among the principal activities of ŠGÚDŠ, along with geological research and exploration belong creation and application of the information system in geology. Some results are open to public through the project "Geological Information System" (GeoIS) which started at the end of 2005 and its mission is to develop a web application, providing access to spatial geological information – regional geological, engineering geological, hydrogeological, geochemical and geophysical maps.

One important service named Landslides was provided to the public in May, 2010. The Geofond register keeps evidence of documented slope deformations in Slovakia. As a groundwork of digital layers serve the data from the aforementioned project Landslide Atlas.

To each slope failure an attribute table is assigned, which contains the following information: identification number in the register of landslides, geomorphological unit, engineering geological area, source of information, type of slope deformation, degree of activity, geological formation, geological setting, hydrogeological conditions, size, slope, endangered objects, cause, remediation, etc.

According to the Landslide Atlas database, the slope deformations endanger 98.8 km of highways and roads of first class, 571 km of roads, of second and third class, 62 km of railways, 11 km of overhead lines, 3.5 km of crude oil pipelines, 101 km of gas pipelines, 291 km of water supply and nearly 30,000 constructions.

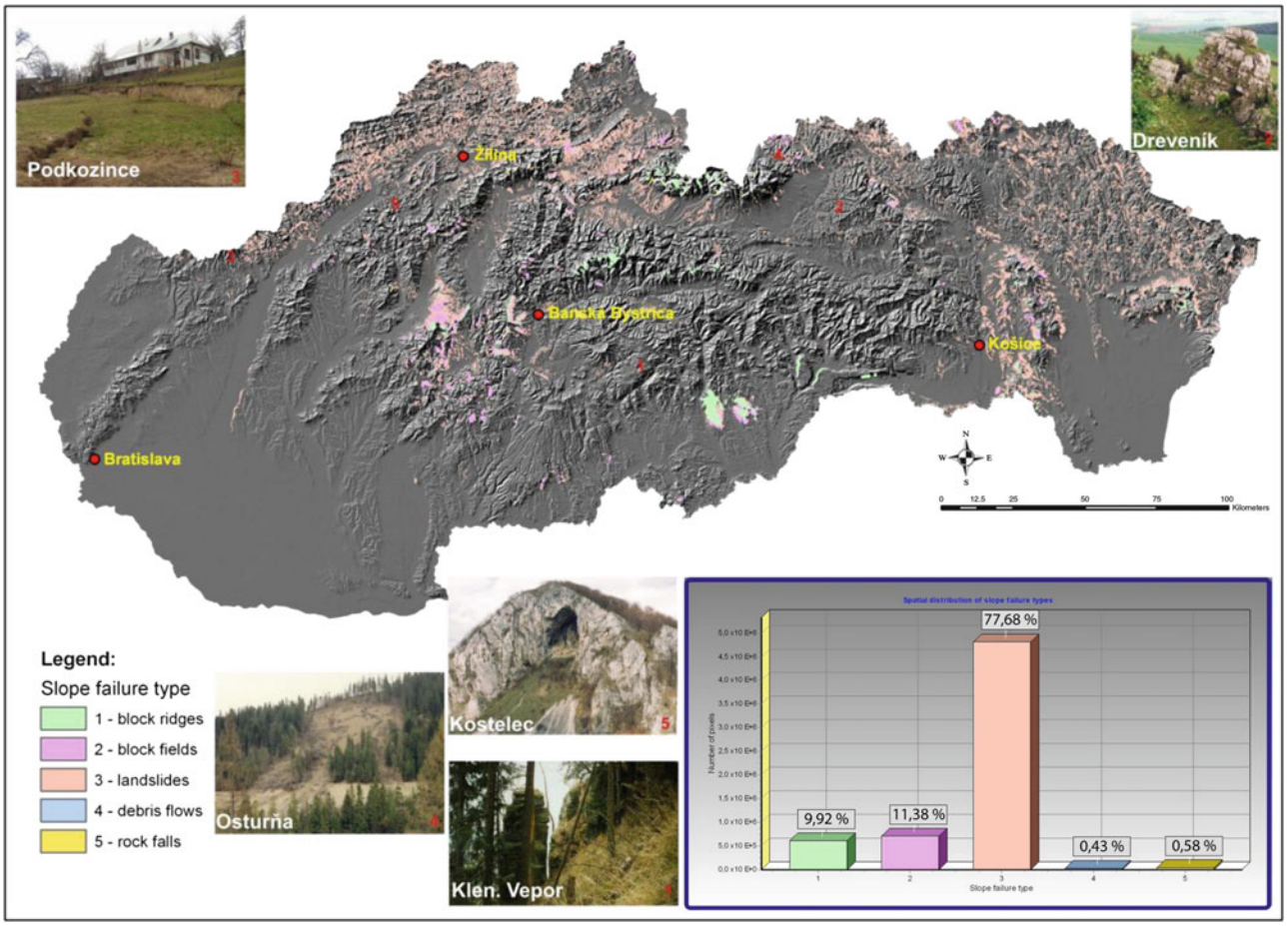

Fig. 1 Slope deformations distribution according to Landslide Atlas (Modified from Bednarik and Liščák 2010)

Metadata, upgrade, searching and visualisation services and access to the landslide application are in accord with professional and technological aspects of the INSPIRE Regulation. Besides the data upgrade the Network services (storing and transformation) and Interoperability of files and services are in the phase of testing.

The Landslides application is available on the web address: http://mapserver.geology.sk:8080/zosuvy (in Slovak) and the Map server that is based on ESRI technologies ArcGisServer ver.10 is available on the web address: http://www.geology.sk/?pg=geois.map_server.

Slope Deformations Inventory in 2010

In May/June 2010, we experienced an unprecedented generation of slope failures, which has been undoubtedly subject to extremely high rainfall in the month of May, in many places exceeding long term means four to five times. Particularly affected were mainly the territories of Eastern Slovakia (Košice and Prešov regions), especially the territories of the Central Carpathian Palaeogene Basin, the Flysch Belt, and also a narrow zone of the Klippen Belt.

Soon afterwards, by the mid of June the Government addressed the Slovak Geological Institute of Dionýz Štúr to carry out an inventory of landslide in order to get figures on the scale of damage.

In principle, the methodology of inventory consisted of the following successive steps in the field survey with subsequent analysis of the results:

(a) Identification of slope deformations in the field;
(b) Levelling of slope deformations using a GNSS device;
(c) Detailed photo documentation of the landslide body and damaged or threatened infrastructure;
(d) Completion of the special-purpose data sheet with emphasis on the infrastructure damaged/threatened.

Identification of Slope Deformations in the Field

Given the urgency of the situation, we first registered landslide sites in which an emergency situation was identified. In addition, we have co-registered other slope failures, because we assumed that not in all locations such emergencies have been reported, which has been also confirmed in several locations, We prepared the first set of

primary information for the Division of Geology and Natural Resources of the Ministry of Environment SR with the identification of critical landslides:

1. With immediate damage/threat to lives and property;
2. With immediate damage/threat to infrastructures;
3. With immediate damage/threat to above-ground and under-ground pipelines (transmission lines, pipelines, water pipelines, telecommunications cables, etc.).

After providing initial information and rough estimate of the damage scale for the Ministry we continued registering of landslides in areas which have not been mapped yet. In many cases, we communicated with the local administration, or directly with affected citizens. By 29/10/2010, we registered 551 slope deformations, the vast majority of landslides which have arisen in the period May–July 2010 (Liščák et al. 2010). A component of the inventory was a photo documentation of slope deformations registered.

Methodology: Levelling of Slope Deformations Using a GNSS Device

In the course of field mapping, provided the conditions were acceptable, we used a Trimble GNSS unit GeoXT/GeoXH 2005, GIS category with sub-meter accuracy of recording. This device made records of linear trajectories of all major elements of landslide morphology – main scarps, transverse and longitudinal cracks and edges of the accumulation zones. In case of unavailability of these elements we have recorded with the highest possible precision pinpoint within an apparent geometric centre, or on conspicuous elements of landslides (usually in the centre of head scarp or accumulation zone). Since the accuracy of recorded data depends on the quality and intensity of the satellite signal, which varies depending both on terrain conditions (relief topography, vegetation density, etc.), as well as on the fluctuating availability and configuration of the satellites during the day, we divided the data into the following Six classes of GIS database field "kvalita":

Class 1: Data recorded with the highest possible precision of the instrument, with an average error of up to 1,5 m, assuming the availability of signals from more than five GPS satellites and additional signals from the European Geostationary Navigation Overlay Service EGNOS. The accuracy of orientation was close to 0.5 m level. Thus, the recorded data are virtually "scaleless" and can be used in accordance with arbitrarily precise map data, including cadastral maps at the largest scales, for example in quantification of damage on individual lots, without the need for additional geodetic survey. With such accuracy 173 slope deformations were recorded. An example of a contour line retrieved from a GPS measurement is given on Fig. 2a; the same object with a smoothed line is on Fig. 2b.

Class 2: Data with relatively high accuracy with an error ranging from 1.5 to 7 m. The error was caused in most cases due to unavailability of sufficient number of satellites due to improper daytime (usually around noon), due to dense vegetation or to improper configuration of terrain (steep slopes with a strong signal shielding effect). The leap in accuracy compared to the class 1 was mainly due to the unavailability of the signal from the European EGNOS satellites. The data are compatible with the geo map data at scales smaller than 1: 2,000. All in all we have recorded 227 slope deformations of this quality.

Class 3: Linear elements with the lowest precision recorded, yet acceptable with an adequate "safe" device sensitivity reducing. This way recorded data were collected in areas with very unfavourable terrain configuration (usually in a forest on steep slopes) where it was necessary to record at least any indication. Deviations within acceptability limits ranged from 7 to 20 m. Data can be considered spatially compatible with maps at scales 1: 5,000–1: 10,000. With such low accuracy 12 objects were recorded.

Class 4: Slope deformations recorded as single point or more points on significant landslide morphology elements, for example, one point on head scarp (highest point), one in an accumulation zone and two points on side edges, etc. The reasons for single point measurements could be various: the unavailability of sufficient number of satellites, even during prolonged observations are (more than 5 min – in this case point entry was the only one that could be obtained), or unavailability of all elements of the slide – dense stand of bush, shrubs, fenced private property, interference with the watercourse etc. The body of the slope deformation was plotted on the basis of these point measurements within the orthophoto at scale 1:5,000, or within digital matrix ZM10 maps at scale 1:10,000. In this class of accuracy 31 slope deformations were recorded.

Class 5: Slope deformations recorded as single point using less accurate GPS devices (tourist navigation devices, PDA devices, car navigation, etc.). Despite the fact that for these data we do not have available information on the mean error, their accuracy can be assessed still compatible with the maps in scale 1:10,000, like in class 4. The number of objects thus recorded is 18.

Class 6: Within this category we include slope deformations, which were plotted in a map without GPS levelling, either on the ground or in the office. We usually drew them into base map 1:10,000 (ZM10), or in orthophotos (1:5,000) and subsequently digitized into a vector format required. This way 90 slope deformations were plotted, particularly in the Košice Region.

Beside the division into classes the database contains the exact figure of the average positional accuracy (median difference in m) as well as the maximum error observed

Fig. 2 Accuracy of GNSS levelling, class 1. (**a**) Rough line of GNSS measurement; (**b**) Smoothed line of GNSS measurements

during the observations for the device Trimble Geo (fields "horz_avg" and "horz_worst").

GIS Database

The GNSS data measured in the field were converted into GIS format using the utilities supplied to the GPS device Trimble GeoXT. Since this device is capable of ground-based recording in the form of vector lines, conversion into GIS was relatively trivial operation.

However, the original lines measured in the field were retrieved in the "raw" form, it means they contained errors and various variations due to sudden changes in the quality of the record ("jagged" lines during the loss of satellites under the trees etc.); thus they were not appropriate for the final drawings into the GIS database. Therefore it was necessary to make additional corrections, particularly those in classes 2 and 3 of the recording quality. Thus additionally smoothed lines were converted into closed polygons representing the final shape of the landslide. For each polygon the tabular data were assigned.

Data on area and perimeter of individual landslides have been derived from the classical features of GIS programmes (MapInfo Professional and ESRI ArcGIS). Similarly, other data resulting from the geographical location of landslides (cadastral territory, district, map sheet ZM 10, etc.) were automatically derived from the GIS documents (SVM 50 database).

Information on the geological setting of the slope deformation was derived through a combination of field records and the digital geological map at scale 1:50,000 (Káčer et al. 2005). As the relative positional accuracy of this map does not correspond to the accuracy of our data retrieved from GPS contouring, we could not proceed in this case automatically using GIS spatial functions. The geological map was compared with each mapped slope deformation separately and the corresponding geological map unit was assigned to the relevant slope deformation based on our expertise.

For each polygon there were also assigned the values of the average slope gradient and average slope aspect (fields "slope_avg" and "aspect_avg"). These values were derived from a raster Digital Elevation Model at a scale of 1:10,000 (drawn from the documents of ZM10, Esprit, Ltd., B. Štiavnica), elaborated in the scope of the project Integrated Landscape Management, (Malík et al. 2007) with positional resolution of the corresponding grid cell size of 20 × 20 m.

The mean values of slope gradient and exposure were assigned to each slope deformation on the basis of average values in all grid cells located inside the slope deformation body. For this purpose, there were standard statistical programmes implemented in GRASS GIS, version 6.2.

The final GIS database consists of 66 data fields; 36 of them contain data of technical character (accuracy of GPS record, date and time of observation, author of the record, etc.) and the rest of the fields store information on the slope deformation from the geological point of view (engineering geological, hydrogeological, geomorphological, etc.).

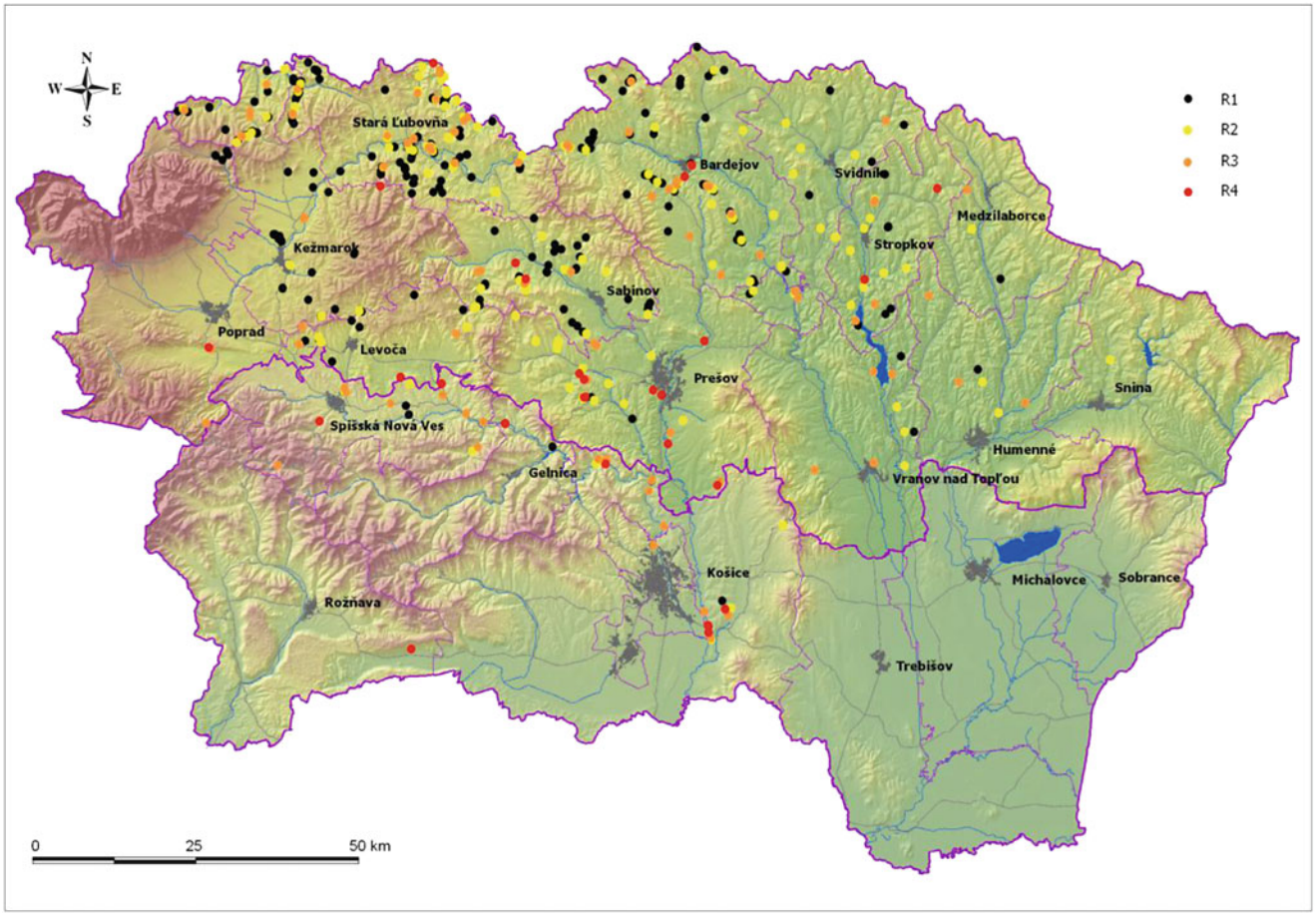

Fig. 3 Slope deformations distribution during the May–June 2010 period in Eastern Slovakia

Socio-Economic Relevance

The whole set of registered slope deformations was divided in accordance with the purpose-made categorization of socio-economic significance (threat to life and property) and consequent risk of landslide on the scale recommended by the European Commission for multirisk evaluation (Marzocchi et al. 2009) as follows:

- Moderate (R1): social, economic and environmental damages are marginal – 273 slope deformations;
- Medium (R2): minor damages to buildings, infrastructures and environment are possible. No significant effect on people, functionality of buildings and economic activities – 151 slope deformations;
- High (R3): concern exists on people's safety. Functional damages to buildings and infrastructures are possible as well as interruption of the economic activities and relevant damages to the environment – 98 slope deformations;
- Very high (R4): expected damages include casualties and injuries, serious damages to buildings and infrastructures, destruction of the environment and of the socio-economic activities – 29 slope deformations.

Table 1 Distribution of slope deformations of 2010 according to their socio-economic relevance in the districts of Košice and Prešov regions

District	Count	R1	R2	R3	R4
Gelnica	3	1	0	0	2
Košice – okolie	21	2	5	9	5
Košice I	2	1	0	1	0
Rožňava	1	0	0	0	1
Sp. N. Ves	17	2	3	10	2
Košice in total	44	6	8	20	10
Bardejov	101	58	26	15	2
Humenné	6	1	2	3	0
Kežmarok	74	51	11	11	1
Levoča	23	11	7	4	1
Medzilaborce	3	1	1	1	0
Poprad	10	7	0	2	1
Prešov	37	3	20	5	9
Sabinov	51	31	14	4	2
Snina	1	0	1	0	0
Stará Ľubovňa	154	90	41	22	1
Stropkov	21	7	8	4	2
Svidník	17	5	9	3	0
Vranov n. Topľou	9	2	3	4	0
Prešov in total	507	267	143	78	19

Overview of single categories within regions and districts is in Table 1, the arrangement of individual socio-economic categories is illustrated in Fig. 3.

Conclusions

The most important benefit of the inventory is "instant" information on the status and impact of slope deformations, occurred or reactivated in May and June 2010 due to climate extremes. The inventory, categorization and update of the current status of landslide sites enable the government and local authorities to effectively lead the necessary funds for exploration and remediation of the affected areas. The way of data collecting and processing, "scalelessness" of topographic information, registration of damaged or endangered buildings allow to incorporate this accurate documentation into land use planning documents, regardless of the detail of the processing and geodetic survey (cadastral maps of lots C and E categories, geometric plans, detailed maps of engineering networks utilities, different land maps, documents of Territorial System of Ecological Stability and General Principles of Functional Arrangement, forestry maps, etc.). Thus, based on a compliance with the cadastral map it is possible to quantify precisely the size of damage to a lot with a possibility of identifying the owner, etc.; this is such an important input for documentation for insurance claims, identification of the extent of damage to gas pipelines, water pipes and so on.

At the same time an extensive GIS database has been created containing information about the date of slope failures generation, the first of its kind in Slovakia, which becomes a fundament for future research on the recovery of such phenomena and their more reliable forecasting.

References

Bednarik M, Liščák P (2010) Landslide susceptibility assessment in Slovakia. Mineralia Slovaca 42(2):193–204, ISSN 0369–2086

Káčer Š et al (2005) Digital geological map of Slovakia at scale 1:50 000. http://www.geology.sk/?pg=geois.ms_gm50. Accessed on June 2011

Kopecký M, Martinčeková T, Šimeková J, Ondrášik M (2008) Landslide atlas – results of the geological project. In: Proceedings of the 6th conference geology and environment, Bratislava, pp 105–110, ISBN 978-80-89343-06-5

Liščák P, Pauditš P, Petro Ľ, Iglárová Ľ, Ondrejka P, Dananaj I, Brček M, Baráth I, Vlačiky M, Németh Z, Záhorová Ľ, Antalík M, Repčiak M, Drotár D (2010) Registration and evaluation of newly evolved slope failures in 2010 in Prešov and Košice regions. Mineralia Slovaca 42(2):393–406, Dionýz Štúr Publishers, ISSN 1338–3523

Malík P, Bačová N, Hronček S, Ivanič B, Káčer Š, Kočický D, Maglay J, Marsina K, Ondrášik M, Šefčík P, Černák R, Švasta J, Lexa J (2007) Creation of geological maps at scale 1:50 000 for the needs of integrated landscape management. Manuscript – Geofond Archive ŠGÚDŠ, archive number. 88158, Bratislava, 552p

Martinčeková T, Šimeková J et al (2007) Atlas of slope stability SR 1:50 000. Final report of engineering geological investigation, INGEO – ighp, spol. s.r.o., Žilina

Marzocchi W, Mastellone ML, Di Ruocco A, Novelli P, Romeo E, Gasparini P (2009) Principles of multi-risk assessment. Interaction amongst natural and man-induced risks. EC, Directorate-General for Research, Environment Directorate (ISBN 978-92-79-07963-4) 450p

Nemčok A (1982) Landslides in the Slovak Carpathians, Veda, vyd. SAV 1982, 319p

Záruba Q, Mencl V (1969) Landslides and their control. Academia, Praha, p 205p

Landslide Impacts in Europe: Weaknesses and Strengths of Databases Available at European and National Scale

Daniele Spizzichino, Claudio Margottini, Alessandro Trigila, and Carla Iadanza

Abstract

Landslides represent a major threat to human life, property, buildings, infrastructure and natural environments in most mountainous and hilly regions of the world. The purpose of this work is to present the results of the analysis carried out by ISPRA on main landslide events and available databases in Europe. The major landslide phenomena occurred in Europe have been collected from the analysis of global disaster databases. For the period 2003–2010, 112 major landslides were recorded. These events, which often occurred at multiple sites for the same triggering factor, claimed a total of 152 fatalities and damaged or destroyed several buildings and transportation infrastructure.

Keywords

Landslide • Database • Europe • Events • Impacts

Introduction

Landslides represent a major threat to human life, property, buildings, infrastructure and natural environments in most mountainous and hilly regions of the world. Landslides are defined as the gravitational movement of a mass of rock, earth or debris down a slope (Cruden 1991), which are basically described by two characteristics: (1) the material involved (rock, debris, earth) and (2) the type of movement (falls, topples, slides, spreads, flows) (Cruden and Varnes 1996). The above classification (e.g. rockfall, debris-flow, earth-slide) facilitates the understanding of the failure mechanism. The occurrence and reactivation of landslides are conditioned by a number of contributing factors related to bedrock and soil properties, slope angle, relief energy or land-use cover. In Europe, most catastrophic landslides are associated with heavy and/or prolonged rainfalls. Other important triggering factors include earthquakes, snow melt and slope toe erosion by rivers or sea waves, thawing mountain permafrost, volcanic eruptions (Hervás 2003), and man-made activities such as slope excavation and loading, land use changes, or water leakage from aqueducts and sewerage. The distribution of landslide hazards over Europe is strongly linked to the geological and relief conditions as well as seismicity and precipitation. Therefore, mountainous areas, such as the Alps, the southern part of Europe and Norway are most prone to landslides. Central Europe is only marginally affected, as Eastern Europe with the exception of Romania and Bulgaria (EEA 2004; Jelínek et al. 2007; Schweigl and Hervás 2009). The purpose of this work is to present the results of the analysis carried out by ISPRA (Italian National Institute for Environmental Protection and Research) on main landslide events and databases in Europe. This activity has been started during the implementation of the EEA technical report 2010 "Mapping the impacts of natural hazards and technological accidents in Europe – An overview of the last decade" (Spizzichino et al. 2010).

D. Spizzichino (✉) • C. Margottini • A. Trigila • C. Iadanza
ISPRA, Italian National Institute for Environmental Protection and Research, Geological Survey of Italy, Via Vitaliano Brancati 48, 00144 Rome, Italy
e-mail: daniele.spizzichino@isprambiente.it

C. Margottini et al. (eds.), *Landslide Science and Practice*, Vol. 1,
DOI 10.1007/978-3-642-31325-7_9,

Table 1 Major landslide events collected during 2010

Date of event	Location	Impact	Source
06 January 2010	Northumberland, England	Fisherman killed when cliff collapsed near Newbiggin	http://news.bbc.co.uk/2/hi/uk_news/england/tyne/8444741.stm
07 January 2010	Arta, Greece	Falling rocks create traffic hazard on highway	http://archive.ekathimerini.com/4dcgi/_w_articles_politics_100006_08/01/2010_113856
13 January 2010	Medveda, Serbia	Landslides are endangering about 2,000 residents from 12 villages in the Medvea municipality	http://www.b92.net/eng/news/society-article.php?yyyy2010&mm=01&dd=13&nav_id=64438
16 January 2010	Scotland	Overnight flooding caused a landslide in southern Scotland and the closure of several roads, including a section of the M74	http://news.bbc.co.uk/2/hi/uk_news/scotland/8462994.stm
01 February 2010	Eskoriatza, Spain	Homes half buried in Basque country – 15 families who live in a block of flats affected by a landslide have been moved to local hotels and nine more are staying with friends or relatives	http://www.thinkspain.com/news-spain/17603/homes-half-buried-in-basque-country-landslide
15 February 2010	Maierato, Italy	Heavy rain causes several mudslides and prompts evacuation of thousands of people; dozens of homes damaged	http://gsc.nrcan.gc.ca/andslides/in_the_news_e.php
19 February 2010	Drautalstraße, Austria	Massive landslide leaves 35,000 cubic metres of debris Landslide closes Drautalstraße (B100) near Leisach	http://austriantimes.at/news/General_News/2010-02-22/20865/Massive_landslide_leaves_35,000_cubic_metres_of_debris
20 February 2010	Patarlagele, Romania	Households flooded, landslides due to rains and snow-melting. The National road 10 Buzau-Brasov blocked by landslide	http://www.financiarul.ro/2010/02/22/households-flooded-landslides-due-to-rains-and-snow-melting/
21 February 2010	Madeira, Portugal	Rescue crews find body in car buried by landslide	http://www.guardian.co.uk/world/2010/feb/22/madeira-floods-landslides-car-death
22 February 2010	Macedonia	Several roads damaged by landsliding	http://gsc.nrcan.gc.ca/landslides/in_the_news_e.php
23 February 2010	Rubite, Spain	A British couple were killed when the roof of a Spanish farmhouse collapsed on top of them	http://www.thisislondon.co.uk/standard/article-23809115-roof-collapse-kills-britons-as-they-watch-tv.do
25 February 2010	Purfleet, England	Two cars damaged in rock fall	http://www.thurrockgazette.co.uk/news/5031501.Landslide_in_Purfleet/
1 March 2010	Azores islands, Portugal	A mudslide swept a school bus off a road, killing the driver and sending two children to hospital	http://www.thestar.com/news/world/article/773603-sleeping-families-die-as-sea-walls-collapse-in-france
2 March 2010	Buzau, Romania	Prime Minister Emil Boc on Monday afternoon toured the village of Odaile, southern Buzau County, that was badly hit by landslides in the past days	http://www.financiarul.ro/2010/03/02/pm-boc-tours-landslide-stricken-odaile/

(continued)

Table 1 (continued)

Date of event	Location	Impact	Source
7 March 2010	Dorset, England	Two children have been rescued after being stuck in a mound of mud following a landslide	http://news.bbc.co.uk/2/hi/uk_news/england/dorset/8554510.stm
11 March 2010	Italy	Landslide (6,000,000 cubic meters) invaded national railway Benevento – Foggia	http://napoli.repubblica.it/dettaglio-news/foggia-10:32/3760496
12 March 2010	Krilo Jesenice, Croatia	Couple injured when rocks hit their car during landslide	http://www.croatiantimes.com/news/General_News/2010-03-12/9554/Couple_injured_in_landslide
16 March 2010	Macedonia	Four people injured when a landslide derailed a passenger train between Skopje and Kicevo	http://gsc.nrcan.gc.ca/landslides/in_the_news_e.php
27 March 2010	Paignton, England	A family had the fright of their lives when a landslide stopped only a foot from their kitchen door	http://www.thisissouthdevon.co.uk/news/Family-s-shock-garden-landslide/article-1951020-detail/article.html
12 April 2010	Merano, Italy	A landslide hit and derailed a train killing 11 people and leaving some 30 injured	http://www.lfpress.com/news/world/2010/04/12/13552636.html
20 April 2010	Ventotene island, Italy	Coastal cliff rockfall killed two students in Cala Rossano beach	http://espresso.repubblica.it/dettaglio/litalia-frana/2125443
7 May 2010	Switzerland	Locarno-Domodossola railway line interrupted by a landslide	http://www.romandie.com/infos/ats/display2.asp?page=20100507174634120172019048164_brf049.xml
28 May 2010	Bastia, France	Spectacular landslide at the foot of a building in Pietranera	http://www.corsematin.com/article/faits-divers/bastia-spectaculaire-glissement-de-terrain-au-pied-dun-immeuble-de-pietranera
9 September 2010	Atrani, Italy	An extremely rapid debris flow triggered by intense rainfall hit Atrani village in Costiera Amalfitana causing one fatality	http://www.repubblica.it/cronaca/2010/09/09/news/frana_sulla_costiera_amalfitana_travolte_diverse_auto-6918660/
31 October 2010	Massa, Italy	Three people killed in Massa (Toscany) by extremely rapid landslides	http://www.gulf-times.com/site/topics/article.asp?cu_no=2&item_no=395883&version=1&template_id=39&parent_id=21
3 November 2010	Turkey	Turkish authorities say a village digging project triggered a landslide, killing six people and injuring four	http://gsc.nrcan.gc.ca/landslides/in_the_news_e.php
16 November 2010	Cornwall, England	The overnight downpours triggered a landslide which blocked the train line linking England's most south westerly county to the rest of Britain	http://www.gulf-times.com/site/topics/article.asp?cu_no=2&item_no=399273&version=1&template_id=38&parent_id=20
05 December 2010	Bosnia Herzegovina	Three people have been killed when their house collapsed due to a landslide triggered by heavy rains.	http://www.presstv.ir/detail/154097.html
13 December 2010	France	The ski resorts of l'Alpe d'Huez, les Deux Alpes and La Grave were cut-off by a major landslide on the RN91 at 8 a.m. on Monday	http://www.skiclub.co.uk/skiclub/news/story.aspx?storyID=1917

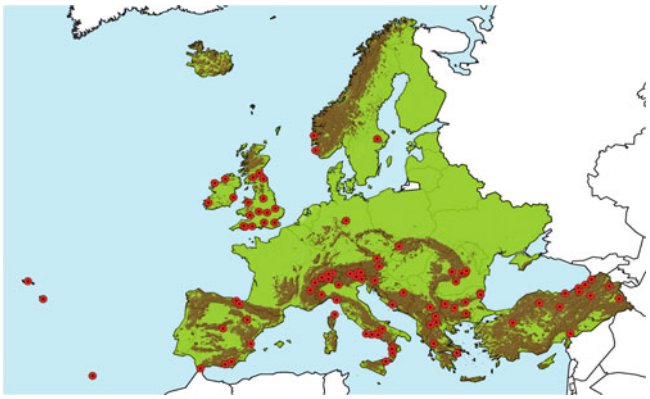

Fig. 1 Major landslide events in EEA countries 2003–2010

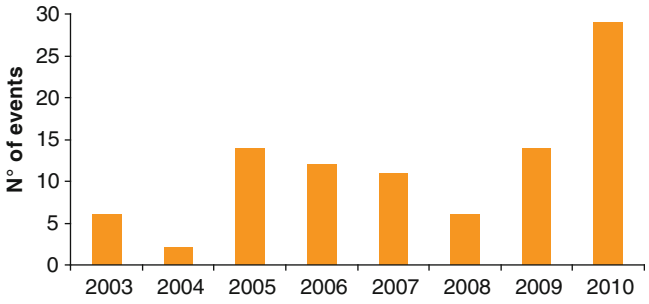

Fig. 2 Temporal distribution of major landslide events in Europe 2003–2010

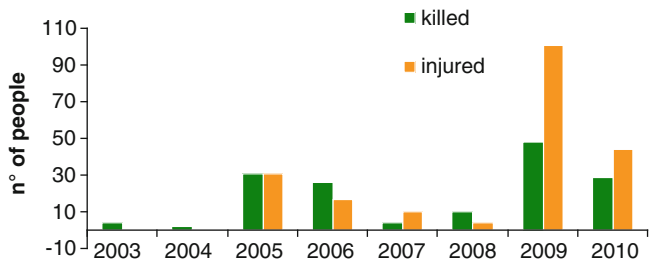

Fig. 3 Fatalities and injured in Europe 2003–2010

Materials and Data Source

The major landslide phenomena that occurred in Europe during the period 2003–2010 were compiled from an analysis of global disaster databases, such as the EM-DAT (2011), NatCatSERVICE (2011), International Consortium on Landslide (ICL) and the Geological Survey of Canada (GSC) as well as by review of the scientific literature and the web press news (Table 1). Last but not least, a special enquiry was carried out in 2009 by ISPRA with the support of the EuroGeoSurveys (Geological Surveys of Europe) to get a more comprehensive picture of landslide events at national or regional scale. The different sources of information varied significantly in their representation of the problem, due to different data entry criteria (e.g. number of fatalities and/or affected people, declaration of a state of emergency, call for international assistance). The major landslide events 2003–2010 represent only a glimpse of the real impact of landslides in Europe. Instead national databases, such as in the case of the Italian Landslide Inventory (Trigila and Iadanza 2008; Trigila et al. 2008), provide a much more comprehensive picture of the frequency, distribution and impact of landslides compared to global databases. This is not surprising, as most landslides are small and localized events that produce, very few fatalities and/or slight economic damage per event. Therefore these events are likely to fall below the threshold values used in the global disaster databases. For example in the EM-DAT database at least one of the following criteria must be fulfilled: (a) 10 or more people reported killed, (b) 100 or more people reported affected (c) declaration of a state of emergency, (d) call for international assistance.

Major Landslide Events 2003–2010

Spatial and Temporal Distribution of Landslides

An overview of the major landslide events reported in the period 2003–2010 by the different information sources is presented in Fig. 1 and in Table 1. As mentioned before, mountainous areas are most prone to landslides. Figure 2 identifies the temporal distribution of major landslide events during the period 2003–2010. The limited number of events does not permit any interpretation of temporal trends.

Landslide Impacts: Fatalities and Economic Losses

In general, fatalities due to landslides are a consequence of rapid and extremely rapid slope movements such as debris and mud flows, triggered by high intensity precipitation.

From 2003 to 2010, 152 fatalities were recorded in 112 events (Fig. 3). This number is much higher than that stated in EM-DAT (2010) for the same period, and certainly

Table 2 Summary of landslide inventories available at European Geological Services

Countries	Presence of landslide inventories	Level of detail (L = only location, C = complex inventory)	Number of landslides (L), landslide events (E)	Map scale	Coverage (%)	Format: D = digital, P = paper	Data of creation	Last updates	Main organization (s) in charge
Austria	Yes	–	30,000	1:25,000, 1:50,000	National	P, D	2002	–	GBA
Albania	Yes	L	250	1:25,000	23 %	D	2007	–	GSA
Belgium	Yes	C	236	All scale levels	5.30 %	D	2007	2009	GSB
Bulgaria	Yes	–	–	1: 500,000	National	D (not georeferenced), P	1999	July 2007	MOEW
Bosnia-Herzegovina	–	–	–	–	–	–	–	Not updated	–
Croatia	Yes	L = 1258; C = 201	1,603	1:25,000 = 1258; 1:5,000 = 201	20 %	D = 1088; P = 371	2001–2008	–	HGI
Cyprus	Yes			1:5,000, 1:10,000		P, D	1986	1998–2008	GSD
Czech Republic	Yes	C	ca 15,000	1:50,000	100 %	D	1960	Not specified	CGS
Denmark	No	L	Very few		<1 %			2008	GEUS
Estonia	–	–	–	–	–	–	–		EGK
Finland	Yes	L	56	No	100 %	D, P	1999	–	SYKE/ MMM.FI
France	Yes	C	>17,000	1:25,000	96 %	D	1994	1999	BRGM, LCPC, RTM, MEEDDM
Germany	No national inventory; only existing in some Federal States	No information	No information	No information	No assessment possible	D, P	No information	August 2009	BGR
Greece	Yes	C	1,850 (D)–5,000(P)	1:50,000	100 %	D	2007	No information	IGME
Hungary	Yes	L	364	1:100,000	100 %	D	–	2009	MBFH
Iceland	Yes					D	2002	Continuous	ISOR
Ireland	Yes	L, C	422	1:2,250,000	80–90 %	D	2005		GSI
Italy	Yes	C	480,000	1:10,000, 1:25,000	National	D	1999	September 2009	ISPRA
Latvia	–	–	–	–	–	–	–	2006	LEGMA
Liechtenstein	–	–	–	–	–	–	–	–	
Lithuania	–	–	–	–	–	–	–	–	LGT
Luxembourg	Yes	L, C	100	1:20,000	60 %	D	2003	–	SGL
Macedonia	–	–	–	–	–	–	–	2009	
Malta	–	–	–	–	–	–	–	–	
Montenegro	–	–	–	–	–	–	–	–	
Netherlands	No	–	–	–	–	–	–	–	TNO

(continued)

Table 2 (continued)

Countries	Presence of landslide inventories	Level of detail (L = only location, C = complex inventory)	Number of landslides (L), landslide events (E)	Map scale	Coverage (%)	Format: D = digital, P = paper	Data of creation	Last updates	Main organization (s) in charge
Norway	Yes	C	33,000	1:50,000	100 %	D	2001	–	NGU
Poland	Yes	C	7,000	1:10,000	5 %	D	2007	2009 (continuously)	PGI
Portugal	No	–	–	–	–	–	–	December 2009	INETI
Romania	Yes			1: 25,000	National	P, D	2001	–	GIR
Serbia									
Slovakia	Yes	L	12,000	1: 250,000	National	P, D	1960		
Slovenia	Yes	L	3,500	1: 250,000	100 %	D	2005	Continual update	GeoZS
Spain	Yes	L, C	About 400	1:200,000	100 %	P, D	2003	2009	IGME
Sweden	No	–	–	–	–	–	–		SGU
Switzerland	Yes	C	12,000	–	National	D	1996	–	FOEN
Turkey	Yes	C	55,608	1:25,000	National	P, D	1997	Continual update	MTA
United Kingdom	Yes	C	14,000	1:10,000, 1: 50,000	100 % of Great Britain not UK	D	1995	In progress	BGS

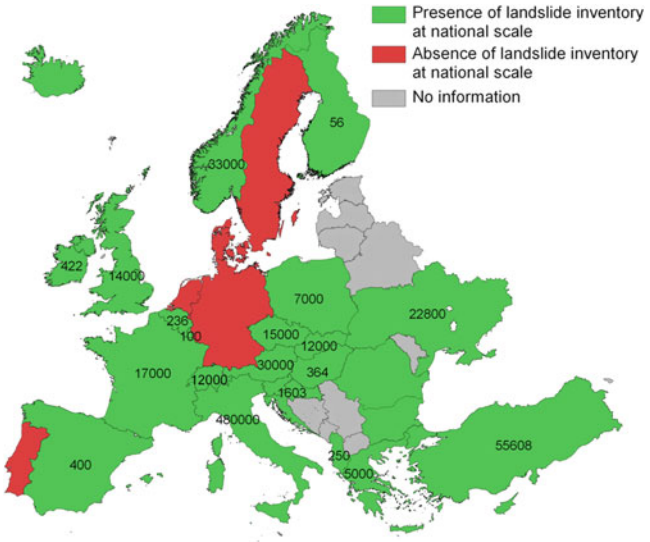

Fig. 4 Availability of a national landslide inventory in European Countries and related number of detected landslides (Spizzichino et al. 2010)

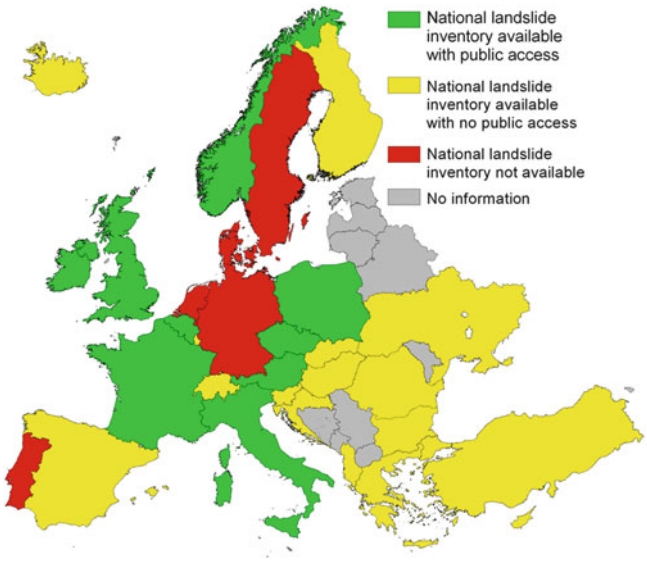

Fig. 5 Availability of landslide inventory and public access in European Countries (Spizzichino et al. 2010)

provides a more comprehensive picture of the major events in Europe at that time.

Currently, there is no comprehensive overview of the overall economic losses resulting from landslides in Europe. The main reasons for this is that landslides are generally managed by different institutions at the local level including local municipalities, road authorities, railway authorities etc. (Sidle and Ochiai 2006). However, figures are available for several European member states, e.g. Spain (EUR 170 million/year), Sweden (EUR 8–15 million/year), and Norway (EUR 6.5 million/year) (Schuster 1996). Italy spent approx. EUR 146 billion between 1957 and 2000 as a result of damage caused by landslides and floods (Cellerino 2006), plus an estimate of approximately EUR 44 billion Euros calculated by the Italian River Basin Authorities to make the entire country safe.

National Landslide Databases in Europe

As landslides are generally local phenomena, it is particularly important to collect information on past events at a local scale, fully involving local Authorities in the process. The questionnaire developed by ISPRA with the support of EuroGeoSurvey, has provided, for the first time at the European scale, an assessment of the availability, limits and potentialities of national landslide inventories for the whole continent. The enquiry yielded a total of 712,089 recognised mass movements in Europe (Table 2).

The results reveal that landslide inventories exist in many European countries, but that they are not homogeneous with regard to the resolution and level of information. Many of these inventories are not available to the public (Figs. 4 and 5).

These shortcomings and the lack of a comprehensive database at the European level are two major impediments to a more comprehensive overview of landslide events and their impact at the European scale.

Conclusion

Landslides are complex phenomena based on the interaction of various factors including material type, bedrock, slope and triggers such as heavy rainfall. As landslides are generally local phenomena, it is particularly important to collect past events and produce detailed landslide maps fully involving local authorities in the process. The present analysis reveals that landslide inventories exist in many European countries, but they are highly variable with regard to the resolution and level of information. Many of these inventories are not available to the public. These shortcomings and the lack of a comprehensive database at the European level are two major impediments to a more comprehensive overview of landslides and their impact at the European scale. As indicated above, an overview based on global databases is considered to be too coarse to provide an integral overview. Such an overview would, however, be highly desirable in further improving of safety measures for landslide risk mitigation in Europe.

Acknowledgments The authors would like to acknowledge Luca Demicheli Secretary General of EuroGeoSurveys, (Geological Surveys of Europe) for the success of the enquiry on national landslide inventories. Special thanks to Peter Bobrowsky (Geological Survey of Canada – GSC) for the information provided on the GSC Landslide Events Worldwide database.

References

Cellerino R (2006) Scuola superiore della pubblica amministrazione La difesa del suolo in Italia: aspetti economici ed amministrativi

Cruden DM (1991) A simple definition of a landslide. Bull Int Assoc Eng Geol 43:27–29

Cruden DM, Varnes DJ (1996) Landslide types and processes. In: Turner AK, Schuster RL (eds) Landslides investigation and mitigation. Special report 247, Transportation Research Board, Washington, DC, pp 36–75

EEA (2004) Europe's environment: the third assessment report (Environmental assessment report No 10). European Environment Agency, Copenhagen, 343p

EM-DAT (2011) Disaster in Number 2010 The OFDA/CRED – International Disaster Database Université catholique de Louvain Brussels – Belgium. www.emdat.be. 12p

Hervás J (ed) (2003) NEDIES project – lessons learnt from landslide disasters in Europe. Report EUR 20558 EN, Office of Official Publications of the European Community, Luxembourg, 91p

Jelínek R, Hervás J, Wood M (2007) Risk mapping of landslides in New Member States. European Commission, Joint Research Centre (EUR 22950 EN – 2007), 34p

NatCatSERVICE/MunichRe (2011) Topics Geo 2010 – Analyses, assessments and positions about the year of natural hazards. www.munichre.com/touch/naturalhazards, 50p

Schuster RL (1996) Socioeconomic significance of landslides. In: Turner AK, Schuster RL (eds) Landslides investigation and mitigation. Special report 247, Transportation Research Board, Washington, DC, pp 12–35

Schweigl J, Hervás J (2009) Landslide mapping in Austria, Joint Research Centre – European Commission (EUR 23785 EN – 2009), 61p

Sidle RC, Ochiai H (2006) Landslides: processes, prediction, and land use. Water Resources Monograph 18, American Geophysical Union, Washington, DC, 312p

Spizzichino D, Margottini C, Trigila A, Iadanza C, Linser S (2010). Chapter 9 Landslides. In: Mapping the impacts of natural hazards and technological accidents in Europe. An overview of the last decade. EEA technical report No 13/2010. ISBN 978-92-9213-140-1, pp 83–91

Trigila A, Iadanza C (2008). Landslides in Italy – Special Report 2008 (Rapporti ISPRA 83/2008), 34p

Trigila A, Iadanza C, Spizzichino D (2008) IFFI Project (Italian landslide inventory) and risk assessment. In: Proceedings of the first world landslide forum, United Nations University, Tokyo, ICL (International Consortium on Landslides) – ISDR (International Strategy for Disaster Reduction), 18–21 Nov 2008, pp 603–606

The Use of PSInSAR™ and SqueeSAR™ Techniques for Updating Landslide Inventories

Claudia Meisina, Davide Notti, Francesco Zucca, Massimo Ceriani, Alessio Colombo, Flavio Poggi, Anna Roccati, and Andrea Zaccone

Abstract

Measurements of ground deformation with millimetric accuracy and the reconstruction of the history of deformations in the last 20 years with Persistent Scatterer techniques have a high potential for landslides studies. In this work we analyze pro and cons of PSI techniques to update the Italian Inventory of Landslides (IFFI) using data from ERS 1/2 (1992–2001) and RADARSAT (2003–2010) satellites. The study area is located in North-Western Italy and belongs to three regions: Piemonte, Lombardia and Liguria.

Keywords

Landslides mapping • Persistent scatterer • NW Italy

Introduction

The Persistent Scatterer Interferometry applied to landslides studies have shown a rapid growth in the last years. Applications of the PSI techniques to landslide research can be found in Colesanti and Wasowsky (2006); Meisina et al. (2006, 2008); Pancioli et al. (2008); Herrera et al. (2011); Cascini et al. (2010); and Righini et al. (2010).

The PSInSAR™ technique developed by Ferretti et al. (2001) and the most recent SqueeSAR™ technique (Ferretti et al. 2011) allow measures of ground displacement by means of traditional permanent scatterers (PS) like buildings, rock and debris as well as from distributed scatterers (DS), which are homogeneous areas spread over a group of pixels in a SAR image such as rangeland, pasture, shrubs and bare earth. The SqueeSAR™ technique allows an increase of density of the points that register ground displacement especially in non-urban areas, as alpine sparse vegetation landscapes.

In this work we analyze benefits and limitations of two approaches (PSInSAR™ and SqueeSAR™) to update the Italian Inventory of Landslides (IFFI) (APAT 2007) using data from ERS 1/2 (1992–2001) and RADARSAT (2003–2010) satellites. The study area is located in North-Western Italy and belongs to three regions: Piemonte, Lombardia (Pavia province) and Liguria (Imperia province).

The Study Area

Geological, Geomorphological and Land Use Settings

The study area is wide, more than 29,000 km^2, and marked by different geological and geomorphological processes and land use settings, which have a strong influence on the landslide typology, on associated risk and on the efficiency of the advanced SAR analysis. Nearly 18,000 landslides are mapped in IFFI inventory of working area.

C. Meisina (✉) • D. Notti • F. Zucca
University of Pavia Earth and Environmental Sciences Department, via Ferrata, 1, Pavia, Italy
e-mail: claudia.meisina@unipv.it

M. Ceriani • A. Zaccone
Regione Lombardia, Milan, Italy

A. Colombo
ARPA Piemonte, Biella, Italy

F. Poggi • A. Roccati
Regione Liguria, Genoa, Italy

C. Margottini et al. (eds.), *Landslide Science and Practice*, Vol. 1,
DOI 10.1007/978-3-642-31325-7_10,

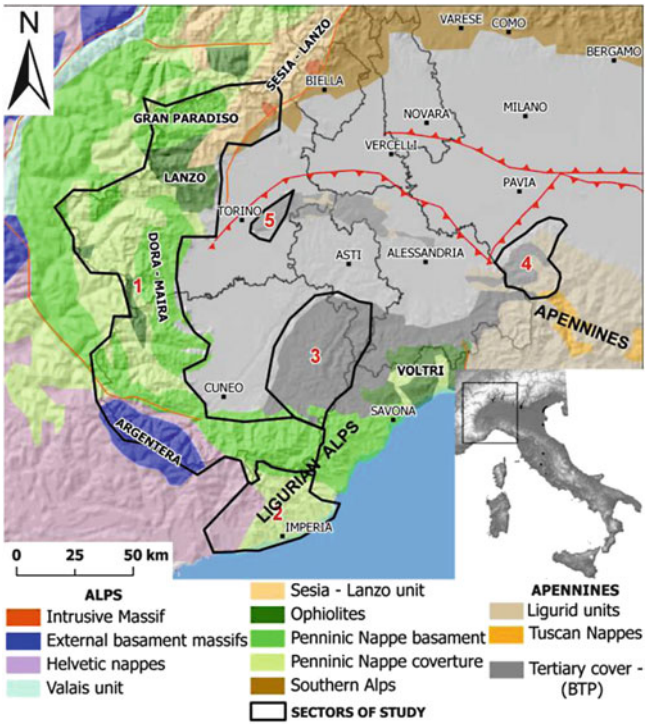

Fig. 1 Study area: *1* Alps, *2* Ligurian Alps, *3* Langhe Hills, *4* Oltrepo Pavese Apennines, *5* Turin Hills (Adapted from Handy et al. 2010)

It is possible to identify five main sectors (Fig. 1):

The Alps (sector 1). In the western sector the geological formations are represented by basement and covertures of Penninic nappes. It is possible to indentify from North to South: the Gran Paradiso gneiss massif, the ophiolitic massif of Lanzo, the calch-schist covertures of Susa Valley, the Dora-Maira gneiss massif. In the southern parts (Cuneo) we can find the Argentera external crystalline massif with a carbonatic – evaporitic coverture. The Alps are characterized by high slope gradients modelled by glacial action and many scarps are covered by talus debris. The main landslide processes are rock falls, complex landslides, debris flows and DSGSD (Deep Seated Gravitational Slope Deformations). The anthropic settlements have a medium-low density and they are concentrated along the valleys. The land use is mainly represented by woods, grassland, pasture, rock outcrop and debris.

In the Imperia Province (sector 2) four areas can be distinguished: (a) the "chaotic complex" area (Baiardo Flysch) with complex landslides; (b) the calcareous-marly flysch (Sanremo Flysch) characterized by DSGSD and large relict landslides; (c) the Ligurian Alps with complex landslides and slow flow of debris; (d) the coastal sector where rockfalls are dominant. The geomorphological setting is characterized by steep slopes modelled by fluvial erosion. The anthropic settlements are concentrated along the coast and in correspondence of gentle slope generally related to old landslide deposits. The land use at low altitude presents a Mediterranean environment, there are many flower greenhouses and terraces retained by stone made walls for olive cultivations. At a higher altitude land use is mainly woods and grassland.

The Langhe Hills (sector 3) correspond to the tertiary sedimentary basin (BTP) made of sandstone, marl and siltstone with monocline structure. The NW gentle slopes are affected by planar slides. The anthropic settlements are concentrated on the ridge of the hills; the land use shows many vineyards, walnuts and cultivated fields.

In the Apennines, in the southern part of Pavia Province (also Oltrepo Pavese) (sector 4) Ligurid nappes (Flysch, Chaotic Complex and shale) and Epi-ligurid nappes (marl, sandstone) outcrop. The slopes are usually gentle and affected by roto-translational slides, slow earth flows and complex landslides. The anthropic settlements are sparse and built often on relict landslides. The land use shows a prevalence of vineyards, cultivated fields at low altitude and woods towards higher altitude.

The Turin Hills (sector 5) present a geological setting similar to the Apennines with marl and sandstone and the main landslides are represented by shallow landslides and roto – translational slides. In this sector we have many sparse buildings in the proximity of Turin City.

The IFFI Landslide Inventories

IFFI is the Italian Landslide Inventory made on a regional scale for the whole country; it is based on aerial photos interpretation, field surveys and collection of historical data. For the study area landslides density ranges from 6 % in Imperia Province to 20 % in Apennines.

For the PSI analysis we consider only extremely slow and very slow-type landslides, as defined by Cruden and Varnes (1996): DSGSD, slow flows, roto-translational slides, complex landslides and the areas potentially affected by planar slides specific for Langhe Hills.

Some sectors of the study area are interesting for concentration of slow landslides: the calc-schists formation in the western Alps, which is affected by many DSGSD, or the shale and flysch formations (i.e. Val Luretta formation) in the Apennines affected by complex landslides.

The PSI Data

The regional study of PSI data was part of a project concerning the geological interpretation of PSInSAR™ and SqueeSAR™ data, carried out in collaboration with local regional environment agencies (ARPA Piemonte, Lombardia Region and Liguria Region). A big set of SAR scenes acquired

Table 1 Density of PS and DS in a sample area of Piemonte Alps

Land use	Density PS/km^2			% PS
	PS + DS	PS	DS	
Buildings	571.5	190.1	381.4	33.3
Highway	511.0	160.6	350.3	31.4
Railways	391.6	49.9	341.8	12.7
Urban area general	299.2	56.4	242.8	18.9
Mountains Grassland	83.9	3.4	80.5	4.1
Debris and rock	81.1	4.2	76.9	5.2
Grass land	51.6	3.5	48.1	6.8
Cultivate field	48.0	7.5	40.4	15.7
Beachwood	16.1	0.8	15.3	4.9
Chestnut wood	13.3	1.1	12.2	8.2
Larch wood	8.2	0.2	8.0	2.6
All area	63	8	54	13

between May 1992 and December 2000 by the ERS 1/2 satellite of the European Space Agency along ascending orbits and a set of scenes acquired between April 2003 and June 2010 by RADARSAT satellite along descending and ascending orbits were used by TeleRilevamento-Europa for a PSInSAR™ and/or SqueeSAR™ analysis. The RADARSAT PSI analyses for Piemonte and Liguria regions have been commissioned within the activities of the RISKNAT Alcotra Strategic Project, co-financed by the EU.

The analysis of PS/DS data showed that the landslide detection depends by some factors:

- Scatterers distribution (Table 1): the presence of natural scatterers (i.e. debris in alpine area and in Ligurian Alps) generally increases the number of landslides suitable for analysis, because debris (glacial, rock falls deposits) is a very good reflector. The presence of vegetation (i.e. Apennine and Langhe) led to a general lack of PS/DS;
- Typology of scatterer: some anthropic structures are very good reflectors (i.e. greenhouses, shacks with tin roofs or dry stone walls in Liguria), but they generally have a limited reliability as ground displacement markers;
- The type of sensor, which determines the incidence angle of LOS (Line of Sight): Radarsat sensor with an incidence angle of 34° allows to reduce the topographic effects on image respect to the incidence angle (23°) of ERS. In addition, ERS data present good quality only in descending geometry so many eastern slopes were not investigated;
- The type of technique: the SqueeSAR™ processing increases the density of information in the area covered by debris and mountain grassland, so in the Alps the increase of PS + DS density was very good (Table 1). In the area covered by buildings and in Apennines the density of SqueeSAR™ data, respect to the older PSInSAR™ processing, shows instead a weak increase.

The slow moving landslides suitable for a PSInSAR™ and/or SqueeSAR™ analysis are then a percentage of total. If we consider the landslides percentage with at least 2 PS and with a density over 30 PS/km^2 (we used these empiric thresholds to eliminate landslides with insufficient number or complete absence of PS/DS within the already mapped landslides). The best results concern the Imperia Province and the Alps; this may be related to the fact that landslides involve often urban areas with a high density of radar targets (e.g. Imperia province) or to the presence of debris deposits (e.g. Alps), which is a very good reflector. DSGSD are frequently covered by debris (due to the high deformation of rock mass), that is well distributed on slope, and then they are particularly suitable for a PSI analysis.

Updating the Landslide Inventories with PSI Data

The improvement to a landslide inventory can be in terms of identification of new landslides, modification of the boundaries of pre-existing landslides and assessment of their state of activity.

Identification of New Landslides and Modification of the Boundaries of Pre-existing Landslides

For the identification of new landslides and for the modification of the boundaries of pre-existing landslides a procedure was adopted based on the "anomalous areas" (Meisina et al. 2008).

The "anomalous areas" consist of clusters of minimum three PS, with a "search radius" of 50 m among the points, characterized by displacement rates over to 2 mm/year that are above a significant threshold background related to the technique precision. Interpretation phase of the anomalous areas was done through the integration in a GIS environment of the PS/DS data with topographic maps at 1:10,000 scale, aerial orthophotos of different periods, geological map, Digital Elevation Model (20 × 20 m or 10 × 10 m), landslide inventory and geotechnical and monitoring database.

The PSInSAR™ and SqueeSAR™ analysis estimate the Line Of Sight (LOS) surface displacement rate, which is a percentage of the real movement in relation to the slope orientation towards the LOS (Fig. 2). This can result in an underestimation of the landslide displacement rates.

To take into account the above consideration, the LOS velocity vector (Vel LOS) was then projected along the slope (Vel Slope) on the basis of slope and aspect models derived from DEM (Fig. 3). Nevertheless, this procedure is useful only when the displacement is quite parallel to the slope.

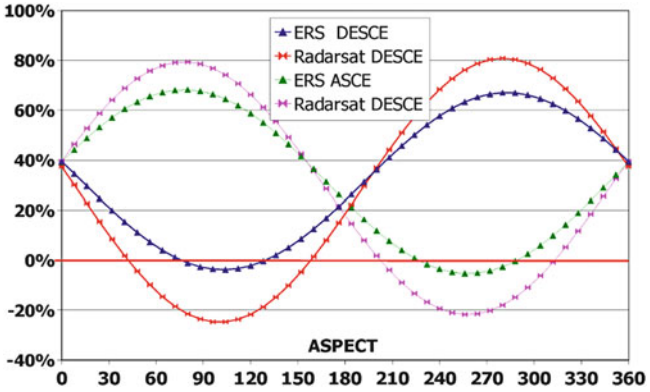

Fig. 2 Percentage of the movement along the slope registered along the LOS, for a slope of 20° with different satellites and geometries of acquisitions

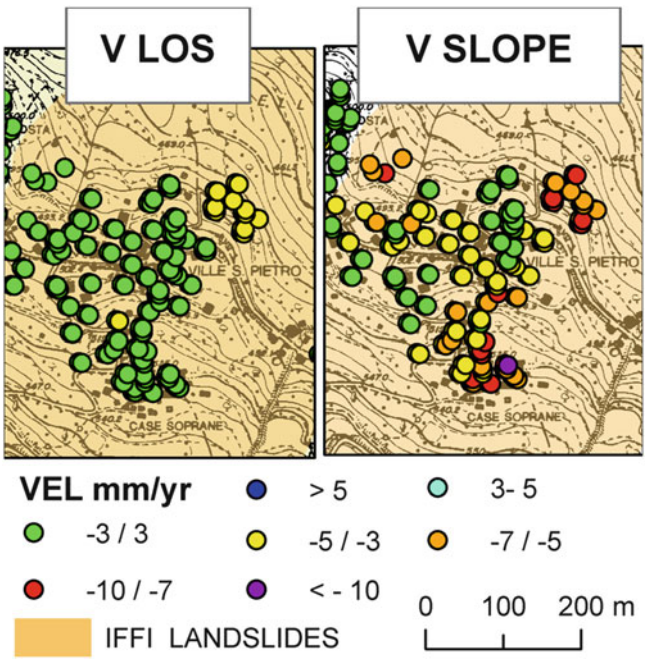

Fig. 3 Landslide of Ville San Pietro (Ligurian Alps). The projection of the velocity along the slope allows to detect a sector with movement not visible in LOS geometry

Using the velocity projected along the slope of both acquisition geometries new "advanced anomalous areas" were then created. An example is represented by the Susa Valley (Fig. 4), where the results show a clear correlation between the Vel slope and the presence of landslides.

The presence of horizontal component is another important evidence in the interpretation of landslide processes and in the detection of new landslides. The availability of PS/DS data in both ascending and descending geometries enhanced the coverage of the study area and enabled the estimation of vertical and E-W horizontal

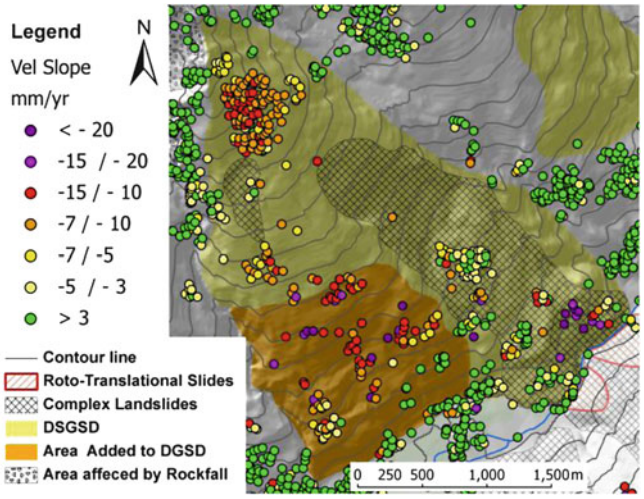

Fig. 4 The DSGSD of Serlavoute in the Susa Valley (Turin). The boundary of this deformation was updated using the SqueeSAR data

displacement components. Due to the LOS geometry of the sensors it is not possible to determine the N-S component of the movement. In order to combine the ascending and the descending data raster maps of interpolated values of the ascending and descending velocity were created. Then the two raster maps were combined with a trigonometric algorithm only for the area where the PS/DS data had high density (i.e. >50 PS-DS/km^2) (Fig. 5). This procedure is important because it was possible to know if the movement registered by PS/DS was also compatible with landslides kinematics and to define the typology of the landslide phenomenon. The calculation of vertical and horizontal E-W deformation components showed good results in the Apennines and Langhe Hills where the gentle slopes allow to have many areas with both ascending and descending geometries.

Another problem in the landslides inventory updating is the interpretation of the movement detected by PS/DS. On such regional analysis only for few sites it is possible to have detailed studies or other geological – monitoring data. This results in the difficulty to discriminate the movement due to landslide from that due to other phenomena, so for many anomalous areas it was not possible to classify them as "new" landslides. For instance in some areas like in Alps and in Liguria it was difficult to distinguish local debris movements or soil/ice creep from a landslide movement. On the other hand, in the areas where PS are mainly buildings, it is important to take also in account the movements related to settlement or structural problem of single buildings.

In addition to geomorphological evidences, some PS/DS parameters were used to discriminate between landslides and other processes. A high average velocity, the homogeneity of the movement (homogeneity index = PSmov/PStot),

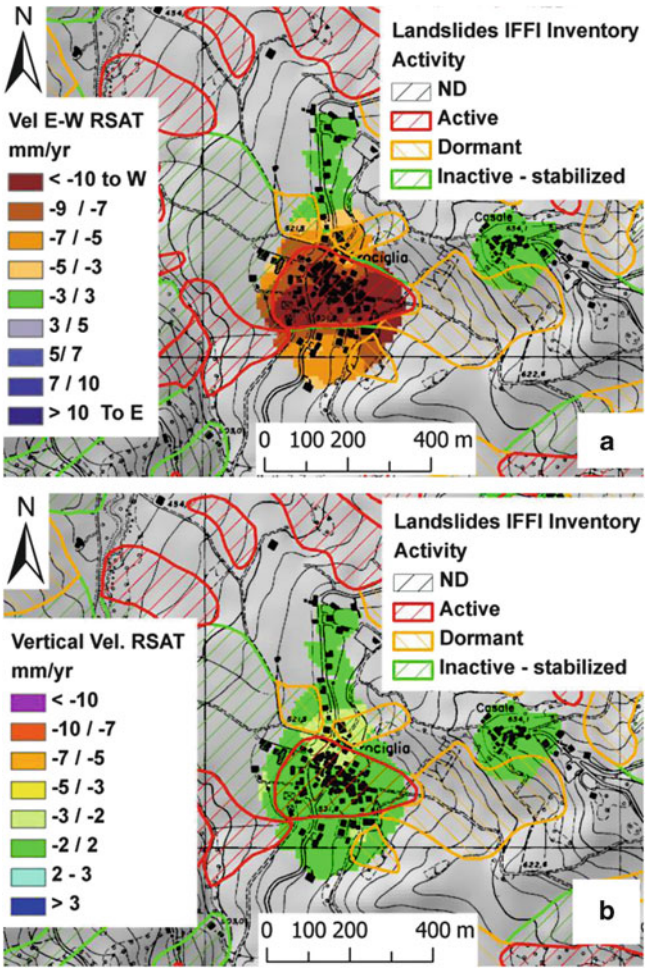

Fig. 5 Crociglia landslide (Pavia Apennines). By resolving the components of the velocity it was possible to observe a strong West component (**a**) and a weak vertical component (**b**), which was compatible with a translational slide on the gentle slope toward West. A new landslide was then added

the areal extensions and, where it was possible to resolve the velocity, the presence of horizontal component, were index of a possible landslide. An example is represented by south-eastern slope of M. Gerbonte in Ligurian Alps (Fig. 6), made of limestone dipping towards NW and covered by large size debris in a finest matrix with a thickness up to 3 m. The high values of vlos (−8 mm/year), the homogeneity of the movement (homogeneity index = 89 %), coupled with geomorphological evidences derived by aerial photointerpretation, allow us to map new landslides classified as slow flow of debris.

Nevertheless, in some cases it was not possible to recognize geologic and geomorphologic evidences of the movement, even if the PS/DS indicators of movement were present; then we introduced for these areas the term "areas with some evidences of instabilities", which require more detailed studies at local scale.

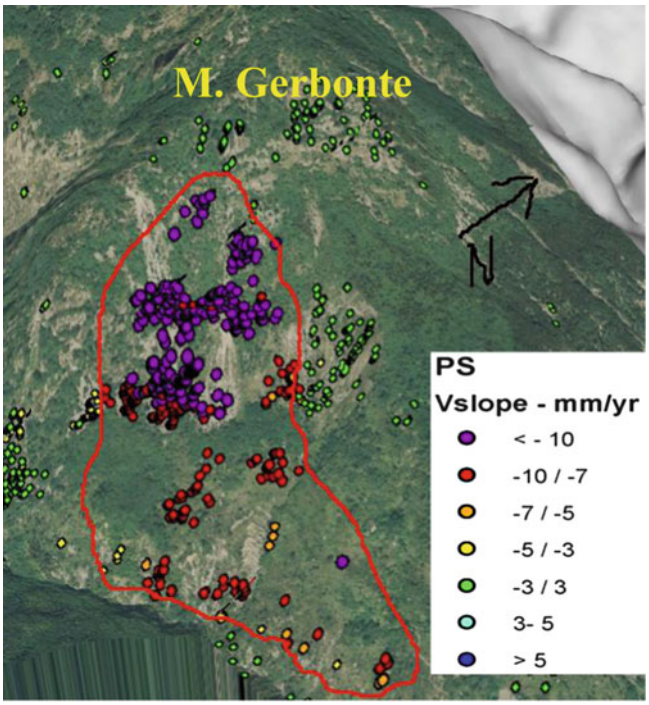

Fig. 6 New landslide in the Ligurian Alps

Assessment of the State of Activity

The assessment of the state of activity of a landslide with PSI data requires to take into account the following factors:

1. The satellite orbit (approximately N-S) strongly limits the technique capabilities for detecting processes with N-S direction of movements; if the true movement direction is not along the LOS, the velocity is then an underestimate of the true velocity. This especially for processes with large horizontal component (e.g. translational slide);
2. All values are relative to a reference point assumed to be stable;
3. Standard deviation of velocity errors increases with distance from the reference point, which could be quite distant from the area of interest.

The above considerations result in limitation to assess the state of activity of landslides at regional scale. In the study area, when the inventory was not in agreement with PS/DS data each landslide was separately analyzed. Generally the previous state of activity of dormant or active landslides was not lowered even if PS data did not register movement rates. For the assessment of the state of activity, it is often necessary to compare the PS data, in particular their time series, with field evidences and in situ monitoring data where available.

The Imperia Province and the Oltrepo Pavese were characterized by the presence of high number of inactive or relict landslides within urban areas (the gentle slopes and the water availability are favourable conditions for human

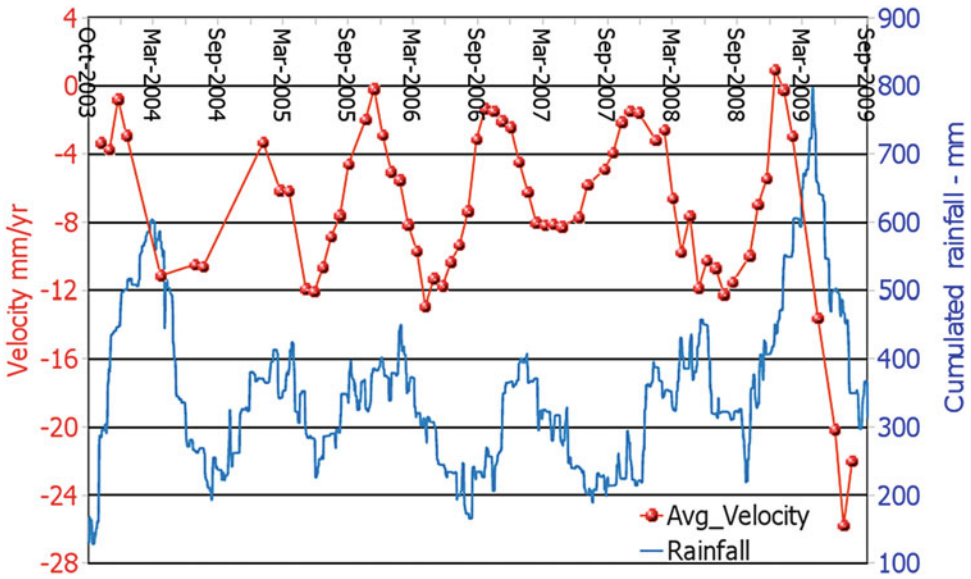

Fig. 7 Landslide of Crociglia. Comparison between the velocity of PS calculated with time series of RADARSAT descending data (2003–2009) and the rainfall cumulated in the previous 6 months

settlement). Within these landslides the PS/DS data often registered important movement rates, not in agreement with the inventory state of activity.

An example is represented by the Crociglia landslide located in the Oltrepo Pavese, on the right side of Morcione Stream at 500–600 m a.s.l. (Fig. 5). From the geological point of view the area is characterised by the presence of a shale succession covered by limestone, marl sandstone and thin shale. Colluvium and landslide deposit cover most of the area, with a thickness ranging between 3 and 12 m. The IFFI landslide database identifies the presence of a large complex landslide classified as inactive – stabilized, that affect the slope; some minor reactivation may be present at the toe of the slope.

The PS/DS data show displacement rates with maximum value in the central area of Crociglia village (Vlos for descending dataset = −6/−7 mm/year; Vslope = −10/−15 mm/year). The vertical and horizontal E-W deformation components, calculated with RADARSAT data, showed a strong horizontal component (8–10 mm/year toward West) and a limited vertical component (1–2 mm/year), in agreement with a movement along the slope with an inclination angle between 5° and 10° (translational slide).

The time series of ERS data show two clear trends, one in the period May 1995–May 1997 with a an average velocity up to −10 mm/year, the second in the period 1997–2000 with an average velocity of −3 mm/year and an acceleration at the end of 2000. These trends can be correlated with long term rainfall.

The RADARSAT data, characterized by less noised data, result in better time series (Fig. 7). Also in this case it is possible to find different trends. A notable acceleration of movement up to −20 mm/year is evident in the period 2008–2009 and can be related with a very wet and snowy period from December 2008 to April 2009. Seasonal trends are also evident. It is possible to distinguish two period per year: from June to October a "dry" period when the velocity is usually less than −4 mm/year (along LOS), while in the winter – spring period the velocity is between 10 and 15 mm/year (along LOS).

The analysis of advanced SAR data, coupled with observation of aerial photos and field surveys, suggest us to don't change the state of activity for the large inactive landslide but to add to the IFFI inventory, a new landslide corresponding to a shallow translational slide in correspondence of the Crociglia village, with displacement strongly related to the rainfall events. Its presence is also confirmed by trench pits which identify a possible sliding surface at a depth of 4–5 m.

Conclusion

The outcomes of this study demonstrate that the Persistent Scatterer Interferometry (PSInSAR™ and SqueeSAR™) can give important contributions in updating landslide inventories. We improve also our methodology of SAR data analysis and interpretation by creating the "advanced anomalous areas" using some tools to project the velocity along the slope and to resolve the vertical and E-W component.

The advanced SAR data were used to map new processes, to modify landslide boundaries, to assess their state of activity and to better understand sliding kinematics. However these techniques are limited to very slow processes. Moreover on a regional scale the different geological-geomorphological-land-use settings and type of processes have a strong influence on the PSI efficiency in updating the landslide inventory. In the whole study area the PSI allows to obtain different results in the different geological and geomorphological contexts:

– Alps: this sector is the most suitable for the persistent scatterers application; due to the presence of debris, the density of PS/DS data is very high. More than 30 % of slow landslides are characterized by PS/DS data, for DSGSD the percentage is up to 50 %. In Piemonte Alps the preliminary results show that about 50 probable new landslides could be added to pre-existing inventory and that the boundaries of about 100 landslides had to be updated. It is important to remind however, that the majority of the new landslides are slow flows affecting talus debris in areas without human settlements. The new landslides detected are not very interesting from geological – risk planning point of view, but they may be interesting for scientific studies;
– Imperia province (Maritime Alps): in this sector the density of PS/DS data is high, scatterers are represented by both debris and anthropic structures. Also in this sector about 30 % of landslides have significant PS/DS data and most of these landslides involve urban area. The interpretation of PSI data allow us to map a limited number of new landslides;
– Langhe hills, Oltrepo Pavese (Apennines) and Turin hills: in these sectors the density of PS/DS data is much lower than in the Alps and the percentage of the landslides suitable for a PS/DS analysis is between 3 % and 20 %. However, in this sector the scatterers are represented mainly by buildings and other infrastructures, so the movements detected are important from the point of view of risk management.

In the Oltrepo Pavese, as in the Imperia province, many large landslides, affecting entire villages, are classified as relict or inactive by pre-existing landslide inventory, nevertheless, some of these show high PS/DS displacement rates. From the hazard-risk planning point of view a landslide with a movement of few mm/year is considered active but the related damages may be absent or not relevant, on the other hand a landslide with stable PS may be more dangerous in case of re-activation. The assessment/change of the state of activity of a landslide with PSI data requires to be carefully done and it is often necessary to compare the PS data with field evidences and in situ monitoring data where available.

References

APAT (2007) Rapporto sulle frane in Italia. Il progetto IFFI: metodologia, risultati e rapporti regionali – Rapporti – 78/2007, ISBN 978-88-448-0310-0

Cascini L, Fornaro G, Peduto D (2010) Advanced low- and full-resolution DInSAR map generation for slow-moving landslide analysis at different scales. Eng Geol 112:29–42

Colesanti C, Wasowsky J (2006) Investigating landslides with space-borne Synthetic Aperture Radar (SAR) interferometry. Eng Geol 88:173–199

Cruden DM, Varnes DJ (1996) Landslide types and processes. In: Turner AK, Shuster RL (eds) Landslides: investigation and mitigation. Special Report 247, Transport Research Board, pp 36–75

Ferretti A, Prati C, Rocca F (2001) Permanent scatterers in SAR interferometry. IEEE Trans Geosci Remote Sens 39:8–20

Ferretti A, Fumagalli A, Novali F, Prati C, Rocca F, Rucci A (2011) A new algorithm for processing interferometric data-stacks: squeeSAR. IEEE Trans Geosci Remote Sens 49(9):3460–3470

Handy MR, Schmid SM, Bousquet R, Kissling E, Bernoulli D (2010) Reconciling plate-tectonic reconstructions of Alpine Tethys with the geological-geophysical record of spreading and subduction in the Alps. Earth-Sci Rev 102:121–158

Herrera G, Notti D, Garcıa-Davalillo JC, Mora O, Cooksley G, Sanchez M, Arnaud A, Crosetto M (2011) Analysis with C- and X-band satellite SAR data of the Portalet landslide area. Landslides 8(2):195–206

Meisina C, Zucca F, Fossati D, Ceriani M, Allievi J (2006) Ground deformation monitoring by using the permanent scatterers technique: the example of the Oltrepo Pavese (Lombardy, Italy). Eng Geol 88:240–259

Meisina C, Zucca F, Notti D, Colombo A, Cucchi A, Savio G, Giannico C, Bianchi M (2008) Geological interpretation of PSInSAR data at regional scale. Sensors 11:7469–7492

Pancioli V, Raetzo H, Campolmi T, Casagli N (2008) Terrafirma landslide services for Europe based on space-borne InSAR data. In: Proceedings of the first world landslide forum, United Nations University, Tokyo, pp 81–84

Righini G, Pancioli V, Casagli N (2010) Updating landslide inventory maps using Persistent Scatterers Interferometry (PSI) in the Biferno River Basin (Central Italy). Geophys Res Abstr 12, EGU2010-2676, EGU General Assembly 2010

Combining Multiple Change Detection Indices for Mapping Landslides Triggered by Typhoons

Alessandro C. Mondini, Kang-tsung Chang, Hsiao-Yuan Yin, and Fausto Guzzetti

Abstract

An important part of landslide research is the interpretation and delineation of landslides, which has increasingly been based on high-resolution satellite images in recent years. Using pre- and post-event FORMOSAT-2 satellite images as the data sources, this study presents a new method that combines four change detection techniques for mapping shallow landslides triggered by typhoons in Taiwan. The four techniques are normalized differential vegetation index (NDVI), spectral angle, principal component analysis, and independent component analysis. We applied the Multiple Change Detection (MCD) technique to map landslides triggered by typhoons. Comparisons were then made between MCD results with landslide inventory maps compiled by using a single index (NDVI). Comparison results show that MCD can perform better than a single index in dealing with old landslides and landslides with non-homogeneous spectral responses. MCD is also able to detect small landslides, which are often missed by visual analysis. Additionally, landslide maps prepared by MCD include runout features of sediment deposits from debris flows. A relatively fast processing chain, MCD is expected to become a useful new tool for emergency management after a typhoon event, which occurs on average four to five times a year in Taiwan.

Keywords

Landslide • Remote sensing • Change detection

Introduction

Landslides are triggered by earthquakes, storms, rapid snow melt, human activities such as timber clearcut or road construction, or a combination of these factors (Aleotti and Chowdhury 1999). Landslides are classified by morphology, material, mechanism of initiation, and other criteria (Cruden 1991; Dikau et al. 1996). This paper focuses on shallow landslides. Shallow landslides, either new or reactivated, refer to failures on soil mantled slopes with depths generally less than 2 m. Shallow landslides on steep slopes may evolve into debris flows as geomaterials break up, mix with water, move downslope, and deposit on lowland areas (Takahashi 1978). Landslide mapping is an important part of landslide research because maps showing observed landslides are the necessary input for calibration and validation of landslide susceptibility models (Guzzetti et al. 2006; Chang et al. 2007; Rossi et al. 2010). For evaluation of the model performance, predicted landslides must be directly compared with observed landslides; therefore, unless observed landslides are correctly mapped, they cannot be used as a basis for comparison. Traditionally, landslides are interpreted and delineated manually on stereoscopic aerial photographs

A.C. Mondini (✉) • F. Guzzetti
CNR, Consiglio Nazionale delle Ricerche, Istituto di Ricerca per la Protezione Idrogeologica, 06128 Perugia, Italy
e-mail: alessandro.mondini@irpi.cnr.it

K.-t. Chang
Kainan University, 33857 Taoyuan County, Taiwan

H.-Y. Yin
Soil and Water Conservation Bureau, 54044 Nantou County, Taiwan

C. Margottini et al. (eds.), *Landslide Science and Practice*, Vol. 1,
DOI 10.1007/978-3-642-31325-7_11,

by an experienced interpreter using morphologies typical of slope movements such as scarps, deposit zones, disturbed vegetation, and disturbed channels or roads as visual cues (Dikau 1999; Saba et al. 2010). Manual interpretation, however, is tedious and expensive. Moreover, aerial photographs can cover only small areas and the revisiting interval of aerial coverage is limited and irregular.

In recent years, high-resolution (HR) satellite images have started to replace aerial photographs for mapping landslides (van Westen et al. 2008; Saba et al. 2010). Various techniques, including visual analysis, image differencing, change vector analysis, maximum likelihood classifier, normalized differential vegetation index, principal component analysis, and object-based image analysis, have been used to interpret landslides from satellite images (Petley et al. 2002; Cheng et al. 2004; Haeberlin et al. 2004; Nichol and Wong 2005; Rosin and Hervás 2005; Restrepo and Alvarez 2006; Borghuis et al. 2007; Martha et al. 2010; Tsai et al. 2010).

This paper uses a *multiple change detection (MCD)* technique, a data processing chain, which makes use of HR satellite images and combines four change detection techniques to semi-automatically recognize and map landslides triggered by a single event. A case study is presented: it involves landslides triggered by the record-breaking Typhoon Morakot. The technique performs well and it shows its capability in interpreting new landslides, old landslides, and sediment deposits of debris flows. Locally, runout features can be separated from landslides. Additionally, the technique is relatively fast in data processing, making it useful for emergency management after a major event such as Typhoon Morakot.

Method

MCD combines four different techniques for detecting changes occurring between pre- and post-event VHR or HR images through a supervised or unsupervised classification (Mondini et al. 2011) to identify and map new shallow landslides triggered by typhoons or strong and prolonged rainfalls.

MCD involves two spectral indices, Normalized Differential Vegetation Index (NDVI) and Spectral Angle (SA), and two geometric transformations, Principal Component Analysis (PCA) and Independent Component Analysis (ICA).

Change in NDVI (δNDVI) between the pre- and post-event images is defined as:

$$\delta NDVI = NDVI_{\text{pre}} - NDVI_{\text{post}} = \left(\frac{NIR - red}{NIR + red}\right)_{\text{pre}} - \left(\frac{NIR - red}{NIR + red}\right)_{\text{post}}$$

where NIR is the radiance in the near-infrared band (0.76–0.90 μm) and red is the radiance in the red band (0.63–0.69 μm). Loss of vegetation caused by new landslides corresponds to large negative δNDVI.

Spectral angle (SA) is an index expressing the difference of the spectral values between homologous pixels in the pre- and post-event images (Sohn et al. 1999; Sohn and Rebello 2002; Masek and Sun 2004):

$$SA = \arccos\left(\frac{u \cdot v}{|u| \cdot |v|}\right)$$

where $u = [\tilde{n}_{\text{blue}}, \tilde{n}_{\text{green}}, \tilde{n}_{\text{red}}, \tilde{n}_{\text{NIR}}]_{\text{pre}}$ and $v = [\tilde{n}_{\text{blue}}, \tilde{n}_{\text{green}}, \tilde{n}_{\text{red}}, \tilde{n}_{\text{NIR}}]_{\text{post}}$ are the spectral vectors from the pre- and post-event images. SA is a metric of spectral changes between pre- and post-event images. It is less sensitive than δNDVI but it can detect new landslides in non-vegetated areas.

PCA and ICA are both linear combinations of the original variables (pre- and post-event multispectral images), projected along new orthogonal axes, obtained by exploiting the criteria of maximum variance (Richards 1984) with PCA, or independence (Hyvärinen et al. 2001; Robila 2005) with ICA.

δNDVI and SA measure changes between homologous single pixels in the pre- and post-event images, whereas PCA and ICA extract global parameters from the whole images for each spectral band. δNDVI and SA produce one image each, and PCA and ICA produce four component images each. Based on a previous study (Mondini et al. 2011), which used the same four techniques for multivariate classification of landslide and stable cells, only one each of the PCA and ICA components are needed as inputs for the next step of data analysis. The component to be selected is the one that has the highest correlation coefficient, either positive or negative, with δNDVI and SA. Thus, the component can complement δNDVI and SA in detecting and delineating landslides.

An unsupervised classification method such as Isodata (Interactive Self-Organizing Data Analysis) (Richards and Jia 1999) clusters pixels into distinct classes, each with similar change detection index values. For this study, the inputs to the unsupervised classification comprised: (1) δNDVI image, (2) SA image, (3) one Principal Component image, and (4) one Independent Component image. An Isodata classification initially grouped pixels into ten classes. These ten classes were then collapsed into two in this study: new landslides and stable areas. Post-processing of classification results included sieving and clumping to remove isolated pixels (the "salt and pepper effect"), contouring, and converting to vector format. The final product was a landslide inventory map outlining all changes in the study area due to landslides.

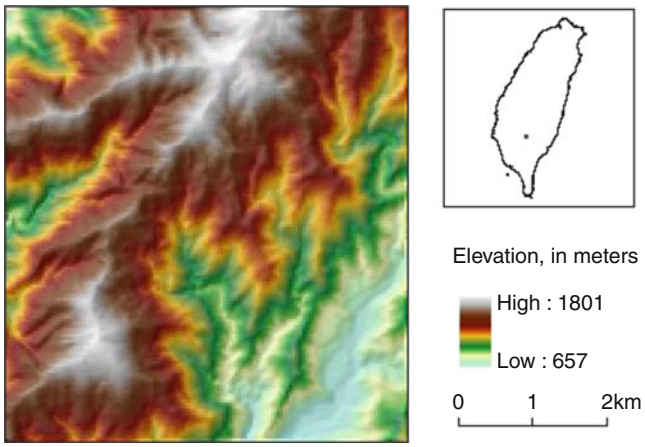

Fig. 1 Study area

Test Cases

Area

The 31.8 km^2 study area, defined by the availability of orthophotos, is located within the region badly affected by Typhoon Morakot in southern Taiwan. Elevations in the study area range from 650 to 1,800 m a.s.l., with generally rugged topography (Fig. 1). Slopes derived from a 20 m DEM have an average of 29°, with 72 % of the study area between 20° and 40°. The mean monthly temperature is 26 °C in July and 17 °C in January. The annual precipitation averages 2,200 mm of which 90 % come from thunderstorms and typhoons between May and October.

The study area is dominated by an early middle Miocene formation, which is composed of black to dark gray arigillite, slate, and phyllite, with sandstone interbeds. The 2007 land use map from Taiwan's Ministry of Interior shows 90 % of the study area covered by natural or plantation bamboo and 6 % by a recreation area in the north. The remaining area is classified as exposed or abandoned land, agriculture, road, and water.

Typhoon Morakot (6–10 August 2009) traversed the island of Taiwan during a 5-day period. Accompanied with strong southwesterly monsoon, Typhoon Morakot set many new records in Taiwan, including 2,885 mm rainfall in 100 h recorded at a gauging station 50 km north of the study area. A vast area over the western hilly regions of the Central Mountain Range received more than the 1-year average precipitation (2,000 mm) in just 3 days (7–9 August). Thousands of landslides were triggered in mountainous terrains and large areas of lowlands were blanketed by severe flooding.

Data

Two FORMOSAT II level-4 multispectral (MS) images, dated July 3, 2007 and November 5, 2009, were used for the case study. Both images were taken at nadir. The co-registration error between the two images was less than one pixel with a standard deviation also below one pixel for both coordinates. It was verified by means of 15 homologous control points with an image-to-image procedure. Small local distortions were still experienced. These distortions could be caused by the loss of some ground control points during the typhoon event or the difference between the pre-event DEM and the post-event conditions.

The set of four digital orthophotos, taken on August 28, 2009, was made available from the Aerial Survey Office of Taiwan's Forestry Bureau These colour orthophotos were compiled from the stereo pairs of 1:5,000 aerial photographs. They have a pixel size of 0.35 m and an estimated horizontal accuracy of 0.5 m. Taiwan's Soil and Water Conservation Bureau (SWCB) provided this study with an inventory map showing landslides triggered by Typhoon Morakot in Taiwan (Fig. 3). According to the SWCB report, landslide areas were interpreted from FORMOSAT-2 images taken between August 17 and October 18, 2009. The analysis technique included the thresholding of NDVI values, removal of clouds and shadows, and manual adjustment of interpretation results. Interpreted landslide areas were post processed by using a slope filter ($<10°$) to remove agricultural fields and built-up areas and a minimum mapping unit of 24 m $\times$ 24 m (12 $\times$ 12 pixels).

Results

Figure 2 shows the result of three change detection layers in a composite red-green-blue image, the red represents δNDVI, the green the fourth ICA component, and the blue the fourth PCA component. In the composite, new landslides are colored blue and azure (due to the relative predominance of δNDVI and the fourth ICA component), old landslides are in white and pink (due to no strong predominance of δNDVI, the fourth ICA component, or the fourth PCA component), and stable areas are shown in green and maroon (due to the relative predominance of the fourth PCA component). Stable areas, whether vegetated or not, show very low and non-homogeneous index values (i.e., small changes in general). In contrast, pixels inside new landslides generally have high values of δNDVI (negative), SA (positive), PCA (positive), and ICA (negative). These pixels are typically grouped into two or three classes, instead of a single class, because of some non-homogeneous spectral response

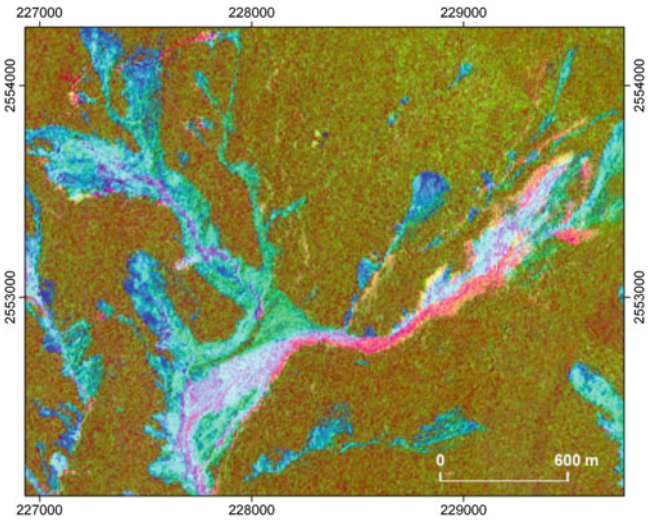

Fig. 2 Three change detection layers in a composite red-green-blue image, in which the *red* represents δNDVI, the *green* the fourth ICA component, and the *blue* the fourth PCA component

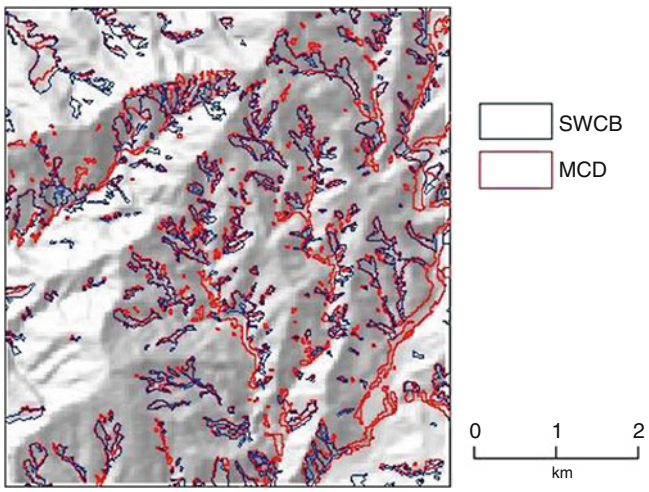

Fig. 3 Landslides mapped by MCD and landslides from the SWCB inventory map for the study area

Table 1 Statistical comparison between the SWCB inventory and the inventory obtained through the MCD technique

MCD results	SWCB	MCD
Smallest mapped landslide	311 m^2	64 m^2
Largest mapped landslide	246,809 m^2	418,208 m^2
N of landslides	302	343
Mean (area)	11,998 m^2	13,225 m^2
Total unstable area	3,623,283 m^2 (11.34 % of total area)	4,536,200 m^2 (13.69 % of total area)
SWCB ∩ MCD	2,373,222 m^2 (65.50 % of total unstable area)	2,373,222 m^2 (52.32 % of total unstable area)
Number of landslides intersects landslides in the other layer	247 out of 302 (81.79 %)	197 out of 343 (57.43 %)

in landslide areas and thus non-homogeneous behaviour in the pixels. Old landslides are more difficult to classify, depending on the vegetation condition. If the vegetation is not yet grown, an old landslide tends to have very low and uniform index values. But if the vegetation is already grown, an old landslide tends to have a high but positive δNDVI value, both behaviours allow to discriminate between new and old landslides. Locally, runout features can be separated from landslides through dedicated classification analysis. From the post-event image, the histograms of the red and green bands and the relative scatterplot of the pixels inside all three preselected unstable areas by MCD show two distinct classes. From a visual inspection, one can be mostly associated to landslides, the other, to runouts.

Figure 3 displays landslides mapped by MCD and landslides from the SWCB inventory map for the study area.

For statistical comparison, a filter with slopes lower than 10° was applied to the MCD results, similar to the post-processing for the SWCB inventory map. The filter removed large part of changes due to human activities and stream channels; however, most runouts were above 10°. Table 1 summarizes the statistical comparison. The MCD results have larger and more landslides than the SWCB inventory map. The overlapped area between the two accounts for 66 % of landslide areas in the SWCB inventory map and 52 % in the MCD results. 82 % of landslides in the SWCB inventory map intersect with landslides in the MCD results, while 57 % of landslides in the MCD results intersect with landslides in the SWCB inventory map.

Several other large runouts are also found within the study area. Together, these runouts, which are not included in the SWCB inventory map, explain the larger total landslide area and mean landslide area in the MCD results.

The MCD results also have more, small polygons than the SWCB inventory map. Some of these missing small landslides in the SWCB inventory map are probably due to the use of a single change detection index, while others because of the minimum mapping unit.

Some landslides are present in the SWCB inventory map but not in the MCD results. A visual inspection suggests that many of them are old landslides that are already present in the pre-event image (and then not related to the event) and others are not visible in the processed images.

Conclusions

Results have demonstrated that MCD can perform better than NDVI thresholding in presence of old landslides and, in particular, landslides with non-homogeneous spectral responses. At the same time, a semi-automatic method such as MCD can detect small landslides, which are often neglected in visual analysis.

When new landslides show homogeneous spectral response, results of PCA, ICA, *δNDVI*, and *SA* are similar and highly correlated. In general, landslides show non-homogeneous spectral responses due to the presence of shadow, different sun angles between the pre- and post-event images, different landslide disturbance patterns, different soil covers, or a combination of these effects. Under these conditions, the selection of an adequate threshold in a single index product image (like NDVI) becomes an hard or perhaps impossible task while MCD combined with a classification gets good results automatically by finding classes of unstable pixels still distinguishable from classes of stable one's.

In this study, we used the fourth PCA component and the fourth ICA component, which had the highest correlation coefficients with *δNDVI* and *SA*. The first three components in the PCA and ICA analysis contained limited information on new landslides because they either overlapped with other information sources or contained noise. At present, there is no evidence that the fourth component of ICA and PCA must always be related to new landslides even if it did happen in our case study. It cannot be excluded that some useful information for landslide recognition and mapping are present in the remaining components.

References

Aleotti P, Chowdhury R (1999) Landslide hazard assessment: summary review and new perspectives. Bull Eng Geol Environ 58:21–44

Borghuis AM, Chang K, Lee HY (2007) Comparison between automated and manual mapping of typhoon-triggered landslides from SPOT-5 imagery. Int J Remote Sens 28:1843–1856

Chang K, Chiang S, Hsu M (2007) Modeling typhoon- and earthquake-induced landslides in a mountainous watershed using logistic regression. Geomorphology 89:335–347

Cheng KS, Wei C, Chang SC (2004) Locating landslides using multi-temporal satellite images. Adv Space Res 33:296–301

Cruden DM (1991) A simple definition of a landslide. Bull Int Assoc Eng Geol 43:27–29

Dikau R (1999) The recognition of landslides. In: Casale R, Margottini C (eds) Floods and landslides: integrated risk assessment. Springer, Berlin, pp 39–44

Dikau R, Cavallin A, Jager S (1996) Databases and GIS for landslide research in Europe. Geomorphology 15:227–239

Guzzetti F, Reichenbach P, Ardizzone F, Cardinali M, Galli M (2006) Estimating the quality of landslide susceptibility models. Geomorphology 81:166–184

Haeberlin Y, Turberg P, Retiere Senegas O, Parriaux A (2004) Validation of SPOT-5 satellite imagery for geological hazard identification and risk assessment for landslides, mud and debris flows in Matagalpa, Nicaragua. In: Proceedings of the XXth ISPRS Congress, Istanbul. http://www.isprs.org/proceedings/XXXV/congress/comm1/papers/51.pdf. Accessed 4 Feb 2011

Hyvärinen A, Karhunen J, Oja E (2001) Independent component analysis. Wiley, New York

Martha TR, Kerle N, Jetten V, van Westen CJ, Kumar KV (2010) Characterising spectral, spatial and morphometric properties of landslides for semi-automatic detection using object-oriented methods. Geomorphology 116:24–36

Masek JG, Sun G (2004) Technical note: a spectral-angle methodology for mapping net forest cover change in northeastern China. Int J Remote Sens 25:5629–5636

Mondini AC, Guzzetti F, Reichenbach P, Rossi M, Cardinali M, Ardizzone F (2011) Semi-automatic recognition and mapping of rainfall induced shallow landslides using optical satellite images. Remote Sens Environ 115:1743–1757

Nichol J, Wong MS (2005) Satellite remote sensing for detailed landslide inventories using change detection and image fusion. Int J Remote Sens 26:1913–1926

Petley DN, Crick WDO, Hart AB (2002) The use of satellite imagery in landslide studies in high mountain area. In: Proceedings of the 23rd Asian conference on remote sensing (*ACRS 2002*), Kathmandu, Nepal. http://www.gisdevelopment.net/aars/acrs/2002/hdm/48.pdf. Accessed 4 Feb 2011

Restrepo C, Alvarez N (2006) Landslides and their contribution to land-cover change in the mountains of Mexico and Central America. Biotropica 38:446–457

Richards JA (1984) Thematic mapping from multitemporal image data using the principal components transformation. Remote Sens Environ 16:35–46

Richards JA, Jia X (1999) Remote sensing digital image analysis. Springer, Berlin

Robila SA (2005) Using spectral distances for speedup in hyperspectral image processing. Int J Remote Sens 26:5629–5650

Rosin PL, Hervás J (2005) Remote sensing image thresholding methods for determining landslide activity. Int J Remote Sens 26:1075–1092

Rossi M, Guzzetti F, Reichenbach P, Mondini A, Peruccacci S (2010) Optimal landslide susceptibility zonation based on multiple forecasts. Geomorphology 114:129–142

Saba SB, van der Meijde M, van der Werff H (2010) Spatiotemporal landslide detection for the 2005 Kashmir earthquake region. Geomorphology 124:17–25

Sohn Y, Rebello NS (2002) Supervised and unsupervised spectral angle classifiers. Photogramm Eng Remote Sens 68:1271–1280

Sohn YS, Moran E, Gurri F (1999) Deforestation in north-central Yucatan (1985–1995): mapping secondary succession in forest and agricultural land use in Sotuta using the cosine of the angle concept. Photogramm Eng Remote Sens 65:947–958

Takahashi T (1978) Mechanical characteristics of debris flow. J Hydraul Div 104:1153–1169

Tsai F, Hwang JH, Chen LC, Lin TH (2010) Post-disaster assessment of landslides in southern Taiwan after 2009 Typhoon Morakot using remote sensing and spatial analysis. Nat Hazards Earth Syst Sci 10:2179–2190

van Westen CJ, Castellanos E, Kuriakose SL (2008) Spatial data for landslide susceptibility, hazard, and vulnerability assessment: an overview. Eng Geol 102:112–131

Very-High Resolution Stereoscopic Satellite Images for Landslide Mapping

Francesca Ardizzone, Federica Fiorucci, Michele Santangelo, Mauro Cardinali, Alessandro Cesare Mondini, Mauro Rossi, Paola Reichenbach, and Fausto Guzzetti

Abstract

Landslide inventory maps are essential for geomorphological studies, and to evaluate landslide hazard, vulnerability, and risk. Landslide maps, including geomorphological, event, seasonal, and multi-temporal inventory maps, are prepared using different techniques. We present the results of an experiment aimed a testing the possibility of using very high resolution, stereoscopic satellite images to map rainfall induced shallow landslides. Three landslide inventory maps were prepared for the Collazzone study area, Umbria, Italy. Two of the maps were prepared through the visual interpretation of stereoscopic satellite images and cover the periods January to March 2010, and March to May 2010. The third inventory map shows landslides occurred in the period January to May 2010, and was obtained through reconnaissance field surveys. We describe the statistics of landslide area for the three inventories, and compare quantitatively two of the landslide maps.

Keywords

Landslide inventory map • Satellite image • GIS

Introduction

A landslide inventory map is the simplest form of landslide map (Guzzetti et al. 2000), and shows the location and, where known, the date of occurrence, and the types of mass movements that have left discernable traces in an area. A landslide map is essential for geomorphological and ecological studies, and to evaluate landslide hazard, vulnerability, and risk. Landslide maps, including geomorphological, event, seasonal, and multi-temporal inventory maps (Cardinali et al. 2001; Guzzetti et al. 2006), are traditionally prepared exploiting different techniques, including the visual interpretation of stereoscopic aerial photographs (Bucknam et al. 2001; Cardinali et al. 2001), reconnaissance field survey (Dapporto et al. 2005; Cardinali et al. 2006; Santangelo et al. 2010), and analysis of archive information on historical landslide events (Taylor and Brabb 1986; Guzzetti et al. 2000; Salvati et al. 2009).

Availability of high resolution (HR) and very-high resolution (VHR) satellite images, and improved digital visualization and analysis techniques, has encouraged investigators to exploit satellite images to detect and map landslides (e.g., Mantovani et al. 1996; Saba et al. 2010). Stereoscopic and three-dimensional (3-D) models obtained from HR and VHR images can be examined visually to detect individual landslides, or groups of landslides, and to prepare landslide inventory maps (Alkevli and Ercanoglu 2010).

We present the results of an experiment aimed at testing the possibility of using VHR stereoscopic satellite images,

F. Ardizzone (✉) • M. Cardinali • M. Rossi • P. Reichenbach • F. Guzzetti
Consiglio Nazionale Delle Ricerche – Istituto di Ricerca per la Protezione Idrogeologica, Via della Madonna Alta 126, 06128 Perugia, Italy
e-mail: Francesca.Ardizzone@irpi.cnr.it

F. Fiorucci • M. Santangelo • A.C. Mondini
Consiglio Nazionale Delle Ricerche – Istituto di Ricerca per la Protezione Idrogeologica, Via della Madonna Alta 126, 06128 Perugia, Italy

Università degli Studi di Perugia, Piazza dell'Università1, 06123 Perugia, Italy

C. Margottini et al. (eds.), *Landslide Science and Practice*, Vol. 1,
DOI 10.1007/978-3-642-31325-7_12,

and innovative 3-D visualization technology, to prepare landslide inventory maps. The experiment was conducted in Umbria, Italy, where two inventories were prepared exploiting multiple sets of stereoscopic satellite images. A third inventory was obtained through a reconnaissance field survey conducted after a rainfall period that resulted in landslides. We measured the degree of matching between two inventories adopting the method proposed by Carrara et al. (1992) and Galli et al. (2008).

Study Area

The study area is in Umbria, Italy (Fig. 1), and extends for about 90 km^2, including 78.9 km^2 of hilly terrain. Sedimentary rocks, Cretaceous to Recent in age, crop out in the area, and comprise recent fluvial deposits, continental gravel, sand and clay, travertine, layered sandstone and marl, and thinly layered limestone (Servizio Geologico Nazionale 1980). Soils in the area range in thickness from a few decimeters to more than one meter. In Umbria, climate is Mediterranean with most of the precipitation falling from October to December, and from February to May. Landslides are abundant in the area, and are caused by meteorological triggers i.e., prolonged rainfall and rapid snowmelt. Mass movements in the area include shallow soil slides and flows, deep-seated slides and flows, and compound failures (Guzzetti et al. 2006; Galli et al. 2008). Shallow landslides occur primarily on cultivated or abandoned areas, and are rare in forested terrain. In the cultivated areas, mechanical ploughing and harrowing obliterate landslides features. For this reason, the lifetime of the individual shallow landslides rarely exceeds a few seasons, although reactivations and new slope failures are common where previous landslides have occurred (Fiorucci et al. 2011).

Materials and Methods

We prepared three inventory maps using two different methods: (1) visual interpretation of VHR stereoscopic satellite images, and (2) reconnaissance geomorphological field mapping. In this section, we first describe the satellite images, the hardware (HW) and software (SW) visualization technology, and the interpretation criteria used to prepare the landslide maps. Next, we discuss the production of the reconnaissance inventory map through field surveys, and we provide information on the rainfall history that has resulted in the mapped landslides.

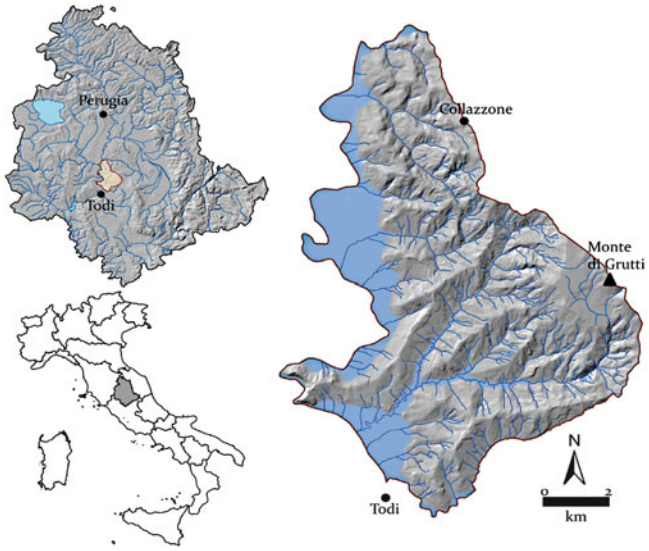

Fig. 1 Location and morphology of the Collazzone study area

VHR Stereoscopic Satellite Images

For our experiment, we used VHR panchromatic images taken (1) by the GeoEye-1 satellite on 12 August 2009 and on 27 May 2010, and (2) by the WorldView-1 satellite on 8 March 2010. GeoEye-1 was launched in September 2008. Flying at an altitude of 681 km, it captures images at 0.41-m panchromatic (black & white, resampled at 0.50-m) and 1.65-m multispectral (resampled at 2-m) resolution. WorldView-1 was launched in September 2007. Operating from an altitude of 496 km, it takes images at 0.50-m panchromatic and 2-m multispectral resolution. Table 1 lists the main characteristics of the stereoscopic images taken by the two satellites and used to detect and map landslides in our study area.

Rational Polynomial Coefficients (RPCs) for the satellite images were available to us. RPCs provide a representation of the ground-to-image geometry, allowing for photogrammetric processing. We used the RPCs to generate 3-D models of each pair of stereoscopic satellite images. We estimated the accuracy of operation using eight check points. Horizontal accuracy of the models, measured by the root mean square error (RMSE), was 2.2 m for GeoEye-1 and 1.12 m for WorldView-1. Vertical accuracy was 2.0 m for GeoEye-1, and 1.9 m for WorldView-1. The Bi-dimensional RMSE was 2.9 m for GeoEye-1, and 2.2 m for WorldView-1. The obtained values are within the accuracy of a 1:10,000 topographic map.

Table 1 Characteristics of the stereoscopic satellite images acquired by the GeoEye-1 and the WorldView-1 satellites, and used in our work

	Date	Overlap (%)	Azimuth Angle (°)	Elevation Angle (°)
GeoEye-1	12/08/2009	90	45.18	86.18
GeoEye-1	12/08/2009	90	189.90	62.3
GeoEye-1	12/08/2009	90	349.99	61.97
GeoEye-1	12/08/2009	90	244.90	13.80
WorldView-1	08/03/2010	70	77.30	57.90
WorldView-1	08/03/2010	70	141.1	52.70
GeoEye-1	27/05/2010	95	8.41	72.26
GeoEye-1	27/05/2010	95	199.51	71.99

Hardware and Software Visualization System

We used ERDAS IMAGINE® and Leica Photogrammetry Suite (LPS) SW for block orientation, and Stereo Analyst for ArcGIS® SW for image visualization and landslide mapping. To obtain 3-D views of the VHR satellite images, we used the StereoMirrorTM HW technology (Fig. 2).

Using Stereo Analyst for Arc ArcGIS®, we studied the 3-D views of the topographic surface created with the oriented satellite images, and we collected 3-D geographical information on the landslides. The SW allowed preparing multiple sets of oriented images all having the same reference system. To map the landslides in real-world three-dimensional geographical coordinates, a 3-D floating cursor was used. When using a floating cursor, it is important that the cursor stays on the topographic surface. The SW facilitates the task with an automatic terrain following mode. We used image correlation to obtain elevation information using the floating cursor.

The StereoMirrorTM technology allows for the 3-D visualization of large areas. For our experiment, the area covered by the GeoEye-1 stereoscopic images was 13 × 17 km (160 km^2), and the area covered by the WorldView-1 stereoscopic images was 24 × 24 km (576 km^2). The ability to analyse in 3-D multiple sets of stereoscopic images for a large area proves important for landslide mapping, chiefly for multi-temporal mapping. The HW and SW technology simplified the acquisition of landslide information from stereoscopic images. Further, the landslide and morphological information was obtained in 3-D and stored directly in a GIS database, reducing the acquisition time and the problems (and errors) associated with the manual digitization of the landslide information and the construction of the geographical database (Galli et al. 2008).

Visual Interpretation Criteria

To recognize the landslides in the digital stereoscopic satellite images, we used the same interpretation criteria adopted by geomorphologists to identify landslides on stereoscopic aerial photographs. The interpreter detects and classifies a landslide based on experience, and on the visual analysis of a set of characteristic features (the landslide "signature") that can be identified on the images. These include: shape, size, tone, colour, mottling, texture, pattern of objects, site topography, and setting (Ray 1960; Allum 1966; Rib and Liang 1978; van Zuidam 1985). Because of the vertical exaggeration of stereoscopic vision, shape is the single most useful characteristic for the identification and classification of a landslide from aerial or satellite stereoscopic images. These photo-interpretation criteria were used to prepare the landslide inventory maps for the Collazzone area.

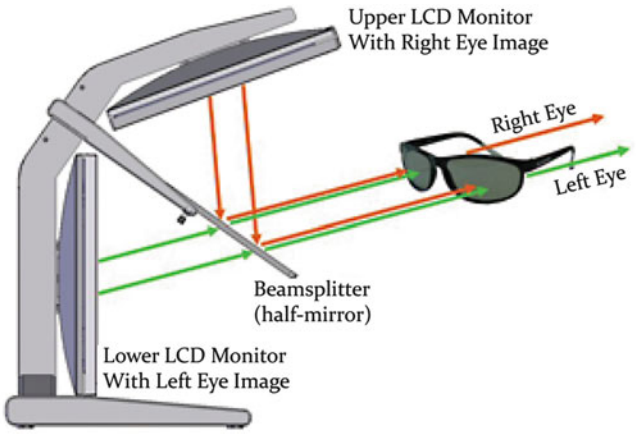

Fig. 2 Sketch of the StereoMirrorTM technology

Field Surveys

Following rainfall events in December 2009 (Fig. 3), we performed reconnaissance field surveys to identify and map rainfall-induced landslides in the study area. Four geomorphologists searched an area of about 90 km^2 in 4 days between January and March 2010. They drove and walked along roads, stopped where single or multiple landslides were identified, and at viewing points to check the slopes. Landslides were mapped in the field at 1:10,000 scale. Single and pseudo-stereoscopic colour photographs of landslides were taken with digital hand-held cameras. The cartographic and photographic information obtained

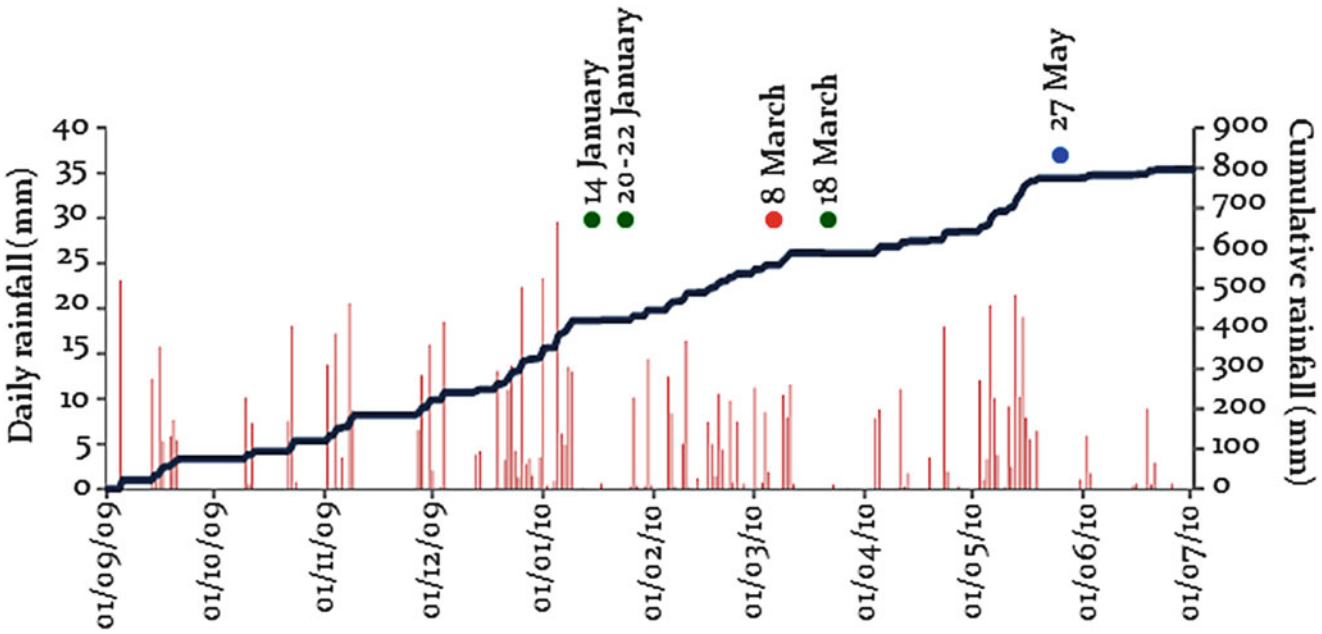

Fig. 3 Todi rain gauge (Fig. 1). Rainfall history in the period 1 September 2009–1 July 2010. *Bars* show cumulated daily rainfall. *Blue line* shows total cumulate rainfall. *Green dots* show dates of field surveys. *Red dot* shows date of WorldView-1 image. *Blue dot* shows date of GeoEye-1 image (Table 1)

in the field was used in the laboratory to map visually the individual landslides on 1:10,000 scale orthophotographs. The landslide and morphological information was then stored digitally in a GIS database.

Rainfall History

To investigate the rainfall conditions that have resulted in landslides in the study area in the period from September 2009 to May 2010, we used rainfall measurements obtained by the Todi rain gauge, located 3 km south of the study area (Fig. 1). In autumn 2009, the rain gauge measured 194 mm of rain, with 34.37 mm in 4 days between 14 and 17 September 2009. In the 2009–2010 winter, the rain gauge recorded 323.84 mm, with 170.86 mm in 22 days from 19 December 2009 to 9 January 2010. In the spring of 2010, the rain gauge measured a cumulated rainfall of 205 mm, with 132.34 mm in 17 days, 3–19 May 2010 (Fig. 3).

Results

For the Collazzone study area, we prepared three landslide inventory maps. Two maps were obtained through the visual interpretation of VHR stereoscopic satellite images taken on 12 August 2009 and 8 March 2010 by the GeoEye-1 and the World-View-1 satellites, (MAP A), and on 27 May 2010 by the GeoEye-1 satellite (MAP B). The third map (MAP C) was obtained through a reconnaissance field survey conducted between 14 of January and 18 of March 2010.

To detect and map the rainfall induced shallow landslides on 3-D digital representations of the stereoscopic satellite images, we adopted a multi-temporal approach (Fiorucci et al. 2011), and we recognized new landslides by comparing images of different dates. To prepare MAP A, we compared visually the GeoEye-1 images taken on 12 August 2009 t0 the World-View-1 images taken on 8 March 2010. Thus, MAP A is a seasonal landslide inventory covering the period August 2009–March 2010. Inspection of the rainfall record (Fig. 3) indicates that most of the landslides mapped in this inventory occurred presumably in the period between the end of December 2009 and the first decade of January 2010.

To obtain MAP B, we compared visually the World-View-1 images taken on 8 March 2010 with the next images obtained on 27 May 2010 by the GeoEye-1 satellite. Therefore, MAP B is a seasonal landslide inventory covering the period March–May 2010, with most of the landslides presumably occurred in the first half of May (Fig. 3). To obtain MAP C a reconnaissance field survey was carried out on 14, 20 and 22 January, and 18 March, 2010 with most of the landslides in the period between the end of December 2009 and the first decade of January 2010.

MAP A shows 159 shallow landslides (Fig. 4) ranging in size from 3.7×10^1 m^2 to 1.51×10^4 m^2, for a total landslide area ALT $= 2.94 \times 10^5$ m^2, 0.37 % of the hilly portion of the study area, an average of 2.0 landslides per square

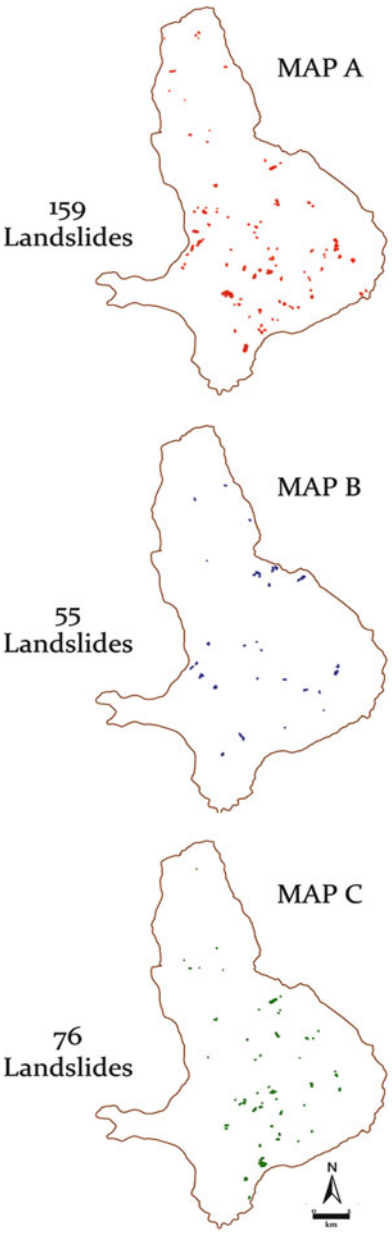

Fig. 4 Landslide inventory maps for the Collazzone study area. *MAP A* shows landslides mapped through the visual interpretation of the WorldView-1 stereoscopic images taken on 8 March 2010. *MAP B* shows landslides mapped through the visual interpretation of the GeoEye-1 stereoscopic images taken on 27 May 2010. *MAP C* shows the landslide inventory prepared through field surveys in the period January–March 2010

kilometre (Table 2). MAP B shows 55 shallow landslides (Fig. 4), with individual landslides in the range from 2.98×10^1 m^2 to 1.16×10^4 m^2, for a total landslide area ALT $= 8.52 \times 10^4$ m^2. This corresponds to 0.11 % of the hilly portion of the study area, an average of 0.7 landslides per square kilometre. The reconnaissance inventory shown in MAP C shows 76 landslides (Fig. 4) in the range of area from 4.59×10^1 m^2 to 1.89×10^4 m^2, for a total landslide area ALT $= 1.37 \times 10^5$ m^2, 0.17 % of the hilly portion of the study area, and an average of 0.04 landslides per square kilometre (Table 2).

Table 2 Descriptive statistics for the three landslide inventory maps available for the Collazzone study area

	MAP A	MAP B	MAP C
Area covered (km^2)	90.0	90.0	90.0
Hilly area (km^2)	78.9	78.9	78.9
N_L (#)	159	55	76
Min A_L (m^2)	3.7×10^1	2.98×10^1	4.59×10^1
Max A_L (m^2)	1.51×10^4	1.16×10^4	1.89×10^4
Mean A_L (m^2)	1.86×10^3	1.55×10^3	1.81×10^3
Median A_L (m^2)	1.01×10^3	9.78×10^2	9.82×10^2
St. Dev. A_L (m^2)	2.5×10^3	2.05×10^3	2.68×10^3
A_{LT} (m^2)	2.94×10^5	8.52×10^4	1.37×10^5
$\delta(A_L)$ # km^{-2}	2.0	0.7	0.04

Analysis of the Landslide Inventories

We analyse the landslide inventory maps studying the statistics of landslide area, and we compare quantitatively MAP A and MAP C that show landslides presumably occurred in the same period.

For each landslide map, the planimetric area was obtained in a GIS. Table 2 lists summary statistics for the mapped landslides in the three inventories. We estimated the frequency density distribution of the landslide areas for the three maps using the Inverse Gamma (IG) and the Double Pareto (DP) functions (Stark and Hovius 2001; Malamud et al. 2004) (Fig. 5). The two distributions provide similar results for the three inventories (Fig. 5, Table 3), with the standard error largest for MAP B, the map with the least number of landslides. In the three inventory maps the "rollover" in the distribution of landslide area is distinct. A problem exists with the estimation of the Double Pareto function for MAP B and MAP C, probably because of the limited number of landslides in these two maps.

To evaluate the geographical mismatch between MAP A and MAP C we use the Error index proposed by Carrara et al. (1992), and the corresponding Matching index proposed by Galli et al. (2008). The two indices quantify the degree of similarity between the different landslide maps, using:

$$E = \frac{(A \cup C) - (A \cap C)}{(A \cup C)} \quad 0 \le E \le 1 \qquad (1)$$

$$M = 1 - E \qquad 0 \le M \le 1 \qquad (2)$$

We applied (1) and (2) to the entire study area, and to individual landslides in the two inventories (MAP A and MAP C). Geographical union ($\cup$) and intersection ($\cap$) of

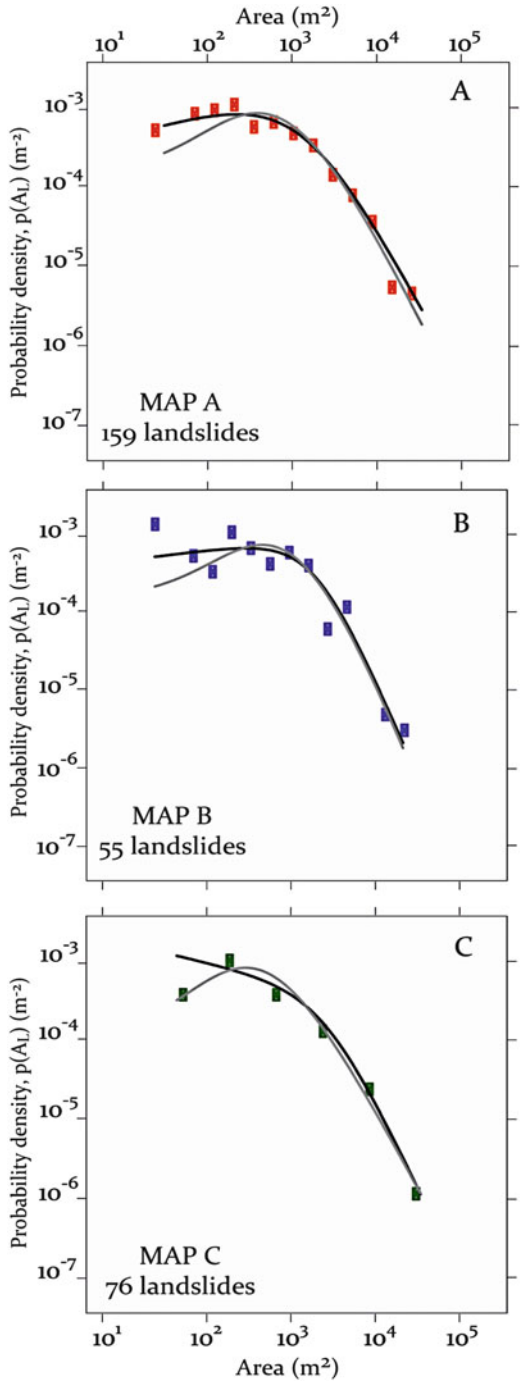

Fig. 5 Statistics of landslide size. The graphs show the probability density of landslide area, p(AL) for the three maps. *Coloured squares* are frequency values calculated by means of histogram estimation of logarithm of the data. *Black lines* are Double Pareto, and *grey lines* are Inverse Gamma models of p(AL) obtained through maximum likelihood estimation

MAP A and MAP C were obtained in a GIS. Geographical union of MAP A and MAP C was 3.73×10^5 m^2, and the landslide area common to both inventories was 5.89×10^4 m^2. The error index E was 0.84, and the corresponding match index M was 0.16. These values indicate a significant discrepancy between the two inventories (Galli et al. 2008). E indices (and M indices) for individual homologous landslides range from E = 0.35 to E = 0.90 (mean = 0.65, $\sigma = 0.15$), and M = 0.10 to M = 0.65 (mean = 0.35, $\sigma = 0.15$). The figures are similar to the values obtained by Santangelo et al. (2010) in a nearby area.

Table 3 Parameters estimated for the double Pareto (Stark and Hovius 2001) and the inverse Gamma (Malamud et al. 2004) models for the probability density of landslide area, p(AL)

	IG		DP	
	$\alpha + 1$ (ε)	$\bar{A}_L$ (m^2)	$\alpha + 1$ (ε)	$\bar{A}_L$
MAP A	2.45 (0.25)	325	2.24 (0.28)	201
MAP B	3.06 (0.65)	393	2.79 (0.55)	270
MAP C	2.20 (0.28)	250	2.49 (0.26)	270

Discussion and Conclusion

In the literature, most of the attempts to detect and map landslides using satellite imagery (Mantovani et al. 1996; Singhroy 2005) consisted in the recognition and mapping of slope failures that have left easily recognizable morphological signs, essentially evident changes in land cover (e.g., from dense forest to exposed soil and rock). In our experiment, VHR stereoscopic satellite images were used to detect and map landslides that did not result in distinct morphological or land cover signatures. This is an advancement compared to previous results.

The HW and SW used in the experiment allowed for the effective 3-D visualization of a large territory (>100 km^2), and simplified the acquisition of 3-D landslide information and storage in a GIS database. Advantages of the system include: (1) the ability to examine a large study area, (2) the possibility to dynamically zoom in and out and to change the image contrast during the visual inspection, facilitating the mapping of landslide of different sizes, and (3) the ability to digitize in 3D during the image interpretation phase, reducing the time and errors associated with the acquisition of landslide information in digital format (Galli et al. 2008).

The landslide inventory produced by visual interpretation of stereoscopic satellite images (MAP A) showed 109 % more landslides, and 114 % more landslide area than the reconnaissance landslide inventory (MAP C). We attribute the difference to the possibility of recognizing slope failures in the VHR stereoscopic images. The spatial resolution of the satellite images, 0.5×0.5 m for GeoEye-1 and WorldView-1, are adequate to detect and map the smallest landslides in the study area. Further, the vertical exaggeration of stereoscopic vision allowed for the detection of small (faint) morphological features related to landslides.

The area covered by the satellite stereoscopic images (>100 km^2) is comparable to the area covered by small-scale aerial photographs (1:50,000 and 1:75,000), and allows for obtaining enlargements up to 1:10,000 scale. The use of RPC information to generate the 3-D models allowed for obtaining accuracy levels comparable to the accuracy of 1:10,000 topographic base maps.

We estimated the probability density of landslide area $p(A_L)$ for the different landslide maps (Fig. 5, Table 3). Inspection of the probability density curves reveals similarities in the density distribution of landslide area, $p(A_L)$. All he empirical distributions exhibit the same general shape, with the density for large and very large landslides obeying a negative power law trend. The Double Pareto function revealed estimation problems for MAP B and MAP C, due to the reduced number of landslides in the two maps.

The geographical mismatch between landslide maps computed using the method proposed by Carrara et al. (1992) and Galli et al. (2008) revealed a discrepancy between the two inventories (MAP A and MAP C). The large error index, $E = 0.84$ depends chiefly on differences in the number of the mapped landslides in the two inventories. Cartographic mismatch for single landslides is smaller, $E = 0.65$ because of the better accuracy obtained by detecting, mapping, and digitizing directly the landslide information, when using the stereoscopic satellite images.

The experiment showed that VHR stereoscopic satellite and adequate 3-D viewing technology facilitates the production of accurate landslide inventory maps, even in areas where slope failures have left subtle signatures. This is an important step towards the systematic production of multi-temporal landslide inventories, seasonal landslide maps, and event landslide inventory maps. GeoEye-1 and WorldView-1 satellite sensors have revisiting times of only a few days (2 to 8 days for GeoEye-1, and 1.5 to 5 days for WorldView-1) allowing for the potential production of multi-temporal inventories and their rapid and frequent update. This is a mandatory step for landslide hazard and risk assessment, and for erosion and landscape evolution studies.

Acknowledgments Work conducted in the framework of the ASI MORFEO project. FF and ACM supported by a grant of the Italian Space Agency. MS and MR supported by a grant of the Italian Department for Civil Protection.

References

Alkevli T, Ercanoglu M (2010) Assessment of ASTER satellite images in landslide inventory mapping: Yenice-Gökçebey (Western Black Sea Region, Turkey). Bull Eng Geol Environ. doi:10.1007/s10064-011-0353-z

Allum JAE (1966) Photogeology and regional mapping. Institute of Geological Sciences, Photogeological Unit. Pergamon Press, Oxford (ISBN 9780080120324), 107p

Bucknam RC, Coe JA, Chavarria MM, Godt JW, Tarr AC, Bradley LA, Rafferty S, Hancock D, Dart RL, Johnson ML (2001) Landslides triggered by Hurricane Mitch in Guatemala – inventory and discussion. U.S. Geological Survey Open File Report 01–443

Cardinali M, Ardizzone F, Galli M, Guzzetti F, Reichenbach P (2001) Landslides triggered by rapid snow melting: the December 1996–January 1997 event in Central Italy. In: Proceedings of 1st EGS Plinius conference, Bios Publisher, Cosenza, 14–16 Oct 1999, pp 439–448

Cardinali M, Galli M, Guzzetti F, Ardizzone F, Reichenbach P, Bartoccini P (2006) Rainfall induced landslides in December 2004 in south-western Umbria, central Italy: types, extent, damage and risk assessment. Nat Hazard Earth Syst Sci 6:237–260

Carrara A, Cardinali M, Guzzetti F (1992) Uncertainty in assessing landslide hazard and risk. ITC J 2:172–183

Dapporto S, Aleotti P, Casagli N, Polloni G (2005) Analysis of shallow failures triggered by the 14–16 November 2002 event in the Albaredo valley, Valtellina (Northern Italy). Adv Geosci 2: 305–308

Fiorucci F, Cardinali M, Carlà R, Rossi M, Mondini AC, Santurri L, Ardizzone F, Guzzetti F (2011) Seasonal landslide mapping and estimation of landslide mobilization rates using aerial and satellite images. Geomorphology 129:59–70

Galli M, Ardizzone F, Cardinali M, Guzzetti F, Reichenbach P (2008) Comparing landslide inventory maps. Geomorphology 94:268–289

Guzzetti F, Cardinali M, Reichenbach P, Carrara A (2000) Comparing landslide maps: a case study in the upper Tiber River Basin, central Italy. Environ Manage 25(3):247–363

Guzzetti F, Galli M, Reichenbach P, Ardizzone F, Cardinali M (2006) Landslide hazard assessment in the Collazzone area, Umbria, central Italy. Nat Hazard Earth Syst Sci 6:115–131

Malamud BD, Turcotte DL, Guzzetti F, Reichenbach P (2004) Landslide inventories and their statistical properties. Earth Surf Proc Landf 29:687–711

Mantovani F, Soeters R, van Westen C (1996) Remote sensing techniques for landslide studies and hazard zonation in Europe. Geomorphology 15:213–225

Ray RG (1960) Aerial photographs in geological interpretation and mapping. Geological Survey Professional Paper 373, Washington, USA

Rib HT, Liang T (1978) Recognition and identification. In: Schuster RL, Krizek RJ (eds) Landslide analysis and control. Special Report 176, Transportation Research Board, National Academy of Sciences, Washington, DC, pp 34–80

Saba SB, van der Meijde M, van der Werff H (2010) Spatiotemporal landslide detection for the 2005 Kashmir earthquake region. Geomorphology 124:17–25

Salvati P, Balducci V, Bianchi C, Guzzetti F, Tonelli G (2009) A WebGIS for the dissemination of information on historical landslides and floods in Umbria, Italy. Geoinformatica 13:305–322

Santangelo M, Cardinali M, Rossi M, Mondini AC, Guzzetti F (2010) Remote landslide mapping using a laser rangefinder binocular and GPS. Nat Hazards Earth Syst Sci 10:2539–2546

Servizio Geologico Nazionale (1980) Carta Geologica dell'Umbria. Map at 1:250,000 scale (in Italian)

Singhroy V (2005) Remote sensing of landslides. In: Glade T, Anderson M, Crozier MJ (eds) Landslide hazard and risk. Wiley, New York, pp 469–492

Stark CP, Hovius N (2001) The characterization of landslide size distributions. Geophys Res Lett 28:1091–1094

Taylor F, Brabb EE (1986) Map showing landslides in California that have caused fatalities or at least $1,000,000 in damages from 1906 to 1984. U.S. Geological Survey Miscellaneous Field Studies Map, MF-1867

van Zuidam RA (1985) Aerial photo-interpretation in terrain analysis and geomorphologic mapping. ITC Smits, The Hague, p 442p

Mapping of Landslides Under Dense Vegetation Cover Using Object-Oriented Analysis and LiDAR Derivatives

Miet Van Den Eeckhaut, Norman Kerle, Javier Hervás, and Robert Supper

Abstract

Light Detection and Ranging (LiDAR) and its wide range of derivative products have become a powerful tool in landslide research, particularly for landslide identification and landslide inventory mapping. In contrast to the many studies that use expert-based analysis of LiDAR derivatives to identify landslides, only few studies, all pixel-based, have attempted to develop computer-aided methods for extracting landslides from LiDAR. So far, it has not been tested whether object-oriented analysis (OOA) could be an alternative. Therefore, this study focuses on the application of OOA using LiDAR derivatives such as slope gradient, curvature, and difference in elevation (2 m resolution). More specifically, the focus is on the possible use for segmentation and classification of slow-moving landslides in densely vegetated areas, where spectral data do not allow accurate landslide inventory mapping. The test areas are the Flemish Ardennes (Belgium) and Vorarlberg (Austria). In a first phase, a relatively qualitative procedure based on expert-knowledge and basic statistical analysis was developed for a test area in the Flemish Ardennes. The procedure was then applied without further modification to a validation area in the same region. The results obtained show that OOA using LiDAR derivatives allows recognition and characterization of profound morphologic properties of deep-seated landslides, because approximately 70 % of the landslides of an expert-based inventory were also included in the object-oriented inventory. For mountain areas with bed rock outcrops like Vorarlberg, on the other hand, it is more difficult to create a transferable model.

Keywords

Deep-seated landslides • LiDAR • Segmentation • Characterisation • Geomorphometry

Introduction

Since the availability of Light Detection and Ranging (LiDAR), shaded-relief, slope, surface roughness and contour maps, and other derivatives have regained popularity for landslide inventory mapping, especially in forested areas (Schulz 2004; Van Den Eeckhaut et al. 2007, 2011).

Many studies have used expert-based analysis of LiDAR derivatives to identify landslides, while only few studies have attempted to develop computer-aided methods for extracting landslides from LiDAR data (McKean and Roering 2004; Booth et al. 2009). Promising results were obtained with

M. Van Den Eeckhaut (✉) • J. Hervás
Institute for Environment and Sustainability, Joint Research Centre (JRC), European Commission, 21027 Ispra, Italy
e-mail: miet.van-den-eeckhaut@jrc.ec.europa.eu

N. Kerle
Faculty of Geo-Information Science and Earth Observation, University of Twente, Enschede, The Netherlands

R. Supper
Geological Survey of Austria, Vienna, Austria

C. Margottini et al. (eds.), *Landslide Science and Practice*, Vol. 1,
DOI 10.1007/978-3-642-31325-7_13,

Table 1 Maps used in the Flemish Ardennes

Map	Additional information
Image layer (2 × 2 m resolution)	
DTM (m)	
Slope gradient (%)	
Plan- and profile curvature ()	
Edge_slope	Map obtained through edge detection (pixel min/max filter in eCognition) on Slope gradient map
Edge_slopecl	Expert-based classification of Edge_slope map
Dif_DTM_DTMki (m) with i = 15, 25, 50, 75	Difference between original DTM and DTMki, where DTMki is a raster map where each grid cell represents the mean value of a moving window with kernel size ki with i = 15, 25, 50, 75 (best result was obtained with i = 50)
Thematic layer (vector map)	
River	Derived from the DTM using the hydrology toolbox in ArcGIS

surface roughness parameters. So far, all these automated attempts have been carried out in a pixel-based analysis. However, with high resolution topographical data such as LiDAR, object-based or object-oriented analysis (OOA) might provide better results. OOA rests upon two inter-related methodological steps: (1) segmentation or regionalization of pixels, if necessary on different scales, into meaningful, homogeneous objects that reduce the noise inherent in pixel-based analysis, and that facilitate a multi-scale analysis (Blaschke 2010); and (2) rule-based classification incorporating spectral, textural, morphometric and contextual landslide features. It is clear that the quality of the segmentation largely controls the classification.

OOA has gained increased attention for (semi-) automated landslide identification from passive optical airborne and satellite sensor data (Barlow et al. 2003; Martha et al. 2010; Stumpf and Kerle 2011; Lu et al. 2011). These studies have proven the potential for creation of inventories of recent landslides of different types. However, until now Digital Terrain Models (DTMs) have only been used in the second step, the classification. The identification of old vegetated landslides, not detectable from passive optical images, has not been investigated so far. Van Asselen and Seijmonsbergen (2006) used LiDAR derivatives in an OOA for semi-automated geomorphological mapping. Their classification included slopes with mass movement. They did not focus on individual landslides as separation of individual landslides was considered difficult. Nevertheless, the objective of this study is to test OOA for landslide inventory mapping using only LiDAR data for both the segmentation and classification steps. As such we enter in the field of geomorphometry. More specifically, we will exploit the profound morphologic manifestation of old, densely vegetated landslides to semi-automatically map their extent using LiDAR derivatives, and we will outline the pros and cons of the methodology. We focus on two study areas: the Flemish Ardennes (Belgium) and Vorarlberg (Austria).

Materials and Methods

Data

The Flemish Ardennes is a hilly region characterised by loose tertiary lithology (alternation of clays and more sandy lithology) affected by more than 200 landslides (Van Den Eeckhaut et al. 2011). We refer to Van Den Eeckhaut et al. (2007) for a detailed description of the LiDAR data used for this region (AGIV 2005).

For Vorarlberg, an Alpine region with bedrock outcrops, we use more detailed LiDAR data provided by VoGIS (Rieger 2005). From the LiDAR point data, available in .txt format for the Flemish Ardennes and in ASCII format for Vorarlberg, 2 m resolution DTMs were created and after low pass filtering (kernel size 3) different LiDAR-derivatives were produced. The maps evaluated in this study (Table 1) are focussing on the lower order derivatives, which the human brain also uses for delineating landslide boundaries and classifying landslide parts (Minar and Evans 2008). The OOA was carried out in eCognition Developer 8.

Conceptualization of Landslides and Translation to OOA

The ultimate benchmark of OOA is human perception (Lang 2008). It has been widely recognized that compared to grid cells, objects are closer to human perception and patterns better represent real landscapes, if the scale is appropriate (Goodchild et al. 2007; Drăguţ et al. 2011). Our visual sense of any kind of object is a common experience, yet not always easy to communicate and even more difficult to translate into rule sets. Hence, (semi-)automated classification of landslides, almost always represents an attempt to replicate subjective landslide recognition (e.g. Martha et al. 2010). Stumpf and Kerle (2011) provide an overview

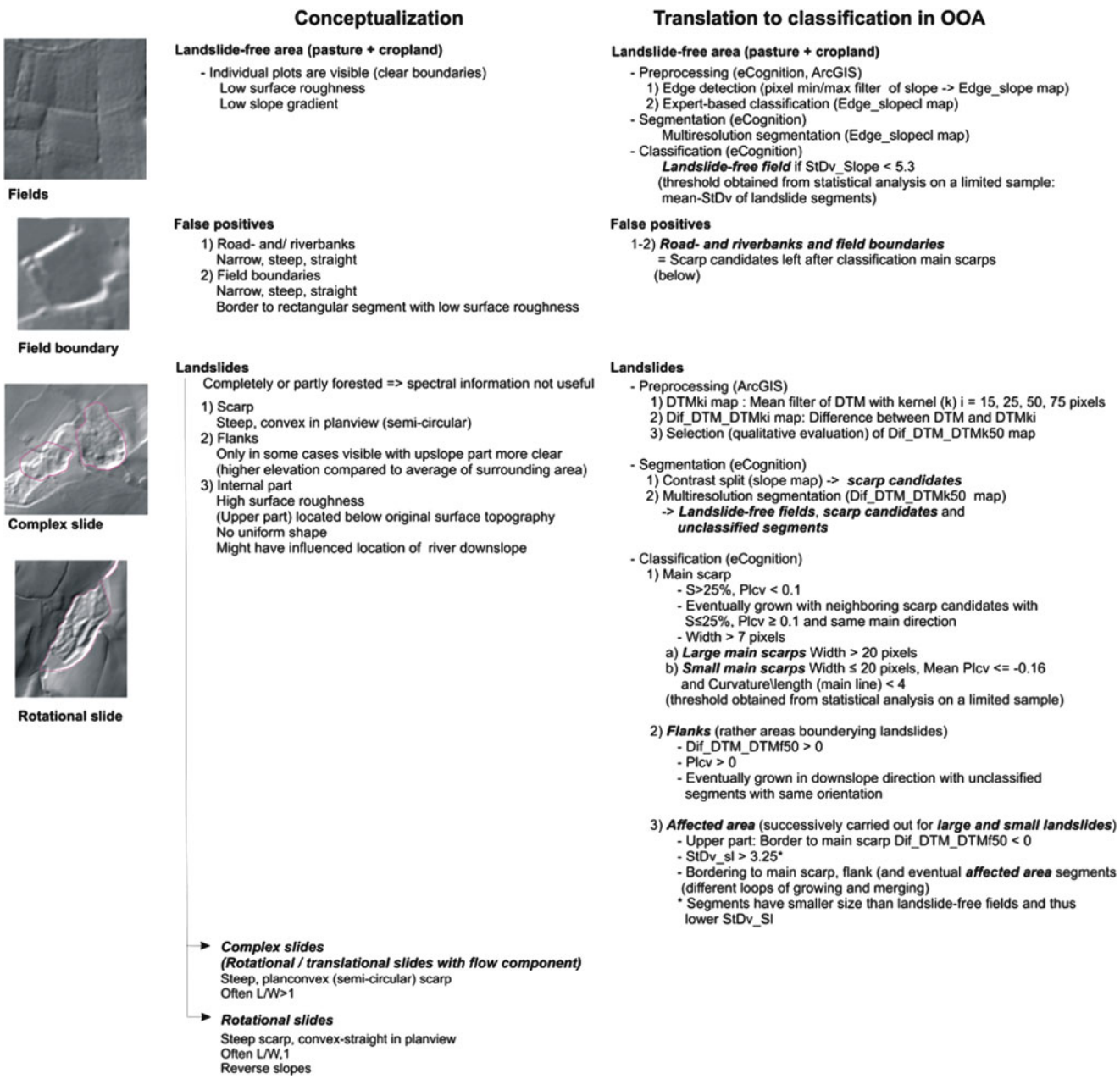

Fig. 1 Human conceptualisation of landslides and translation to object oriented analysis (*S*: slope gradient, *StDv_Slope*: standard deviation of slope gradient; *Plcv*: plan curvature)

of image object features previously used in OOA-based landslide inventory studies. Most of these features are not solely characteristic for landslides, and many are related to passive optical images (i.e. spectral information) making them not very useful in a LiDAR oriented approach where the focus should be put on identification of geomorphometric features. Figure 1 contains the conceptualisation of landslides typically found in the Flemish Ardennes, including old deep-seated rotational/translational slides with a flow characteristic (i.e. complex slides) and rotational slides. The figure also shows the conceptualisation of landslide-free terrain (mainly cropland and pastures) and possible false positive landslides (road-and riverbanks and field borders). The ultimate objective is to find a classification rule set based on the listed characteristics.

Translation of the landslide concept in eCognition starts with segmentation. Multiresolution segmentation was used in combination with Contrast Split segmentation (Fig. 1). The scale factor is the most important factor influencing the segmentation (Drăguţ et al. 2010). Although a relatively high number of studies have focussed on the influence of scale/resolution in terrain analysis, attempts to produce strategies for more objective selection of optimal scales are limited. Only recently several procedures for objective

selection of appropriate scales for multiresolution segmentation have been suggested (Martha et al. 2011; Stumpf and Kerle 2011). For this first analysis we used the estimation of scale parameter tool (ESP; Drăguţ et al. 2010).

For the study area in the Flemish Ardennes, the segmentation and classification procedure was calibrated for a 10 km^2 test area. It was then applied to the 50 km^2 area surrounding the test area (Fig. 2a). For the test and validation area, the existing landslide inventory map obtained through visual inspection of LiDAR derivative maps and field surveys (Van Den Eeckhaut et al. 2007) contains 4 and 14 rotational slides, 10 and 16 complex slides, 4 and 6 possible slides (less clear geomorphic manifestation) and 2 and 15 shallow slides, respectively. The latter are not taken into account in this study.

Results

Landslide Identification

Figure 1 shows the procedure followed for segmentation and classification. First, landslide-free agricultural fields were extracted. The segmentation procedure for this included detection of edges on the slope map and subsequent multiresolution segmentation using the resulting map (Edge_slopecl). Then, a sample of landslide-free field segments and landslide-affected segments was analysed and segments with a standard deviation of slope gradient below 5.3 were found to be landslide-free fields.

For extraction of landslides, the most distinct landslide characteristics, the main scarps, were extracted first, followed by the flanks and finally the landslide-affected area. Contrast Split segmentation of the slope map was carried out to separate steep (classified scarp candidates) from flatter terrain. The flatter terrain in this map was subsequently split with multiresolution segmentation of the Dif_DTM_DTMk50 map (Table 1) and the river map (Fig. 2a).

Main scarp segments were extracted from scarp candidates using their concave planform. As individual scarps could consist of several segments a growing procedure was subsequently used. Based on their width, large and small main scarp segments were separated, because during the calibration procedure more false positives were obtained for smaller main scarps.

Compared to main scarps, the morphologic manifestation of flanks is much less clear. No appropriate procedure has been found for segmentation of flank candidates yet, and thus the focus was not put on landslide flanks itself but on segments bordering the sides of the landslides. Especially for the upper part of the landslide, these segments are located above the surrounding segments (i.e. have mean

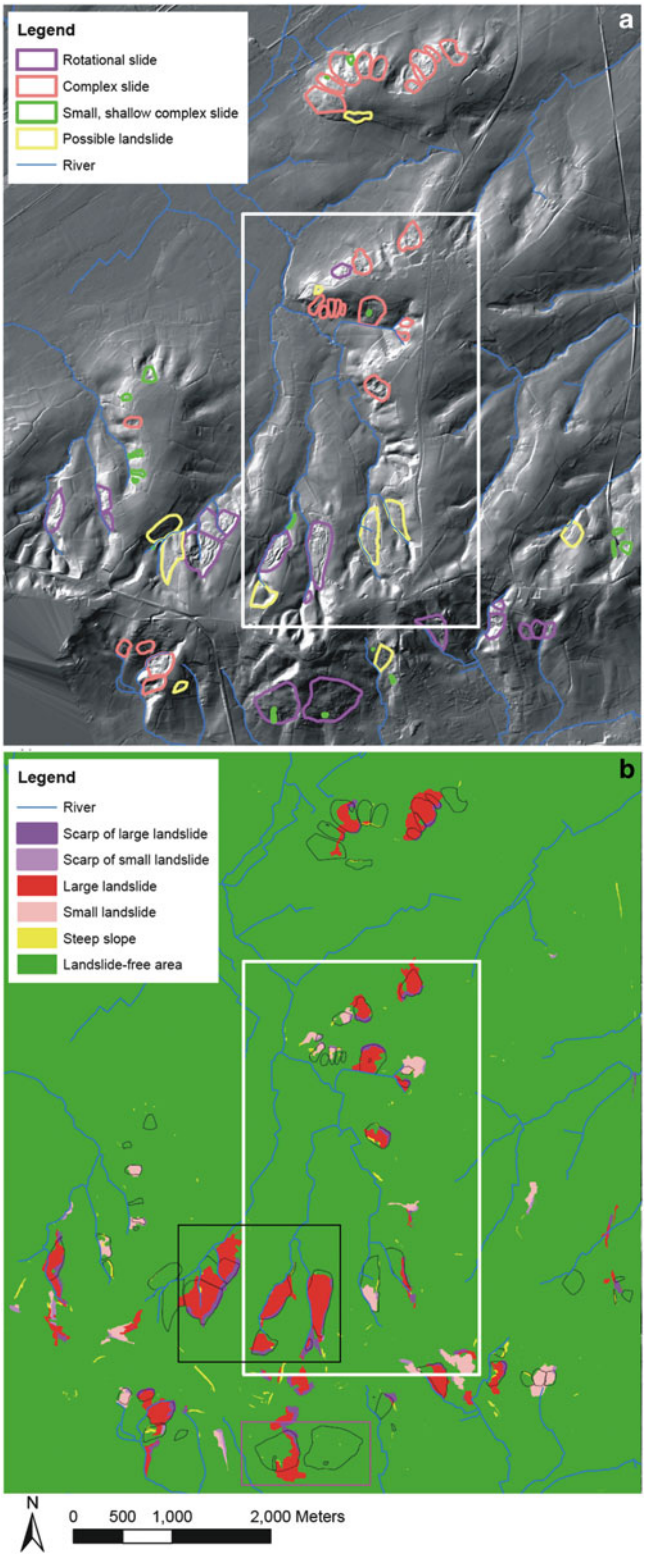

Fig. 2 Test (*white rectangle*) and validation area in the Flemish Ardennes: (**a**) The shaded relief map (LiDAR data © AGIV) is overlaid with the expert-based landslide inventory map created by Van Den Eeckhaut et al. (2007); (**b**) Preliminary landslide inventory obtained with OOA. *Black and purple rectangle* represent correctly identified and missed landslides, respectively

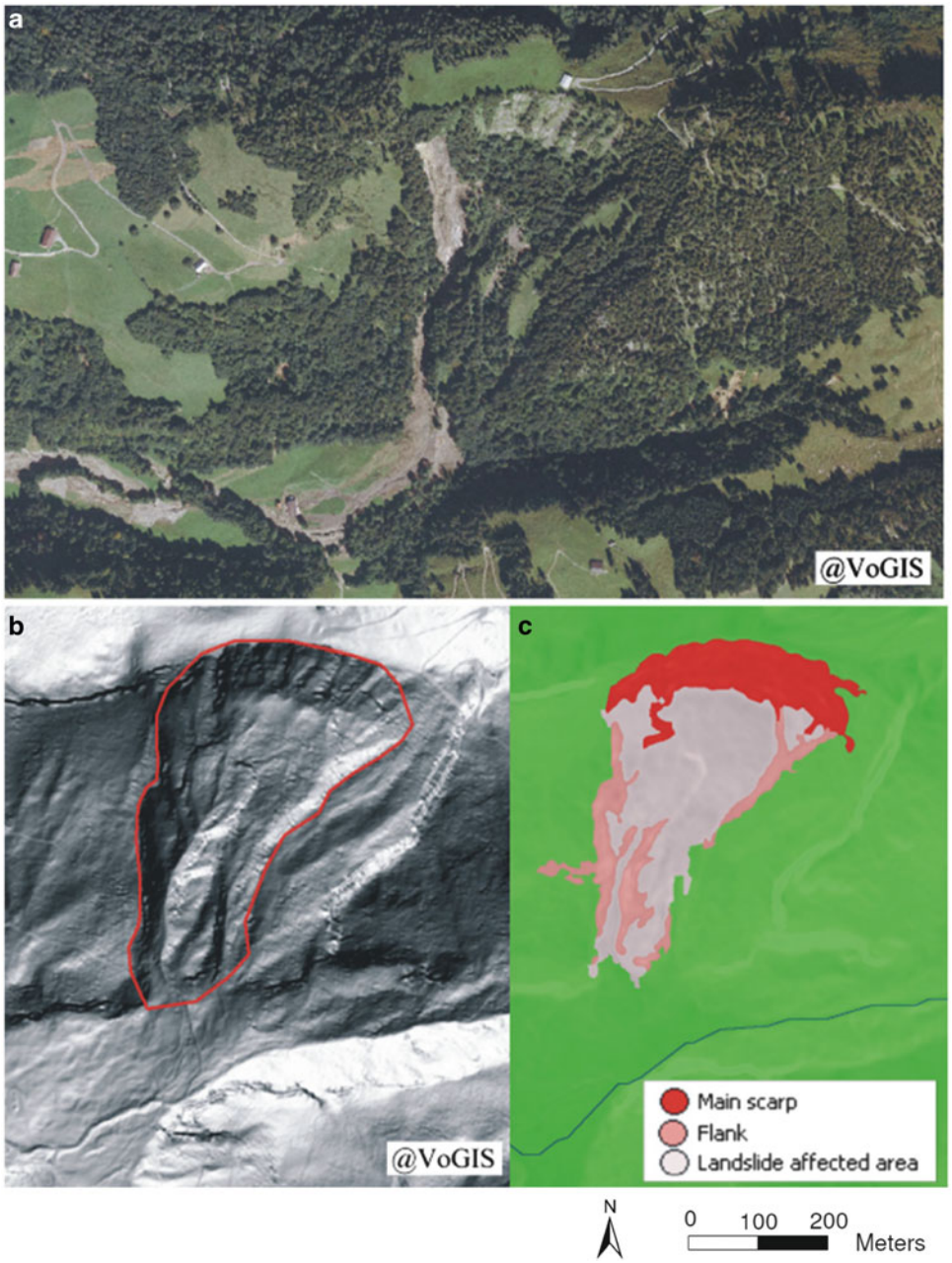

Fig. 3 Landslide under vegetation in Vorarlberg: (**a**) Orthophoto, (**b**) LiDAR-derived hillshade map; (**c**) preliminary result of segmentation and classification of the landslide (LiDAR data @ VoGIS)

Dif_DTM_DTMk50 > 0). The classification of the affected area started from the main scarp (first for the large and subsequently for the small) in downslope direction. Finally, the unclassified segments were classified as landslide-free field. The results obtained are shown Fig. 2b.

Accuracy Assessment

Accuracy assessment of geometric analysis is difficult to perform. First, there is no "completely perfect landslide inventory map" to compare the results against, as landslide inventory maps created from LiDAR analysis by different experts result in inventory maps with considerable differences (Van Den Eeckhaut et al. 2007). Second, currently there is no standard evaluation method for the assessment of the quality of image segmentation, let alone for multiresolution segmentation (Drăguţ et al. 2011).

A first accuracy assessment can be carried out by comparing the landslide inventory obtained with OOA (Fig. 2b) with the expert-based inventory (Fig. 2a). No difference in accuracy was found for the calibration and validation area. The rotational slides in the central south of the study area (i.e. black rectangle) are for example in agreement with the expert-

based inventory. The two large complex slides in the south (i.e. purple rectangle), however, are not identified with OOA. Their surface morphology is probably too subdued and affected by anthropogenic interventions (construction of houses and roads in the lower deforested part of the landslides).

The extent of about 70 % of the landslides was correctly identified with little differences between the accuracy obtained for complex and rotational slides. These results are in the same order as the results obtained by Martha et al. (2010). False negatives (unidentified landslides) are always landslides for which the main scarp was not correctly identified. In most cases the main scarps were initially identified as scarp candidates though later omitted because of a plan convex morphology. The observation that these false negatives generally have smaller main scarps supports the idea of distinguishing between large and small main scarps.

The OOA landslide inventory contains also about ten misclassified zones (group of segments incorrectly classified as main scarp and landslide). These are either steep valley heads (where some slope failure might not be excluded) or zones where a road bank or earthen bank bordering a field was misclassified as a main scarp and subsequently grown into a landslide. Generally, this last group of false positives has an irregular form.

Discussion

For (semi-)automatic mapping of densely vegetated landslides, an alternative to passive optical sensors has to be found for production of landslide inventory maps. Using LiDAR derivatives in an OOA we obtain similar accuracy results (i.e. approximately 70 %) compared to previous studies using OOA and passive optical remote sensing data (e.g. Martha et al. 2010), and thus it is worthwhile to further exploit the possibilities of OOA with LiDAR data.

In soil covered areas such as Flanders, landslides are generally characterized by a much higher surface roughness compared to the surrounding landslide-free areas, and therefore good first results were obtained with slope gradient and surface roughness (standard deviation of slope gradient) maps. The downslope part of old landslides, like those studied here, often has a poor geomorphometric signature. However, this problem has been reported for expert-based landslide inventory mapping to (e.g. Schulz 2004). For delineation of landslide boundaries also several edge detection procedures have been tested, but so far without great success.

In more mountainous areas, such as our second study site in Vorarlberg (Fig. 3), it is more difficult to distinguish landslides from non-landslide areas, because stable bed rock outcrops around landslides also have high topographic roughness. Additionally, the number of false positive main scarps is higher due to the presence of steep cliffs. As in the Flemish Ardennes also in Vorarlberg many landslides have flanks with a subdued morphologic signature. In some cases an internal drainage system has developed (Fig. 3), which further complicates the landslide classification process. Overall, compared to the case-study in Flanders transferability is more difficult. A rule set calibrated for one or two landslides does not work for many other landslides.

Some differences between the use of passive optical remote sensing data and active optical remote sensing data such as LiDAR were observed. The most important one is that when using passive optical remote sensing data, fresh landslides generally consist of one or a few segments only. However, landslides are geomorphologically complex and consist of different parts with different geomorphological characteristics. Hence, they are not represented by one single segment when obtained from LiDAR derivatives, and the aggregation from different segments into one final landslide segment is difficult.

Recent studies have focussed on objective classification of segments. Martha et al. (2011) used k-Means cluster analysis and Stumpf and Kerle (2011) random forests. It should be further investigated whether these approaches are also useful in the context of this study. Similar to Martha et al. (2010), so far thresholds were only obtained through basic statistical analysis of limited samples selected in the test area, but future research will focus on quantification of the process and transferability.

Conclusions

The results obtained show that OOA using LiDAR derivatives (such as slope gradient, curvature and difference in elevation) and edge detection allows recognition and characterization of profound morphologic properties of deep-seated landslides. Main scarp, landslide boundary, and landslide segments were successively classified. Overall about 70 % of the landslides of an expert-based inventory were also included in the object-oriented inventory. Unidentified landslides were misclassified, because they had a less profound or plan convex main scarp. Some plan concave road banks or river valley heads, on the other hand, were incorrectly classified as landslides.

Ongoing research mainly focuses on improvement of the segmentation and automating the classification procedure, both with the objective of increasing transferability.

Acknowledgments This study has been carried out in the framework of the EU-FP7 project SafeLand: Living with landslide risk in Europe: Assessment, effects of global change, and risk management strategies (Grant Agreement 226479; http://www.safeland-fp7.eu/). The authors thank VoGIS for providing the LiDAR data in Vorarlberg, and Prof. J. Poesen for his contribution to the creation of the expert-based landslide inventory of the Flemish Ardennes.

References

AGIV (2005) LIDAR hoogtepunten – brondata van Digitaal Hoogtemodel Vlaanderen (CD-ROM). MVG-LIN-AMINAL-afdeling Water en MVG-LIN-AWZ-afdeling Waterbouwkundig Laboratorium en Hydrologisch onderzoek, Brussel

Barlow J, Martin Y, Franklin SE (2003) Detecting translational landslide scars using segmentation of Landsat ETM + and DEM data in the northern Cascade Mountains, British Columbia. Can J Remote Sens 29(4):510–517

Blaschke T (2010) Object based image analysis for remote sensing. ISPRS J Photogramm Remote Sens 645:2–16

Booth AM, Roering JJ, Perron JT (2009) Automated landslide mapping using spectral analysis and high-resolution topographic data: Puget Sound lowlands, Washington, and Portland Hills, Oregon. Geomorphology 109:132–147

Drăguţ L, Tiede D, Levick S (2010) ESP: a tool to estimate scale parameters for multiresolution image segmentation of remotely sensed data. Int J Geogr Inf Sci 24:859–871

Drăguţ L, Eisank C, Strasser T (2011) Local variance for multi-scale analysis in geomorphometry. Geomorphology 130(3–4): 162–172

Goodchild MF, Yuan M, Cova TJ (2007) Towards a general theory of geographic representation in GIS. Int J Geogr Inf Sci 21:239–260

Lang S (2008) Object-based image analysis for remote sensing applications: modeling reality – dealing with complexity. In: Blaschke T, Lang S, Hay G (eds) Object-based image analysis spatial concepts for knowledge-driven remote sensing applications. Springer, Berlin/Heidelberg, pp 3–27

Lu P, Stumpf A, Kerle N, Casagli N (2011) Object-oriented change detection for landslide rapid mapping. IEEE Geosci Remote Sens Lett 8:701–705

Martha T, Kerle N, van Westen CJ, Kumar K (2010) Characterising spectral, spatial and morphometric properties of landslides for semi-automatic detection using object-oriented methods. Geomorphology 116(1–2):24–36

Martha T, Kerle N, van Westen CJ, Jetten V, Kumar K (2011) Segment optimisation and data-driven thresholding for knowledge-based landslide detection by object-based image analysis. Trans Geosci Remote Sens 49(12):4928–4943

McKean J, Roering JJ (2004) Objective landslide detection and surface morphology mapping using high-resolution airborne laser altimetry. Geomorphology 47:331–351

Minar J, Evans IS (2008) Elementary forms for land surface segmentation: the theoretical basis of terrain analysis and geomorphological mapping. Geomorphology 95:236–259

Rieger W (2005). Laserscanning-Befliegung Vorarlberg – Regionen Oberland und Walsertal sowie Erstellung vond Digitalen Gelandemodellen, Zl. LVA 603.02.04.04.09.08. Amt der Vorarlberger Landesregierung

Schulz WH (2004) Landslides mapped using LIDAR imagery, Seattle, Washington. U.S. Geological Survey Open-File Report 2004–1396, 11p, 1 plate

Stumpf A, Kerle K (2011) Object-oriented mapping of landslides using random forests. Remote Sens Environ 115(10):2564–2577

Van Asselen S, Seijmonsbergen AC (2006) Expert-driven semi-automated geomorphological mapping for a mountainous area using a laser DTM. Geomorphology 78:309–320

Van Den Eeckhaut M, Poesen J, Verstraeten G, Vanacker V, Nyssen J, Moeyersons J, Van Beek LPH, Vandekerckhove L (2007) The use of LIDAR-derived images for mapping old landslides under forest. Earth Surf Proc Landf 32:754–769

Van Den Eeckhaut M, Poesen J, Gullentops F, Vandekerckhove L, Hervás J (2011) Regional mapping and characterisation of old landslides in hilly regions using LiDAR-based imagery in Southern Flanders. Quat Res 75:721–733

Assessment of Landslides Activity in Maily-Say Valley, Kyrgyz Tien Shan

Romy Schlögel, Anika Braun, Almaz Torgoev, Tomas M. Fernandez-Steeger, and Hans-Balder Havenith

Abstract

There is a strong possibility that environmental change (whether climate or land use) will be manifest as changes in the size-frequency distribution of landslides in Maily-Say Valley, Kyrgyzstan. The evolution of the landslide activity over the past 50 years has been analysed on the basis of five landslide inventories of 1962, 1984, 1996, 2002 and 2007. Their size-frequency analyses show that both the number and size of unstable slopes are increasing from 1962 (162 objects) to 2007 (208 objects) and the power-law exponent is decreasing over time. This might indicate that there is an evolution in size probably corresponding to an increase of landslide-related hazards. Remote sensing and spatial analysis through the image subtraction method based on NDVI allowed an accurate detection of new sliding activation in that area. Another aim is to evaluate if and how Data Mining, with its wide range of tools, may support automatic landslide recognition.

Keywords

Landslide activity • Frequency density function • Data Mining • Kyrgyzstan

Introduction

Kyrgyz Tien Shan is prone to different natural hazards due to high seismicity, active tectonics, glacier retreat, and locally intense rainfall (Torgoev et al. 2002). Due to the high landslide activity along the rim of the Fergana Basin in the southern part of the country (Roessner et al. 2002), disasters causing social and economic losses occur almost each year. Especially, the Maily-Say Valley can be considered as a geological and environmental hazard hotspot within the Tien Shan Mountains.

In order to detect those landslides, which might be dangerous for population, two methods are processed. Normalized Differenced Vegetation Index (NDVI), including specific spectral signature of new landslides, were calculated for two images (taken at different times) and subtracted. The second process was to evaluate how Data Mining, may support automatic landslide recognition (e.g. from remote sensing data), for susceptibility mapping or knowledge discovery regarding the causes of landslides. Data Mining is the application of specific algorithms, under acceptable computational efficiency limitations, for extracting patterns from data (Fayyad et al. 1996). Here, the Data Mining approach allows the prediction of landslides using classification methods (Fernandez-Steeger et al. 2002).

R. Schlögel (✉)
Department of Geology, Georisks and Environment, University of Liège, B20 Sart Tilman, 4000 Liège, Belgium

School and Observatory of Earth Sciences, University of Strasbourg, 5 rue Descartes, 67084 Strasbourg Cedex, France
e-mail: schlogel@unistra.fr

A. Braun • T.M. Fernandez-Steeger
Department of Engineering Geology and Hydrogeology, RWTH Aachen University, Lochnerstraße 4-20, 52064 Aachen, Germany

A. Torgoev • H.-B. Havenith
Department of Geology, Georisks and Environment, University of Liège, B20 Sart Tilman, 4000 Liège, Belgium

C. Margottini et al. (eds.), *Landslide Science and Practice*, Vol. 1,
DOI 10.1007/978-3-642-31325-7_14,

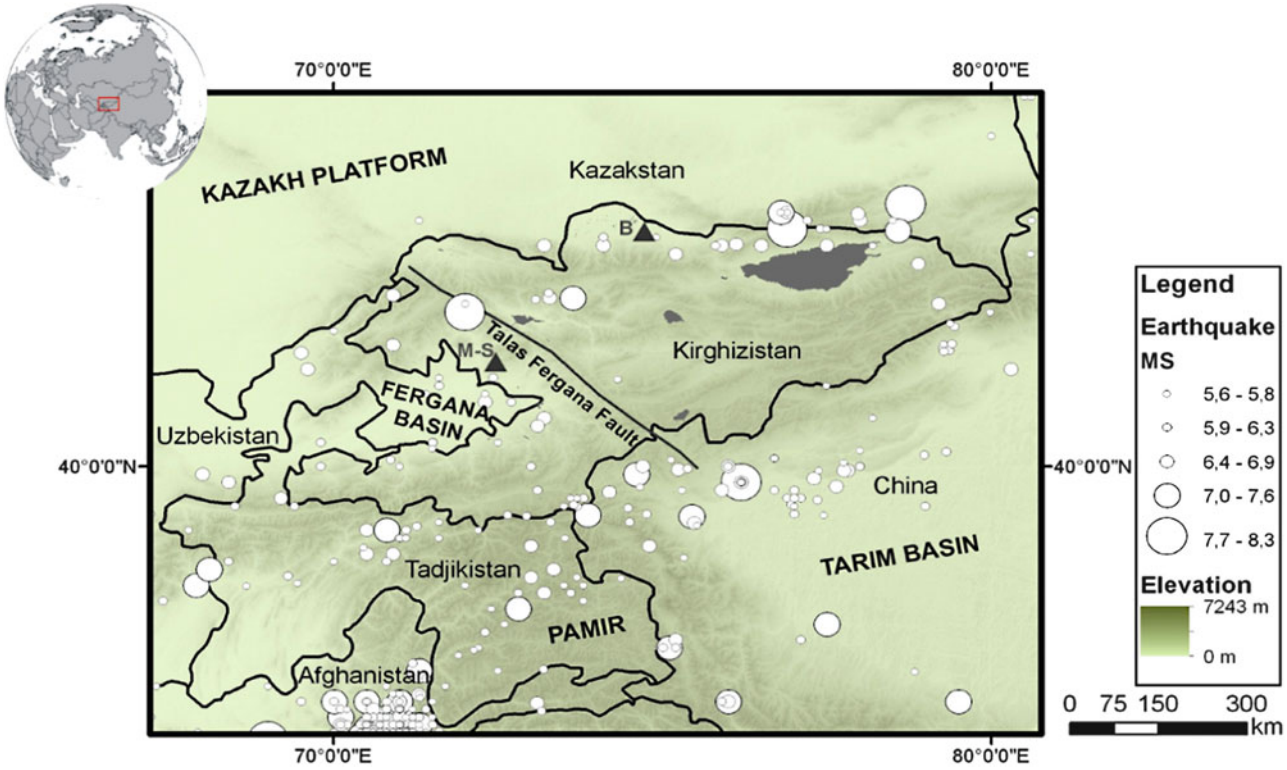

Fig. 1 Topographic map of the Kyrgyz Tien Shan and neighbouring regions. The location of Maily-Say (MS) and the capital city (Bishkek) is indicated by a *black triangle*. The map also shows all historical and instrumental earthquake events with Ms > 5.5 (Schlögel et al. 2011)

Study Area

The Maily-Say Valley is situated in the north of the Fergana Basin, about 25 km from the border with Uzbekistan. The study area is located in a transitional zone bounded in the northeast by the Talas-Fergana Fault (Fig. 1) and in the western foothills of the seismically active Tien Shan mountain belt. Bedrock geology is constituted of Cenozoic and Mesozoic sedimentary rocks (Vandenhove et al. 2003; Havenith et al. 2006). The relief is rough with heights culminating at an altitude ranging from 700 to 4,000 m.

Over the last decades, the town of Maily-Say (estimated population 10,000) has experienced a series of environmental disasters related to earthquakes, landslides and groundwater pollution (in particular by radioactive waste). According to Abdrakhmatov et al. (2003), the seismic hazard of the region is moderate to high. The last strong earthquake (Ms 6.2) hit the region on May 15, 1992, and was located at about 30 km south-southeast of the town of Maily-Say. Evidence for high landslide activity and slope instability is observed throughout the area. Today, more than 200 landslides are located in the vicinity of the town, 80 of which are unstable and have the potential to move under adverse conditions.

The largest landslide in the region, located about 7 km east of the town of Maily-Say, is the Kochkor-Ata landslide, was activated as a whole on April 13, 1994, forming an almost 4 km long earth flow with a total volume of about 10 Mm^3 (Roessner et al. 2002).

Data and Pre-processing

Multi-temporal, remotely sensed images were collected to detect landslides and to determine their evolution. Aerial photographs of the years 1962, 1984 and 1996 (panchromatic, approximate 1:21,000 scale, roughly 2 m ground-resolution) for the Maily-Say Valley were studied in detail and compared with panchromatic and multi-spectral 10.3 by 11.1 km Quickbird images of 2002 and 2007. The multi-spectral images provide four spectral bands, (blue, green, red, near-infrared) with a spatial resolution of 2.44 m; while panchromatic Quickbird images have a spatial resolution of 0.61 m.

Quickbird imagery was pre-processed with the ENVI software before being classified (unsupervised) through the image subtraction in order to make radiometrically and geometrically comparable 2002 and 2007 scenes. Factors affecting geometry can be related to the sensor system, due to variations in platform altitude, in the sensor view angle or caused by the rotation of the earth (Gupta 2003). The images were orthorectified on the basis of a 20 m resolution Satellite Pour l'Observation de la Terre (SPOT)

digital elevation model (DEM) and georeferenced to UTM zone 43 north. Panchromatic and multi-spectral images were co-registered separately to allow superimposition of multi-spectral images. In addition, the images were normalized using a relative radiometric correction process. Gains and offsets were applied to create a normalized image of the 2007 scene while the 2002 image is taken as reference as it shows the larger contrasts (Jensen 1996).

Methods

Landslide Inventories

Landslide inventories are the simplest form of landslide susceptibility mapping (Guzzetti et al. 1999). Two new landslide inventories were created by remote sensing analysis from the Quickbird images for the Maily-Say Valley, verified by field observations and used in specific techniques of landslide detection described further. Using Geographical Information System (GIS) tools, a total of 189 and 208 landslides were mapped from 2002 and 2007 images, respectively.

The initial inventories were created by local scientists through field surveys and air photo interpretation, and corrected by comparison with recent data to make them accurate and comparable (Brardinoni et al. 2003). Previous landslide inventories (already used by Havenith et al. 2006) were improved to produce new ones for the years of 1962 (162 landslides), 1984 (206 landslides) and 1996 (222 landslides). All five inventories contain only landslides that could be identified from remote imagery of a certain year and, therefore, are likely to have been (re-)activated in recent times.

Evolution of Landslides

The landscape in the Maily-Say Valley is continuously changing owing to the high landslide activity. The total area affected by landslides increased from 1.0 % (~1.2 km^2) in 1962 to 3.3 % in 1984, 4.5 % in 1996, 4.3 % in 2002 and 5.6 % (~6.5 km^2) in 2007 compared to the entire investigated area along the Maily-Say Valley. The slight decrease of 0.2 % from 1996 to 2002 is likely to be related to the changed dataset used for mapping (aerial photographs and existing inventories in 1996 and before, Quickbird imagery for 2002 and 2007). The mean landslide size increased from 15,170 m^2 in 1962 to 31,000 m^2 in 2007. Landslide size is quite variable; it ranges from 335 m^2 for the smallest detected landslide to 348,425 m^2 for the largest one in 2007. The evolution of the formation of the largest mass movement is marked by the formation of landslide Tektonik in 1992. Due to this, the maximum landslide size increased from 110,000 m^2 in 1984 to 325,000 m^2 in 1996.

NDVI Subtraction

Methodology

The NDVI, initially developed for classification of vegetation type and health, is here applied to detect fresh translational mass movements (Chang and Liu 2004) such as debris flows and earth flows which are quite common in Maily-Say valley. It is calculated on the basis of the red and near-infrared bands which depend strongly on the presence of vegetation, according to the following equation:

$$\mathrm{NDVI} = (\mathrm{NIR} - \mathrm{R})/(\mathrm{NIR} + \mathrm{R})$$

This processing allows for improved differentiation between spectrally-different surfaces, compared to the use of one band only. Further, band ratioing greatly mitigates shadow effects that sometimes make visual interpretation difficult. The values of this index, also an indicator of biomass, are in the range between − 1 and 1; negative values indicate bare land and positive values indicate a greater level of photosynthetic activity due to the presence of vegetation (often included between 0.2 and 0.8).

Image differencing, or subtraction, is based on a pair of co-registered raw or transformed images of the same area collected at different times. The process simply subtracts pixel values on a pixel-by-pixel basis to generate a third image composed of numerical differences between the pairs of pixels (Ridd and Liu 1998).

The process leading to a new image, using the available Quickbird satellite images of these two periods, can be quantified by the following the equation (here applied to the b-band of the images):

$$\mathrm{Dx}^{b}{}_{ij} = \mathrm{x}^{b}{}_{ij}(t_{2007}) - \mathrm{x}^{b}{}_{ij}(t_{2002}) \quad (1)$$

where $x_{ij}{}^{b}$ (t_{2007}) and $x_{ij}{}^{b}$ (t_{2002}) are the digital numbers (DNs) of a pixel (i,j) of b-band for the 2007 and 2002 images, respectively. In the new image ($Dx_{ij}{}^{b}$), positive or negative values denote the region whose radiation value has increased or decreased, respectively, between 2002 and 2007; a 0-value corresponds to no change in the region.

A suitable threshold value allows us to distinguish the areas of 'real' changes from those marked by the impact of random factors. One interesting application of this method is to apply it to images acquired before and after landslide events in order to identify landslides according to their NDVI value (Lin et al. 2005). In the frame of this study, we analysed where new landsides appeared or old ones were reactivated between 2002 and 2007. A number of 11 classes with 7 negative classes give the most representative results to recognise change in the vegetation canopy due to the disrupted vegetation because of landslide activation. The pre- and post-NDVI images have been created following the equation:

$$\Delta\mathrm{NDVI} = \mathrm{NDVI}_{2007} - \mathrm{NDVI}_{2002} \quad (2)$$

Data Mining Approach

Data Mining uses computational techniques (algorithms) from advanced statistical methods and employs pattern recognition such as neural network techniques. Data Mining also allows discovering previously unknown relationships among the data (pragmatic approach). In contrast to classical modelling attempts or statistical analysis, Data Mining is output-driven. This means that each successful strategy is allowed if it fulfils the previously defined aims and respects the requirements of the applied tools.

Since this method can handle large input datasets, multiple factors such as spectral information (from Quickbird images), recent landslide inventory, and data from the DEM (slope, curvature, topographic roughness index, landform index) were used as input data. The preparation of the data for modelling requires generally various adjustments, which have to be made to the data prior to modelling. Datasets were compiled on a GIS platform and transformed into raster data. The powerful sample command from ArcInfo GRID was used to export the raster in a flat file (like CSV for comma separated values) that could be directly imported in Data Mining tool PASW Modeler. The software then guides the planning in a systematic way to the goal of the study: detecting landslide. It focuses on the process of running data through a series of nodes, referred as a stream. Whereas ANN (Fernández-Steeger et al. 2002; Falaschi et al. 2009) and more recently Bayesians networks (Braun et al. 2011) have successfully been implemented for landslide susceptibility analysis, decision trees (C5.0, CHAID) were developed for landslides recognition in the framework of this study. The models use in advance digitised landslides to train and develop the model in a well-known area. Afterwards the model is tested in another area to evaluate the model skills.

Results

Size-frequency Distribution of Landslides

The frequency-area distribution quantifies the number of landslides per class of surface area. Following the method of Malamud et al. (2004), the size-frequency relationships of these five datasets described earlier were analysed in terms of the frequency density function (f) of the landslide areas (A_L) using the following equation:

$$f(A_L) = \delta N_L / \delta A_L \quad (3)$$

where δN_L is the number of landslides with areas between A_L and $A_L + \delta A_L$. δA_L is the width of the respective area class. In a log-log graph (Fig. 2), this function shows a more-or-less linear tail (in log-log graph) which can be fit by a power-law (Turcotte 1997). A rollover (inflection) is observed for smaller events and objects, here represented by the decreasing frequency density for very small landslide areas (Malamud et al. 2004; Havenith et al. 2006). The deviation from the power-law trend on the left part of the graph is partly explained by undercounting of the small landslides. As discussed by Malamud et al. (2004), many factors cause the incompleteness, such as the quality of imagery, landslide age and freshness and the potential removal of geomorphologic and spectral properties, the experience of the scientist involved. Pelletier et al. (1997) attributed the rollover shown by the probability density function of landslide areas, to a transition from a resistance controlled chiefly by friction (for large landslides) to a resistance controlled by cohesion (for small landslides).

Here, only the linear trend of the size-frequency relationships (e.g. for a size greater than the rollover, which is roughly 10,000 m^2) of the five inventories has been considered, which should be complete above that threshold. The fits of these linear tails of a complete relationship by a power-law are characterized by coefficients of determination, R^2, larger than 0.8.

From the size-frequency analysis presented in Fig. 2, it can be seen that the trends slightly but constantly change over time. The related exponent-values continuously decrease from 1.93 in 1962 to 1.73 in 2007. The value obtained for the 2002 dataset, 1.8, is similar to the power-law exponent determined by Havenith et al. (2006) for Maily-Say landslide records obtained from field observations in 2003, which is equal to 1.9. This confirms the observed trend indicating the more frequent formation of large landslides (in terms of objects and not in terms of events or movements) in the region. The increasing frequency of large landslides can be related to the growth of existing landslides or the coalescence of smaller landslides, as already suggested by Havenith et al. (2006). The latter process probably also contributes to the fact that the number of small landslides is decreasing over time.

NDVI Subtraction

The results of the NDVI calculation for the 2007 Quickbird image (Fig. 3) show that values close to zero represent landslides partly denudated or sites covered by sparse vegetation. The histogram analysis of the NDVI map of the entire zone shows that, the average NDVI is lower in 2007 (NDVI of 0.26) than in e (NDVI of 0.32). This difference may be due in part to the increasing landslide activity and to minor differences in vegetation growth stage. The mass movements of the Valley are generally complex combining deep-seated deformation with surficial erosion. Stable bare soil may be misclassified as landslides.

Figure 3 shows low NDVI where no landslide is located, but some of these false positives can be excluded from the difference map. The NDVI 2007–2002 subtraction maps

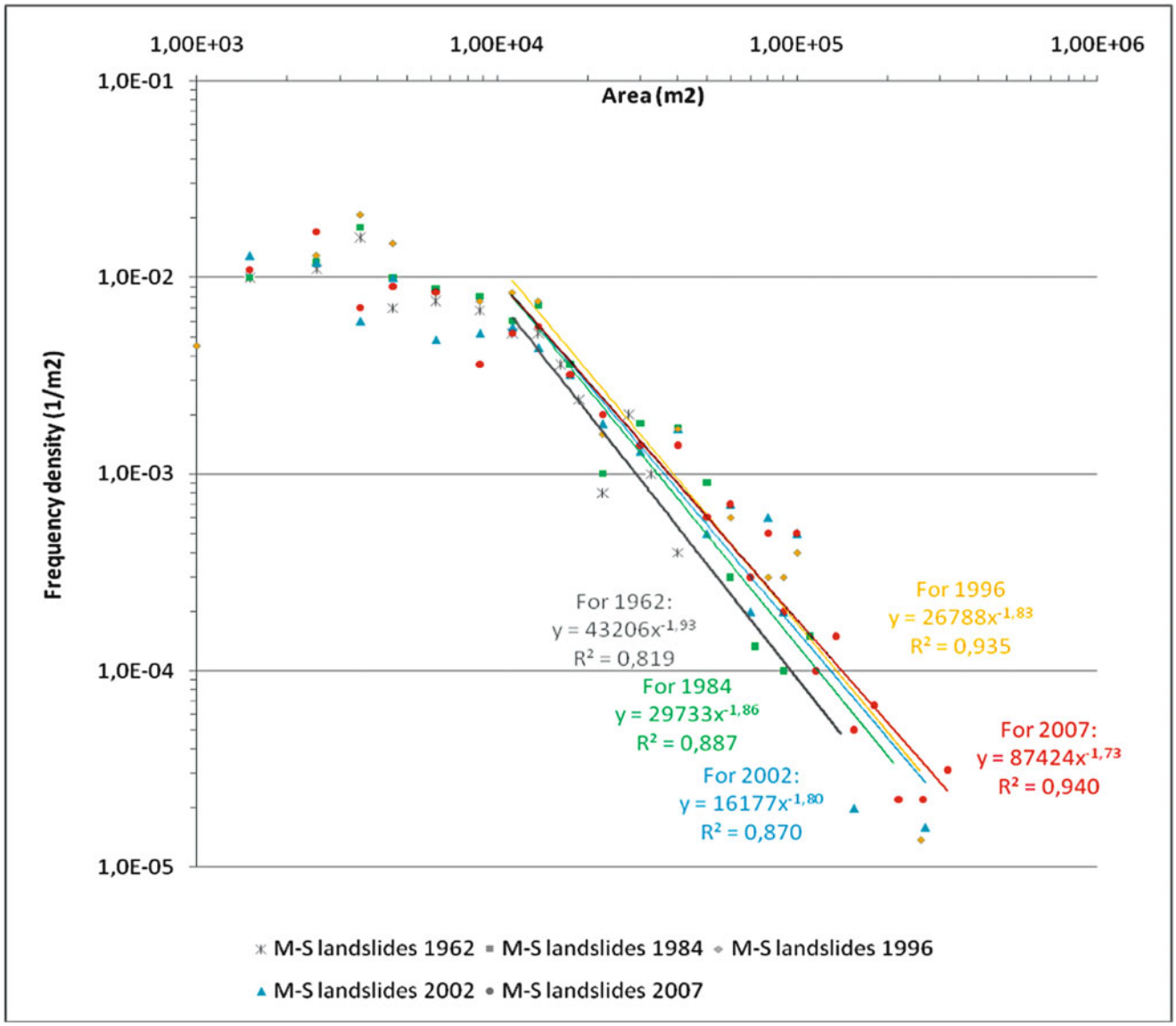

Fig. 2 Frequency density function for landslide areas in the Maily-Say Valley in 1962 (162 objects), 1984 (206 objects), 1996 (222 objects), 2002 (189 objects) and 2007 (208 objects)

show that in general, a strong decrease of NDVI could be attributed to the loss of vegetation due to recent activation of landslides. However, a simple correlation between the decrease of vegetation and the presence of a landslide cannot be established. Each landslide has particular characteristics due to its type of movement (fall, topple, slide, slump, spread or flow) and its type of material (rock, debris, earth material). In addition, the age of a landslide must be considered. With this method, primarily, fresh earth flows can be detected.

By visual analysis, it seems that new activations are represented by the classes 7 to 10, i.e. by the NDVI change values of −0.1 to −0.5. A statistical analysis shows that 88 % of the landslide areas are marked by NDVI change values of 0.0 to −0.5. However, only 27 % of the pixels inside the landslides belong to the NDVI change values of −0.1 to −0.5. This shows that only parts of the landslides can be clearly detected by the method.

Data Mining Using Decision Trees

The CHAID model was largely used to recognize if a pixel corresponds to a landslide area or not in the Maily-Say Valley.

In this study, additionally advanced parameters were taken into account to improve the modelling. This are the band 2 of 2007 and 2002 images, the slope, the topographical roughness index and the aspect. They contribute to about 80 % of the detections of landslide and no landslide using the CHAID algorithm as modelling tool. In addition, other types of models have been created and tested trying to improve the results. With the C5.0 model, the obtained results are quite good and

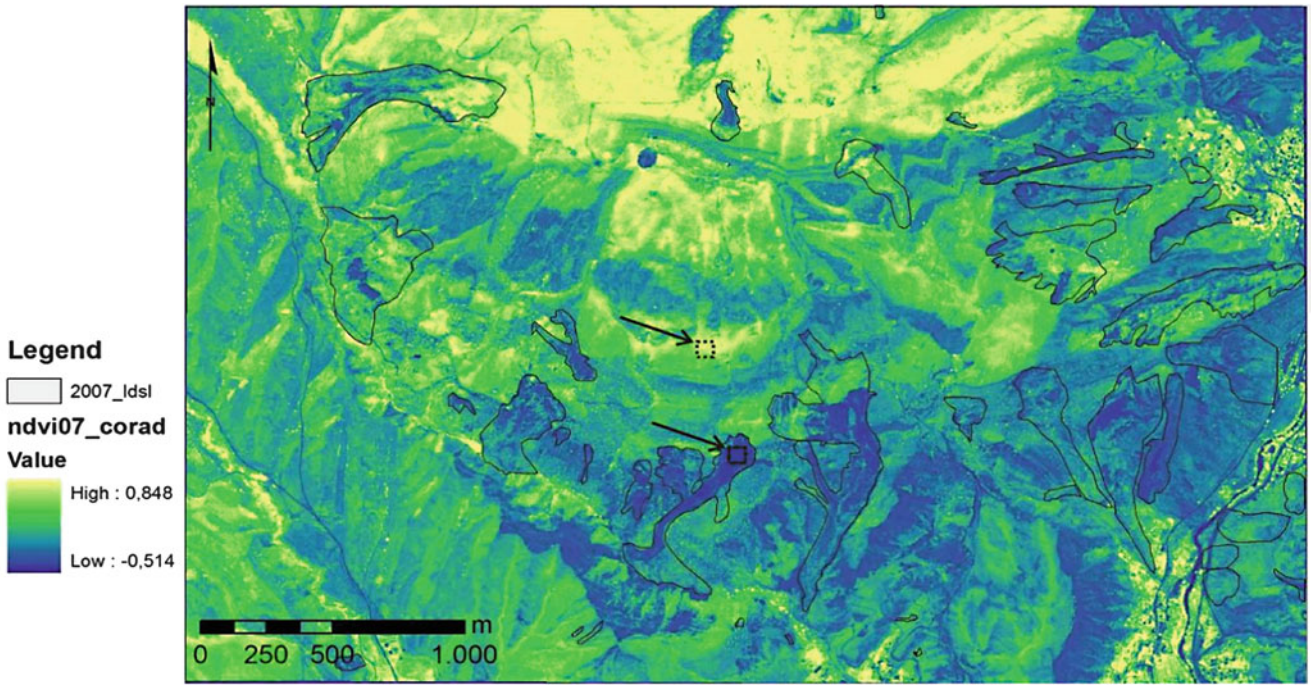

Fig. 3 NDVI of the radiometrically corrected 2007 Quickbird image of the Bedre Coupola area where *bluish* colours represent low NDVI and *greenish* to *yellow* colours represent high NDVI, and the 2007 landslide inventory for the zone (see also an example of denudation processes with low NDVI outlined by a *dashed ellipse*)

probably more relevant to detect landslides but it is often easier for the models to detect places where there are no landslides.

Following a partition at random of 30 % for testing and 70 % for training, concentrated on landslides, the model is only 69 % relevant. In inverting this partition (training area becoming testing area), the model accuracy reveals a more performing model with 82 %. Unfortunately, only 75 % of the pixels are well classified in the training model compared to 79.5 % obtained if we consider the test model. But the latter allows us to detect landslides in a defined environment which is the most interesting in detection.

Discussion and Conclusion

All statistics of the evolution of landslides indicate that the hazard is likely to increase in the Maily-Say Valley. Size-frequency analyses applied to landslide datasets of 1962, 1984, 1996, 2002 and 2007 show that the exponent-values of the power-law fits to the linear tails continuously decrease from 1.93 in 1962 to 1.73 in 2007. This reveals a trend towards the formation of increasingly larger landslides on the Maily-Say slopes.

The size-frequency behaviour of the landslides in Maily-Say can be compared with some observations made by other researchers concerning landslide distributions. All exponent-values obtained for the five inventories are well below those calculated by several other researchers, e.g., by Malamud et al. (2004) studying landslide inventories of landslide types and distributions as well (the values are between 2.11 and 2.48). However, the exponent values of the five inventories presented here compare well with those calculated by Chen (2009) for the landslides triggered by the 1999 Chi-Chi earthquake (value of 1.8). He noted that the exponent value increased for post-seismic landslides triggered by Typhoons in 2001 and 2004 (values of 2 to 2.1). This change of the exponent values of about 0.2–0.3 considered as significant by Chen (2009) is similar to the one observed for the Maily-Say landslides.

Here, we relate the continuous decrease of the exponent value of the landslide size-frequency distribution to the growth and coalescence of existing landslides which are relatively more frequent than the formation of new small slope instabilities. In this regard, it can be assumed that the changing size-frequency distribution of the landslide bodies in Maily-Say is related to the increasing density of slope instabilities. We think that a certain landslide density threshold has been surpassed, beyond which landslide occurrences become interdependent and are not only related to changing environmental conditions and external triggers. Furthermore, power-law exponent-values decreasing over time could indicate a trend towards a cataclysmic situation – this means that in near future larger parts of slopes could fail catastrophically. However, to be able to confirm this, we will also quantitatively assess changes in the landslide sizes and continuously monitor landslide reactivations in hazardous places. Therefore, automatic detection methods are needed.

As many new landslides are translational and constituted by clay and loess deposits, a change detection method, based on image subtraction to detect (re)activations was developed. Differencing of NDVI values determined from the multispectral Quickbird images ($NDVI_{2007} - NDVI_{2002}$) allowed us to outline zones with removed vegetation due to active slope failures considering inherent errors of commission in mapping. This analysis allows us to demonstrate that the multi-temporal differencing method is quite useful to detect both (re)activations of landslides and stabilizing slopes (marked by re-vegetation). However, it is not well adapted to map landslides or to create an inventory of them. For that purpose, a uni-temporal method is more appropriate such as Data Mining, which is able to combine many different parameters influencing slope stability and/or affected by the presence of landslides (e.g. spectral bands, curvature, slope, roughness). The data mining approach is also promising for the task of predicting landslide susceptibility but it requires more time and mathematical skills.

Acknowledgments These studies have been supported by the NATO Science for Peace Project 'Prevention of landslide dam disasters in the Tien Shan, LADATSHA'. We would like to thank reviewers of the 2nd World Landslide Forum for their helpful comments.

References

Abdrakhmatov K, Havenith H-B, Delvaux D, Jongmans D, Trefois P (2003) Probabilistic PGA and arias intensity maps of Kyrgyzstan (Central Asia). J Seismol 7:203–220

Brardinoni F, Slaymaker O, Hassan MA (2003) Landslide inventory in rugged forested watershed: a comparison between air photo and field survey data. Geomorphology 54:179–196

Braun A, Fernandez-Steeger TM, Havenith H-B, Torgoev A, Schlögel R (2011) Analysing the landslide susceptibility in Maily-Say, Kyrgyzstan, with statistical methods. In: Proceedings of the 2nd INQUA-IGCP-567 international workshop on active tectonics, earthquake geology, archaeology and engineering, Corinth

Chang KT, Liu JK (2004) Landslide features interpreted by neural network method using a high-resolution satellite image and digital topographic data. Int Arch Photogramm Remote Sens Sp Inf Sci 35:574–579

Chen CY (2009) Sedimentary impacts from landslides in the Tachia River Basin, Taiwan. Geomorphology 105:355–365

Falaschi F, Giacomelli F, Federici PR, Pucinelli A, D'Amato Avanzi G, Pochini A, Ribolini A (2009) Logistic regression versus artificial neural networks: landslides susceptibility evaluation in a sample area of the Serchio River valley, Italy. Nat Hazards 50:551–569

Fayyad U, Piatetsky-Shapiro G, Smyth P (1996) From data mining to knowledge discovery in databases. AI Mag 17(3):37–54

Fernández-Steeger TM, Rohn J, Czurda K (2002) Identification of landslide areas with neural networks for hazard analysis. Landslides. In: Proceedings of the first European conference on landslides, Prague, Czech Republic; Rotterdam, Balkema, pp 163–168

Gupta RP (2003) Remote sensing geology, 2nd edn. Springer, Berlin, p 655p

Guzzetti F, Carrara A, Cardinali M, Reichenbach P (1999) Landslide hazard evaluation; a review of current techniques and their application in a multi-scale study, central Italy. Geomorphology 31:181–216

Jensen JR (1996) Introductory digital image processing: a remote sensing perspective, 2nd edn. Prentice Hall, Upper Saddle River, p 316

Havenith H-B, Torgoev I, Meleshko A, Alioshin Y, Torgoev A, Danneels G (2006) Landslides in the Maily-Say valley, Kyrgyzstan: hazards and impacts. Landslides 3:137–147

Lin WT, Chou WC, Lin CY, Huang PH, Tsai JS (2005) Vegetation recovery monitoring and assessment at landslides caused by earthquake in Central Taiwan. For Ecol Manage 210:55–66

Malamud BD, Turcotte DL, Guzzetti F, Reichenbach P (2004) Landslide inventories and their statistical properties. Earth Surf Proc Landf 29:687–711

Pelletier JD, Malamud BD, Blodgett T, Turcotte DL (1997) Scale-invariance of soil moisture variability and its implications for the frequency-size distribution of landslides. Eng Geol 48:255–268

Ridd MK, Liu J (1998) A comparison of four algorithms for change detection in an urban environment. Remote Sens Environ 63:95–100

Roessner S, Wetzel HU, Kaufmann H, Sarnagoev A (2002) Satellite remote sensing for regional assessment of landslide hazard in Kyrgyzstan (Central Asia). Zweites forum katastrophenvorsorge. In: Tetzlaff G, Trautmann T, Radktke KS (eds) Deutsches komitee für Katastrophenvorsorge e.V. (DKKV). Boon. pp 433–441

Schlögel R, Torgoev I, De Marneffe C, Havenith HB (2011) Evidence of a changing size-frequency distribution of landslides in the Kyrgyz Tien Shan, Central Asia. Earth Surf Proc Landf 36(12), pp 1658–1669

Torgoev IA, Alioshin YG, Havenith H-B (2002) Impact of uranium mining and processing on the environment of mountainous areas of Kyrgyzstan. In: Merkel BJ, Planer-Friedrich B, Wolkersdorfer C (eds) Uranium in the aquatic environment. Springer, Berlin/Heidelberg/New York, pp 93–98

Turcotte DL (1997) Fractals and chaos in geology and geophysics, 2nd edn. Cambridge University Press, Cambridge, p 398p

Vandenhove H, Quarch H, Clerc J, Lejeune J, Sweeck L, Sillen X, Mallants D, Zeevaert T (2003) Remediation of uranium mining and milling tailing in Maily-Say district of Kyrgyzstan. Final report of EC-TACIS Project N°SCRE1/N°38, Vandenhove H Q H, Mol (Belgium), 614p

Improving Landslide Inventory with Persistent Scatterers in Calabria, Italy

Silvia Bianchini, Francesca Cigna, and Nicola Casagli

Abstract

Landslide inventory maps can benefit from the contribution of remote sensing technologies. We exploit PSI (Persistent Scatterer Interferometry) data extracted from ERS1/2 and RADARSAT-1 satellite images acquired in the intervals 1992–2001 and 2003–2010 respectively, for the detection and mapping of landslide ground displacements at regional scale. We propose a PSI-based procedure, based on the exploitation of activity matrices and intensity scales, combining the information coming from available pre-existing inventories and PSI average velocities. We apply this approach on the test area of Northern Calabria (Southern Italy), extended 4,410 km^2 and extensively affected by landslide hazard, finally updating and improving the landslide inventory of this area and assessing the spatial distribution, state of activity and intensity of 1,196 landslides, corresponding to 4.3 % of the whole investigated territory.

Keywords

Landslide • Inventory maps • Persistent Scatterer Interferometry • State of activity • Intensity • Landslide mapping • SAR Interferometry

Introduction

Systematic investigation and characterization of landslide phenomena at regional scale represent an essential requirement for risk assessment and for consequent planning of proper hazard-reduction resources and actions. Inventory maps of landslide processes deal with the detection of ground mass movements since they provide spatial distribution and parameters of each landslide (e.g. extension, typology, and state of activity).

Landslide inventories are usually based on conventional geomorphologic studies, which rely on intensive field surveys and on time-consuming manual interpretation of aerial and satellite optical images. Technical problems of spatial accessibility and related economical efforts of field campaigns and surveys can be considerably reduced thanks to the contribution of high precision, wide area coverage, non-invasiveness, and cost-efficiency of remote sensing technologies.

Persistent Scatterer Interferometry (PSI) is a multitemporal interferometric technique which analyzes long temporal series of satellite SAR (Synthetic Aperture Radar) data, and provides annual velocities and time series of ground deformation on dense grids of point-wise targets, the so-called PS or Persistent Scatterers (e.g. Ferretti et al. 2001; Colesanti and Wasowski 2006). The PS analysis has recently demonstrated to be a valuable and useful tool to detect surface dis placements with millimetre precision, and has turned out tobe successfully used for identification and mapping of slow-moving landslide phenomena and for evaluation of their state of activity and intensity, at regional and local scale (e.g. Farina et al. 2006; Meisina et al. 2006; Casagli et al. 2008; Pancioli et al. 2008; Herrera et al. 2009; Cigna et al. 2010; Notti et al. 2010; Greif and Vlcko 2011; Righini et al. 2011).

In this paper we present an innovative methodological approach for the updating and improvement of landslide

S. Bianchini (✉) • F. Cigna • N. Casagli
Department of Earth Sciences, University of Firenze,
Via La Pira 4, 50121 Firenze, Italy
e-mail: silvia.bianchini@unifi.it

C. Margottini et al. (eds.), *Landslide Science and Practice*, Vol. 1,
DOI 10.1007/978-3-642-31325-7_15,

inventories by means of PSI analysis, using radar images acquired by satellites ERS1/2 in 1992–2001 and RADARSAT-1 in 2003–2010.

Test Area and Input Data

The test area is the northern part of the Calabria Region, southern Italy. This area has an extension of 4,410 km^2 and includes part of the provinces of Cosenza (CS) and Crotone (KR). The geological background of the Calabrian peninsula shows a sheet pile of basement thrust units piled up and overthrust toward the Apulian foreland during the Neogene (Cucci and Cinti 1998). The outcropping terrains consist of Hercinian crystalline and metamorphic basement units and overlying Mesozoic and Tertiary sedimentary rocks (Amodio Morelli et al. 1976), covered by recent (mostly Upper Neogene) sediments. Northern Calabria is characterized by mountainous and hilly morphology and is extremely susceptible to landsliding because of high slope gradient, intense rainfalls, presence of weathered and faulted crystalline-metamorphic rocks and weakly-consolidated sedimentary sequences; these factors, when associated with extensive human activity (including unsuitable urban expansion and systematic deforestation), have played an important role in producing steep and highly unstable slopes (Carrara and Merenda 1976).

The available input data for the Northern Calabria case study include ancillary data, two pre-existing landslide inventory databases and PSI data. The ancillary data consist of topographic maps (1:10,000 and 1:25,000), geological map (1:25,000), DTM (Digital Terrain Model) with 20 m resolution and its derived maps, and aerial orthophotos with 1 m resolution (*Volo Italia IT2000*). The accessible pre-existing inventory maps are PAI (*Piano Stralcio di Assetto Idrogeologico*) and IFFI (*Inventario Fenomeni Franosi in Italia*). These inventories include spatial distribution of mass movements with related records (e.g. type, extension and state of activity of each phenomenon). They are based on aerial photo-interpretation, field campaigns and local databases and their quality depends strongly on the scale of resolution. PAI inventory reference date is 2001, while IFFI inventory was published afterward, updating PAI database, in 2007. IFFI inventory includes a total of 1,167 landslides, 371 (32 %) of which are classified as 'active' (including active, suspended and reactivated phenomena, according to the multilingual landslide glossary WP/WLI 1993), and 796 (68 %) as dormant. Stabilized phenomena (artificially stabilized, abandoned and relict; WP/WLI 1993) are not mapped. Landslides cover a total area of 168.4 km^2, corresponding to 4.1 % of the whole investigated territory and the most represented landslide typologies are roto-translational slides, complex movements, deep-seated and shallow landslides; these landslide phenomena mainly involve crystalline metamorphic rocks, terrigenous tectonized flysches and recent marine and continental deposits.

PSI ground deformation data consist of present and historical measures derived from two different satellites: present RADARSAT-1 data in the interval 2003–2010 and processed by e-GEOS with the PSP (Persistent Scatterers Pairs) technique (Costantini et al. 2000), and historical ERS1/2 data, acquired in 1992–2001 and processed with the PSInSAR (Permanent Scatterers Interferometric SAR) technique by TRE S.r.l. (Ferretti et al. 2001), in the framework of the PST-A (*Piano Straordinario di Telerilevamento Ambientale*) project. Both ERS and RADARSAT products are characterized by the map distribution of PS benchmarks, and the information provided for each target are: geographic coordinates (latitude, longitude, elevation), LOS (Line Of Sight) yearly velocity and displacement time series.

Within Northern Calabria, we selected two sample sites that are geologically and morphologically representative of most of the region and that are significant because of their landslide assortment in terms of typology, activity and intensity: Verbicaro site and San Lorenzo Bellizzi site, both located in CS province, respectively in the northwest and in the north-central portion of the test area (Figs. 1a and 2a).

PSI-based Methodological Procedure

The approach is based on photo- and radar-interpretation and combines conventional thematic data (topographic, geological and land use maps, and optical images) with deformation measures obtained with the PSI analysis. This integrated analysis leads to: (1) landslide detection and mapping, which consist in the boundaries confirmation or updating of pre-mapped phenomena and in the recognition of new landslides; (2) landslide activity and intensity assessment, which consists in the evaluation of the state of activity and intensity of each mapped phenomenon.

The entire process of acquisition, analysis and interpretation of all the available data is carried out in a Geographic Information System (GIS) environment, which properly combines radar measurements with the other maps and thematic layers.

Landslide Detection and Mapping

Landslide detection and mapping is carried out through the evaluation of boundaries and spatial distribution of each landslide within the test area. This spatial investigation relies on the ancillary data integrated with the pre-existing landslide inventory and with PS ground displacement measurements.

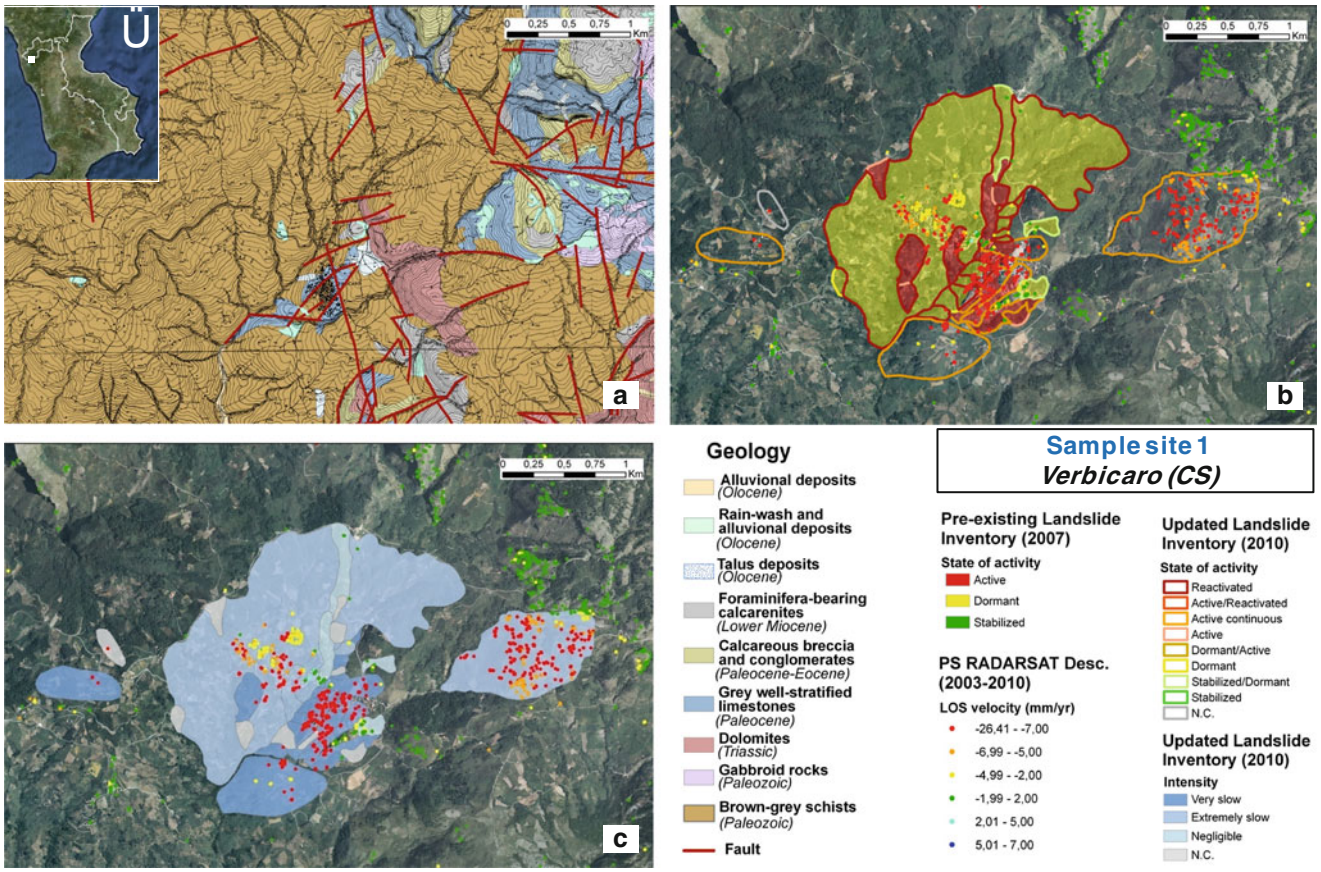

Fig. 1 Sample site of Verbicaro, Northern Calabria (Italy). (**a**) Geological map, 1:25,000; (**b**) Pre-existing and updated inventory map showing landslide state of activity; (**c**) Updated inventory map showing landslide intensity

On the basis of the pre-existing inventory map and PS distribution, the methodology consists of the radar-interpretation and aerial photo-interpretation procedures (Farina et al. 2006; Casagli et al. 2008; Pancioli et al. 2008; Herrera et al. 2009) that allow us to evaluate and spatially extend the point-wise ground motion rates provided by the PS deformation data.

Landslide mapping is mainly obtained by the individuation of geomorphologic evidences related to landslide phenomena, through the use of aerial imagery and through land deformation measurements over the space grid of PS points. Starting from the already mapped landslides, the presence of PS data within (or very close to) their boundaries can result in two conditions: confirmation of boundaries, when the inventory information is in agreement with PS data, or change (usually enlargement) of boundaries, when PS data suggest the modification of the pre-mapped area. No additional information can be given when PS data are not sufficient for radar interpretation or even when they are not present at all inside the already mapped area (Not Classified, N.C.). The presence of PS data outside the previous mapped areas can result in new landslide detections, when significant PS velocities and also geological and geomorphologic evidences suggest the presence of a landslide.

Landslide Activity and Intensity Assessment

Once mapped the spatial distribution of landslides in the area of interest, representative ground displacement values are determined, for each landslide, through the analysis of available PS data.

Landslide activity and intensity assessment is then performed by a PSI-based matrix approach, an advanced methodology for the evaluation of the state of activity and intensity of slow moving landslides, exploiting PS measures of present RADARSAT (2003–2010) and historical ERS (1992–2001) data. The evaluation of activity and intensity is computed by analyzing separately RADARSAT and ERS data for each landslide, and by calculating the average velocity of the PS identified within its boundary, V_P and V_H which are referred, respectively, to the two temporal coverages, *P*resent 2003–2010 and *H*istorical 1992–2001. These representative velocities (V_P and V_H) are then compared with the activity and intensity thresholds, which are chosen for this area as ± 2 mm/year and ± 10 mm/year, away or towards the satellite.

The state of activity of landslides is assigned through two activity matrices: the first one (Fig. 3a) is used for pre-mapped phenomena and it is based on the information

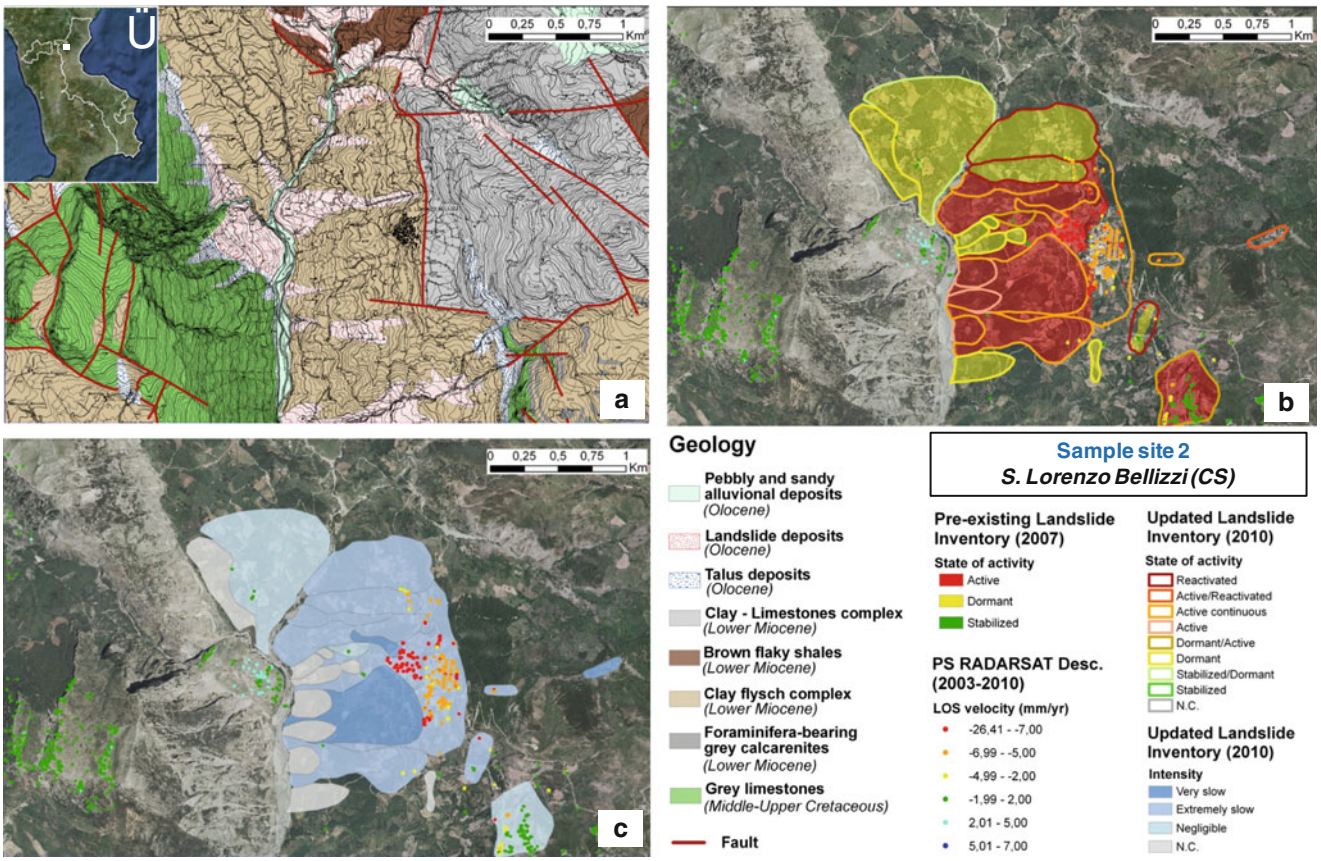

Fig. 2 Sample site of S. Lorenzo Bellizzi, Northern Calabria (Italy). (**a**) Geological map, 1:25,000; (**b**) Pre-existing and updated inventory map showing landslide state of activity; (**c**) Updated inventory map showing landslide intensity

coming from the pre-existing inventory map (reference data: 2007) and present RADARSAT PS measures (2003–2010). The second one (Fig. 3b) is used for new phenomena and it is based on PS measures derived from two distinct time intervals, present RADARSAT 2003–2010 and historical ERS 1992–2001. In the resulting inventory, using a simplified version of the official classification of the landslide states of activity as defined in WP/WLI 1993, two states of activity are distinguished: ACTIVE (currently moving) – including 'active continuous' (constantly moving or suspended) and 'reactivated' (moving after being inactive) phenomena – and INACTIVE (not moving in the last 12 months) – including 'stabilized' (not affected by their original causes anymore) and 'dormant' (potentially being reactivated) phenomena. The reference year of the classified activity is also pointed out in every cell-grid of the matrices.

The evaluation of the intensity of landslides is performed by an intensity scale (Fig. 3c), which is based on PS mean velocity (V_P or V_H) and consists of three classes: negligible ($V < 2$ mm/year), extremely slow (2 mm/year $\leq V < 10$ mm/year) and very slow (V $\geq$ 10 mm/year). When PS number or density is insufficient within the landslide boundaries, the phenomenon is not classified (N.C.).

Results and Discussion

Sample Site 1 – Verbicaro Site (CS)

The first sample site lies in the municipality of Verbicaro (CS province) and is characterized by a mountainous morphology with a dense network of narrow rivers and waterways (Fig. 1a). The site is affected by several large landslides, classified in the pre-existing landslide inventory as roto-translational slides and complex movements. These phenomena mainly involve low-grade metamorphic rocks and occasionally well-stratified limestones.

Pre-existing landslide delineation turned out to be incomplete, and photo- and radar-interpretation complementarity allowed the recognition of four new phenomena (Table 1). Monoscopic aerial photos, together with topographic maps, DTM and derived layers, allowed the detection of soil erosion evidences, vegetation coverage anomalies, and counterslopes along the longitudinal profile as landslide indicators; conventional photo-interpretation permitted to map land movements in natural and rural environments where geomorphologic features were easy to be observed, but where a low density

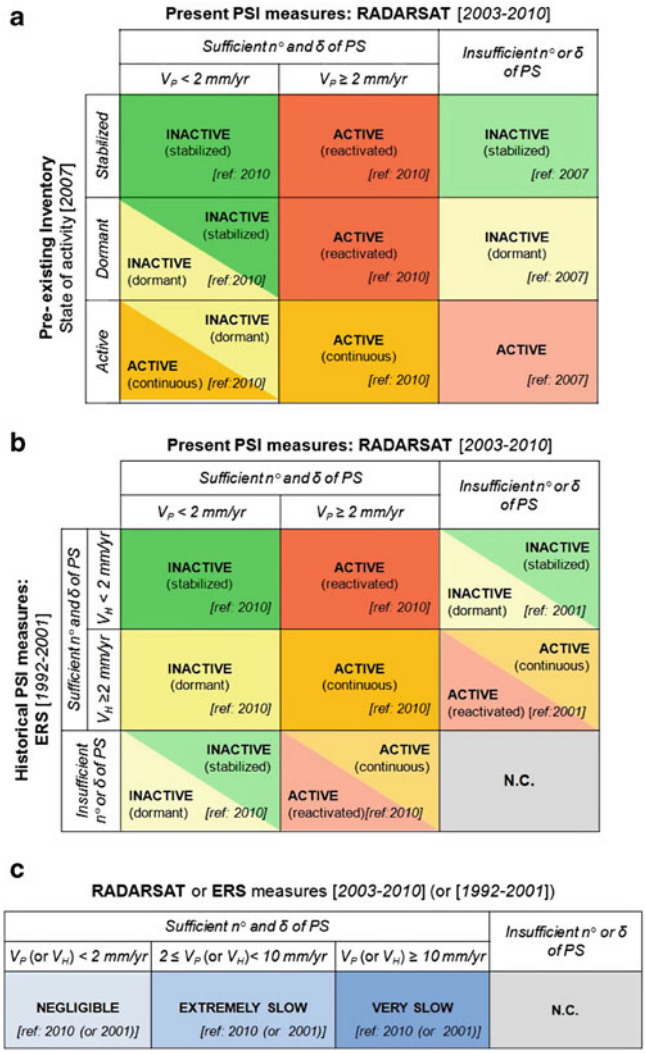

Fig. 3 Activity matrices and intensity scale based on the exploitation of PSI measures. (**a**) Matrix defined for landslides mapped in the pre-existing inventories; (**b**) Matrix employed for new detections, comparing historical ERS and recent RADARSAT measures; (**c**) Intensity scale

of radar targets was identified. On the other hand, radar-interpretation turned out to be very useful and suitable for mapping ground displacements in urbanized and artificial areas where much more PS benchmarkers (buildings or other infrastructures) were retrieved. In particular, aerial photos contribute to better identify landslides in the vegetated areas outside Verbicaro village, such as to the NW, where one new phenomenon was detected, even if it was classified as N.C. because of the presence of only one radar target (Figs. 1b and 3b). In fact, in order to reach a reliability of representative velocity evaluations, at least three radar targets were considered for both state of activity and intensity assessment (Meisina et al. 2006; Notti et al. 2010), and those phenomena not meeting the requirement were not classified (N.C.). The other three new landslides were identified through the orthophotos and the PS data, and show average velocities of 8–16 mm/year, which permit to classify two of them as very slow, and one as extremely slow (Figs. 1c and 3c). It is worth highlighting that the acquisition parameters of the currently available SAR sensors (i.e. temporal sampling and signal wavelength) do not allow the measurements and consequent classification of deformations that are faster than few tens of cm/year (LOS rates in C-band satellites up to 15 cm/year, falling in the class of very slow phenomena, i.e. 16 mm/year to 1.6 m/year, according to Cruden and Varnes 1996).

Moreover, some pre-mapped landslide boundaries were modified and enlarged by means of PS ground deformation data, especially in the Verbicaro urban fabric, which turned out to be unstable (Fig. 1b). For those PS located outside pre-mapped phenomena, when geomorphologic and geological setting and/or the PS velocity distribution did not show the presence of a landslide, no additional phenomenon was mapped. Other geological processes (e.g. subsidence or erosion) may, in fact, induce spatially distributed deformation; moreover, single unstable targets may not be indicative of a real landslide process, but more likely can be due to settlements of single structures.

In the western portion of the urbanized area, the state of activity of many pre-mapped phenomena was changed from dormant to reactivated; while in the eastern portion three landslides were classified as stabilized/dormant since their average ground deformation velocities ranged from 0.9 to 1.5 mm/year. This ambiguous classification is due to the "conservative" approach proposed in the activity matrix, which shows a double name in the two lowermost-left cells (Fig. 3a). For pre-mapped landslides, if PSI data register movements lower than ±2 mm/year, the state of activity recorded in the pre-existing inventory should be theoretically lowered from dormant to stabilized, or from active to dormant, respectively; however, real lowering of the state of activity can be eventually performed and confirmed afterwards, by means of field evidences and focused in situ monitoring (Cigna et al. 2010).

Sample Site 2 – San Lorenzo Bellizzi Site (CS)

The second sample site, located in the municipality of San Lorenzo Bellizzi (CS province), lies at the mountainside of Mt. Pollino and is characterized by steep slopes which reach heights of 1,300 m a.s.l., to both W (at Mt. Timpa di Cassano) and E (at Mt. Serra di Paola) (Fig. 2a). The western sector of Mt. Serra di Paola is affected by several landslides, which are predominantly deep-seated slope gravitational deformations, complex movements and roto-translational slides, as recorded in the pre-existing landslide inventory. These landslides involve terrigenous flysches and were

Table 1 Updating the pre-existing landslide inventory in Verbicaro (Site 1) and San Lorenzo Bellizzi (Site 2): number and percentage of landslide state of activity, intensity and main modifications implemented to the pre-existing inventory

Landslides		Site 1		Site 2	
		N°	%	N°	%
Pre-existing inventory		24	100	21	100
Active		14	58	10	48
Dormant		10	42	11	52
Stabilized		0	0	0	0
Updated inventory		28	100	23	100
Comparison	Confirmed	6	21	7	30
	Modified boundaries	5	18	0	0
	Modified activity	3	11	2	9
	Modified activity + boundaries	1	3	1	4
	New	4	14	2	9
	N.C.	9	33	11	48
State of activity	Reactivated	4	14	3	13
	Active/Reactivated	0	0	1	4
	Active continuous	10	36	5	22
	Active	6	21	4	17
	Dormant/Active	1	3	2	9
	Dormant	3	11	7	31
	Stabilized/Dormant	3	11	1	4
	Stabilized	0	0	0	0
	N.C.	1	4	0	0
Intensity	Negligible	4	14	3	13
	Very slow	11	39	3	13
	Extremely slow	3	11	7	30
	N.C.	10	36	10	44

confirmed or modified by means of photo- and radar-interpretation (Table 1): the state of activity of three phenomena was changed from dormant to reactivated and the deep-seated landslide located W of San Lorenzo Bellizzi village was enlarged to include the urbanized area, which showed a ground average velocity of 6–7 mm/year (Fig. 2b). PSI analysis also allowed the identification of two new phenomena E of San Lorenzo Bellizzi village: one of these was classified as Active/Reactivated with reference year 2001 because of the presence of historical ERS data, but absence of any recent RADARSAT targets. Regarding new detections, the lack of one of the two temporal evaluations of activity – past or present – of ground displacements, due to absence of benchmarks – RADARSAT or ERS respectively – prevents to discern between stabilized and dormant, or between active continuous and reactivated phenomena; for this reason, four cells in the activity matrix in Fig. 3b show double classification, reflecting the uncertainty in the assessment of the state of activity.

On outcropping rocks of Mt. Timpa di Cassano, which is oriented E-NE, some RADARSAT descending PS show positive velocities (blue colour; motion toward the satellite; Fig. 2b), while available ascending ERS data show opposite rates. This is because PSI measures are the one dimension (1D) projection along the satellite LOS, of 3D ground deformation. Slope orientation combined with LOS orientation may cause significant underestimation of land motions, or even may prevent at all the identification of PS within the observed scene, due to foreshortening, layover and shadowing effects (Colesanti and Wasowski 2006). The geometrical visibility of an area depends on its slope and on its aspect with respect to the satellite LOS orientation. The use of appropriate satellite geometry (i.e. along ascending or descending orbits) for the investigated area is therefore fundamental for each PSI-based analysis: generally, ascending acquisition modes are suitable for E-facing slopes, while descending modes are suitable for W-facing slopes.

Conclusions

The improvement of landslide inventory map in Northern Calabria was successfully carried out by means of the PSI technique. The availability of recent RADARSAT PS data (2003–2010) allowed the updating of the landslide inventory up to 2010. The comparison of recent PS data with the information coming from the pre-existing landslide database referred to 2007 and with historical PS measures (PS ERS data spanning 1992–2001) permitted the spatial detection and, when it was possible, the evaluation of present-day and past landslide activity and intensity of the phenomena in the area of interest. In particular, the PSI-based methodological procedure, based on the exploitation of activity matrices and

intensity scales, lead to the assessment of the spatial distribution, state of activity and intensity of a total of 1,196 landslides, that cover 177.5 km^2 (4.3 % of the whole investigated territory).

This PSI-based methodology demonstrated to be highly valuable and helpful for improving landslide inventory maps, especially in urban areas, in order to support the management and planning of risk-reduction measures and strategies.

A future enhancement of the proposed PSI-based methodology would consist in the exploitation of new SAR data (e.g. TerraSAR-X) with a higher spatial resolution (up to 1 m) and with a better acquisition frequency (up to 3–4 measures per month), allowing the identification of more recent and faster landslide phenomena with improved resolution and precision.

Acknowledgments This work is carried out within the SAFER (Services and Applications For Emergency Response) project, funded by the European Community's Seventh Framework Programme (FP7/2007–2013) under EC-ESA Grant Agreement n.218802. RADARSAT-1 data provided by the ESA managed GSC-DA, funded by the FP7/2007–2013 under EC-ESA Grant Agreement n.223001. RADARSAT-1 images were processed by e-GEOS with the PSP-DIFSAR technique. ERS PSI products were made available through the PST-A (*Piano Straordinario di Telerilevamento Ambientale*) project and the WMS service of the Italian Ministry for the Environment, Land and Sea. Access to IFFI (*Inventario dei Fenomeni Franosi in Italia*) was performed through the ISPRA's WMS service, while PAI (*Piano Stralcio di Bacino per l'Assetto Idrogeologico*) was made available by the Italian Civil Protection Department.

References

Amodio Morelli L, Bonardi G, Colonna V, Dietrich D, Giunta G, Ippolito F, Liguori V, Lorenzoni S, Paglionico A, Perrone V, Piccarretta G, Russo M, Scandone P, Zanettin Lorenzoni E, Zuppetta A (1976) L'arco Calabro-Peloritano nell'orogene Appenninico-Maghrebide. Mem Soc Geol Ital 17:1–60

Carrara A, Merenda L (1976) Landslide inventory in Northern Calabria, Southern Italy. Geol Soc Am Bull 87:1153–1162

Casagli N, Colombo D, Ferretti A, Guerri L, Righini G (2008) Case study on local landslide risk management during crisis by means of remote sensing data. In: Proceedings of first world landslide forum, Tokyo, Japan, Parallel Session Vol, 18–21 Nov 2008, pp 125–128

Cigna F, Bianchini S, Righini G, Proietti C, Casagli N (2010) Updating landslide inventory maps in mountain areas by means of persistent scatterer interferometry (PSI) and photo-interpretation: Central Calabria (Italy) case study. In: Malet JP, Glade T, Casagli N (eds) Proceedings of mountain risks: bringing science to society, Florence, Italy, 24–26 Nov 2010, pp 3–9

Colesanti C, Wasowski J (2006) Investigating landslides with space-borne synthetic aperture radar (SAR) interferometry. Eng Geol 88: 173–199

Costantini M, Iodice A, Magnapane L, Pietranera L (2000) Monitoring terrain movements by means of sparse SAR differential interferometric measurements. In: Proceedings of IGARSS 2000, Honolulu, Hawaii, 24–28 July 2000, pp 3225–3227

Cruden DM, Varnes DJ (1996) Landslide types and processes. In: Turner AK, Schuster RL (eds) Landslides: investigation and mitigation. Special Report 247, Transportation Research Board, National Research Council. National Academy Press, Washington, DC, pp 36–75

Cucci L, Cinti FR (1998) Regional uplift and local tectonic deformation recorded by the quaternary marine terraces on the Ionian coast of the northern Calabria (southern Italy). Tectonophysics 292: 67–83

Farina P, Colombo D, Fumagalli A, Marks F, Moretti S (2006) Permanent Scatterers for landslide investigations: outcomes from the ESA-SLAM project. Eng Geol 88:200–217

Ferretti A, Prati C, Rocca F (2001) Permanent scatterers in SAR interferometry. IEEE Trans Geosci Remote Sens 39(1):8–20

Greif V, Vlcko J (2011) Monitoring of post-failure landslide deformation by the PS-InSAR technique at Lubietova in Central Slovakia. Environ Earth Sci. doi:10.1007/s12665-011-0951-x

Herrera G, Davalillo JC, Cooksley G, Monserrat O, Pancioli V (2009) Mapping and monitoring geomorphological processes in mountainous areas using PSI data: Central Pyrenees case study. Nat Hazards Earth Syst Sci 9:1587–1598

Meisina C, Zucca F, Fossati D, Ceriani M, Allievi J (2006) Ground deformations monitoring by using the permanent scatterers technique: the example of the Oltrepo Pavese (Lombardia, Italy). Eng Geol 88:240–259

Notti D, Davalillo JC, Herrera G, Mora O (2010) Assessment of the performance of X-band satellite radar data for landslide mapping and monitoring: Upper Tena Valley case study. Nat Hazards Earth Syst Sci 10:1865–1875

Pancioli V, Raetzo H, Campolmi T, Casagli N (2008) Terrafirma landslide services for Europe based on space-borne InSAR data. In: Proceedings of first world landslide forum, Tokyo, Poster Session Vol, 18–21 Nov 2008, pp 81–84

Righini G, Pancioli V, Casagli N (2011) Updating landslide inventory maps using persistent scatterer interferometry (PSI). Int J Remote Sens. doi:10.1080/01431161.2011.605087

WP/WLI – Working Party on World Landslide Inventory (1993) Multilingual glossary for landslides. BiTech Publisher, Richmond, The Canadian Geotechnical Society

The Debris Flows Inventory of the Aosta Valley Region: An Integrated Natural Hazards Assessment

Marco Giardino, Sara Ratto, Mauro Palomba, Walter Alberto, Marco Armand, and Martina Cignetti

Abstract

The Aosta Valley (NW-Italy) is an alpine region where debris flows frequently occur, interacting with human activities and structures. For a best debris flow hazard assessment, research and mapping activities have been organized. First, aerial photo-interpretation and DEMs analyses were performed at a regional scale to inventory alluvial fans. Second, data on debris flow events have been collected from different sources, such as bibliographic and historical data, municipality hazard maps and drainage basin technical studies. For each event photo-interpretation and geomorphologic analyses have been performed to validate historical data and finally GIS statistical analysis have been carried out. The analysis led to the identification of about 200 single events, thus successfully upgrading a regional database on natural instabilities. Collected data allowed improvements to local knowledge on debris flows, through the recognition of multiple events in the same alluvial fan. Estimation of temporal occurrences led to more precise hazard assessment, useful for proper land planning.

Keywords

Debris flows • Geodatabase • GIS • Geomorphologic mapping • Natural hazards assessment

M. Giardino (✉)
Department of Earth Sciences, University of Torino, Via Valperga Caluso 35, 10125 Turin, Italy

Natrisk Inter-department Research Centre, University of Torino, Turin, Italy

Imageo Srl, Spin-off Company, University of Torino, Turin, Italy
e-mail: marco.giardino@unito.it

S. Ratto • M. Armand
Centro Funzionale, Regione Autonoma Valle d'Aosta, Aosta, Italy

M. Palomba
Department of Earth Sciences, University of Torino, Via Valperga Caluso 35, 10125 Turin, Italy

Natrisk Inter-department Research Centre, University of Torino, Turin, Italy

W. Alberto • M. Cignetti
Department of Earth Sciences, University of Torino, Via Valperga Caluso 35, 10125 Turin, Italy

Imageo Srl, Spin-off Company, University of Torino, Turin, Italy

Introduction

Debris flows are among the most hazardous geomorphologic processes occurring in mountain areas during intense and concentrated rainfalls. Their high mobility is cause of damages not only inside and closest to the torrent incisions, but often farther down on the alluvial fans.

In Northwestern Italy the occurrence of debris flow is one of the most significant natural hazard of the alpine valleys during either heavy, prolonged meteorological events or short and localized storms (Tropeano et al. 1995, 2001, 2006). Indeed, when tributary drainage paths intersect major valley bottoms, debris flows can represent a source of serious risk for structures and infrastructures located on the slopes or along the valley bottoms, especially on the alluvial fans (Mortara and Turitto 1989).

The simultaneous occurrence of several debris flows added to their rapidity, can lead to severe losses to large territories

C. Margottini et al. (eds.), *Landslide Science and Practice*, Vol. 1,
DOI 10.1007/978-3-642-31325-7_16,

and sometimes claim victims. In the recent past, this happened many times in Northwestern Italy, namely during the September 1993, July 1996, October 2000 and November 2002 events (Tropeano et al. 1995, 2001; Tropeano and Turconi 2001).

Consequently, preventive studies aimed to improve knowledge on debris flow processes and resulting effects are necessary to obtain better detailed hazard assessments, in order to protect population and infrastructures against future debris flows by better management of the related risks.

Recently, the knowledge on debris flow has strongly improved by the publication of dedicated studies including insights on hazard and risk assessment methodology and applications (e.g. Jakob and Hungr 2005). Currently, many scientific institutions and administrative agencies in Italy are conducting landslide hazard assessment studies: new methodologies for data collection and analysis, inventories creation and risk management have been made available. In particular, the IFFI Project ("Inventario dei Fenomeni Franosi in Italia"; Amanti et al. 2001; Trigila and Iadanza 2008) has produced a detailed and homogeneous landslide inventory over the whole Italian territory. This can be an important tool for hazard and risk assessment and subsequently for land use planning.

Unlike the national IFFI project, in the Aosta Valley Region debris flow events were excluded from the first edition of the landslide inventory. This choice was related to the peculiar characteristics of a debris flow: a natural instability phenomenon that propagates as an hyperconcentrated fluid along fluvial incisions, even if it usually derives from shallow landslides on slopes. Studies on debris flows are performed differently than those on other landslides. In the Alpine environment the persistence time of landforms related to debris flows can be very short if compared to that of rock falls or other landslides; it is difficult to recognise traces of previous events from aerial photographs, due to the rapid environmental changes and also to the obliteration operated by following events occurred in the same basins.

About debris flows accumulation area, the alluvial fans cover a considerable portion of the entire surface of the Aosta Valley Region, which become even more significant if we consider only the urban areas, mainly located along or near the valley bottoms.

For these reasons a research project has been carried out to improve the knowledge on debris flow hazard in the Aosta Valley by the creation of an inventory at a regional scale, combining historical data, technical maps and geomorphological analysis, as an upgrade of the Regional database for management of natural instabilities (DB "Catasto Dissesti").

Geological and Geomorphological Settings

The Aosta Valley Region is a major alpine valley system, corresponding to the Dora Baltea hydrographic basin. The elevations range from 400 m a.s.l., at the valley mouth into the Po Plain, to 4,810 m a.s.l., at the Mont Blanc, the highest peak of the whole European Alps.

From the geological point of view, the Aosta Valley belongs to the axial zone of the Western Alps, an imbricated stack of continental and oceanic metamorphic complexes (Dal Piaz 1992).

Among the morphodynamic agents of the Aosta Valley, the glaciers played the most important role, by modelling both erosional and depositional landforms (Carraro and Giardino 2004) and influencing indirectly the past and present-day slope dynamics (Panizza 1974).

The geomorphic activity of watercourses greatly affects the Aosta Valley's territory through the progressive erosional deepening of valleys. Also alluvial and "mixed" fans are widespread, mainly created by debris-flow phenomena, as shown during recent heavy meteorological events (i.e. 13–16 October 2000; Ratto et al. 2003).

A fundamental role in the geomorphology of the Aosta Valley is also played by gravitational phenomena, which vary in size and typology: from simple, shallow landslide to large slope instabilities At least 18 % (580 km^2) of the whole regional area is involved in gravitational dynamics (Ratto et al. 2007). A large percentage of landslides are represented by rainfall-induced small slides and soil slips which are often the main sources for debris flows.

Methods

A complex methodology for data collection, analysis and management has been developed to create a debris flow inventory at a regional scale and to improve knowledge on natural instability events in order to enhance hazard and risk assessment studies in the Aosta Valley region.

The data collection has been structured in two different stages. First, a regional fans inventory has been created and second, a GIS system including base and thematic maps have been associated to the geodatabase containing the debris flow events occurred in the region. The preliminary version of the inventory has been carried out only on some test areas of the Aosta Valley Region. To correctly represent all the environmental contexts of the Aosta Valley territory, four key sectors had been chosen (Fig. 1):

Fig. 1 The location of the Aosta Valley Region (NW Italy); the four test areas chosen for the preliminary version of the fans inventory are also indicated in *red* colour

1. The middle Aosta Valley (sector including Fénis and Pollein settlements), as an example of high urbanization on alluvial fans of the main bottom valley;
2. The sector of the middle Aosta Valley including Chambave and Saint Denis settlements, as an example of high urbanization area with debris flow distributed at different elevations, often associated to deep-seated gravitational slope deformation;
3. The Rhêmes Notre Dame valley sector, as an example of tributary valley with frequent and well-documented instabilities on the alluvial fans,
4. The Veny and Ferret valleys, as a case of high mountain area where frequent instability phenomena occurred, closely related to climate variables of glacial and periglacial environments.

First Step: A Regional Fans Inventory

After the preliminary "test" version, a complete fans inventory has been carried out at a regional scale. The identification of geomorphologic elements has been performed combining several methods, including traditional aerial photointerpretation (1997 flight Aosta Valley Autonomous Region) and Digital Elevation Models analysis (both 10 m- and 2 m-DEMs from LIDAR data were used).

Fans boundaries have been mapped by integrating expert visual DEM recognition of maximum slope gradients and aerial photointerpretation; this overcome difficulties in defining the exact geometry of the geomorphologic elements. The study allowed the identification of the lower limit of the alluvial fans and their relationships with fluvial deposits of the valley bottoms.

All the fans have subsequently been identified by an alphanumeric code and included in a database, containing information about watercourses and incisions feeding the alluvial fans. A total number of 620 fans distributed on the entire region has been inventoried, which cover a total area of about 81 km^2.

Second Step: Regional Geodatabase on Debris Flow Events

As a second step, data on debris flow events occurred in fan areas of the whole Aosta Valley Region have been collected from different sources, such as: bibliographic, historical and cartographic data. In particular, a great amount of data has been acquired from:

- Reports from the Regional Forestry Survey network.
- "AVI" database (Inventory of Italian affected sites by mass-movements and floods, by the National Research Council).
- "PAI" maps and reports ("Piani di Assetto Idrogeologico": Hydrogeological setting Plan, by the Po River Basin Authority).
- Municipality hazard maps and studies for land planning restrictions.
- Drainage basin technical studies, reviewed by regional agencies.

Further information have been also acquired through the analysis of the regional inventory maps compiled mostly during and immediately later major flood events occurred in the last decades, the most detailed being the one related to the 13th–16th October 2000 flood.

For each individualized debris flow event, aerial photointerpretations have been performed to validate bibliographic and historical data, both through orthophotos and traditional aerial photographs analysis. In many cases this procedure allowed to upgrade the bibliographic information, usually resulting as point data related to the damages caused by the event, to areal data for the correct definition of the affected area by the event. Often it has been also possible to verify the accuracy of the different data sources considered in the research and to choose the best information available.

Subsequently, the collected debris flow events have been formally organized in a GIS system to perform spatial and statistical analysis, in order to obtain and to identify the most affected sectors of the Region.

As it regards cartographic data, in the GIS structure has been included the fans boundaries, the fans identification points, the limits of the single debris flow events and the events identification points.

Each event has been included in a geodatabase associated to the GIS, where the single record is identified by an alphanumeric code; information on the event date, the municipality and the fan are also included. Within the database, records on debris flows have been divided into three different categories: point data, linear data and areal data. The events collected with an accurate cartographic information, useful to describe the involved area by the debris flow, have been catalogued as areal data; on the contrary when only partial information are available (i.e. damaged bridge or buildings) the record has been considered as a point one.

Finally all the records have been incorporated in the regional database for management of natural instabilities (DB "Catasto Dissesti"). Currently this archive contains about 9,000 records, structured in different categories (landslides, floods, debris flows); information on fans and watercourses characteristics, on damages amount and on remedial measures carried out for every single phenomenon are also available.

Results

The preliminary results of the research activity are outlined below. The methodology of data collection and analysis applied during this study led to the identification of over 220 single debris flow events in the whole area of Aosta Valley Region. Among these data, 23 records doesn't have a reliable chronological reference, while 11 events are missing the cartographic information ("point data"). The remaining data include a precise cartographic reference for the GIS system ("areal data") and reliable features description in the database, so it was possible to perform some spatial and statistical analysis.

As it regards the data temporal distribution, we can observe that most of the new acquired records are connected to the 13th–16th October 2000 flood event, one of the most severe flood of the last century, characterized by 270 different debris flow phenomena occurred on fans (Tropeano et al. 2001; Giardino and Ratto 2007) and 17 victims claimed. At least 171 single phenomena related to this event have been inventoried in the entire Aosta Valley Region, with remarkable differences in the geographical distribution of the natural instability events. The south eastern sector of the region has been the most affected

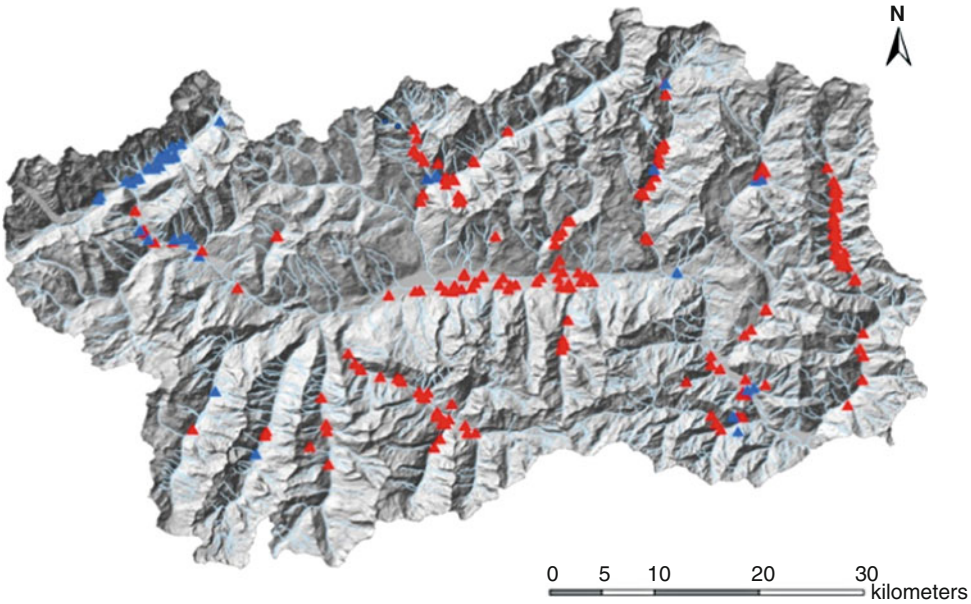

Fig. 2 Spatial distribution of the debris flow events in the Aosta Valley; *red* colours indicate the most severe flood episodes induced events, more frequent in the south-east sector of the region and along the main bottom valley; *blue* colours the ones related to brief and intense rainfalls

by the flood event, including both side of the main valley bottom and several tributary valleys; in particular, the locations with the highest number of observed events have been Gressoney-Saint-Jean (35 events) and Cogne (16 events), but a great number of debris flows have been reported also in Fenis, Arnad (main valley), Ayas, Antey-Saint-André and Valtournenche municipalities (tributary valleys).

The other records inventoried are related to the last decades events and in some cases they match with various large regional flood episodes which affected the Aosta Valley, as for example on October 1977 or on September 1993.

If we compare the new data collected within our research with the records already included in the regional database we can carry out some further observations about the data temporal distribution. Among the over 700 single debris flow events included in the regional database, it's clear the predominant information on the October 2000 event; obviously, this is related not only to the magnitude of the flood itself, but also to the great amount of data available nowadays, a really higher number of documents and reports, if compared to older events (e.g. October 1846, June 1957 or September 1993). However, data on previous natural instability events are still available. The 16th–18th October 1846 event, for example, was one of the most severe historical flood episode in the Aosta Valley, similar to the October 2000 one, both for magnitude and affected areas extent; several bibliographic sources report about the serious damages happened to numerous buildings, roads and bridges, following the flood event. Fewer effects occurred in the Aosta Valley during the June 1957 event, which didn't involve the whole regional territory with equal intensity, but mainly affected valleys of the Gran Paradiso and Monte Rosa sectors. Very severe episodes in terms of extent and damages amount were also the October 1977 and the September 1993 events. In both cases the Cogne Valley and part of the middle main Aosta valley were deeply involved (Blanchet et al. 1994); during the 1977 episode also the highway crossing the main bottom valley was seriously damaged by a large debris flow occurred in the Molinaz Creek (Pontey) (Tropeano et al. 1999).

Discussions

The collected data analysis allowed the identification of the most affected areas by debris flow events; on average all the south-eastern part of the Region is generally affected by the greatest number of natural instability phenomena: in particular some sectors of the middle and low main valley bottom and several tributary valleys, such as Lys Valley, Valtournenche Valley and Cogne Valley; with less intensity also Ayas Valley and Valpelline Valley.

As well, the observed geographical distribution of the debris flow events seems to be different during most of the prolonged and large extent rainfall episodes ("A") in comparison to brief and intense rainstorms ones ("B") (Fig. 2).

(A) In the former cases, the spatial distribution of debris flow phenomena reflects rather well the pluviometric distribution pattern of most severe flood events occurring in Northwestern Italy. Indeed, the most damaging floods take place usually in spring or in autumn when the main atmospheric streams flow comes from south/

southeast, carrying very humid air masses from the Mediterranean sea to the Italian side of the alpine chain; in these cases the highest precipitation peaks are on the internal side of the chain, upwind to the streams, and rainfalls decreases moving towards north/northwest (France and Switzerland boundaries). So, in the Aosta Valley Region the highest precipitation peaks are usually located in the south-eastern sector, particularly along Lys Valley and Champorcher Valley. This distribution has been observed also during the October 2000 event, when the rainfall maximum (up to almost 600 mm in 2 days) was situated at Pontboset (Champorcher Valley); on the contrary, on the western sector of the region the total precipitation amount was around 200–300 mm in 2 days (Ratto et al. 2003, Mercalli at al. 2003; Mercalli and Cat Berro 2001). More recently, a similar rain distribution pattern has been recognized during several intense rainfall events occurred in the last decade, for example June 2002 (Luino et al. 2003; Tropeano et al. 2006), November 2004, September 2006 and on May and November 2008. Moreover, these prolonged rainfall events are capable to simultaneously activate within the region natural instability phenomena in several drainage basin, usually with an area of over 10 km^2.

(B) On the contrary, in the second case, the spatial distribution of debris flows events is more irregular as a consequence of brief and intense rainfall episodes distribution. Therefore a more prominent role is played by local geological and geomorphologic features, as debris load availability or basin slope.

Numerous debris flows events occur in single small basins of many tributary valleys all over the region following rainstorm episodes, taking place typically during the summer season. As an example, we can remember the August 7th, 2004, event occurred in the Grand Valey basin (Saint-Vincent) (Tropeano et al. 2006), or the one on July 20th, 2006, occurred in the Cuneaz basin (Ayas) (Savio and Turconi 2006); more ancient events have been identified too, as the one on August 11th, 1986, occurred in Ferret Valley (Courmayeur) or the one on August 13th, 1972 in Colomba basin (Morgex). These events normally involve rather small basins (area up to 5–10 km^2) and the western part of the Region is regularly involved, as for example the Courmayeur area (August 1986, July 1991 and 1998 events) or the Rhêmes and Valsavaranche Valleys (July 1996 and June 2002 events); the geomorphologic context of these recently deglaciated areas often facilitate brief and intense rainfalls-triggered events: the enhanced activity of these younger basins is related to their greater debris load availability, and to the possible contribution of snow melting and glacial outburst at the higher elevations.

The study carried out at a regional scale showed the great importance of the combined use of different sources of information, such as historical, bibliographic and cartographic data. Even if most of the oldest historical data was only related to point records, they resulted very useful to assess temporal variation in local hazards by comparing ancient and recent events. Moreover, bibliographic data often included an event description, fundamental to understand which kind of natural instabilities occurred (debris flow vs water flood), normally of not clear interpretation by aerial photographs analysis only; for example, indication of duration and characteristics of the instability process can help to distinguish between a debris flow or an hyperconcentrated flow, as that occurred in the Saint Barthelemy basin on October 2000. Also information on damages caused to buildings can be useful, for instance to evaluate if a debris flow or a normal water flood occurred, as in the cases of Bioley basin (Fenis), Arly and Septumian basins (Chambave) on October 15th 2000.

The recognition of multiple occurrences in the same alluvial fan has been possible through the interpretation of documents from different sources; debris flow paths analysis on the fans led to a preliminary estimation of their magnitude and temporal occurrence, helpful to a more precise hazard assessment and consequently to a proper land planning (Fig. 3).

The comparison of different information sources also allowed estimation of their reliability degree. This was possible principally through orthophotos analysis by checking the real occurrence or the correct spatial representation of the events already included in different archives (Fig. 4); for this reason identification of erosion and depositional features characteristics of debris flow processes, such as debris levees and lobes and deep channel scouring, has been performed.

The higher number of reports available for more recent events is generally coupled to a higher level of damages too. For interpreting this fact we have to take in account not only possible implications of global climate changes, but also huge environmental and territorial modifications taken place in the last decades. The fast growth of urbanisation in the limited available space of the valley floors have remarkably altered the land use cover and increased the need to construct buildings on the alluvial fans; consequently, natural risk increased mainly related to debris flows.

Interactions between debris flows events on the fans and large landslides have been observed too. In the case of Bosmatto site (Gressoney-Saint-Jean, Lys Valley) an

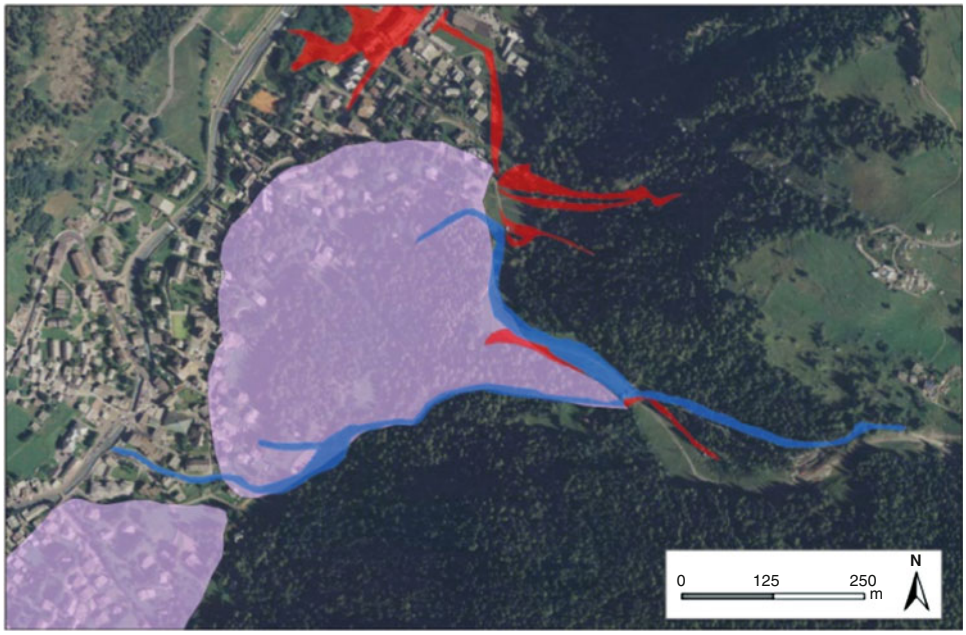

Fig. 3 Multiple debris flows occurrences on the Champoluc alluvial fan (Ayas Valley). With the *red* colour the October 2000 debris flows are indicated, with the *blue* colour the July 2006 ones

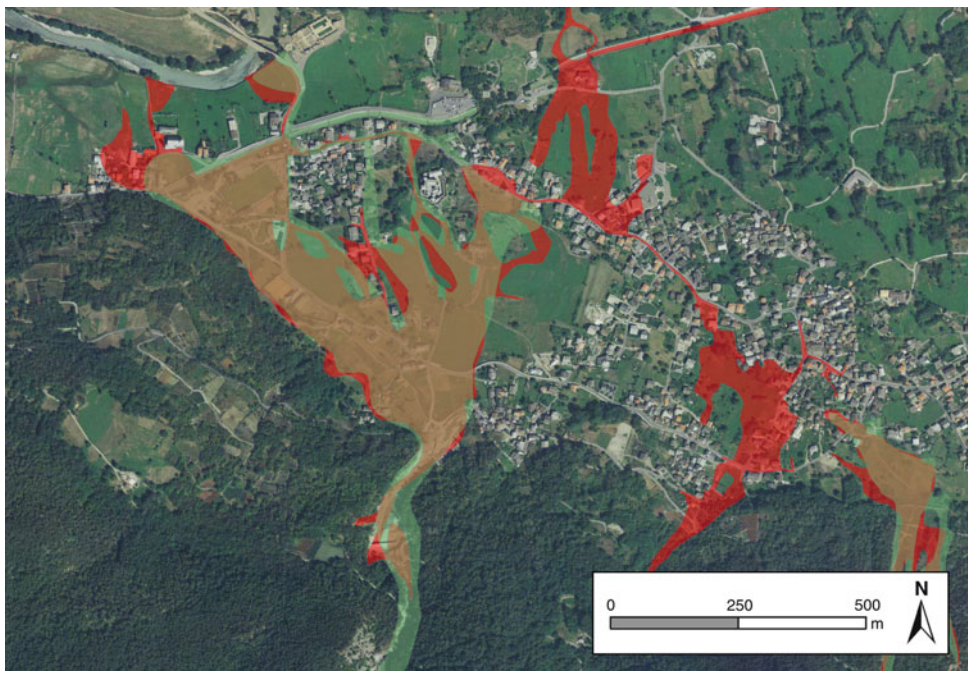

Fig. 4 Comparison of different maps of the same debris flow event from different sources (Arly fan; Fenis, main valley bottom). *Red* colour area from the regional map of the October 2000 event; *green* colour area from the Fenis municipality map for the land use; *brown* colour is the overlap area

impressive debris flow affected the Letzé basin, causing serious damages to the buildings located on the fan, on October 2000. The magnitude of the phenomenon (~200 km^3 of debris on the fan), unusual for a small basin like the Letzé one (<2 km^2), is related to the reactivation of the ancient Mussolier landslide (Fig. 5).

Application of the methodology to the complete Aosta Valley Region dataset involved also the overcoming of some difficulties:

1. *Correct identification of repeated events from different sources*. Aerial photographs analysis allowed to select the most accurate cartographic source; only when chronological references weren't available it had been very difficult to individualize debris flow events.
2. *Exact recognition of small phenomena*. Images resolution is a crucial parameter limiting results from photointerpretation.
3. *Rapid landforms obliteration*. Phenomena identification can be enhanced by availability of aerial photographs taken closer to the event.

Some final remarks are possible. The geodatabase associated to a GIS system enhanced organization and

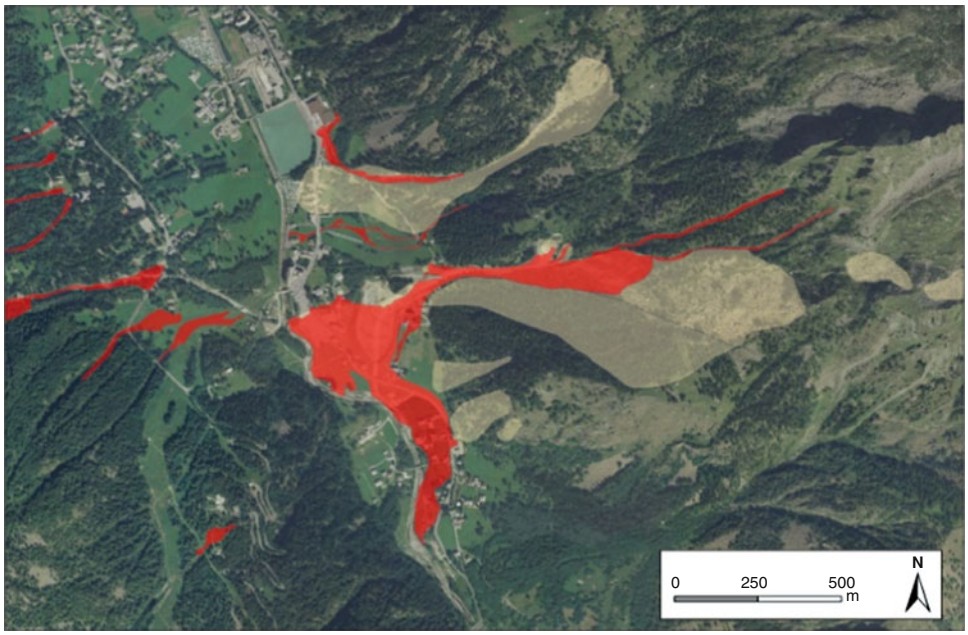

Fig. 5 Interactions between large landslides and debris flow events: the Bosmatto case (Lys Valley). *Red* colours indicate debris flows occurred on October 2000, *pale yellow* the Bosmatto landslide, as surveyed by IFFI project

management of the great amount of collected data. The regional debris flow inventory is ready for upgrades derived from the ongoing drainage basin technical studies, soon available for a great number of municipalities in the Aosta Valley Region. This will offer more detailed information on debris flow factors controlling typical activation thresholds, as for example those related to lithology, structural conditions, debris load potential, climatic fluctuations.

Acknowledgments This work was funded by the Regione Autonoma Valle d'Aosta within research agreements (2008–2010) with the University of Torino, concerning the Regional Landslide Inventory (IFFI Project).

References

Amanti M, Bertolini G, Ceccone G, Chiessi V, De Nardo MT, Ercolani L, Gasparo F, Guzzetti F, Mandrini C, Martini MG, Damasco M, Redini M, Venditti A (2001) Progetto IFFI. Scheda di censimento dei fenomeni franosi, versione 2.33. Presidenza del Consiglio dei Ministri, Dipartimento per i Servizi Tecnici Nazionali, Servizio Geologico, Roma

Blanchet G, Mercalli L, Spanna F, Pellegrino L (1994) Caratteri pluviometrici di settembre-ottobre 1993 sulle Alpi occidentali. Nimbus 2:28–30

Carraro F, Giardino M (2004) Quaternary glaciations in the Western Italian Alps. A review. In: Ehlers J, Gibbard PL (eds) Quaternary glaciations extent and chronology. Part 1 Europe. Elsevier, Amsterdam/San Diego, pp 201–208

Dal Piaz GV (1992) Le Alpi dal M. Bianco al Lago Maggiore. Società Geologica Italiana. Guide Geologiche Regionali. Be-ma (eds) Milano, 3, 311p

Giardino M, Ratto S (2007) Analisi del dissesto da frana in Valle d'Aosta. in Trigila A. (a cura di): Rapporto sulle frane in Italia, APAT Rapporti, 78/2007:121–150

Jakob M, Hungr O (2005) Debris-flow hazards and related phenomena. Springer, Berlin, 739p

Luino F, Chiarle M, Audisio C (2003) Mass movements in small alpine watersheds: a common but underestimated risk. The case of the Savaranche Valley (Aosta Valley) on June 23, 2002. In: Picarelli L (ed) Fast slope movements. Prediction and prevention for risk mitigation. Pàtron, Bologna, pp 325–331

Mercalli L, Cat Berro D (2001) L'evento alluvionale del 13–17 ottobre 2000 nel bacino del Po: analisi pluviometrica. Nimbus 21–22:33–40

Mercalli L, Cat Berro D, Montuschi S, Castellano C, Ratti M, Di Napoli G, Mortara G, Guindani N (2003) Atlante Climatico della Valle d'Aosta. SMS, Torino, 405p

Mortara G, Turitto O (1989) Considerazioni sulla vulnerabilità di alcuni siti adibiti a campeggio in ambiente alpino. Suolosottosuolo, Congresso Internazionale di Geoingegneria, Torino, 27–30 settembre 1989, pp 137–144

Panizza M (1974) Fenomenti franosi connessi ad azioni di glaciopressione. Boll Com Glac It 22:45–48

Ratto S, Bonetto F, Comoglio C (2003) The October 2000 flood in Valle d'Aosta (Italy): event description and land planning measures for the risk mitigation. Intl J River Basin Manag 2:105–116

Ratto S, Giardino M, Giordan D, Alberto W, Armand M (2007) Carta dei fenomeni franosi della Valle d'Aosta, scala 1:100.000. Regione Autonoma Valle d'Aosta Assessorato Territorio, Ambiente e Opere Pubbliche, Tipografia Valdostana, Aosta

Savio G, Turconi L (2006) Eventi di colata detritica osservati nell'estate 2006 in Italia Nord-occidentale. Estratto GEAM. a. XLIII, 3:37–46

Trigila A, Iadanza C (2008) Landslide in Italy. Special report 2008 (Rapporti 83/2008), ISPRA, Roma, 32p

Tropeano D, Turconi L (2001) Alluvione del 14–15 ottobre 2000 nell'Italia nord-ovest: cronaca di sintesi e commenti. Nimbus 21–22:53–85

Tropeano D, Arattano M, Deganutti AM, Luino F, Cirmatori L, Dutto F (1995) L'evento alluvionale del 23–25 settembre 1993 in Liguria, Piemonte e Valle d'Aosta. Aspetti idrologici e geomorfologici. Quad di studi e Documentazione, 18, Suppl. a GEAM, a XXXII, 2–3, 43p

Tropeano D, Govi M, Mortara G, Turitto O, Sorzana P, Negrini G, Arattano M (1999) Eventi alluvionali e frane nell'Italia Settentrionale. Periodo 1975–1981. CNR IRPI di Torino, GNDCI, 279p

Tropeano D, Luino F, Turconi L (2001) Evento alluvionale del 14–15 ottobre 2000 nell'Italia Nord-Occidentale. Fenomeni ed effetti. Geoingegneria Ambientale e Mineraria (GEAM) 101:203–216

Tropeano D, Luino F, Turconi L (2006) Eventi di piena e frana in Italia settentrionale nel periodo 2002–2004. SMS, Torino, 158p

The Integration Between Satellite Data and Conventional Monitoring System in Order to Update the Arpa Piemonte Landslide Inventory

Luca Lanteri and Alessio Colombo

Abstract

Arpa Piemonte is in charge of the maintenance of the framework about the hydrogeological instability of the Piemonte region. One of the main goal of working package B2 of the ALCOTRA European Project RISKNAT is focused to improve the knowledge of the SIFRAP (the landslide inventory of Piedmont region), in particular on the more serious phenomena where detailed examination is needed. The update is mainly carried out by the integration of different kind of data in order to obtain an effective knowledge of phenomena: detailed morphological analysis, carried out mainly by air-photo interpretation and some aimed field survey, are coupled with the outcome of the monitoring system of Arpa Piemonte. Thanks to the found of RISKNAT project also space borne radars data are available: in 2010, we covered an Alpine area of about 13,000 km^2 using data sets from Canadian RADARSAT satellite, covering the time span from 2002 to 2009. The survey was made using a newly patented processing algorithm (the SqueeSAR™) and identified more than 2 millions PS. Also a previous in coverage was made over the entire region (~25,000 km^2) using data sets from ERS-1 and ERS-2 radar satellites, covering the time span from 1992 to 2001. The main activity is now pointed out to analyse and integrate together all these different data in order to obtain meaningful landslides interpretations and an efficient way to make available all data to citizen and regional authorities.

Keywords

Landslide inventory • Risknat • SAR • Permanent scatterers • GPS • Inclinometers • Open source • Geodatabase

Introduction

Starting from the end of 1970, the Geological Survey of Piemonte Region collects information concerning flooding, landslides, geomechanical characteristics of earths and rocks and is in charge of the management and the development of the regional landslide-monitoring system. In 2002 all this topics was moved into the ARPA Piemonte (Regional Agency for Environmental Protection) where the Thematic Department "Geologia e Dissesto" continues to maintain this valuable resource up to date. A first 1:100,000 regional landslide mapping was carried out for the entire regional territory in the first part of 1980s.

From 2000 to 2005 the IFFI project (The Italian landslide Inventory) contributes to increase the level of knowledge and allow to product a national homogeneous landslide information system. The number of mapped landslides has grown considerably compared to the first regional inventory. In 2005, on the bases of IFFI results, about 35,000 single phenomena have been identified and analysed (Fig. 1).

L. Lanteri (✉) • A. Colombo
ARPA Piemonte (Regional Agency for Environmental Protection), via Pio VII 9, 10135 Torino, Italy
e-mail: l.lanteri@arpa.piemonte.it

C. Margottini et al. (eds.), *Landslide Science and Practice*, Vol. 1,
DOI 10.1007/978-3-642-31325-7_17,

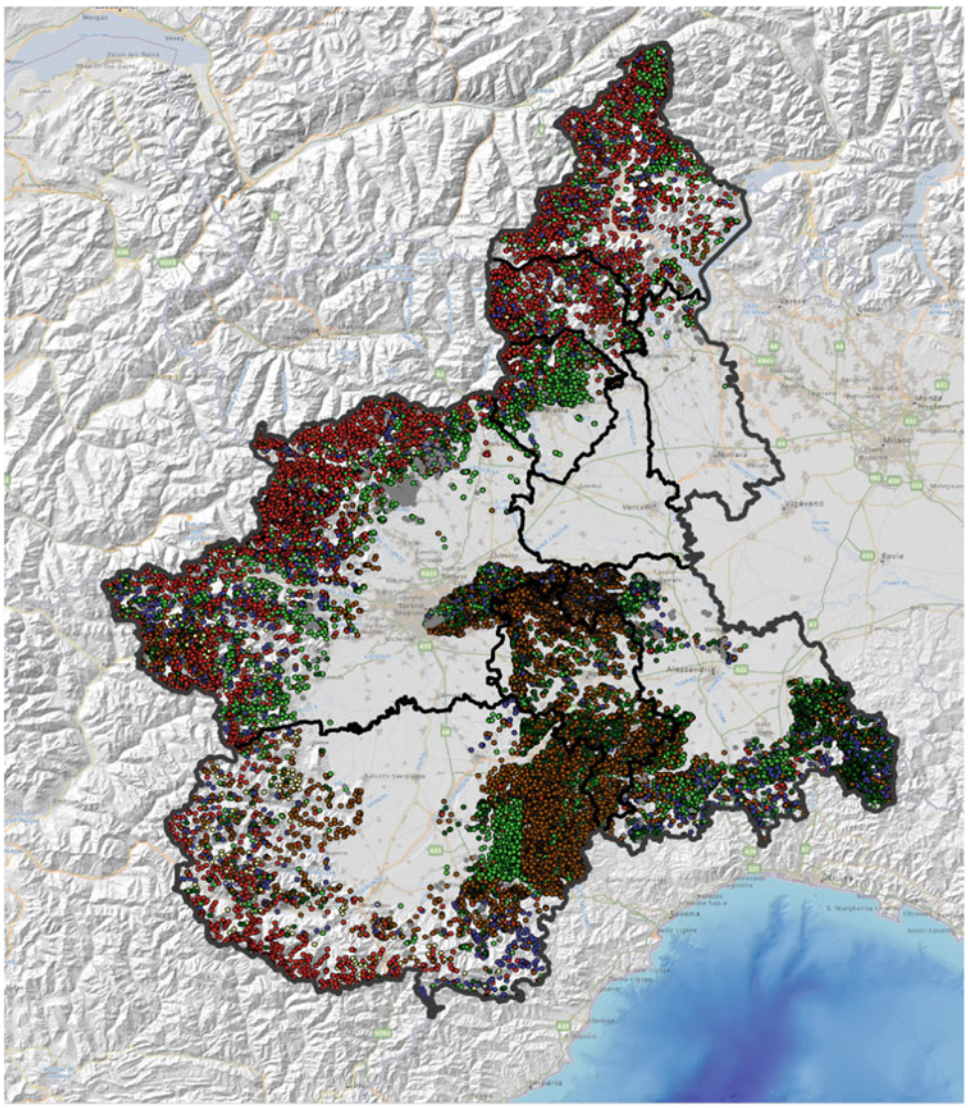

Fig. 1 Distribution of landslide in Piedmont identified by IFFI project in 2005. Due to the scale all landslides are represented as *points*

The knowledge also increased in terms of data quality: the old 1:100,000 landslide mapping was simply cartographic description with a distinction of landslide type (Colombo et al. 2005). A first level of knowledge, which defines a basic landslide classification (shape, location, state of activity and typology), was reached on the whole region.

Now, the strategic Project RISKNAT, a programme for Italian–French cooperation (Objective 3 ALCOTRA) founding the developing of operative tools that can be helpful for land planning and risk management. Especially the B2/C2 working package is aimed to improve the knowledge of the hydro-geological risks in the alpine region and to make available an easy to use and updated framework about natural risks both to common people and administrations.

Therefore, the activity of Arpa Piemonte is focused to improve the knowledge on the more serious phenomena where detailed examination is needed.

The Landslide Inventory

The present landslide inventory of Arpa Piemonte is mainly based on the IFFI project specification, in order to maintain full compatibility with the national inventory. However, from the 2005, when the IFFI project was ended, the inventory has grown significantly both in term of number of collected information and integration with the other components of Arpa geological information system. A strong effort was made to introduce all the missing information necessary to have a complete and exhaustive description of landslides. The geographic data, has been now integrated with information about: detailed morphological elements, location of damages, slope-protection measures and position of detailed geological/structural site survey.

The existing multiple choice field was mainly integrated with some text fields (eg: "*general description*",

"m*orphological description*", "*detailed damages*", "*monitoring data interpretation*" etc.), that allow a more detailed definition of the phenomena.

Some specific section was added to describe the characteristic distinctive for every landslide movement; e.g. for rock-fall is now possible to insert the block shape and volume or to describe impact trace, and other specific information; for other typology such translational landslide is possible to store more specific morphometric information as multiple sliding planes.

Another specific section was added in order to describe the outcome of the monitoring system. In this section it's possible to browse directly from SIFRAP the most significant instrumental data and to plot graphics as cumulative displacement, or polar direction of movement. A detailed analysis of the instrumental data is described into the text field.

A big improvement in comparison to the previous IFFI inventory was made also regarding the data-store infrastructure. All data are now stored in a geographic PostgreSQL/PostGIS database, also containing the whole geological information system of Arpa. Adopting a single geo-database that contain all geo-thematic data allow to reach an higher level of integration with all landslide description ancillary data contained into the Arpa information system such as: monitoring data, borehole log, historical bibliographic data, etc. All the related information can now be simply linked together by the user and become automatically available from one component of information system to another.

Moreover, is it possible to automatically intersect the most significant data with landslide geometry: as an example a simple statistic about PSInSAR™ data, with n° of PS that falls into the landslide, their average, min and max velocity and other basic information was calculated immediately at the end of geometry digitalization. The same thing was made with other data as: environmental or land use regulations, land cover and the nearest meteorological station in order to have a fast landslide characterization, or with element at risk as anthropic infrastructure, dam etc., so that basic statistics were disposable just in real time.

Furthermore, some tools was developed in order to allow data analysis and plotting data directly with an open source GIS and others common commercial and open source instrument. The potential of the integration of these tools made it possible to create an environment, practical, efficient and extremely dynamic in which all data can be effectively post-processed in order to provide the information necessary for understanding the phenomenon.

Satellite Data

Space borne radars have sensibly increased the potentialities of remote sensing opening to a wide range of applications up to now unavailable. Unlike the optical ones, radar images are independent of lighting or weather conditions; hence a regular collection of scenes can be acquired over the same area, basically providing a measurement of the distance between the sensor and the ground target. The specific orbit allows to repeat the measurement in a defined time span, thus, if the target is situated in an area subject to surface deformation, the sensor will detect the variation in the distance by comparing different acquisitions. Different methods for SAR data processing have been recently developed, such as the PSInSAR™ (Permanent Scatterers technique) (Ferretti et al. 2000) analysis, based on the processing of long series of radar data (min. 25–30) acquired in the same geometry over the same area in order to single out those pixels, referred to as Permanent Scatterers (PS), that have a "constant" electromagnetic behavior in all the images. PS can be rock outcrops or large boulders, metal or concrete power poles, buildings, manufactures. PSInSAR™ is a tool for quantitative measurements on a point-wise basis, somehow similar to a GPS network but where each record corresponds to a satellite acquisition depending on the revisiting time of the adopted satellite. The technique has several applications the most important of which is, to our purposes, the analysis of large areas in order to measure slow surface deformation phenomena, such as subsidence, landslides and seismic faults.

Thanks to Space borne radars we were able to increase the potentialities of the monitoring network in order to update and improve the knowledge on the instability framework into the whole region. In Piemonte we realized, in 2007, a PSInSAR™ survey over the entire region (~25,000 km^2) using data sets from ERS-1 and ERS-2 radar satellites, covering the time span from 1992 to 2001. The survey used about 390 radar scenes and identified about 2.5 millions PS. In the framework of an European Project (Alcotra Risknat), in 2010, we covered an Alpine area of about 13,000 km^2 using data sets from Canadian RADARSAT satellite, covering the time span from 2002 to 2009. The survey was made using a newly patented processing algorithm (the SqueeSAR™) by the Politecnico of Milano and identified more than 2 millions PS. SqueeSAR™ (Ferretti et al. 2011) is a second generation PSInSAR™ analysis: exploiting both 'point wise' PS and 'spatially distributed scatterers' (DS). The new algorithm provides information in low-reflectivity homogeneous areas by identifying DS–previously unidentified with PSInSAR™. The availability of such a great amount of high quality data of a new type, however, poses us, landslide-geologists, the hard but challenging task of converting a tool developed by electronic engineers in a tool usable for us. So we did move on the totally unbeaten trail by: defining some guidelines for data use; understanding and defining the limits of the technique; using PS data to integrate at a regional scale the landslide inventory; using PS data for detailed analyses on critical landslides; comparing PS data with data from conventional landslide-monitoring systems; processing the data for

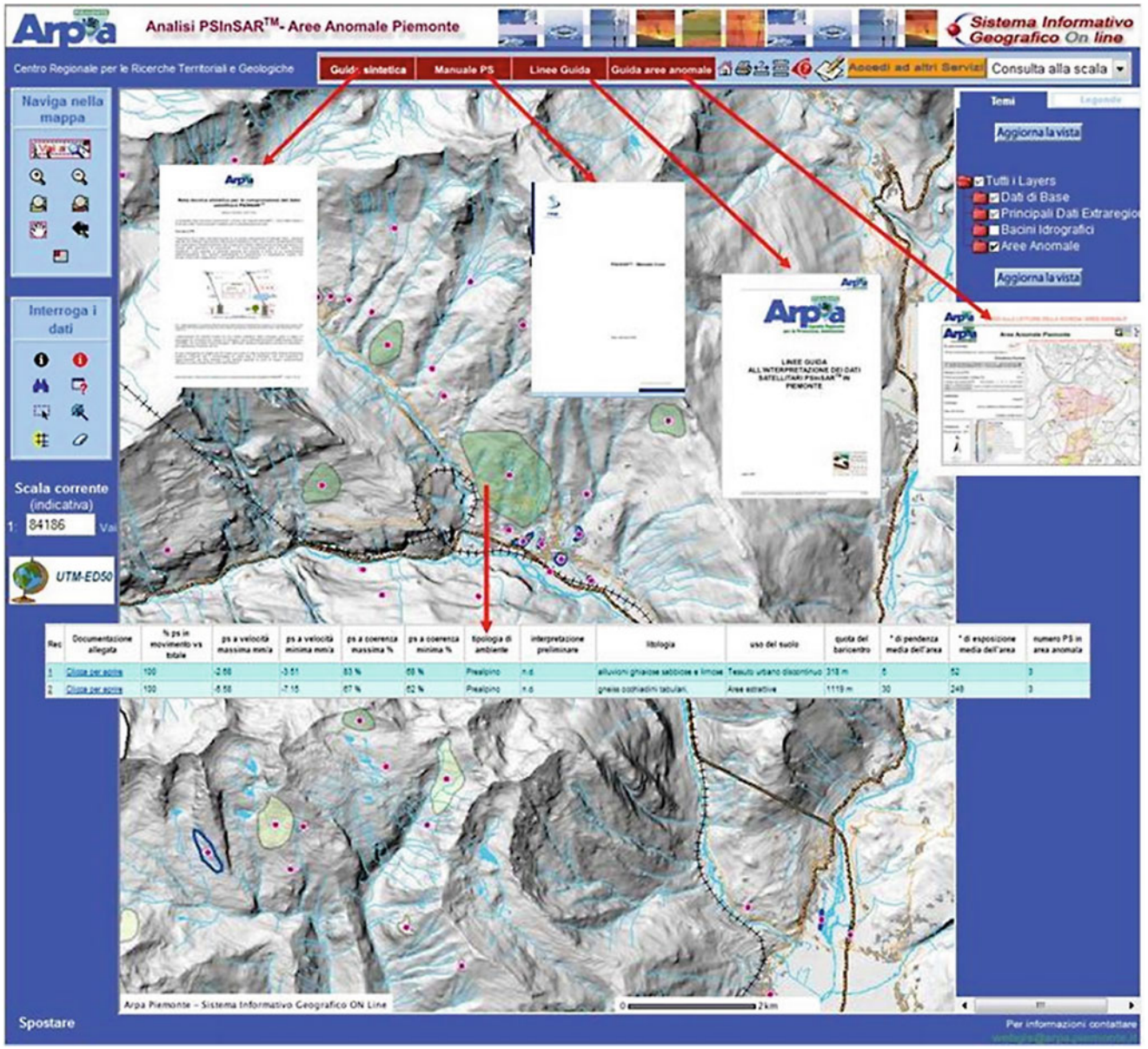

Fig. 2 Data about the geological interpretation of ERS satellite data are diffused by the Arpa Piemonte WebGIS service "Anomalous Areas". The web page also allows to reach technical documents about PSInSAR technique and their correct interpretation

diffusion by webGIS services (as far as we know, our service http://marcopolo.arpa.piemonte.it/ps_ers06/w_ps_ers06.php is unique) (Fig. 2); developing some tools useful for data analyses; defining some specification for public agencies who may need to perform a PS survey; organizing formation seminars for geologists and engineers who may use PS data for risk analyses. In general the analysis of PS/DS data showed that the detection depends by some factor

- Scatterer distribution: the presence of natural scatterers generally increases the number of landslides suitable for analysis. The presence of vegetation limits the presence of PS.
- Geometry of acquisition: the use of two geometries of acquisition (ascending and descending) can reduce the topographic distortions of SAR image (layover and foreshortening) that affect steep slope areas (Alps). So it is possible to detect more landslides. Moreover the availability of PS data in both geometries allows estimating vertical and E-W horizontal displacement components;
- Velocity of the landslide: SAR data analysis is suitable only for very slow landslides with constant movement (DSGSD and complex landslides) that usually represent a small percentage of all landslides

The PS density depends mainly on the presence of targets (rocks, debris, buildings), on the topographic effects (layovering, shadowing, etc.), on the vegetation and snow cover and also on the numbers of scenes elaborated, this results that in some environment, e.g. Apennine, the PS are distributed along the valley bottom where the density of man-made structures is the highest. Another problem is the difficulty in discriminating ground deformation due to different processes, as local settlement of man-made structure (e.g. Apennine and Langhe) or the shallow deformations caused by seasonal processes in debris (Alps) (Meisina et al. 2008).

Landslide Inventory Updating

The inventory defining three levels of landslide knowledge, depending on the available information. The first level defines a basic landslide classification (shape, location, state of activity and type); the second level includes more detailed data from field surveys; the third includes data available from the pre-existing detailed studies. The first level was completed after the end of the IFFI project, and it has allowed reaching a basic level of knowledge on the whole region. Now the activity is pointed to improve the knowledge on the more serious phenomena where detailed examination is needed and to maintain the whole database up to date.

A first step is based on the analysis of monitoring data. Arpa manage several devices installed all over Piemonte to monitor landslides that occur close to facilities or built-up areas. The network includes about 300 monitored sites, up to now. The monitoring network includes many sites with few, mostly conventional instruments (inclinometers, piezometers, extensometers, and topographic benchmarks).

The monitoring data was coupled with detailed morphological analysis, carried out mainly by air-photo interpretation and, in second place, with some aimed field survey. Also the analysis of the geotechnical database of Arpa has allowed to obtain a more exhaustive geo-mechanical framework.

The contribution that SAR interferometry made in updating Arpa Piemonte landslides inventory was supported by the help and the knowhow of the university of Pavia group. By the contribution of Anomalous Areas interpretation (Meisina et al. 2008) we were able to integrate and up to date about 900 phenomena around the whole region. The updating of landslides inventory can be made in these terms:

- Detecting of new landslides: The PS data give information about movements of the surface even where it is not possible to discriminate with other traditional observations;
- Change of the boundaries and/or the typology of old landslides: the PS data, always combined with geomorphological analysis or other data, can be used to redefine the boundaries of the landslides already present in the database. Sometimes the PS data allow to redefine and to improve the interpretation of landslides. For instance this situation is typical of the big rock-fall – rock avalanche accumulations that are also affected by other processes like slow flow or complex landslides. We can use PS data even to change the landslide type according to the landslides classification by velocity proposed by Cruden and Varnes (1996). As previous reported the PS techniques are suitable to study of slow landslides, rapid flow, and rock-fall or in general faster landslides must be mapped by means of other methodologies;
- Determinate the state of activity of landslides: according to other authors (Meisina et al. 2008; Cascini et al. 2009; Righini et al. 2010) PS data are useful to compare and update the state of activity by the movements detected but it is very important point out many limitation such as the period of observation (1992–2009), the coverage quality of PS data, the fact that PS are measured along the LOS directions (1D dimension) and finally the thresholds. Actually it is not an easy task to define a sharp threshold of velocity between stable or dormant and active landslides, and this threshold depends also on the type of landslides. The integration between the PS velocity value and the landslide geomorphological approach (Giglia et al. 2003) seems to be useful to evaluate the residual condition of the slopes;
- Individuate the possible buildings damaged by landslides displacement: The buildings are one of the more suitable targets to be detected as persistent scatterers. The presence of buildings on landslides in many areas (Langhe Hills in Piedmont or Apennines chain) is the only chance to have data of displacement using the SAR techniques. At the same time PS technique may be used in a faster way and on a large scale to detect the buildings potentially damaged by landslides movements.

As for the scatterers on debris, the distribution of the value of the PS velocity on buildings may be also used to discriminate geological process. For instance a strong movement distributed over all the buildings of village is with high probability related to a landslide; a pattern of irregular movements is probably related to a local geotechnical or structural problem (Notti 2010).

The potentiality of PS techniques is clearer when it's compared with the traditional monitoring system. Considering the landslides with at least 3 PS, a density greater than 20 PS/km^2 and of a suitable typology for PS techniques, the 23 % of landslides can be studied and actually monitored with SqueeSAR™ technique. Only 2 % of landslides have a traditional monitoring system.

It's also important to remark that also the stable PS are important, in fact they confirm that a landslide is stable during the time of analysis.

As PS data became a more familiar measurement technology, opportunities emerged for its conjunctive use with GPS and in general geodetic surveying systems. This was stimulated largely by the fact that the strengths of one technology were complemented by the weaknesses of the other. In particular the synergistic use of all type of ground deformation monitoring systems allows:

- Temporal sampling integration: the integration of measures frequent but limited in time with longer time series but monthly cadenced;
- Spatial sampling integration: PS data have a high density of measurement points even if it is not possible to discriminate between different types of deformation on the base of PS position on buildings but no site work needed on the other hand geodetic systems have a low density of measurement points but the measuring station is quite identified and usually accompanied by a monographic book on the other hand there are often some problems due to difficulties during stations set up;
- Precision: PS data due to the low angle of acquisition have millimetric displacement accuracy in vertical direction joined with the spatial positioning accuracy in millimeters derived from GPS measurements.

Therefore the results of this integrated approach are extremely good, the benefit-cost ratio is favourable and the interferometric radar technique proved extremely useful for: identification of formerly unknown slow-moving landslides; proper definition of large alpine deep seated gravitational deformation; definition of the state of activity; landslides zoning; landslide monitoring; detailed investigation of large landslides. The comparison of data from different monitoring system has allowed to obtain an important cross-validation, especially for the brand new SqueeSAR™ technique, where there are few case studied.

In conclusion Regional landslides inventories can be partly updated by PSInSAR™ and SqueeSAR™ interferometry. Nevertheless, the integration with traditional methods such as aerial photo interpretation, field surveys, monitoring and collection of historical data is primary to aid geologists to a correct inter-operation of landslides mechanisms.

Data Dissemination

A proper webGIS service allow to access to all the data. The main service is available from the institutional website of Arpa Piemonte and now also from the RISKNAT project geoportal. The webGIS service allows browsing and searching, in addition to landslide geometry and location, even a set of basic information of 34,000 phenomena, such as the state of activity, the activation date, the methodology of survey, and other correlated data. In order to make available a set of detailed data that can't be spread by webGIS technologies a detailed PDF form was made. Up to now it is possible to download this detailed form for about 180 phenomena, and it will be about 300 at the end of the project.

Acknowledgements This work has been co-funded by European Union – European funds for regional development IT-F ALCOTRA Programme – 2007–2013 Project RISKNAT.

A sincere thanks to all people who worked in the Thematics Department "Geologia e Dissesto" of Arpa Piemonte and the University of Pavia.

References

Cascini L, Fornaro G, Peduto D (2009) Analysis at medium scale of low-resolution DInSAR data in slow-moving landslide-affected areas. ISPRS J Photogramm Remote Sens 64:598–611

Colombo A, Lanteri L, Ramasco R, Troisi C (2005) Systematic GIS-based landslide inventory as the first step for effective landslide-hazard management. Landslides 2(4):291–301. doi:10.1007/s10346-005-0025-9

Cruden DM, Varnes DJ (1996) Landslide types and processes. In: Turner AK, Schuster RL (eds) Landslides investigation and mitigation. Special Report 247, Transportation Research Board, National Research Council, Washington, pp 36–75

Ferretti A, Prati C, Rocca F (2000) Nonlinear subsidence rate estimation using permanent scatterers in differential SAR interferometry. IEEE Trans Geosci Remote Sens 38:2202–2212

Ferretti A, Fumagalli A, Novali F, Prati C, Rocca F, Rucci A (2011) A new algorithm for processing interferometric data-stacks: SqueeSAR™. IEEE Trans Geosci Remote Sens 49(9):3460–3470

Giglia A, Paro L, Ramasco M (2003) Determinazione dello stato di attività dei fenomeni gravitativi nella scheda di 1° livello, Arpa Piemonte. Internal report. http://webgis.arpa.piemonte.it/website/geo_dissesto/link_iffi/allegati/det_stato_attivita.pdf

Meisina C, Zucca F, Notti D, Colombo A, Cucchi A, Savio G, Giannico C, Bianchi M (2008) Geological interpretation of PSInSAR data at regional scale. Sensors 8(11):7469–7492

Notti D (2010) Landslides mapping and analysis by means of Persistent Scatterers SAR data: approaches at different scales. Tesi di Dottorato inedita, Dipartimento di Scienze della Terra, Università degli studi di Pavia a.a. 2009–2010

Righini G, Pancioli V, Casagli N (2010) Updating landslide inventory maps using Persistent Scatterers Interferometry (PSI) in the Biferno River Basin (Central Italy). In: Proceedings of EGU 2010 General Assembly, Vienna, 3–7 May 2010

Landslide Inventory and Susceptibility Mapping in a Mexican Stratovolcano

Gabriel Legorreta Paulín, Marcus Bursik, M.T. Ramírez-Herrera, J. Lugo-Hubp, J.J. Zamorano Orozco, and I. Alcántara-Ayala

Abstract

This paper provides an overview of the on-going research project from the Institute of Geography at the National Autonomous University of Mexico (UNAM) that seeks to conduct multi-temporal landslide inventories and produce landslide susceptibility maps by using Geographic Information Systems (GIS). The Río Chiquito-Barranca del Muerto watershed on the southwestern flank of Pico de Orizaba volcano in Mexico is selected as a case–control study area. First, the project aims to derive a landslide inventory map from a representative sample of landslides using aerial photography and field work. Next, Multiple Logistic Regression (MLR) is used to examine the relation between landsliding and several independent variables (elevation, slope, contributing area, land use, geology, and terrain curvature) to create the susceptibility map. Finally, the model is compared with the reality expressed by the inventory map. In this study, the results of the landslide inventory and susceptibility mapping techniques are presented and discussed.

Keywords

GIS • Landslide inventory • Landslide susceptibility • Multiple logistic regression

Introduction

In volcanic environments, stratovolcanoes have great potential to produce landslides and debris flows due to their high relief, deposition of voluminous pyroclastic deposits on steep slopes, progressive weakening of a volcanic edifice by hydrothermal alteration, etc. On one hand, their volcanic activity can trigger voluminous landslides along stream systems by sector and flank collapse (Siebe et al. 1992, 1993; Capra et al. 2002); however, these are rather infrequent. On the other hand, during the volcanic repose period, small but hazardous landslides and debris flows occur continually. Their study is important to assess the potential damage to human settlements, industrial development, agricultural activities, cattle raising, and silviculture.

In Mexico, Pico de Orizaba, the highest stratovolcano (5,675 m a.s.l.) presents the greatest potential threat for the formation of landslides and debris flows triggered by non-volcanic activity because of its large area of weakened rocks at high altitudes and under high seasonal rainfall. This stratovolcano creates a potentially hazardous situation for 500,000 people living within a radius of 27 km of Pico de Orizaba. The Río Chiquito-Barranca del Muerto watershed on the southwestern flank of Pico de Orizaba has been selected as a case study. The watershed is prone to landsliding due to the

G.L. Paulín (✉)
Instituto de Geografía, Universidad Nacional Autónoma de México, Laboratorio de Análisis Geo-espacial, Circuito Exterior, Ciudad Universitaria, Coyoacán 04510, México, D.F., Mexico
e-mail: legorretag@igg.unam.mx

M. Bursik
Department of Geology, University at Buffalo, SUNY Buffalo, Buffalo, NY, USA 14260

M.T. Ramírez-Herrera
Centro de Investigaciones en Geografía Ambiental, UNAM, Ciudad Universitaria, Morelia, Michoacán, Mexico

J. Lugo-Hubp • J.J.Z. Orozco • I. Alcántara-Ayala
Instituto de Geografía, Universidad Nacional Autónoma de México, Departamento de Geografía Física, Circuito Exterior, Ciudad Universitaria, Coyoacán 04510, México, D.F., Mexico

C. Margottini et al. (eds.), *Landslide Science and Practice*, Vol. 1,
DOI 10.1007/978-3-642-31325-7_18,

combination of several factors such as high rainfall during the wet season, loose pyroclastic deposits, a high degree of weathering, and steep slopes. The present analysis divides the watershed into geologic units to analyze landslide behavior. A landslide inventory map created from multi-temporal aerial photographs and field investigations is used for the subsequent analysis: sampling design and landslide susceptibility calibration, and its validation. The landslide susceptibility is modeled by using Multiple Logistic Regression (MLR) implemented in a GIS platform LOGISNET (Legorreta Paulin and Bursik 2008, 2009).

Background

During the past 30 years, most of the research at Pico de Orizaba has focused on the volcanic history to establish the possible mechanisms and eruptive styles that explain the present morphology of the landscape and the potential hazard of volcanic events and flank collapse (Siebe et al. 1992; Carrasco-Núñez et al. 1993; Carrasco-Núñez and Rose 1995; De la Cruz-Reyna and Carrasco-Núñez 2002; Macías 2005). Several approaches have been proposed for assessing hazards of catastrophic voluminous landslides and debris flows (Hubbard 2001; Sheridan et al. 2001; Concha-Dimas et al. 2005; Hubbard et al. 2007). Each uses GIS applications to assess hazard at local or regional scale, and each has advantages and limitations. Based on previous geological studies and computer simulations with GIS and remote sensing, lahar hazard maps along stream systems of Pico de Orizaba have been created (Hubbard 2001; Sheridan et al. 2001; Hubbard et al. 2007). In spite of this, there is no practical and standardized landslide mapping method using GIS for small non-volcanic triggered landslides that occur continually along the stream systems. As a result, there is a lack of landslide inventory maps and related geo-databases that support the prediction of future slope instability in volcanic terrains.

Based on previous experience of landslide susceptibility and hazard zonation projects (Angeli et al. 2000; Washington State Department of Natural Resources (DNR), Forest Practices Division 2006; Galli et al. 2007; Weirich and Blesius 2007; Hervás and Bobrowsky 2009; Blahut et al. 2010), this project addresses the landslide and susceptibility mapping issue by compiling a multi-temporal landslide inventory and modeling landslide instability by using a MLR. MLR was selected because evaluation under natural conditions has suggested that it is fairly successful at identifying slopes where landsliding has been observed if sampling strategy and sample size are adequate, and if sets of variables that are strongly related to landslides are used (Ohlmacher and Davis 2003; Can et al. 2005).

Study Area

The Río Chiquito-Barranca del Muerto watershed covers 111 km^2 and lies within Veracruz and Puebla states, Mexico. It is a tributary of the Río Blanco, which flows into the Gulf of Mexico (Fig. 1). The watershed is located on the southwestern flank of Pico de Orizaba volcano which is located in the Mexican Volcanic Beld (MVB) physiographic province. The MVB is an active volcanic chain that extends 1,000 km from west to east across central-southern Mexico, from the Pacific Ocean to the Golf of Mexico. The study area is prone to landsliding due to the combination of several factors: (a) In the study area, the mean annual precipitation is 1,000–1,100 mm/year at >4,000 m a.s.l. and 927 mm/year at <1,500 m a.s.l. (Palacios et al. 1999), with most falling as rain during seasonal storms in the wet season, between May and November. (b) The relief is characterized by hilly and steep terrain with elevations from 1,340 to 5,675 m a.s.l. (c) Some slopes are steep (>60° in mountainous terrain). (d) There is a high degree of weathering of volcanic and sedimentary rocks. The stream channel of Río Chiquito-Barranca del Muerto erodes a weathered and highly dissected, folded, and faulted Cretaceous basement of limestone and shale (29.7 %) that has been covered by Tertiary (60.3 %) and Quaternary (2.4 %) lavas, pyroclastic flows, fall deposits, and alluvium (7.6 %) (Fig. 2).

During the present study, more than 400 landslides were mapped using aerial photographs and field verification.

Methodology

Background information was collected to establish a generalized characterization of landslide processes within the watershed. Background information includes geology, land use, climate and hydrology, and reports. The information was georeferenced and incorporated into the GIS ArcMap. Six independent variables used for the analysis were obtained. Digital elevation data (resolution 10 m) from topographic maps of the area at a scale of 1:50,000 were obtained from the Instituto Nacional de Estadística y Geografía (INEGI). Three data layers were obtained from these elevation data, namely slope angle, slope curvature, and contributing area. Other digital coverage was obtained from paper maps of geology and land use at a scale of 1:250,000 by conversion to a 10 m raster format and incorporation in the GIS.

Landslides in the study area were identified by multi-temporal photo-interpretation and field checking. Two sets of aerial photographs were used: from 1994 at a scale of 1:20,000, and from 2008 at a scale of 1:10,000. The landslides were classified into shallow landslides, debris flows, debris slides, deep-seated landslides, earthflows, and rock falls.

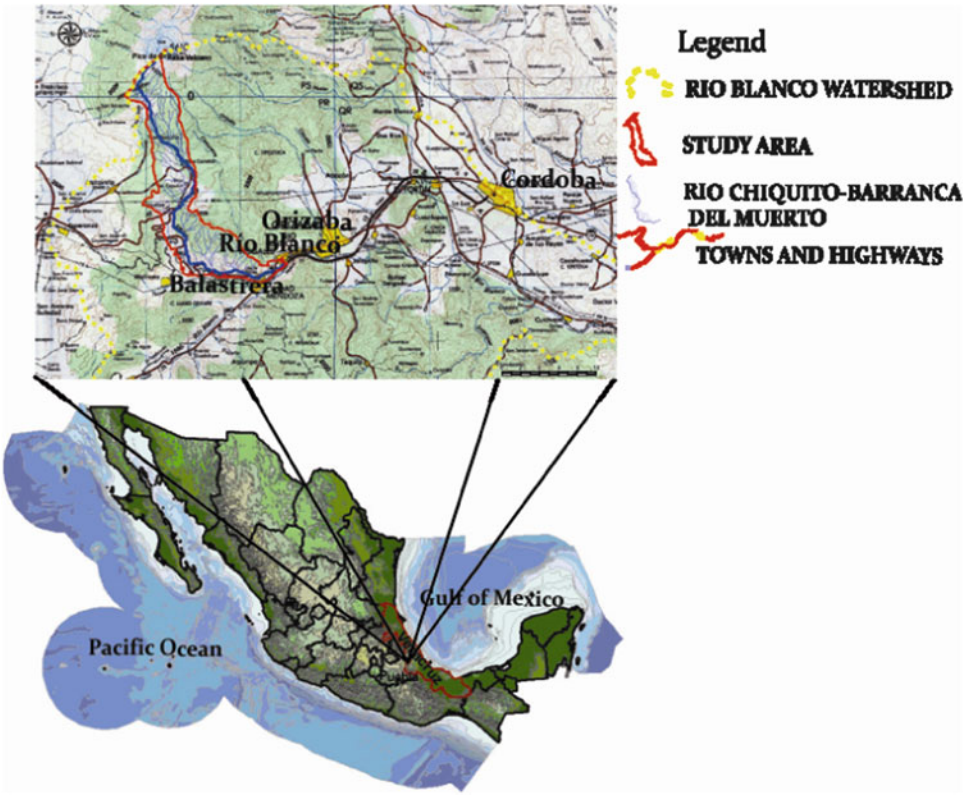

Fig. 1 Localization of the study area

Slope movements were classified according to the landslide hazard zonation protocol (2006) of Washington State DNR Forest Practices Division, Cruden and Varnes (1996) and Wieczorek (1984). All landslides were identified on photo transparencies and directly digitized onto the screen into GIS at the same scale as the photographs. In parallel, the spatial geo-database of landslides was constructed. The following attributes: (1) mass wasting process, (2) level of certainty of the observation, (3) photo identification date, (4) landslide size, (5) landslide activity, (6) landslide parts (head, evacuation zone, deposit), (7) slope shape, (8) field slope gradient, (9) map slope gradient measured from the 10 m digital elevation model (DEM), (10) landslide delivery, (11) land use, (12) elevation at which the landslide started, (13) aerial photograph identification number, (14) landslide area, and (15) researcher comments were standardized by using pre-defined values which are controlled by the geo-dataset domains in the GIS system.

Concurrent with landslide mapping, field reconnaissance provides a realistic view of the watershed and the types of landslide and landforms. The amount of field verification was 37 % of all mapped landslides, which enhances confidence in the landslide assessment.

For the statistical analysis, a multicollinearity diagnostic was calculated by using the variance inflation factor (VIF). Multiple logistic regression landslide susceptibiliy analysis was calculated and mapped by using the LOGISNET GIS system (Legorreta Paulin and Bursik 2009) and SPSS statistical package.

Comparison of the MLR model susceptibility map and the inventory map was used to evaluate the model results. A two-class classification scheme (landslide and non-landslide) was used for the MLR model susceptibility map to facilitate the comparison (Fig. 3) with the inventory map. For MLR, the two-class classification scheme classifies the probability into classes of landslide and non-landslide using a probability of 0.5 as the break point (Dai and Lee 2002); values higher than 0.5 were classified as landslide and those lower than 0.5 as non-landslide. The evaluation of the MLR model vs. the landslide inventory was carried out in terms of producer's accuracy (calculated as the ratio of the number of correctly classified pixels in each category to the total number of true pixels for that category), user's accuracy (calculated as the ratio of the number of correctly classified pixels in each category to the total number of pixels that are classified by the model in that category), and model efficiency (calculated as the ratio of correctly minus incorrectly indicated landslide pixels to the total number of true landslide pixels mapped in the inventory map) (Van Den Eeckhaunt et al. 2005).

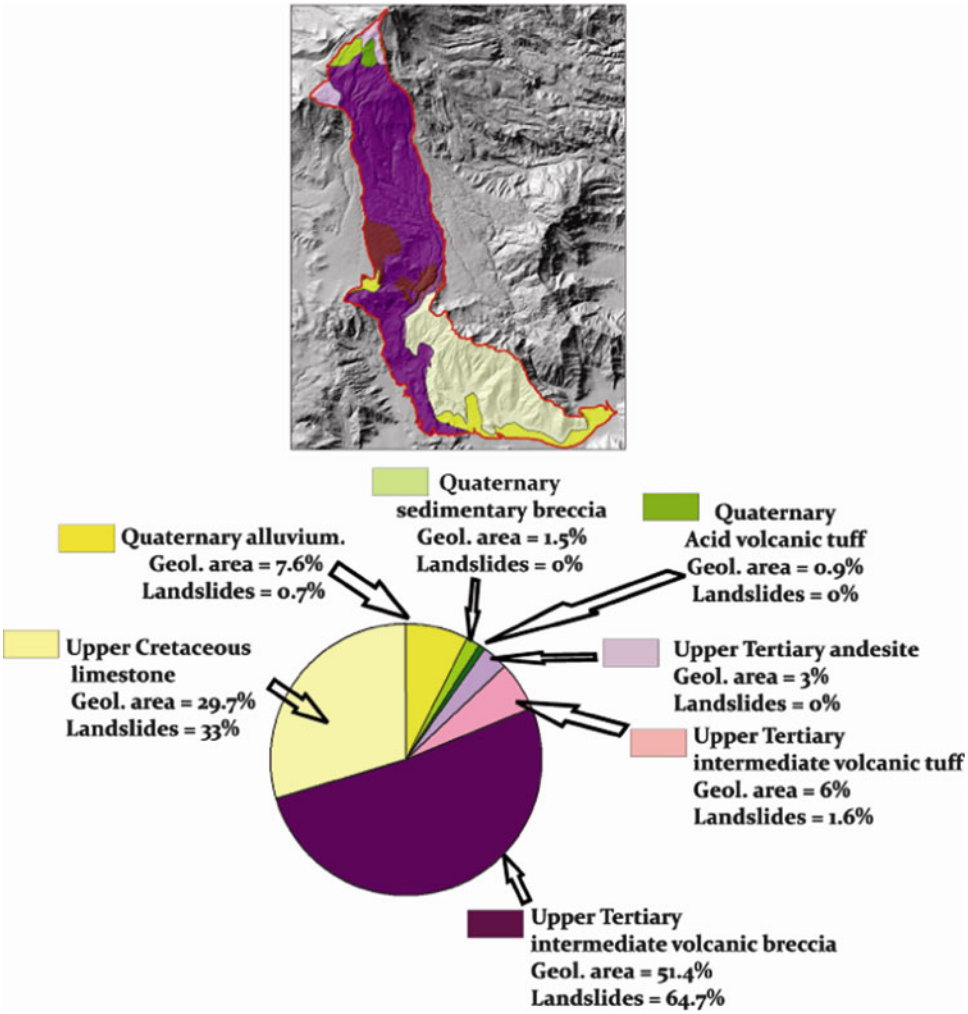

Fig. 2 Distribution and spatial proportion of the geologic rocks and deposits

Results

The study shows that volcanic and/or sedimentary deposits have a different pattern of resistance to erosion processes and a different type of mass movement due to its specific geotechnical properties. In the study area, geological conditions control the abundance of landslides in the catchment. Of the 442 mapped landslides, 66.3 % are in volcanic rock or deposits, 33 % in weathered limestone and shale, and 0.7 % in a sedimentary deposit. By number in the watershed, shallow landslides (including debris slides and debris flows) are the predominant type (91.4 %), followed by rock falls (7.5 %) and deep-seated landslides (including earthflows) (1.1 %). More than 60 % of the landslides are in volcanic material (Fig. 2).

In the upper portion of the watershed, andesitic lava flows do not readily erode and they act as sponges to hold the surface water. Hence, shallow landslides are not frequent.

In the middle portion of the watershed (1,600–4,000 m a.s.l.), lava flows are covered by ash fall deposits and pyroclastic flows that are prone to shallow slides. Also, lava flows form steep steps along the channel of the watershed. For example, in the main stream more than seven steep steps (>10 m high) are found. These steep steps are prone to rock fall, as are also the debris flow deposits. This middle part of the watershed is the point of contact between volcanic and sedimentary rock (2,600–1,600 m a.s.l.). Here, the intrinsic properties of the rock in conjunction with anthropogenic land use trigger shallow, deep-seated, and earthflow landslides. More than 40 % of landslides are in areas of subsistence agriculture and another 40 % in disturbed areas of fir and oak forest.

The VIF showed that elevation, slope, contributing area, land use, geology, and terrain curvature can be used in the MLR analysis. These six variables are strongly related to the probability of distribution for the dependent variable (landslide or non-landslide) but not strongly related to each other.

After the evaluation of multicollinearity, MLR is calculated and mapped pixel-by-pixel on the basis of the logit function: $1/1 + \mathrm{Exp}-(-1.622 + \text{Elevation}$ map

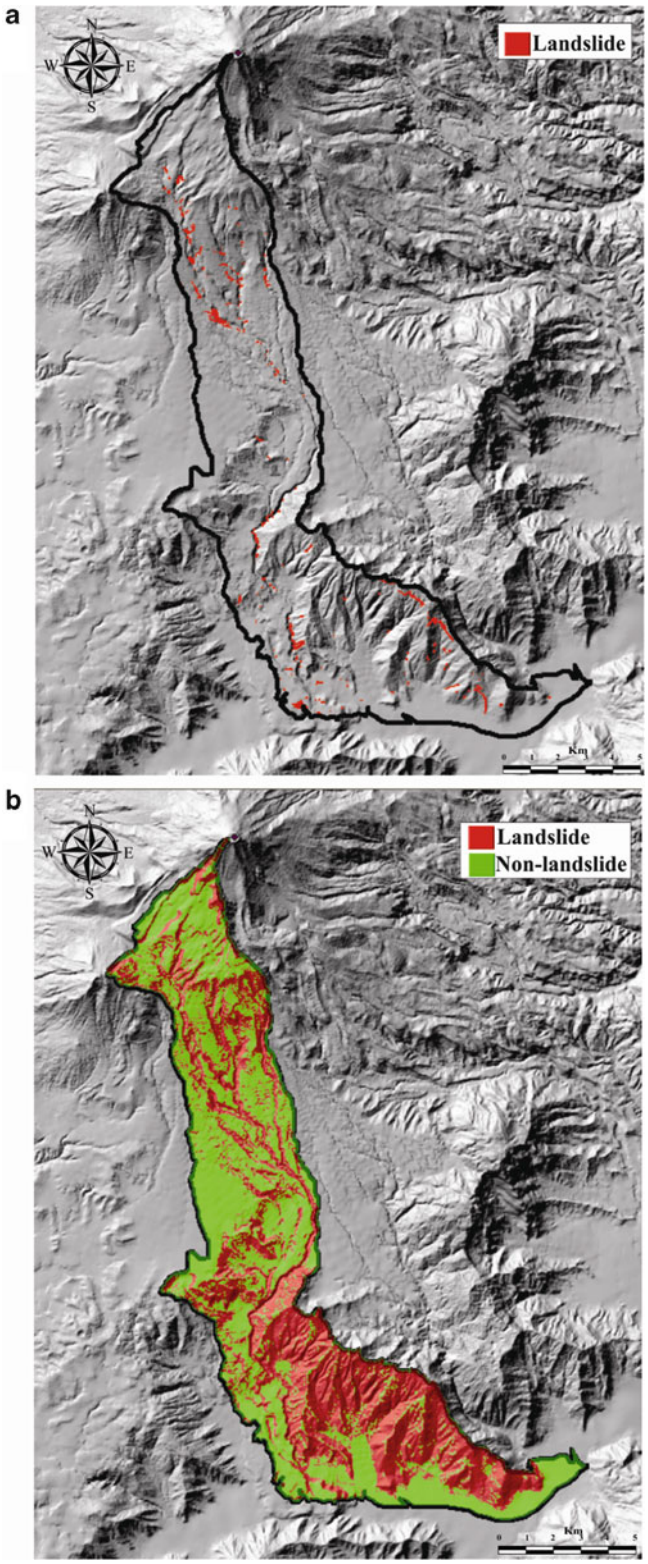

Fig. 3 (**a**) Landslide Inventory map, (**b**) MLR susceptibility model with a two-class classification scheme

(−3.5E−04) + Slope map (0.120) + Contributing Area map(7.6E−07) + Land use map(−0.151) + Geology map (0.190) + Curvature map (−0.433)). The resulting map at 10 m resolution of MLR was compared with the inventory map. To facilitate the comparison and contrast between maps, a two-class classification scheme is used (Fig. 3). MLR model was evaluated in terms of producer's accuracy, user's accuracy, and model efficiency. A cross table that shows the amount of overlap and relation between inventory and predicted maps was used to calculated accuracies and model efficiency.

The producer's accuracy shows that MLR had a high coincidence (72.33 %) between predicted unstable slopes and landslide area in the inventory map. This "good match" of model-inventory prediction is due to its over-prediction which is shown by a low user's accuracy (0.42 %) and negative model efficiency value (−170.32).

Conclusions

In this paper we briefly introduce and review the implementation of a method for landslide mapping and susceptibility assessment of potentially unstable areas in volcanic terrain.

The study at Rio Chiquito-Barranca del Muerto is an attempt to produce the prototype of such standardized methodology for future landslide inventory maps of volcanic regions in Mexico. The method is achieved through the standardization and integration of thematic layers and their related geo-database in a GIS-based system. By directly addressing the landslide mapping issues, local authorities in Mexico such as the civil protection agencies of Puebla and Veracruz states and other governmental organizations will benefit with regard to landslide hazard mitigation and planning.

We emphasize the fact that the study is the first prototype in Mexico to develop a GIS methodology for a systematic landslide inventory and landslide susceptibility maps. Hence, it is subject to being adapted, modified, and improved with further application in other watersheds. We acknowledge the technical limitation of the landslide inventory, whose quality depends on the skills and experience of the investigators, the complexity of the study area, and the reliability of available information including the aerial photographs to identify the landslides. The use of a 10 m resolution DEM for the MLR analysis is also a limitation, since at this resolution all types of landslide can sometimes lose cartographic representation and it is difficult to train the model to separate landslide from non-landslide areas (Legorreta Paulin et al. 2010).

The analysis by MLR has shown the occurrence of landslides in the region of interest to be correlated with the six variables: elevation, slope, contributing area, land use, geology, and terrain curvature. The evaluation shows that the match of MLR model-inventory is not perfect and an overprediction is evident. The over-prediction could

be explained by the different thematic map scales, mapping precision, and degree of update. For instance, the topographic map is old (dated 2006), thus, the derived DEM has no expression of recent shallow landslides. Nevertheless, the overprediction is prefered in this work because the model fairly defines and matches the areas which appear to be susceptible to landsliding. The MLR model achieves the required scientific accuracy and technical accessibility to address issues of hazard mitigation and planning in areas with scarce information.

Regardless of the limitations, the authors foresee the landslide inventory of Rio Chiquito-Barranca del Muerto as an integrated methodology to handle and support prognostic studies of slope instability. Future research will involve the modeling of individual landslide types, the characterization of geologic units (landforms) and landslide types, the inclusion of other thematic variables or the update of existing ones, and the processing of this information to obtain a hazard map.

Acknowledgements The authors thank authorities from the Department of Geology at the University of Buffalo, the International Consortium on Landslides (ICL), the Washington State Department of Natural Resources (DNR) Forest Practices Division, the WA-DNR Geology & Earth Resources Division and the Geo-Spatial Analysis Laboratory from the Institute of Geography, UNAM for their approval and help. This research was supported by the iniciativa de apoyo complementario a la realización de las obras determinadas (IACOD), UNAM, Grant no. IA100711 and the International Programme on Landslides (IPL).

References

Angeli MG, Pasuto A, Silvano S (2000) A critical review of landslide monitoring experiences. Eng Geol 55:133–147

Blahut J, Van Westen CJ, Sterlacchini S (2010) Analysis of landslide inventories for accurate prediction of debris-flow source areas. Geomorphology 119(1/2):36–51

Can T, Nefeslioglu HA, Gokceoglu C, Sonmez H, Duman TY (2005) Susceptibility assessments of shallow earth flows triggered by heavy rainfall at three catchments by logistic regression analyses. Geomorphology 72:250–271

Capra L, Macías JL, Scott KM, Abrams M, Garduño-Monroy VH (2002) Debris avalanches and debris flows transformed from collapses in the Trans-Mexican Volcanic Belt, México. Behavior, and implication for hazard assessment. J Volcanol Geotherm Res 113(1/2):81–110

Carrasco-Núñez G, Rose WI (1995) Eruption of a major Holocene pyroclastic flow at Citlaltépetl volcano (Pico de Orizaba), México, 8.5–9.0 ka. J Volcanol Geotherm Res 69(3/4):197–215

Carrasco-Núñez G, Vallance JW, Rose WI (1993) A voluminous avalanche-induced lahar from Citlaltépetl volcano, Mexico: implications for hazard assessment. J Volcanol Geotherm Res 59 (1/2):35–46

Concha-Dimas A, Cerca M, Rodríguez-Elizarrarás S, Watters RJ (2005) Geomorphological evidence of the influence of pre-existing basement structure on emplacement and deformation of volcanic edifices at the Cofre de Perote-Pico de Orizaba chain and implications for avalanche generation. Geomorphology 72:19–39

Cruden DM, Varnes D (1996) Landslide types and processes. In: Turner AK, Shuster RL (eds) Landslides: investigation and mitigation. Special Report 247, Transportation Research Board, pp 36–75

Dai FC, Lee CF (2002) Landslide characteristics and slope instability modeling using GIS, Lantau Island, Hong Kong. Geomorphology 42:213–228

De la Cruz-Reyna S, Carrasco-Núñez G (2002) Probabilistic hazard analysis of Citlaltépetl (Pico de Orizaba) Volcano, eastern Mexican Volcanic Belt. J Volcanol Geotherm Res 113:307–318

Galli M, Ardizzone F, Cardinali M, Guzzetti F, Reichenbach P (2007) Comparing landslide inventory maps. Geomorphology 94:268–289

Hervás J, Bobrowsky P (2009) Mapping: inventories, susceptibility, hazard and risk. In: Sassa K, Canuti P (eds) Landslides – disaster risk reduction. Springer, Berlin, pp 321–349. ISBN 978-3-540-69966-8

Hubbard BE (2001) Volcanic hazard mapping using aircraft, satellite and digital topographic data: Pico de Orizaba (Citlaltépetl), México. Thesis, Department of Geology, SUNY, at Buffalo

Hubbard BE, Sheridan MF, Carrasco-Nunez G, Díaz-Castellon R, Rodriguez S (2007) Comparative lahar hazard mapping at Volcan Citlaltépetl, Mexico using SRTM, ASTER and DTED-1 digital topography. J Volcanol Geotherm Res 160(1):99–124

Legorreta Paulin G, Bursik M (2008) Logisnet: a tool for multimethod, multiple soil layers slope stability analysis. Comput Geosci 35 (5):1007–1016

Legorreta Paulín G, Bursik M (2009) Assessment of landslides susceptibility: LOGISNET: a tool for multimethod, multilayer slope stability analysis. VDM Verlag Dr. Müller, Saarbrücken, p 360. ISBN 9783639154771

Legorreta-Paulin G, Bursik M, Lugo HJ, Zamorano-Orozco JJ (2010) Effect of pixel size on cartographic representation of shallow and deep-seated landslide, and its collateral effects on the forecasting of landslides by SINMAP and multiple logistic regression landslide models. Phys Chem Earth 35:137–148

Macías JL (2005) Geología e historia eruptiva de algunos de los grandes volcanes activos de México. Boletín de la Sociedad Geológica Mexicana. Volumen Conmemorativo del Centenario Temas Selectos de la Geología Mexicana. LVII(3):379–424

Ohlmacher GC, Davis JC (2003) Using multiple logistic regression and GIS technology to predict landslide hazard in northeast Kansas, USA. Eng Geol 69:331–343

Palacios D, Parrilla G, Zamorano JJ (1999) Paraglacial and postglacial debris flows on Little Ice Age terminal moraine: Jamapa Glacier, Pico de Orizaba (Mexico). Geomorphology 28:95–118

Sheridan MF, Carrasco-Nuñez G, Hubbard BE, Siebe C, Rodriguez-Elizarraraz S (2001) Mapa de peligros del Volcan Citlaltépetl (Pico de Orizaba). Inst Geog, Univ Nac Autonoma Mexico, 1:250,000 scale

Siebe C, Komorowski JC, Sheridan MF (1992) Morphology and emplacement collapse of an unusual debris avalanche deposit at Jocotitlán Volcano, Central Mexico. Bull Volcanol 54:573–589

Siebe C, Abrams M, Sheridan MF (1993) Major Holocene block-and-ash fan at the western slope of ice-capped Pico de Orizaba volcano, Mexico: implications for future hazards. J Volc Geotherm Res 59:1–33

Van Den Eeckhaunt M, Poesen J, Verstraeten G, Vanacker V, Moeyersons J, Nyssen J, Van Beek LPH (2005) The effectiveness of hillshade maps and expert knowledge in mapping old deep-seated landslides. Geomorphology 67:351–363

Washington State Department of Natural Resources (DNR), Forest Practices Division (2006) Landslide hazard zonation (LHZ) mapping protocol, version 2.0. http://www.dnr.wa.gov/BusinessPermits/Topics/LandslideHazardZonation/Pages/fp_lhz_review.aspx

Weirich F, Blesius L (2007) Comparison of satellite and air photo based landslide susceptibility maps. Geomorphology 87:352–364

Wieczorek GF (1984) Preparing a detailed landslide inventory map for hazard evaluation and reduction. Bull Assoc Eng Geol 21:337–342

Landslide Mapping Using SqueeSAR Data: Giampilieri (Italy) Case Study

Federico Raspini, Sandro Moretti, and Nicola Casagli

Abstract

Multi-temporal analysis of space-borne radar images through Persistent Scatterer Interferometry (PSI) is exploited for detecting and mapping slope instability at basin scale in the south-western part of the province of Messina, hit by the intense storm events on October 1st 2009. Available PSI data provide estimates of yearly deformation velocity, referred to both historical (1992–2001; ERS images) and recent (2003–2009; ENVISAT images) scenarios. PSI techniques have recently demonstrated their suitability for the analysis of extremely to very slow moving landslides, and their complementarity with field campaigns, at both regional and local scales, allowing spatial and temporal characterization of the detected phenomena. Coupling and integrating deformation measurements extracted by means of SqueeSAR technique, thematic maps and optical data enabled to identify 26 sites (*hotspot mapping*), characterized by high hydro-geological hazard related to the occurrence of pre-event, extremely to very slow moving landslides.

Keywords

Landslide • Permanent Scatterers (PSInSAR) • Persistent Scatterer Interferometry • SqueeSAR • Giampilieri • Hotspot mapping

Introduction

In the late afternoon of October 1st 2009, a high intensity storm hit the Ionian side of Sicily, particularly affecting a limited area in the south-western part of Messina province, between the Peloritani Mountains ridge and the coastline. At the St. Stefano di Briga rain gauge a rainfall of 225 mm in 8 h, with a peak of 115 mm in 3 h, was recorded. The heavy precipitation of October 1st further deteriorated the critical state caused by the significant accumulation of rainfall occurred during the month of September which led the soil to complete saturation. During of the night, the persisting rainfall in the coastal areas between Galati and Scaletta Zanclea triggered slope failures, mainly shallow soil slides and debris flows on an area of about 50 km^2. The worst damages were reported in the villages of Giampilieri, Scaletta Zanclea, Guidomandri, Pèzzolo, Altolìa, and Itàla. Landslides closed off many roads as well as the railway and main highway. The assessed number of fatalities caused by landslides and inundation amounts to 37 (including 31 deaths and 6 missing persons), with 122 injured people and 2,019 evacuated people.

Following the described event, in the framework of the post-disaster initiatives led by the National Department of Civil Protection, several activities were performed aimed at supporting local authorities in the hydro-geological risk assessment. In particular, a detailed geomorphologic analysis, exploiting the contribution of PSI technique and photo interpretation, was performed by the Earth Science

F. Raspini (✉) • S. Moretti • N. Casagli
Department of Earth Sciences, University of Firenze, Via La Pira, 4, Florence, Italy
e-mail: federico.raspini@unifi.it

C. Margottini et al. (eds.), *Landslide Science and Practice*, Vol. 1,
DOI 10.1007/978-3-642-31325-7_19,

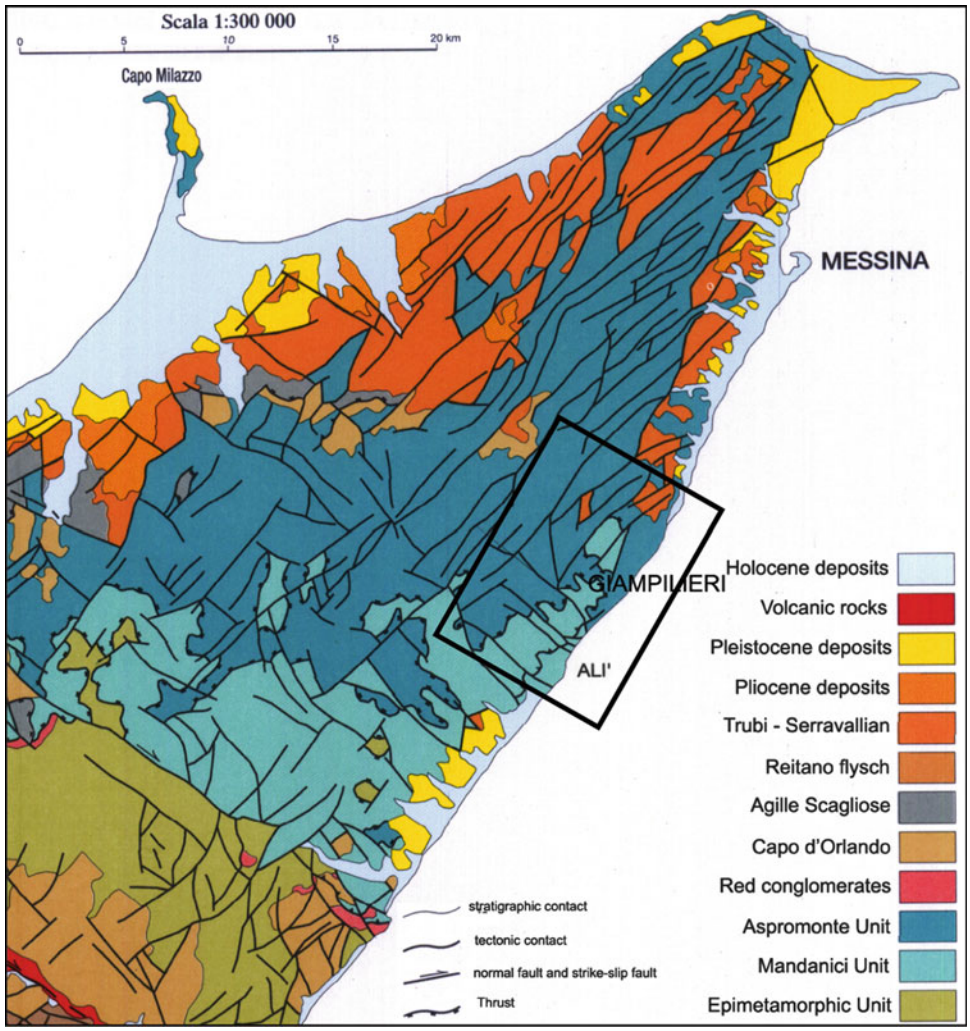

Fig. 1 Simplified geological map of north-east Sicily (From Lentini et al. 2000)

Department of the University of Florence (Centre of Competence of the Italian Civil Protection for geo-hazards) in order to identify slow moving pre-existing landslides affecting the whole territory hit by intense rainstorm.

The Study Area

The investigated area, with an extension of about 75 km^2, is located in a narrow coastal area south of the suburbs of the city of Messina, delimited by the Ionian sea on the East side and by the Peloritani ridge on the West side. The area includes the following five municipal towns, entirely belonging to the Messina district: Alì, Alì Terme, Itala, Scaletta Zanclea and Messina. The main inhabited centres are concentrated along the strongly urbanized coastal area. The middle hill area is characterized by the presence of smaller settlements, connected with the populated coastal area by a single road axis climbing upward along very steep slopes.

Geological Setting

The north-eastern sector of Sicily (Fig. 1), located along the boundary between the African and Eurasian plates, is characterized by a very complex tectonic setting in the central Mediterranean.

In Sicily, three nappe complexes, deriving from three different palaeogeographic domains, have been recognised (Lentini et al. 1995, 2000). In particular, from the Internal to the External domain, the tectonic pile comprises the following Units: the *Kabilo-Calabride Units*, formed by pre-Mesozoic igneous and metamorphic basement fragments (deriving from the European margin), with relative Meso-Cenozoic covers; the *Apenninic-Maghrebid Units*, south-verging thrusts sheets formed by pelagic sediments and fragments of African continental crust; and the *Hyblean Units*, a Meso-Cenozoic sequence of limestone with few mafic intercalations. From a tectonic point of view, the most impressive regional feature of eastern Sicily is

represented by a series of normal faults related to an ESE-WNW regional extensional tectonic regime (Tortorici et al. 1995). This fault belt strongly controls the morphology of the area running more or less continuously from the Hyblean Plateau to the Strait of Messina. In the eastern-facing Peloritani mountain slope area, the Quaternary activities of the Messina-Taormina normal fault influenced seismic activities, sea-level change and uplift.

Geomorphological Setting

The Peloritani Mountain forms a ridge stretching in SW-NE direction made up of a long series of peaks with an average height of 800–1,000 m. The highest peaks in the investigated area are Monte Scuderi (1,253 m a.s.l.) and Pizzo Bottino (1,076 m a.s.l.). The mountain range runs parallel to the Ionian coastline, from Capo Peloro to North to the Alcantara River basin to South dividing the territory of the province of Messina in two sides: the Tyrrhenian side and the Ionian side. Along the two mentioned sides a number of catchment areas were formed subtended by flowing streams, channelling water and debris to the Tyrrhenian and Ionian seas.

The geo-structural conditions, the crystalline competence of the outcropping rock (mainly medium grade metamorphic rocks) and the recent tectonic activity strongly influenced the geomorphology of the investigated area. Landscape, especially towards the Ioinian Sea, is typical of the recently uplifted areas: steep slopes, narrow valleys and high relief energy are the main geomorphologic feature. The short distance separating the watershed from the coast influenced the morphometric characteristics of the river basins. The watercourse network is formed by regular and parallel paths, perpendicular to the Peloritani ridge, leading to the coast. River catchments have a reduced concentration time with a significant transport of solid materials, incisions are short and deeply entrenched into V-shaped valleys, especially in the mountainous sector. Towards the sea riverbeds become over-flooded, forming small alluvial plains. The presence of the so-called "fiumare", straight, steep course, gravel-bed river draining mountain areas is typical of Mediterranean climate region. Their flow varies seasonally and their regime is torrential with catastrophic transport of solid materials following heavy rainfall, causing severe damages if flooding occurs close to populated centres.

Input Data and Methods

Point-wise ground motion information provided by SqueeSAR algorithm can have a purely geological or anthropogenic origin as well as a combination of both. As a consequence, as support to the results provided by the PSI dataset, a series of auxiliary data, relevant for identification of the ground displacement triggers, were acquired, integrated within a Geographical Information System (GIS), and finally analyzed.

Table 1 Number of images, time period, number of identified DS and average DS density for ERS and ENVISAT data stacks used for the PSI analysis

Satellite and orbit	N° images	Time range	N° DS	DS density (DS/km^2)
ERS ascending	48	08/09/1992	6,607	96.2
		24/11/2000		
ENVISAT ascending	55	22/01/2003	30,411	414.9
		20/05/2009		

Radar Satellite Datasets

Satellite analysis of land deformation was performed using the new SqueeSAR approach, a second generation PSInSAR (Permanent Scatterers InSAR) algorithm (Ferretti et al. 2001), one of the several multi-interferometric techniques available today to process long series of SAR images.

Developed by T.R.E., the SqueeSAR approach identifies both point-wise Permanent Scatterers (as previous PSInSAR technique) and spatially Distributed Scatterers (DS), providing a significantly increased coverage of ground deformation measurement points (Ferretti et al. 2011), especially over non-urban areas. DS are identified in low-reflectivity homogeneous areas, scattered outcropping rocks, debris flows, non-cultivated lands and desert areas. The SqueeSAR algorithm is applied to several SAR datasets acquired by different ESA missions. These data allow to carefully measure ground motion since 1992 and to obtain a temporal evolution of the investigated events.

To solve the spatial variability and temporal evolution of ground displacements affecting the investigated area, both historical (1992–2001; ERS1/2 images) and recent (2003–2009; ENVISAT images) scenarios are analyzed (Table 1). Forty-eight SAR images acquired in 1992–2001 by ERS1/2 satellites along ascending orbits were used to study historic ground displacements. Afterwards, 55 SAR images acquired by ENVISAT satellite along ascending orbits were used to monitor recent land deformation.

Ancillary Data: Thematic Maps and Optical Images

Ancillary data include several thematic information and optical images. In particular, for Giampilieri and Briga river basins the following auxiliary data were available:

- A digital colour ortophoto from Volo Italia 2000 (1 m pixel resolution);
- VHRI Quickbird panchromatic images acquired on September, 6th 2006 and October, 9th 2009;
- A high-resolution Digital Elevation Model (1 × 1 m), acquired by the Friuli Venezia Giulia Region by means of an airborne Lidar sensor survey for the National Department of Civil Protection;
- A pre-event topographic map at 1:10,000 scale from the Regional Cartographic Centre;
- The Geological Map of Italy (1:50,000 scale), used to collect geological information of the study area;
- Multi-temporal stereoscopic, black and white aerial photographs taken in 1954, 1995 and 2005, at about 1:33,000 scale and acquired from the Italian Geographical Military Institute (IGM);
- Several sets of post-event digital stereoscopic photographs, including a set of colour images (1:3,500 scale), acquired from helicopter from October 5th to 7th by the Friuli Venezia Giulia Region for the National Department of Civil Protection, and a second set at 1:4,500 scale acquired one month later;
- The October, 1st event landslides map made by the Regional Department for Civil Protection;
- Hydrogeological Setting Plan (PAI) of Sicilia Region;
- IFFI (Landslide Inventory in Italy), a national database published in 2007;
- The landslide inventory map of Briga and Giampilieri catchments, made by the Earth Sciences Department of University of Firenze and CNR-IRPI of Perugia, providing information on both the main landslide events triggered by heavy rainfall of 1st October 2009, on the pre-existing gravitational instability phenomena and other geomorphologic elements related to several geomorphic processes (fluvial and marine dynamics and effects of bedrock structure upon the relief).

Methodology

According to Farina et al. (2004, 2006, 2008), "radar interpretation" is a methodological approach consisting on the possibility of assigning a geomorphologic meaning to the point-wise information provided by PSI technique, through the analysis of ancillary thematic data and photo-interpretation activities. This approach, providing information on the spatial distribution of slope instability events both at regional and local scale, is aimed at improving pre-existing landslide inventories through the integration of stereoscopic photo-interpretation of multi-temporal aerial and/or satellite optical imagery and field survey, in order to identify terrain features and landforms related to mass movements.

Hotspot Mapping

Coupling and integrating deformation measurements extracted by means of SqueeSAR technique, thematic maps (topographic and geological maps) and optical data (ortophoto, VHR optical satellite images and multi-temporal aerial photo), it has been possible to identify 26 sites characterized by high hydro-geological hazard (*hotspot mapping*).

On the basis of available multi–interferometric data these sites were assessed as the most critical in terms of hydro-geological hazard, both for the type of instability events and/or extent of the detected phenomena and/or measured deformation velocities and/or presence of elements at risk (Fig. 2). Two validated *hotspot analyses* (Altolia and Upper Schiavo basin test site), representatives of the type of identified phenomena in the whole study area, are presented. The presented case study shows the fundamental contribution of PSI data to the mapping and analysis of landslide-induced movements at both regional and local scale.

Altolia Case Study

Altolia (identified with number 14 in Fig. 2), is a hill district in the Messina municipality with 460 inhabitants, located 16 km south of the municipal capital city and 5 km from the Eastward State Highway n. 114, crossing Giampilieri Marina along the coastline. The settlement has developed along the right bank of Giampilieri river, among citrus, grapevine and olive groves. Figure 3 shows the results from photo and radar interpretation for Altolia. Pre-existing landslide inventory maps (PAI and IFFI) report two small instability events in the study area: a stabilized complex landslide in the northern part of the settlement and an active rock fall along the right bank of Giampilieri river immediately upstream of Altolia (Fig. 3a).

An overview of the SqueeSAR results both for ERS and ENVISAT datasets is shown in Fig. 3b, c, as measured by the SAR sensor along the satellite's line of sight and expressed in mm/y. The colour scale indicates green points as stable. The gradation from yellow to red represents increasing deformation rates, moving away from the sensor. The density varies with the presence of backscattering structures at the surface and therefore an increased density of DS prevails in the settlement area. The PSI results highlighted ground motion displacements in both historical (1992–2001; ERS images) and recent (2003–2009; ENVISAT images) scenarios. In particular, available datasets allow to identify a large sector in the south-eastern part of the village characterized by a displacement with an average velocity ranging from 2 to 10.7 mm/year in the ERS dataset, and from 2.2 to 8.9 mm/year in the ENVISAT dataset.

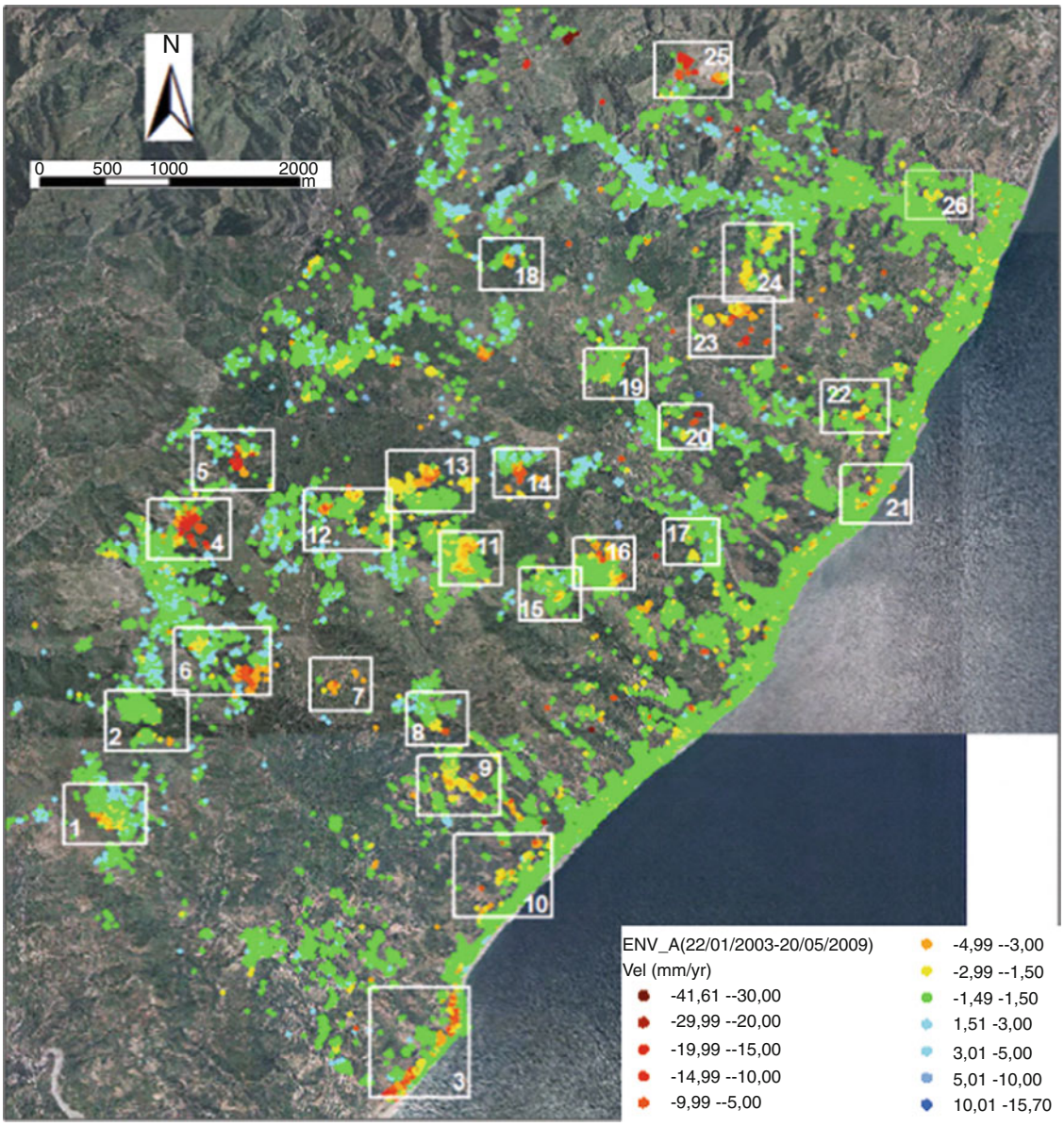

Fig. 2 Location of the 26 sites characterized by high hydro-geological hazard (*hotspot mapping*). *1* M. Santo; *2* P.le Puzzu; *3* Alì Terme; *4* P.le Seddiri; *5* P.le Cimmario; *6* P.le Pitarra; *7* Culma Caravagi; *8* Itàla; *9* Croce; *10* Itàla Marina; *11* M. Pietralunga; *12* P.le Lanzaro; *13* P.zzo Scapola; *14* Altolia; *15* Monticeddu; *16* P.le Laridda; *17* Giampilieri; *18* P.le Dinareddi; *19* Pezzolo; *20* Briga Superiore; *21* San Paolo; *22* San Placido; *23* Upper Schiavo river basin; *24* S. Stefano; *25* P.le Furcu; *26* Villa Parotta

Photo-interpretation of stereoscopic colour images (1:3,500 scale) and field surveys allow to detect and map a large active continuous slide affecting the south-eastern part of Altolia village (Fig. 3d). During field campaign, carried out in the framework of the post-disaster activities and aimed at validating SqueeSAR results, several effects on infrastructures (cracks and damages on houses) were detected. A detailed study of landform features (scarps, counterscarps, tension cracks) led to a complete characterization of the landslide, which could be divided in different sectors characterized by homogenous morphologic behaviour (crown and accumulation zone).

Upper Schiavo Basin Case Study

The investigated area (identified with number 23 in Fig. 2), belongs to the Messina municipality and is characterized by the presence of several elements at risk, including isolated buildings and many minor settlements connected by stretches of paved roads.

Figure 4 shows the results from photo and radar interpretation for the upper Schiavo river basin. Pre-existing landslide inventory maps (PAI and IFFI) do not report instability events in the study area (Fig. 4a). On the contrary, the PSI results show a large sector in the upper part of the basin

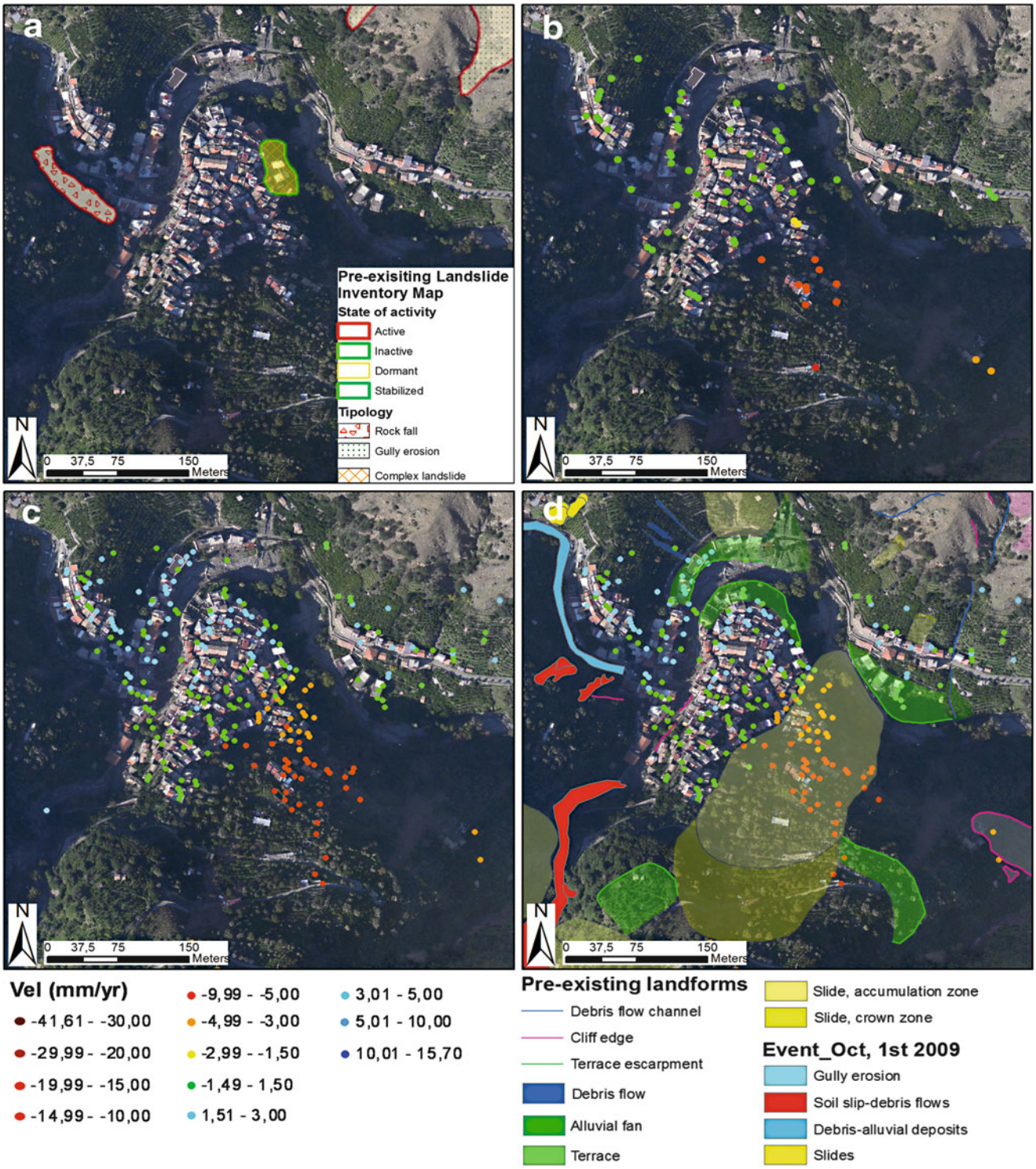

Fig. 3 Results for Altolia (Messina). (**a**) Pre-existing landslide inventory map; (**b**) ERS dataset; (**c**) ENVISAT dataset; (**d**) *hotspot analysis*

characterized by a displacement with an average velocity ranging from 1.6 to 3.9 mm/year in the historical dataset (1992–2001; ERS images), and from 1.5 to 13.9 mm/year in the recent dataset (2003–2009; ENVISAT images). Photo-interpretation of stereoscopic colour images (1:3,500 scale) and analysis of information provided by PSI results allow to detect and map a large complex system of active continuous slides affecting the upper part of the Schiavo river basin

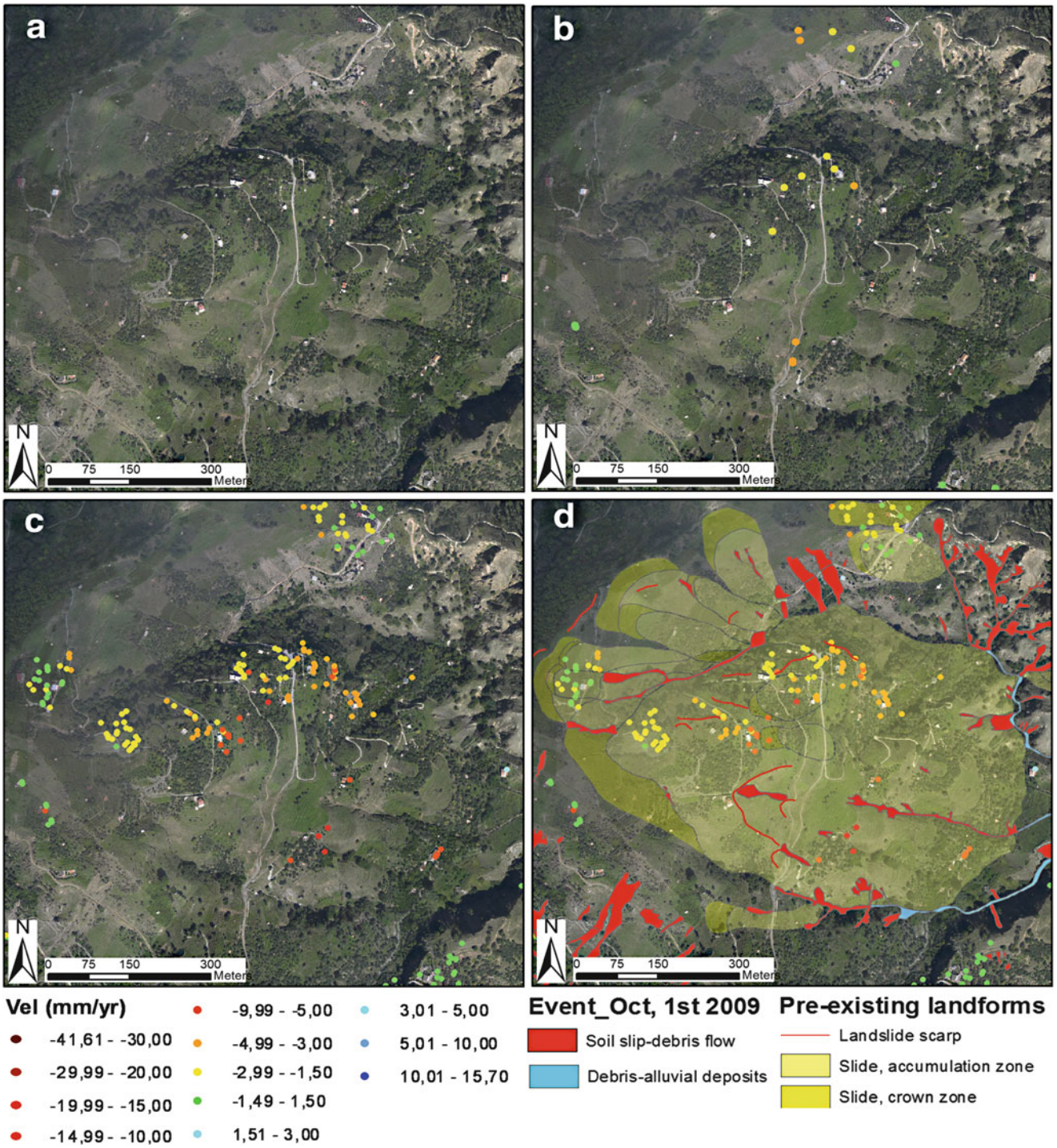

Fig. 4 Results for upper Schiavo basin (Messina). (**a**) Pre-existing landslide inventory map; (**b**) ERS dataset; (**c**) ENVISAT dataset; (**d**) *hotspot analysis*

(Fig. 4d), with the occurrence of many superficial debris flow related to the 1st October event. The field survey confirmed the presence and the extension of the detected phenomena through the identification of tension cracks, scarps and counterscarps.

Discussion and Conclusion

The outcomes of this integrated study provide useful information on the spatial distribution of landslide events. Effectiveness and limitation of the SqueeSAR technique for slope

instability detection at basin scale are mainly related to the different landslide typologies and kinematics. This case study demonstrated the suitability of SqueeSAR data for detection of extremely to very slow moving landslides. On the contrary, fast mass movements with intermittent deformation velocity (such as debris flows triggered by heavy rainfall) cannot be detected.

On the basis of available multi–interferometric data it was possible to identify 26 sites, characterized by high hydro-geological hazard, related to the occurrence of pre-event active landslides.

Photo and radar interpretation shows that populated settlements along the Ionian coastline are built in landslide-prone areas and without taking into account slope instability hazards and their potential consequences on human activities.

Photo-interpretation and field survey highlight that the presence of wide soil layers covering the bedrock on steep slopes, the saturated state of the terrain and the high amounts of rainfall determined the widespread collapse of land masses sliding downhill, hitting the inhabited areas and infrastructures and filling the river beds. Several debris flows occurred along pre-existing landslide flanks, where instability is accentuated by the presence of mobilized material. In addition to natural predisposing factors, that make the slope prone to failure, field survey highlighted that this intrinsic weakness was accentuated by the expansion of the built-up areas and by bad urban planning. Human activities, such as roads cutting across steep slopes, drainage system modification, reduction of river bed cross-section and building area developed close to the main water courses, exacerbated the instability conditions of the area.

Spatial distribution of mass movement phenomena (pre-existing landslides and debris flow events), together with a proper urban planning, could represent a starting point for future implementation of best strategies for risk mitigation, land use planning and consequent reduction of potential consequences on population, infrastructure damage and economic and social losses.

References

Farina P, Moretti S, Colombo D, Fumagalli A, Manunta P (2004) Landslide risk analysis by means of remote sensing techniques: results from the ESA/SLAM project. In: Proceedings of international geoscience and remote sensing symposium, IGARSS, Anchorage, Alaska, 20 Sept 2004, pp 62–65

Farina P, Colombo D, Fumagalli A, Marks F, Moretti S (2006) Permanent scatterers for landslide investigations: outcomes from the ESA-SLAM project. Eng Geol 88:200–217

Farina P, Casagli N, Ferretti A (2008) Radar-interpretation of InSAR measurements for landslide investigations in civil protection practices. In: Proceedings of the 1st North American landslide conference, Vail, 3–7 June 2007, pp 272–283

Ferretti A, Prati C, Rocca F (2001) Permanent scatterers in SAR interferometry. IEEE Trans Geosci Remote Sens 39(1):8–20

Ferretti A, Tamburini A, Novali F, Fumagalli A, Falorni G, Rucci A (2011) Impact of high resolution radar imagery on reservoir monitoring. Energy Procedia 4:3465–3471

Lentini F, Carbone S, Catalano S, Grasso M (1995) Principali lineamenti strutturali della Sicilia nord-orientale. Studi Geologici Camerti 2:319–329

Lentini F, Catalano S, Carbone S (2000) Note illustrative alla carta geologica della Provincia di Messina, Scala 1:50.000, SELCA, Firenze

Tortorici L, Monaco C, Tansi C, Cocina O (1995) Recent and active tectonics in the Calabrian arc (Southern Italy). Tectonophysics 243:37–55

Landslide Inventory in the Area of Zagreb City: Effectiveness of Using LiDAR DEM

Snježana Mihalić, Hideaki Marui, Osamu Nagai, Hiroshi Yagi, and Toyohiko Miyagi

Abstract

Preliminary results of landslide mapping in the City of Zagreb (Croatia), obtained in the frame of the Japanese-Croatian scientific project, are presented in this paper. The aim of this research is to develop a method for landslide delineation in order to enable land use officials to implement this data to create more useful measures for landslide risk management. Selected landslides in the hilly zone of Mt. Medvednica were identified visually using LiDAR bare-earth DEMs. The results of data analysis will be implemented to perform a more comprehensive study of landslides in the entire pilot area (total area is 180 km^2).

Keywords

Landslide inventory • Stereo aerial photographs • LiDAR

Introduction

Landslide hazard mapping is one of the key objectives of the Japanese-Croatian 5-year scientific joint-research project 'Risk Identification and Land-Use Planning for Disaster Mitigation of Landslides and Floods in Croatia'. Landslide hazard zonation will aid development of guidelines for use in urban planning in Croatia. In order to make reliable maps that predict the landslide hazard and risks in a certain area, it is crucial to have insight into the spatial distribution and temporal frequency of landslides. Therefore, each landslide hazard or risk study should start by making a landslide inventory that is as complete as possible in both space and time (Van Westen et al. 2008; Harp et al. 2011).

The activities related to development of landslide inventories by using visual interpretation and automated landslide mapping, followed by development of methodologies of landslide hazard analysis and zonation, have been implemented in the frame of the Projects' Working Group 3 (WG3). Software and hardware, as well as input data (including stereo pairs of aerial photos, digital elevation models, Light Detection and Ranging - LiDAR data and satellite images) will be donated by the Japanese government for three pilot areas in Croatia, two in Primorsko-Goranska County and one in the City of Zagreb. Preparation of a landslide inventory for three pilot areas is planned for the period from 2011 to 2013 based on geomorphic interpretation using stereo pairs of aerial images and from high resolution Digital Elevation Models (DEMs). LiDAR scanning will be performed in March 2012 which will enable analyses of the high resolution DEMs of all pilot areas (total area 246 km^2).

S. Mihalić (✉)
Faculty of Mining, Geology and Petroleum Engineering, University of Zagreb, Pierottijeva 6, 10000 Zagreb, Croatia
e-mail: smihalic@rgn.hr

H. Marui
Niigata University, Research Institute for Natural Hazards and Disaster Recovery, Nishi-ku, Ikarashi ni-no-cho 8050, 950-2181 Niigata City, Japan

O. Nagai
International Consortium on Landslides, Tokyo, Japan

H. Yagi
Lab. Geomorphology, Yamagata University, 1-4-12 Kojirakawa, 990-8567, Yamagata, Japan

T. Miyagi
Department of Geography, Tohoku Gakuin University, 2-1-1 Tenjinsawa, Izumi-ku, Sendai 981-3193, Japan

C. Margottini et al. (eds.), *Landslide Science and Practice*, Vol. 1,
DOI 10.1007/978-3-642-31325-7_20,

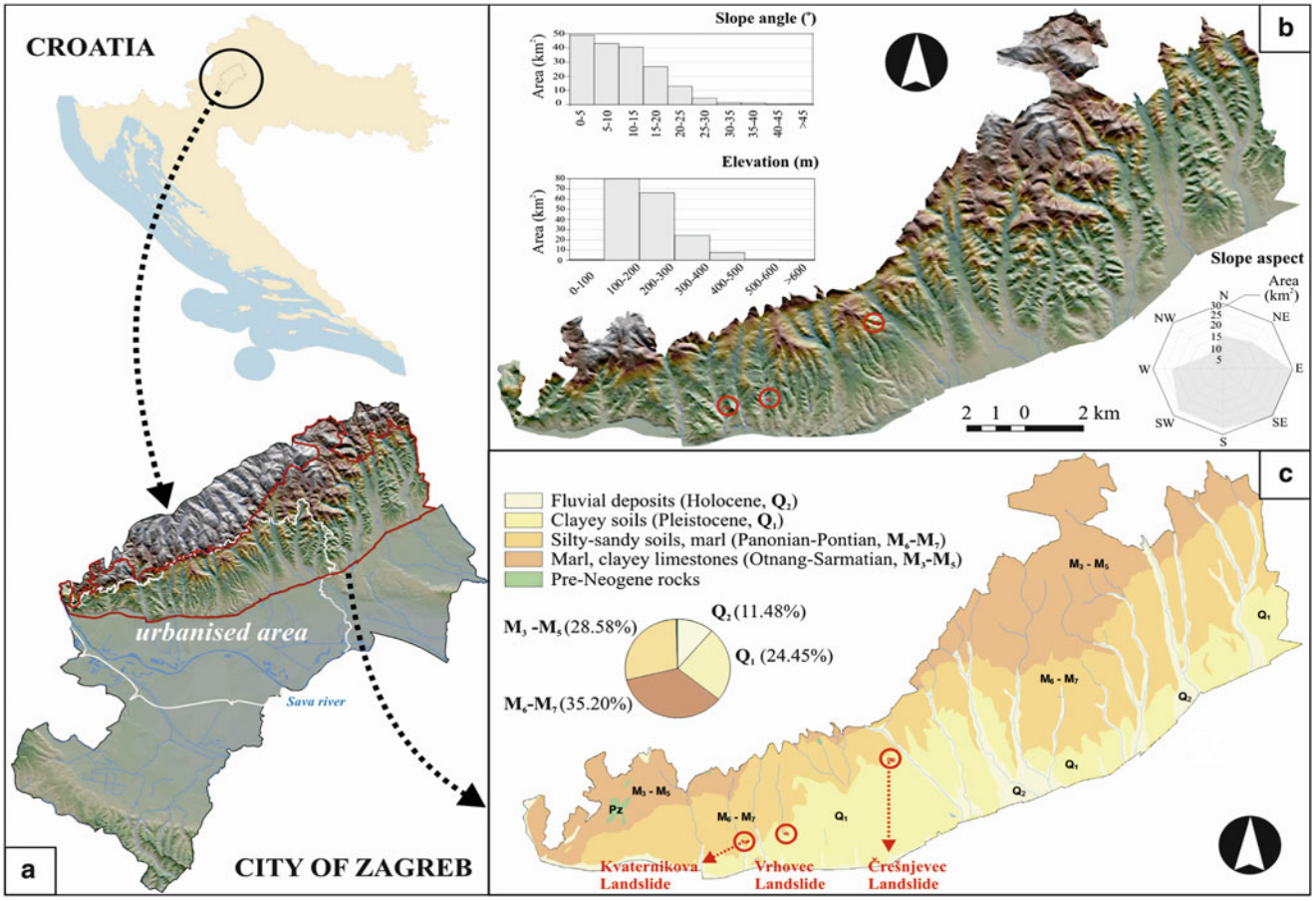

Fig. 1 Thematic data available for the hilly area of the City of Zagreb. (**a**) Geographic location of administrative unit of the City of Zagreb showing the urbanized area (in *white*) and the borders of the pilot area (in *red*). (**b**) Elevation map from the 25 × 25 m DEM. *Histograms* show the distribution of elevation and slope angle computed from the DEM. *Rose diagram* shows the distribution of slope aspect (in km^2). (**c**) Geological map showing the main stratigraphic units. The original scale of the geological map is 1:100,000

The pilot area in the City of Zagreb is a hilly area of Mt. Medvednica (180 km^2) which is a densely populated area with dominant small and shallow landslides that mostly endanger residential structures. Increasing urbanization of this area without strategic measures of risk mitigation has had significant economic costs for the local government as well as for citizens. The local authorities introduced measures for landslide risk management caused by intensive construction activities and the increased population density in the hilly areas, especially in the last 10 years. The main problem with the current practice of landslide risk prevention in the City of Zagreb is the lack of a suitable landslide inventory and landslide hazard and risk maps. Existing landslide maps are derived from direct geomorphological mapping in the field in 1979 and 2007. This implies a high level of uncertainty of landslide interpretation because of the high level of urbanization. Additonally, the criteria used for the delineation of landslides in 2007 were inconsistent and poorly defined.

This paper describes results of the interpretation of three known landslides on the basis of visual inspection of high resolution DEM derived from an airborne LiDAR survey conducted in March 2011 just for a test area (24 km^2). An evaluation of the effectiveness of using topographic derivative maps is part of an investigation on the possibility of using LiDAR for landslide identification and mapping in the hilly area of Mt. Medvednica. It is concluded that LiDAR imagery is a valuable tool for preparation of landslide inventory in the City of Zagreb.

Hilly Area of Mt. Medvednica (City of Zagreb)

The City of Zagreb is located in northwest Croatia in the western part of the Pannonian Basin. The city covers an area of 640 km^2 and includes the urban area and 69 settlements (Fig. 1a) with 77,145 residents. The current land-use includes 205 km^2 of agricultural land, 195 km^2 of forest and 240 km^2 of other use types. The urbanized area (220 km^2) is located below the forest region of Mt. Medvednica to the north and extends to the flood plain of the Sava River in the south. Landslides are a dominant

active geomorphological process in all the Mt. Medvednica stream catchments where approximately 40 % of the urban area is located.

The pilot area of the Croatian–Japanese Project encompasses the middle and lower parts of the catchments shown in Fig. 1b, c, which cover an area of 180 km^2. The elevations in this area range from 115 to 612 m a.s.l., the prevailing slope angles (62 %) range from 5° to 20° and 27 % slopes have slope angles <5°. The pilot area is located in the area composed of Upper Miocene and Quaternary sediments (Fig. 1c). The Upper Miocene deposits are stratified marls, silts and sands with moderately to slightly inclined bedding (slope angle in range 10°–20°). The topmost part of Miocene deposits are fine-grained soils, mostly clays. The Quaternary deposits are heterogeneous mixtures of unfoliated, mostly impermeable clayey soils. The geologic contact between the Miocene sandy silt soils and the Miocene or Quaternary clayey soils is highly susceptible to sliding. The preparatory causal factors of slope instabilities in this zone include the engineering properties of the soils, geomorphological processes (fluvial erosion of the slope toe) and man-made processes of different types (loading of the slopes, defective maintenance of drainage systems, leakage from the water supply system and vegetation removal). The most frequent triggering factors are rainfall and man-made processes. A potential cause is shaking due to earthquakes.

Landslides in the hilly area of Zagreb are mostly small and shallow movements of superficial deposits along contacts with fresh deposits of soil. Despite this, they cause significant economic losses by damaging properties, mostly private houses and the urban infrastructure. The local authorities manage landslide risk by implementating measures for prevention of potential landslides and remediation of activated landslides. Preventive measures rely on a landslide inventory map at a scale of 1:5,000 to differentiate areas where a detailed geotechnical investigation will be required for individual development and areas where no geotechnical assessment is required. This inventory was prepared by the Croatian Geological Survey in 2007 in the form of a data base in which 707 landslides are recorded (Miklin et al. 2010). The landslide map was constructed using geomorphological field mapping and data from existing geotechnical reports. Only 30 landslides have been previously investigated by detailed investigations and just 13 of them are fully or partially stabilised by remedial works. Existing schemes of landslide risk prevention are expensive to implement in terms of total cost because they do not differentiate areas for which some general developmental controls are required, such as limiting the height of cuts and fills, but no detailed geotechnical assessment of hazard or risk assessment is needed. Additionally, they potentially categorize as equally susceptible areas which have different frequencies of landsliding and as a result different levels of hazards. This type of information is also required by the City Office of Emergency Management which is interested in assessment of the risk of injured persons and development of emergency measures.

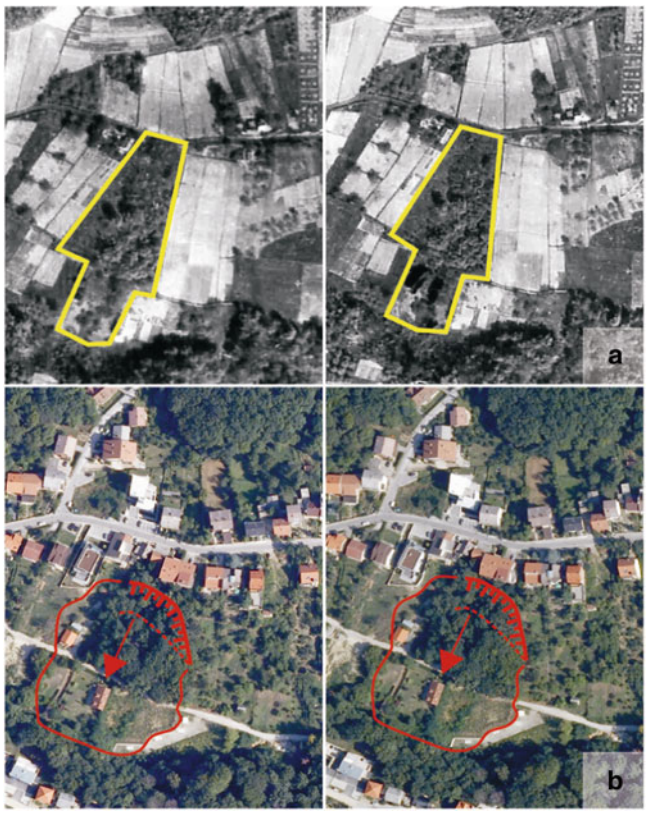

Fig. 2 Stereo pair aerial photographs of the Črešnjevec Landslide from 1967 and 2008. (**a**) Densely vegetated area (inside *yellow frame*) is presumed to be left derelict because unstable slope is useless land. This area is considered as landslide origin. (**b**) Landslide topography composed of main scarp and relatively gentle slope covered by forest is easy to identify at photos from 2008. The area of artificial modification in the bottom of the valley is clearly visible

Figure 1c shows locations of three typical landslides in the hilly area of Zagreb: Črešnjevec Landslide, Vrhovec Landslide and Kvaternikova Landslide. The following discussion presents overview of the three landslides.

Description of Landslides

Črešnjevec Landslide

The Črešnjevec Landslide is a reactivated landslide with unknown precise location, time and cause of initial landslide movement. The dense vegetation typical of the Zagreb hilly area obscures morphology of the Črešnjevec Landslide in aerial photographs from 1967 to 2008 (Fig. 2). Landslide topography encompasses set of horse-shoe shaped steep

scarps; and gentle inclined slopes are at upper and lower part respectively. Densely vegetated areas along the valley are presumed to be left derelict because of instability. The sliding primarily occurred in the middle part of the slope, with the slip surface at the contact between younger clayey soils and Upper Pontian (Pliocene) sandy/clayey silts. The primary movement is easily observed from the surface as a rotational landslide due to its sizable main scarp. The characteristic bulging landslide foot has been removed mostly by artificial modification of the slope. Propagation of the landslide is retrogressive with development of the most recent main scarp near the crest of the hill. Detailed geotechnical investigations were undertaken in 1982 and 2001. Landslide remedial works encompassed regulation of the stream in the valley bottom and construction of drainage wells in the valley (Fig. 2b). Today's geometry of the lower part of the slope is significantly changed by multiple artificial and natural processes such as creeping of superficial deposit from NW direction. After more than 20 years of continuous damaging private houses in the upper part of the landslide are fully destroyed and the City financed new accommodation for the residents. Currently the velocity of the Črešnjevec Landslide is very slow (Cruden and Varnes 1996).

Vrhovec Landslide

The Vrhovec Landslide is a single landslide activated in the last 7 years, and it is caused by artificial works related to the construction of residential buildings above the Vrhovec road. The exact time of activation is not known. It is clearly visible on aerial photographs from 2008 due to the removal of vegetation cover by the sliding. The landslide extends from 164 to 206 m above sea level. The total length of the landslide is approximately 140 m. Detailed geotechnical investigations of the landslide have not been conducted until today. The landslide potentially endangers the Vrhovec road which is located immediately upslope of the main scarp. The whole slope is covered by forest and scrub, and according to the City's urban plan this area is a green urban area. The area of the landslide is composed of Pliocene sandy/clayey silts. The movement is easily observed from land surface due to clearly expressed main scarp, flanks and bulge in the zone of accumulation of displaced material. The Vrhovec Landslide is currently naturally stabilised by the change of geometry, but there is a potential hazard of retrogressive reactivation.

Kvaternikova Landslide

The Kvaternikova Landslide is at least 20 years old but the exact time of initial movement is unknown. It is visible on aerial photographs from 2008. The landslide is formed in a valley with very steep slopes (30°–40°) which was used as an uncontrolled waste disposal. Road fill and waste deposit in the upper part of the landslide caused landslide movement and damaged the Kvaternikova road. Landslide materials, artificial fills and Pleistocene fine-grained soils slip above Upper Pontian (Pliocene) sandy/clayey silts. Detailed geotechnical investigations were undertaken in 2003 and 2006. Landslide remedial works encompassed stabilisation of the upper part of the landslide by constructing a complex geotechnical construction using pile frame construction and pre-stressed ground anchors in combination with drainage system. Today's geometry of the upper part of the landslide is significantly changed by the remedial works, but downslope a characteristic bulge is still clearly expressed. The state of activity of the Kvaternikova Landslide is not known, but most likely the main landslide body is moving extremely slow or very slow (Cruden and Varnes 1996). Small landslides have formed along the landslide flanks and they are also active.

Analyses of LiDAR-derived DEMs

Data and Methods

LiDAR (Light Detection and Ranging) is a remote sensing technique that uses pulses of light to gather information about the surface of the Earth. In this study, high-resolution DEM derived from airborne LiDAR surveys serve as the base data set for creating topographic derivative maps. LiDAR typically provides higher resolutions than other remote sensing techniques and allows the visualization of geologic features at a smaller scale than other remote sensing techniques (Chen et al. 2006; Glenn et al. 2006; Amudsen et al. 2010). Higher resolution data could facilitate the discovery of new landslides and provide more information about existing landslides. Similar techniques were used by Ardizzone et al. (2007), Van Den Eeckhaut et al. (2007) and Schulz (2007) to conduct a landslide inventory in Italy, Belgium and in Seattle (Washington).

The high resolution data became available in Croatia in 2011 only for the part of the pilot area of the Japanese-Croatian Project, i.e., for the test area of 24 km^2 in the City of Zagreb. The LiDAR data were acquired by Goefoto company on April 1, 2011, which corresponds to the leaf-off period in Croatia. LiDAR ground-surface measurements for Zagreb were acquired from the aircraft at an average density of 5 points per square meter. The data were processed to remove vegetation, buildings, and other above-ground features, thus creating a bare-earth DEM. The derived bare-earth DEM has vertical accuracy that is typically about 30 cm, but it is considerably less accurate in some areas, particularly those with dense vegetation due

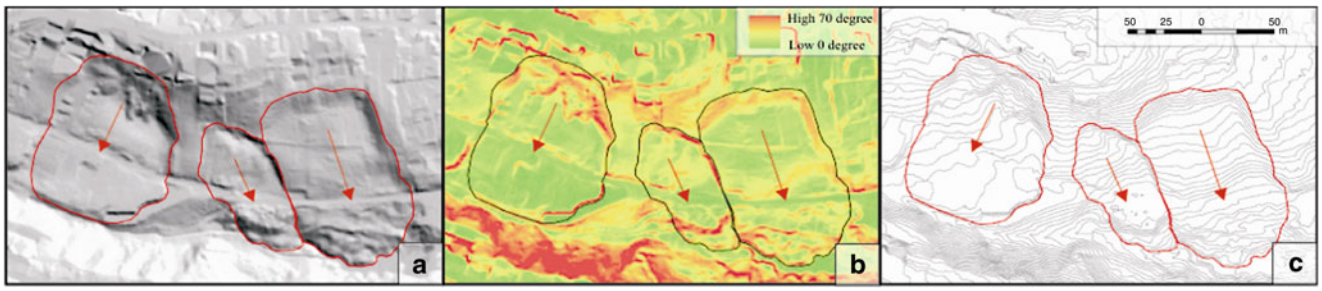

Fig. 3 Composite display of three different topographic derivative maps of the Črešnjevec Landslide (*left* side of the maps) and two successive landslides (Cruden and Varnes 1996) in the *middle* and on the *right* side of the maps. The estimated extent of the landslides has a *red* contour. (a) Hillshade map generated with an azimuth of 315° and a sun angle of 45° draped over a bare earth DEM. (**b**) Slope map showing areas of high slope angle in warmer colors (*red, orange, yellow*) and areas of low slope angle in cooler colors (*green*). (**c**) Contour map generated with a 1 m contour spacing

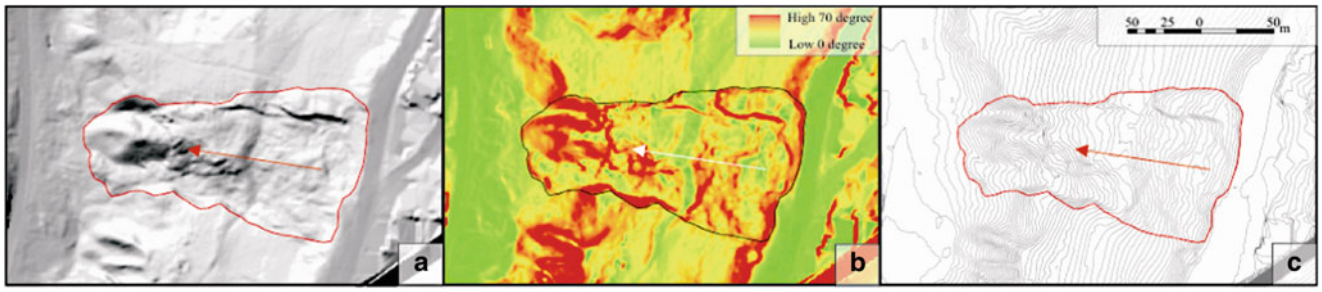

Fig. 4 Composite display of three different topographic derivative maps of the Vrhovec Landslide. The estimated extent of the landslide has a *red contour*. (**a**) Hillshade map generated with an azimuth of 315° and a sun angle of 45° draped over a bare earth DEM. (**b**) Slope map showing areas of high slope angle in warmer colors (*red, orange, yellow*) and areas of low slope angle in cooler colors (*green, blue*). (**c**) Contour map generated with a 1 m contour spacing

to reduced ground-surface measurements in these areas. Preprocessed DEMs with a horizontal resolution of 1 m were used for most of the analysis and supported by data from the raw LAS files that were processed independently using SAGA GIS.

Preliminary analysis encompassed landform mapping performed on three known landslides using an ESRI ArcInfo v. 10 geographic information system (GIS). LiDAR-derived imagery that was used for mapping included shaded relief, slope, and topographic contour maps, as well as topographic profiles. These maps and profiles were visually evaluated for topographic characteristics indicative of landslides, such as scarps, hummocky topography, convex and concave slope areas, midslope terraces, and offset drainages. Mapping was generally performed at 1:2,500 scale. Mapped landforms were evaluated in the field during May 2011 and the maps were revised based on field observations, although very little revision was necessary. Figures 3, 4 and 5 show composite displays of three different topographic derivative maps of landslides Črešnjevec, Vrhovec and Kvaternikova.

Results

Due to the unusual height of the main scarp of the first movement, the Črešnjevec Landslide is readily visible on hillshade, slope and contour maps (Fig. 3, left side of figures). The slope angle of the main scarp is considerably higher than the slope itself with local values up to 25°–45°. In the slope map these appear as the warmer colors of yellow, orange, and red while in the contour map the scarp is identified by a clustering of elevation contours. The flanks of the landslide are also visible on all three maps, but the toe part of landslide is inferred on the basis of the position of a superficial stream and the location of drainage wells. Newly developed scarps in the upper part of the reactivated landslide are not visible because of their limited height (10–20 cm). Similar landslides were also recorded at the same slope (Fig. 3).

The Vrhovec Landslide is readily visible on the hillshade, slope and contour maps (Fig. 4a, b, c). The slope angle of the main scarp is considerably higher than the slope itself with

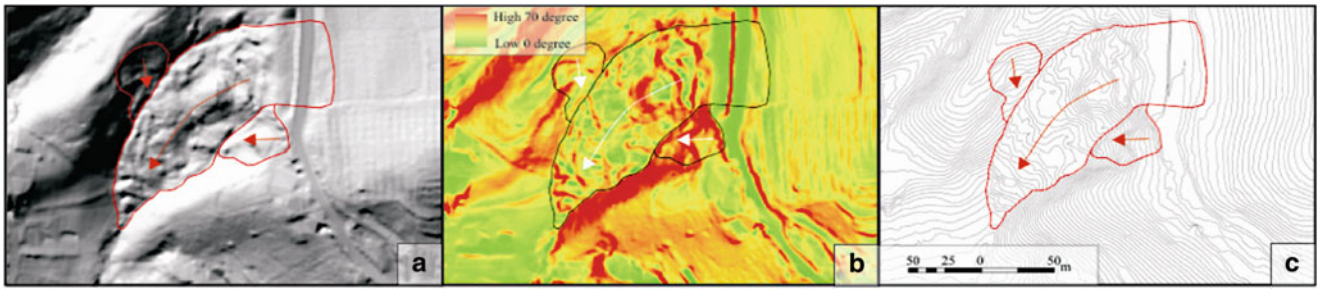

Fig. 5 Composite display of three different topographic derivative maps of the Kvaternikova Landslide. The estimated extent of the landslide has a *red contour*. (**a**) Hillshade map generated with an azimuth of 315° and a sun angle of 45° draped over a bare earth DEM. (**b**) Slope map showing areas of high slope angle in warmer colors (*red, orange, yellow*) and areas of low slope angle in cooler colors (*green, blue*). (**c**) Contour map generated with a 1 m contour spacing

local values up to 25°–45°. In the slope map these appear as the warmer colors (yellow, orange, red) while in the contour map the scarp is identified by a clustering of elevation contours. Hummocky topography, the flanks and the toe of the landslide are also visible.

Due to the unusual height of the valley flanks, the Kvaternikova Landslide is readily visible on hillshade, slope and contour maps (Fig. 5a, b, c). The slope angle of the valley flanks is considerably higher than the slope itself with local values up to 30°–40°. In the slope map these appear as the warmer colors (yellow, orange, red) while in the contour map flanks are identified by a clustering of elevation contours. The displaced mass of the landslide is also visible on all three maps, but the position of the main scarp of landslide is inferred, because this area is artificially modified by remedial works. Smaller landslides were also recorded, but their directions of movement are diagonal to the displacement direction of the main landslide body.

Discussion and Conclusion

The preparation of a landslide inventory in the hilly area of the City of Zagreb on the basis of geomorphic interpretation of stereo pairs of aerial images is limited due to characteristics of landslides (small and shallow landslide bodies), high level of urbanization (modification of natural landscape) and dense vegetation cover (forested areas). The dense vegetation, typical for the Zagreb hilly area, obscures the morphology of landslides both in the field and on aerial photographs. LiDAR data can be processed to reveal the topography beneath vegetation. This technology was useful in the test area for identifying the shape and spatial distribution of historical landslides, identify previously unmapped landslides, and other geomorphic landforms. DEMs of the bare-earth surface derived from LiDAR data express topographic details sufficiently well to identify landslide bodies. Three typical landslides were mapped using LiDAR imagery and field verified. We relied almost entirely on derivatives of LiDAR data for our mapping, including topographic-contour, slope, and hillshade maps. Each mapped landslide was assigned a level of "high" or "moderate" confidence based on the LiDAR characteristics and on field observations and it could be concluded that LiDAR imagery does effectively "remove" vegetation that obscures many landslides. It is therefore a valuable tool for preparation of landslide inventories and investigations in heavily vegetated regions such as the hilly area of Mt. Medvednica.

Further research will focus on the interpretation of the spatial frequency of landslides in the entire pilot area in the City of Zagreb (180 km^2). Future studies will seek to: (1) create a landslide inventory map using the LiDAR-derived imagery scheduled in early March 2012 and to evaluate the relative quality of the LiDAR-derived map against existing landslide inventory maps created by field mapping, (2) create a landslide susceptibility map using LiDAR imagery and records of historical landslides, and (3) evaluate results in the context of landslide causation. A secondary goal is to evaluate the locations and characteristics of historical landslides in relation to stratigraphic conditions along with landslide-related landforms mapped using LiDAR imagery. Interpretation of LiDAR data will be followed by a systematic field checking and geomorphic interpretation of stereo pairs of aerial photos from different periods during the last 50 years.

The results of WG3 of the Japanese-Croatian project, in the form of a landslide inventory and landslide susceptibility and hazard maps, have wide applications in the local administration of the City of Zagreb. Landslide maps that depict the locations of past and current landslides, as well as the relative potential for future movements, will be used as base maps for information about constraints on land-use development, the development of landslide risk prevention measures in the early phases of construction and the development of measures to mitigate losses from present and future landslides by developing crisis response plans. Customized landslide zonation maps are important because they will influence the system of risk prevention and mitigation by introducing new measures or improving existing measures in the land-use planning and civil protection systems in

the City of Zagreb. The Croatian–Japanese joint research project is an opportunity for scientists to derive direct social benefits for Croatian society through the application of the results of scientific research. The project results will be shared with stakeholders, relevant institutions, governments, organizations, individuals, and most importantly the residents that are endangered by landslides in the pilot areas.

The landslide inventory needs to develop in the future to become more reflective of the City of Zagreb situation and necessities. The data collected through scientific research needs to be achieved in a database in the form of accurate, consistent and complete landslide records. The aim of the Japanese-Croatian project is to provide an up-to-date and comprehensive database to the public as soon as possible.

Acknowledgments Results presented herein have been obtained with the financial support from JST/JICA's SATREP Program (Science and Technology Research Partnership for Sustainable Development). This support is gratefully acknowledged.

Authors want to thank the Geofoto Company (Zagreb, Croatia) for giving us promotional price of LiDAR scanning as well as to our colleague P. Ferić for help and support in LiDAR analyses.

References

Amudsen J, Johnson S, Rousea K, Wang H (2010) Using LiDAR-derived DEM's to delineate and characterize landslides in Northern Kentucky and Hamilton County, Ohio. http://www.trishock.com/academic/pdf/lidar_landslides.pdf. Accessed 12 June 2011

Ardizzone F, Cardinali M, Galli M, Guzzetti F, Reichenbach P (2007) Identification and mapping of recent rainfall-induced landslides using elevation data collected by airborne Lidar. Nat Hazard Earth Syst Sci 7:637–650

Chen R-F, Chang K-J, Angelier J, Chab Y-C, Deffontaines B, Lee C-T, Lin M-L (2006) Topographical changes revealed by high-resolution airborne LiDAR data: The 1999 Tsaoling landslide induced by the Chi-Chi earthquake. Eng Geol 88:160–172

Cruden DM, Varnes DJ (1996) Landslide types and processes. In: Turner K, Schuster R (eds) Landslides, investigation and mitigation. Special Report 247, Transportation Research Board, Washington, ISBN 0-309-06151-2, pp 36–75

Glenn NF, Streutker DR, Chadwick DJ, Thackray GD, Dorsch SJ (2006) Analysis of LiDAR-derived topographic information for characterizing and differentiating landslide morphology and activity. Geomorphology 73:131–148

Harp EL, Keefer DK, Sato HP, Yagi H (2011) Landslide inventories: the essential part of seismic landslide hazard analyses. Eng Geol 122(1/2):9–21. doi:10.1016/j.enggeo.2010.06.013

Miklin Ž, Ortolan Ž, Hećimović I, Podolszki L (2010) Preliminary hazard map of the „Sljeme suburban area". In: Proceedings of 4th Croatian geological congress, Šibenik, 14–15 Oct 2010, pp 174–175 (in Croatian)

Schulz WH (2007) Landslide susceptibility revealed by LIDAR imagery and historical records, Seattle, Washington. Eng Geol 89:67–87

Van Den Eeckhaut M, Poesen J, Verstraeten G, Vanacker V, Nyssen J, Moeyersons J, van Beek LPH, Vandekerckhove L (2007) Use of LIDAR-derived images for mapping old landslides under forest. Earth Surf Proc Landf 32:754–769

Van Westen CJ, Castellanos E, Kuriakose SL (2008) Spatial data for landslide susceptibility, hazard, and vulnerability assessment: an overview. Eng Geol 102:112–131

Usage of ASTER Level 3A Stereo Data in Landslide Inventory Mapping: Visual Determination Versus Fieldwork

Tolga Alkevli and Murat Ercanoğlu

Abstract

Studies related to natural hazards have become an extremely important issue among the geoscientists for the last few decades. Particularly after the mid 1980s, developments in computer technology, GIS (Geographic Information Systems), and RS (Remote Sensing) have provided rapid and detailed analysis of different natural hazards such as landslides, earthquakes, floods, and so on, in larger areas. Combined with field observations, these analyses may provide important knowledge in assessing natural hazards. Landslides are one of the most destructive parts in natural hazards. Similar to many countries in the world, Turkey, a landslide suffering country, faces this problem. In Turkey, landslides are of great importance among the natural hazards, and the Western Black Sea region is one of the major landslide prone areas. For this reason, in this study, we selected an area in the Western Black Sea region, in order to investigate the usage of ASTER (Advanced Spaceborne Thermal Emission and Reflection Radiometer) satellite imagery in preparing landslide inventory maps. For this purpose, two- and-three dimensional visual image interpretation was performed at different scales varying from 1:15,000 to 1:50,000. Particularly VNIR (Visible Near Infrared) bands of the ASTER images were used in the analyses. Field studies were also carried out in the study area to map landslides and to compare different landslide inventories. Based on the analyses, it was revealed that the best method to prepare landslide inventory maps by visual interpretation was found as stereoscopic (three dimensional) image analysis at 1:15,000 scale. ASTER Level 3A data were used to create stereo images, RGB (433) in other words ASTER 3N (Nadir) and 3B (Backward) bands can be used to produce stereo images. The smallest mapped landslide was determined as 58,885 m^2, covering approximately 262 pixels. As a result of the assessments, it is considered that ASTER satellite imagery can successfully be used in regional and medium scale landslide inventory studies.

Keywords

ASTER • Stereo data • Landslide inventory

Introduction

The term landslide explains the movement of a mass with rock and debris down a slope (Cruden 1991). The earth materials related to the landslide may fall down in differentways like toppling, sliding, spreading, flowing or a combination of these. The occurrence of landslides is dependent on the different parameters such as geological and/or

T. Alkevli (✉)
Remote Sensing Division 06800, MTA General Directorate of Mineral Research and Exploration Center, Çukurambar, Ankara, Turkey
e-mail: alkevli@mta.gov.tr

M. Ercanoğlu
University of Hacettepe, Ankara, Turkey
e-mail: murate@hacettepe.edu.tr

C. Margottini et al. (eds.), *Landslide Science and Practice*, Vol. 1,
DOI 10.1007/978-3-642-31325-7_21,

geomorphological conditions. Also heavy precipitation, human activity and vegetation cover changes play an important role to trigger landslide activity. In addition to loss of lives, landslides destroy residential and industrial areas as well as agricultural and forest lands, and negatively affect water quality in rivers and streams (Schuster 1996). From another aspect, landslides are natural events and play an important role in the evolution of landforms (Harmon and Doe 2001). Because of landslides can change the surface of the earth, RS (Remote Sensing) is an important tool to assess landslide activity. Furthermore, RS techniques are preferable for landslide assessments because of their updateable features and ability to show large areas, when integrated in a GIS environment (Alkevli and Ercanoğlu 2011). Thanks to the advances in RS, landslide researchers begin to prepare more sophisticated landslide maps. But most of these maps require very detailed information such as precipitation period, topographical variations, rock-soil separations etc. Most of the remote sensing satellites can not supply this information together for landslide mapping. Acquiring the earth data in considerable short temporal frequencies is one of the main advantages of satellite remote sensing. ASTER (Advanced Spaceborne and Thermal Emissivity Raidometer) satellite imagery is 16 days temporal resolution. The visible bands of ASTER are utilized to determine landslide inventory mapping. Landslide inventories are essential to understand the evolution of landscapes, and to ascertain landslide susceptibility and hazard (Galli et al. 2008). In addition, in order to make a reliable map that predicts the landslide susceptibility, hazard or risk in a certain area, it is crucial to have insight into the spatial and temporal frequency of landslides (Van Westen et al. 2008). The main purpose of this study was to determine the use of ASTER imagery to prepare a landslide inventory map in the Western Black Sea region of Turkey. According to this purpose, stereoscopic visual interpretations were carried out to map landslides at scales of 1:15,000, 1:25,000, 1:35,000, and 1:50,000. In addition, a detailed inventory map was produced directly in the field, and then the field inventory was correlated with the inventory maps in different scales prepared by satellite remote sensing.

Study Area

The study area approximately covers 520 km^2 in Western Black Sea Region and is located among the three major cities in Turkey (Fig. 1). The mean annual precipitation in the region is over 1,000 mm (http://tumas.meteoroloji.gov.tr). The topography of the study area varies from 60 to 1,198 m.

The study area is located in Pontid Region, which is one of four major tectonic belts in Turkey. Precambrian and Palaeozoic age rocks constitute base units of stratigraphy in the study area as metagranitoids and marbles. When

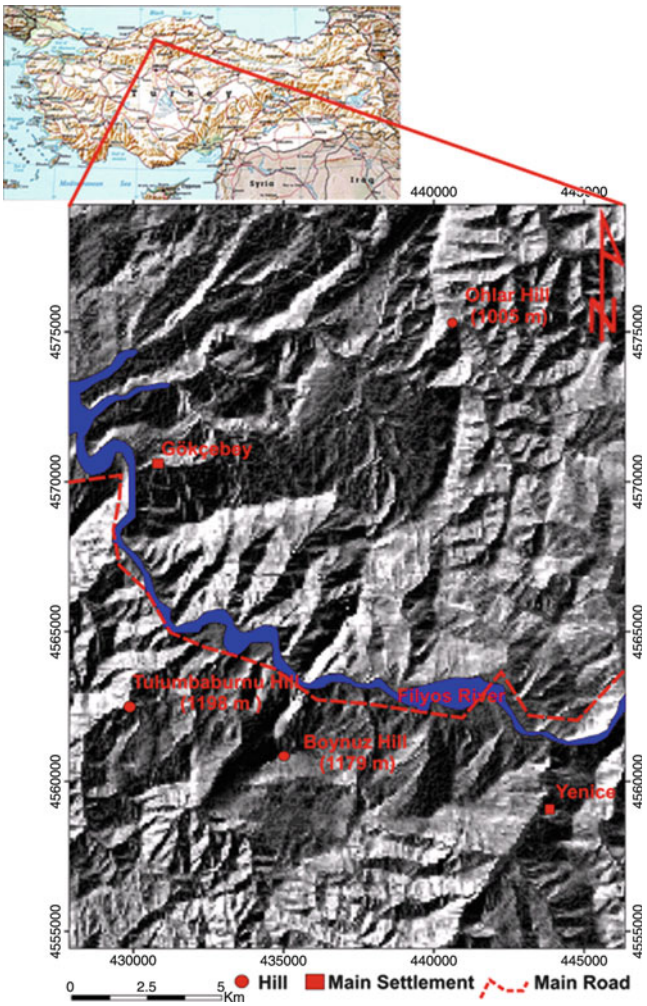

Fig. 1 Location map of the study area

passing through to the younger units, Mesozoic age rocks cover Paleozoic age rocks unconformably. Ahmetusta conglomerates of Lower Cretaceous age are coming after Mesozoic rocks. The most susceptible formation to landsliding is known be the Ulus Formation. It is composed of flysch, sandstone, limestone, marl and shales of Upper Cretaceous age. The Yemişliçay formation is extended between Yenice and Gökçebey region in NE-SW direction and contains different volcanics and sedimentary rocks. The Akveren formation includes basalts and clay rocks.

The Lower-Middle Eocene aged Çaycuma formation is well known with flysch characteristics including conglomerate, limestone, and shales. Çaycuma formation is located in Gökçebey region. The Eocene aged Yığılca formation is extended NW of Gökçebey and represented by neritic limestone, sandstone and siltstone and pyroclastic materials. Quaternary age alluvium and debris flows are located along the Filyos River (see Fig. 2). There are several fault systems associated with the North Anatolian Fault Zone (Herece 1990). Also strike slip faults and dragged zone can be seen in Fig. 2.

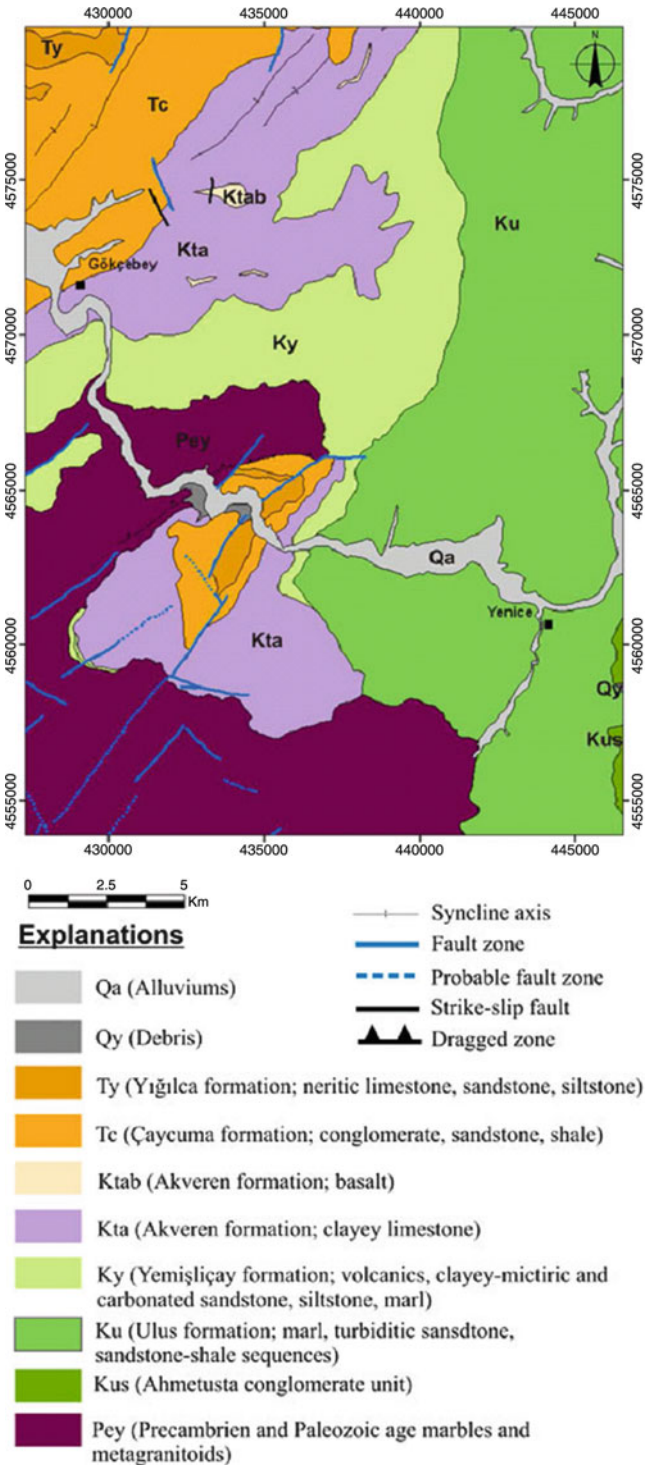

Fig. 2 Geological map of the study area (MTA 2004)

Methodology

Use of ASTER satellite imagery has increased in geological applications because it allows to create stereo images and DEM products (Hirano et al. 2003; Fujisada et al. 2005). ASTER satellite imagery is one of the cheapest among medium spatial resolution data. ASTER Level 3A data have a great utilization in landslide applications because of their spectral and spatial features, DEM capability and stereoscopic views (Liu et al. 2004; Fourniadis et al. 2007; Weirich and Blesius 2007).

ASTER Level 3A data acquired on 5 May 2007 is used for this study. ASTER has 14 spectral bands with different spectral and spatial resolutions. It has three radiometers including VNIR (Visible and Near Infrared Radiometer; wavelength: 0.56–0.86 μm and spatial resolution of 15 m), SWIR (Short Wavelength Infrared Radiometer; wavelength: 1.60–2.43 μm and spatial resolution of 30 m), and TIR (Thermal Infrared Radiometer; wavelength: 8.125–11.65 μm and spatial resolution of 90 m), (ERSDAC 2003). ASTER's backward and nadir telescopes have been used to create stereo imagery which is helpful in landslides inventory mapping by visual interpretation. In this study a landslide inventory map is created in three different ways with stereo-based maps using 3B and 3N bands; a False Color Composite (FCC) using the 3N, 2, 1 in RGB (Red, Green, Blue) order and the 3N in grey scale which is highly susceptible to the water and vegetation cover and all of these maps were correlated with the field inventory.

Stereo image is created using the VNIR portion of ASTER images. The stereo image of the study area can be seen in Fig. 3. Additionally visual interpretations were carried out with the help of ArcGIS 9.3 software taking into consideration four different scales: 1:15,000, 1:25,000, 1:35,000, and 1:50,000. As a result of visual interpretation 12 different landslide inventory maps were prepared. But smaller scales, less than 1:15,000 showed that FCC and infrared band were not sufficent to recognize and determine the landslides. Therefore, six landslide inventory maps (four of stereoscopic images in four different scales, one of FCC at 1:15,000 scale, and one of 3N band at 1:15,000 scale) were produced (Fig. 4). The landslides were classified according to Cruden and Varnes (1996).

After consideration of the results of visual interpretations the Minimum Identified landslide Area (MIDA) is found to be 58,885 m^2 and includes approximately 262 pixels in 1:15,000 scale stereo image. But landslides types such as rotational or earthflows were not recognized with visual interpretation. As for the Minimum Interpreted landslide Area (MINA) with the size of 70,861 m^2 was determined with 1:25,000 scale stereo image. Because of drainage conditions, morphological and vegetational anomalies could be separated from the surrounding area. FCC and 3N bands did not give exact information which is related to landslides. Table 1 gives detailed information about properties of landslides during fieldwork.

The next step was to carry out fieldwork in the study area in 2008 and 2009. There were five field trips to map

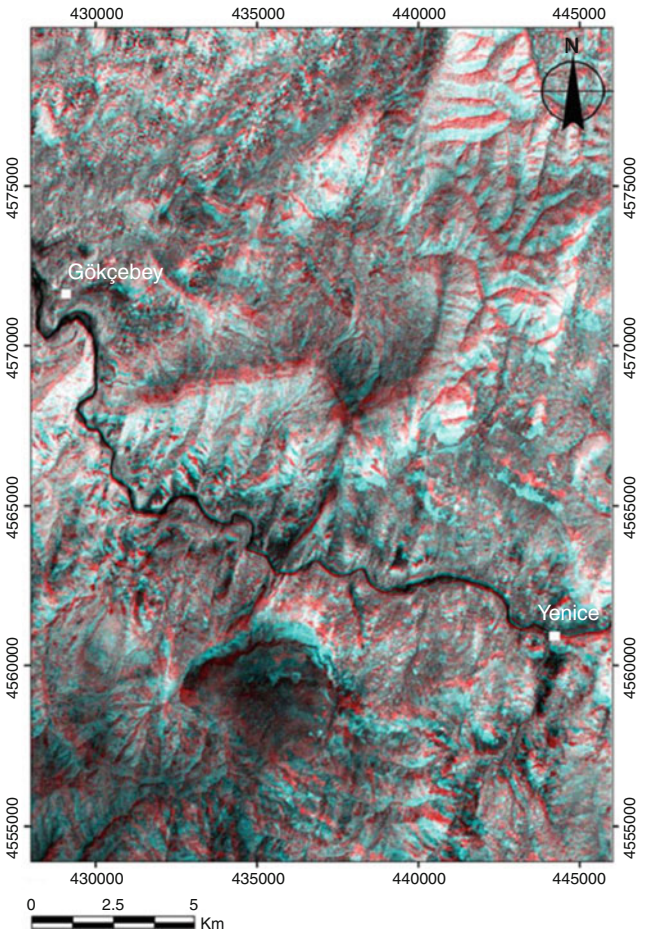

Fig. 3 Stereo image of the study area (rotate the image 90° clockwise and use cyan-red eye glasses)

landslide locations and prepare the landslide inventory map in the study area. A hand-held GPS (Global Positioning System) with the accuracy of 3–6 m was used for the mapping process. During the fieldwork features of landslides such as boundary, location and types of landslides were registered in the landslide inventory form. Totally 68 landslides of three different types according to Cruden and Varnes (1996) were mapped (Fig. 5) and transferred into the GIS (Geographic Information System). The large majority of landslides are rotational slides while the other types are debris flows and complex movements (see Fig. 5). The features and types of the mapped landslides are summarized in Table 2. During the field study the smallest mapped landslide of earth flow type was 7,655 m^2.

The whole correlation processes were carried out according to Carrara et al. (1992) using (1) and (2):

$$E = [(A_1 \cup A_2) - (A_1 \cap A_2)]/[A_1 \cup A_2] \quad (1)$$

$$M = 1 - E \quad (2)$$

For all these equations, E is the relative value error index in the range of 0 and 1, M is the degree of match ranging between 0 and 1, A1 and A2 are the total number of landslide areas in the landslide inventories. After consideration of these if the two inventories are the same, M values are equal to 1 (based on the E = 0); if they are different, M and E are equal to 0 and 1 relatively. As it can be seen from Table 2, the best matching maps couples were Map 3 and Map 4 which have the best correlation M value equal to 0.69.

Results and Discussions

(a) Landslide inventory maps were prepared in two different ways, ASTER Level 3A visual interpretations and direct field mapping. According to the field studies, 68 different landslides were determined in the study area; rotational earth slides (37), flows (earthflows and some debris flows), and complex (7).

(b) Based on the two-dimensional visual interpretation processes FCC and infrared band images were not clear enough and informative even at the bigger scales such 1:15,000. As can be seen on Fig. 4e, f there are few landslides which could be detected by visual interpretation as undetermined types. This situation is also corrected with detection of M values for Map 5 and 6 are correspondingly 0.11 and 0.08 (see Table 2). It can be said that two-dimensional visual interpretation of ASTER imagery is not giving sufficient information for landslide inventories.

(c) The best observation method with ASTER imagery is 3D assessments. As can be seen from Table 2, the best M value was calculated 0.31 at 1:15,000 scale with comparison of Map 1 and Map 7. (Map 1) assuming Map 7 represents "ground truth". As can be seen from Table 2, the best method for preparing landslide inventory map with visual interpretation is ASTER 3D stereoscopic image process at the scale of 1:15,000.

(d) The most significant finding was the compatibility between the smallest mapped landslide (#20 see Fig. 4a) on Map 1 and the g7 landslide of Map 7 (see Fig. 5). The size of this landslide was calculated as 58,885 m2. The type was not clear, although in the field it was classified as a rotational earth slide. The smallest identified and interpreted landslide was on Map 2 (see Fig. 4b, #13) which was produced by 1:25,000 scale stereoscopic image analysis. This flow type landslide was 70,861 m^2 in size; the location and the type were confirmed by fieldwork (y17 in the Map 7). Therefore, it can be concluded that the MIDA is 58,885 m^2 and the MINA is 70,861 m^2 for the ASTER Level 3A data. It should be noted that these values are only valid for the landslides and landslide characteristics of the present study area (Alkevli and Ercanoğlu 2011).

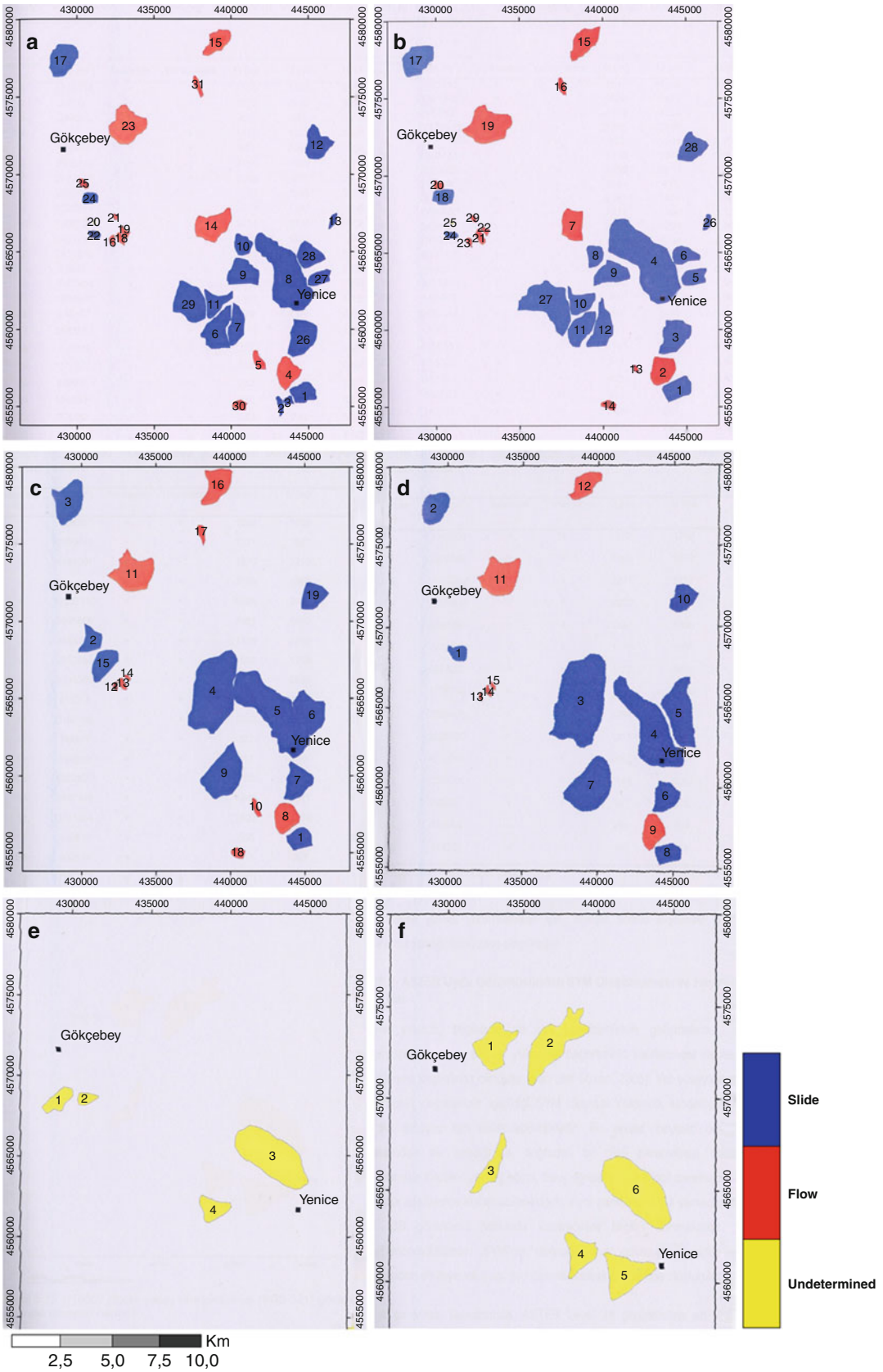

Fig. 4 Landslide inventory maps (prepared with visual interpretation); (**a**) 1:15,000 stereo image, (**b**) 1:25,000 stereo image, (**c**) 1:35,000 stereo image, (**d**) 1:50,000 stereo image, (**e**) FCC image, (**f**) infrared image

Table 1 Properties of the mapped landslides from fieldwork

Material	Number of landslides	Width (m)			Length (m)			MIDA (m^2)	MINA (m^2)
		Min	Max	Ave	Min	Max	Ave		
Field work	Total: 68	85	2,360	598.6	50	2,190	685.3	7,665	7,665
	Slide: 37	155	1,970	642.6	140	2,110	753.2		
	Flow: 24	85	598	264.1	50	1,293	333.3		
	Complex: 7	350	2,360	992.4	617	2,190	1,033		

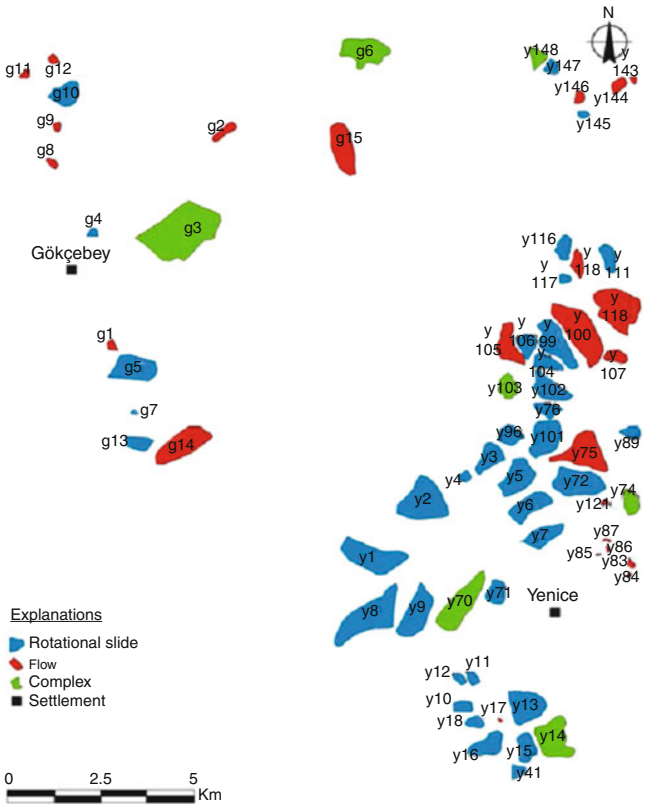

Fig. 5 Landslide inventory map prepared by fieldwork (Alkevli and Ercanoğlu 2011)

Table 2 E and M values of the compared landslide inventory maps

	Map 1	Map 2	Map 3	Map 4	Map 5	Map 6	Map 7
Map 1	E M						
Map 2	0.62 0.38	E M					
Map 3	0.48 0.52	0.50 0.50	E M				
Map 4	0.51 0.49	0.55 0.45	0.31 0.69	E M			
Map 5	0.83 0.17	0.87 0.13	0.84 0.16	0.87 0.13	E M		
Map 6	0.86 0.14	0.83 0.17	0.85 0.15	0.89 0.11	0.65 0.35	E M	
Map 7	0.69 0.31	0.80 0.20	0.87 0.13	0.86 0.14	0.89 0.11	0.92 0.08	

Acknowledgments The authors would like to thank Assoc. Prof. Dr. M. Lütfi Süzen for his encouraging support and suggestions Assoc. Prof. Dr. Ergün Tuncay and Ahmet Temiz are also acknowledged for their help during the field studies. Finally, athe authors would like to thank Mr. Rüçhan Haktanır and Mr. Orhan Toptan for their logistic support.

References

Alkevli T, Ercanoğlu M (2011) Assessment of ASTER satellite image in landslide inventory mapping: Yenice-Gökçebey (Western Black Sea Region, Turkey). Bull Eng Geol Environ 70(4):607–617

Carrara A, Cardinali M, Guzzetti F (1992) Uncertainty in assessing landslide hazard and risk. ITC J 2:172–183

Cruden DM (1991) A simple definition of a landslide. Bull Int Assoc Eng Geol 43:27–29

Cruden DM, Varnes DJ (1996) Landslide types and processes. In: Turner AK, Shuster RL (eds) Landslides: investigation and mitigation. Special Report volume 247, Transp Res Board, pp 36–75

ERSDAC (2003) Earth Remote Sensing Data Analysis Center, ASTER Reference Guide (Version 1.0)

Fourniadis IG, Liu JG, Mason PJ (2007) Regional assessment of landslide impact in the Three Gorges area using ASTER data: Wushan-Zigui. Landslides 4:267–278

Fujisada H, Bailey G, Kelley GG, Hara S, Abrams MJ (2005) ASTER DEM performance. IEEE Trans Geosci Remote Sens 43:2707–2713

Galli M, Ardizzone F, Cardinali M, Guzzetti F, Reichenbach P (2008) Comparing landslide inventory maps. Geomorphology 94:268–289

Harmon RS, Doe WW (2001) Landscape erosion and evolution modeling. Springer, Berlin

Herece E (1990) 1953 Yenice-Gönen deprem kırığı ve Kuzey Anadolu fay sisteminin Biga yarımadasındaki uzantıları. MTA Dergisi 111:47–59 (in Turkish)

Hirano A, Welch R, Lang H (2003) Mapping from ASTER stereo image data: DEM validation and accuracy assessment. ISPRS J Photogramm Remote Sens 57:356–370

Liu JG, Mason PJ, Clerici N, Chen S, Davis A, Miao F, Deng H, Liang L (2004) Landslide hazard assessment in the three Gorges area of the Yangtze river using ASTER imagery: Zigui–Badong. Geomorphology 61:171–187

MTA (2004) 1/25000 ölçekli Türkiye jeoloji veri tabanı F28 paftası (in Turkish)

Schuster RL (1996) Socioeconomic significance of landslides. In: Turner AK, Schuster RL (eds) Landslides: investigation and mitigation. Special report no. 247, Transportation Research Board, National Academy of Sciences, Washington, pp 12–35

Van Westen CJ, Castellanos E, Kuriakose SL (2008) Spatial data for landslide susceptibility, hazard and vulnerability assessment: an overview. Eng Geol 102:112–131

Weirich F, Blesius L (2007) Comparison of satellite and air photo based landslide susceptibility maps. Geomorphology 87:352–364

Mechanism and Triggering Factors of the Maierato (VV) Landslide

Paola Gattinoni and Laura Scesi

Abstract

A large landslide formed at Maierato (Vibo Valencia, Southern Italy) on February 15, 2010, when rapid failure occurred after several days of preliminary movements. The present paper covers: (1) identification of the landslide mechanism and triggering factors, (2) slope stability back-analysis using a finite-element-based shear strength reduction method, and (3) mapping of the landslide susceptibility on the basis of the main geological and hydrogeological controlling factors. The aim of the paper is to explain the mechanism of occurrence of the February 2010 landslide, in order to assess the landslide susceptibility in the whole urban area of Maierato, and then to propose risk mitigation actions.

Keywords

Groundwater flow • Numerical modelling • Stability analysis • Italy

Introduction

On February 15, 2010, a large landslide (estimated volume 10 Mm^3) occurred in the municipality of Maierato (Vibo Valencia), Southern Italy (Fig. 1). This landslide, a roto-translational slide that evolved into a flow (maximum width = 500 m, and length = 1,200 m, Fig. 2), caused the evacuation of nearly 2,300 inhabitants and high economic loess.

The landslide was a manifestation of a larger deep seated gravitational movement. All the Municipaly of Maierato stands on a big paleolandslide being a part of the previously cited deep seated gravitational movement. The presence of other older landslides suggests that the area has a high susceptibility to deep-seated landsliding, which may be linked to its geological and structural setting, in particular to the presence of very weak rocks and to the changes in groundwater level. More in detail, the main preconditioning factor is the presence of weak rocks (both the evaporitic limestone and the Miocenic sandstone), with a stratigraphic succession characterized by alternating more permeable rocks (i.e. limestone and Miocenic sandstone) and impermeable ones (i.e. Miocenic and Pliocenic clays). The most probable trigger of the landslide was the cumulative precipitation over the preceding 20 days (having a return period of more than 100 years), which followed a long period of 4–5 months of heavy rainfall (of about 150 % of the average rainfall of the period). The heavy and prolonged rainfall brought about a great recharge to the deep and the shallow aquifers, generating pressure in the aquifer layers, especially within the Miocenic sandstone, which during the motion could have undergone liquefaction. As a result, the kinematism of the event was at first put down to a roto-translational sliding in a SW direction, then evolving in a flow, as a consequence of the high water content. This conceptual model of the event was reconstructed by the coupling of the geotechnical and groundwater flow modeling. In particular, the slope stability modeling was carried out considering different groundwater level, in order to identify the groundwater conditions triggering the instability. Finally, the landslide susceptibility for the whole urban area of Maierato has been inferred based on: (1) the geological conceptual model reconstruction which allowed

P. Gattinoni (✉) • L. Scesi
DIIAR, Politecnico di Milano, p.zza L. Da Vinci 32, Milan, Italy
e-mail: paola.gattinoni@polimi.it

C. Margottini et al. (eds.), *Landslide Science and Practice*, Vol. 1,
DOI 10.1007/978-3-642-31325-7_22,

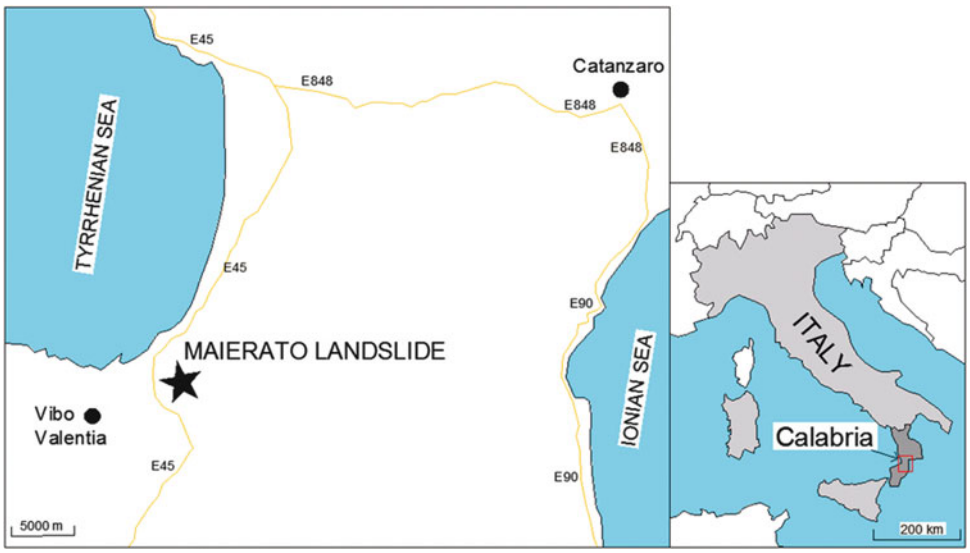

Fig. 1 Location of the Maierato landslide (Southern Italy)

Fig. 2 Panoramic photograph of the Maierato landslide

to identify the weak rocks levels distribution, (2) the main groundwater flow directions identified through a detailed hydrogeological survey.

Geological and Hydrogeological Setting

The landslide is located within the central sector of the Calabria Region (Fig. 1), on the Southeast face of a horst and graben structure. The landslide moved in a Northwest to Southest direction. The area around the landslide is part of a larger area of deep-seated gravitational movement (Guerricchio et al. 2010) covering around 7.5 × 3.5 km with extension towards the Southeast. The deep-seated gravitational movement is probably a consequence of tectonic uplift. The latter has produced a system of normal faults with a Northeast-Southwest direction including the formation of an asymmetric horst separating the Tyrrhenian slope of Pizzo Calabro from Maierato (Van Dijk and Okkes 1991).

According to the Geological Map of Italy (Cassa per il Mezzogiorno 1968), the detailed geological survey showed the following sequence of rock types (Fig. 3) (from the top to the bottom): (1) Pleistocene eluvio-colluvial deposits of variable thickness (0 to 10 m) with a predominance of conglomerates in a silt-sandy matrix of typical red color; (2) Middle Pliocene deposits of alternating clayey sands with macrofossils and clay layers having light grey or brown color with thicknesses of 5–25 m; (3) highly porous Upper Miocene evaporitic limestone with clayey and marl-clayey layers, with thicknesses varying between 25 and 45 m; (4) Late Miocene clays that are well consolidated with thin sand-silty layers and a thickness of 10 to 20 m; (5) Middle to Late Miocene alternating sandstone and grey sandy clays, poorly cemented, with thicknesses from 10 to 40 m; (6) Middle to Late Miocene conglomerates with rounded clasts and blocks of bedrock within a gravel-sand matrix, 0–5 m thick and with limited lateral continuity; (7) Paleozoic crystalline metamorphic bedrock, very fractured and weathered; it forms the Cresta Basilica Plateau and the slopes having a dip greater than 30°. All the sedimentary succession is characterized by a very low dip (from 15° dip to horizontal) towards ESE. Locally gravitational movement

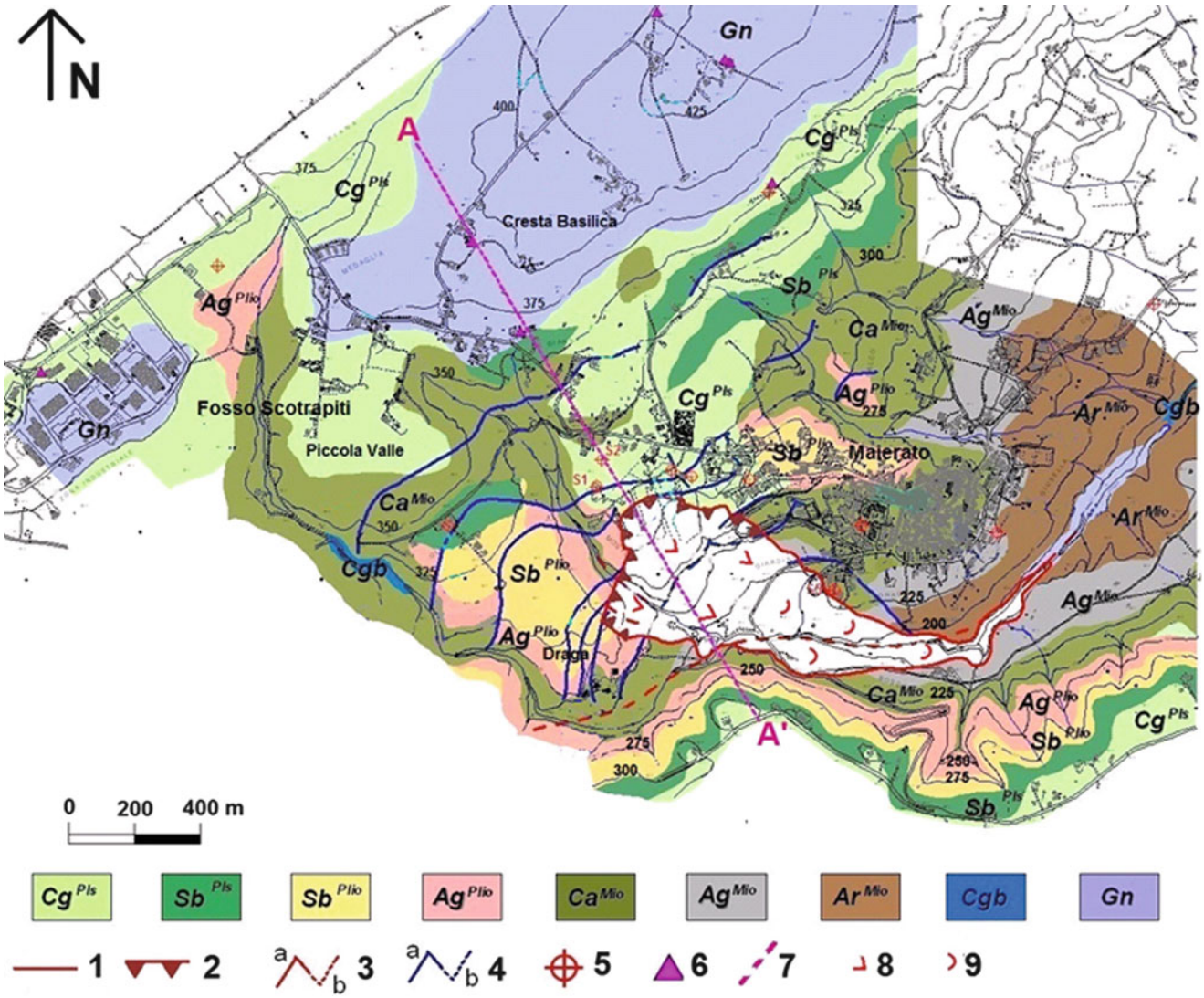

Fig. 3 Geological map. Legend: (Cg^{Pls}) continental conglomerates (Pleistocene), (Sb^{Pls}) continental sands (Pleistocene), (Sb^{Plio}) clayey sands with macrofossils and (Ag^{Plio}) clays (middle Pliocene), (Ca^{Mio}) evaporitic limestone (upper Miocene), (Ag^{Mio}) clays (late Miocene), (Ar^{Mio}) sandstone and sandy clays (middle-late Miocene), (Cgb) conglomerates (middle-late Miocene), (Gn) crystalline metamorphic bedrock (Paleozoic), (*1*) landslide area, (*2*) landslide main scarp, (*3*) faults (a = surveyed, b = supposed), (*4*) sliding surfaces (a = surveyed, b = supposed), (*5*) drillings and piezometers, (*6*) wells, (*7*) A-A′ cross-section trace, (*8*) sliding, (*9*) flow

has produced small dislocations in the sedimentary formations and results in increased thicknesses of some units in some areas (Fig. 3).

As far as the hydrogeological setting is concerned, a deep aquifer, within the metamorphic bedrock, has been utilised to supply the waterworks of Maierato. This aquifer is recharged by rainfall infiltration on the Cresta Basilica Plateau. It has a main flow direction from Northwest to Southeast and it is locally under pressure with an artesian head of around 15 m. This aquifer supplies aquifers within the Miocene sandstone and evaporitic limestone, which subsequently supply springs (Fig. 3). The presence of springs and green vegetation was a prominent feature of the area affected by the 15 February 2010 landslide and demonstrates that the area of the landslide was one with prominent groundwater discharges.

Slope Stability Back-Analysis

Geotechnical Characterization

In the landslide area eight investigation boreholes were drilled (Fig. 3), and piezometric monitoring installed. In situ permeability tests were undertaken in the boreholes and samples were taken for geotechnical characterization.

The data from the boreholes: (1) confirmed the stratigraphic succession previously described (Fig. 3); (2) allowed evaluation of the units thickness; (3) provided information on bedrock depth; (4) identified aquifer layers and allowed the measurement of groundwater levels; and (5) provided information on the weathering and degree of fracturing in the rock mass.

Lefranc tests in the boreholes gave, for the evaporitic limestone, a permeability ranging from 3E−8 to 4E−7 m/s, whereas for the Miocene sandstone an average permeability of around 5E−8 m/s.

Finally, shear tests and triaxial tests were carried out on limestone and sandstone samples. The laboratory results emphasized the very poor mechanical properties of the material involved in the landslide. For the limestone a cohesion of 10 kPa was obtained, with an average friction angle of 33° and very low Young's Modulus (between 6 and 24 MPa). For the Miocene sandstone a friction angle of 37° (with zero cohesion) was observed with Young's Modulus between 70 and 175 MPa.

Landslide Triggering Factors

The main preconditioning factor of the Maireto landslide is the presence of weak, permeable rocks (the evaporitic limestone and the Miocene sandstone), alternating in a stratigraphic succession with impermeable rocks (i.e. Miocene and Pliocene clays).

The instability was possibly initiated by increases in the pore-water pressure due to the rising groundwater levels from the heavy rainfall and prolonged rainfall which characterized the season and, in particular, the month preceding the landslide (Felice et al. 2010). The rainfall recharged both the deep and the shallow aquifers, generating additional pore-water pressures in the aquifer layers, especially within the Miocene sandstone.

Finite-element Modelling

For slope stability a back stress–strain analyse was conducted using a 2D Finite Element Method MIDAS/GTS (2010) to calculate the factor-of-safety with the Shear Strength Reduction Method (Dawson et al. 1999). The analysis was conducted along the cross-section A-A′ (Fig. 4), with geotechnical parameterization utilizing the results of laboratory tests (Table 1).

The following initial boundary conditions were considered: (1) null horizontal displacements along the vertical boundaries of the domain; (2) null displacements both horizontal and vertical along the domain bottom; (3) initial stress conditions dependant on the self-weight and groundwater pore-pressure. For the numerical analysis, the domain was divided using a quadratic mesh having elements of minimum dimension of 1 m in the most interesting zone and maximum dimension of 10 m at the domain border.

The modeling was carried out using different groundwater levels, in order to identify the groundwater conditions that triggered the instability. The results showed that in dry conditions the slope is stable with a safety factor Fs greater than three and with a very localized rupture within the Evaporitic Limestone (Fig. 5a).

The sensitivity analysis carried out on friction angles showed that the slope stability is more affected by the friction angle of the Miocene Sandstone than by the Evaporitic Limestone one (Fig. 6). The presence of groundwater flow obviously decreases the slope stability. However, using the observed water table levels, the factor-of-safety decreases by 20 %. A further decrease of about 20 % is reached considering a rise in the water table level of 10–15 m in the head-scarp area. Nevertheless, in these pessimistic groundwater conditions, the limit equilibrium of slope stability ($F_s = 1$) can be reached only by considering a great decrease in the friction angle of the Miocene Sandstone. In particular, the numerical modeling showed that the instability is reached when there is a decrease in the friction angle of the Miocene Sandstone by 50–60 % (compared to the friction angles obtained in laboratory tests).

The kinematics of the instability event is a roto-translational slide localized along the contact between the Miocene Sandstone and the metamorphic bedrock. If the friction angle of the Evaporitic Limestone is also reduced (in the order of about 50 % of the friction angle observed in the laboratory tests) the modeling showed another surface of rupture at the contact between the Limestone and the Miocene clays (Fig. 5b). As a consequence an instability mechanism involving the liquefaction of the Miocene sandstones can be hypothesized, also explaining the flow-like kinematics observed in the videos of the event.

Landslide Susceptibility Mapping

Based on the slope stability analysis results, in order to assess the landslide susceptibility in the whole urban area of Maierato, the following main controlling factors (in addition to surface geology and slope dip) were mapped:

- The presence of weak rocks (i.e. Miocene sandstones) and their thickness;
- The main groundwater flow paths.

The first one is the main geological predisposing factor and it was analysed on the basis of the geological survey and stratigraphical data obtained from drillings. Then, once the geological conceptual model was reconstructed, the areas characterised by the presence of Miocenee sandstones were identified and mapped, considering different thickness (higher and lower than 5 m, Fig. 7).

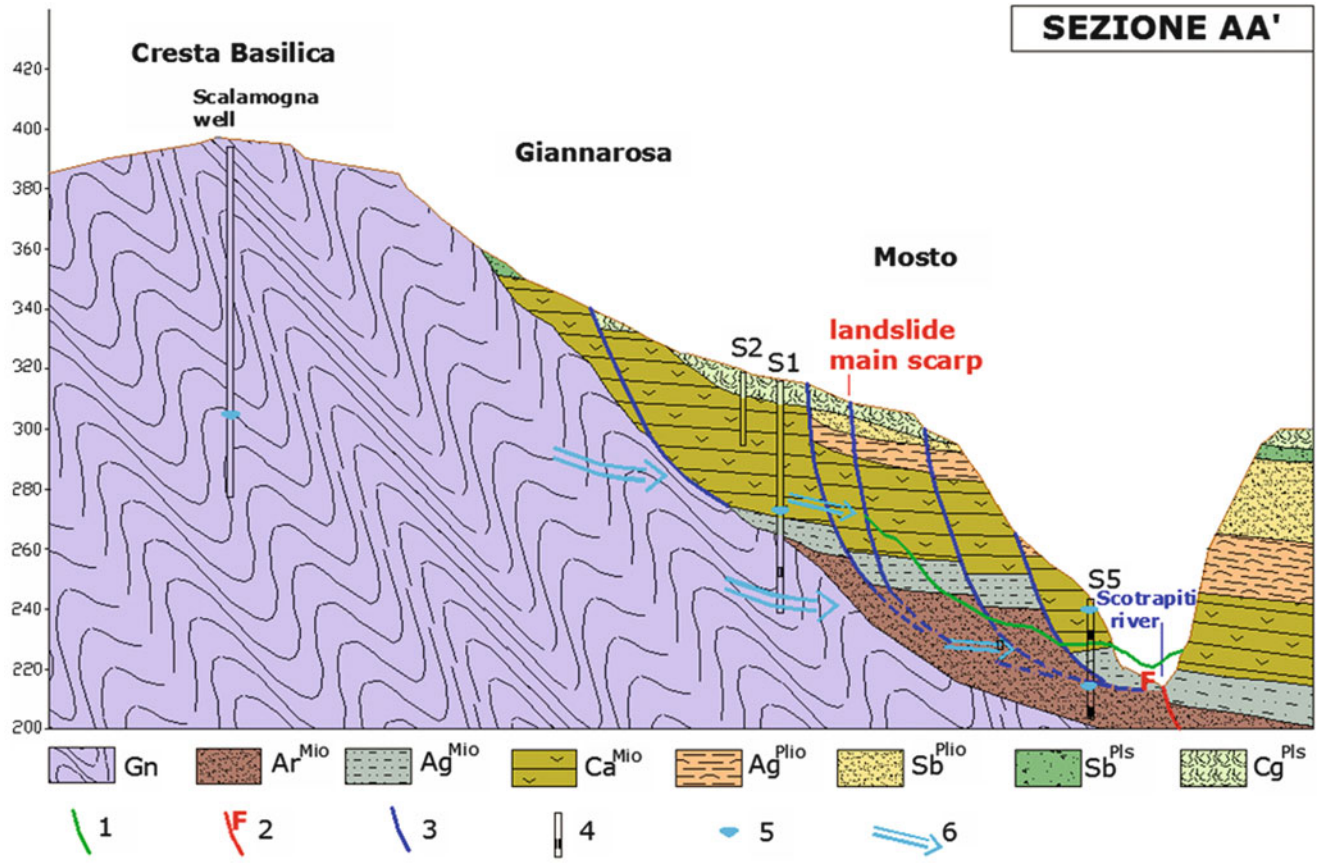

Fig. 4 Geological cross-section before the landslide. Legend: (*Gn*) crystalline metamorphic bedrock (Paleozoic), (Ar^{Mio}) sandstone and sandy clays (middle-late Miocene), (Ag^{Mio}) clays (late Miocene), (Ca^{Mio}) evaporitic limestone (upper Miocene), (Ag^{Plio}) clays (middle Pliocene), (Sb^{Plio}) clayey sands (middle Pliocene), (Sb^{Pls}) continental sands (Pleistocene), (Cg^{Pls}) continental conglomerates (Pleistocene), (*1*) actual topographic surface, (*2*) faults, (*3*) sliding surfaces, (*4*) piezometers with their filters, (*5*) post-landslide water table, (*6*) groundwater flow direction

Table 1 Geotechnical parameters used in the stress–strain analysis, with reference to a Mohr-Coulomb constitutive model (see Fig. 3 for a key to the formation symbols)

	Gn	Ar^{Mio}	Ag^{Mio}	Ca^{Mio}	Ag^{Plio}	Sb^{Plio}	Cg-Sb^{Pls}
Dry specific weight (kN/m^3)	28.5	19.44	22.95	21.06	16.2	21.6	17.55
Satured specific weight (kN/m^3)	29	22.2	24.4	23.2	20.1	23.6	21.0
Friction angle (°)	37	37	28	33	26	35	30
Cohesion (kPa)	0	0	20	10	15	0	0
Young's modulus (MPa)	2,000	70	200	10	100	1,000	600
Poisson's modulus	0.3	0.3	0.3	0.3	0.3	0.3	0.3
Hydraulic conductivity (m/s)	1E−8	5E−8	1E−9	1E−7	2E−9	1E−6	1E−5

Afterward, the hydrogeological triggering factor was analysed through in situ survey of piezometrical levels and springs location; also, in all springs, wells and piezometers) measures of pH, temperature and electric conductivity were carried out, allowing the identification of the main groundwater flow paths (Fig. 7).

Coupling the geological predisposing factor and the hydrogeological triggering one, the landslide susceptibility map of the whole urban area of Maierato has been drawn. Obviously, for the susceptibility mapping also other more general factors have been considered, i.e. the slope dip. The so obtained map (Fig. 8) shows that the hazard interests all the urban zone, involving large areas.

Risk Mitigation Actions

The dimension and the typology of the landslide interesting Maierato don't allow the realization of only structural works to actively prevent the landslide risk. Also, the economic

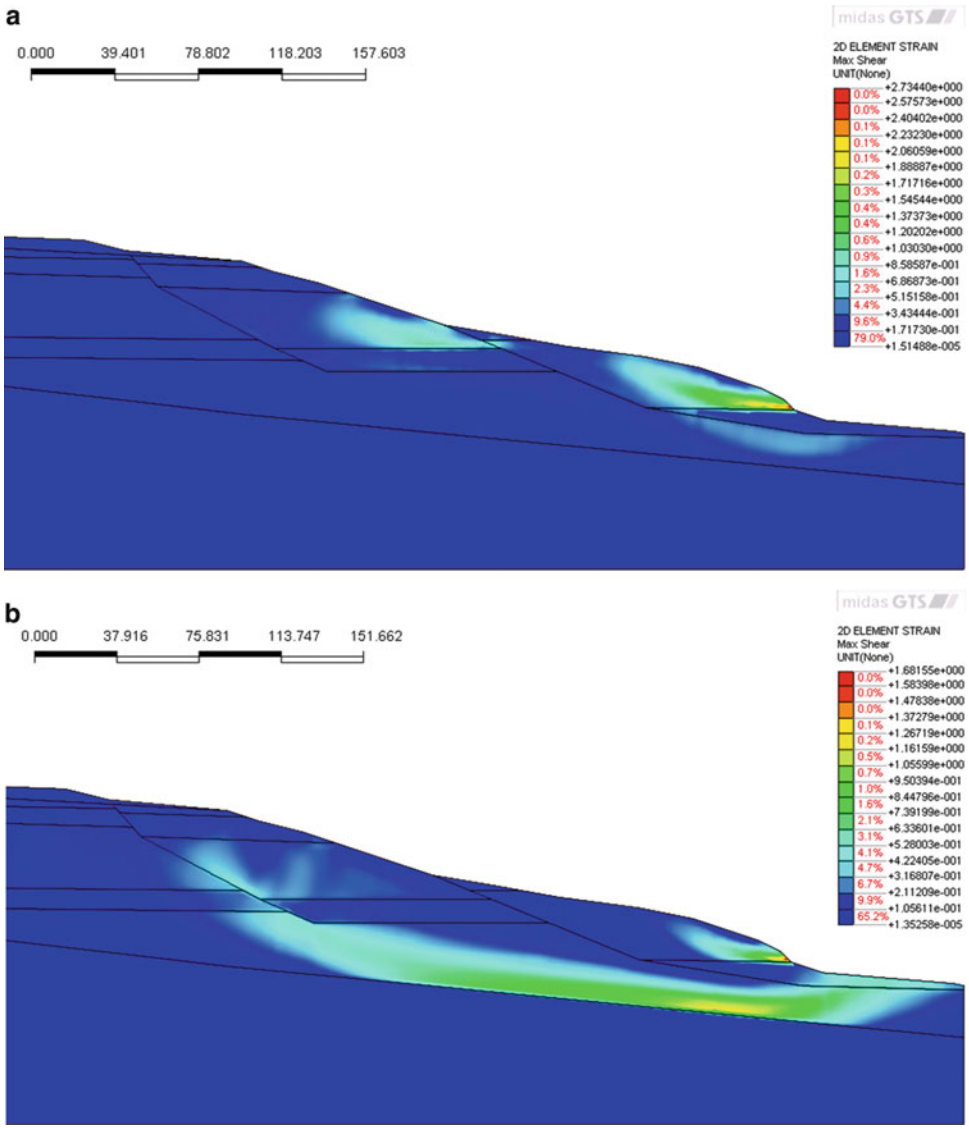

Fig. 5 Max shear increments obtained by the finite element modelling: (**a**) for the geotechnical parameters listed in Table 1 and in dry condition ($F_s = 3.36$); (**b**) considering very low values of the friction angles of both the Miocene Sandstone and the Evaporitic Limestone and the most pessimist groundwater condition ($F_s = 0.99$)

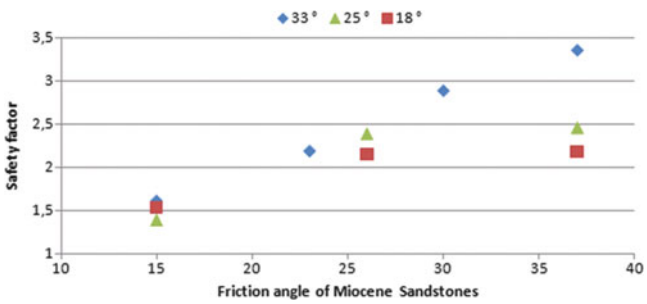

Fig. 6 Safety factor values obtained through finite element modelling (in dry conditions) versus the friction angle of the Miocene Sandstone for different values of the friction angle of the Evaporitic Limestone

situation cannot guarantee with only structural works an effective reduction of the geological risk. Therefore, in addition to structural works (mainly drainage works), a monitoring system has to be considered essential for risk mitigation.

Structural Works

The previously described study allowed to identify groundwater as the main triggering cause of the landslide. As a consequence, drainage is the most important structural works. As the economical conditions doesn't allow the

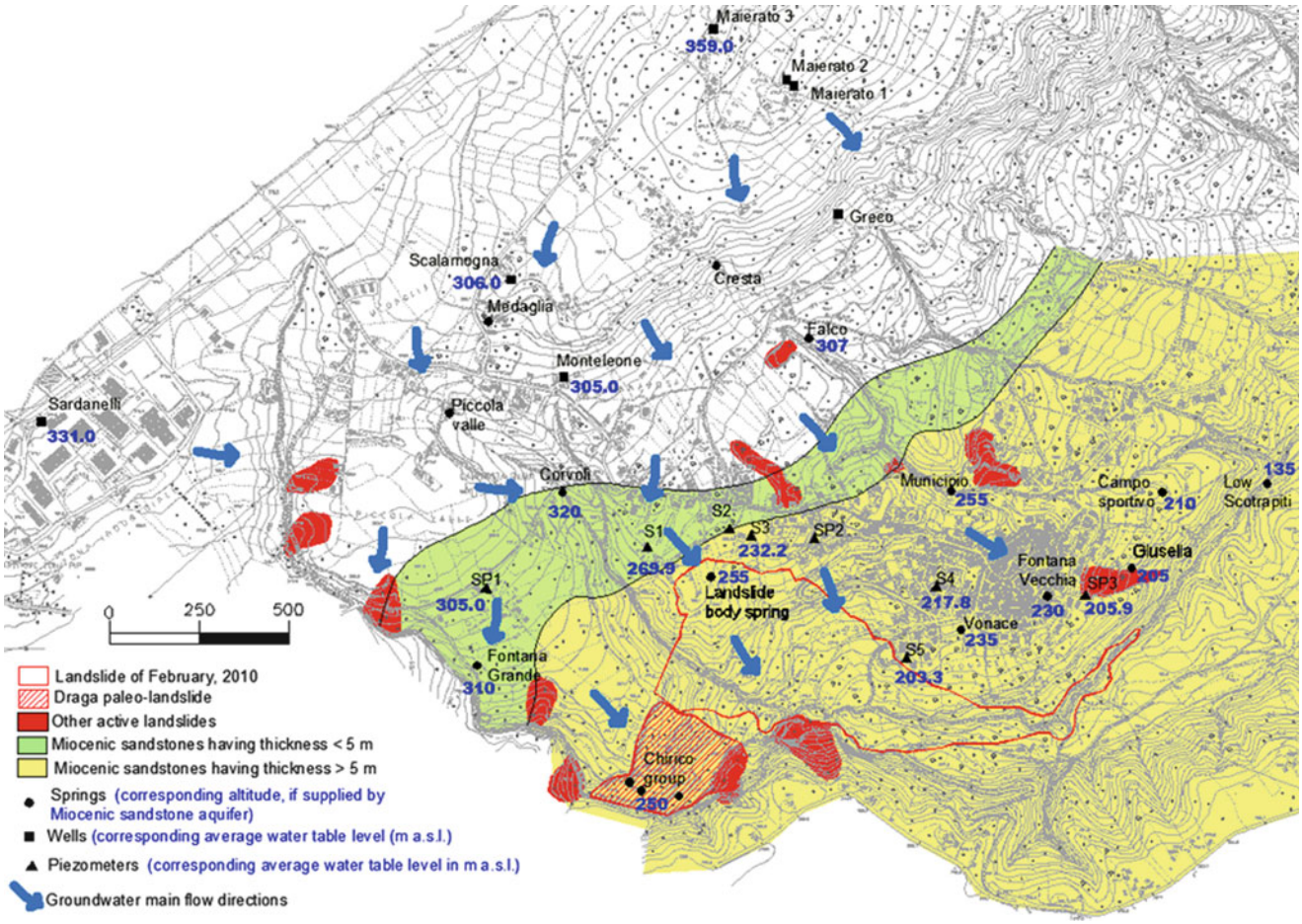

Fig. 7 Map with the main factors controlling landslide susceptibility

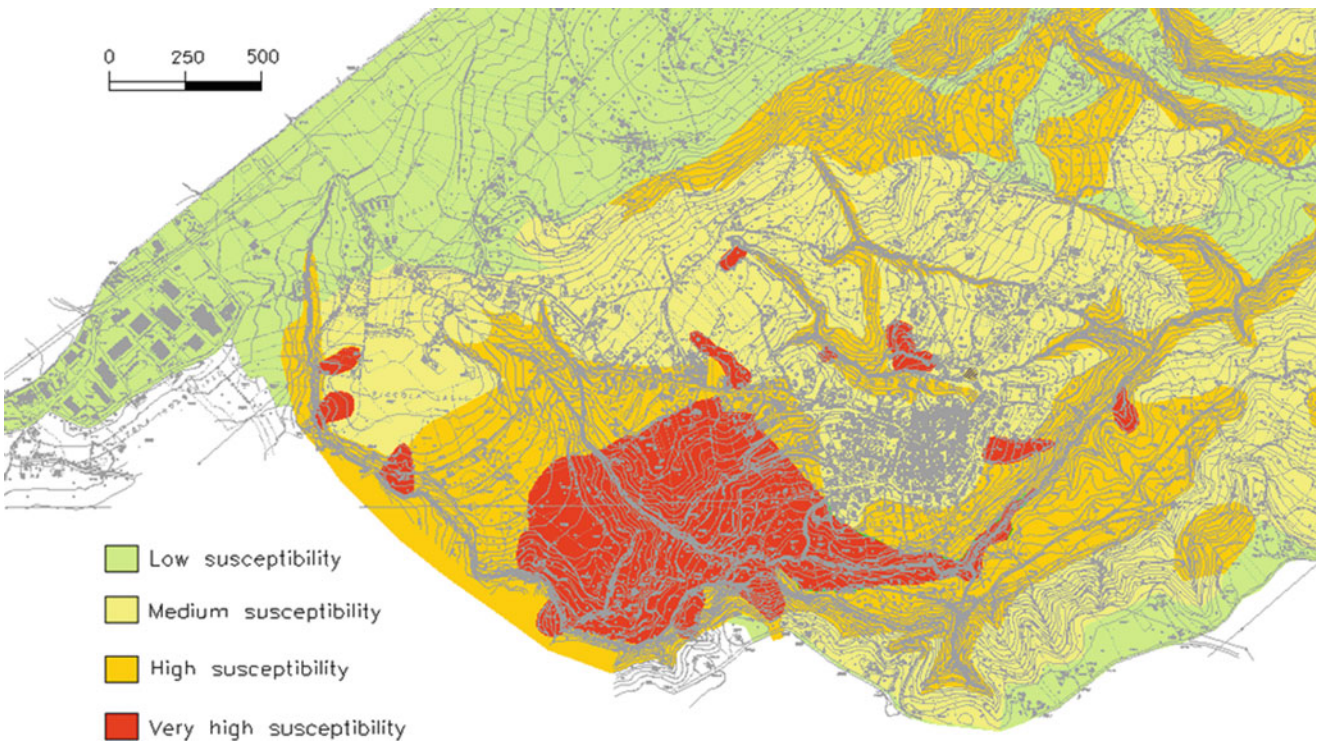

Fig. 8 Landslide susceptibility map of Maierato

realization of big works (i.e. drainage tunnels or structural wells), more economic solutions were considered as sub-horizontal tubular drains and hydraulic barrier wells. In particular, a pilot project consisting of ten tubular drains, a trench and a well was pointed in emergency for preventing the backward of the main scarp. The estimated cost is about 300,000 Euro.

Not Structural Works

A monitoring system was designed, including:
- Surface displacements monitoring through terrain radar interferometer for all the urban area;
- In depth displacements monitoring within the inclinometer tubes already present, coupled with piezometrical monitoring.

The expected cost for the first years of monitoring is about 100,000 Euro, and it will allow in the following years an effective risk mitigation through the activation of civil protection plans.

Conclusions

The Maierato landslide, pre-conditioned for failure by the intrinsic geological weaknesses in the area, was triggered by increased in groundwater flows in the evaporitic limestone and Miocenic sandstone where the aquifers are locally under pressure. The increased groundwater flows were a consequence of the heavy and prolonged rainfall in the Calabrian Region in the period from August 2009 to February 2010.

The presence in the area of larger, older landslides, and the possibility of further retrogression of the head-scarp requires installation of both a monitoring system and a drainage network. The monitoring system needs to capture surface and subsurface displacements and groundwater levels. Data from the monitoring will allow better definition of the landslide conceptual model. A back-analysis on the February 2010 slope failure mechanism using numerical modeling was carried out to quantitatively determine the influence of the various factors that contributed to the failure Afterward, on the basis of the controlling factors distribution a landslide susceptibility map has been produced and the relevant risk mitigation actions has been projected. Actually, the worry for a new backing of the main scarp and for the development of new ruptures brings about the necessity to install, in addition to a draining system, a monitoring system both for the surface and in depth displacements and for the groundwater levels. Data and information arising from the monitoring will allow to define the displacement values and the pluviometrical/piezometrical thresholds useful in an alarm system.

Acknowledgments We thank the Maierato Municipality for providing assistance during fieldwork and Dr. Silvestri for logistical support.

References

Cassa per il Mezzogiorno (1968) Carta Geologica della Calabria scala 1:25.000. Foglio 241 – Settore III SE – Vibo Valentia. Poligrafica & Cartevalori Ercolano (Na)

Dawson EM, Roth WH, Drescher A (1999) Slope stability analysis by strength reduction. Géotechnique 49(6):835–840

Felice E, Cundari L, Lepera G (2010) Frana di Maierato. Analizzate le cause pluvio. ARPACAL Report, Anno I Numero III del 22 maggio 2010

Guerricchio A, Fortunato G, Guglielmo EA, Ponte M, Simeone V (2010) Condizionamenti idrologici da DGPV nell'attivazione della grande frana di Maierato (VV) del 2010. Preeceding of the conference Tecniche per la difesa dall'inquinamento. Nuova Editoriale Bios

MIDAS/GTS (2010) MIDAS/GTS, 2010 – User's guide

Van Dijk J, Okkes M (1991) Neogene tectonostratigraphics and kinematics of Calabria arc basin: implications for the geodynamics of the central Mediterranean. Tectonophysics 196:23–60

Multidisciplinary Study of the Torrio Landslide (Northern Apennines, Italy)

Giulio Masetti, Giuseppe Ottria, Franco Ghiselli, Aldo Ambrogio, Gianluca Rossi, and Lanfranco Zanolini

Abstract

The multidisciplinary approach (geological and geomorphological studies, structural analysis, geoelectrical and seismic surveys, borehole data) utilized in this research allowed the definition of a reliable geological model of the Torrio landslide, one of the largest mass movements of the whole Northern Apennines occurring in the Aveto valley (Emilia-Romagna Region) and that determined the inclusion of the Torrio old villages in the "List of inhabited centres to be transferred". The results indicate that the Torrio mega-landslide is actually composed by three superposed main landslide bodies characterized by different genetic mechanisms, timing of emplacement and state of activity, but all showing deep sliding surfaces (from 30–40 m up to 250 m). This study represents a considerable improvement for the objective of achieving the landslide risk assessment mapping of the territory surrounding the Torrio inhabited centre, according to the Emilia-Romagna Region legislation.

Keywords

Geological structure • Geomorphology • Geophysical methods • Composite mega-landslide • Northern Apennines • Italy

Introduction

Since 1993 the Emilia-Romagna Region has introduced a specific legislation, modified in 2004 (Regional Law No. 7/2004), that identifies in landslide hazard and risk assessment mapping a key instrument for planning the correct land use in the territories of inhabited centres affected by landslides.

One of these centres is Torrio (Emilia-Romagna Region, Ferriere Municipality) which is affected by one of the largest mass movements of the whole Northern Apennines, involving an area of about 3 km^2. Despite being historically known since 1600, the Torrio landslide is little studied, so much so that it is generally reported as a single landslide (e.g. Atlas of unstable inhabited centres of Emilia-Romagna; Malaguti and Zampiga 1993) and as a single active complex landslide is also recorded in the 2010 last update of the Landslide Inventory of the Emilia-Romagna Region (www.regione.emilia-romagna.it/wcm/geologia/canali/cartografia/sito_cartografia/web_gis_dissesto).

G. Masetti
CNR, Institute of Geosciences and Earth Resources, Via Moruzzi 1, Pisa, Italy

G. Ottria (✉)
CNR, Institute of Geosciences and Earth Resources, Via S. Maria 53, Pisa, Italy
e-mail: ottria@dst.unipi.it

F. Ghiselli
Servizio Difesa del Suolo, della Costa e Bonifica, Regione Emilia-Romagna, Via della Fiera 8, Bologna, Italy

A. Ambrogio
GEOINVEST s.r.l., Via della Conciliazione 45/a, Piacenza, Italy

G. Rossi • L. Zanolini
Servizio Tecnico dei Bacini degli affluenti del Po, Regione Emilia-Romagna, Via Santa Franca 38, Piacenza, Italy

C. Margottini et al. (eds.), *Landslide Science and Practice*, Vol. 1,
DOI 10.1007/978-3-642-31325-7_23,

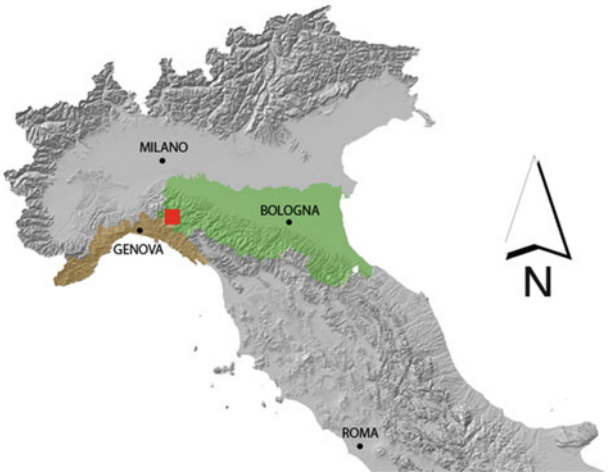

Fig. 1 Location of the study area

The Torrio landslide damaged villages and roads several times and it is still active even if with slow movements. Since 1922, the Torrio old villages were included in the "List of inhabited centres to be transferred" according to the Italian National Law No. 445/1908 which is still in force. In 1975 the Torrio new village was included in the "List of inhabited centres to be consolidated" according to the same Law No. 445/1908.

In this contribution we present the results of a multi disciplinary study targeted to the definition of the overall geometry of the Torrio landslide and its genetic mechanisms. In particular, data from geological and geomorphological surveys, brittle structure analysis and multitemporal aerial photo interpretation, have been integrated with the results of two different geophysical methods, the electrical resistivity tomography and the seismic refraction.

The Torrio landslide develops in the northeastern sector of the Emilia-Romagna Region, at the boundary with the Liguria Region, on the right side of the Aveto valley (Fig. 1).

Geological Setting

The Torrio area belongs to a sector of particular interest for the geology of the Northern Apennines: the Bobbio tectonic window (Elter et al. 1997 and references therein). In this tectonic window, the structural stacking of the belt is displayed completely, from the deepest Trebbia Unit, which represents the Tuscan foredeep units, to the Subligurian Units and the External Ligurian Units, derived from the transitional paleogeographic domains between the Ligurian oceanic basin and the Tuscan continental domain. The Subligurian Units and the External Ligurian Units characterize the upper part of the nappe pile and particularly the External Ligurian Units are the substrate of the thrust-top basin deposits forming the Epiligurian Succession. In the Torrio area the outcropping units are exclusively the Aveto Unit, belonging to the Subligurian Units, and the Vico and Helminthoid Flysch units which represent the External Ligurian Units. The deformation structure of the Aveto Unit is characterized by a tectonic stacking of thrust sheets folded by upright anticline/syncline systems divided by high angle thrusts. This stacking is cut by the low angle basal overthrust of the Vico Unit which locally shows a more inclined attitude as result of a subsequent deformation. The External Ligurian Units are characterized by an even more severe polyphase deformation developing overthrusts and isoclinal overturned mega-folds after again affected by folds and thrusts.

Regarding lithology, the Aveto Unit is mainly composed by sandstone turbidites (Aveto Fm.); the Vico Unit is formed by marly-calcareous turbidites (Vico Flysch; Eocene) with a lower member characterized by arenaceous-pelitic turbidites; the Helminthoid Flysch Unit is represented by the typical Campanian-Maastrichtian marly-calcareous turbidites overlying the basal complex made up of a thick ophiolite-bearing sedimentary melange (Casanova Complex).

The Torrio landslide involved all the outcropping geological units which show very different geomechanical properties. These characyeristics are extremely variable mainly in the Casanova Complex that comprises pelitic matrix-supported polymict breccias with very poor/poor rock quality and brecciated basalts with better quality.

According to the qualitative GSI classification, the polymict breccias have a range value from 15 to 25 while the brecciated basalts can be assigned to values ranging from 45 to 65 (Marinos and Hoek 2000; see also Brideau et al. 2009). The turbidites of Helminthoid and Vico flysch, characterized by the alternation of competent limestones with less competent lithologies (marls, siltstones, claystones), show intermediate geomechanical properties with GSI average values from 25 to 40 (see also Morales et al. 2004). The development of slope instabilities in these formations depends strongly on their structural setting, i.e. the orientation of discontinuities (bedding, faults, joints).

The Aveto Fm. is overall formed of thick-bedded sandstones showing good quality (GSI $>$ 50).

The geological study was integrated by a structural analysis of brittle structures (faults and joints) affecting the lithofacies of the Casanova complex outcropping at the detachment zone of the Torrio landslide and thus the measurement stations were located around the N-S ridge of the Mt. Ciapa Liscia. The elaboration of the collected data (total number about 100 with more than 60 faults) allows to identify three main discontinuity sets, respectively directed WNW-ESE (K1), NNW-SSE (K2), and NE-SW (K3), characterized by high angle (on average $>70°$) joints and strike-slip and normal faults.

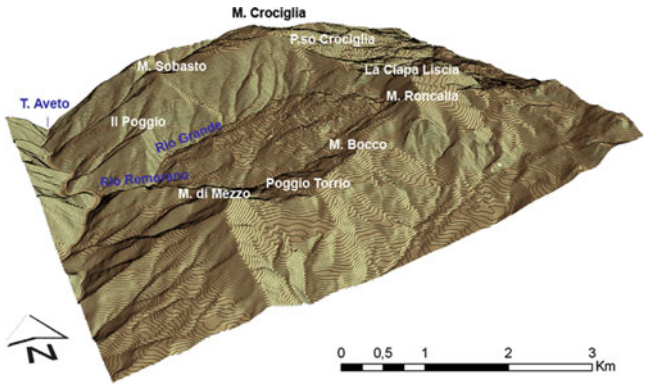

Fig. 2 Block diagram showing the position of the Torrio landslide on the right side of the Aveto valley

Geomorphology

The examined slope is bounded to the north and to the south respectively by Rio Grande and Rio Remorano valleys; downstream of the Torrio landslide toe, the Rio Grande stream flows into the Rio Remorano which is a right-hand tributary of the Aveto river (Fig. 2). The hydrographic basin of the Torrio valley is bounded northward by the southern sides of Mt. Crociglia and Mt. Sobasto and southward by the northern sides of Mt. Bocco and Mt. di Mezzo. The valley-head is represented by the ophiolitic ridge of the Mt. Ciapa Liscia (1,682 m asl) being part of the main drainage divide between Aveto and Nure valleys. The Torrio slope has high relief energy ranging in elevation between 620 m and 1,682 m asl (Mt. Ciapa Liscia) with a maximum elevation difference of 1,062 m.

The main geomorphological features of the Torrio area, derived from the field surveys carried out at 1:5.000 scale as well as from the analysis of the aerial photos, are reported in the geological-geomorphological scheme of Fig. 3. The study area is characterized by a great spreading of landslides and other slope gravitational movements which points to a complex evolution developed during the Late Pleistocene and Holocene in a context strongly influenced by the structural-geological setting and the neotectonic evolution.

Morphotectonic Setting

The watershed divides and more generally the uppermost portions of the slopes, including the highest peaks, show a smooth morphology, contrasting with the "young" morphology of the surrounding slopes and valleys. Likewise, several terraced debris accumulations, characterized by areas of low slope steepness delimited by slope breaks, lay in the middle portions of the slopes that limit N and S the Torrio landslide.

These morphological features suggest the occurrence of two major morphogenetic cycles (Perotti et al. 1988): the late evolution of the 1st morphogenetic cycle would have resulted in a "mature" morphology with the development of a sub-horizontal planation surface. This interpretation is supported by the recognition in this sector of Northern Apennines of a summital paleo-surface. Studies on geographical and height distribution of the highest peaks (Bernini et al. 1977; Brancucci and Motta 1989) indicate that in fact the relict surfaces likely represent residues of a single sub-horizontal surface, then incised by stream action during the 2nd morphogenetic cycle, which began in the Pleistocene with a phase of marked uplift which is still active.

The strong vertical incision of rivers, due to a renewal of erosion, created the conditions for landsliding, with both deep and superficial mechanisms (i.e. rock blocks slide and debris flow), as the main process that have affected the slope evolution. Paleo-landslides are widely represented; their crown zones have been affected by remodeling processes (also anthropogenic) and in many cases are no longer recognizable. Often the current landsliding refers to the reactivation of old landslide deposits already stabilized.

Among other aspects that are more directly related to morphotectonic rejuvenation, the deepening of watercourses and the general lack of current alluvial deposits are clear signs of a strong erosive phase which is still active.

Geophysical Surveys

With the principal aim being to provide additional constraints about the landslide geometry, a geophysical survey was performed applying two different methods: electrical resistivity tomography and seismic refraction. These methods have been pointed out in order to investigate the lateral continuity of the stratigraphic units allowing the management of information mainly regarding the thickness of the sliding material.

The location of the geophysical profiles is given in Fig. 3.

Electrical Resistivity Tomography

The electrical resistivity tomography (ERT) is an active geoelectrical prospecting technique used to obtain 2D and 3D images of the subsurface electrical resistivity distribution. It was used to characterize and map the lithological units involved in the Torrio landslide along two main profiles oriented respectively transversal (E01; 725 m) and parallel (E02; 2,625 m) to the main landslide axis.

Data were recorded using a multielectrode basic system with 126 electrodes at 11 m spacing connected to an AGI SuperSting R1/IP resistivity meter for data acquisition and

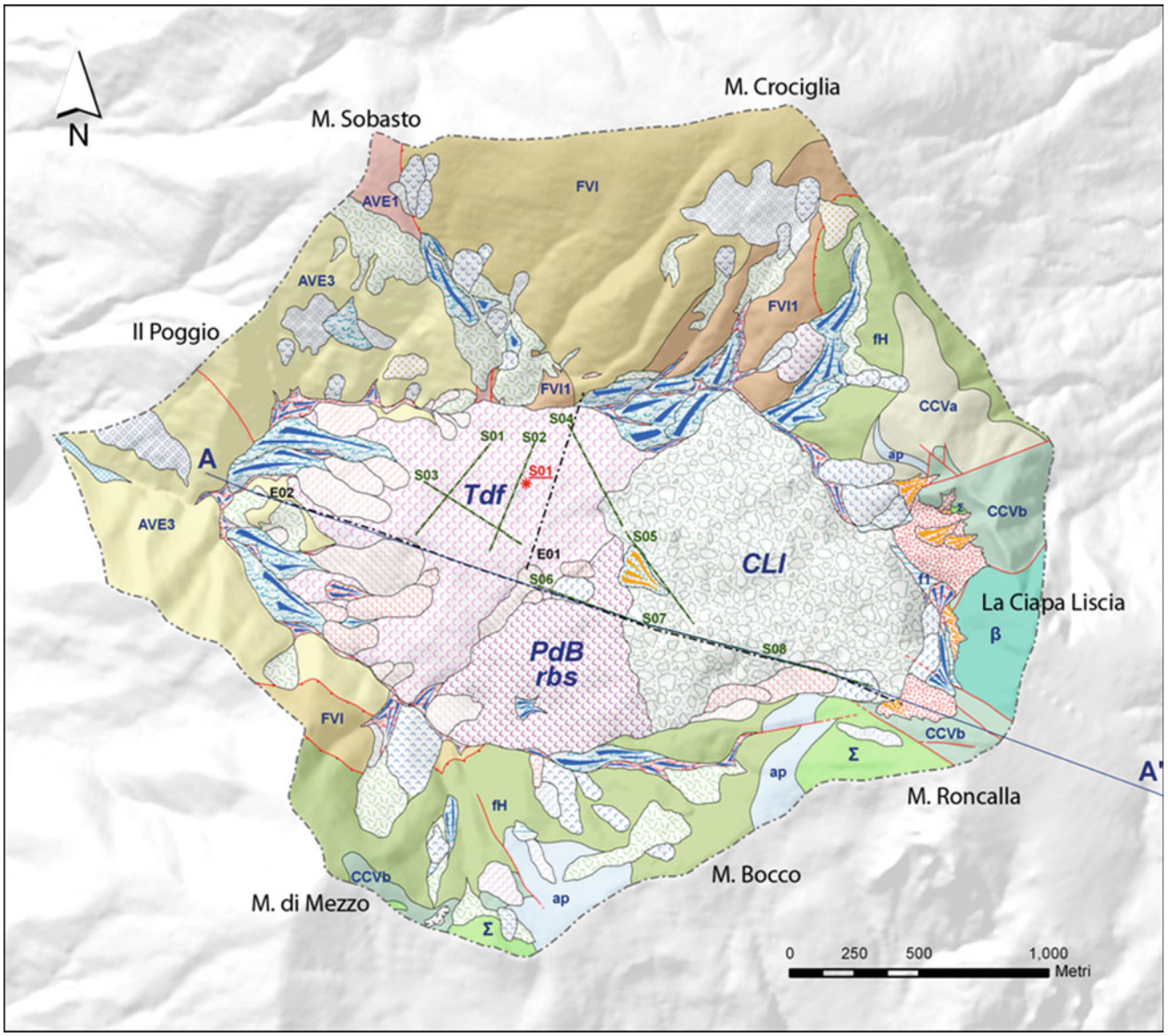

Fig. 3 Geological-geomorphological scheme of the Torrio landslide area. Aveto Fm.: pelitic-arenaceous member (*AVE1*), sandstone member (*AVE3*); Vico Flysch (*FVI*): pelitic-arenaceous member (*FVI1*); Helminthoid Flysch (*fH*); Casanova Complex: ophiolitic sandstones (*CCVa*), matrix-supported polymict breccias (*CCVb*), basaltic breccias (β), serpentinites (Σ), Palombini shale (*ap*). *Tdf* Torrio debris flows, *CLI* Ciapa Lisca landslide, *PdB* Pian di Bosco rock block slide. Location of drilled borehole (*S01*), geophysical profiles (S seismic refraction, E geoelectrical tomographies) and geological-geomorphological cross-section A-A′ is provided

the RES2DINV software (Loke and Barker 1996) for data inversion. The Schlumberger array with a maximum AB of 1,400 m allowed a penetration depth of more than 200 m.

The geoelectrical sections show the presence of three different types of resistivity units:

- Conductive units, characterized by resistivity values lower than 50 Ωm, related to mainly clay lithologies and/or to the presence of water-saturated debris deposits;
- Resistive units, characterized by resistivity values higher than 500 Ωm, that can be associate to calcareous or ophiolitic formations forming the bedrock not involved in the landslides or occurring as huge blocks inside the landslides;
- Intermediate units which can be related to transitional conditions where the resistivity values are generally function of clay content and degree of saturation of groundwater.

As most meaningful example, we describe the longest E02 profile (Fig. 4) that crosses longitudinally almost the entire Torrio landslide. In the east area (mountain sectors) it shows massive accumulations of landslide deposits consisting mostly of brecciated basalts and pillow basalts with high

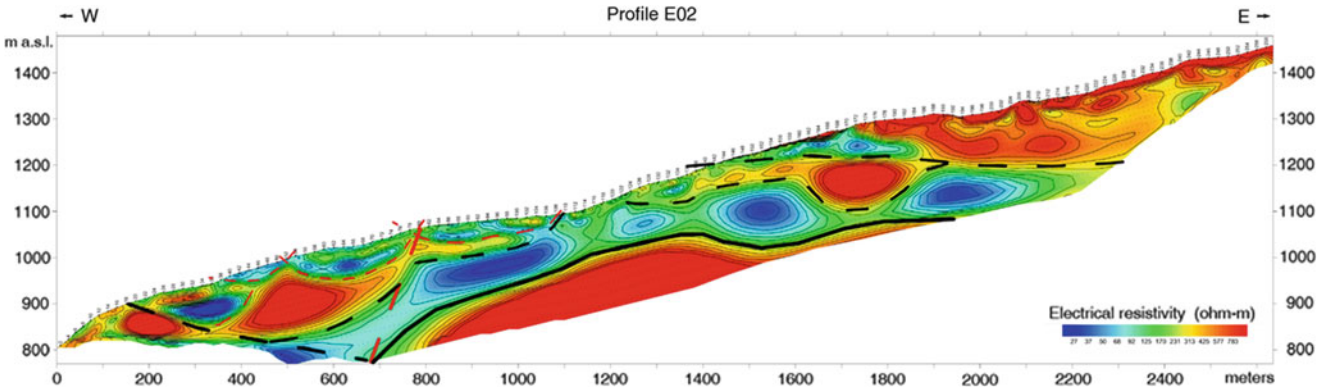

Fig. 4 Geoelectrical tomography section E02 (location on Fig. 3)

resistivity (red/orange/yellow areas), above a level with low resistivity (green/light blue/blue areas) which may indicate the presence of groundwater inside the sliding deposits. Further downstream the areas of highest resistivity can be interpreted as ophiolite and/or limestone rock blocks involved in the landslide and bounded by finest deposits soaked in water with a lower resistivity. In the central part of the profile, below the low resistivity areas, it is clear an area of high resistivity that can be referred to the bedrock, whose upper surface describes a gentle asymmetric antiform. The resistivity contrasts also allow to identify possible secondary landslides in the shallower portions of the main landslide that generally fit with the morphology and have been recognized as active or dormant landslides.

Seismic Refraction

The 2D surface refraction survey was performed along five profiles for a total length of about 4 km to integrate the resistivity survey and map the "bedrock" within the Torrio old villages and surrounding area.

A 24-channel seismograph was used for registration; geophone spacing was 20 m; the seismic source was generated by explosive charges. The survey was performed by forward and reverse intra-spread shots, including off-end shots outside the profiles.

The raw data were processed using both the GRM tecnique and the ray tracing tomography.

The results show two main reflectors; the lower one represents the top of the bedrock characterized by seismic velocities higher than 3.8–4.0 km/s while the upper reflector separates the upper debris deposits with velocities ranging between 1.2 and 2.2 km/s and the lower landslide body characterized by middle-high seismic velocities (2.6–3.4 km/s), directly overlying the bedrock.

The main seismic refraction section is the composite profile S06-S07-S08 (Fig. 5), which proceeds in the direction WNW-ESE covering in the southern sector of the Torrio landslide a length of about 1,400 m and corresponding to the upper part of the E02 geoelectrical profile. The limits between the seismic units roughly follows the trend of the morphology except in the range between the progressives of about 750 m and 1,100 m, where the boundaries are subhorizontal; the result is a gentle antiform-synform pair. In particular the depth of the bedrock varies from less than 80 m (progressive 540) to about 150 m (upstream sector) and 120 m (downstream sector). The thickness of the upper landslide deposits varies from about 15 m in the downstream sectors to about 40 m (upstream sector) with an area of thickening up to approximately 60 m at the progressive 1,050.

Results

The geological-geomorphological data supplemented with the results of the geophysical surveys allowed the elaboration of an integrated geological-geomorphological cross-section showing the new interpretation of the Torrio landslide which can be considered a composite mega-landslide corresponding to the superimposition of three major landslide bodies identifiable for different genetic mechanisms, emplacement time and state of activity (Figs. 3 and 6).

The "Ciapa Liscia landslide" characterizes the upper portion of the Torrio valley, while the "Torrio debris flows" are developed in the northwestern and lower part of the Torrio valley. The "Torrio debris flows" and the "Ciapa Liscia landslide", which are directly responsible for damages to the buildings of Torrio villages, are superimposed on the oldest landslide body, the "Pian di Bosco rock block slide", in the southern sector of the Torrio area.

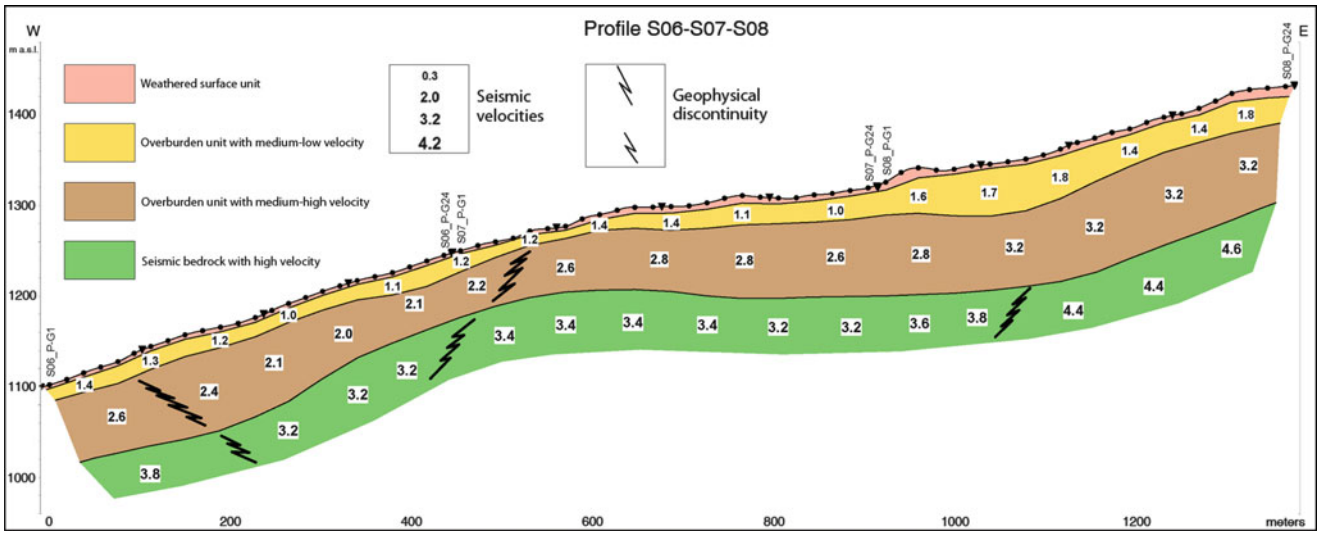

Fig. 5 Seismic refraction profile S06-S07-S08 (location on Fig. 3)

The "Pian di Bosco Rock Block Slide"

This landslide involved mainly the Helminthoid Flysch and is characterized by a sliding surface located at a depth of 120–130 m. This rock block slide, possibly developed during the Lateglacial age (Late Pleistocene-Holocene transition), represents an element of the landscape pre-existing the other two, more recent, Holocene landslides, of which it controlled the emplacement.

This morphological unit, maintaining a certain structural continuity, belongs to an old landslide body that would act as "shoulder" for the emplacement of the "Torrio debris flows" and that successively suffered strong river erosion resulting in morphological terraces and secondary landslides.

The "Torrio Debris Flows"

With this denomination we indicate a complex system of landslides that were subsequently terraced as a result of the neotectonic uplift. On the lower part of these debris flows the Torrio old villages were built and several times destroyed by multiple reactivation events.

The debris flows are made up of ophiolite, sandstone and limestone blocks, lithologies related to the Casanova Complex (CCV), Helminthoid Flysch (fH) and Vico Flysch (FVI), in an abundant clay matrix. They derived from the evolution of ancient landslides, affecting the northwest sector of the old valley-head that is now partly buried by the "Ciapa Liscia landslide". In particular, in the context of glacial and post-glacial climate, in the northwest old valley-head, in a more advanced position than the current one, the landslide deposits mainly due to sliding of marly-calcareous and sandstone formations, were involved in debris flows together with the thick debris accumulations derived from the polygenic breccias of the Casanova Complex.

The fluvial incision connected to the neotectonic uplift produced the terracing of these debris flows, marked by the pronounced slope break observed between 1,025 and 1,050 m that abruptly interrupts the gentlysurface. This slope break is partly withdrawn and attenuated by secondary landslides which involved the frontal part of the Torrio debris flows up to deeply affect the sandstone bedrock (Aveto Fm.) (Fig. 6).

Borehole Data

After the detailed geological-geomorphological and geophysical field investigations of the Torrio debris flows, a borehole (S01) was drilled slightly upstream the Torrio old villages (location on Fig. 3) during December 2009. The borehole was drilled up to the depth of 123 m and equipped with an inclinometer.

The deepest sliding surface has been directly checked at a depth of about 105 m, corresponding to the interface landslide/bedrock. The drilled bedrock is formed by lithologies referable to the Vico Flysch. The borehole stratigraphy indicates that the landslide body is characterized by the occurrence of huge (thickness of more meters) rock blocks mainly made up of limestones and siltstones from Vico and Helminthoid flysch, intercalated at various levels in the landslide deposits characterized by clay matrix. Groundwater was detected at 30 m below ground level.

The inclinometer data allow to define multiple sliding surfaces inside the landslide body (Fig. 7). Referring to a 13 month period of landslide monitoring, the displacement rates reach values of more than 8 cm/year along the shallower sliding surfaces above the 22 m of depth; at the deepest sliding surface the inclinometer was broken after 6/7 months (July/August 2010).

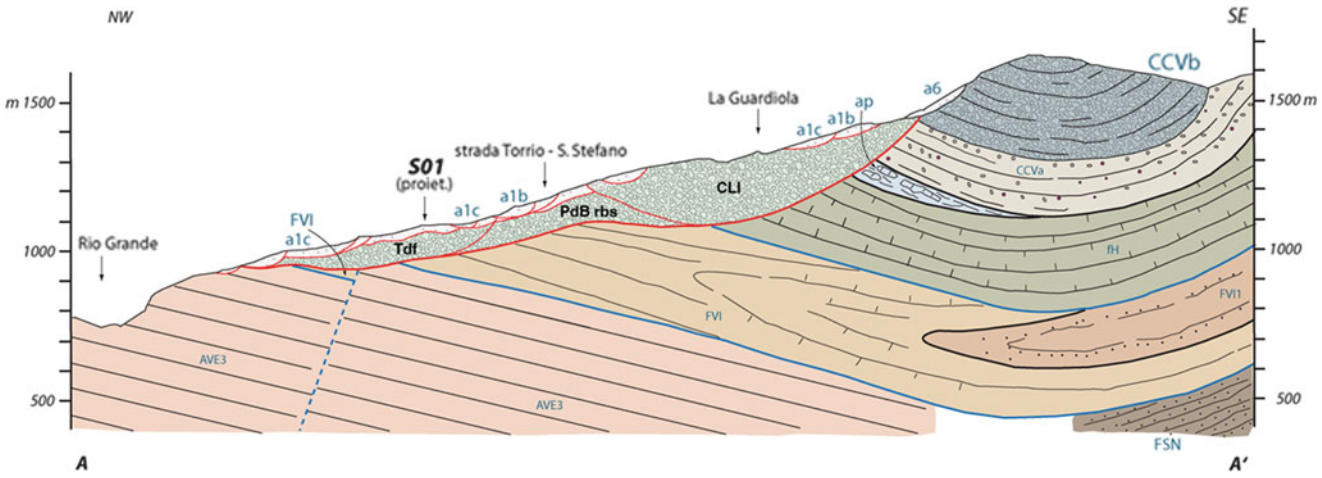

Fig. 6 Geological-geomorphological cross-section A-A′ (location on Fig. 3). Abbreviations as in Fig. 3

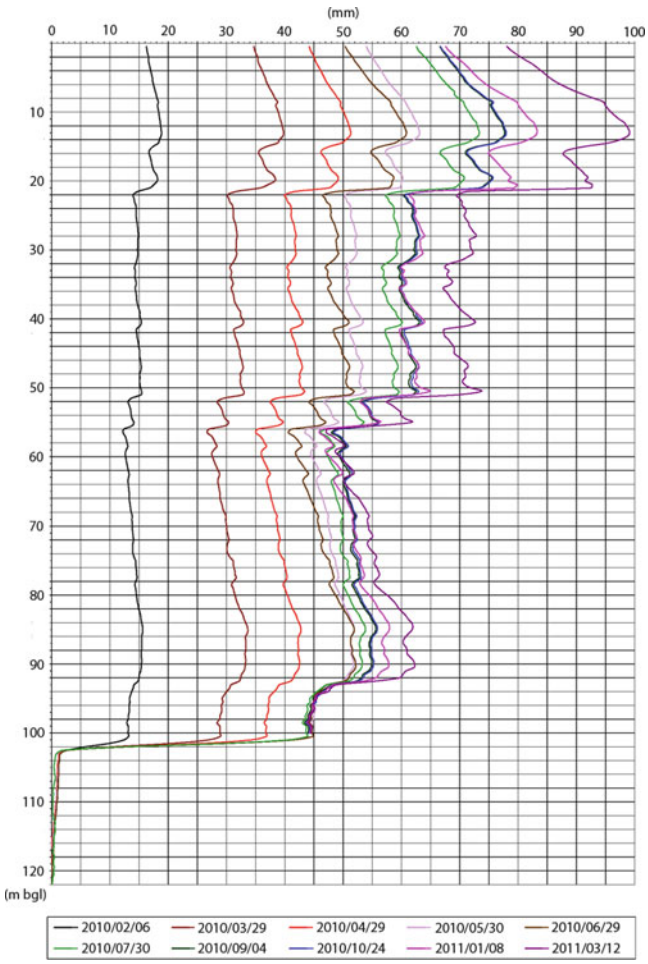

Fig. 7 Inclinometric measures from borehole S01

The "Ciapa Liscia Landslide"

This landslide, occurring in the upper portion of the study area, characterizes the entire Torrio valley. It consists of a huge pile of large blocks of basaltic pillows and breccias, whose origin is later than the Torrio debris flows and have caused their reactivation.

Behind the Ciapa Liscia landslide deposits stands the about 300 m high steep wall below the Mt. Ciapa Liscia, displaying massive basaltic breccias (β) and matrix-supported polymict breccias (CCVb). This wall represents the release area of the landslide and substantially coincides with the tectonic contact between the two lithologies.

A wide trench, partly filled by fine marsh deposits and talus cones, occurs between the release area and the deposit head.

Downstream from the trench area, the landslide body is developed for about 1,300 m with well defined morphological and textural characteristics: the upper part maintains a certain unity while, downstream, the ophiolitic blocks occur progressively more scattered and spaced from each other in a more and more abundant matrix consisting of small clasts derived from their disgregation.

The Ciapa Liscia landslide is partly superimposed on the pre-existing Torrio debris flows, which acted as "conveyor belt" of the blocks under the action of gravity and softening induced by the pressure of the ophiolitic masses.

According to the proposed kinematic model, the Ciapa Liscia landslide consists in a rotational sliding developed along a upward concave surface deriving from the integration of the W-dipping high angle fault between basaltic and polymict breccias and the lower E-dipping low angle tectonic contact between the Helminthoid Flysch and the underlying Vico Flysch. In the carried out geological-geomorphological cross-section the sliding surface reaches the maximum depth at about 250 m bgl (Fig. 6).

As the rear release was provided by the fault between basaltic and polymict breccias, the lateral release surfaces could have been provided by the faults respectively directed ENE-WSW (northern boundary) and WNW-ESE (southern

boundary) roughly corresponding to the K1 discontinuity set (Fig. 3). Therefore the Ciapa Liscia landslide was strongly influenced by brittle structures (strike-slip and normal faults) detected during field investigations and that reflect the regional tectonic pattern already reported by Perotti et al. (1988).

Conclusions

The kinematic and evolutionary model obtained from the multidisciplinary approach of this study indicates that the Torrio mega-landslide can no more be considered as an unitary phenomenon. Actually it is the result of the superposition of three major landslides ("Pian di Bosco rock block slide", "Torrio debris flows" and "Ciapa Liscia landslide") with different genetic and evolutionary mechanisms and especially characterized by a long evolution linked to the neotectonic uplift and also affected by periglacial climatic conditions.

This study confirms the integration of structural-geological-geomorphological analyses, mechanical drilling and geophysical surveys as the most suitable approach to obtain reliable geological models and global interpretations of composite and complex sliding areas.

A better definition of landsliding affecting Torrio area and villages is provided, representing the background for a correct landslide risk assessment mapping according to the Emilia-Romagna Region legislation. Moreover, it represents a contribution for updating the Landslide Inventory of the Emilia-Romagna Region territory.

Acknowledgments This research was carried out within an agreement between Emilia-Romagna Region (Direzione generale Ambiente, difesa del suolo e della costa) and CNR (Institute of Geosciences and Earth Resources). We would like to remember Francesco Baldacci, whose unpublished studies have given a fundamental contribution for achieving the presented results.

References

Bernini M, Clerici A, Papani G, Sgavetti M (1977) Analisi della distribuzione planoaltimetrica delle paleosuperfici nell'Appennino emiliano occidentale. Acta Naturalia de "l'Ateneo Parmense" 13(4):645–656

Brancucci G, Motta M (1989) Morfoneotettonica della Val Fontanabuona e delle aree limitrofe. Mem Acc Lunigianese di Scienze "G. Capellini" 57–58:101–122

Brideau MA, Yan M, Stead D (2009) The role of tectonic damage and brittle rock fracture in the development of large rock slope failures. Geomorphology 103:30–49

Elter P, Ghiselli F, Marroni M, Ottria G (1997) Note illustrative del Foglio 198 "Bobbio" della Carta Geologica d'Italia in scala 1:50.000. Istituto Poligrafico e Zecca dello Stato, Roma, 106p

Loke MH, Barker RD (1996) Rapid least-squares inversion of apparent resistivity pseudosections using a quasi-Newton method. Geophys Prospect 44:131–152

Malaguti C, Zampiga M (1993) Torrio. Sintesi delle conoscenze. In: Annovi A, Simoni G (eds) Atlante dei centri abitati instabili dell'Emilia-Romagna. Provincia di Piacenza. CNR-G.N.D.C.I., Regione Emilia-Romagna, pp 26–27

Marinos P, Hoek E (2000) GSI: a geologically friendly tool for rock mass strength estimation, GEOENG 2000, Melbourne, 19p

Morales T, Uribe-Etxebarria G, Uriarte JA, Fernandez de Valderrama I (2004) Geomechanical characterisation of rock masses in Alpine regions: the Basque Arc (Basque–Cantabrian basin, Northern Spain). Eng Geol 71:343–362

Perotti CR, Savazzi G, Vercesi PL (1988) Evoluzione morfotettonica recente della zona compresa tra la testata del T. Nure e la Val d'Aveto (Appennino piacentino). Suppl Geogr Fis Dinam Quat 1:121–140

Advance in the Mapping of the 1717 AD Triolet Rock Avalanche Deposit (Mont Blanc Massif, Italy) Using Cosmogenic Exposure Dating

Philip Deline, Naki Akçar, Susan Ivy-Ochs, Vasily Alfimov, Irka Hajdas, Peter W Kubik, Marcus Christl, and Christian Schlüchter

Abstract

The granitic deposit of the upper Val Ferret was shown in 1980 to result from a large September 1717 rock avalanche. A huge volume of rock and ice travelled onto the Triolet Glacier $>$ 7 km downvalley. Boulder accumulations and irregular ridges spread out over a distance of 2 km on the valley floor terminate with an arcuate front. A 2009 reconstruction with radiocarbon dating proposed a smaller lateral extension of the landslide on the valley floor preserving Lateglacial moraines, but cosmogenic exposure dating questions it. Consistency of ^{10}Be dates suggests that the deposit results from the 1717 rock avalanche, with a rock volume $> 10 \times 10^6$ m^3, and a likely similar ice volume. The importance of rock avalanches has to be emphasised to help to prevent risk in inhabitated valleys. Even for the recent period, the contribution of cosmogenic exposure dating to geomorphological analysis of complex landform assemblages is valuable.

Keywords

Rock avalanche • Natural hazard • Surface exposure dating • Western Alps • Mont Blanc massif

Introduction

In inhabited mountain valleys, rock avalanching, i.e. the extremely rapid flow movement of fragmenting rock particles, represents a potential high risk for growing infrastructure and people living in high mountain areas. This hazardous process is due to steep slopes, high relief, intensive rock fracturing, seismicity, paraglacial control, periglacial climatic conditions and the presence and interaction of snow, glaciers, and permafrost. The timing of rock avalanche recurrence intervals is essential and can be determined by surface exposure dating of head scarps, sliding planes, or large boulders of the deposits. Despite potential complications, several landslides have been exposure dated in various mountain areas (e.g. Hermanns et al. 2004; Prager et al. 2009) with cosmogenic nuclides (Ivy-Ochs and Schaller 2010 and references therein).

Several rock avalanches occurred in the Mont Blanc massif (western European Alps) in the late Holocene (Deline 2009), especially on its south-east, Italian side (Fig. 1). Scientists have debated for a long time on the extension of the deposit in the upper Ferret Valley that records a rock avalanche which occurred on the night of September 12th 1717 AD (Deline and Kirkbride 2009). Surface exposure dating with in-situ cosmogenic ^{10}Be provides new information about this deposit extension.

P. Deline (✉)
EDYTEM Lab, Université de Savoie, CNRS, Le Bourget-du-Lac 73376, France
e-mail: pdeli@univ-savoie.fr

N. Akçar • C. Schlüchter
Institute of Geological Sciences, University of Bern, Bern 3012, Switzerland

S. Ivy-Ochs • V. Alfimov • I. Hajdas • P.W. Kubik • M. Christl
Institute of Particle Physics, ETH Hönggerberg, Zürich 8093, Switzerland

C. Margottini et al. (eds.), *Landslide Science and Practice*, Vol. 1,
DOI 10.1007/978-3-642-31325-7_24,

Fig. 1 Italian Val Ferret, on the south-east side of the Mont Blanc massif. Strong contrast between the steep crystaline side on the left, affected by several rock avalanches during the Holocene as shown by their deposits on the valley floor, and the metasedimentary gentle side on the right. The Triolet studied deposit is located on the floor of the upper end of the Val Ferret valley, in the background

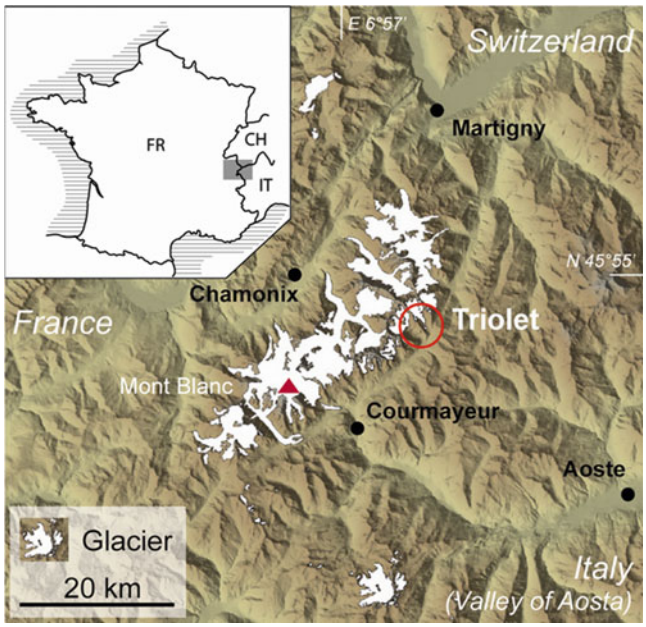

Fig. 2 Location map of the Mont Blanc massif. The studied area is shown by the *red circle*

Studied Area

The Mont Blanc massif has an area of about 550 km^2, 40 % of which is glacierized (Fig. 2). Its highest point is 4,810 m a.s.l., and many of its fractured granite faces, peaks and crests stand well above 3,000 m. The drainage divide between Rhône and Pô rivers forms a 35 km long crest line which is continuously above 3,300 m a.s.l. High elevation is responsible for the massif's extensive glacierization, with 12 glaciers > 5 km^2 bordered by steep rockwalls with a relative relief of 500–1,000 m. The northwest side has relatively gentle slopes and has the largest glaciers, nourished by the dominant westerly winds and protected by their shaded northern aspect. The southeast flank is very steep, with small glaciers bounded by high, subvertical rockwalls (Fig. 1).

Fig. 3 View of the upper Val Ferret, from the Grandes Jorasses (4,208 m a.s.l., left) to the Mont Dolent (3,823 m a.s.l., right). Glaciers are (from left to right) Frébouze, Triolet, and Pré-de-Bard. The studied deposit is located on the valley floor, at the right of the large cone of Frébouze located at the center

Geological Setting

The northern side of the upper Val Ferret which rises up to 2,000 m above the present valley floor consists of coarse-grained porphyritic granite, as the main part of the Mont Blanc massif (Fig. 3). The opposite side of the valley is composed of metasedimentary rocks: massive beds of limestones and calcschists alternate at the base, and are topped by the so-called 'Flysch de Tarentaise' Sequence (conglomerate, limestones, calcschists, and sandstones). Triolet and Pré-de-Bar Glaciers are the largest glaciers, since the others are separated from the main valley by a bedrock barrier.

Characteristics of the Deposit

The floor of the upstream part of the valley is overlain by the recent moraine complex of these two glaciers (Fig. 4). Downstream, the valley floor is covered by an assemblage of units comprising granitic boulders over a distance of 2 km from the recent moraine complex of the Triolet Glacier (Fig. 4). In its distal sector, this deposit is a chaotic accumulation of blocks of all dimensions, with an open-work structure partly filled by alluvium which resulted in the formation of smooth plains. Linear ridges standing as

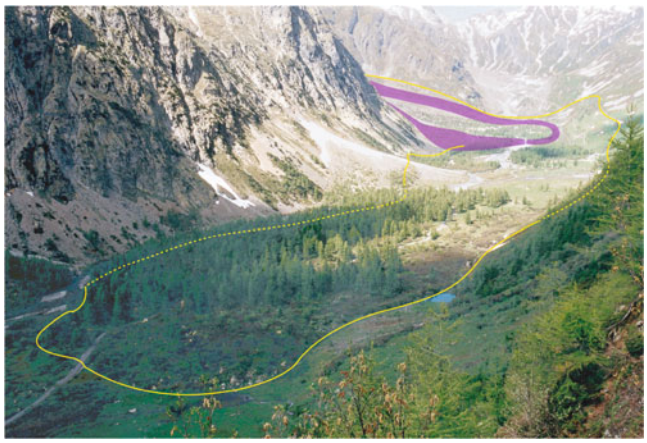

Fig. 4 View of the Upper Val Ferret from downstream. *Yellow line*: limit of the granitic deposits (*dashed line*: hidden limit). *Purple ribbon*: limit of the recent morainic complex of Triolet Glacier. Distance from the morainic complex to the toe of deposit is 2 km (Deline 2009)

much as 4 m above the average surface are found; the more obvious are concentric segments, 10–30 m wide, 1–10 m high, and 100–800 m long, with large boulders on their crests. Upstream, the deposit is overlain by two polygenetic debris cones originating from both sides of the valley (Figs. 3 and 4). Finally, close to the recent Triolet moraine complex, there is an assemblage of alluvial terraces, chaotic boulder accumulations, and coarse or small ridges (Deline and Kirkbride 2009).

Previous Geomorphological and Dating Studies

Since the nineteenth century, the deposits of the upper Ferret Valley were interpreted as a glacial outburst flood, a glacial drift deposited during the Little Ice Age or the Lateglacial, or from both glacial and rockfall origin, until Porter and Orombelli (1980) attributed the whole deposit to a rock avalanche onto the Triolet Glacier, historically dated from 1717 AD and corroborated by dendrochronology and lichenometry. They concluded that the event had a volume of (16–20) $\times$ 10^6 m^3 and covered the valley floor over an area of 2.7 km^2, after having descended from 3,600 m a.s.l. down to 1,740 m, travelling a runout distance of 7.2 km with a travel angle of 13°, typical for large rock avalanches onto glacier.

Aeschlimann (1983) refuted this interpretation mainly on the base of an older than 1717 AD ^{14}C date from a peat located immediately downstream Trio-8 (Fig. 5); he argued that the main part of the boulder deposit resulted from two Lateglacial advances. Orombelli and Porter (1988) performed other radiocarbon dating of peat and Schmidt hammer measurements, and reassert that the entire accumulation of

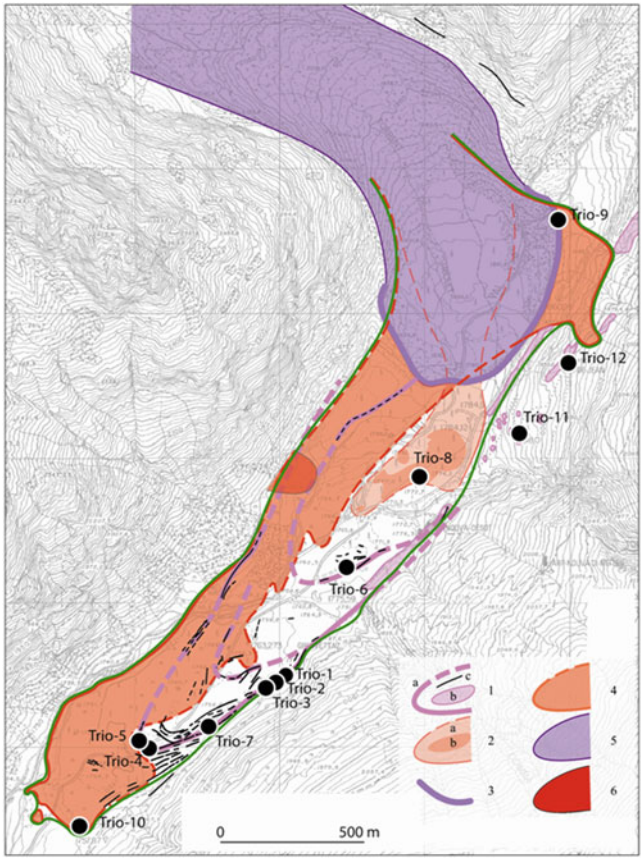

Fig. 5 Map of the deposits of Haut Val Ferret as interpreted by Deline and Kirkbride (2009), with location of the samples used for the surface exposure dating (SED). *1* Late-glacial moraine complex (*a* limit; *b* till veneer; *c* moraine crest); *2* Holocene rock-avalanche deposit older than 1000 AD (*a* limit; *b* chaotic boulder accumulation); *3* outermost moraine postdating the older than 1000 AD rock avalanche; *4* rock avalanche deposit of 1717 AD; *5* recent moraine complex of Triolet Glacier (18th–20th centuries); *6* local rock avalanche deposit after 1717 AD; *7* SED sample sites. The *green line* is the revised outer limit of the 1717 AD rock-avalanche deposit, as reconstructed on the base of the SED (Modified from Deline and Kirkbride 2009)

boulders is a single body of rock avalanche sediment of Late Holocene age.

Deline and Kirkbride (2009) supplied a new interpretation of the deposit (Fig. 5). They provided evidence for the deposition age based on the new ages. Based on new ^{14}C age evidences, Schmidt hammer rebound values, boulder edge-roundness measurements, and geomorphological characteristics of the deposit, Deline and Kirkbride (2009) argued that the deposit of the 1717 AD catastrophe was less extensive than interpreted by Porter and Orombelli (1980): (i) the rock avalanche would have been depleted by one side of the valley so that older deposits – supposed to be Lateglacial moraines – along the other side were preserved; and (ii) an earlier rock avalanche collapsed onto the Triolet Glacier before 1000 AD.

Table 1 ^{10}Be exposure ages. Exposure ages are corrected for erosion and snow; external uncertainties are reported in parentheses. Trio-8 and 8A: sample processed twice (see details in Akçar et al. 2012)

Sample name	Apparent exposure age (year)	Corrected exposure age (year)
Trio-1	854 ± 249 (266)	872 ± 255 (272)
Trio-2	335 ± 176 (184)	342 ± 180 (188)
Trio-3	465 ± 211 (221)	474 ± 215 (225)
Trio-4	412 ± 136 (145)	420 ± 139 (148)
Trio-5	333 ± 105 (112)	339 ± 107 (114)
Trio-6	474 ± 121 (131)	483 ± 123 (134)
Trio-7	326 ± 72 (86)	332 ± 80 (87)
Trio-8	347 ± 88 (95)	354 ± 90 (97)
Trio-8A	324 ± 22 (36)	330 ± 23 (37)
Trio-9	240 ± 96 (101)	244 ± 97 (103)
Trio-10	338 ± 43 (58)	345 ± 44 (54)
Trio-11	9300 ± 400 (900)	9700 ± 400 (1000)
Trio-12	10400 ± 300 (1000)	10900 ± 400 (1000)

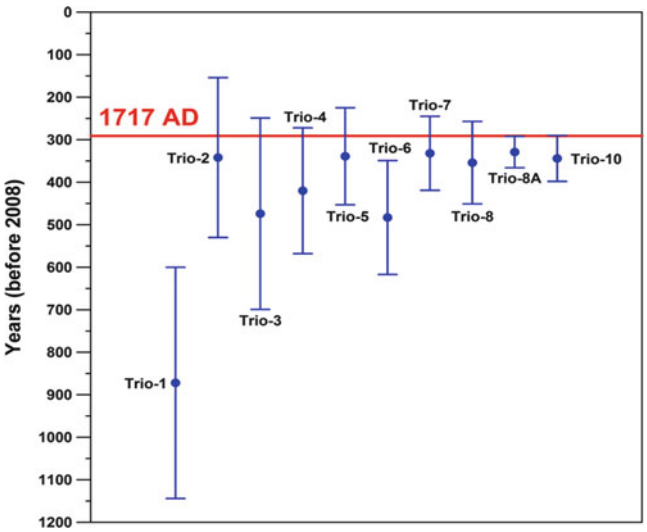

Fig. 6 Plot of the apparent exposure ages (1-σ uncertainty) for the boulders sampled in the upper Val Ferret deposit.Trio-11 and Trio-12 are not depicted here because deposited in other process and time conditions

Surface Exposure Dating Method and Results

Twelve granitic boulders in the upper Ferret Valley were carefully chosen with respect to the aim of the study, geomorphic setting, lithology and size (Fig. 5). Trio-1 to Trio-7 are located on ridges supposed to be Lateglacial moraines; Trio-8 and Trio-10 were sampled on chaotic accumulation of blocks in the proximal and distal areas of the deposit, respectively; Trio-9 was collected from a boulder embedded into the northeastern part of the Triolet morainic complex; finally, Trio-11 and Trio-12 are perched on the metasedimentary side at 50–100 m above the valley bottom (Akçar et al. 2012).

The samples were prepared at the Surface Exposure Laboratory of the University of Bern. Details are exposed in Akçar et al. (2012). Purified quartz from Trio-1 to Trio-8, and from Trio-10 to Trio-12 and Trio-8A, were processed following two different lab protocols. An erosion rate of 0.3 ± 0.5 mm/ka and a 4 months per year snow cover of 30 cm were estimated. Amount of the dissolved quartz and ^{9}Be spike, and ^{10}Be concentration, are given for each sample in Akçar et al. (2012).

Apparent exposure ages from boulders Trio-1 to Trio-10 vary from 244 ± 97 to 483 ± 123 years except for Trio-1 (872 ± 255 a) (Table 1). These results indicate that nearly all the sampled boulders result very likely from the 1717 AD rock avalanche (Fig. 6). Corrected exposure ages for Trio-11 and Trio-12 indicate that perched granite deposits are not related to it.

Discussion and Conclusions

Our ^{10}Be exposure ages from seven (Trio-2–5, 7–8, and 10) boulders indicate that the chaotic granitic deposit with irregular, subconcentric ridges is a deposit of the 1717 AD rock avalanche. These dates, which confirm the interpretation by Porter and Orombelli (1980), are in agreement with the existing ^{14}C dates of wood samples, but samples of the peat bog are considerably older and inconsistent (Deline and Kirkbride 2009). It could be explained by reworked organic matter from the catchment basin; in this case, granitic hummocky accumulations located downstream would be also a part of the 1717 AD rock avalanche. By contrast, right peat ^{14}C ages would mean that a section of the southern edge of the 1717 AD rock avalanche is formed by the preserved peat bog, which was in place before the rock avalanche; this is supported by an electrical tomography profile that shows a low resistivity up to 10 m deep in the peat bog, suggesting the absence of a rock debris layer. In both cases, the boulder deposit that Deline and Kirkbride (2009) proposed to predate 1000 AD is part of the 1717 AD rock avalanche.

The younger age of Trio-9 in the Triolet LIA moraine could result from either an englacial transport of the boulder deposited onto the glacier in 1717 AD, or a recent exhumation and exposition of the boulder deposited by the glacier with the moraine earlier than 1717 AD. Finally, Trio-1, and possibly in Trio-6, present inheritance.

Taking into account the deposit upon the glacier that supplied the morainic complex in the following two centuries, the total deposited rock volume was probably larger than 10×10^6 m^3, mixed with a huge volume of glacier ice – e.g. ice was 70–75 % of the total volume of the 1920 and 1997 Brenva rock avalanches (Deline 2009).

Results from this study contribute to improve our skill to distinguish between rock avalanche deposits and moraine sets in valleys of glaciated mountains – two assemblages of landforms which often look alike –, and to the assessment of related natural risks.

Acknowledgments The authors thank A. Franchino for his assistance on the field, and an anonymous referee for improving the manuscript.

References

Aeschlimann H (1983) Zur Gletschergeschichte des italienischen Mont Blanc Gebietes Val Veni – Val Ferret – Ruitor. Ph.D. Thesis, University of Zurich, Zurich

Akçar N, Deline P, Ivy-Ochs S, Alfimov V, Hajdas I, Kubik P W, Christl M, Schlüchter C (2012) The 1717 AD rock avalanche deposits in the upper Ferret Valley (Italy): a dating approach with cosmogenic ^{10}Be. J Quaternary Sci 27(4):383–392

Deline P (2009) Interactions between rock avalanches and glaciers in the Mont Blanc massif during the late Holocene. Quaternary Sci Rev 28(11–12):1070–1083

Deline P, Kirkbride MP (2009) Rock avalanches on a glacier and morainic complex in Haut Val Ferret (Mont Blanc Massif, Italy). Geomorphology 103:80–92

Hermanns RL, Niedermann S, Ivy-Ochs S, Kubik PW (2004) Rock avalanching into a landslide-dammed lake causing multiple dam failure in Las Conchas valley (NW Argentina) – evidence from surface exposure dating and stratigraphic analyses. Landslides 1:113–122

Ivy-Ochs S, Schaller M (2010) Examining processes and rates of landscape change with cosmogenic radionuclides. Radioactiv Environ 16:231–294

Orombelli G, Porter SC (1988) Boulder deposit of upper Val Ferret (Courmayeur, Aosta Valley): deposit of a historic giant rockfall and debris avalanche or a Lateglacial moraine? Eclogae Geol Helv 81:365–371

Porter SC, Orombelli G (1980) Catastrophic rockfall of September 12, 1717 on the Italian flank of the Mont Blanc massif. Zeitschrift für Geomorphologie 24:200–218

Prager C, Ivy-Ochs S, Ostermann M, Synal HA, Patzelt G (2009) Geology and radiometric C-14-, Cl-36- and Th-/U-dating of the Fernpass rockslide (Tyrol, Austria). Geomorphology 103: 93–103

Amplification of the Destructive Effects of Rock Falls by Sliding on Volcanic Soils: Examples from the Anaga Massif (Tenerife Island, Spain)

Jorge Yepes Temiño, Martín Jesús Rodríguez-Peces, Sara Marchesini, Sergio Leyva, and José Luis Díaz-Hernández

Abstract

This paper provides geomorphological and geotechnical observations on the amplification of the destructive behaviour of rock falls on rocky slopes in the Anaga massif (Tenerife Island, Spain) covered with soils rich in organic matter, within a high rainfall regime. The soil organic matter would be the determinant factor of this process, because it would reduce the soil strength as a result of overcoming the liquid limit during heavy rains. Thus the soil could develop a semi-fluid consistency, triggering a more efficient sliding of the blocks of rock along the slope and, hence, amplifying the destructive effect of the rock falls. Other potential determinant factor would be that the soil fine fraction could undergo a sudden change in its microfabric related to the dynamic load caused by the rock fall, similar to the mechanism described to explain the landslides developed in clayey soils.

Keywords

Canary Islands • Clay • Humus • Rock fall • Tenerife • Volcanic soil

Introduction

Rock falls are very frequent in the rocky massifs of volcanic islands during the erosion stages, when the volcanic activity is absent. These periods are characterised by effective and progressive erosion and the development of steep relief with sub-vertical cliffs. In this geomorphological context, rock-fall events are particularly intense in the steepest slope areas, where lava and pyroclast layers alternate, and in colluvial sediments of low strength which contain large blocks of rock. The rock-fall deposits are accumulated on the bottom of the steep slopes by means of isolated events in areas of low to moderate rock-fall susceptibility. (Ayenew and Barbieri 2005) In zones of high susceptibility, repeated rock falls from the same cliff ultimately form extensive talus screes at the bottom of the slope. The main type of rock-fall movement is bouncing, but locally can be rolling and sliding (Huang et al. 2010). The travel path of these processes often remain visible for several years, since the mobilized blocks of rock can open a corridor on its way through a dense forest. To be able to prevent the potential human and economical losses related to the rock-fall

J.Y. Temiño (✉)
Department of Civil Engineering, University of Las Palmas de Gran Canaria, Las Palmas 35017, Spain
e-mail: jyepes@dic.ulpgc.es

M.J. Rodríguez-Peces
Department of Geodynamics, University Complutense of Madrid, Ciudad Universitaria s/n, Madrid 28040, Spain
e-mail: martinjr@geo.ucm.es

S. Marchesini
Laboratory of Concretes, Soils and Asphalts, University of Las Palmas de Gran Canaria, Las Palmas 35017, Spain

Department of Civil Engineering, Polytechnic University of Marche, Ancona, Italy
e-mail: sarasclera@gmail.com

S. Leyva
Technical Road Maintenance and Exploitation Service, Local Government of Tenerife, Santa Cruz de Tenerife, Spain
e-mail: sergiolc@tenerife.es

J.L. Díaz-Hernández
Research and Training Institute for Agriculture and Fishery (IFAPA), Junta de Andalucía, Granada 18080, Spain
e-mail: josel.diaz@juntadeandalucia.es

C. Margottini et al. (eds.), *Landslide Science and Practice*, Vol. 1,
DOI 10.1007/978-3-642-31325-7_25,

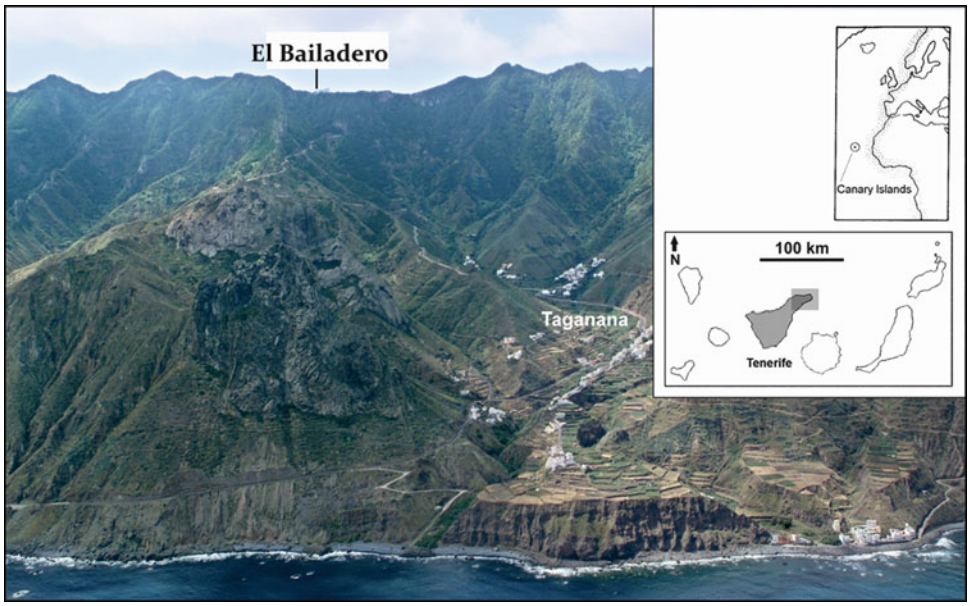

Fig. 1 Panoramic view of the steep slopes of the Anaga massif, located at the northeastern part of the Tenerife Island. The location of the El Bailadero is depicted

phenomena, it is crucial to understand and be able to recognize the determinant factors that could trigger and amplify the dangerous effects of this type of rapid mass movement.

Tenerife (Canary Islands, Spain) is a volcanic island with more than 7 Ma, which was built during four main volcanic stages (Ancochea et al. 2004). There are recognized remains of three old volcanic edifices (Anaga, Teno and Roque del Conde) which were originally disconnected from each other, forming three isolated islands, but were later partially covered by the materials of the recent volcanic stages. These old volcanic massifs comprise a very thick succession of basaltic lavas alternating with pyroclasts, typical of basaltic shield volcanoes. The lack of recent volcanic activity in these three sectors of the island has made possible the geomorphological context described above with effective erosion and steep rocky slopes.

The risk related to the rock falls in Tenerife Island is accentuated by several factors: (a) the existence of many sections of road running through the old basaltic massifs which have a significant sub-vertical jointing; (b) the strong gusts of wind that affect the northern side of Tenerife Island, mostly in a northwest trend, which can reach 147 km/h in the rainy season, according to the Spanish Meteorological Agency (AEMET 2004), (c) the existence of a soil layer rich in organic matter widely covering the northern side of island.

In this paper, we have studied the potential amplification of the destructive effect of rock falls in the Anaga massif, located at the northeastern flank of Tenerife (Fig. 1). In this island sector the average annual rainfall reaches 557 mm, with a maximum monthly rainfall record of 448 mm (AEMET 2004). In addition, the action of the trade winds between 1,000 and 1,500 m above sea level produces an increase in the relative humidity, as large masses of water vapour are retained by the steep slopes. Both phenomena have favoured the intense weathering of the rock masses, the colonization of woody vegetation and the subsequent development of a residual soil rich in humus. The rate of the rock-fall events has been assessed by means of field surveys, consulting the incident reports of the Technical Road Maintenance and Exploitation Service of the Local Government of Tenerife, surveying the neighbours of the area and studying the aerial photographs of the last 40 years. The main geotechnical properties of the soil layer have been also analyzed to assess the potential amplification factors of the destructive effect of rock fall.

El Bailadero Rock Fall

On 16 November 2009, following a week of heavy rains, a large massive block (150 m^3) of olivine-pyroxene basalt fell from the rocky cliff face of the El Bailadero area, located in the Anaga massif at the northeast sector of Tenerife Island (Fig. 2), impacting on the TF-134 regional road, close to the kilometric point 1 + 500. The collision broke the block of rock into several pieces and triggered the slide of a section, about 15 m wide, of the embankment on which the road was supported. The block of rock had a volume of about 150 m^3 and an estimated unit weight between 25 and 30 kN/m^3. The vertical distance between the road and the source area of the block is 110 m. The first 25 m are related to a sub-vertical scarp and the

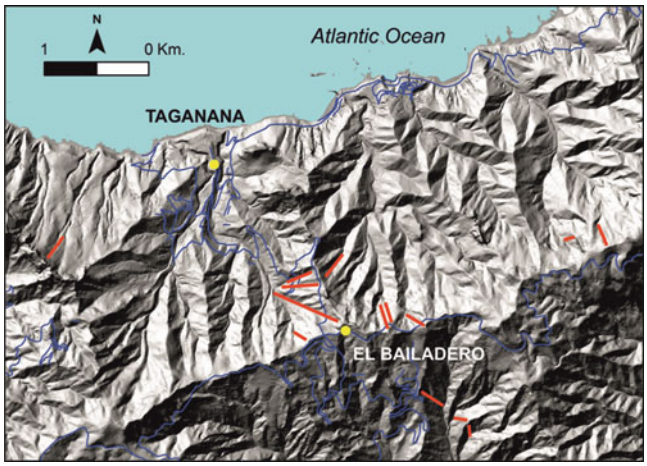

Fig. 2 Map showing the main paths related to rock falls (*red lines*) which were found in the Anaga massif after the heavy rainfalls recorded during the winter of 2009

Fig. 3 Open corridor developed in the laurissilva forest by the sliding of a fallen block of basalt from the cliff face of the El Bailadero on 16 November 2009

following 85 m are a steep slope covered by a dense forest. The travel distance of the block prior to impact with the road was 110 m, measured in plan, and other additional 110 m after the impact. During transport, the block of rock dragged the vegetation and a soil layer of about 50 cm thick across a 20 m wide corridor. The visual aspect developed by the trace of the block is similar to a firewall (Fig. 3).

The field surveys and aerial photographs show that this type of phenomenon is very common on the steep rocky slopes of Tenerife and Madeira Islands which are exposed to intensive precipitation, particularly in the old basaltic rock masses (Fig. 3). The forest consists of laurissilva of faya and tree heath (*Myrico fayae* and *Ericetum arboreae*) with a size between 2 and 15 m in height. This laurissilva

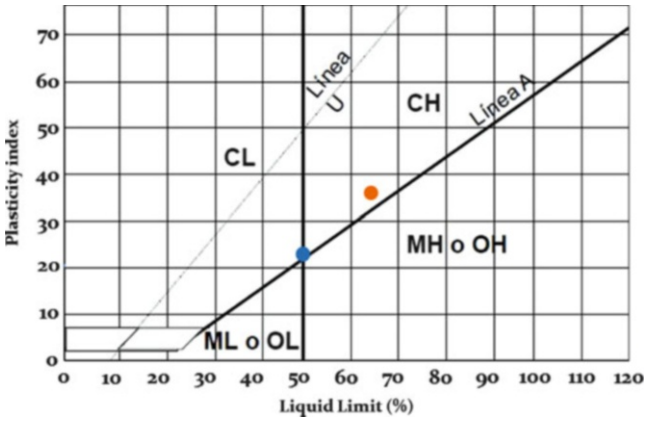

Fig. 4 Casagrande's chart corresponding to the clay content of the soil layer related to the sliding of the El Bailadero rock fall

forest is native to Macaronesia region, which comprises the Azores, Madeira and Canary Islands. In this landscape, residual soils are continuous layers rich in organic matter.

Geotechnical Investigations

We have characterized the mechanical behaviour of materials involved in the amplification of the destructive effect of the El Bailadero rock fall. Their geotechnical properties have been determined through a number of laboratory tests developed on soil samples taken from the rock fall area.

The geotechnical test focused in the characterisation of the soil type comprises unit weight and specific gravity determination (AENOR 1994a, b), Atterberg limits determination (AENOR 1993, 1994c) and engineering classification of soils following the Unified Soil Classification System (USCS) criteria (ASTM 2000) The strength of the soil was derived by means of direct shear test of soils under unconsolidated undrained (UU) and consolidated drained (CD) conditions (AENOR 1998). The deformability and potential of swelling of the soil was evaluated using both the Lambe (AENOR 1996) and oedometer tests (AENOR 1994d).

The soil samples were also examined by powder X-ray diffraction in order to obtain their global mineralogy, specially the amount of clay minerals in the soil. Data processing was performed using the XPowder® software (Martín-Ramos 2004), based on a proper database of diffractograms and following the process designed by Snyder and Bish (1989) and Downs and Hall-Wallace (2003).

The grain size analysis following the USCS classification indicates a soil mainly composed of silty sand with low clay content. However, the existence of a small amount of clayey material could reduce the geotechnical quality of the complete soil. In fact, the fine content could be regarded as high plasticity clay (CH), according to the Casagrande's chart (Fig. 4). In addition, the clay material has a significant

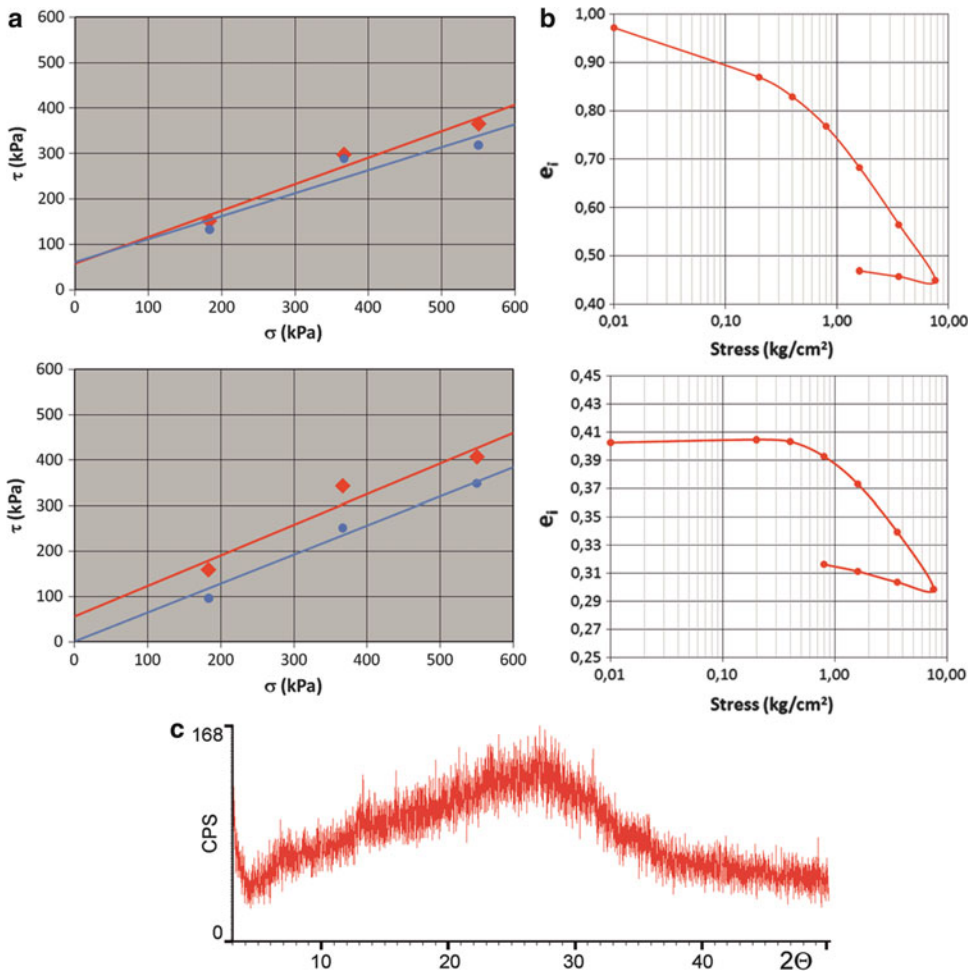

Fig. 5 Results of the main geotechnical tests performed to obtain the mechanical behaviour of the volcanic soil involved in the sliding of the El Bailadero rock fall. (**a**) Direct shear strength test. The *red* and *blue lines* are referred to peak and residual conditions, respectively; (**b**) Oedometer test showing the compressibility of the soil samples; (**c**) Diffractogram obtained by X-ray diffractometry of the clay fraction (oriented aggregates)

plasticity index ranging from 24 % to 37 % and high activity (1.6–9).

The values of cohesion and friction angles derived by means of the direct shear tests range between 0 and 58 kPa and 27° and 34°, respectively (Fig. 5a). These shear strength parameters are in agreement with the particle size obtained above. We have obtained a swelling index between marginal and critic (0.12–0.17 MPa) by means of the Lambe test and a compression ratio obtained in the oedometer test ranging between 0.11 and 0.34, which are characteristic of soils with low to medium compressibility (Fig. 5b).

The above-mentioned values are an evidence of a certain degree of plasticity and swelling that could have the soil. This behaviour has not been able to be related to the existence of clay minerals linked to materials of volcanic origin potentially expansive, because the X-ray diffractometry analysis supports the total absence of clay minerals in the soil (Fig. 5c). The shape of the diffractogram is typical of a sample of low crystallinity, suggesting the existence of amorphous minerals in the soil, likely organic matter and/or iron oxides and oxyhydroxides. This fact is in agreement with a moist ambient, whose soils are rich in organic matter and oxides. These observations agree with the existence of leafy vegetation developed in the residual soil, as in the case studied here.

The existence of a great proportion of organic matter as humus in the fine fraction of the soil could justify the low strength and compressibility found in the soil. In addition, we can assume that the soil could be susceptible to swelling processes during the rainy season, resulting in an isotropic and very open microfabric, comparable to the flocculated structure of clay minerals.

Discussion and Conclusions

The block of rock related to the El Bailadero rock fall slid over the slope as a consequence of a suddenly reduction of the shear strength of the soil (about 19–66 kPa), which has been assessed from data obtained in the direct shear test. This loss of strength would have undergone by the weathered soil layer as a result of overcoming the liquid limit during the heavy rainfall. This would be the determining

factor by which the soil developed a semi-fluid consistency, triggering a more efficient sliding of the block of rock along the slope and, hence, amplifying the destructive effect of the rock fall. The layer of soil which developed a semi-fluid consistency was thin (<0.5 m thick), but enough to slide successfully the entire block of rock along the slope. The rest of the substrate remained with a consistency between semi-rigid and plastic.

Another potentially determinant factor to explain the process described above, and pending a more detailed study, would be that the fine fraction of the soil underwent a mechanism of structural collapse similar to that has been described to explain the landslides developed in clayey soils (Perret et al. 1996; Okamoto et al. 2004; Khaldoun et al. 2009). Following this hypothesis, the dynamic load caused by the rock fall would have triggered the sudden collapse of the isotropic and open microfabric, resulting in an anisotropic and dense structure (scattered structure) with the soil particles oriented in a plane parallel to the topography. This phenomenon would trigger a significant reduction of the shear strength parameters of the soil as well as a more efficient sliding of the block of rock along the slope and, hence, amplifying the destructive effect of the rock falls.

Taking into account the hazard of this type of processes and the existence of a lot of segments of road extending through the old basaltic rock masses, it is recommended to develop a comprehensive geotechnical and mineralogical characterization of the alteration layers linked to volcanic materials. These further studies would be very useful to get more detailed insight into the mechanism of generation of the process described in this work, and to perform hazard maps to improve the landslide risk mitigation and the land-use planning on volcanic terrain.

References

AEMET (2004) Guía resumida del clima en España: 1971–2000. Plan Estadístico Nacional 2001–2004. Dirección General del Instituto Nacional de Meteorología, Ministerio de Medio Ambiente (ed), Madrid, Spain. (DL M3219-93), 257p

AENOR (1993) UNE 103-104/93. Test for the plastic limit of a soil. Asociación Española de Normalización y Certificación (ed), Madrid, Spain. (DL M3219-93), 2p

AENOR (1994a) UNE 103-301/94. Determination of a soil density. Method of the hydrostatic balance. Asociación Española de Normalización y Certificación (ed), Madrid, Spain. (DL M5292-94), 2p

AENOR (1994b) UNE 103-302/94. Determination of the relative density of the particles of a soil. Asociación Española de Normalización y Certificación (ed), Madrid, Spain. (DL M5293-94), p 3

AENOR (1994c) UNE 103-103/94. Determination of the liquid limit of a soil by the Casagrande method. Asociación Española de Normalización y Certificación (ed), Madrid, Spain. (DL M5291-94), 9p

AENOR (1994d) One-dimensional consolidation test in an oedometric cell. UNE 103-405-94, Asociación Española de Normalización y Certificación (ed), Madrid, Spain. (DL M21118-94), 10p

AENOR (1996) Determination of expansivity in a soil in the Lambe apparatus. UNE 103-600-96, Asociación Española de Normalización y Certificación (ed), Madrid, Spain. (DL 16171:1996), 10p

AENOR (1998) UNE 103-401/98. Determination of the shear strength of a soil with the direct shear box. Asociación Española de Normalización y Certificación, Madrid (ed), Madrid, Spain. (DL M29325:1998), 34p

Ancochea E, Barrera JL, Bellido F, Benito R, Brändle JL, Cebriá JM, Coello J, Cubas CR, De La Nuez J, Doblas M, Gómez JA, Hernán F, Herrera R, Huertas MJ, López-Ruiz J, Martí J, Muñoz M, Sagredo J (2004) Canarias y el vulcanismo neógeno peninsular. In: Vera JA (ed) Geología de España. IGME-SGE, Madrid. (ISBN 84-7840-546-1), pp 637–671

ASTM (2000) ASTM-D 2487/00. Standard classification of soils for engineering purposes (Unified soil classification system). American society for testing and materials, West Conshohocken, PA. (ISBN D2487/00), 11p

Ayenew T, Barbieri G (2005) Inventory of landslides and susceptibility mapping in the Dessie area, northern Ethiopia. Eng Geol 77:1–15

Downs RT, Hall-Wallace M (2003) The American mineralogist crystal structure database. Am Mineral 88:247–250

Huang RQ, Liu WH, Zhou JP, Pei XJ (2010) Experimental field study of movement charateristics of rock blocks falling down a slope. J Earth Sci 21(3):330–339

Khaldoun A, Moller P, Fall A, Wegdam G, De Leeuw B, Méheust Y, Fossum JO, Bonn D (2009) Quick clay and landslides of clayey soils. Phys Rev Lett 103(188301):1–4

Martín-Ramos JD (2004) Using XPowder®, a sofware package for powder X-ray diffraction analysis. D.L.GR-1001/04. Spain. (ISBN: 84-609-1497-6), 10p

Okamoto T, Larsen JO, Matsuura S, Asano S, Takeuchi Y, Grande L (2004) Displacement properties of landslide masses at the initiation of failure in quick clay deposits and the effects of meteorological and hydrological factors. Eng Geol 72:233–251

Perret D, Locata J, Martignonib P (1996) Thixotropic behavior during shear of a fine-grained mud from Eastern Canada. Eng Geol 43:31–44

Snyder RL, Bish DL (1989) Quantitative analysis. In: Bish DL, Post JE (eds) Modern powder diffraction. Reviews in Mineralogy 20. Mineralogical Society of America, pp 101–143

Creation of Landslide Inventory Map for the Toktogul Region of Kyrgyzstan, Central Asia

Namphon Khampilang and Malcolm Whitworth

Abstract

This project is reliant upon the use of remote sensing for the detection and delineation of landslides. Therefore optical satellite images, such as medium resolution ASTER, and high resolution SPOT 5, will be combined with topographic data to analyse the landslide prone areas. The specific objectives are to generate a landslide inventory distinguishing between different landslide types, and to use this map for GIS based spatial landslide hazard modelling in the Toktogul region of Kyrgyzstan. The project steps include: (1) detection and mapping of landslides at different scales using high resolution imagery and DEM data to generate a GIS landslide inventory database for the area, (2) ground truthing of this landslide inventory using field reconnaissance, (3) integrating morphological, lithological, structural, land use, hydrological and seismic data within a GIS environment (DEM data from SPOT will form an important component of this dataset), and (4) derivation of statistical landslide hazard models through the integration of the landslide inventory with the GIS datasets. The results will be shown in the form of landslide inventory maps including a GIS database at various scales and a landslide hazard model showing landslide prone areas and distinguishing different hazard levels. Consequently, these mapping results will be used to assist in making rational decisions regarding local evacuation plans in areas susceptible to slope failure.

Keywords

Landslide hazard assessment • ASTER • SPOT

Introduction

A landslide is a downward and outward movement of slope forming materials under the influence of gravity (Varnes 1978). Each year, landslides claim thousands of casualties and cause billions of dollars in infrastructure and property damage, a total that is, worldwide, larger than that from any other natural disasters (Guzzetti et al. 1999; Yang and Chen 2010). From a different point of view, landslides are natural events and play an important role in the evolution of landforms. Landslide occurrence depends upon different parameters such as geological and geomorphological processes, changes in vegetation cover, land use and hydrologic conditions. Landslides are triggered by many factors including heavy precipitation, earthquakes and human activities (Safae et al. 2010; Alkevli and Ercanoglu 2011).

Landslide detection including recognition and classification is a basis of the spatial and temporal occurrence which leads to the understanding of Landslide hazard and risk management (Martha et al. 2010). Many researchers have identified, classified and studied landslides and for this, they have produced landslide maps at different scales depending on the purpose and the available resources, using a variety of techniques, including the analysis of stereoscopic aerial photographs, geological and geomorphological field mapping,

N. Khampilang (✉) • M. Whitworth
University of Portsmouth, ad, Portsmouth PO1 3QL, UK
e-mail: namphon.khampilang@port.ac.uk;
Malcolm.whitworth@port.ac.uk

C. Margottini et al. (eds.), *Landslide Science and Practice*, Vol. 1,
DOI 10.1007/978-3-642-31325-7_26,

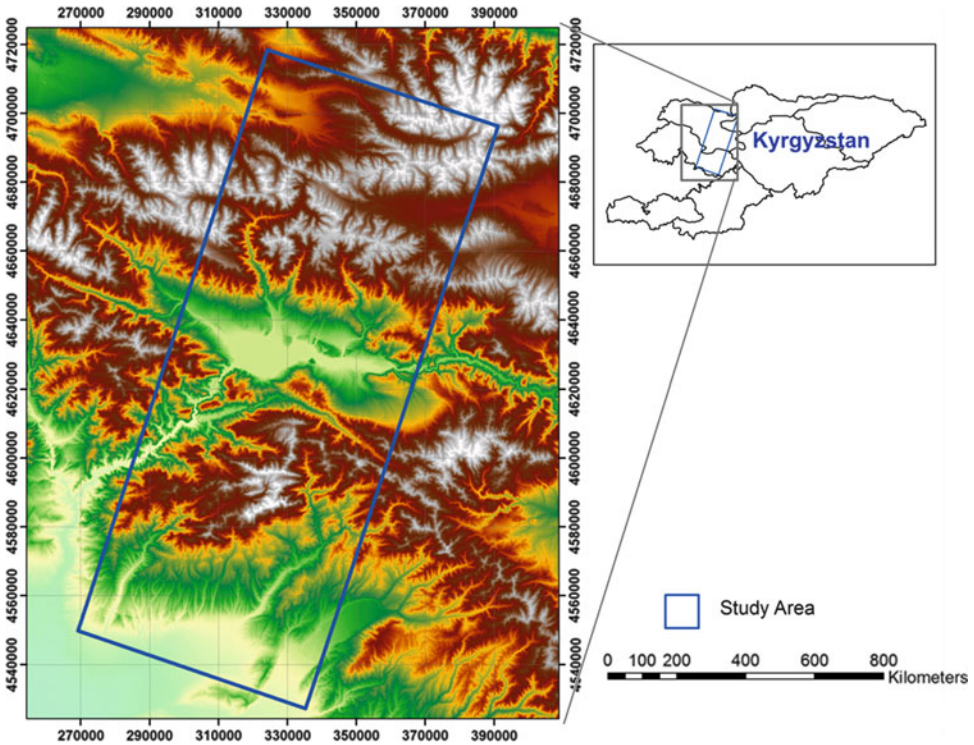

Fig. 1 Location map of the study area

engineering-geological slope investigations, and the examination of historical archives (Guzzetti et al. 1999; Galli et al. 2008). In addition, tools for handling and analyzing spatial data such as Remote Sensing software packages and GIS may facilitate the application of quantitative techniques in both landslide inventory mapping and hazard assessment. Several studies have been performed using remotely sensed data and GIS data integration in landslide assessment (Guzzetti et al. 1999; Ostir et al. 2003; Qi et al. 2010). Remote sensing techniques are preferable for landslide assessments because they provide up to date data and have the ability to show large areas, when integrated into a GIS environment (Alkevli and Ercanoglu 2011).

The data used in this paper was collected from the Advanced Spaceborne Thermal Emission and Reflection Radiometer (ASTER), using level 1B at 15 m resolution; the ASTER Global Digital Elevation Model (ASTER GDEM) at 30 m resolution; the SPOT-5 panchromatic at 2.5 m resolution and SPOT DEM at 20 m resolution. The purpose of this study was to investigate the use of ASTER and SPOT-5 satellite imageries to prepare landslide inventory maps in a landslide prone area in the Toktokul region of Kyrgyzstan in Central Asia. For this purpose, 2D and 3D visual interpretations were created to map landslides using the remote sensing programme ENVI 4.3. The landslide inventory map itself was produced using Arc GIS 10.2 software programme.

Study Area

The study area is situated in the Toktokul hydroelectric and irrigation scheme which is the largest in Central Asia, with a reservoir containing almost 20 km^3 of impounded water behind a 230 m-high dam. Annually, the scheme generates 1,200 MW of electricity that is distributed over Kyrgyzstan, Uzbekistan, Tajikistan, Kazakhstan and Russia. This area is located in the technical and seismically active Tien Shan Mountains (Havenith et al. 2006). The Tien Shan is a Cenozoic orogenic belt in Central Asia with a basin and range structure caused by the post-collisional convergence of India with Asia. A major tectonic feature in the Tien Shan is the active Talas-Fergana fault crossing the mountain belt from NW to SE (Fig. 1). Due to being situated in a seismically active area, coupled with the complex interactions between tectonic, geological, geomorphological and hydrological factors present in the region, landslides frequently lead to serious damage to property, infrastructure and associated loss of life (Roessner et al. 2005). The area is associated with numerous deep-seated slope deformations, landslides, disruptions to superficial deposits and long run out debris flows. Although landslides have been identified in the Tien Shan mountains (Wetzel et al. 2000; Havenith et al. 2002; Roessner et al. 2005; Havenith et al. 2006; Roessner et al. 2006; Strom and Korup 2006; Torgoev et al. 2006;

Table 1 Technical specifications of ASTER sensor and Terra satellite orbital parameters (Hirano et al. 2003)

Technical specifications	Terra ASTER stereo
VNIR 0.52–0.86 μm, 15 m	3
SWIR 1.600–2.430 μm, 30 m	6
TIR 8.125–11.65 μm, 90 m	5
Stereo capability	Yes
	Bands 3N and 3B (nadir and aft-looking telescopes)
	0.78–0.86 Am
Stereo imaging geometry	Along-track
Base-to-height (B/H) ratio	0.6
Pixel size	15 m
Scene coverage	60 × 60 km
Orbital path	Near-polar sun-synchronous
Orbital altitude	705 km
Orbital inclination	98.2°
Repeat cycle	16 days

Danneels et al. 2008; Strom 2010) no detailed landslide inventory is available to assist in the risk assessment for the area, mostly due to a restrictive data policy during the period of Soviet occupation (Roessner et al. 2005; Strom and Korup 2006).

Data

This study was undertaken to investigate the use of medium resolution ASTER satellite images and high resolution SPOT-5 satellite images to determine landslide locations. ASTER is a high performance optical sensor with 14 spectral bands that range from visible to thermal infrared bands (Table 1). It uses three radiometers such as VNIR (Visible and Near Infrared Radiometer; wavelength: 0.56–0.86 μm; spatial resolution: 15 m), SWIR (Short Wavelength Infrared Radiometer; wavelength: 1.60–2.43 μm; spatial resolution: 30 m), and TIR (Thermal Infrared Radiometer; wavelength: 8.125–11.65 μm; spatial resolution: 90 m) (Fourniadis et al. 2007). Hirano et al. (2003) states that a major advantage of the along-track mode of data acquisition (as compared to cross-track) is that the images forming the stereopairs are acquired a few seconds apart (rather than days apart) under uniform environmental and lighting conditions, resulting in stereopairs of consistent quality that are well suited for DEM generation by automated stereocorrelation techniques which provides a greater amount of useful geomorphological information. This is a helpful feature in landslide studies (Alkevli and Ercanoglu 2011).

Eight scenes of ASTER Level 1B data (Fig. 2) provided by NASA for educational purposes were used in the study ASTER Global Digital Elevation Model (DEM) at 30 m resolution was also used in association with ASTER images in order to create 3D views.

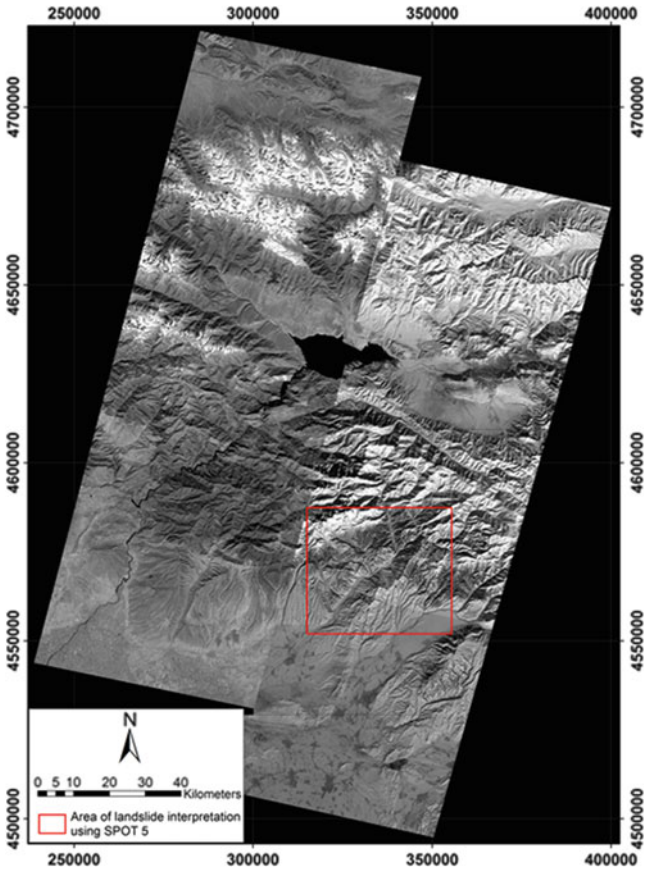

Fig. 2 Mosaic ASTER image of the study area band 3N

Furthermore, for a part of the study area (15 %) SPOT-5 panchromatic images at resolution 2.5 m will also be used to identify and classify landslides. Figure 3 shows the example of SPOT-5 image covering part of the study area.

Methodology

ASTER imagery is increasingly used in geological applications as it is one of the least expensive medium resolution satellite images available (Alkevli and Ercanoglu 2011). In order to investigate the use of ASTER images for landslide mapping by visual interpretation, four different data sets were used:

1. False Colour Composites (FCC) using the 3N, 2, 1 bands in red, green, blue order. Different image processing techniques were applied to enhance the multispectral images. Only the VNIR portion of ASTER images was considered in the analyses because of their relative higher resolution when compared with the SWIR and TIR portions;
2. The 3N infrared band;
3. The Principal Component (PC) transformation. For the visual interpretation, only the first three PC images extracted

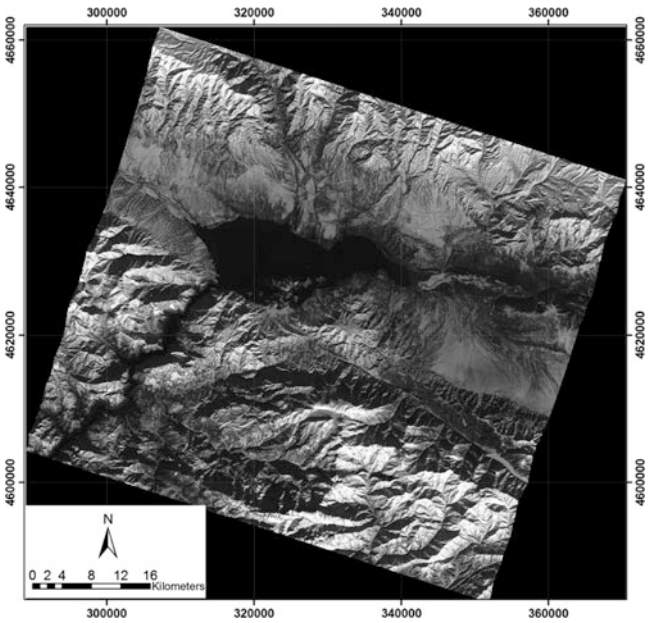

Fig. 3 Example of SPOT 5 image part of the study area

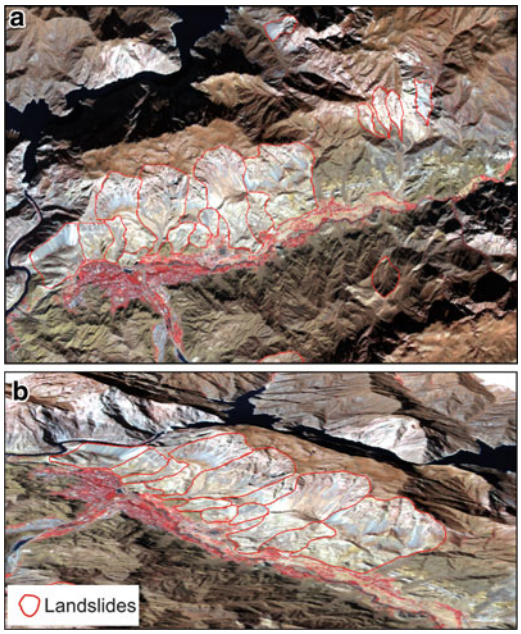

Fig. 4 Example of landslides overlaying on ASTER image (**a**) 2D view (**b**) 3D view

from the combination of the 3 VNIR and 6 SWIR bands were used because of their higher quality; and

4. The merged ASTER images and ASTER DEM to produce 3D view.

The different image processing techniques were performed using ENVI 4.3. Additionally, the visual interpretations were created and interpreted using Arc GIS 10.2 software.

Landslide information identified by remote sensing product using visual interpretation is related to the morphology, vegetation and drainage condition of the slope. In addition, tone and pattern of the surface, such as hummocky topography, may be taken into account as it may be related to slope failure. However, scales smaller than 1/15,000 demonstrated that FCC and infrared band assessments were insufficient to recognize landslide-related features during the visual interpretation.

SPOT-5 panchromatic band images at 2.5 m resolution (Fig. 3) are also used in this project. The image processing techniques such as interactive stretching will be used to enhance the spatial resolution of the image in order to easier identify landslides.

Results and Discussion

The landslide inventory map was produced by visual interpretation of ASTER level 1B data. Based on the 2D and 3D visual interpretation, 348 active and dormant landslides were identified in the study area. These are shown in the landslide inventory map (Fig. 5). The landslides identified are rotational slides, debris flows and rock falls, however, this information on landslide type could only be determined for large landslides. Small landslides did not produce sufficiently distinctive features to confirm whether they were rotational slides, debris flows or rock falls. The largest landslide found in the area was 15,869,692 m^2 and the smallest was 51,973 m^2. The landslide interpretation resulted as a landslide inventory map combining all data sets which were FCC, 3N infared band, PC and 3D view (Figs. 4 and 5).

Based on 2D visual interpretation, FCC was found to be more useful than the 3N infared band because landslides could be identified more easily due to their higher contrast to surrounding area in FCC images. However, for scales more detailed than 1/15,000, FCC, 3N infrared band and PC images derived from ASTER were considered insufficient for landslide identification and mapping. For identification of landslides on a larger scale, higher resolution remote sensing images are needed. Nevertheless, it could be sufficient in other areas depending on reflection of the landslide surface shown on the images.

In some areas landslides were difficult to detect on the 2D ASTER images due to a lack of distinctive traces, whereas the 3D view was consistently useful at showing the morphology of the landslides. Hence, 3D visual interpretation performed on ASTER imagery and ASTER DEM is useful for landslide inventory mapping.

SPOT-5 panchromatic 2.5 m resolution has shown a significantly more detailed representation of landslide features and morphological structures (Fig. 6). Consequently, the mapping of landslide location using SPOT-5 will be carried out in more detail at a later point and the landslide inventory map based on SPOT-5 interpretation will be produced in a larger scale.

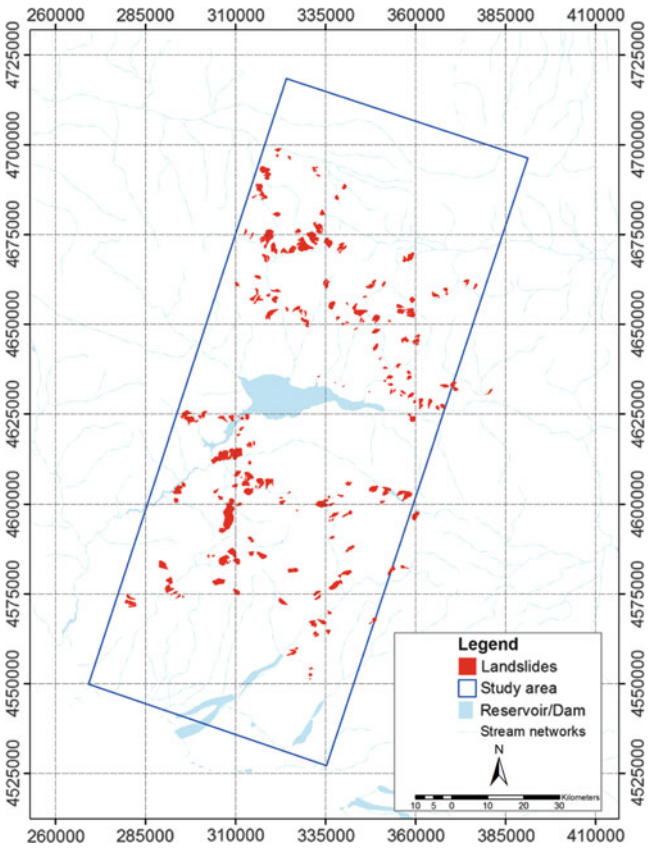

Fig. 5 Landslide inventory map of the study area produced from ASTER imagery

However, visual interpretation is a subjective methodology mostly depending on the interpreter's knowledge and experience using different criteria defined for the identification of landslides. The errors inherent in visual image interpretation may produce differences of between 60% and 90 % when different researchers are doing the interpretation (Saba et al. 2010). Therefore, field verification is needed in order to correct any errors in image interpretation.

Conclusion and Further Works

The purpose of this study was to investigate the use of ASTER and SPOT satellite imagery to prepare a landslide inventory map in a landslide prone area in the Toktokul region of Kyrgyzstan in Central Asia. The results showed that available ASTER images are suitable for identification of large (greater than 50,000 m^2) landslides in the Toktokul region and that satellite remote sensing data are valuable in allowing better mapping and understanding of landslides especially when being merged with DEMs to produce 3D views.

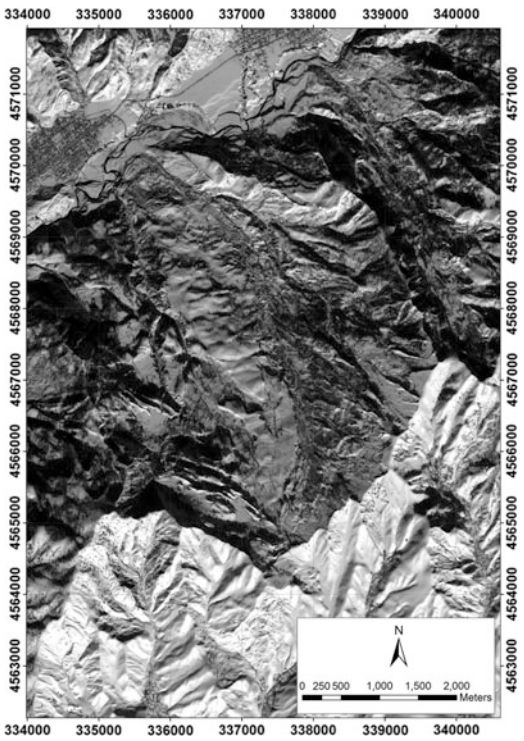

Fig. 6 Complex landslide identified on SPOT 5 Panchromatic image

Further Work

To complete the landslide hazard assessment of the area, the following work needs to be done:

1. Identify landslides from SPOT 5 data and produce a landslide inventory map from SPOT images,
2. Ground truth this landslide inventory using field reconnaissance,
3. Integrate morphological, lithological, structural, land use, hydrological and seismic data within a GIS environment. DEM data from SPOT will form an important component of this dataset, and
4. Derive statistical landslide susceptibility models through the integration of the landslide inventory with the GIS datasets.

The expecting results will be shown in form of a landslide inventory map including a GIS database at various scales and a landslide hazard map showing different levels of hazard prone areas. Consequently, this mapping result will be used to assist in making rational decisions regarding local evacuation plans in areas susceptible to slope failure.

Acknowledgments The authors would like to thank the Royal Thai government for providing PhD funding and University of Portsmouth staff for creating a warm and supportive working environment. Furthermore, the authors would like to give credit to NASA for providing free ASTER images through the Land Processes Distributed Active

Archive Center (LP DAAC) and to the Incentive for the Scientific use of Images from the Spot system (ISIS programme) for providing SPOT data at a reasonable rate. Finally, the authors would like to thank Institute of Communication and Information Technologies for the geological data support. And most importantly, the authors would like to thank the reviewer who revised and did the hard work in order to improve this paper.

References

Alkevli T, Ercanoglu M (2011) Assessment of ASTER satellite images in landslide inventory mapping: Yenice-Gökçebey (Western Black Sea Region, Turkey). Bull Eng Geol Environ 70(4):607–617

Danneels G, Havenith HB, Strom A, Pirard E (2008) Landslide detection methods, inventory analysis and susceptibility mapping applied to the Tien Shan, Kyrgyz Republic. In: Proceedings of the first world landslide forum, 18–22 Nov 2008, Tokyo, pp 426–429

Fourniadis IG, Liu JG, Mason PJ (2007) Landslide hazard assessment in the Three Gorges area, China, using ASTER imagery: Wushan-Badong. Geomorphology 84(1–2):126–144

Galli M, Ardizzone F, Cardinali M, Guzzetti F, Reichenbach P (2008) Comparing landslide inventory maps. Geomorphology 94:268–289

Guzzetti F, Carrara A, Cardinali M, Reichenbach P (1999) Landslide hazard evaluation: a review of current techniques and their application in a multi-scale study, Central Italy. Geomorphology 31: 181–216

Havenith HB, Jongmans D, Faccioli E, Abdrakhmatov K, Bard PY (2002) Site effect analysis around the Seismically induced Ananevo rockslide, Kyrgyzstan. Bull Seismol Soc Am 92(8):3190–3209

Havenith HB, Torgoev I, Meleshko A, Alioshin Y, Torgoev A, Danneels G (2006) Landslides in the Mailuu-Suu valley, Kyrgyzstan-Hazards and impacts. Landslides 3:137–147

Hirano A, Welch R, Lang H (2003) Mapping from ASTER stereo image data: DEM validation and accuracy assessment. ISPRS J Photogramm 57(5–6):356–370

Martha TR, Kerle N, Jetten V, van Westen CJ, Kumar KV (2010) Characterising spectral, spatial and morphometric properties of landslides for semi-automatic detection using object-oriented methods. Geomorphology 116(1–2):24–36

Ostir K, Veljanovski T, Podobnikar T, Stancic Z (2003) Application of satellite remote sensing in natural hazard management: the Mount Mangart landslide case study. Int J Remote Sens 24(20): 3983–4002

Qi S, Xu Q, Lan H, Zhang B, Liu J (2010) Spatial distribution analysis of landslides triggered by 2008.5.12 Wenchuan Earthquake, China. Eng Geol 116:95–108

Roessner S, Wetzel HU, Kaufmann H, Sarnagoev A (2005) Potential of satellite remote sensing and GIS for landslide hazard assessment in Southern Kyrgyzstan (Central Asia). Nat Hazards 35:395–416

Roessner S, Wetzel HU, Kaufmann H, Sarnagoev A (2006) Satellite remote sensing and GIS for analysis of mass movements with potential for dam formation. Italian J Eng Geol Environ Special Issue (1):103–114

Saba SB, van der Meijde M, van der Werff H (2010) Spatio-temporal landslide detection for the 2005 Kashmir earthquake region. Geomorphology 124:17–25

Safae M, Omar H, Yousof ZBM, Ghias V (2010) Applying geospatial technology to landslide susceptibility assessment. Electron J Geotech Eng 15:677–696

Strom AL (2010) Uniform inventory of the Tien Shan rockslides: basis of the rockslide disaster mitigation strategy. URl: http://www.interpraevent.at/palm-cms/upload_files/Publikationen/Tagungsbeitraege/2010__902.pdf. Last accessed 20 Mar 2011

Strom AL, Korup O (2006) Extremely large rockslides and rock avalanches in the Tien Shan Mountains, Kyrgyzstan. Landslides 3:125–136

Torgoev IA, Aleshin YG, Meleshko AV, Havenith HB (2006) Hazard mitigation for landslide dams in Mailuu-Suu valley (Kyrgyzstan). Italian J Eng Geol Environ Special Issue (1):99–102

Varnes DJ (1978) Slope movements, type and processes. In: Schuster RL, Krizek RJ (eds) Landslide Analysis and Control. Transportation Research Board, Special Report 176, pp 11–33

Wetzel HU, Roessner S, Sarnagoev A (2000) Remote sensing and GIS based geological mapping for assessment of landslide hazard in Southern Kyrgyzstan (Central Asia). International conference on management information systems incorporating GIS & remote sensing, Lisbon, 14 June 2000, pp 355–366

Yang X, Chen L (2010) Using multi-temporal remote sensor imagery to detect earthquake-triggered landslides. Int J Appl Earth Obs Geoinf 12(16):487–495

Residual Strength Measurements for Some British Clays

Seyyedmahdi Hosseyni, Nobuyuki Torii, and Edward N. Bromhead

Abstract

Since Skempton presented his theory of residual strength in clay soils in 1964 (with a consolidation of ideas in 1985), a huge body of results for the residual strength of many clays has been published. Nowhere is this more marked than in Britain. The datasets available have been derived from a variety of methods, including back analysis, laboratory tests on natural and reconstituted soils. Laboratory tests have included tests with broadly unlimited deformation (e.g. ring shear tests), tests on sampled shear surfaces, tests with slip surfaces pre-formed mechanically in the laboratory, and tests on undisturbed specimens (for example, reversal tests in the shear box). This paper concentrates on the results from back-analyses.

It has been observed (for example, by Bromhead, Ibsen (2004) Bedding-controlled coastal landslides in Southeast Britain between Axmouth and the Thames Estuary. Landslides 1(2):131–141) that very many of the landslides investigated around the South and East coasts of England are compound landslides with extensive sub-horizontal basal shear surfaces in locations that conform to the bedding. In some strata (e.g. Barton et al. (2006) The slip surface in the D zone of the Barton Clay. QJEGH 39(4):357–370) the basal shear occurs in a thin stratum of noticeably higher plasticity than above or below. It has also been observed that similar bedding control is exerted on the position of compound landslide basal shear surfaces in inland landslides, most noticeably in connection with failures of cut slopes for transportation infrastructure (roads and railways). Experience suggests that the results from a back-analysis are dominated by the properties of these strata where the bedding-controlled basal shear surface constitutes a significant fraction of the total length.

The paper presents an analysis of the data from published back analyses, supplemented with some of the more reliable laboratory testing that has been specifically recorded as being on samples from bedding-controlled basal shear surfaces, and compares datasets from a number of stiff fissured over-consolidated clays of very different ages. Inferences

S. Hosseyni (✉)
Azadshahr Branch, Islamic Azad University, Azadshahr, Iran

School of Civil Engineering and Construction, Kingston University, Kingston upon Thames, UK
e-mail: M.Hosseyni@Kingston.ac.uk

N. Torii
Department of Civil Engineering, Graduate School of Engineering, Kobe University, Kobe, Japan

E.N. Bromhead
School of Civil Engineering and Construction, Kingston University, Kingston upon Thames, UK

C. Margottini et al. (eds.), *Landslide Science and Practice*, Vol. 1,
DOI 10.1007/978-3-642-31325-7_27,

are drawn from these results about the mode of formation of what are taken to be sedimentologically-controlled weak horizons occurring throughout the geological record.

Keywords
Residual shear strength • London clay • Gault • Lias

Introduction

It has often been observed that in Britain, there are a significant number of landslides of compound form, where the basal shear surface follows a weak bed in the geological sequence on site. Of course, the geology of southern and central Britain is conducive to the occurrence of this type of landslide, as it is composed of numerous clay strata separated by sands and limestones, with dips typically less than 2°. As well as papers that review the generic similarities between landslides, numerous papers describe a single instance, or a small geographical area in which there are a small number of related landslides. In addition to landslides in natural slopes, particularly on the coast, but also in some inland locations, the literature also describes slides in infrastructure cuttings and other excavations.

In addition, the gently-sloping and not particularly high hillsides in many areas of central England were left mantled with drapes of shallow landslides after the retreat of the last glaciations and its associated post-glacial periglacial conditions. These mantles are readily disturbed by cuts, fills, and changes to the groundwater. Because these landslides do not follow a single stratigraphic level in the Lias, the residual strength mobilized along the basal shear surface represents an average value for a range of material types.

Back Analysis Technique

The back analysis technique was reviewed by Chandler (1977) but not originated by him. It is a technique for determining the operative shear strength of the basal slip surface of a slowly-moving landslide as the shear strength that produces F = 1. Some techniques involved in the analysis are given by Bromhead (2005). The normal procedure employed in Britain is to determine the average shear stress (τ_{av}) and average normal effective stress (σ'_n) acting on the slip surface, and then to plot these values on a graph as though they were a single determination of shear strength in a geotechnical test. By the time a family of landslides in a particular stratum has been analysed, especially if they have a range of sizes, a scatter of data points is found, from which typical residual shear strength parameters (c'_r and ϕ'_r) can be determined – or more usually ϕ'_r alone, as c'_r is commonly found to be negligible in these studies.

We see such a synthesis being performed for landslides in London Clay by James (1970), extended by inter alia Bromhead (1978), Skempton (1985), Bromhead and Dixon (1983) and Dixon and Bromhead (2002). James concentrated on slides in railway cuttings, Bromhead on the coastal landslides east of Herne Bay, and Dixon on the coastal landslides of a small area adjacent to Warden Point, on the Isle of Sheppey. Both the latter sites are on the south coast of the Thames Estuary (Fig. 1).

An additional body of data comes from the study of shallow landslides that move sub-parallel to the topographic slope, and which are therefore not specifically related to a particular soil horizon, but rather relate on average to larger stratigraphic units such as "Lias clay" (Chandler 1969, 1970). Inevitably, given the generally low relief and flat slopes in southern and central Britain, the stress levels in these slope failures are very low, and equate to the results from small infrastructure cuttings. The highest stress levels come from a very small number of large coastal landslides or from moderately-sized landslides where the piezometric pressures are very low due to undrained unloading (Bayley 1972; Chandler 1982a).

A majority of published back analyses have been performed using an "advanced" method of limit-equilibrium analysis, such as that published by Morgenstern and Price (1965), which satisfies both force and moment equilibrium criteria. However, the sophistication of such methods is lost upon the shallowest slides, which might just as well be analysed with the "infinite slope method" (Haefeli 1948; Skempton and Delory 1957).

In this paper, we have examined a total of 135 papers which describe the measurement of residual strength including back analyses and laboratory tests. It was determined that the majority of back analyses related to the following strata:

- London Clay (Eocene, Tertiary)
- Gault Clay (Lower Cretaceous)
- Lias Clay (Jurassic)

For brevity in this paper, we have only considered those results (Fig. 1). We have not knowingly omitted any of the published results for these strata, but are aware of missing data.

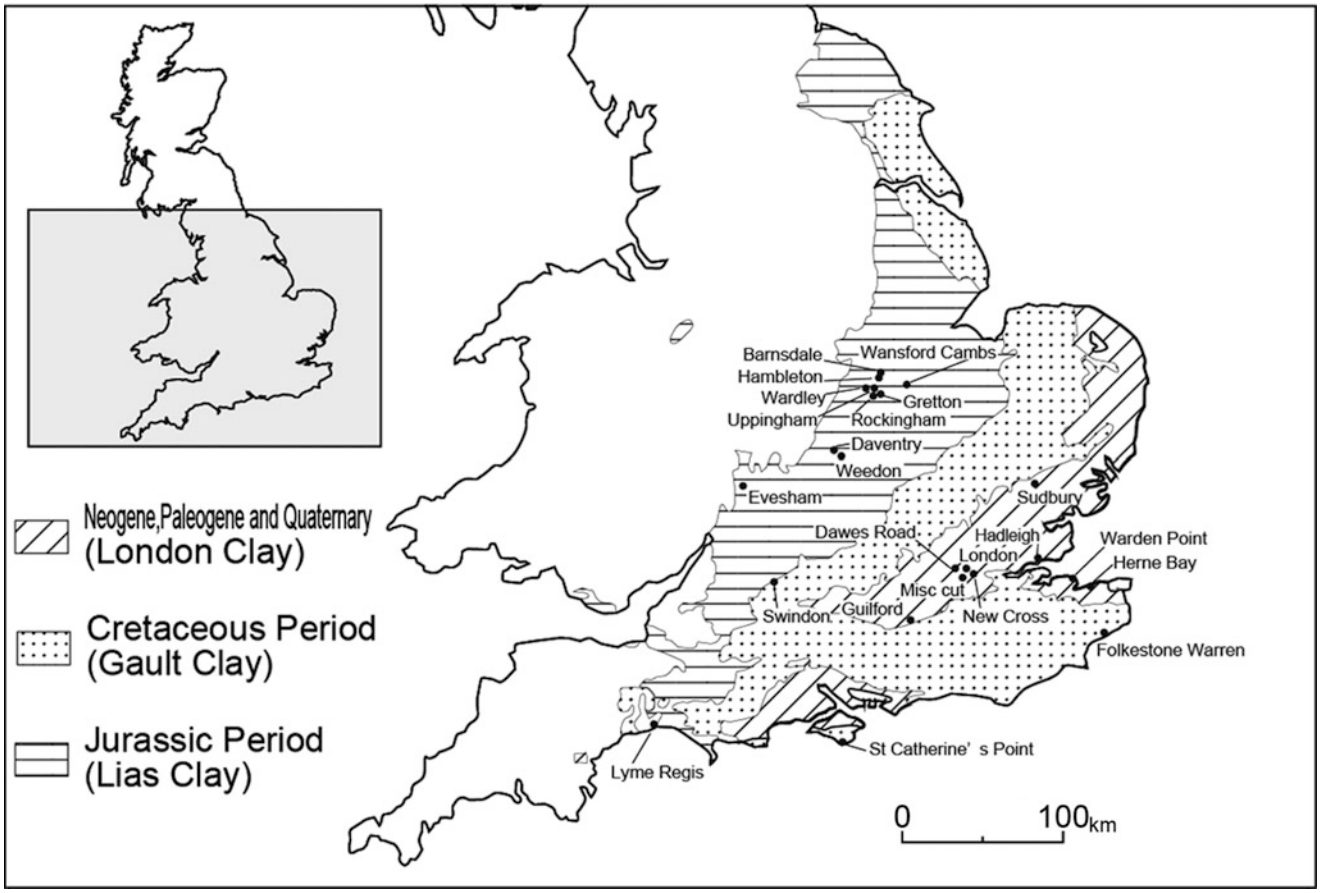

Fig. 1 Geological map of S.England showing outcrops of strata referred in text, and location of principle sites (After British geological survey)

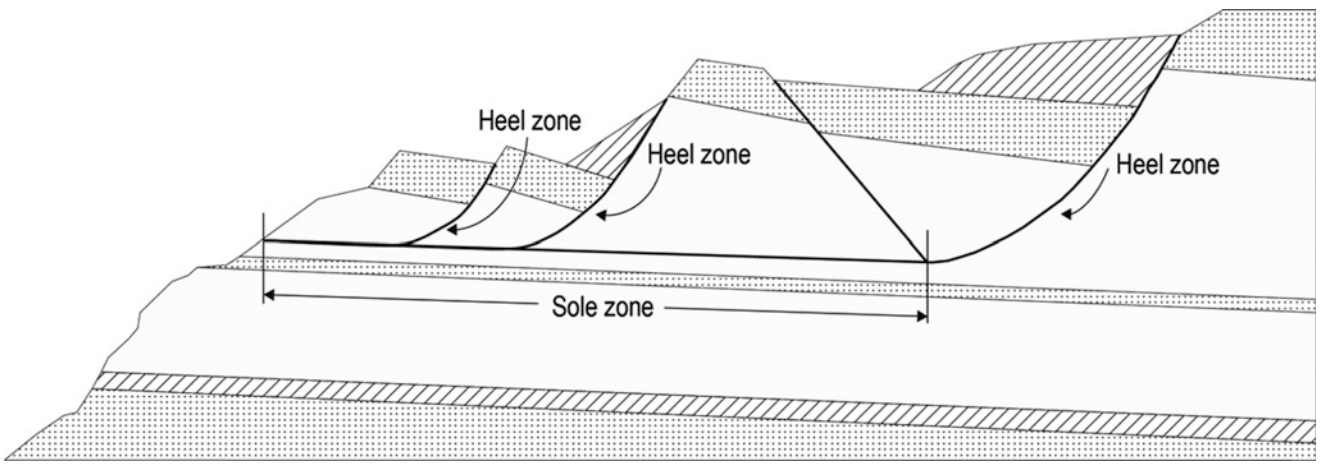

Fig. 2 Example is the compound slide at Jordan Cliff, Dorset (Stability of slopes by Bromhead)

The back analysis results from a compound landslide relates closely to the residual shear strength of the weak basal bed, but not exactly. The reason for this is that a uniform shear strength is assumed in the "heel" zone (Fig. 2), the "sole", and where present, the "toe", whereas the "heel" and the "toe" are probably running through a stronger material. Inaccuracies occur partly because of errors in the estimation of groundwater pressures, and partly – but commonly – from the errors resulting from treating the landslide in two dimensions not three.

The back analysis results in the literature fall into several classes. The best data values for the purpose of this survey are

listed numerically in the source papers, and are published with an account of the on-site investigations into the geometry of the slip, and the corresponding piezometric conditions. Some accounts simply list the equivalent ϕ'_r value, without the corresponding mean stresses, or show the points on a low-resolution graph (Chandler 1977, 1982b). We have extracted these results as accurately as we are able. There are number of case records published where there is an accurate cross section, complete with piezometric data, but no analyses. In a continuation of the project we hope to analyse these cases, but for reasons of brevity and auditability, we have confined ourselves to published data values for this paper. Equally frustrating are the numerous cases that we are aware of, but which remain unpublished, or where publication does not extend to the analyses. Landslides in Britain relate to strata as old as the Carboniferous.

Criticism of the Published Back-Analyses

London Clay (150 m Thick)

London Clay outcrops mainly along extensive lengths of both sides of the Thames Estuary, and in the London area, but to a lesser extent in the Hampshire Basin, and for extremely short lengths on the Isle of Wight.

James' (1970) analyses of slides in railway cuttings have surveyed profiles, slip surface locations and shapes established from instruments and direct observations – sometimes during remediation. However, the piezometric levels are usually obtained from very few instruments, of the "standpipe" type, and where the piezometric data were lacking, an average pore pressure ratio (r_u) equal to 0.3 was assumed. Undoubtedly, the assumption of a high pore pressure ratio leads to high back analysed ϕ'_r, and where the slides occurred before full equalisation of initially undrained piezometric conditions has took place, then this is the source of some error. Furthermore, the slides commonly are not very laterally-extensive, and a three-dimensional effect (where in particular the analyses are done on a principal, or centreline, section) again leads to a small overestimate of ϕ'_r.

The dataset does contain a few results from shallow "solifluction" type landslides, notably at Hadleigh Castle (Hutchinson and Gostelow 1976; Skempton 1977).

The Herne Bay analyses (Bromhead 1978) provided at one time the main corpus of high stress-level data for the London Clay (Dunbaven 1980). The analyses are of three coastal landslides. Of these, the Miramar landslide is the one with the most "bedding control". It is also wide laterally, so 3-D effects are small. The topography for all three landslides is good, the slip surfaces are well-identified, and the piezometric conditions are not only determined through multiple piezometers, but they are to some extent (especially in the case of the Miramar landslide) controlled by the proximity of the underlying Oldhaven Beds (Lambeth Group). However, the Queen's Avenue and Beacon Hill landslides are not laterally-extensive, and there is a possible 3-D effect there (explored briefly by Bromhead et al. 2001). Furthermore, the Beacon Hill landslide extends significantly under the foreshore, and in retrospect, the pore pressures used for this zone are probably overestimated.

The stability analyses for the landslides at Warden Point, Isle of Sheppey, have even better piezometric data, good topography and slip surface positioning. Like some of the Miramar slide analyses, an effort has been made to back-figure the pore pressures through time, and thus to provide data for stages in the evolution of the landslide for which a profile, but no directly measured piezometric conditions, were available. Some of the residual strength data appears in papers that do not, at first sight seem to relate to residual strength. An example of this is Skempton and Petley (1967).

Gault (45 m Thick)

The Gault Clay outcrops (as shown by Hutchinson et al. 1980) along two "ribbons" on the geological map, and at the coast at Folkestone, Eastbourne, and the south of the Isle of Wight. It is present on Dorset's "Jurassic Coast" in the upper parts of cliffs, but facies changes lead to it not forming important landslides. High effective stress level data comes from the deep-seated landslides at Folkestone and the Isle of Wight – the former being published in detail, and the latter not so well. In order to extend the dataset slightly, we have included the back analysis for the St Catherine's Point landslide (Hutchinson et al. 1991; Hutchinson and Bromhead 2002), the basal shear of which follows a clay bed in the Sandrock series, which is stratigraphically beneath the Gault. This clay is similar in appearance and plasticity to the Gault, and is close stratigraphically.

The analyses for small landslides tend to come from shallow, topographically controlled landslides. Several of the examples were disturbed slopes reactivated by excavations associated with motorway construction. There does not seem, in general, to be a body of case records for landslides in highway or railway cuttings similar to that for the London Clay, although the controlled slope failure at Selborne (Cooper et al. 1998) was effectively of that type.

The largest landslide in Gault is Folkestone Warren, and back analyses are presented by Hutchinson (1969) and Hutchinson et al. (1980). The latter paper took the opportunity to correct some misinterpretations in the earlier paper, notably in the inclusion of a large "first time" element of failure on one of the sections, and in an averaging procedure.

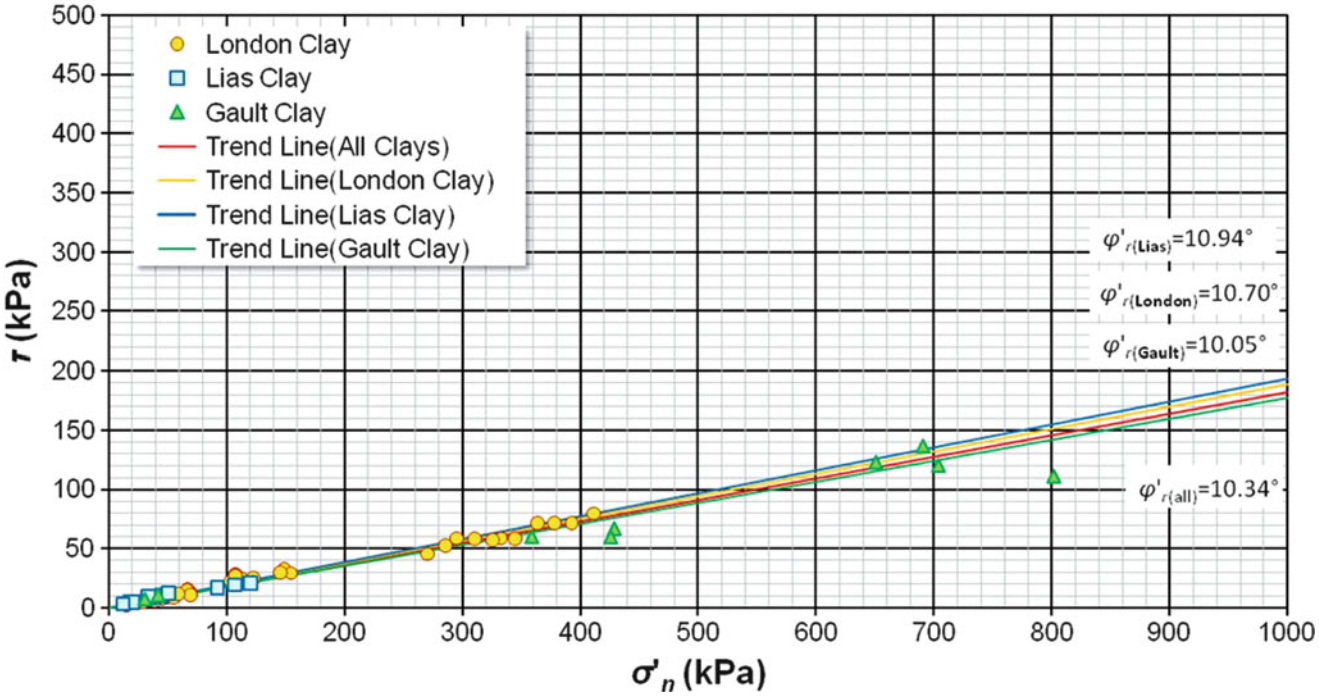

Fig. 3 The best fit straight lines through the origin for each set of data

However, the main sections are limited to the western part of the Folkestone Warren landslide. Moreover, it is likely that the construction of drainage adits has had an effect on the pore pressure conditions used in the analyses.

An extension of the analyses at Folkestone Warren to back-analyse the cross sections after the large displacement failures may have underestimated the "overshooting" caused by the failure of part of the rear scarp.

Lias (>250 m Thick)

In this paper "Lias" is used as a shorthand name for the late Triassic–early Jurassic clays and limestones forming the lower part of the very extensive Lias Formation that outcrops on the English coast in Dorset and Yorkshire, and stretches in a broad band across central England. It is also present, but to a lesser degree, in south Wales and western Scotland, as well as in parts of northern Europe. On the Dorset coast the Lias exhibits alternating bands of limestone and weak mudstone. Where these limestones are widely spaced, the mudstones are weak enough to permit the development of landslides in coastal cliffs and inland slopes. Investigations in the coastal cliffs at Lyme Regis show that the landslides are controlled in shape by weak beds in the sequence; inland, in the English Midlands, this is less evident, and shallow mudslides following the terrain slope are evident (Chandler et al. 1973), although occasionally, bedding-control is evident in deeper-seated landslides (Chandler 1979).

Back analysis of failed Lias clay slopes in the English Midlands (Chandler 1971, 1976) has concentrated on shallow reactivated mudslide remnants of periglacial origin, as many of the larger slides on the Dorset coast have not been subject to detailed sub-surface investigation, and although numerous records of the investigations in the Lyme Regis area have been published, these do not extend to the engineering analyses. The Lias is a rather thick sequence, with great variability in its lithologies. Work is in hand to re-analyse the slopes at Lyme Regis, and this new data will appear when completed. However it would be out of place to insert new results in the graph (Fig. 3) which comprises exclusively already published data.

Results

The three datasets can be analysed independently or together. The best fit straight lines through the origin for each set have the following slopes (see Table 1 and Fig. 3 and indicating the best estimate for ϕ'_r):

Indeed, the main outlier data points seem to be those for the Folkestone Warren sections, using both (a) the minimum piezometric levels, and (b) the after (or "post-") sliding profile (after the major, large displacement, landslide of 1915). Reflection on the groundwater conditions (e.g. Bromhead and Ibsen 2007) renders it highly improbable that this is a realistic interpretation of the piezometric levels operating. Without those outliers, the three datasets are indistinguishable to the unaided eye when plotted on the same graph.

Table 1 ϕ'_r value, number of points and r^2 for three different clays

Clay	ϕ'_r	No. of points	r^2
London clay	10.70	44	0.985
Gault clay	10.05	9	0.928
Lias clay	10.94	11	0.971
All	10.34	64	0.971

Interpretation

The British clays are dominated by illitic and chloritic minerals, with small and variable contents of smectite and kaolinite. In a few cases, the beds containing the basal shear surfaces are observed to have subtly different colour, or noticeably different plasticity to adjacent material (e.g. in the Barton Clay (Barton and Garvey 2011); in the Atherfield Clay in South Kent (Bromhead et al. 1998), or at Folkestone Warren (Hutchinson et al. 1980)), but mainly, the "slide prone horizon" (Hutchinson and Bromhead 2002) is indistinguishable except by very careful sampling and testing. Nature, however, finds these slide prone horizons easy to detect.

Bromhead (2007) speculated publicly that they may well be the results of small additions of volcanic ash at the time of deposition: these ashes weather to smectites, and could be a mechanism for producing very localised effects, but given the distance to likely ash sources, they are unlikely to produce thick deposits (although one such is known from Walton on the Naze).

Generally, however, smectites evolve into illite and chlorite, so there is little difficulty in seeing why those minerals dominate: not only are they a maturation product, but also there is some evidence of "recycling", where the erosion of some older strata creates the sediment supply for younger. This process today is putting all of the British clays into new sediments, much as Italian clays are being deposited, for example, in the Adriatic, where Niedoroda et al. (2005) has reported the accumulation of c 50 m of clayey sediments in places since the recovery of sea level after the LGM (i.e. in the past 22 ka, and most probably, in the past 10 ka or so).

The mean figure from all three datasets is likely to be the effective lower bound for the residual shear strength of a dominantly illitic clay, containing sufficient smectite to distinguish it from the adjacent material, but insufficient to give it smectite properties. The rather stronger adjacent materials demonstrate the (unquantifiable) effects of silt and sand content, and of the various cementitious minerals such as calcite, gypsum and various iron compounds.

This paper is concerned with a small number of research questions, and it attempts to provide answers not by the collection of new, primary, data but instead by reviewing a corpus of already published data. We find that, at a practical, engineering, level, the residual shear strengths of these three strata appear to be the same. This leads us to conclude that the hypothesis above is likely to be correct.

Future work

Work is in hand to provide an analysis for every published section for which data from back analysis is not available. However, for this paper, and to permit the logic of its analyses to be audited, we have used exclusively the published data. We are aware that some of the information is duplicated (for example, the "Misc Cut Slopes" of (Bromhead 2004) are known to be a subset of James's (1970) data), and where possible, we have "weeded out" known duplicates.

None of the other strata for which data points and case records are available are as comprehensive as for the three strata dealt with in this paper, nor are they so consistent internally or with each other. A future paper will include details for all cases available to us, and will contain new back analyses done by us where the available sources permit.

While British clays are dominated by illite, a small number of strata are dominated by smectites. This may even be true of the Fuller's Earth of Jurassic age, but certainly includes examples from the Panama Canal (Lutton and Banks 1970), from western Canada (Cruden et al. 1991) and Japan (Gibo et al. 2002). Preliminary indications are that the latter class also cluster closely around a single value for ϕ'_r.

References

Barton ME, Garvey PM (2011) Reactivation of landsliding following partial cliff stabilisation at Barton-on-Sea, Hampshire. QJEGH 44 (2):233–248

Bayley MJ (1972) Cliff stability at Herne Bay. Civ Eng Public Works Rev 67:788–792

Bromhead EN (1978) Large landslides in London clay at Herne Bay, Kent. QJEGH 11:291–304

Bromhead EN (2004) Reflections on CH Gregory's new cross landslide of 1841. In: Paper presented at the advances in geotechnical engineering: the Skempton conference, London, pp 803–814

Bromhead EN (2005) Geotechnical structures for landslide risk reduction. In: Glade T, Malcolm GA, CM J (eds) Landslide hazard and risk. Wiley, New York, pp 549–594

Bromhead EN (2007) Unpublished keynote lecture at 200th anniversary conference of the Gelogical Society of London

Bromhead EN, Dixon N (1983) The field residual strength of London clay and its correlations with laboratory measurements, especially ring shear test. Géotechnique 36(3):449–452

Bromhead EN, Ibsen M-L (2007) Folkestone Warren landslide and the impact of past and future rainfall. Paper presented at the landslides and climate change – challenges and solutions, Isle of Wight, pp 17–24

Bromhead EN, Hopper AC, Ibsen M-L (1998) Landslides in the Lower Greensand escarpment of south Kent. B Eng Geol Environ 57 (2):131–144

Bromhead EN, Fourlas G, Zemichael A (2001) Applications of 3D slope stability analysis. Paper presented at the geotechnical engineering: meeting societies' needs, Hong Kong, pp 685–690

Chandler RJ (1969) The effect of weathering on the shear strength properties of keuper marl. Géotechnique 19(3):321–334

Chandler RJ (1970) A shallow slab slide in the Lias clay near Uppingham, Rutland. Géotechnique 20(3):253–260

Chandler R J (1971) Landsliding on the Jurassic escarpment near Rockingham, Northamptonshire. In: Brunsden D (ed), Institute of British geographers, vol 3, special publication, London, pp 111–128

Chandler RJ (1976) The history and stability of two clay slope in the upper Gwash valley, Rutland. Philos T Roy Soc A 283:463–491

Chandler RJ (1977) Back analysis technique for slope stabilization works: a case record. Géotechnique 27(4):479–495

Chandler RJ (1979) Stability of a structure constructed in a landslide. In: Proceedings of the 7th European conference on soil mechanics and foundation engineering, vol 3, Brighton, pp 175–182

Chandler RJ (1982a) Recent European experience of landslides in overconsolidated clays and soft rocks. Paper presented at the proceedings of the 4th international symposium on landslides, Toronto, pp 61–81

Chandler RJ (1982b) Lias clay slope sections and their implication for the prediction of limiting or threshold slope angles. Earth Surf Proc Land 7(5):427–438

Chandler RJ, Pachakis M, Mercer J, Wrightman J (1973) Four long-term failures of embankments founded on areas of landslip. QJEGH 6(August):405–422

Cooper MR, Bromhead EN, Petley DJ, Grant I (1998) The Selborne cutting stability experiment. Géotechnique 48(1):83–101

Cruden DM, Thomson S, Hoffmann BA (1991) Observation of Graben geometry in landslides. Paper presented at the the international conference on slope stability, Isle of Wight, pp 33–36

Dixon N, Bromhead EN (2002) Landsliding in London clay coastal cliffs. QJEGH 35(4):327–343

Dunbaven M (1980) Discussion on large landslides in London clay at Herne Bay. QJEGH 13:63–65

Gibo S, Egashira K, Ohtsubo M, Nakamura S (2002) Strength recovery from residual state in reactivated landslides. Géotechnique 52 (9):683–686

Haefeli R (1948) The stability of slopes acted upon by parallel seepage. Paper presented at the proceedings of the second international conference on soil mechanics and foundation engineering, Rotterdam, pp 57–62

Hutchinson JN (1969) A reconsideration of the coastal landslides at Folkestone Warren, Kent. Géotechnique 19(1):6–38

Hutchinson JN, Bromhead EN (2002) Keynote Paper: Isle of Wight Landslides. Conference on instability. Paper presented at the conference on instability, planning & management, pp 291–298

Hutchinson JN, Gostelow TP (1976) The development of an abandoned cliff in London clay at Hadleigh, Essex. Philos T Roy Soc A 283:557–604

Hutchinson JN, Bromhead EN, Lupini JF (1980) Additional observation on the Folkestone Warren landslides. QJEGH 13 (1):1–31

Hutchinson JN, Bromhead EN, Chandler MP (1991) Investigations of the landslides at St Catherine's Point. Paper presented at the slope stability engineering, Isle of Wight, pp 169–179

James PM (1970) Time effects and progressive failure in clay slopes. Ph.D., Imperial college, London University

Lutton RJ, Banks DC (1970) Study of clay shale slopes along the Panama canal. Waterways experiment station technical, report S-70-9, p 285

Morgenstern NR, Price VE (1965) The analysis of the stability of general slip surfaces. Géotechnique 15(1):79–93

Niedoroda AW, Reed CW, Das H, Fagherazzi S, Donoghue JF, Cattaneo A (2005) Analysis of a large-scale depositional clinoformal wedge along the Italian Adriatic coast. Mar Geol 222–223:179–192

Skempton AW (1964) Fourth Rankine lecture: long-term stability of clay slopes. Géotechnique 14(2):77–102

Skempton AW (1977) Slope stability of cuttings in brown London clay. Paper presented at the 9th international conference on soil mechanics and foundation engineering, Tokyo, pp 261–270

Skempton AW (1985) Residual strength of clay in landslides, folded strata and laboratory. Géotechnique 35(1):3–18

Skempton AW, Delory A (1957) Stability of natural slopes in London clay. Paper presented at the 4th international conference soil mechanics and foundation engineering, London, pp 378–381

Skempton AW, Petley DJ (1967) The strength along structural discontinuities in stiff clay. Paper presented at the geotechnical conference, Oslo, pp 29–46

Gravitational Processes in the Eastern Flank of the Nevado de Toluca México

José Fernando Aceves-Quesada, Víctor Manuel Martínez Luna, and Gabriel Legorreta Paulín

Abstract

Landslides in volcanic mountainous terrains covered by poorly consolidated materials are common in Mexico. This investigation illustrates the landslides and geomorphologic changes of debris flow deposits in the town of Santa Cruz Pueblo Nuevo, State of Mexico, by using a multicriteria analysis in Geographic Information Systems (GIS) to obtain a potential hazard map.

The volcano has the fourth-highest elevation in Mexico (4,662 m a.s.l.) and it is in the geologic province of the Transmexican Volcanic Belt in the center of Mexico. The volcano is prone to landslides due to its loose vulcanoclastic sediments that are dragged by the streams and torrents during the rainy season. The basin extends from the rim of the volcano to the foothills at an altitude of 2,850 m a.s.l.

Unstable areas are mainly along first-order tributary streams and meander bends developed on lahars, pyroclastic flows, and pumice fall deposits whose stability has decreased in the basin. The unstable areas frequently create debris flows and debris slicing affecting the human settlements. On June 24, 1940, a large debris flow partially destroyed the town of Santa Cruz Pueblo Nuevo. Today, the town is settled in the alluvial fan of the old debris flows deposit. It is a highly probable that the town will be affected again by landslides and debris flows. As a prevention to future debris flow, have been constructed walls of containment (gabions) along the principal channel of the river La Ciénaga, nevertheless in every rainy season the gabions are saturated and frequently destroyed, which shows the intense activity of the remove gravitational processes.

Keywords

Landslides inventory map • Modeling • Multicriteria Evaluation • Nevado de Toluca Volcano

Introduction

In Mexico, volcanic regions are common and prone to landslides and debris flows along the stream systems. These slope failures create a potentially hazardous situation for people and property down the valleys. The basin of La Cienaga is located on the eastern flank of the Nevado de Toluca Volcano (NTV). This volcano, located in central Mexico, is a large stratovolcano with an explosive history, and the fourth highest mountain in Mexico (4,662 m.a.s.l). The highest point is the Fraile Peak with 4,660 m.a.s.l. and

J.F. Aceves-Quesada • V.M.M. Luna
Departamento de Geografía Física, Instituto de Geografía, Universidad Nacional Autónoma de México, Circuito Exterior,Ciudad Universitaria, México, Coyoacán, D.F 04510, Mexico

G. L. Paulín (✉)
Laboratorio de Análisis Geo-espacial, Instituto de Geografía, Universidad Nacional Autónoma de México, Circuito Exterior, Ciudad Universitaria, México, Coyoacán, D.F 04510, Mexico
e-mail: legorretag@igg.unam.mx

C. Margottini et al. (eds.), *Landslide Science and Practice*, Vol. 1,
DOI 10.1007/978-3-642-31325-7_28,

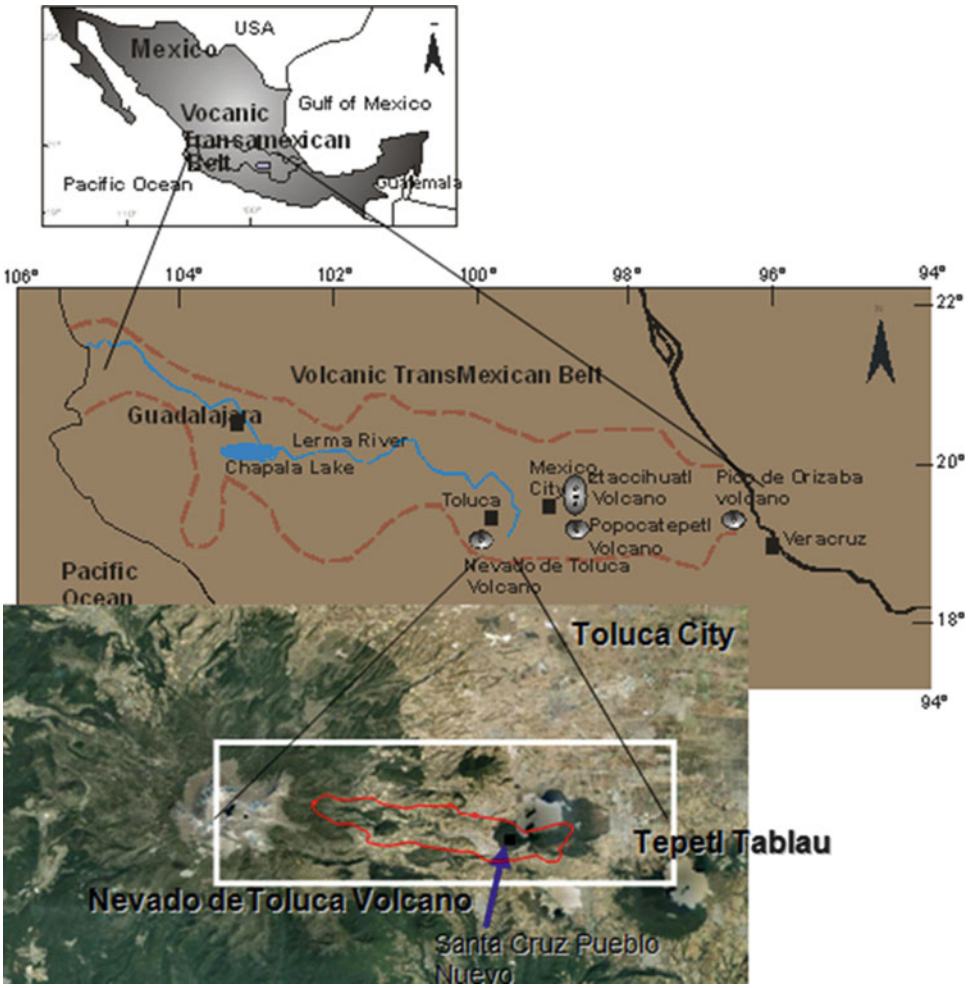

Fig. 1 Localization map

de lower point is in the Toluca Valley at 2,650 m.a.s.l. The volcano lies in the southeastern part of the Toluca Basin, 70 km east of Mexico City. The volcano is mainly composed of pyroclastic flows, lahars, debris avalanches and pumice falls. The slope (Fig. 1) is a large piedmont composed of coalescent fans of pyroclastic materials, landslides deposits, and alluvial sediment. The ravines along the volcano east flank are long, narrow, and deep (100–300 m). The heads of these ravines start in old glacial cirques and continue downstream forming a long dendritic drainage system. The slope is 20–35° in the elevated portions while in the piedmont it is 6–12° (Aceves-Quesada et al. 2007a).

The town of Santa Cruz Pueblo Nuevo is located in the Municipality of Tenango del Valle (in the State of Mexico). It has 1,098 inhabitants is located at 2,880 m.a.s.l., and is settled on the alluvial fan of the river la Ciénaga (Fig. 1). This fan is composed of old debris flows and lahar deposits. On June 24, 1940 a torrential rain triggered a large debris flow that destroyed the town. The mean annual precipitation is high (1,200–1,100 mm/year at > 4,000 m.a.s.l), with temperature between −2 °C to 12 °C -E(T)H-, and 1,100 to 800 mm/year at elevations between 2,650 and 4,000 m.a.s.l. (García-Enriqueta 2004), the bulk of which falls as rain during seasonal storms in summer.

The objective of this project is to identify areas prone to landslides and debris flows in La Ciénaga basin by applying a geomorphologic cartography and multi-critiria analysis.

In this proceeding we show the first results obtained from the geomorphologic analysis.

Justification

- The town of Santa Cruz Pueblo Nuevo has a potentially landslide hazardous situation.

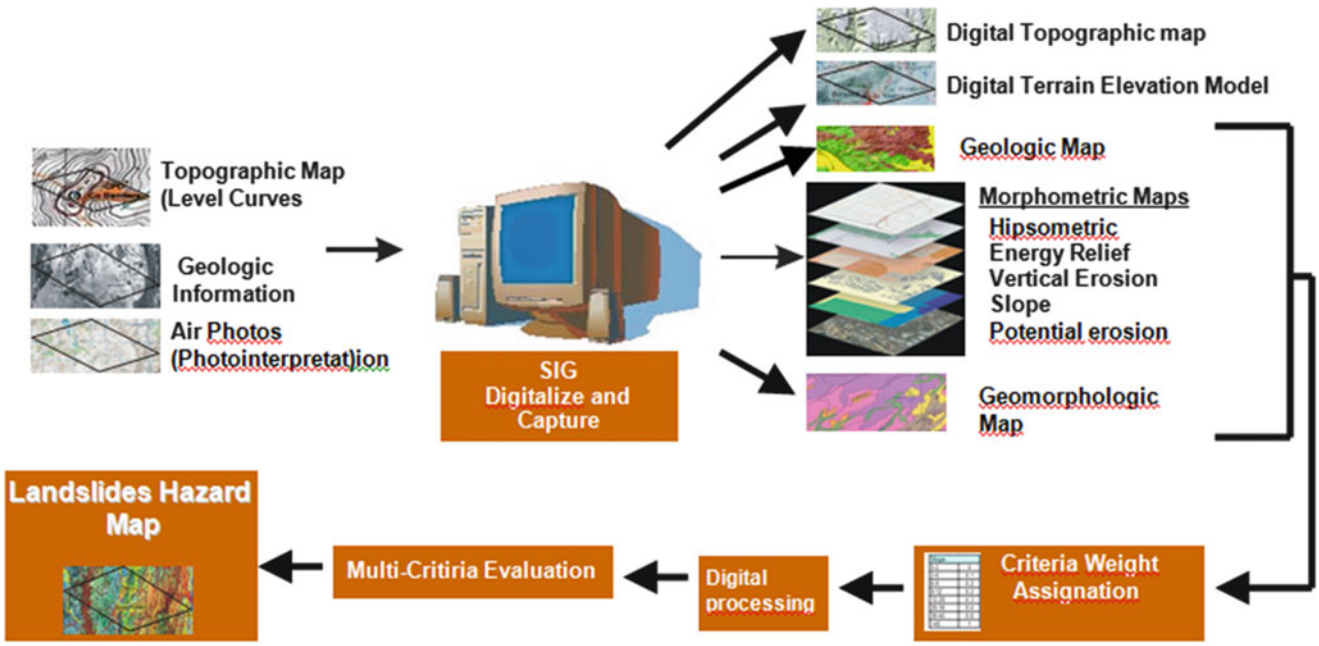

Fig. 2 Methodology diagram flow

- More than 1,000 inhabitants are living within a fan composed of old debris flows deposits.
- On June 24, 1940 a torrential rain triggered a large debris flow that destroyed the town.
- Santa Cruz Pueblo Nuevo inhabitants do not seem aware or ignore the risk of debris flows. No preventive measures have been taken by the local inhabitants or the authorities to restrict further building in hazard zones.
- There is a lack of landslide inventory maps.
- No practical methodology to map landslide susceptibility has been established in this area with scarce information.

Goal

The goal of this project is to applied a geomorphologic cartography and Multicritiria Evaluation for La Ciénaga basin to identified areas that prone to landslides and debris flows.

Methodology

The methodology encompasses four main steps of analysis

Step 1: Gathering the basic information and create new thematic GIS information layers.

- Paper geologic and topographic base maps at a scale of 1:50,000 were obtained. The information was georeferenced and incorporated into the ILWIS GIS.
- Digital elevation and slope data (resolution 10 m) from topographic map was obtained.

Step 2: Using GIS, photo interpretation, and fieldwork geology, morphometric and geomorphology cartography is elaborated. Six maps were elaborated.

Step 3: Integrate in a GIS the obtained information and simultaneously assess groups, factors, and standardized and weighted constraints.

Step 4: Elaboration the potential hazard map applying Multicitiria Evaluation in the ILWIS GIS module that apply hierarchies heuristic decision rules in order to solve land-suitability problems (Fig. 2).

Geology

The study area is in the lower part of a small endorheic basin La Ciénaga on the eastern flank of Nevado de Toluca volcano (NTV). NTV in central Mexico is a large stratovolcano with an explosive history. Eruptions produced a complex sequence of pyroclastic deposits that have affected the area at least 18 times during the last 100,000 year. Thirteen eruptions (eight vulcanian, four plinian and one ultraplinian) and the destruction of at least three domes have all occurred in the last

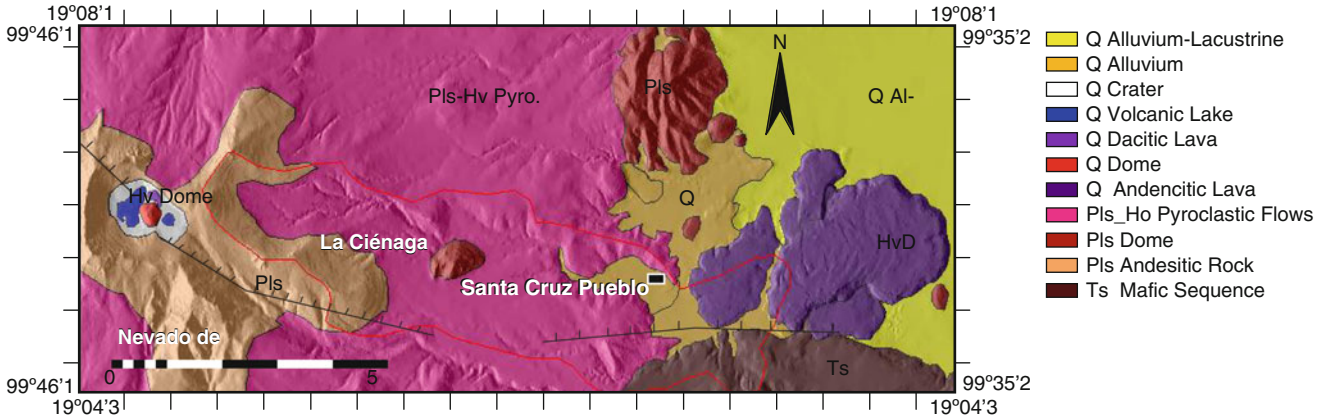

Fig. 3 Geologycal map

42,000 year as well as two sector collapses in the last 100,000 year. NTV rises 2,100 m above the upper basin of the Lerma River, and 3,100 m above Ixtapan de la Sal and Tonatico. The summit was destroyed by the 10,445 ± 95 year eruption. The reconstructed height for NTV by slope reconstruction was 5,000 and 5,050 m a.s.l and with morphoisohipses was 5,080 m a.s.l. The volcano was built upon the intersection of three fault systems: Taxco-Queretaro (NNW–SSE), San Antonio (NE–SW) and Tenango (E–W). The North-eastern Slope is a large piedmont composed of coalescent fans of pyroclastic materials and landslides. Fluvial erosion has removed the recent sediments. To the east, the volcanic piedmont continues with active fans composed of pyroclastic materials and alluvial sediment. These ravines are deeper (100–300 m), start in old glacial cirques and continue through a long dendritic drainage. The slope is 20–35° in the elevated portions while in the piedmont it is 6–12° and I n the plain it is 2–6°. Pyroclastic flow deposits are widely spread around the volcano, filling the stream valleys. In the basin of La Ciénaga have an average thickness of 5 m; the maximum distance reached by these deposits is 12 km from the crater towards the eastern.

The block and ash flows form massive units interstratified with surge horizons and its covered by lahars. These deposits are related to dome collapses (Fig. 3).

Lahars at NTV are wide spread around the volcano filling new and old valleys. Lahars have rounded and subrounded dacite lithics (15–25 cm), small pumice fragments (<5 cm) fixed in a muddy-sand sized matrix. To the south, the lahar thickness is more than 30 m, but in the basin are less than 5 m. The oldest lahars are made up of rounded and subrounded gray and red andesite blocks fixed in red clay sized matrix with scarce pumice fragments. The recent deposits contain subangular and subrounded blocks of gray and red dacite, with pumice fragments, some of which is hydrated, fixed in a silt-clay sized matrix.

The flow direction of these lahars was controlled by the topography, principally deep tectonic, glacial and fluvial valleys. In distal areas, the lahar deposits were transformed into fluvial mixing with the stream and river waters. To the east, the lahars contain more pumice fragments in a pale brow silt-clay matrix. There is a lahar with large hydrated pumice fragments (20–30 cm) at the south-eastern of the la Ciénaga Basis. In this area, many secondary lahars exist, such as the one deposited in 1940. These secondary lahars are not related to volcanic activity and represent an increased hazard. On the top of this deposits are covered by ash falls and pumice falls. In the Ciénaga basin the most important deposit is the Upper Toluca Pumice, composed by the alternation of layers of thick and thin pumice with surges (in some places thicknesses are 7 m) (Aceves-Quesada et al. 2007b).

Results

Using the ILWIS GIS morphometric maps were elaborated: hypsometric, energy relief, vertical erosion map, slope and potential erosion. Geomorphological was digitalized in screen.

1. The *hypsometric map* was heuristically classify to highlight the volcanic landforms, the lower point located is 2,620 m a.s.l. in the basin of Toluca, and the higher is the Eagle peek at 4,660 m a.s.l. in the top of the Nevado de Toluca volcano (Fig. 4).
2. An *Energy Relief Map* was calculated by applying a filter.
3. This map represents the maximum elevation change within 1 hectare. The biggest differences, which represent the highest values, happen in the steep hillsides of the basin and the zones of ravines where there present to themselves more assets the processes of slides and rock falls (Fig. 5).
4. *A Vertical Erosion Map* was calculated by splitting the study area into boxes of 1 km^2, and the maximum vertical

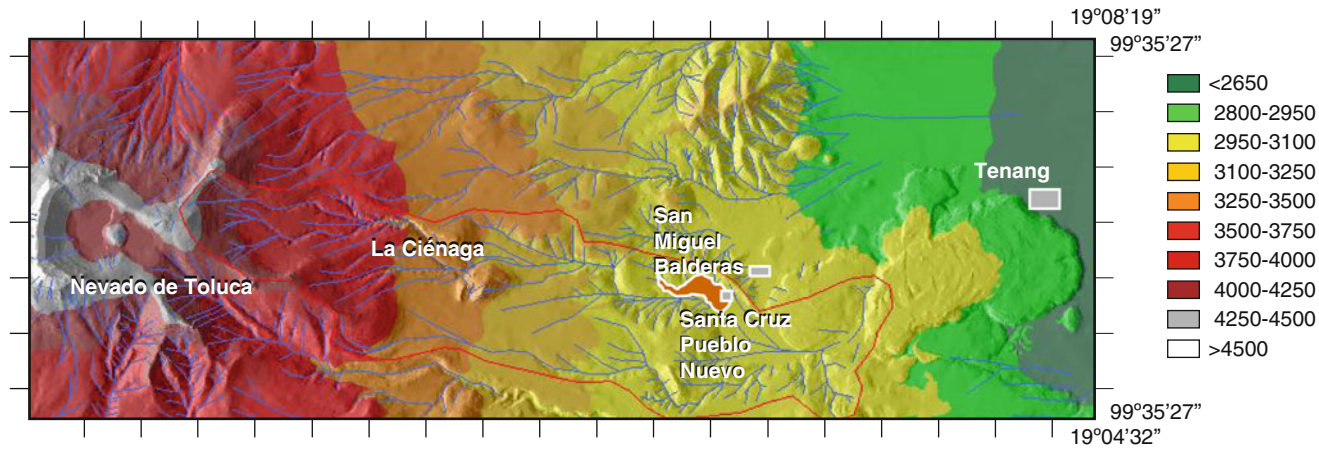

Fig. 4 Hipsometric map

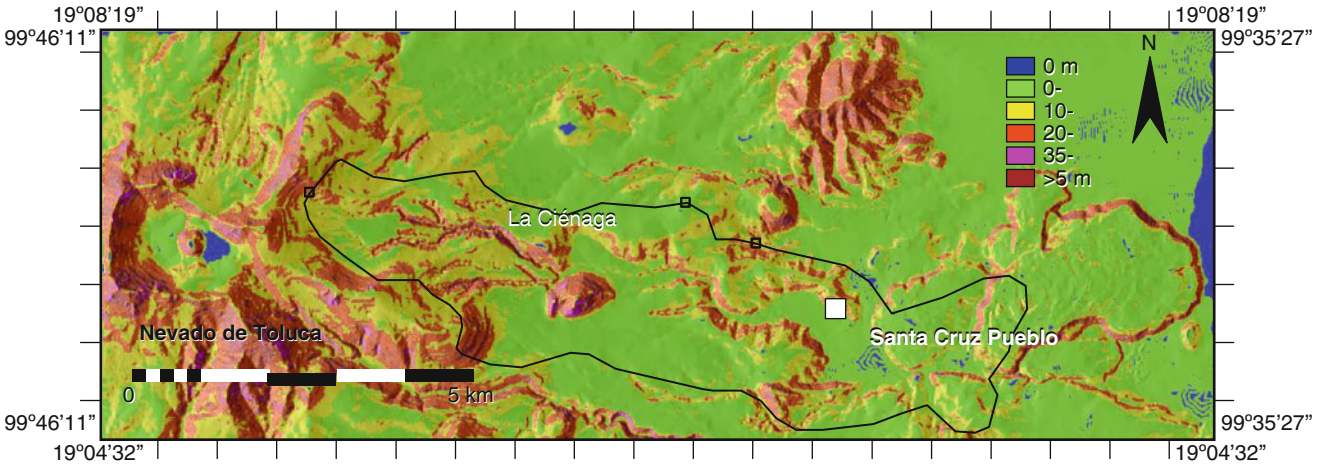

Fig. 5 Energy relief map

distance was obtained in each. The values obtained were interpolated by kriging. The map represents the average vertical height between the talweg and the watershed. In this map the values of major depth of ravines find inside the values from 100 to 150 m, which are located in the high average part of the basin represented by the orange colors (Fig. 6).

5. *A Slope map* was heuristically reclassified to highlight the difference in the relief. In this map we see that the values that to predominate in the basin are 12°, nevertheless inside the ravines the slopes can reach values of 20–45° (Fig. 7).
6. *The potential erosion* was obtained to reclassify the slope map, applying the recommendations of Palacio (1983) and Van Zuidam (1985) to define the zones prone to intensive erosion. In this the highest values of erosion it corresponds to the zone of the river bed. In this zone the values incremented by the slope and the poorly consolidated materials (Fig. 8).
7. *A Geomorphologic map* was heuristically derived by interpretation of aerial photographs, DEM, geology, and morphometric maps in order to highlight external and internal landform processes, to obtain the relevant forms in the basin (Fig. 9).

Muti-Critiria Evaluation and Landslide Hazard Map

A database has been built, classified and analyzed within a GIS environment; additionally, MCE aided hazard mapping, four morphometric maps (hypsometric, gradient, internal and potential erosion) were produced, and maps of geology and geomorphology (Table 1). These maps were obtained from hardcopies of thematic maps at 1:50,000 scale from the Instituto Nacional de Estadística, Geografía e Informática agency (INEGI), from air photography and from field work. This information generated a digital database that has been

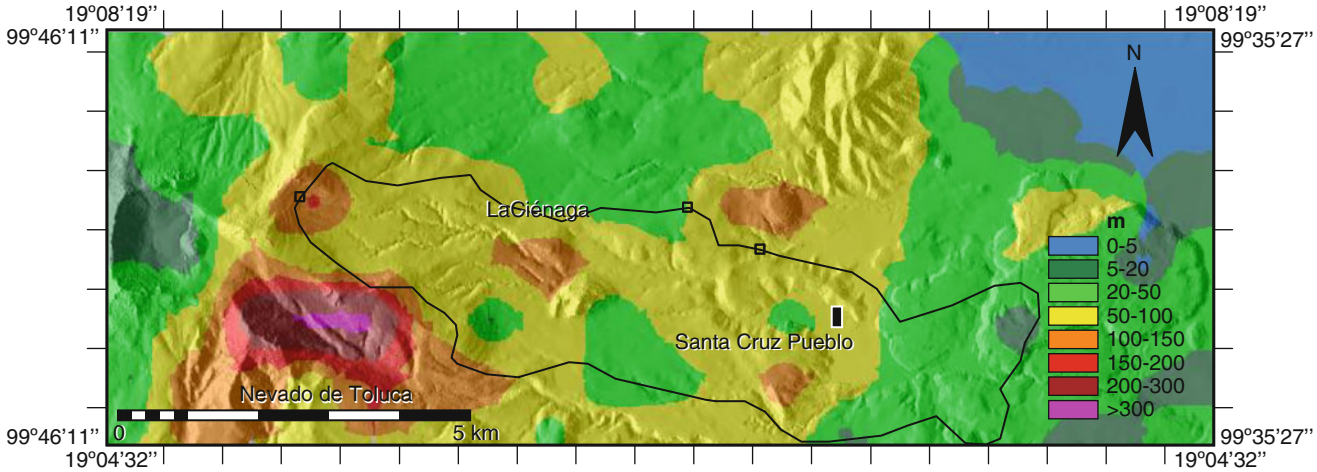

Fig. 6 Vertical erosion map

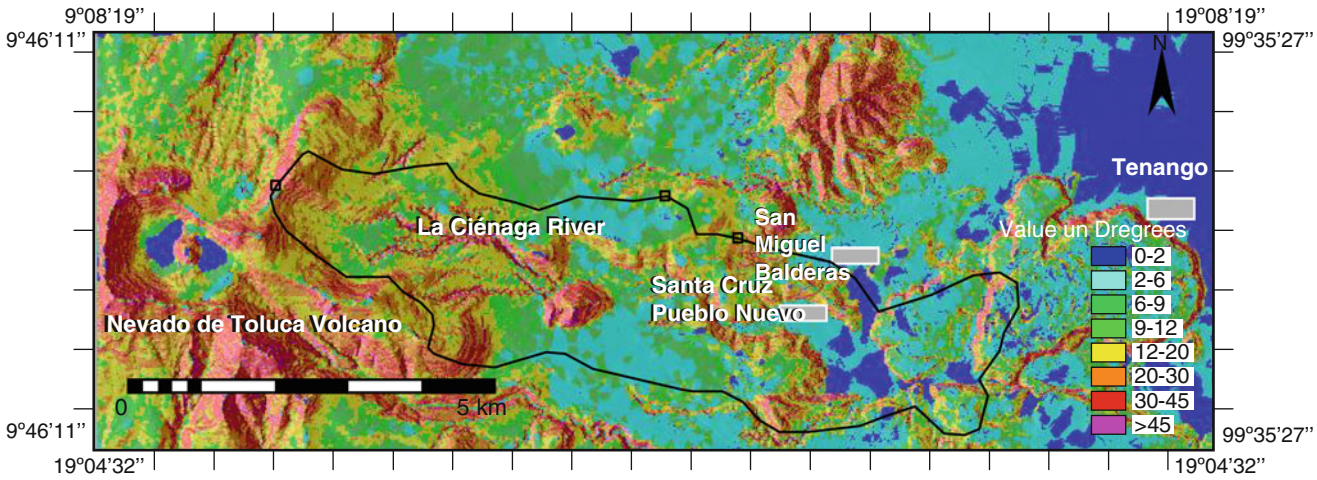

Fig. 7 Slope map

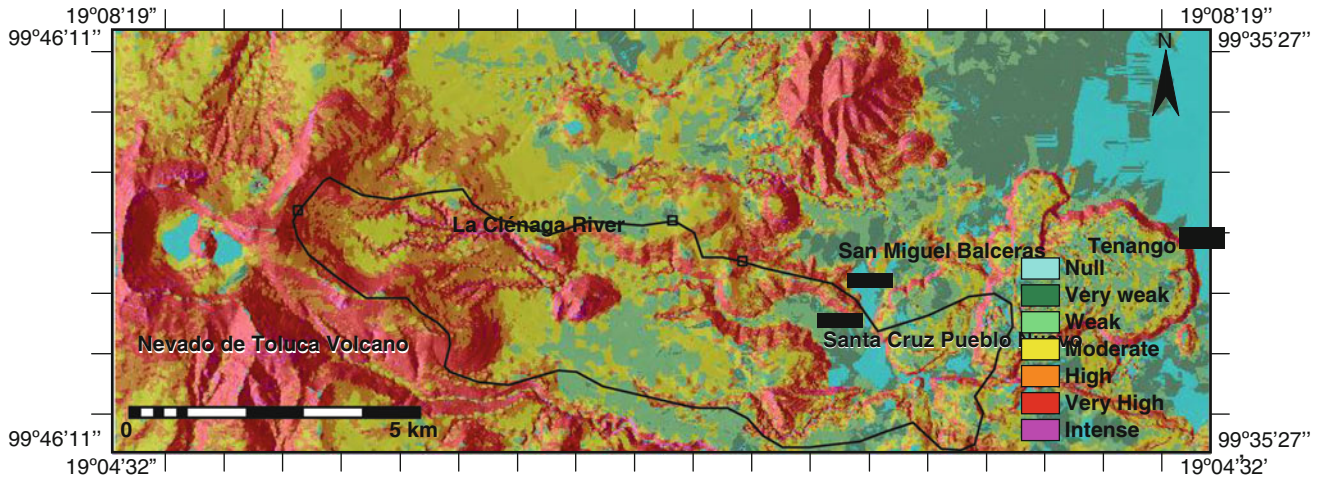

Fig. 8 Potential erotion map

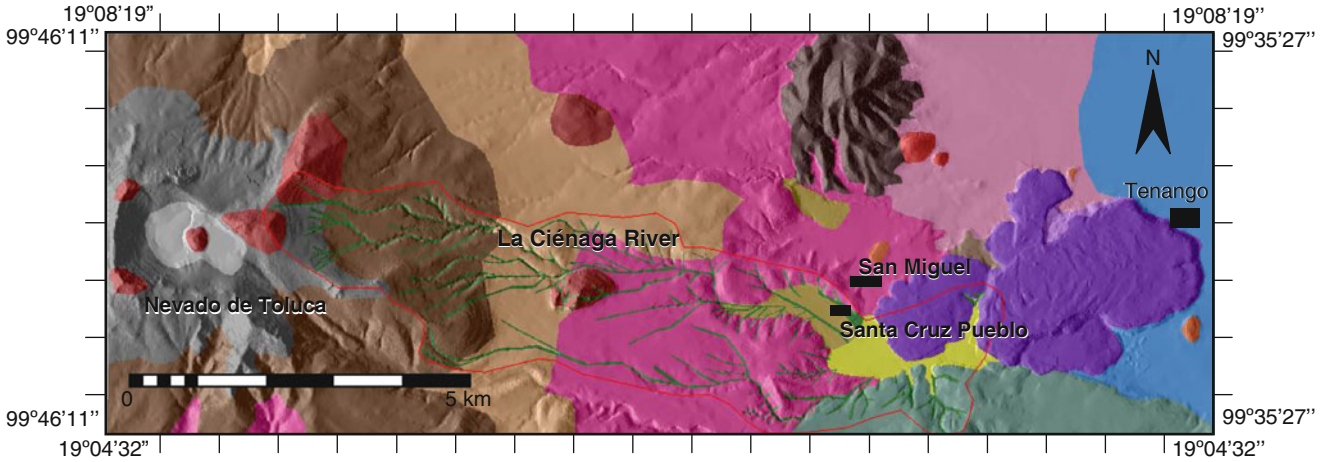

Fig. 9 Geomorphological map

Table 1 Weights for the alternatives (maps) using for the landslide hazard map

Alternatives	Weight
Geomorphology	0.408
Vertical erosion	0.200
Energy relief	0.200
Geology	0.103
Potential erotion	0.061
Slope	0.028

Table 2 Weights for the geology map

Geology	Weight
Q Alluvium-Lacustrine	0.2
Q Alluvium	0.6
Q Crater	0
Q Volcanic lake	0
Q Dacitic lava	0
Q Dome	0.3
Q Andencitic lava	0.1
Pls_Ho Pyroclastic flows	1
Pls Dome	0.4
Pls Andesitic rock	0.2
Ts Mafic sequence	0

Table 3 Weights for the internal relief map

Internal relief	Weight
0	0
0–10	0.1
10–20	0.2
20–35	0.3
35–50	0.6
>50	1

Table 4 Weights for the vertical erosion map

Vertical erosion	Weight
0–5	0
5–20	0.1
20–50	0.2
50–100	0.2
100–150	0.3
150–200	0.4
200–300	0.6
>300	1

Table 5 Weights for the slope map

Slope	Weight
0–2	0
2–6	0.1
6–9	0.2
9–12	0.2
12–20	0.3
20–30	0.4
30–45	0.6
>45	1

used to apply MCE. This method has been used to integrate in a Gis the obtained information and simultaneously assess a series of elements oriented towards a specific objective, applying decision rules, based on analysis, discussion and hierarchies of alternatives in order to make decisions on land-suitability problems. Based on the objective of evaluating the vulnerability associated with landslides hazards, a decision rule set was chosen and structured, which integrates the assessment and ranking criteria (in this case five) established from the outlined objective, and the selection of alternatives, represented by the spatial objects (pixels) contained in the thematic layers (digital maps).

Table 6 Weights for the geomorphology map

Geomorphology	Weight
Alluvial fan	0.0125
Alluvial plain	0
Alluvio-Lacustrine plain	0
Tephra plain	0
Buried Cinder cone	0.0125
Cinder cone	0.0125
Crater	0
Dome	0.0125
Stratovolcano	0.03125
Upper slope	0.0625
Lower slope	0.125
Lava hills buried by Tephra	0.03125
Lava hillslope	0
Lava plateu	0
Nevado de Toluca cone	0.0625
Pyroclastic hillslope	0.125
Volcanic Piedmont	0.0125
Gully	0.5

Table 7 Weights for the potential erosion map

Potential erosion	Weight
Null	0
Very weak	0.1
Weak	0.1
Medium – high	0.3
High	0.5
Very high	0.5
Intense	1

Thus, each criterion constitutes a thematic map in the GIS database, and in this phase, we understood the major importance for the total evaluation, of the factor selection process (criteria) in a consistent and objective way.

The MCE is based on integrating all criteria and alternatives in a pair-comparison matrix (PCM), where criteria are in the main column and alternatives in the main row, and in the inner cells punctuations derived from the assessment resulted from the expert's evaluation. These punctuations represent the value, preference level, degree of attraction or significance that each alternative has obtained in each criterion. This study is a first step towards more comprehensive researches on vulnerability assessment as input to determinate the landslides hazard on one of the highest volcanoes in Mexico (Aceves-Quesada et al. 2007a).

The most important factor determining the landslide hazard was the geomorphologic map, followed by the vertical erosion and the energy relief maps.

This study is a first step towards a more comprehensive research on assessing landslide hazard on one of the highest volcanoes in Mexico. The method applied here is an alternative procedure for the construction of risk-prevention maps in areas where information is scarce and of low spatial resolution.

By directly addressing the landslide characterization of the historical debris flows, local authorities in Mexico such as the civil protection agencies of the State of Mexico and other governmental organizations as well as the inhabitants will benefit with regard to landslide hazard mitigation and planning.

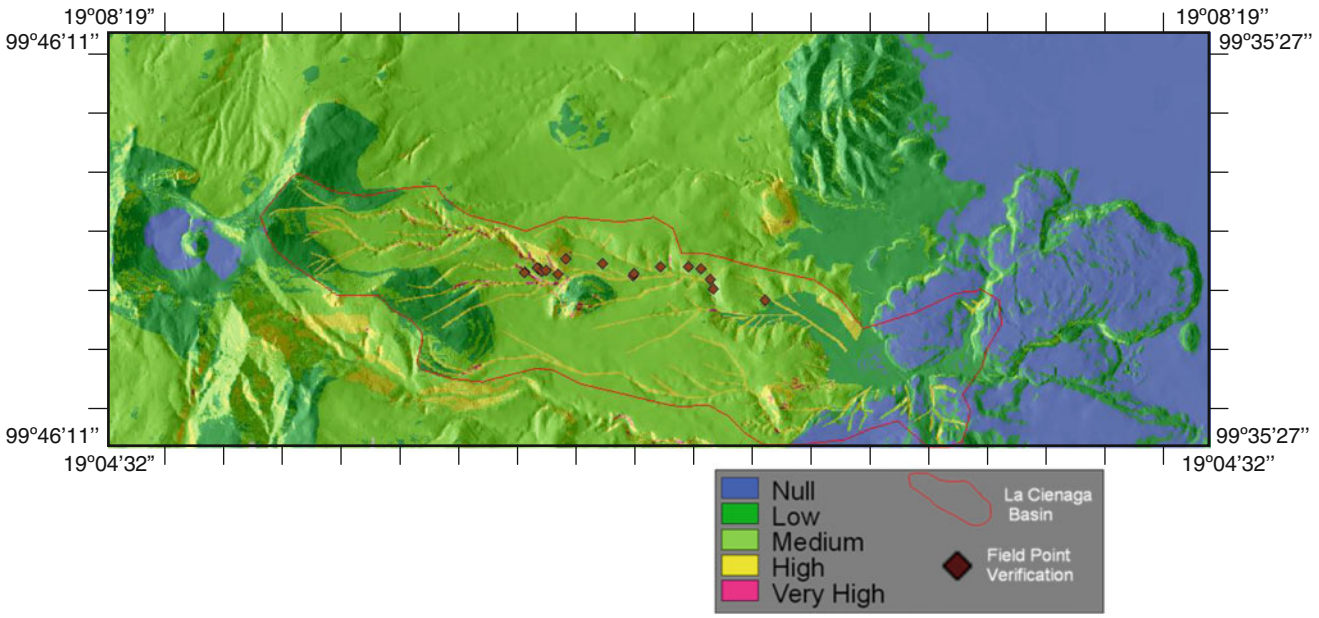

Fig. 10 Landslide hazard map

The information was Integrated in a GIS the obtained information and simultaneously assess groups, factors, and standardized and weighted constraints. Weighth values were assigned for the Multi-criteria Evaluation. The values were assigned in accordance with the importance of the factors to trigger landslides (Tables 2, 3, 4, 5, 6, and 7).

In this map the application of the Evaluation multi-criterion we see as the important zones that contribute the material that it goes away to deposit in the low part of the basin and that is a part of the fan it is along the river bed is located the critical points where so much the type of material, the morphology of the ravine, as the slopes, the vertical erosion and the energy of the relief present the highest values and therefore these spots in red color indicate the most unstable zones where the biggest number of slides appears throughout the year, this result happened in field (orange points in the maps) there being obtained a certainty of 75 % (Fig. 10).

Conclusions

The most important factor determining the landslide hazard was the geomorphologic map, follow by the vertical erosion and the energy relief maps.

This study is a first step towards a more comprehensive research about hazard landslides assessment in one of the highest volcanoes in Mexico.

The methodology applied here is an alternative procedure for the construction of risk-prevention maps in areas with a scarce and of low spatial resolution information.

By directly addressing the landslide characterization of the historical debris flows, local authorities in Mexico such as the civil protection agencies of the state of Mexico and other governmental organizations as well as the inhabitants will benefit with regard to landslide hazard mitigation and planning.

Acknowledgements The authors thank authorities from the International Consortium on Landslides (ICL) for their approval and help. This research was supported by the Programa de Apoyo a Proyectos de Investigación e Innovación Tecnológica (PAPIIT) de la modalidad de Iniciativa de Apoyo Complementario a la Realización de las Obras Determinadas (IB100412), UNAM, and the International Program on Landslides (IPL). We also acknowledge the assistance of of Yarummy Álvarez Ruiz.

References

Aceves-Quesada F, Díaz-Salgado J, López-Blanco J (2007a) Vulnerability assessment in a volcanic risk evaluation through a multi-criteria-gis approach in Central Mexico. Nat Hazards 40(2):339–356

Aceves-Quesada F, Martin del Pozzo AL, López-Blanco J (2007b) Volcanic hazards zonation of the Nevado de Toluca volcano, center of Mexico. Nat Hazards 41(1):159–180

García, Enriqueta (2004) Modificaciones al sistema de clasificación climática de Köopen: para adaptarlo a las condiciones de la República Mexicana. Enriqueta García (5ta Edición). México

Palacio-Prieto JL (1983) Metodología para el desarrollo de trabajos geomorfológicos a escala 1: 50 000 Primer Congreso del Instituto de Geografía. UNAM, pp 52–72

Van Zuidam RA (1985) Aerial photointerpretation in terrain analysis and geomorphologic mapping. ITC. Smits Publishers, The Hague, p 442

Causes of Small Scale Landslides in Flysch Deposits of Istria, Croatia

Željko Arbanas, Sanja Dugonjić, and Čedomir Benac

Abstract

In this paper we will present the overview of recent landslides in the Istria Peninsula, Croatia. The central area of the Istrian Peninsula is situated from the Trieste Bay in the west to the Učka Mountain in the east and is called Gray Istria according to gray colour of the Paleogene flysch sediments. Flysch rocks mostly consist of claystones, siltstones with intercalated calcareous sandstones and breccia-conglomerates. During the last two decades many small scale landslides occurred in the area. Based on field investigations conducted during remedial works designing, a data base of investigated landslides was established. Landslides in flysch slopes of Gray Istria are mostly rotational slides, falls and debris flows of small scale. The sliding surface is typically on the contact of the superficial deposits and flysch bedrock which is almost impermeable below the superficial deposits with low permeability. Due to the inconvenient geological conditions, long term intensive rainfall and anthropogenic influence mostly during road construction, the natural balance in the slope was disturbed, and instabilities occurred.

Keywords

Landslide • Flysch • Triggering mechanism • Rainfall

Introduction

This paper presents the overview of recent landslides occurring in the central and northern part of the Istrian Peninsula, so called Gray Istria, in the last two decades. The Istrian Peninsula is situated in the north-western part of the Adriatic Sea. The investigation area of 550 km^2 is situated from the Trieste Bay in the west to the Učka Mountain in the east, while in the northern part it borders on the Ćićarija Mountain range. In geological sense the area is formed in flysch rock mass deposits called Gray Istria due to gray color of the flysch rock mass.

Landslides in the area are relatively numerous, types and mechanisms of occurrence are similar, generally rotational and translational slides and falls. Debris flows were registered only at few locations. Landslide occurrences are mostly conditioned by an unfavorable geological setting and triggered by infiltration and groundwater level rising caused by heavy rainfall during relatively long periods of time prior to sliding.

A data base of investigated landslides in Gray Istria, made at the University of Rijeka, contains the basic information about the location, type, dimensions, and time of occurrence of the landslide, together with geotechnical properties of the soils and rocks and other relevant data. During the field investigations, it was determined that many slopes have been stable for a long time period before the sliding. Disturbance of a naturally established balance inside the slope generated by infiltration of a great amount of precipitation caused instabilities in most of the locations. Long rainy periods are crucial for sliding initiation. Infiltration of surface water is relatively slow due to the low hydraulic conductivity of clayey material in the superficial deposit. However the

Ž. Arbanas (✉) • S. Dugonjić • Č. Benac
Faculty of Civil Engineering, University of Rijeka, Viktora Cara Emina St. 5, 51000 Rijeka, Croatia
e-mail: zeljko.arbanas@gradri.hr

C. Margottini et al. (eds.), *Landslide Science and Practice*, Vol. 1,
DOI 10.1007/978-3-642-31325-7_29,

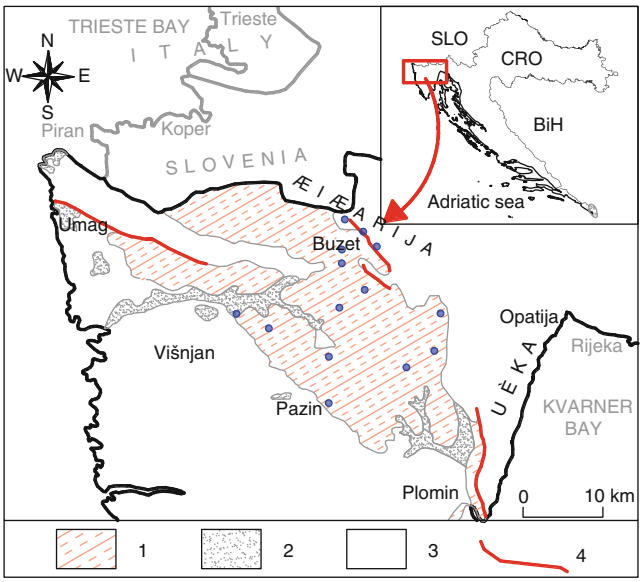

Fig. 1 Geological map of Gray Istria: *1* Paleogene flysch, *2* Alluvium, *3* Limestone, *4* Fault lines. *Blue dots* represent landslide locations

intensive, but short term rainfall considerably influences the erosion processes.

Geological Setting of the Gray Istria

From the geological point of view, the Istrian Peninsula can be generally divided into three geological units: area of the Red Istria situated in the southern and south-western part of the peninsula built in carbonate rocks and covered by the red colored deposits of Mediterranean soil, or so called *terra rossa*; area of the White Istria that covers the Ćićarija Mountain range and part of Učka Mountain with carbonate rocks visible in the surface; and Gray Istria area in the central part of the peninsula built in Paleogene flysch deposits (Fig. 1).

The flysch area is situated from the Trieste Bay in the west to the Učka Mountain in the east and on the contact with limestones of Ćićarija Mountain in the north (Fig. 1). The shelf is formed in the foraminiferal limestone; it's top, however, is located in the siliciclastic rocks with flysch characteristics. The bottom of the flysch series is lithologically mostly homogeneous and marly and the upper series is lithologically heterogeneous. It contains mostly claystones and siltstones with calcitic sandstones and breccia conglomerate interbeds (Velić et al. 1995).

The geological cross section (Fig. 2) of the investigated landslides mostly consists of two characteristic layers: colluvium and/or residual soil forming the superficial deposits and the bedrock formed in clastic Paleogene deposits, respectively flysch of different weathering grade (Arbanas et al. 2006). The cover is formed of clays with intermediate

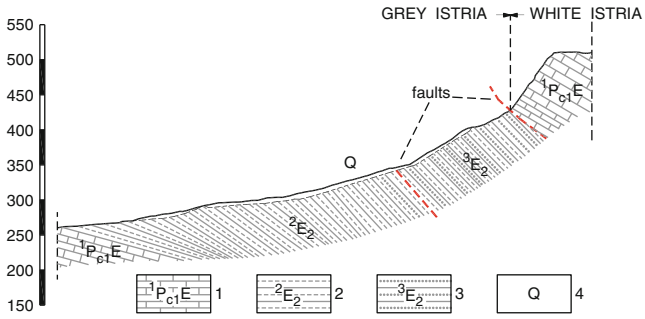

Fig. 2 Geological cross section on the landslide Krbavčići: *1* Paleogene limestones, *2* Paleogene marls, *3* Paleogene flysch, *4* superficial quaternary deposits (Arbanas et al. 2006)

Table 1 Dimension of characteristic landslides in the area according to Multilingual landslide glossary (WP/WLI 1993)

Landslide dim. (m)	Krbavčići (1979)	Drazej (2005)	Brus (2005)	Marinci (2006)	Juradi (2010)
L	242	48	208	23	63
L_d	240	45	142	21	55
L_r	220	25	142	20	60
W_d	55	50	37	15	150
W_r	45	49	37	14.5	145
D_d	10.0	4	8–10	2	8
D_r	12.5	8	10	8.5	11

(CI) to high (CH) plasticity, and semisolid to plastic consistency, depending on the water content. Residual soils are product of flysch rock mass weathering and consist of silty clays with low (CL) to high (CH) plasticity and without rocky fragments. It is possible to distinguish different flysch weathering grades over the geological cross section. From deeper layers to the surface of terrain one can find: fresh rock mass (F), slightly weathered (SW), moderately weathered (MW), highly weathered (HW), and completely weathered (CW) to residual soil (RS) (ISRM 1981). The slip surface was usually formed on the contact between the superficial deposit formed of residual soil (RS) or colluvium, and the completely weathered rock mass (CW) and layers of different weathering grade (from HW to F).

A typical cross-section on flysch slopes has two zones of different hydraulic conductivity: colluvium and flysch bedrock. Clayey and silty cover layers have low hydraulic conductivity while flysch rock complex in the bed can be considered as completely impermeable.

Properties of Landslides in the Area

Flysch deposits have heterogonous geotechnical properties and exposed to water and air a flysch rock mass is prone to chemical weathering and decomposition, especially leaching of $CaCO_3$ component, oxidation and swelling,

Fig. 3 Photo of the landslides in the area: (**a**) Juradi landslide, (**b**) Krbavčići landslide, (**c**) Krušvari landslide, (**d**) Drazej landslide, (**e**) Brus landslide, (**f**) Marinci landslide

which considerably affect changes in physical and mechanical properties. Chemical weathering is mostly expressed in fine-grained members, especially varieties of siltstones. Due to the mentioned processes, the flysch rock mass increases its volume in time, and disintegrates into silt or clay. By this gradual degradation physical and mechanical properties of clayey silt materials become more like engineering soil. Consequence of these geomorphological processes is a sporadic accumulation of eroded deposits on the slopes that can potentially be susceptible to sliding (Arbanas et al. 2007).

Landslides in the area generally overtake relatively small slope areas and are caused by unfavorable hydrological conditions, very often in combination with human activities on the slope (construction of roads and facilities) (Arbanas et al. 2007). The analyzed landslides are generally of multiple style and retrogressive distribution. Sliding of clayey talus cover on the contact with flysch bedrock is typical (Arbanas et al. 1999).

Strength parameters of soils in the landslide bodies show considerable variations and it is very hard to determine the acceptable area of the values that can generally be adopted as characteristic values for all soil types in flysch superficial deposits. Dimensions of some characteristic landslides are shown in Table 1 and volume of investigated instabilities varies from 1,000 to 175,000 m^3. Average slope angle is between 15 % and 30 %, and thickness of superficial deposits varies from 0.5 to 11 m.

The landslide types and mechanisms in the area are generally rotational and translational slides and falls. Debris flows were registered only at few locations (Arbanas et al. 2006). The reactivated translational Juradi slide, the Krbavčići rotational slide and earth flow, the translational Brus slide and the rotational Drazej the Marinci slides (Fig. 3) are five of the most important landslides in the area. The dimensions of these landslides are present in Table 1 according WP/WLI (1993).

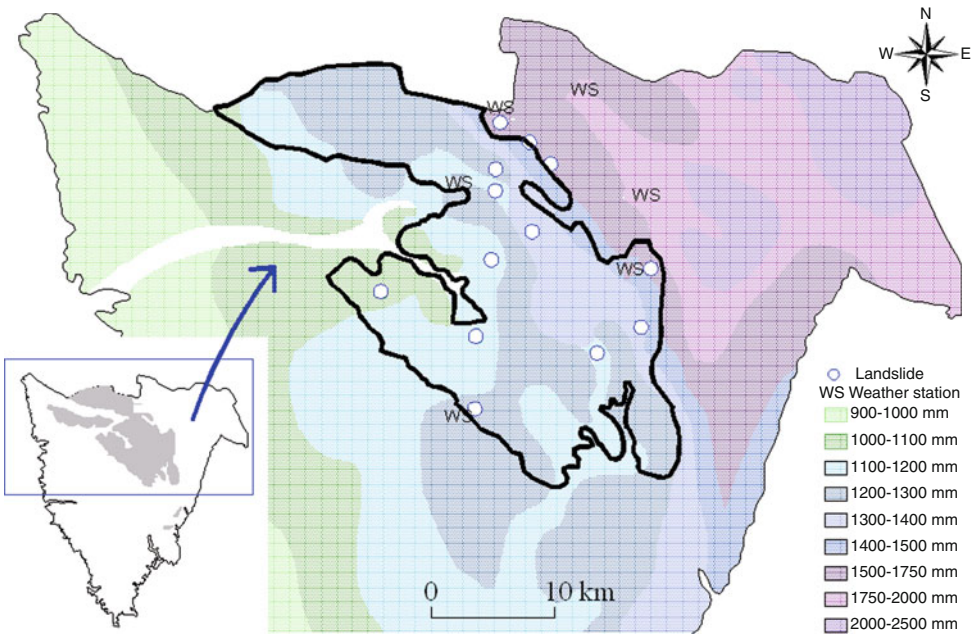

Fig. 4 Mean annual precipitation map of central and north Istria (1961–1990) (After Gajić-Čapka et al. 2003)

The Juradi Landslide is located in the central part of the Istrian Peninsula and it is a translational slide that reactivated many times in last 80 years. The last reactivation occurred on 1st December 2010. The main scarp of the landslide divided the Juradi Village in two parts (Fig 3a). The Juradi Landslide was formed in a typical geological setting of Paleogene flysch deposits and the landslide occurrence was the result of clayey cover sliding over the siltstone and marl layers in the bedrock. The landslide affected a 11 m thick sliding body mass with total volume of 47,000 m^3 on a slope of average inclination of 5–7 %. The sliding occurred due to the soil strength decrease on the contact between the superficial deposit and the bedrock, caused by an increase in the pore water pressures and unfavorable hydrodynamic forces during the infiltration process. Further movements were reduced by effective surface drainage and consequent lowering the ground water level.

The first large movement at the slope near the Krbavčići village, in vicinity of the Buzet city (Fig. 1) occurred in 1961. After this initial appearance the landslide was naturally suspended without significant consequences. The landslide was reactivated as a multiple retrogressive sliding type in the night between 30th and 31st of January 1979 (Arbanas et al. 2006). The last reactivation of the Krbavčići Landslide occurred in winter 2003 with main activity in the upper part of the slope above the viaduct is shown in Fig. 3b. The moving mass endangered the stability of the viaduct. It was saved by excavating and removing a large amount of material from the upper part of the landslide body. The landslide body was 220 m long with a total volume of 105,000 m^3 on a slope with an average inclination of 15–30 %.

The Drazej Landslide on the local road near the City of Pazin was occurred on 2nd January 2005 and the sliding overtook the road embankment (Fig. 3d). Based on field investigation results it was established that the sliding body volume of approximately 10,000 m^3 and slip surface on the contact of clayey superficial deposit and flysch bedrock were formed. Field investigations further indicated that multiple reactivated sliding had occurred on same location in the history.

The Brus Landslide is located near the Brus village. The sliding occurred on 9th April 2005. This landslide presents a typical translational block sliding with a landslide body consisting of almost one unique flysch rock mass block (Arbanas et al. 2010). The rock mass block, 150 m long and 30 m wide, was moved 33 m down the slope (Fig. 3e). The upper part of the landslide was located near the top of the slope and the main scarp damaged the local road.

Another instability in the area occurred at the end of April 2006, near the Marinci village, where the landslide affected the road embankment on a relatively steep slope on the regional road (Fig. 3f). The landslide body was 10 m deep and the volume of the sliding mass was about 1,800 m^3 (Arbanas et al. 2007), which is a representative volume of small shallow landslides in the area of Istria.

Sliding Causes and Triggering Factors

By analyzing the sliding causes and triggering factors it was concluded that almost all landslides in the investigated area were caused by a rising of the groundwater level in the slope by water infiltration during long time rainy periods, and consequently by a decrease of effective strength caused

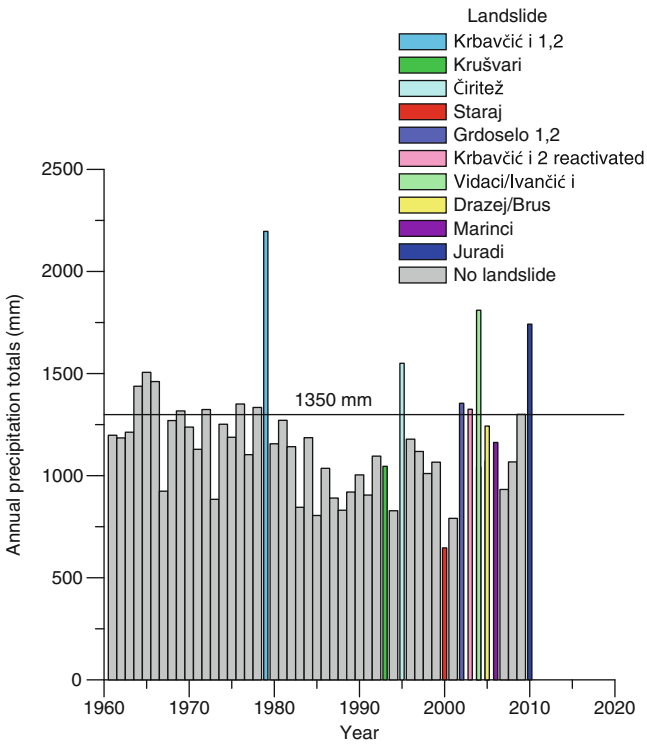

Fig. 5 Cumulative annual precipitations in relation with year of the landslide event. The line shows average annual precipitation value of 1,350 mm for whole area

by pore pressure increasing. A certain number of landslides were triggered by human activity that "helped" lead and retain the surface water in the sliding zone and enabled intensive wetting and infiltration (Arbanas et al. 2007).

Precipitation data for a 50 years period (1960–2010), from six weather stations in the investigated area (Abrami, Rakitovec, Vodice, Lanišće, Lupoglav, Pazin) (Fig. 4) were analyzed to reconstruct correlations between precipitations and landslide triggering.

Analyzing initiation date of 16 landslides, it could be concluded that only a few landslides occurred in a year with extremely high annual precipitation (Fig. 5). Further analyses were conducted analyzing cumulative precipitation prior to sliding appearance. It was established that high precipitation in approximately the last 3 months before landslide initiation was a better indicator. The analyzed landslides are mostly activated during winter period when the number of rainy days during a 3-month-period was large and the evapotranspiration values were small. It was also deduced, that relatively short, but intensive rainfall events (days to several weeks) did not influence landslide occurrence in the region, probably because the small hydraulic conductivity of clayey layers disabled fast infiltration. The long term period of surface water presence is necessary for infiltration and ground water level rising. The high cumulative value of precipitation observed in approximately 3 months before sliding was detected as a triggering factor for investigated landslides in Gray Istria.

Conclusions

A data base of investigated landslides in the north-eastern part of the Istrian Peninsula was made based on available results of field investigations conducted during the designing of remediation measures on buildings, facilities and infrastructure. Soil instabilities are mostly slides and falls in flysch deposits. It was determined that unfavorable geomorphological and hydrogeological conditions are the main causes of landslide occurrence, while rainfall and anthropogenic influences are the main triggering factors.

Precipitation recorded close to the landslides was analyzed to establish the influence of rainfall on the triggering of the landslides. It is clear that landslides occurred after long rainy periods, while short term rainfalls have significant influence on erosion. It is concluded that the analyzed landslides are mostly activated in winter when the number of rainy days and associated total rainfall amount during a 3-month-period were high and the evapotranspiration values small. More specifically landslides are caused by water infiltration in the slope, rising of groundwater level and decreasing of strength as a consequence of pore water pressure increasing.

It can be assumed that new landslides on flysch slopes will occur under the same or similar conditions as those under which the recent landslides occurred (Dugonjić et al. 2008). Sufficiently long rainy periods present the main triggering factor for (re)activation of small shallow landslides on flysch slopes of Gray Istria.

References

Arbanas Ž, Benac Č, Jardas B (1999) Small landslides on the flysch of Istria. In: Proceedings of 3rd conference of Slovenian geotechnical society, vol 1, Sloged, Ljubljana, pp 81–88

Arbanas Ž, Benac Č, Jurak V (2006) Causes of debris flow formation in flysch area of North Istria, Croatia. Monitoring, simulation, prevention and remediation of dense and debris flows. In: Lorenzini G, Brebbia CA, Emmanouloudis DE (eds) WIT transaction on ecology and the environment, vol 90, pp 283–292

Arbanas Ž, Grošić M, Goršić D, Griparić B (2007) Landslides remedial works on small roads of Istria. In: Proceedings of 4th Croatian roads congress. Cavtat, Croatia. Croatian Road Society, Zagreb, 28–31 Oct 2007, pp 38–45

Arbanas Ž, Mihalić S, Grošić M, Dugonjić S, Vivoda M (2010) Brus landslide, translational block sliding in flysch rock mass. In: Proceedings of the European rock mechanics symposium rock mechanics in civil and environmental engineering, Lausanne, Swiss. CRC/Balkema, London, pp 635–638

Dugonjić S, Arbanas Ž, Benac Č (2008) Assessment of landslide hazard on flysch slopes. In: Proceedings of 5th conference of Slovenian geotechnical society. Nova Gorica, Slovenia. Sloged, 12–14 June 2008, pp 263–272

Gajić-Čapka M, Perčec Tadić M, Patarčić M (2003) A digital annual precipitation map of Croatia. Croatian Meteorolog J 38:21–33 (in Croatian)

ISRM, Commission on standardization of laboratory and field test (1981) Suggested methods for the quantitative description of discontinuities in rock masses. In: Brown ET (ed) Pergamon, Oxford, UK, p 211

WP/WLI, International Geotechnical Societies UNESCO Working Party on World Landslide Inventory (1993) Multilingual landslide glossary. The Canadian geotechnical society. BiTech Publishers Ltd., Canada

Velić I, Tišljar J, Matičec D, Vlahović I (1995) General review of the geology of Istria. Excursion guide-book. In: Vlahović I, Velić I (eds) Institute of Geology, Zagreb, pp 5–20

Landslide Controlling Factors in Catchments with High Deforestation

Guns Marie and Vanacker Veerle

Abstract

Many tropical mountain regions experience rapid land cover change and natural hazards like landslides. In this work, landslide controlling factors in two Andean catchments with different land cover dynamics were analysed using rare event logistic regression with replications. Our results show that topographical factors alone cannot explain the observed landsliding pattern. We suggest that major changes in soil properties and hydrology after deforestation play a role in accelerating landslide activity.

Keywords

Landslides • Controlling factors • Rare event logistic regression • Deforestation • Andes

Introduction

Many tropical mountain regions experience rapid land cover change and are prone to natural hazards like landslides. In Ecuador, the demographic growth in the early twentieth century and the agrarian reforms of the 1960s and 1970s have forced people to look for new agricultural land. Numerous inhabitants migrated to marginal steep uplands which are highly sensitive to soil erosion (Molina et al. 2008). This migration induced rapid land cover changes (Vanacker et al. 2007), including massive deforestation of primary forest. Moreover, natural hazards and risks are increasing, especially in developing countries (Alcántara-Ayala et al. 2006). Understanding the factors that control landslide hazards is therefore essential.

G. Marie (✉)
Georges Lemaître Centre for Earth and Climate Research, Earth and Life Institute, Université catholique de Louvain, Place Louis Pasteur 3 boîte L4.03.08, 1348 Louvain-la-Neuve, Belgium

Fund for Scientific Research – FNRS, Rue d'Egmont 5, 1000 Brussels, Belgium
e-mail: marie.guns@uclouvain.be

V. Veerle
Georges Lemaître Centre for Earth and Climate Research, Earth and Life Institute, Université catholique de Louvain, Place Louis Pasteur 3 boîte L4.03.08, 1348 Louvain-la-Neuve, Belgium

Various techniques have been used in the past to analyse landslide controlling factors (see overviews of Guzzetti et al. 1999; Dai and Lee 2002; Huabin et al. 2005). Logistic regression is interesting as it models the relationship between a dichotomous variable (e.g. presence or absence of landslides) and a set of independent variables (e.g. controlling factors). This statistical technique has to be adapted for landslide analysis as landslides, like many other natural hazards, are rare events (Van Den Eeckhaut et al. 2006).

The main purpose of this work is to analyse the controlling factors of landslides in two Andean catchments with different land cover dynamics. We developed a new technique based on Monte Carlo simulation and rare event logistic regression (Guns and Vanacker 2012). This technique, called rare event logistic regression with replications, allows correcting bias of using rare event data, and offers a robust detection of factors controlling landsliding patterns.

Study Area

General Description

The study area is located in the Ecuadorian Andes, in the south of the Cordillera Real (Fig. 1). It is composed of two watersheds: Ingapata (4.8 km^2) and Llavircay (24.8 km^2)

C. Margottini et al. (eds.), *Landslide Science and Practice*, Vol. 1,
DOI 10.1007/978-3-642-31325-7_30,

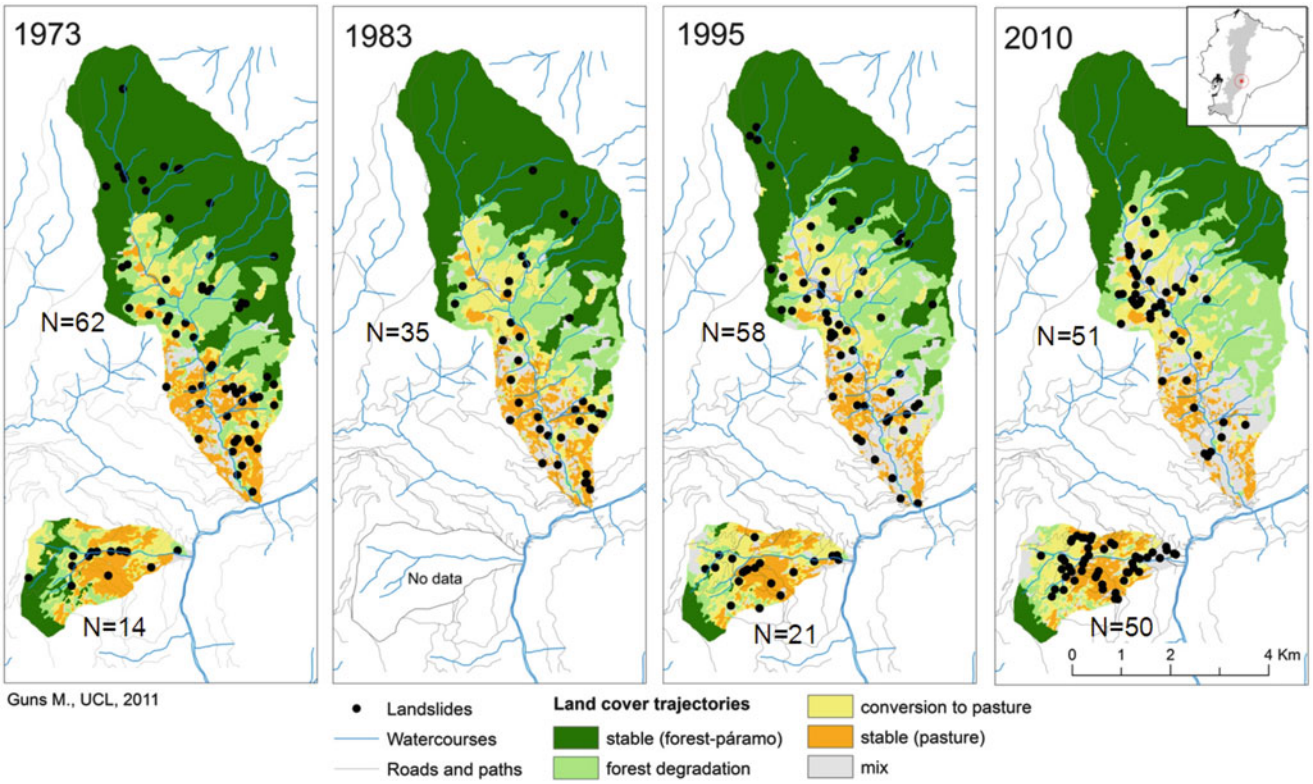

Fig. 1 Land cover trajectories and landslides in Ingapata (southern catchment) and Llavircay (northern catchment)

located 2 km downstream. Both rivers are tributaries of the Paute River that drains in the Namangoza, Santiago and Maranon Rivers and finally in the Amazon River. The study area is exposed to the Amazonian influence and is thus subjected to a warm and humid tropical climate (Winckell et al. 1997).

Relief in Ingapata catchment varies from 2,020 to 3,384 m and from 2,017 to 3,736 m in Llavircay catchment. The study area possesses natural slopes up to 55°. With a mean slope of 25°, the area is considered as very steep. One third of the total study area is constituted of slopes higher than the stability angle (estimated at 30° according to Basabe 1998).

The study area is underlain by metamorphic rocks of the Jurassic-Lower Cretaceous (BGS and CODIGEM 1994). Lithology includes meta-volcanic rocks (meta-andesitic and meta-basaltic at low metamorphism), meta-sedimentary rocks (phyllite, shales and quartzite) and marble (Cando Jácome 2004). Outcrop shows that foliation direction is variable but that fracturation and weathering are very high.

Landslides

Mass movements and creep are abundantly present. Inventories of mass movements created from aerial photographs interpretation and field campaigns revealed 291 landslides (reactivation excluded) between 1973 and 2010 (Fig. 1). They are mainly earth slides (translational slides) and earth slumps (rotational slides) according to Cruden and Varnes (1996) classification.

Land Cover

Land cover evolution has been reconstructed for five periods of times from aerial photo interpretation and field campaigns. Spectral response patterns, texture analysis of the photographs (Gagnon 1974; Lillesand and Keifer 1994) and field validation allow distinguishing six land cover classes: (1) dense forest, (2) degraded forest, (3) bushes or so called matoral, (4) pasture with sporadic trees, (5) pasture and (6) subpáramo and páramo. Páramo is the natural shrub and grassland found at high altitudes in the Andes (Luteyn 1999).

Two different patterns of land cover change are apparent: in the less accessible catchment (Llavircay), deforestation started only in the mid-twentieth century while deforestation started few decades earlier in the other one (Ingapata). Half of the primary forest (824 ha) in Llavircay catchment has disappeared since 1963 and all of it (172 ha) in Ingapata catchment. In 2010, half of Llavircay catchment was still covered by trees but less than 15 % in Ingapata, where 60 % of total area was used directly for agricultural purpose.

Table 1 Summary of all variables tested their resolution and source

Variable		Resolution (m)	Source of the data
Slope		20	Derived from a Digital Elevation Model (DEM) based on contour lines of digital topological map (Instituto Geográfico Militar 1992)
Distance to watercourse		1	Euclidian distance calculated in ArcGIS9.3 from features of the digital topological map (Instituto Geográfico Militar 1992)
Distance to path		1	
Distance to road		1	Euclidian distance calculated in ArcGIS9.3 from features token by GPS during field campaign in Ingapata [no road in Llavircay]
Curvature	Concave	20	Reclassification of the curvature grid derived from the DEM based on contour lines of digital topological map (Instituto Geográfico Militar 1992)
	Rectilinear		
	Convex		
Land cover trajectory	Stable (forest-páramo)	20	Field observations taken during three campaigns in summer 2008, 2009 and 2010 + digitalization of orthorectified aerial photographs of 1963, 1973, 1983, 1995 and 2000 (Instituto Geográfico Militar)
	Forest degradation		
	Conversion to pasture		
	Stable (pasture)		
	Mix		

Trajectories of Land Cover Change

Land cover maps give information for a specific year and do not represent the dynamic evolution of land cover. Trajectory maps were created to analyse the temporal changes in land cover. Five trajectories were created (Fig. 1): (1) stable (forest-páramo), (2) stable (pasture), (3) forest degradation, (4) conversion to pasture and (5) others (mixed land cover changes). The two first ones represent unchanged land covers while the three last ones correspond to changes in vegetation cover.

Materials and Methods

Data Preparation

The environmental controlling factors are spaced in maps in a grid-cell mapping unit (Guzzetti et al. 1999) as it is very common nowadays with GIS utilisation. A conversion from GIS grid-data (maps) to a table is necessary for the statistical approach in R software. The resulting matrix form is an attribute table in which each line represents a 20 m resolution pixel of the catchment and every column represents the value of a variable. All variables, which were identified as possible controlling factors, are listed in Table 1.

In order to avoid auto-correlation and to focus on landsliding controlling factors, every landslide is represented by only one grid-cell (pixel) located in the centre of its shear plane. The dependent variable is dichotomous, and equals '1' when a landslide is present and equals '0' when no landslide is present. Proportion of landslide affected pixels compared to non-affected pixels is about 58/61.657 for Llavircay and 28/11.928 for Ingapata.

For every time period under analysis, a new attribute table is created with the appropriate landslide inventory. Those attribute tables are imported in R software for the statistical analysis.

Rare Event Logistic Regression with Replications: Theory

Ordinary logistic regression is a common statistical method to determine the relationship between a dichotomous variable, landslide presence/absence, and a set of explanatory variables.

King and Zeng (2001a, b) have shown that ordinary logistic regression underestimates the probability of occurrence of an event if the number of events (1) is very small in comparison to the number of non-events (0). This is often the case with natural hazards, as in our study where the amount of events is less than 1 % of the amount of non-events. King and Zeng (2001a, b) developed for political science the 'rare event logistic regression' which applies the following three corrections measures for rare event data: (1) an endogenous stratified sampling of the dataset, (2) a prior correction of the intercept and (3) a correction of the probabilities to include the estimation uncertainty.

Van Den Eeckhaut et al. (2006) were the first authors to use this methodology for landslides. Since then, and to our knowledge, only Bai et al. (2011) and Vanwalleghem et al. (2008) used rare event logistic regression for geomorphologic studies. The application of rare event logistic regression to our

database shows that the factors that are identified to significantly control landslide occurrence vary strongly according to the endogenous stratified sample chosen. This sample dependence was already pointed out by Demoulin and Chung (2007).

In order to avoid sample dependence, we adapted the rare event logistic technique by incorporating aspects of Monte Carlo simulation techniques (Guns and Vanacker 2012). The principal idea is to average the results of 50 replications of an ordinary rare event logistic regression made with 50 different endogenous stratified samples. This technique allows overcoming sample-dependency and offers a robust detection of the factors controlling landsliding patterns.

Rare Event Logistic Regression with Replications: Implementation

R software and the package Zelig (Imai et al. 2007) are used for the entire processes. The preliminary step is to create the choice-based (or case–control) samples which are the result of an endogenous stratified sampling scheme (Ramalho 2002). It consists of taking all the events (1) and a random selection of the non-events (0). The proportion of events to non-events was set at one to ten (Beguería 2006).

The first steps of rare event logistic regression with replications are similar to those of the ordinary rare event logistic regression (Van Den Eeckhaut et al. 2006): (1) multicollinearity detection with a linear regression and calculation of Variation Inflation Factors (VIF) and Tolerance (TOL), (2) influencing variables detection with a stepwise logistic regression and (3) rare event logistic regressioncalculation with the variables kept (significance level of 0.05).

We repeat these steps 50 times on different sub-samples of non-events (0) taken randomly in the study area. For the final result, only variables with a p-value of 0.05 and present in at least five replications are kept (Begueria 2006). Their average will form the resultant regression.

Results and Discussion

The results of the rare event logistic regression with replications are regrouped in Table 2. As no multicollinearity was detected, all the variables were used.

The importance of each controlling factor can be evaluated based on: (1) *count* that gives percentage of replications in which this controlling factors was significant, (2) *p-value* that gives an idea of its significance in the model and (3) *MPI* the measure of parameter importance that evaluates the potential influence of the variable on the probability of event occurrence (Vanwalleghem et al. 2008).

Ingapata Catchment

All periods of time confounded, only four different variables out of twelve are significant in Ingapata catchment (Table 2): *slope*, *distance to watercourse*, *distance to road* and *conversion to pasture*. There is an important shift in the factors that are identified to significantly control landslide occurrence. In 1973, only the environmental factor *distance to watercourses* explains landslide presence. The topographical factor *slope* is the major controlling factor (MPI = 7.491) for 1995. Although significant, the anthropogenic variable *conversion to pasture* does not appear in a lot of replications (34 % only). However, the construction of an asphalt road between 1995 and 2010 significantly (p-value < 0.001) altered slope stability in Ingapata catchment.

Llavircay Catchment

All periods of time confounded, six different variables out of eleven are significant in Llavircay catchment (Table 2): *slope*, *distance to watercourse*, *distance to path*, *conversion to pasture*, *stable (pasture)* and the trajectory *mix*. Only three variables are always present: the two trajectories directly linked with (conversion to) pastures and the topographical variable *slope*. The variable *distance to path* and the trajectory *mix* are present three times out of four. The variable *distance to watercourse* is present only once, in 2010. In general, for every year, the number of anthropogenic controlling factors is much more important than the number of natural environmental factors.

Catchment Comparison: Natural Controlling Factors

Three potential controlling factors (Table 1) can be considered as natural factors: *slope, curvature* and *distance to watercourse*.

Curvature has never appeared as a significant controlling factor in this tropical mountainous region (Table 2). Landslides are likely to occur on concave slopes but also on planar and convex slopes (Sidle 2007). This was observed

Table 2 Summary of the rare event logistic regressions with replications showing, for both catchments, percentage of replications in which the variable entered (count), logistic coefficient (β) and its standard error (S.E), Wald statistic, variable significance (P-value), Odd ratio, maximum value of explanatory variable in dataset (MPV) and measure of parameter importance (MPI = β*MPV)

	Count	β	S.E	Wald	P-value	Odd ratio	MPV	MPI
Ingapata catchment								
1973 (14 landslides)								
Intercept	100	−5,515	0.419	−13,193	< 0.001	0.004		
Distance to watercourse	100	−0.007	0.003	−2,358	0.021	0.993	982	−6,585
1995 (21 landslides)								
Intercept	100	−10,908	1,358	−8,094	< 0.001	0.000		
Slope	100	0.153	0.042	3,613	< 0.001	1,165	49	7,491
Conversion to pasture	34	1,106	0.494	2,238	0.028	3,023	1	1,106
2010 (50 landslides)								
Intercept	100	−5,674	0.627	−10,401	< 0.001	0.003		
Distance to road	100	−0.004	0.001	−4,494	< 0.001	0.996	1,459	−5,654
Slope	82	0.059	0.024	2,434	0.018	1,061	49	2,905
Llavircay catchment								
1973 (62 landslides)								
Intercept	100	−8,957	0.611	−14,685	< 0.001	0.000		
Slope	100	0.080	0.018	4,520	< 0.001	1,083	55	4,395
Conversion to pasture	94	1,167	0.368	3,162	0.008	3,213	1	1,167
Distance to path	78	−0.001	0.000	−2,736	0.010	0.999	2,721	−2,721
Stable (pasture)	32	1,049	0.384	2,742	0.014	2,855	1	1,049
1983 (35 landslides)								
Intercept	100	−9,885	0.691	−15,361	< 0.001	0.000		
Conversion to pasture	100	2,660	0.557	4,772	< 0.001	14,294	1	2,660
Stable (pasture)	100	2,681	0.586	4,575	< 0.001	14,599	1	2,681
Mix	100	2,198	0.624	3,525	0.001	9,007	1	2,198
Slope	54	0.058	0.025	2,342	0.022	1,060	55	3,212
1995 (58 landslides)								
Intercept	100	−8,034	0.550	−14,989	< 0.001	0.000		
Slope	98	0.045	0.017	2,690	0.012	1,046	55	2,464
Conversion to pasture	98	1,255	0.338	3,668	0.004	3,507	1	1,255
Distance to path	76	−0.001	0.000	−2,867	0.005	0.999	2,721	−2,994
Mix	20	1,299	0.384	3,375	0.001	3,664	1	1,299
stable (pasture)	18	1,511	0.489	3,084	0.003	4,531	1	1,511
2010 (51 landslides)								
Intercept	100	−8,058	0.593	−16,215	< 0.001	0.000		
Conversion to pasture	100	2,929	0.566	5,327	< 0.001	18,709	1	2,929
Stable (pasture)	92	2,738	0.668	4,065	0.003	15,455	1	2,738
Distance to watercourse	86	−0.005	0.002	−2,845	0.008	0.995	1,219	−5,608
Mix	52	2,776	0.769	3,622	0.002	16,057	1	2,776
Distance to path	24	−0.003	0.001	−3,067	0.015	0.997	2,721	−7,076
Slope	22	0.047	0.020	2,366	0.023	1,048	55	2,558

in the study area where 45 % of the landslides were on concave slopes, 16 % on planar slopes and 39 % on convex slopes. However it might be difficult to represent changes in curvature adequately, given the fact that the resolution of the DEM is only 20 m.

Distance to watercourse is significant only once in every catchment (1973 for Ingapata and 2010 for Llavircay). According to our results (Table 2), part of the landslides observed in 1973 might have been triggered by undercutting of Ingapata River banks. This might be related to land cover change in the upper part of the catchment but is also a phenomenon frequently observed in active mountain belts (Korup et al. 2007). With a MPI absolute value of 5.654 (Table 2), the proximity to watercourse is the second major controlling factor in Llavircay in 2010. However we should be careful with this value (as well as the one of *distance to path* in 2010) as it may come from data collection bias. In contrast to the other landslide inventories, the 2010 landslide repertory was made by field mapping. A bias due to less visibility and accessibility may explain why more landslides

were observed close to paths and watercourses, the two most accessibility corridors, in Llavircay in 2010.

In both catchments and for all time periods studied (except in Ingapata for 1973 when few landslides were observed), the *slope* is significantly controlling the landslide occurrence. This is not surprising as the greater the slope angle is, the greater the vertical component of gravity (Donati and Turrini 2002). Interestingly, the analysis of the absolute value of MPI (Table 2) shows that the influence of the variable *slope* is decreasing with time in both catchments. In Llavircay catchment, for example, slope was considered as the major controlling factor in 1963 (MPI = 4.395) but has less predictive power in 2010 (MPI = 2.558). That means that even though this controlling factor is important for landsliding, other variables are getting more important in the recent years.

Catchment Comparison: Anthropogenic Controlling Factors

Distance to path can be considered as a landsliding controlling factor in Llavircay catchment at every time (except 1983). Due to its construction design, the asphaltic *road* could only have played a significant role in Ingapata catchment in 2010 and it significantly did (Table 2). The effects of roads or trails on slope stability are well documented in Sidle and Ochiai (2006) and could be summarized in three points: (1) natural hydrologic pathways alteration, (2) unstable slope undercutting and (3) fillslope overloading and oversteepening. Our field expertise also noticed improper design of drainage measures that may have caused an increased pore pressure.

The last variables considered as anthropogenic controlling factors are the ones linked with land cover trajectories. We do not observe correlation between the presence of forests (and páramo) and the spatial pattern of landslides. Moreover, according to our results, *forest degradation* seems not to be a controlling factor for landslides. This suggests that a significant reduction in the density of trees does not directly lead to a measurable increase in landslide occurrence. A possible explanation could be that the root density in a degraded primary forest is still high enough to ensure slope stability. However few studies exist on the influence of temporal and spatial variations of forest densities on root strengths and landslide occurrences.

If we consider that *conversion to pasture* in Ingapata (1995) is not very important (significant in only 34 % of the replications – Table 2), it could be said that the three variables linked with pastures and dynamics of vegetations are important controlling factors in the Llavircay catchment only. In other words, in the catchment with the most recent deforestation, the conversion from forest to pasture in the period of time observed (*conversion to pasture*) or that occurred before 1963 (*stable(pasture)*) control the presence of landslides. Moreover, an area with high fluctuations of vegetation cover (*mix*) is important for landslide occurence. We do not observe this pattern in Ingapata which only differs from Llavircay by its smaller size and its initial deforestation time.

As catchment size does not explain the different pattern of landslide controlling factors (Guns and Vanacker 2012), we suggest that the shorter deforestation time lag in Llavircay could explain why land cover change plays an important role in controlling landslides. Tasser et al. (2003) have shown that rooting density and distribution are controlled by land cover type and not only by soil conditions. The conversion from forest to agricultural land modifies rooting strength but also soil moisture regime (Sidle and Ochiai 2006). Our analyses of 50 soil samples randomly taken in the two catchments indicate that a linear relation exists between bulk density and the time elapsed since deforestation. This suggests that major changes in soil properties after deforestation play a role in accelerating landslide activity.

Conclusion

Controlling factors of landslides in two Andean catchments with different land cover dynamics were analysed using rare event logistic regression with replications. The results show that topographical factors alone cannot explain the observed landsliding pattern. Our data show that the construction of asphaltic roads significantly alters slope stability in the area. Forest conversion to agricultural land highly controls landslide occurrence in the catchment with recent deforestation only. Importantly, we observe no correlation between the degradation of forest and the spatial pattern of landslides. This suggests that a significant reduction in the density of trees in forests does not lead to a measurable increase in landslide occurrence. We suggest that major changes in soil properties and hydrology after deforestation play role in accelerating landslide activity.

Acknowledgments Funding for this research was provided by the Fonds National de la Recherche Scientifique (FNRS, Brussels). This study was supported by the Belgian Science Policy grant SR/00/133 FOMO and the CUD-PIC project 'Strengthening the scientific and technological capacities to implement spatially integrated land and water management schemes adapted to local socio-economic and physical settings'. The authors would like to thank Pr. D. Alvarado and Ing. P. Borja (Universidad de Cuenca, Ecuador), engineers of CGPaute (Ecuador), Ing. L. Jerves (Celec – Hidropaute, Ecuador) and Dr. A. Molina (KUL) for their precious help on the field.

References

Alcántara-Ayala I, Esteban-Chávez O, Parrot JF (2006) Landsliding related to land-cover change: a diachronic analysis of hillslope instability distribution in the Sierra Norte, Puebla, Mexico. Catena 65:152–165

Bai S, Lü G, Wang J, Zhou P, Ding L (2011) GIS-based rare events logistic regression for landslide-susceptibility mapping of Lianyungang, China. Environ Earth Sci 62:139–149

Beguería S (2006) Changes in land cover and shallow landslide activity: a case study in the Spanish Pyrenees. Geomorphology 74:196–206

Basabe P (1998) Prevención de desastres naturales en la Cuenca del Paute – Informe final: Proyecto Precupa. Swiss Disaster Relief Unit (SDR/CSS), Cuenca, Ecuador

BGS, CODIGEM (1994) Geological and metal ocurrences maps of the southern Cordillera real and El Oro Methamorphic Belts, Ecuador

Cando Jácome M (2004) Consejo de programación de obras de emergencia de la cuenca del Rio Paute y sus afluente – COPOE, Proyecto de Desarrollo de la Cuenca del Paute, Componente Geológico, Quito, 36 p

Dai FC, Lee CF (2002) Landslide characteristics and slope instability modeling using GIS, Lantau Island, Hong Kong. Geomorphology 42:213–228

Demoulin A, Chung C (2007) Mapping landslide susceptibility from small datasets: a case study in the Pays de Herve (E Belgium). Geomorphology 89:391–404

Donati LM, Turrini C (2002) An objective method to rank the importance of the factors predisposing to landslides with the GIS methodology: application to an area of the Apennines (Valnerina; Perugia, Italy). Eng Geol 63:277–289

Gagnmon H (1974) La photo aérienne son interprétation dans les études de l'environnement et de l'aménagement du territoire, Édition HRW, Montréal, 278p. ISBN 0039282481

Guns M, Vanacker V (2012) Logistic regression applied to natural hazards: rare event logistic regression with replications. Nat Hazards Earth Syst Sci 12:1937–1947

Guzzetti F, Carrara A, Cardinali M, Reichenbach P (1999) Landslide hazard evaluation: a review of current techniques and their application in multi-scale study, Central Italy. Geomorphology 31:181–216

Huabin W, Gangjun L, Weiya X, Gonghui W (2005) GIS-based landslide hazard assessment: an overview. Prog Phys Geog 29:548–567

Imai K, King G, Lau O (2007) Zelig: everyone's statistical software. http://GKing.harvard.edu/zelig

Instituto Geográfico Militar (1992) Mapa topografica Taday (Cola de S. Pablo). Ñ V-C4, escala 1:50 000, 2 edición, Ecuador

King G, Zeng L (2001a) Explaining rare events in international relations. Int Organ 55:693–715

King G, Zeng L (2001b) Logistic regression in rare events data. Polit Anal 9:137–163

Korup O, Clague J, Hermanns R, Hewitt K, Strom A, Weidinger J (2007) Giant landslides, topography, and erosion. Earth Planet Sci Lett 261:578–589

Lillesand TM, Keifer JW (eds) (1994) Remote sensing and image interpretation, 3rd edn. Wiley, New York, p 750. ISBN 0471305758

Luteyn JL (1999) Páramos: a checklist of plant diversity, geographical distribution and botanical literature, vol 84. Memoirs of the New York Botanical Gardens, New York, p 278

Molina A, Govers G, Poesen J, Van Hemelryck H, De Bièvre B, Vanacker V (2008) Environmental factors controlling spatial variation in sediment yield in a central Andean mountain area. Geomorphology 98(3–4):176–186

Ramalho EA (2002) Regression models for choice-based samples with misclassification in the response variable. J Econometrics 106:171–201

Sidle RC, Ochiai H (2006) Landslides: processes, prediction, and land use. American Geophysical Union, Washington, DC, p 312. ISBN 978-0-87590-322-4

Sidle RC (2007) In: Sivakumar MVK, Ndiang'ui N (eds) Climate and land degradation. Springer, Berlin/New York/Heidelberg, p 623. ISBN 978-3-540-72438-4

Tasser E, Mader M, Tappeiner U (2003) Effects of land use in alpine grasslands on the probability of landslides. Basic Appl Ecol 4: 271–280

Vanacker V, Molina A, Govers G, Poesen J, Deckers J (2007) Spatial variation of suspended sediment concentrations in a tropical Andean river system: the Paute River, southern Ecuador. Geomorphology 87(1–2):53–67

Van Den Eeckhaut M, Vanwalleghem T, Poesen J, Govers G, Verstraeten G, Vandekerckhove L (2006) Prediction of landslide susceptibility using rare events logistic regression: a case-study in the Flemish Ardennes (Belgium). Geomorphology 76: 392–410

Vanwalleghem T, Van Den Eeckhaut M, Poesen J, Govers G, Deckers J (2008) Spatial analysis of factors controlling the presence of closed depressions and gullies under forest: application of rare event logistic regression. Geomorphology 95:504–517

Cruden D, Varnes D (1996) Landslides: investigation and mitigation. In: Turner A, Schuster R (eds) Transportation Research Board, National Research Council, 673p

Winckell A, Zebrowski C, Sourdat M (1997) Los paisajes naturales del Ecuador; Las regiones y paisajes del Ecuador; Geografía básica del Ecuador, Tomo IV, Volumen 2, Geografía física. Centro Ecuatoriano de Investigación Geográfica, IPGH, IGM, ORSTOM, Quito, 417p

Characterizing Tree Growth Anomaly Induced by Landslides Using LiDAR

Khamarrul A. Razak, Alexander Bucksch, Michiel Damen, Cees van Westen, Menno Straatsma, and Steven de Jong

Abstract

Disrupted vegetation is often used as an indicator for landslide activity in forested regions. The extraction of irregular trees from airborne laser scanning data remains problematic because of low quality of observed data and paucity of field data validation. We obtained high density airborne LiDAR (HDAL) data with 180 points m^{-2} for characterizing tree growth anomalies caused by landslides in the Barcelonnette region, the Southern French Alps. HDAL allowed the mapping of a complex landslide and its three kinematic zones. The TreeVaW method detecting trees from the HDAL data and determined their position and height, while the SkelTre-skeletonization method extracted the tree inclination. The tree growth anomalies are parameterized by tree height dissimilarities and tree inclinations. These parameters were successfully extracted from the HDAL and compared with field data. We revealed that the distribution of LiDAR-derived tree growth anomalies was statistically different for landslide areas as compared to stable areas.

Keywords

Forested landslides • Drunken trees phenomena • LiDAR-derived tree irregularities

Introduction

The characterization of tree growth anomalies caused by landslides is a key component in the assessment of landslide activity in forested mountainous landscapes. The so-called "drunken trees" phenomenon is often associated with landslide-originating landforms and the biotopes occurring within them. However, there is limited research published on this topic. Tree irregularities are typically visible in the bending and tilting of the tree stem, and are essential factors for determining the tree stability (Lundstrom et al. 2008). To relate tree anomalies to landslides occurrence and its activity, the identification of disrupted trees in forested landslides is crucial.

Landslide mapping has traditionally been undertaken by visual interpretation on stereoscopic images, in concert with field verification. Image analysis using aerial photographs, satellite, and radar images can efficiently cover a large area, but is less effective in accurately mapping the landslides in forested terrain (Wills and McCrink 2002; Van Den Eeckhaut

K.A. Razak (✉)
Faculty of ITC, University of Twente, Enschede, 217, 7500AE, The Netherlands

UTM IC- Razak School, Universiti Teknologi Malaysia, Jalan Semarak, Kuala Lumpur 54100, Malaysia
e-mail: razak@itc.nl

A. Bucksch
Delft University of Technology, Delft 2629 HS, The Netherlands

School of Biology and School of Interactive Computing, Georgia Institute of Technology, Atlanta, GA, USA

M. Damen • C. van Westen • M. Straatsma
Faculty of ITC, University of Twente, Enschede, 217, 7500AE, The Netherlands

S. de Jong
Department of Physical Geography, Utrecht University, Utrecht, The Netherlands

C. Margottini et al. (eds.), *Landslide Science and Practice*, Vol. 1,
DOI 10.1007/978-3-642-31325-7_31,

et al. 2007). Field mapping yields greater accuracy, but is somehow limited in terrain coverage and at the expense of high labor costs (Haneberg et al. 2009) particularly identifying the location and geometric of disrupted trees.

High resolution LiDAR data is capable of revealing landslide morphological features beneath dense vegetation (McKean and Roering 2004; Schulz 2007; Van Den Eeckhaut et al. 2007; Kasai et al. 2009; Razak et al. 2011). However, many researchers neglect the LiDAR point cloud which represents the vegetation structures for landslide recognition. Mackey and Roering (2011) addressed the difficulty to distinguish active and dormant landslides without additional information on feature activity. Mackey et al. (2009) manually recognized trees on the single LiDAR-derived image and five historical aerial photos and tracked tree displacement over 42 years in order to quantify decadal-scale slide deformation and observed the long-term sediment flux in earthflow-prone terrain. They also remarked that many trees could not be visually identified on LiDAR and aerial photos. Although topographic laser scanning systems have undergone phenomenal developments in recent years resulting in a wide variety of applications, extraction of irregular vegetation related to landslides still remains difficult because of the required high point density of LiDAR data and lack of field validation.

A drunken trees phenomenon is described as a stand of trees displaced from their normal vertical alignment or growing and tilted at various angle (De Villiers 2001; Alexandrowicz and Margielewski 2010). Typically, this phenomenon is caused by melting permafrost, frost heaving, forested active rock glaciers, earthquakes and landslides. Parise (2003) described that trees can be an indicator of local deformation and different episodes of displacement. Stoffel (2006) summarized the most typical responses of trees to landslide activity that is often used in dendrogeomorphology. However, few studies have been published related to landslide-drunken forests phenomena. So far, no literature was found relating laser-derived parameters to tree growth anomalies caused by landslides in a forested mountainous landscape.

The present study aims at the utilization of high density airborne LiDAR data to accurately map a complex landslide and its kinematic zones, and to characterize the drunken trees associated to tree growth anomalies induced by landslides. Tree growth anomalies in the form of tree height dissimilarity and tree inclination are extractable from HDAL and quantified with respect to landslide activity in the forested catchment in the Barcelonnette basin, France.

Study Area

The study area is situated on the north-facing slope of the Barcelonnette Basin, 2.5 km to the south-east of Jausiers, France. The area consists of Callovo-Oxfordian unstable black marls, overlaid by deposits of reworked glacial till. The climate is characterized by strong inter-annual rainfall variability. Predisposing geomorphic and climatic influences triggered various types of landslides in the area mostly covered by deciduous and coniferous forests. This area is largely covered by *Pinus Nigra* (black pine tree). We selected an area consisting of a complex landslide located beneath 100 years old forest in the Southern French Alps (Fig. 1).

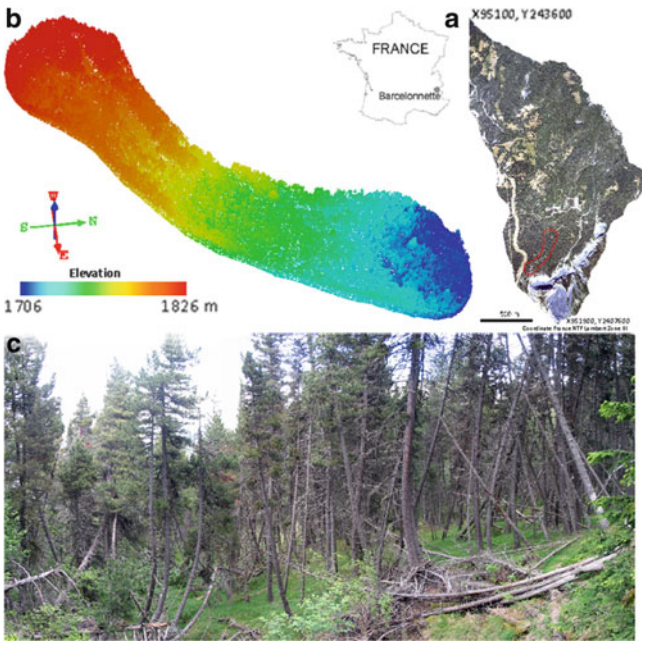

Fig. 1 Location of forested landslide in the Barcelonnette basin, France (**a**) 8.09 million LiDAR point cloud with elevation (**b**) Field photos showing the drunken trees phenomena caused by landslides (**c**)

Table 1 Metadata for the airborne LiDAR campaign

Acquisition (month/year)	July 2009
Laser scanner	RIEGL VQ480i
IMU system	IMAR FSAS (record up to 500 Hz)
Positional system	Topcon legacy (record up to 5 Hz)
Laser pulse repetition rate	300 kHz
Beam divergence	0.3 mrad
Laser beam footprint	75 mm at 250 m
Field of view	60°
Scanning method	Rotating multi-facet mirror

Methods

LiDAR Measurement

An HDAL dataset was acquired in July 2009 using a hand-held laser scanning system. This system consists of a RIEGL VQ-480 laser scanner, a Topcon Legacy GGD GPS and an

iMAR FSAS inertial measurement unit (IMU). Specifications are given in Table 1. An airborne LiDAR campaign was carried out under snow-free conditions using a helicopter flying about 300 m above the ground. Several flight lines were acquired over the same area to increase the point density over the forested terrain. Here we used about eight million points with a mean point density of 180 points m^{-2}.

Field Data Validation

Two field campaigns were carried out in June 2009 and 2010 to measure tree location, tree height and inclination of 110 individual trees. Two local geodetic stations were setup near the landslide area using a Leica differential GPS system 1200 in which a 24-h static observation was carried out for each geodetic station. The geodetic base stations were later used to transform the coordinates of the two local geodetic stations. Horizontal and vertical accuracy of these stations are on average 13 and 22 mm, respectively.

A total station was used to transform the coordinates of the local networks inside the forest for measuring each individual tree location. Tree heights were observed using a Nikon laser rangefinder and the tree inclination angles were measured at tree breast height (1.3 m) using a Suunto PM-5. We collected detailed tree data in six sampling plots in the landslide area as shown in Fig. 3.

Recognition of the Forested Landslide

We used the landslide filter as described in Razak et al. (2011) to automatically extract the ground points and to generate a 25 cm LiDAR derived DTM for recognizing landslides under forest. We utilized the LiDAR-derived topographic openness which was stereoscopically visualized coupled to a color composite image. The interpretation of the landslide margins and a subdivision in kinematic zones was done by image interpretation experts using both 2D and 3D products of the LiDAR-derived images, created with the ILWIS software. The 2D terrain expression was enhanced using a script in which shadow filters from three different directions (west, north-west, and north) were applied. The resulting maps were linearly stretched and displayed as a hill-shade color composite. This map was combined with the LiDAR-derived DTM to create a 3D anaglyph image.

The visual interpretation was based on the analysis of morphometric terrain features such as slope steepness, length and form. These factors are indicative for various landslide processes, such as debris flow movement, surface cracking, and block tilting. Areas with the same or similar terrain features were delineated using on-screen digitizing from the 2D and 3D image products. We subdivided the landslide into three landslide kinematic zones: a head-scarp or source zone, a long narrow transport zone, and a depositional zone.

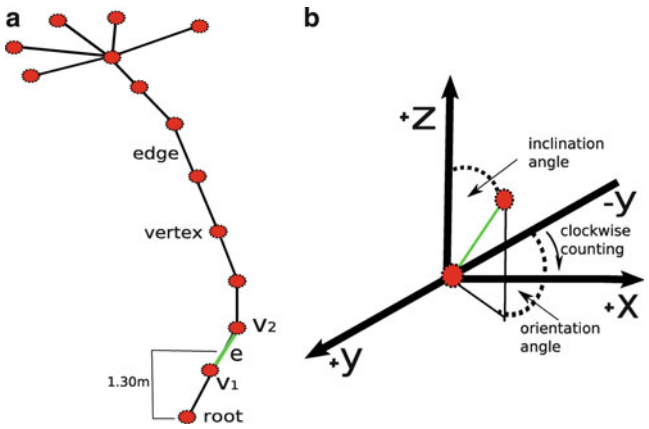

Fig. 2 (**a**) A schematic skeleton graph of a delineated tree. The edge *e* connecting the vertices v1 and v2 around 1.30 m is shown in *green*. (**b**) Calculation of the inclination angle

Tree Detection, Height and Delineation Using LiDAR Data

We utilized the TreeVaW (**Tree Va**riable **W**indow) method for detecting individual trees and estimating the dominant tree height (Popescu et al. 2002; Popescu and Wynne 2004). This method implies a variable window technique with local maximum (LM) focal filtering and yields consistent results for all situations with R^2 of 84 %. The program was performed in IDL and outputs are delivered as position (x, y) of single trees, tree height, and crown width. The LIDAR-derived digital canopy model (DCM), with a grid resolution of 25 cm was used as a data input. DCM was computed by subtracting the digital terrain model (DTM) from the digital surface model (DSM), representing the surface of the tree crowns.

In order to assign point clouds to particular single trees, manual tree delineation was carried out using the Quick Terrain Modeler software. This software has the capability to deal with enormous 3D point clouds. We carefully identified point clouds located on the tree crown, branches, stem, and ground-below tree and stored the point clouds (xyz-coordinates) in a single ASCII file. This step is required for providing a single tree as a data input for the SkelTre-skeletonization approach.

Extraction of Single Tree Inclination

This section describes the extraction of the inclination angle of a delineated tree. The parameters are calculated by analyzing a skeleton, which is derived from the point cloud for each individual tree.

A skeleton is a line describing the tree shape. Ideally, it is centred within the object and is connected whenever the object is connected. In this study, we used the so-called SkelTre-skeleton (Bucksch et al. 2009, 2010; Bucksch 2011). The output of SkelTre-skeletonization is a graph consisting of vertices and edges (Fig. 2a). Each vertex is embedded into a local weighted centre of gravity of the point cloud and is associated with a Cartesian *xyz*-coordinate in Euclidean space. The neighbourhood relation between the vertices is expressed by linking neighbouring vertices with an edge. This particular skeleton was previously used to extract the diameter at tree breast height from high density airborne LiDAR data, (Bucksch et al. 2010; Bucksch 2011).

The skeleton-graph is rooted at the vertex having the lowest z-coordinate value (Fig. 2a), which is assumed to be the start of the tree trunk on the ground. The inclination is the angle derived from analyzing the edge e covering 1.3 m tree height from the root vertex (Fig. 2a). e connects two embedded vertices v_1 and v_2, where the z-value of v_1 is smaller than the z-value of v_2. The vector $m_e = (v_2\_v_1)$ is taken to compute the inclination of the tree trunk around 1.3 m tree height as the deviation from the vertical in degrees (Fig. 2b).

Statistical Measures of LiDAR-derived Tree Growth Anomalies

The quality of LiDAR-derived tree growth anomalies was evaluated. Firstly, LiDAR-derived tree height and inclination were compared with the field measurement data. The statistical measures are presented in the form of mean absolute percentage error (*MA%E*), root mean square error (*RMSE*), and coefficient of determination (R^2). Secondly, we analyzed the tree height and inclination in relation to landslide activity. LiDAR-derived trees were subset based on the landslide map (Fig. 3). In addition, 29 trees in the stable area were manually delineated to determine the natural tilt variation. All trees were analysed using the SkelTre-skeletonization method. Location of sampled areas is given in Fig. 3.

We expected that the trees in the landslide area differ in tree height and inclination compared to the trees in the stable area. The independent-samples Mann-Whitney U test was applied to evaluate the statistical significance between the two datasets: trees on landslides and trees on non-landslide areas.

Results and Discussions

Internal Morphology of Forested Landslide

The visual interpretation of the LiDAR-derived images of the area resulted in the subdivision of the landslide in three kinematic zones with rotational and earthflow movement merging towards the north into one complex movement. Figure 3 shows the margin of a complex landslide and three kinematic zones mapped by an expert image interpreter as indicated on the 25 cm shaded relief image in the Bois Noir catchment, France. Area of the landslide source, transport, and depletion zones is about 11,710, 2,385, and 11,675 m^{-2}, respectively. Six tree sampling, stable tree plots used for vegetation analysis and a transport zone profile are also highlighted. Main- and side-scarps could be recognized in the zones. At places back- and forward tilted blocks could be identified most prominently in the south-west part of the landslide area.

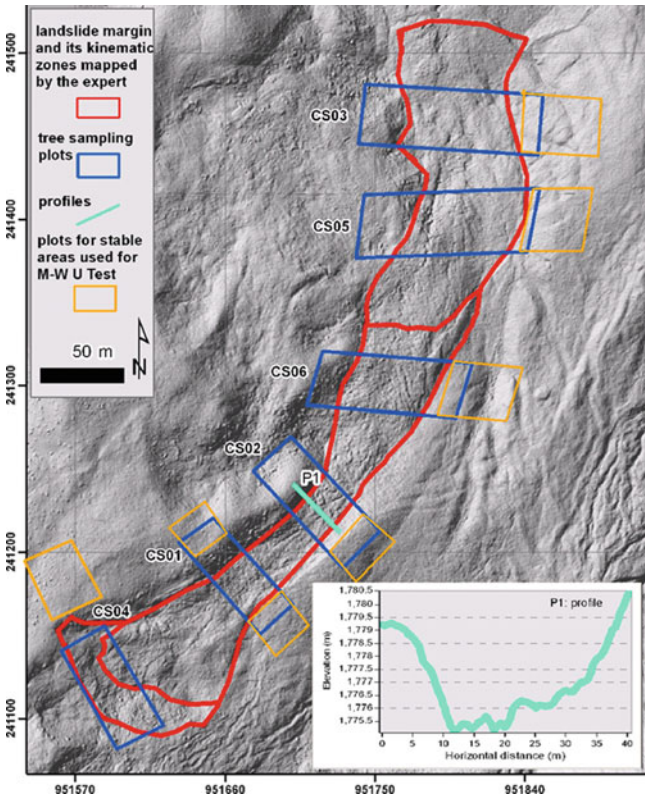

Fig. 3 Landslide and its kinematic zones mapped by an expert image interpreter in the Bois Noir catchment, France. Tree sampling plots used for vegetation analysis, stable tree plots and a transport zone profile are also presented

Accuracy of LiDAR-derived Tree Growth Anomalies

The quality of extracted parameters of tree irregularities (tree height and inclination) is presented in this section. Figure 4 shows the scatter plot of LiDAR-derived single tree heights versus tree heights from field data. Tree heights of the 110 trees measured in the field ranged from 6.8 to 19 m, with an average of 11.9 m. The coefficients of determination for tree height were 0.91, 0.72, and 0.82 for

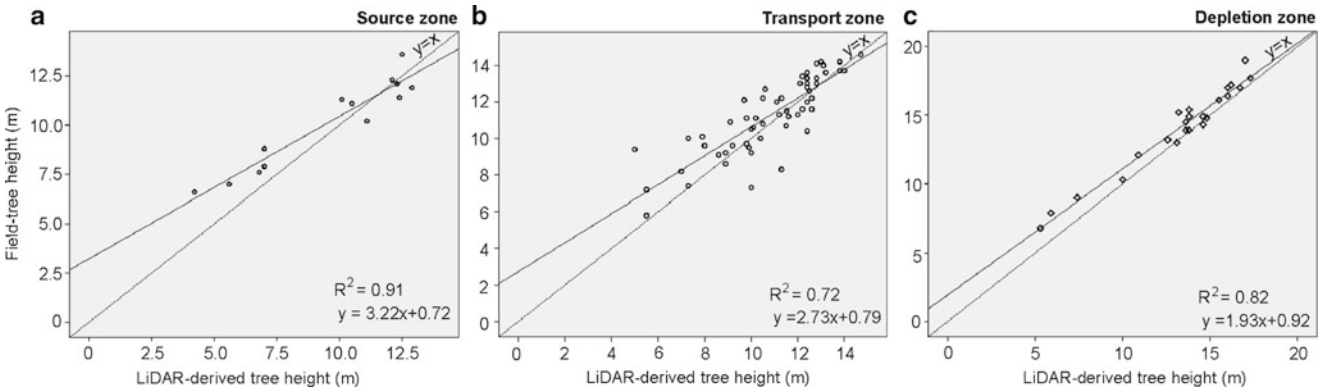

Fig. 4 Scatter plots of LiDAR-derived tree heights versus field-derived tree heights for three landslide kinematic zones

Table 2 Statistical measures of tree height demonstrated in three landslide kinematic zones

Landslide zones	n	*MA%E*	*RMSE*	R^2
Source	14	0.17	1.19	0.91
Transport	72	0.09	1.28	0.72
Depletion	24	0.07	1.07	0.82

landslide source, transport, and deposition zones, respectively (Table 2). This result is comparable to Popescu et al. (2002), who predicted dominant tree height, with R^2 value of 0.84 in the healthy forest characterized by gentle slopes.

Here the accuracy of estimated tree heights was slightly lower because most of the trees are located on the undulated terrain with steep slope and surface roughness. For instance, we estimated slope of up to 50° and surface roughness of up to 40 cm in the transport zone. We also observed that a large number of the trees are irregular (e.g. bended or tilted) and tend to entangle their crown areas. These factors have direct impact on the accuracy of tree height.

The SkelTre-skeletonization method is capable to extract the tree inclination from the high density LiDAR data (Fig. 5). The 1:1 relationship lines are also indicated in Fig. 5. SkelTre mostly under-predicts the inclination, which is more prominent in the source zone tree inclination below 40°. Furthermore, Table 3 shows the deviance measures (*MA%E* and *RMSE*) and linear regression of tree inclination. The coefficients of determination for tree inclination were 0.82°, 0.60° and 0.83° for source, transport, and deposition zones, respectively. We found about 16 % of the single trees could not be processed by this method. More than half of these trees are located in the transport zone. It is because of insufficient points on the tree particularly at the lower tree stem and complexity of tree structure.

These factors also caused large residuals in the tree inclination prediction. Trees will continue to grow vertically upright after the movement stops and show bended tree trunks may also difficult to extract from the LiDAR data. We observed in the field that most of the irregular trees are bended trees, over-tilted trees, and back-tilted. Furthermore, trees located on steep slopes or areas with a high local surface roughness are hard to delineate and therefore could limit the performance of the SkelTre-skeletonization method.

So far, we used manual tree delineation for providing the input data for the SkelTre-skeletonization, which requires the point cloud of a single tree as a data input. Manually delineating single trees is very time consuming. We spent about 18 h for manually delineating 110 single trees. The quality of delineated data has a direct impact on the quality of extracting tree inclination. Although, manual tree delineation employs the human cognitive process to distinguish between points belonging to a particular tree, a (semi) automatic single trees delineation is required when huge data sets of eventually larger areas are analyzed.

Tree Irregularities in Relation to Landslide Occurrences

We observed in the field that trees inside the landslide zones have a lower height, dissimilarity height, and are more inclined. To support the field evidence, we performed a statistical Mann-Whitney U test for tree height and inclination in three kinematic zones.

With a p-value < 0.05, we found that the tree height is lower and dissimilar in the landslide than in the stable areas (Table 4). This holds for all landslide kinematic zones. Trees are also more inclined in the landslide area than in the stable area (Table 5) at the 95 % confidence level. Our results refuted the initial hypothesis that no differences are present. In total we analyzed about 1,701 and 121 trees for tree height and inclination, respectively.

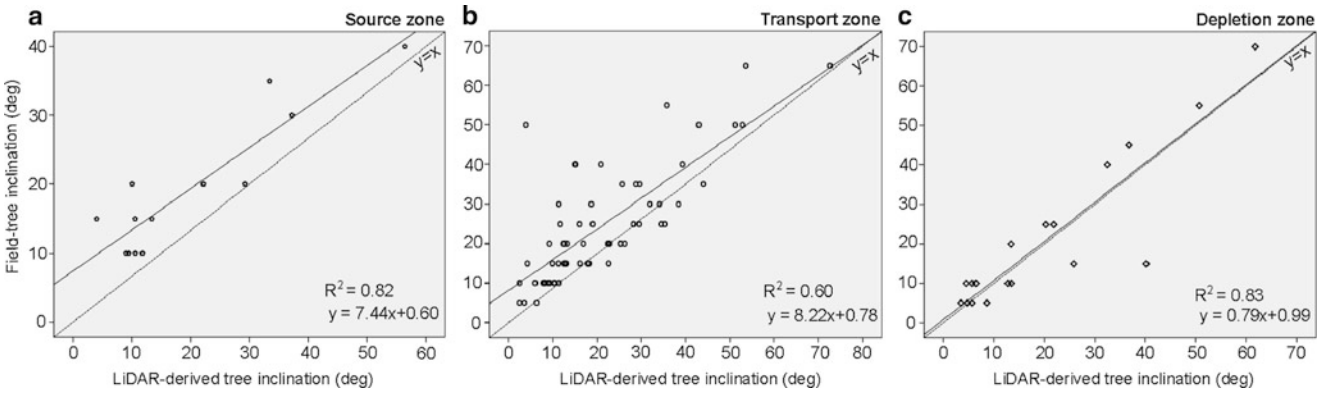

Fig. 5 Scatter plots of LiDAR-derived tree inclination versus field data (**a**) source (**b**) transport, (**c**) depletion zone

Table 3 Accuracy of SkelTre-skeletonization inclination prediction for three landslide kinematic zones

Landslide zones	n	*MA%E*	*RMSE*	R^2
Source	13	0.25	7.14	0.82
Transport	61	0.28	10.27	0.60
Depletion	18	0.38	7.94	0.83

Table 4 Mann-Whitney U Test for tree height presented in three landslide kinematic zones

Landslide zones	Landslide area		Stable area		*P-value*
	n	Mean rank	n	Mean rank	
Source	100	60.93	55	109.04	$P < 0.001$
Transport	235	255.53	430	375.34	$P < 0.001$
Depletion	343	398.13	538	468.33	$P < 0.001$

Table 5 Mann-Whitney U Test for tree inclination presented in three landslide kinematic zones

Landslide zones	Landslide area		Stable area		*P-value*
	n	Mean rank	n	Mean rank	
Source	13	11.15	5	5.20	$P < 0.034$
Transport	61	43.20	14	15.32	$P < 0.001$
Depletion	18	17.39	10	9.30	$P < 0.013$

Parise (2003) addressed that vegetation with a certain degree of disturbance could reveal different phases of movement, indicates amounts of movement, and relative age of these movements. In spite of assumption that landslides under forest are often to be dormant, Van Den Eeckhaut et al. (2009) proved that local reactivations within the landslide zones are likely to occur. LiDAR-derived tree growth anomalies and their spatial distribution may potentially be used to identify patterns of landslide activity that influence long-term movement in forested mountainous landscapes.

Conclusions

In this study, we have shown that high density LiDAR is capable to objectively map the margin of a complex landslide and its kinematic zones, and to characterize tree growth anomalies caused by landslides beneath 100 years old forest in the Barcelonnette basin, the Southern French Alps.

High resolution LiDAR-derived images allow us to digitally map landslides over complex landscape with unprecedented resolution and accuracy, particularly in vegetated older dormant slides which may not unrecognizable on aerial-photos or multispectral digital imagery (Wills and McCrink 2002). The generation of a detailed landslide inventory in forested mountainous area is considered important for landslide hazard assessment.

We used the TreeVaW method to automatically extract the tree height from HDAL data. We predicted dominant tree height in landslide source, transport, and deposition zones, with R^2 values of 0.91, 0.72, and 0.82, respectively. We observed that many trees are irregular and tend to entangle their crown areas in the transport zone which may influence the estimation of tree height. The SkelTre-skeletonization method is capable to reveal the tree inclination from the HDAL data. The coefficients of determination for tree inclination were 0.82, 0.60, and 0.83 for source, transport, and deposition zones, respectively. This method have tendency to under-predict the tree inclination. In an active landslide zone, the *MA%E* and *RMSE* for tree inclination prediction are 0.28 and 10.27, respectively. However, this method is depending on sufficient number of points on the tree stem and quality of delineated point clouds.

The tree growth anomalies are parameterized by tree height dissimilarities and tree inclinations. These parameters were successfully extracted from the HDAL data and revealed the underlying landslide activity. More

research is required to improve the tree detection algorithm and skeletonization method. Further study is planned to increase the number of field validation data and to expand the tree growth anomaly parameters into tree orientation at different tree heights, local tree density, tree diameter at breast height, and stem biomass. Differentiating the tree shape in response to earth surface processes in a larger area such as pressure of snow-pack, wind, rockfall, creep of sub-soil, and slope inclination also require further research work.

Acknowledgments This work was supported by the Malaysia Fellowship (Ministry of Higher Education and Universiti Teknologi Malaysia), ITC-University of Twente in collaboration with Department of Physical Geography, Utrecht University, the Netherlands. The authors are grateful to Jean Philippe Malet (University of Strasbourg) for managing the airborne LiDAR campaign under funding from the French Project ANR Risk-NatSISCA 'Système Intégré de Surveilllance de Glissements de Terrain Argileux' (2009–2021) and Restauration des Terrains de Montagne (RTM, Division of Barcelonnette). This research also contributes to the EU FP7 Safeland project.

References

Alexandrowicz Z, Margielewski W (2010) Impact of mass movements on geo- and biodiversity in the Polish Outer (Flysch) Carpathians. Geomorphology 123:290–304

Bucksch A (2011) Revealing the skeleton from imperfect point clouds. Ph.D. Thesis at Delft University of Technology, Dr. Hut, Munich. ISBN:978-3-86853-877-9

Bucksch A, Lindenberg R, Menenti M (2010) Robust skeleton extraction from imperfect point clouds. Visual Comput 26(10):1283–1300

Bucksch A, Lindenberg R, Menenti M, Rahman MZA (2009) Skeleton-based botanic tree diameter estimation from dense LiDAR data. In: Upendra N. Singh (ed) Lidar remote sensing for environmental monitoring. Proceedings of SPIE, vol 7460

De Villiers M (2001) Water - the fate of our most precious resource. Mariner Book, Boston, p 352. ISBN 0-618-12744-5

Haneberg WC, Cole WF, Kasali G (2009) High resolution lidar-based landslide hazard mapping and modeling, UCSF Parnassus Campus, San Francisco, USA. Bull Eng Geol Environ 68(2):263–276

Kasai M, Ikeda M, Asahina T, Fujisawa K (2009) LiDAR-derived DEM evaluation of deep-seated landslides in a steep and rocky region of Japan. Geomorphology 113:57–69

Lundstrom T, Stoffel M, Stockli V (2008) Fresh-stem bending of silver fir and Norway spruce. Tree Physiol 28:355–366

Mackey BH, Roering JJ (2011) Sediment yield, spatial characteristics, and the long-term evolution of active earthflow determined from airborne LiDAR and historical aerial photographs, Eel River, California. Geol Soc Am Bull. doi:10.1130/B30306.1.1

Mackey BH, Roering JJ, McKean JA (2009) Long-term kinematics and sediment flux of an active earthflow, Eel River, California. Geology 37:803–806

McKean J, Roering JJ (2004) Objective landslide detection and surface morphology mapping using high-resolution airborne laser altimetry. Geomorphology 57:331–351

Parise M (2003) Observation of surface features on an active landslide, and implications for understanding its history of movement. Nat Hazards Earth Syst Sci 3:569–580

Popescu SC, Wynne RH, Nelson RF (2002) Estimating plot-level tree heights with lidar: local filtering with a canopy-height based variable window size. Comput Electron Agr 37:71–95

Popescu SC, Wynne RH (2004) Seeing the trees in the forest: using lidar and multispectral data fusion with local filtering and variable window size for estimating tree height. Photogramm Eng Rem S 70(5):589–604

Razak KA, Straatsma MW, van Westen CJ, Malet J-P, de Jong SM (2011) Airborne laser scanning of forested landslide characterization: terrain model quality and visualization. Geomorphology 126:186–200

Schulz WH (2007) Landslide susceptibility revealed by LIDAR imagery and historical records, Seattle, Washington. Eng Geol 89:67–87

Stoffel M (2006) A review of studies dealing with tree rings and rockfall activity: the role of dendogeomorphology in natural hazard research. Nat Hazards 39:51–70

Van Den Eeckhaut M, Poesen J, Verstraeten G, Vanacker V, Nyssen J, Moeyersons J, Van Beek LPH, Vandekerckhove L (2007) Use of LIDAR-derived images for mapping old landslides under forest. Earth Surf Proc Land 32:754–769

Van Den Eeckhaut M, Muys B, Van Loy K, Poesen J, Beeckman H (2009) Evidence for repeated re-activation of old landslides under forest. Earth Surf Proc Land 34:352–365

Wills CJ, McCrink TP (2002) Comparing landslide inventories, the map depends on the method. Environ Eng Geosci 8(4):279–293

A GIS Method for Obtaining Geologic Bedding Attitude

Ivan Marchesini, Michele Santangelo, Federica Fiorucci, Mauro Cardinali, Mauro Rossi, and Fausto Guzzetti

Abstract

Landslide susceptibility assessment at different scales and in different physiographic environments requires quantitative information on multiple thematic environmental data. Information on bedding attitude proves necessary to define the structural and geological setting of an area. In this study, we developed a procedure to obtain bedding attitude data exploiting aerial photo-interpretation and a GRASS GIS script. Results show that our procedure provides bedding attitude information in good agreement with data acquired during field surveys. We foresee the possibility to generate dense spatial distributions of bedding attitude data, useful for spatial interpolation and landslide susceptibility assessments.

Keywords

Landslides • Susceptibility • Bedding attitude • GIS • Aerial photo-interpretation

Introduction

Bedding attitude (BA) information is useful to define the structural and geological setting of an area, and is important for the determination of landslide susceptibility (Guzzetti et al. 2006). Bedding attitude can be defined as the spatial arrangement of the bedding planes, and is commonly expressed by dip direction and dip angle (inclination) values. BA measurements can be collected during structural surveys, or through the interpretation of aerial photographs (API). The first method provides quantitative local (point) measures of bedding attitude that may not be representative of the regional structural setting. The second method provides semi-quantitative BA information representative of a general geological and structural arrangement, suitable for medium- to small-scale assessments.

The intersection line between a bedding plane and topography (i.e., the bedding trace, BT) allows to (1) infer the bedding surface (BS), the flat surface that locally approximates the bedding plane, and (2) estimate the bedding attitude (Fig. 1). The method is known as "structure contours" (e.g. Rowland and Duebendorfer 1994). In the literature, little exists on the development of systems to exploit GIS methods and API to obtain quantitative BA information (Cardinali et al. 2001). For the purpose, we present a procedure in two steps: (1) a preliminary API of an image dataset, performed by trained geomorphologists, and (2) the subsequent processing of bedding traces through a script implemented in a GIS environment.

Materials and Methods

Bedding Trace Mapping

API criteria to detect and map bedding traces (BTs) are based mainly on the morphoselection principle. Sequences of rock layers with different strength, grain size, and mineralogical

I. Marchesini (✉) • M. Cardinali • M. Rossi • F. Guzzetti
I.R.P.I. – C.N.R, Via Madonna Alta 126, Perugia, Italy
e-mail: Ivan.Marchesini@irpi.cnr.it

M. Santangelo • F. Fiorucci
I.R.P.I. – C.N.R, Via Madonna Alta 126, Perugia, Italy

Dipartimento di Scienze della Terra, Università degli Studi di Perugia, Piazza dell'Università 1, Perugia, Italy

C. Margottini et al. (eds.), *Landslide Science and Practice*, Vol. 1,
DOI 10.1007/978-3-642-31325-7_32,

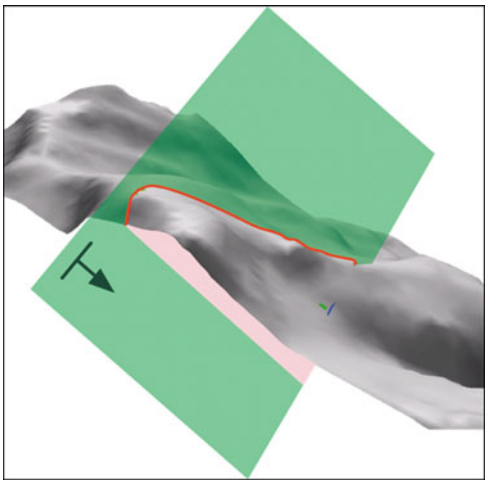

Fig. 1 Example of bedding trace (BT, *red line*), bedding surface (BS, *green plane*), and bedding attitude (BA, symbol with *arrow*)

composition, have a distinct morphological and photographic signature. Such characteristics are shown in stereoscopic aerial photographs. Hence, a trained geomorphologist is capable to detect the BTs, and to define the related qualitative BAs. In particular, bedding traces can be identified by photographic and morphological elements such as: (1) sub-parallel bands having different colour tones in unvegetated areas, (2) the presence of sub-parallel vegetation bands, (3) the repetitive variations in terrain gradient along a slope, and (4) geomorphological considerations on the asymmetry of a relief.

The vertical exaggeration typical of stereoscopic view allows detecting very subtle morphological features. Figure 2a shows a 2D view of a satellite image where BTs are represented by numerous sub-parallel linear bands of different shades of colour. In the 3D image (Fig. 2b), the intersection of bedding traces with topography provides clear information on bedding attitudes.

Bedding Attitude Estimation

We implemented a GIS tool using shell scripting in GRASS GIS environment (GRASS Development Team 2010) and GNU-Linux OS. The script returns a vector map of points whose attributes contain information on dip angle, dip direction, and associated uncertainty. A bedding traces map (represented by open and closed lines), and a DEM are necessary to execute the code.

The script is in five steps, which are replicated for each BT. In the first step, the bedding trace is draped on the DEM becoming a 3D linear feature (Fig. 3a). If the BT is an open line, (second step) the script draws a three-dimensional segment to join the two end nodes of the line representing the bedding trace (Fig. 3b). The new line and the BT form a polygon. In the third step, the 3D polygon boundary is sampled to obtain a sequence of regularly spaced points. Point spacing depends on the resolution of the DEM. A 3D Delaunay triangulation (Davis 1973) is then performed. The Delaunay triangulation method was selected because it limits user subjectivity. The result is a nearly flat surface corresponding to the bedding surface – BS (Figs. 3c and 4a). The fourth step consists in calculating the BS slope (Fig. 4b) and aspect (Fig. 4c) raster maps. The mean values for the dip angle and the dip direction of the bedding surface are estimated in the fifth step. The average BS inclination is the median of the slope map values. Then, the standard deviation (a measure of uncertainty) of the slope map is calculated.

Average bedding trace dip direction is calculated following the method proposed by Davis (1973). Sine and cosine of the aspect map are calculated. The average aspect (dip direction) of the BS is determined using mean sine and cosine values. The statistical spread of the dip direction is calculated in two methods. In the first method, circular variance (V) is calculated as:

$$V = \frac{1 - R}{n}$$

where n is the number of cells of the bedding surface aspect map, and R is the modulus of the resultant vector of the unitary vectors of each aspect map cell. V can take values in the range from 0 to 1. Low V values indicate a nearly flat surface, and higher values indicate a steep surface (Davis 1973; Nichols 2009). The second method estimates the angular standard deviation of the aspect map as (Butler 1992):

$$S = \frac{1}{(\mathrm{n} - 1)} \sum_{i=1}^{n} \Delta_i^2$$

where, Δ_i is the angle between the aspect of the i-th cell and the average aspect, and n is the number of the aspect map cells.

All the values (i.e. median slope, slope standard deviation, average aspect, circular variance, angular standard deviation) are assigned to a bedding attitude point-vector layer. Each point in the layer is the centroid of the bounding box of the corresponding bedding trace.

Results

We tested the procedure in the Collazzone study area, Umbria, central Italy. Two geomorphologists interpreted stereoscopic b/w aerial photographs taken at 1:33,000 scale in 1954. The images proved effective for the analysis because forest cover was sparse at the time of the photographs, allowing for the recognition of geomorphological features even in forested areas. The bedding traces (BTs) were drawn on a transparent film superimposed on the aerial photographs.

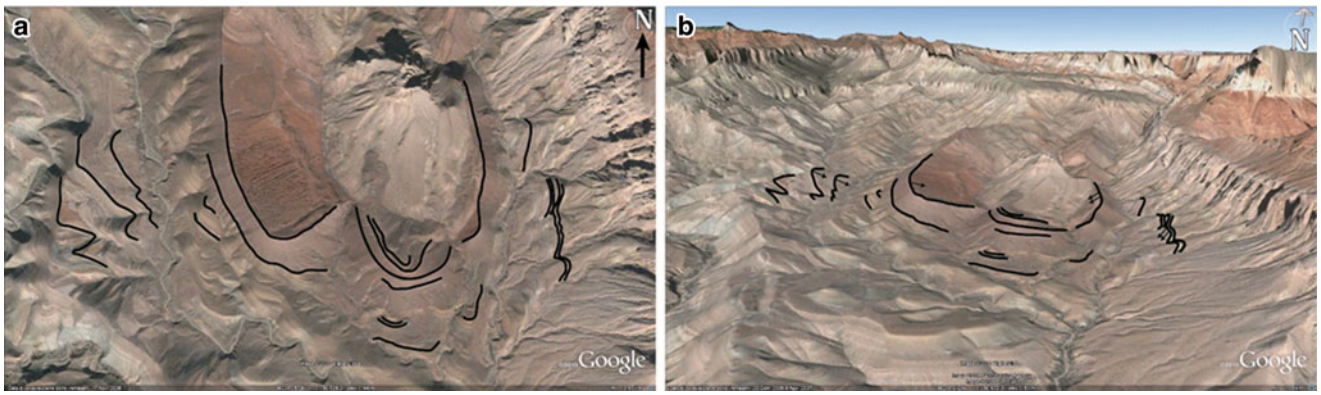

Fig. 2 Example of bedding traces detected by photointerpretation criteria on a GoogleEarth image of Grand Canyon, (AZ). (**a**) The bedding traces are recognizable even by photographic elements alone. (**b**) The three-dimensional view emphasizes the intersection of the same BTs with topography and allows to estimate the dip and dip direction of bedding planes (BA)

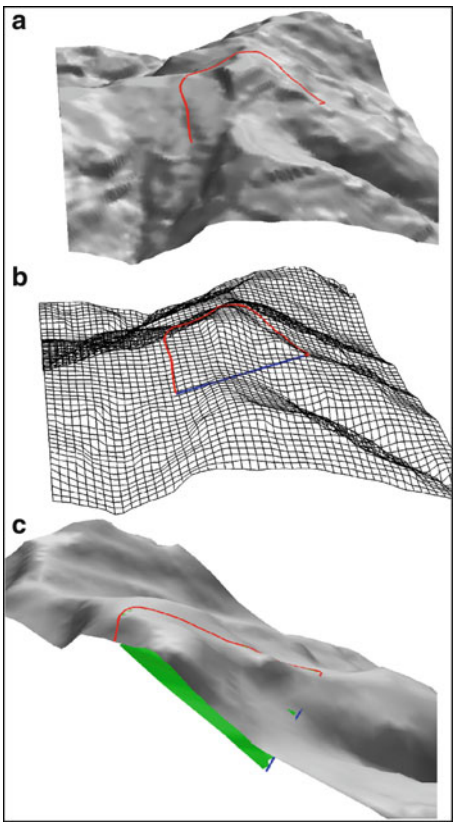

Fig. 3 (**a**): Bedding trace draped on the DEM, (**b**): bedding trace nodes joining, (**c**): bedding surface (BS) is drawn in *green*

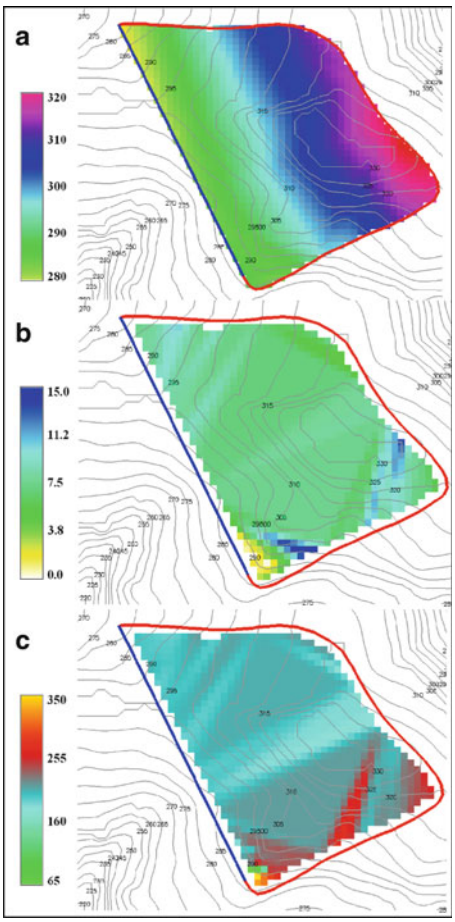

Fig. 4 (**a**): BS elevation map (meters a.s.l.), (**b**): BS slope map (degrees), (**c**): BS aspect map (degrees, CCW from east)

In a second step, the mapped features were visually transferred (re-drawn) on a transparent non-deformable plastic sheet superimposed on a 1:10,000 scale topographic base map. Then, the transparent sheet was scanned and geo-referenced to enable digitization and storage of the information in a GIS vector layer. When transferring the information from the aerial photographs to the GIS dataset, errors can occur due to e.g.: (1) the change in scale, from the smaller scale of the aerial photographs (1:33,000) to the larger scale of the topographic map (1:10,000 scale), (2) object deformation on the stereoscopic model, due to the vertical exaggeration and the conical projection of the aerial photographs, (3) differences in

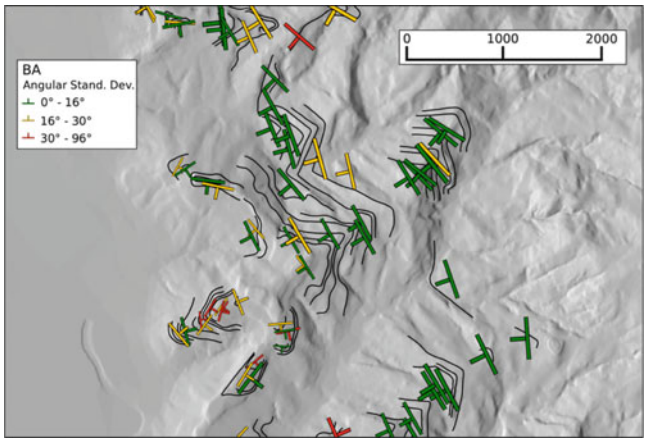

Fig. 5 BAs can be represented by means of oriented symbols (according to dip direction), different dimensions (proportional to the inclination value), and different colours (according to three different levels of dip direction angular variance)

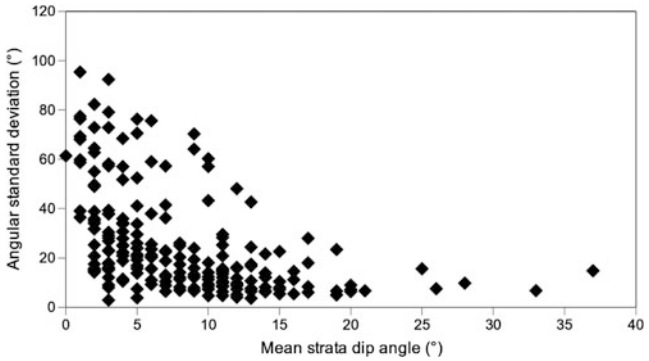

Fig. 6 The graph shows the BSs angular standard deviation against the mean inclination of the BSs for the Collazzone BTs dataset. The angular standard deviation (V) of the BSs dip direction is generally high only when the BSs dip is low

topography in the different cartographic media (aerial photographs and base maps) (Ardizzone et al. 2007), (4) the absence in the topographic base map of BTs' photographic elements. This results in mapping errors (positioning and shape) of the single bedding trace.

After the interpretation of aerial photographs (API), the GRASS script was executed obtaining a preliminary bedding attitudes layer. The layer was then analysed by the geomorphologists to identify bedding traces that needed corrections. We used a 3D digital model obtained from a pair of stereoscopic VHR satellite images taken by the GeoEye satellite in May 2010. The three-dimensional BTs were superimposed to the oriented stereoscopic model, and the error corrected. Where necessary, new 3D bedding traces were digitized directly on the oriented stereo pair. Finally, a second run of the script was executed using the revised BTs dataset to produce a new BA layer. Figure 5 shows details of the obtained bedding attitude map. In the Figure BAs are represented by oriented symbols, scaled to the inclination value.

Bedding inclination spans the range from 1° (small bedding symbol) to 20° (large bedding symbol). The angular standard deviation (S) is less than 16° for half of the BAs dataset, and less than 30° for 75 % of the BA data. Most of the bedding attitudes that have high values of S are characterized by low values of the mean slope (sub-horizontal layers, see chart in Fig. 6). This explains the strong directional variability. Inclination values are less scattered. About 75 % of the values of the dip standard deviation are smaller than 2°, with a maximum value of 8°.

A quality assessment of the results obtained was performed through a visual inspection carried out by the same geomorphologists who performed the API. The representation, with colours and oriented symbols, has proved particularly useful in facilitating the verification of the degree of matching between BAs and the geomorphologists' expectations.

The obtained bedding attitude data (red symbols in Fig. 7) were further compared to data obtained during geological field surveys (yellow symbols in Fig. 7). Visual comparison of the two datasets indicates that the BAs obtained through the API and GIS procedure are more widespread and consistent with the dominant structures in the study area (a syncline is highlighted in Fig. 7).

Discussion and Conclusion

We developed a procedure to obtain bedding attitude data from aerial photo-interpretation using a GRASS GIS script. Advantages of the procedure include: (1) a quantitative estimation of the inclination and dip direction of multiple BTs mapped trough API, (2) a significant increase in the number of bedding attitude features compared to those obtained during field surveys, (3) the rapid execution of the procedure, compared to long and expensive field surveys, and (4) the fact that the obtained BA features are not influenced by local anomalies.

Bedding attitudes obtained exploiting API and the GRASS GIS script are quantitative, distributed geographically, and representative of the dominant geological structures in the study area. Using the proposed method it is possible to obtain a dense spatial distribution data, useful for BAs spatial interpolation (Meentemeyer and Moody 2000; Günther 2003; Günther et al. 2004; Ghosh et al. 2010).

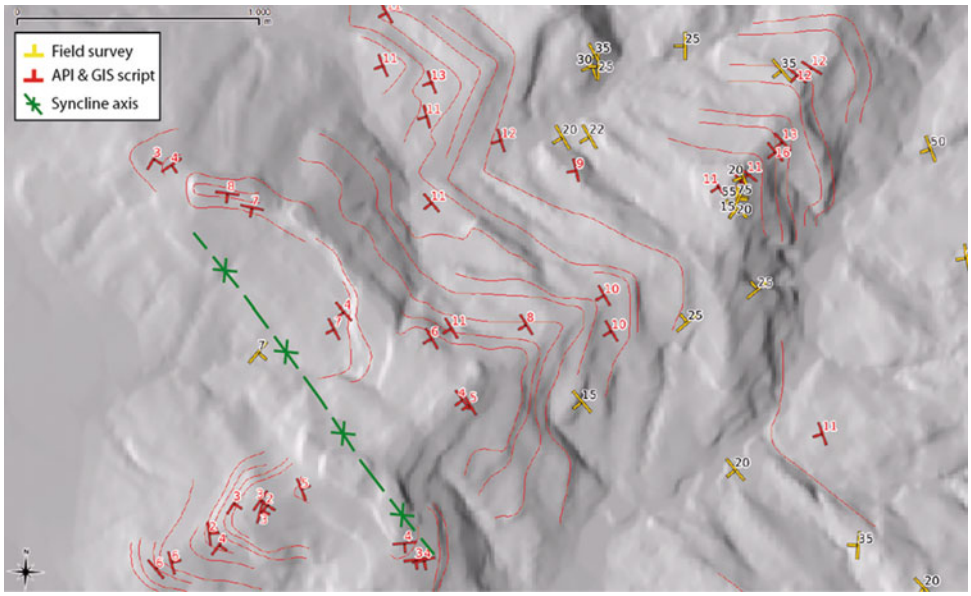

Fig. 7 Comparison of the BAs obtained by means of the procedure (*red symbols*) with data relating to a detailed geological survey (*yellow symbols*). In *green synclyne axis* is drawn. Inclination values are labelled

The GRASS shell script has not been tested in areas characterized by steeply inclined bedding planes, and is available (http://geomorphology.irpi.cnr.it/tools) under the terms of the GPL licence.

References

Ardizzone F, Cardinali M, Galli M, Guzzetti F, Reichenbach P (2007) Identification and mapping of recent rainfall-induced landslides using elevation data collected by airborne Lidar. Nat Hazards Earth Syst Sci 7:637–650

Butler RF (1992) Paleomagnetism: magnetic domains to Geologic Terranes. Blackwell Scientific Publications – Boston. Oxford. http://www.geo.arizona.edu/Paleomag/book/

Cardinali M, Antonini G, Reichenbach P, Guzzetti F (2001) Photo geological and landslide inventory map for the Upper Tiber River basin. Publication CNR GNDCI n. 2116, Scale 1:1,200,000

Davis JC (1973) Statistics and data analysis in geology, 2nd edn. Wiley, New York

Ghosh S, Günther A, Carranza EJM, van Westen CJ, Jetten VG (2010) Rock slope instability assessment using spatially distributed structural orientation data in Darjeeling Himalaya (India). Earth Surf Proc Land 35:1773–1792

GRASS Development Team (2010) Geographic Resources Analysis Support System (GRASS) Software, Version 6.4.0. Open Source Geospatial Foundation. http://grass.osgeo.org

Günther A (2003) SLOPEMAP: programs for automated mapping of geometrical and kinematical properties of hard rock hill slopes. Comput Geosci 29:865–875

Günther A, Carstensen A, Pohl W (2004) Automated sliding susceptibility mapping of rock slopes. Nat Hazards Earth Syst Sci 4:95–102

Guzzetti F, Reichenbach P, Ardizzone F, Cardinali M, Galli M (2006) Estimating the quality of landslide susceptibility models. Geomorphology 81:166–184

Meentemeyer RK, Moody A (2000) Automated mapping of conformity between topographic and geological surfaces. Comput Geosci 26:815–829

Nichols G (2009) Sedimentology and stratigraphy. Wiley/Blackwell, Chichester/UK

Rowland SM, Duebendorfer EM (1994) Structural analysis and synthesis: a laboratory course in structural geology. Blackwell, Malden, USA

DP Test in Geotechnical Characterization of Shallow Landslides Source Area: Results and Perspectives

Giacomo D'Amato Avanzi, Yuri Galanti, Roberto Giannecchini, Susanna Duchi, Diego Lo Presti, and Daria Marchetti

Abstract

Aiming at improving the knowledge on the source areas of shallow landslides, this research deals with the geotechnical characterization of the debris slope cover of arenaceous formations, by means of low cost dynamic penetration tests (Dynamic Probing – DP).

The knowledge of strength parameters of this material is fundamental to understand the triggering mechanisms of the shallow landslides. Therefore, in order to determine the typical values of relative density (D_R) and internal friction angle (ϕ'), many tests were performed and the results of 132 Dynamic Probing tests, 74 Standard Penetration Tests (SPT) and 14 laboratory shear tests, were analysed. The comparison between the ϕ' values obtained by DP tests with those resulting from direct shear tests evidenced a good linear correlation. This confirmed the satisfactory and repeatable results of DP tests. Therefore, Dynamic Probing can be an effective, simple, practical and inexpensive tool for the geotechnical characterization of hazardous slopes.

Keywords

Dynamic Probing test • Friction angle • Shallow landslide • Source area • Tuscany

Introduction

In Italy and all over the world, severe rainfall events produce many rapid shallow landslides, mostly soil slip-debris flows, which often cause victims and huge damage (Campbell 1975; Hutchinson 1988; Crosta et al. 1990; Sassa 1998; Hungr et al. 2001). Many meaningful examples of disasters caused by rapid shallow landslides and debris flows may be mentioned in several areas: China (Tang et al. 2011), Japan (Wang et al. 2002), New Zealand (Ekanayake and Philipps 2002) and USA (Ellen and Wieczorek 1988). Other examples come from Italy, such as Campania (Del Prete et al. 1998; Cascini 2004; Guadagno and Revellino 2005), Northern Tuscany (Delmonaco et al. 2003; D'Amato Avanzi et al. 2004; Casagli et al. 2006), Ischia Island (De Vita et al. 2007). Once more, in October 2010 some rapid landslides caused three deaths in the Massa-Carrara Province (North-Western Tuscany). In Northern Tuscany the soil slip-debris flows mainly involve the colluvium/debris slope cover of arenaceous or arenaceous-pelitic formations, which largely crop out in mountains areas, where the rainfall events triggering landslides are frequent (Giannecchini 2005, 2006).

High destructive power and spatial-temporal unpredictability make the rapid shallow landslides very dangerous and hard to oppose, mainly due to the following factors: extremely rapid triggering and evolution, difficulty of prediction, lack of knowledge about triggering mechanisms, high areal frequency and high run-out distance. Furthermore, rainfall data are often lacking, especially in mountain areas. Then, critical rainfall threshold assessment and civil protection planning become difficult operations. Therefore, a deep

G.D. Avanzi • Y. Galanti (✉) • R. Giannecchini • S. Duchi • D. Marchetti
Earth Sciences Department, University of Pisa, Via S. Maria, Pisa 53-56126, Italy
e-mail: galanti@dst.unipi.it

D.L. Presti
Civil Engineering Department, University of Pisa, Via Carlo F. Gabba, Pisa 22-56122, Italy

C. Margottini et al. (eds.), *Landslide Science and Practice*, Vol. 1,
DOI 10.1007/978-3-642-31325-7_33,

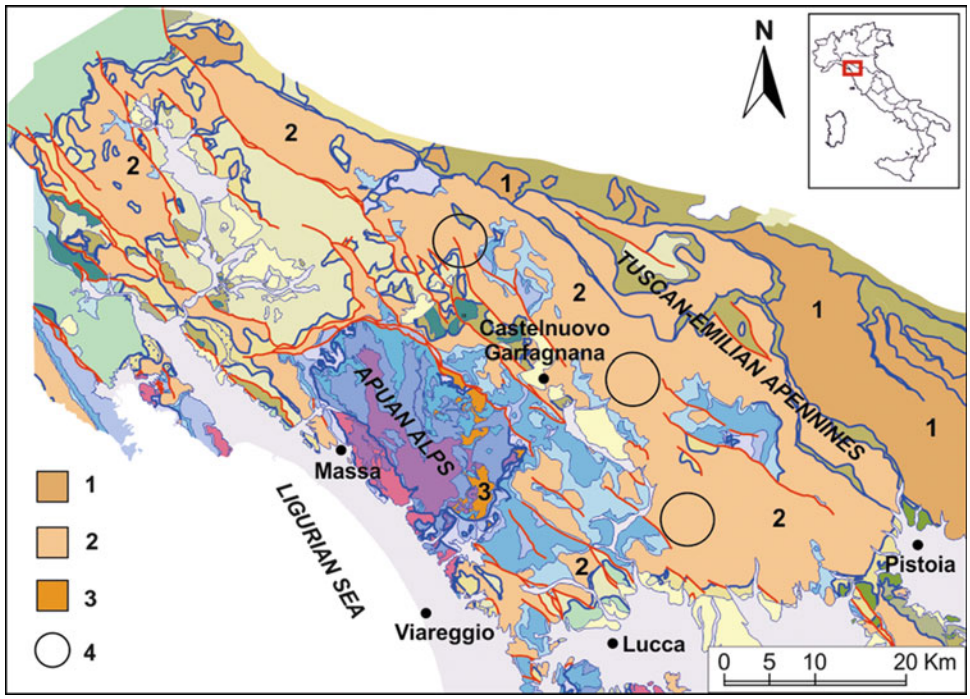

Fig. 1 Geologic sketch of the Northern Tuscany (After Carmigmani and Lazzarotto 2004, modified). *1* external sandstone flysch, *2* internal sandstone flysch (mainly Macigno Fm.), *3* meta-sandstone (Pseudomacigno Fm.), *4* sample areas

study of the physical-mechanical characteristics of the source areas is needed, in order to understand the triggering mechanisms of the shallow landslides and to contribute to the assessment of the hazard.

This paper aims at contributing to the characterization of the source area of the shallow landslides by means of Dynamic Probing (DP) tests. These tools are particularly suitable in scarcely accessible and impassable slopes, to obtain data on soil geotechnical properties and thickness. Original data collected on site and coming from databases are presented and discussed. They refer to limited but representative areas of the Northern Tuscany and the related experiences and considerations can be of general interest.

Geological Setting

The Northern Tuscany falls within the Northern Apennines, a fold-and-thrust belt, which mainly formed during the Upper Cretaceous-Upper Miocene. Since the Upper Miocene, tensional tectonics originated to several tectonic depressions bounded by NW-SE trending normal faults, in which either marine or continental successions deposited. The chain originated from the consumption of the Liguria-Piedmont oceanic basin, located in the western Tethys, and the consequent collision between the Adria and the European plates, which started in the Upper Cretaceous (Elter et al. 1975; Carmignani et al. 2004; Conti and Lazzarotto 2004).

On the Tuscan side of the Apennines, from the Upper Cretaceous to the Mid-Upper Miocene-Lower Pliocene a mainly compressive style was responsible for piling up and positioning of tectonic units coming from different paleogeographic domains (from west to east: Ligurian Domain, Sub-Ligurian Domain, Tuscan Domain). Since the Upper Miocene-Lower Pliocene extensional tectonics gave rise to tectonic depressions, in which neo-autochthonous sequences were deposited.

Since this paper deals with shallow landslides, the research focused on colluvium/debris slope covers of some peculiar arenaceous formations, well represented in Northern Tuscany. Among them the Macigno Fm. (Tuscan Nappe Unit) forms the main Apennines ridge and crops out for hundreds of square kilometres; therefore, it was firstly considered. This formation consists of siliciclastic turbidites made of grey-brown sandstone and normally shows a high sandstone/shale ratio and thick to very thick, coarse-grained strata. The sandstone is mainly composed of quartz, feldspar and mica, with high percentage of carbonate cement; the depositional environment is mainly referable to channelled submarine fans (Pandeli et al. 1994). Figure 1 shows the geological sketch map of the Northern Tuscany, highlighting the sandstone formations and the zones investigated.

Large debris slope covers characterize the Macigno Fm. and often completely mantle vast slopes and hide the bedrock. They mainly consist of sand and gravel with a minor portion of fine material. This considerable production of debris and colluvium results from several factors, such as:

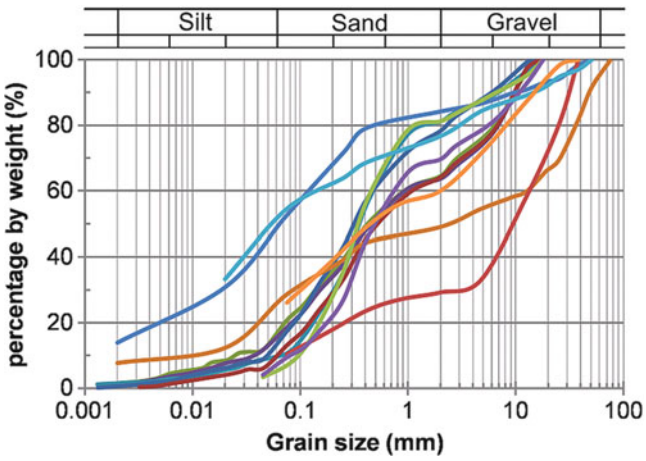

Fig. 2 Grain size distribution of the samples collected on slopes involving landslides

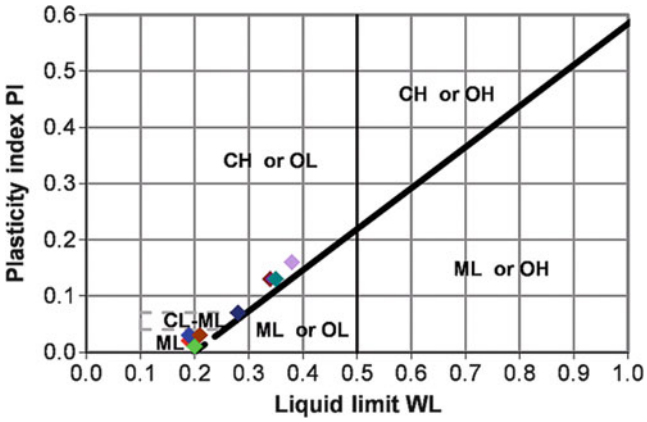

Fig. 3 Representation of the samples collected in the landslides source areas in the Plasticity Chart

morpho-climatic conditions of the Northern Tuscany, where the mountains intercept Atlantic and Mediterranean humid air masses, forcing their adiabatic lift and condensation in abundant precipitations; the particular composition of the Macigno Fm., sensible to chemical alteration in a temperate climate; tectonic evolution, which determined slow but continuous uplift and intense rock deformation and fracturing, so favouring its fragmentation.

Research Methods

Firstly, many technical reports were collected and analyzed in order to quantify the main physical and mechanical parameters of the Macigno Fm. debris cover, such as relative density (DR) and internal friction angle (ϕ'). Among them, 133 reports provided the results of 220 tests, subdivided into 91 Medium Dynamic Probing tests (DPM), 41 Super Heavy Dynamic Probing test (DPSH), 74 Standard Penetration Test (SPT) and 14 direct shear tests.

Moreover, in order to calibrate the penetration data, several soil samples were collected in the source areas of landslides (circled areas, Fig. 1), close to the penetration test sites. By laboratory tests their physical properties (index properties, grain size distribution, Atterberg limits) were determined.

Laboratory Analysis

The samples were usually collected using cylindrical samplers, 4.2 cm wide and 19.7 cm long. In consideration of the dimensions of the samplers and the technique of inserting, the material collected in situ was considered as disturbed. Other data come from professional reports including results of laboratory tests on undisturbed soil samples.

Figure 2 shows the grain size distribution of the materials analyzed. According to the USCS classification, the samples usually fall into the SM class (silty sand with gravel), whereas few samples fall into the SW-SM class (well-graded gravelly sand with silt) or in GP-GM class (poorly-graded gravel-sand mixture with silt). These soil classes were used in the geotechnical characterization.

Moreover, the Atterberg limits were analyzed in order to identify the plasticity properties of the Macigno Fm. debris (Fig. 3). The Atterberg limits plotted on the Casagrande plasticity chart show that the tested samples may be defined as low plasticity soils (liquid limit WL less than 50 %).

Dynamic Probing Tests

Methodology

There are not so many published data in literature about the mechanical characterization of coarse-grained soils, (e.g. Kokusho et al. 1995). This is mainly because of difficulties or impossibility of undisturbed sampling for laboratory test and intrinsic limits of the dynamic penetration tests. On the contrary, many dynamic penetration data are often available and may constitute an important basement for an areal characterization of the slope materials. In fact, the dynamic penetrometer is a practical, simple, quick and inexpensive tool for testing soil properties.

The test is based on the count of how many blows the penetrometer hammer needs to insert a probe for a prefixed length. The probe may consist of either a steel cone (Dynamic Probing) or a sampler (Standard Penetration Test). The Dynamic Probing (DP) test may be directly executed on the natural ground surface, whilst the Standard

Table 1 Classification of the dynamic penetrometers (Stefanoff et al. 1988)

Type	Acronym	Hammer mass (M, Kg)
Light	DPL	$M \leq 10$
Medium	DPM	$10 < 40$
Heavy	DPH	$40 \leq M < 60$
Super Heavy	DPSH	$M \geq 60$

Penetration Test (SPT) generally needs a borehole to perform the test in; therefore, easiness of transport, installation and use makes DP very suitable and cheaper than SPT. Nowadays dynamic penetration tests are commonly used to determine some soil properties such as thickness, internal friction angle and consistency. DP tests are suitable for any loose soil and very weak rocks, but are more proper for coarse-grained soils (Lo Presti and Squeglia 2008).

Nevertheless, many questions come from the use of DP tests: above all, in Italy and worldwide Dynamic Probing instruments have different characteristics and different methods of investigation may be used; this causes significant problems of standardization and comparability of results. Stefanoff et al. (1988) proposed a classification of dynamic penetrometers, based on the mass of the hammer (Table 1) and this is now commonly used worldwide. In Italy penetrometers of DPSH type are frequently used, while the DPM are mainly used in difficult to access areas, such as slopes, forested areas, etc.

As above mentioned, dynamic penetrometers are often used to estimate important geotechnical properties of soils, such as relative density (D_R) and angle of internal friction (ϕ'). This implies use of empirical correlations, which are not always particularly accurate, because of the lack of a complete standardization.

In a dynamic penetration test the worker counts the number (N_{DP}) of blows necessary to drive the probe for a prefixed length (step – 0.1 m for DPM test and 0.2 m for DPSH test) till the required depth is completed. In order to favour the comparison between results obtained by different penetrometer types, normalization with SPT is however necessary, determining the number of blows (N_{SPT}) referred to the SPT. The normalization uses the CF factor, namely the ratio between the specific energy per blow of DP (Q_{DP}) and SPT (Q_{SPT}). CF is calculated as follows:

$$CF = \frac{Q_{DP}}{Q_{SPT}} = \frac{(M_{DP} \times H_{DP})/(A_{DP} \times \delta_{DP})}{(M_{SPT} \times H_{SPT})/(A_{SPT} \times \delta_{SPT})} \quad (1)$$

where, $M_{DP\text{-}SPT}$: hammer mass (Kg); $H_{DP\text{-}SPT}$: mass falling height (cm); $A_{DP\text{-}SPT}$: area of the steel cone (cm^2); $\delta_{DP\text{-}SPT}$: cone penetration depth (cm) for DP and SPT, respectively.

The N_{SPT} is then calculated by the following relation:

$$N_{SPT} = CF \times N_{DP} \quad (2)$$

CF was calculated by the (1) obtaining 1.48 for DPSH and 0.76 for DPM. Usually the N_{SPT} is normalized to a standard penetrometer efficiency (ER) of 60 % (Skempton 1986) and an atmospheric pressure of 98.1 kPa (Liao and Whitman 1986). The penetrometer efficiency depends on the hammer system of the instrument and on the interaction between hammer and anvil. Most of the penetrometers used in Italy for SPT test have an equipment efficiency of 60 %, the same of the standard; for DPSH and DPM tests it is possible to consider an efficiency of 74 % (Pagani 2011) and 80 %, respectively.

The N_{SPT} value should be corrected also for a number of site-specific factors, to improve its comparability and repeatability (Rogers 2006), obtaining the final $(N_1)_{60}$. Therefore, the corrected $(N_1)_{60}$ represents the normalized value of N measured in situ and may be obtained as follows (Robertson and Wride 1997):

$$(N_1)_{60} = N_{SPT} \times C_N \times C_E \times C_B \times C_R \times C_S \quad (3)$$

where N_{SPT}: number of SPT blows; $C_N = (Pa / \sigma'_{V0})^{0.5}$: correction factor for effective overburden stress, with Pa: reference pressure (98.1 kPa); σ'_{V0}: vertical effective stress; $C_E = ER/60\%$: correction factor for hammer efficiency with ER: actual energy ratio (%) of the penetrometer used (C_E is 1.33 for DPM, 1.22 for DPSH and 1.00 for SPT); C_B: correction factor related to the borehole diameter; C_R: correction factor related to the drill rod length; C_S: correction factor for the sampler type. Table 2 shows the correction values commonly used.

The knowledge of $(N_1)_{60}$ allows calculating the relative density D_R by the following relation (Skempton 1986):

$$\frac{(N_1)_{60}}{D_R^2} = a + b \quad (4)$$

expression (4) may be written as:

$$D_R = \left(\sqrt{\frac{(N_1)_{60}}{a+b}}\right) \times 100 \quad (5)$$

Skempton (1986) took up the ratio $(N_1)_{60}/D_R{}^2$ as a parameter affected by overburden pressures, ageing and grain size of sands. The parameter (a + b) for sandy soils assumes a value of 55, 60 or 65 for fine, medium and coarse sand, respectively (Skempton 1986). In this study, such values were attributed to silty sand with gravel (SM), gravelly sand with silt (SW-SM) and gravel and sand with silt (GP-GW), respectively. These soil classes come from

Table 2 Recommended correction factors for SPT and DP blow-count values (After Robertson and Wride 1997, and Yound and Idriss 2001, modified)

Factor	Equipment variable	Term	Correction
Overburden stress		C_N	$(98.1/\sigma'_{v0})^{0.5}$
Borehole diameter	65–115 mm	C_B	1.00
	150 mm		1.05
	200 mm		1.15
Rod length	10–30 m	C_R	1.00
	6–10 m		0.95
	4–6 m		0.85
	3–4 m		0.80
	<3 m		0.75
Sampling method	Standard sampler	C_S	1.00
	Sampler without linears		1.1–1.3

Table 3 Empirical relations for estimating ϕ′ according to relative density and grain size (Schmertmann 1978)

Grain size	ϕ′ (°)
Fine sand	$28 + 0.14 \times D_R$
Medium sand	$31.5 + 0.115 \times D_R$
Coarse sand	$34.5 + 0.1 \times D_R$
Gravel and sand	$38 + 0.08 \times D_R$

laboratory tests on the considered soils, according to the USCS classification.

The knowledge of D_R indirectly allows obtaining the internal friction angle (ϕ′) using the Schmertmann's (1978) empirical relation. Table 3 shows the equations mainly used for coarse-grained soils.

Results

The estimation of geotechnical parameters requires classification of the soil into homogeneous layers, according to their values and trend of $(N_1)_{60}$ with depth. A grain size category, selected among silty sand with gravel (SM), gravelly sand with silt (SW-SM) and gravel and sand with silt (GP-GM), is attributed to each layer by comparing the $(N_1)_{60}$ values with the soil profile, coming from on site observation and boreholes close to the DP test. This is essential to calculate D_R and ϕ′ by means of the Skempton's (1986) and the Schmertmann's (1978) empirical relations, respectively, as above mentioned.

For each soil type the average values of D_R and ϕ′ were calculated, together with their standard error and standard deviation value. These values were obtained for all layers probed by DPSH and DPM tests; they are listed in Table 4 and 5, respectively.

Figure 4 shows the distribution of ϕ′ values for each soil type, according to the probing depth. The ϕ′ values show a considerable but reasonable dispersion, which is rather typical for data coming from indirect investigations, such as DP tests. Nevertheless, the ϕ′ mean values coming from DPM and DPSH tests remain comparable. The ϕ′ values show an increase in scattering around the mean values with increasing in grain size and sorting; DPM tests (Table 5; Fig. 4a) show this trend more clearly then DPSH tests (Table 5; Fig. 4b). The presence of pebbles in a silty-sand material, even in low percentage probably, causes a significant increase of N_{DP} (number of blows, coming from DP tests), and consequently in the D_R and ϕ′ values. Furthermore, at the little depth commonly investigated by Dynamic Probing tests (usually less than 5–6 m when investigating cover materials involving shallow landslides), the D_R and ϕ′ values of each soil type do not show significant increase with depth.

In order to validate the results, the values of D_R and ϕ′ obtained by DPSH and DPM tests were also compared with the results obtained in similar materials by SPT tests (Fig. 5). This comparison shows small differences: the SPT tests provided slightly higher internal friction angles (ϕ′) than DP tests and therefore seem to be less conservative; this is mainly true for silty sand. The ϕ′ values obtained by DP tests were compared with those resulting from direct shear tests performed on undisturbed samples, collected close to the DP sites, in the same soil type and the same depth and stress conditions. The comparison evidences a good linear correlation between the results of these different tests (Fig. 6), confirming the satisfactory and repeatable results of Dynamic Probing tests.

Table 4 Average values of D_R and related standard error and standard deviation values for the three considered soil types

Soil type	DP type	Average (%)	Standard error	Standard deviation
SM	DPSH	31.5	0.965	5.459
	DPM	32.8	0.766	9.030
SW-SM	DPSH	44.1	1.338	8.358
	DPM	48.5	0.944	10.889
GP-GM	DPSH	58.5	2.224	13.711
	DPM	67.9	1.943	15.178

Table 5 Average values of ϕ′ and related standard error and standard deviation values for the three considered soil types

Soil type	DP type	Average (°)	Standard error	Standard deviation
SM	DPSH	32.4	0.138	0.793
	DPM	32.6	0.107	1.264
SW-SM	DPSH	36.6	0.153	0.957
	DPM	37.1	0.109	1.252
GP-GM	DPSH	40.8	0.289	1.780
	DPM	41.5	0.223	1.739

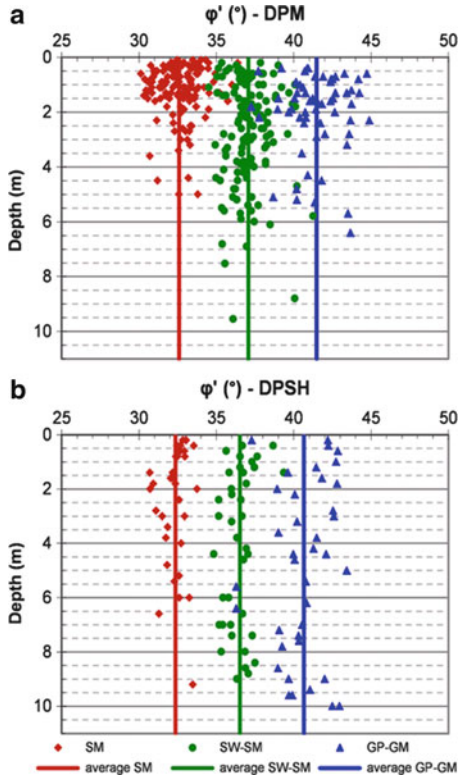

Fig. 4 Distribution of φ′ values for each soil type, according to the probing depth, obtained by DPM (**a**) and DPSH (**b**) tests, respectively. SM: silty sand with gravel; SW-SM: gravelly sand with silt; GP-GM: gravel and sand with silt

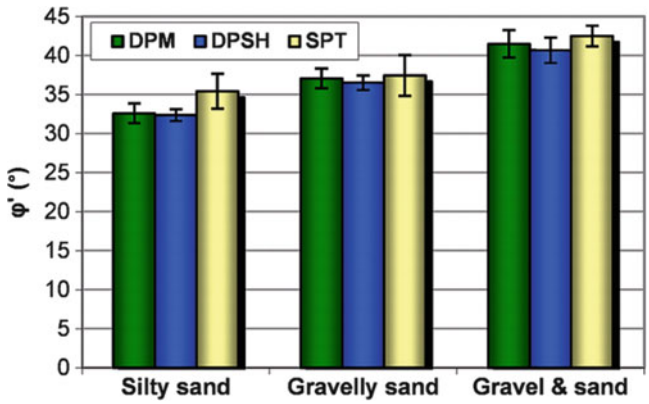

Fig. 5 Comparison between the φ′ values obtained for each soil type by DPM, DPSH and SPT tests. The little bars show the standard deviation

Final Remarks and Perspectives

The usefulness, suitability and adaptability of the penetration tests in characterizing the debris slope cover of sandstone sequences in the Northern Tuscany was tested in this paper. The study mainly focused on the debris formed by the most typical arenaceous formations, such as the Macigno Fm., vastly cropping out in the study area. The characterization based on Dynamic Probing tests (DPSH and DPM types), commonly used by geologists because of their numerous advantages. Even though literature does not offer so many data on mechanical properties of these particular granular materials, DP tests supplied useful data, providing a reliable characterization of the materials. In detail, 91 DPM, 40 DPSH, 74 SPT and 14 shear strength tests performed in this material were analysed. The data discussed above show good consistency. If considered together with geological and morphological features of the source area of shallow landslides, they allow at identifying typical slope profiles, under both geotechnical and geometrical points of view.

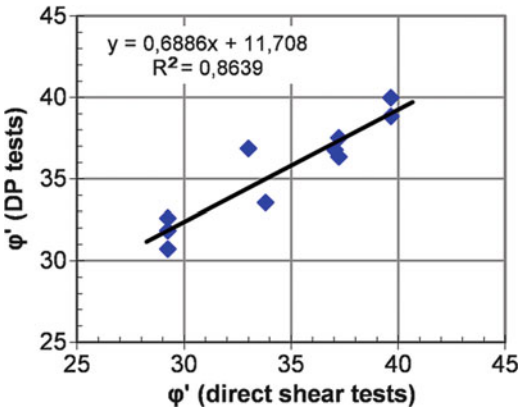

Fig. 6 Correlation between the φ′ values resulting from DP tests and direct shear tests in similar conditions

By means of DP tests a lot of data may be easily and quickly acquired, so characterizing wide areas and the parameter variability instead of disposing of few spotty data from boring, undisturbed sampling and laboratory tests. A limited number of in situ direct and indirect tests (drilling, seismic survey, etc.) may calibrate and improve the empirical relations used to obtain the required geotechnical properties. Difficulties or impossibility of undisturbed sampling in coarse-grained soils might be surmounted by in situ shear tests. The in situ direct measurement of shear strength represents a possible improvement in the knowledge of debris soils behaviour and may also give data on the residual strength of debris. Undisturbed sampling by in situ freezing may be another effective approach to obtain suitable materials for laboratory testing. In this way actual and reliable parameters may be achieved, and susceptibility and hazard maps may be based.

References

Campbell RH (1975) Soil slip, debris flows and rainstorms in the Santa Monica mountains and vicinity, southern California. U. S. Geological Survey Professional Paper, 851, 51p

Carmignani L, Conti P, Cornamusini G, Meccheri M (2004). The internal northern Apennines, the northern Tyrrhenian Sea and the Sardinia-Corsica Block. In: Crescenti V, D'Offizi S, Merlino S, Sacchi L (eds), Geology of Italy, Soc. Geol It., Spec. Vol. for 32th IGC Florence 2004, pp 59–77

Carmignani L, Lazzarotto A (2004) Geological Map of Tuscany (Italy). Regione Toscana, Spec. Edition for the 32nd IGC, Florence. Tip. L.A.C., Firenze

Casagli N, Dapporto S, Ibsen ML, Tofani V, Vannocci P (2006) Analysis of the landslide triggering mechanism during the storm of 20th-21st November 2000, in Northern Tuscany. Landslides 3:13–21

Cascini L (2004) The flowslides of May 1998 in the Campania region, Italy: the scientific emergency management. Rivista Italiana di Geotecnica 2:11–44

Conti P, Lazzarotto A (2004) Geology of Tuscany: evolution of the state-of- knowledge presented by geological maps and the new geological map of Tuscany, 1:250,000 scale. In: Morini D, Bruni P (ed) The Regione Toscana project of geological mapping. Spec. Vol. for the 32nd IGC, Florence, pp 25–50

Crosta G, Guzzetti F, Marchetti M, Reichenbach P (1990) Morphological classification of debris-flow processes in South-Central Alps (Italy). In: Proceedings of the 6th International IAEG Congress, Balkema, Rotterdam, pp 1565–1572

D'Amato Avanzi G, Giannecchini R, Puccinelli A (2004) The influence of the geological and geomorphological settings on shallow landslides. An example in a temperate climate environment: the June 19, 1996 event in the north western Tuscany (Italy). Eng Geol 73:215–228

Delmonaco G, Leoni G, Margottini C, Puglisi C, Spizzichino D (2003) Large scale debris-flow hazard assessment: a geotechnical approach and GIS modelling. Nat Hazards Earth Syst Sci 3:443–455

Del Prete M, Guadagno FM, Hawkins AB (1998) Preliminary report on the landslides of 5 May 1998, Campania, southern Italy. Bull Eng Geol Environ 57:113–129

De Vita P, Di Clemente E, Rolandi M, Celico P (2007) Engineering geological models of the initial landslides occurred on April 30 2006, at Mount di Vezzi (Ischia Island, Italy). Italian J Eng Geol Environ 2:119–141

Ellen SD, Wieczorek GF (1988) Landslides, floods, and marine effects of the storm of January 3–5, 1982, in the S. Francisco Bay Region, California. U.S. Geological Survey Professional paper, 1434, 310p

Elter P, Giglia G, Tongiorgi M, Trevisan L (1975) Tensional and compressional areas in the recent (Tortonian to present) evolution of the Northern Apennines. Bollettino di Geofisica Teorica ed Applicata 17:3–18

Ekanayake JC, Philipps CJ (2002) Slope stability thresholds for vegetated hillslopes: a composite model. Can Geotech J 39:849–862

Giannecchini R (2005) Rainfall triggering soil slips in the southern Apuan Alps (Tuscany, Italy). 6th Plinius Conf. on Mediterranean Storms (EGU), Mediterranean Sea, 17–24 October 2004. Adv Geosci 2:21–24

Giannecchini R (2006) Relationship between rainfall and shallow landslides in the Southern Apuan Alps (Italy). Nat Hazards Earth Syst Sci 6:357–364

Guadagno FM, Revellino P (2005) Debris avalanches and debris flows of the Campania Region (southern Italy). In: Jakob M, Hungr O (eds) Debris-flow Hazard and related phenomena. Springer, pp 489–518

Hungr O, Evans SG, Bovis M, Hutchinson JN (2001) Review of the classification of landslides of the flow type. Environ Eng Geosci 7:221–238

Hutchinson JN (1988) Morphological and geotechnical parameters of landslides in relation to geology and hydrogeology. In: Bonnard C (ed) Proceedings of the 5th international symposium on landslides, vol 1, Balkema, Rotterdam, pp 3–35

Kokusho T, Tanaka Y, Tadashi K, Kouji K, Kouichi S, Shinji T, Shintaro A (1995) Case study of rock debris avalanche gravel liquefied during 1993 Hokkaido-Nansei-Oki earthquake. Soil Found 35:83–95

Liao SSC, Whitman RV (1986) Overburden correction factors for SPT in sand. J Geotech Eng 112(3):373–377

Lo Presti D, Sqeglia N (2008) Prove penetrometriche dinamiche. Hevelius (ed) Benevento, Italy, (in Italian)

Pagani (2011) DPSH Dynamic penetrometers (TG 63–100; TG 63–150; TG 63–200). URL: http://www.pagani-geotechnical.com/index.php?id=67. Accessed 24 June 2011

Pandeli E, Ferrini G, Lazzari D (1994) Lithofacies and petrography of the Macigno formation from the Abetone to the Monti del Chianti areas (Northern Apennines). Memorie della Società Geologica Italiana 48:321–329

Robertson PK, Wride CE (1997) Cyclic liquefaction and its evaluation based on the SPT and CPT. In: Proceedings of the NCEER workshop on evaluation of liquefaction resistance of soils: technical report NCEER-97-0022, National Center for Earthquake Engineering Research, Buffalo, pp 41–87

Rogers DJ (2006) Subsurface exploration using the Standard Penetration Test and the Cone Penetration Test. Environ Eng Geosci 12 (2):161–179

Sassa K (1998) Recent urban landslide disasters in Japan and their mechanisms. In: Proceedings of the 2nd international conference environmental management, vol 1, Balkema, Rotterdam, pp 45–78

Schmertmann JH (1978) Use of SPT to measure dynamic soil properties? Yes, but...!. In: Dynamic geotechnical testing, ASTM STP 654, pp 341–355

Skempton AW (1986) Standard penetration test procedures and the effects in sands of overburden pressure, relative density, particle size, ageing and overconsolidation. Geotecnique 36 (3):425–447

Stefanoff G, Sanglerat G, Bergdhal U, Melzer KJ (1988) Dynamic probing (DP): international reference test procedure. In: De Ruiter (ed) Proceedings of ISOPT-I, vol 1, Balkema, pp 53–70

Tang C, Zhu J, Ding J, Cui X, Chen L, Zhang J (2011) Catastrophic debris flows triggered by a 14 August 2010 rainfall at the epicenter of the Wenchuan earthquake. Landslides. doi:10.1007/s10346-011-0269-5

Youd TL, Idriss IM (2001) Liquefaction resistance of soils: summary report from the 1996 NCEER and 1998 NCEER/NSF Workshops on Evaluation of Liquefaction Resistance of Soils. J Geotech Geoenviron Eng 127(4):297–313

Wang FW, Sassa K, Wang G (2002) Mechanism of a long-runout landslide triggered by the August 1998 heavy rainfall in Fukushima Prefecture, Japan. Eng Geol 63:169–185

Quantitative Geomorphological Analysis Based on Wavelet Transforms

Angelo Doglioni and Vincenzo Simeone

Abstract

The identification and quantitative study of important geological discontinuities, like those related to large landslides constitutes a paramount problem, which claims for a careful, detailed and, if possible, quantitatively based geomorphologic analysis. Numerical geomorphic analyses represent an interesting approach to these studies, allowing for a detailed and pretty accurate identification of hidden topographic anomalies that may be related to large landslides or other hidden geological structures. Geomorphic numerical analyses herein presented, are performed on the digital elevation model, based on the 2D discrete wavelet transform. This analysis is applied to a case study related to the middle-south Apennine at the front of the Apennine, whereas a really large deep-seated large landslide has been previously identified on the base of different geomorphic analysis. Finally, the analysis emphasizes some peculiar aspect of the buried front of the Apennine, which can potentially bias the landslide.

Keywords

Geomorphic analysis • Wavelet transform • Deep-seated landslide

Introduction

The quantitative analysis of landforms to identify element related to large landslides and hidden geological structure is a hot topic. Indeed, a large availability of digital models of the topography, which are often quite accurate, fosters these approaches. Digital Elevation Models (DEM) notoriously provide a representation of the earth surface in terms of a grid, or a mesh of triangles. DEMs are also georeferenced, thus providing an elevation schema of surface topology. These representations can be seen as matrixes of real numbers, which can be processed according to the approaches of signal processing to find evidence of unclear geomorphological elements.

Numerical geomorphic analyses of DEMs represent an interesting approach to these studies, allowing for a detailed and pretty accurate identification of hidden topographic anomalies that need a geologically-based interpretation and for instance may be related to large landslides. The earlier attempts of numerical analysis of DEMs proved to be particularly effective at the identification of the stream networks (Helmlinger et al. 1993). Multi-scale analysis constitutes a further interesting approach to DEM processing. In fact, topographic attributes extracted from DEMs are dependent on the resolution of the elevation data from which they are computed (Gallant and Hutchinson 1997).

In particular, the hierarchical analysis of DEMs can be used to define landform-based units that act as basic spatial and structural entities for soil, terrain or ecological maps, see MacMillan et al. (2004). Hierarchical analysis of DEMs allows for a multi level identification of geomorphic and hydrological entities, which constitute an inventory of landforms and natural resources. As pointed out by Gallant and Hutchinson (1997), a regular rectangular grid may not

A. Doglioni (✉) • V. Simeone
Engineering Faculty of Taranto, Technical University of Bari, viale del Turismo 8, Taranto, Italy
e-mail: a.doglioni@poliba.it

C. Margottini et al. (eds.), *Landslide Science and Practice*, Vol. 1,
DOI 10.1007/978-3-642-31325-7_34,

prove an ideal representation of topographic surfaces for the study of scale effects. Therefore, spectral and wavelet techniques (Priestley 1981; Daubechies 1992) are obvious alternatives but have several deficiencies, particularly in their use of oscillatory basis functions. The positive wavelet representation has very attractive properties of localization and feature representation. Applications to 1D topographic data show useful results, including the identification of changes in topographic structure with scale. Extension to 2D analysis allows for the quantification of characteristic shapes, scales and orientations in the landscape.

Here DEM analysis is pursued according to the approach of discrete wavelet transform (DWT) (Daubechies 1992). Scientific literature provides a number of works based on 2D continuous wavelet transform (Antoine et al. 2003; Bruun and Nilsen 2003; Booth et al. 2009) aimed at constructing a hierarchical Digital Terrain Model. Wavelet analysis is commonly used for data denoising and principal components analysis (Aminghafari et al. 2006).

Wavelet analysis of DEM was undergone for the identification of anomalies of unique features of the surficial topography. Jordan and Shott (2005) present an application of wavelet analysis to morphotectonic lineament investigation, i.e. tectonic faults, associated with characteristic geomorphological features such as linear valleys, ridgelines and slope breaks. Booth et al. (2009) analyse power spectra produced using the two-dimensional discrete Fourier transform and the two-dimensional continuous wavelet transform to delineate the characteristic spatial frequencies of deep-seated landslide morphologic features such as ridges, scarps, and displaced blocks of material. In fact, spectral power shows characteristic frequency bands of spatial patterns, thus highlighting past slope instabilities and allowing the delineation of landslide terrain. Kalbermatten et al. (2009) showed how wavelet analysis of high-resolution DEMs is complimentary to classic morphometric indicators. They introduce various methods using wavelets and structure tensors in order to show the multi-scale nesting of landscape features.

Here an approach for geomorphic numerical analyses is presented. The hierarchical representation of the DEM, can provide evidences of anomalies or singularities of the land surface, which are not directly evident from the DEM as it is, or from a slope and curvature analysis (Porres de la Haza and Pardo Pascual 2002).

The introduced approach is applied to an interesting case study at the front of the Apenine chain of south Italy for which a 40 m-resolution DEM is available. Moreover, the wavelet transforms are performed on multiple levels, thus trying to address the problem of which is the level extent for an accurate analysis fit to a specific problem.

The Wavelet Transform

Wavelet transform is a methodology for analysing localized variations of power within a series of data. Given a set of spatial data, e.g. an elevation profile, it can be dealt as a signal, which is decomposed into space–frequency space. This allows for determining both the dominant modes of variability and how those modes vary in space. In fact, as reported by Daubechies (1992), wavelet transform allows for decomposing data into different frequency components, which can be studied and analysed with the proper resolutions matching to their scales. Wavelet transform is particularly popular for the analysis of time-evolving signals, which are notoriously dependent on two variables: scale, i.e. frequency, and time. Therefore wavelets are capable to provide accurate time-frequency localization. However, this approach can be easily fitted to other distributed data, in particular topographic data coming from a grid-based description of earth surface.

Discrete Wavelet Transform (DWT) is an orthogonal function applied to a finite set of data. DWT resembles the Discrete Fourier Transform (DFT), in that the transforming function is orthogonal, a signal passed twice through the transformation is unchanged, and it is assumed the input signal as a set of discrete-time samples. However, while DFT is based on a sinusoid, DWT is based on a set of functions defined by a recursive difference equation:

$$\phi(x) = \sum_{k=0}^{M-1} c_k \phi(2x - k) \tag{1}$$

where M is the specified number of nonzero coefficients, which is arbitrary, and referred to as the order of the wavelet. On the other hand, the values of the coefficients are not arbitrary, but determined by constraints of orthogonality and normalization. Moreover, the area under the wavelet is required to be one, which implies:

$$\sum_{k} c_k = 2 \tag{2}$$

This class of wavelet functions is bounded to be zero outside of a small interval. This is what makes the wavelet transform able to operate on a finite set of data, i.e. compact support. The functions commonly used for performing transforms consist of a few sets of well-chosen coefficients resulting in a function, which has a discernible shape. A number of mother wavelets exist, the specific choice of a mother wavelet must be made according to the features of

the data to be analysed. The choice of the mother wavelet for DEM analysis is also dependent of the resolution of the elevation models, which affects the description of terrain detail. For the analysis of large landslides influenced by tectonical displacements, medium-low resolution DEMs can be used. Therefore, the biorthogonal 1.1 mother wavelet (Daubechies 1992) is here chosen. Biorthogonal Wavelets are families of compactly supported symmetric wavelets. Biorthogonal wavelets use two scaling functions, which may generate different multiresolution analysis and then two wavelets, one for decomposition and the other for reconstruction instead of the same single one, are used, thus implying interesting properties. Biorthogonal wavelets show linear phase, which is necessary for signal and image reconstruction. The biorthogonal discrete wavelet transform analysis and reconstruction equations are:

$$a_{j,k} = \int x(t) 2^{j/2} \tilde{\phi}\left(2^j t - k\right) dt \tag{3a}$$

$$b_{j,k} = \int x(t) 2^{j/2} \tilde{\psi}\left(2^j t - k\right) dt \tag{3b}$$

$$x(t) = 2^{\frac{N}{2}} \sum_k a_{N,k} \phi\left(2^N t - k\right) + \sum_{j=N}^{M-1} 2^{\frac{j}{2}} \sum_k b_{j,k} \psi\left(2^j t - k\right) \tag{4}$$

where $x(t)$ is the signal, $\phi(t)$ and $\psi(t)$ are the reconstruction scaling and wavelet functions, while $\tilde{\phi}(t)$ and $\tilde{\psi}(t)$ are the analysis scaling and wavelet functions, $a_{j,k}$ and $b_{j,k}$ are the scaling and wavelet coefficient respectively, which form the biorthogonal discrete wavelet transform of $x(t)$. M and N are two integer values related to the dimension of the compact support. When $j = N$ the transform reproduce the coarse information, while when $j = M - 1$, the transform has to stop at some finest scale. $M - N$ represents the number of decomposition levels of the discrete wavelet transform.

How DWT Is Applied to a DEM

A geomorphic numerical analyses is here attempted. In particular, the analysis is based on a hierarchical representation of the DEM. This can evidence anomalies or singularities of the land surface, which are not immediately readable from the DEM as it is, or from a simple slope and curvature analysis. Can also give quantitative evidence of the result of geologically-based observational approach. This means that discontinuities and/or singularities are quantified and highlighted in terms of detail coefficients of the DWT, see (3a) and (3b). These are represented as topographic data, overlapped for instance on a DEM, or on whatever thematic map can be interesting to compare. Therefore, this comparison makes it possible to locate and emphasize the anomalies and then their correlation to landforms or other data coming from different investigations. It is noteworthy that 2D wavelet transform preserves the average values of the elevation at different scales, and this is particularly suitable for grid-based DEM. The grid-based DEM can be assumed as a matrix, where a DWT is performed columnwise and linewise, which basically represent horizontal (west–east) and vertical directions (north–south). The significant outcomes of this analysis are low-frequency approximation coefficients and high-frequency detail coefficients, see (3a) and (3b). The detail coefficients in particular are analysed, whereas sudden and wide variations of these coefficients are related to the variations and discontinuities of the DEM. Detailed coefficients are therefore 2D-plotted both on the horizontal and vertical direction, thus allowing to visualize and quantify potential anomalies of the land surface. Moreover, a further level wavelet analysis can be performed on the matrix of the approximation coefficients, which represent a smoothed representation of the land surface. This allows for the construction of a further level detail coefficients matrix, which can provide further information about the land surface.

The Case Study: Low Biferno Valley

The study area covers the lower valley of Biferno river downstream of Ponte Liscione Dam in Southern Italy, which is located at the transition zone between the Apennine chain and the Adriatic foredeep domains (Figs. 1 and 2), where allochthonous nappes are partially buried under Pleistocenic foredeep deposits (Fig. 1). The internal part of river Biferno catchment is part of the Apennine chain. The outcrops of allochthonous flysch clay shales. Downstream of Ponte Liscione dam, there is the zone of the passage from the chain domain to the foredeep deposits domain; also if there is a zone where tectonic nappe of allochtonous deposits are partially buried under foredeep ones (Fig. 1). The southern right side of the valley shows the outcropping of allochthonous nappe of Apennine front more rearward than on the left side (Guerricchio et al. 2010) (Fig. 2).

Going down towards the coast, on both sides of the valley Plio-Pleistocenic foredeep deposits outcrop. There is a general gradual gentling of the shapes, which shows the typical configuration of the foredeep deposits: conglomerate regressive terraces rest on the sub-Apennine grey-blue clays. The left riverside is higher and steeper than the right one (Fig. 2) and it is strongly affected by large retrogressive landslides up to Guglionesi town. On the right side between Biferno and Cigno valleys, there is the so-called Larino Plateau (Fig. 2). It is a large regressive terrace

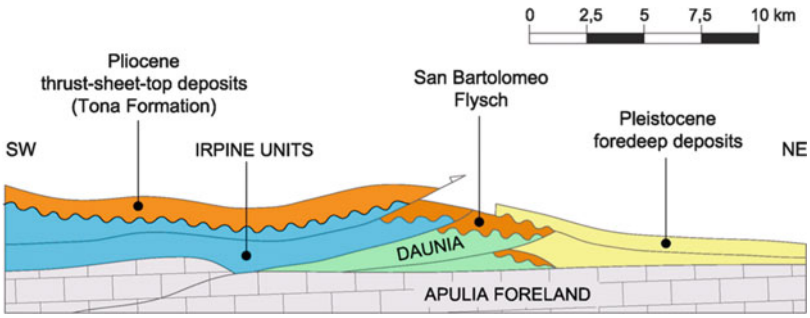

Fig. 1 Schematic geological cross-section of Appennine-Foredeep domains in Biferno valley area (After Patacca and Scandone 2007). The direction of the section is SW to NE

(Pleistocene). Larino Plateau gently slopes (about 1°) NE toward the confluence of Cigno stream with Biferno river. On the southern side of this plateau, there is the valley of Cigno stream and an high scarp up to a crest where the towns of Ururi, San Martino in Pensilis and Portocannone are located, and where regressive sandy-gravelly soils deposits, similar to those of Larino Plateau crop out.

The particular geomorphological characters of the study area are here intended as consequence of a huge deep-seated landslide on the right side of Biferno valley (Guerricchio et al. 2010). This involved foredeep deposits at the front of the Apennine ridge and it is due to the underthrusting of allochthonous nappe due to Apennine orogenesis (Fig. 1). Several large landslides, involving foredeep Plio-Pleistocenic deposits along the Adriatic coast (Cancelli et al. 1984; Guerricchio et al. 1996; Doglioni et al. 2011) can be partially related to the effects of the compression of Apennine chain on foredeep deposits (Guerricchio 2000; Doglioni and Simeone 2011).

The morphological characters of the lower Biferno valley as well as the paths of Biferno river and Cigno stream are analysed through a wavelet analysis of a medium resolution (40 m square cells) grid-based DEM (Fig. 3) to give the evidence of this large deep-seated landslide, also affecting the landslide hazard on the left bank of low Biferno valley.

Results and Discussion

A 2D wavelet decomposition based on biorthogonal 1.1 wavelet function is undergone. The investigated area covers a surface of about 1,340 km^2, see Fig. 3, from the coastline towards the Apennines. The decomposition was performed on 4 levels, starting from a 1,173 × 1,611 grid, see Fig. 3, each of them associated to horizontal and vertical wavelet transforms. Looking at the section AA of Fig. 3, the following Fig. 4 shows a 1D DWT applied to the aforementioned section. It is clearly visible how the detail coefficients are correlated with the discontinuities and/or sudden variations of the terrain altitude. This particularly allows for emphasizing those points whereas these discontinuities are not clearly evident from the analysis of the DEM. Moreover it is possible to quantify these discontinuities and then to classify their entities.

Looking at Fig. 4b, it is possible to observe that the flat areas, for instance the river valley and Larino Plateau, corresponds to low magnitude detail coefficients, see Fig. 4a. On the other hand, the upstream zone, corresponding to the Apennine, is characterized by higher, in terms of absolute values, detail coefficients. Moreover, the oscillations of the detail coefficients are particularly wide, whereas the terrain tends to rapidly change its elevation. It is noteworthy that detail coefficients oscillate also where the terrain locally change its elevation. These kinds of oscillations, which somehow break the continuity of the topography, are not easily recognizable just looking at the DEM. However, DWT allows for a quick quantitatively-based identification of these local discontinuities, see Fig. 4. The next step is to extend this analysis to the entire DEM and then try to address the problem of how the detail coefficients vary on a 2D domain. This may help to investigate the evolution of the landforms and to identify potential large anomalies on the DEM, or potential structural features of the DEM, or even correlations with the regional tectonics. The following Figs. 5 and 6 show level 1 absolute values of detail coefficients of Biferno valley in the order for the vertical and the horizontal transform, for the investigated DEM. Level 1 coefficients seem to provide a clearer and sharper characterization of the landforms than the further levels of DWT. The colour map of the figure represents the detail coefficients of the DWT. In particular the meaning of these coefficients is: the higher is their value the sharper is the discontinuity of the section. On the other hand, the lower is the detail coefficient, more regular is the surface of the terrain. Indeed looking both at

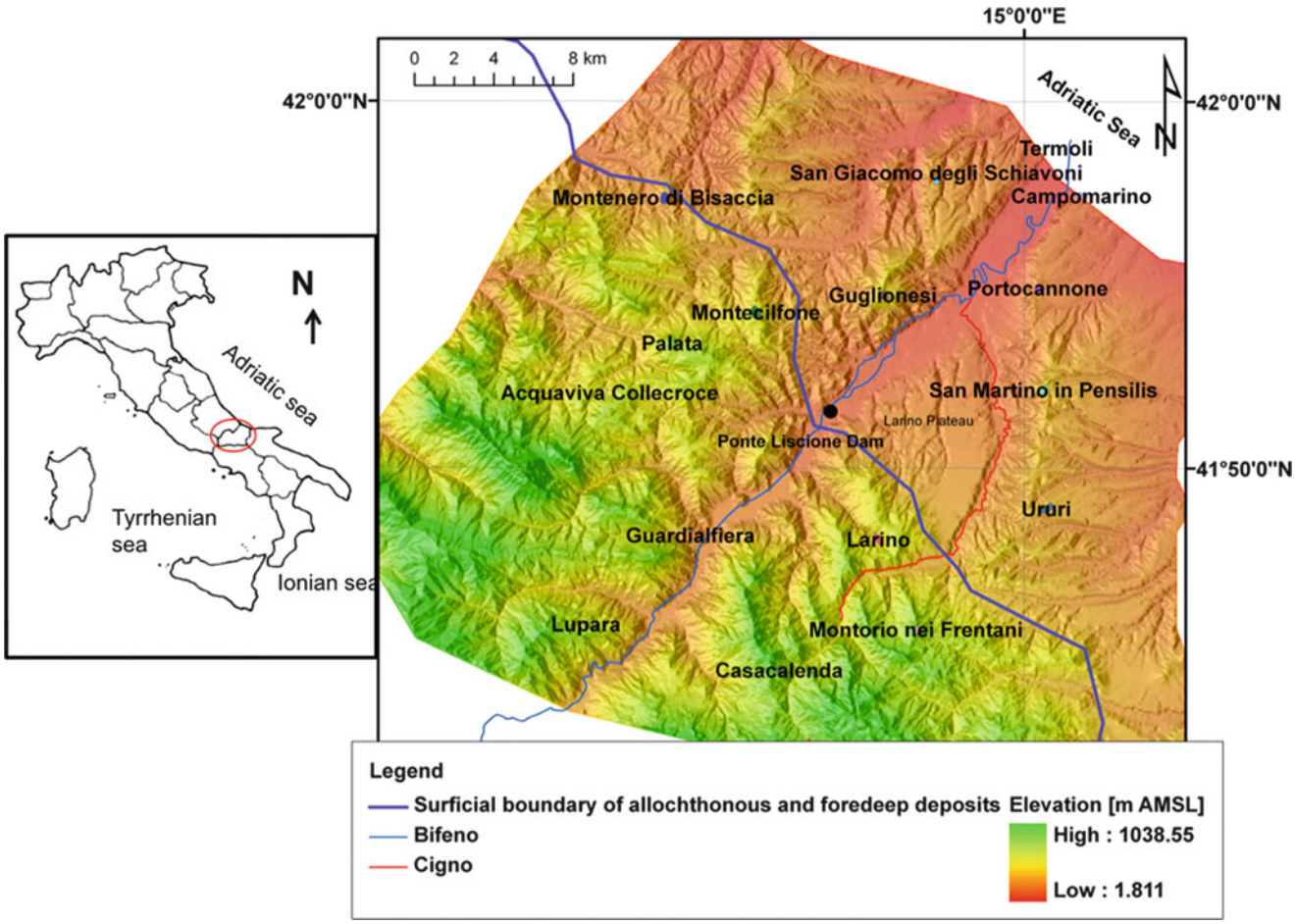

Fig. 2 Low Biferno valley

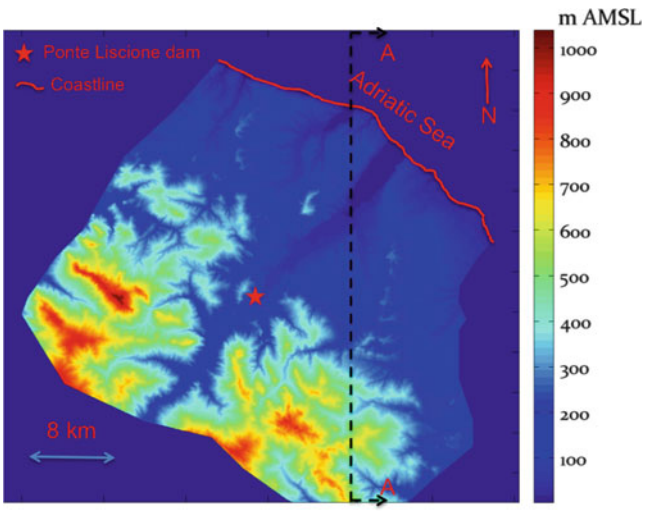

Fig. 3 DEM of Biferno valley and example section

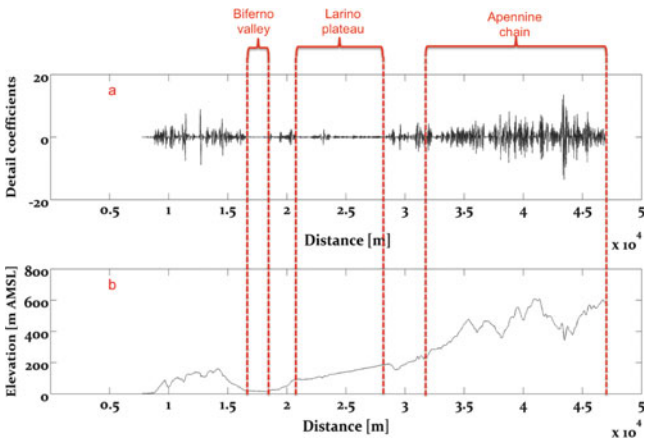

Fig. 4 1D DWT (**a**) and vertical cross section AA of the investigated area (**b**)

Figs. 5 and 6, it is clear that the south-west area of the figures is characterized by high values of detail coefficients, and this is consistent with the presence of the Apennine. These two figures clearly show a sort of hole, which corresponds to Larino plateau, whereas it is somehow east crowned by Cigno stream.

This large anomaly is asymmetrical with respect to Biferno valley, being right hand to the river. This area is surrounded by the dotted rectangle. It is clearly visible

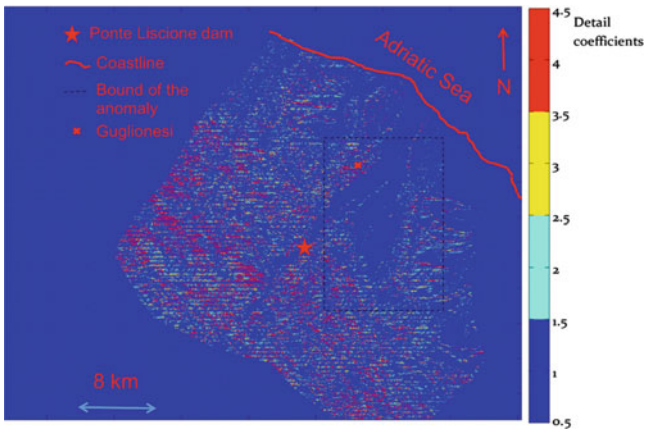

Fig. 5 Details coefficient of level 1 vertical DWT

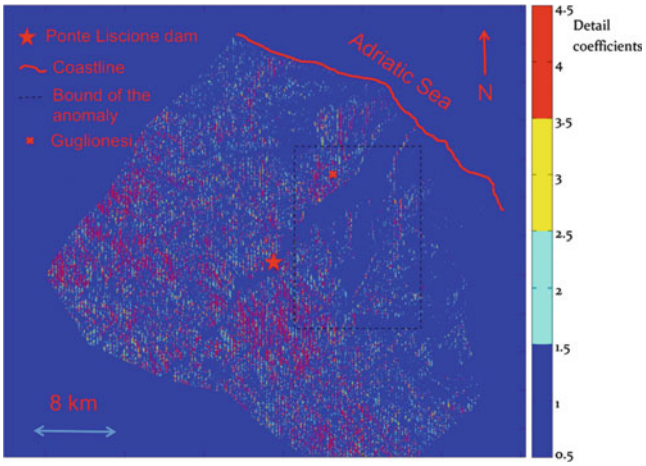

Fig. 6 Details coefficient of level 1 horizontal DWT

on the central right part of the image a large almost flat area crowned by higher points on the right and bounded on the left, according to the south-west to north-east direction by the Biferno valley. This sort of anomalous hole represents the main body of the giant landslide identified on the base of an observational geologically-based approach by Guerricchio et al. (2010) and the low-resolution image sharply evidences its bounds and shape. It is evident also the crown of this landslide. On the left side of Biferno valley, in front of the landslide, the low-resolution image shows the presence of the peak of Guglionesi (Figs. 5 and 6), which is quite well outlined as the only one anomalous zone in the background scenario of lower elevated foredeep deposits areas. It is due to the erosion of Biferno river at the base of the valley bank that is forced to flow in that position by the giant landslide toe (Guerricchio et al. 2010). This analysis shows that the instability of the foredeep deposits hills

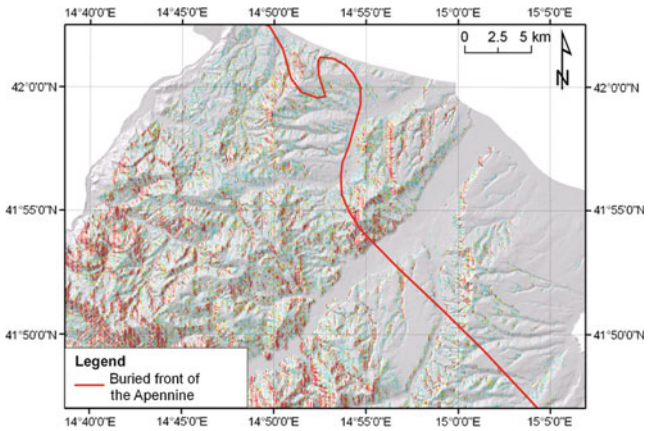

Fig. 7 Overlapping of DEM, level 1 horizontal detail coefficient of DWT and buried front of the Apennine

may be conditioned by their complex geomorphological and tectonic evolution. In fact, there are discontinuities due to tectonic phenomena related to the powerful horizontal thrust related to the Apennine layer on the foredeep deposits. The presence of this complex of tectonic tangential stresses affects the stability of these slopes, in particular whereas other factors occur, like localized erosion. Therefore, the main mechanism is likely conditioned by the uplift of plio-pleistocenic deposit due to the thrust of Apennines. A further interesting feature emphasized by level 1 coefficients is their overlapping with the buried front of the Apenine chain as reconstructed in the structural map of Italy (Patacca and Scandone 2007). Figure 7 shows a relatively clear correlation between the buried front and the higher values of the detail coefficient. This potential correlation may reveal a likely relation between the surface landforms and the buried front. Moreover, it is quite evident how the higher values of the coefficient are close to the south-west bounds of the large deep seated landslide of the low Biferno valley as well as, going north, close to the landslides of the Adriatic coast. This correlation highlights an important and extremely interesting point: the Adriatic coast landslides, an in particular those of the middle low Adriatic, may be related to the presence of deformations and fractures induced by tectonic actions and tectonic horizontal stresses. In particular, Fig. 7 shows how the shape of the front and the back high value detail coefficients follow similar parallel tracks, which sometime, see north part of the figure, overlap. So that the irregular structural asset of foredeep deposits can be correlated to the deformation induced by the thrust of the buried front of the Apennine. Looking at the large landslide of Biferno valley, this proves the tectonic origin of the landslide and its consistency with the buried front of the Apennine.

Conclusions and Future Developments

This work tries to address the problem of the geomorphic quantitative analysis for the identification of special geomorphic element, using an approach based on the 2D DWT applied to the DEM of the area under investigation. The methodology is applied to the case study of low Biferno valley, where a giant deep-seated landslide is located and investigated. The methodology attempts to emphasize how the terrain forms can be consistent with the local tectonic, which can affect the presence of giant deep landslides. The proposed methodology is of particular use whereas an accurate and reasonably detailed DEM exists. DWT allows for identifying the anomalies and/or singularities of the DEM in terms of detail coefficients of the transform. Detail coefficients represent the high frequency variations of the terrain elevation. Therefore, after an appropriate choice of the wavelet function, it is possible to emphasize where the terrain abruptly changes its profile, due to local or large-scale factors. This approach, which is usually applied to a cross section of the DEM (Booth et al. 2009), is here extended to the entire DEM, thus allowing for visualizing and quantifying the 2D variations of DEM in terms of detail coefficients. The study of the 2D variations highlighted large singularities of the DEM, which are likely correlated to landforms consistent with large deep landslides.

In particular, the presence of a large singularity in the low right Biferno valley, proves the hypothesis of a large deep-seated landslide involving the area between Cigno stream and Biferno river. The high value details coefficients mark the bound of this landslide and than allow for estimating the involved area. Besides emphasizing the large singularities, 2D DWT applied to the DEM allows for correlating the values of the detail coefficients with the tectonic structures, identified by indirect observations, or interpolating direct observations. In particular, here it is emphasized how the buried front of the Apennine follows a track which is similar to that of the high value detail coefficients. So that the anomalous deformation distribution can be correlated to buried tectonic geological structures. This analysis fosters the quantification of the surface landforms in terms of study of the tectonic interaction between the Apennine and the foredeep area. Moreover, this interaction is likely related to the occurrence of a series of deep-seated landslides, which characterize the middle-low Adriatic coast of Italy. The analysis of DEM by DWT is therefore potentially a very powerful approach, which may reveal details, which helps in the reconstructions of deep landslides and of ongoing tectonic phenomena. In this scenario, further investigations on high resolution DEM of middle-low Italian Adriatic coast are currently being processed, thus trying to address the relationship between the Apennine and the known coastal landslides.

References

Aminghafari M, Cheze N, Poggi JM (2006) Multivariate denoising using wavelets and principal component analysis. Comput Stat Data An 50(9):2381–2398. doi:10.1016/j.csda.2004.12.010

Antoine JP, Carrette P, Murenzi R, Piette B (2003) Image analysis with two-dimensional continuous wavelet transform. Signal Process 31(3):241–272. doi:10.1016/0165-1684(93)90085-O

Booth AM, Roering JJ, Taylor Perron J (2009) Automated landslide mapping using spectral analysis and high-resolution topographic data: Puget Sound lowlands, Washington, and Portland Hills, Oregon. Geomorphology 109(3–4):132–147. doi:10.1016/j.geomorph.2009.02.027

Bruun BT, Nilsen S (2003) Wavelet representation of large digital terrain models. Comput Geosci 29(6):695–703. doi:10.1016/S0098-3004(03)00015-3

Cancelli A, Pellegrini M, Tonnetti G (1984) Geological feature of landslide along the Adriatic coast (Central Italy). In: Proceedings of the international symposium on Landslide, vol 2, Toronto, pp 7–12

Daubechies I (1992) Ten Lectures on Wavelets. SIAM, Philadelphia, p 377. ISBN 0-89871-274-2

Doglioni A, Fiorillo F, Guadagno FM, Simeone V (2011) Evolutionary polynomial regression to alert rainfall-triggered landslide reactivation, Landslide. doi: 10.1007/s10346-011-0274-8 (in press)

Doglioni A, Simeone V (2011) Large landslides along the Adriatic coastline in Southern Italy. In: Proceedings of the EGU General Assembly, Vienna, 3–8 April 2011, 13, EGU2011-13491, 2011

Gallant JC, Hutchinson MF (1997) Scale dependence in terrain analysis. Math Comput Simulat 43(3–6):313–321. doi:10.1016/S0378-4754(97)00015-3

Guerricchio A, Melidoro G, Simeone V (1996) Le grandi frane di Petacciato sul versante costiero adriatico (Molise). Mem Soc Geol It 51:607–632

Guerricchio A (2000) La fragilità del territorio dell'Italia centro-meridionale desumibile da immagini da satellite. X Congresso Nazionale dei Geologi, International conference, Roma, pp 443–482

Guerricchio A, Doglioni A, Galeandro A, Simeone V (2010) Deep seated gravitational slope deformation and hydraulic vulnerability of the lower Biferno valley (Southern Italy) In: Proceedings of the 2010 IAEG conference, Geologically Active, Taylor & Francis Group, Auckland NZ, 5–10 Sept 2010, pp 683–689

Helmlinger KR, Kumar P, Foufoula-Georgiou E (1993) On the use of digital elevation model data for Hortonian and fractal analyses of channel networks. Water Resour Res 29(8):2599–2613. doi:10.1029/93WR00545

Jordan G, Schott B (2005) Application of wavelet analysis to the study of spatial pattern of morphotectonic lineaments in digital terrain models. A case study. Remote Sens Environ 94(1):31–38. doi:10.1016/j.rse.2004.08.013

Kalbermatten M, Van De Ville D, Joost S, Unser M, Golay F (2009) Laplace-gradient wavelet pyramid and multiscale tensor structures applied on high resolution DEMs, Geomorphometry 2009, August 31 - September 2. Zurich, Switzerland, pp 124–132

MacMillan RA, Keith JR, McNabb DH (2004) Defining a hierarchy of spatial entities for environmental analysis and modeling using digital elevation models (DEMs), Computers. Environ Urban Syst 28(3):175–200. doi:10.1016/S0198-9715(03)00019-X

Patacca E, Scandone P (2007) Geology of the southern Apennines. In: Mazzotti A, Patacca E, Scandone P (eds) Results of the

CROP Project, Sub-project CROP-04 So, Special Issue 7(2007), pp 75–119

Porres de la Haza MJ, Pardo Pascual JE (2002) Comparison between the different curvature models of terrain for determining the degree of soil humidity, in Recent Advances in Quantitative Remote Sensing, Publicacions de la Universitat de València, pp 238–245

Priestley MB (1981) Spectral analysis and time series, Academic Press, London, 1–2., ISBN 0125649010 (v. 1) 0125649029 (v. 2), 890 p

The Role of Inherited Structures in Deep Seated Slope Failures in Kåfjorden, Norway

Halvor Bunkholt, Tim Redfield, Per Terje Osmundsen, Thierry Oppikofer, Reginald L. Hermanns, and John Dehls

Abstract

From studies of orthophotos and through field work, a complex deformation pattern has been recognized in the Lyngen area, Troms, Norway. The area is among the most alpine in Norway and contains a strong clustering of rock slope failures. The rock slope failures are characterized by two different deformation styles, and the difference in style is geographically separated by a fjord and valley lineament. Field studies suggest that two directions of tension oriented almost perpendicular to each other, utilize pre-existing brittle to brittle/ductile fabrics inherited from much older deformation events. The NE-SW direction of tension is parallel to the average displacement vector pointing down-dip along inherited faults. This vector is gravitationally controlled. The NW-SE displacement vector trends strike-parallel along the inherited faults. The presence of the latter appears to be confined geographically.

Keywords

Brittle deformation • Sackung • DSGSD • Neotectonic

Introduction

Troms County in Northern Norway is particularly well suited for integrated studies of landslide processes. Due to the region's high latitude, the tree line lies between 200 and 600 m above sea level; the area thus provides premium exposures of bedrock discontinuities that are easily visible on aerial photographs and accessible targets for field work. The area in focus (Fig. 1c) consists mainly of well-foliated, high-grade metamorphosed schists, paragneisses and other supracrustal rocks on both sides of an alpine ridge that contains the Lyngen Ophiolite (Fig. 1b) (Furnes et al. 1980). The eastern side of the Lyngen Ophiolite may be controlled by a major N-S striking east-dipping normal fault (Osmundsen et al. 2009; Hansen et al. 2011) (purple line in Fig. 1b). If so, the Lyngen Ophiolite could also be considered a horst block. By applying the term fault to discontinuities in the bedrock across which there has been a relative displacement, proven by kinematic indicators as described by Petit (1987), or an off-set between lithological units, unambiguous evidence for this fault has not yet been observed in the field. Regional to semi-regional lineaments have been mapped in previous and ongoing works (Sigmond et al. 1984; Tolgensbakk and Solli 1988; Zwaan 1988; Brekke et al. 1992; Dehls et al. 2000b; Mosar 2000; Mosar et al. 2002; Osmundsen et al. 2009, 2010; Hansen et al. 2011). Figure 1b, c shows a subset of these lineaments containing all faults that clearly offset lithological units on the published maps.

The timing of last movement of these onshore faults is not established, but in the nearby offshore region, a N-S trending E-dipping regional normal fault clearly offsets Carboniferous to Mid Jurassic supracrustal rocks against Precambrian to Devonian metamorphic and sedimentary rocks (Brekke et al. 1992). The pink lines of Fig. 1c define landslide related lineaments. These are undifferentiated

H. Bunkholt (✉) • T. Redfield • P.T. Osmundsen • T. Oppikofer • R.L. Hermanns • J. Dehls
Geological Survey of Norway, Leiv Eriksons vei 39, Trondheim NO-7040, Norway
e-mail: halvor.bunkholt@ngu.no

C. Margottini et al. (eds.), *Landslide Science and Practice*, Vol. 1,
DOI 10.1007/978-3-642-31325-7_35,

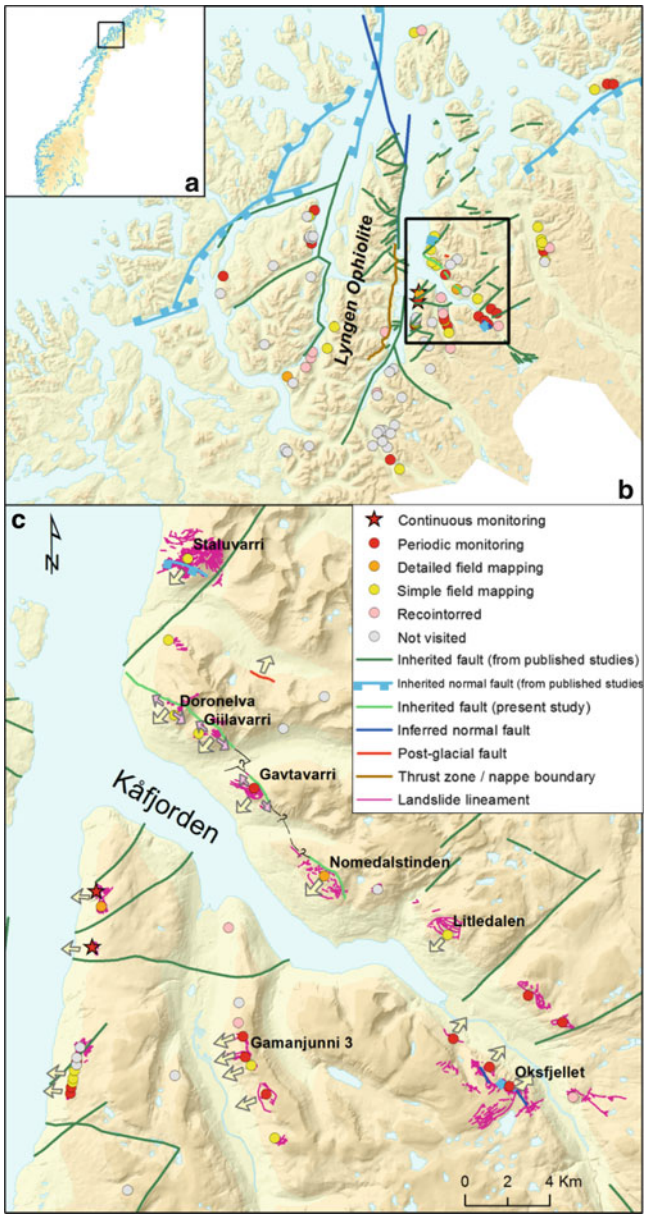

Fig. 1 (**a**) Location map; (**b**) the greater Lyngen area with unstable slopes and main lineaments; (**c**) area in focus along Kåfjorden. Legend applies to both maps

geomorphic linear features, trenches, fractures, gravitational sliding planes related to the landslide, or faults. The area is characterized by high alpine mountains flanking glacially over-steepened valleys and fjords. Several fjord valleys strike off the eastern side of the Lyngen Ophiolite at high angles, and these valleys contain 51 % of the 106 currently mapped rock slope instabilities in Troms County (Fig. 1b). The small area of focus shown in Fig. 1c around Kåfjorden contains 34 % of the mapped slope failures in the County.

A high concentration of structures due to tectonics and glacial unloading in the bedrock, and the steepness of the relief, are described as two main parameters that facilitate

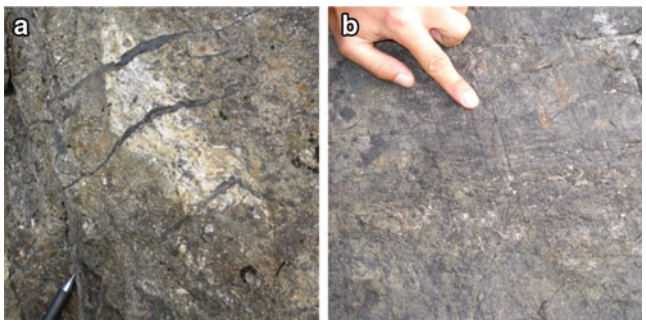

Fig. 2 (**a**) Pseudotachylite filled tension cracks at Staluvarri; (**b**) physical grooves caused by rocksliding scratched into the fault plane surface, overprinting the mineralized lineations

development of large gravitational rock-slope deformation (e.g. Braathen et al. 2004; Saintot et al. 2011; Böhme et al. 2011; Henderson and Saintot 2011). The ongoing work in the area focus on mapping of the rock slope failures, where data collection for use in risk and hazard classification of the unstable slopes is the primary goal (Hermanns et al. this volume). Nevertheless, we also look more closely at the pattern of landslide clustering, searching for an understanding of which underlying controlling factors may cause the high density of rock slope failures, giving the apparent difference in deformation style within the area. This work has just started.

Geological Setting

Terrain Morphology

A dip threshold for when a slope is considered unstable varies from province to province, depending on local geological and morphological conditions. In the study area rock slope failures are both present in slopes dipping shallower than 40° and absent in slopes dipping steeper than 60°, within similar lithologies. We therefore suggest that strong relief caused by glacial over-steepening are not the primary cause for the large density of landslides in the study area, but we certainly do acknowledge it as a contributing factor that amplifies the deformation effects caused by the brittle and brittle-ductile fabrics in the bedrock.

Bedrock Lineaments

Hansen et al. (2011) present a preliminary data compilation from ongoing work that suggests the NE-SW to E-W striking onshore faults in Troms follow pre-existing ductile shear zones in the basement rocks. Direct correlation between onshore and offshore basement controlled faults and

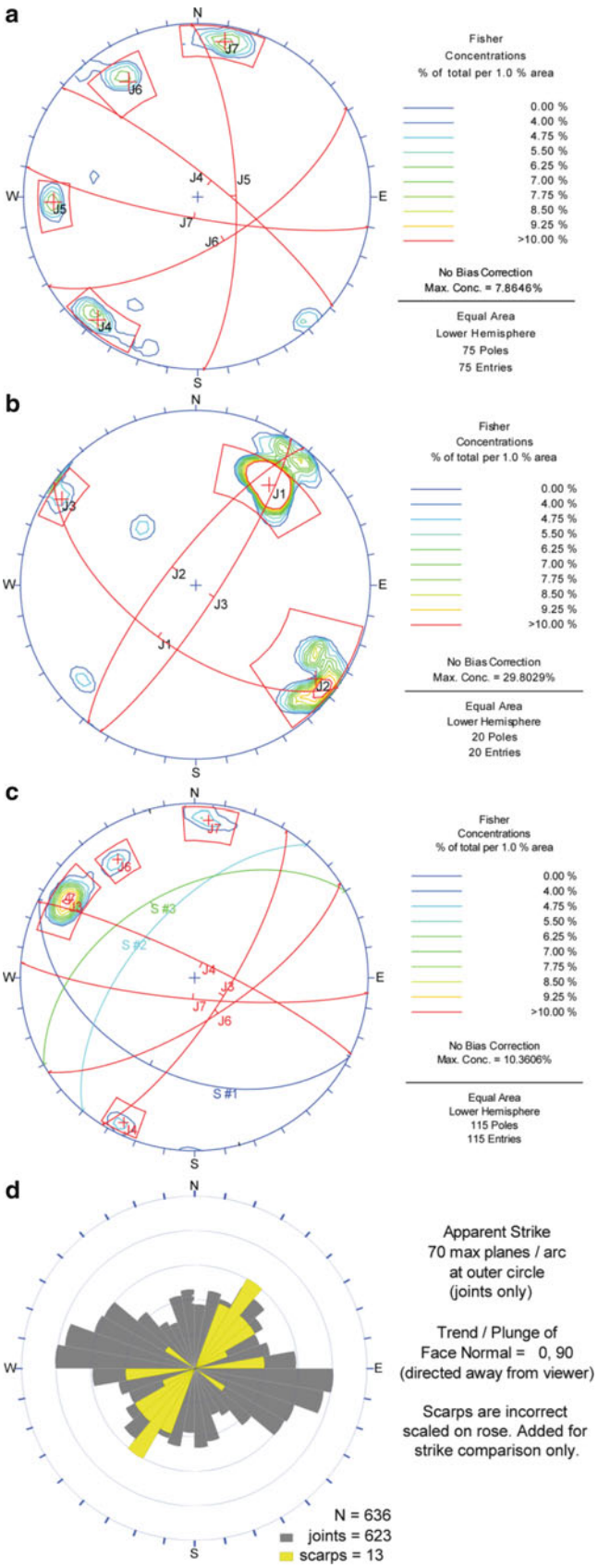

Fig. 3 Kinematic analysis of fractures and sliding planes at three selected sites. (**a**) Oksfjellet; (**b**) Staluvarri; (**c**) Gamanjunni 3. S#1-S#3 refer to the back scarps; (**d**) rose plot of all joints and fractures (*grey*) and scarps (*yellow*) in field area recorded in 2010

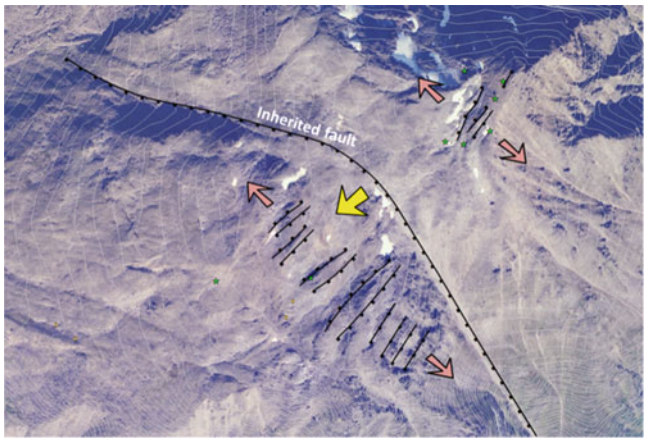

Fig. 4 Giilavarre. Gravitational driven tension (*yellow arrow*) acts above an inherited fault. Secondary tension is set up normal to this (*pink arrows*). *Black line*: assumed inherited fault

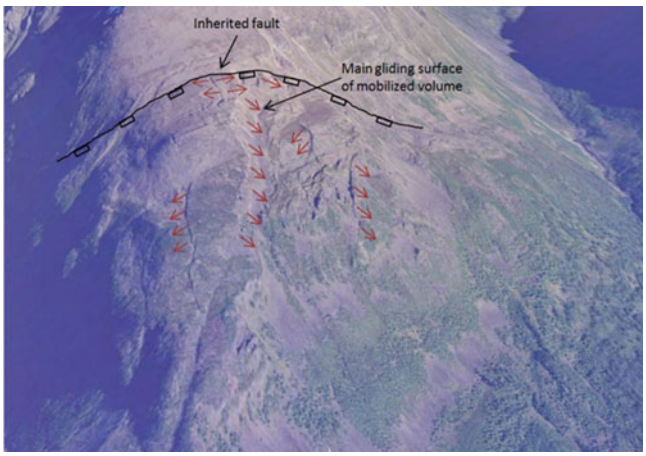

Fig. 5 Gavtavarre. Gravitational driven displacement vectors marked in *red*. *Black line*: assumed inherited fault. Screenshot from www.norgei3d.no

ongoing dating of fault gouge, suggest these faults may have been active between the collapse of the Caledonides and the Eocene (Hansen et al. 2011). Our field observations are not incompatible: at Staluvarre we have identified pseudotachylite-filled tension cracks at a sliding plane at the blue lineament in Fig. 1c, and mineral growth slickenlines at several sliding planes. At Revdalsfjellet, rockslide related frictional striations were observed to cross-cut older down-dip mineral growth slickenlines (Fig. 2a, b). These observations suggest the larger faults in the area have been active earlier at depth in the crust.

Post-glacial faults have been identified in at least 14 localities in Fennoscandia. These post-glacial faults generally strike SW–NE and they are interpreted to be thrust faults (Kukkonen et al. 2010).

However, the NW-SE striking Nordmannvikdalen Fault (drawn in red in Fig. 1c) is an exception, and is

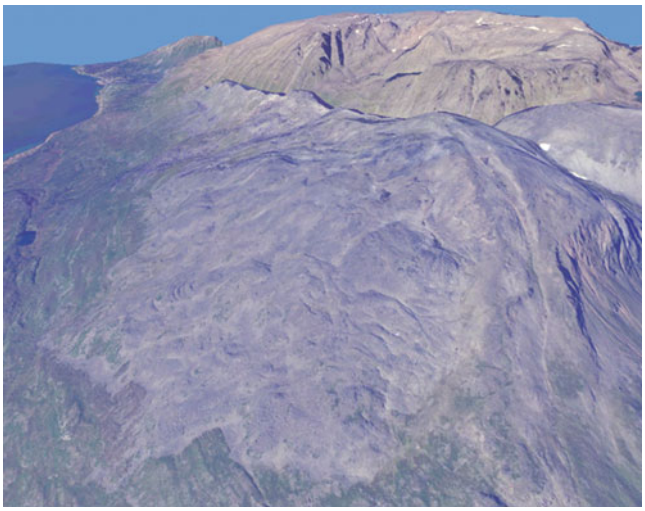

Fig. 6 Nomedalstinden. The whole slope is decomposing while moving downwards with creep velocity. Screenshot from www.norgei3d.no

interpreted as a normal fault (Tolgensbakk and Solli 1988; Dehls et al. 2000a). Published literature mostly suggests that the post-glacial faults are reactivated pre-existing structures, with a long history that may extend back to the Precambrian (Kukkonen et al. 2010).

Landslide Lineaments

Site analyses of local discontinuities (joints, fractures, sliding planes and faults within and adjacent to several of the unstable slopes), return a pattern of dominantly ESE-WNW to SW-NE orientation (Bunkholt et al. 2011), whereas larger scarps and main scarps mainly follow the SW-NE orientation trend were measured (Fig. 3c, d). At Staluvarri (Fig. 3b), mineral growth slickenlines on several fractures within set J1 provide kinematic indicators of down-dip movement on the sliding planes. These faults strike NW-SE, parallel to the inherited lineament displayed in blue in Fig. 1c. The majority of the measured joints and fractures (Fig. 3d) strike NW-SE to W-E, sub-parallel to the Nordmannvikdalen Fault and at a locally high angle to the main valley trends.

Discussion

Difference in Deformation Styles

There are several different styles of gravitational slope failures in the greater Lyngen area, and particularly in the study area (Bunkholt et al. 2011). All slope failures lie

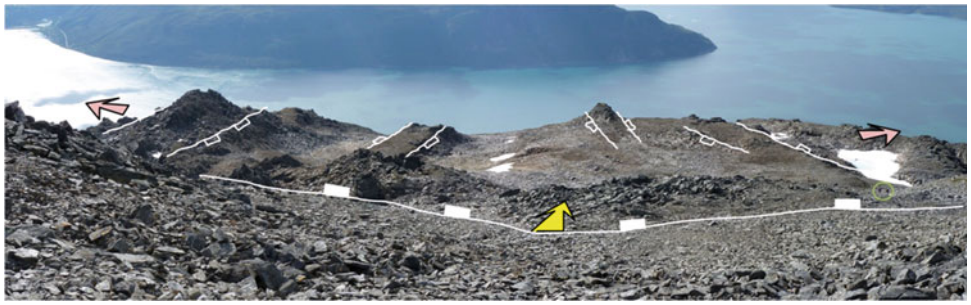

Fig. 7 Giilavarre. Classical horst-and-graben system indicates tension direction (*pink arrows*) parallel with the strike of the inherited fault (*white line*). *Yellow arrow*: gravitational tension perpendicular to the fjord, down-dip the inherited fault. The inherited normal fault cross-cut at least two valleys and three slopes

Fig. 8 Array of sinkholes at Gavtavarri tells of fjord-parallel tension in the subsurface, down-dip the fjord-perpendicular main sliding plane

in glacially steepened or over-steepened valley sides, and the destabilized volumes range from a few millions to hundreds of millions of cubic meters. The average annual displacement velocities are measured with interferometric synthetic aperture radar (InSAR), terrestial laser scanning (TLS) and/or differential global positioning system (dGPS). The velocities range from below detection limit to several tens of millimetres per year. Daylighting of the basal sliding surfaces or basal zones of weakness are nowhere observed, and they all appear to penetrate deeply.

Northeast of Kåfjorden: DSGSD

Following the characterization of Agliardi et al. (2001), the unstable slopes along the north-eastern part of Kåfjorden may be addressed as deep-seated gravitational slope deformations (DSGSD). They exhibit the classical morpho-structures with doubled ridges, trenches, scarps and counterscarps, and the sizes of the instabilities are on the order of the total slope. Present-day velocities vary within sub-domains of each slide, but may be generalized as between a few and more than 20 mm/year. Other morpho-structures such as large sinkholes and several meters wide open trenches tell of past or ongoing tension. In some places, e.g. Giilavvari (Fig. 5), Gavtavarri (Fig. 6) and Doronelva, down-dip movement occurs along valley-parallel inherited lineaments (green lines Fig. 1c). These inferred inherited normal faults are interpreted to cross-cut at least these three mountains, capturing the unstable areas including the main sliding planes in its hanging wall (Fig. 1c). Similar normal faults are also identified elsewhere. These inherited fault planes are steeply dipping and do not daylight. Within the unstable areas, several meters wide and many tens of meters deep trenches have opened up parallel to the strike of the slope. Long arrays of large sinkholes appear in the bedrock both parallel and perpendicular to the strike of the slope (Fig. 8), even in flat areas. These geomorphic features trend parallel to the slope gradients and at high angles to the inherited faults. We suggest gravitational down-dip tension is occurring along sliding planes above the inherited faults and perpendicular to Kåfjorden (yellow arrows), at the same time as fjord-parallel tension (pink arrows) in Figs. 1c, 4 and 7. The fjord-parallel tension direction in thus strike-parallel to the inherited faults, and may be an effect of topography. As gravity pulls on the bulk rock mass above the inherited faults, sideways flexure of the slope may be initiated on each of the flanks, as the contour lines bend around the convex slope (Fig. 4) and provide a free surface for lateral spreading (Fig. 5).

However, deformation structures caused by tension strike parallel to the inherited faults (pink arrows) are also observed on both sides of the inherited faults (Fig. 4), behind the main sliding planes of the fjord-perpendicular tension (yellow arrows). This area is not affected by gravitational deformation related to the fjord-perpendicular rock slide movements, which we interpret to occur above the inherited faults only.

At Nomedalstinden (Fig. 6) a well-defined back scarp provides an upper limit for an almost completely disintegrated slope. Abundant block rotations, ridges, scarps and counter-

scarps dominate the slide area. Equal surface expressions are also observable at the other DSGSDs on the north-eastern side of Kåfjorden labelled in Fig. 1. Moreover, morphologies similar to horst-and-graben systems, relay ramps and normal faults are also clearly present in many of these slopes. Such morphologies are usually known from extensional settings like rift zones. In particular the slopes Giilavarri (Fig. 7), Doronelva, Staluvarri and Gavtavarri (Fig. 8) exhibit well-expressed normal fault morphologies.

Southwest of Kåfjorden: Planar, Wedge and Toppling Failures

Unstable slopes with a different deformation style are present on the opposite, south-western side of Kåfjorden. Here, the morphologic elements characteristic for DSGSDs (Agliardi et al. 2001) are not commonly identified. Their absence suggests that the Kåfjord valley and fjord act as a geographic boundary between two sub-regions characterized by notably different styles of deformation. For example, at Oksfjellet and Gamanjunni 3, the main scarps appear to follow the same directions as those of the DSGSDs along the north-eastern side of Kåfjorden, but the response of the slope to gravitational failure is distinctly different. At Oksfjellet, well-defined systems of relay ramps can be mapped, but rock toppling and planar sliding appear to represent the fundamentally important failure mechanisms. At Gamanjunni 3, planar sliding on differently oriented sliding planes appears to control the movement, leading to wedge failure of a large rigid block down-slope (Bunkholt et al. 2011).

At these sites the rock mass do not disintegrate as occurs north of Kåfjord valley (Figs. 7 and 8). Rather, the unstable areas are more precisely delimited both vertically and laterally. From InSAR, the areas with high rate of movement are very well confined within delimiting structures mapped in field and on aerial photos (Henderson et al. 2011). More work needs to be done to understand the reasons for the difference in deformation style across the Kåfjord valley, but we notice from Fig. 4a, c that the brittle structures at Oksfjellet (J4 & J7) and Gamanjunni 3 (J3 & J6) are mainly oriented NE-SW, whereas the brittle structures at Staluvarri (J1 & J2) are oriented both NE-SW and NW-SE, parallel with the inherited faults. Thus, it may seem that the NW-SE fracture set is less present in the southwest of Kåfjorden. More field work is needed to better constrain our interpretation.

Inherited Structures and Sliding Planes

Among the mapped rockslide-related lineaments (Fig. 1c) are both smaller and larger fractures and sliding surfaces. The larger lineaments commonly act as either main scarps or intra-slide transverse scarps or sliding planes. We notice that the E-W to SW-NE striking basement-related lineaments assigned to older deformation events, also are present as the dominating orientation in the stereonets of Fig. 3 of the landslide-related lineaments of brittle fractures. Observations from both Revdalsfjellet and Staluvarri point towards a kinematic relationship between the tectonic lineaments of Fig. 1b, and the currently gravitationally driven rockslide-related lineaments (Fig. 1c). Based on the observations from Staluvarri and Revdalsfjellet, coupled with results from previous studies, we suggest that both the major and minor sliding planes of the rock slope failures utilize inherited lineaments from older deformation events.

Inherited Faults and Neo-tectonic Faults

Three kilometers away from Kåfjorden in map view, the neotectonic Normannvikdalen Fault trends parallel to the large inherited normal faults that run through the unstable slopes. The dip of the Normannvikdalen Fault is calculated at 28° and it is interpreted as a normal reactivation of an older existing (possibly reverse) fault (Dehls et al. 2000a). The fault is sub-parallel to several of the inherited faults interpreted to control much of today's slope failures (Fig. 1c), and we currently do not rule out that some of the unstable slopes and their deformation morphologies not only are a result of gravitational processes alone, but may also be under the influence of neotectonic forces deforming the mountain sides at a deeper level. The proximity and parallelism between the Nordmannvikdalen Fault and the green-colored assumed inherited fault in Fig. 1c, point towards linkage of such kind.

Conclusion

We observe that there is a remarkable clustering of rock slides in the greater Lyngen area (Fig. 1b), and in particular the Kåfjord area (Fig. 1c). We observe that there is a relationship between the orientations of regional bedrock lineaments assigned old deformation events, and smaller local fracture sets on intra-rockslide scales. Field evidence allow us to establish a clear kinematic relationship between the regional lineaments and the local rock slide lineaments, as the latter appear to utilize the former, highlighted by overprints of old kinematic indicators (mineral lineations) with recent kinematic indicators (rockslide-generated grooves). We have further observed a clear difference in slope deformation style between several rockslides, where the Kåfjord valley and fjord lineament appear to divide areas with different deformation styles. Based on current field data, it may seem that this discrepancy is connected to a difference in inherited structures. Our studies on the underlying causes for the high density of rock slope

failures in the region have just started, and much more work is needed. At the current stage, therefore, we do not rule out that more profound mechanisms other than topography and tectonic fabrics may contribute, such as ongoing neotectonic activity. To follow this path though, much more work is required.

Acknowledgments This work is part of the project ROS Fjellskredanalyse i Troms, a collaboration project between the Norwegian Geological Survey (NGU) and the Norwegian Water Resources and Energy Directorate (NVE). The project is fully financed by NVE.

References

Agliardi F, Crosta G, Zanchi A (2001) Structural constraints on deep-seated slope deformation kinematics. Eng Geol 59:83–102

Böhme M, Henderson I, Saintot A, Hermanns RL, Henriksen H (2011) Rock-slope instability investigations in Sogn & Fjordane County, Norway: a detailed structural and geomorphological analysis. In: Jaboyedoff M (ed) Slope tectonics, vol 351. Geological Society, London, pp 97–112, Special Publication. ISBN 978-1-86239-324-0

Brekke H,Kalheim JE, Riis F, Egeland B, Blystad P, Johnsen S, Ragnhildstveit J (1992) Two-way time map of the unconformity at the base of the Upper Jurassic (north of 69° N) and the unconformity at the base of the Cretaceous (south of the 69° N), offshore Norway, including the main geological trends onshore. Scale 1:2 million NPD Continental Shelf Map No. 1., The Norwegian Petroleum Directorate/The Geological Survey of Norway

Braathen A, Blikra LH, Berg SS, Karlsen F (2004) Rock-slope failures in Norway; type, geometry, deformation mechanisms and stability. Norwegian J Geol 84:67–88

Bunkholt H, Osmundsen PT, Redfield T, Oppikofer T, Eiken T, L'Heureux J-S, Hermanns R, Lauknes TR (2011) ROS Fjellskred i Troms: status og analyser etter feltarbeid 2010. Norwegian Geological Survey Report No. 2011–031, 135 p

Dehls J, Olesen O, Olsen L, Blikra LH (2000a) Neotectonic faulting in northern Norway; the Stuoragurra and Nordmannvikdalen postglacial faults. Quatern Sci Rev 19:1445–1460

Dehls JF, Olesen O, Bungum H, Hicks EC, Lindholm CD, Riis F (2000b) Neotectonic map: Norway and adjacent areas. Geological Survey of Norway, Notway

Furnes H, Roberts D, Sturt BA, Thon A, Gale GH (1980) Ophiolite fragments in the Scandinavian Caledonides. In: Panayioutou A (ed) Ophiolites – proceedings of the international Ophiolite symposium, Nicosia, Cyprus, 1979, Geological Survey Department of Cyprus, pp 582–600

Hansen J-A, Bergh SG, Henningsen T, Davids C (2011) Brittle fault zones in North Norway: onshore-offshore link and regional implications. NGF abstracts and proceedings of the Geological Society of Norway, vol 1, pp 37

Henderson IHC, Saintot A (2011) Regional spatial variations in rockslide distribution from structural geology ranking: an example from Storfjorden, western Norway. In: Jaboyedoff M (ed) Slope tectonics, vol 351. Geological Society, London, pp 79–96, Special Publication. ISBN 978-1-86239-324-0

Henderson IHC, Laukens TR, Osmundsen PT, Dehls J, Larsen Y, Redfield TF (2011) A structural, geomorphological and InSAR study of fractures in the development of rock slope failures. In: Jaboyedoff M (ed) Slope tectonics, vol 351. Geological Society, London, pp 185–201, Special Publication. ISBN 978-1-86239-324-0

Kukkonen IT, Olesen O, Ask, Maria VS and the PFDP Working Group (2010) Postglacial faults in Fennoscandia: targets for scientific drilling. GFF 132(1):71–81

Mosar J (2000) Depth of extensional faulting on the Mid-Norway Atlantic passive margin. Geol Surv Norway Bull 437:33–41

Mosar J, Eide EA, Osmundsen PT, Sommaruga A, Torsvik TH (2002) Greenland-Norway separation: a geodynamic model for the North Atlantic. Norwegian J Geol 82:281–298

Osmundsen PT, Henderson I, Lauknes TR, Larsen Y, Redfield TF, Dehls J (2009) Active normal fault control on landscape and rock-slope failure in northern Norway. Geology 37:135–138

Osmundsen PT, Redfield TF, Hendricks BHW, Bergh S, Hansen J-A, Henderson I, Dehls J, Lauknes TR, Larsen Y, Anda E, Davidsen B (2010) Fault-controlled alpine topography in Norway. J Geol Soc 167(1):83–98

Petit JP (1987) Criteria for the sense of movement on fault surfaces in brittle rocks. J Struct Geol 9:508–698

Saintot A, Henderson I, Derron M-H (2011) Inheritance of ductile and brittle structures in the development of large rock slope instabilities: examples from Western Norway. In: Jaboyedoff M (ed) Slope tectonics, vol 351. Geological Society, London, pp 27–78, Special Publication. ISBN 978-1-86239-324-0

Sigmond EMO, Gustavsen M, Roberts D (1984) Bedrock map of Norway, 1: 1 million. Geological Survey of Norway

Tolgensbakk J, Solli JL (1988) Kåfjord, kvartærgeologi og geomorfologi, 1:50 000, 1634 II. Geografisk Institutt/University of Oslo, Oslo

Zwaan KB (1988) Nordreisa, bedrock map, M 1: 250 000. Geological Survey of Norway

Tectonics and Large Landslides in the Northern Apennines (Italy)

Alessandro Chelli, Andrea Ruffini, Paolo Vescovi, and Claudio Tellini

Abstract

This work was aimed to highlight the spatial relationships between large-scale gravitational phenomena and tectonic uplifted structures in the area between Enza river valley and Taro river valley in the Northern Apennines. The structural-tectonic map of the investigated area and the inventory map of the large landslides and DSGSDs were made. The analysis of the structural map highlighted the existence of antiforms with axes roughly SE-NW. The comparison between the large landslides and the antiforms has shown that a spatial relationship between large complex landslides (earth/rock slides – earth flows) and positive geological structures exists.

Keywords

Large landslide • Deep seated gravitational slope deformation • Tectonic structure • Northern Apennines

Introduction

The Northern Apennines is a mountain chain characterized by distensive regime in the Tyrrhenian side and by a compressive one in the Adriatic side (Bernini and Papani 2002; Argnani et al. 2003). Several geomorphic features support the evidence that the Adriatic side of the Apennines experienced uplift since the Pliocene, with remarkable increases in the uplift rate in Late Pliocene and Middle-Late Pleistocene (Bartolini 1999). The uplift occurred as a consequence of the NE-verging thrust fronts propagation. Recent studies integrating existing and new data have accounted for the mechanism and for the 1 mm/year rate of the uplift for the external front of the Northern Apennines (Picotti and Pazzaglia 2008).

From the geomorphological point of view, the erosive processes, leading to the evolution of the slopes, are one of the principal effects of the uplift. In the study area, landslides are the main erosive process and they transport the earth material from the slopes to the streams. Nevertheless, the correlation between the landslides and tectonic uplift is in turn related to the links between landslides and tectonic features. Tectonics play a key role in the evolution of large-scale gravitational phenomena mainly through the formation of steep slopes and intense fracturing of the rock mass (Galadini 2006).

This work was aimed to reveal, if they exist, spatial relationships between large landslides and Deep-seated Gravitational Slope Deformation and tectonic uplifted structures.

General Features of the Area

The area considered in this study lies approximately between 44° and 45° N and 9° and 10° E, in the Emilia Apennines between the courses of Enza and Ceno torrents (Fig. 1). It is a mountainous area whose altitude exceeds 1,800 m a.s.l. in correspondence of the NW-SE divide between the Tyrrhenian and Adriatic sides of the belt, while it reaches about 700 m a.s.l. in the northeastern portion of it.

A. Chelli • A. Ruffini (✉) • P. Vescovi • C. Tellini
Department of Earth Sciences, University of Parma, V.le G.P. Usberti 157/A, Parma, Italy
e-mail: a.ruffini@provincia.parma.it

C. Margottini et al. (eds.), *Landslide Science and Practice*, Vol. 1,
DOI 10.1007/978-3-642-31325-7_36,

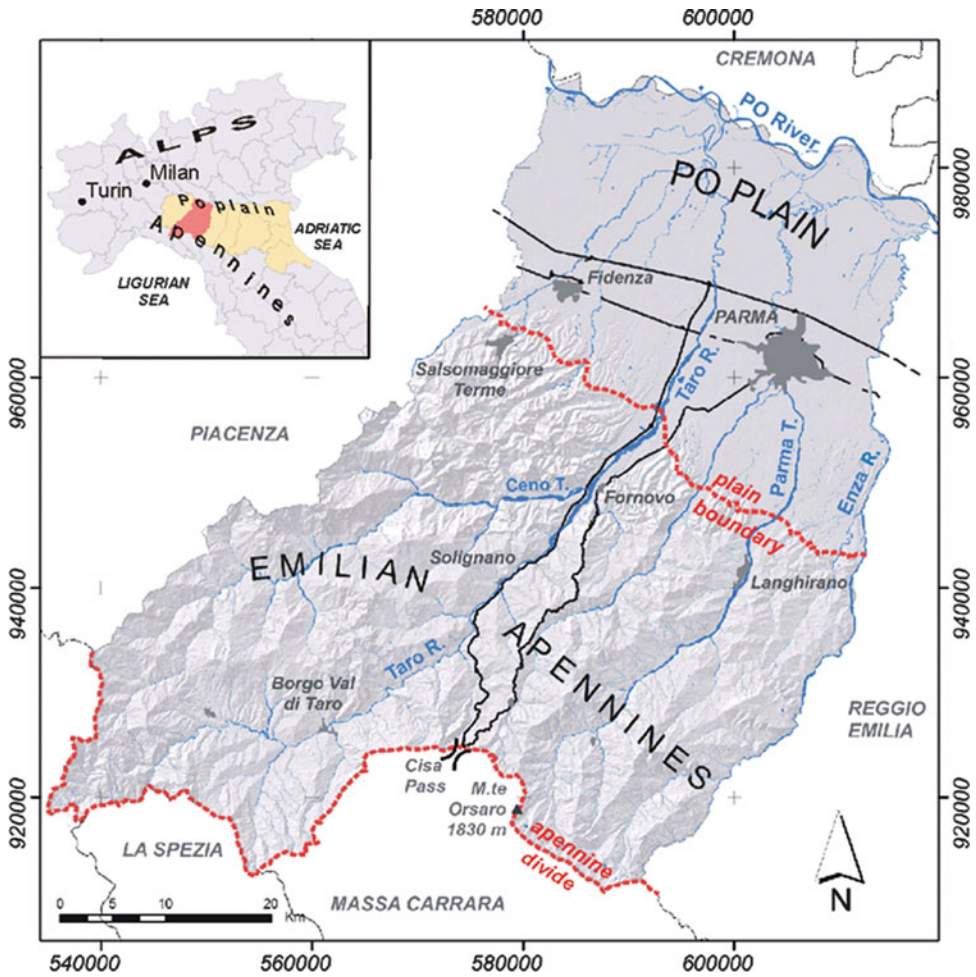

Fig. 1 Geographical sketch map of the area

The Northern Apennines are a folded and thrusted belt separating the extensional, back-arc basin of the Tyrrhenian Sea to the west from the Adriatic foredeep to the east. They started to develop in the Upper Cretaceous, by the convergence of the Adria and Africa plates, culminating in continent-to-continent collision starting in the Middle Eocene.

In most of the study area, the units of the Ligurian s.l. (allochthonous) and Epiligurian sequences of the Northern Apennines outcrop. They are characterized by the high content of weak rocks highly tectonized as ductile and fragile styles. In correspondence of the area across the Apennine main divide, the sandstone units (i.e. Macigno Fm and the Cervarola Fm) outcrop. They represent the foredeep deposits and the deepest units of the tectonic stack, tectonically uplifted during Plio-Pleistocene (Argnani et al. 2003).

As result of the predisposing geologic factors and meteorological conditions, the Emilia Appenines are largely imprinted by landsliding. In fact, the mean annual rainfall varies roughly from 1,000 to 2,000 mm throughout the area, while prolonged and/or intense rainfalls can occur mainly in Autumn and Winter. Sometimes, these extreme meteorological events may deliver in 2 or 3 months quantities of rainfall exceeding half of the mean annual value. These rainfalls increase the water content of soil whose water charge is already high because of the seasonal maximum of rainfall, causing the increase of soil pore pressure.

The rising up of pore pressure can cause earth flows or complex landslides (rock or earth rotational or translational slides-earth flows) other than soil slips and debris flows. Complex landslides are the most common landslides in this area and the reactivation of one or more parts of large complex landslides can also occur, as happened several times in the last 20 years.

Large complex landslides or huge rock slides are present throughout the Emilia Apennines. Several slopes are affected by large landslides as a whole but, in some cases, the presence of clear signs of collapse upslope does not correspond downslope to the existence of a clear shear surface emerging from the ground surface. This fact was interpreted as indicator of probable occurrence of a Deep-Seated Gravitational Slope Deformation (DSGSD).

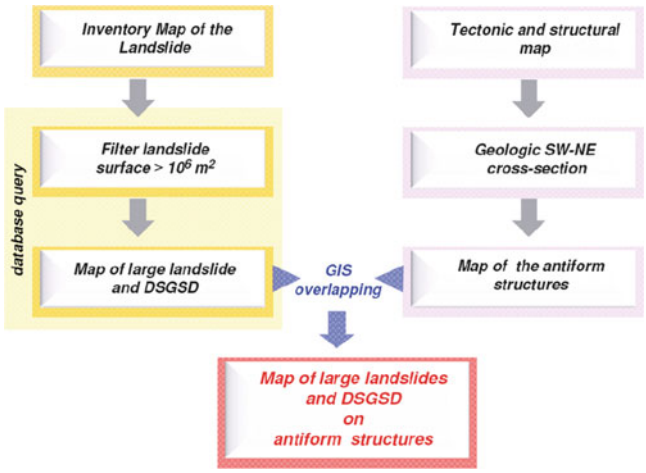

Fig. 2 Work flow

Material and Methods

To detect the relationships among tectonic structures and large landslides and to investigate them, a work plan has been followed (Fig. 2).

The geologic and morphologic analyses have been performed separately, to test the truth of the results at the end of the workflow. The geologic and geomorphologic maps were performed both at the scale 1:50,000.

The structural-tectonic map of the investigated area was compiled after the Structural Map of the Northern Apennines, the geologic maps of the CARG-project (1:50,000) for this part of the Emilia Romagna region (www.regione.emilia-romagna.it/SGSS) and unpublished surveys by one of the authors. The map shows the outcropping rocks grouped as structural-stratigraphic units while only the tectonic features (faults, thrusts and fold axes) significant at the used map scale were drawn.

Four SW-NE geologic cross-sections were drawn throughout the area roughly perpendicular to the strikes of the main tectonic and structural features of the Northern Apennines. The spatial arrangement of the cross-sections was retained the most appropriate to highlight the tectonic structures consequent to the compressive tectonic style of the Adriatic side of the Apennines and their lateral continuity.

The Landslide Inventory Map of the Parma Province (Enza, Parma and Taro valleys) was realized in the years from 2002 to 2004 by the Department of Earth Science, Parma University from detailed aerial photographs (year 2001, scale 1:13,000) and field surveys. The landslides have been classified using material and type of movement, and their state of activity (active, inactive, dormant, relict) has been also identified. The landslide map was georeferenced and the landslides were digitised using GIS software (ArcMap 9.2, ESRI). Finally, a database containing the landslides and their attributes was created. Types of movement and materials, state of activity, geographic coordinates and size (length, width and area) of the landslides were the main attributes inserted in the database.

The volume of displaced material should be the parameter used to choose large landslides from the population of landslides of the area. Nevertheless, the lack of subsurface data for most of the landslides and of knowledge about the thickness of their body prevented the use of the landslide volume as discriminating parameter.

Korup (2005) stated that empirical scaling relationships show that large landslides involve $>10^6$ m^3 of material. The same author considered as large landslides those with a planform area exceeding 1 Km^2.

Guzzetti et al. (2009) have compiled a dataset on volume and area of slides from worldwide literature founding that the relationship between them is a power-law equation. Following this equation a landslide volume of an order of magnitude of 10^6 m^3 generally corresponds to an area of an order of magnitude of 10^5 or more m^2. Carraro et al. (1979) have indicated as large a landslide with, at least, an area of 0.5–5 Km^2.

So, in this work we consider large landslides those with a planform area $\geq 10^6$ m^2. A semi-automatic procedure was adopted to extract large landslides from the database of the Parma Province Landslides Inventory. In fact a query was made to select polygons (landslides) with an area $\geq 10^6$ m^2. A tolerance of -5 % (5×10^4 m^2) in the measure of the planform area was admitted because the uncertainty introduced with the digitization process. Then, a check was made on the selected large landslides and if landslides with minor area but in close spatial relationship with those of large dimensions existed, they were adjoined to the population considered for the study, constituting "groups" of landslides.

Results

More than 30 large landslides were finally extracted (Fig. 3) from the Landslide Inventory Map of Parma Province. Principally, they are earth flows or complex landslides (rock/earth slides-earth flows) in which the volume of displaced material may reach up to 10^6 m^3: i.e. the landslide of Corniglio, one of the most relevant of the entire Northern Apennines, reaches 100×10^6 m^3 of displaced material that becomes 200×10^6 m^3 if the total amount of material moved by the secondary landslides correlated with the principal one is accounted for (Larini et al. 2001). In fact, many of the large landslides have a "cortege" made by several minor landslides activated as consequence of the principal one that can be considered as a part of it.

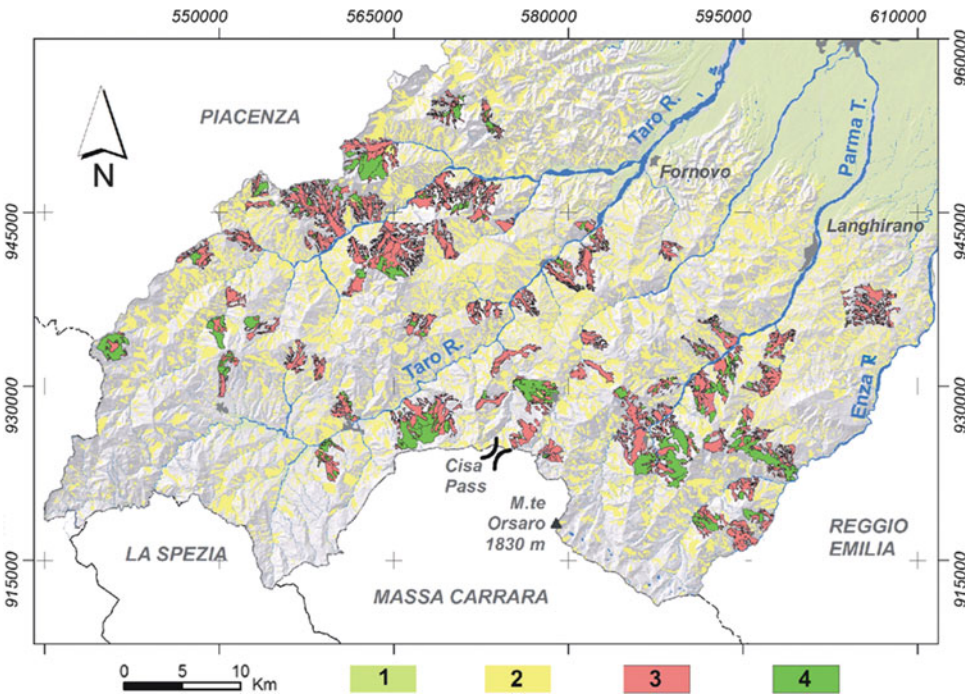

Fig. 3 The landslide inventory map of the Parma Province. Legend: *1* alluvial plain, *2* minor landslides, *3* and *4* respectively large landslides and rock slides – DSGSD treated in this work

More than 20 large landslides involve, as part of them, rock slides which have undergone a moderate displacement moving almost as a single mass and maintaining its integrity. In one case, the morphological features have allowed to recognize a DSGSD.

The principal evidence resulting from the large landslides map (Fig. 3) is that in several cases two or more landslides are very close one to the other constituting real clusters of landslides.

The structural-tectonic map and the four geologic cross-sections (Fig. 4) have highlighted the existence of several antiforms involving geologic units at different levels in the tectonic stack.

On the basis of the tectonic units involved and of some features of the deformation, four principal types of antiforms can be recognized which, from 1 to 4, involve deeper structural levels:

1. Antiforms involving Ligurian s.l. units, affecting the reverse limb of already overturned succession;
2. Antiforms involving, in their cores, lower Ligurian units;
3. Antiforms where the deepest allochtonous units (Subligurian) outcrop in tectonic window;
4. Antiforms involving, in their cores, the deepest foredeep units outcropping in tectonic window.

The strikes of the axes of these antiforms are roughly NW-SE (Fig. 4) with a mild arched planimetric shape. As highlighted in the cross-section shown in Fig. 4, these structures generally correspond to thrust surfaces that emerge at the ground surface with high angles. They represent the youngest deformations of the Apennine structural frame, along which the late compressive stages occurred in the Adriatic side of the Northern Apennines, resulting in the uplift of the chain since the Middle Pleistocene (Bartolini 1999).

Discussion and Conclusions

As result of the overlapping between the Inventory Map of the Large Landslides and DSGSDs and the Structural-Tectonic Map (Fig. 2), it is remarkable the appearance of a sort of coincidence among late antiforms and some large landslides (bright colour) (Fig. 5). In fact, about in the centre and in the southeastern part of the investigated area, large landslides occur along the axes of the antiforms or in the area immediately close to them. So, a spatial relationship seems to exist (Fig. 5) among landslides and antiforms and this relationship could be due to the role as preparatory causal factor, with respect to the landslide movements, played by the uplift occurred in correspondence of the tectonic structures. In fact, the landslides may be the slope response to the disequilibrium induced by the increase of the energy relief due to the tectonic uplift.

In the investigated area, the large landslides connected with the tectonic structures are usually rock slides, often followed in sequence by earth flows (complex landslides), with their surface of rupture at variable depth but generally exceeding 15–20 m below the ground surface. These large slides, involving the outcropping rocks, seem more related to the structural and tectonic features (joints, schistosity, faults) that the substrate acquired during the tectonic stress, than

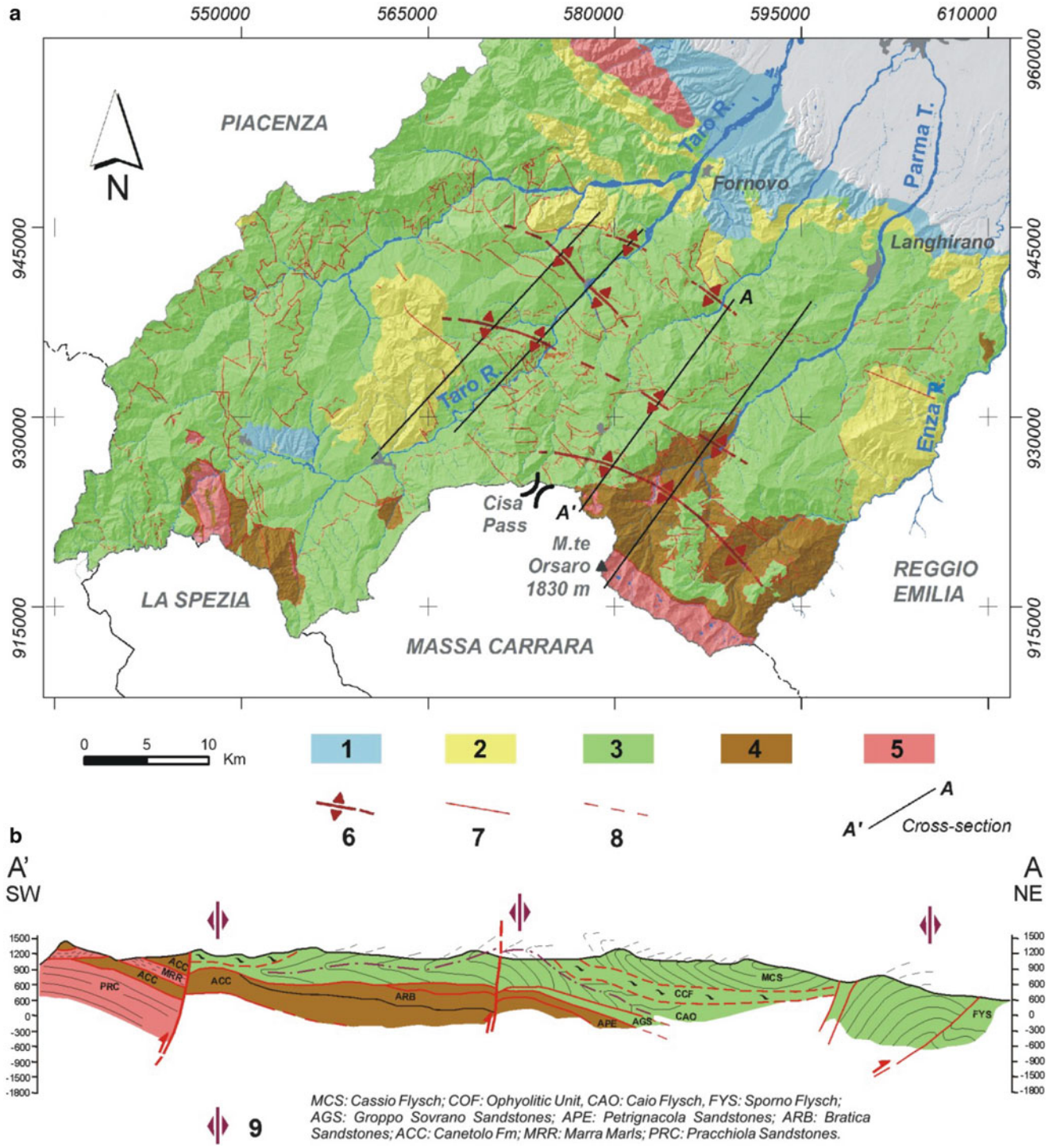

Fig. 4 (**a**) Structural tectonic map of the area. The *black solid line* represents the geologic cross section. Legend: *1* Pliocene-Quaternary deposits, *2* Epiligurian sequences, *3* Ligurian sequences, *4* Subligurian sequences, *5* Tuscan-Umbrian sequences, *6* Antiform axis, *7* Fault, *8* Thrust. (**b**) geologic cross-section (A'-A) illustrated in the text, *9* Antiform axis

the more widespread earth flows. In fact, the latter ones generally involve weathered rock that periodically flows usually because of prolonged or intense rainfalls. Therefore, they seem to be caused by the lithologic feature of the slopes (e.g.: presence of clay, claystone and shales) where the outcropping rocks are often deeply weathered as response to the periods occurred during the late Quaternary, characterized by deterioration of the climate conditions (Tellini and Chelli 2003).

For instance, in Fig. 5b it is shown the southeastern portion of the investigated area. Here, the large landslides occur in

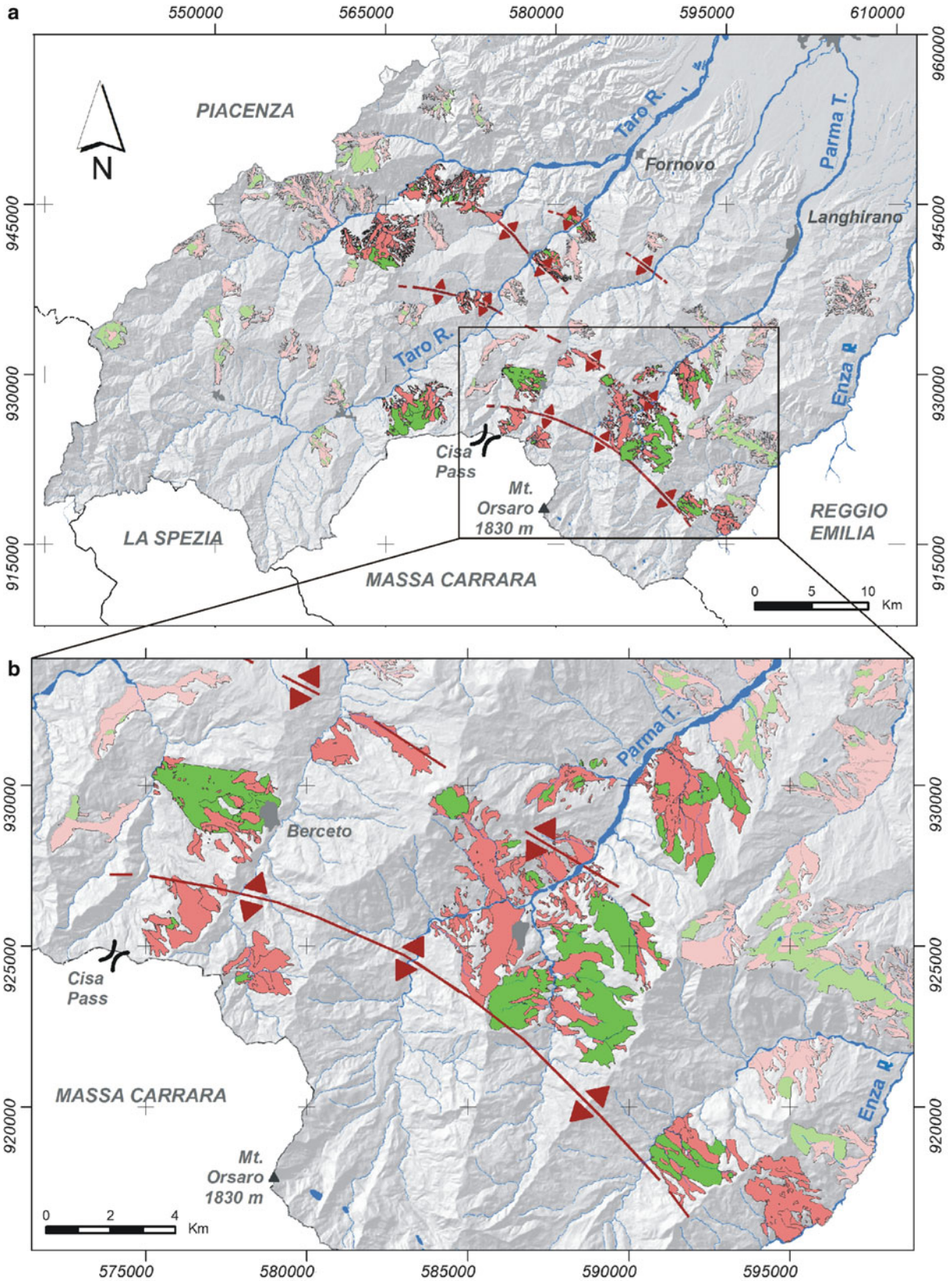

Fig. 5 (**a**) Result of the overlapping between the inventory map of large landslides and DSGSDs and the antiform axes. (**b**) focus on the SE part of the study area (the colours used for the landslides have the same meaning of those used in Fig. 3; the landslides in bright colour are discussed in the text)

correspondence of the limbs of antiforms, especially in the area lying between the two axes of the antiforms themselves. In this area the uplift and the presence of jointed and faulted rocks promoted the instability of the slopes.

The evident spatial relationships between large landslides and tectonic structures highlighted in this work for a portion of the Emilian Apennines lay the basis for future researches on this topic. So, they should be aimed to investigate the connection existing at the slope scale between landslides and tectonic features.

Acknowledgments Dr. Giacomo Guidetti is gratefully acknowledged for his help in the work. The research was funded by FIL2009 University of Parma (Head: A. Chelli).

The authors thank Javier Hervas whose comments and suggestions greatly improve the manuscript.

References

Argnani A, Barbacini G, Bernini M, Camurri F, Ghielmi M, Papani G, Rizzini F, Rogledi S, Torelli L (2003) Gravity tectonics driven by quaternary uplift in the Northern Apennines: insights from the La Spezia-Reggio Emilia geo-transect. Quatern Int 101–102:13–26

Bartolini C (1999) An overview of Pliocene to present-day uplift and denudation rates in the Northern Apennine. In: Smith BJ, Whalley WB, Warke BA (eds) Uplift, erosion and stability: perspectives on long-term landscape development, vol 162. Geological Society, London, pp 119–125, Special Publications

Bernini M, Papani G (2002) La distensione della fossa tettonica della Lunigiana nord-occidentale (con carta geologica alla scala 1:50.000). Boll Soc Geol It 121:313–341

Carraro F, Dramis F, Pieruccini U (1979) Large-scale landslides connected with neotectonic activity in the Alpine and Apennine range. In: Proceedings of the I.G.U.U.N.E.S.C.O. Commission on geomorphological survey and mapping, 15° Plenary meeting, Modena, 7–15 Sept 1979, pp 1–16

Galadini F (2006) Quaternary tectonics and large-scale gravitational deformations with evidence of rock-slide displacements in the Central Apennines (central Italy). Geomorphology 82:201–228

Guzzetti F, Ardizzone F, Cardinali M, Rossi M, Valigi D (2009) Landslide volumes and landslide mobilization rates in Umbria, central Italy. Earth and Planet Sci Lett 279:222–229

Korup O (2005) Distribution of landslides in southwest New Zealand. Landslides 2:43–51

Larini G, Malaguti C, Pellegrini M, Tellini C (2001) La Lama di Corniglio (Appennino parmense), riattivata negli anni 1994–1999. Quaderni di Geologia Applicata, vol 8–2. Pitagora Editrice, Bologna, pp 59–114

Picotti V, Pazzaglia FJ (2008) A new active tectonic model for the construction of the Northern Apennines mountain front near Bologna (Italy). J Geophys Res 113:B08412. doi:10.1029/2007JB005307

SGSS-RER Geologia. URL: http://www.regione.emilia-romagna.it/geologia

Tellini C, Chelli A (2003) Ancient and recent landslide occurrence in the Emila Apennines (northern Apennines, Italy). In: Proceedings of the workshop on geomorphological sensitivity and system response, Camerino-Modena Apennines, Italy, 4–9 July 2003, pp 105–114

Landslide Inventories for Reliable Susceptibility Maps in Lower Austria

Helene Petschko, Rainer Bell, Philip Leopold, Gerhard Heiss, and Thomas Glade

Abstract

Landslide inventories, their accuracy and the stored information are of major importance for landslide susceptibility modelling. Working on the scale of a province (Lower Austria with about 10,000 km^2) challenges arise due to data availability and its spatial representation. Furthermore, previous studies on existing landslide inventories showed that only few inventories can be used for statistical susceptibility modelling. In this study two landslide inventories and their resulting susceptibility maps are compared: the Building Ground Register (BGR) of the Geological Survey of Lower Austria and an inventory that was mapped on the basis of a high resolution LiDAR DTM. This analysis was performed to estimate minimum requirements on landslide inventories to allow for deriving reliable susceptibility maps while minimizing mapping efforts. Therefore a consistent landslide inventory once from the BGR and once from the mapping was compiled. Furthermore, a logistic regression model was fitted with randomly selected points of each landslide inventory to compare the resulting maps and validation rates. The resulting landslide susceptibility maps show significant differences regarding their visual and statistical quality. We conclude that the application of randomly selected points in the main scarp of the mapped landslides gives satisfactory results.

Keywords

Landslide inventory mapping • Minimum requirements • Archive data • LiDAR DTM • Lower Austria

Introduction

Landslide inventories form the most important data basis for subsequent landslide susceptibility, hazard or risk analysis. Therefore, their quality regarding location and representativeness of the recorded events highly affects the possible quality of its further applications. Working on the scale of a province (in this case Lower Austria), it is of high importance to have data that represents the actual landslide density. Depending on the available archives and their particular purpose the data may show a large range in information quality and quantity. Therefore, a major drawback may be the locally restricted information (Glade 1996). Traditionally landslide inventories consist either of archive data collected in a database from different data sources such as newspapers, archives of churches or national and municipal authorities (Guzzetti et al. 1994; Glade 1996; Glade et al. 2001) or of landslides mapped by the interpretation of topographic maps or aerial photographs (Brardinoni et al. 2003; Duman et al. 2005). New methods for landslide inventory mapping arose with the availability of high resolution

H. Petschko (✉) • R. Bell • T. Glade
Department of Geography and Regional Research, University of Vienna, Universitaetsstrasse 7, 1010 Wien, Vienna, Austria
e-mail: helene.petschko@univie.ac.at

P. Leopold • G. Heiss
Health and Environment Department, Environmental Resources and Technologies, AIT – Austrian Institute of Technology GmbH, Konrad Lorenz Straße 24, 3430 Tulln, Austria

C. Margottini et al. (eds.), *Landslide Science and Practice*, Vol. 1,
DOI 10.1007/978-3-642-31325-7_37,

remote sensing data, e.g. satellite imagery and LiDAR data, resulting in a "revolution in geomorphology" (Anders and Seijmonsbergen 2008) and in increasing levels of sophistication in terrain mapping (Petley 2010). These new methods contain the identification and mapping of landslides on the hillshade of a LiDAR DTM (Chigira et al. 2004; Schulz 2004; Ardizzone et al. 2007; Bell 2007; Van Den Eeckhaut et al. 2007) and the semi-automated object based mapping of landslides on LiDAR and/or satellite images (van Asselen and Seijmonsbergen 2006; Booth et al. 2009; Martha et al. 2010; Mondini et al. 2011).

As a detailed knowledge on the inventories used for susceptibility modelling is important and as we want to reduce the mapping effort to its possible minimum we set the following three objectives for this study: (1) to analyse the database and documents of the Building Ground Register regarding further information on main triggers and size of events and to identify points that store information on landslide events, (2) to map landslide polygons by interpreting the morphology provided by hillshades of the LiDAR DTM and (3) to compare the resulting inventories and thereby to identify minimum requirements of a landslide inventory for subsequent statistical landslide susceptibility modelling. These minimum requirements may help to define future steps of landslide inventory mapping for the entire province of Lower Austria with respect to the implementation of the resulting susceptibility maps for spatial planning strategies.

This study is part of the project MoNOE (Method development for landslide susceptibility modelling in Lower Austria) that is presented by Bell et al. (this volume).

Study Area

The study area is Lower Austria and focuses particularly on the districts which are identified as prone to landslides according to the prevalent lithology and morphology. In a first project phase, three districts (Amstetten, Waidhofen/Ybbs and Baden) are chosen as test study area to develop a methodology for inventory homogenization and mapping. The three districts have been selected according to their geological setting and landslides based on the number of present entries in the Building Ground Register. All main geological units of Lower Austria are covered and the landslide density differs significantly. In Amstetten and Waidhofen/Ybbs numerous landslide information is available. In contrast, Baden has a similar geological setting but only very few reported landslides. The area of these districts totals 2,072 km^2. For a detailed map on the distribution of the landslide inventories in Lower Austria refer to Bell et al. (this volume).

In Lower Austria, several extensive inventories are available: the "Building Ground Register" (BGR) is a database maintained by the Geological Survey of Lower Austria and consists of reports on landslide events recorded since 1953; the "GEORIOS" database and the "Map of sedimentary deposits" are both provided by the Geological Survey of Austria and contain mainly polygons but also lines and points on mapped landslides. Detailed analysis of these inventories in a previous study showed that these are of varying quality (Petschko et al. 2010) so that the way they are used for landslide susceptibility modelling has to be adopted.

Materials/Data

For a general overview on geodata applied in this study refer to Bell et al. (this volume). In the present study the LiDAR DTM with a resolution of 1 × 1 m and its derivatives (hillshade, slope map, contour lines) were the most important data source. Furthermore orthophotos with a resolution of 25 × 25 cm (taken in the period 1999–2005) and of 12.5 × 12.5 cm (taken in the period 2007–2009) were used during the mapping as a reference on the current land cover.

Landslide Inventory: Building Ground Register

The archive of the Building Ground Register stores reports and studies on e.g. supervision of quarries or underground investigations of parcel land since 1953. Additionally, this archive contains approx. 1,500 studies on reported landslide events (slide, fall) until the year 2009 (Pomaroli et al. 2011). The minimum information provided for each landslide event is a short report that includes the date or the period (month, season and year) of occurrence, the location, the geological setting and a comment on the event trigger (Schwenk 1992). The main information on each event is available in a database which is connected to a point shape-file. Originally the points were mapped at a scale of 1:50,000, but nowadays they are mapped on orthophotos (spatial resolution 25 cm) and on the parcel land map of Lower Austria (1:1,000) with higher accuracy.

Methods

Building Ground Register

The Building Ground Register database is complemented with additional information stored in the event related analogue documents and reports. The entries of the database are analysed with respect to date, main trigger, size and setting (natural or engineered slope) of the event. Especially the latter information is important for the selection of points for

the modelling: only the points indicating landslides on natural slopes are selected as input data to model the susceptibility of natural slopes. The anthropogenic engineered slopes are not considered (Pomaroli et al. 2011).

Inventory Mapping on LiDAR DTM

The method for landslide inventory mapping on the basis of a LiDAR DTM and its derivatives was earlier described in Petschko et al. (2010) and tested for the district Waidhofen/Ybbs. This method is now applied for the districts Amstetten and Baden; therefore we summarize the main details on the mapping method here. The mapping is based on the visual interpretation of the morphology that is visualized by hillshades with different azimuth angles and contour lines, both calculated from the LiDAR DTM (Petschko et al. 2010). With respect to the application of the resulting inventory in statistical modelling we decided to map landslide polygons with a representative density while covering each lithological unit (Petschko et al. 2010). Furthermore, several landslide types are differentiated: slide, flow and complex (following Cruden and Varnes 1996). In case of large areas with several slides of different ages one large polygon was mapped covering the entire area and attributed as "area of slides" (Petschko et al. 2010).

Comparison and Minimum Requirements of Inventories

The resulting inventories are analysed regarding their differences and possible advantages or drawbacks of using the one or the other dataset for modelling landslide susceptibility. Besides the accuracy of the location of the landslides and the density of information also the effort of mapping and the implementation of the resulting maps in spatial planning are important. Therefore, the visual differences of the maps have to be taken into account.

This comparison is facilitated by fitting a number of different models with logistic regression (generalized linear models in R) (e.g. Atkinson et al. 1998; Brenning 2005). For a detailed description of the logistic regression modelling method used here refer to Leopold et al. (this volume). The input datasets for the models are: aspect, flow accumulation, slope angle, slope length, land cover, geology, landform classification and the topographic wetness index as explanatory variables and landsides as dependent variable. Three landslide input parameters are used: (1) randomly selected points form the BGR; (2) points that are randomly sampled in the entire slide polygon and (3) points that are randomly sampled in the main scarp of the slide. For the inventory mapped on the basis of the LiDAR DTM we only use landslides classified as "slide" in the model.

The resulting landslide susceptibility maps are compared both statistically and visually. Therefore the statistical significance of the input datasets and the area-under-ROC (AUROC) values of all maps are compared. The validation of the resulting maps is performed by calculating a ROC plot and the AUROC that allows evaluating the model's performance independently of determined thresholds in the probability values (Beguería 2006). By the usage of training datasets (for each inventory) and the same independent test dataset that is derived of the entire landslide body a "success" and a "prediction" rate was calculated (Chung and Fabbri 2003). Furthermore, the resulting map is also visually evaluated according to geomorphological "quality" (Bell 2007) and to major differences between the susceptibility maps modelled with points from BGR and LiDAR mapping. Therefore, the aimed user-optimized visualisation (Bell et al. this volume) is applied to the resulting maps and the differences between the maps are analysed.

Results

Building Ground Register

The analysis of the completed database of the Building Ground Register shows that 694 events have been reported in the three test districts (BGR green points in Amstetten and Waidhofen/Ybbs are shown in Fig. 1d). It is obvious that these are purely the reported events; the real number of failures can be assumed to be much higher. Landslides that occurred in anthropogenic engineered slopes can successfully be identified by the review of the reports and are excluded from this analysis. The main trigger of the reported events was rainfall (76 %) and snow-melt (12 %). The landslides occurred on pasture (43 %) and affected infrastructure (23 %). The maximum reported landslide size was 75,000 m^2 but the average size is 1,885 m^2 with an average depth of 1.9 m^2 only. During the completion of the BGR database it was noticed that the location of the points (at the main scarp, the parcel land, or at the location of damage) differs and is not exact at each point.

Inventory Mapping on LiDAR DTM

The landslide inventory mapping resulted in a total number of 2,014 polygons. The main mapped landslide type is "slides" (1,518 polygons). 413 polygons are classified as "area with

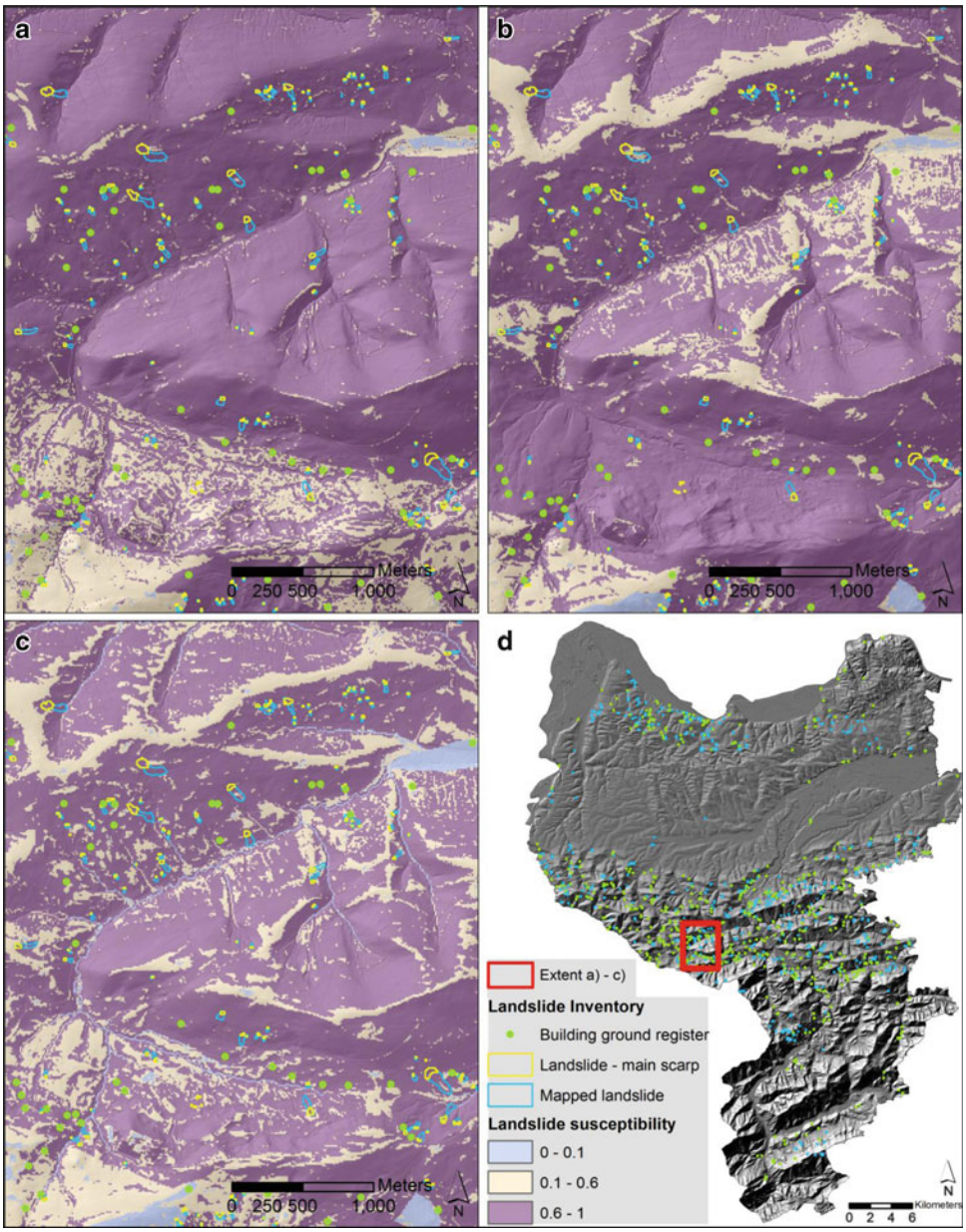

Fig. 1 Comparison of results from logistic regression modelling with (**a**) Points of the Building Ground Register, (**b**) randomly selected points within the mapped landslide polygons and (**c**) randomly selected points within the main scarp of the mapped landslides and the parameters: aspect, slope angle, slope length, lithology, landform classification, land cover, flow accumulation and topographic wetness index. The same classification according to probability values is applied to each susceptibility map. Figure 1. (**d**) shows the landslide inventories (BGR and mapped landslides) in Amstetten and Waidhofen/Ybbs superimposed on the LiDAR hillshade map (Data source: DTM – Provincial Government of LowerAustria)

slides". The resulting inventory on "slides" is presented in Fig. 1d with blue polygons.

During the mapping on the basis of the LiDAR DTM, the respective results have been compared with the points from the BGR. This comparison showed, that only few points can be related to a morphological feature visible on the hillshade. This may be mainly due to the BGR mapping scale (1:50,000) or the size or the age of the event. In some cases agricultural land use is another possible reason for the disappearing of landslides. It was observed that landslides that are mainly located on pastures are very quickly remediated (Bell et al. in prep.).

Comparison and Minimum Requirements of Inventories

In Table 1 a comparison of the analysed Building Ground Register and the mapped landslide inventory regarding number of landslides is presented. In general, more landslides have been mapped than there are stored in the BGR. This is of major advantage in the district Baden where only little information on landslides was available. Furthermore, the representativeness of the BGR could be tested by the comparison of the percentage of landslides mapped (LiDAR) and

Table 1 Comparison of building ground register and mapped landslide inventory for the districts Amstetten, Baden and Waidhofen/Ybbs regarding number of entries/mapped polygons and percentage of these in the three districts. Additionally, the area of the district is stated

District	Number of mapped polygons	Mapped polygons (%)	Number of entries in BGR	BGR entries (%)	District area (km^2)
Amstetten	1,213	60	535	77	1,187
Baden	107	5	7	1	754
Waidhofen/ Ybbs	694	34	151	22	131

Table 2 Comparison of the results of the validation of the modelling results. The "success rate" was calculated with the training dataset on landslides (BGR, scarp or body) and the "prediction rate" was calculated with the test dataset from points from the entire landslide (body). (*not enough observations)

Landslide inventory	"Success rate" AUROC training	"Prediction rate" AUROC test (with landslide bodies)
BGR	–*	0.76
Landslide body	0.87	0.87
Landslide scarp	0.89	0.84

reported in the BGR. This shows that the reported landslide density in Baden is lower than the mapped landslide density.

In Table 2 the comparison of the calculated area-under-ROC values is presented. The "prediction rate" was calculated with a test dataset with points in the landslide body as general reference. The prediction rate is significantly lower in the model with the BGR as input data than at the models of the mapped landslides.

Figure 1 shows the results of the landslide susceptibility modelling with the different landslide inventory point samples. The visual differences of these maps are related to the susceptibility zones. When modelling with the mapped landslides, the susceptibility of the hill slopes is more differentiated between high and medium classes. These differences are particularly occurring at upper and local ridges since the geomorphological quality of the maps (b) and (c) can be stated as higher than the quality of map (a). Comparing the results from modelling with landslide body or main scarp it is shown (Fig. 1b, c) that fewer areas are classified as highly susceptible but the overall impression is similar.

Discussion and Conclusions

The BGR contains very important information at least on the year of occurrence and its major advantage is the long timeline it covers. Some drawbacks are the accuracy of the location of the points that were mapped on a scale of 1:50,000 and the fact that only reported events are stored in this database.

Nevertheless, as the comparison of BGR and mapped inventory particularly for the district Baden shows, the mapping on LiDAR DTM is a valuable additional data source in areas with sparse information on landslides. Furthermore, a higher mapping accuracy can be achieved within short time due to the availability of LiDAR data with a high resolution. Therefore, the landslide mapping can be performed to obtain a representative landslide density and distribution over the entire province with high accuracy regarding the location of the points.

The visual comparison of the landslide susceptibility maps is of course highly dependent on the chosen classification thresholds. As they are once defined (refer to Bell et al. (this volume)) the differences in the possible resulting map can be analysed. This comparison shows that the differences between the usage of BGR or mapped landslides are significant, whereas the maps derived from the usage of points in the entire landslide body or main scarp are quite similar.

Keeping in mind the limited resources and the end-user optimized visualization of the maps we conclude that mapping landslide points in the main scarp area gives satisfying results to derive a representative landslide density in the entire province, which subsequently leads to reliable landslide susceptibility maps. Thus, for the rest of the districts a LiDAR mapping based landslide inventory will be prepared by mapping landslide points in the main scarp area instead of complete landslide polygons. The latter would not be feasible for such a large area, mainly due to limited resources.

Acknowledgments The authors thank several institutions and individuals for their support: the colleagues from the Geological Survey of Austria and from the Austrian Service for Torrent and Avalanche Control for providing inventory data; the Provincial Government of Lower Austria in particular the colleagues from the Geological Survey and the Department of Spatial Planning and Regional Policy for inventory data. Thanks to them also for supporting the MoNOE-project and for numerous fruitful discussions. Thanks also to the Department for Hydrology and Geoinformation for providing LiDAR and orthophoto data.

Finally, the authors are grateful for financial support of the Provincial Government of Lower Austria.

References

Anders NS, Seijmonsbergen H (2008) Laser altimetry and terrain analysis – a revolution in geomorphology. GIM International. November 2008, pp 36–39

Ardizzone F, Cardinali M, Galli M, Guzzetti F, Reichenbach P (2007) Identification and mapping of recent rainfall-induced landslides using elevation data collected by airborne Lidar. Nat Hazards Earth Syst Sci 7(6):637–650

Atkinson P, Jiskoot H, Massari R, Murray T (1998) Generalized linear modelling in geomorphology. Earth Surf Proc Land 23 (13):1185–1195

Beguería S (2006) Validation and evaluation of predictive models in hazard assessment and risk management. Nat Hazards 37(3):315–329

Bell R (2007) Lokale und regionale Gefahren- und Risikoanalyse gravitativer Massenbewegungen an der Schwäbischen Alb. Dissertation thesis, Rheinische Friedrich-Wilhelms-Universität Bonn, Bonn, Germany. http://hss.ulb.uni-bonn.de/2007/1107/1107.pdf

Bell R, Petschko H, Röhrs M Dix A (in prep) Assessment of landslide age, human impact and landslide persistence using airborne laser scanning DTMs. Geografiska Annaler Series A

Bell R, Glade T, Granica K, Heiss G, Leopold P, Petschko H, Pomaroli G, Proske H, Schweigl J (this volume) Landslide susceptibility maps for spatial planning in Lower Austria. In: Proceedings of the 2nd world landslide forum, Rome, 3–7 Oct 2011

Booth AM, Roering JJ, Perron JT (2009) Automated landslide mapping using spectral analysis and high-resolution topographic data: Puget Sound lowlands, Washington, and Portland Hills, Oregon. Geomorphology 109(3–4):132–147

Brardinoni F, Slaymaker O, Hassan MA (2003) Landslide inventory in a rugged forested watershed: a comparison between air-photo and field survey data. Geomorphology 54(3–4):179–196

Brenning A (2005) Spatial prediction models for landslide hazards: review, comparison and evaluation. Nat Hazards Earth Syst Sci 5:853–862

Chigira M, Duan F, Yagi H, Furuya T (2004) Using an airborne laser scanner for the identification of shallow landslides and susceptibility assessment in an area of ignimbrite overlain by permeable pyroclastics. Landslides 1(3):203–209

Chung CJF, Fabbri AG (2003) Validation of spatial prediction models for landslide hazard mapping. Nat Hazards 30(3):451–472

Cruden DM, Varnes DJ (1996) Landslide types and processes. In: Turner AK, Schuster RL (eds) Landslides, investigation and mitigation. National Academy, Washington, D.C., pp 36–75

Duman TY, Çan T, Emre Ö, Keçer M, Dogan A, Ates S, Durmaz S (2005) Landslide inventory of northwestern Anatolia, Turkey. Eng Geol 77(1–2):99–114

Glade T (1996) The temporal and spatial occurrence of landslide-triggering rainstorms in New Zealand. Heidelberger Geographische Arbeiten 104:237–250

Glade T, Frances F, Albini P (eds) (2001) The use of historical data in natural hazard assessments. Kluwer Academic Publishers, The Netherlands

Guzzetti F, Cardinali M, Reichenbach P (1994) The AVI project: a bibliographical and archive inventory of landslides and floods in Italy. Environ Manage 18(4):623–633

Leopold P, Heiss G, Petschko H, Bell R, Glade T (this volume) Susceptibility maps for landslides using different modelling approaches. In: Proceedings of the 2nd world landslide forum. Rome, 3–7 Oct 2011

Martha TR, Kerle N, Jetten V, van Westen CJ, Kumar KV (2010) Characterising spectral, spatial and morphometric properties of landslides for semi-automatic detection using object-oriented methods. Geomorphology 116(1–2):24–36

Mondini AC, Guzzetti F, Reichenbach P, Rossi M, Cardinali M, Ardizzone F (2011) Semi-automatic recognition and mapping of rainfall induced shallow landslides using optical satellite images. Remote Sens Environ 115(7):1743–1757

Petley D (2010) Landslide hazards. In: Alcántara-Ayala I, Goudie AS (eds) Geomorphological hazards and disaster prevention. Cambridge University Press, Cambridge, NY, pp 63–75

Petschko H, Glade T, Bell R, Schweigl J, Pomaroli G (2010) Landslide inventories for regional early warning systems. Malet JP, Glade T, Casagli N (eds) In: Proceedings of the international conference "Mountain risks: bringing science to society". CERG Editions, Strasbourg

Pomaroli G, Bell R, Glade T, Heiss G, Leopold P, Petschko H, Proske H, Schweigl J (2011) Darstellung der Gefährdung durch gravitative Massenbewegungen im Bundesland Niederösterreich als Grundlage der Raumplanung. Skolaut C (ed) Wildbach- und Lawinenverbau - Zeitschrift für Wildbach-, Lawinen-, Erosions- und Steinschlagschutz. Verein der Diplomingenieure der Wildbach und Lawinenverbauung Österreichs, Villach, pp 198–212

Schulz WH (2004) Landslides mapped using LIDAR imagery, Seattle, Washington. US Geological Survey Open-File Report, 1396(11)

Schwenk H (1992) Massenbewegungen in Niederösterreich 1953–1990. Jahrbuch der Geologischen Bundesanstalt. Geologische Bundesanstalt, Wien, pp 597–660

Van Asselen S, Seijmonsbergen AC (2006) Expert-driven semi-automated geomorphological mapping for a mountainous area using a laser DTM. Geomorphology 78(3–4):309–320

Van Den Eeckhaut M, Poesen J, Verstraeten G, Vanacker V, Nyssen J, Moeyersons J, van Beek LPH, Vandekerckhove L (2007) Use of LIDAR-derived images for mapping old landslides under forest. Earth Surf Proc Land 32(5):754–769

Landslide Susceptibility Mapping at National Scale: The Italian Case Study

Alessandro Trigila, Paolo Frattini, Nicola Casagli, Filippo Catani, Giovanni Crosta, Carlo Esposito, Carla Iadanza, Daniela Lagomarsino, Gabriele Scarascia Mugnozza, Samuele Segoni, Daniele Spizzichino, Veronica Tofani, and Serena Lari

Abstract

Landslide susceptibility maps are key tools for land use planning, management and risk mitigation. The Landslide susceptibility map of Italy, scale 1:1,000,000 is being realized by using the Italian Landslide Inventory – *Progetto IFFI* and a set of contributing factors, such as surface parameters derived from 20 to20 m DEM, lithological map obtained from the geological map of Italy 1:500,000, and land use map (Corine Land Cover 2000). These databases have been subjected to a quality analysis with the aim of assessing the completeness, homogeneity and reliability of data, and identifying representative areas which may be used as training and test areas for the implementation of landslide susceptibility models. In order to implement the models, physiographic domains of homogeneous geology and geomorphology have been identified, and landslides have been divided into three main classes in order to take into account specific sets of conditioning factors: (a) rockfalls and rock-avalanches; (b) slow mass movements, (c) debris flows. The modelling tests performed with different techniques (Discriminant Anaysis, Logistic Regression, Bayesian Tree Random Forest) provided good results, once applied with the appropriate selection of training and validations sets and with a significant number of statistical units.

Keywords

Landslide • Susceptibility • Italy • Landslide inventory

Introduction

Landslides are among the most problematic natural hazards in Italy, in terms of both casualties and economic losses. The management of landslide risk requires suitable actions at different levels, from national to municipal. In particular, at national level it is mandatory to correctly allocate the limited budget available for mitigation, thus recognizing the most critical areas where funds should be allocated. Moreover, it is important to know the fragility of the territory at trans-regional level in case of large disasters that require the intervention of National Civil Protection. For both needs, a map reporting the susceptibility of landslides at national scale is fundamental.

Some experiments of landslide susceptibility mapping at national scale have been already presented in the literature in Italy (Delmonaco et al. 2002; Günther et al. 2008) and in other

A. Trigila (✉) • C. Iadanza • D. Spizzichino
ISPRA – Italian National Institute for Environmental Protection and Research, Geological Survey of Italy, Via V. Brancati, 48, Rome 00144, Italy
e-mail: alessandro.trigila@isprambiente.it

P. Frattini • G. Crosta • S. Lari
Department of Geological Sciences and Geotechnologies, University of Milano-Bicocca, Piazza della Scienza, 4, Milan 20126, Italy

N. Casagli • F. Catani • D. Lagomarsino • S. Segoni • V. Tofani
Department of Earth Sciences, University of Florence, Via La Pira, 4, Florence 50121, Italy

C. Esposito • G.S. Mugnozza
Department of Earth Sciences, University of Rome "Sapienza", Piazzale Aldo Moro, 5, Rome 00185, Italy

C. Margottini et al. (eds.), *Landslide Science and Practice*, Vol. 1,
DOI 10.1007/978-3-642-31325-7_38,

countries (Malet et al. 2010). However, these maps have been produced using heuristic methods based on multi-criteria analysis of contributing factors and subjective judgement. None of these maps have been produced by systematically exploiting national-scale landslide inventories that are becoming available in many countries.

The aim of the work is to present the methodology adopted by ISPRA (Italian National Institute for Environmental Protection and Research) with the University of Florence, University of Milano-Bicocca and University of Rome "La Sapienza" for the development of a Landslide susceptibility map of Italy at 1:1,000,000 scale. This research is carried out in the framework of the European Thematic Strategy for Soil Protection and in particular in the activities of the JRC European Landslide Expert Group dealing with the definition of guidelines for delineating landslide prone areas in Europe and the development of preliminary models for landslide susceptibility assessment at European and national scale (Hervas 2007; Hervás et al. 2010; Van Den Eeckhaut et al. 2010).

The "Landslide susceptibility map of Italy" project activities include: (1) analysis and quality assessment of existing datasets for geology, land use, land surface and landslides; (2) identification of "homogeneous" physiographic settings, (3) test of different susceptibility models to assess advantages, disadvantages and the applicability at the scale of the analysis; (4) selection of an optimal model; (5) application of selected model to the entire area and production of Landslide Susceptibility Map of Italy. This paper presents the results of the first four activities.

Contributing Factors

Considering the expected significance in controlling landslides and the availability of complete datasets for the entire country, it has been decided to use as contributing factors the lithology, the land use and selected land surface parameters.

The lithological map was obtained from the 1:500,000 Geological Map of Italy (Compagnoni et al. 1976–1984) by reclassifying the 128 geological units in 16 classes, according with similar lithological and geomechanical characteristics. The geological classification is consistent and homogeneous for the entire area, even if not always optimized for landslide susceptibility (e.g., talus and alluvial deposits are not distinguished, pyroclastic soils around Vesuvius Volcano are not well classified). In some portions, the accuracy of the map is moderate, with errors in mapping limits higher than 50 mm, which correspond to acceptable graphicism error at 1:1,000,000 scale.

Land use was obtained by reclassified 1:100,000 Corine Land Cover Map (Büttner et al. 2002) in 11 classes based on

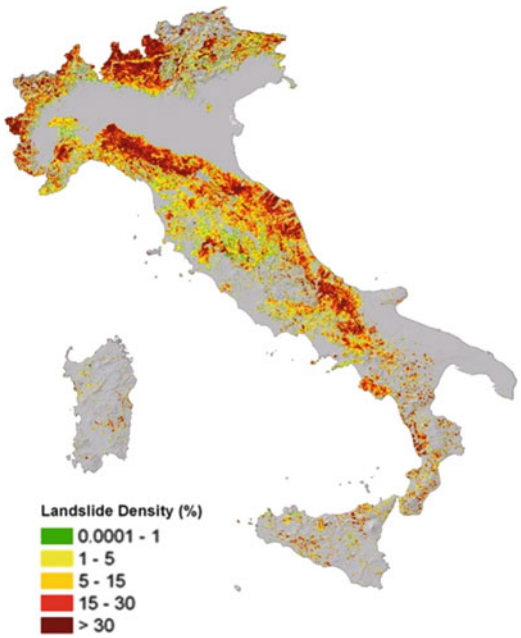

Fig. 1 Landslide density in Italy (From Trigila et al. 2010)

landslide density and spatial significance of similar units in the area. The map is high homogeneous, and the resolution of boundaries is high for the scale of the analysis.

A 20 × 20 m DEM (IGM) was adopted for the description of land surface. This DEM derives from the interpolation of 25 m interval contour lines. Although the resolution is optimal for the scale of the analysis, the quality of the DEM is low in some sectors due to interpolation problems (e.g., terrace effect) and a strong smoothing effect. A number of DEM-derived variables have been created within GIS: slope gradient, aspect, curvatures, contributing area, topographic wetness index (Beven and Kirkby 1979), roughness (VRM, Sappington et al. 2007).

The Italian Landslide Inventory

The Italian Landslide Inventory (*Progetto IFFI – Inventario dei Fenomeni Franosi in Italia*) has been used for the analysis (Fig. 1). This inventory includes 486,336 landslides which affect an area of about 20,800 km^2 (6.9 % of Italy). The main types of movement are: rotational/translational slides (32.5 %), slow earth flows (15.3 %) and rapid debris flows (14.6 %).

The inventory has been developed by ISPRA and 21 Regions and self-governing Provinces following a common protocol for both the geometric representation and the landslide attributes. Landslides have been identified using field surveys, historical documents, and aerial photo interpretation, and mapped within a GIS environment as polygon (78 %),

line (11 %) or points (11 %), according to the shape, the typology and the dimension of the landslides.

The mapping scale is 1:10,000 in the most part of Italian territory. Less resolution scale (1:25,000) has been used in mountain and sparsely populated areas.

The attributes associated to each landslide are organised in three different levels of increasing detail. The 1st level contains the basic data on landslide location, type of movement and state of activity; the 2nd level provides data on geometry, lithology, geotechnical properties, land use, causes and activation date; the 3rd level gives detailed information on damages, investigations and remedial measures (Trigila and Iadanza 2008). For most of landslides, only the 1st level information is available.

The pre-existing degree of knowledge on landslides among the Regions was extremely different before the Project began. Despite the adoption of a common protocol for landslide identification and mapping, currently there is still a lack of homogeneity of the inventory, especially in terms of landslide density (ls/km^2) (Trigila et al. 2010).

A further analysis allowed to recognize that this incompleteness is due to three main problems: (1) sources of information, (2) landslide size resolution, (3) interpretation of landslide typology.

Regions where landslide have been recognized mainly based on historical data report only events in urban areas and along the transportation network, thus neglecting all landslide bodies that can be recognized in sparsely populated areas by aerial photo-interpretation or field survey. Susceptibility models based on such limited information roughly describe the susceptibility of most active slopes, but generally underestimate the overall landslide potential (Carrara et al. 2003).

The size–frequency relationship allows to determine the resolution of the inventory and to estimate the completeness, under the assumption that a complete inventory should follow a power-law relationship for a wide range of orders of magnitude (Malamud et al. 2004). The analysis has been performed for all Regions and all landslide typologies (Fig. 2). In general, it is possible to observe a systematic difference in the modal size of landslides, and a strong deviation from power law below a certain threshold, which regionally varies.

Problems related to the interpretation of landslide typology has been observed in a few cases. In Apennine areas, slides, earthflows and complex landslides (mostly slide-earthflows) are not consistently classified among the Regions (Fig. 3a). However, this problem was overcome by grouping the three typologies together. The same occurs for rockfalls and complex landslide in the Alpine areas.

DSGSDs pose several problems of consistency. Some Regions considered DSGSDs as very large phenomena involving entire slopes and characterized by clear morpho-structural features (Agliardi et al. 2001). In other Regions, relatively small phenomena that are elsewhere considered as rock slides are classified as DSGSD. Although a susceptibility model for DSGSD will not be developed, this problem is important for the susceptibility model of slides, because an overestimation of DSGSD imply an underestimation of slides (cfr. Piemonte inventory in Figs. 2e and 3c).

Concluding, the non-homogeneity of the IFFI inventory requires a careful selection of training and validation sets for the susceptibility models, in order to avoid systematic errors in the analysis.

Moreover, to reduce problems related to the classification of landslides, the typologies have been reclassified into three classes: (1) slow-moving landslides (herein SML, including rotational and translational slides, earthflows and Apenninic complex landslides), (2) rockfalls and rock-avalanches (herein RRA, including rockfalls and Alpine complex landslides), and (3) debris flows (herein DF).

Susceptibility Modelling Tests

The strong geological and morphological heterogeneity of Italy required a subdivision of the area in 5 relatively homogeneous domains to be used for the training of the models: the Alps, the Northern Apennines, the foredeep-foreland (Apennine eastern slope until the Adriatic coast), the inner chain (Apennine western slope until the Tyrrhenian coast) and the Calabrian Arc (Calabria region and north-east Sicily). For each area and for each landslide typology class (SLM, RRA, DF), training and validation zones are identified according to the completeness and quality of database, and further refined based on the results of susceptibility modelling tests. Models developed for the training areas will then be applied to the entire domains and finally joined to develop the final Landslide Susceptibility Maps of Italy.

In order to be consistent over the entire areas, it was decided to adopt the same modelling techniques, for the choice of which a number of tests have been performed using Discriminant Analysis, Bayesian Tree Random Forest (BTRF) and Logistic Regression.

The modelling tests have been performed to analyse several issues that are relevant for susceptibility modelling:

- The suitability of different terrain units (slope-units vs. grid cells)
- The effect of different training and validation sets
- The effect of different independent variable set
- The effect of the size of the terrain units
- The effect of different sampling techniques and density of points

The type and size of terrain units strongly affect the results and the quality of susceptibility models (Carrara et al. 2003). The optimal terrain units should be selected

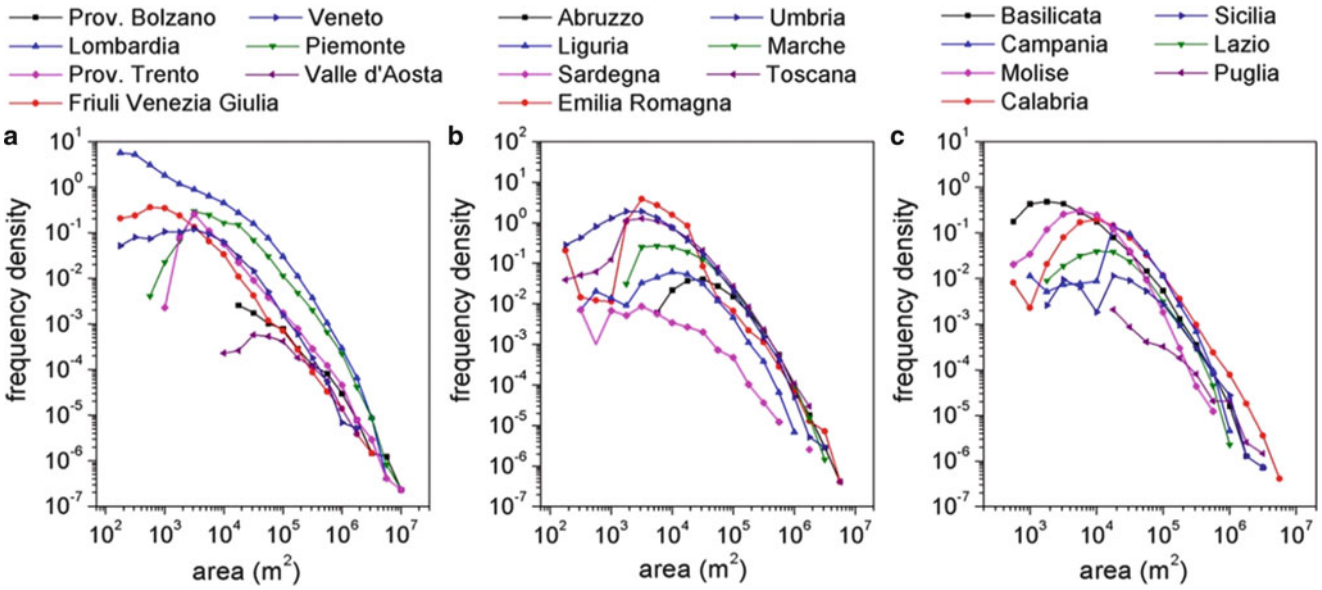

Fig. 2 Size-frequency curves for rotational and translational slides for Italian regions. Some regions present a censoring for landslides above 10,000 m^2, which is due to an adoption of previous protocol for landslide mapping. For most regions, the size-frequency curve shows a deviation from power-law for landslides smaller than about 500,000 m^2

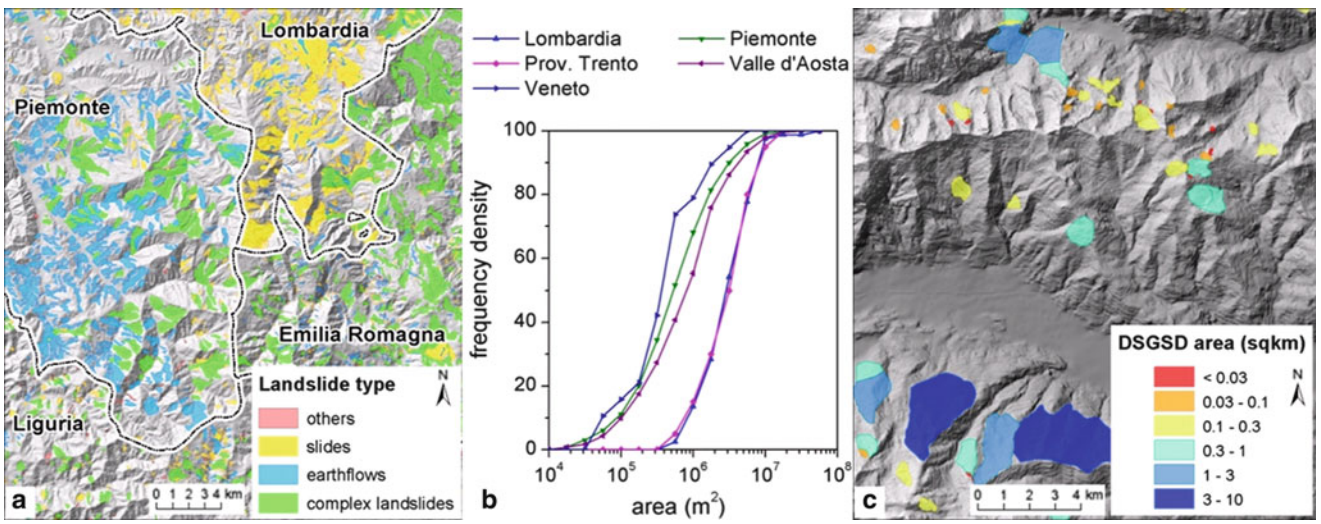

Fig. 3 Example of problems related to the interpretation of landslide typology. (**a**) unclear distinction among earthflows, slides and complex landslides in the Apennine area; (**b**) cumulative probability as a function of size for DSGSD, showing different approaches to DSGSD mapping; (**c**) extract of DSGSD inventory in Regione Piemonte, with polygons reclassified according to planar area, showing the presence of extremely small DSGSD bodies

according to the typology and the mean size of landslides. For instance, grid-cells are suitable for debris flows and small landslides, whereas slope-units may be preferable for large slides. In some cases, however, the selection of a terrain unit is forced by data availability, or by the scale of the analysis.

For our modelling, it has been decided to adopt large grid cells as terrain units. Although geomorphologically not significant, these units can be used easily for extremely large areas. In order to assess the suitability of these terrain units, Discriminant Analysis was applied to 500 × 500 m grid-cells and to hydrologically significant slope units. As a results, the large grid-cells model performed as good as the slope-unit model, especially for SML (Fig. 4) and RRA.

The selection of appropriate training and validation sets is also fundamental.

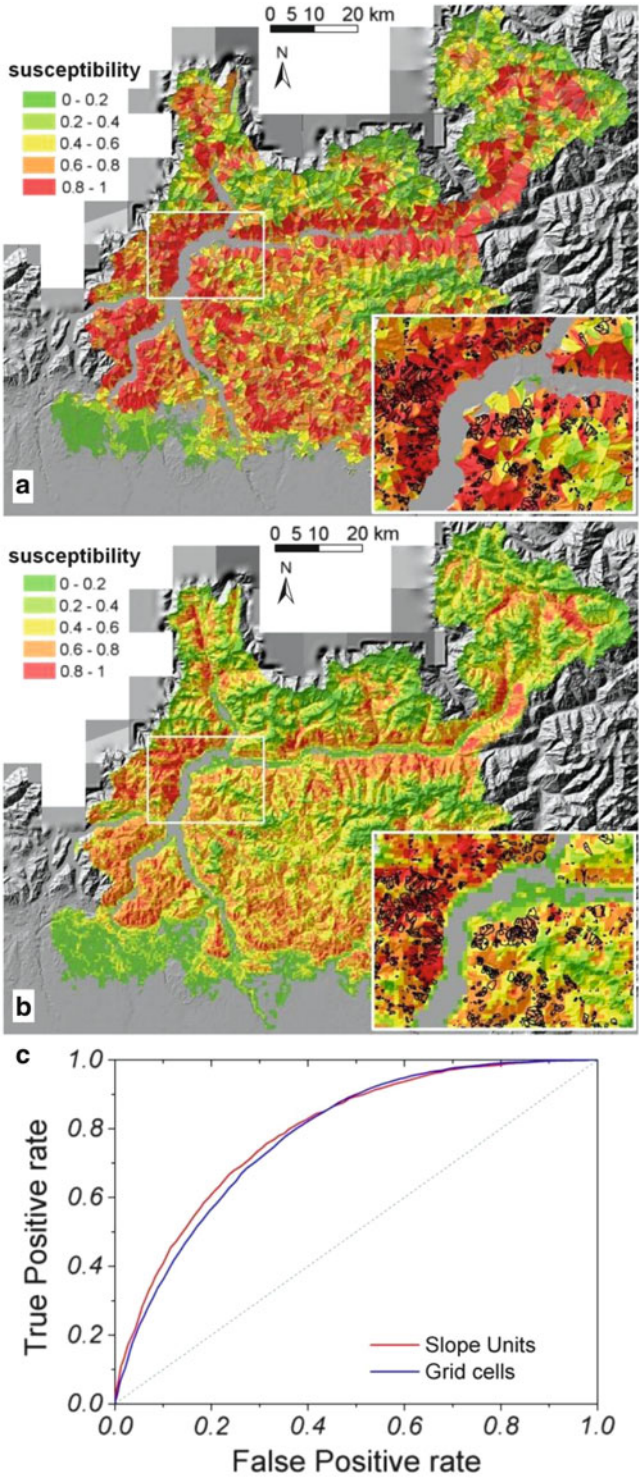

Fig. 4 Rotational and translational slide susceptibility maps developed by using Discriminant Analysis and different terrain units. (**a**) slope-units; (**b**) 500 × 500 m square cells. (**c**) ROC curves for the two models, showing a similar performance

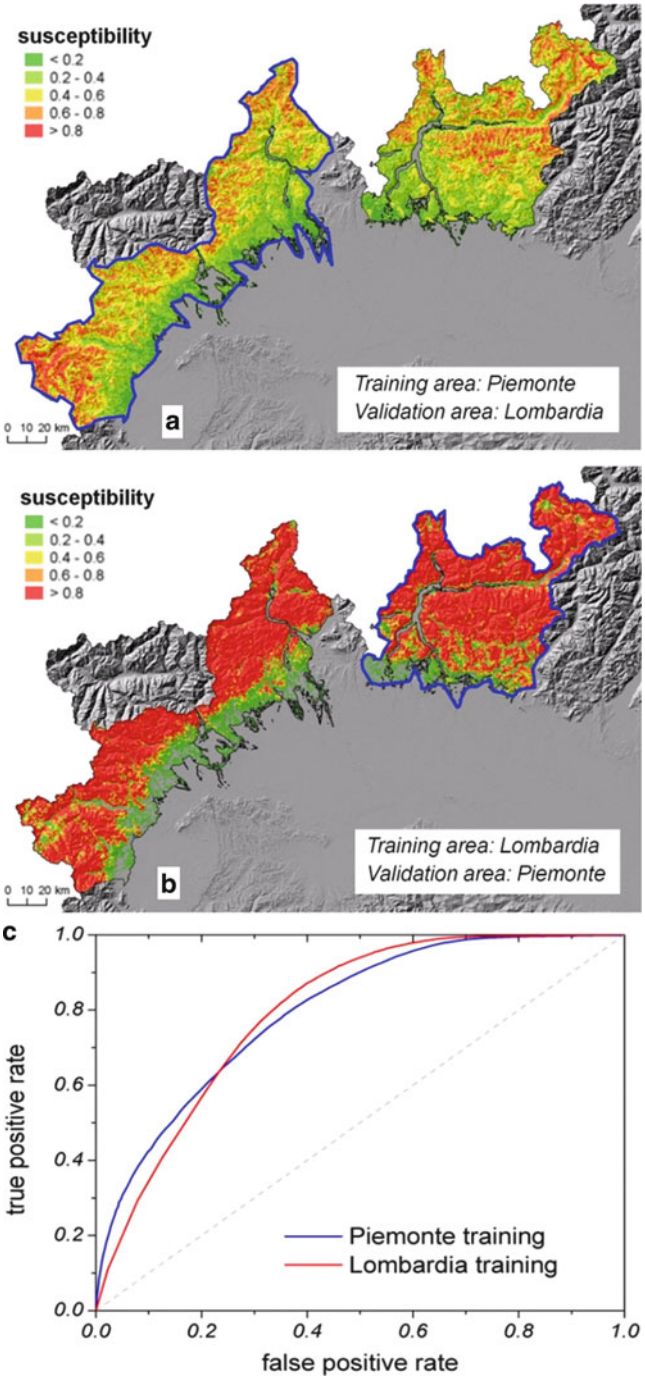

Fig. 5 Rockfall and rock-avalanche susceptibility maps developed by using Discriminant Analysis and different training and validation sets. Model (**b**), developed by using Lombardia as training set, strongly overestimate susceptibility due to problems related to rockfall inventory mapping. A visual comparison of the two maps shows strong differences that are not appreciable with ROC curves (**c**)

Especially with small scale models, this issue can be extremely complex. Discriminant analysis was used for RRA susceptibility modelling of a large area that includes part of Lombardy and part of Piemonte. A first model was trained in Lombardy and validated in Piemonte, and the second vice versa (Fig. 5).

The two models are very different, with the model trained in Lombardy strongly overestimating the landslide

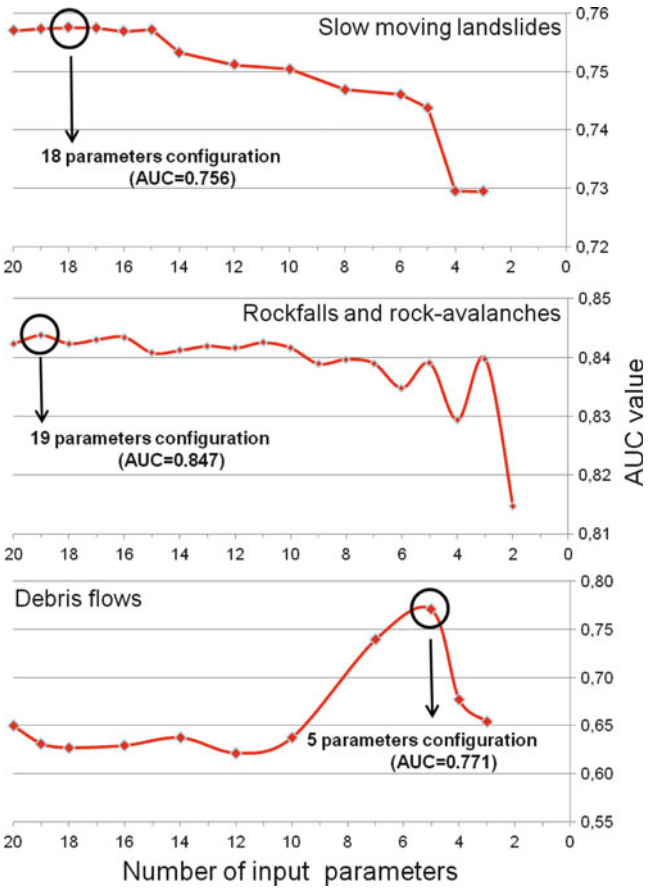

Fig. 6 Iterative procedure for the determination of the optimal configuration of the Bayesian Tree Random Forest model

susceptibility. In spite of these differences, the ROC curves of the two models are very similar, thus demonstrating how difficult is the assessment of model quality when training and validation are performed with non-homogeneous datasets deriving from different sources.

The analyses performed in the Northern Apennine with the Bayesian Tree Random Forest (BTRF henceforth) focused on the estimation of the importance of the single input parameters and on the selection of the optimal configuration of a regression model. The results of these tests are displayed in Fig. 6. The model was initially applied using the complete set of input parameters at disposal (full version), automatically assigning them a rank by relevance and calculating the Receiver Operating Characteristic (ROC) curve (with relative Area Under Curve, AUC) using an independent testing dataset. Subsequently, reduced versions of the BRTF model were applied taking into account a progressively lower number of parameters. Step by step the least relevant

Table 1 Ranking of the most important parameters involved in landslide susceptibility modelling in the Northern Apennine homogeneous domain

RANK	SML	RF\RRA	DF
1st	Prevailing lithology	Prevailing lithology	Prevailing lithology
2nd	Mean contributing area	Mean slope gradient	Prevailing land cover
3rd	Mean slope gradient	Prevailing land cover	Mean profile curvature
4th	Mean profile curvature	Standard deviation of curvature	Mean TWI

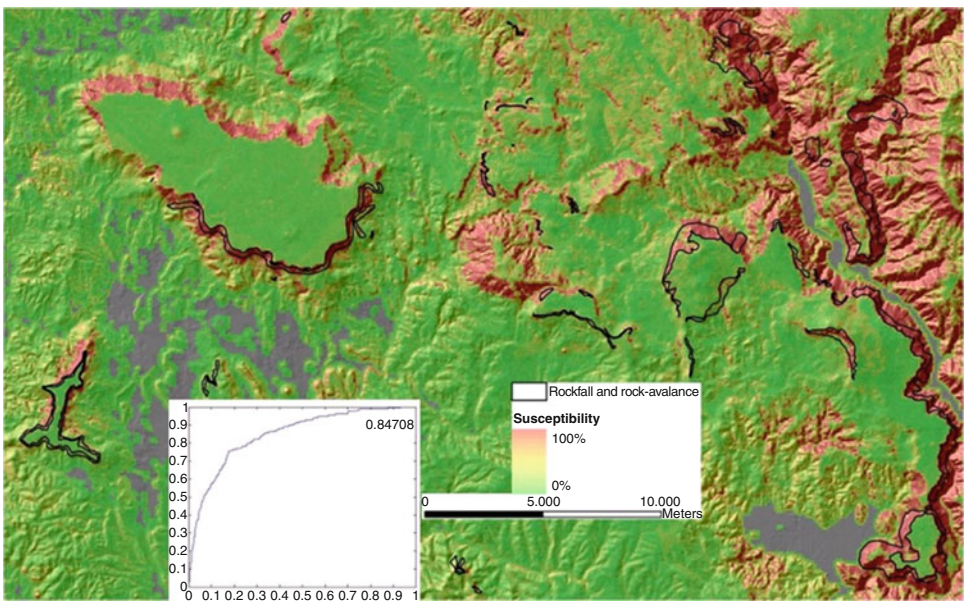

Fig. 7 Application of the Bayesian Tree Random Forest model in a test area

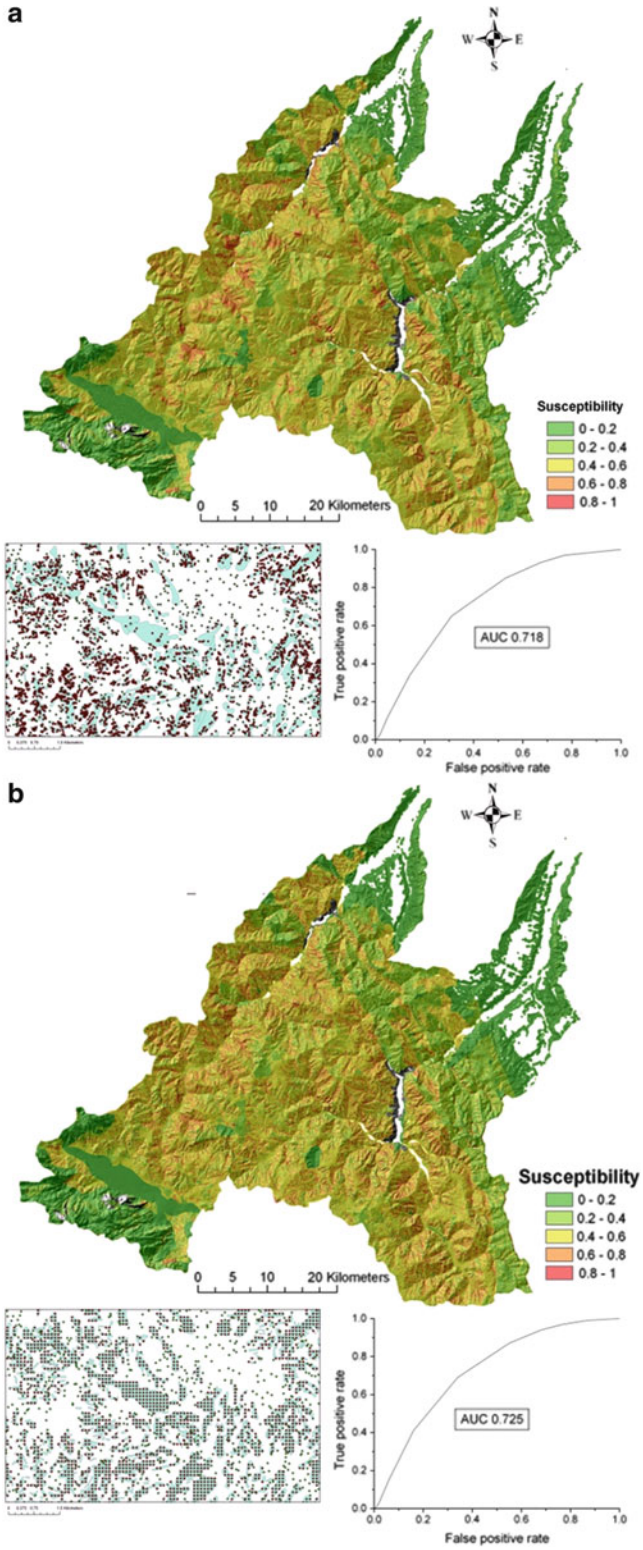

Fig. 8 Example of SML susceptibility maps obtained by applying the logit function with two different sampling strategies (sketch in the *lower left corner*), with related ROC curves: (**a**) randomly placed points; (**b**) "gridded" points

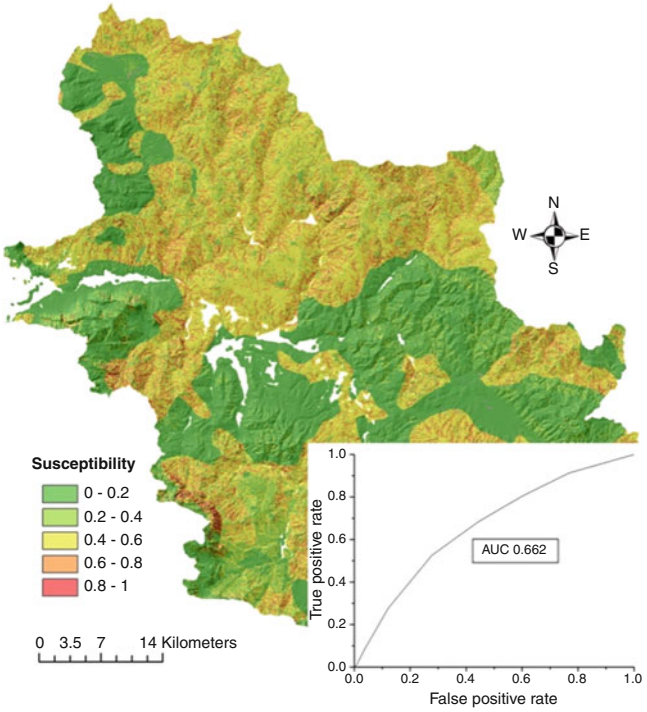

Fig. 9 Results of the RRA susceptibility logit function with "gridded" points applied in the test area

parameters were discarded and the AUC values of every run was used to assess the effectiveness of the regression model.

This procedure, applied separately for each landslide typology in every homogeneous domain, allows to:

– Sort the variables by relevance, determining the most important ones (an example is shown in Table 1);
– Decide how many and which parameters need to be taken into account to best assess the landslide susceptibility (optimal configuration of the BTRF regression model) (Fig. 6).

Finally, the optimal configuration of the BTRF was applied to the whole study area (Fig. 7).

The southern Italy represented a sort of test site for evaluating the performance of the Logistic Regression approach in the susceptibility assessment at the national scale. In particular, many tests have been performed in order to verify differences and analogies among the results which derive from different sampling strategies and/or different resolutions of the maps representing the contributing factors.

On one hand, a comparison was made of the models where the explanatory variables were sampled at different resolutions: the highest one (20 × 20 m) and the one resampled at 100 × 100 m. On the other hand, different approaches in terms of sampling strategy were carried out by varying the sampling pattern (random or systematic) (Figs. 8 and 9), the total number of sampled points

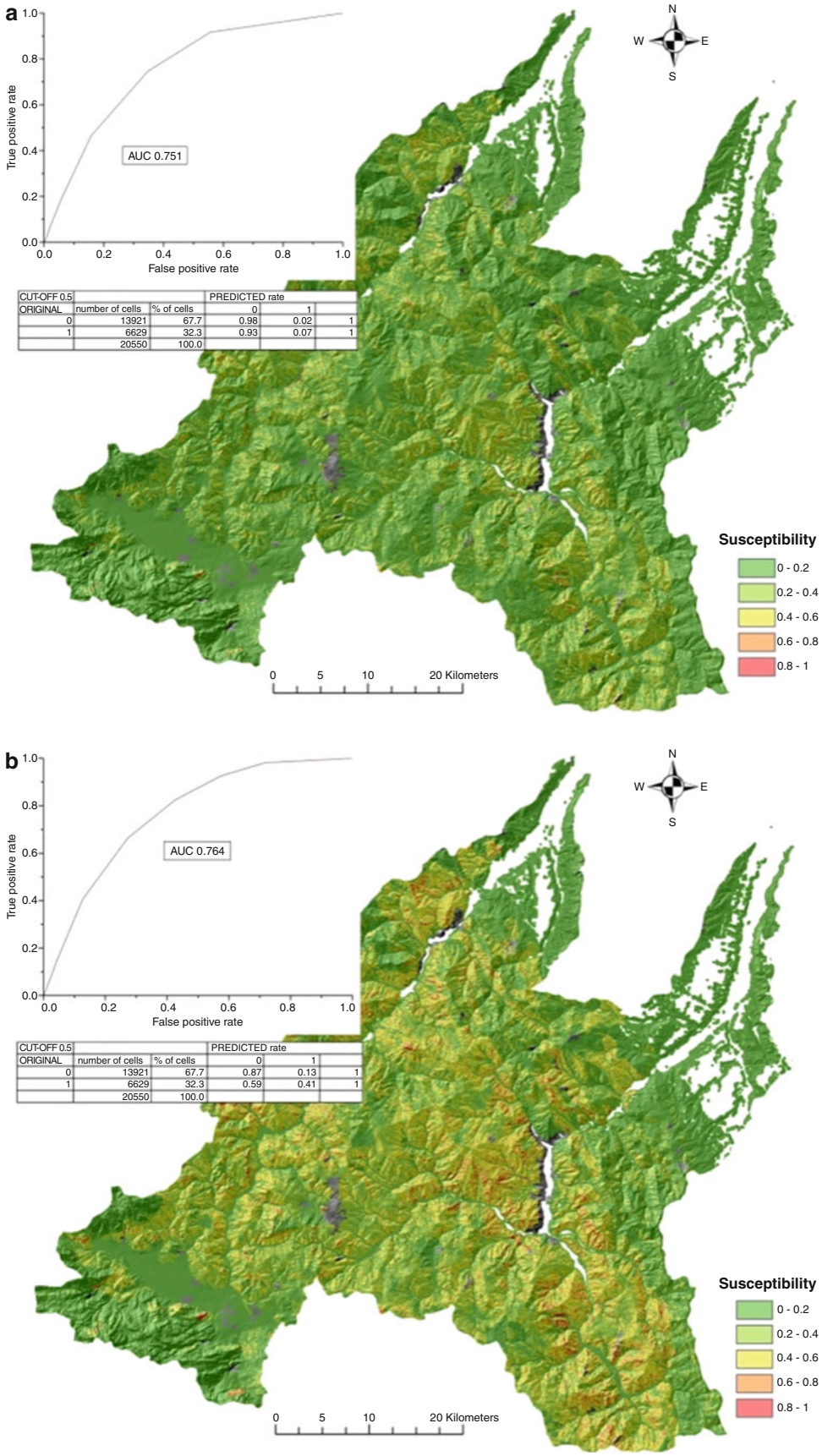

Fig. 10 Example of DF susceptibility maps obtained by applying the logit function with two different datasets (in terms of total number of sampled points), with related ROC curves and frequency tables: (**a**) one point is sampled in each scar area after applying a zonal statistic within the scar area itself; (**b**) all the landslide points are sampled. Despite the similar ROCs and AUCs, the results are markedly different as observable in the maps and frequency tables

(Fig. 10), the proportion between "landslide" and "no landslide" points.

Significant differences also come out by analyzing the results in the training areas as well as in the test ones. The ROC curves and the observation of true and false positive rates for specific cut-off values highlighted that the most reliable results are obtained with a systematic sampling on the 100 × 100 resolution grids, with a ratio of "landslide" points to "no landslide" points of at least 0.5. The ROC curves have been always coupled with the analysis of each single contingency table used to build them, in order to assess the actual efficiency and reliability of selected models, as the curves themselves do not always explicitly detect the real differences between different models.

Finally, it is possible to observe that logistic regression model is reliable even for large scale susceptibility assessment, where only a part of the territory is sampled and analyzed. Notwithstanding, it is important to emphasize that the coefficients of categorical variables (dummies) can assume negative values, thus estimating the inhibitory effect of a given land-use or lithology class on landslides, rather than the contributing effect.

Conclusion

The modelling tests performed for selected sub-areas of Italy provided good performance with all techniques, once applied with the appropriate selection of training and validations sets and with a significant number of statistical units.

These tests also demonstrated that large grid-cells (100 × 100 m, 500 × 500 m) are suitable terrain units for the scale of the analysis. Moreover, they showed that accuracy statistics or ROC curves are not sufficient to evaluate the models, since the same quality was assigned to extremely different models. A careful quality assessment needs an evaluation of geomorphologic significance of predicting variables and an appraisal of modeling results according to the sensibility of the operator.

Considering the results of the tests, the Bayesian Tree Random Forest model was selected to develop the national scale susceptibility map. The model will be applied to 100 × 100 m grid cells and then resampled up to 500 × 500 m. The models will be independently trained for the different physiographic settings and finally joined to produce the 1:1,000,000 susceptibility map of Italy.

References

Agliardi F, Crosta G, Zanchi A (2001) Structural constraints on deep-seated slope deformation kinematics. Eng Geol 59(1–2):83–102

Beven KJ, Kirkby MJ (1979) A physically-based variable contributing area model of basin hydrology. Hydrol Sci Bull 24(1):43–69

Büttner G, Feranec J, Jaffrain G (2002) Corine land cover update 2000 technical guidelines. European Environmental Agency technical report 89, 56 pp

Carrara A, Crosta G, Frattini P (2003) Geomorphological and historical data in assessing landslide hazard. Earth Surf Process Landf 28:1125–1142

Compagnoni B, Damiani AV, Valletta M, Finetti I, Cirese E, Pannuti S, Sorrentino F, Rigano C (1976–1984) Carta Geologica d'Italia alla scala 1:500,000 (5 fogli). Servizio Geologico d'Italia, Roma

Delmonaco G, Leoni G, Margottini C, Puglisi C (2002) La propensione del territorio italiano ai fenomeni franosi. Ital J Eng Geol Environ 1:111–116

Günther A, Reichenbach P, Hervás J (2008) Approaches for delineating areas susceptible to landslides in the framework of the European soil thematic strategy. In: Proceedings of the first world landslide forum, Tokyo, 18–21 Nov 2008, pp 235–238

Hervás J (ed) (2007) Guidelines for mapping areas at risk of landslides in Europe. In: Proceedings of the experts meeting held on 23–24 October 2007. Institute for Environment and Sustainability Joint Research Centre (JRC), Ispra, Italy EUR 23093 EN – 2007

Hervás J, Günther A, Reichenbach P, Malet JP, Van Den Eeckhaut M (2010) Harmonised approaches for landslide susceptibility mapping in Europe. In: Malet JP, Glade T, Casagli N (eds) Proceedings of international conference on mountain risks: bringing science to society, Florence, 24–26 Nov 2010. CERG Editions, Strasbourg, pp 501–505

Malamud BD, Turcotte DL, Guzzetti F, Reichenbach P (2004) Landslide inventories and their statistical properties. Earth Surf Process Landf 29(6):687–711

Malet JP, Thiery Y, Hervàs J, Günther A, Puissant A, Grandjean G (2010) Landslide susceptibility mapping at 1:1M scale over France: exploratory results with a heuristic model. In: Malet JP, Glade T, Casagli N (eds) Proceedings of the international conference mountain risks: bringing science to society, Florence, Italy, 24–26 Nov 2010. CERG Editions, Strasbourg, pp 315–320

Sappington JM, Longshore KM, Thompson DB (2007) Quantifying landscape ruggedness for animal habitat analysis: a case study using bighorn sheep in the Mojave Desert. J Wildl Manage 71(5):1419–1426

Trigila A, Iadanza C (2008) Landslide in Italy – special report 2008 (Rapporti 83/2008). ISPRA, Roma, 32 pp. URL: http://www.isprambiente.gov.it/site/it-IT/Pubblicazioni/Rapporti/Documenti/rapporto_83_08_landslides.html

Trigila A, Iadanza C, Spizzichino D (2010) Quality assessment of the Italian landslide inventory using GIS processing. Landslides 7(4):455–470

Van Den Eeckhaut M, Hervás J, Jaedicke C, Malet JP, Picarelli L (2010) Calibration of logistic regression coefficients from limited landslide inventory data for European-wide landslide susceptibility modelling. In: Malet J P, Glade T, Casagli N (eds) Proceedings of the international conference mountain risks: bringing science to society, Florence, Italy, 24–26 Nov 2010. CERG Editions, Strasbourg, pp 515–521

New Developments in Harmonized Landslide Susceptibility Mapping over Europe in the Framework of the European Soil Thematic Strategy

Andreas Günther, Miet Van Den Eeckhaut, Paola Reichenbach, Javier Hervás, Jean-Philippe Malet, Claire Foster, and Fausto Guzzetti

Abstract

In the context of the European Soil Thematic Strategy, and the formulation of a draft of a European framework directive devoted to the sustainable use of soil, landslides are recognized as one of the eight soil threats requiring harmonized spatial hazard assessments over the EU territory. The general framework for such assessments consists of a nested geographical approach based on "Tiers", where a low-resolution (1:1 Million) evaluation ("Tier 1") using already available pan-European datasets should enable the delineation of priority areas requiring more detailed assessments with additional data ("Tier 2"). In this contribution, we present new developments in the elaboration of a "Tier 1" generic landslide susceptibility evaluation based on a heuristic modelling approach exploiting the most important landslide conditioning factors. Extensive landslide locations available at small spatial scales have been collected and harmonized over the EU territory to be used for input parameter specification and model calibration, evaluation and classification. Since the analyzed area is highly complex in terms of climato-physiographic conditions controlling landslide occurrences, a preliminary landslide terrain differentiation is proposed consisting of eight calibration zones where specific predictor class weights have been allocated through a heuristic indexing approach. The spatially combined preliminary pan-European susceptibility estimate classifies 13 % of the EU territory as prone to landslides, thus requiring more detailed, quantitative inventory-based susceptibility evaluations ("Tier 2").

Keywords

Landslides • Susceptibility map • Heuristic model • Soil Thematic Strategy • Continental scale

A. Günther (✉)
Federal Institute for Geosciences and Natural Resources (BGR), Stilleweg 2, D-30655 Hannover, Germany
e-mail: a.guenther@bgr.de

M. Van Den Eeckhaut • J. Hervás
Institute for Environment and Sustainability, Joint Research Centre (JRC), European Commission, Ispra, Italy

P. Reichenbach • F. Guzzetti
Research Institute for Hydrogeological Protection (CNR-IRPI), National Research Council, Perugia, Italy

J.-P. Malet
Institut de Physique du Globe de Strasbourg (CNRS) and University of Strasbourg (EOST), Strasbourg, France

C. Foster
British Geological Survey (BGS), Nottingham, UK

Introduction

The relevance of landslide zoning for environmental policy and decision making in Europe is above all set forth in the framework of the European Union's Thematic Strategy for Soil Protection, adopted on 22 September 2006 (EC 2006a). This Strategy considers landslides as one of eight soil threats in Europe for which identification of areas where they are likely to occur in the future (so-called priority areas in the Strategy) and design of risk reduction measures is needed. To achieve these objectives, the Soil Framework Directive was proposed as a legislative instrument (EC 2006b).

C. Margottini et al. (eds.), *Landslide Science and Practice*, Vol. 1,
DOI 10.1007/978-3-642-31325-7_39,

For the identification of priority areas for soil threats, the Soil Information Working Group (SIWG) of the European Soil Bureau Network (ESBN) selected a set of common thematic data (i.e., landslide occurrence or density, topography, bedrock, soil type, land cover, land use, climate and seismicity; Eckelmann et al. 2006) and envisaged a nested geographical assessment scheme based on "Tiers", where a "Tier 1" assessment is aimed for the general delineation of areas prone to the generic landslide threat at the continental scale. The initial work of SIWG in ESBN on the landslide threat was put forward by the European Landslide Expert Group (http://eusoils.jrc.ec.europa.eu/library/themes/Landslides) created in 2007.

In this paper, the recent developments in the preparation of a continent-wide "Tier 1" generic landslide susceptibility map are presented. Since the European territory covered by the 27 EU member states, Norway, Switzerland and the Balkan countries is highly complex in terms of climatological, physiographical and seismotectonical conditions, we suggest a preliminary landslide terrain differentiation over the study area resulting in eight distinct model zones. We then briefly introduce the thematic data representing the landslide conditioning factors for a "Tier 1" susceptibility evaluation as well as the results of an extensive survey undertaken to collect available landslide locations from national and regional databases held by different institutions.

We finally present a preliminary pan-European landslide susceptibility estimate produced from spatial combination of the results obtained for each model zone using a heuristic model, in which the collected landslide locations were used for landslide conditioning factor class weight calibrations, and model evaluations and classifications.

Data and Thematic Information

Climato-physiographic Landslide Regions

A preliminary attempt to delineate climato-physiographic regions with broadly distinct landslide controlling characteristics was done through aggregation of the 36 climatic areas of the "Soil Regions Map of Europe 1:5 M" (BGR 2005) into seven model regions (Fig. 1). Additionally, the coastal areas have been extracted as a separate model zone using a 1 km buffer landward from the coastline (Malet et al. 2009). This seems important since coastal landslides and their controlling/triggering characteristics are not comparable to inland phenomena. For landslide susceptibility evaluations, each of the eight model zones is treated separately.

When examining the terrain differentiation shown in Fig. 1, it can be inferred that the delineated zones display individual characteristics in terms of the spatial distribution

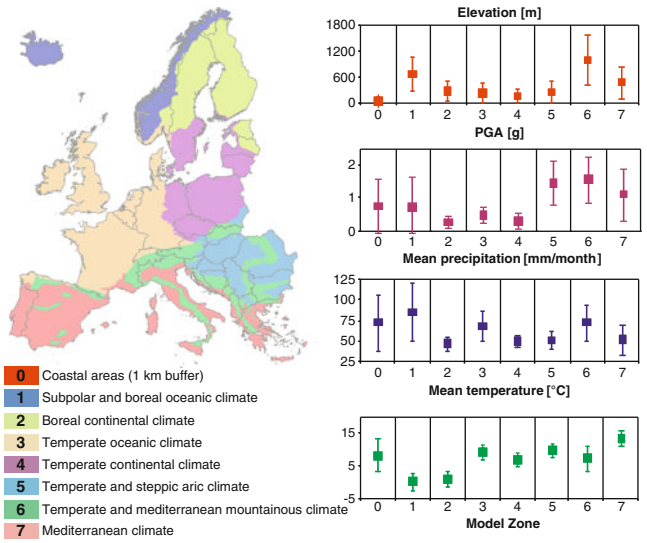

Fig. 1 Preliminary climato-physiographic terrain differentiation resulting in eight individual model zones (*left*) and basic zonal statistics (mean values with standard deviations) of important first-order morphologic, seismologic and climatic factors attributed t0 landslide occurrence (*right*)

of important geofactors and climatic attributes, whereas within most zones especially elevation and precipitation show a high degree of intercorrelation. However, the zonation shown in Fig. 1 must be considered preliminary mainly because it does not show a good differentiation in central Europe since not sufficiently considering physiographic characteristics.

Landslide Conditioning Factors

According to the specifications for a "Tier 1" assessment over Europe, the three most important landslide conditioning factors, slope gradient, lithology and land cover, are used for susceptibility evaluation (Hervás 2007; Günther et al. 2008; Hervás et al. 2010) (Fig. 2). At the given analysis scale, these factors can be assumed to have a high degree of conditional independence and also can be considered the major predisposing elements controlling the occurrence of all types of landslides. All input parameters derived from common pan-European or global datasets have been selected against alternative data based on their individual predictive capability to the compiled landslide database (see below). More specifically, the data used for this assessment consists of (Fig. 2):

- A slope gradient map derived from the EU27 DEM (Reuter 2009). This DEM covers the 27 EU member states and Norway and Switzerland as well as the non-EU Balkan countries, but lacks information on Iceland

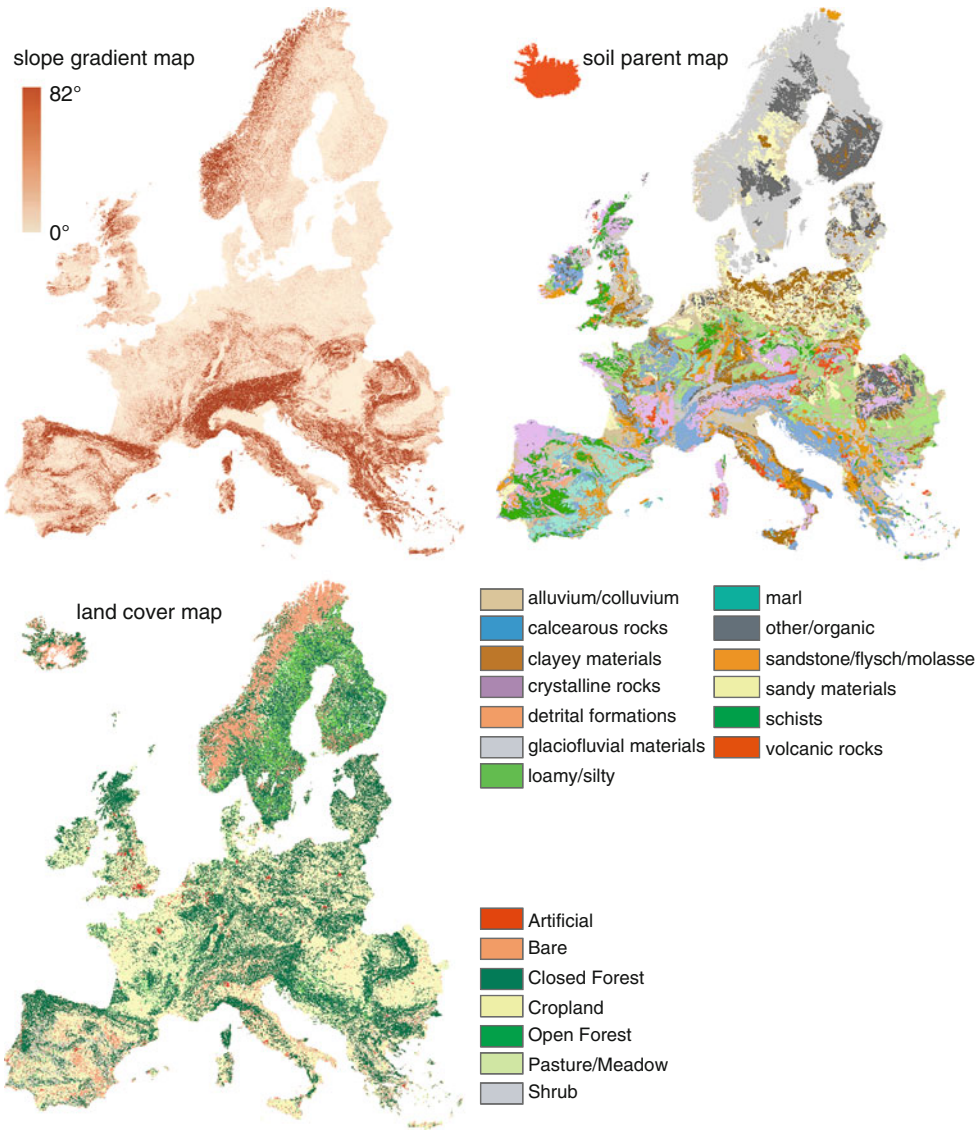

Fig. 2 Thematic information of the landslide conditioning factors used for the continental level "Tier 1" analysis

and Cyprus. The continuous slope raster derived from this dataset was classified into eight slope classes using the frequency distribution of the landslides over the integer slope.

- A soil parent material map derived from the "Soil Geographical Database of Europe 1:1 M" (Panagos et al. 2012). The dominant parent material information stored as attributes of soil typological units (STU's) was further aggregated from 42 classes available at level 2–13 classes based on expert knowledge, landslide distribution and class size. The vector data was rasterized to a grid with a cell size of 1 × 1 km.
- A land cover map derived from the global land cover dataset GlobCover produced by the European Space Agency (ESA) (http://ionia1.esrin.esa.int/_). The 23 classes have been aggregated into seven land cover classes for this assessment. The grid cell size of the GlobCover dataset is 300 m.

Landslide Information

Throughout the EU, vast information on landslides is available from national and regional level landslide inventories compiled for different purposes with different levels of detail by different institutions (Van Den Eeckhaut et al. 2011), but so far no attempt has been made to harmonize this information to produce a homogeneous pan-EU landslide location coverage. For this study, we conducted an extensive survey collecting landslide point information from different sources that can be used for the establishment and evaluation of susceptibility estimations.

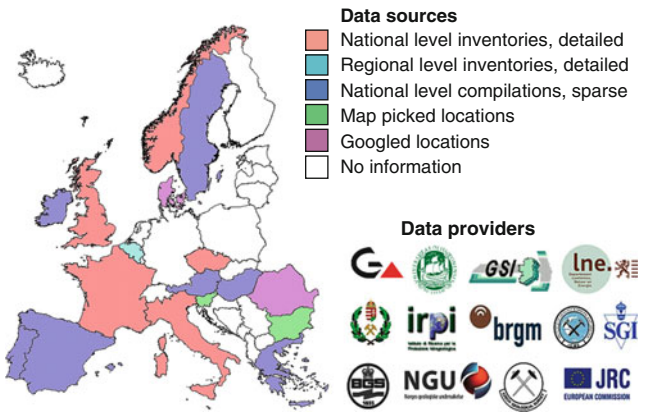

Fig. 3 Current status of landslide location information used in this study for individual European countries compiled from different sources

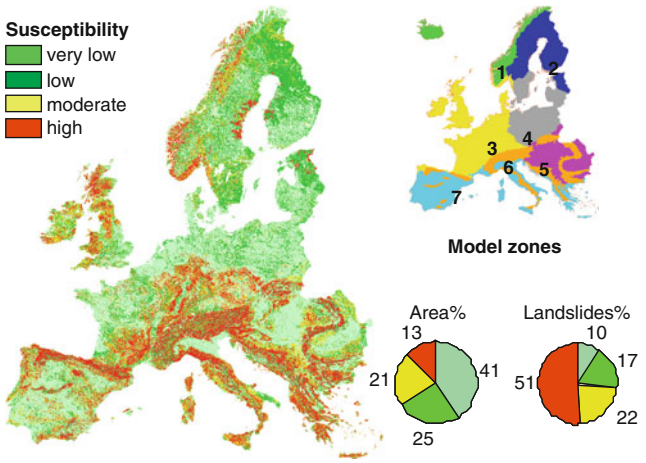

Fig. 4 Preliminary landslide susceptibility map obtained from spatial mosaicking of zone-specific reclassified susceptibility indices

Figure 3 shows the current state of the landslide inventory compiled. It can be seen that many areas (especially north-eastern Europe and the Balkan region) lack information and that the landslide locations show a highly uneven distribution throughout the model zones in terms of level of detail. However, most of the area not covered by landslide information belongs to model zones 2 and 4 which can be considered comparably less affected by the landslide threat over the majority of the area. In a whole, more than 100,000 landslide points have been integrated into the assessment by now.

Landslide Susceptibility Evaluation

For landslide susceptibility mapping, each model zone is treated separately and a first pan-European map was produced by spatial mosaicking of the individual zone-specific estimates. The preliminary susceptibility evaluation and classification process consists of a heuristic assessment involving the following steps:

- Assignment of global parameter weights (w_j) through pairwise comparison of the three predictors, where the highest importance is given to the slope parameter (Malet et al. 2009, 2011).
- Zone-specific allocation of standardized parameter class weights (x_{ij}) utilizing landslide frequency ratios derived from the harmonized landslide inventory and expert knowledge combined with trial-and-error model runs and analysis of false negatives.
- Calculation of a landslide susceptibility index S for each model zone using

$$S = \sum_{j=1}^{n=3} w_j \cdot x_{ij} \quad (1)$$

where w_j is the weight of predictor j and x_{ji} is the weight of class i in predictor j.

- Evaluation of the zone-specific susceptibility index grids using ROC curves and slicing into four susceptibility levels at True Positive Ratios (TPR) breaks of 0.5, 0.75, 0.9.
- Spatial mosaicking of the resulting zone-specific susceptibility maps (Fig. 4).

Preliminary Conclusions and Work in Progress

The preliminary pan-EU susceptibility map shown in Fig. 4 has certain important limitations, but is able to classify 13 % of the area as comparably landslide prone since >50 % of the landslide points are situated therein. In many portions of the study area, even this preliminary assessment has a reasonable performance. The preliminary estimate chiefly suffers from the fact that the model zone delineation needs to be improved, and that the zone-specific susceptibility maps cannot be straightforwardly associated through spatial mosaicking since the susceptibility classes must be assumed to differ in terms of landslide intensity across the model zones. Moreover, there is need for further elaboration of the heuristic analysis scheme, and validation of the results against other assessments. Currently, the following improvements are carried out:

- Delineation and testing of alternative and more appropriate model zones across Europe.
- Incorporation of additional landslide locations (especially in underestimated areas) and enhancement of data standardization to increase the signal obtained form landslide occurrence.
- Implementation of a more advanced heuristic analysis scheme employing spatial multi-criteria evaluation

(Malet et al. 2009, 2011) also considering more appropriate spatial associations of the zone-specific estimates.

- Cross-validation of the heuristic model with multivariate statistical analyses (stepwise logistic regression, Van Den Eeckhaut et al. 2010) using the same data in representative areas of the model zones where the inventory information has a high level of completeness.

In a future stage, it also seems important to produce landslide-type specific susceptibility estimates (Malet et al. 2009, 2011). This may be considered a general advancement in EU-wide "Tier 1" landslide susceptibility evaluations since the information for a rough typological differentiation (e.g., flows, slides and falls/topples) is available in or may be assigned to most of the inventory data collected for this study.

Acknowledgments This work is part of the European Landslide Expert Group on 'Guidelines for Mapping Areas at Risk of Landslides in Europe' coordinated by JRC Ispra since 2007, and part of the ICL-IPL project IPL-162 *"Tier-based harmonized approach for landslide susceptibility mapping over Europe"*. We like to thank the members of the European Landslide Expert Group (http://eusoils.jrc.ec.europa.eu/library/themes/landslides/wg.html) for all the fruitful discussions.
We are highly indebted to the institutions sharing landslide location information with us and supporting this study. These are: Geologische Bundesanstalt, Austria (GBA, Nils Tilch); Hungarian Office for Mining and Geology (Tamás Oszvald); Czech Geological Survey (Dana Čápová); Geological Survey of Ireland (GSI, Ronnie Creighton); Geological Survey of Norway (NGU, Thierry Oppikofer and Reginald Hermanns); Institute of Geology and Mineral Exploration, Greece (IGME, Eleftheria Poyiadji); Swedish Geotechnical Institute (SGI, Mats Öberg); Environment, Nature Energy Department, Flemish Government, Belgium (LNE, Liesbet Vanderkerckhove), Albanian Geological Survey (AGS, Mimoza Jusufati); Sächsisches Landesamt für Umwelt, Landwirtschaft und Geologie, Germany (LfULG, Peter Dommaschk); Instituto de Geografia e Ordenamento do Território, University of Lisbon, Portugal (IGOT, José Luis Zêzere); Federal Office for the Environment, Switzerland (BAFU, Hugo Raetzo and Bernard Loup).

References

BGR (2005) Soil regions map of the European Union and adjacent countries 1:5M (version 2.0). Special publication, Ispra. EU catalogue number S.P.I.05.134

EC (2006a) Thematic strategy for soil protection. COM(2006)231 final. Commission of the European Communities, Brussels, Belgium

EC (2006b) Proposal for a directive of the European parliament and of the council establishing a framework for the protection of soil and amending directive 2004/35/EC. COM(2006)232 final. Commission of the European Communities, Brussels, Belgium

Eckelmann W, Baritz, R, Bialousz S, Bielek P, Carre F, Houskova B, Jone RJA, Kibblewhite MG, Kozak J, Le Bas C, Toth G, Varallyay G, Yli Halla M, Zupan M (2006) Common criteria for risk area identification according to soil threats. European oil Bureau Research Report no. 20, EUR 22185 EN. Office for official publications of the European Communities, Luxembourg

Günther A, Reichenbach P, Hervás J (2008) Approaches for delineating areas susceptible to landslides in the framework of the European Soil Thematic Strategy. In: Proceedings of the first world landslide forum, Tokyo, 18–21 Nov 2008, pp 235–238

Hervás J (2007) Guidelines for mapping areas at risk of landslides in Europe. In: Proceedings of the experts meeting, 23–24 Oct 2007, Ispra, Italy. JRC Report EUR 23093 EN, Office for official publications of the European Communities, Luxembourg, 53p

Hervás J, Günther A, Reichenbach P, Malet J-P, Van Den Eeckhaut M (2010) Harmonised approaches for landslide susceptibility mapping in Europe. In: Malet JP, Glade T, Casagli N (eds) Proceedings of the international conference mountain risks: bringing science to society, Florence, Italy, 24–26 Nov 2010. CERG Editions, Strasbourg, pp 501–505

Malet JP, Thiery Y, Puissant A, Hervás J, Günther A, Grandjean G (2009) Landslide susceptibility mapping at 1:1M scale over France: exploratory results with a heuristic model. In: Proceedings of the international conference on landslide processes: from geomorphologic mapping to dynamic modelling. A tribute to Prof. Dr. Theo van Asch, Strasbourg, France, 6–7 Feb 2009, pp 315–320

Malet JP, Puissant A, Mathieu A, Van Den Eeckhaut M, Fressard M (2011) Integrating spatial multi-criteria evaluation and expert knowledge for national-scale landslide susceptibility analysis: application to France. In: Proceedings of the 2nd world landslide forum, Rome, 3–7 Oct 2011 (this volume)

Panagos P, Van Liedekerke M, Jones A, Montanarella L (2012) European soil data centre: response to European policy support and public data requirements. Land Use Policy 29(2):329–338

Reuter HI (2009) A Europe-wide digital elevation model based on SRTM and Russian topographic contours. Data set and documentation for the contract 2007-4500049350. BGR Hannover

Van Den Eeckhaut M, Hervás M, Jaedicke C, Malet JP, Picarelli L (2010) Calibration of logistic regression coefficients from limited landslide inventory data for European-wide landslide susceptibility modelling. In: Malet JP, Glade T, Casagli N (eds) Proceedings of the international conference mountain risks: bringing science to society, Florence, Italy, 24–26 Nov 2010. CERG Editions, Strasbourg, pp 515–521

Van Den Eeckhaut M, Hervás J, Montanarella L (2011) Landslide databases in Europe: analysis and recommendations for interoperability and harmonization. In: Proceedings of the 2nd world landslide forum, Rome, 3–7 Oct 2011 (this volume)

Integrating Spatial Multi-criteria Evaluation and Expert Knowledge for Country-Scale Landslide Susceptibility Analysis: Application to France

Jean-Philippe Malet, Anne Puissant, Alexandre Mathieu, Miet Van Den Eeckhaut, and Mathieu Fressard

Abstract

Information on landslide susceptibility and hazard at the national scale is of fundamental importance for the design and implementation of risk management policies and the prioritarization of the allocation of resources. Lack of such information in Europe and the implementation of the European Union's Thematic Strategy for Soil Protection (Commission of the European Communities, Thematic strategy for soil protection. COM (2006)231 final. Brussels, 2006a; Commission of the European Communities, Proposal for a Directive of the European Parliament and of the Council establishing a framework for the protection of soil and amending directive 2004/35/EC. COM(2006)232 final. Brussels, 2006b) let to an initiative of *JRC* (*Joint Research Centre*, European Commission) to setup a European *Landslide Expert Group* in order to identify the areas in Europe where landslides are likely to occur. In this context, this work presents the method developed for the creation of the 'Tier 1' landslide susceptibility map for France at a 1:1M scale, where susceptibility is defined as the spatial probability of occurrence of an event. The method is applied by differentiating three categories of landslide types, namely slides, falls and flows. More specifically, the method combines a weighting-rating procedure of both factors and classes of factors using a spatial-multi-criteria evaluation technique (SMCE) and an objective calibration of the weights based on statistics on the distribution of observed landslides per slope angle, lithology and landcover classes. The quality of the nation-scale map is evaluated with references (1) to the French landslide inventory map BDMvT, and (2) to regional or local susceptibility maps available in the literature or created for planning purposes.

J.-P. Malet (✉) • A. Mathieu
Institut de Physique du Globe de Strasbourg, CNRS UMR 7516, Université de Strasbourg, Ecole et Observatoire des Sciences de la Terre, 5 rue Descartes, Strasbourg F-67084, France
e-mail: jeanphilippe.malet@unistra.fr

A. Puissant
Laboratoire Image, Ville, Environnement, CNRS FRE 7230, Université de Strasbourg, 3 rue de l'Argonne, Strasbourg F-67084, France

M. Van Den Eeckhaut
Institute for Environment and Sustainability, Joint Research Centre (JRC), European Commission, Ispra (VA) 21027, Italy

M. Fressard
Géographie Physique et Environnement, CNRS UMR 6554, Université de Caen-Basse-Normandie, Esplanade de la Paix, Caen Cedex F-14032, France

C. Margottini et al. (eds.), *Landslide Science and Practice*, Vol. 1,
DOI 10.1007/978-3-642-31325-7_40,

Keywords
Landslide • Susceptibility map • Heuristic model • Expert knowledge • Spatial multi-criteria evaluation

Introduction

Landslide susceptibility maps usually cover areas between local and regional scales (Guzzetti et al. 1999), and only very few attempts have been realized to delineate landslide susceptibility at national (Dikau and Glade 2003; Creighton 2006; Castellanos Abella and van Westen 2007; Foster et al. 2008; Blteanu et al. 2010; Salvati et al. 2010), continental (Guenther et al. 2008; Hervás et al. 2010) and even worldwide scales (Nadim et al. 2006; Hong et al. 2007; Kirschbaum et al. 2009).

Information on landslide susceptibility at national scales is of fundamental importance for the design and implementation of risk management policies and the prioritarization of the allocation of resources. Lack of such information in Europe and the implementation of the *European Union's Thematic Strategy for Soil Protection* (Commission of the European Communities 2006a, b) let to an initiative of *JRC* (*Joint Research Centre, European Commission*) to setup a *European Landslide Expert Group* in order to identify the areas in Europe where landslides are likely to occur (Hervás 2007).

In this context, given that spatio-temporal information on landslides are currently not available in many European areas or are not harmonized, guidelines for landslide susceptibility mapping across Europe have been proposed, and are based on the use of common datasets and a nested approach in 'Tiers' (Eckelmann et al. 2006; Hervás et al. 2010; Fig. 1).

This manuscript presents the method developed for the creation of the 'Tier 1' landslide susceptibility map for France at a 1:1M scale. It can be considered as an exploratory work to critically assess the methodology in order to create in a near future the European map (Hervás et al. 2010). The method is applied by differentiating three categories of landslide types, namely slides, falls and flows (Malet et al. 2009). The method combines a weighting-rating procedure (type of factors, class of factors) using a spatial-multi-criteria evaluation technique (SMCE) and an objective calibration of the weights from the statistics of observed events (per slope angle, lithology and landcover classes).

The quality of the nation-scale map is evaluated with references (1) to the French landslide inventory map and (2) to regional or local susceptibility maps available in the literature or created for planning purposes by the French Geological Survey (*BRGM*; *Bureau des Recherches Géologiques et Minières*).

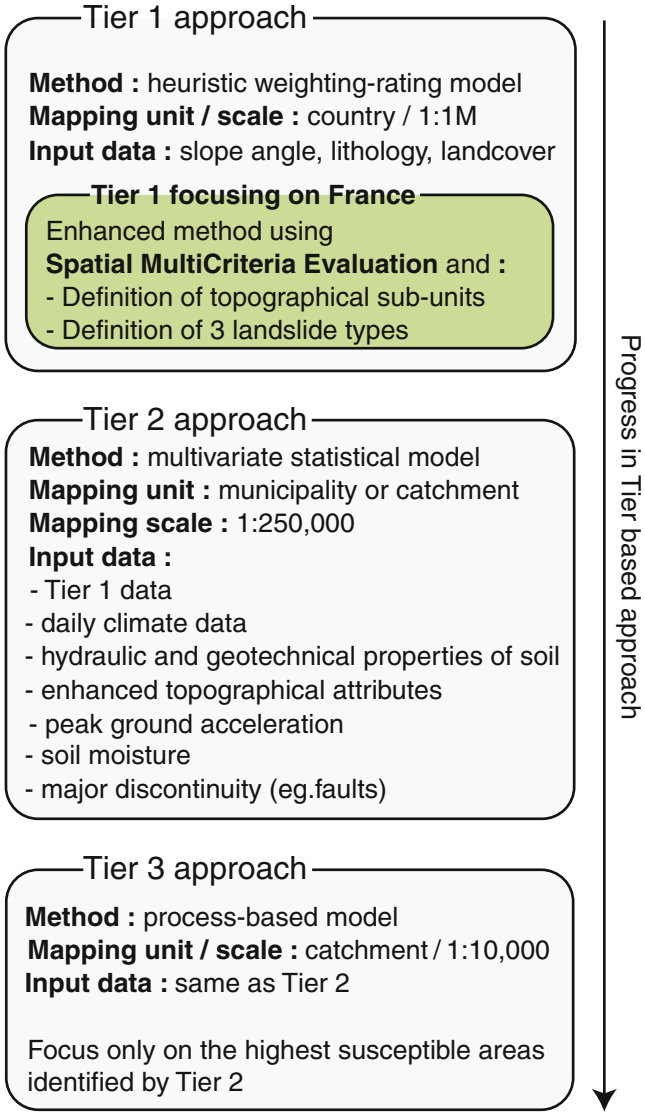

Fig. 1 Methodological framework for the country and continent-wide landslide susceptibility assessment (Adapted from Hervás et al. 2010)

Data Used for the Creation of the Susceptibility Map

Thematic Maps of Predisposing Factors

According to the recommendations for the Tier 1 assessment (Günther et al. 2008), a limited set of data has been used, and consisted of the three most important landslide predisposing factors (Fig. 2):

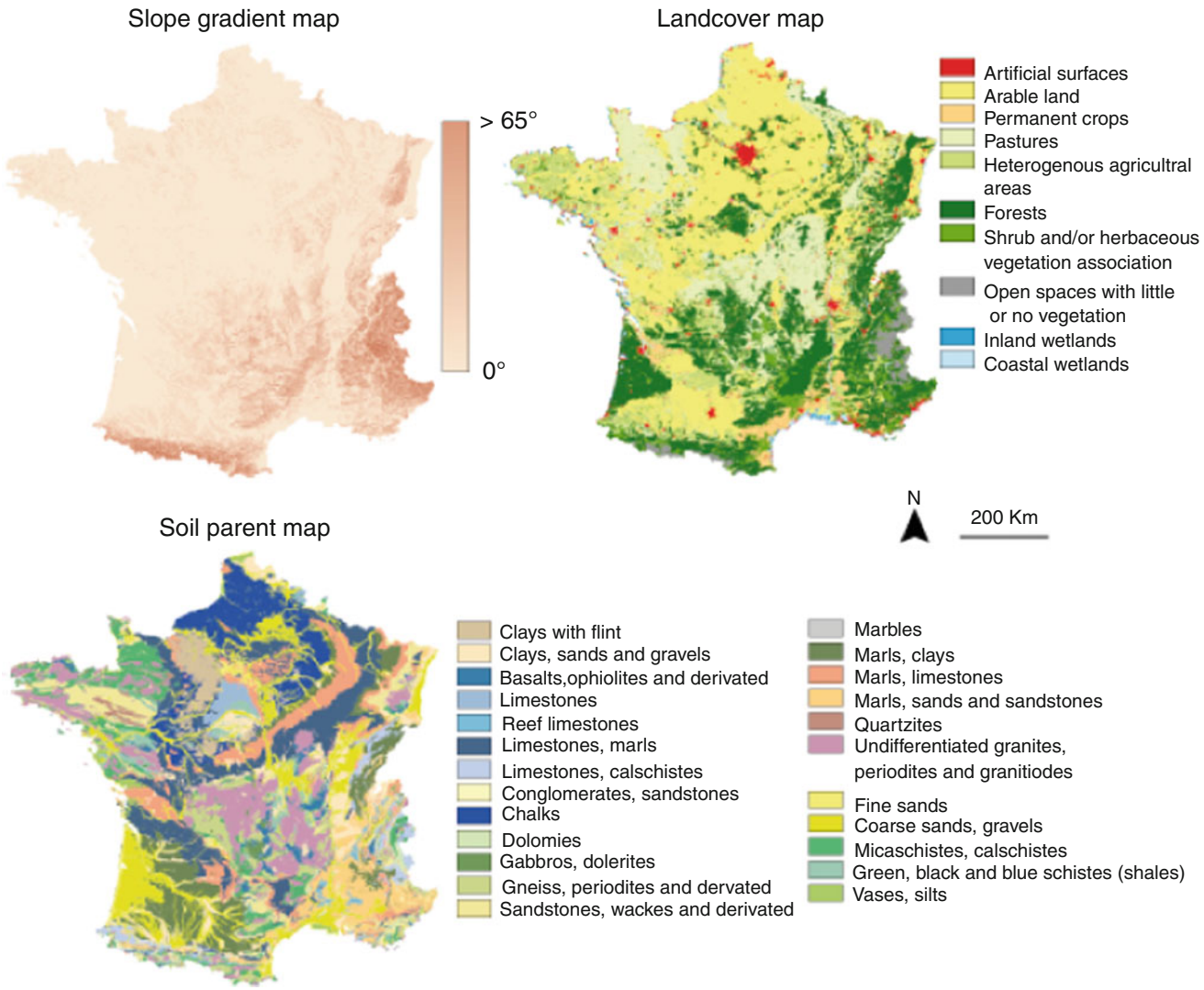

Fig. 2 Thematic maps of the landslide conditioning factors used for the Tier 1 susceptibility analysis over France

- A slope gradient map, classified in 13 classes with an interval of 5°. This map is derived from the NASA SRTM (Shuttle Radar Topographic Mission) DEM with 90 × 90 m cell size;
- A soil parent map classified in 24 classes according to the main lithological units observed in France in terms of lithology, structure and age. This map is derived from the geological database of the French Geological Survey at 1:1M scale;
- A landcover map derived from the Corine Land Cover dataset (CLC2000) available for Europe at 1:100,000 scale. The database is obtained by combination of Landsat MSS and Spot XS imageries. An update with Landsat ETM+ imageries from 2006 has been performed. Level 1 of this database, which consists in ten classes, is used in this work.

All the data have been rasterized to a grid-based (raster) mapping unit of 90 m, corresponding to the resolution of the DEM.

Landslide Inventory Map

The French landslide inventory map (BdMvT; www.bdmvt.net) has been used in order to define the weights associated to each factor and classes of factors using class-frequency ratios. The inventory is not exhaustive and some errors (incorrect location, incorrect landslide type) or incompleteness of the database are observed. These uncertainties have been addressed for the calculation of the different statistical indicators to introduce in the model (Fig. 3).

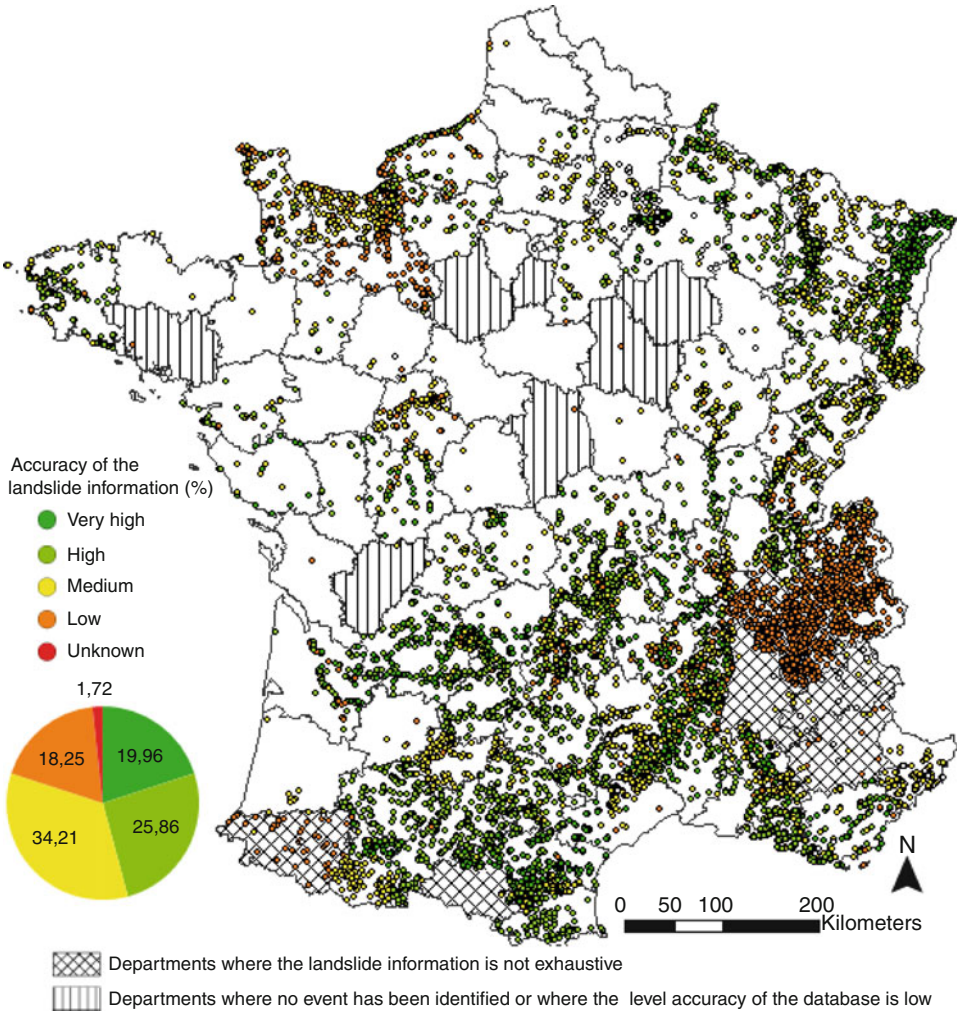

Fig. 3 Accuracy of the French landslide inventory for the three landslide types considered in the analysis

The landslide types considered in our analysis are:

- Falls (e.g. rockfalls and topples affecting hard rocks);
- Slides (e.g. rotational and translational slides affecting soils, cohesive sediments and hard rocks);
- Flows (e.g. mudflows, earthflows, debris flows and debris avalanches affecting soils, cohesive sediments and hard rocks).

A frequency analysis has been carried out for the three landslide types, and all the classes of factors in order to investigate the distribution of events per slope gradient, lithology and landcover and to define a hierarchy among the different factors.

Methodology: Spatial Multi-criteria Evaluation

Methodological Workflow

The statistical technique used for the analysis is a Spatial Multi-Criteria Evaluation model based on an analytical hierarchy process and the use of a tree-shaped structure to organize the thematic data and to associate a weight to each factor and class of factor. The workflow is structured in several stages (Fig. 4):

- The division of the application domain of the model in three topographic experiment units to take into account the influence of different topographical conditions favourable to landslide occurrences (Fig. 5). Coastal areas have been defined by using a 1 km-buffer along the coastline; plain and mountain areas have been distinguished according to the criteria proposed by Nordregio (2004);
- The definition of a susceptibility model for three landslide types (i.e. falls, slides, flows);
- The transformation of the input data in Boolean value for each class, and a standardization of the data;
- The definition of the weights attributed to each predisposing factor and to each class. A pairwise comparison method has been used for the factors whereas a direct method has been used for the classes. More importance has been given to the slope gradient in the pairwise comparison. The weighting procedure (Fig. 6) for the classes has been performed (1) by using class-frequency ratios, and (2) by adjusting the weights through expert-based corrections and the analysis of false negatives;

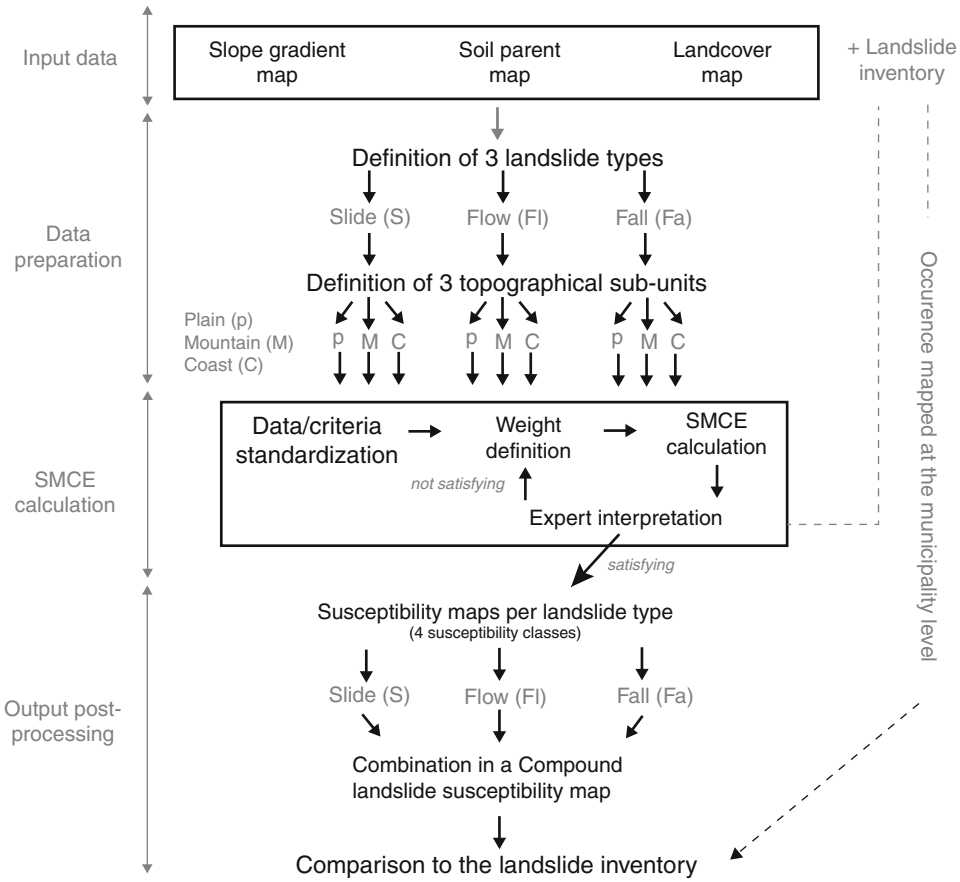

Fig. 5 Representation of the topographical experiment units used in the analysis (the coast unit is not represented)

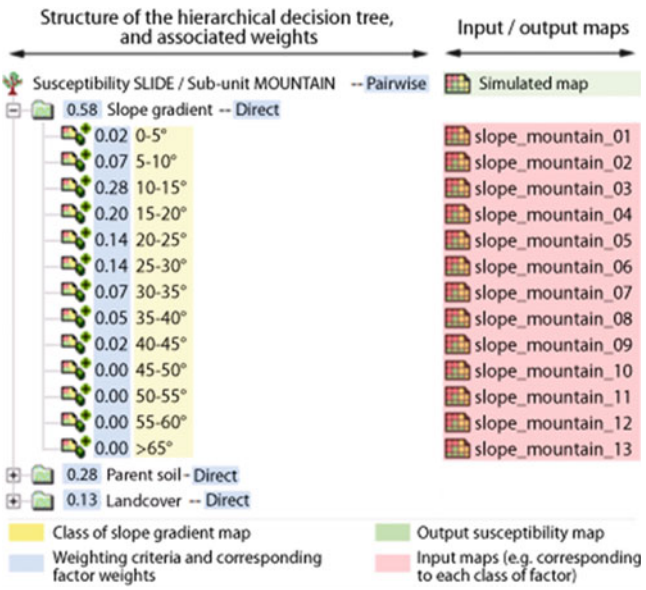

Fig. 6 Criteria tree used for the calculatrion of the susceptibility map for the landslide type 'slide' and the experiment unit 'mountain', and associated weights (factors, classes)

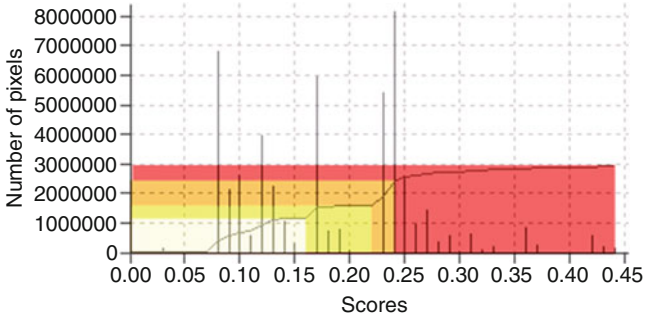

Fig. 7 Determination of four susceptibility classes from the distribution of scores (example of the model performed for the landslide type 'flow' in the experiment unit 'plain'). The *colors* refer to the caption of Fig. 8

- The creation of a series of susceptibility models (with a cell size of 90 m) for each landslide type by using a slicing procedure to define four susceptibility classes (e.g. null, low, moderate, high). At the end, the susceptibility models obtained for the plain, mountain and coastal units are combined in one compound susceptibility map for each landslide type. In the association procedure, more importance is given to the highest susceptibility class observed for each cell;

Definition of Susceptibility Classes

The scores obtained for each output maps have been classified using a slicing method. Four susceptibility classes have been defined because it provides a good representation of the value distribution for most of the events observed in plain and mountain areas (Fig. 7).

Results: Susceptibility Maps for France

The compound landslide susceptibility map (Fig. 8a) corresponds to the combination of the three susceptibility maps calculated for the type 'slide', 'flow' and 'fall' (Fig. 8b); the association rule of Fig. 8c has been used.

The precautionary principle has been considered to define the association rule used to combine the landslide susceptibility maps. The association rule gives higher possibilities of presence for the high and moderate susceptibility classes; 44 % and 31 % of the 16 association possibilities result respectively in a high and moderate susceptibility, whereas only 19 % and 6 % result in a low and null susceptibility.

Following the guidelines of Hervás (2007), the susceptible and non-susceptible areas have been differentiated; the class of high susceptibility provides a good assessment of the major areas prone to landsliding (Fig. 9). For a qualitative evaluation

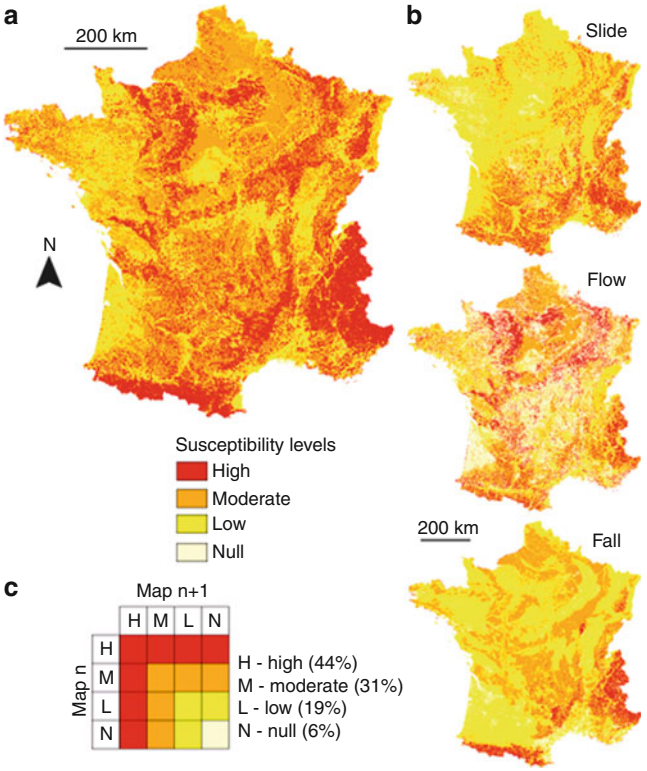

Fig. 8 Susceptibility maps for France. (**a**) Compound landslide susceptibility map; (**b**) Individual landslide susceptibility maps; (**c**) Association rule used to combine the individual maps

of the performance of the model, a comparison with the information available in the French landslide inventory (e.g. a binary map representing the municipalities affected by at least one landslide whatever its type) is proposed (Fig. 9). The municipalities affected by landslide events in the past are well predicted by the susceptibility model. However, for several departments, the model overestimates the landslides susceptibility in comparison to the recorded events. This may be explained by:

- The low accuracy or the incompleteness of the BDMvT database in some departments. This is particularly true for some departments located in mountain areas which are known to be highly prone to landslides;
- The criteria used in the association rule for the combination of the individual susceptibility maps which favours the highest susceptibility class calculated for each cell;
- The generalization of the input data in broad classes which does not allow to predict correctly local environmental conditions.

For a quantitative evaluation of the model, the susceptibility maps have been compared to published regional assessments performed with the same type of factors, but using other sources of data (provider, resolution, scale, information content) or other types of modelling approaches.

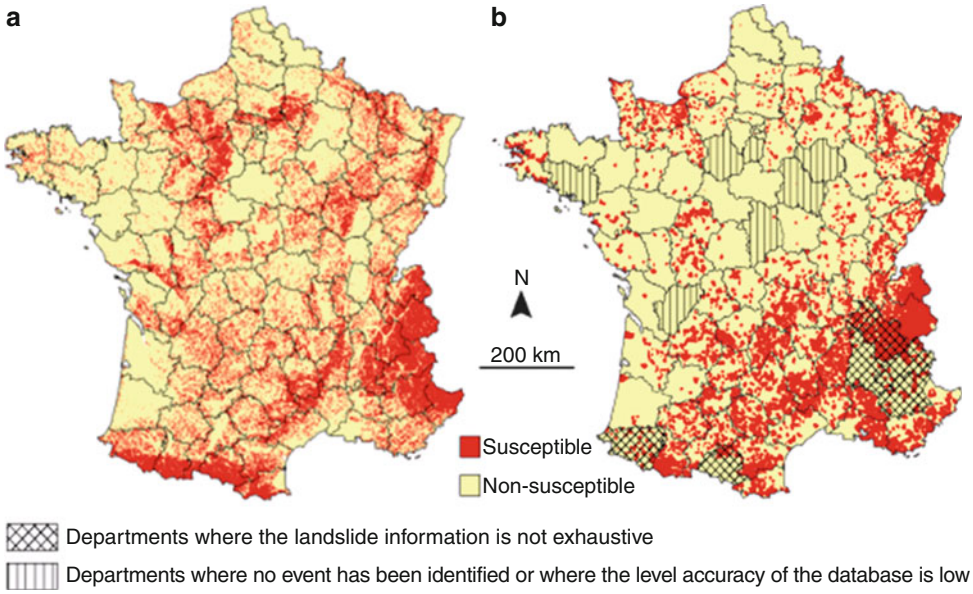

Fig. 9 Susceptible and non susceptible landslide areas for France. (**a**) Compound landslide susceptibility map corresponding to the high susceptibility class of Fig. 8a. (**b**) Municipalities affected or not by landslides in the past

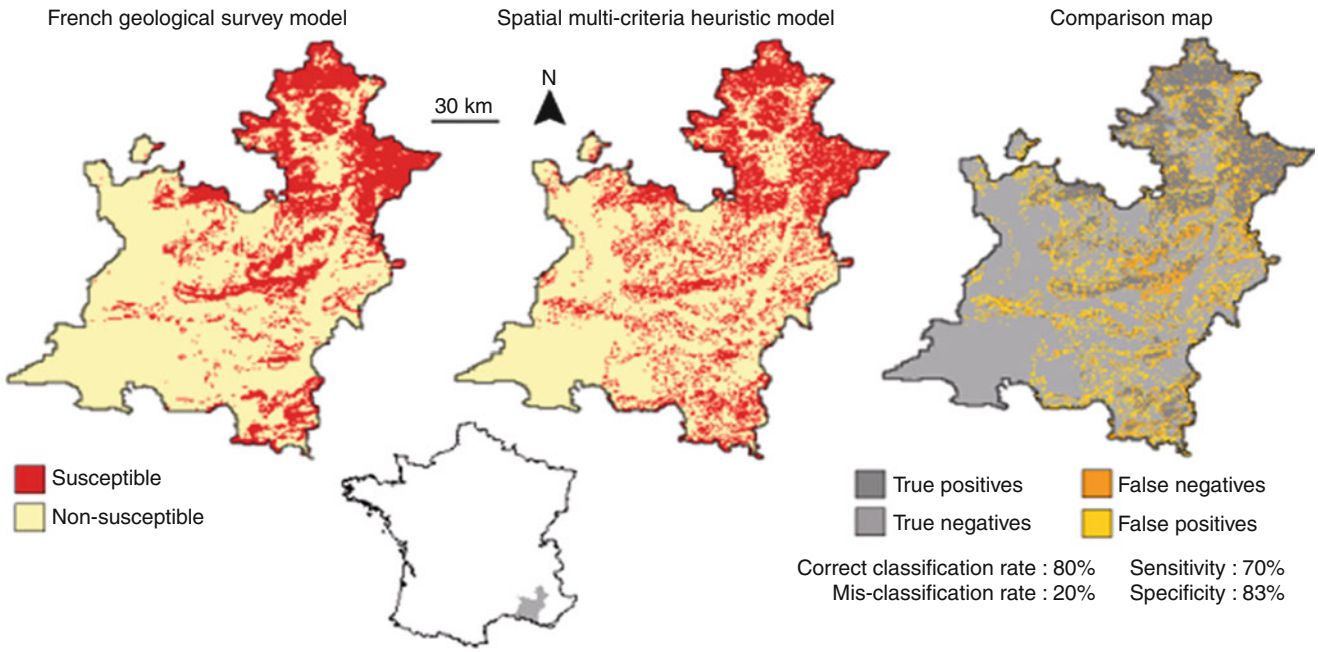

Fig. 10 Evaluation of the compound susceptibility map with an assessment provided by BRGM in the Western part of the Region Provence Alpes Côte d'Azur

The evaluation is based on a cross operation providing a confusion matrix from which some statistics are calculated, such as classification rates, sensitivity and specificity index. Depending on the map available the evaluation has been performed for the compound landslide susceptibility map (Fig. 10) and for the individual landslide susceptibility maps (Fig. 11).

The compound susceptibility map (Fig. 9a) has been compared to an assessment carried out by the French Geological Survey (*BRGM*) in 2007 in Region Provence Alpes-Côte d'Azur at a spatial resolution of 50 m. This assessment is the only map available in France that proposes a global susceptibility analysis for the three landslide types.

Figure 10 indicates that 80 % of the areas are well classified by the spatial multi-criteria evaluation model. It corresponds to plain areas (true negatives in light grey) and mountain areas (true positives in dark grey). The model also provides a good assessment of the major areas known to be prone to landsliding. Incorrectly classified observations (20 % of the simulated area) seem to correspond to

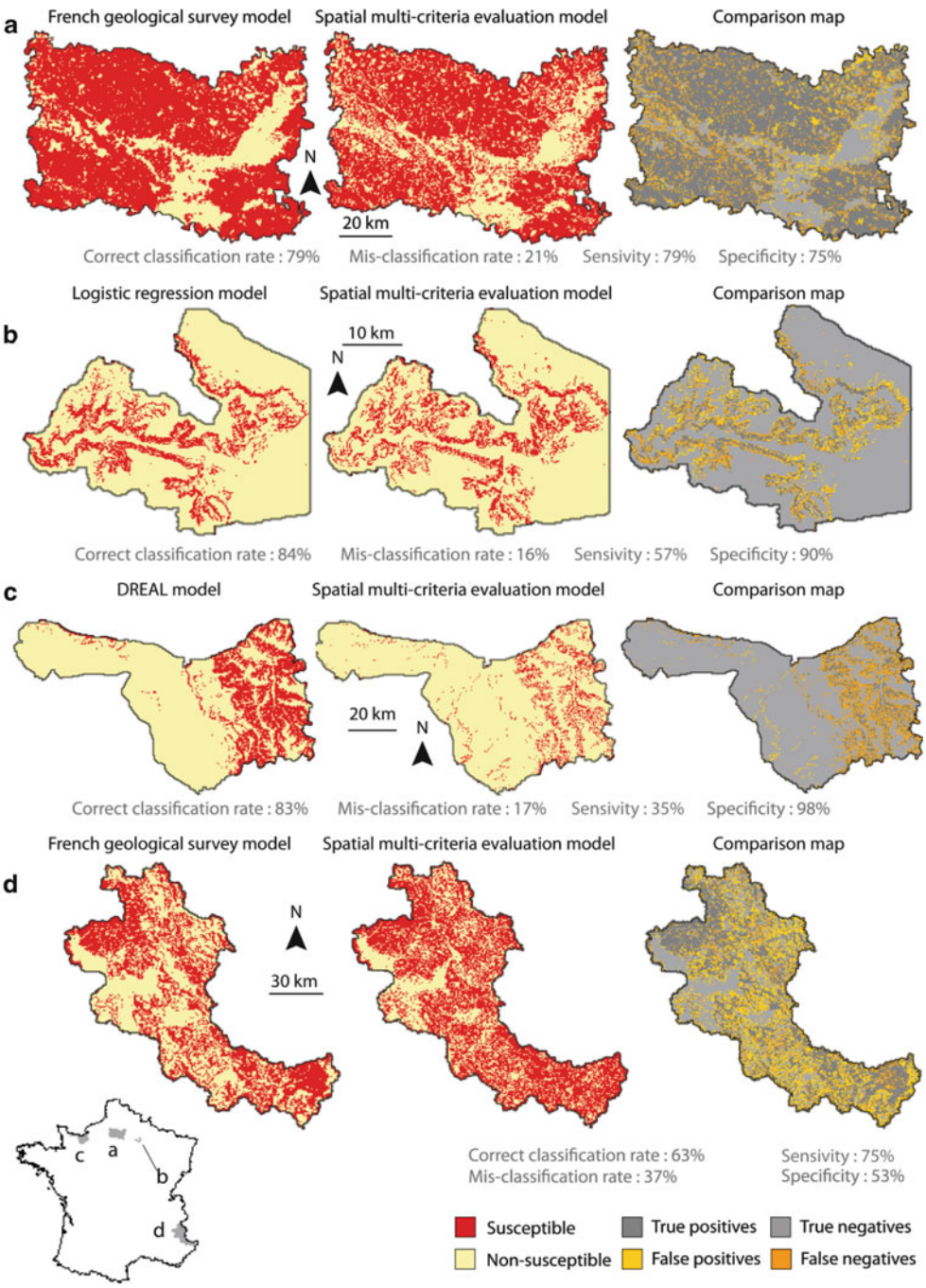

Fig. 11 Evaluation of the individual landslide susceptibility maps with different assessment at local scales for (**a**) flow-type landslide in the Department Oise, (**b**) slide-type landslide in the region of Montagne de Reims, (**c**) slide-type landslide in the North east part of the Department of Calvados, (**d**) for fall-type landslide in the region Ecrin-Queyras-Mercantour in the Western French Alps

intermediate areas. Despite of these observations, the proportion of positive and negative cases correctly predicted is respectively of 70 % and 83 % (Fig. 10). The predictive power of the SMCE model can therefore be considered as good taking into account the limited numbers of input data.

The individual landslide susceptibility maps have been compared to local susceptibility assessments (Fig. 11) in the Department of Oise for the evaluation of the flow-type susceptibility map (Fig. 11a), the region of Montagne de Reims (Van Den Eeckhaut et al. 2010) and the North east part of the Department of Calvados for the slide-type susceptibility map (Fig. 11b, c), and the region Ecrin-Queyras-Mercantour in the Western French Alps for the fall-type.

Taking into account the few numbers of input data, and the scale of analysis, the spatial multi-criteria evaluation model is in fair agreement with the local susceptibility maps produced at higher scale (1:100,000–1:250,000), with correct classification rate of ca. 80 % for the flow and slide susceptibility maps. The fall susceptibility map simulated with the spatial multi-criteria evaluation model identifies more possible fall prone areas than the local assessment,

but this can be explained by the use of more detailed information on geological discontinuities and local soil characteristics such as compressive strengths of the parent rocks.

Conclusion

In this contribution, the recent approaches towards the establishment of a common methodology for the assessment of landslide susceptibility within the European Union's Soil Thematic Strategy are presented. The focus was on the development of a simple heuristic methodology based on expert knowledge and simple spatial multi-criteria evaluation, and its test over France at a 1:1M scale. The results demonstrated the necessity to differentiate the analysis per landslide types and topographic experiment units (plain, mountain, coast).

In the near future a Tier 1 landslide susceptibility map for the whole Europe is expected to be prepared by the *Landslide Expert Group* by using a large landslide dataset actually compiled for Europe and the definition of more complex physio-geographic units taking into account topographical regions and climate regions for the subdivision of the continent. Possibly, landslide triggers such as cumulated rain maps or peak acceleration maps may be introduced in the analysis in a later phase.

Although this contribution does not focus on medium-scale Tier 2 and large scale Tier 3 assessments, it might be required to apply such more detailed inventory-based and physically-based susceptibility and hazard analysis for different types of landslides and triggering factors within areas of high landslide susceptibility as delineated by Tier 1.

Acknowledgments This work is part of the *European Landslide Expert Group* on '*Guidelines for Mapping Areas at Risk of Landslides in Europe*' coordinated by the *JRC* since 2007, and has been partly supported by the CERG (*European Centre on Geomorphological Hazards*) through the *European and Mediterranean Major Hazards Agreement* (EUR-OPA) of the Council of Europe. The members of the *European Landslide Expert Group* are thanked for all the fruitful discussions.

References

Blteanu D, Chendeş V, Sima M, Enciu P (2010) A country level spatial assessment of landslide susceptibility in Romania. Geomorphology 124:102–112

Castellanos Abella EA, van Westen CJ (2007) Generation of a landslide risk index map for Cuba using spatial multi-criteria evaluation. Landslides 4:311–325

Commission of the European Communities (2006a) Thematic strategy for soil protection. COM(2006)231 final. Brussels

Commission of the European Communities (2006b) Proposal for a Directive of the European Parliament and of the Council establishing a framework for the protection of soil and amending directive 2004/35/EC. COM(2006)232 final. Brussels

Creighton R, Irish Landslides Working Group (2006) Landslides in Ireland. Geological Survey of Ireland, Dublin

Dikau R, Glade T (2003) Nationale Gefahrenhinweiskarte gravitativer Massenbewegungen. In: Liedtke H, Mäusbacher R, Schmidt KH (eds) Relief, Boden und Wasser. Nationalatlas Bundesrepublik Deutschland. Institut für Länderkunde, Leipzig, pp 98–99

Eckelmann W, Baritz R, Bialousz S, Bielek P, Carre F, Houskova B, Jones RJA, Kibblewhite MG, Kozak J, Le Bas C, Toth G, Varallyay G, Yli Halla M, Zupan M (2006) Common criteria for risk area identification according to soil threats. European Soil Bureau Research Report no. 20, EUR 22185 EN. Office for Official Publications of the European Communities, Luxembourg

Foster C, Gibson A, Wildman G (2008) The new national landslide database and landslide hazard assessment of Great Britain. In: Proceedings of the first world landslide forum, Tokyo, 18–21 Nov 2008, pp 203–206

Günther A, Reichenbach P (2010) Landslide susceptibility assessment over Europe according to the 'Tier 1' approach: experiment and perspectives. In: European landslide experts group meeting on harmonised landslide susceptibility mapping for Europe. Ispra, Italy, 25–27 May 2010. (http://eusoils.jrc.ec.europa.eu)

Günther A, Reichenbach P, Hervás J (2008) Approaches for delineating areas susceptible to landslides in the framework of the European Soil Thematic Strategy. In: Proceedings of the first world landslide forum, Tokyo, 18–21 Nov 2008, pp 235–238

Guzzetti F, Carrara A, Cardinali M, Reichenbach P (1999) Landslide hazard evaluation: a review of current techniques and their application in a multi-scale study, Central Italy. Geomorphology 31(1–4):181–216

Hervás J (2007) Guidelines for mapping areas at risk of landslides in Europe. In: Proceedings of experts meeting, Ispra, Italy, 23–24 Oct 2007. JRC Report EUR 23093 EN. Office for Official Publications of the European communities, Luxembourg

Hervás J, Günther A, Reichenbach P, Malet JP, Van Den Eeckhaut M (2010) Harmonised approaches for landslide susceptibility mapping in Europe. In: Malet JP, Glade T, Casagli N (eds) Proceedings of the international conference mountain risks: bringing science to society, Florence, Italy, 24–26 Nov 2010. CERG Editions, Strasbourg, pp 501–505

Hong Y, Adler R, Huffman G (2007) Use of satellite remote sensing data in the mapping of global landslide susceptibility. Nat Hazards 43:245–256

Kirschbaum DB, Adler R, Hong Y, Lerner-Lam A (2009) Evaluation of a preliminary satellite-based landslide hazard algorithm using global landslide inventories. Nat Hazards Earth Syst Sci 9:673–686

Malet JP, Thiery Y, Hervás J, Günther A, Puissant A, Grandjean G (2009) Landslide susceptibility mapping at 1:1M scale over France: exploratory results with a heuristic model. In: Proceedings of the international conference on landslide processes: from geomorphologic mapping to dynamic modelling. A tribute to Prof. Dr. Theo van Asch, Strasbourg, France, 6–7 Feb 2009

Nadim F, Kjekstad O, Peduzzi P, Herold C, Jaedicke C (2006) Global landslide and avalanche hotspots. Landslides 3:159–173

Nordregio (2004) Mountain areas in Europe: analysis of mountain areas in EU member states, acceding and other European countries, Report 2004:1. Nordic Centre for Spatial Development, Stockholm, Sweden

Salvati P, Bianchi C, Rossi M, Guzzetti F (2010) Societal landslide and flood risk in Italy. Nat Hazards Earth Syst Sci 10:465–483

Van Den Eeckhaut M, Marre A, Poesen J (2010) Comparison of two landslide susceptibility assessments in the Champagne-Ardenne region (France). Geomorphology 115:141–155

Digital Rock-Fall and Snow Avalanche Susceptibility Mapping of Norway

Jan Høst, Marc-Henri Derron, and Kari Sletten

Abstract

Norway is prone to a variety of different landslide types. Despite this fact, inferior efforts have been undertaken to establish a national overview of which areas can be considered safe and which have a potential landslide hazard. As a consequence, many municipalities have allowed construction of buildings and infrastructure in landslide hazardous areas. In 2007, Geological Survey of Norway initiated a project to develop susceptibility maps for rock-fall and snow avalanche, on the basis of a 25 × 25 m digital terrain model covering the whole country. The GIS algorithms were developed in a consensus driven approach involving universities, research institutes, consultancies and several public authorities. The produced maps aim to raise awareness of possible landslide hazards in municipality land-use planning.

Keywords

Landslide • Susceptibility • Mapping • Modelling

Introduction

Landslides are recurrent phenomena onshore and offshore Norway, and lives and properties are lost every year. Despite this fact, governmental authorities have been reluctant to establish a national overview of landslide susceptibility.

In 2007, in the framework of the project "National Susceptibility Mapping of Geohazards" at NGU, it was decided to draw maps of susceptibility for rock falls and snow avalanches for the whole Norwegian mainland territory. These maps aim to provide a first overview (screening) of the entire country, in a relatively short time, at reduced costs, and with an automatic procedure applied homogeneously to the whole country. The main requirements for these maps were:

- To cover the entire Norwegian territory (385,000 km^2)
- To assess in a simple way the susceptibility of an area of being affected by a rock fall or snow avalanche
- To provide maps at an indicative scale of around 1:50,000 within a short time frame (ca. 2 years)
- To use only use data already available for the entire area

A large part of this work was achieved within a co-operation between the Geological Survey of Norway (NGU) and the Institute of Geomatics and Risk Analysis (IGAR) of the University of Lausanne, including the development of new methods and softwares. The University of Oslo, Norwegian Geotechnical Institute (NGI), Directorate for Water Resources and Energy Directorate (NVE) and Norwegian University of Science and Technology (NTNU) also participated in establishing the framework for the analyses.

Methods

The method used to draw these susceptibility maps is an extension to 2D (maps) of the alpha-beta method designed initially to work along profiles (Lied and Bakkehøi 1980;

J. Høst (✉) • K. Sletten
Geological Survey of Norway (NGU), Leiv Eirikssons vei 39, Trondheim N-7491, Norway

M.-H. Derron
Institute for Geomatics and Risk Analysis, University of Lausanne, Lausanne, Switzerland

C. Margottini et al. (eds.), *Landslide Science and Practice*, Vol. 1,
DOI 10.1007/978-3-642-31325-7_41,

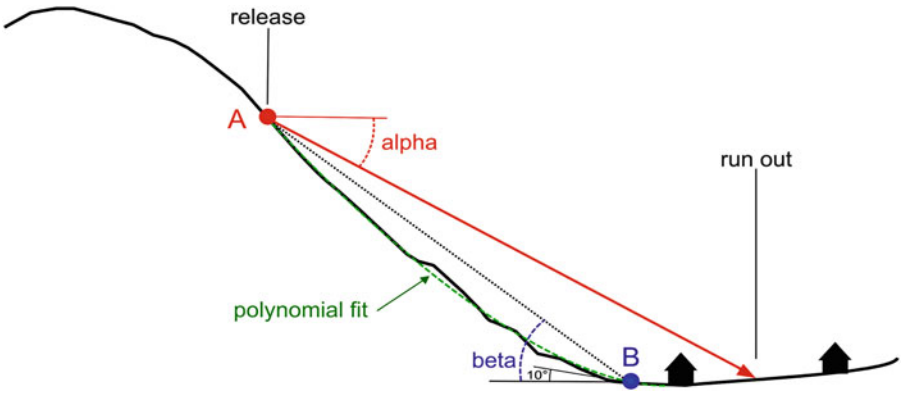

Fig. 1 Basics of the alpha-beta method (Lied and Bakkehøi 1980; Bakkehøi et al. 1983)

Bakkehøi et al. 1983). The main principles of the alpha-beta method are shortly reminded here (Fig. 1):

1. A release point, A in Fig. 1, is selected
2. The rock-fall/avalanche path starting from A is manually selected and its topographical profile is drawn. For snow avalanche this profile is smoothed according to a polynomial fitting (2nd or 4th degree)
3. The point B is then located on the smoothed profile where the slope angle = 10° (snow) or = 23° (rock-fall)
4. The angle beta is measured as the angle between the line AB and the horizontal
5. The angle alpha is then estimated using a statistical relationship between alpha and beta. The simplest relationships are of the type: alpha = m*beta-n, where m and n are empirical coefficients
6. Finally the potential propagation of the avalanche is estimated using the angle alpha as a shadow angle from A.

The classical alpha-beta method requires to define manually the possible avalanche corridors. But for the purpose of this project, to cover the entire Norway, the processing had to be fully automated, without requiring any human interaction or interpretation.

Practically the amount of data to be processed makes it very difficult to use common GIS softwares like ArcGIS. Therefore an independent code was developed at NGU and IGAR specifically for this project (Derron 2010).

In outline, the processing used for this project has two main steps: (1) the determination of release areas, i.e. the areas from which an avalanche/rock fall can initiate, and (2) the estimation of the propagation zone.

Datasets

Input Datasets

The main dataset used is the digital elevation model (DEM) provided by Statens Kartverk which is an elevation grid of 25 m cell size, projected and georeferenced in UTM/WGS84 – zones 32, 33 and 35 N. No other dataset or avalanche inventories were used.

For the rock-fall modelling, input data also involved:

- The geological bedrock map N250 provided by NGU.
- The map of superficial cover – mosaic of various scales provided by NGU

Output

All the processing is done in raster mode and the results of the computations are raster files (geotiff format) in the same projection and coordinate systems than the input data (UTM 32, 33, 35 N/WGS84). At the end of the processing, all the cells of the initial DEM were classified according to three categories:

1. Cell included in a release area
2. Cell included in a propagation zone
3. Cell not included in a release or propagation area

In order to make the results easier to handle in GIS environment, the release areas and propagation zones were finally vectorized in polygons (without any smoothing) (Fig. 2).

Rock-Fall Release Areas

The potential rock-fall release areas were automatically detected by the method of slope analysis of Loye et al. (2009), taking into consideration the slope angle, the DEM cell size, the type of bedrock and the outcropping conditions. The main idea of this method is that slope angle thresholds can be used to divide the relief in geomorphologic classes. In order to fix the threshold values, the slope angle distribution is decomposed in Gaussian populations (Fig. 3).

In conclusion the criteria to determine if a cell of the DEM is in a potential release area is:

Cell in a release area IF:

(slope angle $> \delta_{rockface}$) OR

[(slope angle $> \delta_{side}$) AND "on bare rock"]

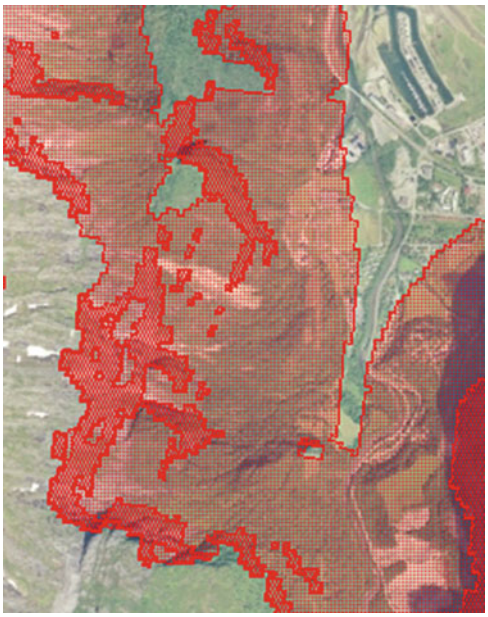

Fig. 2 The final map product is not smoothed, to ensure that users understand that the modelling is very rough (M 1:50,000)

With:

$\delta_{rockface}$ = lower limit angle of the "steep rock face" class (43° in the example)

δ_{side} = mode angle of the "steep valley side" class (34° in the example)

Finally, we must be aware that the slope angle thresholds defined above are *strongly dependant on the resolution of the DEM and the type of rock*. The larger the cell size of the DEM, the more underestimated is the slope angle of a steep slope. That is why the thresholds angles must be defined using the DEM and values measured in the field cannot be directly used. The mechanical properties of the rocks will influence the values of the slope thresholds too. Consequently, this slope analysis has to be performed for the different types of rocks in order to define proper thresholds for each lithology.

Snow Avalanche Release Areas

The method to define if a cell in included in a release area is a simple thresholding of its slope angle value. A cell of the DEM is in a release area if:

$$30° <= \text{ slope angle } <= 55°$$

The lower and upper limit values were selected according to McClung and Schaerer (1993) and Lied and Kristensen (2003) showing that almost all the avalanches are released from areas with slope from 30° to 55°.

The slope angle is estimated with a 3 × 3 moving filter, with the algorithm of Horn (1981).

The potential release areas for snow avalanches were extracted for the entire country. Examples of release areas are presented in Fig. 4.

Propagation Zones Estimation

The estimation of propagation is based on an adaptation of the shadow angle method and more precisely of the alpha-beta method used for snow avalanches (Fig. 1). For the present project, two aspects have to be improved compared to the initial shadow angle method: (1) the new method must produce maps and not only profiles, (2) the processing has to avoid any manual operation and be entirely automatic to be able to cover very large regions.

The steps of the processing used to estimate the rock-fall propagation zones are illustrated in the flow chart of Fig. 5, whereas for snow avalanche the steps are shown in Fig. 6.

A flow path is computed from each release cell of the DEM with the algorithm D8 (Jenson and Domingue 1988): the flow passes from one cell to the lowest of its eight neighbouring cells. The flow path is stopped when the path reaches a cell that belongs to one of the large flat areas defined in the previous step (point B in Figs. 1 and 10). Finally, one cell B is associated to each release cell A.

Cone of Propagation

The cone propagation technique was developed for rock falls first by Jaboyedoff and Labiouse (2003). Once a value of alpha angle is attributed to a release cell, a vertical cone can be drawn (Fig. 7, left), with its apex located in the release cell. The zone of potential propagation from a release cell is delimited by the intersection of the cone with the DEM (Fig. 7, right).

The propagation can also be constrained laterally by an opening angle δ (or dispersion angle), whereas the actual opening is 2∗δ (Fig. 8). The angle δ defines how far the blocks can deviate from the steepest flow path (path AB). Crosta and Agliardi (2004) propose a maximum value of 15° for δ. A very conservative value δ = 30° was selected for the final maps. Tests have shown that this parameter is by far not critical and that the results are only very slightly sensitive to its value.

Final Propagation Zones

The final propagation zones are defined by the union of all the cone propagation areas. If a cell of the DEM is in *at least one cone of propagation*, then this cell is considered as "susceptible" and then included in a final propagation zone. A cell in a propagation zone can be included in only

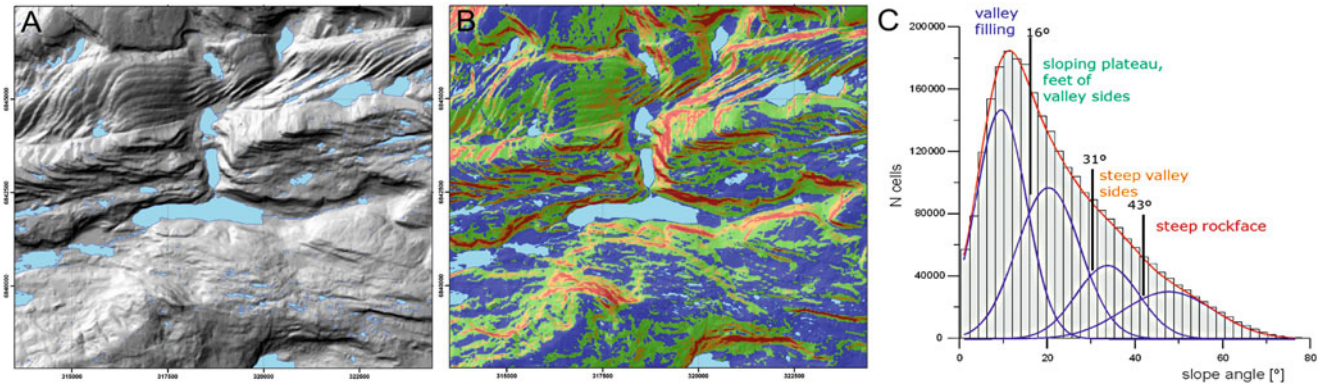

Fig. 3 *Top left*: shaded relief based on the 25 m cell size DEM, *Top right*: segmentation of the relief in four classes according to the slope angle populations, *Bottom right*: histogram of slope angle and decomposition in four Gaussian population. *Blue lines* = Gaussian populations used to decompose the histogram. *Red line* = sum of the Gaussian populations. *Black vertical lines* indicate the threshold values of slope angle

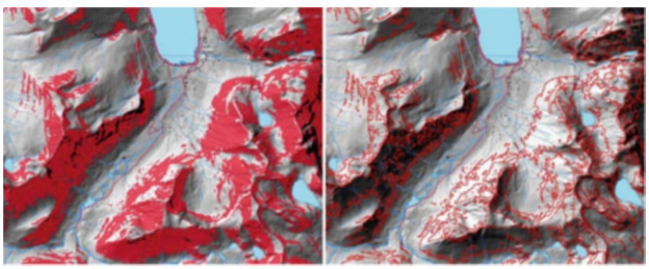

Fig. 4 *Left*: release areas (*red*) based on the slope angle thresholding (30–55°), *Right*: edges of the release areas

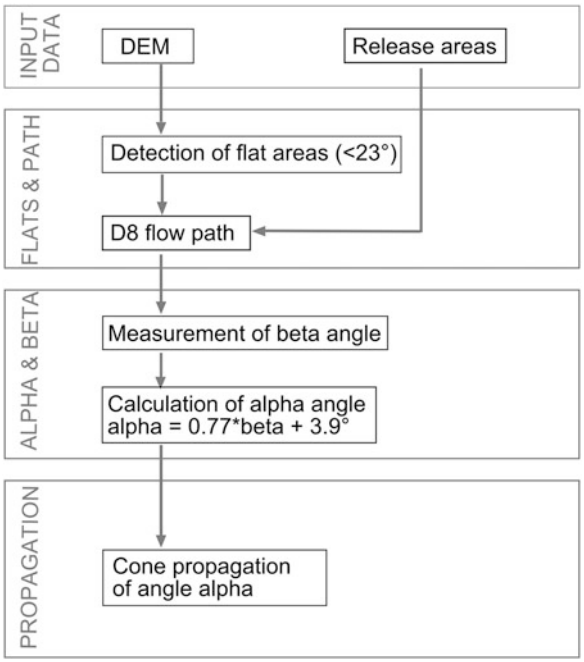

Fig. 5 Flow chart of the rock fall propagation calculation

one cone or be at the intersection of several propagation cones. There is no distinction of the number of release cells that may reach a propagation cell in the final product.

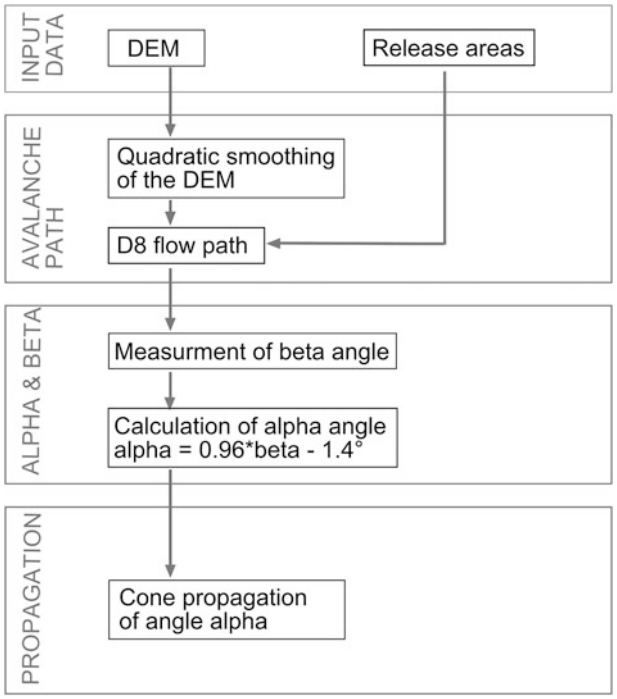

Fig. 6 Flow chart of the snow avalanche propagation calculation

The final susceptibility map for rock fall (below) is a binary map: inside/outside an area susceptible to be reached by a rock fall (Fig. 9).

Discussion

The final products can be seen (in Norwegian) at the following web map services (zoom in to 1:200,000 or better):

- Snow avalanche: http://www.ngu.no/kart/skrednett/?map=Snøskred – aktsomhetskart
- Rock fall: http://www.ngu.no/kart/skrednett/?map=Steinsprang – aktsomhetskart

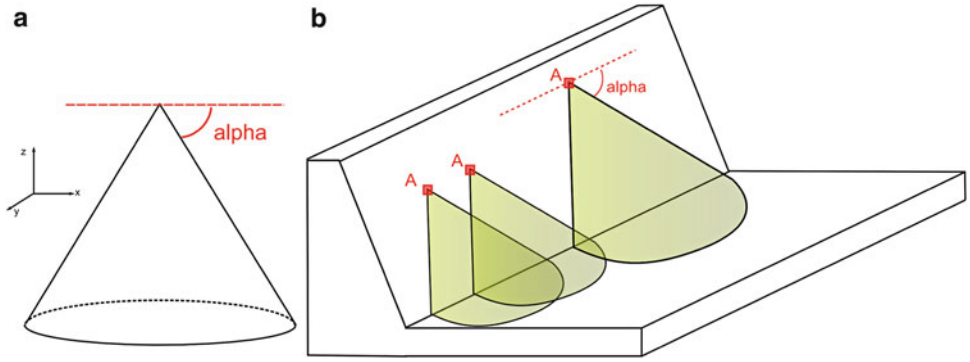

Fig. 7 *Left*: cone of propagation with an angle of propagation alpha; *Right*: intersection of some propagation cones on a simplified topography

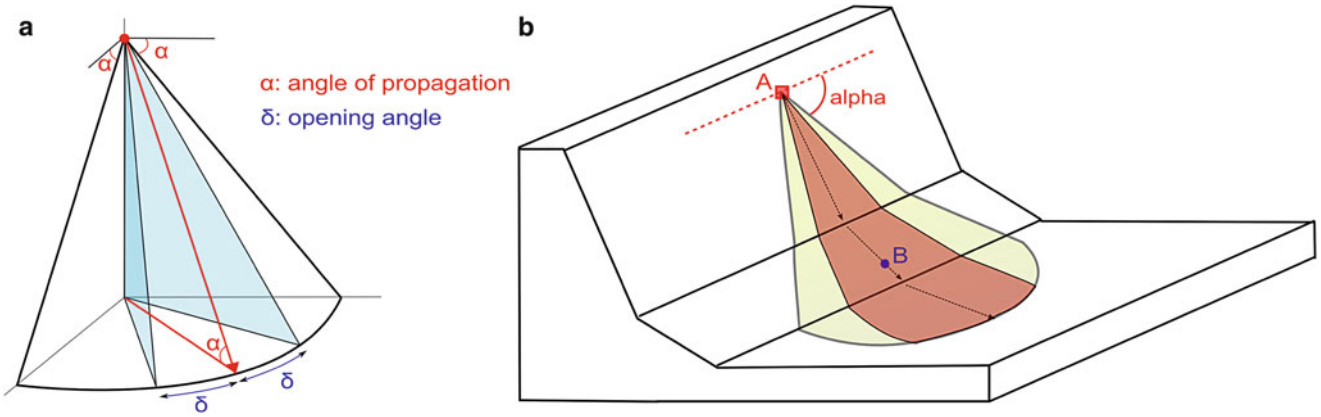

Fig. 8 *Left*: principle of the limiting opening angle used to reduce the possible dispersion of a rock fall from its main path. *Right*: application of the opening angle on a simplified topography (*yellow*: full cone propagation, *red*: propagation reduced laterally to the opening angle)

The technical description of the procedure used to draw these susceptibility maps is provided in the previous chapter, and technical reports can be downloaded (see References).

It is now important to discuss some issues related to the use of these maps. Modelling a complex geohazard phenomenon at the applied scale implies strong simplifications, and technical and strategic choices. All these factors will influence the final product and define its potential field of applications.

Information Content

The maps produced in this project provide a *qualitative assessment of the susceptibility* for a location to be affected by a snow avalanche or rock fall (in/out). They do not include any information about: the probability of occurrence of an event, its return period, its intensity or the consequences of an event on the elements at risk (population and infrastructures).

DEM Resolution and Error

The most important input data is the 25 m gridded DEM provided by Norwegian Mapping Authority. Some limitations are inherent to the quality of this DEM: (1) some errors were detected in the original DEM (unrealistic pits) and corrected, (2) the relatively low resolution of the DEM (one point each 25 m) is a more important limiting factor. As the DEM surface is a simplified representation of the real topography, some morphological features may be missing. In particular, steep slope calculation can be affected by strong underestimations (Fig. 4). It has for main consequence that short steep cliffs can be missed during the detection of release areas.

Forest Cover

It was decided in this project not to take into account the forest cover. The main reasons for this choice are:

- No dataset of the forest cover and suitable for our purpose is available for the whole country. In addition such a dataset should be periodically updated to take into consideration land-use changes.
- Even if such a dataset was available, then the impact of forest cover on rock fall propagation should have been defined. This interaction is quite complex and many parameters are required to model it (trunk diameters, restitution coefficients . . .). This was beyond the scope of this project, as it was decided to always consider the worst case scenario.

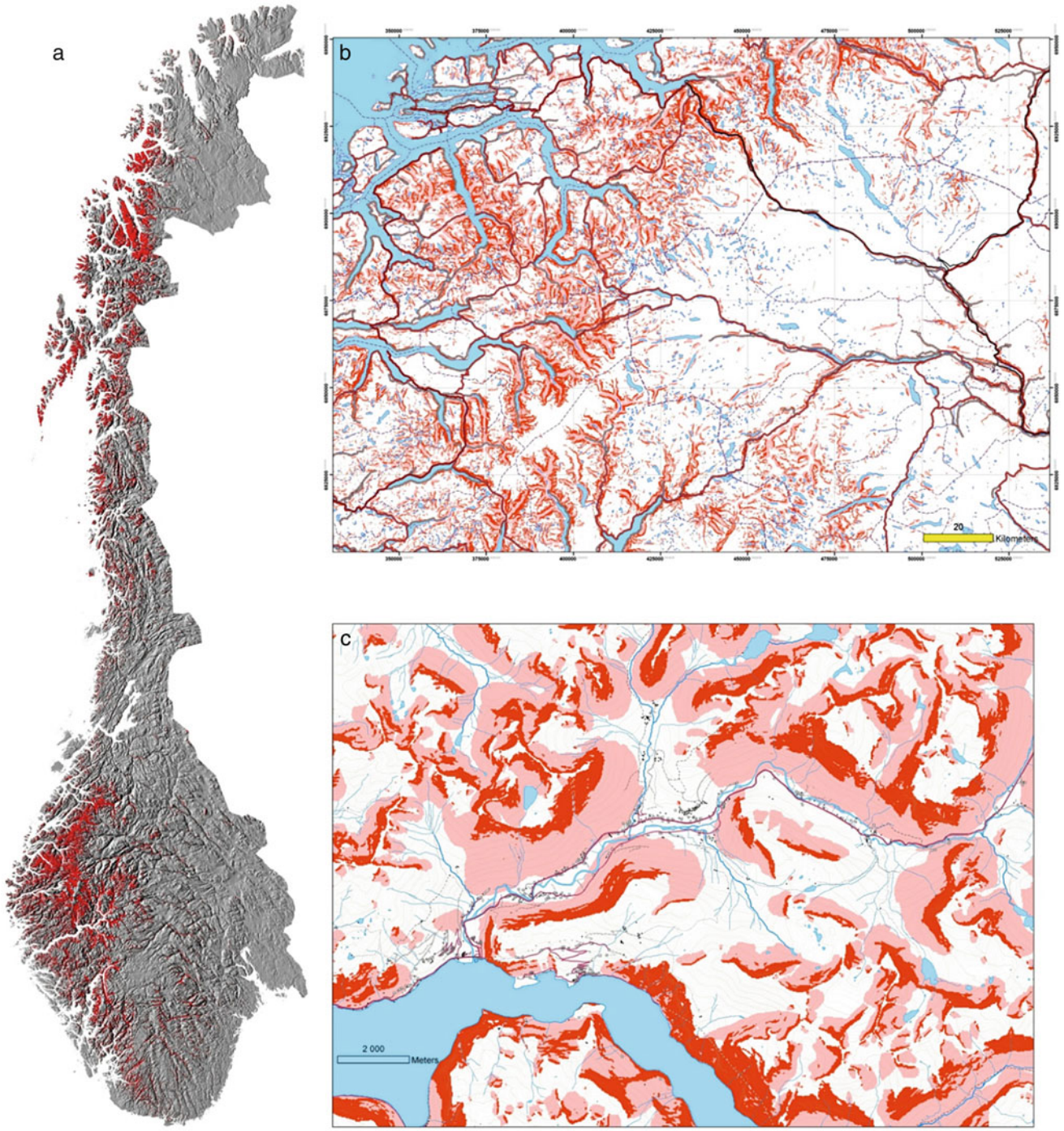

Fig. 9 *Right*: overview of the final susceptibility map for rock falls overlain on a shaded relief map of Norway. *Left*: extracts of the rock fall susceptibility map. *Red*: release areas, *pink*: propagation zones

Parameters Choice

As such small scale (= large area, few details) susceptibility assessments are made to be conservative: we prefer to overestimate rather than underestimate the potential hazardous zones. All the parameters used during the processing were selected along this conservative line. Hence, the final result aims to represent the worst case possible scenario. It means that some propagation areas may be overestimated.

In particular, a frequent drawback of shadow angle models is the overestimation of the propagation when a high and steep cliff is over a flat bottom valley. Technical solutions exist to correct partly these drawbacks. They have not been tested or applied to the present product but should be considered for a next version.

Operational Use

A particular caution must be taken not to over-interpret these susceptibility maps. The maps aim to provide a first overview, a screening over the entire country, of the regions that may be exposed to rock falls or snow avalanches. They can be used to identify risk hotspots at regional scale and to help prioritizing future more detailed hazard assessment.

Even if they are in a digital format, they must not be used at scale more detailed than 1:50,000. They do not replace in any way fieldwork, detailed mapping and specific site investigations. In particular, these maps cannot be used for detailed planning such as house- or road construction.

Credit

The development of the above methods and maps is attributed to Marc-Henri Derron.

References

Bakkehøi S, Domaas U, Lied K (1983) Calculation of snow avalanche run-out distances. Ann Glaciol 4:24–30

Crosta GB, Agliardi F, Frattini P, Imposimato S (2004) A three-dimensional hybrid numerical model for rockfall simulation. Geophysical Research Abstracts 6, n. 04502

Cruden D, Varnes D (1996) Landslide types and processes. In: Turner K, Schuster R (eds) Landslides investigation and mitigation. Special report 247, Transportation Research Board, pp 36–75

Derron M-H (2010) Method for the susceptibility mapping of rock falls in Norway, NGU. Download from: http://www.ngu.no/website/common92/skrednett/TekniskRapportSkredSteinAkt.pdf

Derron M-H (2010) Method for the susceptibility mapping of snow avalanches in Norway, NGU. Download from: http://www.ngu.no/website/common92/skrednett/TekniskRapportSkredSnoAkt.pdf

Horn B (1981) Hill shading and reflectance map. Proc IEEE 69 (1):14–47

Jaboyedoff M, Labiouse V (2003) Preliminary assessment of rockfall hazard based on GIS data. ISRM 2003 – technology roadmap for rock mechanics. South African Institute of Mining and Metallurgy, Johannesburg, pp 575–578

Jenson S, Domingue J (1988) Extracting topographic structures from digital elevation data for geographic information system analysis. Photogramm Eng Remote Sens 54:1593–1600

Lied K, Bakkehøi S (1980) Empirical calculations of snow avalanche run-out distances based on topographic parameters. J Glaciol 26:165–177

Loye A, Jaboyedoff M, Pedrazzini A (2009) Identification of potential rockfall source areas at a regional scale using a DEM-based geomorphometric analysis. Nat Hazards Earth Syst Sci 9:1643–1653

Mc Clung DM, Schaerer PA (1993) The avalanche handbook. The Mountaineers, Seattle, 271 pp

Mapping Mass Movement Susceptibility Across Greece with GIS, ANN and Statistical Methods

Maria Ferentinou and Christos Chalkias

Abstract

In this paper Geographic Information Systems (GIS) are applied to map the spatial zonation of mass movement susceptibility in national scale via artificial neural networks (ANN), and spatial statistical modelling that is, frequency ratio and Logistic Regression (LR). For this purpose 16 potential factors were identified to map mass movement susceptibility across Greece mainland. Among these, seven factors: elevation, slope, precipitation, geology, land cover, terrain forms and seismic acceleration, were ranked as the most important, applying susceptibility index (s_{ij}) and standard deviation criterion. The output mass movement susceptibility map derived from (LR) model showed 85.33 % in prediction accuracy of the total area of Greece. Frequency ratio showed 71.62 % and ANN showed 60 %. According to the obtained results LR model is the most accurate, while the two other models gave reasonable results. Future work will focus on regional scale in order to refine the proposed models in landslide prone regions.

Keywords

Mass movements • Susceptibility mapping • Greece • GIS based modelling • Frequency ratio • Logistic regression • Artificial neural network

Introduction

Mountainous or rural environments confront landslides, as a major natural disaster. Following Cruden and Varnes (1996) and Dikau et al. (1996), the term landslide is used for soil, debris and rock travelling by sliding, flow, and complex movement. Rock fall events are very common in Greece, and were also recorded in the examined landslide inventories. In this paper the term mass movements is generally used in order to cover both landslides and rockfalls. Land use change, overexploitation of natural resources, deforestation, construction of transportation facilities required by expanding population, climate change and the potential for extreme weather conditions have contributed to the increase of mass movement frequency globally, during the last decades. This means, that it is likely the geographic distribution of such natural hazards, will alter since their occurrence seems to be on the rise.

Mass movement susceptibility mapping is commonly based on the relations between mass movements occurrence and the distribution of various environmental variables in the area under investigation.

Different ways of approaching mass movement hazard assessments on a global (Nadim et al. 2006) and national scale are given using examples from Germany (Glade et al. 2003), Australia (Leventhal and Kotze 2008), and Cuba (Castellanos and Van Western 2008).

Many approaches have been developed for landslide susceptibility assessment mapping. Landslide susceptibility approaches divided in two general categories: qualitative and quantitative methods. The most important difference between these methods is their degree of objectivity.

M. Ferentinou (✉) • C. Chalkias
Department of Geography, Charokopio University of Athens, 70, El. Venizelou, Athens, Greece
e-mail: mferen@hua.gr

C. Margottini et al. (eds.), *Landslide Science and Practice*, Vol. 1,
DOI 10.1007/978-3-642-31325-7_42,

General overviews are presented in, Hansen (1984), Carrara et al. (1991), Leroi (1996), Soeters and Van Western (1996), Aleotti and Chowdhury (1999), Guzzetti et al. (1999), Van Westen et al. (2003), Lee and Jones (2004) Ayalew and Yamagishi (2005), Ercanoglu and Gokeoglou (2001) and Yilmaz (2009).

In Greece, a first attempt on a compilation of a mass movement hazard zonation map at a national original scale was accomplished by (Koukis and Ziourkas 1991; Koukis et al. 2005), using the geographical distribution of the recorded cases. Papadopoulos and Plessa (2000), studied earthquake related landslides in Greece. Gournelos et al. (2006) produced a landslide hazard map at national scale using fuzzy rules.

In the current paper, national hazard zonation mapping scale, is implemented for Greece, with intend to reveal general hot spots of the instability areas for the entire country.

Mass Movements in Greece

In Greece, mass movements are a repeated and persistent natural hazard. The highly active geoenvironment produces 'rough' terrestrial and subaqueous topography, along with intense seismicity and precipitation pattern are among the factors that contribute to landsliding. The wildfires and post-fire erosion processes, the climate change, and the expansion of transportation network, may also be contributing factors. An increment of about 20 % of the mass movement occurrences was recorded during the last 20 years. All the recorded cases constitute occurrences that have mostly affected inhabited areas and transportation network. The magnitude of these instability zones, varies considerably from thousands of m^3 to several million m^3. The main types of mass movements concerning the total number of recording cases are slumps (40 %), creep (20 %), and earth flows (18 %), while falls (22 %) is the main type of movement in rock formations (Koukis et al. 1997). The predominant factors are intense erosion, human activities and heavy rainfalls. Koukis et al. (1996), found that in Achaia County located in southwestern Greece, an area of high mean annual rainfall, the dominant factor contributing to landsliding is precipitation and lithology. The same authors report that there is high correlation between mass movement manifestation and precipitation.

Mass Movement Inventory and Preparation of Parameter Maps

In this study the examined factors contributing to landslides were all converted to raster format, using rectangular grids, with cell size 250 m as the basis for the analysis. The whole

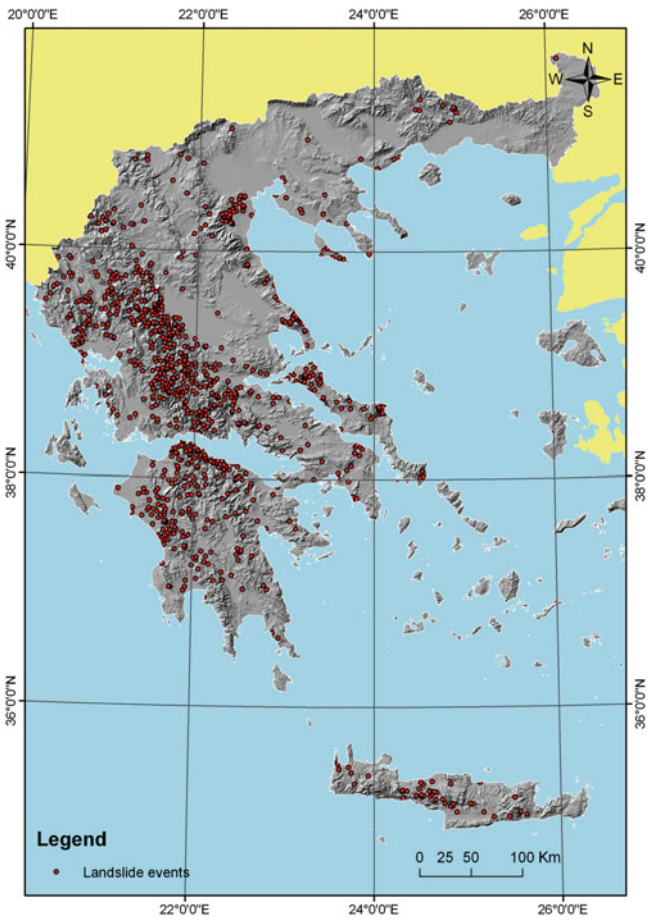

Fig. 1 The study area with mass movement locations

data set in the official Greek reference system – HGSR8.

Two mass movement inventory datasets were used with a total of 1,200 cases. 90 % of these data were used as a training set for FR, LR and ANN method, and 10 % of events were kept for test set. The inventories cover the period from 1950 to 2003. The first database maintained by the Institute of Geology and Mineral Exploration (IGME) is mainly formed only from the recent historical record, covering a time period (1910–1995), (Koukis et al. 1997). A second inventory covering events from 1995 to 2003, was also used which was developed from field mapping, remote sensing data and other records. In Fig. 1 the study area is presented with mass movement events.

The intrinsic causal factors that were proposed to be utilized in the analysis are geological (lithology) geomorphological (topographic elevation, slope, slope aspect, terrain forms, curvature, plan and profile curvature, proximity to drainage network, proximity to coastline, topographic wetness index), environmental (land cover), and anthropogenic (vicinity to road network). Seismic intensity was also proposed. The triggering factors that were implemented in the analysis

procedure were seismic acceleration and mean annual precipitation. These are common variables for controlling mass movement hazard (Soeters and Van Western 1996; Carrara et al. 1991).

A satellite derived Digital Elevation Model (DEM) was used for digital representation of the surface elevation, as topography is one of the major factors in mass movement analysis. The source was a global elevation data set the Shuttle Radar Topography Mission (SRTM)/SIR-C band data, (with 3 arc seconds) released from (NASA) in 2003. The DEM derivatives (slope, aspect, curvature, plan and profile curvature), were calculated using functions implemented in ArcMap 9.3 and SAGA GIS software.

The Geological Map of Greece at 1/500,000, published (Bornovas and Rondoyanni-Tsiambaou 1983) was also used in this study. The main types of identified alpine basement rocks in the map are Upper Cretaceous limestones, transition zone of Mesozoic limestones and schist – cherts, Semi-metamorphic and metamorphic rocks (phyllites, sipolines, gneisses marbles), marbles, volcanic rosks, ophiolites, and granites. These rocks are usually overlain by Neogene sediments and Quaternary deposits.

For the study area CORINE (Coordinate of Information on the Environment) database was used. Land cover project legend was followed and (Cumer 1994; Heyman et al. 1994).

Seismic intensity data were retrieved from earthquake data maintained from Geodynamic Institute of Greece.

Proximity to drainage network was also implemented in the analysis in order to investigate the effect of regional geomorphology and local erosional characteristics and mass movement occurrence. The source data were 1:50,000 maps from Hellenic Army General Service.

Vicinity to roads was selected in order to explore the relationship between anthropogenic activities with shape topographic surface and mass movements generation. The data were acquired from OpenStreetmap.

Precipitation is a fundamental slope instability triggering factor. It is widely common that areas receiving higher rainfall relative to the region depict a higher probability of mass movement occurrence. As a general trend pattern in Greece, there is a clear contrast between the more rainy western Greek area (rainside) and the drier eastern one (rainshadow), whereas there is little precipitation over the islands, particularly in the southern parts. The source of data used in this study was mean annual precipitation based on time series (1950–1974) from Public Power Company.

The map of expected Peak Ground Acceleration (PGA) with 475 – year return period (10 % probability of exceedance in 50 years) was launched in 1992 from the Technical chamber of Greece.

Methodology

General Concepts

Data preparation and coding depends on the application and the characteristics of the particular study. Data coding is necessary to convert the variables to such a form that the computational tools (statistical methods, logistic regression, artificial neural networks) can be best utilized, as they can only utilize numerical information.

The preparation of the mass movement susceptibility map in this study, involves the following steps:

Identification of the parameter maps together with mass movement inventories, and creation of the spatial database. The number of classes for all the parameters was (subjectively chosen) based on the physical meaning of the attributes.

The background data (parameter maps) were combined with the landslide inventory map to produce spatial correlations. Frequency ratio (FR) and susceptibility index $s_{i,j}$ were calculated.

The next step was rating the 16 initially identified parameters and the selection of the 7 most important among them according to the integrated susceptibility index (SI) and standard deviation.

One of the crucial steps in landslide susceptibility assessment is the identification of landslide areas and the definition of non landslide areas which would be used for training, in order to derive a predictive relationship for landslide occurrence. This sampling data set was used as input for LR and ANN methodologies. Alternative sampling datasets were created within GIS environment. Each of these datasets consists of points (samples) with a binary landslide indication field. The landslide samples (value: 1) originated from landslide inventory sources, while non-landslide samples (value: 0) were randomly located across Greece.

A sampling function was applied to the parameter maps in order to prepare a matrix of samples of landslide and non landslide areas with seven dimensional vectors. For ordinal and ratio type variables sampling was done in the original data grids, though in nominal variables sampling was done to the reclassified grids which obeyed landslide density through $s_{i,j}$ value (details in the next section). The produced ASCII file was exported to a statistical package (SPSS) in order to perform a LR, and to MATLAB in order to use ANN algorithm.

Computation of weight values was done though through LR and ANN for the various parameter maps, to produce a resultant landslide susceptibility index (LSI) map, which was classified to five susceptibility classes.

The results, were validated through the evaluation of the prediction for the 10 % test set of the initial data set.

Frequency Ratio Analysis

The Frequency Ratio (FR) is the ratio of the area where mass movements occurred in the total study area, and also, is the ratio of the probabilities of a mass movement occurrence to a non-occurrence for a given attribute (Lee and Talib 2005). Equation 1 shows the formulation of FR.

$$FR = \left(\frac{N_{i,j}}{A_{i,j}} \div \frac{N_T}{A_T}\right) \quad (1)$$

The factors analyzed, were evaluated using the FR method to determine the level of correlation between the location of the mass movements in the study area and these factors.

Susceptibility index $s_{i,j}$ was also estimated for all the aforementioned parameters subclasses, defined as

$$s_{i,j} = \ln\left(\frac{N_{i,j}}{A_{i,j}} \div \frac{N_T}{A_T}\right) \quad (2)$$

The index of susceptibility ($s_{i,j}$) was applied to indicate the weight of an individual category for any parameter through the comparison of mass movement density in the spatial extent associated with the category with the mean mass movement density in the whole research area. Equation 2 was applied and the grids referring to the various parameters were reclassified according to susceptibility index value. Each pixel was assigned a susceptibility value $s_{i,j}$ based on its underlying factor category. The final susceptibility map was produced summing the reclassified grids of each data layer.

Integrated susceptibility (SI), was also performed in order to rate the importance of the various parameters to landsliding and select the most important (Table 1).

$$SI = \ln\left(\frac{N_s}{A_s} \div \frac{N_T}{A_T}\right) \quad (3)$$

The standard deviation (σ) of the susceptibility index for the parameters involved is was calculated as an index to compute influence on landsliding.

$$\sigma_i = \sqrt{\frac{\sum_{j=1}^{n} \left(x_{i,j} - \overline{x_1}\right)^2}{n}} \quad (4)$$

Where, σ_i is the standard deviation of the susceptibility of the i_{th} factor, n is the number of grid cells in the susceptibility map associated with the ith factor, x_i is the mean susceptibility of the factor and $x_{i,j}$ is the susceptibility of the j_{th} grid cell for the ith factor.

Table 1 Integrated susceptibility and standard deviation for mass movement factors

	Parameters	SI	σ_i
1	Geology GEO	0.63	0.62
2	Precipitation PRE	0.40	0.65
3	Elevation ELEV	0.36	0.49
4	Land cover LC	0.31	0.48
5	Slope angle SL	0.29	0.67
6	Terrain forms TF	0.23	0.45
7	Seismic acceleration ACC	0.15	0.35
8	Vicinity to road	0.21	0.38
9	Plan curvature	0.19	0.13
10	Topographic wetness index	0.13	0.31
11	Proximity to coast line	0.13	0.25
12	Seismic intensity	0.12	0.31
13	Proximity to drainage network	0.07	0.11
14	Aspect	0.04	0.51
15	Profile curvature	0.01	0.22
16	Curvature	0.00	0.26

Among the initial data set comprising 16 environmental factors, 7 factors: elevation, slope, precipitation, geology, land cover, terrain forms, and seismic acceleration, were the most important factors, coupling SI index and σ_i (Table 1).

Logistic Regression

In order to estimate the landslide susceptibility for the Greek territory the Logistic Regression Model (Hosmer and Lemeshow 1989) was also adopted. Logistic Regression (LR) is a multivariate analysis model for predicting the presence (or the absence) of a phenomenon (in this case of a landslide) based on the values of predictor variables. The main idea is to assess a predictive relationship – via formulation – between landslides and factors influencing landsliding. Logistic regression modelling incorporates effectively different kind of variables (continuous / discrete). Additionally, in this method the variables do not have to follow normal distribution. As landsliding is a complex multivariate geomorphological procedure, and the factors contributing to landlsiding are nonlinear in nature, LR is a powerful method for landslide susceptibility assessment.

The logistic regression formula is the following:

$$y = \frac{1}{1 + \exp(-\sum a_i x_i)} \quad (5)$$

where a_i = regression coefficients. x_i = variables. a_o the zero coefficient (constant) and $x_o = 1$.

The sumGRID is calculated through (6):

$$sumGRID = -4.418 + (0.006GEO) + (0.011LC) + + (0.004TC) + (0.048SL) + (0.210ACC) + (0.002PRE) + +(-0.001ELEV) \quad (6)$$

The map of probability for landslide occurrence is calculated. The final output is in raster format with values between 0 (minimum landslide susceptibility) and 1 (maximum landslide susceptibility), (7):

$$LSI = \frac{1}{1 + \exp(sumGRID \times (-1)} \quad (7)$$

Artificial Neural Networks Model

Artificial neural networks (ANNs), take their name after the networks of biological nerve cells. Back-propagation (BP) algorithm is the most widely used of the supervised learning neural network paradigms and was successfully applied in many fields of model free function estimation. BP ANN follow a three layer architecture fully connected below and above. The first layer is the input layer, it is the only layer in the network that can receive external input. The second layer is the hidden layer in which the processing units are interconnected to layers below and above. The third layer is the output layer. Units are not connected to other units in the same layer. Each interconnection has associative connection strength, given as weight w. Weights are adjusted during training of the network. The basic mathematical concepts of the back-propagation algorithm are found in Hush and Horne (1993).

A network is said to generalize when it appropriately classifies vectors not in the training set. The common technique is to divide the input vectors available for training into two disjoint sets and use just one of these, for training and a second one (10 % in this case), for test set. The data set used in LR method was also used for training with ANN. After training is the test set is used, so as to evaluate prediction efficiency of the network.

A network structure of 7-200-1 was created and trained with BP Levenberg – Maquardt, algorithm. using learning rate 0.1. The initial weights were random. The training data set were normalized between [−1. 1]. Trying to achieve the best network's performance, several networks with different architectures were developed using the variations of the back-propagation algorithm available in MATLAB. The number of epochs was set to 5,000 and the root mean square error goal for stopping criterion was set to 0.2. The network converged after 2,000 epochs. The mean square error for the training is also calculated through linear regression with R = 0.78.

The final weights were applied to the entire data set and the landslide susceptibility index (LSI) was then calculated, for the whole data set, according to (8).

$$LSI = (0.16 \times GEO) + (0.14 \times LC) + (0.15 \times TF) + (0.14 \times SL) + +(0.16 \times ACC) + (0.15 \times PRE) + (0.14 \times ELEV) \quad (8)$$

Results: Validation

Using the methodologies described above, three different mass movement susceptibility maps were created for Greece. Geographic representations of the model predictions show satisfactory results for the three models. This emerges from the comparison between the mass movement inventory map (Fig. 1) and the mass movement susceptibility maps resulting from FR, LR, and ANN (Fig. 2). The mass movement susceptibility analysis result was verified using the test set (10 % of the initial training set). Validation was performed by comparing the location of test data and the final maps. The density of mass movement occurrences was highly correlated to medium to high susceptibility levels, Table 2 summarize the results of the analysis. The output mass movement susceptibility map produced according to Logistic Regression (LR) model showed 85.33 % of the events coincide with medium to very high susceptibility class. in prediction accuracy of the total area of Greece. The susceptibility index model showed s_{ij} 71.62 % and Artificial Neural Network (ANNs) showed 60 %. The map obtained from LR is more accurate than the other models. Accuracies of the two other models can be evaluated relatively similar.

The areas of very high susceptibility are more or less located in the same geographic regions across Greece for all methods. These areas are in the western and mountainous part of Greece (Pindos ridge and its south expansion in Peloponnese), in Crete and some other pockets across Greece mainland.

Discussion: Conclusions

The developed susceptibility maps show that area classified as medium to very high susceptibility contain 60–85 % of the mass movements of the test set. The combined maps produced from the three models gave a prediction accuracy of 74.67 %. These areas generally have elevation 300–1,100 m, slope angle 9–25°, mean annual precipitation 300–600 mm, they are mainly dominated, from flysch or

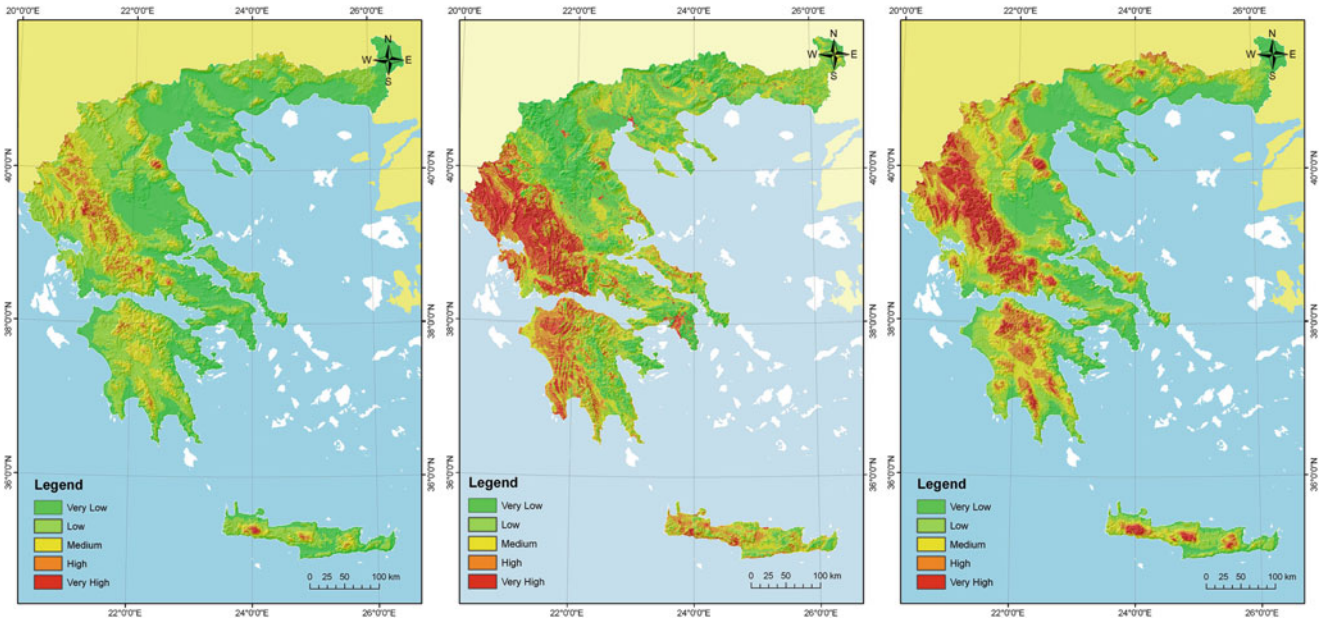

Fig. 2 Mass movement susceptibility mapping based on FR, LR and ANN

Table 2 Mapping results for test set

Susceptibility	Statistical index		Logistic regression		Artificial neural network	
	Nr of landslides	Percentages	Nr of landslides	Percentages	Nr of landslides	Percentages
Very low	2	2.67	4	5.33	16	21.33
Low	20	27.03	7	9.33	14	18.67
Medium	26	35.14	17	22.67	15	20.00
High	22	29.73	14	18.67	18	24.00
Very high	5	6.76	33	44.00	12	16.00

transition zone formations and Neogene sediments, and are used as agricultural areas.

It can be concluded that most of the predictions is related to the noise that characterizes data due to very small scale of study, with reference to both input and output variables. The output value, in particular, could be affected by two different kinds of noise: the first, which is relevant also to input variables, is essentially connected to inherent inventory mistakes. The inefficiency in accuracy of ANN is probably attributed to the internal rating of the parameters from each methodology. ANN rate elevation as an important factor, though LR model coefficient for elevation is very low. Precipitation is high according to ANN and a very low value according LR. The coding of the parameters could also affect, the results, of the ANN prediction, as the parameters were coded through landslide density.

The methods used in this study are valid for generalized planning and assessment purposes, although they may be less useful at the site-specific scale, where local geological and geographic heterogeneities may prevail. For the method to become more efficient and increase prediction results more mass movement data are needed in order to retrain the models in a more realistic mode, following less assumptions, and study more parameters taking advantage of ANN model free capabilities.

References

Aleotti P, Chowdhury R (1999) Landslide hazard assessment: summary review and new perspectives. Bull Eng Geol Environ 58:21–44

Ayalew L, Yamagishi H (2005) The application of GIS-based logistic regression for landslide susceptibility mapping in the Kakuda-Yahiko Mountains, Central Japan. Geomorphology 65 (1–2):15–31

Bornovas I, Rondoyanni-Tsiambaou T (1983) Geological map of Greece, scale1:500,000. IGME, Athens

Carrara A, Cardinali M, Detti R, Guzzetti F, Pasqui V, Reichenbach P (1991) GIS techniques and statistical models in evaluating landslide hazard. Earth Surf Process Landf 16:427–445

Castellanos EA, van Western CJ (2008) Qualitative landslide susceptibility assessment by multicriteria analysis: a case study from San Antonio del Sur. Guantánamo. Geomorphology 94(3–4):453–466

Cruden DM, Varnes DJ (1996) Landslide types and processes. In: Turner AK and Schuster RL (eds) Landslides investigation and mitigation. Special report 247, Transportation Research Board. National Academy of Sciences, Washington, DC

Cumer A (1994) Il progetto CORINE Land cover in Italia: un modello da seguire Documenti del territorio Anno VIII N. 28/29 giugno/dicembre (in Italian)

Dikau R, Brunsden D, Schrott L, Ibsen M (eds) (1996) Landslide recognition, identification movement and causes. Wiley, Chichester, 251 pp

Ercanoglu M, Gokceoglu C (2001) Assessment of landslide susceptibility for landslide-prone area (north of Yenice, NW Turkey) by fuzzy approach. Environ Geol 41:720–730

Glade T, Dikau R, Bell R (2003) National landslide susceptibility analysis for Germany. In: European Geophysical Society (eds) Abstracts – Joint Assembly, Nice (Frankreich) 10 April

Gournelos T, Chalkias C, Tsagkas D (2006) Landslide susceptibly zonation of Greece using fuzzy logic rules and GIS. Geographies 12:114–126 (in Greek)

Guzzetti F, Carrara A, Cardinali M, Reichenbach P (1999) Landslide hazard evaluation: a review of current techniques and their application in a multi-scale study. Geomorphology 31:181–216

Hansen A (1984) Landslide hazard analysis. In: Brundsen D, Prior DB (eds) Slope instability. Wiley, New York, pp 523–602

Heyman Y, Steenmans C, Croisille G, Bossard M (1994) "CORINE land cover project" technical guide. European Commission, Directorate General Environment, Nuclear Safety and Civil Protection, ECSC-EEC-EAEC, Brussels/Luxembourg, 136 pp

Hosmer DW, Lemeshow S (1989) Applied logistic regression. Wiley, New York

Hush DR, Horne GB (1993) Progress in supervised neural networks "What's new since Lipman". IEEE Signal Process Mag 8–39

Koukis G, Ziourkas C (1991) Slope instability phenomena in Greece: a statistical analysis. Bull Int Assoc Eng Geol 43:47–60

Koukis G, Tsiambaos G, Sabatakakis N (1996) Landslides in Greece: research evolution and quantitative analysis. In: Senneset K (ed) Proceedings of the 7th international symposium on landslides, Balkema, Rotterdam, pp 1935–1940

Koukis G, Rozos D, Hadzinakos I (1997) Relationship between rainfall and landslides in the formations of Achaia. In: Marinos PG, Koukis GC, Tsiambaos GC, Stournaras GC (eds) Proceedings of the symposium on engineering geology and environment, Balkema, Rotterdam, pp 793–798

Koukis G, Sabatakakis N, Nikolaou N, Loupasakis C (2005) Chapter 37, Landslide hazard zonation in Greece. In: Proceedings of the open symposium on landslide risk analysis and sustainable disaster management by international consortium on landslides, Washington, DC, USA, pp 291–296

Lee EM, Jones DKC (2004) Landslide risk assessment. Thomas Telford, London, pp 454

Lee S, Talib JA (2005) Probabilistic landslide susceptibility and factor effect analysis. Environ Geol 47:982–990

Leroi E (1996) Landslide hazard – risk maps at different scales: objectives, tools and developments. In: Senneset K (ed) Landslides-Glissements de terrain. VII international symposium on landslides, Trondheim, Norway. Balkema, Rotterdam, pp 35–51

Leventhal AR, Kotze GP (2008) Landslide susceptibility and hazard mapping in Australia for land-use planning – with reference to challenges in metropolitan suburbia. Eng Geol 102:238–250

Nadim F, Kjekstad O, Peduzzi P, Herold C, Jaedicke C (2006) Global and avalanche hotspots. Landslides 3:159–173

Papadopoulos GA, Plessa A (2000) Magnitude – distance earthquake-induced landslides in Greece. Eng Geol 58:377–386

Smith K, Petley DN (2009) Environmental hazards. Routledge, New York

Soeters R, van Westen CJ (1996) Slope instability recognition. Analysis and zonation. In: Turner AK, Schuster RL (eds) Landslides, investigation and mitigation. National Academy Press, Washington, DC (Transportation Research Board, National Research Council, Special report, 247), pp 129–177

Van Westen CJ, Rengers N, Soeters R (2003) Use of geomorphological information in indirect landslide susceptibility assessment. Nat Hazards J Int Soc Prev Mitig Nat Hazards 30(3):399–419

Yilmaz I (2009) Landslide susceptibility mapping using frequency ratio, logistic regression, artificial neural networks and their comparison: a case study from Kat landslides (Tokat – Turkey). Comput Geosci 35:1125–1138

Probabilistic Landslide Hazard for El Salvador

Carlos Eduardo Rodríguez-Pineda and Jairo Yepes-Heredia

Abstract

A new method for assessing landslide hazard was proposed and implemented in El Salvador. In this method hazard is defined as a conditional probability of failure due to rainfalls or earthquakes which are in turn dependent on the slope susceptibility.

Total probability was obtained considering probability and susceptibility functions for different slope failure mechanism, this is: coherent, disrupted slides, and flows; and using conditional probability for conditioned events. The application for El Salvador evaluated the landslide hazard for cells of 1 × 1 km; topographical, rainfall and seismicity data was obtained from the SNET in El Salvador.

Probability of failure for rainfall-induced and earthquake-induced landslides and total probability of failure was calculated for the whole country and spatial hazard distribution was plotted and hazard maps for each case were obtained. Hazard maps fit very well with rainfall-induced and earthquake-induced distribution of historical landslides in El Salvador and can be used as a risk management tool.

Keywords

Probabilistic landslide hazard • Rainfall induced landslides • Earthquake-induced landslides • Landslide hazard in El Salvador

Introduction

In this paper a method for assessing landslide hazard was developed and applied to El Salvador. This method calculates slope failure probability taken into account rainfalls and earthquakes as conditional events prior the landslide failure.

El Salvador is a small Central American country which has been historically affected by large and destructive landslides triggered by rainfalls as those induced during the Mitch Hurricane (Crone et al. 2001), and by moderate and strong earthquakes as those induced during the 1986 and 2001 earthquakes (Rodríguez 2007).

The main factors, besides rainfalls and earthquake, which conditioned landslide occurrence in El Salvador, are the topography, soil susceptibility and land cover and use (Baroň et al. 2007). Some previous hazard maps have been proposed for the country mainly based on previous events distribution (SNET 2011). Application of heuristic models as that proposed by Mora and Varhson (1994) have also been modified and used in order to produce landslide hazard maps in this country (Escobar et al. 2003), however a quantitative model as that proposed in this paper have not been used so far in this region.

Rainfall-induced probability was obtained by multiplying the probability of occurrence of a critical rainfall by the probability of landslide given that critical rainfall by a

C.E. Rodríguez-Pineda (✉)
Departamento de Ingeniería Civil, Pontificia Universidad Javeriana, Calle Calle 40 No 5-50, Bogotá D.C, Colombia

Universidad Nacional de, Bogotá, Colombia
e-mail: crodriguezp@javeriana.edu.co

J. Yepes-Heredia
Universidad Nacional de, Bogotá, Colombia

C. Margottini et al. (eds.), *Landslide Science and Practice*, Vol. 1,
DOI 10.1007/978-3-642-31325-7_43,

susceptibility factor. The probability of occurrence of the critical rainfall was obtained from an analysis of historical cases in El Salvador and using I-D-F curves; the probability of slope failure given the critical rainfall was obtained from a statistical analysis of rainfall-induced landslides in volcanic soils in Central America; finally, the susceptibility factor is based on a exponential function of the slope angle which was obtained from statistical analysis of landslide events.

The earthquake-induced probability of failure was calculated by multiplying the probability of occurrence of a given earthquake by the probability of the slope failure given this earthquake by a susceptibility factor. The probability of occurrence of a given earthquake acceleration at the slope site was obtained by considering the spatial distribution of different seismic sources, the recurrence function for each of those sources and appropriated attenuation relationships for El Salvador; the probability of slope failure for a given earthquake was obtained by statistical analysis of magnitude-landslide distance values from historical earthquakes worldwide; susceptibility was defined as an exponential function of slope angle.

Hazard maps for rainfall- and earthquake-induced landslides were obtained. The combined effect of rainfalls plus earthquakes was also used to generate landslide hazard maps. These maps were compared with landslide distribution during rainfalls and earthquakes and with previous hazard maps, it can be see that these maps may be useful in order to define critical areas to be considered in risk mitigation strategies for the country.

General Setting

Topography, seismicity, and rainfall data was supplied by the SNET in El Salvador, a brief description of the general setting is included in this section.

Physiography

Figure 1 shows the morphological map of El Salvador where different geographic regions can be identified.

In El Salvador four physiographic zones can be identified which have in general east–west trend and are almost parallel to the Pacific Coast to the South.

North area in the country is a mountainous zone called *Montaña Fronteriza* where landslides have been associated with intense rainfalls. Southward the cordillera a wide valley, *Interior Valley*, is formed between the north cordillera and the volcanic chain, rainfall and earthquake landslides are common in this area. *Central zone* is a volcanic area where active volcanoes; in this area rainfall and earthquake induced landslides have been triggered in the past

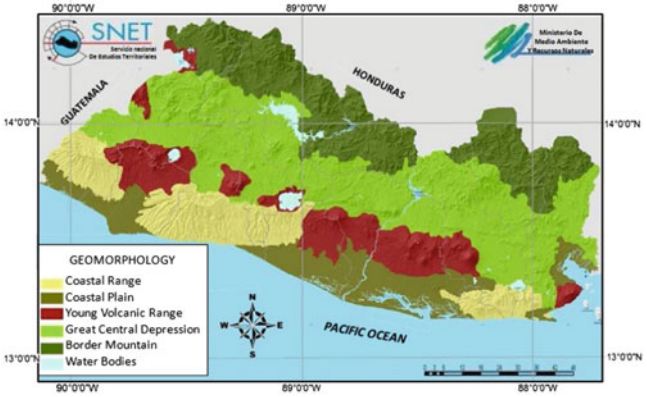

Fig. 1 Physiographic map of El Salvador (Modified from SNET 2011)

(Rodríguez 2007; Crone et al. 2001). In the southern area three different *coastal cordilleras* are observed, near Guatemala the Tacuba, in the central zone the El Balsamo and near the Fonseca Golf the Jucuarán Cordilleras, earthquake and rainfall-induced landslides have been reported in this region; some flat areas are also identified near the Pacific coast where alluvial and coastal deposits are common, no landslides have been reported in this area except those related to river banks erosion.

Geology

Most superficial lithological units in El Salvador are from the Pleistocene period, whereas deeper units are from the Pliocene and Miocene periods. Sedimentary and volcanic units are the most common units. Marine sedimentary units have been identified only to the north of the country near Metapán. Fluviatile and lacustrine sedimentary units can also be observed which usually include beds of pyroclastic deposits which come from volcanic activity. In flat zones alluvial deposits of the main rivers are common.

Most of the country shows volcanic extrusive units mainly interbedding of andesites and basalts, which can be observed in the southern cordilleras and along the volcanic chain, recent pyroclastic deposits are common in these regions. Some intrusive units can be identified particularly forming the northern cordillera near Metapán and Chalatenango (Baxter 1999).

Climate

Due to the Pacific Ocean influence the climatic conditions in El Salvador are controlled by the Inter-tropical Confluence Zone and by some local anomalies. This country shows a dry season between November and April, and a rainy season between May and October. Average annual rainfalls vary

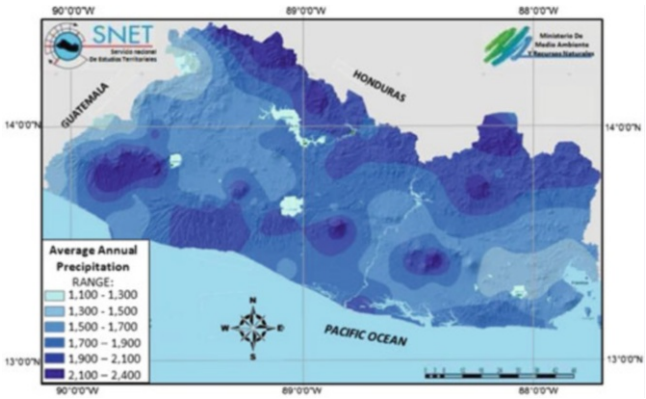

Fig. 2 Average annual rainfall distribution in El Salvador. Average for data between 1971 and 2001 (Modified from SNET 2011)

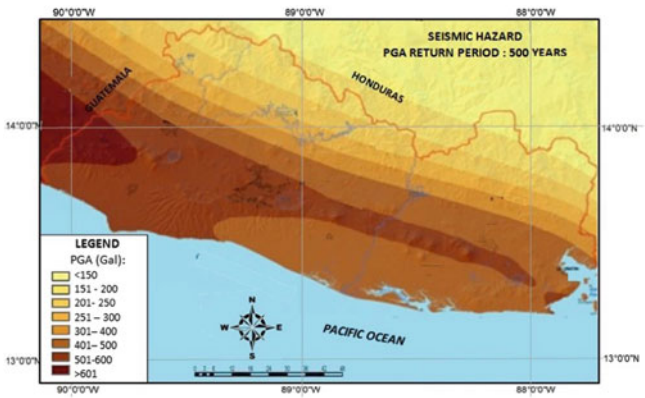

Fig. 3 Seismic hazard map for a return period of 500 years in El Salvador (From SNET 2011)

between 1,100 and 2,500 mm. Figure 2 shows the spatial distribution of average annual rainfalls in the country. Mean temperature is about 27.5 °C in the coastal zone with maxima between march and April, 38 °C to the east and 32 °C in the central and western zones; minimum temperature values range between 16 °C and 18 °C in January. Northen cordillera controls the influence of the trade winds from the Caribbean Ocean, inducing a low rainfall in the country compared with those that have coast along the Caribbean Ocean as Costa Rica (Yepes 2009).

Seismicity

Deep focus earthquakes (h > 200 km) are related to the subduction of Cocos Plate beneath the Caribbean Plate along the Central American Fault (Burbach et al. 1984) and are events of large magnitudes, commonly higher than 6.0 reaching values as high as 8.0.

Shallow earthquakes (h < 20 km) are tectonic events linked to the volcanic chain (White 1991), magnitude of these events range between 5.5 and 6.5 (White 1991). Intermediate depth earthquakes occur along the subduction zone with magnitudes larger than 6.0 (Dewey and Suárez 1991).

El Salvador seismic activity is also influenced by activity along the boundary between the Caribbean and the North American plate, however this seismogenic source have not produced important effects in the country. Figure 3 shows the seismic hazard map for a return period of 500 years in El Salvador.

Analysis Method

Landslide hazard was defined as failure probability taken into account rainfall, earthquake and slope susceptibility effects. In this section the method used to obtain that probability is briefly explained.

Total Probability

Total probability of failure of a given slope is obtained with (1), where the probability of failure due to a given rainfall and that due to an earthquake are considered statistically as exclusive events.

$$P_t(F) = P(R) + P(S) - (P(R) \cdot P(S)) \tag{1}$$

Pt(F) is the total probability of failure, P(R) is the probability of failure due to rainfalls and P(S) is the probability of failure due to earthquakes.

P(R) is obtained by using (2), where p^r is the probability of occurrence of a given critical rainfall, p^{fr} is the probability that the critical rainfall induce landslide in the slope, and S is a function that defines the slope susceptibility to landsliding.

$$P(R) = p^r \cdot p^{fr} \cdot S \tag{2}$$

P(S) is obtained by using (3), where p^s is the probability of excedence of a given earthquake magnitude, p^{fs} is the probability that the seismic events induce the slope failure, and S the slope susceptibility, in this paper S was consider the same for rainfall- and earthquake-induced landslides.

$$P(S) = p^s \cdot p^{fs} \cdot S \tag{3}$$

Probability of Failure Due to Rainfalls

Probability of a given rainfall (p^r), was obtained from I-D-F curves supplied by SNET for different rainfall stations around El Salvador. I-D-F curves include data for return periods between 5 and 50 years.

In order to define critical rainfalls allowable to induced landslides, a database of rainfall-induced landslides in volcanic ashes in Central America was compiled, and rainfall

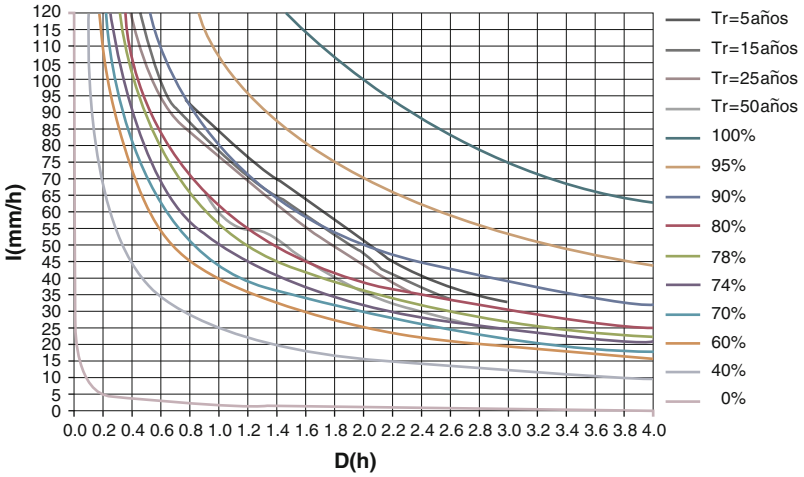

Fig. 5 Critical rainfalls and landslide density curves for the Observatorio Station in San Salvador

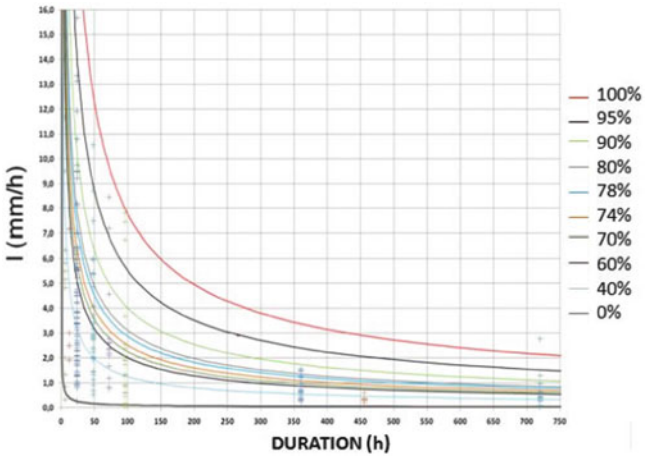

Fig. 4 Landslide density curves for rainfall-induced landslides in Central America

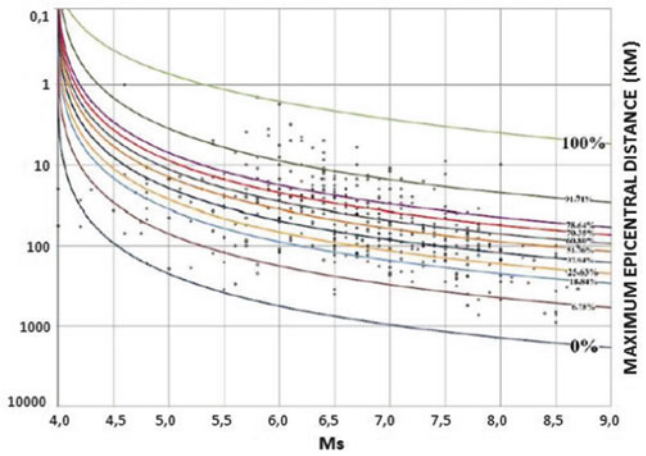

Fig. 6 Landslide density as a function of earthquake magnitude and epicentral distance

intensity vs rainfall duration for each case was plotted in order to obtain curves of density of landslides, defined as upper limit lines that involve a given percentage of the events in the database. Those curves are shown in Fig. 4.

Crossing I-D-F- curves with landslide density curves allows defining the probability that a given rainfall induce landslide in a given slope (p^{fr}), as shown in Fig. 5 for the Observatorio Station in San Salvador.

Probability of Failure Due to Earthquakes

Probability of excedence of a given earthquake with magnitude M (p^{s}) was obtained considering a Poisson model and an appropriate recurrence functions as the Gutemberg-Richter type, for different seismogenic sources for El Salvador. Data for obtaining probability of seismic events was obtained from the Regional Seismic Hazard Project for El Salvador from Benito (2009).

Probability of failure of a given slope due to an earthquake of magnitude M (p^{fs}) was obtained using the database obtained by Rodriguez (2001) and complemented by Yepes (2009). Maximum epicentral distance of different landslide mechanism, as defined by Keefer (1984), was obtained from the database and plotted as a function of earthquake magnitude, and different landslide density curves were defined as upper limit lines that involved a given percentage of cases into the database, as shown in Fig. 6. Total probability was obtained integrating along the whole area of seismic sources, which were divided in unit areas of 1 km^2.

Slope Susceptibility

In order to consider slope susceptibility into the analysis a function was obtained from a landslide database compiled by Rodríguez (2001). A sinus function was initially used but that gives too high weighting values for low slope angles,

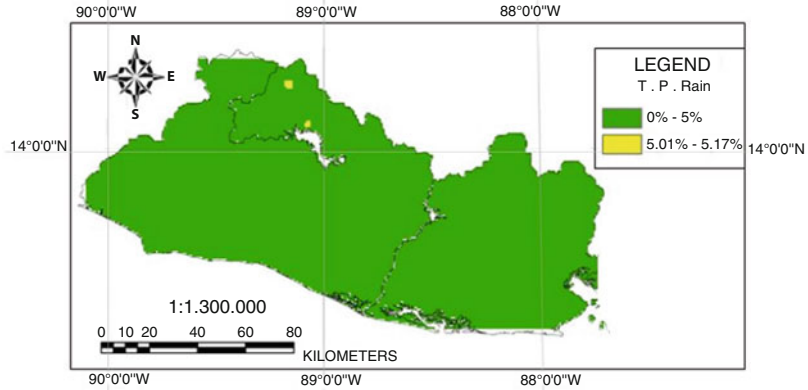

Fig. 7 Hazard map for rainfall-induced landslides due to a rainfal of 1 year of return period

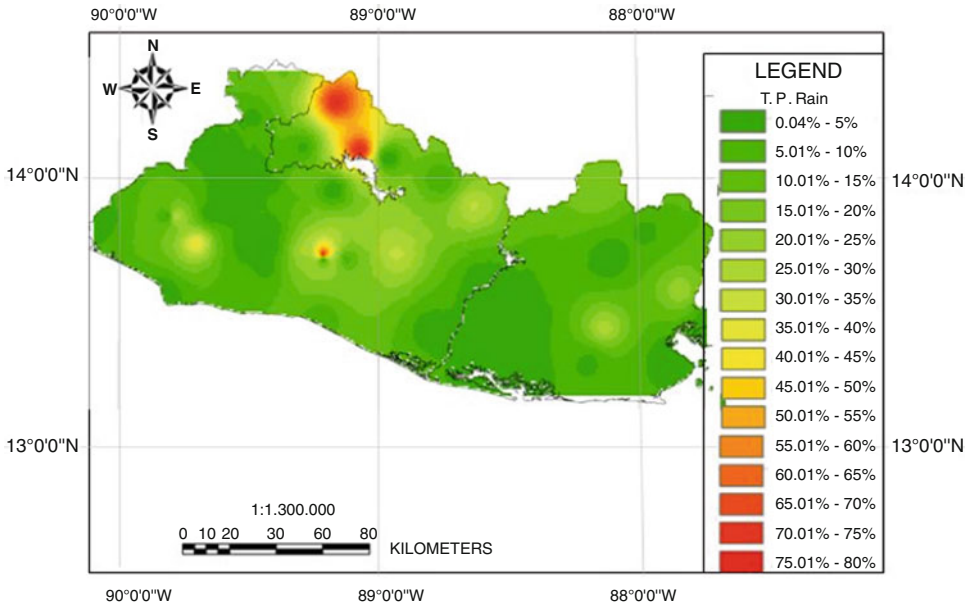

Fig. 8 Hazard map for rainfall-induced landslides for a rainfall with return period of 50 years

than an exponential function was tested and good results were obtained. Function used is included as (4).

$$S = 1 - e^{-10 \cdot \theta^4} \tag{4}$$

where θ is the slope angle in radians.

Results

Previous method was used in El Salvador in order to obtain landslide hazard maps for events induced by rainfalls, by earthquakes and combining rainfalls and earthquakes.

Hazard Maps for Rainfall-induced Landslides

Maps were obtained for events with different return periods. Hazard map for a rainfall with 1 year of return period is shown in Fig. 7, whereas map for a rainfall of 50 years of return period is shown in Fig. 8.

These maps show the spatial distribution of slope failure probability. For a rainfall with a short return period, that is a low intensity and short duration rainfall, slope failure probability is very low (less than 5 %), whereas for a large return period rainfall, that is a very intense and large duration rainfall, northen cordillera and central volvanic areas show high slope failure probabilities (larger than 30 %) in most areas. These maps show that north western zone and central volcanic zones, are highly susceptible to rianfall-induced landalides.

Hazard Maps for Rainfall-induced Landslides

For earthquake-induced landslides hazard maps, for earthquakes of 1 year and 50 years of return period are shown in Figs. 9 and 10, respectively.

For low magnitude earthquakes Fig. 9 shows for most of the country low slope failure probabilities, however even for

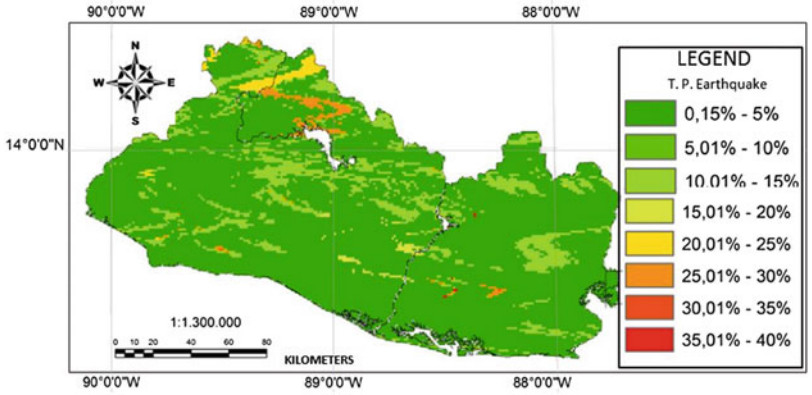

Fig. 9 Hazard map for earthquake-induced landslides for an earthquake with return period of 1 year

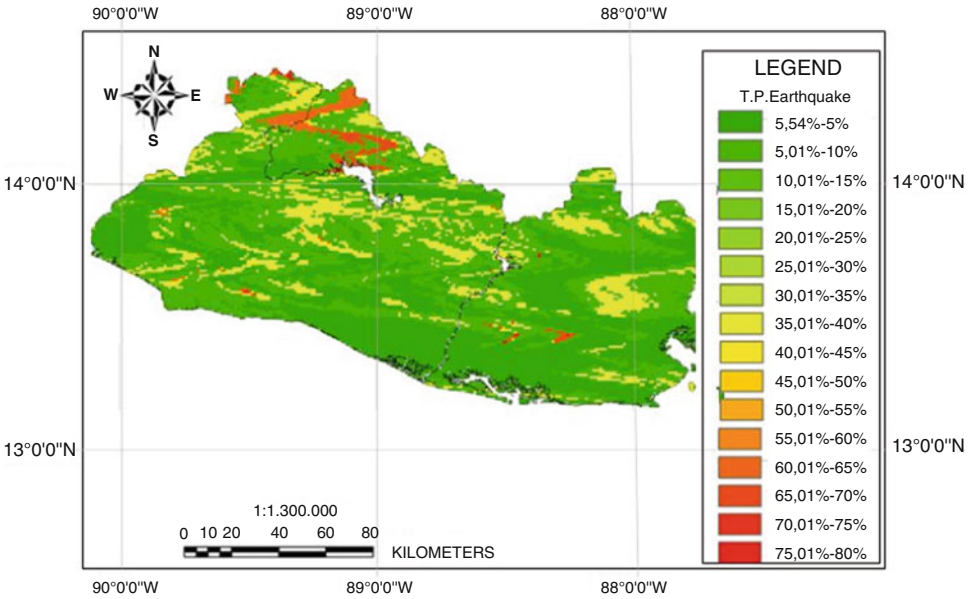

Fig. 10 Hazard map for earthquake-induced landslides for an earthquake with return period of 50 years

these small earthquakes it can be seen some spot areas where failure probability are quite high, for instance in the north western area (boundary coordillera) and along central volcanic chain, probabilities ah high as 25 % were obtained.

For earthquakes with return period of 50 years high failure probabilities, larger tha 30 %, are widespread around the country showing a very high slope susceptibility to earthquakes.

Hazard Maps Combining Rainfall and Earthquake Effects

The combined effect of rainfall and earthquake in landslide hazrd was calculated by using the total probability of independent events as it was explained above. Figures 11 and 12 show hazard maps for events with a return period of 1 year and 50 years, respectively.

Figures 11 and 12 show that the comibined effect of rainfall and earthquakes increased significantly slope failure probability.

Slope Susceptibility Map for El Salvador

The SNET has published a slope susceptibility map showing the areas more susceptible to landsliding around the country, this map is included as Fig. 13. It can be seen that north western area of the boundary coordillera and central volcanic area are the most susceptible to landslides showing a good agreement with maps obtained with present method, this suggesting that this method may be applied with reasonable reliability to obtain hazard maps including the combined effect of rainfalls and eartquakes.

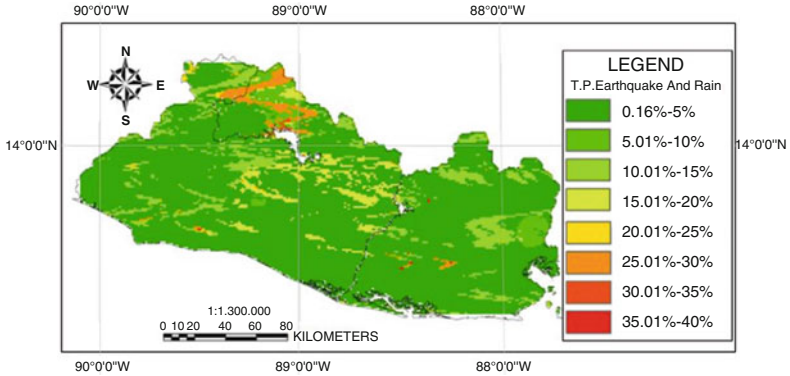

Fig. 11 Landslide hazard map including the combined effect of earthquake and rainfalls with a return period of 1 year

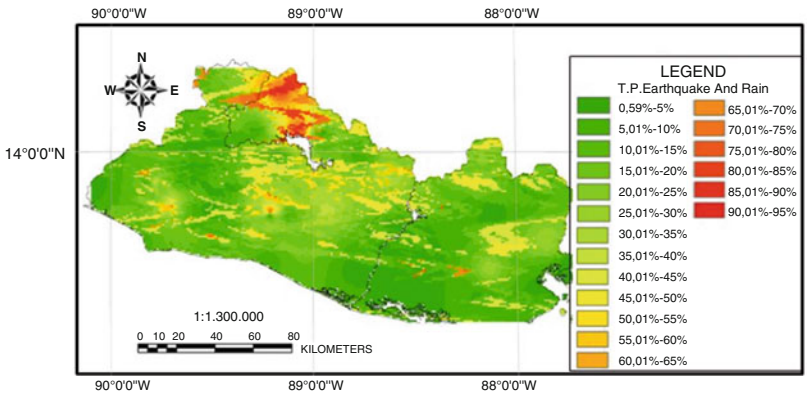

Fig. 12 Landslide hazard map including the combined effect of earthquake and rainfalls with a return period of 1 year

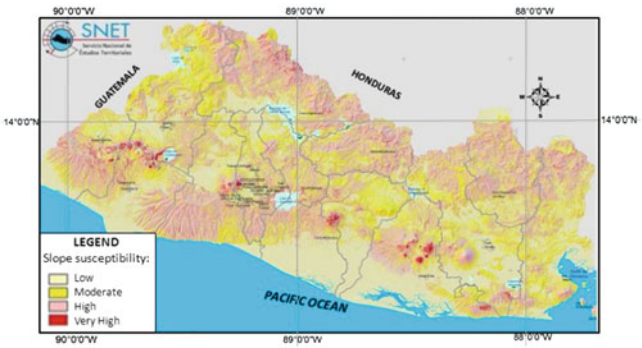

Fig. 13 Slope susceptibility map for El Salvador (Modified from SNET 2011)

Conclusions

A new method for landslide hazard assessment is presented in this paper, this method calculates the slope failure probablity conisdering the combined effect of rainfalls and earthquakes with different return period, which allows obtaining hazard maps for different total probabilities.

The method was applied in order to produce hazard maps for El Salvador, obtaining that the north western area of the boundary coordillera and central volcanic area are the most susceptible regions to landsliding. This result is in a good agreement with the slope susceptible map published by SNET (2011).

Acknowledgments Authors wish to thank the Servicio Nacional de Estudios Territoriales (SNET) from El Salvador for the support in obtaining important data for this paper, special thanks are given to Manuel Diaz and Raquel Orellana who supplied unpublished data. Thanks are also given to Juan Camilo Pineda for editing figures for this paper.

References

Baroň I, Kycl P, Hradecký P, Metelka V, Vorel T, Šebesta J, Hernández W, Chávez G, Alvarado A, Huapaya S (2007) Identifying the areas susceptible to landsliding and other hazardous processes in El Salvador, Nicaragua and Costa Rica, Central America. In: Proceedings of the 1st North American landslide conference, Vail

Baxter S (1999) Geologic map of El Salvador Scale 1:500000. Instituto Internacional HERMES

Benito B (2009) Evaluación Regional de la Amenaza Sísmica en Centroamérica - Proyecto RESIS II Final Report. Universidad Politécnica de Madrid, Madrid, 21p

Burbach GV, Forhlich C, Pennington WD, Matumoto T (1984) Seismicity and tectonics of the subducted Cocos Plate. J Geohys Res B 89(B9):7719–7735

Crone AJ, Baum RL, Lidke DJ, Sather DND, Bradley LA, Tarr AC (2001) Landslides induced for Hurricane Mitch in El Salvador-An inventory and descriptions of selected features. Open-File Report 01–444. U.S. Geological Survey. Denver, 24p

Dewey JW, Suárez G (1991) Seismotectonics of middle America. In Neotectonics of North America, Slemmons et al. (eds) Geological Society of America, Decade Map, vol 1. pp 309–321

Escobar HE, Escobar MR, Rendón JR (2003) Caracterización geotécnica de las formaciones geológicas del área metropolitana de San Salvador y aplicación a la evaluación de amenaza por deslizamientos. Civil Engineering Dissertation, Universidad Centroamericana "José Simeón Cañas", San Salvador, El Salvador

Keefer DK (1984) Landslides caused by earthquakes. Geol Soc Am Bull 95:406–421

Mora S, Vahrson W-G (1994) Macrozonation methodology for landslide hazard determination. Bull Assoc Eng Geol 31(1):49–58

Rodríguez CE (2001) Hazard assessment of earthquqake-induced landslides on natural slopes. Ph.D. thesis, Imperial College, University of London, London, UK

Rodriguez CE (2007) Earthquake-induced landslides in Central America. In: Bundschuh J, Alvarado GE (eds) Central America geology resources hazards. Taylor and Francis, London, 1331p. ISBN 13:978-0-415-41647-4

SNET. Servicio Nacional de Estudios Territoriales (2011) URL:http://www.snet.gov.sv. Last accessed 26 June 2011

White RA (1991) Tectonic implications of upper-crustal seismicity in Central America. Neotectonics of North America, Slemmons et al. (eds) Geological Society of America, Decade Map, vol 1. pp 323–338

Yepes JE (2009) Implementacion De Un Modelo Estocástico Para Evaluar Amenaza De Deslizamientos. M.Sc. dissertation, Universidad Nacional de Colombia, Bogotá

Hazard Zoning in Areas with Major Deep-Seated Landslides: Case Study from Switzerland

Daniel Tobler and Hans-Rudolf Keusen

Abstract

The large, deep-seated Gryfenbach landslide in Lauterbrunnen, Switzerland, endangers part of the village as well as the main entrance to the whole valley. A mass of about 25 million m^3 is situated at the left valley entrance and moves with an average of cm a year. In the steep frontal part of the sliding mass two large spontaneous landslides have been recorded (secondary processes). Following the abnormally intensive snowmelt in spring 1999 the movement increased 30-fold. Important infrastructures within the landslide were destroyed. A complicated monitoring system has been installed to understand the landslide's behaviour and hazard potential in detail.

At the same time the authorities start to elaborate the hazard map of the valley. Through extensive field investigations, analyses of monitoring data and conclusions by analogy from other large landslides the relevant scenarios for the hazard assessment have been formulated. In 2003 the first draft of the hazard map existed GEOTEST AG (Technischer Bericht zur Gefahrenkarte Lauterbrunnen, Nr. 00063.5, Zollikofen (unpublished), 2003), see Fig. 10). In 2011 a revised hazard map has been published GEOTEST AG (Lauterbrunnen, Naturgefahren, Bericht zur Teilrevision Gefahrenkarte, Nr. 10151.01, Zollikofen (unpublished), 2011). This product is based on today's hazard assessment methods. The paper focuses on the Swiss hazard assessment methodology, on the scenario definition of large, deep-seated landslides illustrated on the case study in the Lauterbrunnen valley.

Keywords

Landslide hazard assessment • Hazard map • Case study

Introduction

A thorough assessment of the prevailing hazards and risks in a specific region is imperative for any kind of development activity that has a spatial impact. This is particularly important in disaster-prone areas, like narrow valleys dominated by landslides and rock fall processes (Bonnard et al. 2004). Today, a number of tools and instruments are available to analyse, visualize and evaluate major hazards and risks (Lateltin 2009; PLANAT 2011).

In the past few years, Switzerland developed a number of such instruments (e.g. BUWAL 1998, 1999a; PLANAT 2003, 2005a, 2005b; OFAT, OFEE and OFEFP 1997 or Wilhelm 1999). They serve as an indispensable basis for an integrated disaster reduction approach, which is not only being discussed presently in Switzerland, but equally on an international level. The methodology fulfils many of the demands but also gives rise to a number of problems and disadvantages. This refers to the production of the instruments as well as the implementation and transformation of the hazard information into practical use.

D. Tobler (✉) • H.-R. Keusen
GEOTEST AG, Birkenstrasse 15, CH-3052 Zollikofen, Switzerland
e-mail: daniel.tobler@geotest.ch; hansrudolf.keusen@geotest.ch

C. Margottini et al. (eds.), *Landslide Science and Practice*, Vol. 1,
DOI 10.1007/978-3-642-31325-7_44,

The new Federal Ordinances on Flood and Forest Protection (OACE 1994) require the cantons to establish hazard maps which have to be incorporated in regional master plans and local development plans. The cantons are responsible initiating hazard mapping.

Landslide Hazard Assessment

Landslide Classification

The Swiss classification of landslides for hazard mapping relies on AGN (2004). Landslides can be classified according to their estimated depth of the slip surface (<2 m: shallow; 2–10 m: intermediate; >10 m: deep) and the long-term mean velocity of the movements (<2 cm/year: substable; 2–10 cm/year: slow; >10 cm/year: active). Depth and velocity parameters are not always sufficient to estimate the potential danger of a slide. Differential movements must also be taken into account as well as the potential of reactivation of a sliding mass (Lateltin et al. 2005).

Due to heavy precipitation, debris flows and very shallow slides are frequent in Switzerland. Most of them are moderate in volume (<20,000 m^3) and of rapid velocity (1–10 m/s). Debris flows and shallow slides are dangerous and annually cause fatalities and traffic disruptions.

Landslide Phenomena Map

A map of landslide phenomena and an associated technical report record evidence and indications of slope instability as observed in the field. The map presents phenomena related to dangerous processes (e.g. Fig. 1 example of a map of mass movements and water hazard processes) and delineates vulnerable areas.

Field interpretations of these phenomena allow landslide-prone areas to be mapped, based on the observation and interpretation of landforms, on the structural and geotechnical properties of slope instabilities and on historical traces of previous slope failures (Riemer et al. 1988). The different phenomena are represented by different colors and symbols (Lateltin et al. 2005). The recommendations for the uniform classification, representation and documentation of natural processes have been established by the federal administration (OFEE and OFEFP 1995).

Landslide Hazard Map

Hazard assessment implies the estimation of the intensity of an event over time. The hazard is defined as a threatening event or as the probability of a potentially damaging natural

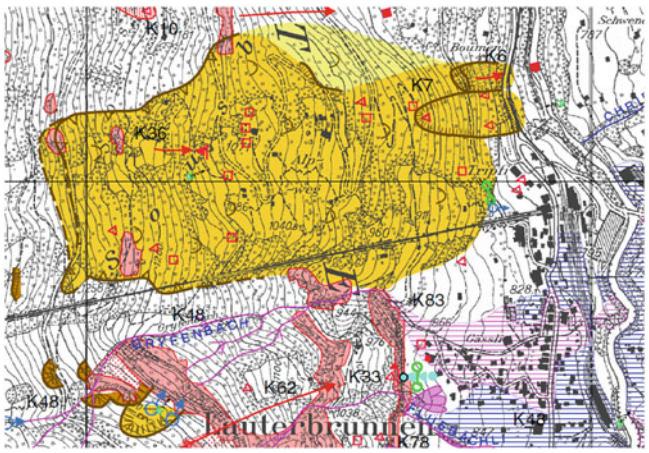

Fig. 1 Landslide phenomena map of the Gryfenbach landslide in Lauterbrunnen (Bernese Oberland, central Swiss Alps). The phenomena map is a major product in hazard assessment (GEOTEST AG 2003). For the legend see OFEE and OFEFP (1995)

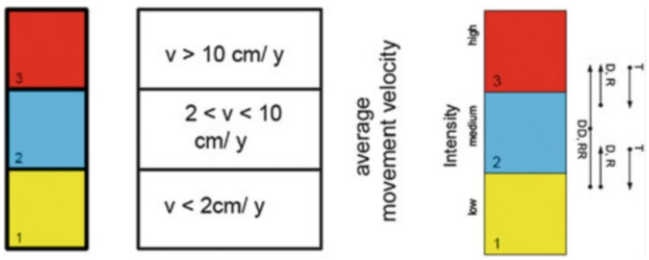

Fig. 2 Classification of landslides for hazard maps (AGN 2004). $_D$, $_R$ and $_T$ indicate an intensification/decrease of the hazard level depending on the reactivation potential ($_R$), the amount of differential movements ($_D$) or the depth of a moving mass ($_T$). Deep-seated landslides (RT) may have code like $RT2_{DR}$

phenomenon within a specific period of time in a given area (IDNDR 1993). Landslides normally correspond to gradual phenomena (constant slides) or unique events (spontaneous, shallow landslides). It is indeed difficult to make an assessment of the return period of a large rock avalanche, or to predict when a dormant landslide may reactivate (Raetzo et al. 2002; AGN 2004).

Most slides are characterized by continuous movements, sometimes with associated phases of reactivation. Herefore three levels of intensity are considered, high, medium and low (Fig. 2).

A low intensity movement has an annual mean velocity of less than 2 cm/year. A medium intensity corresponds to a velocity ranging from 2 to approximately 10 cm/year. The high intensity class is usually assigned to shear zones or zones with clear differential movements. It may also be assigned if reactivated phenomena have been observed or if horizontal displacements greater than 1 m per event may occur (AGN 2004; Lateltin et al. 2005). In the area affected by slides, field intensity criteria can be directly converted to

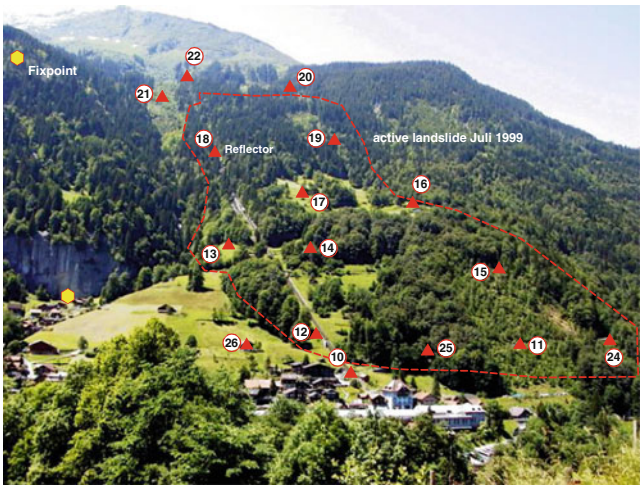

Fig. 3 Landslide of Gryfenbach as an example of a continuous landslide with indication of boundaries and tachymetric measuring points. Without the tachymetrc dataset velocities can hardly defined

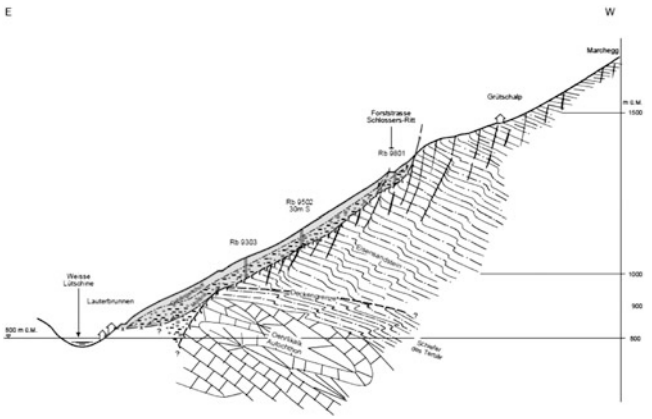

Fig. 4 Geological cross-section through the landslide of Gryfenbach with indication of borehole locations (GEOTEST AG 2007). The weathered and jointed bedrock shows a high hydraulic conductivity which leads to high pore water pressures in the depth. It is one of the major causality for this mass movement

danger classes. Especially with large, deep-seated landslides the difficulty is to define the velocity. The larger the slide the harder is the estimation of velocity without technical support (recordings, surveys, monitoring data, Fig. 3, see also Korup 2006).

Gryfenbach Landslide, Lauterbrunnen

History: Location

The Gryfenbach landslide is located in the sedimentary Helvetic nappes of the Canton Bern, in the central Swiss Alps (Fig. 1). This deep-seated, creeping landslide is extraordinary in many ways, chief amongst which is its

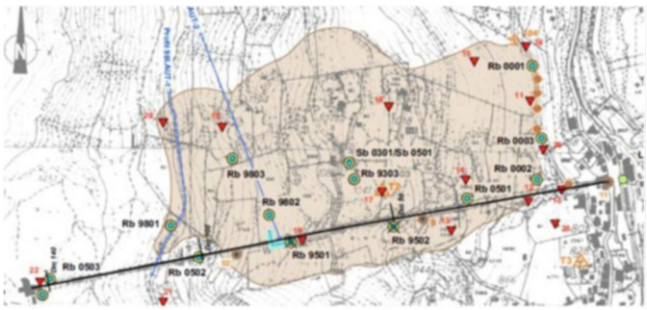

Fig. 5 Landslide with indication of all components of the monitoring system (*circles* = boreholes with inclinometer; *red triangle* = reflector for tachymetric measures, *blue lines* = seismic profiles, *black line* = Lauterbrunnen-Mürren railway; GEOTEST AG 2007)

immense size. The slide mass reaches depths of more than 60 m and incorporates approximately 25 million m^3 of quarternary sediments and weathered bedrock (Fig. 4; Keusen 2000). The bedrock consists of fractured and sagged limestones (Strozzi et al. 2005).

The large, deep-seated landslide endangers part of the village Lauterbrunnen as well as the main entrance to the whole valley. Based on surveys, it could be registered that the average displacement lies between 1 and 2 cm a year. Measurements all over the 30–40 ha landslide area, show an increase of movement in springtime (snow melt) and a decrease in autumn. In the steep frontal part of the sliding mass two large spontaneous landslides have been recorded in 1966 and 1983 (secondary processes, CSD 1973 and CSD 1983). These events buried the two lifelines (main road, railway) for several days. Fortunately there were no fatalities. Following the abnormally intensive snowmelt in spring 1999 the movement increased 30-fold. Important infrastructures within the landslide were destroyed. Interactions with a nearby creek, which is prone to debris flow tightened the situation even more.

Landslide Monitoring

A complicated monitoring system (Fig. 5), consisting of inclinometer drillings, tachymetric measures, pore water pressure measurements, has been installed in the years 1999–2003 to measure the movement and to understand the landslide's behaviour and hazard potential in detail.

The hydrogeological situation is complex (Fig. 6). The water infiltrates in a higher valley, the Soustal. From there the groundwater flows through fractures of the sagged bedrock into the sliding mass and produces an uplift (high pore water pressure) in the frontal part of the landslide.

In the field, the evidences for movements concentrate along the border of the landslide. Within the sliding mass there are nearly no indications of movement. This can be

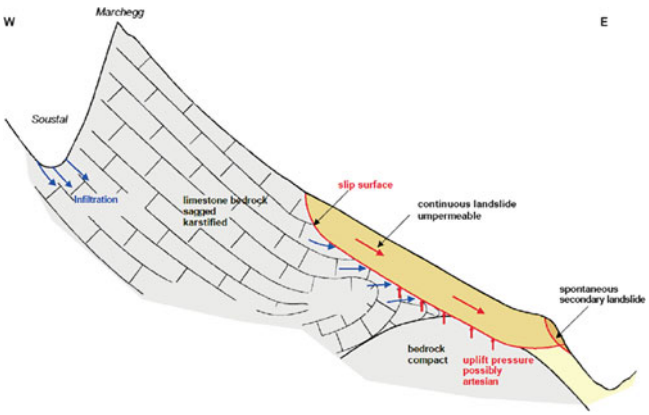

Fig. 6 Schematic cross-section with indication of hydrogeological situation. Water from the Sous valley infiltrates and leads to high pore water pressures at the slip surface (GEOTEST AG 2007)

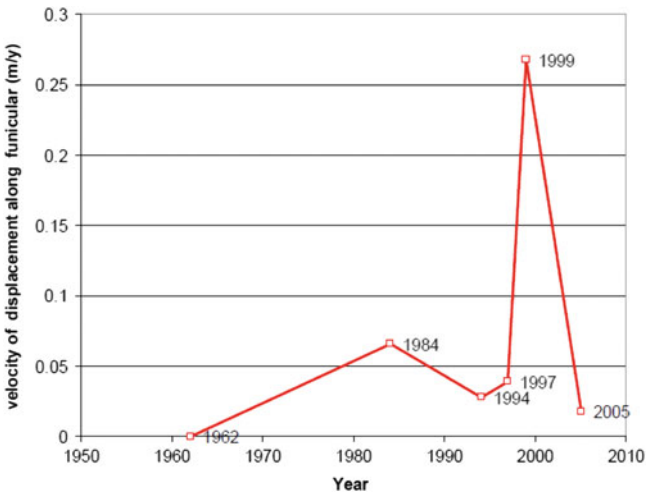

Fig. 7 Velocity of the funicular's displacement during the last 60 years (GEOTEST AG 2007)

justified on one hand by the big depth of the mass; on the other hand through the compact landslide body which moves as a whole.

Landslide Intensity

The first section of the Lauterbrunnen-Mürren Mountain Railway (BLM), which was built in 1891 to facilitate the access to the village of Mürren located on a plateau above Lauterbrunnen, is crosscutting the landslide on its southern fringe (Fig. 3). Whereas average rates of displacement measured on the railway superstructures in the last 100 years were in the order of 20 mm/year before 1999, in the spring of that particular year a displacement rate of 10 mm/day was observed over a short time period (Fig. 7). Overall, a displacement of several decimetres was observed, threatening the operation of the funicular (Strozzi et al. 2005).

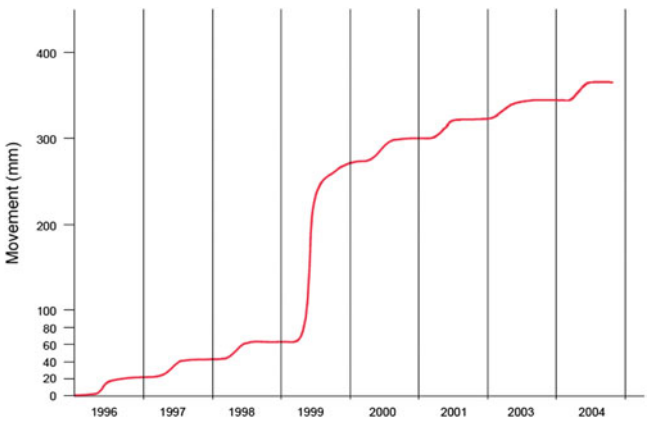

Fig. 8 Monitoring of the landslide's movement between 1996 and 2004. The abnormally intensive snowmelt in spring 1999 intensified the movement to the decuple (10 mm/day) of a normal year

During snowmelt period there seems to be a rapid build-up of pore pressure. It becomes manifest in an acceleration of the movement in early summer (May to June). After the snowmelt the velocities decrease and in winter time the landslide is normally nearly stable (Fig. 8).

The inclinometer measures were carried out once to twice a year. The results confirm the mean yearly displacement rates of the tachymetric measures. In the inclinometer data two different sliding surfaces are visible; a minor one in a depth of about 30 m and the major rupture in 60 m (Fig. 9).

Landslide Hazard Map

With all the information of the monitoring, the field investigations, the historic dataset of past events (spontaneous, secondary landslides in the frontal part) and the recording of the movements before the 1999 event, it is possible to draw the hazard map of the Gryfenbach landslide (Fig. 11).

The average displacement velocities of the deep-seated landslide (RT) are in the central part around 2 cm/year, in the frontal part between 1 and 2 cm/year. According to the Swiss landslide classification for hazard maps (Fig. 2) these movements lead to low (yellow, 1) and medium (blue, 2) hazard intensities. It is well known that this landslide is prone to reactivations (e.g. 1999, indicated by $_{R}$ in the map). This fact will raise the hazard level for one class (yellow to blue, blue to red). The immense depth of the landslide (indicated by $_{T}$ in the map) decreases the hazard level again. The major body of the landslide show a medium hazard level ($RT2_{RT}$).

The frontal part of the landslide is prone to spontaneous secondary slides. This fact was taken into consideration in the hazard map (indicated by D). The depth of the mass movement is here about 10 m. According the recommendations (AGN 2004 and Fig. 2) the hazard level will increase (yellow to blue [$RT1_{DR}$], blue to red [$RT2_{DR}$]) (Figs. 10 and 11).

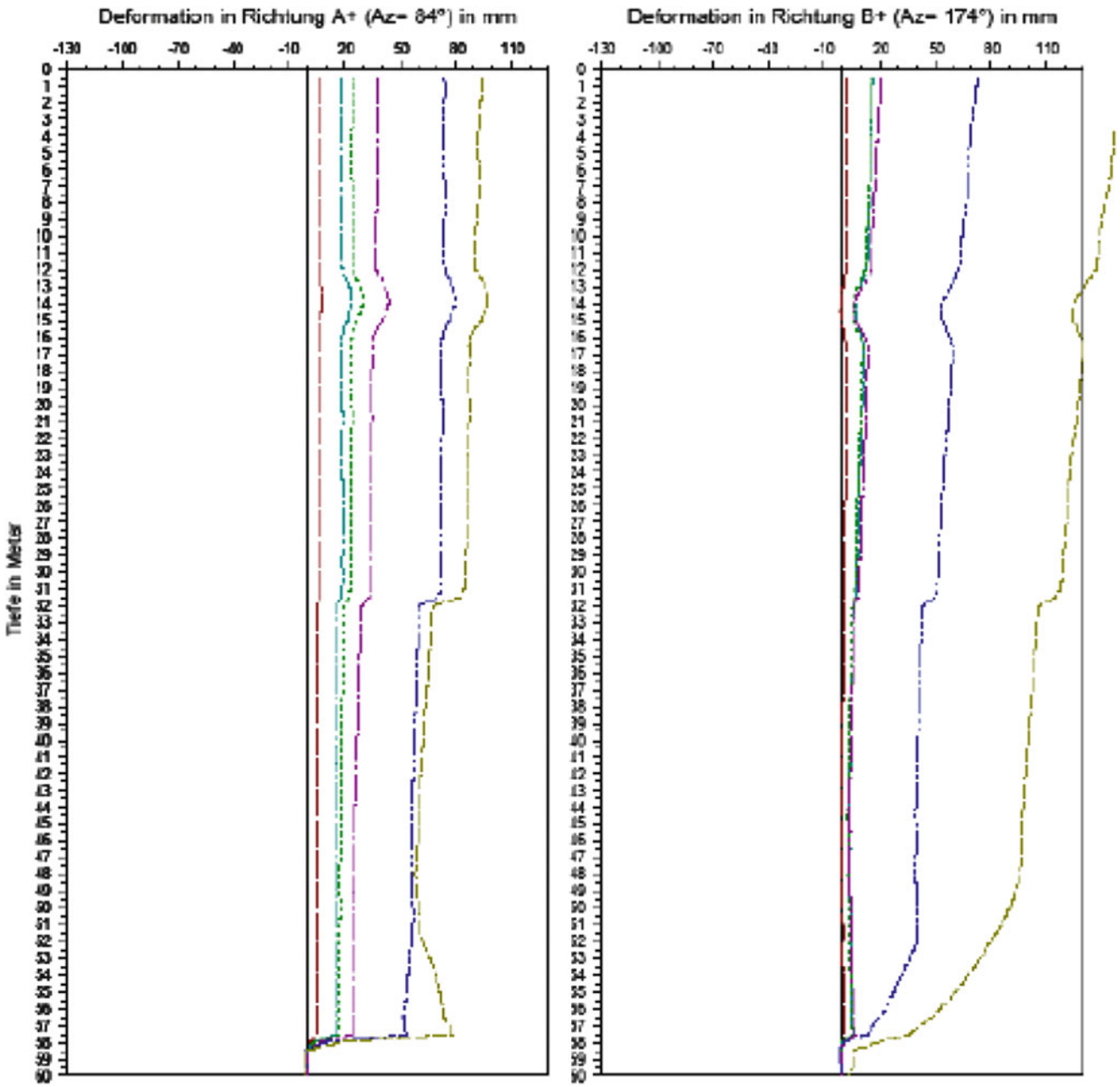

Fig. 9 Inclinometer dataset of a borehole in the frontal part of the landslide. The major slip surface can be located in a depth of about 60 m (GEOTEST AG 2007)

Conclusions

In the year of 2000 the authorities started to elaborate the hazard map of the valley. Through extensive field investigations, analyses of monitoring data and conclusions by analogy from other large landslides the relevant scenarios for the hazard assessment have been formulated. In 2003 the first draft of the hazard map existed (GEOTEST AG 2003). During the next years the Swiss authorities issued a uniform guidance for the assessment of landslide hazards (AGN 1998, 2004). Different types of landslides have to be evaluated separately. In the Lauterbrunnen area three types exist: shallow rapid landslide, rapid deep slides and slow deep-seated landslides. The overlay of these processes leads to a very complex and highly sophisticated hazard assessment. The product of this guideline is shown in the 2011 released and revised hazard map (GEOTEST AG 2011) with depth -, reactivation – and differential movement dependent hazard levels.

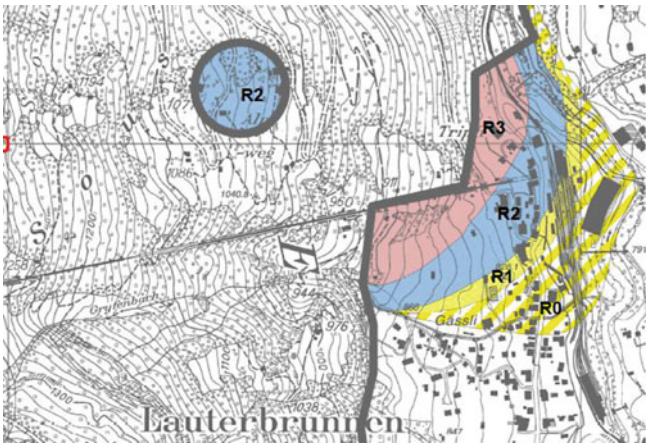

Fig. 10 Original hazard map 2003, section Gryfenbach for continuous landslides with hazard levels within the investigation area (GEOTEST AG 2003) Numbers indicate the average velocity of the moving mass (*1* low, *2* medium, *3* high)

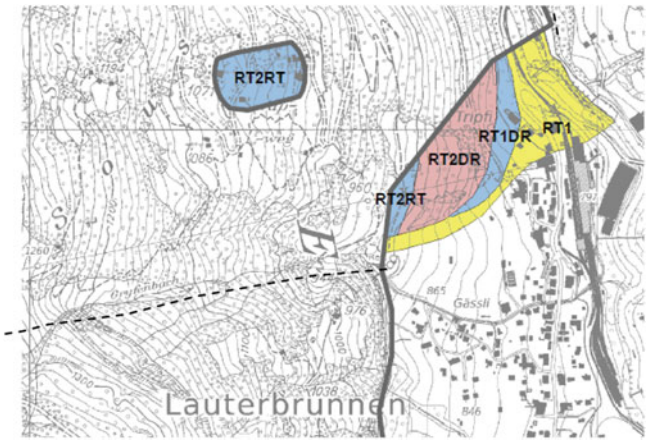

Fig. 11 Revised hazard map, section Gryfenbach for continuous landslides with hazard levels within the investigation area (GEOTEST AG 2011). RT indicates the deep-seated landslide. Numbers (*1* and *2*) indicate the average velocity of the moving mass (*1* low, *2* medium) and $_{R, D}$ indicate the intensification/decrease of the hazard level depending on the reactivation potential ($_R$) and amount of differential movements ($_D$)

Nowadays detailed displacement data are essential to elaborate a trustful hazard map. Especially in cultivated areas official measurement datasets are available nearly nationwide. Based on this data long term information of landslide displacement may be generated (Eberhardt et al. 2007).

References

AGN (1998) Geologische Naturgefahren in der Schweiz. Bulletin angew. Geologie, Separatdruck 3/1, Bern

AGN (2004) Gefahreneinstufung Rutschungen i.w.S. Permanente Rutschungen, spontane Rutschungen und Hangmuren. Entwurf. Bern

Bonnard C, Dewarrat X, Noverraz F (2004) The sedrun landslide. Identification and mitigation of large landslide risks in Europe. Advances in risk assessment. IMIRILAND project. Balkema, Leiden, pp 227–252

BUWAL (1998) Swiss agency for the environment, forest and landscape. Methoden zur Analyse und Bewertung von Naturgefahren. BUWAL Umweltmaterialien, vol 85, Bern

BUWAL (1999a) Swiss agency for the environment, forest and landscape. Risikoanalyse bei gravitativen Naturgefahren. Methode, Fallbeispiele und Daten. BUWAL Umweltmaterialien, vol 107/I and 107/II, Bern

CSD (1973) Tripfirutsch I, Bericht über die Baugrunduntersuchung. Bern (unpublished)

CSD (1983) Tripfirutsch II, Bericht über die erste Beurteilung. Bern (unpublished)

Eberhardt E, Bonzanigo L, Loew S (2007) Long-term investigation of a deep-seated creeping landslide in crystalline rock. Part II. Mitigation measures and numerical modelling of deep drainage at Campo Vallemaggia. Can Geotech J 44:1181–1199

GEOTEST AG (2003) Technischer Bericht zur Gefahrenkarte Lauterbrunnen, Nr. 00063.5, Zollikofen (unpublished)

GEOTEST AG (2007) Lauterbrunnen, Rutschung Gryfenbach, Synthese und Prognosen, Report Nr. 94152.26, Zollikofen (unpublished)

GEOTEST AG (2011) Lauterbrunnen, Naturgefahren, Bericht zur Teilrevision Gefahrenkarte, Nr. 10151.01, Zollikofen (unpublished)

IDNDR (1993) International agreed glossary of basic terms related to disaster management. Department of Humanitarian Affairs, DHA-Geneva

Keusen HR (2000) Die Rutschung Gryfenbach (Lauterbrunnen, BE) – ihre dramatische Entwicklung im Jahr 1999. Bulletin angew Geologie 5(1):73–83

Korup O (2006) Effects of large deep-seated landslides on hillslope morphology, western Southern Alps, New Zealand. J Geophys Res 111(F01018):18

Lateltin O (2009) Natural Hazards, Switzerland, Recommendations - Taking account of the Hazards caused by ground movement in the land-use planning framework. English translation by S. Jewell. Federal Office for Environment, Forests and Countryside (OFEFP); Federal Office for Saving Water (OFEE); Federal Office for Land Use Planning (OFAT), Switzerland

Lateltin O, Haemmig C, Raetzo H, Bonnard C (2005) Landslide risk management in Switzerland. J Int Consort Land 2(4):313–320

OACE (1994) Ordonnance sur l'aménagement des cours d'eau (Ordinance on Land-use Planning) du 2 novembre 1994

OFAT, EFEE, OFEFP (1997) Prise en compte des dangers dus auxh mouvements de terrain dans le cadre de l'aménagement du territoire (Consideration of Landslide Hazard in Land-use Practice). Recommandations. Office fédéral de l'aménagement du territoire (OFAT), Office fédéral de l'économie des eaux (OFEE), Office fédéral de l'environnement, des forêts et du paysage (OFEFP), OCFIM Nr. 310.023f, Berne, Switzerland

OFEE, OFEFP (1995) Dangers naturels, légende modulable pour la cartographie des phénomènes. Recommandations. (Natural Hazards, Legend for Hazard Mapping, Guidelines). Office fédéral de l'environnement, des forêts et du paysage (OFEFP), Office fédéral de l'économie des eaux (OFEE), OCFIM Nr. 310.022f, Berne, Switzerland. (in French; German version also available). www.bwg.admin.ch/themen/natur/f/index.htm

PLANAT (2003) Sicherheit vor Naturgefahren – Vision und Strategie der PLANAT. Nationale Plattform Naturgefahren. http://www.planat.ch

PLANAT (2005a) Strategie Naturgefahren Schweiz. Synthesebericht., Tech. rep., National Platform for Natural Hazards, http://www.planat.ch/ressources/planat product de 543.pdf

PLANAT (2005b) VADEMECUM, Hazard maps and related instruments. PLANAT, Bern, 34 p

PLANAT (2011) National Platform for Natural Hazards. www.planat.ch; http://www.planat.ch/en/specialists/risk-management/

Raetzo H, Lateltin O, Bollinger D, Tripet JP (2002) Hazard assessment in Switzerland – codes of practice for mass movements. Bull Eng Geol Env 61:263–268

Riemer W, Locher T, Nunez I (1988) Mechanics of deep seated mass movements in metamorphic rocks of the Ecuadorian Andes. In: Ch. Bonnard (ed) Proceedings of the 5th international symposium on Bonzanigo et al. 1179 2007 NRC Canada Landslides, Lausanne, vol 1, A. Balkema, Rotterdam, pp 307–310

Strozzi T, Keusen HR, Graf K (2005) Analysis of the displacement along a funicular with large baseline interferograms on point targets. ESA SP-572

Wilhelm C (1999) Kosten-Wirksamkeit von Lawinenschutz-Massnahmen an Verkehrsachsen 1999 Vorgehen, Beispiele und Grundlagen der Projektevaluation. Bern. BUWAL

Overview of Landslide Risk Reduction Studies in Sri Lanka

R.M.S. Bandara and K.M. Weerasinghe

Abstract

Sri Lanka, is located in the Indian Ocean between northern latitudes of 5°51′ and 9°51′ and eastern longitudes of 79°40′ and 81°55′ approximately 24 km to the southeast of India. Sri Lanka occupies an area of nearly 65,000 sq km stretching to 435 km from North to South and 224 km from West and East.

The climate of Sri Lanka varies from semi-arid to mild temperature. The mountains located in the central part of the island are surrounded by low land that extends up to the shores. Those climatologic and morphological variations influence two monsoonal and inter-monsoonal periods. Country's annual rainfall varies from 2,500 to over 5,000 mm in the south-western part of the island, while in the north-west and south-east, rainfall averages less than 1,250 mm annually. Mean annual temperature is 27 ° C in the lowlands of Sri Lanka and in the central highland with an altitude up to 400 m; the mean annual temperature is 15 ° C.

The excessive rainfall and varied climate has contributed to the land degradation, especially in the mountainous region of the country where rainfall is the major triggering factor of landslides. With the disastrous landslides that occurred in mid 1980s, the Government of Sri Lanka took the initiates of studying the landslide phenomena in the country and as a result about 70 % of the landslide prone districts have been mapped in terms of their landslide potential and general guidelines for construction and development have been prepared in order to reduce the landslide risk http://www.nbro.gov.lk/web/index.php?option=com_content&view=article&id=168&Itemid=192&lang=en (2011). Landslide early warning is issued for ensuring the safety of the people who live in the central highlands and the mountainous communities are being educated on the measures they can take to halt or reduce the landslide threat. Since recently, the country has also stepped into the mitigation of landslides that have imparted a threat on human settlements, public thoroughfares, public buildings etc. This paper provides an overview of Sri Lanka's efforts in landslide risk reduction studies.

Keywords

Landslides • Hazard zonation mapping • Landslide risk reduction

Landslides: A Pressing Problem

More than 390 lives were lost and about 175,000 people became homeless during the last three decades in Sri Lanka because of landslides. As a result of the historic heavy

R.M.S. Bandara • K.M. Weerasinghe (✉)
Landslide studies and Services Division, National building Research Organisation, 99/1 Jawatta Road, Colombo 05, Sri Lanka
e-mail: kmweera@yahoo.com

C. Margottini et al. (eds.), *Landslide Science and Practice*, Vol. 1,
DOI 10.1007/978-3-642-31325-7_45,

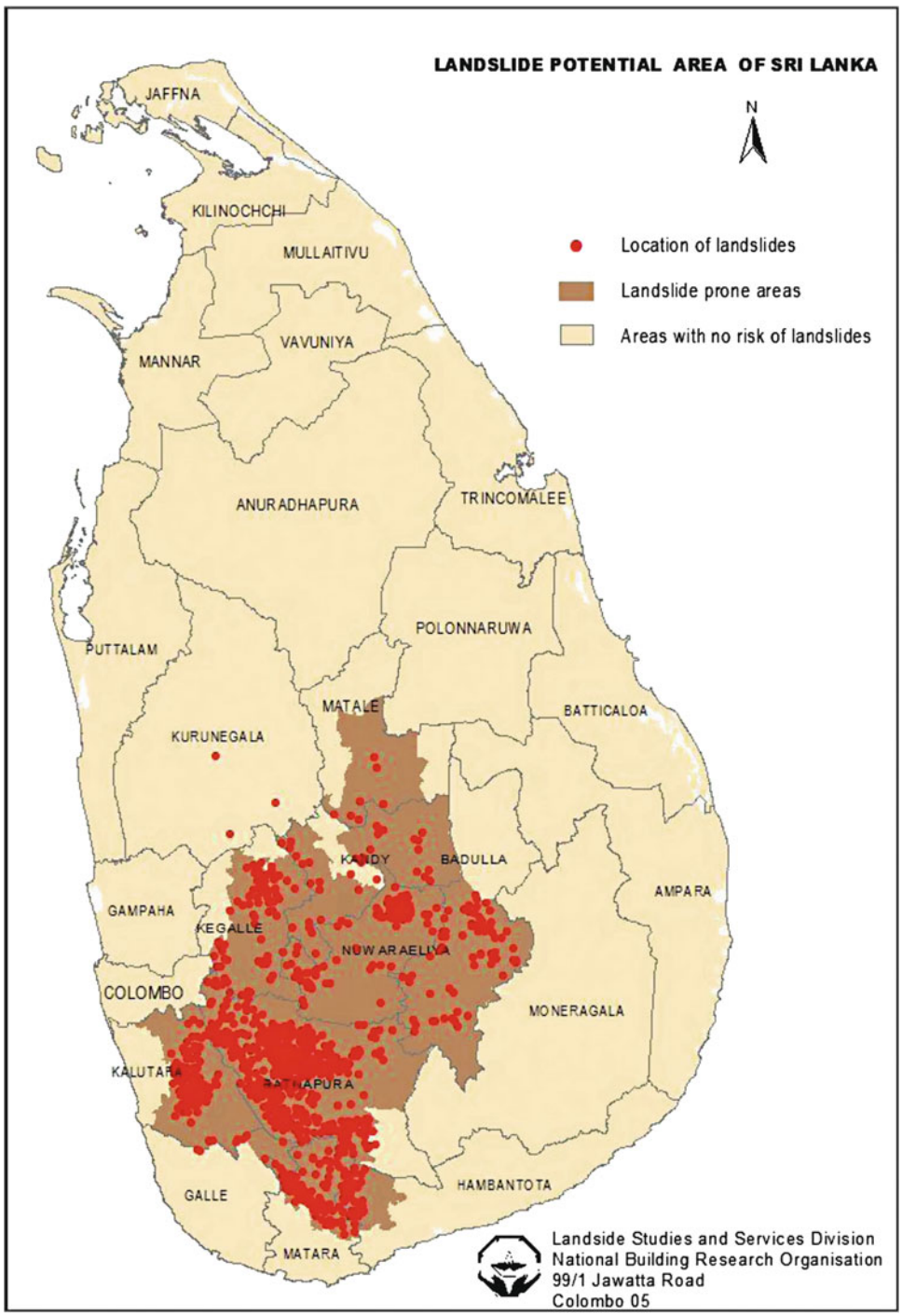

Fig. 1 Locations of landslides recorded between 1947 and 2011

precipitation in May 2003 alone, 191 persons were killed and 3,000 families were severely affected by landslides while their dwellings were destroyed. Similar results were encountered due to heavy precipitation in January 2007, November 2010 and January to February, 2011. More than 70 persons were killed and nearly 5,000 families were severely affected due to the landslides that occurred between 2007 and 2011.

Landslides are a pressing environmental problem of the hill country of Sri Lanka, an area of nearly 20,000 km^2 spread over ten districts (Badulla, Nuwara Eliya, Ratnapura, Kegalle, Kandy, Matale, Kalutara, Galle, Matara and Hambantota) (Fig. 1). They have caused a substantial damage to life, farmlands, communication systems; engineering constructions, infrastructure such as educational facilities, domestic and industrial supply systems, roads, railway lines, and forest

growth etc., and therefore a significant impact on the economy of the country both nationally as well as regionally.

The excessive rainfall and varied climatologic and morphological conditions have contributed to the massive land degradation experienced by the central region of the country where rainfall is the major triggering factor of landslides. The central region of Sri Lanka is hilly and mountainous with highly fractured and folded basement rock overlain by residual soil and colluviums. The elevation of the hilly region ranges from 185 to 2,717 m above MASL. This region is occupied by about 30 % of the total population of the country. Landslides, including slope failures and rock falls both new ones and reactivations of existing landslides, are a frequent phenomenon in these areas. They are likely to have a greater economic impact in the urban and semi urban environment when there is a possibility of damage and losses to investments on various development projects, infrastructure facilities and more important to lives. The total extents of loss of forest cover, wild life and damage to the eco-system by landslides cannot be estimated and will probably remain unknown.

A Proactive Approach

With the disastrous landslides that occurred in mid 1980s, the Government of Sri Lanka took the initiatives of studying the landslide phenomena in the country. On June 16th 1986, the Cabinet of Ministers of the Sri Lankan Government decided (Cabinet Paper 116 of 16th June 1986) to launch Landslide Hazard Zonation Mapping Project (LHMP) to study and identify the distribution of landslide potential in the central highlands. Phase I of LHMP was carried out between 1990 and 1995 with technical and financial assistance from UNDP and UNCHS. The National Building Research Organisation (NBRO) was selected as the executing agency of LHMP, mainly due to availability of multidisciplinary expertise at NBRO. During the 5 year period that Phase I of LHMP was in operation, 2,114 landslides in Badulla and Nuwara Eliya administrative districts were extensively studied to identify the major causative factors of landslides and their relative contribution (Manual on landslide hazard zonation 1995). The result of those field studies along with both national and international expertise in the fields of Geology, Geography, Geotechnical Engineering, Hydrology and Sociology were heavily utilized and a probabilistic methodology for lanadslide hazard zonation was developed at NBRO (Manual on field mapping 1995). Generation of 30 landslide hazard zonation map sheets covering 1,200 km^2 at 1:10,000 scale, development of general guidelines for construction and development in landslide prone areas, and building the capacity of NBRO to continue the subsequent Phases were the other major outputs of the LHMP-Phase I (Arambepola and Weerasingh 1998). Subsequent to the completion of LHMP Phase I, with the financial support of the Government of Sri lanka, the Landslide Studies and Services Division (LSSD) of NBRO continued the studies of landslides and related geohazards in the hilly areas covering the districts of Ratnapura, Kegalle, Matale, Kandy and Kalutara http://www.nbro.gov.lk/web/index.php?option=com_content&view=article&id=173&Itemid=133&lang=en. With the approval of the Cabinet of Ministers of the Sri Lankan Government (Cabinet Paper 03/1372/111/061 dated 17.07.2003), NBRO was requested to extend the landslide hazard zonation mapping programme to the southern districts of Matara, Galle and Hambantota also. Presently, LSSD of NBRO is successfully in the process of establishing sustainable, long-term and short-term mechanisms for landslide disaster management in Sri Lanka (Arambepola and Weerasingh 1998).

Influencing Factors

LHMP studies reveal that intensive heavy rain is the major triggering factor of landslides in Sri Lanka (Mohottala and Chandrapala 1994). However, changes resulting from undue human intervention such as improper land use and cropping practices, unplanned human settlements in unstable areas, obstructions to the normal drainage courses, non-engineered practices used in development have caused a phenomenal increase in the incidence of landslides in hilly areas. This is clearly exemplified by the fact that landslides observed in the initial mapping stages in 1990s were found to be mainly due to natural causes whereas those which occurred within the last decade were mainly due to manmade causes such as modification of hill slopes for development work, haphazardly built human settlements, obstructions to the natural drainage paths etc.

Based on the studies carried out by NBRO, Slope category, Bedrock Geology and Structure, Type and spread of overburden deposit, Landforms and Hydrology have been identified as the major natural causative factors of landslides (Manual on landslide hazard zonation 1995). In addition to these natural factors, Land use and land management are also incorporated in the NBRO's methodology (Fig. 2) for landslide hazard zonation mapping to account for the human influence in causing landslides. Those causative factors have been assigned weights and ratings based on their relative contribution to causing a landslide. The weights and ratings have been decided on considering expert opinion and statistical analysis of historical data (Table 1).

Through an extensive field study, a site is rated against each of the above mentioned causative factors and states of nature (SON) maps of each factor are prepared (Manual on field mapping 1995). These SON maps are then digitally captured into a GIS database along with their attribute data and assigned ratings. The digitally captured data are then

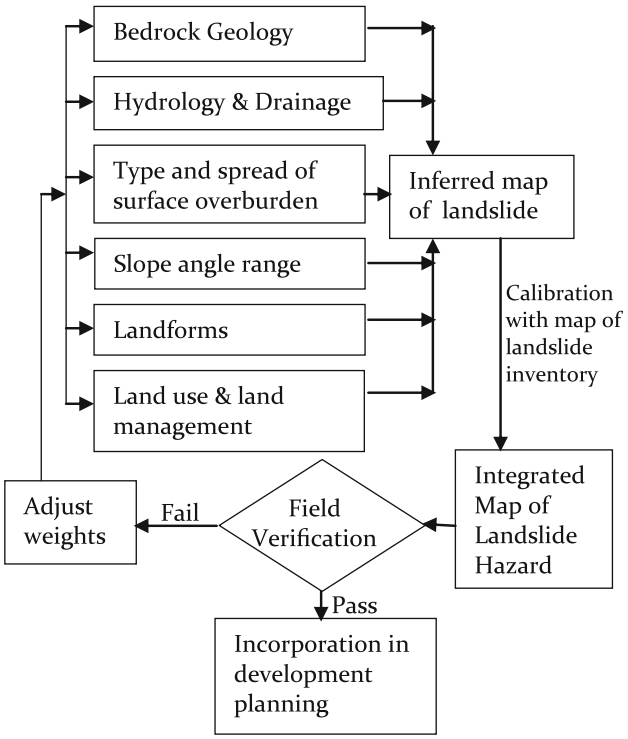

Fig. 2 Methodology of landslide hazard zonation mapping (Manual on landslide hazard zonation 1995)

analyzed separately to prepare the derived map of respective factors (Manual on field mapping 1995). The derived maps represent the distribution of landslide hazard potential based only on one causative factor, independent of the influence of other factors. The derived maps are then overlaid using GIS and, for each resulting polygon, the cumulative hazard rating value (R) is computed by adding up the ratings. The overlaid map is then classified into landslide hazard zones based on the cumulative hazard rating value R (Table 2). A sample landslide hazard zonation map is shown in Fig. 3.

Considering the fuzzy nature of landslide potential which is highly dependent on the changes of the causative factors the predicted landslide hazard zones are expressed in descriptive terms such as landslides are most likely to occur etc. (Fig. 3 and Table 2) rather than crisp terms such as high, medium and low etc (Manual on landslide hazard zonation 1995).

Landslide hazard zonation maps are intended to be used as a planning tool which identifies the degree of hazard associated with a specific area (Arambepola and Weerasingh 1998). Thus, the maps are utilized in planning human settlements, infrastructure and other development activities within the hilly area of the country. Guidelines that are needed to be strictly followed when any development is planned within each landslide hazard zone are also provided along with the landslide hazard zonation maps (Table 3). The maps can also be utilized for policy making, selecting suitable land to relocate highly vulnerable communities and infrastructure, economical distribution of relief aids, identifying economical mitigatory measures and issuing landslide early warning (Bandara 2002).

Preparedness Through Education

NBRO's experience in landslide related issues within the past 25 years revealed that all stakeholders from decision makers to grass root level communities serving and living in the landslide prone areas are lacking the required awareness on landslides (Arambepola and Weerasingh 1998). Therefore, NBRO conducts many awareness programmes to educate all levels of the society in the landslide prone areas on identifying the pre warning signals of landslides, avoiding inappropriate land utilization practices and adopting suitable land management practice. In combination with these educating activities, many awareness documents have been prepared by NBRO in the form of posters, booklets, guidelines, videos and board games http://www.nbro.gov.lk/web/index.php?option=com_content&view=article&id=176&Itemid=208&lang=en.

In addition, with the support of the Disaster Management Centre (DMC) of Sri Lanka and the Japan International cooperation Agency (JICA), NBRO has formed community based disaster management (CBDM) committees in selected landslide prone areas. The members of those CBDM committees have been educated to identify areas that are vulnerable to landslides and the steps that they can take to reduce the vulnerability and risk associated those areas. The CBDM committees have been educated to identify a safe location for emergency evacuation, in case of a landslide and the safe routes to reach the identified evacuation place. In certain areas, JICA has even supported to restore the safety of such identified evacuation routes by constructing for example roads and foot bridges. These CBDM committees have further been provided with simple rain gauges which can be used to measure rainfall and to issue local level early warning to their community, when the rainfall reaches to the pre-established threshold value.

Mitigation Strategy

Landslide Mitigation plays a key role in NBRO's proactive approach in landslide disaster risk reduction, because most of the landslide potential areas identified by the landslide hazard zonation mapping are already inhibited.

Over the past 20 years, the Sri Lankan government has made a reasonable attempt to compensate the hillside dwellers to abandon the affected slopes and to resettle them on suitable land. Although insurance schemes exist to cover certain types of disasters, disasters due to landslides are not covered by them. Certain initiatives have been made to persuade

Table 1 Weights and ratings assigned for major causative factors and their sub-factor elements (Manual on landslide hazard zonation 1995)

Major factors and maximum weighting	Sub factors and maximum weighting	Sub factor Elements, qualitative ratings, and numerical ratings		
Geology	Lithology	Marble	Very low	0
		Weathered rock	Low	1
	8	All others	Medium	3
		Charnockite, Granulite or bedrock not exposed	High	5
		Quartzite	Very high	8
	Amount of dip and type of slope	Dip and scarp 71–90	Very low	0
20		Dip and scarp 56–70	Low	1
	4	Dip 11–30, scarp 46–55 and all intermediate slopes	Medium	2
		Dip 0–10, scarp 31–45	High	3
		Dip 31–55, scarp 0–30	Very high	4
	Deviation angle (degrees)	Angle 26–120	Very low	0
	6	Angle 11–25 or 121–155	Low	2
		Angle 156–180	High	4
		Angle 0–10	Very high	6
	Other discontinuities	To be decided on case to case basis	Very low	0
	2		Very high	2
Type of natural soil and their thickness	Soil cover (m)	Bare bedrock	Very low	0
		Colluvium <1, Residual <2	Low	2
	10	Colluvium 1–3, Residual 2–8	Medium	8
10		Colluvium 3–8, Residual >8	High	9
		Colluvium >8, Residual >8	Very high	10
Slope range and category	Slope range and category (degrees)	Slope category I (>40)	Very high	25
		Slope category II (31–40)	High	16
		Slope category III (17–31)	Medium	13
25	25	Slope category IV (11–17)	Low	7
		Slope category V (0–10)	Very low	5
Hydrology and drainage	Relief amplitude (m)	Relief >350	Very low	1
		Relief 0–170	Medium	2
20	5	Relief 170–350	Very high	5
	Hydrological map unit area (sq. km)	Area 0–0.07 or > 0.5	Very low	1
		Area 0.07–0.2	Medium	2
	4	Area 0.2–0.5	Very high	4
	Hydrological map unit shape (form factor)	0.6–1.0	Very low	1
		0.3–0.6	Medium	2
	4	< 0.3	Very high	4
	Drainage density (km/sq. km) with or without soil cover	With >5 or without >10	Very low	1
		With 3–5 or without 6-10	Medium	2
	5	With 0–3 or without < 6	Very high	5
	Proximity to water bodies	To be decided on case to case basis	Very low	0
	2		Medium	1
			Very high	2
Land use and management	Land use and management	JT1, JC, JQ, JWb, W1, S1	Very low	3
15	15	JT2,JR,JWp,HP,HK,HM,HW,W2,W3, W4, S2,S4	Medium	8
		HA, G1, G2, S3, N1, N2, N3, N4	Very high	15
Landform	Landform	F11,F12,F31–35,F43,F91–92, F94, A10–13, X1,X2	Very low	1
10	10	F41,F42,F44–48,F53	Medium	3
		F51,F52,F54–58,X13,X14	High	5
		F61,F62,F71–74,F81–83, F92,X11,X15	Very high	10

Table 2 Landslide hazard zonation based on cumulative hazard potential value (Manual on landslide hazard zonation 1995)

Overall hazard rating (R)	Landslide hazard zone
R < 40	Landslides not likely to occur
40 < = R <55	Modest level of landslide hazard exists
55 < = R < 70	Landslides are to be expected
R > = 70	Landslides are most likely to occur

insurance companies to consider the matter and design suitable insurance schemes. Finally, it is also difficult to encourage local conventional hillside cultivators to abandon their cultivated land. Therefore, mitigation of major landslides associated with human settlements and infrastructure is difficult, but it has been emerged as a timely necessity.

Mitigation of the Watawala landslide that slid twice across the Colombo-Badulla railway at Watawala in 1992 and 1993 is the most remarkable example that Sri Lanka has for structural mitigation of landslides. With NBRO's recommendations based on a detailed study conducted on this landslide, an Australian company successfully mitigated the landslide by lowering the ground water table through application of a network of surface and subsurface drainage.

The Road Development Authority of Sri Lanka has also contributed to landslide mitigation by stabilizing the landslides associated with major trunk roads such as Colombo-Wellawaya road and Colombo-Haputale road through lowering of the ground water table associated with these roadside landslides.

With the limited resources that were available at NBRO during the last decades, the NBRO's mitigation strategy had to be limited to soft mitigation approaches such as by making it mandatory to carry out a landslide impact assessment integrated in the environmental impact assessment (EIA) process to be essentially performed prior to planning major development projects. Through such mandatory assessments NBRO was able to implement necessary mitigation methods through the owners of those major projects. In addition, through the acts implemented by the national level environmental management agencies such as Central Environmental Authority (CEA) and Natural Resource Management Centre (NRMC), steps were taken to control slope degradation.

Recently, the National Housing Development Authority of Sri Lanka also has taken necessary steps to design their housing schemes on hill slopes to suit the terrain conditions by including retaining structures and appropriate drainage networks.

With the financial support from the Government of Sri Lanka, in the year 2009, NBRO was able to directly implement four landslide mitigation projects in the towns of Peradeniya, Padiyapelella, and within the districts of Matale and Badulla http://www.nbro.gov.lk/web/index.php?option=com_content&view=article&id=173&Itemid=133&lang=en (2011). Structural mitigation measures are applied for mitigating Peradeniya and Padiyapelella landslides whereas nonstructural measures are applied for mitigation of landslides in

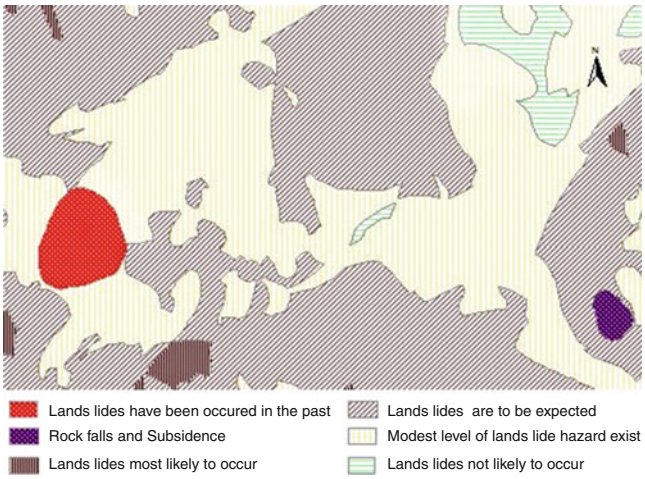

Fig. 3 Sample landslide hazard zonation map prepared by NBRO

Matale and Badulla districts. All four projects are ongoing. With the support of JICA, NBRO was able to implement another structural mitigation project for stabilizing the landslide located in the proximity to a school in Mahawewa, Kumbalgamuwa in Sri Lanka http://www.nbro.gov.lk/web/index.php?option=com_content&view=article&id=173&Itemid=133&lang=en (2011). Sensitive devices for measuring surface movement have been installed accross this Mahawewa landslide and as a result, NBRO was able to issue landslide early warning to the school community during the inclement weather conditions prevailed in January and February of this year. Recognizing the importance of landslide mitigation, the government of Sri Lanka has decided to implement an integrated landslide mitigation project this year. Phase I of this project covers mitigation of landslides in the districts of Badulla, Nuwara Eliya, Kandy and Matale. The cost of the Phase I is estimated to be around US$ 50 Million. The project is still in the planning stage.

Early Warning for Safe Guarding Lives

Almost all Sri Lankan landslides that have been investigated to date are known to be rain induced. Therefore NBRO has taken initiatives for development of an early warning system based on the distribution of inferred landslide potential identified through landslide hazard zonation mapping and the studies on rainfall patterns immediately preceding the slide event. As a result, and also as a part of the landslide risk reduction studies in Sri Lanka, NBRO presently issues landslide early warning to those communities that are vulnerable to landslides during the inclement weather situations http://www.nbro.gov.lk/web/index.php?option=com_content&view=article&id=119&Itemid=206&lang=en (2011). The warning messages are generally issued at three levels namely Alert, Prepare for

Table 3 Guidelines to be followed when developing landslide hazard zones identified by the landslide hazard zonation maps (Manual on landslide hazard zonation 1995)

Landslide hazard zone	Guidelines for development
Landslides not likely to occur	No visible signs of slope instability or danger of landslides exist based on the present state of knowledge. No limitations need to be imposed particularly on well managed lands and engineered construction. Location specific limitations may become necessary particularly for sites that are prone to flooding and erosion
Modest level of landslide hazard exists	Slight danger of landslide hazard exists. Engineered and regulated new construction and well planned cultivation are permitted. Plans for construction should be technically vetted and certified by specialists
Landslides are to be expected	Moderate levels of landslide danger exist. New construction should be discouraged and improved land use planning practices should be introduced to halt and reverse the process of slope degradation. All essential construction, remediation and new projects should be subjected to thorough landslide hazard assessment
Landslides are most likely to occur	Danger and potential threat to life and property exists. No new construction should be permitted. Essential additions in the existing structures may be allowed only after thorough site investigation and adequate precautions which are certified by the specialists. Early warning system should be established if symptoms of landslides are clear and risk levels are high
Landslides, rock falls and subsidence have been occurred in the past	Known danger of landslides and therefore, perennial threat to life and property exists in the area. All new construction should be prohibited and the land use and management practices should be studied and improved to halt and reverse the process of slope degradation. Landslide remediation should be undertaken and early warning systems should be established, if human settlements, buildings and infrastructure exist in the vicinity

Fig. 4 A roadside landslide that occurred in the beginning of 2011

evacuation, and Evacuation. Table 4 further describes those warning levels along with the rainfall threshold values derived for a specific area. The rainfall threshold values may vary from region to region, based on the severity of the landslide potential and the weather patterns.

However, the derivation of local/regional scale effective early warning systems is difficult due to the diverse rainfall patterns prevailing at local scale (Mohottala and Chandrapala 1994). Most rainfall data which have been provided by the Meteorological Department of Sri Lanka had been measured through the rain gauges located in the close proximity of urban centers and the actual rainfall captured by the slopes located a few kilometers away from these gauges are often not reflected in the recorded rainfall data. To overcome this situation, with the support from donor agencies, NBRO is in the process of installing automatic rain gauges on slopes that are highly vulnerable for landsliding. In addition, to increase the effectiveness and to improve the results, communities have also been provided simple rain measuring devices that have already been calibrated according the rainfall threshold values. Proper awareness on critical rainfall values and tools for quantitative measuring of rainfall have been provided to those communities and those devices have been found beneficial for landslide forecasting at village level.

Capacity Building and Experience Sharing

NBRO organized the first National symposium on Landslides as an activity under the Landslide Hazard Mapping Project in 1994 and it provided a forum for all participating institutions and professionals to discuss the problems associated with hill development for the first time. Subsequently NBRO and CHPB organized a workshop on the Role of R & D Institutions in Natural Disaster Management where experts from Sri Lanka, India, and Thailand shared their experiences on landslide related issues. Both these activities were helpful in creating awareness on the subject and in documenting the gaps and constraints in the development process, which has contributed to the natural disasters and environmental degradation (Fernando 1998). In late 1990s, NBRO in collaboration with the two national organizations, namely the Centre for Housing Planning and Building (CHPB) and the Urban Development Authority (UDA), and the Asian Disaster Preparedness Centre (ADPC) in Thailand have introduced two education programs on natural Disaster Management and Community Based Disaster management with the view of increasing the capacity of Government officials, professionals and development workers to face the challenges in natural disaster risk reduction.

In the year 2009, NBRO resumed organizing annual symposia to share the multi faceted research and development knowledge at national level.

Table 4 Landslide early warning levels issued based on rainfall threshold values derived for a specific area and the distribution of landslide potential of that area

Warning level	Warning type	Rainfall threshold value
Level 1	Alert	75 mm cumulative rainfall for 24 h
Level 2	Prepare for evacuation	100 mm cumulative rainfall for 24 h
Level 3	Evacuate	150 mm cumulative rainfall for 24 h or 75 mm rainfall per hour

Favourable Political Will

Being impressed by the success of her initiatives on landslide hazard zonation mapping during 1990–1991,the Government of Sri Lanka extended her support for implementing similar studies in other landslide prone areas of the country. As a result NBRO was able to thoroughly study the landslide phenomena of our country and step into other essential landslide-related topics such as awareness creation, landslide mitigation, and landslide early warning http://www.nbro.gov.lk/web/index.php?option=com_content&view=article&id=173&Itemid=133&lang=en (2011). The most significant development within the entire process is the release of the draft National Disaster Management Plan in January 1992, authored jointly by the Ministries of Reconstruction, Rehabilitation and Social Welfare and the Ministry of Policy Planning and Implementation (Ambalavanar and Lankaneson 1994).

Consequent to a memorandum submitted by NBRO to the government after the flashfloods and landslides occurred in May 2003, cabinet approval was granted by the Cabinet Paper no. 03/1372/111/061 dated 17.07.2003 on "Development of Risk Free Sustainable Human Settlement by Implementing Recommendations of the National Building Research Organization (NBRO) through the Development Planning Process".

The Government of Sri Lanka made another giant step in the year 2005, by finalizing the legal provisions for Disaster Management through the "Disaster Management Counter Measures Bill" which envisaged the setting up of the National Disaster Management Council which is the apex legal body for the formulation of work plans and programmes. The finalized plan for disaster management spells out polices for improved institutional arrangement for disaster management from national to local level. In early 2006, the Government of Sri Lanka established a new Ministry for handing over the responsibilities of disaster management.

Subsequent to the disastrous landslide situations that occurred late last year and early this year (Fig. 4). Identifying the human factor in increased landslide situations in our country, the Government of Sri Lanka issued a circular, making it mandatory for obtaining landslide clearance from NBRO prior to planning and constructions of buildings and other structures in 10 landslide prone district of Badulla, Matale, Kandy, Nuwara Eliya, Kegalle, Ratnapura, Kalutara, Galle, Matara and Hambantota. The objective of implementing this new mandatory rule was to control haphazard planning of human settlements and to ensure regulated planning and engineered construction inclusive of measures to stabilize any slope failures that could be initiated or aggravated by the planned construction http://www.nbro.gov.lk/web/index.php?option=com_content&view=article&id=167&Itemid=210&lang=en (2011).

Acknowledgments The authors wish to acknowledge the support extended by the Government of Sri Lanka, UNDP, UNCHS and JICA for landslide disaster management in Sri Lanka. They also acknowledge the generous support of the Ministry of Disaster Management and the management of NBRO for conducting landslide related research within our country.

References

Ambalavanar V, Lankaneson T (1994) National disaster management plan; current status trends with particular reference to landslide management. In: Proceedings of the national symposium on landslides in Sri Lanka, 17–19 Mar 1994, Sri Lanka, pp 343–348

Arambepola NMSI, Weerasingh, KM (1998) Towards achieving the long term objectives of landslides hazard mapping programme. In: Proceedings of the workshop on the role of R & D institutions in natural disaster management, 10–11 Sept 1998, Sri Lanka, pp 8_1–8_8

Bandara RMS (2002) Hazard mapping for delineating multiple risks of natural disasters under the Sri Lanka urban multi-hazard disaster mitigation project. In: Proceedings of the regional workshop on best practices in disaster mitigation, 24–26, Sept 2004, Indonesia, pp 107–119

Fernando WBJ, (1998) Plan for disaster management. In: Proceedings of the workshop on the role of R & D institutions in natural disaster management, 10–11 Sept 1998, Sri Lanka, pp 26_1–26_3

Landslide Hazard Mapping Project (1995) Manual on landslide hazard zonation, Landslide Studies and Services Division, NBRO, Sri Lanka

Landslide Hazard Mapping Project (1995) Manual on field mapping, Landslide Studies and Services Division, NBRO, Sri Lanka

Mohottala AW, Chandrapala L (1994) Relationship between rainfall and landslides with particular reference to the hilly regions of Sri Lanka. In: Proceedings of the national symposium on landslides in Sri Lanka, 17–19 Mar 1994, Sri Lanka, pp 133–138

National Building Research Organisation (2011) Landslide studies and services. http://www.nbro.gov.lk/web/index.php?option=com_content&view=article&id=173&Itemid=133&lang=en. 12 June 2011

National Building Research Organisation (2011) Landslide studies and services. http://www.nbro.gov.lk/web/index.php?option=com_content&view=article&id=176&Itemid=208&lang=en. 12 June 2011

National Building Research Organisation (2011) Landslide studies and services. http://www.nbro.gov.lk/web/index.php?option=com_content&view=article&id=168&Itemid=192&lang=en. 12 June 2011

National Building Research Organisation (2011) Landslide studies and services. http://www.nbro.gov.lk/web/index.php?option=com_content&view=article&id=167&Itemid=210&lang=en. 12 June 2011

National Building Research Organisation (2011) Landslide studies and services. http://www.nbro.gov.lk/web/index.php?option=com_content&view=article&id=119&Itemid=206&lang=en. 12 June 2011

Susceptibility Maps for Landslides Using Different Modelling Approaches

Philip Leopold, Gerhard Heiss, Helene Petschko, Rainer Bell, and Thomas Glade

Abstract

This study focuses on the comparison of different approaches for landslide susceptibility modelling and is part of the research project "MoNOE" (Method development for landslide susceptibility modelling in Lower Austria). The main objective of the project is to design a method for landslide susceptibility modelling for a large study area. For other objectives of the project we refer to Bell et al. (Proceedings of the 2nd world landslide forum, Rome, 3–7 Oct 2011, this volume). To reach the main objective, the two different statistical models "Weights of Evidence" and "Logistic Regression" are applied and compared. By using nearly the same input data in test areas it is possible to compare the capabilities of both methods. First results of the comparison indicate that in valleys and on south facing slopes the results are quite similar. In contrast, the analysis on north facing slopes shows differences. In the ongoing work the reasons for these differences will be analysed. Furthermore, attention will be paid to finding adequate validation methods for the two modelling approaches.

Keywords

Susceptibility modelling • Weights of evidence • Logistic regression

Introduction

Landslide susceptibility maps can form a powerful tool for preventive spatial planning on a regional scale. Particularly on a regional scale landslide processes and their dynamics are still poorly understood. Susceptibility modelling and the implementation of the resulting maps are challenges for geoscientists. Therefore, it is of high importance to produce a landslide susceptibility model, or a combination of models, that result in robust and reliable susceptibility maps.

This study focuses on the comparison of different statistical modelling approaches as part of the research project "MoNOE" (Method development for landslide susceptibility modelling in Lower Austria). The research project and its objectives are described in detail by Bell et al. in this volume. The main objective of the project is to design a method for landslide susceptibility modelling for a large study area (about 10,200 km^2) and to produce landslide susceptibility maps which are finally implemented in the spatial planning strategies of the Lower Austrian provincial government.

Study Area and Data Collection

The study focuses on 2/3 of the area of the province Lower Austria in the northeast of Austria. It covers districts where landslide events have been recorded by the Lower Austrian provincial government in the past 60 years. The geographical expansion and the position of the study area are shown in Fig 1.

P. Leopold (✉) • G. Heiss
Health and Environment Department, AIT – Austrian Institute of Technology GmbH, Donau-City-Straße 1, Vienna 1220, Austria;
philip.leopold@ait.ac.at

H. Petschko • R. Bell • T. Glade
Department of Geography and Regional Research, University of Vienna, Vienna, Austria

C. Margottini et al. (eds.), *Landslide Science and Practice*, Vol. 1,
DOI 10.1007/978-3-642-31325-7_46,

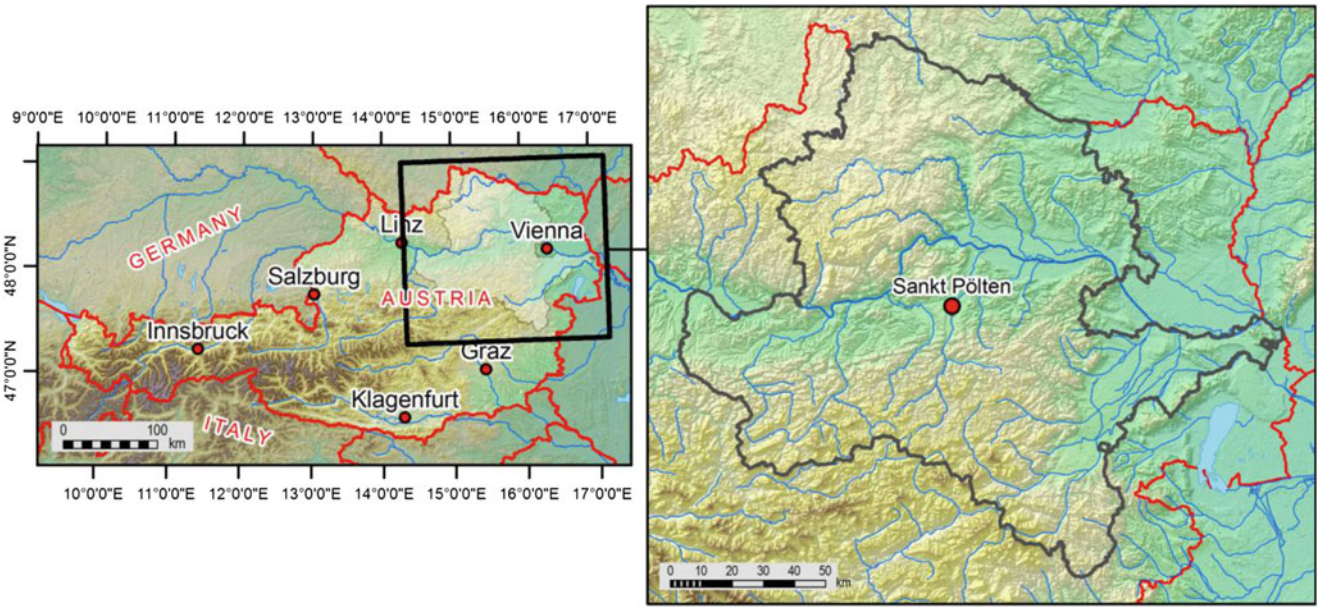

Fig. 1 Study area in the northeast of Austria, covering 2/3 of the area of the province Lower Austria

Methods and models are developed and tested within three test regions of Lower Austria, the districts of Waidhofen/Ybbs, Amstetten and Baden. The optimised methodology will finally be applied to the entire study area, which covers 20 districts.

The entire project focuses on the landslide types fall and slide, whereas in this contribution only slides will be addressed (classification after Cruden and Varnes 1996). To enable susceptibility modelling, landslide inventories were compiled and relevant spatial data (e.g. geology, DTM, orthophotos) was gathered, prepared and homogenized. For a detailed description of the collected data and the landslide inventory refer to Bell et al. and Petschko et al. (this volume). Based on this data, the major aim of this presentation is to provide information on the methodology and on how to choose the "best-fit" modelling method (or a combination of methods) in order to reach the main objective of the MoNOE project. This objective is to design the best modelling procedure for spatial landslide susceptibility maps covering a large region and using the available data sources.

Model Input Data and Landslide Inventory

The high amount of gathered and homogenized spatial data makes the use of various input datasets as model input data possible (Bell et al. in this volume). First modelling tests showed that a comparison of the modelling methods is easier when a reduced set of the most significant input datasets is used. Therefore, for this contribution the following input datasets were applied:

1. Landcover (derived from EOS-ASTER satellite images, reclassified to a resolution of 10 × 10 m)
2. Geology (scale of 1:200,000, simplified to lithological relevant parameters)
3. Slope (derived from the LiDAR DTM, rescaled to 10 × 10 m resolution)
4. Aspect (derived from the LiDAR DTM, rescaled to 10 × 10 m resolution)
5. Landform classification (derived from the LiDAR DTM, 10 × 10 m resolution)

The parameters slope and aspect were computed by using the ArcGIS Spatial Analyst -Extension and the landform classification was derived with the ArcGIS Topographic Position Index -Extension (Jenness 2006).

As mentioned before, the collected data allows additional inputs of datasets to be used in the future, such as distance to geological structures, to rivers, and to very old landslides as well as topographic wetness index and other parameters. However, the benefits of using these datasets for each modelling method have to be evaluated.

As Petschko et al. (this volume) describes, two different landslide inventories were applied within the three test districts: the Building Ground Register of the Geological Survey of Lower Austria, which contains only point information, and a newly prepared landslide polygon inventory based on the interpretation of the multiple hillshade maps of the LiDAR DTM. For the first tests presented in this contribution identical sets of the Building Ground Register were used for both modelling methods.

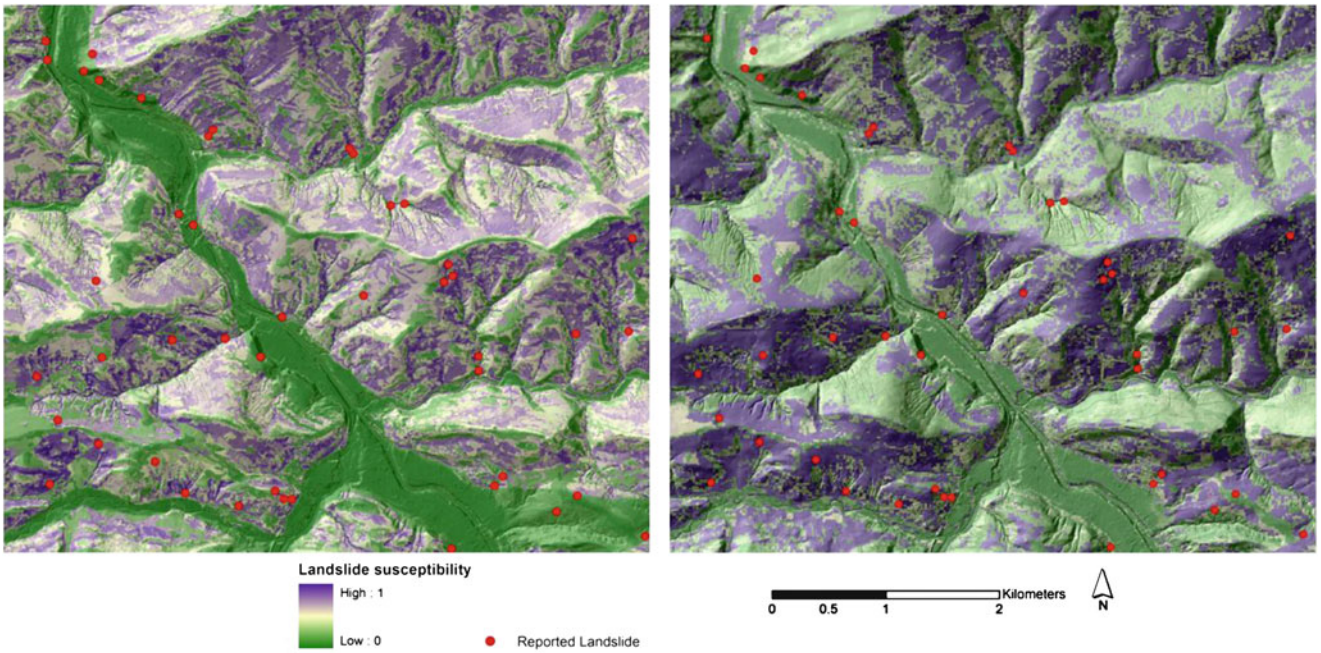

Fig. 2 Comparison of the modelling results in two geographical identical detail test areas. The left side landslide susceptibility map is based on the Logistic Regression method, the right side map is computed with the Weights of Evidence method

Modeling Methods

To reach the previously defined objective the two different statistical models Weights of Evidence (WofE) and Logistic Regression (LR) were applied and the results were compared.

The WofE method was utilized using the "Spatial Data Modeler" Toolbox for ArcGIS 9.3. (Sawatzky et al. 2009). WofE modelling was described by Bonham-Carter et al. (1989) and was used for landslide susceptibility modelling in recent years by different authors (e.g. Neuhäuser and Terhorst 2006). The method is an application of Bayes' Rule of Probability. It is assumed that landslides happen when certain evidential parameters occur, and the causality of this process is time-independent. A set of training points (inventory of landslides) is used to calculate the weights of predictor variables from various evidential themes. Evidential themes are raster maps with the information from the five input datasets mentioned before. The combination of the weights from all used evidential parameters produces a response theme. This is an output map that expresses the probability that a unique cell will contain a landslide event.

Logistic Regression was carried out using a combination of ArcGIS and the Open Source statistics package R. The LR method was described by Atkinson et al. (1998) and Brenning (2005) and was also used by many authors for landslide susceptibility modelling in recent years, e.g. Ayalew and Yamagishi (2005) and Rossi et al. (2010). This method is based on the evaluation of the statistical relationship of explanatory variables which are mainly terrain parameters with the binary dependent variable which contains information on the presence or absence of landslides in the study area. The binary dependent variable consists of the landslide points of the Building Ground Register and the same amount of points that were randomly selected outside of all known landslides. After fitting the model in the open source statistics software "R" the regression coefficients are applied to calculate a landslide susceptibility map for the test study area.

Results

Two geographically identical detail images of the modelling results are presented in Fig. 2. The left image is computed using the LR method, the right image is computed with the WofE method. In both approaches the same input parameters landcover, geology, slope and aspect were used. In the LR modelling the additional parameter landform classification was applied. In both approaches the landslide inventories are used as described before. The authors evaluate this comparison as a first approximation and as a basic approach for the ongoing work.

As shown in Fig. 2, the results in the valleys and on the south facing slopes are quite similar for both models. In contrast, the results for the north facing slopes differ significantly. In the case of WofE modelling, the input dataset aspect shows high contrast values. The northwest, northeast,

and north directions pose strong negative weights and southeast directions pose strong positive weights. As a result, north facing slopes have low susceptibility rates in the final map output. In the case of LR modelling, the input datasets slope and geology pose the highest regression-coefficients. The values of slope and geology are generally equal on north and south facing slopes, so the LR modelling does not distinguish in the final map output between these slopes.

These differences in spatial details must still be carefully analysed in the ongoing work. However, it is now possible to compare the capabilities of the different methods and software solutions.

Discussion and Conclusions

These preliminary results showed that the large study area and very heterogeneous geology pose a huge challenge for landslide susceptibility modelling. Thus, modelling strategies have to be modified. Smaller sub areas should be defined and a simplification of the complex geology to main lithological parameters is required. Considerable efforts will be spent on the validation of the resulting maps for the different modelling methods. The comparison of the first modelling results using WofE and LR performed with nearly identical input parameters, showed quite similar results in the MoNOE project. Nevertheless, some differences can be observed, which need to be further analysed regarding their origin and the statistical and geomorphological quality of each of the maps. This needs to be done especially because of possible adverse effects of choosing the one or the other map for the implementation in the provincial spatial planning strategies.

Acknowledgments This study was performed within the MoNOE project, which is funded by the provincial government of Lower Austria. The input of all MoNOE partners was very supportive and is highly appreciated.

References

Atkinson P, Jiskoot H, Massari R, Murray T (1998) Generalized linear modelling in geomorphology. Earth Sur Proc Land 23(13):1185–1195

Ayalew L, Yamagishi H (2005) The application of GIS-based logistic regression for landslide susceptibility mapping in the Kakuda-Yahiko Mountains, Central Japan. Geomorphology 65(1–2):15–31

Bell R, Glade T, Granica K, Heiss G, Leopold P, Petschko H, Pomaroli G, Proske H, Schweigl J (this volume) Landslide susceptibility maps for spatial planning in Lower Austria. In: Proceedings of the 2nd world landslide forum, 3–7 Oct 2011, Rome

Bonham-Carter GF, Agterberg FP, Wright DF (1989) Weights of evidence modelling: a new approach to mapping mineral potential. Stat Appl Earth Sci 89(9):171–183

Brenning A (2005) Spatial prediction models for landslide hazards: review, comparison and evaluation. Nat Hazard Earth Syst Sci 5:853–862

Cruden DM, Varnes DJ (1996) Landslide types and processes. In: Turner AK, Schuster RL (eds): Landslides – investigation and mitigation. Transportation Research Board Special Report 247. National Academy Press, Washington, DC, pp 36–75

Jenness J (2006) Topographic position index (tpi_jen.avx) extension for arcview 3.x, v. 1.2. Jenness Enterprises. http://www.jennessent.com/arcview/tpi.htm. Last accessed 16th June 2011

Neuhäuser B, Terhorst B (2006) Landslide susceptibility assessment using weights-of-evidence applied on a study site at the Jurassic escarpement of the Swabian Alb (SW-Germany). Geomorphology 86:12–24

Petschko H, Bell R, Leopold P, Heiss, G, Glade T (this volume) Landslide inventories for reliable susceptibility maps in Lower Austria. In: Proceedings of the 2nd world landslide forum, Rome, 3–7 Oct 2011

Rossi M, Guzzetti F, Reichenbach P, Mondini AC, Peruccacci S (2010) Optimal landslide susceptibility zonation based on multiple forecasts. Geomorphology 114(3):129–142

Sawatzky DL, Raines GL, Bonham-Carter GF, Looney CG (2009) Spatial data modeller (SDM). ArcMAP 9.3 geoprocessing tools for spatial data modelling using weights of evidence, logistic regression, fuzzy logic and neural networks. http://arcscripts.esri.com/details.asp?dbid=15341. Last accessed 16th June 2011

Using Remotely Sensed Information for Near Real-Time Landslide Hazard Assessment

Dalia Kirschbaum, Robert Adler, and Christa Peters-Lidard

Abstract

The increasing availability of remotely sensed precipitation and surface products provides a unique opportunity to explore how landslide susceptibility and hazard assessment may be approached at larger spatial scales with higher resolution remote sensing products. A prototype global landslide hazard assessment framework has been developed to evaluate how landslide susceptibility and satellite-derived precipitation estimates can be used to identify potential landslide conditions in near-real time. Preliminary analysis of this algorithm suggests that forecasting errors are geographically variable due to the resolution and accuracy of the current susceptibility map and the application of satellite-based rainfall estimates. This research is currently working to improve the algorithm through considering higher spatial and temporal resolution landslide susceptibility information and testing different rainfall triggering thresholds, antecedent rainfall scenarios, and various surface products at regional and global scales.

Keywords

Landslide nowcasting • Remote sensing • Rainfall-triggered landslide hazards

Introduction

Landslide hazards generate more economic losses and fatalities than is generally acknowledged, due in large part to the reality that most casualties from landslide disasters occur in the developing world. In such areas, complex topographic, lithologic and vegetation signatures coupled with heavy rainfall events can lead to extensive mass wasting. Recent examinations of rainfall-induced landslides have increased understanding of the triggering mechanisms and surface conditions underlying slope instability (Baum et al. 2010; Iverson 2000). However, investigations remain largely site-specific and rely on high-resolution surface observable data, in situ gauge rainfall information and detailed landslide inventories. Such information is frequently unavailable over larger areas (regional to global spatial scales) due to spatial and temporal heterogeneities in surface information, rainfall gauge networks, and sparse landslide inventories.

The increasing availability of remotely sensed surface and atmospheric data offers a new opportunity to address landslide hazard assessment at larger spatial scales. A preliminary global landslide hazard algorithm developed by Hong et al. (2006, 2007) seeks to identify areas that exhibit a high potential for landslide activity by combining a calculation of landslide susceptibility with satellite derived rainfall estimates. The algorithm considers all rapidly-occurring mass movement types (e.g. landslides, debris flows, mudslides) that are directly triggered by rainfall.

This research first presents a regional approach for improving some of the challenges identified in the prototype algorithm. It then provides a discussion of main items to be addressed in a second version of the global algorithm system.

D. Kirschbaum (✉) • C. Peters-Lidard
NASA Goddard Space Flight Center, Hydrological Sciences Branch, Greenbelt, MD, USA
e-mail: dalia.b.kirschbaum@nasa.gov

R. Adler
Earth Science Interdisciplinary Center, University of Maryland, College Park, MD, USA

C. Margottini et al. (eds.), *Landslide Science and Practice*, Vol. 1,
DOI 10.1007/978-3-642-31325-7_47,

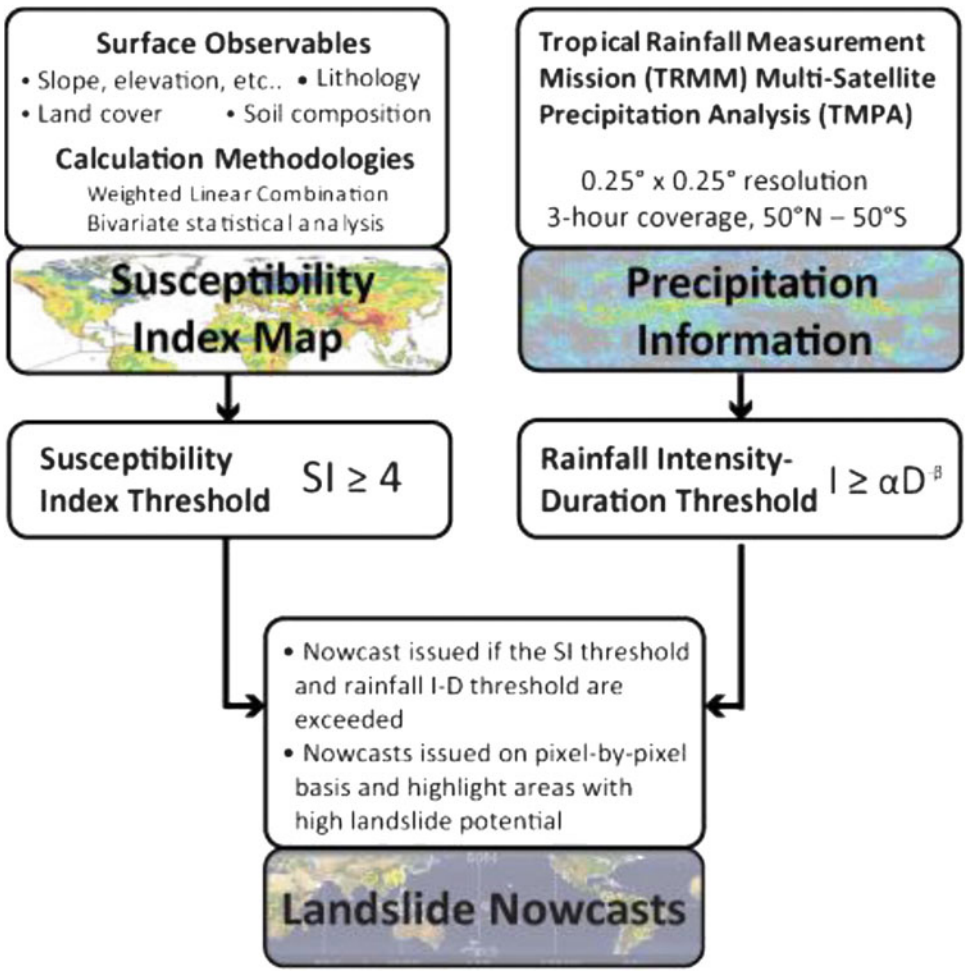

Fig. 1 Framework of the Global Landslide Nowcasting Algorithm. The algorithm uses a threshold approach, considering a relative susceptibility index and precipitation threshold information to identify regions where landslides may occur. *Figure from* Kirschbaum et al. (2011)

The algorithm is currently running in near real-time at http://trmm.gsfc.nasa.gov/publications_dir/potential_landslide.html.

Global Landslide Hazard Algorithm

Algorithm Framework

The global algorithm framework uses a global landslide susceptibility map that was calculated using several remotely sensed and surface products (Fig. 1). Shuttle Radar Topography Mission (SRTM) data at a 3 arc-second (~90 m) resolution is used to derive topographic parameters including elevation, slope, and drainage density. Other products include 1 km Moderate Resolution Imaging Spectroradiometer (MODIS) land cover, and 0.25–0.5° resolution soil characteristics information. Each product is aggregated or interpolated from its base spatial resolution to 0.25° × 0.25°. Soil type (classification of soil clay mineralogy, soil depth, moisture capacity, etc.), soil texture (percentage of sand, clay and loam) and land cover were assigned a qualitative weight derived from previous literature. The six parameters chosen to estimate susceptibility (slope, soil type, soil texture, elevation, land cover, and drainage density) were normalized globally and combined using a weighted linear combination approach. The resulting global susceptibility map includes susceptibility values ranging from 0 (low susceptibility) to 5 (high susceptibility). Hong et al. (2007) provides an in depth discussion of the products and methodologies used to calculate the global susceptibility index.

Hong et al. (2006) developed a rainfall I-D threshold for the global algorithm framework that utilizes satellite-based Tropical Rainfall Measuring Mission (TRMM) Multisatellite Precipitation Analysis (TMPA) product (Huffman et al. 2007) rainfall information. This merged satellite product provides precipitation estimates at 0.25° × 0.25° resolution every 3 h from 50°N to 50°S.

To identify 'nowcast' areas of potential landslide activity, the algorithm couples the static susceptibility map with the rainfall I-D curve, assigning minimum thresholds for susceptibility and rainfall values at specified temporal durations. If a pixel has a susceptibility index value greater than the defined threshold and the rainfall accumulation exceeds the I-D threshold value, then an algorithm 'nowcast' is issued. This approach can be applied over any spatial scale

or resolution and is intended to provide an indication of areas that are likely to experience landsliding conditions.

Landslide Inventory Information

The global algorithm framework was evaluated using a newly compiled global catalog for rainfall-triggered landslide events (Kirschbaum et al. 2009a). Landslide information was obtained from online news reports, hazard databases, and other credible sources. The landslide catalog includes events from 2003, and 2007–2010 and generally provides a minimum number of reported landslide events worldwide due to influencing factors such as regional reporting biases and accuracy of reports. The landslide entries include information on the date of the landslide, the location (both nominal and latitude/longitude), type of movement (if available), and impacts (fatalities, injuries or affected persons, and additional information).

Algorithm Evaluation

Global evaluation of the current algorithm platform identifies several limitations of the system. First, the surface observables are aggregated to a 0.25° resolution, which serves to strongly decrease the strength of surface signals such as topography or slope by averaging values over a large area. Second, the susceptibility map incorporates two fairly coarse resolution soil products, which serves to overemphasize the soils information and bias susceptibility values in many areas. Third, the globally consistent rainfall threshold is shown to under-estimate actual rainfall triggering conditions in many environments. Kirschbaum et al. (2009b) outlines a set of recommendations for improving algorithm performance. These include consideration of surface data products at higher spatial resolutions, employment of a more physically-based methodology for calculating susceptibility, and re-evaluation of the rainfall intensity-duration threshold to better account for regional climatology. The study emphasizes that the validation efforts would be greatly enhanced by using more detailed and comprehensive landslide inventories and that this approach may be better suited for regional scale analysis.

Regional Landslide Hazard Approach

Central America

Drawing upon the recommendations outlined in the global evaluation, the algorithm framework approach was tested for a regional case-study in Central America. The evaluation employs a statistically-based methodology to calculate landslide susceptibility over four Central American countries that were significantly affected by Hurricane Mitch in November 1998. Following the hurricane teams of landslide experts from the U.S. Geological Survey (USGS) and others used multi-temporal aerial photographs and field mapping to estimate the areas and locations of over 24,000 landslides in selected study areas over the four countries (Bucknam et al. 2001; Harp et al. 2002; Rodriguez et al. 2006; Devoli et al. 2007).

The extensive landslide inventory mapped following Hurricane Mitch was evaluated with high resolution surface observable datasets to calculate a landslide susceptibility index. Datasets used included a 90-m SRTM DEM, which was used to derive elevation, slope, curvature (slope concavity), and aspect (slope orientation). Land cover information was re-classified into 10 classes based on a relative landslide susceptibility categorization. Country-level lithologic maps were obtained for each of the four countries, with mapping scales ranging from 1:100,000 for El Salvador to 1:500,000 for Honduras, Guatemala, and Nicaragua. The data were divided into classes according to their lithologic characteristics, rock type and age. Lithologic classes were assigned using information on landslide distribution in a selection of the mapped study areas and classification guidelines from Nadim et al. (2006).

A susceptibility map was calculated using a frequency ratio approach, which considers the presence or absence of landslides within a defined range of cover types to identify the combination of surface types with the highest occurrence of landslides. The frequency ratio value is calculated for every grid within the study area as:

$$Fr_{cb} = \frac{LandslideArea_{cb}/LandslideArea_T}{StudyArea_{cb}/StudyArea_T} \quad (1)$$

where Fr_{cb} is the frequency ratio value for each surface observable or category c = (1,2,...m), at each bin b = (1,2,...n), and T denotes the total area for landslides and study area for the surface observable. The numerical value of the frequency ratio suggests that when Fr ≈ 1, the percent of landslide pixels is proportional to the total pixel area within the bin and when the frequency ratio diverges from Fr = 1, there is a more pronounced relationship between the landslide and total pixel areas. Figure 2 shows the susceptibility map calculated for this evaluation. After calculation at 90 m, the susceptibility map was aggregated to 1 km and divided into five categories based on the distribution of the frequency ratio values.

This statistical approach was chosen because it was both relatively simplistic to calculate within a Geographic Information System (GIS) platform and facilitated testing multiple surface observable categories at varying resolutions. For further information on the evaluation methodology or

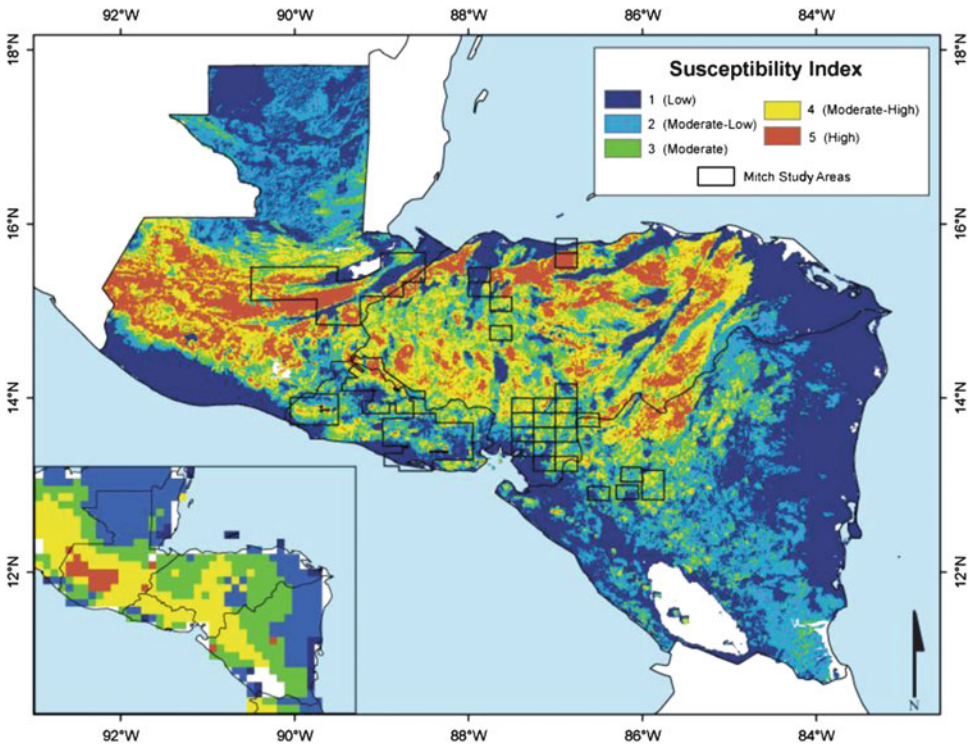

Fig. 2 Regional landslide susceptibility map for four countries in Central America using the Hurricane Mitch landslide inventory. Mapped locations of the inventory are designated with black boxes. The inset map plots the global landslide susceptibility map over the same area. *Figure from* Kirschbaum et al. (2011)

data used in this investigation, please refer to Kirschbaum (2009) and Kirschbaum et al. (2011).

Improvements to the Global Framework

Susceptibility Map

The regional framework indicated that considering landslide susceptibility at regional scales using detailed landslide inventories can greatly improve the accuracy of the landslide nowcasting algorithm. As such, one of the main limitations of the current global susceptibility map is incorporating fairly coarse resolution datasets that contain large uncertainties together with more accurate products. Current research is working to improve upon the data uncertainties by applying remotely sensed data at higher resolution within an intercomparison testing framework. Several models are currently being tested to provide a more physical basis to the susceptibility map. These include methodologies from Nadim et al. (2006), the SINMAP approach outlined in Pack et al. (2001), and Coe et al. (2004). However, as shown in the regional case study, having accurate and sufficient landslide inventory information is critical to both calculating and validating these susceptibility maps. These approaches will first be tested within the United States where several landslide inventories (both static and event-based) are available. Figure 3 highlights the inventories currently available over the United States. This work will first identify several test areas to evaluate the three methodologies. Then results will be extrapolated to the entire continental U.S. and then ultimately to the global scale to determine both the accuracy and efficiency at calculating the susceptibility index at over larger areas.

Rainfall Intensity and Antecedent Moisture

Rainfall Intensity-Duration (I-D) thresholds, such as the one used within the global algorithm framework, are subject to large inaccuracies based both on the data available as well as the very empirical methodology used to calculate these relationships. In theory, the I-D threshold specifies the minimum average rainfall intensity that can cause destabilizing conditions on a hillslope which trigger landslide events. However, this relationship fails to account for previous meterological forcings that can play a critical role in initiating a slope failure. This algorithm framework tests several different indices of soil moisture and antecedent rainfall conditions within the model framework to provide a relative index of the status of the soil prior to the critical rainfall. Potential methods to be tested may include the Antecedent Water Index model proposed by Godt et al. (2006), the Antecedent Daily Rainfall Model by Glade et al. (2000), and a straightforward antecedent rainfall index similar to the relationship approximated by Chleborad et al. (2006). Each of these relationships will be tested and validated with available landslide inventory information over the United States.

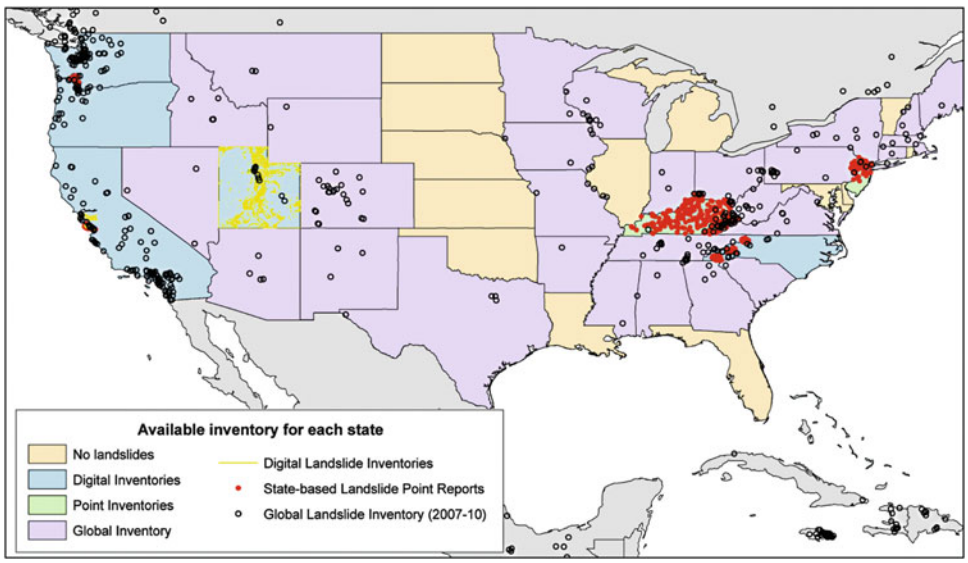

Fig. 3 Available landslide inventory data for the continental United States. The states are highlighted based on the presence of different inventory products: digital inventories are specified in yellow, point-based landslide inventories are shown in red, and the global landslide inventory (shown for 2007–2010) is shown in black circles. The inventory data was compiled from a large number of sources, including several state geological surveys, universities, and the Global Landslide Catalog (GLC) described in Kirschbaum et al. (2009a, 2011)

The rainfall data currently used within the algorithm is at a 3-hourly resolution at 0.25° resolution. Moving forward, this algorithm framework and calculation of both rainfall intensity and antecedent moisture values will be greatly enhanced by products from the Global Precipitaiton Measurement (GPM) mission (http://gpm.nasa.gov). GPM products will provide advanced space-borne measurements of precipitaiton every 2–4 h worldwide using an international constellation of sensors to provide information on rain and snow with greatly improved accuracy and spatiotemporal resolution.

Additional Triggering and Destabilizing Factors

Another challenge of the current algorithm framework is adequately accounting for exogenous factors leading to increased slope instability. At present, the algorithm framework does not account for landslides triggered by seismic activity or anthropogenic impact. Tectonic weakening of the hillslopes can destabilize the surface and failure planes, increasing the potential for a landslide during and subsequent to heavy rainfall events. Anthropogenic impact on surface instability and landslide frequency is somewhat more difficult to quantify. Road cuts, improper building, and inadequate water drainage weakens surface materials, which serves to increase shear stresses and slope instability. While the completeness and accuracy of landslide inventories continues to be a limiting factor in algorithm validation, integrating additional indicators such as population density, proximity to road networks, and economic fragility may help to better constrain locations where populations may be at higher risk to landslide occurrences.

There are several global databases that provide information on road networks, seismic activity, burned areas, and population centers. After a thorough evaluation and improvement of the natural factors contributing to global landslide hazards within the landslide framework, we will begin to consider the role of exogenous variables in both weakening slopes and triggering landslides at various spatial and temporal scales.

Conclusions

This research provides an overview of how remotely sensed data may be used to evaluate landslide hazards at the global scale and provide a "nowcast" of landsliding conditions through exploiting near real-time satellite rainfall information and surface datasets. The first version of this global system shows moderate skill in forecasting active areas for landsliding; however, the algorithm framework is significantly limited by the composition of the susceptibility map, rainfall-triggering relationship, and landslide inventory information for validation. Moving forward, this work seeks to incorporate additional factors contributing to slope instability, including antecedent soil moisture and anthropogenic impacts. Drawing upon other detailed landslide inventories as well as our rainfall-triggered GLC, we will develop a higher resolution, more physically-based evaluation to examine and possibly forecast rainfall-triggered landslide hazards at both regional and global scales. Future missions such as the Global Precipitation Measurement mission (GPM; http://gpm.nasa.gov), will provide higher spatiotemporal precipitation inputs to better characterize landslide-triggering conditions and improve hazard forecasting.

Acknowledgments The authors greatly acknowledge the State Geological Surveys and the individuals who provided landslide inventory information. This work was supported by the GPM mission and NASA's Applied Sciences Program.

References

Baum RL, Godt JW, Savage WZ (2010) Estimating the timing and location of shallow rainfall induced landslides using a model for transient, unsaturated infiltration. J Geophys Res 115(F03013):1–26

Bucknam RC, Coe JA, Chavarria MM, Godt JW, Tarr AC, Bradley L, Rafferty S, Hancock D, Dart RL, Johnson ML (2001) Landslides triggered by Hurricane Mitch in Guatemala – inventory and discussion. US Geological Survey Open-File Report 01–443, pp 1–40

Chleborad AF, Baum RL, Godt JW (2006) Rainfall thresholds for forecasting landslides in the Seattle, Washington, Area—Exceedance and probability. US Geological Survey Open-File Report, 2006–1064

Coe JA, Godt JW, Baum RL, Bucknam RC, Michael JA (2004) Landslide susceptibility from topography in Guatemala. In: Lacerda WA, Ehrlich M, Fontura SAB, Sayao ASF (eds) Landslides: evaluation and stabilization. Taylor & Francis Group, London, pp 69–78

Devoli G, Strauch W, Chavez G, Hoeg K (2007) A landslide database for Nicaragua: a tool for landslide-hazard management. Landslides 4:163–176

Glade T, Crozier M, Smith P (2000) Applying probability determination to refine landslide-triggering rainfall thresholds using empirical 'Antecedent Daily Rainfall Model'. Pure Appl Geophys 157:1059–1079

Godt JW, Baum RL, Chleborad AF (2006) Rainfall characteristics for shallow landsliding in Seattle, Washington, USA. Earth Surf Proc Land 31:97–110

Harp EL, Hagaman KW, Held MD, Mckenna JP (2002) Digital inventory of landslides and related deposits in Honduras Triggered by Hurricane Mitch. US Geological Survey Open-File Report 02–61, pp 1–18

Hong Y, Adler R, Huffman G (2006) Evaluation of the potential of NASA multi-satellite precipitation analysis in global landslide hazard assessment. Geophys Res Lett 33(L22402):1–5

Huffman GJ, Adler RF, Bolvin DT, Gu G, Nelkin EJ, Bowman KP, Hong Y, Stocker EF, Wolff DB (2007) The TRMM Multisatellite Precipitation Analysis (TMPA): Quasi-Global, Multiyear, Combined-Sensor Precipitation Estimates at Fine Scales. J Hydrometeorol 8:38–55

Hong Y, Adler R, Huffman G (2007) Use of satellite remote sensing data in the mapping of global landslide susceptibility. Nat Hazards 43(2):245–256

Iverson RM (2000) Landslide triggering by rain infiltration. Water Resour Res 36(7):1897–1910

Kirschbaum DB (2009) Multi-scale landslide hazard and risk assessment: a modeling and multivariate statistical approach. Doctoral Dissertation, Columbia University

Kirschbaum DB, Adler R, Hong Y, Hill S, Lerner-Lam A (2009a) A global landslide catalog for hazard applications: method, results, and limitations. Nat Hazards 52(3):561–575

Kirschbaum DB, Adler R, Hong Y, Lerner-Lam A (2009b) Evaluation of a preliminary satellite-based landslide hazard algorithm using global landslide inventories. Nat Hazard Earth Syst Sci 9:673–686

Kirschbaum DB, Adler R, Hong Y, Kumar S, Peters-Lidard C, Lerner-Lam A (2011) Advances in landslide nowcasting: evaluation of a global and regional modeling approach. Environmental Earth Sciences 66(6):1683–1696

Nadim F, Kjekstad O, Peduzzi P, Herold C, Jaedicke C (2006) Global landslide and avalanche hotspots. Landslides 3:159–173

Pack RT, Tarboton DG, Goodwin CN (2001) Assessing terrain stability in a GIS using SINMAP. In: Proceedings of the 15th annual GIS conference, GIS 2001, Vancouver, British Columbia, 19–22 Feb 2001, pp 1–9

Rodriguez CE, Torres AT, Leon EA (2006) Landslide hazard in El Salvador. In: Nadim F, Pottler R, Einstein H, Klapperich H, Lillehammer KS (eds) Proceedings of ECI conference on Geohazards, pp 1–10

Modelling Landslides' Susceptibility by Fuzzy Emerging Patterns

Anna Rampini, Gloria Bordogna, Paola Carrara, Monica Pepe, Massimo Antoninetti, Alessandro Mondini, and Paola Reichenbach

Abstract

This contribution proposes an approach to model regional landslide susceptibility, based on a supervised learning technique that mines fuzzy emerging patterns on a set of classified data. In our approach the training set contains positive and negative examples of areas, (i.e., slope units), affected or not affected by landslides. The fuzzy emerging patterns characterise the positive and the negative areas exploiting their ability to discriminate between the two classes. The approach consists first, in inducing a set of fuzzy rules, and then in reducing them by retaining those that identify fuzzy emerging patterns for the given training set. The fuzzy rules define the main characteristics of the slope units that are affected or not affected by landslides and are used to classify other slope units in the same region. The classification technique provides an estimate of the hesitation of the decision process, which is a measure of its ability to uniquely associate a slope unit to the susceptible or not susceptible class. In the paper we describe the approach and discuss the preliminary results.

Keywords

Fuzzy emerging patterns • Fuzzy rules • Trust • Landslide susceptibility • Data mining

Introduction

Landslide susceptibility is the propensity of an area to be subject to landslide occurrence. Susceptibility maps are useful to predict the spatial location of possible future landslide events.

In the literature, many approaches have been proposed to map landslide susceptibility. They are mainly based on statistical, physical modelling and fuzzy logic (Guzzetti et al. 2006; Pradham 2010).

In this contribution we propose a novel supervised learning method that identifies fuzzy emerging patterns on a set of classified data used as training set, containing slope units affected and not affected by landslides (positive and negative examples).

Fuzzy emerging patterns have been first defined by García-Borroto et al. (2010). They are a generalization of emerging patterns, i.e., a combination of variable values that occur mostly in a class, and which barely appear in the remaining classes. The presence of a pattern in an item (an element or instance of the database) gives some evidence about the class the object should belong to. Many authors proposed algorithms to extract and use emerging patterns for supervised classification (Dong and Li 1999; Ramamohanarao and Fan 2007). Two main emerging pattern–based classifiers can be distinguished depending on the different phase of the pattern discovery. The first group

A. Rampini (✉) • P. Carrara • M. Pepe • M. Antoninetti
CNR-IREA, via Bassini 15, Milan 20133, Italy
e-mail: rampini.a@irea.cnr.it; carrara.p@irea.cnr.it; pepe.m@irea.cnr.it; antoninetti.m@irea.cnr.it

G. Bordogna
CNR-IDPA, via Pasubio 5, Dalmine, BG 24044, Italy
e-mail: gloria.bordogna@idpa.cnr.it

A. Mondini • P. Reichenbach
CNR-IRPI, via della Madonna Alta- 126, Perugia 06128, Italy
e-mail: alessandro.mondini@irpi.cnr.it; Paola.Reichenbach@irpi.cnr.it

C. Margottini et al. (eds.), *Landslide Science and Practice*, Vol. 1,
DOI 10.1007/978-3-642-31325-7_48,

(Li et al. 2000) makes a lazy discovery, searching for patterns during the classification stage; the second group (Dong et al. 1999) finds the emerging patterns during the training stage, and applies them for the classification. We use this second approach since it is much more efficient.

Fuzzy emerging patterns have been defined by García-Borroto et al. (2010) as conjunctions of fuzzy predicates such as:

[A_1 *is high*] *and* [A_2 *is medium*] *and* [A_3 *is low*]

where A_1, A_2, A_3 are independent variables of an object, and *high, medium, low* are linguistic values defined as fuzzy subsets on the domain of the variables (Zadeh 1965). Fuzzy emerging patterns can constitute the antecedents of fuzzy rules, i.e., fuzzy conditional propositions, such as the following one:

If [A_1 *is high*] *and* [A_2 *is medium*] *and* [A_3 *is low*]
then C *is high*

where the rule antecedent is "[A_1 *is high*] *and* [A_2 *is medium*] *and* [A_3 *is low*]" and the rule consequent is "C *is high*", with C being the dependent variable.

In our example, for mining the emerging patterns we select as training set of objects, the slope units that are portions of the territory bounded by drainage and divide lines (Carrara 1988; Guzzetti et al. 2006). The slope units are classified *a priori* into two classes, positive and negative (i.e., affected or not affected by landslides, respectively) depending on the percentage of area that has been affected by a landslide in the past. From the training set fuzzy emerging patters are identified as conjunctions of fuzzy predicates over the variables describing the slope units. These Emerging patterns synthesise the main features of either the positive or the negative subsets of the training set.

Once these patterns are identified, we use them in a fuzzy inference process to classify new slope units described by the same variables of the patterns and located in the same territory.

The model classification indicates if the slope unit is low or high susceptible to landslides. Furthermore, it provides an uncertainty degree reflecting the hesitation margin associated with the decision, i.e., a measure of the ability of the decision process to uniquely associate a slope unit with one of the two classes (susceptible and not susceptible to landslides). The objective of our analysis is different the models based on discriminant analysis proposed by Guzzetti et al. (2006), which are aimed at determining the probability of a slope unit to be susceptible or not susceptible to landslide.

The originality of the proposed method for landslide susceptibility mapping is twofold:

1. The identification of fuzzy emerging patterns allows building a synthetic and explicit (thus comprehensible) knowledge-base of the factors that favour/disfavour landslide occurrence, which can aid geologists to integrate and revise their knowledge on landslide controlling factors;
2. The procedure associates to each classified slope unit a hesitation margin that depends on the quality and the reliability of the obtained classification. For example, two slope units can be classified as susceptible to landslides with different hesitation margins, i.e., e1 = 0,9 and e2 = 0,1, respectively. This means that the uncertainty of the classification is high for the slope unit 1 and lower for the slope unit 2; in fact, a high hesitation margin reveals that the available knowledge, expressed by the fuzzy rules, is contradictory. This second situation must be further examined by revising the available knowledge with new training data and new analysis.

The following section briefly describes and formalizes the concept of fuzzy emerging patterns, which is the basic notion for the proposed method. The method is then applied to the Collazzone area and the preliminary results are analysed and discussed.

Basic Notion: Fuzzy Emerging Patterns

Let us consider a set O of objects $o = (v_1, \ldots, v_M, c)$ each one described by both a set of values $v_1 \in D_{A1}, \ldots, v_M \in D_{AM}$ of a set of independent variables $A_1, \ldots, A_M$ and a value c (a class identifier) of a dependent variable C, whose values are defined on a categorical domain with cardinality equal to K.

Further, given a subset of the previous set of variables for which N_A ($1 < N_A < |D_A|$) distinct linguistic values $l_{i,A}$ with membership functions $\mu_{li,A}: D_A \rightarrow [0,1]$ are defined, a fuzzy pattern fp is defined as a conjunction of fuzzy predicates as follows:

$$fp = A_1 \text{ is } l_{i,A1} \text{ and } A_2 \text{ is } l_{j,A2\ldots} \text{ and } A_s \text{ is } l_{h\,As}, \quad (1)$$

fp is a fuzzy emerging pattern for a set of objects O if it is a distinguishing feature of one of the categories in C, i.e., of one class with respect to the other classes.

To define a fuzzy emerging pattern it is necessary to introduce a measure of the discrimination power of a fuzzy pattern fp.

We denote by $sup(o, fp)$ the support of the fuzzy pattern fp by the object $o = (v_1, \ldots, v_M, c)$:

$$sup(o, fp) := min_{li \in fp}\{\mu_{li}(v_i)\} \quad (2)$$

$sup(o, fp)$ is the minimum membership degree among those of the values v_i of o to the linguistic values l_i in fp.

The support of fp with respect to the class $c_i \in C$ is defined as follows:

$$CSup(c_i,fp) = \sum_{o \in ci} sup(o,fp) \quad (3)$$

and the total support of *fp* in all K classes of C is defined as:

$$TSup(fp) = \sum_{ci \in C} CSup(c_i,fp) \quad (4)$$

The *Trust* of a fuzzy pattern is the ratio of the support of *fp* in the class with highest support, with respect to the total support of *fp* in all the classes of C:

$$Trust(fp) = (max_{ci \in C}\{CSup(c_i,fp)\})/TSup(fp) \quad (5)$$

Trust (*fp*) can be interpreted as the degree of membership of *fp* to the fuzzy set of "good patterns for classification" because it measures the ability of *fp* to discriminate among the classes.

When *Trust* (*fp*) = 0 it means that there are no objects in *O* that satisfy at least a little the fuzzy predicates in *fp*. When *Trust*(*fp*) = 1 it means that all the objects of the same class fully satisfy the fuzzy predicates defining *fp,* while the remaining objects of other classes do not. In this case *fp* describes the distinguishing features of the objects of a class C with respect to the other classes.

In the case when a set of fuzzy rules of the kind $fp \rightarrow c$, is available and one wants to select only those rules that have a good ability to discriminate a set of objects among the classes in C, one can evaluate the *Trust (fp)* of the rules' antecedents on a training set of sample objects which are representative of the ones to classify. A selection of the best rules can be applied by imposing that *Trust* (*fp*) $> T > 0.5$, where *T* is minimum threshold value: the greater the *T* threshold, the stronger the ability of *fp* as antecedent of a fuzzy rule to classify objects.

In the context of our application the objects are the slope units and the dependent variable C assumes two values such that a slope unit is either susceptible or not susceptible to landslides. In the following section we describe the method that we applied for inducing a set of fuzzy rules from a training data set from which, then, we selected the best rules by evaluating the condition *Trust (fp)* > 0.5 on their antecedents *fp*.

The Proposed Method: Inducing Fuzzy Rules and Classifying Slope Units

The method proposed exploits the formal notions previously illustrated and in particular the use of fuzzy emerging patterns and their discrimination power. This section describes and discusses its step-by-step application on a study area.

The study area of Collazzone extends for 78.9 km^2 in central Umbria, Italy. In this area, the Institute IRPI of the Italian National Research Council (CNR) collected and organized several thematic data and prepared landslide susceptibility models through discriminant analysis (Guzzetti et al. 2006).

The study area was partitioned in 894 slope units starting from a 10 × 10 m DTM using specialised software. Each slope unit is characterized by 45 variables (see Table 1): a number of morphological and hydrological parameters derived from the specialized software, some corresponding to those acquired by traditional methods, (for example, channel length, stream order, link length), others defined to model the spatial distribution of landslides (for example the slope unit area, the slope unit terrain gradient, the slope unit aspect, the slope unit terrain roughness); The slope units are also characterized by lithological and structural information including bedding attitude and land-use.

First Step: Selection of Learning Training Sets

Slope units were sub-divided into two classes, i.e., units free of landslides (not susceptible slope units) and units with landslides (susceptible slope units).

The assumption was that a slope unit can belong only to one of the two classes. This binary classification was done based on the distribution of landslides derived by a multi-temporal inventory map prepared through the systematic interpretation of five sets of aerial photographs and integrated by field surveys (Guzzetti et al. 2006).

For this classification we have considered only the subset of shallow landslides.

For each slope unit we computed the percentage of coverage with shallow landslides. Slope units having less than 2 % of the area covered by shallow slope failures were considered free of landslides, whilst slope units having 2 % or more of their area covered were considered as containing landslides.

The scope of the models based on discriminant analysis developed in Guzzetti et al. (2006) was to determine the group membership of a slope unit to the class of not susceptible or susceptible units by finding a linear combination of the environmental variables which maximises the difference between the population of slope units affected and not affected by landslides with minimal error. In our method, the objective is different, since the role of the *a priori* classification of slope units is to train a set of fuzzy rules capable to reproduce as much as possible the prior binary classification into not susceptible or susceptible units, and to provide an indication of the uncertainty of the decision for each slope unit. When the uncertainty for a slope unit

Table 1 List of independent variables describing a slope unit

Variable name	Description	Partition number	Best partition method
ALLUVIAL	Recent alluvial deposit	3	Kmeans
SANDST	Sandstone	3	Kmeans
CLAY	Clay	3	Kmeans
LIMES	Limestone	3	Kmeans
CONTI	Continental deposit	3	HFP
GRAVEL	Gravel and coarse continental sediments	3	Regular
MARL	Marl	3	Regular
SAND	Sand	3	HFP
TRAVERTI	Travertine	3	HFP
FOREST	Forested area	3	Kmeans
URB	Urban area	3	HFP
FRUIT	Fruits trees	3	HFP
PASTURE	Pasture	3	HFP
SA	Cultivated area with trees	3	HFP
SS	Cultivated area	3	Kmeans
VIN	Vineyards	3	HFP
REG	Bedding dipping into the slope	3	Kmeans
FRA	Bedding dipping out of the slope	3	Kmeans
TRA	Bedding dipping across the slope	3	Kmeans
FRA_OLD	Deposit of ancient landslides	3	Kmeans
ORDER	Slope unit drainage channel order	3	Kmeans
MAGN	Slope unit drainage channel magnitude	3	HFP
LINK_LEN	Slope unit drainage channel length	3	HFP
AREAT_K	Drainage basins total area upstream the slope unit	3	HFP
R	Slope unit surface roughness index	3	HFP
ELV_M	Slope unit mean elevation	3	HFP
ELV_STD	Slope unit elevation standard deviation	3	Kmeans
SLO_ANG	Slope unit mean terrain gradient	3	Kmeans
ANG_STD	Slope unit terrain gradient standard deviation	3	Kmeans
LNK_ANG	Drainage channel mean slope	3	HFP
SLO_LEN	Slope unit length	3	Kmeans
LEN_STD	Standard deviation of terrain unit length	3	HFP
ANGLE1	Slope unit terrain gradient (lower portion)	3	HFP
ANGLE2	Slope unit terrain gradient (intermediate portion)	3	HFP
ANGLE3	Slope unit terrain gradient (upper portion)	3	Kmeans
TR1	Slope unit facing N-NE	2	Regular
TR2	Slope unit facing S-SE	2	Regular
TR3	Slope unit facing S-SW	2	Regular
CONC	Concave profile downslope	2	Regular
CONV	Convex profile downslope	2	Regular
COV_COC	Concave–convex slope downslope profile	2	Regular
COC_COV	Convex–concave slope downslope profile	2	Regular
RET	Slope unit rectilinear profile	2	Regular
IRR	Slope unit with irregular slope (downslope profile)	2	Regular
CC	Downslope concave slope	3	HFP

classification is high, the computed rules bear some inconsistencies.

To test the procedure, we selected several training sets each one containing the same number N of positive and negative examples, (i.e. Pos and Neg), where Pos contains susceptible units and Neg not susceptible units.

We assume that the slope units affected or not affected by landslides in the past will have the same level of susceptibility are susceptible to landslides also in the future.

For sensitivity analysis we selected several training sets of distinct quality (see details below) containing 10 %, 20 %, 30 %, and 45 % of the total number of classified slope units

(i.e., 894). The quality of a training set is determined by the criterion used for the selection of the examples: we applied three criteria, i.e., a random selection, the best choice and the worst choice. The random selection collects heterogeneous examples of slope units, the best and the worst criteria select slope units having homogenous characteristics. The best choice is aimed at providing the learning mechanism with the best available examples of both not susceptible and susceptible units to test the maximum level of accuracy that the classification can achieve given the best available training set. Conversely, the worst choice is aimed at providing the learning mechanism with the worst available examples to test the level of accuracy that the classification can achieve given the worst available training set.

The best choice aims at selecting the slope units with the clearest classification. It consists in first ordering the slope units in decreasing order considering the area affected by shallow landslides. The last ranked slope units were those corresponding to the less susceptible and most extended units. Large landslides are in this way more likely to be selected in the positive training set. The reason of this ordering is to consider that if a slope unit is fully covered by a landslide, the values of its variables might strongly characterise landslide occurrence, while if a slope unit is marginally covered by landslides its values might weakly characterise landslide occurrence. After ranking, we selected the first N/2 and last N/2 slope units as positive and negative examples, respectively; N is the desired cardinality of the training set; for example, when we generate a training set with the 10 % of slope units (894) N = round (0.1*894) = 89. Positive and negative samples are used to train the learning phase of fuzzy rules. We provide the learning phase with selected training sets containing the slope units that are selected as best examples of susceptible and not susceptible areas.

The worst choice consists in selecting the N central slope units in the previously ordered list, which correspond to the slope units whose classification is most ambiguous since they are only partially covered by past landslides with a percentage of their area around 2 %.

Second Step: Identification of Fuzzy Partitions for each Variable Domain

Given a training set of N positive and negative examples, we first need to determine a good fuzzy partition for each variable A, by defining a given number *h* of linguistic values with their membership functions $\mu_{1A,\ldots}\mu_{hA}$. This choice is particularly difficult and long due to the number of variables describing the units (see Table 1).

For this reason, we used the GUAJE fuzzy data analysis tool (Guaje 2010), making several trials by specifying distinct values for the number of fuzzy partitions, and by applying three distinct partition methods: the regular partition method, in which all the membership functions have the same shape and are homogenously distributed on the variable domain; the Kmeans partition method, that applies the Kmeans clustering algorithm (see *LIMES* and *ELV_STD* in Fig. 1); the Fuzzy Hierarchical Partitioning (FHP) method that applies an agglomerative clustering algorithm (Guaje 2010; Guillame and Magdalena 2006) (see *CC* and *SAND* Fig. 1). Due to their specific properties (Guillame and Magdalena 2006), all the membership functions of the linguistic values of the variables were defined with triangular shape, except those at the domain borders of the variable domains, which were defined with semi trapezoidal shape. We remind that a triangular membership function μ on a domain D is a piecewise linear function represented by three values of the domain D (*left, central, right*) with *left* $\leq$ *center* $\leq$ *right* that define the x coordinate of the points (*left*, 0) (*center*, 1) (*right*, 0) delimiting the four linear pieces of the function.

A semi trapezoidal membership function is a piecewise linear function that can be either descending at the left edge D_{min}, or ascending at the right extreme D_{max} of the variable domain and is represented by four values (D_{min}, *left, right,* D_{max}) defining the x coordinates of the points (D_{min}, *1*) (*left*, 1) (*right*, 0) (D_{max}, 0) for the descending function and (D_{min}, *0*) (*left*, 0) (*right*, 1) (D_{max}, 1) for the ascending function delimiting the three linear pieces.

By applying the three partition methods we generated 12 distinct fuzzy partitions for each of the 45 variables with linguistic values from 2 up to 5. Then, for each variable A we selected the partition with best quality, i.e., the one that has the smallest fuzzy partition Entropy PE, the greatest Partition Coefficient PC and the greatest Chen index *Ch* (Bezdek and Pal 1998; Guillaume and Magdalena 2006) defined as follows, respectively:

$$PE = -\frac{1}{N}\left\{\sum_{k=1,\ldots N}\sum_{i=1,\ldots h}\mu_{iA}(v_k)\log_2(\mu_{iA}(v_k))\right\} \tag{6}$$

$$PC = \frac{\sum_{k=1,\ldots N}\sum_{i=1,\ldots h}\left(\mu_{iA}(v_k)^2\right)}{N} \tag{7}$$

$$Ch = \frac{1}{N}\sum_{k=1,\ldots N}\max_{i=1,\ldots h}\{\mu_{iA}(v_k)\} - \frac{2}{h(h-1)}\sum_{i=1,\ldots h-1}\sum_{j=i+1\ldots h}\frac{1}{N}\sum_{k=1,\ldots N}\min(\mu_{iA}(v_k),\mu_{jA}(v_k)) \tag{8}$$

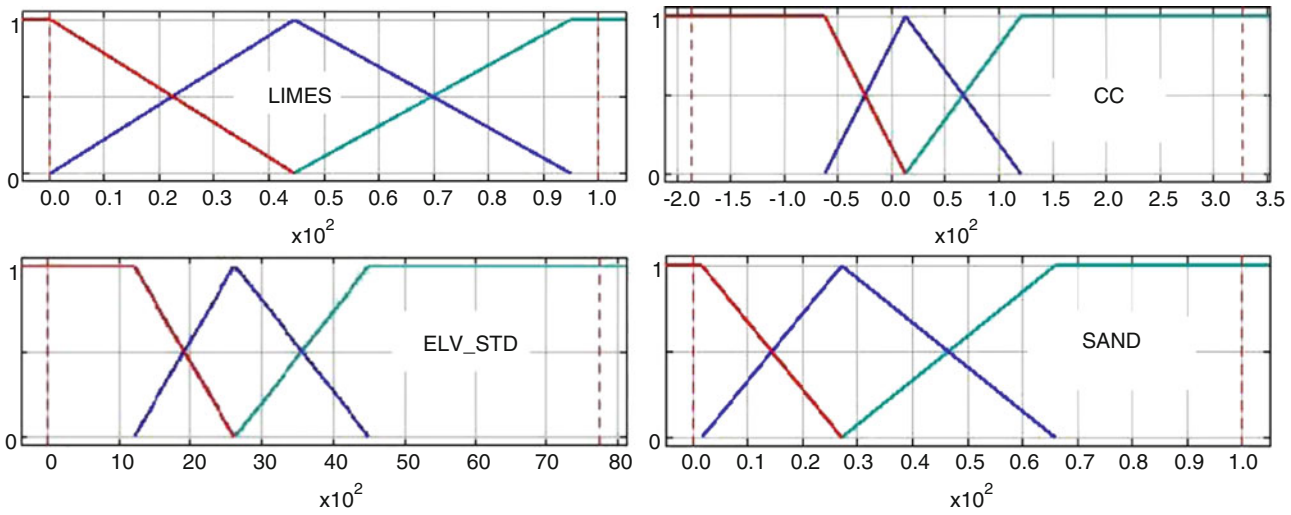

Fig. 1 Membership functions defining the linguistic values *low*, *medium* and *high* of the variables *LIMES* (Limestone) and *ELV_STD* (Slope unit elevation standard deviation) obtained by the Kmeans clustering, and of *CC* (Downslope concave slope), and *SAND* (sand) obtained by FHP method on the 30 % training set with best choice

For each variable of Table 1 the third column reports the number of linguistic values and the fourth column the partition method that has been deemed as providing the best partition on the basis of the quality measures *PE*, *PC* and *Ch*; these values are obtained on the 10 % training set selected with the best choice.

Variables in Table 1 are the so called independent variables, included in the antecedent part of a rule. In our case the consequent part of the rule contains only one variable, which is of course dependent, and giving the final value of susceptibility/non susceptibility. It is called *FRAX*. A fuzzy partition has to be provided also for this variable.

Since the objective of this study is to compare the accuracy of the classification of our method with the truth provided by the *a priori* binary classification of slope units, we defined two complementary membership functions, named *low* and *high* on the unit domain [0,1] with triangular membership functions *low* = (0,0,1) and *high* = (0,1,1). A slope unit of the training set classified as susceptible has maximum membership degree to *high* equal to 1, while it has minimum membership degree to *low* equal to zero, and *viceversa* for the not susceptible units.

Third Step: Fuzzy Rules Induction

After the partition phase, on the basis of the identified best fuzzy partitions for each variable, and the defined fuzzy partition for the dependent variable, we generated a set of fuzzy rules by applying the Fuzzy Decision Tree method implemented by the learning algorithm known as fuzzy ID3 (Ichihashi et al. 1996). A fuzzy rule is a path of the tree from the root to a leaf. The set of fuzzy rules generated was revised and reduced by evaluating the *Trust*, as defined in (1) of their antecedent; the fuzzy rules with trust above 0.5 were retained and stored in the knowledge-base for later use in the fuzzy inference process of classification. In Table 2 the fuzzy rules mined from the 10 % training data set with best choice is depicted. The rule number 2 in the last row means that

"if *LIMES* is *High* then *FRAX* is *low*"

independently from the values of all other variables.

The rule number 1 in the second row from bottom means that

"if *LIMES* is *low* and *ELV_M* is *medium* then *FRAX* is *high*"

independently from the values of all other variables.

Notice that, following the rule revision obtained by applying the *Trust* evaluation, only 6 variables out of 45 play an active role in the classification process.

The rules are reported in decreasing order of the trust of their antecedent (i.e., trust of the fuzzy emerging pattern).

Fourth Step: Classification by Fuzzy Inference with the Generated Knowledge-Base

We used the FISpro tool (Guillame and Chamomordic 2011) to perform the inference process that applies the fuzzy rules, induced in the previous phase, to classify new slope units. We used the Mamdani implication, and choose the "fuzzy output" option in order to obtain a degree of membership of each classified slope unit to both *low* and *high*

Table 2 Fuzzy rules mined from the 10 % training set (89 slope units) selected with best choice (*L low, M medium, H high*)

Rule	LIMES	SAND	ELV_M	ELV_STD	LINK_ANG	TR2	FRAX
3	*L*		*L*	*L*	*M*		*H*
4	*L*	*L*	*L*	*L*	*L*	*L*	*L*
5	*L*		*L*	*M*			*H*
1	*L*		*M*				*H*
2	*H*						*L*

FRAX. A slope unit whose dependent variable *FRAX* has greater membership degree to *low* than to *high* is interpreted as not susceptible; *viceversa* it is considered susceptible to landslides.

The difference between the two membership degrees, which is a value in [0,1], is the complement of the hesitation margin, i.e., the uncertainty u of the classification of the slope unit o:

$$u(o) = 1 - |\mu_{high_{\mathrm{FRAX}}}(o) - \mu_{low_{\mathrm{FRAX}}}(o)| \qquad (9)$$

When $u(o) = 1$ the uncertainty is maximum, thus the classification is completely undetermined since the decision process assigned the slope unit to both classes with same degree. Conversely, when $u(o) = 0$ the decision on the classification is certain. Intermediate values mean partial uncertainty of the classification.

Discussion of the Results

Table 3 reports the summary of the results obtained with distinct training sets, selected based on the distinct criteria described in the previous subsections, namely with random selection, best choice criterion and worst choice criterion, and with distinct number of slope units corresponding to 10 % 20 % 30 %, and 45 % of the available total number of classified data (894). An experiment of rule generation and classification by using all available data for the training was also carried out (the results are shown in Table 3). For each training set Table 3 reports the number of fuzzy rules induced, the number of active variables that these rules use as input variables, the mean accuracy of the classification, and the mean hesitation margin that expresses the uncertainty of the classification.

The mean hesitation margin reaches the maximum for the random selection and the minimum for the best choice of the training set. In the case we used all data as training set we achieved the minimum hesitation margin of 0,04.

Surprisingly, the best accuracy of 96 % is obtained with the smallest training set (10 % of all data), selected by the best choice criterion, which generated the 5 rules reported in Table 2 in decreasing order of their support, with 6 active variables, out of which two are lithological (*LIMES* and *SAND*) and four are morphological (*ELV_M*, *ELV_STD*, *LNK_ANG* and *TR2*). It's worth noticing that the hesitation margin of the classification obtained with this training set is very low (0.14), just second to 0.04 obtained by using all data as training set (last row of Table 2), that, nevertheless, achieved a smaller mean accuracy (94 %) with a much greater number of rules (71) and 28 active variables. This is explained by the fact that providing too many examples the rule induction process is over fitted and thus is unable to synthesise the main characteristics of the phenomenon; conversely, providing a few well characterized examples as those obtained with the best choice, the rule induction process can learn the main discriminating characteristics.

We observed a stability of the rules induction process when using a training set with percentage ranging between 20 % and 30 % based on the best choice criterion. In fact, we obtained the same mean accuracy of 92 % and hesitation margin equal to 0.26, which are a greater accuracy and a smaller hesitation margin with respect to those obtained with other choices of the training set with same percentage. In this case the rules are 11 and the 14 active variables are *LIMES*, *CONTI*, *MARL*, *SAND*, *FOREST*, *FRUIT*, *FRA*, *ELV_STD*, *LNK_ANG*, *LEN_STD*, *ANGLE2*, *ANGLE3*, *IRR*, *CC*. Thus, by duplicating the training set dimension (from 10 % to 20 %) we duplicated the number of rules and increased the active variables. Nevertheless this tendency is not linear.

The worst choice of the 20 % and 30 % training sets produced a worst mean accuracy of 90 % and 87 % respectively with a greater hesitation margin of 0.27 and 0.3 respectively. The number of rules and active variables are more or less susceptible too.

The random choice of the training sets generally produced lower accuracies than the other choices. This could suggest that the random training set might have selected slope units which are too heterogeneous with respect to the dimensions of the landslides than the slope units selected with the other choices. This characteristic does not favour the induction of a synthetic set of good representative fuzzy rules. In fact, the hesitation margins of the classifications obtained with the random sets are also the greatest.

A general observation is that the variables that were most often selected as playing an active role in the fuzzy rules in

Table 3 Classification results obtained on the 894 slope units by applying the fuzzy rules learned with distinct training sets

Training set selection method	% of all data available (%)	Number of fuzzy rules	Number of active variables	Mean accuracy (%)	Mean hesitation margin
Random	10	11	12	87	0.3
	20	14	22	88	0.3
	30	13	27	75	0.43
	45	25	21	82	0.36
Best choice	10	5	6	96	0.14
	20	11	14	92	0.26
	30	11	14	92	0.26
	45	22	25	85	0.35
Worst choice	10	11	12	87	0.3
	20	14	15	90	0.27
	30	11	12	87	0.3
	45	16	20	86	0.31
All data	100	71	28	94	0.04

all the experiments are the following (in decreasing order of frequency): *LNK_ANG*, *FRA*, *TRA*, *LIMES*, *COV_COC*, *SAND*, *REG*, *TR2*, *TR3*, *IRR*, *CLAY*, *CONTI*, *GRAVEL*, *SS*, *R*, *ELV_STD*, *SLO_ANG*, *SLO_LEN*, *ANGLE1*, *ANGLE2*, *ALLUVIAL*, *TRAVERTI*, *FOREST*, *FRUIT*, *SA*, *FRA_OLD*, *ORDER*, *ANGLE3*, *TR1*, *CONV*, *URB*, *LNK_LEN*, *LEN_STD*, *CONC*, *COC_COV*, *CC*.

Conclusions

A supervised learning method of fuzzy rules induction has been proposed for generating a synthetic and comprehensible knowledge-based describing the independent variables that characterise a set of slope units with respect to their susceptibility to the occurrence of landslides.

In order to analyse the sensitivity of the rule induction process, the method has been applied using several distinct training sets, containing already classified examples, and the obtained rules are then tested on a larger set of data. The results obtained, measured in terms of accuracy and hesitation margin, are encouraging; furthermore the experiments caused a strong reduction in the number of variables required to perform the classification. However, the feasibility of the approach on larger dataset needs a confirmation.

References

Bezdek JC, Pal NR (1998) Some new indexes of cluster validity. IEEE Trans Syst Man Cybernetics—Part B: Cybernetics 28(3):301–315

Carrara A (1988) Drainage and divide networks derived from high fidelity digital terrain models. In: Chung CF, Fabbri AG, Sinding-Larsen R (eds) Quantitative analysis of mineral and energy resources, NATO-ASI Series. D. Reidel Publishing Co, Dordrecht, pp 581–597

Dong G, Li J (1999) Efficient mining of emerging patterns: discovering trends and differences. In: Proceedings of the fifth ACM SIGKDD international conference on knowledge discovery and data mining, San Diego, California, United States, ACM, pp 43–52

Dong G, Zhang X, Wong L, Li J (1999) Caep: classification by aggregating emerging patterns. DS'99, vol 1721 of Lecture Notes in Computer Science, Japan

García-Borroto M, Martínez-Trinidad J, Carrasco-Ochoa J, (2010) Fuzzy emerging patterns for classifying hard domains. Knowledge and Information Systems, Springer, London, 0219, Computer Science, pp 1–17

GUAJE (2010) A Java environment for generating understandable and accurate models. In: Alonso JM, Magdalena L (eds) ESTYLF 2010. Proceedings of the XV Spanish conference for fuzzy logic and technology, Huelva, 3–5 Feb, pp 399–404

Guillaume S, Magdalena L (2006) Expert guided integration of induced knowledge into a fuzzy knowledge base, soft computing, 10, 9 pp 773–784

Guillaume S, Charnomordic B (2011) Learning interpretable fuzzy inference systems with FisPro. Infor Sci, doi:10.1016/j.ins.2011.03.025 (in press)

Guzzetti F, Reichenbach P, Ardizzone F, Cardinali M, Galli M (2006) Estimating the quality of landslide susceptibility models. Geomorphology, 81: 166–184. Li J

Ichihashi H, Shirai T, Nagasaka K, Miyoshi T (1996) Neuro-fuzzy id3: a method of inducing fuzzy decision trees with linear programming for maximizing entropy and an algebraic method for incremental learning. Fuzzy Set Syst 81:157–167

Li J, Dong G, Ramamohanarao K (2000) Instance-based classification by emerging patterns. In: Proceedings of the 4th European conference on principles of data mining and knowledge discovery, Lyon, France, September 13–16, 2000. Springer, pp 191–200

Pradham B (2010) Application of an advanced fuzzy logic model for landslide susceptibility analysis. Int J of Comput Intell Sys 3 (3):370–381

Ramamohanarao K, Fan H (2007) Patterns based classifiers. World Wide Web 10(1):71–83

Zadeh LA (1965) Fuzzy sets. Inf Control 8:338–353

Analysis of Landslide Susceptibility Using Monte Carlo Simulation and GIS

Heon-Woo Lee, Hyuck-Jin Park, Ik Woo, and Jeong-Gi Um

Abstract

Since the landslide is one of the repeated geological hazards and causes a terrible loss of life and properties in Korea, many different researches have been carried out to evaluate the hazard and the susceptibility of landslide. The physical landslide model has been suggested to evaluate the factor of safety in previous studies but the deterministic approach has been utilized. However, applying the deterministic model in regional study area can be difficult or impossible because of the difficulties in obtaining and processing of large spatial data sets. With limited site investigation data, uncertainties were inevitably involved with. Therefore, the probabilistic analysis method such as Monte Carlo simulation has been utilized in this study. The GIS based infinite slope stability model has been used to evaluate the probability of failure. The proposed approach has been applied to practical example. The study area in Pyeongchang-gun, Gangwon-do has been selected since the area has been experienced tremendous amount of landslide occurrence.

Keywords

Monte Carlo simulation • Probability of failure • Uncertainty

Introduction

Landslides are one of the repeatedly occurring geologic hazards experienced during the rainy season in Korea. They cause the loss of about 23 human lives each year, which accounts for nearly 25 % of the annual death due to all natural disasters. Regardless of this, the development and urbanization of mountainous areas is continuing, and consequently slope instability is further exacerbated and the potential for landslides is increased.

Landslide occurrence is controlled by spatial and climatic factors such as geology, geomorphology, vegetation, and rainfall, and hence the prediction of, or susceptibility analysis for, landslides is difficult. This is because an enormous amount of spatial data must be acquired from the region and then processed. Consequently, GIS (Geographic Information Systems) has been widely and effectively used in analyzing the spatial information relevant to landslides. A great advantage of using GIS is that all spatial attributes related to a particular area can be presented in the form of a digitized map that can be saved, searched, modified, and updated. It can also cover the general area, allowing regional scale geographic and geologic data to be readily analyzed. This capability has facilitated many studies on landslide hazard assessment using GIS (Carrara et al. 1991; Gokceoglu and Aksoy 1996; Luzi and Floriana 1996; Guzzetti et al. 1999; Jibson et al. 2000; Lee and Min 2001; Gritzner et al. 2001; Lee and Choi 2003).

H.-W. Lee (✉) • H.-J. Park
Department of Geoinformation Engineering, Sejong University, 98 Gunja-dong, Gwangjin-gu, Seoul, Republic of Korea
e-mail: sglee@uos.ac.kr

I. Woo
Department of Coastal Construction Engineering, Kunsan National University, Gunsan, Republic of Korea

J.-G. Um
Department of Energy Resource Engineering, Pukyong National University, Busan, Republic of Korea

C. Margottini et al. (eds.), *Landslide Science and Practice*, Vol. 1,
DOI 10.1007/978-3-642-31325-7_49,

Landslide hazard assessment methods can be divided into two categories: quantitative and deterministic (or geotechnical). The quantitative technique ranges from a stability scoring system based on criteria such as slope, vegetation, parent material, and geometry, to statistical models that link geologic and geomorphologic attributes based on spatial correlation (Chung et al. 1995; Chung and Fabbri 1998, 1999; Dhakal et al. 2000). Most GIS techniques used in numerous previous studies only consider the statistical relationships between landslide occurrences and factors such as soil type, land use, slope geometry, vegetation, and other parameters, but not the failure mechanism. In other words, the relationship between events and the environment has been investigated without reference to a mechanical analysis. In contrast, the geotechnical approach analyzes the mechanical condition of slopes and evaluates their stability through mathematical calculation (Montgomery and Dietrich 1994; Wu and Sidle 1995; Gorsevski 2002). In this approach, the physical properties of a slope are obtained and a mathematical model is used to evaluate the landslide susceptibility and hazard potential. The factor of safety (FS) is calculated in this approach as an index of landslide susceptibility. The geotechnical technique was used in this study in order to overcome the limitation of the quantitative technique. However, the input parameters used in geotechnical technique should be obtained from very broad study area with limited number of sampling and subsequently, the uncertainties were involved. But the deterministic analysis used only mean values for input parameters and consequently could not properly with uncertainties involved in input parameters Therefore, the probabilistic analysis was proposed in this study to control the unceratinties effectively.

Probabilistic Analysis of Landslide Hazard

Physical Landslide Model

In order to utilize the geotechnical failure model and apply the mechanical properties of soil to susceptibility analysis the infinite slope model is used. In this, the slope is assumed to extend infinitely in its dip direction, and sliding is considered to occur along a plane parallel to the face of the slope. This is the most usual approach in landslide analysis (Kamai 1991; Terlin 1996; Pack et al. 1998, 2001). When the lengths of the landslide slip surfaces are large enough compared with their depths, the infinite slope model may be accurately and successfully adapted. This model is appropriate for Korean landslides where the sliding surfaces are commonly located at shallow depth (NIDP 2000).

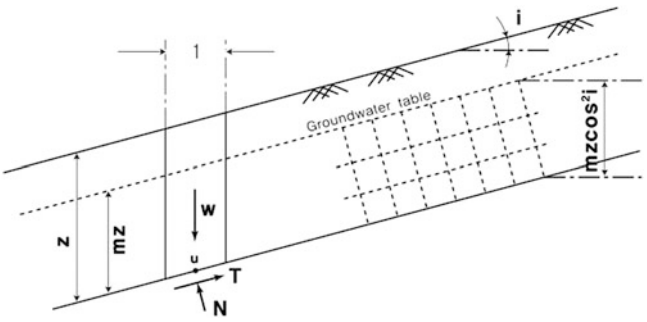

Fig. 1 Infinite slope model

As shown in Fig. 1, the groundwater level in an infinite slope is assumed to be parallel to the surface and to be located at *mz*. In addition, the groundwater flow is parallel to the slip surface. If a slice of infinite slope mass that has unit width is considered, as in Fig. 1, the normal (N) and shear stress (T) at the base of the slope element can be given as:

$$\mathrm{N} = W\cos i = [(1-m)\gamma_t + m\gamma_{sat}]z\cos i \tag{1}$$

$$\sigma = \frac{N}{\sec i} = [(1-m)\gamma_t + m\gamma_{sat}]z\cos^2 i \tag{2}$$

$$\mathrm{T} = \mathrm{W}\sin \mathrm{i} = [(1-m)\gamma_t - m\gamma_{sat}]z\sin i \tag{3}$$

$$\tau = \frac{T}{\sec i} = [(1-m)\gamma_t + m\gamma_{sat}]z\sin i\ \cos i \tag{4}$$

From Fig. 1, the pore water pressure is:

$$\mathrm{u} = \mathrm{mz}\,\gamma_w \cos^2 i \tag{5}$$

Then the shear strength along the failure plane is:

$$\mathrm{S} = \mathrm{c}' + (\sigma - \mathrm{u})\tan\phi \tag{6}$$

The factor of safety on the sliding surface is:

$$\mathrm{FS} = \frac{s}{\tau} = \frac{\mathrm{c}' + (\sigma - u)\tan\phi'}{\tau} \tag{7}$$

where i is the slope angle, γ_t is the total unit weight of soil, γ_w is the unit weight of water, γ_{sat} is the unit weight of saturated soil, z is the soil depth from the ground surface, m is the ratio of the groundwater level to the soil depth, $c'$is the effective cohesion, and $\varphi'$is the effective friction angle.

Probabilistic Approach

The strength parameters of soil, such as cohesion and friction angle are prerequisite to evaluate the factor of safety from the infinite slope model. However, true values of the cohesion and friction angle cannot be obtained from field investigation or laboratory test due to the extensive size of the study area and the limitation of the sampling numbers. Therefore, the uncertainties are involved in the procedure of determination for cohesion and friction angle. Consequently the cohesion and friction angle were considered as random variables in this study and subsequently the probabilistic approaches were implemeneted.

Monte Carlo simulation approach was used as the probabilistic approaches in this study to analyze the probabilistic properties of random variables and evaluate the probability of slope failure. The Monte Carlo simulation is known as the most complete probabilistic analysis since all the random variables are represented by their probability density function and the probability of failure as the result of reliability analysis is represented by the probability density function. The advantages of Monte Carlo simulation are that it is relatively easy to implement on a computer and it can deal with a wide range of functions, including those that cannot be expressed conveniently in an explicit form (Baecher and Christian 2003). Therefore, in this study, Monte Carlo simulation was used in the evaluation of the probability of slope failure. In the simulation procedure, random numbers between zero and one were generated from a uniform distribution. Then, using the cumulative distribution of the probability density function for each variable, a unique value for each variable was selected randomly. The group of randomly selected parameters was combined with the fixed input data to generate a single random value for the factor of safety. This process was repeated many times to generate a sufficient number of different factors of safety.

Study Area

The Pyeongchang-gun area of Korea was selected as a suitable test site for the proposed approach. On July 2006, this locality experienced a large number of landslides following heavy rainfall of 227 mm in 1 day. The bedrock of the study area consists mainly of biotite granite. Aerial photographs and 1:5,000 scale digital topographic maps were examined to locate the landslides. In addition, 1:5,000 scale topographic maps, 1:25,000 scale soil maps, and 1:50,000 scale geologic maps were examined. In order to accurately evaluate landslide susceptibility, the landslide activity was located both by using the aerial photographs and digital topographic maps and by conducting a field survey.

Table 1 Distribution of the slope failure probability for various groundwater levels when COV is 20 %

	m (%)			
Probability of failure (%)	0.0	0.5	0.75	0.9
0 ~ 1	67.0	51.5	43.8	39.5
1 ~ 5	14.1	13.0	11.4	8.0
5 ~ 10	4.2	6.4	5.9	4.3
10 ~ 20	3.9	6.9	7.4	6.2
20 ~ 30	2.0	4.1	4.9	5.0
30 ~ 50	2.5	5.1	6.9	8.0
50 ~ 70	1.7	3.4	4.8	6.8
70 ~ 90	1.8	3.3	4.8	6.4
90 ~ 100	2.8	6.6	10.1	15.8

Landslide Location Detection and Spatial Database Construction

The accurate detection and location of landslides is important for their susceptibility analysis. A field survey is widely considered the most accurate detection method in the landslide inventory process. However, using a field survey as an incipient step in the data collection process is difficult, time consuming, and costly, especially in mountainous areas where access is limited or even impossible. Remote sensing is therefore employed to overcome the lack of field data.

For this work, aerial photographs taken before and after landslides were used to detect event locations. Field surveys were used to verify landslide locations that were indicated by a study of aerial photographs. The slides were determined by a comparison of the sequential images then verified by fieldwork. A photo database was constructed through orthorectification and by merging many images. Recent events were seen as a break in the forest canopy, bare soil, or other geomorphologic characteristics typical of landslide scars; for example, head and side scarps, flow tracks, and soil and debris deposited below the scar. Approximately 40 monochromatic aerial photographs were used to map recent landslides and to assemble a database to assess their surface area and number within the study region. A total of 483 landslides were mapped.

In order to analyze geomorphologic attribute such as slope angle, which is indispensable parameter in the geotechnical technique, digitized information is required. To achieve this, contour and survey base points with an elevation value read from the 1:5,000 scale topographic maps were extracted, and the digital elevation model (DEM) was made with a 5 m resolution. Using the DEM, the slope angle was calculated.

The 1:25,000 scale soil maps were used to acquire the characteristics of the soil, such as the topographic map, the soil texture map, and the effective soil depth. The topographic map was based on the geomorphology of soil

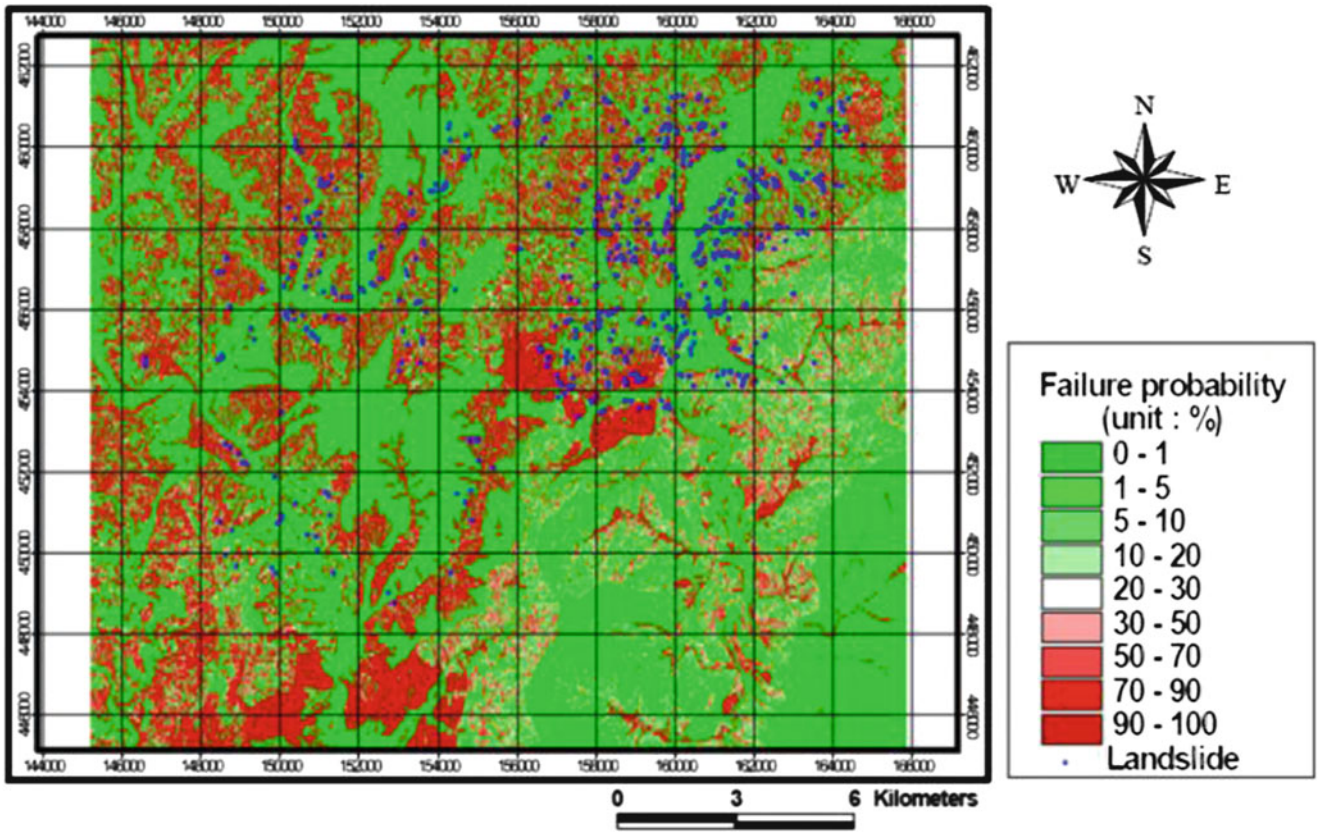

Fig. 2 Failure probability distribution when COV is 0.1. (latitude 37°36′12.16″N, Longitude 128°31′53.81″E)

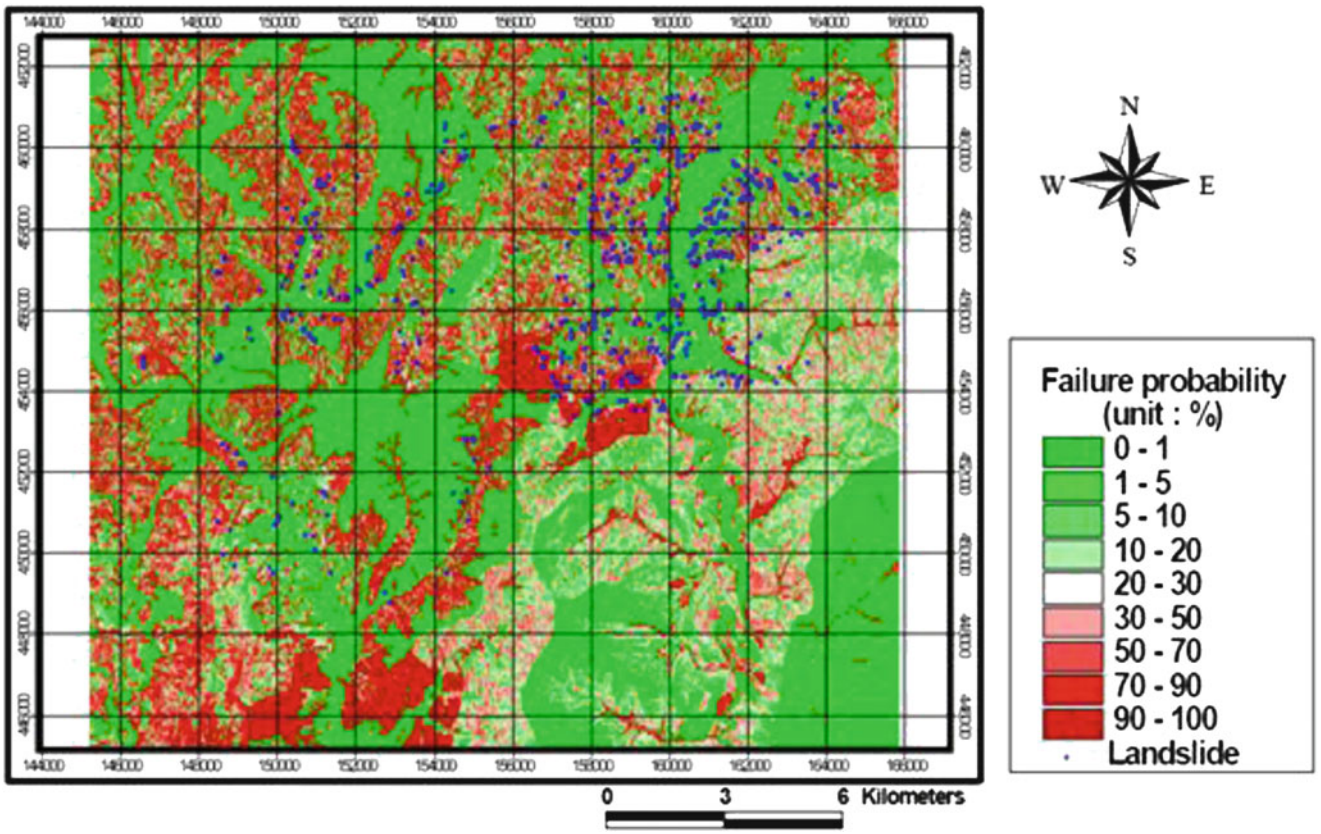

Fig. 3 Failure probability distribution when COV is 0.2. (latitude 37°36′12.16″N, Longitude 128°31′53.81″E)

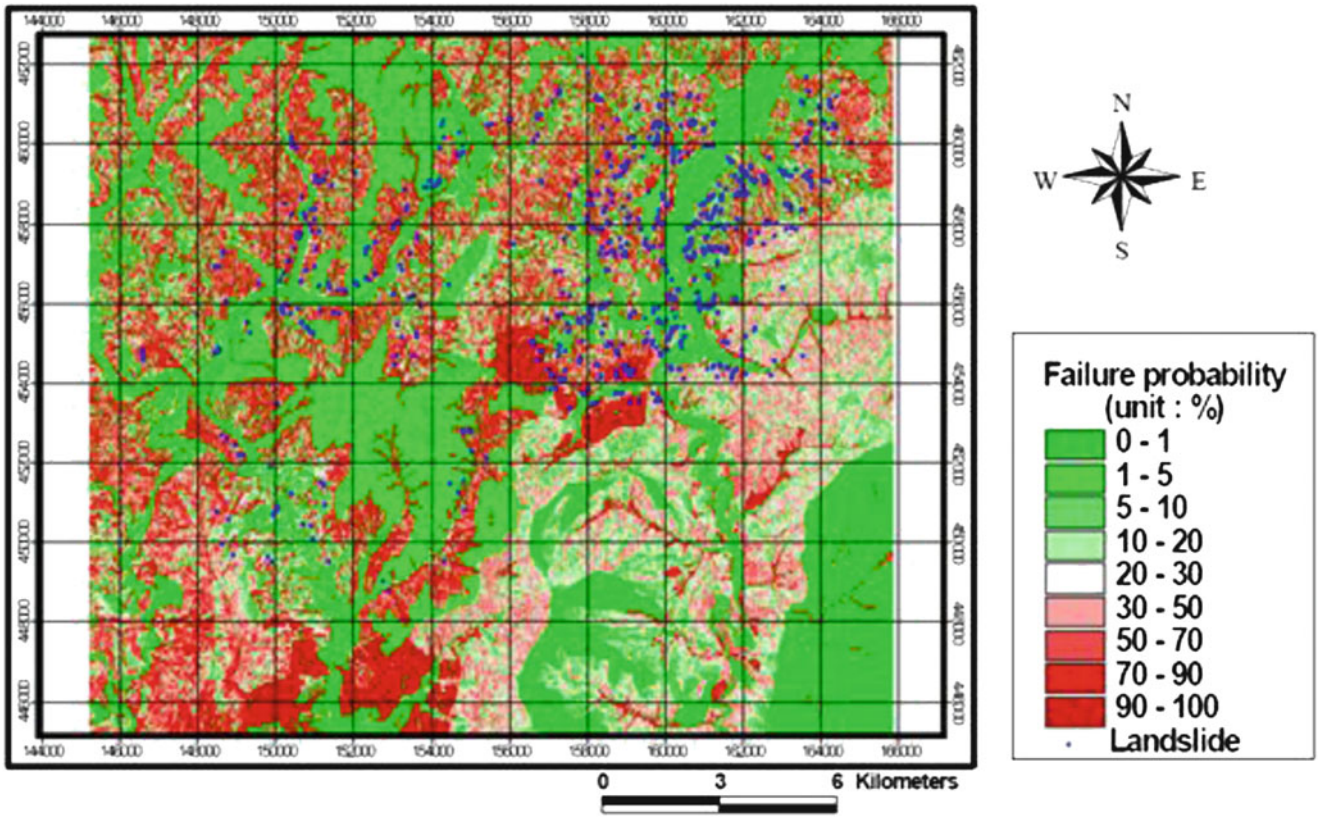

Fig. 4 Failure probability distribution when COV is 0.3. (latitude 37°36′12.16″N, Longitude 128°31′53.81″E)

Table 2 Percentage of landslide cells in hazard class

m (%)	0.0 (%)	0.5 (%)	0.75 (%)	0.9 (%)
COV = 10	17.1	34.0	46.8	59.2
COV = 20	27.5	49.2	60.2	67.5
COV = 30	48.4	63.9	68.9	72.3

distribution, and the soil texture map was based on the soil size distribution. The effective thickness was evaluated from the depth to bedrock. In addition, the geologic map was used to obtain the contributing lithology.

Analysis of Random Properties for Input Parameters and Monte Carlo Simulation

In the geotechnical model, the mechanical input parameters such as the shear strength of the soil, soil thickness, and the groundwater level are the requisite parameters. However, certain input factors such as cohesion and the friction angle of soil can be obtained only by laboratory testing and it is logistically difficult to acquire this information across the wide area of soils in the region. Consequently, the representative values of unit weight, cohesion, and internal friction angle for each soil type were determined from the research results of the Korea Highway Corporation (2009). In this procedure, the uncertainties were involved in cohesion and friction angle and therefore, they were considered as random variables. Then the probabilistic analysis approach was carried out. In order to carry out the probabilistic analysis, the probabilistic properties (that is, mean, standard deviation, and probability density function) of random variables should be determined. However, due to limited amount of data which can be obtained, they were estimated on the basis of judgment, experience, or results published by others (Hoek 2007). From the previous studies (Mostyn and Li 1993; Nilsen 2000; Pathak and Nilsen 2004; Park et al. 2005) the cohesion and friction angle were found to be normally distributed. The mean values of strength parameters for each soil type were estimated from the results of the previous research. However, the standard deviation of each random variable could not be obtained. Therefore, coefficients of variation (COV) for cohesion and friction angle were used. The coefficients of variation (COV) of cohesion and friction angle are known as 10 % in many previous researches (Schulz 1975; Cherubini 2000). However, since the cohesion and friction angle used in this study were estimated from the previous research, the uncertainties could affect the strength parameters more seriously. Therefore, the variances of the strength parameters could be larger than expected, so the larger COV (that is, 20 % and 30 %) was used to analyse in

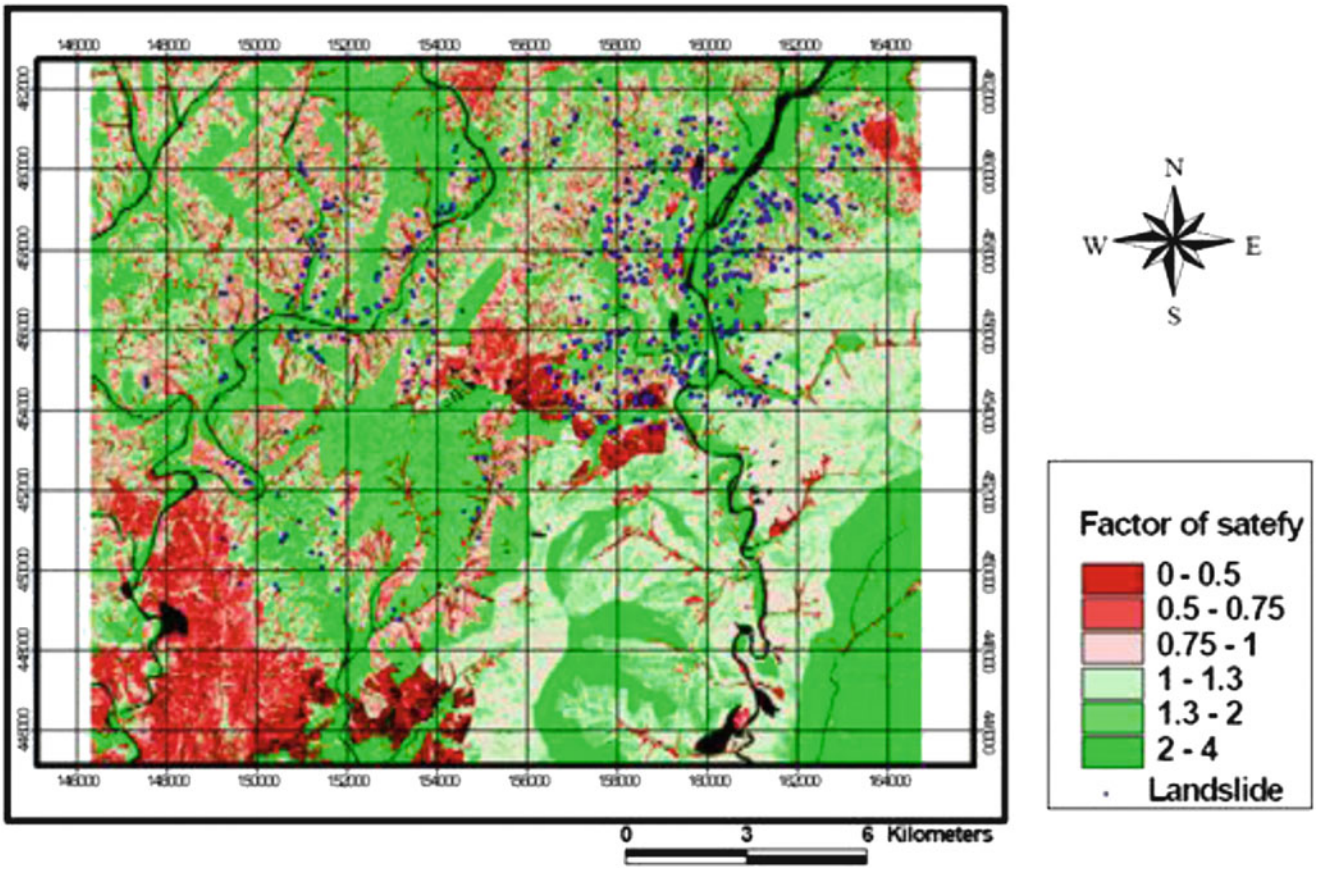

Fig. 5 Factor of safety distribution when m = 0.9. (latitude 37°36′12.16″N, Longitude 128°31′53.81″E)

Table 3 Results of the deterministic analysis

m (%)	0.0 (%)	0.5 (%)	0.75 (%)	0.9 (%)
% of landslide cells in hazard class	10.2	27.0	40.3	57.4

this study. That is, COV whose range were varied from 10 % to 30 %, were used in the probabilistic analysis in order to evaluate the effect of the uncertainties.

Using the probabilistic properties of random variables and other input parameters, the Monte Carlo simulation procedure was implemented in MATLAB software. The Monte Carlo simulation includes the following steps.

1. Generate the random variables such as cohesion and friction angle using random number generator and cumulative distribution function for cohesion and friction angle.
2. Calculate the factor of safety for a pixel using the generated random variables (cohesion and friction angle). After N repeated calculation, the probability distribution curve for the factor of safety is obtained. Then the probability of failure for the cell is evaluated.
3. Repeated the above calculation for all other pixels and produce the slope failure probability map.

In addition, in order to evaluate the effect of the groundwater to the stability of slope, the groundwater level (m in infinite slope model) was varied from 0 % to 90 % in the probabilistic analysis.

Evaluation of Slope Failure Probability

Table 1 shows the distributions of the probability of slope failure for the different groundwater level. As groundwater level rises due to rainfall, the area with high failure probability is increased and the area with low failure probability is decreased. This means the study area is becoming unstable, as expected. Figures 2, 3 and 4 show the calculated probability of slope failure at 90 % groundwater level for the cases of 10 %, 20 % and 30 % COV, respectively.

In order to verify the accuracy of the probabilistic analysis, the hazard class (or unstable cell) was determined. According to previous research (Priest and Brown 1983), 10 % of failure probability is evaluated as unstable.

Therefore, the cell whose probability of failure is larger than 10 % is designated as unstable.

Table 2 shows the percentage of landslide cells in hazard class. As can be observed in Table 2, the percentage of landslide cells in hazard class is increased with COV.

When the groundwater level is 90 %, the accuracy (percentage of landslide cells in hazard class) is 59.2 %, 67.5 % and 72.3 % at 10 % COV, 20 % COV and 30 % COV, respectively. That is, as COV is increased, the accuracy of the analysis is increased.

In order to compare the results of the probabilistic analysis with the deterministic analysis, the factor of safety was evaluated using same input parameters used in the probabilistic analysis. The result shows in Fig. 5 and Table 3. The percentage of landslide cells in hazard class in the deterministic analysis is 57.4 % at 90 % groundwater level. But this value is lower than the results of the probabilistic analysis, which show 59.2 %, 67.5 % and 72.3 % at 10 % COV, 20 % COV and 30 % COV, respectively. That is, the accuracy of the deterministic analysis is lower than the one of the probabilistic analysis. This is because the deterministic analysis used the single fixed mean values for cohesion and friction angle and, subsequently the variance (or uncertainties) of the data was not considered in the analysis. Consequently the probabilistic analysis which effectively deals with the uncertainties shows better outcome in the prediction of landslide hazard.

Results

Many different researches have been used to evaluate the susceptibility of landslide since the landslide is one of the repeated geohazards. The previous studies were mainly focused on the statistical relationship between causative factors and landslide occurrence. However, those approaches were not considered failure mechanisms and engineering properties of geological materials. Therefore in this study the physical landslide model has been suggested and the geotechnical input parameters were evaluated. However, uncertainties were inevitably involved with geotechnical input parameters since large spatial data set for input parameters are difficult to obtain from large study area. Therefore, Monte Carlo simulation, one of the most commonly used probabilistic analysis is used probabilistic analysis, is used. For this, cohesion and friction angle were considered as random variable and their mean values were obtained from soil map and previous researches. In order to evaluate the effect of the groundwater, the groundwater levels were varied from 0 % to 90 %. Furthermore, COV values in the uncertain parameters were varied from 10 % to 30 % to evaluate the uncertainties. The results showed that the probabilistic analysis method showed more accurate than the deterministic analysis.

Acknowledgments This work was supported by the National Research Foundation of Korea (NRF) grant funded by the Korea government (MEST) (No. 2010–0021314) and the project to educate GIS experts.

References

Baecher GB, Christian JT (2003) Reliability and statistics in geotechnical engineering. Wiley, New Jersey, 605

Carrara A, Cardinali M, Detti R, Guzzetti F, Pasqui V, Reichenbach P (1991) GIS techniques and statistical models in evaluating landslide hazard. Earth Surf Proc Land 20:427–445

Cherubini C (2000) Relibability evaluation of shallow foundation bearing capacity on c, phi soils. Can Geotech J 37:264–269

Chung CF, Fabbri AG (1998) Three Bayesian prediction models for landslide hazard. In: Proceedings of the international association for mathematical geology, Italy, pp 204–211

Chung CF, Fabbri AG (1999) Probabilistic prediction models for landslide hazard mapping. Photogramm Eng Rem Sens 65:1389–1399

Chung CF, Fabbri AG, van Westen CJ (1995) Multivariate regression analysis for landslide hazard zonations. In: Carrara A, Guzzetti F (eds) Geographic information system in assessing natural hazards. Kluwer, Dordrecht, pp 107–133

Dhakal AS, Amada T, Aniya M (2000) Landslide hazard mapping and its evaluation using GIS: an investigation of sampling schemes for a grid cell-based quantitative method. Photogramm Eng Rem Sens 66:981–989

Gokceoglu C, Aksoy H (1996) Landslide susceptibility mapping of the slopes in the residual soils of the Mengen region by deterministic stability and image processing techniques. Eng Geol 44:147–161

Gorsevski PV (2002) Landslide hazard modeling using GIS. Ph.D. thesis, University of Idaho, 240p

Gritzner ML, Marcus WA, Aspinall R, Custer SG (2001) Assessing landslide potential using GIS, soil wetness modeling and topographic attributes. Geomorphology 37:149–165

Guzzetti F, Carrara A, Cardinali M, Reichenbach P (1999) Landslide hazard evaluation; a review of current techniques and their application in a multi-scale study, Central Italy. Geomorphology 31:181–216

Hoek E (2007) Rock engineering; Course note by Evert Hoek [Online]. http://www.rockeng.utoronto.ca/Hoekcorner.htm

Jibson RW, Harp LW, Michael JA (2000) A method for producing digital probabilistic seismic landslide hazard maps. Eng Geol 58:271–289

Kamai T (1991) Slope stability assessment by using GIS. Science and Technology Agency of Japan, in Japanese

Korea Highway Corporation (2009) Road design cuideline, p 472

Lee S, Choi U (2003) Development of GIS-based geological hazard information system and its application for landslide analysis in Korea. Geosci J 7:243–252

Lee S, Min K (2001) Statistical analysis of landslide susceptibility at Yongin, Korea. Environ Geol 40:1095–1113

Luzi I, Floriana P (1996) Application of statistical and GIS techniques to slope instability zonation. Soil Dyn Earthq Eng 15:83–94

Montgomery DR, Dietrich WE (1994) A physically based model for the topographic control on shallow landsliding. Water Resour Res 30:1153–1171

Mostyn GR, Li KS (1993) Probabilistic slope analysis – state of play. In: Proceeding of conference on probabilistic method in geotechnical engineering, pp 89–109

NIDP (National Institute for Disaster Prevention) (2000) Fundamental issues for landslide hazard avoidance or mitigation plans. Research report, p 276 in Korean

Nilsen B (2000) New trend in rock slope stability analysis. Bull Eng Geol Environ 58:173–178

Pack TT, Tarboton DG, Goodwin CN (1998) The SINMAP approach to terrain stability mapping. In: Proceedings of the 8th congress of the international association of engineering geology, Vancouver, pp 21–25

Pack TT, Tarboton DG, Goodwin CN, (2001) Assessing terrain stability in a GIS using SINMAP. In: Proceedings of the 15th annual GIS conference, GIS 2001

Park HJ, West TR, Woo I (2005) Probabilistic analysis of rock slope stability and random properties of discontinuity parameters, Interstate Highway 40. Eng Geol 79:230–250

Pathak D, Nilsen B (2004) Probabilistic rock slope stability analysis for himalayan condition. Bull Eng Geol Environ 63:25–32

Priest SD, Brown ET (1983) Probabilistic rock slope stability of variable rock slopes. Trans Inst Min Metall, 92p

Schultz E (1975) The general significance of statistics for civil engineers. In: Proceedings of 2nd international conference on application of statistics and probability in soil and structural engineering, Aachen

Terlin MTJ (1996) Modeling spatial and temporal variations in rainfall triggered landslide. International Institute for Aerospace Survey and Earth Science, Publication no. 32

Wu W, Sidle RC (1995) A distributed slope stability model for steep forested basins. Water Resour Res 31:2097–2110

An Overview of a GIS Method for Mapping and Assessing Landslide Hazards

Gabriel Legorreta Paulín, Marcus Bursik, and José Lugo Hubp

Abstract

In Mexico, numerous GIS-based applications have been used to represent and assess slope stability. However, there is not a practical and standardized landslide mapping methodology under the GIS system. This work aims to illustrate a comprehensive methodology to characterize areas that are prone to slope instability. The Río Chiquito-Barranca del Muerto watershed on the southwestern flank of Pico de Orizaba volcano, the highest mountain in Mexico, was selected as study area. The study area has a combination of several contributing factors to landslides such as high rain fall during the wet season, rock types, high degree of weathering, and steep slopes.

The methodology encompasses three main stages of analysis to assess landslide hazards. The technique and its implementation in a GIS-based technology is presented and discussed.

Keywords

GIS • Landslides inventory • Landslide susceptibility • Multiple logistic regression

Introduction

In Mexico, volcanic regions are common and prone along the stream systems to small and large landslides and debris flows. This creates a potentially hazardous situation for people and property down the valleys. For example, on June 5th, 2003, lives and property were lost at the town of Balastrera (a settlement at the base of Pico de Orizaba volcano) owing to the coalescence of up-stream landslides that increased the destructive power of a debris flow. This debris flow not only produced a flood, but also caused the rupture and explosion of ducts belonging to PEMEX (the oil company in Mexico), located about 300 m from the town. Although authorities and scientists have made efforts to assess slope stability by using Geographic Information Systems (GIS) and remote sensing approaches, no practical GIS methodology is established to map landslide susceptibility and landslide hazard in volcanic terrains.

The objective of this mass wasting project is to provide standardized methods for conducting landslide inventories and landform hazard maps that support governmental authorities for hazard mitigation and landscape planning in Mexico.

This paper summarizes the methodology of the on-going research project from the Institute of Geography at the National Autonomous University of Mexico (UNAM) that seeks to develop technical guidelines to conduct multi-temporal landslide inventories, landslide susceptibility, and hazard maps by using GIS.

G.L. Paulín (✉)
Laboratorio de Análisis Geo-espacial, Circuito Exterior, Ciudad Universitaria, Instituto de Geografía, Universidad Nacional Autónoma de México, Coyoacán, 04510 México, D.F, Mexico
e-mail: legorretag@igg.unam.mx

M. Bursik
Department of Geology, University at Buffalo, SUNY Buffalo, NY 14260, USA

J.L. Hubp
Departamento de Geografía Física, Instituto de Geografía, Universidad Nacional Autónoma de México, Circuito Exterior, Ciudad Universitaria, Coyoacán, 04510 México, D.F, Mexico

C. Margottini et al. (eds.), *Landslide Science and Practice*, Vol. 1,
DOI 10.1007/978-3-642-31325-7_50,

The Río Chiquito-Barranca del Muerto watershed on the southwestern flank of Pico de Orizaba volcano is selected as a case study area. The study area has physiographic conditions which are prone to landslides.

Background Justification

Worldwide, landslide susceptibility and hazard zonation projects have been addressed by compiling multi-temporal landslide inventories and modeling landslides instability using a GIS. (Washington State Department of Natural Resources (DNR), Forest Practices Division 2006; Hervás and Bobrowsky 2009; Blahut et al. 2010).

In Mexico, numerous GIS-based applications have been used to represent and assess slope stability (Capra and Lugo-Hubp 2006; Pérez-Gutiérrez 2007; Secretaría de Protección Civil 2010). These studies include basic concepts and explanations of landslide classification, trigger mechanisms, criteria, considerations, and analysis for landslide hazard reconnaissance, etc.

Based on previous geologic studies and computer simulations with GIS and remote sensing, lahar hazard maps along stream systems of Pico de Orizaba have been created (Sheridan et al. 2001; Hubbard et al. 2007). In 2010, an atlas of geological and hydrometeorological hazards of Veracruz was created by the Secretariat of Civil Protection of Veracruz state in collaboration with other federal and state government agencies. The atlas has a heuristic general framework for GIS landslide risk evaluation at state and municipal level. In spite of this, there is no practical and standardized landslide mapping method using GIS for small non-magmatic landslides that occur continually along the stream systems in volcanic terrains. Also, little work has been done on the systematic comparison of models, in order to outline advantages and limitations of the methods to model the spatial distribution of landslides.

Methodology

The methodology encompasses three main stages of analysis to assess landslide hazards. Stage 1 builds a historic landslide inventory (steps 1–5 in Fig. 1); stage 2 calculates the susceptibility for the watershed (step 7 in Fig. 1); and stage 3 calculates the landform hazard for the watershed (steps 8–11 in Fig. 1). The technique and its implementation in a GIS-based technology is as follows (Fig. 1).

Step 1. Selection of a study area: The Río Chiquito-Barranca del Muerto watershed is selected for the study because it has physiographic conditions which are prone to landslides. The area has high precipitation during the wet season, high degree of weathering, steep slopes, weak rock types, and associated faults. Also, lying in the southwestern flank of Pico de Orizaba volcano, the study area is representative of the typical mexican volcanic watershed landscape.

The watershed is a tributary of the Río Blanco, which flows into the Gulf of Mexico within Veracruz and Puebla states, and it covers 111 km^2 (Fig. 2). The Río Chiquito-Barranca del Muerto watershed is characterized by hilly and steep terrain with elevations from 1,340 to 5,600 m a.s.l. and slopes between 0° (inner valleys of relatively flat plains) and 61° (mountainous terrain). In the study area the mean annual precipitation is high (1000–1100 mm/year at $>$ 4,000 m a.s.l. and 927 mm/year at elevations $<$1,500 m a.s.l.; Palacios et al. 1999), the bulk of which falls as rain during seasonal storms between May and November. In combination with the intense precipitation, the geologic materials (mainly Tertiary (60.3 %) and Quaternary (2.4 %) volcanic terrains overlying weathered Cretaceous sedimentary rocks) have had great influences on the topography and current landforms. These influences are expressed in the patterns of resistance to erosion processes and the types of mass movement. In 2010, more than 400 landslides (shallow, deep-seated, and earthflow landslides) have been mapped.

Step 2. Literature review and data gathering: Background information is collected to provide a generalized characterization of mass wasting processes within the watershed. Background information includes geology, land use, climate and hydrology (including data on large storm events), pre-existing landslide maps and reports, etc.

Step 3. Selection of aerial photographs: Climatic almanacs and storm records guide the geologist in choosing the most complete and relevant time sets of aerial photographs. In the study area, one set of 1:10,000 aerial photographs from 2008 and one set of 1:20,000 photographs from 1994 were analyzed using a mirror stereoscope with 3× magnification and they were used as a layer during GIS analysis and mapping.

Step 4. Selection of GIS layers and evaluation of different landslide susceptibility models: The researcher then retrieves and incorporates digital GIS layers into an ArcGIS base map (Fig. 3a). The digital layers include the watershed boundary, topography, shaded relief, hydrology, roads, geology, previously mapped landslides, orthographic photography, and landslide susceptibility resulting from the best tested model among Multiple Logistic Regression (MLR), LOGISNET, SINMAP, and SLPSTAB (Fig. 3). MLR model was selected because it provides the best scientific accuracy, technical accessibility, and applicability.

Step 5 and 6. Landslide inventory map and field work: A single historic landslide inventory map is created with the two sets of aerial photographs from diferent time. During stereo aerial photographic analysis, all landslides are mapped by "heads-up" digitizing in ArcGIS. "Heads-up" digitizing involves mapping on photo transparencies and

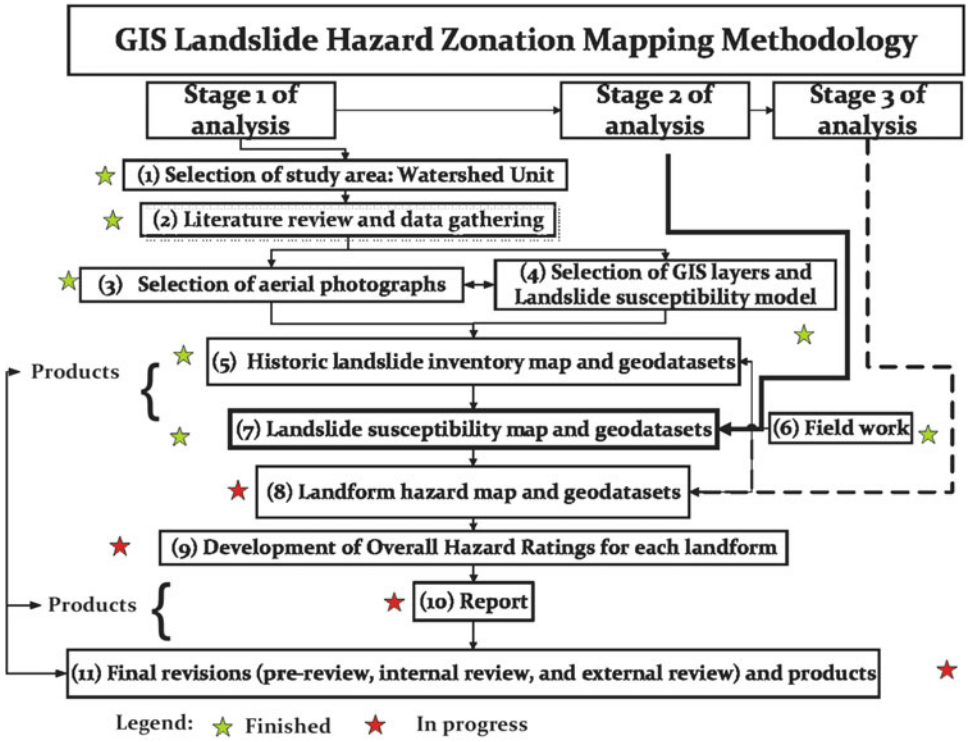

Fig. 1 General procedure for conducting landslide inventories, landslide susceptibility and landform hazard maps

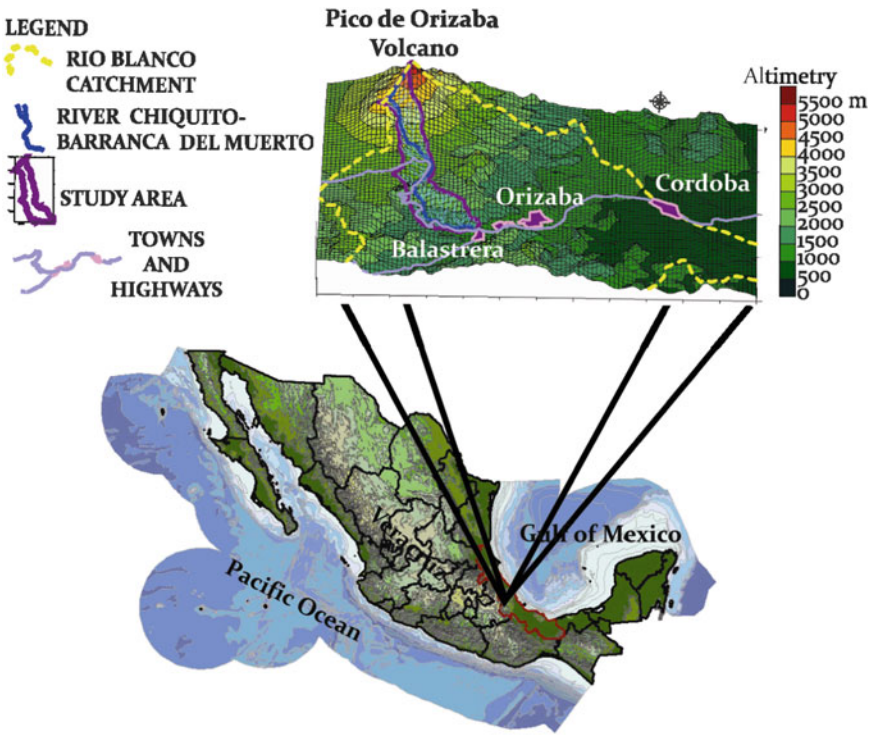

Fig. 2 Localization of the study area

digitizing right onto the screen into GIS at the same scale as the photos. Mapped landslides are interpreted and documented in the geo-dataset. The amount of field verification is held to a reasonable minimum (between 15 % and 25 % of total landslides) which allows for an enhanced degree of confidence in the mass wasting assessment (Fig. 4).

Step 7 and 8. Landslide susceptibility map and landform map: Landslide susceptibility was mapped pixel-by-pixel base on the Multiple Logistic Regression (MLR) function

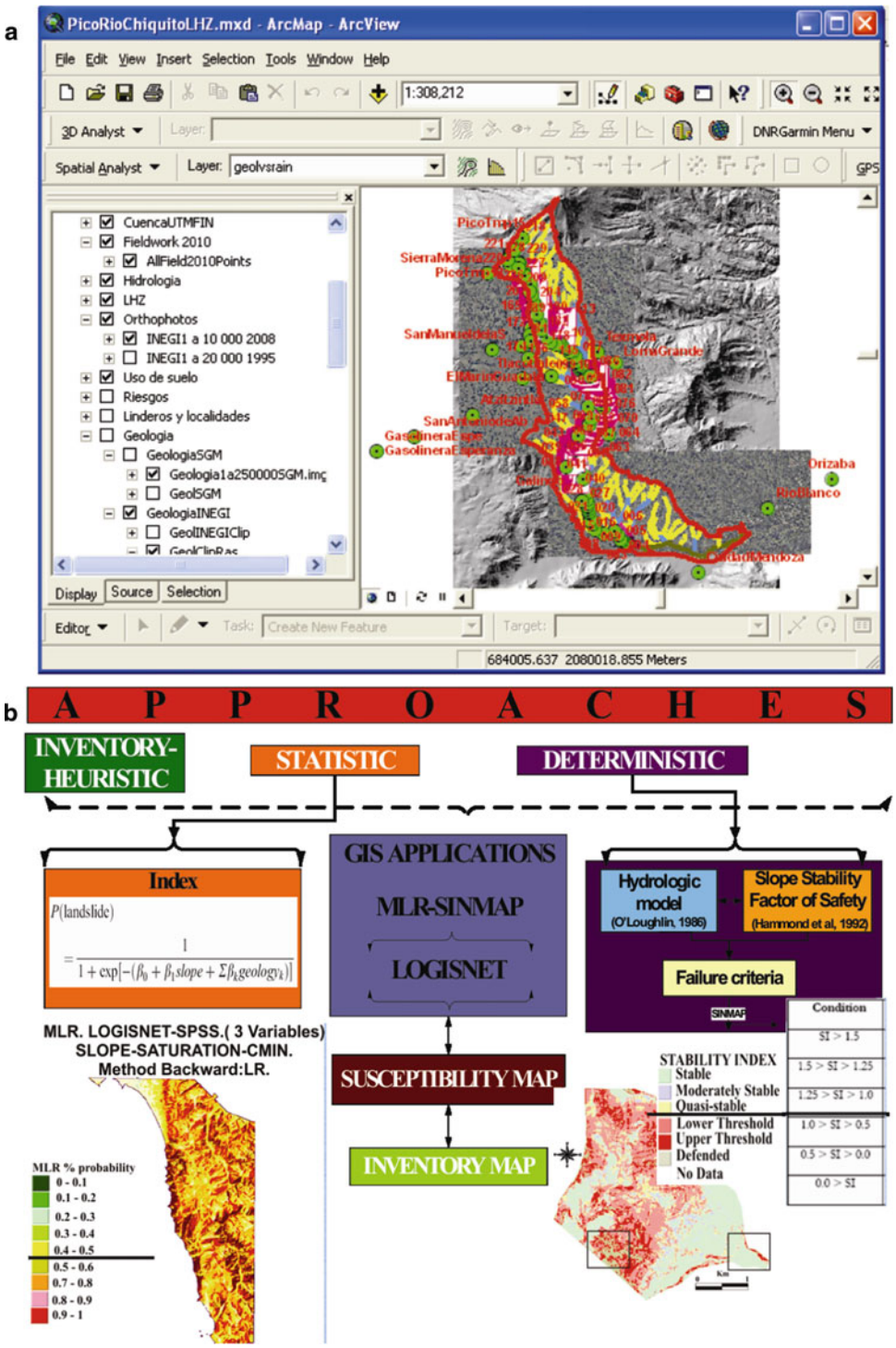

Fig. 3 (**a**) GIS layers for the base map and (**b**) the landslide models selection

(Fig. 5). The resulting map of MLR with DEM at 10 m was compared with the inventory map. The evaluation of the MLR model was in terms of producer's accuracy, user's accuracy, and model efficiency. The model is able to predict 72 % of the existing landslides. In this study, analysis by MLR has shown the occurrence of landslides in the region of interest to be highly correlated with the six variables: elevation, slope, contributing area, land use, geology, and terrain curvature.

Once landslides are mapped and evaluated, areas of similar landslide potential are grouped into individual landforms. Examples of landforms are inner gorges, bedrock hollows, and convergent headwalls. Concurrent to landslide and landform mapping, field reconnaissance is conducted to provide

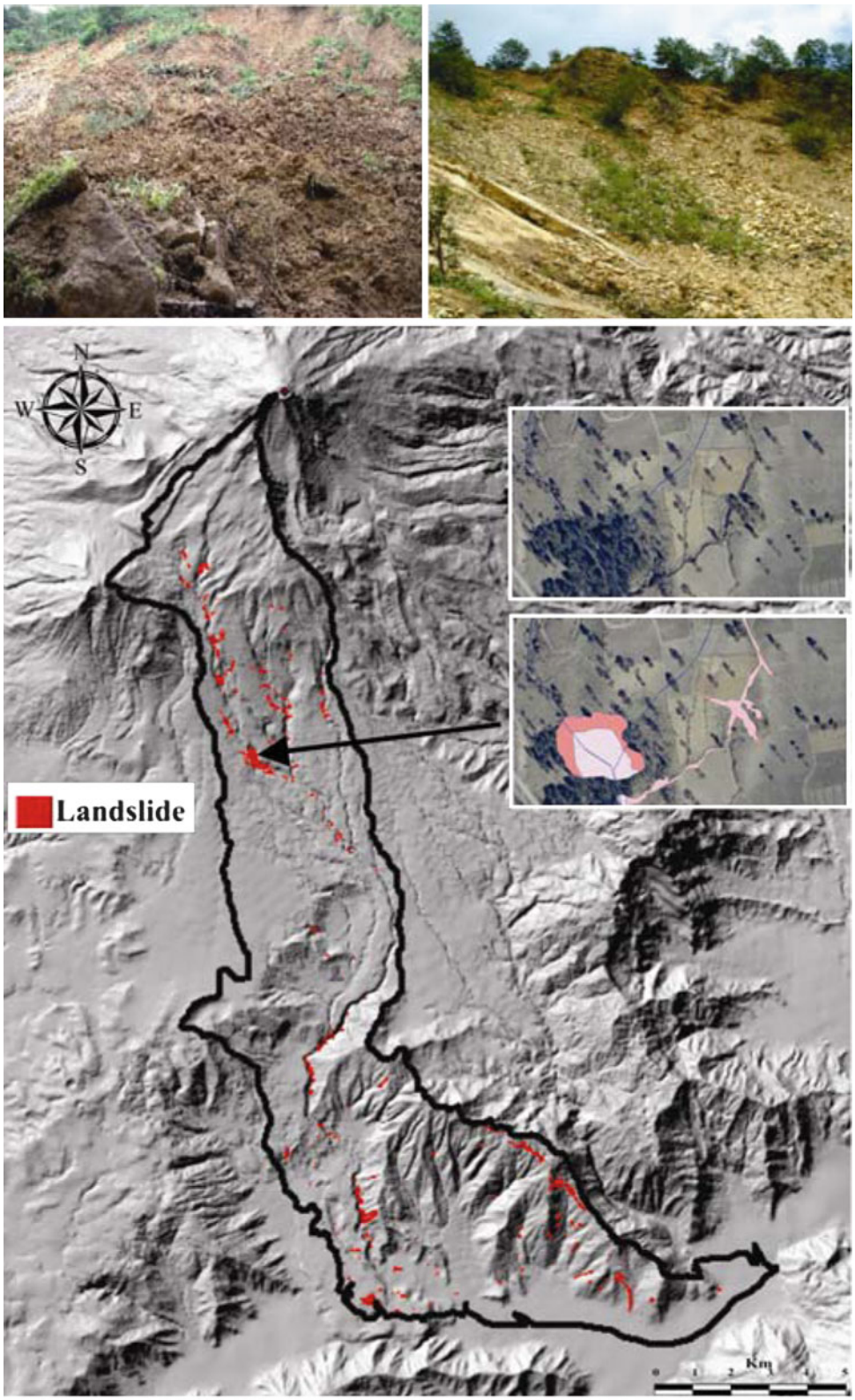

Fig. 4 Example of landslides and its representation on the landslide inventory map

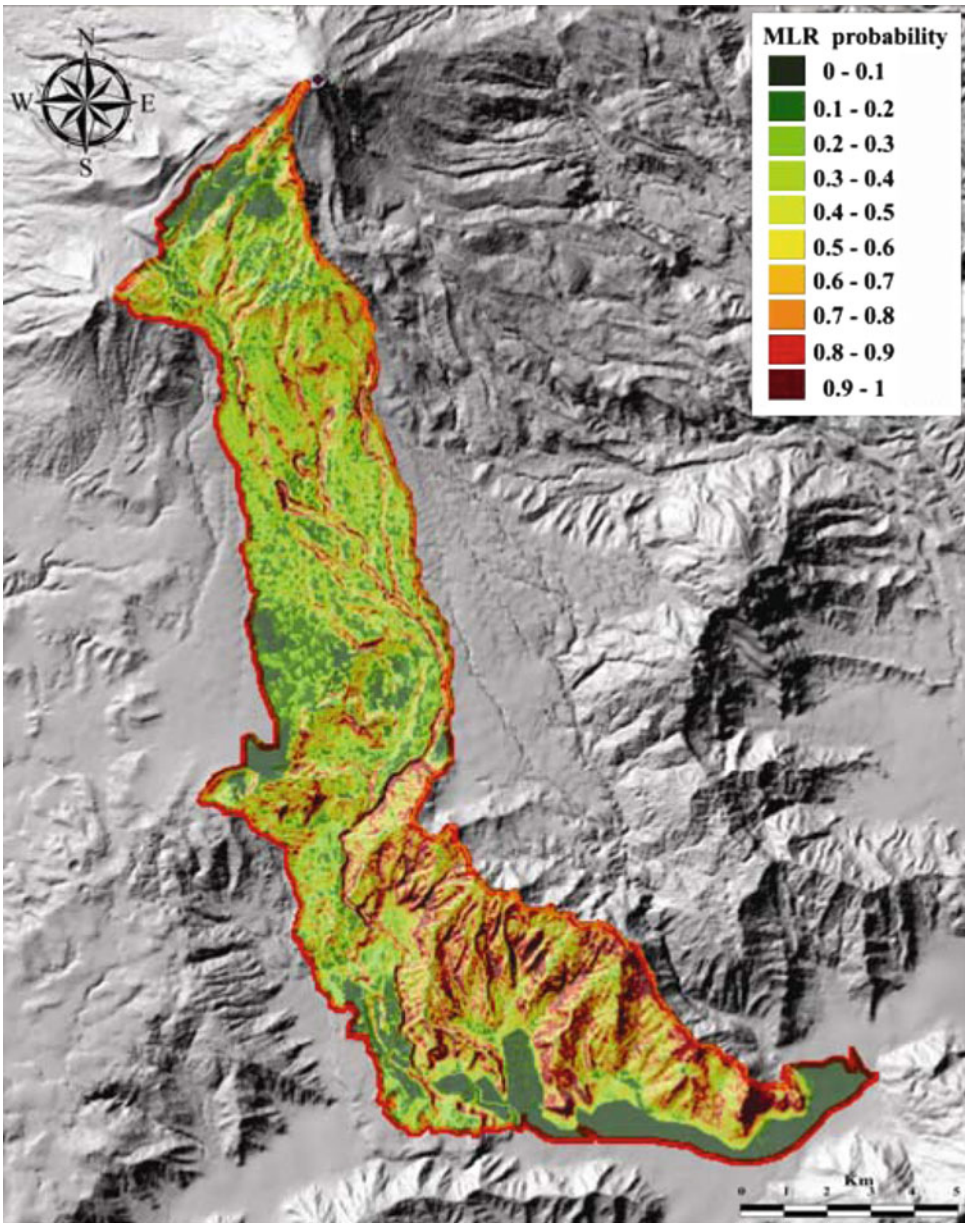

Fig. 5 MLR susceptibility model

the analyst with a realistic view of the watershed and the types of mass wasting and landforms present.

Step 9. Development of Overall Hazard Ratings for Landforms: Semi-quantitative hazard ratings are derived from values that correspond to the number and total area of landslides within each landform, normalized for the total period of time spanned by the aerial photographs, and the area of each landform. These values are referred to as the Landslide Area Rate and the Landslide Frequency Rate, respectively. Because the resulting numbers are always very small fractions, the values are then multiplied by one million and rounded in order to provide single easily-usable number. This procedure is restricted to those shallow landslides that deliver sediment to public resources. Using these semi-quantitative calculations, the Landslide Frequency Rate and Landslide Area Rate for Delivery values are entered into a matrix to determine the Overall Hazard Rating for each landform. As a result, each landform gets a hazard rating of Low, Moderate, High, or Very High (Washington State Department of Natural Resources (DNR), Forest Practices Division 2006).

Step 10. Report: A written report describes the analysis and includes an explanatory text, landform descriptions, landslide triggering mechanisms and the landslide hazard findings for each watershed. The confidence level of the analyst is also discussed.

Step 11. Final revisions and products: Prior to public release of the report and the corresponding 1:50,000 landslide

and landform hazard maps, a tri-level review is conducted. The first two levels are internal peer-reviews carried out by another analyst and a licensed Engineering Geologist. The third review is external and is voluntarily performed by reviewers such as geoscientists, foresters, and other interested parties. The comments received are used to improve the products prior to final public release on the Institute of Geography website.

Acknowledgements The authors thank authorities from the Department of Geology at the University of Buffalo, the International Consortium on Landslides (ICL), the Washington State Department of Natural Resources (DNR) Forest Practices Division, the WA-DNR Geology and Earth Resources Division and the Geo-Spatial Analysis Laboratory from the Institute of Geography, UNAM for their approval and help. This research was supported by the iniciativa de apoyo complementario a la realización de las obras determinadas (IACOD), UNAM, Grant no. I1100711 and the International Programme on Landslides (IPL).

References

Blahut J, Van Westen CJ, Sterlacchini S (2010) Analysis of landslide inventories for accurate prediction of debris-flow source areas. Geomorphology 119(1–2):36–51

Capra L, Lugo-Hubp J (2006) Fenómenos de remoción en masa en el poblado de Zapotitlán de Méndez, Puebla: relación entre litología y tipo de movimiento. Revista mexicana de ciencias geológicas 20(2):95–106

Secretaría de Protección Civil (2010) Atlas de peligros geológicos ehidrometeorológicos del estado de Veracruz. Comp.: Ignacio Mora González; Wendy Morales Barrera, Sergio Rodríguez Elizarrarás. Xalapa: Secretaría de Protección Civil del estado de Veracruz: Universidad Veracruzana: UNAM. 1V

Hervás J, Bobrowsky P (2009) Mapping: inventories, susceptibility, hazard and risk. In: Sassa K, Canuti P (eds) Landslides – disaster risk reduction. Springer, Berlin, pp 321–349. ISBN 978-3-540-69966-8

Hubbard BE, Sheridan MF, Carrasco-Nunez G, Díaz-Castellon R, Rodriguez S (2007) Comparative lahar hazard mapping at Volcan Citlaltépetl, Mexico using SRTM, ASTER and DTED-1 Digital Topography. J Volcanol Geotherm Res 160(1):99–124

Palacios D, Parrilla G, Zamorano JJ (1999) Paraglacial and postglacial debris flows on little ice age terminal moraine: Jamapa Glacier, Pico de Orizaba (Mexico). Geomorphology 28:95–118

Pérez-Gutiérrez R (2007) Análisis de la vulnerabilidad por los deslizamientos en masa, caso: Tlacuitlapa, Guerrero. Boletín de la Sociedad Geológica Mexicana 59(2):171–181

Sheridan MF, Carrasco-Nuñez G, Hubbard BE, Siebe C, Rodriguez-Elizarraraz S (2001) Mapa de peligros del Volcan Citlaltépetl (Pico de Orizaba). Inst Geog, Univ Nac Autonoma Mexico, 1:250,000 scale

Washington State Department of Natural Resources (DNR), Forest Practices Division, (2006) Landslide Hazard Zonation (LHZ) Mapping Protocol, version 2.0. Accessed at: http://www.dnr.wa.gov/BusinessPermits/Topics/LandslideHazardZonation/Pages/fp_lhz_review.aspx

Minimal Standards for Susceptibility and Hazard Maps of Landslides and Rock Falls

Gerlinde Posch-Trözmüller and Richard Bäk

Abstract

Within the scope of the EU program INTERREG IV A (Italy/Austria), the project MassMove – with partners from the regional governments of Carinthia (Austria), and of Friuli Venezia Giulia and Veneto (Italy) – aims at establishing guidelines for the compilation of landslide susceptibility and hazard maps at regional and local scale. Project activities started December 2008; it will be concluded in November 2011.

Keywords

Susceptibility maps • Hazard maps • Inventory maps • Landslide • Rock fall • Landslide inventory

Introduction

Alpine regions have repeatedly been affected by natural geological hazards. Because of the enormous damages and possible catastrophic events, a reduction of the risk potential is highly desirable. Powerful tools for such a program dealing with hazard in context with regional planning or protective measures are susceptibility and hazard maps. Although a variety of methods for hazard assessment exist, and also guidelines for the compilation of landslide susceptibility and hazard maps have been published before (e.g. Fell et al. 2008; Hervás 2007), they haven't been established as an act of law up to now, except in France and Switzerland. In order to develop such guidelines, various study areas in the partner regions Carinthia (Austria), Friuli Venezia Giulia and Veneto (Italy) are being systematically surveyed within MassMove (Bäk, 2011) by universities (Padova, Milano, Trieste) in the Italian regions and the Geological Survey of Austria and Joanneum Research in Carinthia.

Selection of the Study Areas

In a first step, the study areas were selected on the basis of various criteria, which included the variability of the phenomena (shallow landslides, earth flows, rock falls), the documentation of past events, as well as the existence of different geological formations and processes.

In Carinthia, two study areas were chosen (Fig. 1). One, the study area "Auental", is situated in the northeast of Carinthia. The main topic in this area is the assessment of danger due to shallow landslides (Fig. 2), although also deeper seated landslides occur in this area, as it happened in 2005 after intensive rainfall (Fig. 3). The other Austrian study area, "Mölltal", situated in the northwest of Carinthia and encompassing an area of 100 km^2 (Fig. 1), was chosen to study rock fall. Old and recent huge rock fall events (Figs. 4, and 5) are documented in this region characterized by high cliffs. Due to the size of the area and its partial inaccessability, regions for detailed investigations within the study area were chosen.

In the region of Friuli Venezia Giulia three study areas were chosen by each partner, the two partners and their

G. Posch-Trözmüller (✉)
Geological Survey of Austria, Neulinggasse 38, 1030 Wien, Vienna, Austria
e-mail: gerlinde.posch@geologie.ac.at

R. Bäk
Department 15 Environment, Carinthian Government, Klagenfurt, Austria

C. Margottini et al. (eds.), *Landslide Science and Practice*, Vol. 1,
DOI 10.1007/978-3-642-31325-7_51,

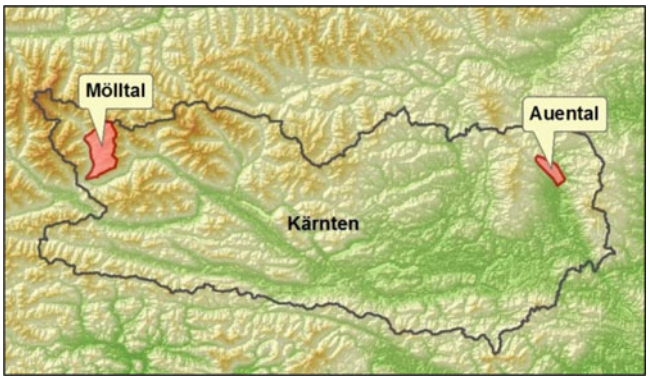

Fig. 1 Study areas in the federal region of Carinthia (Austria): Auental and Mölltal

external experts are working on different processes: Servizio Gestione Territorio is working on shallow landslides in three study areas in Studena (Pontebba), Paularo and Castelnovo del Friuli (which was chosen because of the fact that this area is affected by landslides on a yearly basis; Bäk et al. 2011a), whereas Servizio Geologico is working exclusively on rock fall in three study areas in Timau (Paluzza), Venzone, where a lot of rock falls were triggered by the earthquake of 1976 (Bäk et al. 2011a), and Villa Santina-Caneva di Tolmezzo. The partner Veneto (Direzione Difesa del Suolo) chose to investigate rock fall in four study areas, Perarolo di Cadore, where a rock fall of 4,000 m^3 happened recently and the rock fall hazard is very high (Bäk et al. 2011a), Alleghe, Rocca Pietore, and Valstagna (Fig. 6).

Fig. 2 Shallow landslide in the study area Auental (*top*) and its position on the Laserscan (*yellow arrow*, below; Poltnig and Strobl 2010)

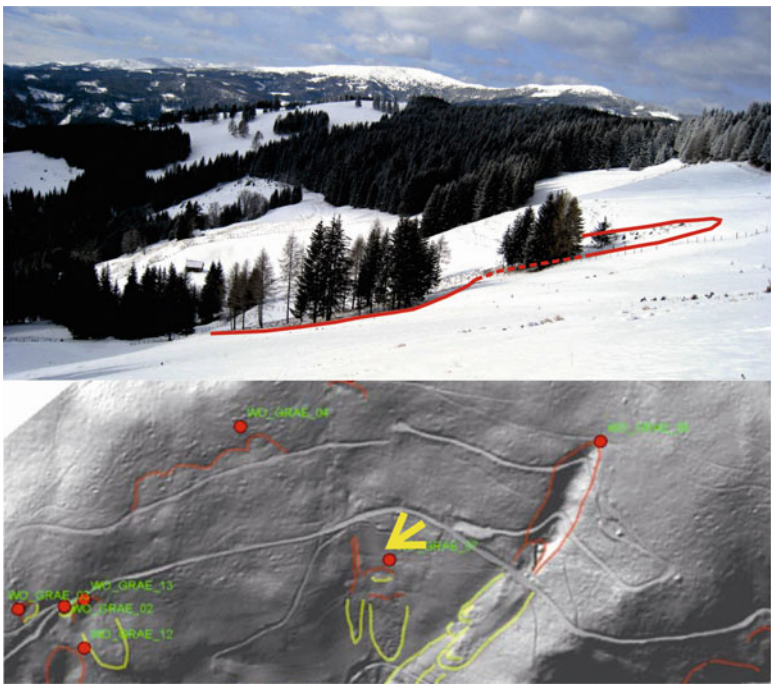

Fig. 3 Landslide in the study area Auental that took place in 2005 after intensive rainfall

Fig. 4 Steep cliffs in the study area Mölltal

Fig. 5 Scar through the wood below a cliff, made by a large block in 2003 in the study area Mölltal

Fig. 6 Hazard due to rock fall from steep cliffs near Valstagna (Veneto, Italy)

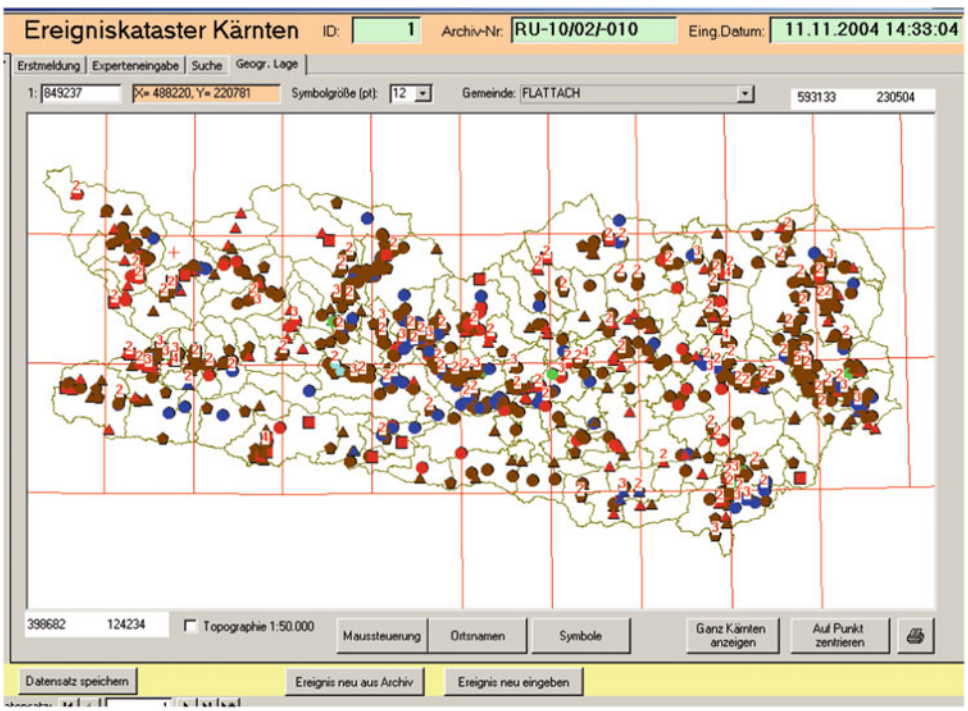

Fig. 7 Digital landslide inventory of Carinthia (Bäk et al. 2005a)

Systematic Investigations

The systematic investigations in the study areas included:

Collection and Digital Registration of Basic Data

DEM, topographic data including slope inclination classes, exposition, cliffs, land use, geological maps, landslide inventory maps and engineering-geological characteristics of the geological units were collected and registered digitally. Landslide inventories were also updated and compared, and additional known mass movement structures as well as historical data that weren't previously included in the database were recorded.

In all the partner regions GIS-based inventories have already been in use for some time. In Carinthia historical events of the last 50 years are recorded (Figs. 7 and 8). Apart from that the Geological Survey of Austria maintains the nationwide landslide database GEORIOS. In the regions Friuli Venezia Giulia and Veneto the national system IFFI is used

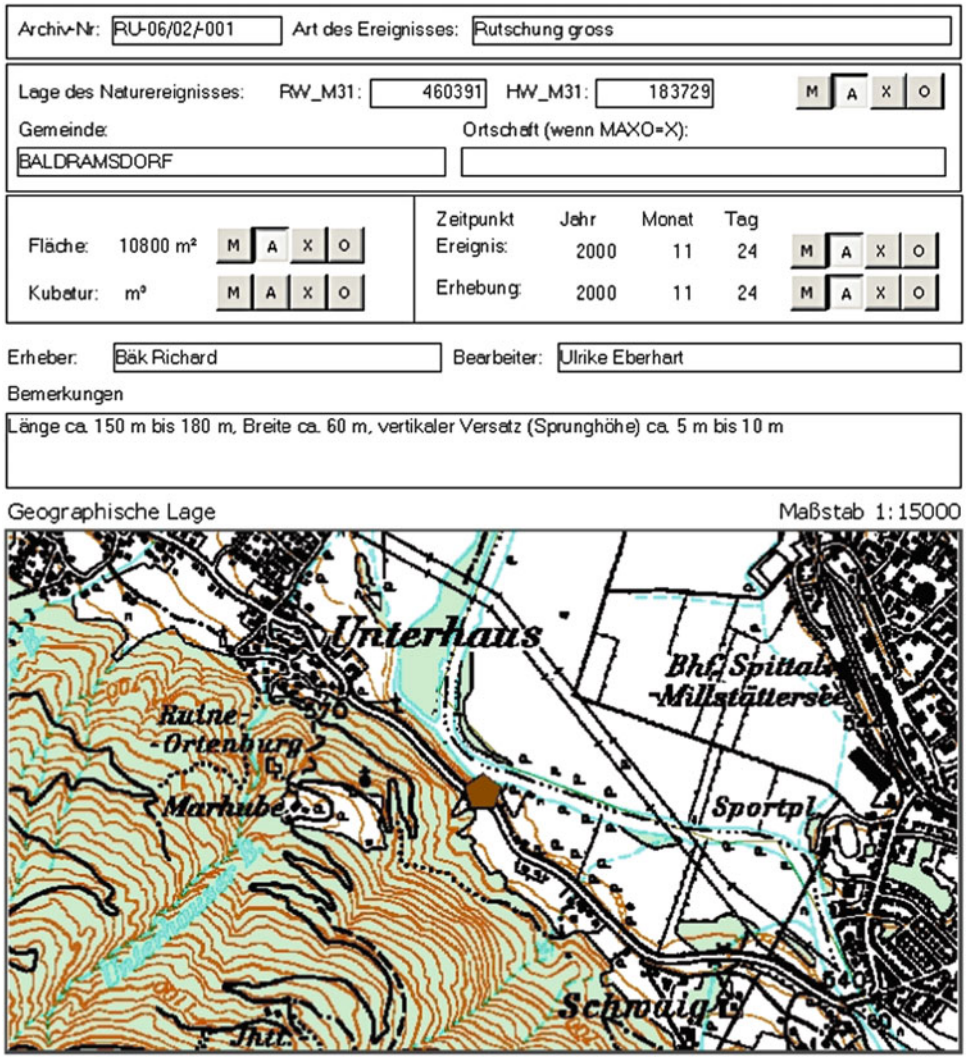

Fig. 8 Detail from the digital landslide inventory of Carinthia (Bäk et al. 2005b)

(Kranitz et al. 2006; Baglioni et al. 2006). Since 2010 the region of Friuli Venezia Giulia also has available the new database SIDS (Integrated System of Soil Protection), consisting of several information layers connected with cartographic data as well as specific information regarding the boundaries of landslides and danger areas, avalanche sites, perimeters of floods, hydraulic structures, etc. (Torresin 2010).

Data Processing and Evaluation

Parameters used for describing mass movements were defined for the categories geology, geomorphology, topography, hydrogeology, vegetation, and anthropogenic influence. Existing database structures were evaluated and a meta-database for the documentation of the results within MassMove was developed.

For this purpose the databases in use in the partner regions were compared. All three databases, IFFI (Italy), GEORIOS (Austria), and the digital landslide inventory of Carinthia (Austria), have some common features as well as some specific ones. The common part of all these databases are basic information (where, when, what, why did something happen, and who recorded the event), connection to GIS – layer with point, line and polygon information and some geological data (Lipiarski 2010).

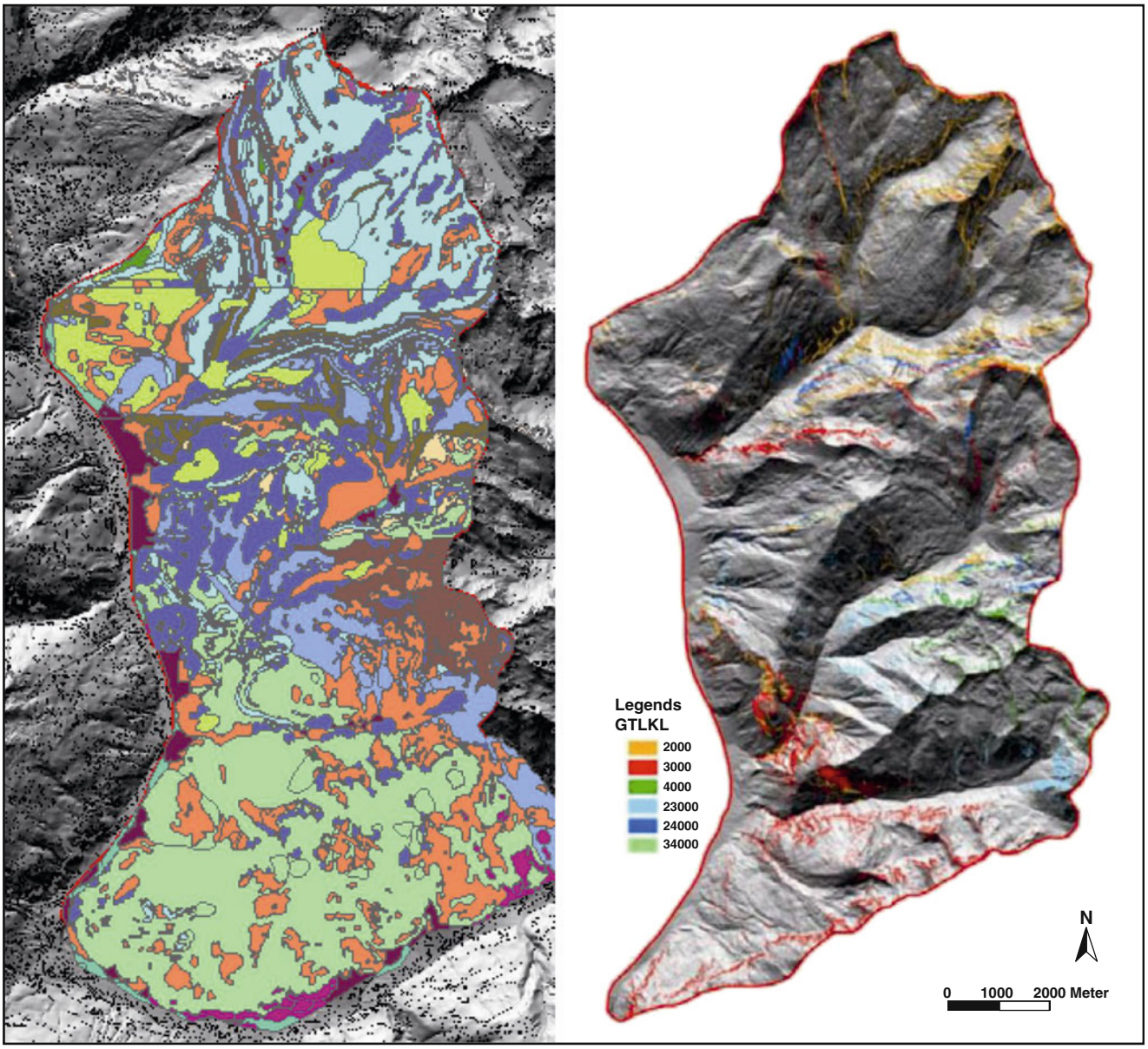

Fig. 9 Preliminary map of geotechnical-lithological units (*left*, Melzner 2009), potential rock fall source areas within the study area Mölltal (*right*, Melzner et al. 2010; Melzner and Kociu 2010), gained by automated, GIS-based identification of threshold slope inclination classes

Recording of Relevant Structures (by Field Work and/or Remote Sensing)

Geological and detailed engineering geological mapping was carried out as well as remote sensing using Lidar (terrestrial and airborne, Figs. 2 and 9), multitemporal aerial photography and infrared thermography. Computer simulations of shallow landslides and rock falls (Figs. 9, and 10) are currently being carried out by experts.

Hazard Assessment on the Basis of Well-Known Methods and Models

In the partner regions susceptibility and/or hazard maps at varying scales have been in use. In the Italian partner regions a modified BUWAL method is used for hazard assessment (Bäk et al. 2011a). In Austria guidelines as legal ordinance on how to deal with hazard only exist concerning floods, avalanches and debris flows (Bäk et al. 2011b). The goal was

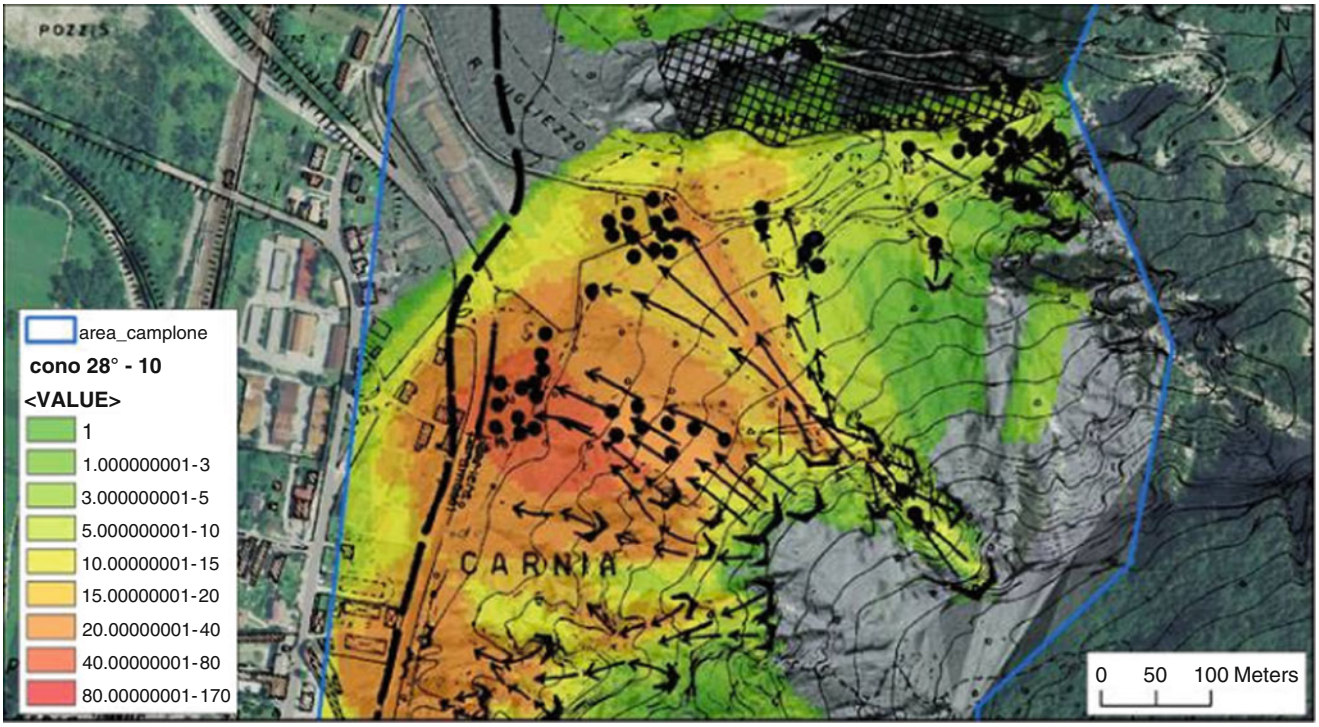

Fig. 10 Rockfall runout modelling: Shadow angle approach model for the study area Venzone; for comparison the blocks from the historical map are included (Crosta et al. 2010)

to improve methods in use and to achieve minimal requirements for susceptibility and hazard assessment for landslides and rock fall.

After clarifying and defining the methods, landslide susceptibility and hazard maps are being created. The results are in the process of evaluation.

The accuracy (and spatial resolution) of the results depends on the scale of the input data, therefore the accuracy of the investigation has to increase with the aim of the intended target: (1) susceptibility, (2) hazard and (3) protection measurements.

Glossary

A glossary of landslide-related technical terms has been established to ensure better communication and understanding.

Results

This systematic work is the basis for the definition of guidelines for landslide susceptibility and hazard mapping. The guidelines should describe the minimum requirements of input parameters and outputs, whereas the used methods should be optional. The presentation of the results of MassMove concerning landslide susceptibility and hazard maps is determined by the requested aim and scale of the project.

Currently the project is still work in progress, so the guidelines for the creation of susceptibility and hazard maps are under construction. Further information on the project, the progress reports and the glossary may be found on the Massmove-homepage (www.massmove.at).

Acknowledgments The project presented is an INTERREG IV A (Italy/Austria) project, funded by the European regional development fund (EFRE).

References

Baglioni A, Tosoni D, De Marco P, Arziliero L (2006) Analisi del dissesto da frana in Veneto. Rapporto IFFI 2006. URL: http://www.isprambiente.gov.it/site/_files/Pubblicazioni/Rapporti/Rapporto_frane/Capitolo_10_Veneto.pdf. Accessed 25 May 2011

Bäk R (2011) MASSMOVE. URL: http://www.massmove.at. Accessed 4 Aug 2011

Bäk R, Eberhardt U, Goldschmidt F, Kociu A, Letouze-Zezula G, Lipiarski P (2005a) Ereigniskataster und Karte der Phänomene als Werkzeuge zur Darstellung geogener Naturgefahren (Massenbewegungen). Arbeitstagung 2005 der Geologischen Bundesanstalt "Blatt 182 Spittal an der Drau" Gmünd/Kärnten, 12–16. Sept 2005, Wien, pp 201–206

Bäk R, Eberhardt U, Goldschmidt F, Letouze-Zezula G, Oswalder H (2005b) GINS. Digitales Geologisches Informationssystem Kärnten – ein Werkzeug für nachhaltige Raumentwicklung. Arbeitstagung 2005 der Geol. Bundesanstalt "Blatt 182 Spittal an der Drau" Gmünd/Kärnten, Sept 2005, Wien, 183–193

Bäk R, Kranitz F, Torresin M, Mariani R (2011a) Minimal standard for creation of hazard maps for landslides as a tool for preventive disaster reduction (INTERREG IV A Italy/Austria, Project Nr. 1381–302, Acronym MassMove). In: Skolaut Ch (Hrsg) Gefahrendarstellungen für Massenbewegungen. Wildbach- und Lawinenverbau, Journal of Torrent, Avalanche, Landslide and Rock Fall Engineering, 74. Jahrgang, Heft Nr. 166, 176–197

Bäk R, Raetzo H, Mayer K, von Poschinger A, Posch-Trözmüller G (2011b) Mapping of geological hazards: methods, standards and procedures (state of development)-overview. In: Skolaut Ch (Hrsg) Gefahrendarstellungen für Massenbewegungen. Wildbach- und Lawinenverbau, Journal of Torrent, Avalanche, Landslide and Rock Fall Engineering, 74. Jahrgang, 166, 30–52

Crosta GB, Frattini P, Agliardi F (2010) Study areas "Venzone - Carnia", "Villa Santina - Caneva di Tolmezzo" and "Timau". In: Posch-Trözmüller G (ed) Third scientific report to the INTERREG IV A project MASSMOVE – Minimal standards for compilation of danger maps like landslides and rock fall as a tool for disaster prevention. Wien. URL: http://www.massmove.at/. Accessed 4 Aug 2011

Fell R, Corominas J, Bonnard C, Cascini L, Leroi L, Savage WZ (2008) Guidelines for landslide susceptibility, hazard and risk zoning for land use planning. Eng Geol 102:85–98

Hervás J (ed) (2007) Guidelines for mapping areas at risk of landslides in Europe. In: Proceedings of the experts meeting, JRC, Ispra, Italy, 23–24 Oct 2007. JRC Report EUR 23093 EN, Office for Official Publications of the European Communities, Luxembourg, 53 pp

Kranitz F, Manca P, Oberti S, Piano C (2006) Analisi del dissesto da frana in Friuli Venezia Giulia. Rapporto IFFI 2006. URL: http://www.apat.gov.it/Media/iffi/Rapporto_Frane_Italia_APAT_78_2007/Capitoli/Capitolo_11_ Friuli_Venezia_Giulia.pdf. Accessed 25 June 2011

Lipiarski P (2010) Comparison of database structures between existing databases of the project partners. In: Posch-Trözmüller G (ed) Third scientific report to the INTERREG IV A project MASSMOVE – Minimal standards for compilation of danger maps like landslides and rock fall as a tool for disaster prevention. Wien. URL: http://www.massmove.at/. Accessed 4 Aug 2011

Melzner S (2009) Mölltal. In: Posch-Trözmüller G (ed) Second scientific report to the INTERREG IV A project MASSMOVE – Minimal standards for compilation of danger maps like landslides and rock fall as a tool for disaster prevention. Wien. URL: http://www.massmove.at/. Accessed 4 Aug 2011

Melzner S, Kociu A (2010) Study area "Oberes Mölltal". In: Posch-Trözmüller G (ed) Fourth scientific report to the INTERREG IV A project MASSMOVE – Minimal standards for compilation of danger maps like landslides and rock fall as a tool for disaster prevention. Wien. URL: http://www.massmove.at/. Accessed 4 Aug 2011

Melzner S, Dorren L, Kociu A, Bäk R (2010) Regionale Ausweisung potentieller Ablöse- und Wirkungsbereiche von Sturzprozessen im oberen Mölltal/Kärnten. Posterpräsentation beim 12. Geoforum Umhausen, Niederthai

Poltnig W, Strobl E (2010) Study area "Auental". In: Posch-Trözmüller G (ed) Third scientific report to the INTERREG IV A project MASSMOVE – Minimal standards for compilation of danger maps like landslides and rock fall as a tool for disaster prevention. Wien. URL: http://www.massmove.at/. Accessed 4 Aug 2011

Torresin M (2010) Study areas "Studena", "Paularo", and "Castelnovo". In: Posch-Trözmüller G (ed) Fourth scientific report to the INTERREG IV A project MASSMOVE-Minimal standards for compilation of danger maps like landslides and rock fall as a tool for disaster prevention. Wien. URL: http://www.massmove.at/. Accessed 4 Aug 2011

Hyperconcentrated Flow Susceptibility Analysis and Zoning at Medium Scale: Methodological Approach and Case Study

Leonardo Cascini, Silvio Di Nocera, Michele Calvello, Sabatino Cuomo, Settimio Ferlisi, and Fabio Matano

Abstract

A methodological approach for the susceptibility analysis and zoning, at medium scale, of hyperconcentrated flows is presented. The adopted procedure comprises the following steps: (1) collection of data useful to acquire detailed knowledge of the slope processes leading to flow-like mass movements in the site; (2) hyperconcentrated flow susceptibility analyses via heuristic and statistic procedures; (3) hyperconcentrated flow susceptibility zoning (1:25,000 scale) at a preliminary/intermediate level. The procedure is applied to the test site of Monte Albino, (southern Italy), which extends over an area of around 400 ha. The obtained results emphasize the potential of an approach which moves from preliminary to intermediate level of susceptibility zoning. The results also highlight the important role played by the combined use of different procedures, based on heuristic and statistical models, in defining a standardised criterion to be adopted in problems dealing with the analysis and zoning of susceptibility to hyperconcentrated flows.

Keywords

Hyperconcentrated flows • Susceptibility • Zoning • Heuristic • Statistical

Introduction

In the last few decades, several methods for landslide susceptibility analysis have been proposed in the scientific literature. Generally, these methods differ depending on the scale and related purposes of the analysis – and, consequently, on the quality/quantity of input data – and on the adopted procedure (heuristic, statistical or deterministic). Owing to the complexity of the problem and the variability of the factors involved in the analyses, standardised methodological criteria are lacking.

This paper shows the results of an ongoing research programme aimed at developing a standardised criterion for landslide susceptibility analysis and zoning at medium scale (1:25,000). To this aim, a methodology is presented embracing the contribution of both geological and geotechnical approaches towards a proper use of the available input data within heuristic and statistical procedures. Then, the different steps described in the proposed methodological approach are applied to a well-documented case study in the Campania region (southern Italy) where different kinds of flow-like mass movements can occur.

The Adopted Methodological Approach

The adopted methodological approach for the flow-like mass movement susceptibility analysis and zoning was conceived on the basis of the recommendations given by the "Guidelines for landslide susceptibility, hazard and risk zoning for land-use planning" (Fell et al. 2008).

L. Cascini (✉) • M. Calvello • S. Cuomo • S. Ferlisi
Department of Civil Engineering, University of Salerno, via Ponte don Melillo 1, Fisciano, SA, Italy
e-mail: l.cascini@unisa.it; mcalvello@unisa.it; scuomo@unisa.it; sferlisi@unisa.it

S. Di Nocera • F. Matano
Department of Earth Science, University of Naples "Federico II", Largo S. Marcellino 10, Naples, Italy
e-mail: sildinoc@unina.it; matano@unina.it

C. Margottini et al. (eds.), *Landslide Science and Practice*, Vol. 1,
DOI 10.1007/978-3-642-31325-7_52,

In particular, the Guidelines suggest that the landslide inventory and susceptibility zoning maps can be developed using methods which are grouped into three different categories: basic, intermediate and advanced. On the basis of the adopted methods, three different zoning levels can be obtained (preliminary, intermediate and advanced). For instance, when using basic methods exclusively, only a preliminary zoning level can be obtained; while intermediate and advanced methods can allow the improvement of the zoning level that, according to the scale of the zoning and the related purpose, could be intermediate or advanced.

According to Cascini (2008), the selection of the most appropriate zoning method depends on several factors such as: availability, quality and accuracy of data; resolution of zoning; required outcomes; scale of zoning, etc. The Guidelines thoroughly discuss this topic as well as the activities that, among others, may be used to map the existing landslides and to define the areas with a potential to experience landsliding in the future. Cascini (2008) also relates methods, input data and procedures that, according to Soeters and vanWesten (1996), are classifiable as heuristic, statistical and deterministic. For instance, methods using heuristic or empirical procedures to process topographic, geological and geomorphological data, are considered as "basic". Methods can be defined "intermediate" when they use more detailed input data and procedures based on statistical analyses. Finally, "advanced" methods need hydrogeological and geotechnical data and the use of deterministic or probabilistic procedures. Independently from the adopted scale and zoning level, the use of "descriptors" to describe the degree of landslide zoning is encouraged.

At medium scale, the Guidelines suggests two possible zoning levels: preliminary and intermediate. It is usually appropriate to carry out the preliminary level of landslide susceptibility as the first stage of the analysis; then, the intermediate susceptibility zoning level may be pursued, having the control of both the process and the cost of zoning (Cascini 2008).

On the basis of the above suggestions, in order to achieve the goal of this work (i.e., hyperconcentrated flow susceptibility analysis and zoning at medium scale), the following methodological approach was adopted:

- Preliminary step: collection of data useful to acquire detailed knowledge of the slope processes leading to flow-like mass movements in the site (this includes knowledge of geology, geomorphology and hydrogeology);
- Step I: hyperconcentrated flow susceptibility analyses via heuristic and/or statistic procedures;
- Step II: hyperconcentrated flow susceptibility zoning (1:25,000 scale) at a preliminary/intermediate level.

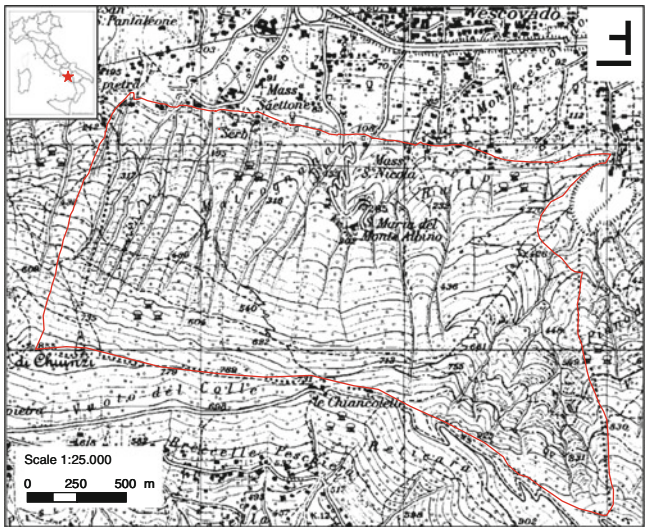

Fig. 1 Study area

Monte Albino Case Study

The selected test site of Monte Albino, located in the municipality of Nocera Inferiore (southern Italy), extends over a total area of around 400 ha, from 90 to 890 m a.s.l. (Fig. 1).

Along the hillslope 10 catchments can be individuated as well as 10 open slopes (Cascini et al. 2008), located in the lower portions of the relief (below 330 m a.s.l.). Over one of these open slopes, a first-failure phenomenon, causing three fatalities and the destruction of some buildings, occurred on March 2005.

On the basis of the proposed methodology, in order to define the geological setting as well as to deepen the knowledge of the different kinds of phenomena which can occur on the slopes, field surveys and studies were firstly carried out following a multidisciplinary approach (involving competences on geology, morphology, hydrogeology, geotechnics, historical data treatment, geomatics, geostatistics, etc.). The main results achieved during this preliminary step of the work are herein presented.

Geological Setting

The Monte Albino massif is constituted by a carbonatic bedrock covered by reworked and in-situ pyroclastic deposits originated from the air-fall deposition of the materials produced by the explosive activity of the Somma-Vesuvius volcanic complex. On the basis of field observations in

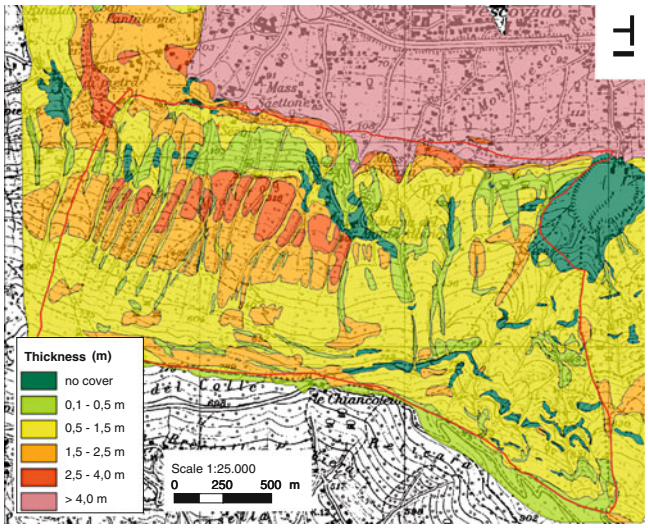

Fig. 2 Soil thickness map (1:25,000 scale)

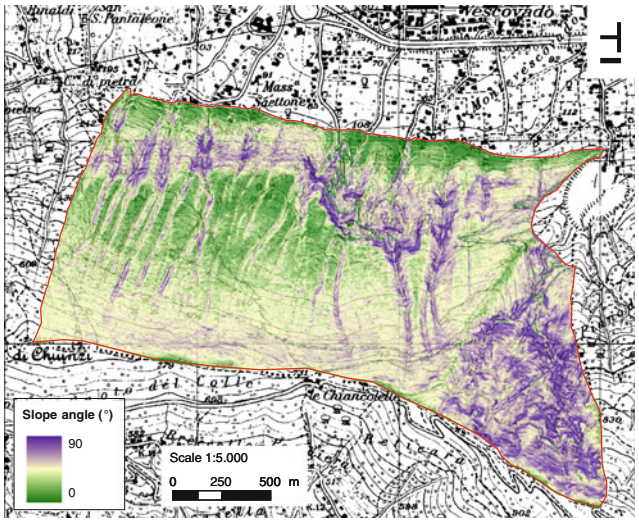

Fig. 3 Slope angle map (1:5,000 scale)

selected areas and morphological analysis extensively carried out on both topographic maps at different scales (1:25,000–1:5,000) and accurate 1998 and 2004 orthophotos, the thickness of the pyroclastic deposits has been estimated and mapped in the study area (Fig. 2). The spatial distribution of the thickness classes is controlled by the morphology of the slope. In particular, the thickness of the pyroclastic deposits reaches values of 4 m in the median part of the western sector of the slope where the slope angles range between 20° and 30° (Fig. 3); on the contrary, the thickness values do not exceed 1.5 m in the eastern part of the slope where slope angles attain the highest values. Moreover, it must be observed that the main vertical discontinuities of the pyroclastic deposits correspond to: (1) "scarps in calcareous rocks" (usually having a structural control due to the presence of fault scarps or thick strata heads) and (2) "erosion scarps along the gullies" (mainly originated by the erosive processes that grooved the pyroclastic covers and, in some cases, allowed the uncovering of the carbonatic bedrock).

Moving from the upper part to the toe of the slope, it is possible to recognise – in the western part of the Monte Albino hillslope – the presence of morphological concavities filled by pyroclastic soils and prone to first-failure phenomena. On the contrary, in the eastern part, streams cutting directly into the carbonatic bedrock are found. In the lateral sectors of the gullies, in the inter-rill areas and along the open slopes there are morphological elements probably related to landslide and erosive processes. The area at the toe of the slope shows a complex array of fans of different origin, on top of which lies a part of the urbanized area of the Nocera Inferiore municipality.

Finally, it is worth to observe that the study area corresponds to the northern part of the hydrogeological Unit of the Lattari Mounts. The groundwater regimen is conditioned by the main tectonic structures, originating springs in the lower part of the slope. Also ephemeral springs related to suspended groundwater can be found in the upper part of the slope.

Flow-Like Mass Movements

Owing to the above described geological predisposing factors, the Monte Albino hillslopes are prone to different kinds of rainfall-induced flow-like mass movements: hyperconcentrated flows, landslides on open slopes and flowslides (Cascini et al. 2010).

With reference to the hyperconcentrated flows, information found in historical documents essentially focuses on the consequences to properties related to the occurrence of these phenomena during the eighteenth and the nineteenth centuries. In particular, the described consequences refer to some exposed urbanised areas (such as the site called "Vescovado") as well as to a consular road (Fig. 4). The documentary sources also revealed that the hyperconcentrated flows mainly originated during autumn-winter periods due to the washing of the air-fall products of the explosive activity of the Vesuvius volcano. In this regard, a strict correlation existed in the past between the eruption events affecting the study area and the occurrence of hyperconcentrated flows. Since the last century, the Vesuvius activity strongly reduced and, during this period, the genesis of hyperconcentrated flows changed being strictly related to rainfall-induced erosion processes affecting the pyroclastic soil deposits.

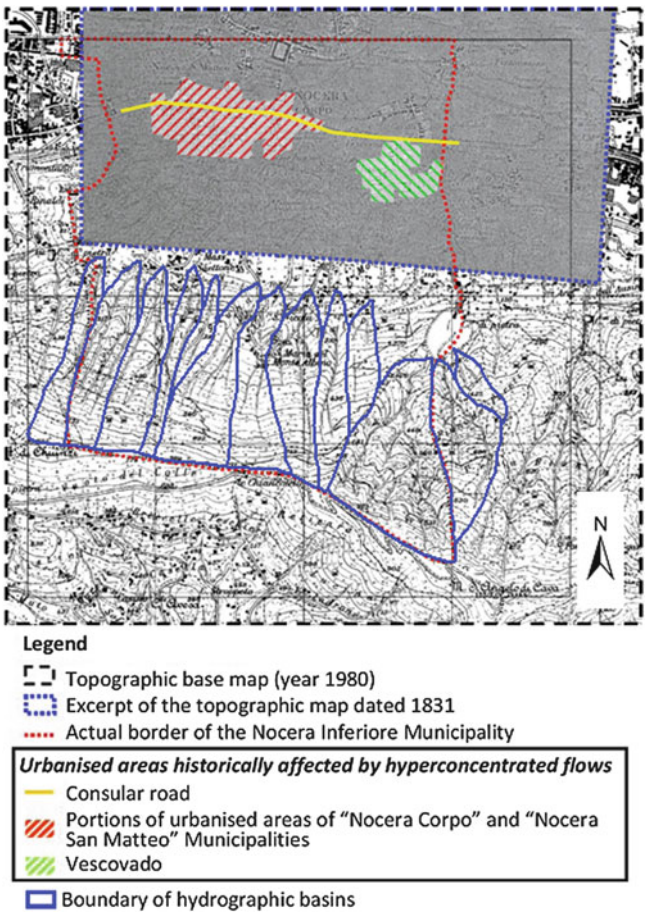

Fig. 4 Urbanised areas affected by hyperconcentrated flows occurred during the eighteenth and the nineteenth centuries

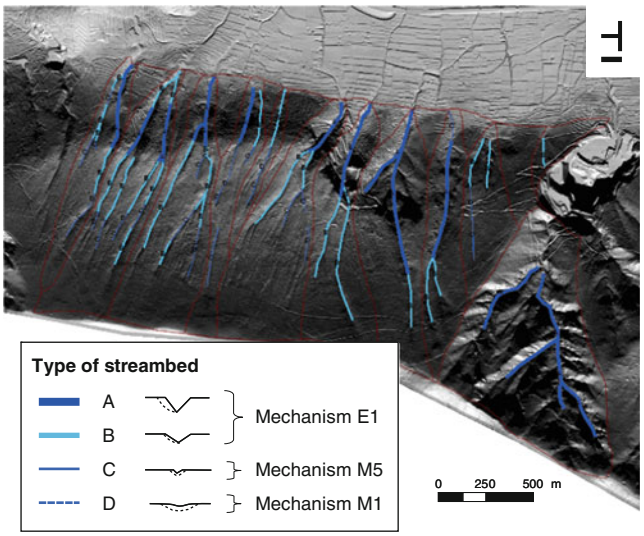

Fig. 5 Characterisation of the streambeds in relation to their geometric features and slope instability mechanisms

Susceptibility Analysis (Step I) and Zoning (Step II)

Towards the susceptibility analysis and zoning of the study area, the streambeds are preliminarily identified and classified in relation to their geometric features and slope instability mechanisms (Fig. 5).

All the main gullies and channels are characterised in relation to the shape of their cross-section (less incise from A to D type). The main instability phenomena affecting the watersheds are: superficial erosion due to rainwater (E1), and slope failure due to rainfall infiltration, with small (M5) or large (M1) soil volumes involved (Cascini et al. 2008). Type A streambeds are mostly located at the toe of the hillslope in the western part while they reach the uppermost portions of the hillslope in the eastern sector.

The analyses (step I) are preliminary carried out using a qualitative heuristic procedure (basic method), which is then followed by a quantitative statistical model (intermediate method). In both analyses, the main features predisposing to erosion are the slope angle and the thickness of the soil cover. In the statistical analysis, however, further independent variables, either derived from the available DEM (obtained from a LIDAR survey of the area) or from the geological, geomorphological and hydrogeological thematic maps, are explicitly considered.

The heuristic procedure takes into account the characteristics of the stream channels (Fig. 5) to classify them on the basis of both the erosion potential of the streambed and the instability potential of the channel's sides. To this aim, within the employed procedure (shown in Fig. 6), the susceptibility is computed, at each stream section, as a function of the following four factors: average longitudinal slope of stream section, average slope of stream sides, average thickness of pyroclastic cover along the streambed, average thickness of pyroclastic cover on the stream sides.

The combination of these factors, each one divided in four classes on the basis of its quartiles distribution over the studied area, first leads to two partial susceptibility estimates (in four classes), respectively related to slope and cover thickness, and then to a final estimate of the total relative susceptibility, S_He, in five classes: from very low (1) to very high (5). The results of the heuristic analysis (step II), in terms of map at a preliminary level of zoning, are shown in Fig. 7.

The statistical analysis is based on a probabilistic multivariate approach which is able to quantitatively relate the analyzed phenomenon, in this case the rainfall-induced erosion of the pyroclastic cover, to different features of the territory (i.e. independent variables). To this aim, the "event map" used as the geo-statistical dependent variable within the analysis is derived from a geomorphologic map of the territory. As for the independent thematic maps,

"Cover thickness" partial susceptibility			Cover thickness along streambed			
			0,1-0,5m	0,5-1,5m	1,5-2,5m	2,5-4,0m
			A	B	C	D
Cover thickness on stream sides	0,1-0,5m	A	L	L	M	M
	0,5-1,5m	B	L	L	M	M
	1,5-2,5m	C	M	M	H	H
	2,5-4,0m	D	M	M	H	H

"Slope" partial susceptibility			Longitudinal slope of stream section			
			<30°	30-35°	35-40°	>40°
			L	M	H	VH
Slope of stream sides	<30°	L	L	L	M	M
	30-35°	M	L	L	M	M
	35-40°	H	M	M	H	H
	>40°	VH	M	M	H	H

Total relative susceptibility (S_He)		"Cover thickness" partial susceptibility		
		L	M	H
"Slope" partial susceptibility	L	1	2	3
	M	2	3	4
	H	3	4	5

Fig. 6 Procedure used for the heuristic analysis

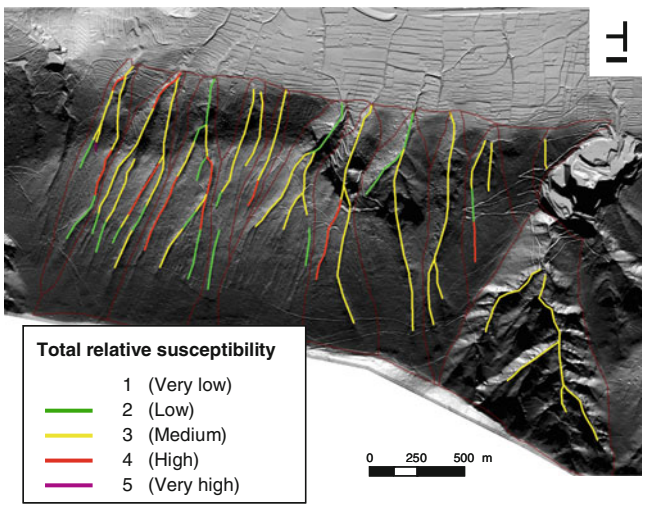

Fig. 7 Susceptibility map at preliminary level of zoning for the triggering of the hyperconcentrated flows

a sensitivity analysis has been carried out, on a large number of DEM-derived and heuristically-developed maps which were available for the study area (i.e. 23 variables), to determine the variables that are most statistically significant for the analysis. The 6 uncorrelated independent variables employed are shown in Table 1 together with the typology of the map, the number of classes into which they have been subdivided for the analysis and the classification method employed for the purpose.

The statistical algorithm used to conduct the susceptibility analysis is often cited in the literature as the "Information Value Method" (e.g., Kobashi and Suzuki 1988; Yin and Yan 1988; Van Western 1993). This method belongs to the

Table 1 Independent variables used in the statistical analysis

Thematic map	Type	Classes	Classification
Slope	Raster	8	Eq. Pop. 12.5 %
Curvature (longitudinal)	Raster	8	Eq. Pop. 12.5 %
Flow accumulation	Raster	8	Natural breaks
Pyroclastic thickness	Shape	6	Heuristic
Geo-structural features	Shape	7	Heuristic
Dist. from streamlines	Raster	8	Eq. Pop. 12.5 %

class of the bi-variate approaches based on the definition of a statistical correlation between the dependent variable and each one of the independent variables. The employed procedure may be divided in three subsequent phases: (1) definition, for each thematic map, of an index of relative weight for each class of the independent variable, (2) production of a map of relative susceptibility related to each significant independent variable, (3) production of a map of global relative susceptibility (i.e. final result of the multivariate statistical analysis) on the basis of a linear combination of the maps produced in the previous phase. The equations used in the analysis are the followings:

$$W_{ij} = \frac{Npix(E_{ij})}{Npix(C_{ij})} \tag{1}$$

$$I_{ij} = \ln\left(W_{ij} \Big/ \frac{\sum_j Npix(E_{ij})}{\sum_j Npix(E_{ij})}\right) \tag{2}$$

$$S_i(k) = I_{ij}(k) \tag{3}$$

$$S - St(k) = \sum_{ij} I_{ij}(k) \tag{4}$$

where: W_{ij} = relative weight of class j of i-th variable; $Npix(E_{ij})$ = number of "event" pixels within class j of the i-th variable; $Npix(C_{ij})$ = number of total pixels within class j of the i-th variable; I_{ij} = normalized susceptibility index of class j of i-th variable; $S_i(k)$ = relative susceptibility of i-th variable within terrain unit k (i.e. 5 × 5 m square cell); S_St(k) = total relative susceptibility within terrain unit k.

The results of the statistical analysis are reported in Table 2 and Fig. 8. The values of the normalized susceptibility indexes shown in the table indicate the relative importance of class j of the i-th variable towards the computation of the susceptibility. The Figure shows the global relative susceptibility map for the study area, drawn by considering 5 × 5 m square cells terrain units (the same used for the computation of all the statistical indicators) and four different susceptibility classes ($S\_St < -0.5$; $-0.5 \leq S\_St < 0$; $0 \leq S\_St < 0.5$; $S\_St \geq 0.5$).

The comparison between the results obtained by the heuristic procedure and the statistical algorithm is not

Table 2 Values of the normalized susceptibility indexes I_{ij}

	Norm. susceptibility index (j = 1,8)							
Thematic map	1	2	3	4	5	6	7	8
Slope	−0.10	0.10	0.05	−0.06	−0.10	−0.04	−0.01	−0.22
Curvature (longitudinal)	−0.10	−0.05	−0.09	−0.15	−0.18	−0.09	0.11	0.24
Flow accumulation	−0.10	−0.21	−0.14	0.14	0.32	0.62	0.72	.062
Pyroclastic thickness	−0.54	0.13	−0.11	0.13	−0.33	−3	N/A	N/A
Geo-structural features	−0.08	0.29	0.23	−2.51	−3	−1.45	−0.48	N/A
Dist. from streamlines	0.64	0.16	−0.40	−0.34	−0.47	−0.46	−0.44	−3

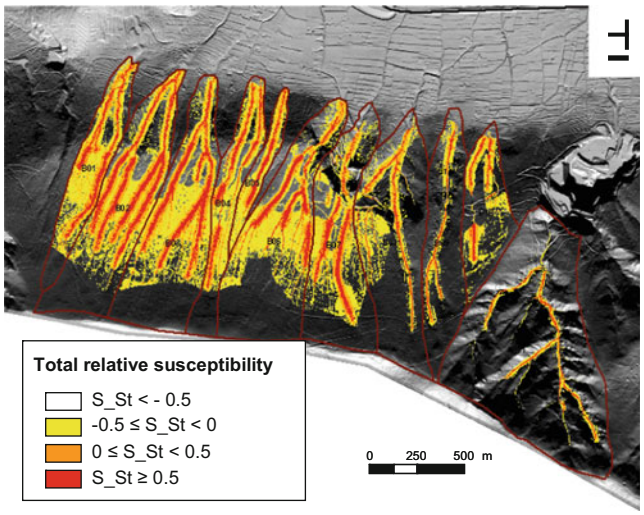

Fig. 8 Susceptibility computational map at intermediate level for the triggering of the hyperconcentrated flows

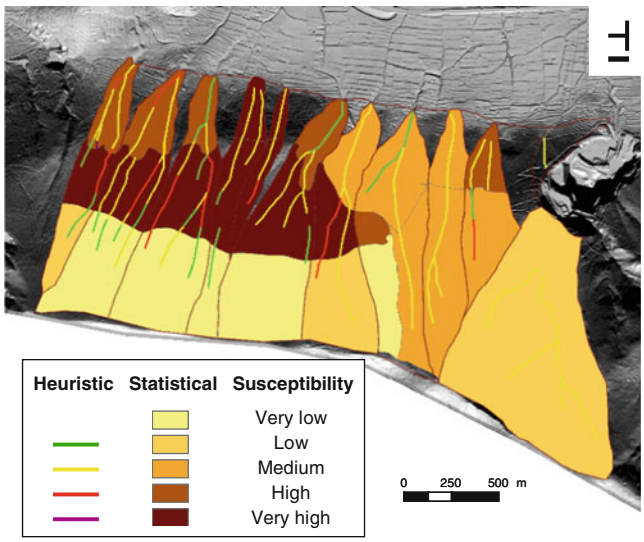

Fig. 9 Susceptibility zoning map of the studied area to the triggering of hyperconcentrated flows at medium scale

straightforward, as the first method only refers to and zones the stream channels (Fig. 8), while the second analysis leads to a total coverage map (Fig. 9). To this aim, however, the heuristic class of S_He can be compared, for each stream channel, with the average value of the total relative susceptibility S_St computed considering a 10 m buffer zone around the channels. The results of this comparison leads to 71.4 % of channels simultaneously classified as susceptible according to both the heuristic (i.e. S_He from medium to very high) and statistical (i.e. S_St > 0) analyses, thus confirming the goodness of both the qualitative and quantitative estimates of susceptibility.

All that considered, the last step of the analysis, which is needed to produce the final susceptibility zoning map (step II), is the combination of the results obtained by the heuristic and the statistical procedures. Indeed, following the procedure proposed by Calvello et al. (2011), who differentiate between Terrain Computational Units (TCUs) and Terrain Zoning Units (TZUs) depending on whether they refer to the homogeneous territorial domains used in the landslide analysis or to the units used to produce a landslide map for zoning purposes, the map shown in Fig. 8 has to be considered a computational map and not a zoning map. The final map of the analysis, i.e. the susceptibility zoning of the studied area to the triggering of hyperconcentrated flows at medium scale, is reported in Fig. 9. In the map, the statistical results are reported by considering litologically-based subdivisions of the basins as TZUs and, similarly to what has been done for the heuristic analysis, five susceptibility classes: very low, low, medium, high and very high. The values of susceptibility assigned to each zoning unit is based on the average value of the total relative susceptibilities S_St computed in 5 × 5 m TCUs within each sub-basin. The map clearly indicates that the most susceptible zones and riverbeds are located in the central and western part of the study area at intermediate elevations between the foot and the crest of the slope.

Concluding Remarks

In this paper, a methodology is presented to analyse and zone the susceptibility of Monte Albino hillslopes (Nocera Inferiore, southern Italy) to hyperconcentrated flows. The proposed approach comes from the recommendations provided by Fell et al. (2008) and comprises some

consequential steps. In particular, susceptibility analyses (step I) are carried out with the purpose of zoning (step II) the slope areas prone to erosion which may originate hyperconcentrated flows (along channels). Within step I, the analyses are preliminary carried out using heuristic procedures and followed by statistical models. In both analyses, the main factors and features predisposing to erosion are the slope angle and the thickness of the soil cover.

The obtained results emphasize the potential of an approach which moves from preliminary to intermediate level of susceptibility zoning. In particular, the multivariate analyses offer a significant contribution for reducing the uncertainties related to the final zoning map taking into account appropriate statistical indicators. Moreover, these results highlight the important role played by the combined use of different procedures in defining a standardised criterion to be adopted in problems dealing with the analysis of susceptibility to hyperconcentrated flows. The role played by a statistically-based quantitative approach on the reliability of the hyperconcentrated flow susceptibility zoning is also highlighted. Finally, it is worth noting that the effectiveness of the proposed procedure is strongly increased by the availability of detailed topographic data (e.g., LIDAR surveys). The latter are becoming progressively common in many areas of the world, thus allowing the use of the adopted procedure to other geo-environmental homogeneous contests affected by similar phenomena.

References

Calvello M, Cascini L, Mastroianni S (2011) Landslide density zoning maps towards susceptibility analyses at small and medium scale. Geomorphology, submitted

Cascini L (2008) Applicability of landslide susceptibility and hazard zoning at different scales. Eng Geol 102:164–177

Cascini L, Cuomo S, Guida D (2008) Typical source areas of May 1998 flow-like mass movements in the Campania region, Southern Italy. Eng Geol 96:107–125

Cascini L, Di Nocera S, Matano F, Calvello M, Cuomo S, Ferlisi S (2010) On the reliability of landslide inventory mapping: the case study of Monte Albino, Nocera Inferiore (southern Italy). In: Proceedings of the 85th national congress of the Italian geological society, pp 573–574

Fell R, Corominas J, Bonnard C, Cascini L, Leroi E, Savage WZ (2008) Guidelines for landslide susceptibility, hazard and risk zoning for land-use planning. Eng Geol 102:85–98

Kobashi S, Suzuki M (1988) Hazard index for judgment of slope stability in the Rokko Mountain Region. In: Proceedings of the Interpraevent, vol 1, Graz, pp 223–233

Soeters R, van Westen CJ (1996) Slope instability recognition, analysis and zonation. In: Turner AK, Schuster RL (eds) Landslides investigation and mitigation, TRB Special Report 247. National Academy Press, Washington, DC, pp 129–177

Van Western C (1993) Application of geographic information systems to landslide hazard zonation. Ph.D. thesis, Technical University Delft, The Netherlands

Yin KJ, Yan TZ (1988) Statistical prediction model for slope instability of metamorphosed rock. In: Proceedings of the 5th ISL, vol 2, Lausanne, pp 1269–1272

Inventory of Landslide Risk to Limit Consequences of Climate Change

Marius Tremblay, Karin Lundström, Victoria Svahn, Charlotte Cederbom, and The Göta älv Working Group

Abstract

A comprehensive inventory of the landslide risk in the Göta älv valley, Sweden, is conducted to limit consequences of climate change on society. Here we present an overview of the project and highlight key problems to be solved. Methodology developments and investigations are performed regarding mapping of quick clay, hydrological and meteorological conditions, erosion and risk analysis. Much of the knowledge and experience gained in the project can be implemented and used elsewhere, nationally and abroad.

Keywords

Landslide • Quick clay • Risk analysis • Consequence • Sweden • Göta älv

Introduction

Landslide scars are frequent along the Göta älv river in southwest Sweden, draining lake Väner (Fig. 1). Several landslides have resulted in casualties and severe damages on buildings and infrastructure during the latest century. Moreover, higher average precipitation and increased occurrence of extreme rainfall events are some expected climate changes in Sweden during the coming 70–100 years (Ministry of the Enviroment 2009; Nikulin et al. 2011). To prevent extensive floodings and damages of cities and infrastructure around Lake Väner, it is necessary to allow controlled overflow from Lake Väner through the river Göta älv. An overflow in the river, in turn, leads to increased risk for erosion and landslides along the Göta älv valley.

The Swedish Government has commissioned the Swedish Geotechnical Institute (SGI) to perform a comprehensive inventory of the landslide potential in the Göta älv river valley, taking predicted climate changes into consideration. This 3-year project, ending 2011, includes site investigations and methodology developments together with analyses of the effects of a changing climate during the coming 100 years. This paper aims to give an overview of the project. We summarize the different parts of the project, and highlight some of the major problems to be solved.

M. Tremblay (✉) • K. Lundström • V. Svahn • C. Cederbom, and • The Göta älv Working Group
Department of Land Use Planning and Climate Adaptation Swedish Geotechnical Institute, Olaus Magnus Road 35, Linköping 591 93, Sweden
e-mail: marius.tremblay@swedgeo.se

The Göta älv Project

Background

The Göta älv river valley is about 90 km long and it extends from the largest lake in Sweden, Lake Väner, in the north to the city of Göteborg in the south. The river valley is an important locality for dwelling, industry and transportation both on land and on the river (Fig. 2).

Thick deposits of marine clay along the entire river valley in combination with human activity result in a number of landslides in the river bank each year. The earliest reported landslide occurred in the middle of the 1,200th century, it was c. 60 ha big and affected an entire village. More recent landslides occurred in the 1950s (Göta and Surte) and in the 1990s (Agnesberg and Ballabo).

Only 22 % of the shoreline had been investigated in terms of landslide risk analysis before 2005. Moreover, none of

C. Margottini et al. (eds.), *Landslide Science and Practice*, Vol. 1,
DOI 10.1007/978-3-642-31325-7_53,

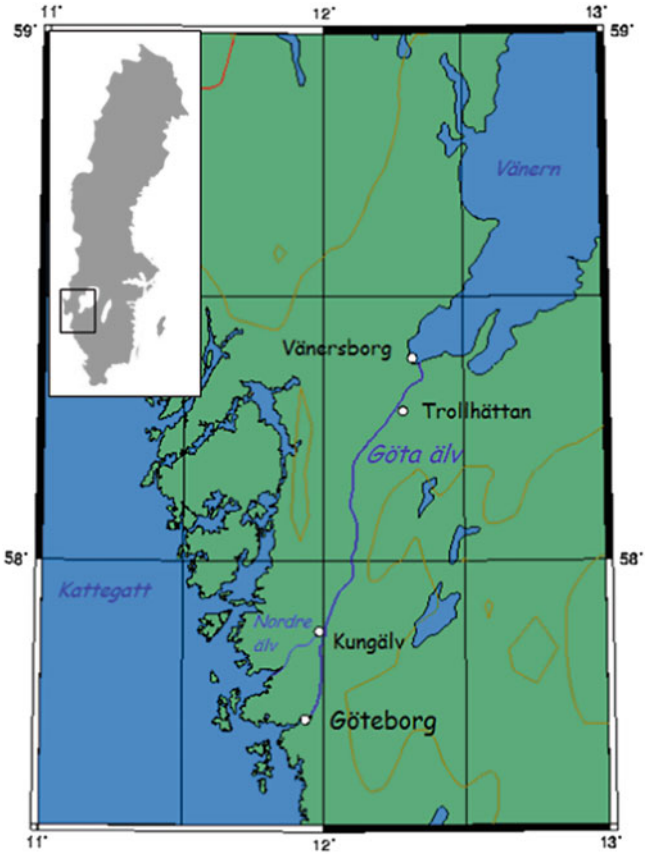

Fig. 1 Location of river Göta älv, extending from lake Vänern to the city of Göteborg

Fig. 2 Photo of Göta älv towards the north. The river valley is an important locality for dwelling, industry and transportation

these separate and local investigations considered changing conditions in a future climate. Based on the sparse data existing until then, SGI analysed the effect of increased tapping from Lake Väner for the geotechnical conditions of the river bank (Hultén et al. 2006).

Analysis suggested that an increase in tapping will lead to a significantly higher risk for landslides, and that new risk areas will emerge (Hultén et al. 2006). However, to meet future climate change, and to handle increased water flow in the river, more comprehensive knowledge of the stability conditions in the river valley is required.

Project Overview

In December 2008, SGI was commissioned to perform the inventory of the Göta älv valley. The project started in January 2009 and is running until December 2011 with a total budget of 100 MSEK.

We have limited the investigation to areas adjacent to the main river and its tributaries. The field area has been divided into ten subareas where sounding, groundwater measurements and sampling have been performed. The samples are investigated further in laboratory.

Recently, high precision elevation data became available for the river valley. To have acces to a complete terrain model, we have mapped the submarine river topography by multi-ray sonar. In addition, automatic stations measuring slope-inclination, groundwater- and porewater pressure and water level are gathering information around and in the river.

Several uncertainties, such as handling and mapping of quick clay, are considered in separate development projects. Moreover, specific investigations focusing on parameters (groundwater, erosion and climate) and methodologies (how to estimate probabilities for and consequences of landslides) are being run as specific projects within the main Göta älv project.

A limited amount of the result from these sub-projects have been published in reports or papers that we refer to here. However, most results are currently only presented in internal reports, that will be available to the public once the project is finished. Hence, we refer to this material as being ‘in preparation’.

GIS Platform

A special GIS platform has been designed for collecting existing data and new data produced in the project. The platform contains a mixture of background data, e.g. topography and geology, and overlying dynamic data. Dynamic data include geotechnical data, environmental data, existing landslide database and project analyses such as stability calculations.

Specific Investigations

Mapping and Handling of Quick Clay

Quick clay is a form of highly sensitive marine clay that change from being relatively stiff to becoming a liquid mass when it is disturbed (for a detailed description of quick clay in Sweden, see Rankka et al. 2004). The presence of quick clay has a major influence on the total area affected by a landslide, and quick clay mapping is therefore one of the most important investigations that is being conducted in our project.

A literature review on the influence of changes in porewater chemistry has been conducted (Larsson 2010) and an additional literature review on the sensitivity of quick clay to disturbance is in preparation.

Another key problem working in areas with quick clay is to predict the extent of a potential future landslide. This is crucial for estimating the consequences of a landslide, and we are currently working on guidelines for how to make such a prediction.

Hydrological and Meteorological Conditions

The hydrological and meteorological conditions for the Göta älv valley have been compiled (in preparation). Present-day climate variabilities are described together with predicted consequences of a future climate based on the latest available climate models. In general, the data compiled span a time period between 1960 and 2100.

The compilation summarizes yearly and seasonal averages of temperature and precipitation, respectively, and extreme precipitation (24 h and 100 year return period). Measurements and predictions of water level in lake Väner, water flow from lake Väner to the Göta älv plus local inflow are considered. Moreover, annual and seasonal average of ground humidity are presented. Finally, observed and predicted sea-levels today and in future, respectively, are shown.

Groundwater- and porewater conditions have a direct impact on slope stability and have therefore been studied in detail. We have judged the groundwater conditions for slopes along the river based on the hydrological predictions until 2100. Moreover, we have analysed observed porewater pressures in two different slopes to better understand the geohydrological conditions along the Göta älv.

Erosion

Several investigations have been made to reveal the conditions of erosion within and along the river. The river banks have been investigated in the field (e.g. erosion marks and existing preventive measures), and the multi-ray sonar image of the river bottom have been analysed. The geology of the river bottom has been mapped using backscatter measurements, and a small study of erosion in cohesive soils has been conducted.

Moreover, the effects of ship-induced erosion has been examined, and we have compiled information about suspended material in the river. Finally, to estimate the effects of a changing climate hydraulic modelling and hydrodynamic calculations are being made.

The findings will be summarized in a report that gives an overview of the present erosion conditions and the potential effects of a changing climate (in preparation).

Risk Analysis

Probability Estimates

One of several challenges in the project is to make realistic estimates of the probability for landslide in the extensive study area with a reasonable working effort. Stability has been calculated for vertical sections across the slope approximately every 500 m along the river. We have chosen to summarize them by selecting a number of 'type sections', for which reliability analyses are perfomed. Obtained performance functions along the type sections are then projected back into areas with similar geological, morphological and hydrological setting.

The method we use for reliability analysis of the selected type sections is an elaboration and simplification of a first order reliability method (FORM) that has previously been succesfully used in the Göta älv setting (Alén 1998).

The uncertainty for each driving parameter is investigated, and the progression of probability for landslide over time due to climate change is accounted for. When the uncertainty is strongly dominated by the undrained shear strength and topography, the method can be simplified. The result is transferred to a 2D map with five classes of probability. (in preparation).

Consequence Estimates

The aim of our work related to consequence estimates has been to update and develop a previously used methodology (Alén et al. 2000). Much work has been invested in identifying relevant factors (e.g. population, property, contaminated land, transportation network, industry), value consequences of importance and to estimate sensitiveness (in preparation).

The consequence is set to be the product of the inventory of elements at risk, value per unit area, the vulnerability and the exposure (Fig. 3). The result is presented in a 2D map with five consequence classes given in MSEK/ha.

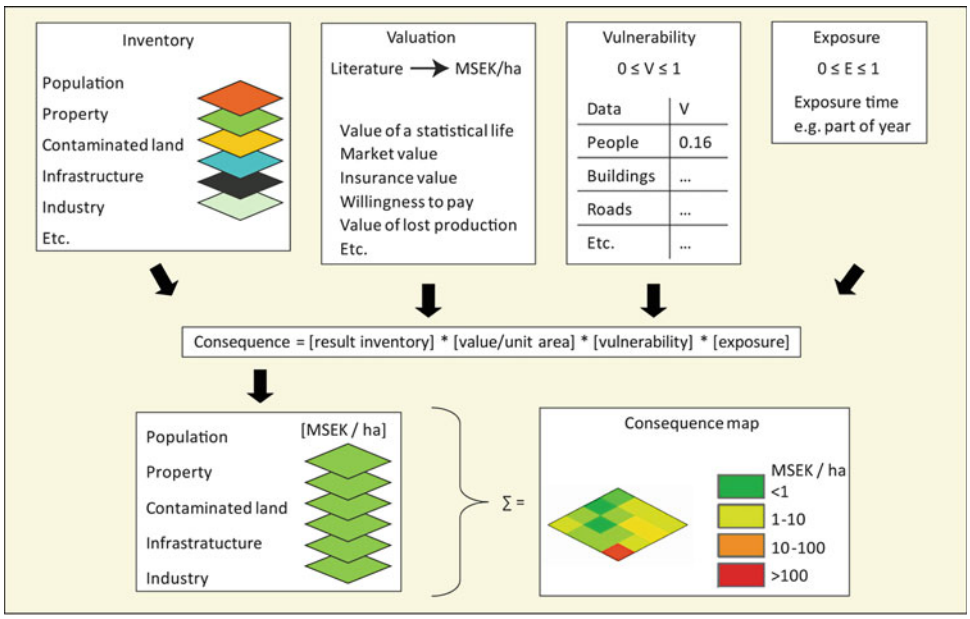

Fig. 3 Schematic sketch of how consequence is estimated and transferred into 2D map. The consequence is set to be the product of the number or density of objects obtained in an inventory, the value per unit area, the relative vulnerability and relative exposure time. The sum of the consequences for all object categories is plotted in a 2D map using GIS techniques

Illustration of Risk

The five classes of probability and consequence, respectively, are combined in a risk matrix from which three classes of risk are identified (Fig. 4);

- Acceptable risk
- Unsafe risk level (investigation required)
- Unacceptable risk level (preventive measures are required).

The outcome of the risk analysis will be presented in maps over the investigation area illustrating the extent of the three risk levels.

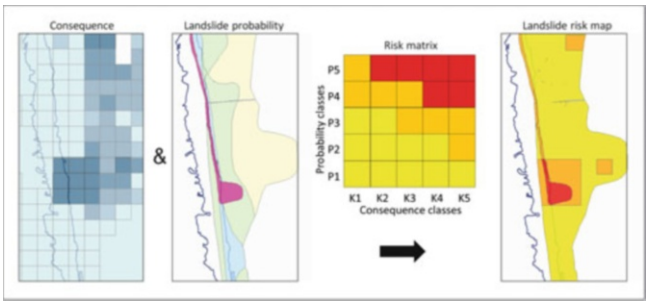

Fig. 4 Illustration of risk analysis. Estimates of consequences of and probabilities for landslide are grouped into five classes and combined by GIS techniques in a risk matrix. The resulting pair of numbers, e.g. (P3,K3) are grouped in three risk classes; acceptable risk (*yellow* color), unsafe risk level (*orange* color) and unacceptable risk level (*red* color). The different risk levels are subsequently illustrated in map view

Concluding Remarks

Much of the knowledge and experience gained during the development projects and specific investigations within the Göta älv project can be implemented and used elsewhere, nationally and abroad.

The outcome of the project will be made public once the project is finished and has been reported to the mandator, the Swedish Government. Hence, we will spread gained knowledge to the geotechnical community by different channels after December 2011. More information about the project and the outcome (publications, reports etc.) is available on our website www.swedgeo.se.

Acknowledgements The complexity of the investigation requires collaboration with other national and international authorities, research institutes and organisations. We thank Chalmers University, Deltares, Göteborg University, Lantmäteriet, Länsstyrelsen Västra Götalands län, Lund University, Myndigheten för Samhällsskydd och beredskap, Norwegian Geotechnical Institute, Swedish Geological Survey, Sjöfartsverket, Svenska Kraftnät, Swedish Hydrological and Meteorological Institute, and Vattenfall for a constructive long-term collaboration extending beyond the Göta älv project.

References

Alén C (1998) On probability in geotechnics. Random calculation models exemplified on slope stability analysis and ground-superstructure interaction. Ph.D. thesis, Chalmers University of Technology, Göteborg

Alén C, Bengtsson P-E, Berggren B, Johansson L, Johansson Å (2000) Skredriskanalys i Göta älvdalen – Metodbeskrivning. SGI Report 58. Linköping. (ISSN 0348-0755). 103 p

Hultén C, Edstam T, Arvidsson O, Nilsson G (2006) Geotekniska förutsättningar för ökad tappning från Vänern till Göta älv. SGI Varia 565. Linköping. (ISSN 1100-6692). 41 p

Larsson R (2010). Inverkan av förändringar i porvattnets kemi – främst urlakning – på naturlig leras geotekniska egenskaper. Litteraturstudie. SGI Varia 611. Linköping. (ISSN 1100-6692)

Ministry of Environment (2009) Sweden's fifth national communication on climate change. Ds 2009:63. Stockholm. (ISSN 0284-6012). 156p

Nikulin G, Kjellström E, Hansson U, Strandberg G, Ullerstig A (2011) Evaluation and future projections of temperature, precipitation and wind extremes over Europe in an ensemble of regional climate simulations. Tellus 63:41–55

Rankka K, Andersson-Sköld Y, Hultén C, Larsson R, Leroux V, Dahlin T (2004) Quick clay in Sweden. SGI Report 65. Linköping. (ISSN 0348-0755). 137p

Probability Maps of Landslide Reactivation Derived from Tree-Ring Records

Jérôme Lopez Saez, Christophe Corona, and Frédéric Berger

Abstract

Probability maps of landslide reactivation are presented for the Aiguettes landslide located in the southern French Alps based on results obtained with dendrogeomorphic analysis. Spatio-temporal activity was derived from tree-ring series of 223 disturbed trees. 355 growth disturbances were identified in the samples indicating 14 reactivation phases of the landslide body between 1898 and 2011. Probabilities of landslide reactivation were computed and illustrated using a Poisson distribution model. For example, in the toe, the probability increases from 0.28 for a 5-year period to 0.99 for a 100-year period. This method differs from conventional approaches, which have demonstrated to have limitations in the prediction of spatiotemporal reactivation of landslides. Based on extensive data and therefore allowing determination of quantitative probability maps of reactivation, this approach is considered a valuable tool for land managers in charge of protecting and forecasting people as well as for those responsible for land-use planning and management.

Keywords

Dendrogeomorphology • Landslide • Return period • Poisson distribution model

Introduction

Each year, mass movements cause considerable financial damage to alpine societies (Hilker et al. 2009). Global statistics show that damage from landslides has risen for the last 30 years in mountain areas (Alexander 2008). In addition, extensive records of landslide activity (Floris and Bozzano 2007) show that new slides are, in many cases, consequent upon partial or complete reactivation of existing landslide bodies. A need therefore exists for the documentation of past events and elaboration of site-specific landslide reactivation maps indicating the degree of stability of specific areas as well as providing information on the probability of landslide reactivation (Varnes 1984). Methods available for the assessment of probabilities of landslide reactivation have been reviewed by Aleotti and Chowdhury (1999). Two independent approaches have been traditionally used: (1) analysis of the potential for slope failure and (2) a statistical treatment of past landslide events.

As complete as possible landslide records covering multiple decades are normally needed to perform a reliable probabilistic analysis, but such data is not normally available with satisfying spatial resolution, over long enough timescales, and as a continuous record (Thiery et al. 2007; Corominas and Moya 2008). The temporal window of the record seldom spans more than a few decades and rarely covers centuries. In order to compute accurate probability maps of landslide reactivation at the local scale, an approach is thus required which offers both an adequate temporal and spatial resolution. On shallow landslide bodies covered with tree stands, dendrogeomorphology may allow such a reconstruction of landslide reactivation with the desired resolution through the analysis of growth disturbances contained in tree-ring records (Alestalo 1971; Stoffel et al. 2010). Indeed, trees suffering from superficial and slow movements may

J.L. Saez (✉) • C. Corona • F. Berger
Cemagref UR EMGR, 2 rue de la papeterie, BP 76 F-38402 Saint Martin d'Hères Cedex, France
e-mail: jerome.lopez@cemagref.fr

C. Margottini et al. (eds.), *Landslide Science and Practice*, Vol. 1,
DOI 10.1007/978-3-642-31325-7_54,

survive reactivation events and conserve evidence of topping, tilting (or S-shaped stems), scarring or root breakage in their increment rings (Carrara and O'Neill 2003). The purpose of this study therefore is to map the probability of landslide reactivation for a site in the Ubaye Valley (French Alps) using dendrogeomorphic techniques. Through an exhaustive sampling of 223 Mountain pines we (1) reconstruct a chronology of past landslide reactivations; (2) derive a high-resolution landslide return period map and finally (3) quantify and map the probability of landslide reactivation for the coming 5, 20, 50 and 100 year.

Study Site

The Aiguettes landslide (44°25′30.8″ N, 6°36′26.7″ E, Fig. 1a) is located in the Riou-Bourdoux catchment, a tributary of the Ubaye River and on the north-facing slope of the Barcelonnette basin, 3 km north of Saint-Pons (Alpes de Haute-Provence, France). The Riou-Bourdoux catchment has been considered the most hazardous area in France (Delsigne et al. 2001) and is well known for its extensive mass-movement activity.

The Aiguettes landslide is 800 m long, 400 m wide (16 ha), and has a depth varying between 4 and 9 m. Its elevation ranges from 1980 to 1740 m asl. The rotational landslide is a slump characterized by 15 m thick top moraine layer underlain by a weathered and unsaturated black marl layer and is very sensitive to mass movement.

The study site is characterized by irregular topography with a mean slope angle of about 20°. Two main scarps (SC) delineate the head of the landslide (Fig. 1b): SC1, located at around 1980 m asl, is 200 m long and 40 m high. SC2, located at around 1880 m asl, is 40 m high, with a slope angle of 70°, and completely void of vegetation. On the landslide body, four recent earth slides and several minor internal scarps and cracks are clearly visible. *Pinus uncinata* has a competitive advantage on these dry, matrix-poor soils (Dehn and Buma 1999) and form nearly homogeneous forest stands outside the surfaces affected by the scarps and recent earth slides. The tilted and deformed *P. uncinata* trees also clearly indicate that the Aiguettes landslide has been affected by multiple reactivations in the past. The climate at the study site is dry and Mediterranean with strong interannual rainfall variability. According to the HISTALP dataset (Efthymiadis et al. 2006), precipitation at the gridded point closest to the Aiguettes landslide (44°25′ N, 6°35′E) is 895 ± 154 mm.yr^{-1} for the period 1800–2003. Rainfall can be violent, with intensities trespassing 50 mm h^{-1}, especially during frequent summer storms. Mean annual temperature is 7.5 °C with 130 days of freezing per year (Maquaire et al. 2003).

Material and Methods

Reconstruction of Landslide Events with Tree-Ring Series

Dendrogeomorphic techniques have been used to date landslide events in several ways. Tree age may supply a first, but important information as the oldest undisturbed tree on a landslide body will provide a minimum age of movement (Carrara and O'Neill 2003). The earliest dendrogeomorphic studies of landslides date back to Alestalo (1971) and the method has been used ever since extensively in the United States (Wieczorek et al. 2006), also in Quebec (Bégin and Filion 1988). In Europe, tree rings have been used to reconstruct the frequency and landslides reactivation in the French (Astrade et al. 1998) and Italian Alps (Stefanini 2004), in the Spanish Pyrenees (Corominas and Moya 1999) and the Flemish Ardennes (Van Den Eeckhaut et al. 2009).

Collection and Preparation of Samples

Based on an outer inspection of the stem, *P. uncinata* trees obviously influenced by past landslide activity were sampled. Normally four cores per tree were extracted; two in the supposed direction of landslide movement (i.e. upslope and downslope cores), and two perpendicular to the slope. To gather the greatest amount of data on past events, trees were sampled within the tilted segment of the stems. To avoid misinterpretation, trees growing in sectors influenced by processes other than landslide or anthropogenic activity (sylviculture) were disregarded systematically for analysis. A total of 223 *P. uncinata* trees were sampled with 892 increment cores. The samples obtained in the field were analyzed and data processed following standard dendrochronological procedures (Stoffel and Bollschweiler 2008) and growth curves of the samples of disturbed trees were then compared with the reference chronology to detect missing, wedging or false rings and to identify reactions to mechanical stress. As no significant correlation was found between the reference chronology and 44 cores from 11 affected trees, these trees were rejected for further analysis.

Sign of Disturbance in the Tree-Ring Record

Landslide movement induces several kinds of growth disturbances (GD) to trees, most commonly in the form of an abrupt reduction in annual ring width and/or the formation of compression wood on the tilted side of the stem. A reduction in annual ring width over several years is interpreted as damage to the root system, loss of a major

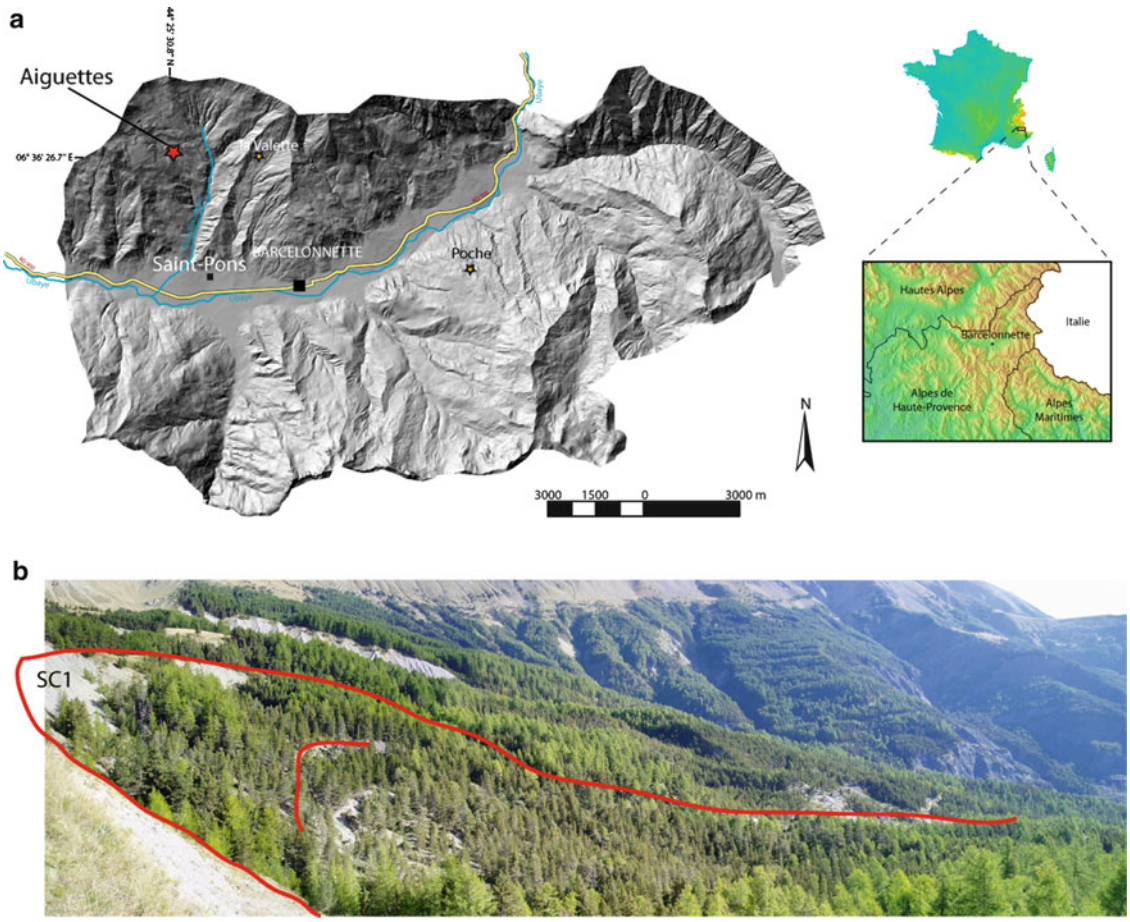

Fig. 1 (**a**) The Aiguettes landslide is located in the Southern French Alps, in the Ubaye Valley, near the village of Saint-Pons. (**b**) View of the main scarp SC1 and of the landslide body. The *red dotted line* delimits the landslide area

limb, or a partial burying of the trunk resulting from landslide activity (Carrara and O'Neill 2003). In this study, growth-ring series had to exhibit (1) a marked reduction in annual ring width for at least five consecutive years such that the (2) width of the first narrow ring was 50 % or less of the width of the annual ring of the previous year. The onset of compression wood is interpreted as a response to stem tilting induced by landslide pressure. Tilted trees try to recover straight geotropic growth (Mattheck 1993) through the development of asymmetric growth rings, i.e. formation of wider annual rings with smaller, reddish-yellow colored cells with thicker cell walls (so-called compression wood; Timell 1986) on the tilted side and narrow (or even discontinuous) annual rings on the opposite side of the tree (Carrara and O'Neill 2003). Finally, the formation of callus tissue was interpreted as a reaction to the corrasion of tree stems by the debris that causes damage and scars (Hupp 1984).

Dating of Events

Determination of events was based on the number of samples showing GD in the same year and on the distribution of affected trees on the landslide body (Bollschweiler et al. 2008). To avoid overestimation of GD within the tree-ring series in more recent years because of the larger sample of trees available for analysis, we used an index value (I_t) as defined Butler and Malanson (1985):

$$I_t = \left(\sum_{i=1}^{n} (R_t) / \sum_{i=1}^{n} (A_t) \right) .100 \qquad (1)$$

Where R is the number of trees showing a GD as a response to a landslide event in year t, and A is the total number of sampled trees alive in year t. In order to minimize the risk that GD caused by other (geomorphic) processes could mistakenly be attributed to a landslide event and to take into account the sampling size, the chronology of past events was based on It $\geq$5 %. However, the strictness of these thresholds and the large sample size may induce a misclassification of minor reactivation. To avoid misclassification, the annual patterns of disturbed trees for years with 2 % $\geq It <$ 5 % and GD in at least five trees were carefully examined. Using geographical coordinates, trees were placed into a Geographical Information System (GIS; ArcGIS 9.3) as geo-objects, and years of GD were linked as attributes to each single tree. We computed

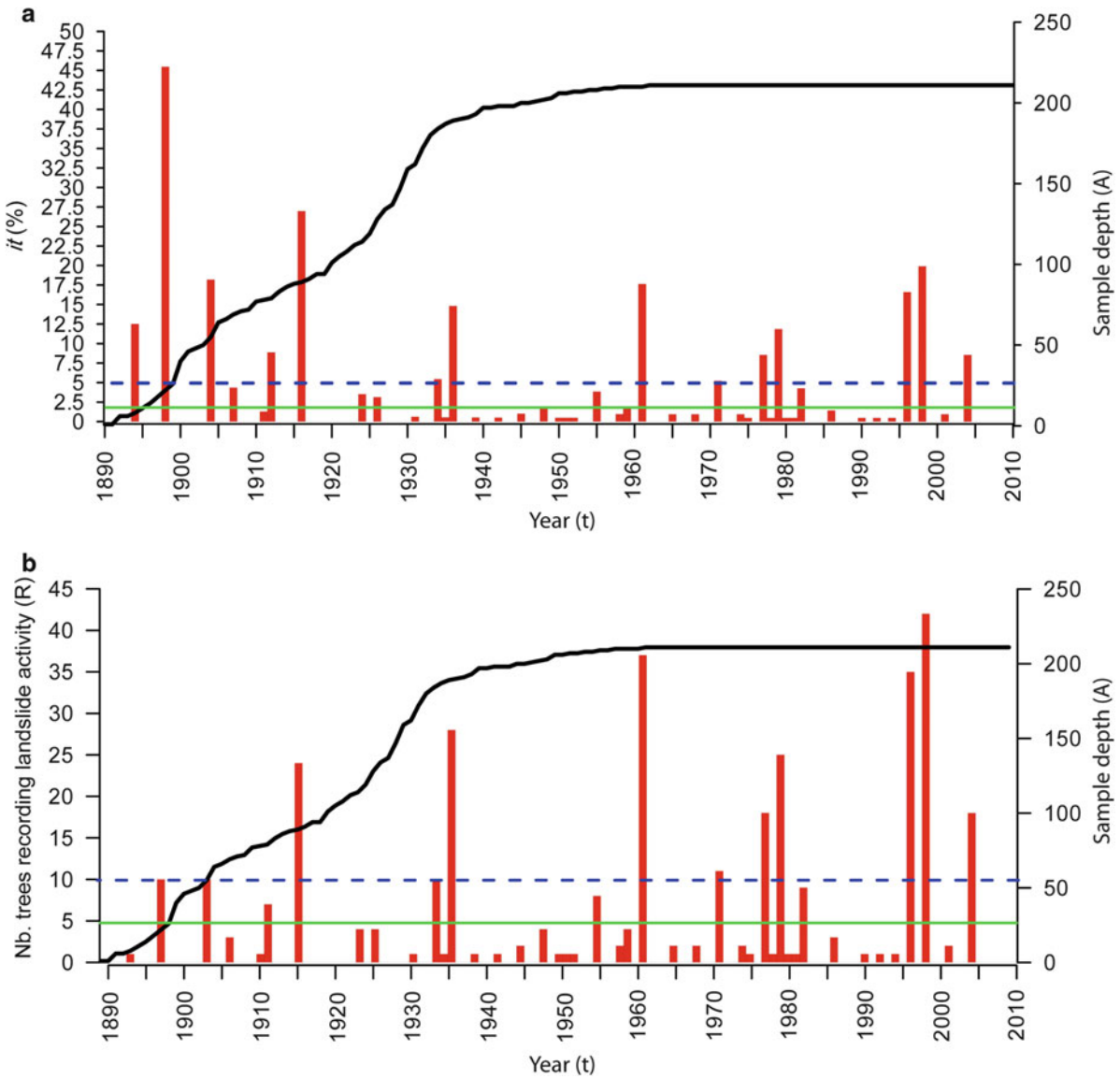

Fig. 2 Event response histograms showing landslide induced growth disturbances (GD) from sampled trees. (**a**) Percentage of trees and (**b**) total number of trees responding to a damage event. *Blue* (*Green*) horizontal *dotted lines* demarcates in (**a**), the 5 % (2 %) sample depth thresholds, and, in (**b**), the n = 10 (n = 5) tree threshold. The *black line* shows the sample depth (i.e. the total number of trees alive in each year)

autocorrelations (feature similarity) based on the location and values of trees with the ArcGIS pattern analysis module and calculated yearly Moran indices (Moran 1950) to evaluate whether the pattern of disturbed trees was clustered, dispersed or random. A Moran index value near 1 indicates clustering while a value near −1 indicates dispersion. Random and dispersed patterns were disregarded from the reconstruction whereas years with clustered patterns were considered as minor or spatially limited movements.

Calculation of Landslide Return Periods and Probabilities of Reactivation

Traditionally, the return period designates the mean time interval at which a material reaches a given point in an avalanche path (Corona et al. 2010). Frequency is usually expressed in years as a 'return period' (i.e. 1/frequency). By analogy, individual tree return periods (*Rp*) were calculated for the Aiguettes landslide from GD frequency *f* for each tree *T* as follows (Reardon et al. 2008):

$$f_T = \left(\sum_{i=T}^{n} GD\right) \div \left(\sum_{i=T}^{n} A\right) \quad (2)$$

Where GD represents the number of growth disturbances detected in tree *T*, and *A* the total number of years tree *T* was alive. Due to the exhaustive sampling and effectiveness of the dendrogeomorphic reconstruction, this approach was used to determine landslide return period.

Complete landslide records covering a long time span may be used to perform probabilistic analyses (Corominas and Moya 2008). The theoretical probability of a landslide to

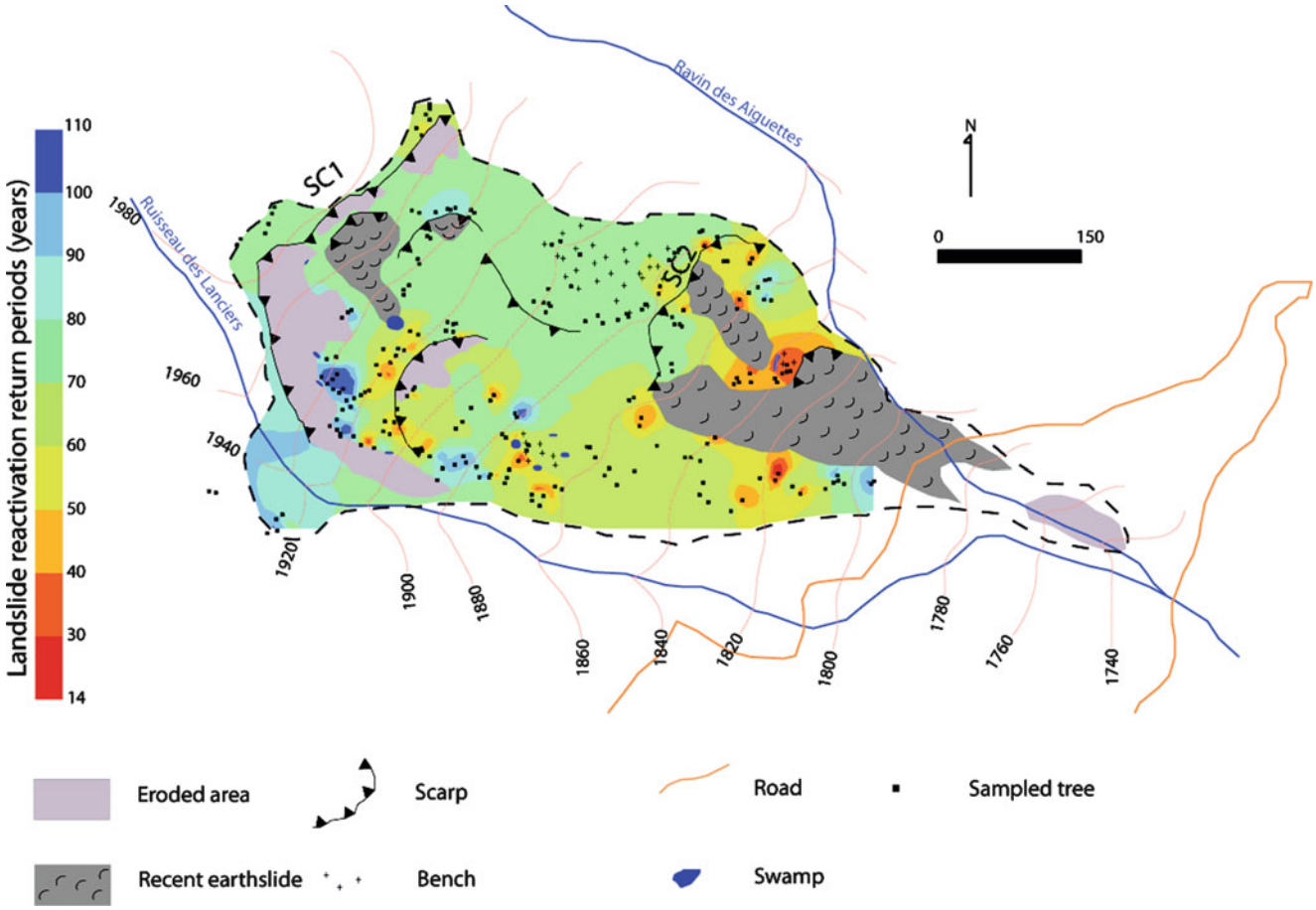

Fig. 3 Interpolated return periods for the sampled area of the Aiguettes landslide. Return period maps were computed with (**a**) the whole sampled trees for the period 1890–2011

occur at Aiguettes was modelled using a Poisson distribution (Corominas and Moya 2008). The Poisson model allows determination of future landslide probability based on the assumption (Guzzetti et al. 2005). The probability (p) for an event with a return period (T) to occur in a given number of years N (fixed to 5, 10, 20 and 100 years) was computed as follows:

$$p = 1 - e^{(-N/T)} \quad (3)$$

According to this distribution, the probability P for a centennial event to occur during the next 100 years is, for example, 0.63.

Results

Growth Disturbances

Pith age data from 223 *P. uncinata* trees sampled at Aiguettes suggest an average age of the sample of 91 ± 16 year. A total of 355 GD related to past landslide event was identified in the 212 *P. uncinata* trees. The most common reaction to landslide events was in the form of abrupt growth reductions with 60 % of all GD (213 GD). The onset of compression wood (142 GD, 40 %) represents another common response of *P. uncinata* to landsliding. The earliest GD observed in the tree-ring series dates back to 1889, however this year was not considered a landslide event as only one tree showed GD (Fig. 2a, b). In 1898, the number of GD surpassed five which was defined the threshold for GD to be considered as a landslide reactivation.

Landslide Events

The 355 GD identified in the tree-ring series allowed dating of 15 landslide reactivation between 1898 and 2011. As can be seen in Fig. 2, the dating of 12 reactivation (1898, 1904, 1911, 1916, 1936, 1961, 1971, 1977, 1979, 1996, 1998 and 2004) was based on $It \geq 5$ % and GD in at least ten trees. In contrast, for the reactivations dated to 1912, 1955 and 1982, the limited number of GD was >5 and 5 % > It > 2 % did not allow for them being considered reactivations with equal confidence. The yearly Moran I statistics computed for these years vary between −0.01 in 1955 (i.e. dispersed distribution

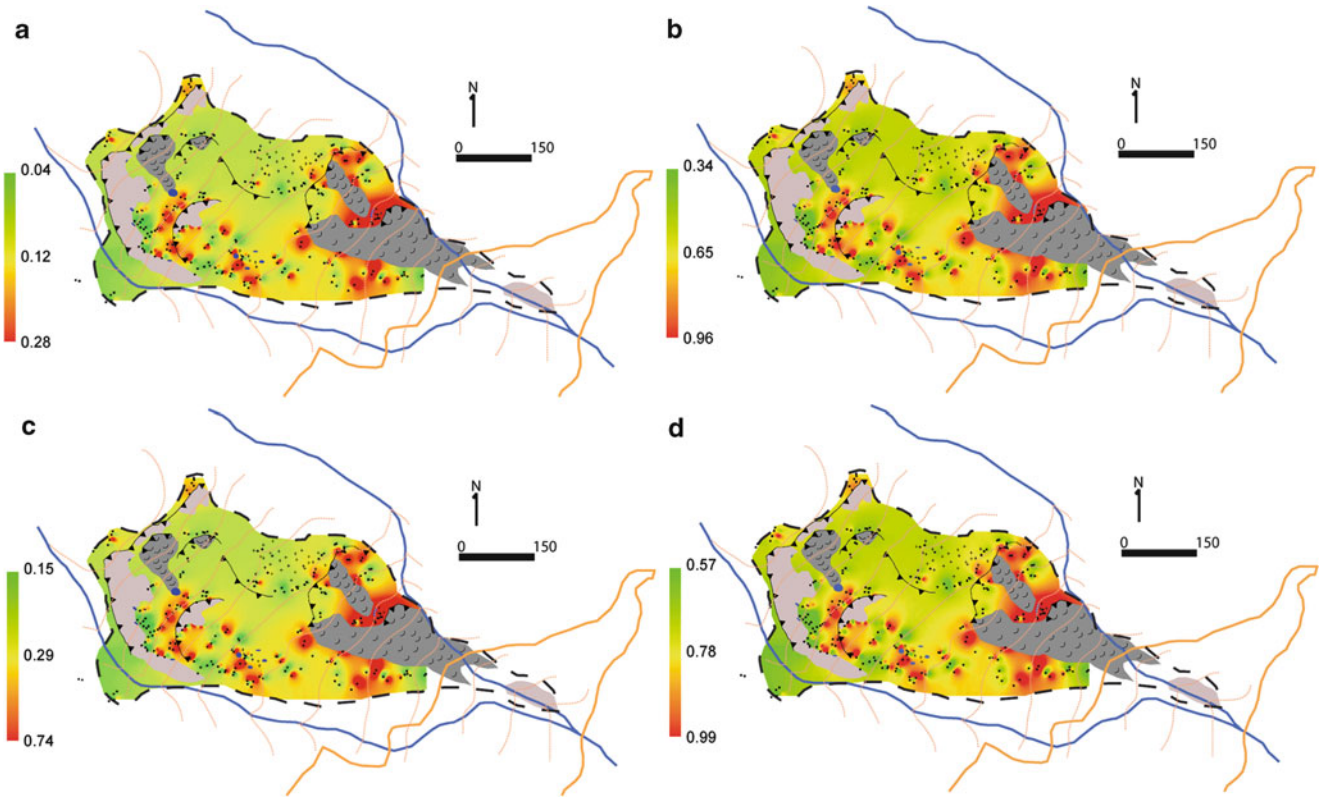

Fig. 4 Probability maps of reactivation for the Aiguettes landslide within (**a**) 5, (**b**) 20, (**c**) 50 and (**d**) 100 years computed using a Poisson distribution model

of affected trees) and 0.18 in 1912 (i.e. spatial clustering of GD). Two react (1912, 1982) display clustered patterns of disturbed trees with sufficient aggregation to be considered landslide reactivation. In 1955, the spatial distribution of disturbed trees does not display any significant pattern and this year was not therefore kept for further analysis.

Return Period and Landslide Probability Maps

Considering the 14 reconstructed events within the sampled area, the mean return period for the Aiguettes landslide is 1.1 10-year for the period 1890–2011.

When analysed spatially, the return period show a clear increase from the main scarp SC2 (14 year) to the upper part of SC1 (>70 year) (Fig. 3).

Return periods of landslide were transformed into landslide occurrence probability using a Poisson distribution. Highly-resolved maps of return period derived from the 223 cross-dated *P. uncinata* trees were then used to represent the probability for a landslide reactivation to occur within 5, 20, 50, and 100 year (Fig. 4a–d).

As expected, the probability for a landslide to be reactivating is highest in SC2 and increases from 0.28 for a 5-year period to 0.99 for a 100-year period. At the margins, the probabilities for an event are lower, yet, they remain >0.57 for the 100-year period.

Discussion

Dendrogeomorphic analysis of 892 increment cores taken from 223 *P. uncinata* allowed reconstruction of 14 events for the Aiguettes landslide between 1890 and 2011. Several limitations are apparent as to the potential of tree-ring analysis to detecting past periods of landslide activity. Reactivation of the landslide body must be on one hand powerful enough to damage a sufficiently large number of trees through stem topping, tilting or root damage. At the same time, more violent and destructive events are likely to kill trees and evidence of this category of events is not likely to be available to the investigator, as dead trees will disappear some time after an event.

Despite these limitations, the methodology deployed in this study enhances the reliability of datasets on past landslide events at the local level. In addition, the *It* and GD thresholds as well as the spatial analysis of event-response maps minimized the risk of GD resulting from non-landslide events to be included in the chronology. The thresholds also allowed rejection of GD related to creep or fall which have

been shown to affect a rather limited number of trees per event.

The reconstruction of spatiotemporal patterns of landslide activity with dendrogeomorphic techniques is recent but has been helpful for the understanding of landslide kinematics and its spatial evolution (Corominas and Moya 2008). Fantucci and McCord (1996), for instance, identified reactivation events of a landslide at Fossatello between 1880 and 1994 and produced maps showing parts of the landslide body reactivated in 10-year periods. In our study, the exhaustive sampling of *P. uncinata* trees allowed computation of a very detailed spatiotemporal chronology of landslide reactivation at Aiguettes. Given the completeness of the reconstruction (since 1898), we were able to map return periods of reactivation. Assuming that landslide recurrence will remain comparable in the future, and adopting a Poisson probability model (Guzzetti et al. 2005), we were also able to determine the probability of having a reactivation in each mapping unit for time intervals varying from 5 to 100 year. Highest return periods associated with major probabilities of reactivation are mapped in the main scarp SC2.

Our approach does not include statistical analysis or physically-based modelling, as these conventional methods have been shown to suffer from major caveats and to predict the spatiotemporal occurrence of landslides with major difficulties (Jaiswal et al. 2011). Most previous work focusing on landslide mapping has been based on susceptibility maps and therefore provide an estimate of where landslides are expected to occur (Guzzetti et al. 2005). Much less work has been done on the establishment of the temporal probability of reactivation (Guzzetti et al. 2005). The approach presented in this paper allows determination of quantitative probabilities of reactivation estimated directly from the frequency of past landslide events and does not require a landslide susceptibility analysis as a complete inventory of past landslide events was reconstructed with dendrogeomorphic techniques (Corominas and Moya 2008).

Conclusion

Because of increased activity in mountain areas, it has become imperative to improve landslide forecasting at the local scale, which is currently difficult using statistical analysis or physically-based models. In this study, we demonstrate the potential of extensive dendrogeomorphic analyses to add substantially to the spatiotemporal record of landslides at a study site. In addition, dendrogeomorphic data have also been shown to add very accurate evidence to the extent of past reactivation where other sources often fail to produce conclusive results. For land-use planning, the identification of endangered areas is paramount importance and dendrogeomorphic mapping should therefore be used systematically for hazard zoning in forested areas affected by shallow landslides. Finally, if coupled with a Poisson model, dendrogeomorphic mapping can improve our knowledge about the probability of reactivation. These probability maps should be used for disaster prevention and generation of risk maps, as well as for the detailed design phase of engineering works and for the construction of slope stabilization works.

Acknowledgments This research has been supported by the PARAmount project, "ImProved Accessibility, Reliability and security of Alpine transport infrastructure related to mountainous hazards in a changing climate", funded by the Alpine Space Programme, European Territorial Cooperation, 2007–2013. It has also been supported by the DENDROGLISS program, funded by the MAIF foundation.

References

Aleotti P, Chowdhury R (1999) Landslide hazard assessment: summary review and new perspectives. Bull Eng Geol Environ 58:21–44

Alestalo J (1971) Dendrochronological interpretation of geomorphic processes. Fennia 105:1–139

Alexander DE (2008) A brief survey of GIS in mass-movement studies, with reflections on theory and methods. Geomorphology 94:261–267

Astrade L, Bravard JP, Landon N (1998) Mouvements de masse et dynamique d'un géosystème alpestre: étude dendrogéomorphologique de deux sites de la de la vallée de Boulc (Diois, France). Géographie Physique et Quaternaire 52:153–165

Bégin C, Filion L (1988) Age of landslides along the Grande Rivière de la Baleine estuary, eastern coast of Hudson Bay, Québec (Canada). Boreas 17:289–299

Bollschweiler M, Stoffel M, Schneuwly DM, Bourqui K (2008) Traumatic resin ducts in Larix decidua trees impacted by debris flows. Tree Physiol 28:255–263

Butler D, Malanson G (1985) A reconstruction of snow-avalanchecharacteristics in Montana, U.S.A., using vegetative indicators. J Glaciol 31:185–187

Carrara PE, O'Neill JM (2003) Tree-ring dated landslide movements and their relationship to seismic events in southwestern Montana. Quaternary Res 59:25–35

Corominas J, Moya J (1999) Reconstructing recent landslide activity in relation to rainfall in the Llobregat river basin, Eastern Pyrenees, Spain. Geomorphology 30:79–93

Corominas J, Moya J (2008) A review of assessing landslide frequency for hazard zoning purposes. Eng Geol 102:193–213

Corona C, Rovéra G, Lopez Saez J, Stoffel M, Perfettini P (2010) Spatio-temporal reconstruction of snow avalanche activity using tree-rings: Pierres Jean Jeanne avalanche talus, Massif de l'Oisans, France. Catena 83:107–118

Delsigne F, Lahousse P, Flez C, Guiter G (2001) Le Riou Bourdoux: un "monstre" alpin sous haute surveillance. Revue forestière française. LIII: 527–540

Dehn M, Buma J (1999) Modelling future landslide activity based on general circulation models. Geomorphology 30:175–187

Efthymiadis D, Jones PD, Briffa KR, Auer I, Böhm R, Schöner W, Frei C, Schmidli J (2006) Construction of a 10-min-gridded precipitation data set for the greater Alpine region for 1800–2003. J Geophys Res 111:D01105. doi:10.1029/2005JD006120

Fantucci R, McCord A (1996) Reconstruction of landslide dynamic with dendrochronological methods. Dendrochronologia 13:33–48

Floris M, Bozzano F (2007) Evaluation of landslide reactivation: a modified rainfall threshold model based on historical records of

rainfall and landslides. Geomorphology. doi:10.1016/j/geomorph.2007.04.009
Guzzetti F, Reichenbach P, Cardinali M, Galli M, Ardizzone F (2005) Probabillistic landslide hazard assessment at the basin scale. Geomorphology 72:272–299
Hilker N, Badoux A, Hegg C (2009) The Swiss flood and landslide damage database 1972–2007. Nat Hazard Earth Syst Sci 9:913–925
Hupp CR (1984) Geo-botanical evidence of late quaternary mass wasting in block field areas of Virginia. Earth Surf Process Land 8:439–450
Jaiswal P, Van Westen CJ, Jetten V (2011) Quantitative assessment of landslide hazard along transportation lines using historical records. Landslides. doi:10.1007/s10346-011-0252-1
Maquaire O, Malet JP, Remaître A, Locat J, Klotz S, Guillon J (2003) Instability conditions of marly hillslopes: towards landsliding or gullying? The case of the Barcelonnette basin, South East France. Eng Geol 70:109–130
Mattheck C (1993) Design in der Natur. Reihe Ökologie 1: Rombach Wissenschaft
Moran PAP (1950) Notes on continuous stochastic phenomena. Biometrika 37:17–23
Reardon BA, Pederson GT, Caruso CJ, Fagre DB (2008) Spatial reconstructions and comparisons of historic snow avalanche frequency and extent using tree rings in Glacier National Park, Montana, U.S.A. Arctic, Antarctic, and Alpine Research, vol 40, pp 148–160
Stefanini MC (2004) Spatio-temporal analysis of a complex landslide in the Northern Apenines (Italy) by means of dendrochronology. Geomorphology 63:191–202
Stoffel M, Bollschweiler M (2008) Tree-ring analysis in natural hazards research – an overview. Nat Hazard Earth Syst Sci 8:187–202
Stoffel M, Bollschweiler M, Butler DR, Luckman BH (2010) Tree rings and natural hazards: a state-of-the art. Springer, Dordrecht/Berlin/London/New York, p 505
Thiery Y, Malet JP, Sterlacchini B, Puissant A, Maquaire O (2007) Landslide susceptibility assessment by bivariate methods at large scales: application to a complex mountainous environment. Geomorphology 92:38–59
Timell TE (1986) Compression wood in gymnosperms. Springer, Berlin
Van Den Eeckhaut A, Muys B, Van Loy K, Poesen J, Beeckman H (2009) Evidence for repeated re-activation of old landslides under forest. Earth Surf Process Land 34:352–365. doi:10.1002/esp.1727
Varnes DJ (1984) Landslide Hazard zonation: preview of principles and practices: Paris, Unesco. In: International association of engineering geologists, commission on landslides and other mass movements on slopes. Natural Hazards, vol 3, 176 pp
Wieczorek GF, Eaton LS, Yanosky TM, Turner EJ (2006) Hurricane-induced landslide activity on an alluvial fan along Meadow Run, Shenandoah Valley, Virginia (eastern USA). Landslides 3:95–106. doi:10.1007/s10346-005-0029-5

Radargrammetric Generation of DEMs from High Resolution Satellite SAR Imagery: A New tool for Landslide Hazard and Vulnerability Assessment

Paola Capaldo, Mattia Crespi, Francesca Fratarcangeli, Andrea Nascetti, and Francesca Pieralice

Abstract

Spatial information acquisition and analysis tools play a fundamental role to supplying the information necessary to produce landslide inventories, which represent the foundations for quantifying landslide hazard and vulnerability. In this frame, fundamental data are Digital Surface Models (DSMs) and Digital Elevation Models (DEMs).

The goal of this paper is just methodological, focused to illustrate the actual potentialities of DSMs generation from high resolution satellite Synthetic Aperture Radar (SAR) imagery with a radargrammetric stereo-mapping approach. The fundamental advantage of this approach is that it can work with just a couple of images (no matter for their coherence), which can be collected in a short time (half day to quite few days) thanks to the independence of satellite radar acquisition from weather (clouds), daylight and logistic constraints (as for airborne data collection).

The suite for the DSMs generation through the radargrammetric approach has been implemented in SISAR (Software per Immagini Satellitari ad Alta Risoluzione), a scientific software developed at the Geodesy and Geomatic Institute of the University of Rome "La Sapienza". In order to demonstrate the radargrammetric mapping potentialities of high resolution SAR data, a test site was established in the area of Merano (Northern Italy), characterized by mixed morphology and land cover. The data available for the experiment were a COSMO-SkyMed SpotLight stereo pair and a LiDAR DEM, used as ground truth. An accuracy better than 3 m has been achieved in open areas and the implemented algorithm appears able to generate DSMs both over open and forested areas, where the accuracy is around 4 m.

Therefore, radargrammetric generation of DSMs from high resolution satellite SAR imagery appears a valuable tool to supply topographic information for landslide inventories at different scales.

Keywords

Landslide hazard • Digital surface and elevation models • Radargrammetry • High resolution SAR • COSMO-SkyMed

Introduction

Landslides result in extensive damages to both properties and lives. Therefore, essential issues both for town-and-country management and planning, and for environmental protection are the evaluation of landslide hazard and the identification of areas vulnerable to future landslides.

P. Capaldo (✉) • M. Crespi • F. Fratarcangeli • A. Nascetti • F. Pieralice
Area di Geodesia e Geomatica, DICEA, Università di Roma "La Sapienza", Rome, Italy
e-mail: paola.capaldo@uniroma1.it

C. Margottini et al. (eds.), *Landslide Science and Practice*, Vol. 1,
DOI 10.1007/978-3-642-31325-7_55,

From two pioneering works (Carrara et al. 1977; Carrara 1983), it was more and more recognized by several authors (Borga et al. 1998; Carrara et al. 1995; Guimarães et al. 2003; Guzzetti et al. 1999; Gritzner et al. 2001; JTC-1 2008; Lee et al. 2002; Lee 2007; Lee et Pradhan 2007; Nichol et al. 2006; Park and Chi 2008; Van Westen et al. 2008) that spatial information acquisition and analysis tools, such as Digital Photogrammetry, Global Navigation Satellite Systems, Digital Image Processing and Geographic Information Systems, play a fundamental role to supplying the information necessary to produce comprehensive landslide inventories, which are a must for quantifying landslide hazard and vulnerability. In this respect, fundamental spatial information are Digital Elevation Models (DEMs) and Digital Surface Models (DSMs), which differ from DEMs since they include vegetation and buildings too. Their importance is clearly evidenced in a recent and very comprehensive review (Van Westen et al. 2008), which underlines DEMs and DSMs contribution for landslide hazard assessment at four mapping scales (small, medium, large, detailed) (Van Westen et al. 2008, Table 5).

In this paper, we show the actual potentialities of DSMs generation from high resolution satellite Synthetic Aperture Radar (SAR) imagery with a radargrammetric stereomapping approach. The fundamental advantage of this approach is that it can work with just a couple of images, which can be collected in a short time (half day to quite few days) thanks to the independence of satellite radar acquisition from weather (clouds), daylight and logistic constraints (as for airborne data collection). Moreover, since the radargrammetric approach deals with the amplitude (not the phase) of the SAR imagery, it does not require coherence between images, as for the most known and used interferometric approach (InSAR).

As a matter of fact, up to now, SAR imagery has been employed for DSMs generation mainly using the InSAR approach. Even special missions have been designed and set up to yield elevation data on world scale, as the Shuttle Radar Topography Mission (SRTM) or TanDEM-X.

On the contrary, radargrammetry was first used in the 1950s with ground and airborne radar; then, it was less and less used, due to the quite low resolution of radar satellite imagery in amplitude, if compared to their high resolution in phase. Only in the very last years, thanks to the very high resolution imagery acquired by new satellite sensors, as COSMO-SkyMed (Italian), TerraSAR-X (German) and RADARSAT-2 (Canadian), which are able to supply imagery with 1 m ground resolution, the radargrammetric approach has been revalued and investigations re-started (Toutin and Chenier 2009; Raggam et al. 2010; Perko et al. 2011).

In analogy to photogrammetry, radargrammetry is based on a stereo pair, which has to be acquired under a suited geometric configuration. As mentioned, only the amplitude information of SAR imagery is used. The gray tones of each SAR image depend on several characteristics of the imaged surface, which reflects a certain amount of radiation according to its geometrical and physical characteristics. Then, as for photogrammetry, two are the basic steps for DSMs generation: stereo pair orientation and image matching for points cloud generation.

The orientation model for SAR imagery implemented in SISAR (Software per Immagini Satellitari ad Alta Risoluzione, developed at the Geodesy and Geomatic Institute of the University of Rome "La Sapienza") is based on the classical Range-Doppler equations proposed in the book of Leberl (Leberl 1990). Moreover, a possible refinement of some radar acquisition parameters has been taken into account to exploit the potentialities of the novel high resolution imagery. In this respect, using a set of Ground Control Points (GCPs), the corrections for three acquisition parameters, whose initial values are supplied within the image metadata, may be estimated during the orientation, if necessary.

As regard the image matching for DSMs generation, an original procedure has been developed for SISAR, based on a coarse-to-fine hierarchical solution with an effective combination of geometrical constrains and an Area Based Matching (ABM) algorithm.

Here it is presented a DSM generated from a COSMO-SkyMed same-side stereo pair acquired in SpotLight mode over the area of Merano (Northern Italy). At first, the results of the stereo pair orientation are shown; the results obtained in the orientation step are representative of the geometric potentialities of SpotLight stereo pairs as regards 3D surface reconstruction, whereas the accuracy of the final product is strictly affected by the quality of the subsequent matching procedure. Therefore, the results of image matching and DSM generation are discussed; accuracy assessment of two DSM tiles with extension of 2–3 Km^2 has been performed using the software DEMANAL, developed by Prof. K. Jacobsen at Leibniz University Hannover, allowing a full 3D DSM comparison to remove possible horizontal biases too. As ground truth it was used the LiDAR DTM by the "Provincia Autonoma di Bolzano", freely available on-line.

Radargrammetric Orientation Model

The radargrammetry technique performs a 3D reconstruction based on the determination of the sensor-object stereo model, in which the object position is computed by the intersection of two radar rays with two different look angles. The model is based on the two fundamental equations (1). The first equation of (1) represents the general case of zero-Doppler projection: in zero-Doppler geometry the target is supposed to be acquired on a heading that is perpendicular to

the flying direction of the satellite; the second equation of (1) is the slant range constraint

$$\begin{cases} V_{XS}\cdot(X_S-X_P)+V_{YS}\cdot(Y_S-Y_P)+V_{ZS}\cdot(Z_S-Z_P)=0 \\ \sqrt{(X_S-X_P)^2+(Y_S-Y_P)^2+(Z_S-Z_P)^2}-(DS+CS\cdot I)=0. \end{cases} \quad (1)$$

where: V_{XS}, V_{YS}, V_{ZS} are the cartesian components of the satellite velocity in the local coordinate system (time dependent); X_S, Y_S, Z_S are the coordinates of the satellite in the local coordinate system (time dependent); X_P, Y_P, Z_P are the coordinates of the generic Ground Point (GP) in the local coordinate system (time independent); DS is the *near-range*, a parameter related to the range measurements whose initial value is available in the metadata; CS is the column spacing; I is the column position of point P on the image.

The satellite orbit can be conveniently modelled with a circle, since the orbital arc related to the image acquisition in SpotLight mode is quite short (about 10 Km); its parameters are estimated in a least squares adjustment using few orbital state vectors available in the image metadata.

The satellite position is related to the acquisition time of each line of the image, which can be computed using the *acquisition start-time* and the *Pulse Repetition Frequency (PRF)*. Initial values for these parameters are available in the metadata too; they can be corrected, if necessary, using a set of GCPs. In particular, the linear relationship between the acquisition time of each GP and its line number *J* (2) reads as follow:

$$t = start\_time + \frac{1}{PRF}\cdot J \quad (2)$$

A third parameter that may be corrected in the least squares adjustment is the already introduced near range.

Data set and Orientation Results

Imagery and GPs Data

The available data for the experiment is a COSMO-SkyMed SpotLight stereo pair acquired over the area of Merano (Northern Italy) (Table 1). The images belong to the Level 1A (SCS) category products, that is focused data in complex format, in slant range and zero-Doppler projection. The area displays mixed morphology and land cover, representing an urban zone (the town of Merano), a small plain (the Adige river valley) and a mountainous zone; the heights range from about 300 m to 2,500 m (Fig. 1 left).

Table 1 Merano stereo pair features

Acquisition data	Coverage [Km^2]	Incidence angle [°]	Orbit and look side	B/H
30/11/2009	10 × 10	25.9	Descending right	0.4
2/11/2009	10 × 10	42.3	Descending right	

The stereo pair orientation was performed with SISAR and its accuracy was evaluated on the basis of 20 GPs, used both as GCPs and Check Points (CPs) (Fig. 1 right; Capaldo et al. 2011): their horizontal coordinates were derived from cartography (scale 1:5,000) whereas the heights came from the LiDAR DTM (mean elevation accuracy of 0.25 m and horizontal spacing 2.5 m), used also for the DSMs assessment; both these data are available for free on the website of the Provincia Autonoma di Bolzano (http://www.provincia.bz.it/urbanistica/cartografia/cartografia.asp).

Orientation Results

To test the effectiveness of the new rigorous model implemented in SISAR, the stereo pairs have been orientated and the model accuracy was analyzed, evaluating the average, the standard deviation (St. Dev.) and the RMSE computed over CPs residuals (RMSE CPs), following the standard Hold-OutValidation procedure for accuracy assessment (Brovelli et al. 2008).

In previous investigations (Capaldo et al. 2010) it was noted that the increase of GCPs number does not improve significantly the orientation accuracy. Therefore the stereo pair has been oriented using 3 GCPs, which can be the appropriate number to estimate the orientation parameters of SAR model, with a good compromise between the accuracy and the number of GCPs which has to be kept low for budget and logistic reasons.

In addition, it has to be noted that some tests were performed using the ground coordinates (on the WGS84 ellipsoid at zero ellipsoidal height) provided for the scene corners directly in the metadata file. These tests highlight that for the COSMO-SkyMed imagery a good accuracy may be achieved just using the information related to scene corners, so that ground surveyed GCPs do not appear necessary, with a remarkable increase in the efficiency, saving the time for their (GPS) surveys and their identification and coordinate measurements on the images. The results, both with three GCPs and with four scene corners, are summarized in Table 2. The accuracy level is around 2.5–3 m in the height component.

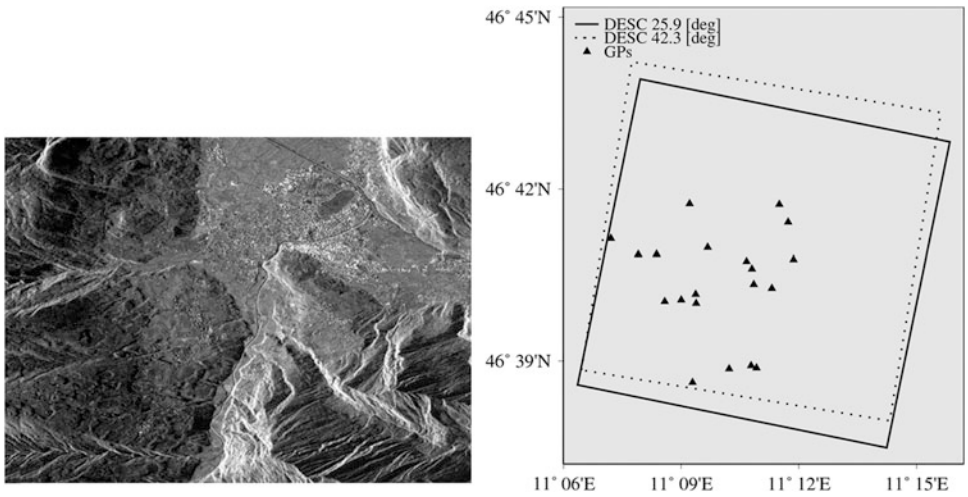

Fig. 1 Merano COSMO-SkyMed SpotLight and Ground Points data set

Table 2 Stereo pair orientation accuracy based on surveyed GCPs (above) and image corners (below)

Radargrammetric model								
Average CPs [m]			St. Dev. CPs [m]			RMSE CPs [m]		
E	N	Up	E	N	Up	E	N	Up
Orientation with 3 GCPs								
2.20	1.90	−0.93	3.13	2.54	2.24	3.83	3.17	2.42
Orientation with 4 image corners								
2.18	−1.16	0.94	3.29	2.36	2.14	3.95	2.62	2.34

DSM Generation

Image Denoising

SAR imagery is affected by a high level of noise (speckle) due to the inherent nature of radar backscatter. The source of this noise is due to random interference between the coherent returns issued from the numerous scatterers present on the imaged surface, at the scale of the wavelength of the incident radar signal.

Speckle noise gives the SAR image a grainy appearance and prevents target recognition and texture analysis efficiently.

Therefore, an image preprocessing step to reduce speckle noise is required before starting the matching procedure.

In order to determine which adaptive image filters allow to get the best results in terms of DSMs accuracy, a series of tests were performed, varying filter type and window size.

In details, the applied filters were: Lee, Gamma Map, Frost, Median; the correlation window size has been changed from a (5 × 5) size to a (11 × 11), considering odd sizes only. Also, the same filter has been passed several times (up to three) over the images. The tests performed show that Gamma Map and Lee filters give approximately the same results in term of RMSE values, and the best are those for a (7 × 7) correlation window.

Future investigations will be useful to assess the potential of more sophisticated image denoising techniques, such as those based on wavelet or frequency domain transforms (Liu et al. 2009).

Image Matching Strategy

As already mentioned, the DSM accuracy is strictly related both to the stereo pair orientation and to the matching process. In order to obtain good stereo geometry, the optimum configuration for the radargrammetric application is when the target is observed in opposite-side view; however it causes large geometric and radiometric disparities, hindering image matching. A good compromise is to use a same-side configuration stereo pair with a base to height ratio ranging from 0.25 to 2 (Meric et al. 2009) in order to increase the efficiency in the matching procedure.

Many different approaches for image matching have been developed in recent years. The main step of image matching process is to define the matching entity, that is a primitive (in the master image) to be compared with a portion of other (slave) images, in order to identify correspondences among different images.

According to the kind of matching primitives, we can distinguish two basic techniques, the already mentioned ABM and the Feature Based Matching (FBM) (Nascetti 2009; Jacobsen 2006). In ABM method, a small image window composed of grey values represents the matching primitive and the principal methods to assess similarity are cross correlation and Least Squares Matching (LSM); on the other hand, FBM uses, as main class of matching, basic features that are typically the easily distinguishable primitives in the input images, like corners, edges, lines, etc.

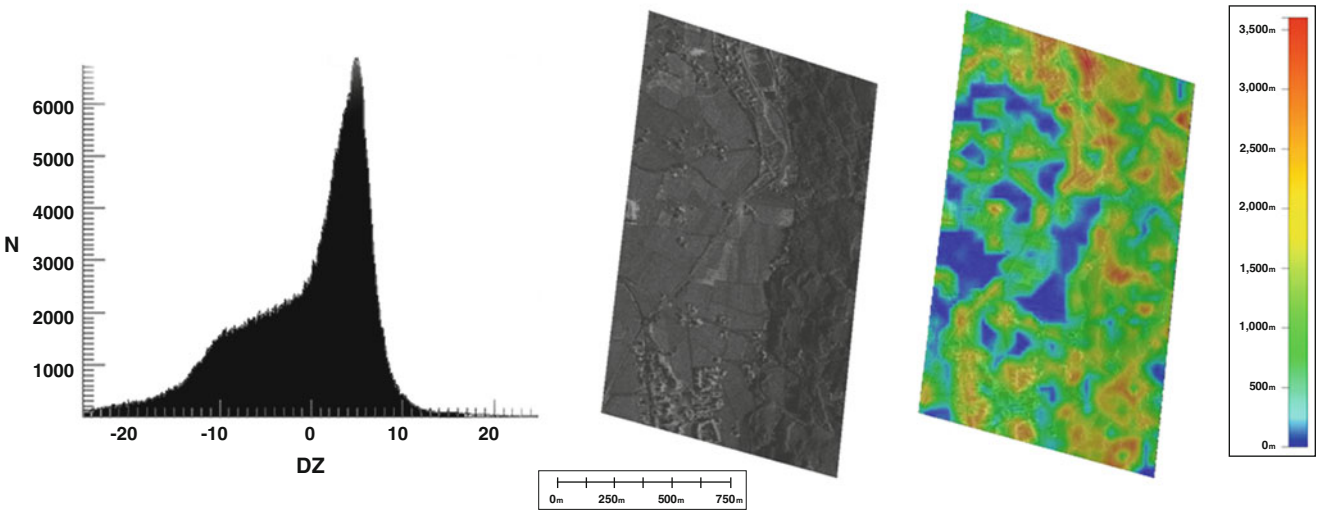

Fig. 2 DSM Tile 1: Histogram of height differences (*left*); tile screenshot (*centre*); points cloud density map (*right*)

These strategies, if separately applied, do not appear suited to manage the strong geometrical deformation (like foreshortening and layover) and the complex and noisy radiometry (speckle) of SAR imagery. Therefore, an original matching procedure has been developed.

This matching method is based on a coarse-to-fine hierarchical solution with an effective combination of geometrical constrains and an ABM algorithm, following some ideas of Zhang and Gruen (2006) but with a complete original procedure and implementation.

After image preprocessing, the two images are resampled reducing at each pyramid level the original resolution resolution. The correspondences between points in the two resampled images are computed by correlation function and finally a LSM refinement is performed to obtain more precise results. In this way the surface model is successively refined step by step, until the last step (corresponding to the original image resolution) where the final dense and accurate DSM is reconstructed. The advantage of this technique is that at lower resolution it is possible to detect larger structures, whereas at higher resolutions small details are progressively added to the already obtained coarser surface.

DSMs Generation Results

In order to evaluate the potentiality of the described matching strategy, two different tiles with extension of 2–3 Km^2 were considered, which were selected in order to test the potentialities of the radargrammetric approach with different morphologies and in some difficult cases for automatic image matching due to SAR imagery distortions (foreshortening, layover).

The extracted DSMs (Fig. 3 left, Fig. 4) have been compared with the reference LiDAR DTM through DEMANAL software, allowing for a full 3D comparison to remove possible horizontal biases too. The height differences are computed interpolating (with a bilinear method) the analyzed DSMs over the reference LiDAR DTM (the value is negative when the extracted DSM is above the reference DTM).

We had to take into account that the generated DSMs were compared with the reference DTM, which do not include vegetation and buildings. This is the reason of a part of the differences between the compared surfaces and this turns of particular interest over forested areas, where the radargrammetric approach was able to generate a dense points cloud, despite the quite low coherence between the stereo images. In these areas the differences are mainly due to the forest and the bias values are representative of the canopy height (apart from the already known effect of radar penetration into the canopy, causing a height underestimation around 25–30 %) (Perko et al. 2011).

The area represented in Tile 1 (Fig. 2 centre) is characterized by a steep rather forested area which slopes down to a plain (Adige river valley) where we can find open areas with poor texture and a small built up zone.

During the matching process the highest density of points has been found over forested and built-up areas (red zone in the points cloud density map, Fig. 2 right). An histogram of the height differences is showed in Fig. 2 (left), indicating a numerical range between −40 and +25 m; the clearly asymmetric error distribution is due to differences between the reference DTM and the extracted DSM, in particular to the effect of the large forested area, which cause a large amount of systematic negative differences. Validation analysis was made with respect to two selected areas over flat and forested

Table 3 DSM Tile 1 accuracy evaluation

Absolute error tile 1 [m]					
Terrain	BIAS	St. Dev.	RMSE	LE95	# Points
Flat	−2.03	1.94	2.80	4.54	48,787
Forested	−14.40	4.28	15.02	9.89	17,745

Table 4 DSM Tile 2 accuracy evaluation

Absolute error tile 2 [m]					
Terrain	BIAS	St. Dev.	RMSE	LE95	# Points
Urban 1	−4.34	3.59	5.63	8.63	159,094
Urban 2	−4.92	3.40	5.98	9.11	159,789

terrain, respectively, and points cloud was interpolated on a regular grid (1.6 × 1.6 m posting, in order to preserve the mean points cloud interdistance) to allow a full comparison.

A sample cut-off at the 95 % probability level was considered, so that the LE95 was evaluated, in order to leave out the outliers from the statistical evaluation (Tables 3, and 4).

The achieved mean accuracy was better than 3 m over flat areas and appears quite consistent with the results of orientation; over the forested terrain the standard deviation goes up to 4 m and a large negative bias is present, amenable to the forest (mean height canopy about 15 m).

Further, a deeper investigation was carried out through a visual inspection of the entire error map (Fig. 3 right); yellow error areas highlight matching failures, probably caused by zone with poor texture; large positive height difference values (blue areas) are mainly due to the presence of narrow gorges, not correctly reconstructed.

The urban area represented in Tile 2 has been chosen because it also contains some of the most common geometric distortions that characterize radar imagery.

In fact, we have here a relief affected by foreshortening and layover: foreshortening compresses features which are tilted toward the radar; furthermore, because of the layover, the top of the feature is displaced towards the radar from its true position on the ground, and "lays over" the base of the feature.

Two urban areas not affected by distortions have been selected in order to evaluate the accuracy of the extracted DSM (Fig. 4); the results are shown in Table 4.

The accuracy in term of RMSE is about 6 m for both areas; in these cases, unlike the forest canopy in Tile 1, the buildings are not correctly reconstructed; in fact, the bias is only 5 m and it is not representative of the average building heights.

Certainly, to model the complicated urban morphology, specific algorithms (probably not fully automatic), which consider also remarkable features as double bounces, must be developed.

Also to see the effect of radar distortions, an image of Tile 2 has been orthorectified using the extracted DSM (see Fig. 5 left); during orthorectification process, layover and foreshortening situations are stretched back to their correct positions and pixels are stretched or smeared, creating areas where the matching algorithm cannot find homologous points because of lack of radiometric information.

These areas are easily recognizable in the error map (Fig. 5 right, red zone) because they are characterized by the highest values of height discrepancies (about 30 m) between the extracted DSM and the reference one. Also, we can see the blue error zone, which is caused by the shadow of the Passirio river high banks.

The use of at least two stereo pairs acquired under different look side seems to be an effective strategy to overcome these kinds of problems, in order to model the terrain surface also in presence of occlusions, distortions and shadows.

Conclusion and Future Work

A new model for radargrammetric processing (orientation and DSM generation) of high resolution satellite SAR stereo pairs was defined and implemented in the scientific software SISAR. An experiment was carried out with a COSMO-SkyMed SpotLight stereo pair collected over the test site of Merano (Northern Italy).

The orientation evaluation shows that the height accuracy is at level of 2.5–3.0 m. A small GCP number is enough to achieve a good accuracy level; in addition, the usage of corner coordinates is certainly suited to the image orientation with COSMO-SkyMed SpotLight imagery; therefore, no surveys of GCPs are necessary.

These results are representative of the geometric potentialities of the rigorous radargrammetric model, whereas the accuracy of the final DSM product is strictly affected by the quality of the subsequent matching procedure.

The DSM evaluation showed that the achievable accuracy is also strictly related to the terrain morphology: over a flat area the RMSE is better than 3 m; moreover, a quite dense point cloud were generated even over forested areas, where it was possible to estimate the average canopy height with a mean error of about 4 m over; on the contrary, the details of building areas were not correctly reconstructed.

Therefore, even if further tests and researches are needed (for example to improve the performances of the matching procedure in urban areas or with more complex morphologies), radargrammetry is likely to became an effective complement/alternative to InSAR, since it may work even with a couple of images with good performances over forested areas too.

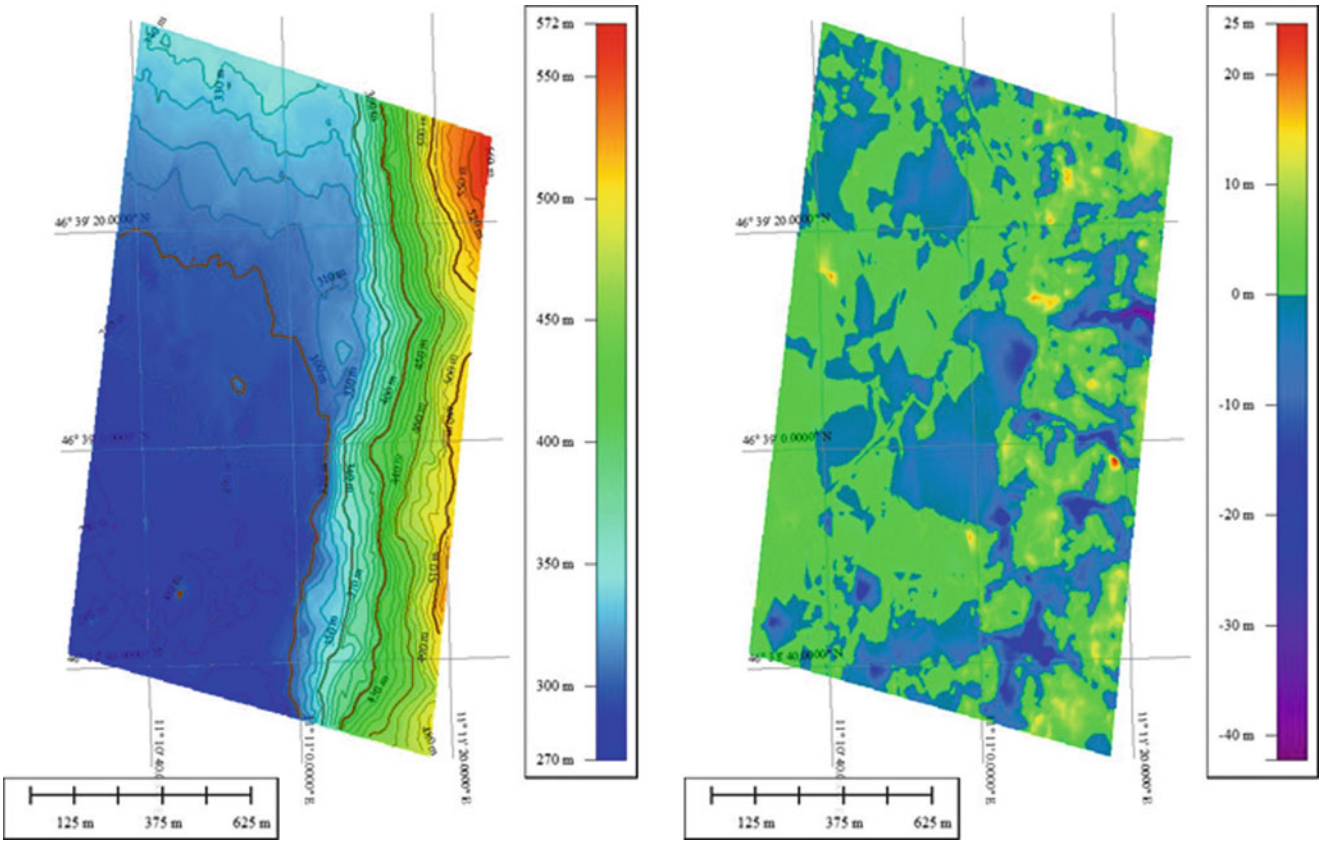

Fig. 3 DSM Tile 1: generated DSM (*left*) and error map (*right*)

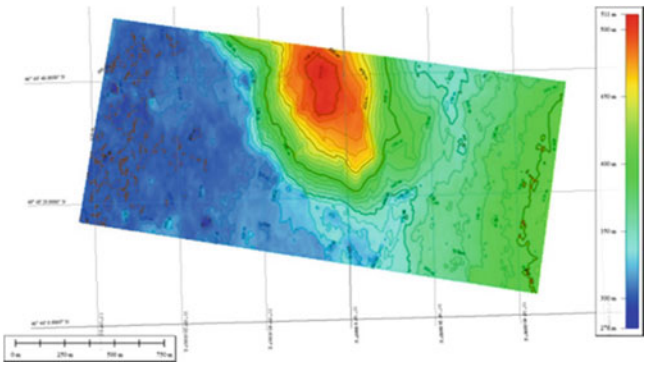

Fig. 4 DSM Tile 2: generated DSM

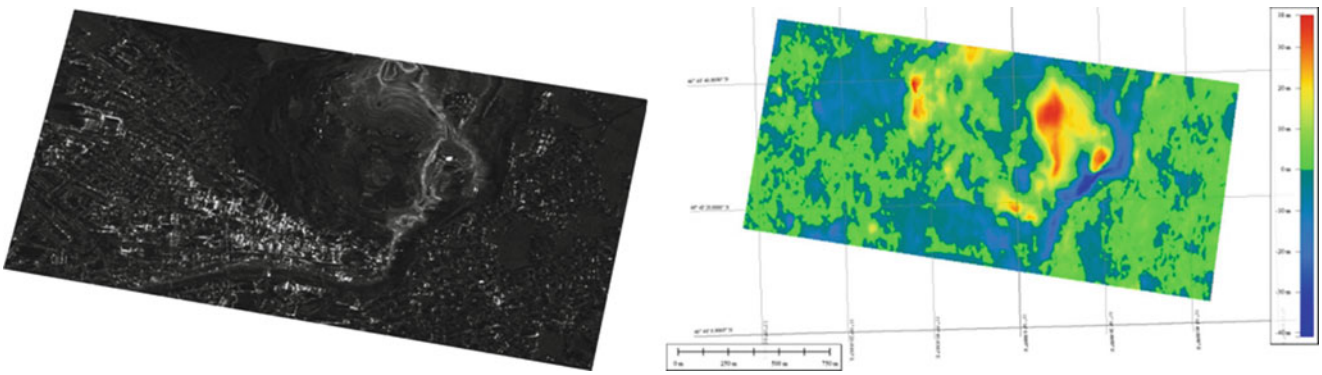

Fig. 5 DSM Tile 2: Orthophoto (*left*) and error map (*right*)

So, radargrammetric generation of DSMs from high resolution satellite SAR imagery appears a valuable tool to supply topographic information (elevation, slope aspect) for landslide inventories at different scales (medium, large), according the classification illustrated in (Van Westen et al. 2008).

Acknowledgements The COSMO-SkyMed stereo pairs were made available by e-Geos S.p.A., Rome (Italy), in the frame of a collaboration agreement; the authors are indebted to e-Geos S.p.A. for this. Moreover the authors thank very much Prof. K. Jacobsen for making available the DEMANAL software.

References

Borga M, Dalla Fontana G, Da Ros D, Marchi L (1998) Shallow landslide hazard assessment using a physically based model and digital elevation data. Environ Geol 35(2–3):81–88

Brovelli M, Crespi M, Fratarcangeli F, Giannone F, Realini E (2008) Accuracy assessment of high resolution satellite imagery orientation by leave-one-out method. ISPRS J Photogramm Remote Sens 63(4):427–440

Capaldo P, Crespi M, Fratarcangeli F, Nascetti A, Pieralice F (2010) Definition of a radargrammetric model and application with COSMO-SkyMed imagery. In: Proceedings of the 2nd EARSeL Joint SIG Workshop, Ghent (Belgium), 22–24 Sept 2010 (in press)

Capaldo P, Crespi M, Fratarcangeli F, Nascetti A, Pieralice F (2011) High resolution SAR Radargrammetry. A first application with COSMO-SkyMed SpotLight Imagery, IEEE GRSL (in press)

Carrara A, Carratelli EP, Merenda L (1977) Computer-based data bank and statistical analysis of slope instability phenomena. Zeitschrift für Geomorphologie 21:187–222

Carrara A (1983) Multivariate models for landslide hazard evaluation. Math Geol 15(3):403–426

Carrara A, Cardinali M, Guzzetti F, Reichenbach P (1995) GIS-based techniques for mapping landslide hazard. In: Carrara A, Guzzetti F (eds) Geographical information systems in assessing natural hazards. Kluwer, Dordrecht, pp 135–176

Crosetto M, Aragues FP (1999) Radargrammetry and SAR interferometry for DEM generation: validation and data fusion. In: Proceedings of the CEOS SAR workshop, ESA-CNES, Toulouse, 26–29 Oct 1999, 6 pages

Guimarães RF, Montgomery DR, Greenberg HM, Fernandes NF, Trancoso Gomes RA, de Carvalho A, Júnior O (2003) Parameterization of soil properties for a model of topographic controls on shallow landsliding: application to Rio de Janeiro. Eng Geol 69:99–108

Guzzetti F, Carrara A, Cardinali M, Reichenbach P (1999) Landslide hazard evaluation: a review of current techniques and their application in a multi-scale study, Central Italy. Geomorphology 31:181–216

Gritzner ML, Marcus WA, Aspinall R, Custer SG (2001) Assessing landslide potential using GIS, soil wetness modeling and topographic attributes, Payette River, Idaho. Geomorphology 37:149–165

Jacobsen K (2006) Digital surface models of city areas by very high-resolution space imagery. In: Proceedings of the 1st workshop of the EARSeL-SIG Urban Remote Sensing, 02–03 March, Berlin, unpaginated CD-ROM

JTC-1 Joint Technical Committee on Landslides and Engineered Slopes (2008) Guidelines for landslide susceptibility, hazard and risk zoning, for land use planning. Eng Geol 103:85–98

Leberl FW (1990) Radargrammetric image processing. Artech House, Norwood, p 595

Lee S, Chwae U, Min K (2002) Landslide susceptibility mapping by correlation between topography and geological structure: the Janghung area, Korea. Geomorphology 46:149–162

Lee S (2007) Application and verification of fuzzy algebraic operators to landslide susceptibility mapping. Environ Geol 52(4):615–623

Lee S, Pradhan B (2007) Landslide hazard mapping at Selangor, Malaysia using frequency ratio and logistic regression models. Landslides 4:33–41

Liu E, Liu H, Zhang Y, Guo Z (2009) An improved method of image denoising base on stationary wavelet. In: Proceedings of the IEEE global congress on intelligent systems. Xiamen, China, pp 379–383

Meric S, Fayard F, Pottier E (2009) Radargrammetric SAR image processing. In: Pei-Gee Peter H (ed) Geoscience and remote sensing. Intech, Vienna, pp 421–454

Nascetti A (2009) A stereo image matching strategy based on corner detection and least squares refinement: algorithm implementation in IDL development environment and testing over high resolution satellite imagery. Degree Thesis (unpublished)

Nichol JE, Shaker A, Wong M-S (2006) Application of high-resolution stereo satellite images to detailed landslide hazard assessment. Geomorphology 76:68–75

Park NW, Chi KH (2008) Quantitative assessment of landslide susceptibility using high-resolution remote sensing data and a generalized additive model. Int J Remote Sens 29(1):247–264

Perko R, Raggam H, Deutscher J, Gutjahr K, Schardt M (2011) Forest assessment using high resolution SAR data in X-Band. Remote Sens 3:792–815

Raggam H, Gutjahr K, Perko R, Schardt M (2010) Assessment of the stereo-radargrammetric mapping potential of terraSAR-X multibeam spotlight data. IEEE Trans Geosci Remote Sens 48(2):971–977

Toutin T, Chenier R (2009) 3D radargrammetric modeling of RADARSAT-2 Ultrafine Mode: preliminary results of the geometric calibration. IEEE Geosci Remote Sens Lett 6(2):282–286

Van Westen CJ, Castellanos E, Kuriakose SL (2008) Spatial data for landslide susceptibility, hazard, and vulnerability assessment. An overview. Eng Geol 102(3–4):112–131

Zhang L, Gruen A (2006) Multi-image matching for DSM generation from IKONOS imagery. ISPRS J Photogramm Remote Sens 60(3):195–211

Slope Angle as Indicator Parameter of Landslide Susceptibility in a Geologically Complex Area

Angelo Donnarumma, Paola Revellino, Gerardo Grelle, and Francesco Maria Guadagno

Abstract

Slope angles are a key parameter in estimating susceptibility to developing earth flows. In this paper, slope angles are used to estimate potential unstable areas in a pilot sector of the Benevento province in (Southern Italy).

Since the study area is characterized by a complex lithological setting, landslide distribution was analyzed within four-groups of homogeneous litho-technical sequences. Slope angle frequency distributions were obtained from a landslide sample in accordance with the Weibull probability density distribution function. Their analysis shows that the largest occurrence of landslides fall within an interval of slope angles ranging from 9° to 14°. As filed surveys confirm, the low frequency of instabilities on steeper slopes can be explained by a deficit of potentially involving materials, partially due to the presence of stony sequences. Consequently, the probability of failure was calculated only on slope angle ranges already affected by existing landslide phenomena.

Keywords

Earth flows • Weibull distribution • Southern Italy

Introduction

Assessment of the landslide susceptibility and identification of potentially landslide-prone areas have both experienced extensive advances in scientific literature. A variety of methods have been developed using deterministic and statistical approaches based on slope angle distribution. Statistical analysis is widely used mainly in large-scale previsional studies, as it allows for a better understanding of the relationship between landslide phenomena and predisposing factors. Furthermore it guarantees a lower degree of subjectivity in contrast to heuristic methods.

However, a key issue is represented by the definition of predictive models founded on statistical bases. The assumptions on which these models are based, are only partially satisfied when the statistical analysis deals with discrete variables such as for example the slope angle. In this case, analyses carried out by Ohmori and Sugai (1995), Iwahashi et al. (2001, 2003), Korup (2005), Xiaoyi and Jianping (2006), Guzzetti et al. (2007) and Lee et al. (2008) were based on the assumption that landslide susceptibility does not monotonically increase with an increase in the slope angle.

Nevertheless, even though landslide evolution is largely connected to the steepness of the slope in geomorphologic environments dominated by slow movements (such as earth flows), it has to be taken into account that high slope angles do not always produce earth flows. High gradients can be often due to the presence of stony layers within sequences, which influence the behavior of the masses (Grelle et al. 2011b)

Based on the above considerations, this paper aims to analyze the influence of the slope angle in earth flow occurrences, which involve structurally and lithologically complex sequences. The study was applied to a pilot area of

A. Donnarumma (✉) • P. Revellino • G. Grelle • F.M. Guadagno
Department of Biological, Geological and Environmental Sciences, University of Sannio, Via dei Mulini, 59/A, Benevento, Italy
e-mail: angelo.donnarumma@unisannio.it

C. Margottini et al. (eds.), *Landslide Science and Practice*, Vol. 1,
DOI 10.1007/978-3-642-31325-7_56,

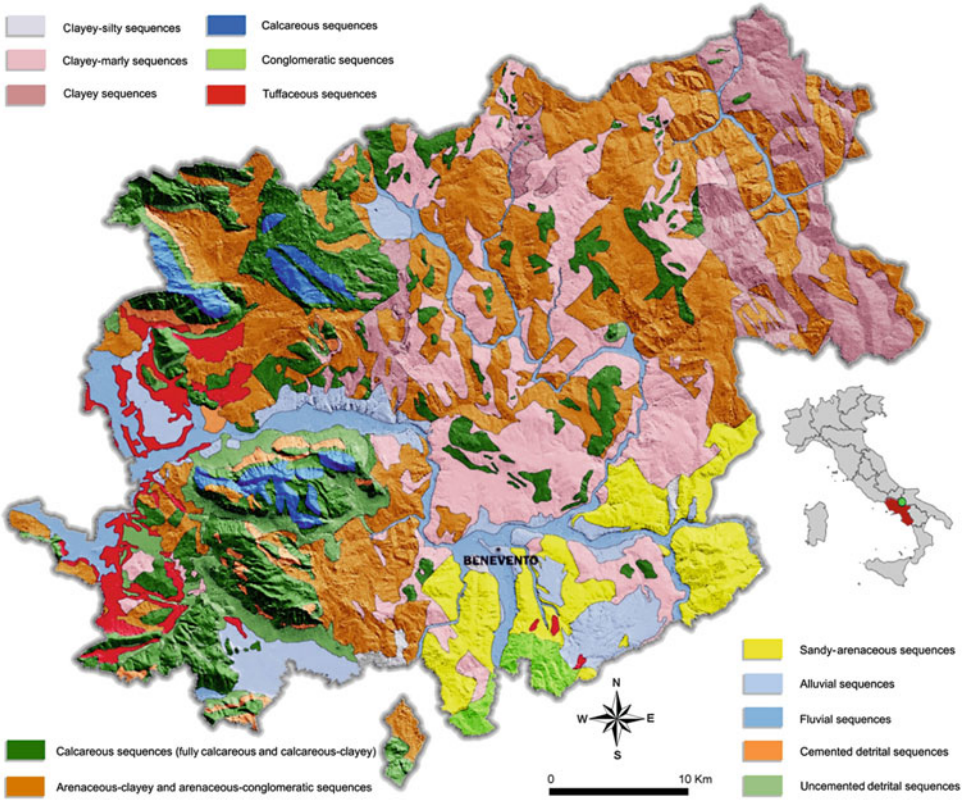

Fig. 1 DEM of the study area and litho-technical sequences outcropping

the Benevento province in Southern Italy, where considerable data relating to slope angles and lithological sequences was available (Guadagno et al. 2006).

Geological Features and Landslide Occurrence in the Study Area

The Province of Benevento (approximately 2,000 km^2) has been historically affected by landslides prevalently of the earth flow type. Its morphological pattern is controlled by both the regional geo-structural setting, and the outcropping terrains which mainly consist of structurally complex formations (*sensu* Esu 1977).

Revellino et al. (2010) grouped these deposits into successions on the basis of their lithological and engineering-geological/geomechanical features (Fig. 1) in order to elucidate the relationship between landslides and the geological formations. Within these groups, the analysis was carried out only on the following sequences affected by earth flows: (1) Clayey sequences (Cl); (2) Arenaceous-clayey-conglomeratic sequences (Ar-Cl-Cg); (3) Clayey-silty sequences (Cl-S) and Clayey-marly sequences (Cl-M)

As regards landslides, recent studies carried out by Guadagno et al. (2006) and Revellino et al. (2010) led to an inventory of more than 3,100 earth flows, covering an approximate area of 358 km^2, approximately 18 % of the entire surface area of the province (Fig. 2). By comparing Figs. 1, and 2, one can note that landslide phenomena are mainly connected to Cl, Ar-Cl-Cg, Cl-S and Cl-M litho-technical sequences.

Landslide distribution activity (sensu WP/WLI 1993) is generally advancing, except in the source area where it is retrogressive.

Moreover, large earth flows usually affect the full slope length, even though smaller and secondary phenomena, which have often different directions and velocities, as highlighted in the literature for similar instabilities (e.g. Corominas et al. 2005; Lollino et al. 2003), take place within the main landslide body. Usually, reactivations involve the full landslide bodies or limited sectors during long and intense storms.

Probability of Failure and Landslide Susceptibility

Scientific Background

Parametric statistical analysis is well suited to addressing landslide susceptibility assessments of geomorphologic environments dominated by recurrent slope instabilities. The experimental results obtained by PWRI (1976), Ohmori

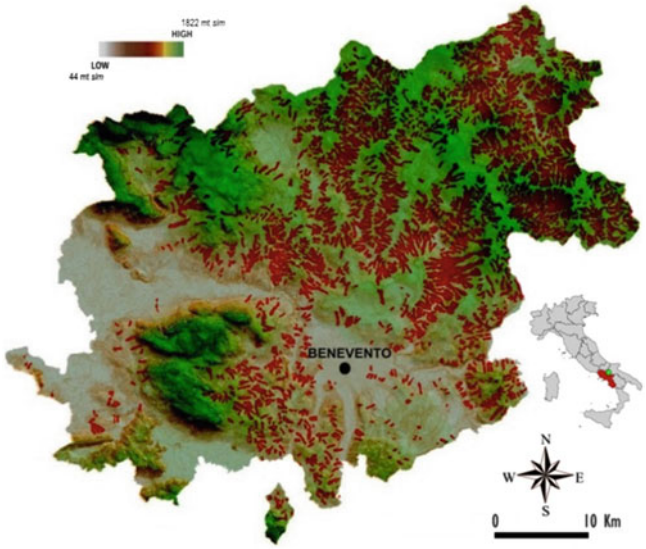

Fig. 2 Landslide distribution on DEM of the study area

and Sugai (1995) and Iwahashi et al. (2003) show that the distribution of the mean slope angle of a landslide population fits a sub-optimal Gaussian function. From a probabilistic point of view, the application of statistical-mathematical algorithms to slope angle data provides an estimate of slope failure proneness.

Since we deal with Gaussian distributions, the Probability Density Functions (PDFs) of Weibull (Weibull 1951) could be well applied, being that the mode angles for whole landslide masses varied in relation to the local geology (Iwahashi et al. 2001).

The mathematical structure of the 2- and 3-parameter Weibull PDFs, respectively, is defined by:

$$f(\alpha) = \left(\frac{\beta\alpha^{\beta-1}}{\eta^{\beta}}\right) \exp\left\{-\left(\frac{\alpha}{\eta}\right)^{\beta}\right\}, \ \alpha > 0 \qquad (1)$$

$$f(\alpha) = \left(\frac{\beta}{\eta}\right)\left(\frac{\alpha-\gamma}{\eta}\right)^{\beta-1} \exp\left\{-\left(\frac{\alpha-\gamma}{\eta}\right)^{\beta}\right\} \qquad (2)$$

where α is the slope angle, β is the shape parameter, η is the scale parameter and γ is the location parameter. Each is a positive number.

As described by Iwahashi et al. (2003):

- β controls the shape of the function. If $\beta = 1$, the Weibull distribution coincides with exponential distribution. If $\beta > 1$, the Weibull distribution shows one peak on a probability density function graph. The situation, $\beta < 1$, indicates early failures; $\beta = 1$ indicates random failures. $\beta > 1$ implies wear-out failures.
- η controls the expansion and the reduction of the probability density function graphs, and moving the peak position, η indicates the theoretical mode of a failure. Iwahashi et al. (2003) clarified that the more fine-grained the geology, the smaller the value of η would thus result;
- γ controls the parallel movement of probability density function graphs.

The cumulative Weibull distribution function F(A) (3) defines the probability of failure (Iwahashi et al. 2003). F(A) is defined by the following equation:

$$F(A) = P(A < \alpha) = \sum_{\alpha_i < \alpha} P(A = \alpha_i) \qquad (3)$$

Probability Density of the Slope Angle (α)

In order to investigate the evolutive character of the instabilities, a PDF of the slope angle (α) was computed in terms of landslides area. A 2-parameter Weibull model was thus applied allowing the PDF of α and the analysis of its spatial distribution to be determined.

Slope angle data was extracted from 1:5,000 scale maps by using an Arcview GIS Platform (ESRI 1999) implemented with Spatial Analyst and Analyst 3D modules. A count map of 10 × 10 m was used to sample the angle distribution.

The data binning was preliminarily made with 1-size, non zero intervals and was characterized by small dispersion. The PDF of α ($p(\alpha)$) was obtained by dividing the area of each interval by its own amplitude. More specifically, we fixed 0° as the starting point of the binning procedure and then we extracted the counts in each bin of a 1° amplitude:

$$p(\alpha) = \frac{1}{A_{LT}} \frac{\delta A_L}{\delta\alpha} \qquad (4)$$

where δA_L is the landslide area between α and $\alpha + \delta\alpha$ and A_{LT} is the full landslide area. Equation (4) is normalized as follows:

$$\int_0^{\pi/2} p(\alpha)d\alpha = 1 \qquad (5)$$

The semi-logarithmic graphs (Fig. 3) show the α PDF of the landslides inventoried in the study area. By investigating the behavior of the PDFs, it was possible to note that the data set presents a double trend. The first, corresponding to the lower angles, has a positive correlation; the second, corresponding to the higher values, has a negative

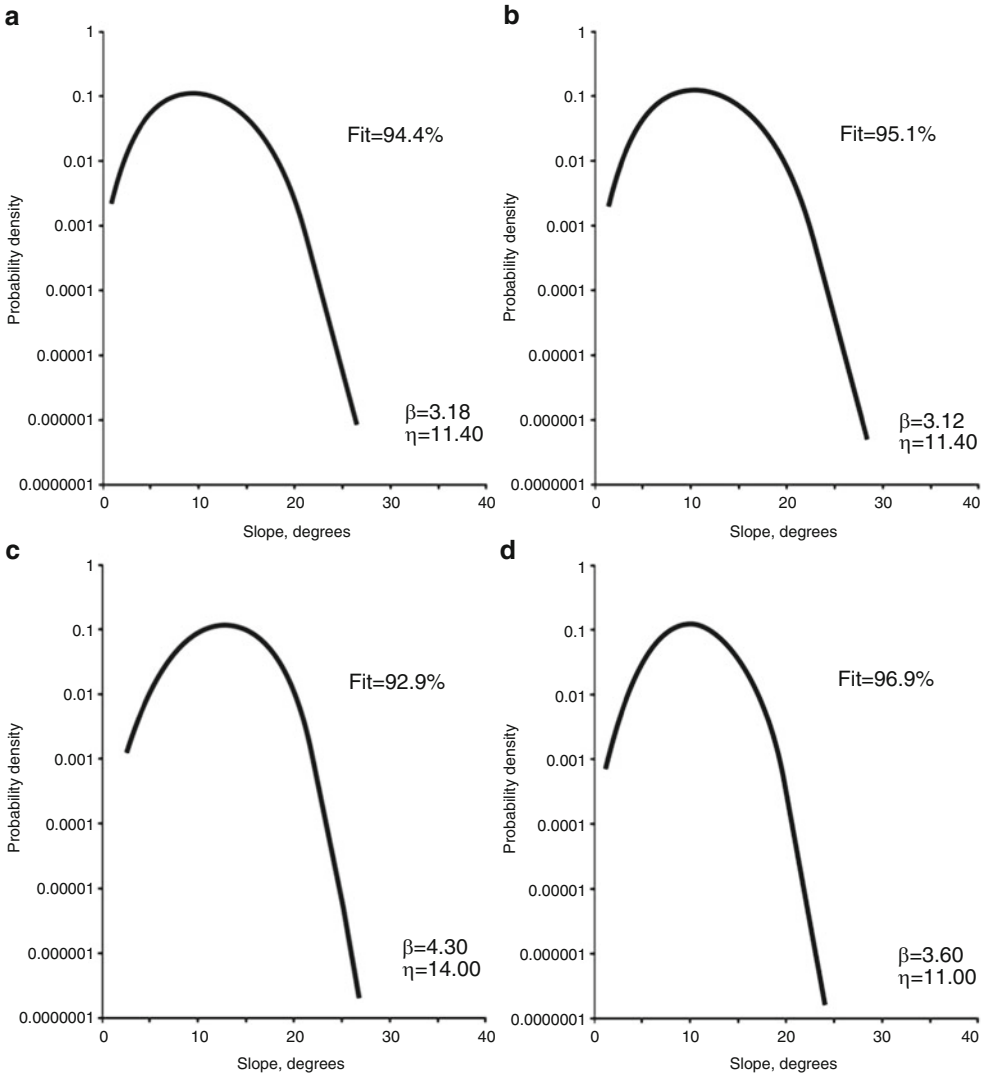

Fig. 3 Probability density function versus slope angle in the landslide area for each litho-technical sequence analyzed: (**a**) Clayey sequences, *Cl*; (**b**) Arenaceous-clayey-conglomeratic sequences, *Ar-Cl-Cg*; (**c**) Clayey-silty sequences, *Cl-S*; (**d**) Clayey-marly sequences, *Cl-M*

correlation. In particular, by approaching the peak, the values strongly decrease. In this way, it was possible to identify the slope sectors where landslides are spatially distributed.

Moreover, the PDFs obtained for each litho-technical sequence show peak values between 9–11°, 11–13° and 14–16° where landslides involved Cl and Cl-M (Fig. 3a, d), Ar-C1-Cg (Fig. 3b) and Cl-S (Fig. 3c) respectively.

Probability Distribution of the Slope Angle (α)

In order to analyze the evolutive trend of slopes induced by instabilities, the spatial distributions of α were compared in both landslide and stable areas. Data was normalized in relation to the max of the two curves, allowing the range of the probability distribution variability to be restricted between 0 and 1.

As shown in Fig. 4a, b, which refer to sequences where the stony component is lacking or poorly present, data appears to be univocally distributed in terms of trend and peak values, being the curves fully overlapped (the average shift is: 5.97 % and 7.52 %, respectively). This result could highlight the fact that the slope steepness was reduced by extreme landslide processes. Indeed, in these areas, the Landslide Index, calculated as the percentage of the area affected by landslide events for a 1 km^2 grid for the whole province, is even more than 70 % (Revellino et al. 2010).

On the contrary, the data-set distributions of Fig 4c, d show a poor agreement of the peak values, which are significantly shifted, and a poor overlapping of the curves (the average shift is: 26.79 % and 13.78 %, respectively), above all in the case of Cl-S sequences (Fig. 4c). Moreover, distribution tails also display a different behavior, which might be influenced by the poor number of events

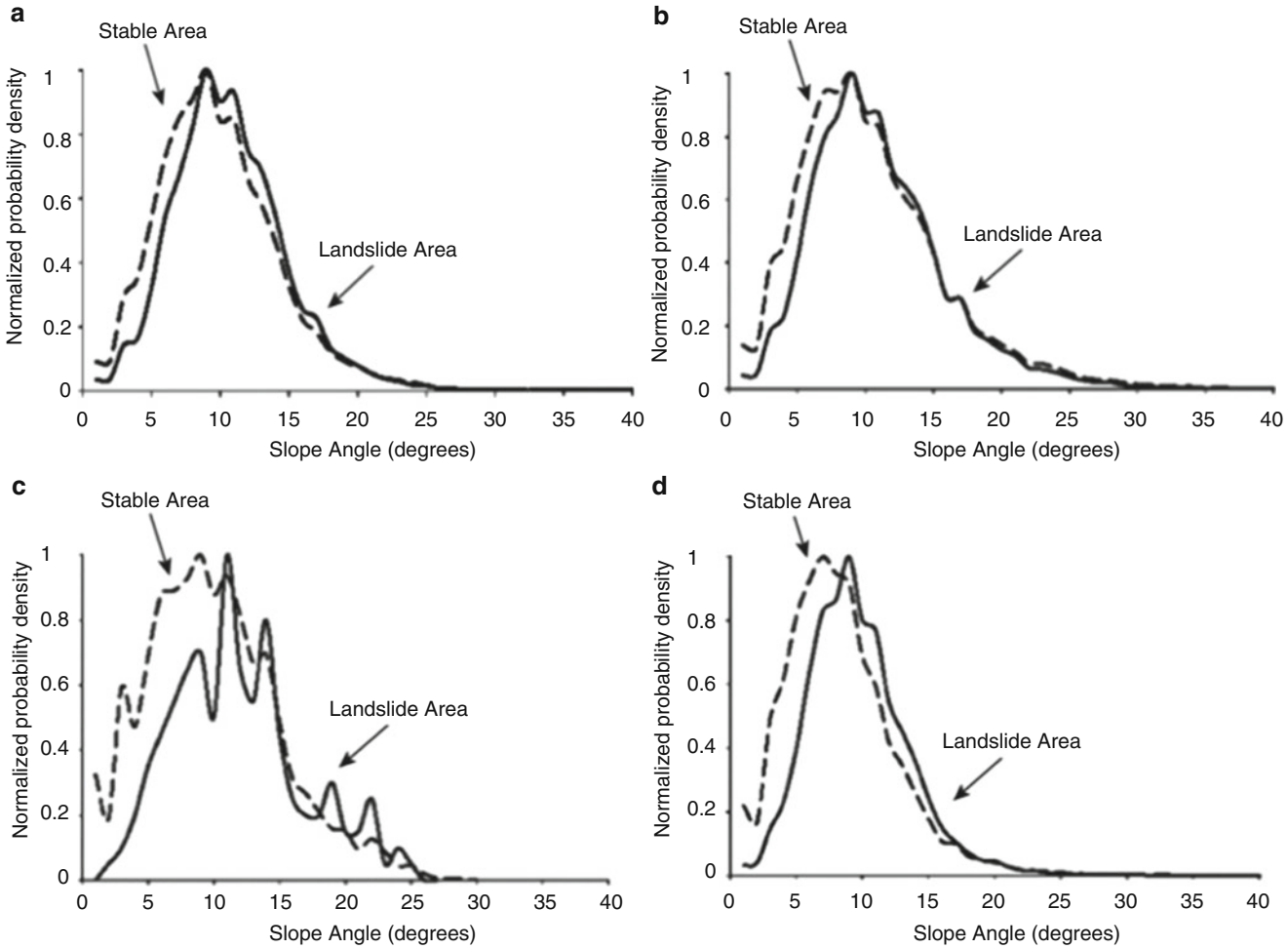

Fig. 4 Area probability density distribution, normalized in relation to the peak, vs slope angles of both landslides and stable area: (**a**) Clayey sequences, *Cl*; (**b**) Arenaceous-clayey-conglomeratic sequences, *Ar-Cl-Cg*; (**c**) Clayey-silty sequences, *Cl-S*; (**d**) Clayey-marly sequences, *Cl-M*

inventoried in this geological context too. As regards Cl-S and Cl-M sequences, landslide area distributions show prevailing slope angles around 10–12°. On the other hand, distributions of the stable areas are characterized by angles between 7° and 9°.

As confirmed by field surveys, it should be noted that landslide source areas are slowly evolving where the stony terrains are prevailing at the top of the sequence involved in landsliding. This field evidence is supported by the distributions of Fig. 5, where slope angles of the landslide source areas are compared with those of the respective channels.

Excluding the analysis on the CL-S sequence, which could be influenced by the poor statistic representativeness of data due to the exiguous number of landslides recorded (# 14), the remaining sequences are characterized by distributions (Fig. 5) that are almost unchanged with respect to those in Fig. 4.

In the case of the Cl-M sequence, the α distribution of the source area is only slightly overlapped and shifted with respect to the slope angle distribution of the entire landslide area. In addition, the peak values of the α probability density of the source areas are significantly higher (13–15°) with respect to those of the channel areas (8–9°). This could probably be related to the geo-mechanical resistance offered by the stony component that, in these sectors, constrains failure along the pre-existing weak surfaces such as fractures or bedding joints (Grelle et al. 2011b). The result is a slow and irregular retrogression, locally influenced by the fracture pattern of the stony terrain. The consequence is high evolutive control on the distribution of the activity as demonstrated by Revellino et al. (2010).

Probability of Failure

A statistical analysis of the frequency-mean slope angle relationship was carried out in order to define the probability of failure. The data fitting was performed by using the 3-parameter Weibull density function (Fig. 6). The result

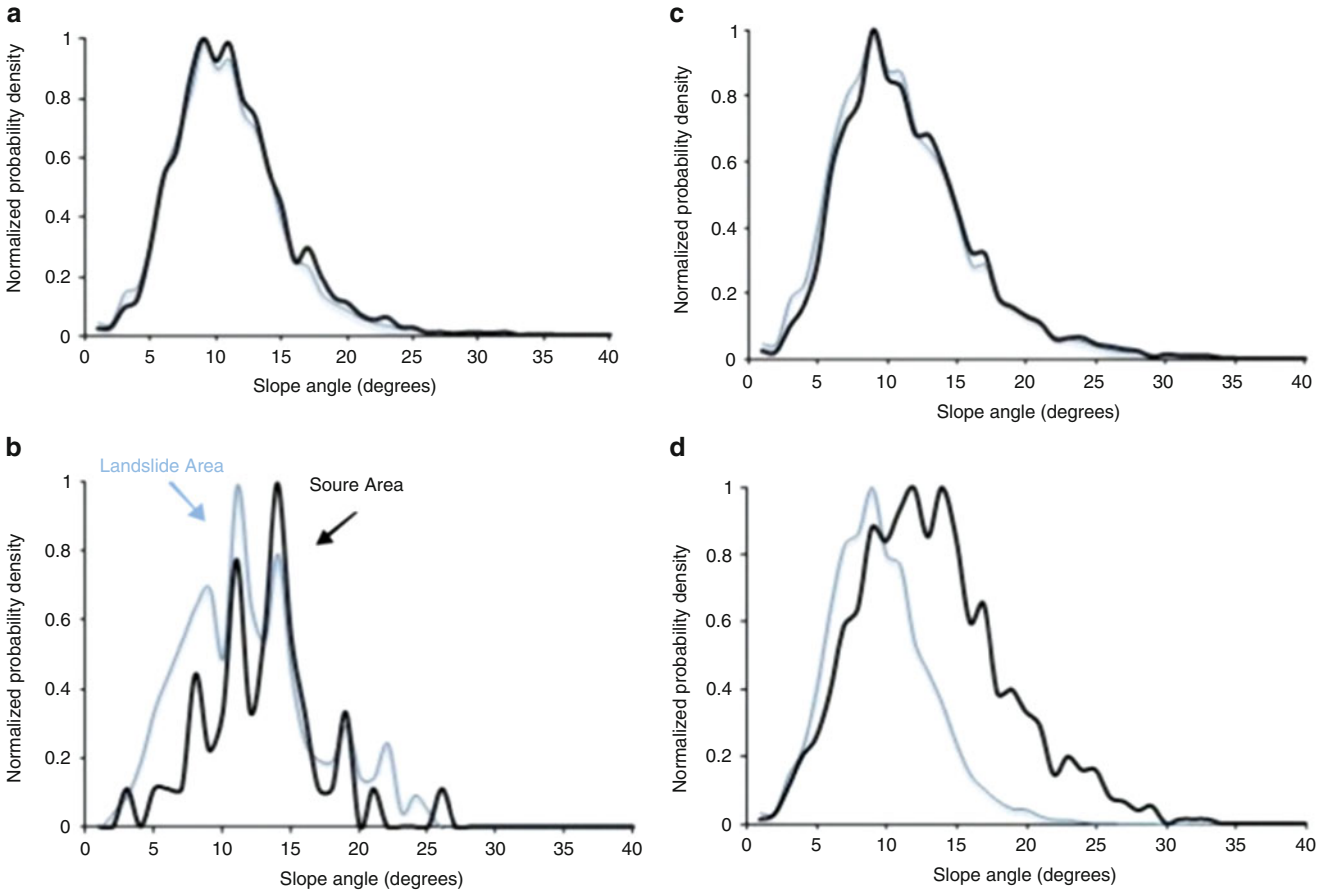

Fig. 5 Area probability density distribution, normalized in relation to the peak, vs slope angles of both landslides and source areas: (**a**) Clayey sequences, *Cl*; (**b**) Arenaceous-clayey-conglomeratic sequences, *Ar-Cl-Cg*; (**c**) Clayey-silty sequences, *Cl-S*; (**d**) Clayey-marly sequences, *Cl-M*

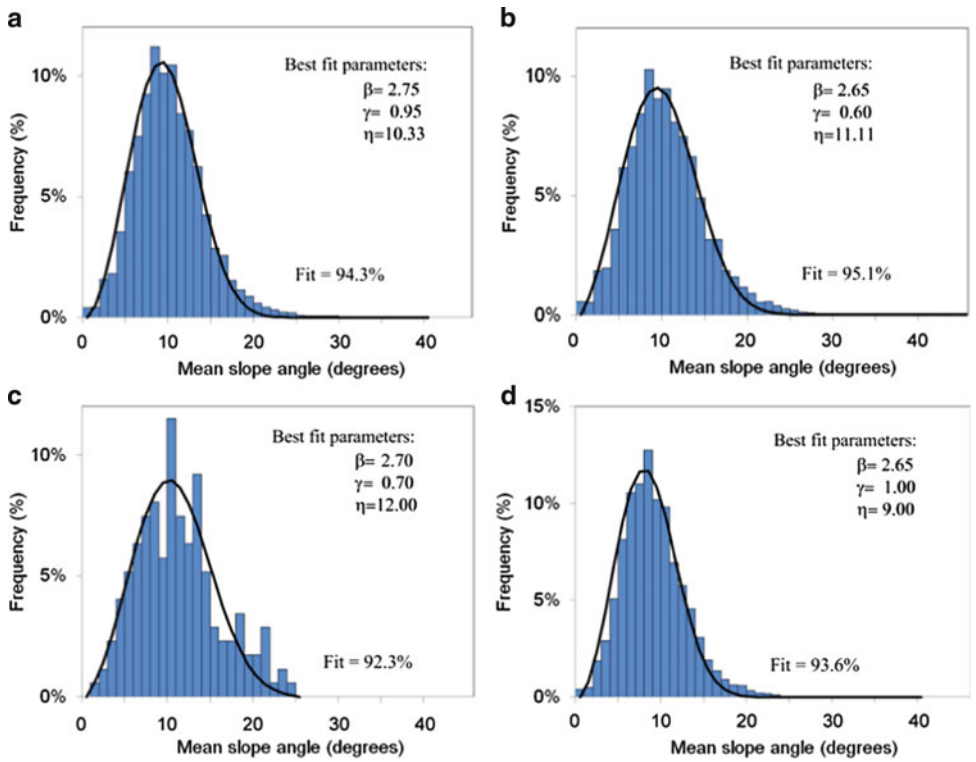

Fig. 6 Mean slope-angle frequency distributions of landslides for each geological sequence: (**a**) Clayey sequences, *Cl*; (**b**) Arenaceous-clayey-conglomeratic sequences, *Ar-Cl-Cg*; (**c**) Clayey-silty sequences, *Cl-S*; (**d**) Clayey-marly sequences, *Cl-M*

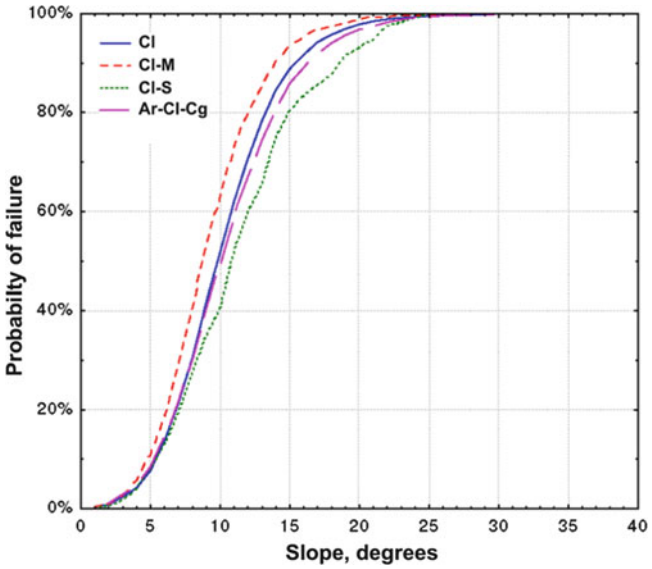

Fig. 7 Cumulative distribution functions of mean slope-angle distributions of landslides for each geological sequence

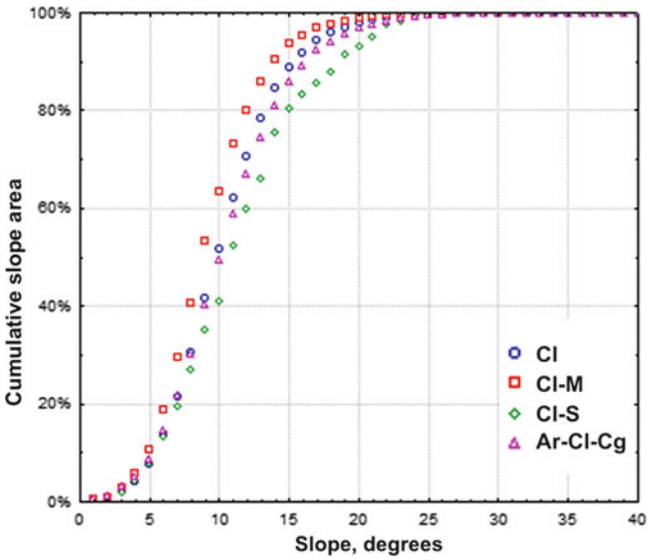

Fig. 8 Cumulative slope angle distribution

shows a unimodal asymmetric shape with peak values generally around 10°.

The cumulative Weibull distribution function F(A) was thus computed for the four litho-technical sequences (Fig. 7). Although the preliminary analysis of the probability of failure curves shows that the model seems to describe well the variability of experimental data, some interpretations should be necessarily made. First, the morpho-structural setting of large-scale areas may influence the slope angles distribution, increasing its variability. Second, the heterogeneous nature and setting of the outcropping sequences play a dominant role in the slope gradient pattern, resulting

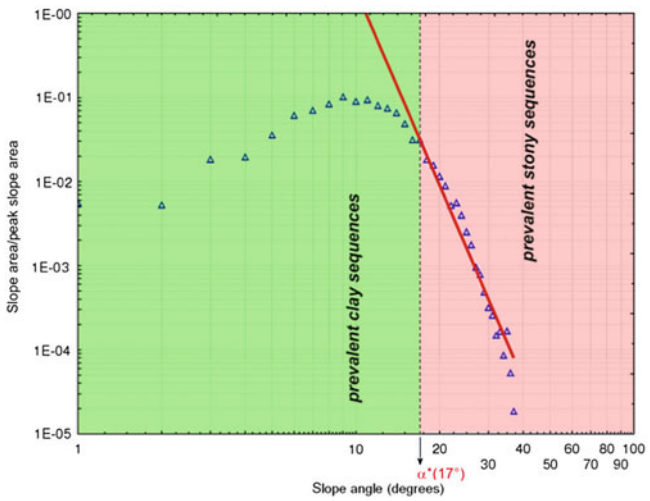

Fig. 9 Distribution curve of the landslide area in relation to the slope angle

in gently slope shapes alternated by rough and steep morphologies. The latter are characterized by a low spatial landslide frequency and, therefore, a lack of materials prone to developing landslides.

Therefore, when operating in geologically complex areas, the probability computed by the Weibull model must be calibrated and interpreted in the specific morphological context. In fact, the cumulative distribution function C(A) (6) shows that more than 95 % of the outcropping of the four litho-technical sequences has slope angles lower than 17° (Fig. 8).

$$C(A) = \sum_{\alpha_i < \alpha} C(A = \alpha_i) \tag{6}$$

This value represents the point of intersection (roll-over, α*) of two data sets in the bi-logarithmic graph of the slope angle (Fig. 9). In particular, the spatial analysis of α shows that the areal frequency distribution beyond the roll-over is controlled by the following power law equation:

$$y = 2E + 08 - 7.909\alpha \; (r^2 = 0.96)$$

This correlation is valid for slope angles ranging between $12° < \alpha < 39°$.

The value $\alpha^* = 17$ aims at identifying the lower threshold defining slope angles influenced by the outcropping of stony sequences. It is assumed that slopes having a slope angle higher than α* correspond to sectors where stony layers are outcropping.

In order to adapt the model to the specific study case, the probability of failure curves were recalculated considering the influence of α*.

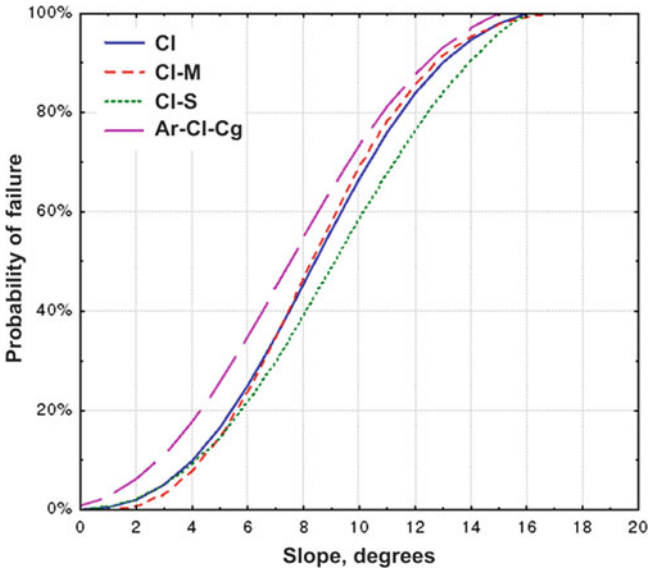

Fig. 10 Curves of probability of failure calculated in relation to the cumulative slope angle distribution

The probability of failure distributions for the four litho-technical sequences is shown in Fig. 10.

Conclusion

The study highlights and confirms that slope angle analysis is a key aspect in landslide susceptibility analysis.

The relationship between landslide frequency and slope angle underlines the role that landslides have in landscape evolution. Generally, slope steepness is significantly influenced by the geological nature of the slope. In the study area the mainly clayey sequences show a good regular Gaussian disposition with peak values, 9–14°, which are included in the shear strength fully-softened to residual range obtained by means of ring shear tests on tipical clayey samples (Grelle and Guadagno 2010; Grelle et al. 2011a).

However, the fitting Weibull functions for the four study sequences, Cl, Ar-Cl-Cg, Cl-S and Cl-M, show a different pattern which is referable both to the interaction between the geo-structural sequence and the slopes and the retrogressive evolution of landslides, which is typical of source areas.

As reported in the literature, the probability failure analysis by considering slope angles only should take into account the real lithology of the slope. In this study the threshold angle between the low and high stony abundance in the terrain sequences was attributed to the roll-over in the bi-log curve of the landslide area in relation to the slope angle. Consequently, the suitable slope failure analysis was performed again on angles under this threshold.

Finally, it is possible to ascertain that earth flows in the study area, or in similar complex geological areas, are not immediately connected to the slope angle distribution. For this reason a preliminary, deep knowledge of the study site and a post-processing analysis addressed to contextualize the output data are needed.

The results obtained indicate that accurate slope angle analyses considerably improve landslide susceptibility studies in areas characterized by complex terrains, evaluating its effective contribution as landslide predisposing factor.

References

Corominas J, Moya J, Ledesma A, Lloret A, Gili JA (2005) Prediction of ground displacements and velocities from groundwater level changes at the Vallcebre landslide (Eastern Pyrenees, Spain). Landslides 2(2):83–96

Environmental Systems Research Institute (ESRI) (1999) Arcview GIS 3.2. Environmental Systems Research Institute Inc, Redlands

Esu F (1977) Behaviour of slopes in structurally complex formations. In: Proceedings of the international symposium on the geotechnics of structurally complex formations, vol 2. Capri, 292–304

Grelle G, Guadagno FM (2010) Shear mechanism and viscoplastic effects during impulsive shearing. Geotechnique 60(2):91–103

Grelle G, Revellino P, Guadagno FM (2011a) Methodology for seismic and post-seismic stability assessment of natural clay slopes based on a viscoplastic behaviour model in simplified dynamic analysis. Soil Dyn Earthq Eng 31(9):1248–1260. doi:10.1016/j.soildyn.2011.05.005

Grelle G, Revellino P, Donnarumma A, Guadagno FM (2011b) Bedding control on landslides: a methodological approach for computer-aided mapping analysis. Nat Hazard Earth Syst Sci 11:1395–1409. doi:10.5194/nhess-11-1395-2011

Guadagno FM, Focareta M, Revellino P, Bencardino M, Grelle G, Lupo G, Rivellini G (2006) La carta delle frane della provincia di Benevento. Sannio University Press, Benevento

Guzzetti F, Ardizzone F, Cardinali M, Galli M, Reichenbach P, Rossi M (2007) Distribution of landslides in the Upper Tiber river basin, Central Italy. Geomorphology. doi:10.1016/j.geomorph.2007.07.015

Iwahashi J, Watanabe S, Furuya T (2001) Landform analysis of slope movements using DEM in Higashikubiki area, Japan. Comput Geosci 27(7):851–865

Iwahashi J, Watanabe S, Furuya T (2003) Mean slope-angle frequency distribution and size frequency distribution of landslide masses in Higashikubiki area, Japan. Geomorphology 50:349–364

Korup O (2005) Distribution of landslides in southwest New Zealand. Landslides 2:43–51

Lee CT, Huang CC, Lee JF, Pan KL, Lin ML, Dong J (2008) Statistical approach to storm event-induced landslides susceptibility. Nat Hazard Earth Syst Sci 8:941–960

Lollino G, Lollino P, Bertolino G (2003) Analysis of the behaviour of a large landslide in structurally complex soils by means of monitoring field data. In: Proceedings of the international conference – Fast slope movements prediction and prevention for risk mitigation – Naples, May 11–13. Vol 1. Ed. Patron. Bologna, pp 317–324

Ohmori H, Sugai T (1995) Toward geomorphometric models for estimating landslide dynamics and forecasting landslide occurrence in Japanese mountains. Zeitschrift fur Geomorphologie 101:149–164, Supplementband

PWRI (1976) Jisuberi no Jittai-toukei (2) (The actual statistics of landslides no.2): Technical Memorandum of PWRI 1121 (in Japanese)

Revellino P, Grelle G, Donnarumma A, Guadagno FM (2010) Structurally-controlled earth flows of the Benevento Province (Southern Italy). Bull Eng Geol Env 69(3):487–500. doi:10.1007/s10064-010-0288-9

Weibull W (1951) A statistical distribution function of wide applicability. J Appl Mech-Trans ASME 18:293–297

WP/WLI (1993) A suggested method for describing the activity of a landslide. Bull of the IAEG 47:53–57

Xiaoyi F, Jianping Q (2006) Effect on stratum gradient frequency distribution of landslides in the three gorges area of northeast Chongqing. Wuhan Univ J Nat Sci 11(4):767–772. doi:10.1007/BF02830162

The Susceptibility Map for Landslides with Shallow Initiation in the Emilia Romagna Region (Italy)

Mauro Generali and Marco Pizziolo

Abstract

The Emilia Romagna Region (RER) is probably one of the most landslide susceptible regions of the world, with ~24 % of the mountain sector covered by landslide accumulations. The regularly updated 1:10,000 Landslides Inventory Map (LIM), managed by the Regional Geological Survey, counts more than 70,000 landslides. Nowadays most land-use planning is based on LIM but this has several intrinsic shortcomings, mainly due to its scale and forecast significativity. This paper presents the methods we used to compile a detailed susceptibility map for the whole RER Apennines.

The triggering mechanism of the most common landslides phenomena in RER, disregarding of the subsequent evolution, is characterized by a first movements that may be described as "shallow phenomena" involving the upper part of the landslides (depletion areas). For this reasons we developed a model for the areas "outside" the LIM mapped landslides aimed to identify the triggering areas for future landslides. For this statistical analysis we used Bivariate Logistic Regression methods. As our aim was to predict triggering phenomena, we calibrated the model on the depletion areas, selected using a semi-automatic GIS procedure. The resulting map can be used for LIM verification and updating and adds it a forecast connotation useful for land use planning; nevertheless it has to be used by experienced users, for this purpose the model advantage and shortcomings will be discussed.

Keywords

Emilia Romagna Apennine • Landslide initiation • Susceptibility • Logistic regression

Introduction

Italy is probably one of the most landslide prone areas of the world (landslides cover ~7 % of entire country) and the Emilia Romagna Region (RER) is one of the most affected regions in Italy (APAT 2007). Like many other Italian regions, nowadays RER has a 1:10,000 Landslide Inventory Map (LIM), which represents the fundamental state-of-the-art knowledge of regional landslides. At present LIM counts more then 70,000 landslide in an area of ~11,000 km^2. It is constantly updated by aerial photo analyses and new field event reports, and it also contains information on historical events (Glade 2001).

The LIM is an irreplaceable document for land use planners, especially because in RER the majority of new landslide events involve the reactivation of past movements. Nonetheless, LIM has intrinsic predictive limitations. On the issue of landslide spatial forecast at regional scale, in the past several attempts have been made in RER to define landslide susceptibility (Bertolini et al. 2002). These are outdated products, however, because they are based on old LIM versions, simple methodologies and usable for "situational overview" (scale up to 1:25,000); they are currently

M. Generali (✉) • M. Pizziolo
Geologic, Seismic and Soils Survey, Emilia Romagna Region (Italy), Viale della Fiera 8, Bologna 40138, Italy
e-mail: mgenerali@regione.emilia-romagna.it

C. Margottini et al. (eds.), *Landslide Science and Practice*, Vol. 1,
DOI 10.1007/978-3-642-31325-7_57,

insufficient for detailed (district to municipality) land use planning. More detailed works have been carried out by several authors but they are territorially restricted and methodologically inhomogeneous so they can neither be merged together, nor extrapolated to the neighbouring areas. With this work we try to fill this gap in spatial prediction through detailed analysis, which is extended to the whole region, focused on the most common landslide type and able to cover the whole RER Apennines. The homogeneous coverage of the ~11,000 km^2 and the analysis detail (usable up to 1:5,000 scale) make these maps a useful contribution to the "local scale" land use planning processes and to hazard and risk mitigation policies for the entire region.

Regional Setting

The Emilia Romagna Region (RER) straddles the northern and central belt of Italy. About half of the >22,000 km^2 of the region and in particular the southern part, is characterized by hilly and mountainous areas, with altitudes ranging from just tens of metres to 2,163 m a.s.l.

The geology differs significantly between the Emilia Apennines (central and western side), and the Romagna Apennines (eastern side): the former is almost completely characterized by sedimentary (and mostly weak) rocks, often formed by Cretaceous-Paleogenic structurally complex clay and clay shale or tectonized alternances (flysch) (Ligurian Units), surmounted by Eocene-Miocene marine deposits (Epiligurian Units), while the latter is dominated by the Oligo-Miocene Flysch deposits (Marly-Sandstone Formation); both are delimited in their frontal side by Plio-Pleistocene marine and transitional deposits (Fig. 1).

The RER Apennines mean Landslide Index (area covered by landslides / total area) is ~24 % but in some municipalities it reaches or exceeds 50 %. Most of the landslides are characterized by slow to extremely slow movement, mainly constituted by slides, earth-flows and complex landslides. They rarely threaten human life directly but often affect property, infrastructure, rivers and landscapes, causing severe damages and high risk levels. The main predisposing factor is the weakness of the bedrock and hillslopes materials, while the main triggering factor is precipitation.

Amongst the predisposal factors, especially for small and medium events, we must not underestimate the great importance of the area's recent history: in recent centuries Man has greatly modified the natural environment, first of all with widespread timber harvesting and conversion to agriculture and later with the construction of many villages, towns and infrastructures. In the past few decades most of the farms and fields have been abandoned and forests have reclaimed many hill slopes, but the resident population has continued to grow nonetheless: at 1/1/2007 the hilly and mountainous areas of the RER had a population of 1,342,149 people, 31.78 % of the whole RER, amounting to an increase of 5 % over 10 years, who are particularly concentrated in hills and larger villages. Nowadays there are >145,000 buildings and > 8,100 km of roads located directly on landslide accumulations or in a meaningful bound but they are certainly underestimated.

Materials and Methods

In this chapter we present the LIM data and the typical landslide processes that we deal with; these are the background for the conceptual framework delineation. We'll then present the identification and/or creation of the data we'll further use in the statistical analysis.

Landslides Inventory Map

Over three decades, RER's Geological Survey (SGSS) has progressively developed an historical LIM which, derived originally from detailed (1:5,000–1:10,000) field surveys in '80 and '90, has been updated with periodical and extensive correction, integration and validation by further field check and multi-temporal aerial photo interpretation. The LIM used in this work dates back to 2006 and counts 70,037 landslide polygons, classified according to type of movement and state of activity. In this map approximately 54.7 % of the landslides (corresponding to ~28 % of the total landslide area) are classified as active[1] and the remaining 45.3 % as dormant; landslides classified as stabilized are negligible.

LIM is one of the main product used by the land use planners due to the Apennine singularity: >80 % of the landslides events with area >5,000 m^2 see a total or partial reactivation of a mapped landslide; but the landslides inventory map has also several shortcomings:

1. Mapping subjectivity, unavoidable in every individual survey and intellectual work, can be reduced but not eliminated;
2. It's lacking in small landslides, especially dormant, due to the difficult reconnaissance and their progressively masking, especially in cultivated slopes;
3. It doesn't give any information about the "out of landslide" areas;
4. It represent a "snapshot" of the moment then:

[1] The State of activity definition doesn't correspond to that used by Varnes (1978), WP/WLI (1993) or Cruden and Varnes (1996), but assume as active a landslide that has shown activity in the last ~30 years.

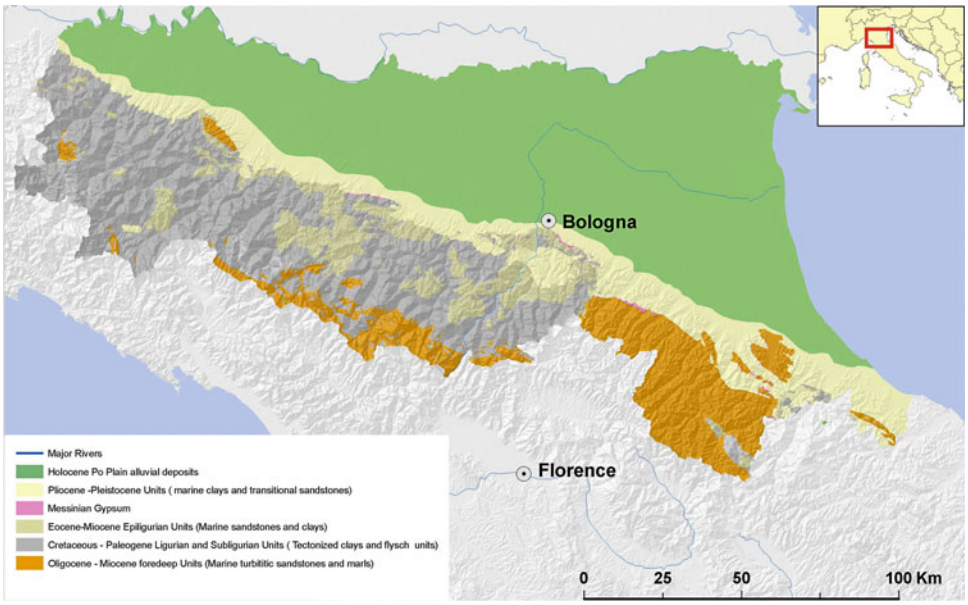

Fig. 1 Structural-Geological Map of the Emilia Romagna Apennines (from Cerrina Feroni et al. 2002)

- It's subject to a pretty fast ageing (mainly regarding the activity state), then it requires a constant updating;
- It doesn't contain forecast information and doesn't provide suggestions on the future landslides evolution.

For these reasons, purely LIM-based land-use planning is still too "risky" and a forecast contribution is generally desirable. Actually, across most of the RER territory, planning is still based on the landslide activity state classification, a characteristic very difficult to assess objectively and subject to suddenly changes that can lead to contradictions like that shown in the example of Fig. 2.

As land use planning in RER underestimates this kind of behaviour, the resulting planning maps overestimate the hazard in recently activated areas and underestimate the risk in many dormant landslides areas. For this reason we believe land-use planning, at every scale, should approach this issue with a less observational and more forecast-oriented approach. Our issue has been to produce a map with the following requirements: (1) coverage of the whole Emilia Romagna Apennines (~11,000 km^2); (2) high detailed resolution, such as can be used up to scale 1:5,000; (3) focused on forecasting the most frequent type of landslide; (4) ability to predict both the areas most prone to landslides outside of mapped landslides and to evaluate the mapped landslide reactivation likelihood; (5) ability to evolve towards relative hazard and specific risk assessment.

Type of Landslide Movement

In RER, most phenomena can be classified as earth-slides, earth-flows and complex landslide. Their triggering phase usually involves the retrogression of pre-existing depletion areas (originating past movements) and the onset of a small first slide movement (Figs. 3 and 4[1]).

The subsequent phase, through an "undrained loading" mechanism (Hutchinson and Bhandari 1971; Hutchinson 1988), sees the partial or total reactivation of the landslide accumulation which is the result of previous reactivations (Figs. 3 and 4[2, 3]).

We should note that even big landslide accumulations can be reactivated by a small retrogression movement (Fig. 3), so it is very important to try to locate even small potential sources of such movements.

Most of the landslides present this kind of evolution and can thus be treated in the same way as regards forecasting their triggering phase, so these are the type of landslides selected and used for the statistical model.

Analysis Methods

Many different methods for assessing landslide susceptibility have been proposed and compared in literature (Carrara 1983; Hutchinson 1995; Aleotti and Chowdury 1999; Chung and Fabbri 1999; Guzzetti et al. 1999; Crosta et al. 2001; Wang et al. 2005; Chung 2006; van Westen et al. 2006). Among these, physically-based and statistical models are the most widely used (e.g., Guzzetti et al. 1999; Dai et al. 2002). The former require detailed geotechnical and hydro-geological data to reproduce the physical processes (white-box models), whereas the latter rely only on comparison with past landslides (black-box models), and are more suitable for modelling susceptibility to landslides in large areas where such knowledge is lacking (Van Den Eeckhaut et al. 2006). Due to the vastness and heterogeneity of the study area,

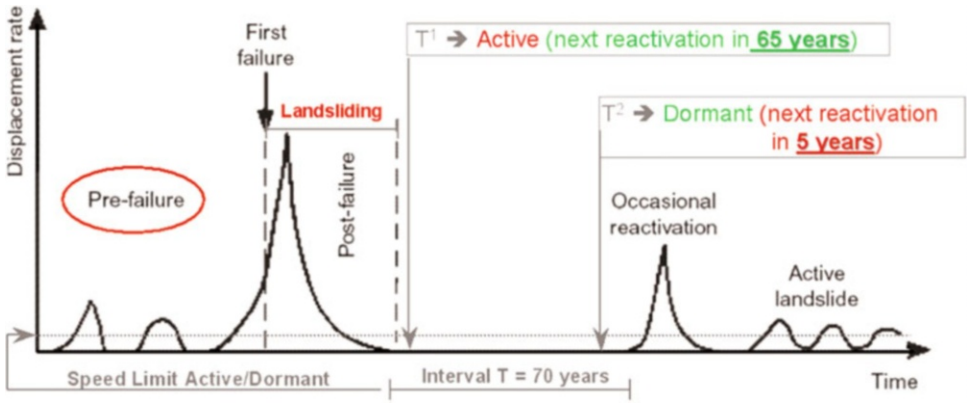

Fig. 2 A classic landslide temporal behaviour (modified from Leroueil et al. 1996). The image shows that in a quite long reactivation period perspective, a landslide mapped as dormant may be more hazardous than one classified as active

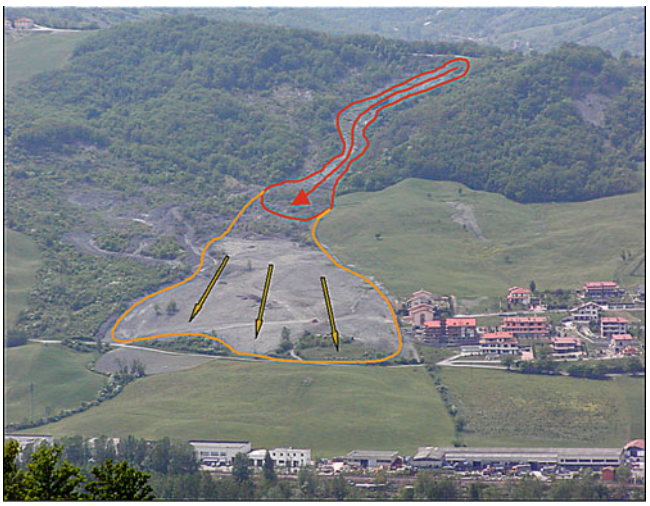

Fig. 3 An example of "undrained loading" reactivation: the Spazzavento Landslide (Bologna Province) of January 2002: the shallow earth-flow (*red boundary*) triggered a dormant landslide of ~20 m thickness (*orange boundary*)

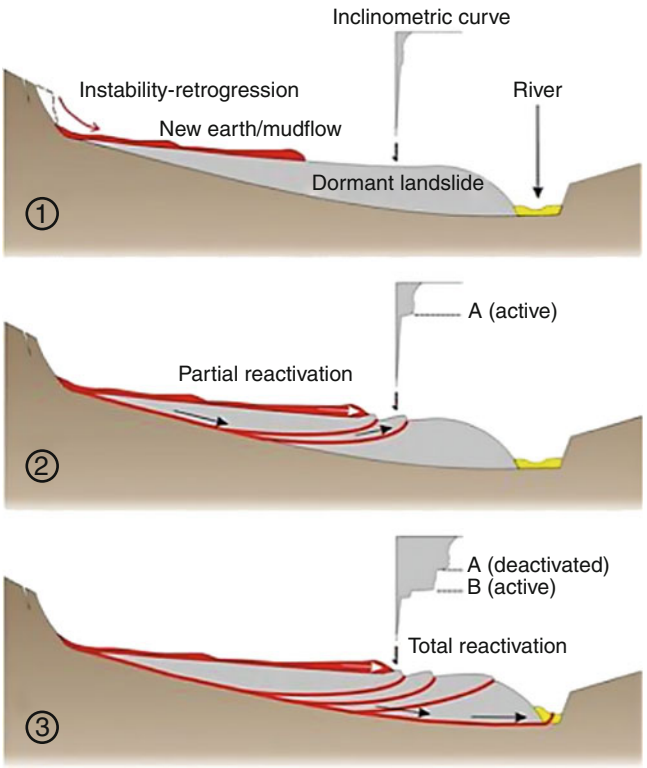

Fig. 4 Schema of the "undrained loading" reactivation mechanism (from Bertolini e Pizziolo 2008). A retrogression of the depletion area, involving a relatively low amount of material, may partially or totally reactivate a dormant landslide with a volume of 2–3 order magnitude higher then the first reactivation movement

we chose the latter method and, in particular, a multivariate regression method.

The conceptual model for all statistical models is that "the past (and present) landslide locations are the key to the future" (Carrara et al. 1995; Zêzere 2002). More specifically, locations susceptible to landslides will be selected because of their similarity in environmental characteristics to those of landslides already mapped in the study area. This basic assumption is one of the greatest limitations because climatic conditions or land use may change, hence the past is not strictly an indicator for the future. Chung and Fabbri (2003b) found some other weak points in statistical modelling practices that can be summarized as follows: (1) Simplification of inputs and categorization of continuous data layers cause the loss of much of the original significance of the data; (2) Assumptions in predictive models are unavoidable but rarely they are discussed in detail by the authors; (3) In any prediction, the methods used to make prediction are of no scientific value unless the validity of the prediction results is measured. In the follows we describe how we tried to overcome these problems.

Conceptual Framework

The conceptual model of every statistical methodology is approximately the same (Carrara et al. 1995; Guzzetti et al. 1999; Van Den Eeckhaut et al. 2006): (1) Identification

of unstable zones in the study area; (2) Mapping of environmental factors which are supposed to be correlated with slope instability; (3) Estimation of the relative contribution of these factors in generating slope-failures; (4) Application of the model and classification of every land unit into domains of different susceptibility levels.

Despite this homogeneity, the results of different frameworks (not just statistical procedures), may differ greatly. According to several authors (van Den Eeckhaut et al. 2009; Rossi et al. 2010; Suzen and Doyuran 2003), backed up by our own tests (section "Multivariate Versus Monovariate Approach"), differences between various statistical methods do not lead to particularly substantial differences in the final map; the real differences come from other matters, namely: (a) the type, amount and quality of the input data; (b) the conceptual framework: model assumptions and construction.

Since the statistical models rely on the assumption that the past is the key of the future (black-box model), the amount and quality of past data bear the greatest importance. Literature abounds with works that discuss statistical questions but show models calibrated on just a few tens or, at best, few hundreds of landslides. Statistical models require "statistical stability", especially when using categorical (dummy) variables; that is why an appropriately large and high quality dataset is the most important starting point.

As to conceptual framework, in literature two different approaches are used to identify "unstable areas": the first specifies landslide accumulation as instability evidence (Carrara et al. 1990; Cardinali et al. 2002; Ayalew and Yamagishi 2005; Lee et al. 2008; Wang et al. 2007); the second uses the depletion areas as unstable zones (Suzen and Doyuran 2003; Van Den Eeckhaut et al. 2006). The two approaches are substantially different: the former focuses on products, the latter on processes. Considering that every statistical regression will find the conditions more likely similar to those used in the calibration phase, even with the same original dataset, the results of the two approaches will differ greatly: the model calibrated on landslide accumulations will likely find other "existing" landslide accumulations while the model calibrated on depletion areas is focused to highlight conditions that can lead to new landslide phenomena. In the study area context we believe the first approach to be quite useless because, aside from being landforms, "landslides" are, first and foremost, a process (landsliding) and landslide accumulations are merely the final result of a process generated elsewhere. Furthermore, if the landslide inventory map on which the model is based is presumed to be essentially complete, it is virtually useless to try to find many other landslide bodies, especially in the absence of any connection between shapes and processes.

Land Unit

Since we wanted to use the depletion zones as unstable areas, and the former are usually much smaller than the produced accumulation, despite the wide area to model (~11,000 km^2), we had to use a high detail land unit for statistical analysis: the 10 × 10 m cells of the DEM derived from the 1:5,000 Regional Technical Maps (CTR), in turn derived from the 1973–1976 1:13,000 aerial photographs. A wider unit (like elementary slopes, UCU – Unique Condition Unit, etc.), could not locate small but important local morphologies; we must indeed bear in mind that many morphometric parameters derived from DEM use a kernel of 3 × 3 cells, so the 10 × 10 m DEM is generally representative of the morphology in a 30 × 30 m area.

Choice of Regression Model

When one decide to approach the landsliding forecast using a statistical approach, he/she wants to solve the following problem: he/she knows the sites where the landslide exists (and where not) and wants to determine why the phenomenon could be found just in those locations and not elsewhere. Once one understand which are the main predisposal factors and how each of them influence the phenomenon, he/she wants to apply this "new knowledge" to outguess the locations where the same phenomena are most likely to occur again. This is the ideal field of application of Binomial Logistic Regression (LogR) which, in this context, can be used to predict the probability that a phenomenon will occur at an unsampled location.

In landslide forecasting, LogR has become popular quite recently (e.g., Carrara et al. 1995; Atkinson and Massari 1998; Begueria and Lorente 1999; Gorsevski et al. 2000; Lee and Min 2001; Dai and Lee 2002; Dai and Lee 2003; Ohlmacher and Davis 2003; Vanacker et al. 2003; Ayalew and Yamagishi 2005; Lee 2005; Akgün and Fikri 2007; Van Den Eeckhaut et al. 2006; Wang et al. 2007; Bai et al. 2008a, b; Rossi et al. 2010), because of its many advantage.

Like all other statistical regression methods, logistic regression requires the independent variables to be statistically independent (Hosmer and Lemeshow 1989). Apart from this, its requirements are much less restrictive than other statistical models (like Discriminant Analysis or OLS), regarding the independent (predictor) variables characteristics: (a) they may be either numerical or categorical (in this case represented by dummy variables); (b) they need not be normally distributed; (c) it does not assume homoscedasticity.

Chung and Fabbri (2003a) highlighted that discretization procedures may lead to the loss of significativity of variables. Furthermore the analysis results may appreciably vary according to different class subdivisions. The possibility in LogR of using both categorical and continuous variables, avoids the necessity of converting continuous variables into discrete (categorical) maps.

A further great advantage of LogR is also that predicted values can be directly interpreted as probability because they are constrained to fall into an interval between 0 and 1. Goodness-of-fit tests such as the likelihood ratio test are available as indicators of model appropriateness.

In LogR landslide presence/absence will be the dichotomous dependent variable (Y): 1 = presence; 0 = absence of landslide. Its presence will be influenced by the existence, in the same location, of (Xi) independent variables (where i = 1, 2, ….. n, are the different predictor variables). The role of the LogR model is to quantify the influence of the Xi variables in order to: (1) evaluate the relative contribution of each variable in helping us understand the process; (2) combine all the influences to obtain the odds of every other area unit to be a landslide prone area.

Logistic regression applies "maximum likelihood estimation" method, after transforming the dependent into a "logit variable" (the natural log of the odds of the dependent occurring or not – (2)). In this way, logistic regression estimates the odds of a certain event occurring. Note that logistic regression calculates changes in the log odds of the dependent, not changes in the dependent itself as OLS (Ordinary Least Square) regression does. The logistic response function can be written as:

$$P_{(Y=1)} = \hat{P} = \frac{1}{1 + e^{-z}} \tag{1}$$

where P is the probability of occurrence of a landslide (Y = 1). The (1) can be linearized with the Logit transformation to obtain the Log odds:

$$z = Log \frac{\hat{P}}{\left(1 - \hat{P}\right)} \tag{2}$$

where (z) is linearly related with the independent variables:

$$z = \beta_0 + \beta_1 X_1 + \beta_2 X_2 + ... + \beta_n X_n \tag{3}$$

Where β_0 is the model intercept and the β_i are the coefficients for the independent variables X_i (i = 1, 2, … n) estimated by maximum likelihood.

As z varies between $-\infty$ and $+\infty$, the probability varies from 0 to 1 on an S-shaped curve (Suzen and Doyuran 2003).

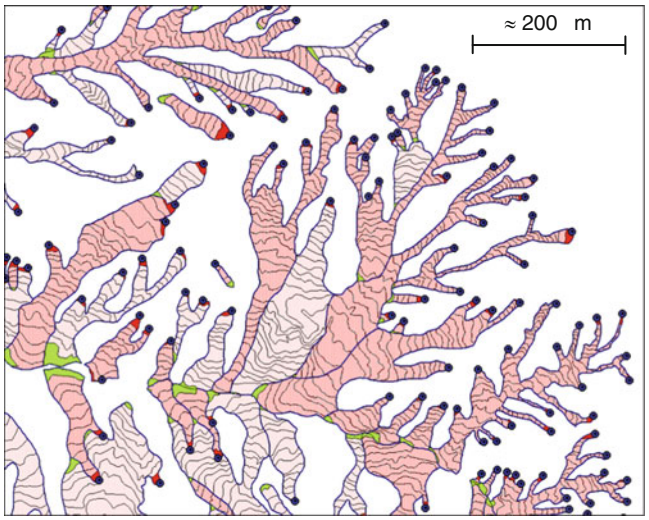

Fig. 5 Identification of unstable areas (*blue dots*) on the LIM polygons

Identification of Unstable Areas

Since the RER LIM derives from the geological map, it only maps landslide accumulations, not their depletion areas. Furthermore, many landslides have a multi-lobed shape, characterized by several branches merging into a single accumulation "GIS-polygon" but each one with its own distinct depletion zone. Mapping all the depletion areas of the >70,000 landslides by aerial photo-interpretation would have been a useful but enormous effort which was not feasible at the time. To solve this issue in the SGSS we wrote a series of GIS procedures (language Avenue for ArcView 3.x) that allowed us to obtain the higher elevation point of each branch of each landslide polygon (Fig. 5). These points usually fall within the depletion area, so the cells corresponding to each of these points have been assumed to be statistically representative of the correspondent landslide initiation conditions.

This procedure gave us further advantages:

1. The possibility to obtain a great number of unstable points in a relatively objective way;
2. The capability to don't lose information and to take the most advantage from the landslide inventory map (if we simply used only the upper point for each landslide polygon we'd have lost many useful information).

After an appropriate semiautomatic cleaning of misplaced points, we got 112,050 unstable points that became the 1's (presence of landslides) in the logistic regression model.

Identification of Stable Points

Despite its popularity, logistic regression may cause some problems if the total area affected by landslides is much

smaller than the total study area. Indeed LogR sharply underestimates probabilities if the number of 1's (presence) in the population is dozens to thousands of times smaller than the number of 0's (absence), (King and Zeng 2001). According to the same authors, the number of non-landslide points should be from equal to five times greater than the number of landslide points. In actual fact in our map, the number of triggering points identified as described in section "Identification of Unstable Areas", is three orders of magnitude lower than the total number of cells of the area. To overcome such a problem, the strategy is to randomly sample on the map a numerical suitable set of "probably stable points". The reason of the random sample is to ensure a distribution of points statistically proportional to the overall presence of each value for each variable, thus to significantly compare the relative presence for landslide and non-landslide points. For this issue, prior to seed random stable points on the map, we had to find the portion of slopes most likely stable through progressive exclusion of non suitable areas. We proceeded as follows: (1) identification of the limit between the Po valley and intravallive plains and the hillslopes, based on geological and morphological evaluations; (2) from the remaining hillslopes, exclusion of some "probably unstable areas"; such areas were set, by experience, as a 30 m buffer around the mapped landslides; in this way we have probably excluded most landslide depletion areas and those areas surrounding the accumulations, often affected by stress detension and retrogression instability phenomena.

At the end of this cleaning operation, we randomly sampled about 140,000 "probably stable points" which will be the "0's" of the LogR model, each of which has been associated with the corresponding set of independent variable values.

Independent Variables

The general consensus is that any independent variable must be: (1) operational (having a certain degree of affinity with the dependent variable); (2) complete (be fairly represented all over the study area); (3) non-uniform (varying spatially); (4) measurable (can be expressed by any of the different types of measuring scales); (5) non-redundant (its effect should not account for double consequences in the final result) (Ayalew and Yamagishi 2005). Variables preparation/generation is therefore an important phase of the modelling process, which has to strike a balance between significativity and spatialization feasibility.

Independent variables maps may be classified in several ways according to their origin as: i. field survey based, ii. DEM based and iii. Remote Sensing based, or according to the data type as: continuous or categorical. Field survey based maps are very time and money consuming ones but they are often fundamental for a landslide model (e.g. geological maps and its derivates). Remote Sensing Based maps are recently on the increase but in landslide models are not widely adopted yet. Finally in the last decade, DEM and digital terrain analysis provided a great contribution to morphometry and hydrology applications and nowadays dozens of variables may be generated from DEM quickly and cost-effectively (Moore et al. 1991; Gallant and Wilson 2000).

In this work we decided to use two field based derived variable maps (lithotechnical and land use maps), and to test a series of DEM-derived continuous maps.

Lithotechnical Map

Based on RER Geological Map (scale 1:10,000), a lithotechnical map was elaborated following these steps: (1) conversion of the >500 geological units into lithological units; (2) GIS-intersection of the lithology with the geo-structural paleo-domain (which strongly influences the diagenesis degree and the structural characteristic of the rock mass); (3) further amalgamation of the still many classes to achieve the more suitable number of 16 lithotechnical classes.

Land-Use Map

The wide use of land-use maps in almost every susceptibility analysis witnesses the importance always given to this parameter. Notwithstanding we agree with those authors that recognized problems in the use of land use maps as predictor variables when applied to landslide susceptibility models (Van Den Eeckhaut et al. 2006). Indeed many ancient or dormant landslides last activated decades or centuries years ago, when the land use (and climate) was very different from the current day. In the RER Apennines, in the last few centuries there has been widespread timber harvesting and agricultural development, more recently followed by a progressive and important abandonment of farming. In these conditions land use tends to be more a dependent variable rather than a causal one and it must be used with awareness. Trying to overcome its limitation, in this work we used the oldest release of the Land Use Map (24 classes), derived by 1976 aerial photo, in order to better represent the pre-landslide condition, at least for recent landslides.

DEM-Derived Maps

Starting from the 10x10m DEM we computed about 30 parameters. For several parameters, we also used different software and algorithms. With ArcGIS® we used the unique standard methods, based on the algorithm of ESRI, "Neighbourhood Method" (Srinivasan and Engel 1991), for basic geomorphometry and "D8" (O'Callaghan and Mark 1984) for basic hydrology. To test more advanced algorithms, we used the software SAGA-GIS (Conrad

2006) and algorithms like that of Zevenbergen and Thorne (1987) for basic geomorphometry and "D∞" (Tarboton 1997), for basic hydrology.

Despite of the large number of geo-morphometric parameters (Gallant and Wilson 2000), in literature we didn't find one able to describe the small scale terrain undulations (hummocky) that characterize areas like landslide accumulations, colluviums deposits, etc., affected by high tension stress/strain and, in general, recognisable as very landslide prone areas in field surveys.

To highlight this distinguishing morphology we had to devise a new parameter, conceptually similar to the Topographic Position Index (TPI) and Slope Position Index (SlPI) (Weiss 2001; Jenness 2006), which we called: Local Roughness Index (LRI) (Fig. 6).

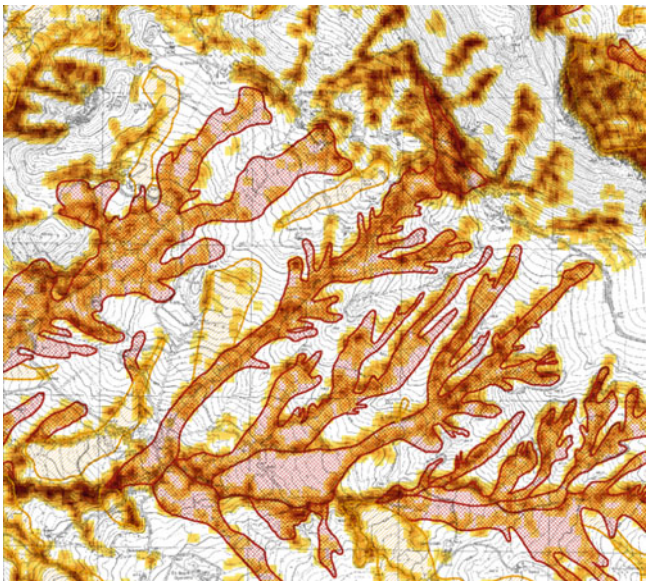

Fig. 6 Comparison between the "Local Roughness Index" (LRI) Map (*yellow to brown raster pixels*) and the LIM (polygons with cross hatch). It's noticeable the good agreement between the DEM-derived parameter and the Landslide Inventory Map

Preliminary Analysis of the Independents

At each point, 1's and 0's of the dataset, the corresponding value of all the variables (continuous and categorical), was extracted, producing the database for model calibration; then, each parameter was subject to several preliminary analyses to decide whether or not it should be included in the multivariate model.

Two different kinds of preliminary analysis were performed on the "candidate" predictor variables: (1) a collinearity matrix analysis between each combination of two variables and (2) a univariate test of association of each independent with the dependent, through a Bayesian analysis.

Independents Correlation

As with other statistical regression methods, logistic regression is sensitive to collinearity among the independent variables (Hosmer and Lemeshow 1989). Many of the independents, even if appreciably correlated with the dependent, should not be used at the same time in a multivariate model. Violating this conditional independence (CI) can severely bias the simulated maps by over- or underestimating landslide probabilities (Thierya et al. 2007). Thus we tested collinearity among all the variables and decided to exclude those with $R^2 \geq 0.5$ and use wisely those with $0.3 < R^2 < 0.5$.

Bayesian Test of Association

A bivariate test of association through the application of the Bayes theorem has been performed between the occurrence of each independent candidate and that of landslides (1's) and non landslide (0's) points. The Bayes Theorem is expressed by (4).

$$P(F|Xi) = \frac{P(Xi|F) \cdot P(F)}{P(Xi)} \tag{4}$$

where: $P(F(\ |\ Xi)$ is the "conditional probability" or "posterior probability", of occurrence of a landslide F, once given the presence of the analysed independent Xi and is constrained between 0 and 1. $P(Xi\ |\ F)$ is the conditional probability of Xi given F, also called "plausibility function"; $P(F)$ is the "prior probability", in the sense that it does not take into account any information about Xi; $P(Xi)$ is the "marginal probability" of Xi and acts as a normalizing constant. The application of (4) leads to graphics like those of Fig. 7. Figure 7 shows that landslide probability does not change significantly with variations in Aspect, whereas an increase in Slope generates a rapid increase in probability, reaching a maximum for about 20°, tending to lower, stabilize and rise again for high slope values (even if it shows an unstable behaviour).

Based on these observations, we can say, for instance, that Slope is an important causal factor and must be used in the LogR model while Aspect contribution is negligible and may be discarded. Graphs like Fig. 7 have been prepared for all variables, taken singularly or in "interference" with lithotechnic; the latter because we presumed the influence of many parameters varies depending on lithotechnical classes and disregarding this issue may lead to an excessive smoothing of the effect of the factors themselves. Figure 8 shows that this is an effective problem and should be considered in the final model.

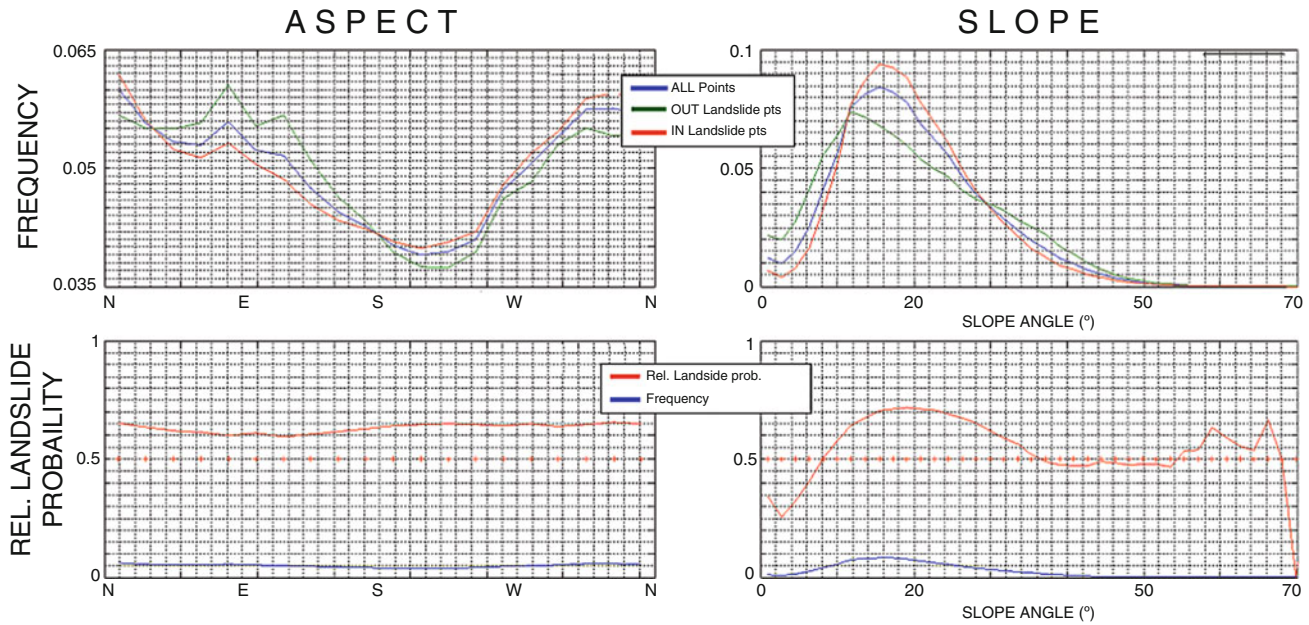

Fig. 7 Frequency distributions of 1's, 0's and total points and the "posterior landslide probability" calculated with (4). The graphs show the different effects of two independents variable on the conditional probability (or relative landslide probability), to have a landslide varying the value of the variable themselves

Logistic Regression Models (Calibration and Validation)

Like every statistical models, landslide prediction models have no scientific value unless the validity of the results is measured (Chung et al. 2002; Chung and Fabbri 2003a, 2005). Given that the "wait and see" validation is not feasible, as is usually done we randomly subdivided the dataset: 80 % of the dataset points were used for calibration and the remaining 20 % for validation. The apportionment of 80/20 has been chosen to maintain a good amount of data for the calibration phase, still leaving enough data for a comprehensible validation.

To test the "goodness of fit" of the model to the calibration data, we used the −2 Log Likelihood (−2LL) while to validate the model prediction performance we used the ROC (Receiver Operating Characteristic) (Swets 1988). ROC curves plot the proportion of false positives against the true positives at each level of the criterion and are an easy numerical and visual approach which compares a Boolean map of "reality" (presence or absence of landslides), with the probability map. The ROC area is the integral of the curve: a value of 0.5 corresponds to a random prediction while 1 equals a perfect model. The closer the result is to 1, the better the prediction performance we obtain.

Even with the same dataset (dependent and independents variables) and the same statistic method (LogR), the results can still be different, depending on the way the variables are combined together. Based on issues discussed before, we chose to test first of all single variable models, then multivariate models, increasing the number of the variables independently onset in the regression, and lastly, complex models with "interference" between variables, such as lithotechnic and slope (Fig. 8); this way we further guide the model, trying to get the best performance from the model itself. Table 1 shows the increase of performance of the different models calibrated on all landslides (irrespective of the activity state), starting from the easiest to the more complex ones.

The last model, that gave us the best prediction performance (0.78), comprises 2 categorical (Lithotechnic and Land-use) and eight continuous DEM derived variables [Elevation, Slope[2], Convergence Index Aspect (CI), Topographic Position Index (TPI), Local Roughness Index (LRI), Topographic Wetness Index (TWI)[3] , annual mean Solar Radiation (SR) and Drainage Density (DD)], and has the following formulation:

[2] We used the Zevenbergen and Thorne (1987) algorithm that performs better then others on sharp slope changes.

[3] For the flow accumulation we used the D∞ algorithm (Tarboton 1997), that performs much better then D8 to identify the accumulation/dispersion of water flow along the hillslopes.

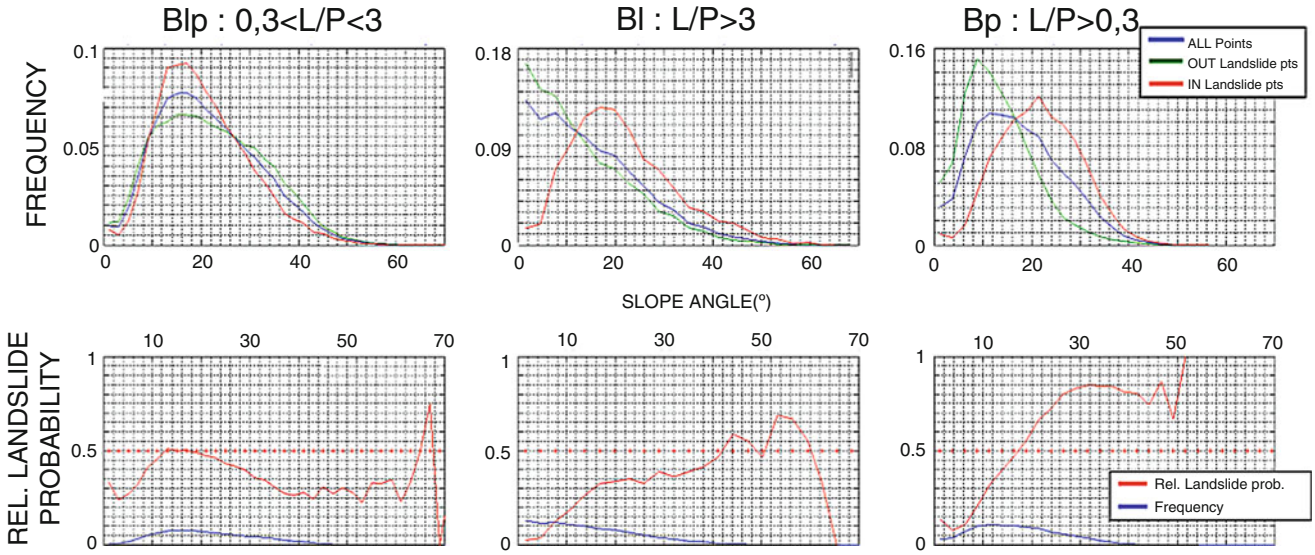

Fig. 8 These graphs are similar to those *right* of Fig. 7 but branched for different lithology (Flysch formations with different Arenitic/Pelitic ratio). We can note how the effect of slope on instability varies significantly on different lithotechnical classes and suggest the use of a multivariate model with "interference" between variables

$$Logit(\hat{P}) = Z = \beta_0 + \sum\sum \beta_{ij} X_i \cdot LIT_j + \sum\sum \beta_{ij} X_i \cdot USE_j \quad (5)$$

where Xi are the continuous variables, $LITj$ are the lithotechnical classes, $USEj$ are the land-use classes and the β are the parameters given by the LogR model for the best calibration fitting; in particular β_0 is the model intercept and β_{ij} are the regression parameters given to the variables combination.

The term "susceptibility" by definition is time-independent (Guzzetti et al. 1999), so that a susceptibility map would foresee the landslide prone areas at "indefinite time". With this assumption, a landslide susceptibility map should be calibrated on all LIM landslides, regardless of their last activation or present activity state. Unfortunately, using all landslides may produce several "side effects":

1. The land-use "independent" variable on ancient landslides is probably more a landslide dependent variable than one affecting them (section ". Land-Use Map");
2. Morphology can slowly evolve due to weathering, erosion, etc. and the depletion area morphology of an ancient landslide may be totally remodelled, especially in a territory like RER Apennines which, over the last few centuries, has undergone important human changes;
3. Reconnaissance of old and ancient landslides may be difficult, so landslide mapping may be much less accurate than for recent or active landslides.

Each of these issues can negatively influence susceptibility map reliability. To overcome all of these problems, we might consider calibrating the model only on landslides mapped as active; this way we can:

1. Be more confident about the reliability of the independent variables significance;
2. We further introduce a sort of "temporal information" which, even if it does not lead to a really definable "hazard map", it gives some more useful information at a time scale compatible with long term land-use planning.

After the modelling described above, we tested the model of (5) only on the 38,178 active landslides and the ROC area lunged up from 0.78 to 0.85. Figure 9 shows that the red line represents much better results: it says that, at a certain level of territory stated as unstable (specificity), the model can locate many more landslide areas (sensitivity); in opposite, to predict a certain amount of landslides (Y), it produces fewer "false alarms"(X). For this performance and for the advantages described above, we decided to adopt this latter model as the final susceptibility model.

Table 1 Index of the models tested and relative improvement in fit (decrease in − 2LL) and prediction performance (ROC area)

Dependent variables		−2LL	ROC area	
Costant		312137.35	0.500	
Slope		310447.42	0.574	Single variable
Convergence index aspect		307924.03	0.610	
Topographic wetness index		310215.97	0.534	
Drainage density		311982.11	0.495	
Solar radiation		312024.55	0.505	
Local roughness index		310295.37	0.562	
Topographic position index		312044.96	0.515	
Lithomap		292630.20	0.659	
Land cover		300084.88	0.635	
Climate		305367.60	0.593	
Slope position index		307445.30	0.554	
Slope	add lithomap	285515.60	0.691	Two summed variables
Convergence index aspect		288682.80	0.681	
Topographic wetness index		289122.20	0.673	
Drainage density		292629.30	0.662	
Solar radiation		292605.20	0.659	
Local roughness index		288889.30	0.678	
Land use		285285.50	0.688	
Slope	interference with lithomap	281285.02	0.703	Two variables with interference
Convergence index aspect		307533.01	0.612	
Topographic wetness index		292501.79	0.663	
Drainage density		294854.76	0.656	
Solar radiation		293446.81	0.657	
Local roughness index		302688.37	0.609	
Topographic position index		309827.62	0.554	
Sum of all the factors stand alone		268332.60	0.747	Complex models
Sum of all the factors stand alone + all the factors with interference with lithomap		260578.34	0.763	
Sum of all the factors with interference with lithomap + all the factors with interference with land use		253929.30	0.780	

Figure 10 shows the differences in the susceptibility frequency distributions calculated for points "outside landslide boundaries" (0's) and "landslide points" (1's). We can note a significant difference between the two groups, nevertheless there are many 0's with high and 1's with low susceptibility. The former is probably because either they are not recognized as landslides or simply have a high level of landslide susceptibility; the latter are more difficult to explain but the reasons may be as follows:

1. They belong to old landslides, probably stabilized or with the original morphology strongly modified;
2. The triggering phase has been affected by local factors not accounted for in the model (like human interference, structural issues, etc.);
3. Because for LIM cartography limits and automation of the points selection, they wrongly fall within stable areas.

Figure 11 breaks down the 1's distribution of Fig. 13 into active and dormant landslide points. Here we can appreciate the greatest significance of active points with respect to the dormant ones (we must, in any case, bear in mind that the model has been calibrated only on active landslides, so this result for dormant landslides was to be expected).

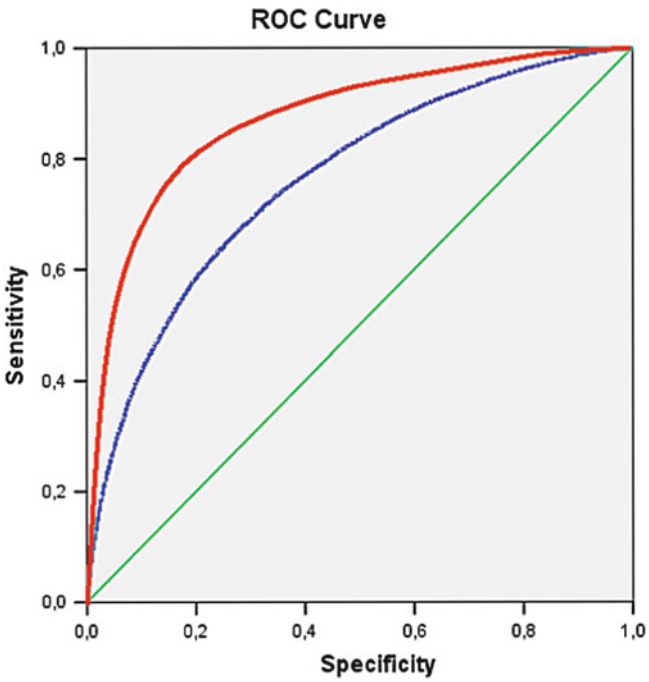

Fig. 9 ROC curves. – the *green* line represents a random forecast (only the intercept is included in the model – area = 0.5). The *blue* line represents the performance of the model calibrated on all landslides (0.78) while the *red* one the model calibrated only on active landslides (0.85)

Multivariate Versus Monovariate Approach

We compared the LogR method with a monovariate approach: the Frequency Ratio model. In this last, every independent variable is categorized and the frequency of observed unstable points is evaluated for each class of each regressor. The final susceptivity index (SI) is obtained by summing the frequency of the regressors values (divided by the variables number).

The comparison shows that considering simpler combination of independent variables, the monovariate approach is even better than the multivariate one, but increasing the complexity (adding more regressors and interactions), the gain of the multivariate approach is higher (Fig. 12).

Results

Combining in ArcGIS the coefficients obtained by LogR with the (5) and performing the inverse transformation of (1), we obtained the map of P which represents the "landsliding susceptibility" of the whole RER Apennine (Fig. 13). The pixel value ranges from 0 to 1 and can be considered as the probability for each cell to be the source of a landslide.

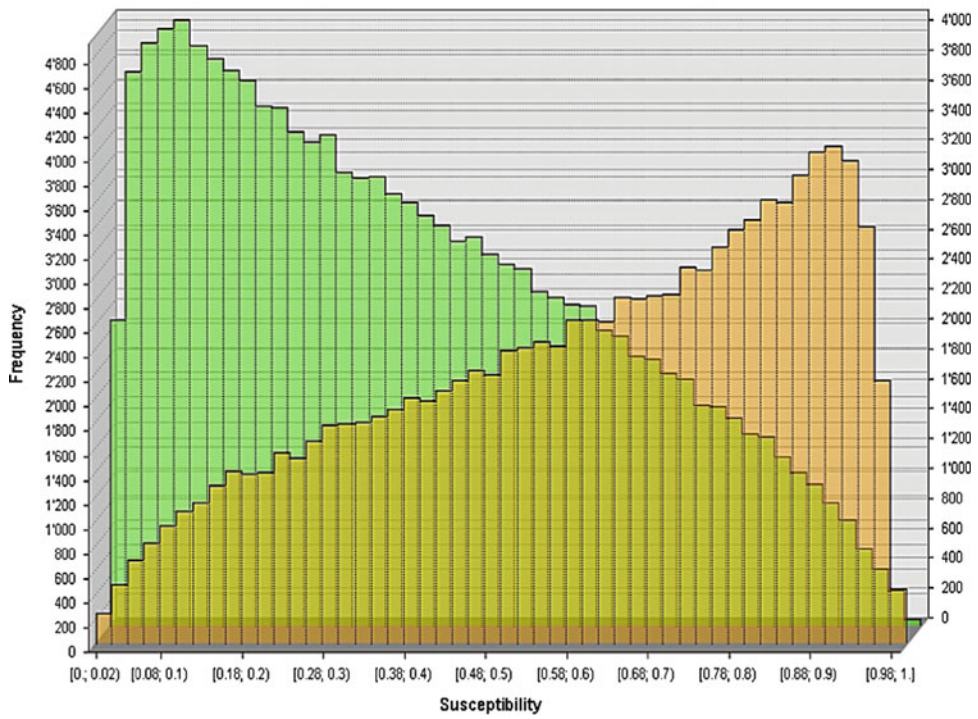

Fig. 10 Comparison between the frequency distributions of susceptibility calculated by the model of (5) for 0's (*green* – mean = 0.37) and 1's without distinction between active and dormant landslides (*orange* – mean = 0.61)

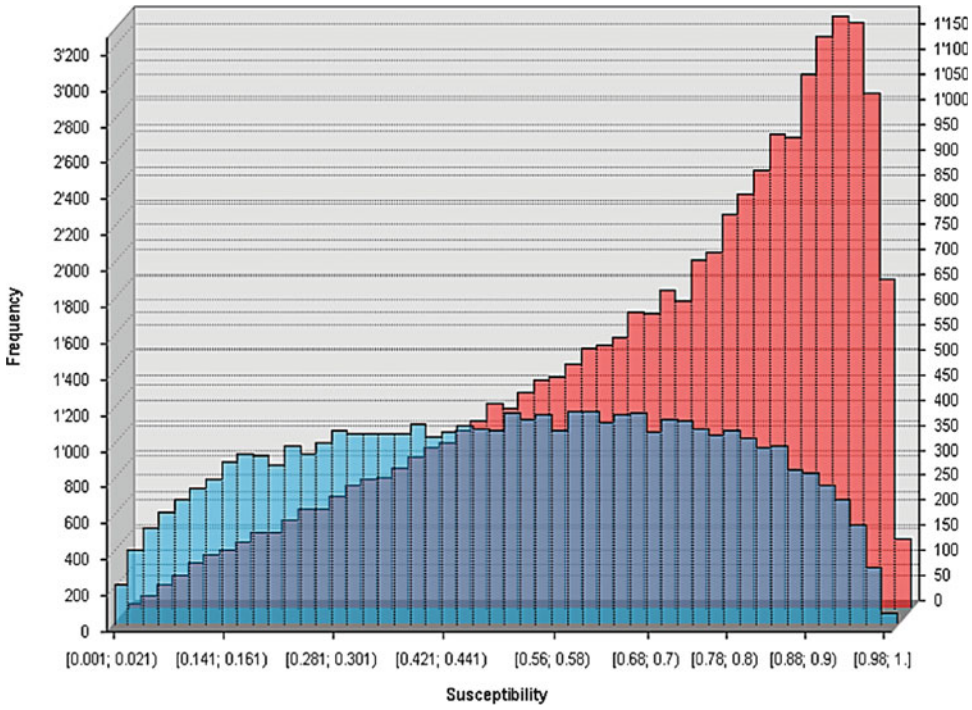

Fig. 11 Comparison of the frequency distribution of susceptibility calculated by the last model for dormant (*blue* – mean = 0.50) and active (*red* – mean = 0.68) landslides

COMPLEXITY

Mod.	LogR	Freq. Ratio
1	0.573 ± 0.004	0.623 ± 0.004
2	0.696 ± 0.004	0.709 ± 0.004
3	0.708 ± 0.004	0.725 ± 0.004
4	0.759 ± 0.004	0.755 ± 0.004
5	0.769 ± 0.004	0.743 ± 0.004
6	0.773 ± 0.004	0.747 ± 0.004

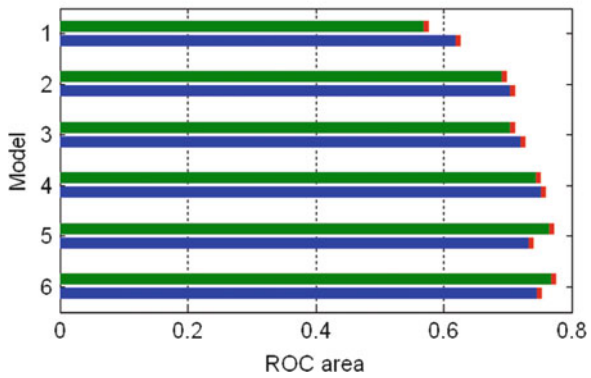

Fig. 12 Comparison of model performance: LogR (*green bars*) verus Frequency Ratio (*blue bars*) models

The resolution in the above image of Fig. 13 doesn't do justice to the product detail but shows the overall area and the lithological guided pattern of susceptibility (compare Figs. 1 and 13). Below there are two subsequent enlargements. In the lower right enlargement the LIM has been overlaid in order to compare the details of the resultant map with the depletion areas of the mapped landslides and their tendency to retrogressive and widening evolutions; note how, in the same lithotechnical class, susceptibility varies rapidly and greatly, concentrating on medium and steep slopes and slightly concave areas. Interpreting the map, in any case, it is crucial to bear in mind that it aims to identify the triggering areas and not the further evolution (runout) of displaced material; for this reason the "green areas" on mapped landslides, particularly if morphologically depressed, must not be presumed to be "stable areas" but areas less prone to be affected by a local landslide activation.

Discussion and Conclusions

RER Apennine is affected by a huge number of landslides which results in a mean landslide index of ~24 %. The absence of a susceptibility map covering the entire RER area with a high detail level and the heterogeneity of the area, led us to develop and apply a statistical method based on the singularity of the territory.

In this work we have tried to emphasize how the appropriateness of modellization relies not so much on statistical method choice, as on:

1. The amount and quality of the LIM input data;
2. The appropriateness of preliminary choices, that can be called the "conceptual framework", to fit the specificity of the target landslide.

In particular, we aimed to predict the areas more likely to generate new landslide events or actual landslide backward

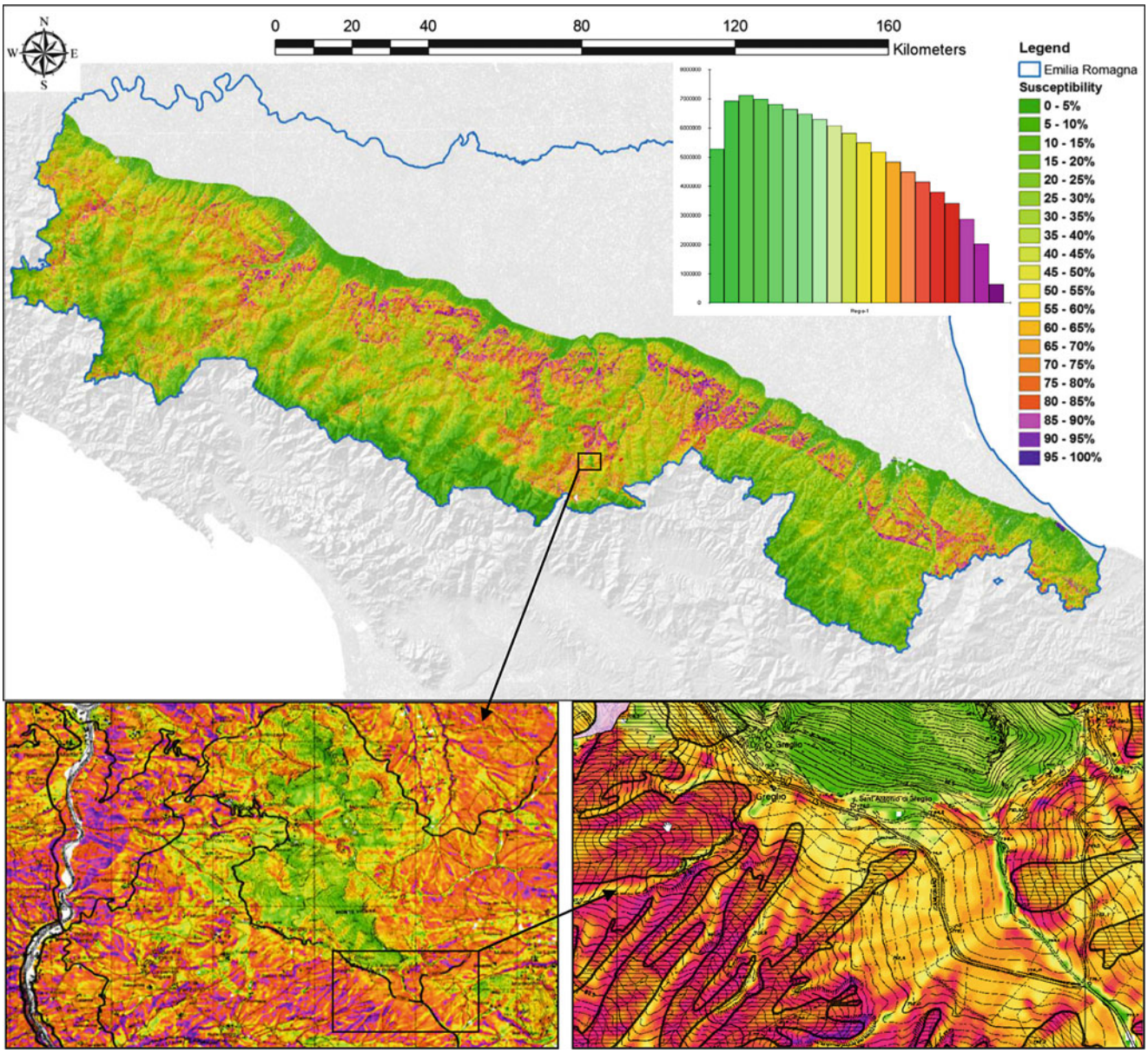

Fig. 13 Susceptibility map of the whole RER Apennine (above: 28,650 × 14,459 10 × 10 m cell map – 113,840,217 actually calculated – mean susceptibility = 0.41; σ = 0.25). The histogram shows the frequency distribution of the susceptibility all over the area. Below two progressive enlargements of the resulting map. On the *lower right* the susceptibility map with the LIM overlaid (*black striped hatch polygons*)

evolution. With the used approach it's been possible to focus the modellization on the starting processes (landsliding), correlated with the triggering area conditions, instead of on the effects (landslides accumulations). We believe that this approach is generally preferable and the result is in any case helpful in identifying the landslides (usually small), not reported in the LIM or improving it's polygons quality (Fig. 13).

Despite of the detailed scale of the input map that it requires, by means of the 10 × 10 m DEM we can develop high resolution maps for detailed field applications; furthermore, unlike a small scale product, which does not allow zooming in for further detail, such a detailed map can be generalized in many ways to be used for smaller scale applications.

On the other hand, as every other kind of model, unavoidable assumptions and simplifications lead to shortcomings and limitations that should be always highlighted by modellers and properly understood by final users. Table 2 briefly summarizes the main assumptions and simplifications of our choices and the shortcomings which each of these produces.

Table 2 Report of the main model shortcomings

Model feature	Shortcomings
Retrogressive triggering model	It cannot predict landslides triggered by slope undercut or for block reactivation of part of the landslide accumulation
Small base unit (cells 10 × 10m)	With this cell dimension the morphometric parameters are often significant for an area just a few dozen linear metres wide, so we cannot foresee landslides which, in the triggering area, present dimensions of many dozens or hundreds of metres[a]
Model with high morphological and no structural components	We cannot foresee landslides which are strongly influenced by structural tectonics, bedrock- strata/ hillslope relationship (like for rock-slides), particular hydro-geological circulations (like permeability contrast, faults circulations, etc.)[a]
Model calibrated on slides, flows and complex landslides	We cannot foresee different types of movements (rockfalls, topples, lateral spreadings, DGPV, etc.)
Model designed to predict the triggering areas	There are no hints about the magnitude of possible landslides, nor about their downslope evolution (runout) or retrogression upslope; It is landscape knowledge that must address an ostensible evolution scenario. Particular attention may be paid in assuming as stable many areas which, for instance because of their low slope, may be classified at low susceptibility: they actually may be landslide accumulations, then the susceptibility map has always to be used in conjunction with LIM

[a]Anyway those kind of landslides would be hardly ascribed to the group of shallow landslides

Some of the issues depicted in Table 2 can be overcome with different (but potentially complementary) approaches and modellizations. It'll be nonetheless easy in a GIS environment to develop different models for different landslide specificity and overlay or merge someway the different results. For instance a further development and application of the presented model we've worked on to overcome the lack of landslide evolution forecast (runoff area), partially uses the output of the presented model to predict the mapped landslides reactivation likelihood.

The mapped landslide reactivation likelihood model will be published in a further paper.

Joining a detailed and updated LIM with the forecast information given by these kind of models (even if black box type), may results in a virtuous growing of knowledge and, hopefully, a better land use planning.

References

Akgün A, Fikri B (2007) GIS-based landslide susceptibility for Arsin-Yomra (Trabzon, North Turkey) region. Environ Earth Sci 51(8):1377–1387

Aleotti P, Chowdhury R (1999) Landslide hazard assessment: summary review and new perspectives. Bull Eng Geol Environ 58:21–44

APAT (2007) Rapporto sulle frane in Italia. Il progetto IFFI: metodologia, risultati e rapporti regionali. Rapporto 78/2007, Roma

Atkinson PM, Massari R (1998) Generalized linear modelling of susceptibility to landsliding in the central Apennines, Italy. Comput Geosci 24(4):373–385

Ayalew L, Yamagishi H (2005) The application of GIS-based logistic regression for landslide susceptibility mapping in the Kakuda-Yahiko Mountains, Central Japan. Geomorphology 65:15–31

Bai SB, Wang J, Pozdnoukhov A, Kanevski M (2008a) Validation of spatial prediction models for landslide susceptibility maps. In: Proceedings of the 8th international symposium on spatial accuracy assessment in natural resources and environmental sciences, Shanghai, 25–27 June 2008, pp 280–286

Bai SB, Wang J, Zhang F Y, Pozdnoukhov A, Kanevski M (2008b) Prediction of landslide susceptibility using logistic regression: a case study in Bailongjiang River Basin. In: Proceedings of the fifth international conference on fuzzy systems and knowledge discovery, Vol4, China, pp 647–651

Begueria S, Lorente A (1999) Landslide hazard mapping by multivariate statistics; comparison of methods and case study in the Spanish Pyrenees. The Damocles Project Work, Contract No EVG1-CT 1999–00007. Technical Report, 20p

Bertolini G, Canuti P, Casagli N, DE Nardo MT, Egidi D, Galliani G, Genevois R, Mainetti M, Pignone R, Pizziolo M, Pomi L, Zinoni F (2002) Carta della Franosità della Regione Emilia-Romagna ai fini di Protezione Civile. Regione Emilia-Romagna e CNR-GNDCI, 110p

Bertolini G, Pizziolo M (2008) Risk assessment strategies for the reactivation of earth flows in the Northern Apennines (Italy). Eng Geol 102(3–4):178–192

Cardinali M, Carrara A, Guzzetti F, Reichenbach P (2002) Landslide hazard map of the upper Tiber River basin, Italy. Publication GNDCI no 2634. SystemCart, Roma

Carrara A (1983) Multivariate models for landslide hazard evaluation. Math Geol 15(3):403–427

Carrara A, Cardinali M, Detti R, Guzzetti F, Pasqui V, Reichenbach P (1990) Geographical information systems and multivariate models in landslide hazard evaluation. In: ALPS 90 Alpine landslide practical seminar, sixth international conference and field workshop on landslides, Università degli Studi di Milano, Milan, 31 Aug–12 Sept, pp 17–28

Carrara A, Cardinali M, Guzzetti F, Reichenbach P (1995) GIS technology in mapping landslide hazard. In: Guzzetti F, Carrara A (eds) Geographical information systems in assessing natural hazards. Kluwer Academic, Dordrecht, pp 135–175

Cerrina Feroni A, Martelli L, Martinelli P, Ottria G (2002) Structural-Geological map of the Emilia-Romagna Apennines. Selca Ed, Firenze

Chung CF, Kojima H, Fabbri AG (2002) Stability analysis of prediction models for landslide hazard mapping. In: Allison RJ (ed) Applied geomorphology: theory and practice. Wiley, London, pp 1–19

Chung CF, Fabbri AG (1999) Probabilistic prediction model for landslide hazard mapping. Photogramm Eng Remote Sensing 65(12)

Chung CF, Fabbri AG (2003a) Validation of spatial prediction models for landslide hazard mapping. Nat Hazards 30:451–472

Chung CF, Fabbri AG (2003b) On some weak points of quantitative landslide hazard zonation. In: Proceedings of the IAMG 2003, Portsmouth, 7–12 Sept

Chung CF, Fabbri AG (2005) Systematic procedures of landslide hazard mapping for risk assessment using spatial prediction models. In: Glade T, Anderson M, Crozier MJ (eds) Landslide hazard and risk. Wiley, Chichester, pp 139–174

Chung CF (2006) Using likelihood ratio function for modeling the conditional probability of occurrence of future landslides for risk assessment. Comput Geosci 32(8):1052–1068

Conrad O (2006) SAGA – Program structure and current state of implementation. In: Böhner J, McCloy KR, Strobl J (eds) SAGA – Analysis and modelling applications, vol 115. Verlag Erich Goltze GmbH, Göttingen, pp 39–52

Crosta G, Frattini P, Sterlacchini S (2001) Valutazione e gestione del rischio da frana. Regione Lombardia, Milano

Cruden DM, Varnes DJ (1996) Landslide types and processes. In: Turner AK, Schuster RL (eds) Landslides: investigation and mitigation, Special report. National Academy Press, Washington, DC, pp 36–75

Dai CF, Lee CF (2003) A spatiotemporal probabilistic modeling of storm-induced shallow landslide using aerial photographs and logistic regression. Earth Surf Proc Land 28:527–545

Dai FC, Lee CF, Ngai YY (2002) Landslide risk assessment and management: an overview. Eng Geol 64(1):65–87

Gallant JC, Wilson JP (2000) Terrain analysis: principles and applications. Wiley, New York, p 472

Glade T (2001) Landslide hazard assessment and historical landslide data – an inseparable couple? In: Glade T, Frances F, Albini P (eds) The use of historical data in natural hazard assessments, Advances in natural and technological hazards research. Kluwer Academic, Dordrecht, pp 153–168

Gorsevski PV, Gessler P, Foltz RB (2000) Spatial prediction of landslide hazard using logistic regression and GIS. In: Proceedings of the 4th international conference on integrating GIS and environmental modeling. Alberta, 9p

Guzzetti F, Carrara A, Cardinali M, Reichenbach P (1999) Landslide hazard evaluation: a review of current techniques and their application in a multi-scale study, Central Italy. Geomorphology 31:181–216

Hosmer DW, Lemeshow S (1989) Applied regression analysis. Wiley, New York, p 307

Hutchinson JN, Bhandari RK (1971) Undrained loading, a fundamental mechanism of mudflow and other mass movements. Geotecnique 21:353–358

Hutchinson JN (1988) Morphological and geotechnical parameters of landslides in relation to geology and hydrogeology. In: Proceedings of the 5th international symposium on landslides, Vol 1. Lausanne, pp 3–35

Hutchinson JN (1995) Landslide hazard assessment. In: Bell DH, Balkema AA (eds) Landslides. Balkema, Rotterdam, pp 1805–1841

King G, Zeng L (2001) Logistic regression in rare events data. Political Anal 9:137–163

Jenness J (2006) Topographic Position Index (tpi_jen.avx) extension for ArcView 3.x, v. 1.3a. Jenness Enterprises. http://www.jennessent.com/arcview/tpi.htm

Lee S (2005) Application of logistic regression model and its validation for landslide susceptibility mapping using GIS and remote sensing data. Int J Remote Sens 26(7):1477–1491

Lee S, Min K (2001) Statistical analysis of landslide susceptibility at Yongin. Korea Environ Geol 40:1095–1113

Lee CT, Huang CC, Lee JF, Pan KL, Lin ML, Dong JJ (2008) Statistical approach to storm event-induced landslides susceptibility. Nat Hazards Earth Syst Sci 8:941–960

Leroueil S, Locat J, Vaunat J, Picarelli L, Lee H, Faure R (1996) Geotechnical characterization of slope movements. In: Proceedings of the 7th international symposium on landslides, Vol 1. Trondheim, pp 53–74

Moore ID, Grayson RB, Ladson AR (1991) Digital terrain modelling: a review of hydrological, geomorphological and biological applications. Hydrol Proc 5:3–30

O'Callaghan JF, Mark DM (1984) The extraction of drainage networks from digital elevation data. Comput Vision Graphics Image Proc 28:328–344

Ohlmacher CG, Davis CJ (2003) Using multiple regression and GIS technology to predict landslide hazard in northeast Kansas, USA. Eng Geol 69:331–343

Rossi M, Guzzetti F, Reichenbach P, Mondini AC, Peruccacci S (2010) Optimal landslide susceptibility zonation based on multiple forecasts. Geomorphology 114:129–142

Srinivasan R, Engel BA (1991) Effect of slope prediction methods on slope and erosion estimates. Appl Eng Agric 7(6):79–783

Suzen ML, Doyuran V (2003) A comparison of the GIS based landslide susceptibility assessment methods: multivariate versus bivariate. Environ Geol 45(8):665–679

Swets JA (1988) Measuring the accuracy of diagonstic systems. Science 204(4857):1285–1293

Tarboton DG (1997) A new method for the determination of flow directions and upslope areas in grid digital elevation models. Water Res Res 33(2):309–319

Thierya Y, Maleta JP, Sterlacchini S, Puissant A, Maquairea O (2007) Landslide susceptibility assessment by bivariate methods at large scales: application to a complex mountainous environment. Geomorphology 92(1–2):38–59

Vanacker V, Vanderschraeghe M, Govers G, Willems E, Poesen J, Deckers J, De Bievre B (2003) Linking hydrological, infinite slope stability and land-use change models through GIS for assessing the impact of deforestation on slope stability in high Andes watersheds. Geomorphology 52:299–315

Van Den Eeckhaut M, Reichenbach P, Guzzetti F, Rossi M, Poesen J (2009) Combined landslide inventory and susceptibility assessment based on different mapping units: an example from the Flemish Ardennes, Belgium. Nat Haz Earth Syst Sci 9:507–521

Van Den Eeckhaut M, Vanwalleghem T, Poesen J, Govers G, Verstraeten G, Vandekerckhove L (2006) Prediction of landslide susceptibility using rare events logistic regression: a case-study in the Flemish Ardennes (Belgium). Geomorphology 76:392–410

Van Westen CJ, van Asch TWJ, Soeters R (2006) Landslide hazard and risk zonation – why is it still so difficult? B Eng Geol Environ 65:167–184

Varnes DJ (1978) Slope movement types and processes. In: Schuster RL, Krizek RJ (eds) Landslides analysis and control: national research council, vol 176, Transportation research board, Special report. Transportation Research Board, Washington, DC, pp 11–33

Wang HB, Sassa K, Xu WY (2007) Assessment of landslide susceptibility using multivariate .logistic regression: a case study in Southern Japan. Environ Eng Geosci 13:183–192

Wang HB, Liu G, Xu WY, Wang G (2005) GIS-based landslide hazard assessment: an overview. Prog Phys Geography 29:548–567

Weiss A (2001) Topographic position and landforms analysis. In: Poster presentation. ESRI User Conference, San Diego

WP/WLI (1993) A suggested method for describing the activity of a landslide. Bull Int Ass Eng Geol 47:53–57

Zevenbergen LW, Thorne CR (1987) Quantitative analysis of land surface topography. Earth Surf Proc Landf 12:47–56

Zêzere JL (2002) Landslide susceptibility assessment considering landslide typology, a case study in the area north of Lisbon (Portugal). Nat Hazard Earth Syst Sci 2:73–82

Methods for Shallow Landslides Susceptibility Mapping: An Example in Oltrepo Pavese

Claudia Meisina, Davide Zizioli, and Francesco Zucca

Abstract

The principal aim of this study is to compare different landslide susceptibility zonation models for predicting areas prone to shallow landsliding using both physically distributed landslide models and artificial neural networks. Necessary geotechnical and hydrological parameters were obtained coupling sample laboratory analysis and in situ measures; soil thickness was estimated using an empirical model while distribution of rainfall intensity was analyzed by performing a spatial interpolation. The predictive capabilities of these models were finally evaluated using a threshold-independent quantitative method (the ROC plot).

Keywords

Shallow landslide • Physically based models • Artificial neural network

Introduction

Shallow landslides are triggered by intense rainfall of short duration. Even though they involve only small portions of hilly and mountainous terrains, they are the cause of heavy damages to people and infrastructures. The identification of shallow landslide-prone areas is a necessity to plan mitigation measures. On a regional scale physically-based models have been extensively used to determine both the timing and the localization of shallow landslides (e.g. Montgomery and Dietrich 1994; Pack et al. 1998; Baum et al. 2002). Statistical spatial models, such as Weight of Evidence, Fuzzy Logic, Logistic Regression, and Neural Networks, have also grown in number in the recent years to predict shallow slides occurrence (Ermini et al. 2004; Gómez and Kavzoglu 2005).

Oltrepo Pavese, which is located in the Northern Apennines of Italy, is characterized by high density of mass movements and has historically suffered from widespread damage from landslides. More recently extreme rainfall events have triggered shallow landslides in areas which were not yet affected by these types of landslides. An important event happened subsequently to rapid snowmelt and intense rainfall in April 2009.

The main goal of this research is to evaluate the predictability of shallow landslide occurrence of April 2009 event using three physically based models: SHALSTAB (Montgomery and Dietrich 1994), SINMAP (Pack et al. 1998) and TRIGRS (Baum et al. 2002), comparing them with the results obtained by Artificial Neural Networks (ANNET), in order to highlight potential and limitation of these models for the forecasting of the potential source areas.

The Study Area

Geological Setting

The Oltrepo Pavese, which is situated in Northern Italy, has an extension of about 1,100 km^2. A test area, corresponding to the surrounding of the Recoaro valley, with an extension of 17.5 km^2, was selected in the sector of Oltrepo Pavese with the highest density of the April 2009 landslides (Fig. 1). The test site slopes are characterized by medium-high

C. Meisina (✉) • D. Zizioli • F. Zucca
Department of Earth and Environmental Sciences, University of Pavia, Via Ferrata n°1, Pavia 27100, Italy
e-mail: claudia.meisina@unipv.it

C. Margottini et al. (eds.), *Landslide Science and Practice*, Vol. 1,
DOI 10.1007/978-3-642-31325-7_58,

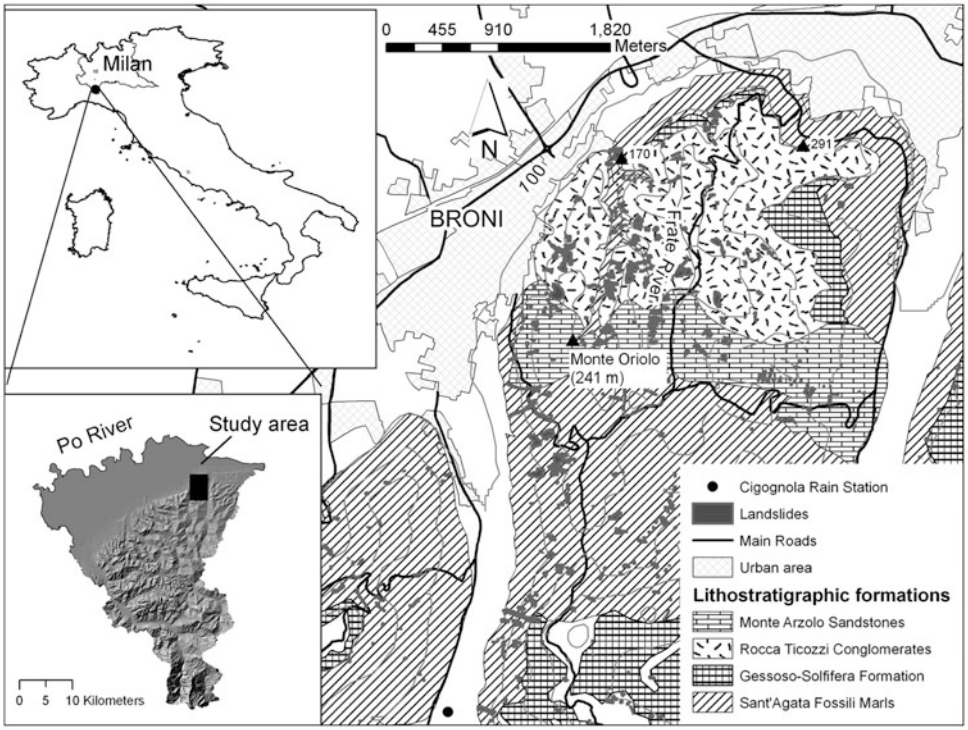

Fig. 1 Geological sketch map and location of the shallow landslides triggered by the 26–27 April 2009 rainfall event

gradient (40 % of the area have slope gradient higher than 15°) and are made up of marls (S. Agata Fossili Marls) and of gravel, sand and poorly cemented conglomerates (M. Arzolo Sandstones and Rocca Ticozzi Conglomerates). A small portion of the area is characterized by the presence of Gessoso-Solfifera Formation (marls, sandy marls and vacuum limestones with lens of gypsum-rudites containing gypsum selenite). The strata dip towards the E-NE. Colluvial soils, derived by the weathering of the bedrock, have a thickness ranging from 0.5 m to 2–3 m at the bottom of the valley.

The April 2009 Event

The 27th and 28th April 2009 the north-eastern sector of Oltrepo Pavese experienced an extreme rainfall event. On April 28th a rain-gauge station (Cigognola) recorded 160 mm of rain in 62 h (~20 % of the annual average amount) with 22 mm/h maximum rainfall intensity. The April 2009 event occurred after a rather wet winter season with intense snowfall. The rainfall data show a distinct rainfall peak occurred at 9 p.m.; after this peak several shallow landslides were triggered causing fatal victim and damaging/blocking roads in several places.

Color aerial photographs taken immediately after the events in the north-eastern part of Oltrepo Pavese with a spatial resolution of 15 cm were studied in order to map the existing landslides.

Detailed field surveys have been carried out to detect: slope failures characteristics, site geomorphology, the thickness of failed soils, the presence or absence of groundwater seepage, and the location of landslides with respect to land use.

For some landslides a detailed stratigraphic profile was constructed and samples were collected for laboratory investigations (grain size distribution, dry densities, Atterberg Limits, direct shear tests).

Aerial photo-interpretation coupled with field surveys revealed that the rainfall event of April 2009 triggered about 1,600 landslides in the north-eastern sector of Oltrepo Pavese. At least 492 landslides occurred in the Recoaro valley and adjacent areas (Fig. 1).

The slides occurred mainly in colluvial soils. Most of the slides were shallow (thickness usually from 0.5 to 2 m) with the failure surface located along the contact between the colluvial cover and the weathered bedrock; sometimes they involved portions of bedrock.

Landslides appear on SW-NE oriented slopes and were observed in the slope range from 16° to 37°. The landslide frequency is higher for slope angles between 25° and 30° and tends to decline with an increasing or decreasing slope angle. Most of the landslides tended to concentrate in areas of slope angle change (e.g., from a gentle slope to a steep slope).

Changes in land cover have played a major role in landslide occurrence and distribution in the study area. From 1980 to 2009 woodland increased from 8 % to 45 % as a consequence of recolonisation of abandoned vineyards. The

roots extend generally in the first meters of the soil profile and are involved in the landslide. In the abandoned vineyards the old tillage pattern oriented across the maximum slope gradient allow also the concentration of water. This explains the occurrence of a great number of landslides in correspondence of the woodlands.

According to USCS classification the majority of the analyzed samples are non plastic or slightly plastic soils (CL). Coarse fragments consisting in marls or sandstone derived from the underlying bedrock are also present in the colluvial deposits. In particular, dry density ranges between 15 and 16.3 kN/m^3 and porosity ranges between 0.38 and 0.48. Shear strength parameters show a friction angle in the range of 23°÷32° (the highest values correspond to the colluvial soils of the Rocca Ticozzi Conglomerates and M. Arzolo Sandstones formations); the effective cohesion ranges between 0 and 10 kPa.

The Materials and Methods

The Models

SINMAP outputs the stability index value (SI) (Pack et al. 1998). The stability index is defined as the probability that a location is stable assuming uniform distributions of the parameters over the uncertainty ranges. This value ranges between 0 (most unstable) and 1 (stable). Where the most conservative set of parameters in the model results in stability, the stability index is defined as the factor of safety at this location.

SHALSTAB predicts the steady state rainfall necessary for slope failure throughout a study area (Montgomery and Dietrich 1994). The output is represented by critical rainfall qcr: areas with lower qcr are interpreted as more susceptible to shallow landsliding, whereas areas with higher qcr are interpreted as more stable, as a less frequent rainfall event would be required to cause instability. Thus the spatial distribution of critical rainfall expresses the potential for shallow landslide initiation. If tanθ (θ = slope angle) equals or exceeds tanϕ (ϕ = soil friction angle) slope instability will occur even under dry conditions according to the model. This category of instability is called "chronic". If tanθ < tanϕ (1 − ρw/ρs) (ρs = wet soil density, ρw = the density of water), then slope instability is unlikely as ground is not expected to fail even at saturation. Grid cells falling into this category are ranked as "stable"

TRIGRS (Transient Rainfall Infiltration and Grid-based Regional Slope-stability analysis) model is coded in Fortran and is designed for modelling the potential occurrences of shallow landslides by incorporating the transient pressure response to rainfall and downward infiltration processes (Baum et al. 2002; Baum et al. 2008). Under assumption of saturated or tension-saturated initial soil conditions, the TRIGRS program computes transient pore-pressure changes to find analytical solutions to partial differential equations, representing one-dimensional vertical flow in isotropic, homogeneous materials due to rainfall infiltration from storms with durations ranging from hours to a few days. The TRIGRS program uses an infinite slope model to compute a factor of safety (FS) calculation for each grid cell.

ANNET landslide susceptibility model employed in this study is based on the general concept of slope stability considering multiple factors acting on slopes, some of which can cause weakness and produce failure, whereas other factors strengthen the slope and thereby protect against movement (Ermini et al. 2004; Gómez and Kavzoglu 2005). A three-layer artificial neural network structure (Multilayer Perceptron, MLP), has been applied to the study area using Trajan 6.0 software (2001) and coupling as inputs terrain parameters derived from DEM and geological-geotechnical characteristics. Many networks have been developed using back propagation algorithm for testing. The best one in terms of accuracy was selected and the ROC curve (Beguería 2006; Cervi et al. 2010) was used to compute the second derivative, in order to obtain appropriate susceptibility classes.

The Input Data

A Digital Elevation Model (DEM) with grid size of 10 × 10 m provides the topographic basis.

For the analysis with TRIGRS and SINMAP the study area was divided into four regions, characterized by quite homogeneous in situ conditions and soil properties and corresponding to the lithostratigraphic units (Tables 1 and 2).

SINMAP allows uncertainty of the variables through the specification of lower and upper bounds. Formally these bounds define uniform probability distributions over which these quantities are assumed to vary at random.

For SHALSTAB the parameters are considered constant and uniformly spatially distributed all over the study domain The geotechnical and hydrological parameters have been calculated as weighted average of all the parameters.

The soil thickness was derived from field data collected after the April 2009 event. We used a geomorphologically indexed model based on the local slope angle, to the elevation (h) and to the topographic position (TP) (Fig. 2):

$$DTB = wm\left[h_{\max} - \frac{Z_i - Z_{\min}}{Z_{\max} - Z_{\min}} - (h_{\max} - h_{\min})\right] + \left[h_{\max}\left(1 - \frac{\tan\theta_i - \tan\theta_{\min}}{\tan\theta_{\max} - \tan\theta_{\min}}\left(1 - \frac{h_{\min}}{h_{\max}}\right)\right)\right] + \left[h_{\max} - \frac{TPn_i - TPn_{\min}}{TPn_{\max} - TPn_{\min}} - (h_{\max} - h_{\min})\right] \quad (1)$$

Table 1 Initial setting for the input parameters for SINMAP. *Cr* root cohesion [N/m^2], *C'* soil cohesion [N/m^2], θ slope angle, ρs wet soil density [kg/m^3], ρw density of water [kg/m^3]; *g* gravitational acceleration (9.81 m/s^2), *D* vertical soil depth [m], f the internal friction angle of the soil, *h [m]* soil thickness, *T* is the soil transmissivity [m^2/h], *R* steady state recharge [m/h]

	ϕ (°)		C = (Cr + C′)/(h g ρs)		T = k D (m2/h)		R (m/h)	T/R (m)	
Region	Min	Max	Min	Max	Min	Max		Min	Max
S. Fossili Marls	24	25.4	0.06	0.8	0.002	0.079	0.00021	11.83	371.88
R. T.Conglomerates	30	33.7	0.05	1.18	0.018	8.64	0.00021	84.52	40568.67
M. Arzolo Sandstones	23.3	29.9	0.03	0.72	0.021	8.64	0.00021	101.42	40568.673
Gessoso-Solfifera F.	22	27	0.09	0.83	0.001	0.086	0.00021	9.29	405.68

Table 2 Input parameters for TRIGRS

	ϕ (°)		C' [N/m^2]		ρs [kN/m^3]		k [m/s]	
Region	Min	Max	Min	Max	Min	Max	Min	Max
S. Fossili Marls	24	25.4	2,000	10,000	17.946	18.701	$1*10^{-6}$	$1*10^{-5}$
R. T.Conglomerates	30	33.7	2,000	10,000	17.455	19.122	$1*10^{-5}$	$1*10^{-4}$
M. Arzolo Sandstones	23.3	29.9	1,400	7,900	17.651	19.907	$1*10^{-6}$	$1*10^{-5}$
Gessoso-Solfifera F.	22	27	3,900	7,500	17.455	19.417	$1*10^{-6}$	$1*10^{-4}$

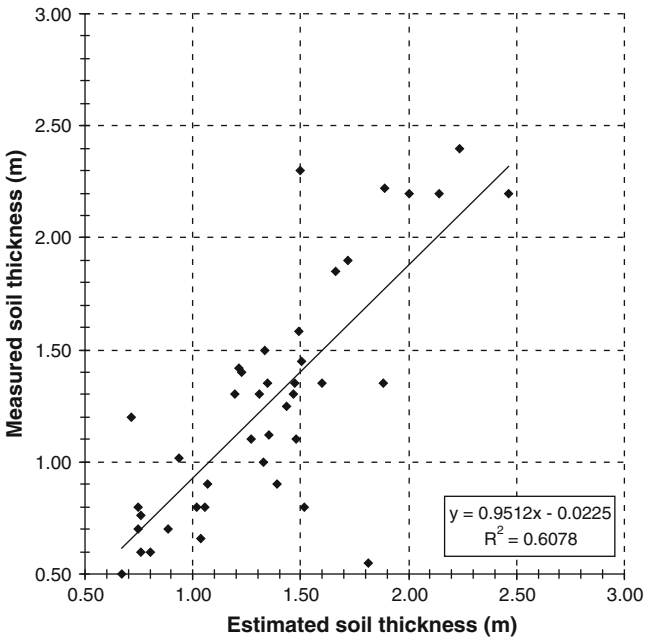

Fig. 2 Measured versus estimated soil thickness

Where *wm* is the weighted mean, h_{max} and h_{min} are maximum and minimum deep to bedrock, Z_i is the elevation in the point *i*, Z_{max}, Z_{min} the maximum and minimum elevations found in the area, θ is the slope angle, while *TPi* and *TPn* represent topographic position and normalized topographic position.

$$TPi = Zi - Mean(Zi) \tag{2}$$

$$TPn = \frac{1}{1 + \exp^{-TPi}} \tag{3}$$

The hourly rainfall intensities recorded in the Cigognola rain gauge during the April 2009 event were assumed as boundary conditions at the slope surface.

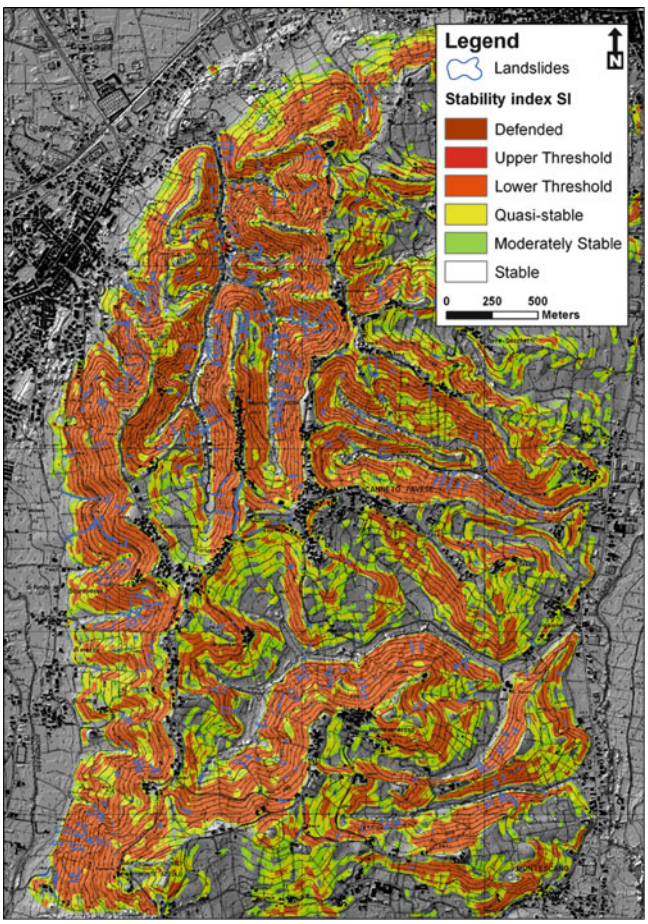

Fig. 3 Stability index map obtained by SINMAP

For SINMAP the ratio R/T combines both climate and hydrogeological factors (Table 1). The transmissivity T represents the water flow within the soil and was derived from the hydraulic conductivity (minimal and maximal). The parameter R (steady state recharge rate) is influenced

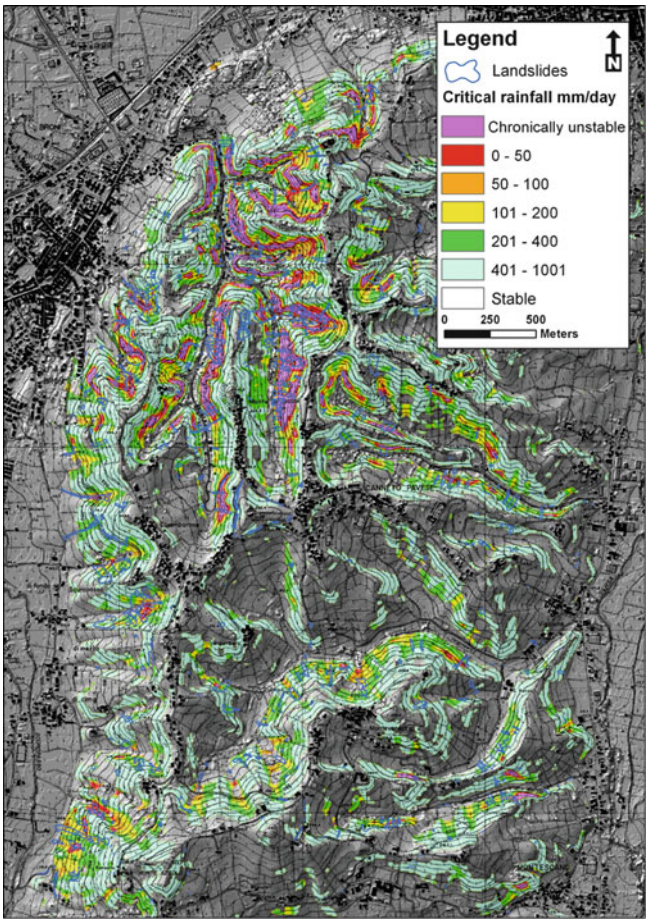

Fig. 4 Critical intensity of rainfall (mm/day) computed by SHALSTAB

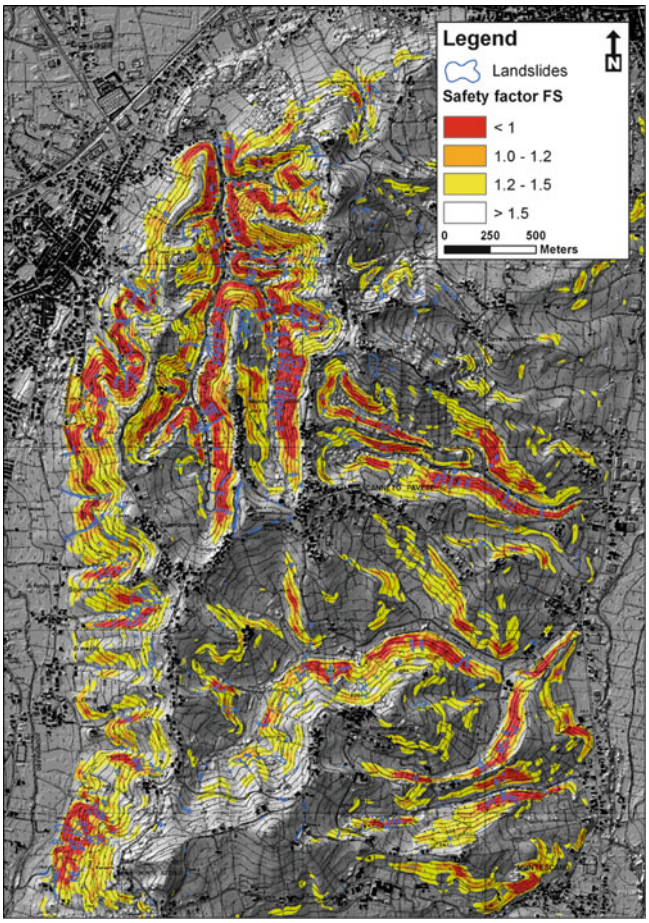

Fig. 5 Safety factor map obtained using TRIGRS

by factors like rainfall intensity and duration. The recharge was assumed to be the effective precipitation. It means rainfall minus evapotranspiration and bedrock infiltration. For each region the potential evapotranspiration was calculated from the rainfall and temperature with the Thornthwaite and Mather method (1957). The land use map allowed determining the water holding capacity necessary for the evapotranspiration calculation. The amount of infiltration depends on slope angle and we supposed that only ¼ of the water infiltrates in the substratum.

As regards TRIGRS initial conditions a water table depth corresponding to the ground level was assumed.

Different factors that contributed to shallow landsliding in the 2009 event in the study area were employed in neural network models (ANNET), including geological formations, land use and those derived from original DEM parameters (slope angle, landform classification, the April potential solar radiation, soil thickness, permeability, topographic ruggedness index, slope position index).

The Results

The Figs. 3, 4, and 5 show the results obtained with the three physically based models; the Fig. 6 represents the output of the neural network model. There is a general agreement between the source areas provided by the used models and the effective landslide source areas.

The predictive capability of the models was compared using the so-called receiver-operating characteristic (ROC) plot (Beguería 2006) (Fig. 7). In the ROC plot the percentage of unstable cells correctly predicted by the model is plotted against the percentage of predicted unstable cells over the total. These values indicate the ability of the model to correctly discriminate between positive and negative observations in the validation sample. The area under the ROC curve (AUC), can serve as global accuracy statistic for the model and it is threshold-independent. This statistic ranges from 0.5 (random prediction, represented by the diagonal straight line) to 1 (perfect prediction) and can be used for models comparison.

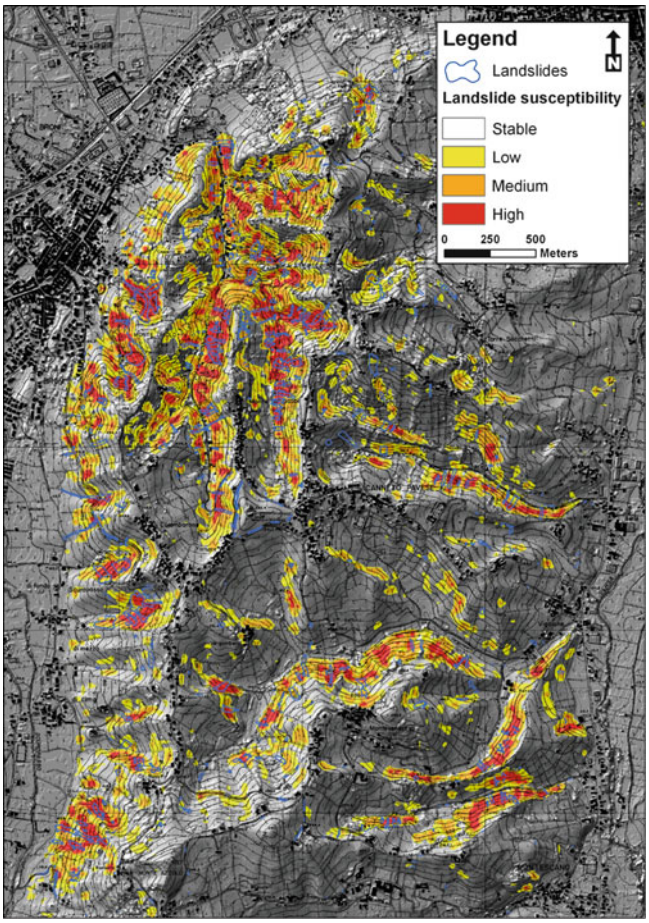

Fig. 6 Shallow landslides susceptibility map obtained using artificial neural networks (ANNET)

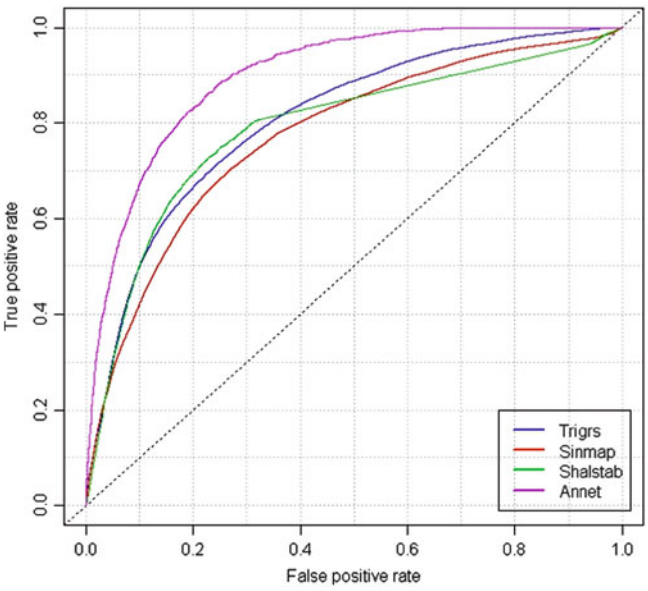

Fig. 7 Comparative ROC curves

Table 3 Parameters derived from ROC curves

Model	AUC	True positive (%)	False alarm (%)
Sinmap	0.773	75	32
Shalstab	0.787	75	25
Trigrs	0.807	75	28
Annet	0.899	75	15

Global accuracy (AUC) is 0.787 for SHALSTAB (Table 3). The incidence of shallow landsliding is high for areas mapped as "chronic" and for areas with critical rainfall lower than 200 mm/day (150 mm of rain in 48 h were recorded in the April 2009 event). This demonstrates that SHALSTAB is successful at identifying the most unstable areas of the landscape.

The global accuracy of SINMAP is quite similar and it is equal to 0.773, although rather conservative. About the 32 % of the study area is classified with SI below one (upper threshold and lower threshold classes), which refer to conditions that are highly unstable and thus critical. A slightly better performance is measured for TRIGRS (0.807).

False positives (over-prediction of landslide areas) are present both in SHALSTAB and TRIGRS; they are generally represented by:

1. Areas with higher slope angles. These zones are specially present in the SHALSTAB model where if tanθ equals or exceeds tanϕ slope instability will occur even under dry conditions;
2. Areas corresponding to south-facing slopes. Due to the different insolation the initial saturation conditions of the soils were different at the beginning of the April 2009 event on south and north–facing slopes;
3. Areas with presence of vegetation with root systems which contribute to soil strength by providing an additional cohesion component (e.g. old woodland).

The different conditions described in points (2) and (3) were not taken into account in the used models.

A relative high number of false negatives are related to shallow landslides triggered by anthropogenic activity such roads, which have not been incorporated within the physically based model approaches. These areas concern rotational slides which developed in presence of road cut and which represent 25 % of the shallow landslides of the test site.

ANNET models, which take into account the most important predisposing factors in the study area, were found promising for future studies in shallow landslide susceptibility zoning (area under the ROC plot = 0.899).

Conclusions

Different landslide susceptibility zonation models for predicting areas prone to shallow landslides were produced using both physically distributed landslide

models and artificial neural networks. The following considerations may be made:

- TRIGRS and SINMAP model the source areas of shallow landslides for a specific event (the April 2009 event). Heterogeneity is accounted for by allowing material properties and other input values to vary from grid to grid.
- SHALSTAB provides the spatial distribution of critical rainfall which expresses the potential for shallow landslide initiation. SHALSTAB assumes constant properties in the whole area.
- Even if the simplified assumptions about slope hydrology and kinematics (steady state slope parallel flow, translational slides) adopted by SHALSTAB and SINMAP are not very realistic in the test site, all the models forecast good agreement with the mapped inventory.
- SINMAP model furnishes more unrealistic scenarios than the others models.
- TRIGRS represents the most adequate physically based model for the analysis of shallow landslide source areas occurred within the study area.
- Physically based models are useful for shallow landslide susceptibility assessment at regional scale, nevertheless they do not take into account some important predisposing factors in the study area, namely the anthropogenic activity (road cutting and particularly those related to vineyards).
- 75 % of true positive rate with 15 % of false alarm, produced by the ANNET models, were found promising for future studies in landslide susceptibility zoning.

Future researches are devoted to the identification of mapping units, which take into account the different land use of the territory, and to the study of the role of the root systems of different typology of vegetation (e.g. old woodland, abandoned vineyard).

Acknowledgments This study has been supported by research projects funded by Broni municipality, Pavia Province and Rotary Club Oltrepo Pavese.

The aerial photographs of 18 May 2009 were taken by Ditta Rossi s.r.l. (Brescia).

References

Baum RL, Savage WZ, Godt JW (2002) TRIGRS – a Fortran program for transient rainfall infiltration and grid-based regional slope-stability analysis, US geological survey open-file report 2002–0424. U.S. Geological Survey, Reston

Baum RL, Savage WZ, Godt JW (2008) TRIGRS – a Fortran program for transient rainfall infiltration and grid-based regional slope-stability analysis, version 2.0, US Geological Survey Open-File Report. U.S. Geological Survey, Reston, 75p

Beguería S (2006) Validation and evaluation of predictive models in hazard assessment and risk management. Nat Hazards 37(3):315–329

Cervi F, Berti M, Borgatti L, Ronchetti F, Manenti F, Corsini A (2010) Comparing predictive capability of statistical and deterministic methods for landslide susceptibility mapping: a case study in the northern Apennines (Reggio Emilia Province, Italy). Landslides 7(4):433–444

Ermini L, Catani F, Casagli N (2004) Artificial neural networks applied to landslide susceptibility assessment. Geomorphology 66:327–343

Gómez H, Kavzoglu T (2005) Assessment of shallow landslide susceptibility using artificial neural networks in Jabonosa River Basin, Venezuela. Eng Geol 78(1–2):11–27

Montgomery DR, Dietrich WE (1994) A physically based model for the topographic control on shallow landsliding. Water Resour Res 30:1153–1171

Pack RT, Tarboton DG, Goodwin CN (1998) The SINMAP approach to terrain stability mapping. In: Moore DP, Hungr O (eds) Proceedings of the 8th congress of IAEG, vol 2. Balkema, pp 1157–1165

Thornthwaite CW, Mather JR (1957) Instructions and tables for computing potential evapotranspiration and the water balance. Climatology 10:311

Trajan Software (2001) Trajan 6.0 professional-neural network simulator (manual). Protaprint, Durham

Application of GIS Techniques for Landslide Susceptibility Assessment at Regional Scale

Goffredo Manzo, Veronica Tofani, Samuele Segoni, Alessandro Battistini, and Filippo Catani

Abstract

We evaluated the landslide susceptibility in Sicily region (Italy) (25,000 km^2) using a multivariate Logistic Regression model. The susceptibility model was implemented in a GIS environment by using ArcSDM (Arc Spatial Data Modeller) to develop spatial prediction models through regional datasets. A newly developed algorithm was used to automatically extract the scarp area from the whole landslide polygon. From the many susceptibility factors which influence landslide occurrence, on the basis of detailed analysis of the study area and univariate statistical analysis, the following factors were chosen: slope gradient, lithology, land cover, a curve number derived index and a pluviometric anomaly index. All the regression logistic coefficients and parameters were calculated using a selected landslide training dataset. Through the application of the logistic regression modelling technique the final susceptibility map was derived for the whole area. The results of the analysis were validated using an independent landslide dataset. On average, the 81 % of the area affected by instability and the 80 % of the area not affected by instability was correctly classified by the model.

Keywords

Landslide • Susceptibility • Logistic regression • GIS • ArcSDM • Sicily

Introduction

Following the formal definition given by Varnes and the IAEG (1984), hazard can be defined as the expected probability of a mass movement of a given intensity which takes place in a certain area within a given time span. This, essentially, means that landslide hazard assessment procedures must take into account both space and time prediction. Predictions based only on spatial probability of occurrence are defined susceptibility analyses (Dai et al. 2002). Spatial prediction can be based on a number of techniques and data. According to Aleotti and Chowdury (1999), they can be classified in heuristic, statistic and deterministic methods. Among the most used methods for the prediction of landslide susceptibility over large areas are those based on the weighting of landslide preparatory factors using statistical methods. The use of multivariate techniques, in which the natural and anthropogenic factors of hillslope instability are evaluated and weighted against each other in order to obtain the best estimation function, have long gained the approval of scientists and risk managers all over the world. Applications can be based on regressive methods (Bernknopf et al. 1988; Jade and Sarkar 1993; Wieczorek et al. 1996), discriminant analysis (Carrara 1983; Carrara et al. 1991; Chung and Fabbri 1995; Baeza and Corominas 1996) or neural networks (Bianchi and Catani 2002; Lee et al. 2003; Lu and Rosenbaum 2003; Ermini et al. 2005; Gomez and Kavzoglu 2005).

G. Manzo (✉)
Department of Earth Sciences, University of Firenze, Via La Pira 4, Florence 52021, Italy

Geodetic Division, Italian Geographic Military Institute, Via di Novoli 93, Florence 50127, Italy
e-mail: goffredo.manzo@gmail.com

V. Tofani • S. Segoni • A. Battistini • F. Catani
Department of Earth Sciences, University of Firenze, Via La Pira 4, Florence 52021, Italy

C. Margottini et al. (eds.), *Landslide Science and Practice*, Vol. 1,
DOI 10.1007/978-3-642-31325-7_59,

Guzzetti et al. (1999) and Van Westen (2004) give a general review of current methodologies used in statistical analysis, and agree upon the necessity of proper calibration and validation of methods in order to obtain useful hazard maps (Catani et al. 2005).

The objective of this work is to assess the landslide susceptibility in the whole Sicily region by means of a multivariate Logistic Regression model. The final output is constituted by a regional landslide susceptibility map (at the 1:100,000 scale) which is the first one realized in Sicily so far. This paper reports first the description of the study area and of the regional landslide inventory map, then the description of the landslide predisposing factors (slope angle, land cover, lithology, CN index and pluviometric anomaly index). The application of the model was entirely carried out in GIS environment, using the ArcSDM (Arc Spatial Data Modeller) integrated module (Sawatzky et al. 2004). The analysis is completed by a detailed validation carried out comparing the final susceptibility map with the landslide inventory.

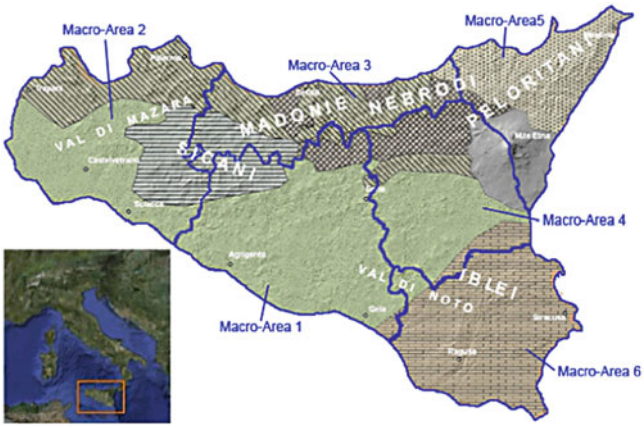

Fig. 1 Study area

Table 1 Landslide types and their percentage

Landslide types	(%)
Slow flows	36.3
Complex movements	32.2
Rotational and translational slides	21.0
Falls and topples	8.7
Rapid flows	1.4
Lateral spreads	0.4

Materials and Methods

Study Area and Landslide Inventory Map

The study area is the Sicily region, which is located in Southern Italy and covers and area of 25,428 km^2 (Fig. 1). The mountain areas occupy the 24 % of the whole region, the hilly areas the 62 % while the flat areas the 14 %.

From a geological point of view the study area can be subdivided into three regions which present different structural and lithological elements.

The northern section (Sicilian Apennines) is constituted by four main Mesozoic ridges: (1) Peloritani chain made up of metamorphic and flysch rocks with a maximum elevation of 1,000 m a.s.l. (2) the Nebrodi chain made up of argillaceous and arenaceous rocks with average elevation higher than the Peloritani chain (3) the Madonie chain constituted by calcareous and arenaceous rocks with a maximum elevation of 2,000 m a.s.l, (4) the Sicani chain made up of flysch rocks.

The central part of the study area is made up of Tertiary sedimentary rocks, constituted mainly by evaporitic rocks. The elevation ranges from 1,200 m a.s.l. to 1,600 m a.s.l.. The Iblei mesa constituted by calcareous and calcarenitic rocks occupies the southern-eastern portion of the Sicily region. The Etna Volcano characterizes the eastern portion of the island, at N of Iblei mesa.

The annual rainfall pattern of the study area can be defined as having two peaks, in November and March, with a dry summer. Mean annual rainfall varies in relation to relief, ranging from 1,300 mm in the Nebrodi and Peloritani chains to about 2,000 mm in the Etna area.

For the application of the susceptibility model the study area was partitioned into 6 macro-zones (with areal extension ranging from 3,000 to 6,000 km^2) according to the Civil Protection Alert Zones (Fig. 1). Each macro-zone was trained independently in order to reduce the computational load and to get more accurate results.

The landslide inventory map of Sicily region comes from the IFFI Project database (Trigila et al. 2010). It counts 3,098 landslides while the area affected by landslides is 291 km^2, the 1.15 % of the total area. Concerning the type, the majority of movements are slow flows and complex movements followed by rotational and translational slides (Table 1). The 61 % of the landslides are active, while the 36.5 % is dormant. Since the majority of the landslides are slow-moving landslides (90 % of the total ones), the susceptibility analysis will concern only these types of phenomena (Fig. 2).

The descriptive statistics highlighted that the lithology more susceptible to landsliding is the flysch-type formation constituted by an alternation of argilloceous and arenaceous layers, while the type of land cover with the highest proportion of landslides is scrub and/or herbaceous vegetation associations.

Given that the susceptibility analysis aims to identify the susceptible areas based on the analysis of the combination of parameters which has led to failure, we developed a simple

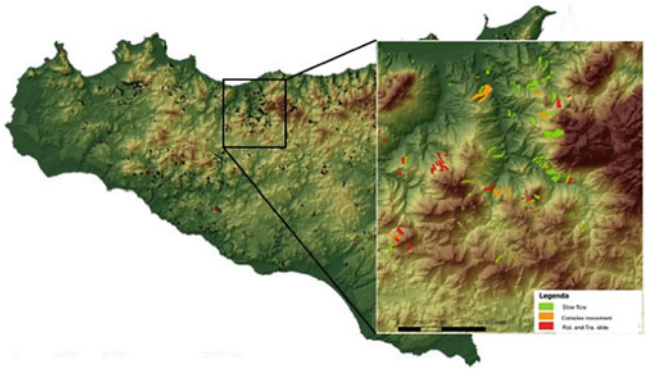

Fig. 2 Landslide inventory map

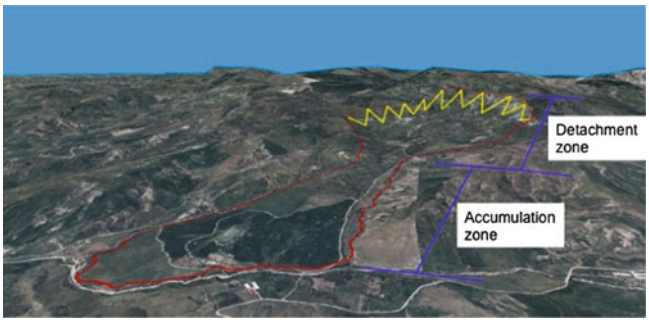

Fig. 3 Identification of detachment zone and accumulation zone. Only the detachment zone is considered in the susceptibility analysis

model to extract the detachment zone from the whole landslide perimeter. This simple model developed in a GIS environment is based on the DTM, with a spatial resolution of 20 m, and the derived map, the slope angle. The detachment zone has been identified for each landslide polygon as the area with the slope angle higher than 5° and elevation higher than the mean elevation inside the landslide perimeter (Fig. 3). Only the detachment zones have been then used to train and validate the susceptibility model.

Input Data

Many different landslide susceptibility parameters have been used in the definition of hazard mapping. Some (e.g. slope gradient and lithology) are widely adopted and accepted while the application of others (e.g. structural settings, higher derivatives of elevation, soil depth) are still debated and basically depend upon the type of phenomenon under investigation (Carrara and Guzzetti 1995; Baeza and Corominas 1996).

On the basis of the landslide types of the Sicily region and the results of a preliminary monovariate statistical analysis of the parameters within mapped mass movements, the following preparatory factors were selected: slope angle, lithology, land cover, CN index and pluviometric anomaly index (I_a).

A brief description of each parameter follows.

Slope Angle

The slope angle has been derived from a DTM with a spatial resolution of 20 m. Five classes have been defined on the basis of the distribution of slope angle inside landslides and on the basis of literature data. In particular the classes are: 0°–5°; 5°–12°; 12°–18°; 18°–32°; >32°.

Land Cover

The vegetation cover and the use of land parcels greatly influence slope behavior at every scale (Varnes and IAEG 1984; Hansen 1984). This is especially true when considering shallow landsliding but it is also of importance for deep-seated mass movements. For the whole territory of the Sicily region the CORINE Land Cover map is available. The CORINE Land Cover map is organized into three levels: the first one (5 items) indicates the major categories of land cover on the planet; the second level (15 items) is for use on the scale of 1:500,000; the third level (44 items) was used in the CORINE Project on a scale 1:100,000. In this work, considering the objective of the study and the extension of the study area, we adopted the second level. The distribution of the 15 classes of land cover over the study site is reported in Fig. 4.

Lithology

Lithology is considered one of the most important predisposing factor and in particular lithotechnical classification, which classifies the different lithologies on the basis of their mechanical behavior. In this work the lithotechnical map was derived from the Geological map of the Sicily region at the scale of 1:100,000. 9 classes have been identified. They are reported in Fig. 5.

CN Index

The runoff curve number (also called a curve number or simply CN) is an empirical parameter used in hydrology for predicting direct runoff or infiltration from rainfall excess. The curve number method was developed by the USDA Natural Resources Conservation Service (Soil Conservation Service 1972). It is a widely used and efficient method for determining the approximate amount of direct runoff from a rainfall event in a particular area. In our work the estimation of CN parameter was done in GIS environment using a toolbox developed by USGS called Arc-CN Runoff (Xiaoyong and Min-lang 2004). The fundamental thematic data are lithology and land cover. In particular to each lithology class a hydrologic soil group has been associated. Then using the toolbox to each class of CORINE land cover and for each hydrologic soil group a CN value was defined (Table 2).

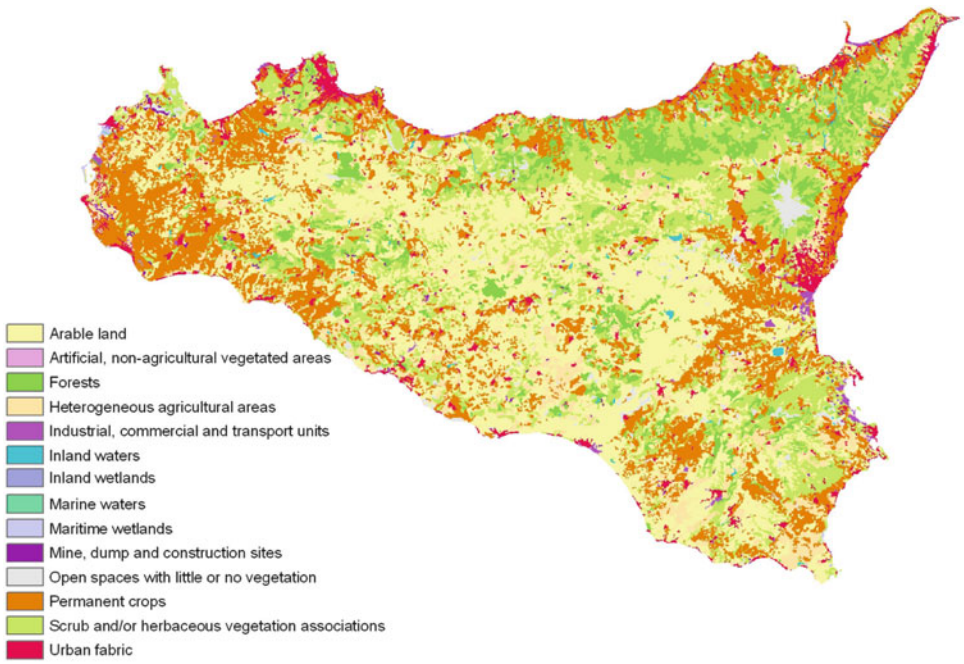

Fig. 4 Land Cover map of the study area

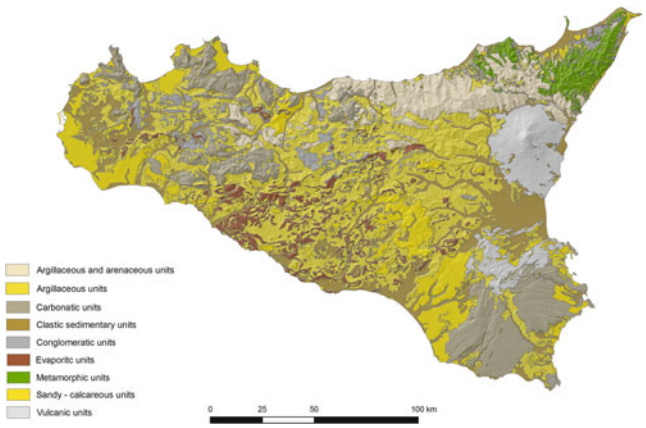

Fig. 5 Lithology map of the study area

The CN values were then organized in 9 classes (0–10; 10–37; 37–51; 51–60; 60–68; 68–76; 76–81; 81–88; 88–98).

Pluviometric Anomaly Index (I_a)

In order to take into account the effect of anomalous rainfalls in the susceptibility model, we defined a pluviometric anomaly index (I_a). This index is reported in (1).

$$I_a = \frac{1}{n}\sum\left(\frac{h_{\max 24_i} - h_{\max 3_i}}{h_{\max 24_i}}\right) \quad (1)$$

The index takes into account the maximum intensity precipitation in 3 h (h_{max3}) and the daily maximum intensity precipitation (h_{max24}). The I_a is computed for each rainfall event and for each rainfall rain gauge station. Rainfall information related to 78 pluviometric stations distributed all over Sicily and related to a period ranging from 1924 to 1995 were collected. The spatialization of the I_a index was carried out using the "Nearest Neighbor" algorithm in GIS environment. Three classes were adopted: low anomaly (0–0.42), medium anomaly (0.42–0.52) and high anomaly (0.52–0.80).

Application of the Susceptibility Model

In this study we adopted a Logistic Regression (LR) model, which is particularly appropriate for regional scale applications. The model was trained using a random selection (70 % of the unstable area) performed independently on each Macro Zone.

The basic analysis unit for the susceptibility modeling is the Unique Condition Unit (UCU). UCUs were outlined by means of GIS analyses, overlapping all the aforementioned thematic maps and considering all the possible combinations of classes.

The susceptibility analysis was carried out using the ArcSDM software (Sawatzky et al. 2004) (which was modified for handling the whole studied area). This software, making use of the Bayes theorem (Bonham-Carter and Agterberg 1990), defines for each class of each susceptibility factor a series of parameters to be used for the computation of the a posteriori probability:

– Positive weight (W^+) is based on the ratio between the probability of having a given class (j) of a given variable (i) in a landslide (F) or not (F^)

$$W_{ij}^{+} = \ln\frac{P(V_{ij}|F)}{P(V_{ij}|F^{\wedge})} \quad (2)$$

Table 2 Classification scheme of CN index

CN values	Hydrologic soil group			
Land Cover classes	A	B	C	D
Inland waters	94	10	10	10
Marine waters	0	10	0	0
Permanent crops	65	71	85	83
Arable lands	81	81	75	79
Heterogeneous agricultural areas	79	68	75	78
Open spaces with little or no vegetation	98	78	74	63
Forests	53	74	71	70
Scrub and/or herbaceous vegetation associations	80	78	73	74
Mine, dump and construction sites	65	78	55	91
Industrial, commercial and transport units	78	93	74	78
Inland wetlands	0	25	25	0
Maritime wetlands	25	25	25	25
Urban fabric	92	63	71	71
Artificial, non-agricultural vegetated areas	0	80	92	58

– Negative weight (W^-) expresses the opposite situation

$$W_{ij}^- = \ln \frac{P(V_{ij}^{\wedge}|F)}{P(V_{ij}^{\wedge}|F^{\wedge})} \quad (3)$$

– Contrast (C) defines the degree of spatial correlation between landslide susceptibility and each class

$$C = W^+ - W^- \quad (4)$$

– Standard deviation of positive and negative weight
– Contrast standard deviation (S_c)
– Studentized contrast (StudC) represents a linkage between contrast and the uncertainty in weights assignment: in the present study the threshold value 2 was used

$$StudC = C/S_c \quad (5)$$

– Generalize class (Gen_class) is basically used to select each class of each factor according to the aforementioned StudC threshold. In the present work, from the original 41 classes only 38 were selected as susceptibility variables.

Generally, the values of weights and contrast of each class show only little variations among the six macro-areas. In particular, regarding the slope factor the highest contrast was observed in the 5°–12° class or in the 12°–18° class; in the lithology factor the clayey class had always the highest contrast (followed by evaporites or sandy-clayey rocks); scrubs and grasslands was the most contrasted land use class (followed by urban areas); about CN the highest contrast values were found in the classes with high CN values (81–88 and 89–98); the anomaly pluviometric index class with the highest value had also the highest contrast.

On the basis of weights, contrast, and generalize classes, the ArcSDM software reclassifies each thematic input raster and determines the UCUs (Unique Condition Units). Theoretically, 18,225 UCUs should be taken into account (from the combination of 5 × 9 × 15 × 9 × 3 classes), actually the number was considerably reduced: some combinations did not occur (e.g. in the macro-area 1 only 2,646 combinations are present); polygons with an area lower than 1 ha were merged to the closest polygons; using the "generalize class" parameter, all the classes without a significant statistical correlation with landslides were grouped into a single class. As an example, in the Macro-area 1 only 712 UCUs were eventually considered.

Subsequently, the ArcSDM software applies the Logistic Regression model and calculates the regression coefficients of every class of each predisposing factor using the Maximum Likelihood technique. Moreover, the software calculates the a posteriori probability of each UCU to contain a landslide. This probability value, ranging from 0 to 1 (or o % to 100 %), represents the final susceptibility output of the Logistic Regression model.

Susceptibility Mapping

To get the final susceptibility map, those probabilistic values were reclassified into four susceptibility levels (from S_0 to S_3) following an approach proposed by Catani et al. (2005). The adopted reclassification scheme is based on the comparison between the cumulative density function of the LR outputs within mapped landslides (cdfL) and the cdf within the total area (cdfT) (Fig. 6). The difference between the derivatives of cdfL and cdfT is used to identify the output values where a sudden increase in the cdfL curve is not accompanied by a similar increase in the cdfT one. Those values can be used as thresholds to separate two different susceptibility classes (Fig. 6).

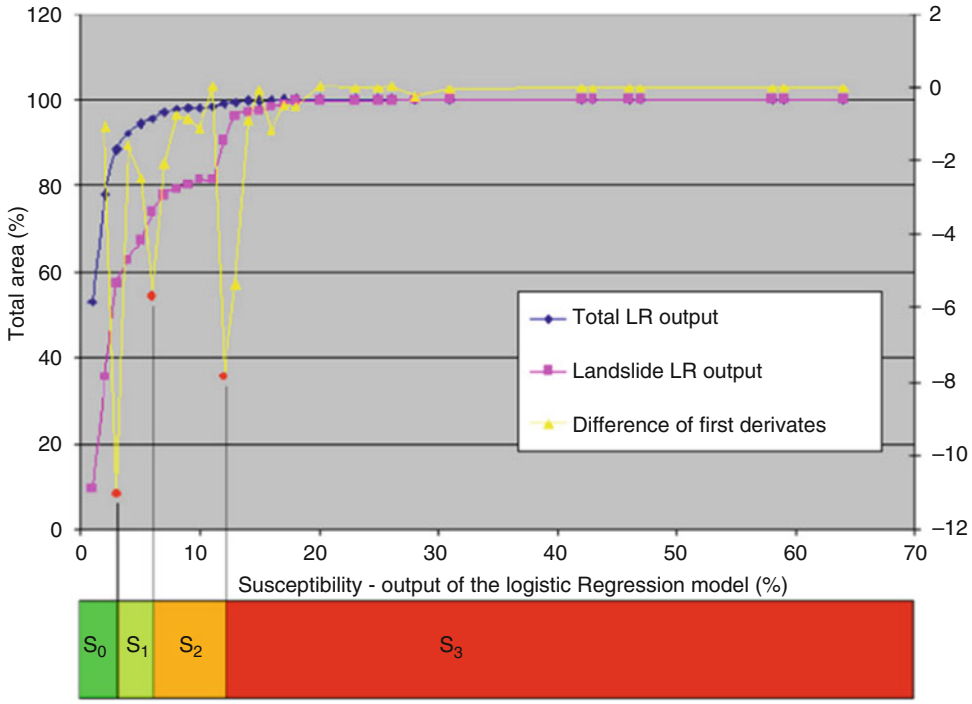

Fig. 6 Identification of susceptibility classes in the macro-area 4 (see text for explanations)

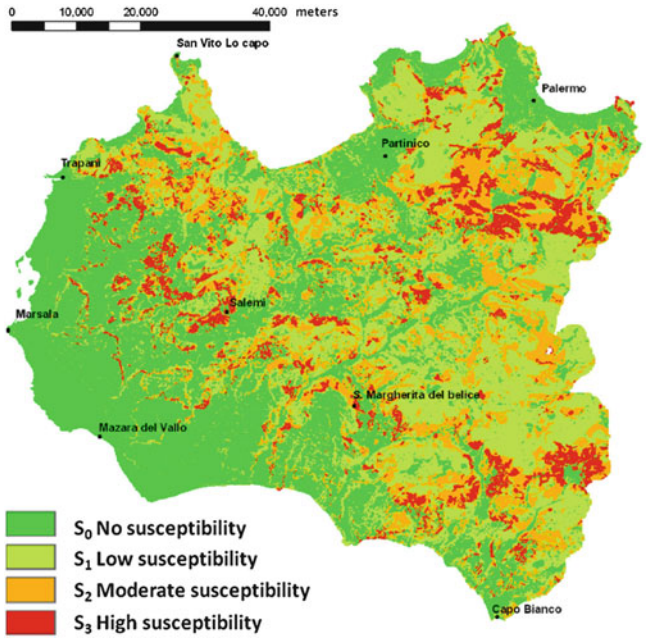

Fig. 7 Susceptibility map of the macro-area 2

In order to obtain the final susceptibility maps (Fig. 7), the LR model and the output reclassification procedure were applied separately to each macro-area on a pixel-by-pixel basis.

Results and Validation

The final regional 1:100,000 susceptibility map was constituted assembling the 6 macro-area maps. The format of the final map was a raster grid with 100 m x 100 m cells.

Table 3 Sensitivity (Se) and specificity (Sp) of the susceptibility model in the six macro-areas

Macro-area	Se (%)	Sp (%)
1	90.62	82.93
2	89.31	74.35
3	83.47	63.78
4	85.30	85.83
5	95.09	70.40
6	65.53	94.61

According to our model, 6 % of the Sicily (1,552 km^2) is exposed to a high susceptibility (S3 class), 15 % moderate, 33 % low and 46 % is considered not susceptible to landsliding.

The effectiveness of the proposed methodology was evaluated comparing the final susceptibility map with the landslide inventory. In the validation process, an independent dataset was compared to the predicted instability (S_2 and S_3) and stability (S_1 and S_0). For each macro-area a confusion matrix was built.

The confusion matrix is based on the calculation of true positives (TP: predicted instability matching with observed instability), true negatives (TN: predicted stability in observed stable areas), false positives (FP: predicted instability in observed stable areas) and false negatives (FN: predicted stability in observed unstable areas) Table 3. Those statistics were combined to calculate the model sensitivity

$$Se = TP/(TP + FN) \quad (6)$$

and specificity

$$Sp = TN/(TN + FP) \quad (7)$$

Discussion and Conclusions

As showed in the materials and methods section, the proposed approach for the assessment of landslide susceptibility of the Sicily region at the scale of 1:100,000 has a relevant degree of objectivity and can be easily applied elsewhere at regional scale. Given the outcropping litholgies, Sicily is particular susceptible to landsliding. The majority of landslides are slow-moving ones, in particular slow flows, complex movements and rotational and traslational slides.

The landslide susceptibility model adopted is a multivariate logistic regression model which has been considered as the most appropriate considering the landslide types and the extension of the study area. The landslide predisposing factors selected are slope angle, lithology, land cover, CN index and pluviometric anomaly index (I_a).

Three different version of the model were applied and validated. The simplest version is based on only three variables: slope gradient, lithology and land use. Another version encompasses Curve Number as fourth variable and the full version of the model was obtained adding the pluviometric anomaly index (PAI) variable. Comparing the validation results of these three versions, it was observed that the fourth variable (CN) adds a considerable predictive power with respect to the basic three variables-model, while the further addition of the fifth (PAI) only slightly enhances the results.

The most innovative aspect of the work is related to the complete implementation of the landslide susceptibility assessment procedure within a GIS environment. This has been possible using ArcSDM (Arc Spatial Data Modeller) (Sawatzky et al. 2004) in order to develop the methodology through regional datasets.

References

Aleotti P, Chowdhury R (1999) Landslide hazard assessment: summary review and new perspectives. Bull Eng Geol Env 58:21–44

Baeza C, Corominas J (1996) Assessment of shallow landslide susceptibility by means of statistical techniques. In: Proceedings of the seventh international symposium on landslides, Trondheim, pp 147–152

Bernknopf RL, Campbell RH, Brookshire DS, Shapiro CD (1988) A probabilistic approach to landslide hazard mapping in Cincinnati, Ohio, with applications for economic evaluation. IAEG Bull 24(1):39–56

Bianchi F, Catani F (2002) Landscape dynamics risk management in Northern Apennines (Italy). In: Brebbia CA, Zannetti P (eds) Development and application of computer techniques to environmental studies, vol 1. WIT Press, Southampton, pp 319–328

Bonham-Carter GF, Agterberg FP (1990) Weights of evidence modeling: a new approach to mapping mineral potential. In: Statistical applications in the earth sciences, Geological Survey of Canada paper. Geological Survey of Canada, Ottawa, pp 171–183

Carrara A (1983) Multivariate methods for landslide hazard evaluation. Math Geol 15(3):403–426

Carrara A, Guzzetti F (eds) (1995) Geographical information systems in assessing natural hazards. Kluwer Academic, Dordrecht

Carrara A, Cardinali M, Detti R, Guzzetti F, Pasqui V, Reichenbach P (1991) GIS techniques and statistical models in evaluating landslide hazard. Earth Surf Proc Land 16:427–445

Catani F, Casagli N, Ermini L, Righini G, Menduni G (2005) Landslide hazard and risk mapping at catchment scale in the Arno River basin. Landslides 2:329–342

Chung CF, Fabbri AG (1995) Multivariate regression analysis for landslide hazard zonation. In: Carrara A, Guzzetti F (eds) Geographical information systems in assessing natural hazards. Kluwer Academic, Dordrecht, pp 107–142

Dai FC, Lee CF, Ngai YY (2002) Landslide risk assessment and management: an overview. Eng Geol 64:65–87

Ermini L, Catani F, Casagli N (2005) Artificial neural networks applied to landslide susceptibility assessment. Geomorphology 66:327–343

Gomez H, Kavzoglu T (2005) Assessment of shallow landslide susceptibility using artificial neural networks in Jabanosa River Basin, Venezuela. Eng Geol 78:11–27

Guzzetti F, Carrara A, Cardinali M, Reichenbach P (1999) Landslide hazard evaluation: a review of current techniques and their application in a multi-scale study, Central Italy. Geomorphology 31:181–216

Hansen A (1984) Landslide hazard analysis. In: Brundsen D, Prior DB (eds) Slope instability. Wiley, New York, pp 523–602

Jade S, Sarkar S (1993) Statistical models for slope stability classification. Eng Geol 36:91–98

Lee S, Ryu J-H, Min K, Won J-S (2003) Landslide susceptibility analysis using GIS and artificial neural networks. Earth Surf Proc Land 28(12):1361–376

Lu P, Rosenbaum MS (2003) Artificial neural networks and grey systems for the prediction of slope stability. Nat Hazard 30(3):383–398

Sawatzky DL, Raines GL, Bonham-Carter GF, Looney CG (2004) ARCSDM3.1: ArcMAP extension for spatial data modelling using weights of evidence, logistic regression, fuzzy logic and neural network analysis. http://www.ige.unicamp.br/sdm/ArcSDM31/

Soil Conservation Service (SCS) (1972) National engineering handbook, section 4, hydrology. United States Department of Agriculture (USDA), Washington, DC

Trigila A, Iadanza C, Spizzichino D (2010) Quality assessment of the Italian Landslide Inventory using GIS processing. Landslides 7(4):455–470

Van Westen CJ (2004) Geo-Information tools for landslide risk assessment: an overview of recent developments. In: Lacerda E, Fontoura S (eds) Landslides: evaluation and stabilization. Taylor & Francis, London

Varnes DJ, IAEG Commission on Landslides (1984) Landslide hazard zonation – a review of principles and practice. UNESCO, Paris, 63p

Wieczorek GF, Gori PL, Jager S, Kappel WM, Negussy D (1996) Assessment and management of landslide hazards near Tully Valley landslide, Syracuse, New York, USA. In: Proceedings of the VII international symposisum landslides, Trondheim, Vol 1, June 1996, Balkema, Rotterdam, pp 411–416

Xiaoyong Z, Min-lang H (2004) ArcCN-Runoff: an ArcGIS tool for generating curve number and runoff maps. Environ Model Software 19:875–879

Landslide Susceptibility Maps for Spatial Planning in Lower Austria

Rainer Bell, Thomas Glade, Klaus Granica, Gerhard Heiss, Philip Leopold, Helene Petschko, Gilbert Pomaroli, Herwig Proske, and Joachim Schweigl

Abstract

Landslides threaten most parts of the provincial state of Lower Austria and cause damage to agricultural land, forests, infrastructure, settlements and people. Thus, the project "MoNOE" (Method development for landslide susceptibility modelling in Lower Austria) was initiated by the provincial government to tackle these problems and to reduce further damage by landslides. The main aim is to prepare landslide susceptibility maps for slides and rock falls and to implement these maps into the spatial planning strategies of the provincial state.

Landslide susceptibility maps are either prepared by statistical (for slides) or empirical or process-based (for rock falls) approaches. Final maps are combined to a single landslide susceptibility map and optimised for the end-users (spatial planners and local authorities). It shows that a difference exists between the best scientific maps and the best maps for spatial planning purposes. This involves questions about the best number of susceptibility classes, its thresholds and ideal colours.

Keywords

Landslide inventory • Landslide susceptibility • Spatial planning • LiDAR DTM • Lower Austria

Introduction

Landslides occur frequently in Lower Austria – a federal province of Austria (e.g. Schwenk 1992). Since 1953 more than 1,500 landslides have been studied by the Geological Survey of Lower Austria and stored in the Building Ground Register (BGR). These landslides mainly have caused damage to agricultural land, forests and infrastructure, but also threaten settlements and people. Therefore, the project "MoNOE" (Method development for landslide susceptibility modelling in Lower Austria) is funded by the provincial government. The main objectives of this project are:

1. Design of a method for landslide susceptibility modelling for a large study area (about 10,200 km^2)
2. Production of landslide susceptibility maps (for rock falls and slides)
3. Implementation of the susceptibility maps into the spatial planning strategies of the provincial state of Lower Austria

R. Bell (✉) • T. Glade • H. Petschko
Department of Geography and Regional Research, University of Vienna, Universitätsstrasse 7, 1010 Wien, Vienna, Austria
e-mail: rainer.bell@univie.ac.at

K. Granica • H. Proske
Joanneum Research Forschungsgesellschaft mbH, DIGITAL - Institute for Information and Communication Technologies, Graz, Austria

G. Heiss • P. Leopold
Health and Environment Department, AIT – Austrian Institute of Technology GmbH, Environmental Resources and Technologies, Tulln, Austria

G. Pomaroli
Department of Spatial Planning and Regional Policy, Office of the Lower Austrian Provincial Government, St. Pölten, Austria

J. Schweigl
Office of the Lower Austrian Provincial Government, Geological Survey, St. Pölten, Austria

C. Margottini et al. (eds.), *Landslide Science and Practice*, Vol. 1,
DOI 10.1007/978-3-642-31325-7_60,

Together with the heterogeneous geology and the aim to implement the landslide susceptibility maps in spatial planning strategies of the state this poses huge challenges towards the development of new and suitable methods for modelling landslide susceptibility. Limitations are given by restricted (digital) data availability for such large areas, e.g. geology is only available at a scale 1:200,000 for the entire study area. Since reliable landslide inventories are an essential prerequisite for high quality susceptibility maps, all available digital landslide information was gathered and evaluated. Furthermore, basic geodata had to be prepared and homogenized.

Subsequently, susceptibility modelling for slides and rock falls was carried out independently. However, since the final landslide susceptibility map shall comprise both processes in one map, approaches for combining single process susceptibility maps have to be developed. Due to the need to optimise final landslide susceptibility maps for spatial planners and local authorities, the maximum number of susceptibility classes and respective thresholds and colours for each class has to be defined. Consequently, the difference between the best scientific landslide susceptibility map and the best map for spatial planning purposes is analysed. Beside all this, human impact on landslides is analysed, mainly at local scale. However, depending on the results it will be tested whether parameters can be derived that can be integrated into regional scale landslide susceptibility modelling.

Study Area

The study area Lower Austria covers an area of approx. 10,200 km^2, which is about 2/3 of the provincial state of Lower Austria. It is located in the northeast of Austria (Fig. 1). Only districts which are prone to landslides and where landslides have been recorded by the Geological Survey of Lower Austria are investigated.

The main geological units of Lower Austria comprise the Northern Calcareous Alps, the Flysch Zone, the Molasse Zone and related units (Vienna basin and Waschbergzone), the Eastalpine Crystalline (Paragneiss and Quarzphyllite), the Bohemian Massif (Granite and Gneiss) and quaternary sediments (fluvial terraces and alluvial deposits) (Fig. 1). Deatails on the geology can be found in Wessely (2006). Based on the BGR inventory most of the registered landslides occurred in the Flysch Zone, followed by the Molasse Zone and the Northern Calcareous Alps (Schwenk 1992, see also Fig 1).

The pattern of total rainfall distribution in the study area follows mainly the topography and shows its maximum in the high mountain area of the Northern Calcerous Alps in the southwest with approx. 1,700 mm and dropping down to the northeast to approx. 500 mm (www.noe.gv.at, 2011).

Detailed information on spatial planning laws in Lower Austria is given in Pomaroli et al. (2011).

Materials/Data

To model landslide susceptibility, essential digital information on landslides and basic geodata must be gathered. Various landslide inventories were available (Table 1). Their spatial representation is shown in Fig. 1. Furthermore, numerous basic geodata was collected, which is listed in Table 2.

Methods

Various methods are applied for the different tasks of the project.

In a first step all available data on landslide inventories were gathered and their potential regarding the applicability for susceptibility modelling was analysed in detail. Furthermore, basic geodata were collected, prepared and homogenised. A new land cover classification was created by deriving it from satellite images.

Whereas slide susceptibility is modelled using statistical approaches (Weights of Evidence and Logistic regression), rock fall susceptibility is modelled based on two steps. First, rock fall release areas are determined by empirical slope thresholds depending on geology (lithology as well as tectonics), followed by modelling the run-out using empirical and process-based run out models. Both susceptibility maps are verified in the field. Furthermore, slide susceptibility maps are validated using common validation criteria like AUROC, success and prediction rate curves.

Final slide and rock fall susceptibility maps are combined and optimised for end-user needs. This is jointly developed with the spatial planners and geologists of the provincial government.

Results

Analysing all available landslide inventories, it turned out that only the landslide inventory based on the Building Ground Register of the Provincial Geological Survey could be used to some extent for slide susceptibility modelling. Furthermore, the need for preparing a new and homogenized landslide inventory based on LiDAR DTM interpretation became evident. Detailed results on the landslide inventories and minimum requirements for susceptibility modelling are presented in Petschko et al. (in this volume).

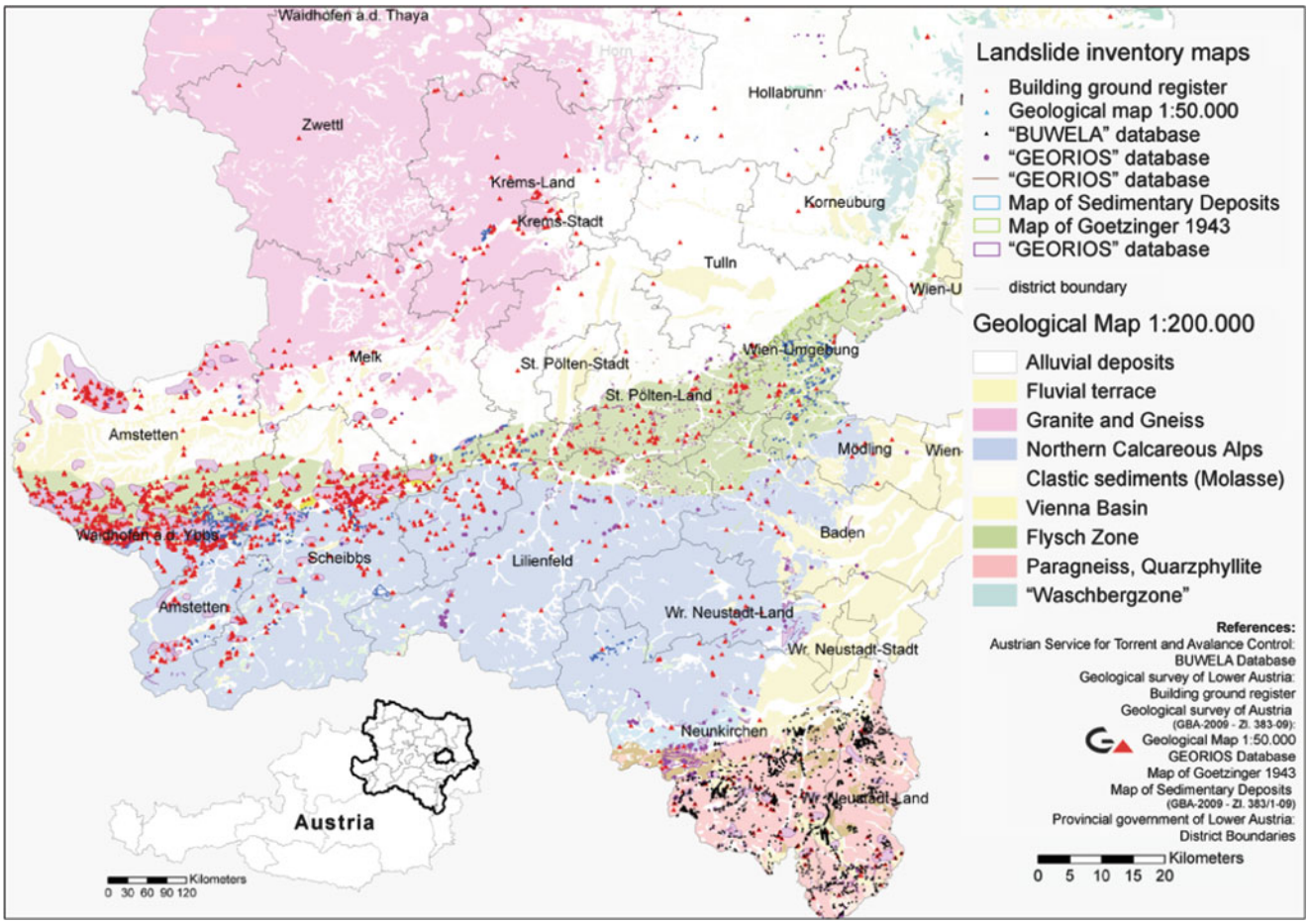

Fig. 1 Location, geology and available landslide inventories of the study area Lower Austria

Table 1 Available landslide inventories in Lower Austria (Note: N.T. = No information on time of mapping/of the events available)

Type	Source	Scale
Building ground register (BGR)	Geological Survey of Lower Austria	1:50,000; Lower Austria; Points; since 1953
Hazard maps and Hazard zoning maps	Austrian Service for Torrent and Avalanche Control – WLV	1:50,000, 1:2,000; Lower Austria – areas surrounding settlements; Polygons (in Tiff); N.T.
Localisation of Slides and Falls	Austrian Service for Torrent and Avalanche Control – WLV	1:50,000; Lower Austria, Points; N.T.
Geomorphological maps (Mapping, archive data)	BUWELA Project WLV, southeast of Lower Austria	ca. 1:50,000, "Bucklige Welt", Points; N.T.
GEORIOS Database	Geological Survey of Austria	1:50,000; Lower Austria, Points, Lines, Polygons; N.T.
Map of unconsolidated rocks	Geological Survey of Austria	1:50,000; Lower Austria, Points, Polygons; N.T.

Table 2 Available basic geodata in Lower Austria (Note: NÖGIS = webgis of the provincial state of Lower Austria, BMLFUW = Federal Ministry for Agriculture, Forestry, Environment and Water Management)

Type	Source	Scale
Geological Map, GK200	Geological Survey of Austria	1:200,000
Geological Map, GK50	Geological Survey of Austria	1:50,000, Parts of Lower Austria
Map of unconsolidated rocks	Geological Survey of Austria	1:50,000
Land cover	Joanneum Research	10 m resolution, derived from satellite data
Various Geodata (Roads, Rivers, Train, Settlements, etc.)	NÖGIS	1:50,000; 1:10.000; 1:1,000
Precipitation and designed rainfall	Hydrology / BMLFUW	Station records, 6 km resolution
Orthophotos	NÖGIS	12.5–25 cm resolution
Digital terrain model	NÖGIS	1 m resolution, Airborne LiDAR

Regarding the preparation of the basic geodata, it turned out that the geological map at a scale of 1:200,000 showed some major errors in representing alluvial areas. These areas reach up to 200 m upslope in many cases. This aspect was corrected within this project. Furthermore, there was the need to simplify the geological map to lithological relevant parameters.

So far, susceptibility modelling was carried out in three test districts (Waidhofen/Ybbs, Amstetten, and Baden) to develop methods to be applied subsequently in the whole study area. Whereas for Waidhofen/Ybbs and Amstetten the BGR landslide inventory shows sufficient landslide information, the district Baden shows only seven entries, but was chosen to test and develope methods in a district with insufficient landslide information.

First results of the comparison of slide susceptibility maps based on Weights of Evidence and Logistic regression show to a great extent quite similar results. However, some differences are significant and must be further analysed. Detailed information on this comparison is given in Leopold et al. (in this volume). Proske et al. (in this volume) concludes that applying first an empirical run-out model for rock fall susceptibility and subsequently a process-based run-out model in hot spot areas of the empirical model provide a reasonable solution for modelling rock fall susceptibility for such large areas. For details it is referred to the respective paper.

This contribution is focussed on the combination of the rock fall and slide susceptibility maps and the end-user optimisation.

Intensive discussions with the representatives of the provincial government resulted first in the decision that the common traffic light colours (green, yellow, red, or dark green, light green, yellow, orange, red) should not be used for the final landslide susceptibility classes ranging from low to high or very low to very high, although these colours are the most intuitive ones, enabling an easy way to read and understand the maps. The reason for this is that the colours yellow and red are used within the hazard zoning maps of the Austrian Service for Torrent and Avalanche Control. Whereas there are strict regulations including e.g. the prohibition of new building activities connected with the different hazard zones, the final landslide susceptibility map will have only a status of indication. To prevent misunderstandings and misinterpretations especially at the local authorities it was decided not to use these colours. Several alternative colour schemes were tested which resulted so far in the usage of the colours beige and purple, in addition to transparent for "susceptibility not to be expected" (Figs. 2b, c, d).

Parallel to the discussion of the colours the final number of different susceptibility classes had to be decided. The scientists preferred four to five classes to more exactly differentiate within areas susceptible to landslides (Fig. 2a). However, this was finally rejected because of the difficulties to define specific options for actions for each class, which would make sense for the end-users. Thus, it was decided to take three classes (susceptibility not to be expected, susceptibility not to be excluded, susceptibility to be expected) for the final maps (Figs. 2b, c, d).

A third question to be answered is the value of the susceptibility class thresholds. In Fig. 2b (conservative),c (progressive) different options are shown based on the percentage of landslide pixels from the landslide inventory used in modelling. The final decision is still being discussed between the scientists and the provincial state government. Fig. 2d presents the first result of a combined rock fall and slide susceptibility map. The high susceptible rock fall areas in the center of the map where slide susceptibility is minor (see Figs. 2b or c) can easily be seen.

Discussion and Conclusions

Analysing all available landslide inventories showed that only the BGR inventory is of some use for landslide susceptibility modelling. It clearly turned out that a new inventory must be prepared. With regard to the available data and especially the large size of the whole study area we decided to prepare such a new landslide inventory based on interpretation of the LiDAR DTM. Historical landslide information (e.g. the BGR) was not directly integrated in the newly mapped inventory since the available information is not comprehensive for the entire study area and has limitations in the accuracy of the location. However, historical landslide information was used as orientation in analysing the LiDAR DTM. Details on the preparation of the LiDAR landslide inventory can be found in Petschko et al. (2010) and in Petschko et al. (in this volume).

First modelling results for rock fall susceptibility as well as slide susceptibility are very promising for the three test districts. However, some more analyses and validations have to be carried out before the developed approaches can be applied to the whole study area.

A major decision regarding the end-user optimisation has already been taken, i.e. the number of susceptibility classes. Final decisions for the ideal colours and the susceptibility class thresholds are shortly before reached.

The project has demonstrated so far that close cooperation between scientists and representatives of the provincial state government is essential to prepare high quality and end-user optimised landslide susceptibility maps. Although the results show that there is a difference between the best

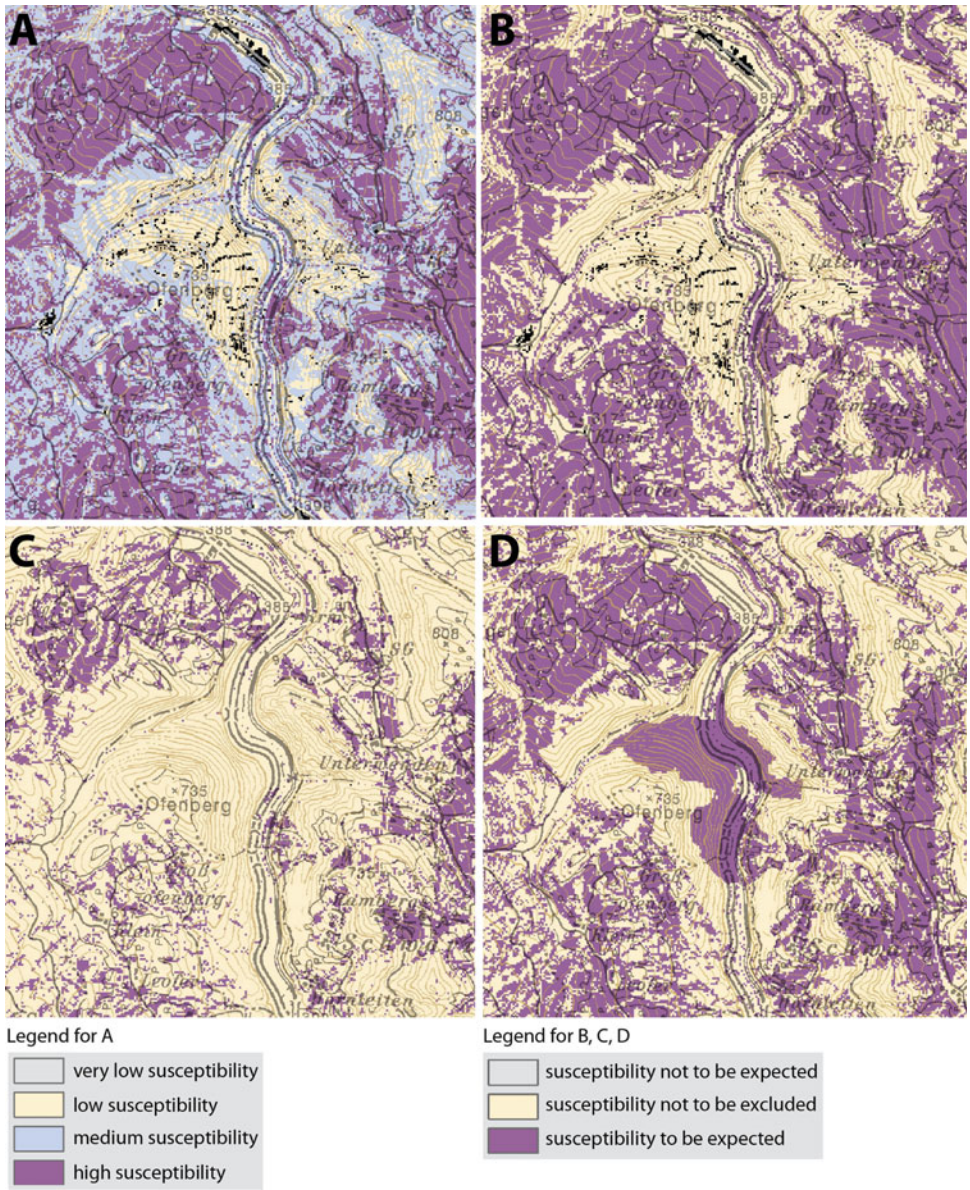

Fig. 2 Different landslide susceptibility maps. (**A**) Slide susceptibility map, example of a preferred scientific map with four classes; (**B**) Slide susceptibility map, example preferred for implementation into spatial planning strategies, class thresholds: lowest class = 1 % of landslide pixels – 40 % of the study area, highest class = 80 % of landslide pixels – 21 % of the study area; (**C**) Slide susceptibility map, like B but class thresholds: lowest class = 0.1 % of landslide pixels – 26 % of the study area, highest class = 50 % of landslide pixels – 8 % of study area; (**D**) Combined slide and rock fall susceptibility map, preferred for implementation into spatial planning strategies

scientific map and the best map for implementation in spatial planning strategies, this way it is ensured that only landslide susceptibility maps are produced which will have clear options for action for each susceptibility class and therefore will be more easily accepted by responsible spatial planners and local authorities.

Acknowledgments The authors thank several institutions and individuals for their support: the colleagues from the Geological Survey of Austria and from the Austrian Service for Torrent and Avalanche Control for providing inventory data; the Provincial Government of Lower Austria in particular the colleagues from the Geological Survey and the Department of Spatial Planning and Regional Policy for inventory data. Thanks to them for supporting the MoNOE-project and for numerous fruitful discussions. Thanks also to the Department for Hydrology and Geoinformation for providing LiDAR and orthophoto data.

Finally, the authors are grateful for financial support of the Provincial Government of Lower Austria.

References

Leopold P, Heiss G, Petschko H, Bell R, Glade T (this volume) Susceptibility maps for landslides using different modelling approaches. In: Proceedings of the 2nd world landslide forum, Rome, 3–7 Oct 2011

Petschko H, Bell R, Leopold P, Heiss G, Glade T (this volume) Landslide inventories for reliable susceptibility maps. In: Proceedings of the 2nd world landslide forum, Rome, 3–7 Oct 2011

Petschko H, Glade T, Bell R, Schweigl J, Pomaroli G (2010) Landslide inventories for regional early warning systems. In: Malet J-P, Glade T, Casagli N (eds) Proceedings of the international conference 'Mountain Risks: Bringing Science to Society', Firenze, 24–26 November 2010, pp 277–282

Pomaroli G, Bell R, Glade T, Heiss G, Leopold P, Petschko H, Proske H, Schweigl J (2011) Darstellung der Gefährdung durch gravitative Massenbewegungen im Bundesland Niederösterreich als Grundlage der Raumplanung. In: Wildbach und Lawinenverbau. Zeitschrift für Wildbach-, Lawinen-, Erosions- und Steinschlagschutz, Society of

Engineers in the Austrian Torrent and Avalanche Control, Wien, 74, 166, pp 198–212

Proske H, Bauer C, Granica K (this volume) Different approaches of Rockfall Susceptibility Maps in Lower Austria. In: Proceedings of the 2nd world landslide forum, Rome, 3–7 Oct 2011

Schwenk H (1992) Massenbewegungen in niederösterreich 1953–1990. In: Jahrbuch der geologischen bundesanstalt. Geologische Bundesanstalt, Wien, pp 597–660

Wessely G (2006) Geologie der österreichischen Bundesländer. Niederösterreich, Wien

www.noe.gv.at (2011) Rainfall for the period 1971–2000 in Lower Austria, http://www.noe.gv.at/ExterneSeiten/Wasserstand/folder_n_lt/niederschlag/bemessung/n_1971_2000.htm. Accessed 25 June 2011

The Geological Hazard Map of Catalonia 1:25,000. A Tool for Geohazards Mitigation

Pere Oller, Marta González, Jordi Pinyol, Marcel Barberà, and Pere Martínez

Abstract

We present the Geological Hazard Prevention Map of Catalonia 1:25,000 (MPRG25M), and in detail, the procedure carried out for landslide hazard determination. As a component of the Geoworks of the Geological Institut of Catalonia (IGC), the MPRG25M is a multi-hazard map at 1:25,000 scale conceived to be used for land use planning. It includes the representation of evidence, phenomena, susceptibility and natural hazards of geological processes. These are the processes generated by external geodynamics (such as slope, torrent, snow, coastal and flood dynamics) and internal (seismic) geodynamics. The information is displayed by different maps on each published sheet. The map is intended to enable government and individuals to have an overview of the territory with respect to geological hazards, identifying areas where it is advisable to carry out detailed studies in case of action planning.

Keywords

Geohazards • Mapping plan • Landslides • Catalonia

Introduction

The Parliament of Catalonia approved, by Law 19/2005, the creation of the Geological Institute of Catalonia (IGC), assigned to the Ministry of Land and Sustainability (TES) of the Catalonian Government.

One of the functions of the IGC is to "study and assess geological hazards, including avalanches, to propose measures to develop hazard forecast, prevention and mitigation and to give support to other agencies competent in land and urban planning, and in emergency management". Therefore, the IGC is in charge of making official hazard maps for such a finality. These maps comply with the Catalan Urban Law (1/2005) which indicates textually that in those places where a risk exists, building is not allowed.

The high density of urban development and infrastructures in Catalonia requires geo-thematic information for planning. As a component of the Geoworks of the IGC, the strategic program aimed at acquiring, elaborating, integrating and disseminating the basic geological, pedological and geothematic information concerning the whole of the territory in the suitable scales for the land and urban planning. Geo-hazard mapping is an essential part of this information. Despite some tests have been carried out on extensive areas (Mountain Regions Hazard Map 1:50,000 (DGPAT 1985), Risk Prevention Map of Catalonia 1:50,000 [ICC 2003]), the MPRG25M, started in 2007, is the first mapping plan 1:25,000 which covers the whole country (Fig. 1).

The conception of the map was a major challenge. Despite the intense documentation search done at the beginning of the project, no similar works, merging such number of phenomena, at land planning scale and in a so wide area, were found.

P. Oller (✉) • M. González • J. Pinyol • P. Martínez
Institut Geològic de Catalunya, Balmes 209, Barcelona, Spain
e-mail: pereo@igc.cat

M. Barberà
Geocat Gestió de Projectes, Barcelona, Spain

C. Margottini et al. (eds.), *Landslide Science and Practice*, Vol. 1,
DOI 10.1007/978-3-642-31325-7_61,

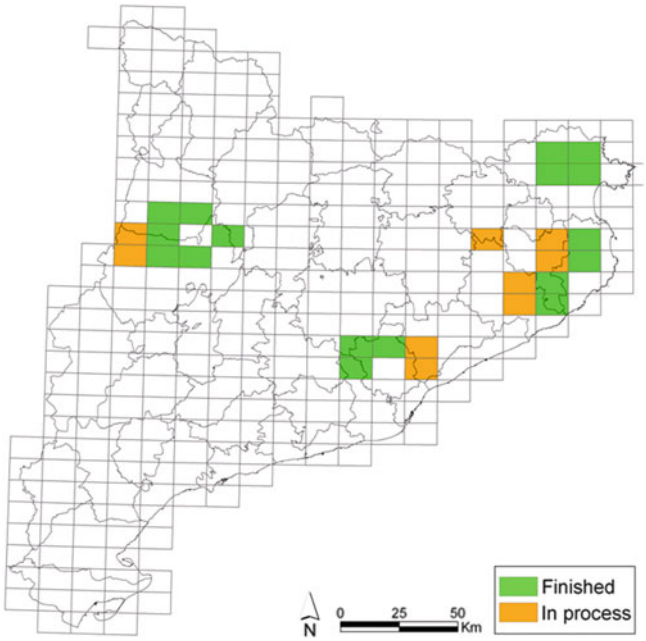

Fig. 1 Map of Catalonia with the MPRG25M mapping plan: 304 sheets 1:25,000, 17 finished (11 published), 9 in progress

Geological Hazard Prevention Map of Catalonia 1:25,000 (MPRGC25M)

The MPRGC25M includes the representation of evidence, phenomena, susceptibility and natural hazards of geological processes. These are the processes generated by external geodynamics (such as slope, torrent, snow, coastal and flood dynamics) and internal (seismic) geodynamics. The information is displayed by different maps on each published sheet. The main map (Fig. 2) is presented on a scale of 1:25,000, and includes landslide, avalanche and flood hazard. Hazard level is qualitatively classified as high (red), medium (orange) and low (yellow). The methods used to analyze hazards basically consist of geomorphological, spatial and statistical analysis.

Several complementary maps on a 1:100,000 scale show hazard caused individually by different phenomena in order to facilitate the reading and understanding of the mapped phenomena. Two additional maps for flooding and seismic hazards, represented on a 1:50,000 scale, are added to the sheet.

The map is intended to enable government and individuals to have an overview of the country, with respect to geological hazards, identifying areas where it is advisable to carry out detailed studies in case of action planning. At the same time a database is being implemented. It will incorporate all the information obtained from these maps. In the future it will become the Geological Hazard Information System of Catalonia (SIRGC).

For hazard evaluation, maximum homogeneity and reproducibility in the mapping procedure is intended, in order to extrapolate it to the entire territory. It consists of a geomorphological approach complemented with GIS analysis and statistical modeling. Terrain susceptibility, frequency, magnitude, and hazard for each different phenomena, are the parameters to be obtained. Of course, expertise is important throughout the entire process. The procedure followed in the main map consists of three steps: (1) catalogue of phenomena and evidences, (2) susceptibility determination, and (3) hazard determination.

The catalogue of phenomena and evidence is the base of the further susceptibility and hazard analysis. It comprises the following four phases: (1) Bibliographic and cartographic search: the information available in archives and databases is collected. (2) Photointerpretation: carried out on vertical aerial photos of flights from different years (1957, 1977, 1985, 2003, etc.). The observation of the topography and the vegetation allows the identification of areas with signs of instability coming from the identification and characterization of events that occurred recently or in the past, and from activity indicators. (3) Field survey: checking in the field the elements identified in the previous phases. Field analysis allows a better approach and understanding, and therefore identifying signs and phenomena not observable through the photointerpretation. (4) Population inquiries: the goal of this stage is to complement the information obtained in the earlier stages, especially in aspects such as the intensity and frequency. It is done through a survey to witnesses who live and/or work in the study areas.

In a second step, areas susceptible to be affected by the phenomena are identified from the starting zone to the maximum extent determinable at the scale of work. Their limits are drawn taking into account the catalogue of phenomena and geomorphological indicators of activity, and from the identification of favourable lithologies and morphologies of the terrain. This phase includes the completion of GIS and statistical analysis to support the determination of the starting and run-out zone. It can be extensively applied with satisfactory results with regard to the scale and purpose of the map.

Finally hazard is estimated on the basis of the analysis of the magnitude and frequency (or activity) of the observed or potential phenomena. Susceptibility areas are classified according to the hazard matrix represented in Fig. 3. Hazard zones are represented as follows: areas where no hazard was detected (white), zones with low hazard (yellow), medium hazard zones (orange), and areas with high hazard (red).

In order to obtain an equivalent hazard for each phenomenon, an effort was made to equate the parameters that define them. The same frequency/activity values were used for all phenomena, but magnitude values were adapted to each of them.

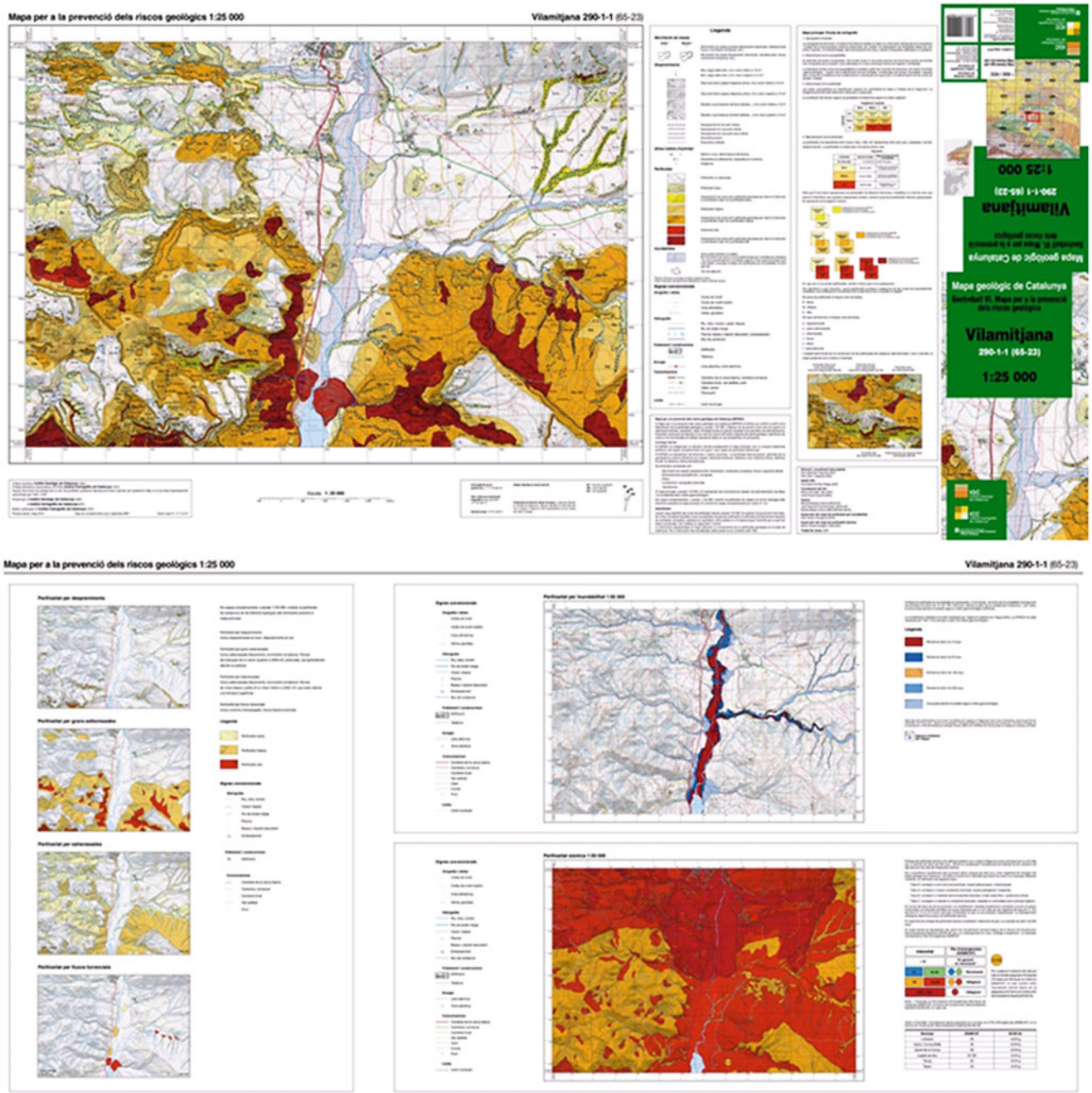

Fig. 2 First published sheet (front and back), Vilamitjana (65-23), in 2010

Each hazard level contains some considerations for prevention (Fig. 4). These considerations inform about the need for further detailed studies and advise about the use of corrective measures.

Hazard from each phenomenon is analyzed individually. The main challenge of the map is to easily present the overlapping hazard of different phenomena. A methodology identifying that this overlap exists has been established with this objective in mind. It indicates what the maximum overlapped hazard is (Fig. 5), but in any case, without obtaining new hazard values.

To identify the hazard level and the phenomena that causes it, especially in overlapping areas, an epigraph is assigned (Fig. 6). This epigraph consists of two characters, the first in capital letters, indicates the value of hazard (A for high hazard, M for medium hazard and B for low hazard), and the second, in lower-case, indicates the type of phenomena (*d* for rockfalls, *s* for slides, *x* for flows, *a* for

		FREQUENCY / ACTIVITY		
		Low	Medium	High
INTENSITY	Low	Low	Low	Low
	Medium	Low	Medium	Medium
	High	Medium	High	High

Fig. 3 Hazard matrix (based on Altimir et al. 2001)

	PREVENTION	
HAZARD	**Detailed studies**	**Hazard management**
Not observed	-	-
Low	Recommendable	Necessary in certain cases
Medium	Essential	Necessary in many cases
High	Essential	Necessary in most of the cases

Fig. 4 Prevention recomendations

avalanches and *f* for subsidence and collapses). The higher the overlapping, the longer the epigraph will be (Fig. 7).

Landslide Hazard Analysis Procedure (Main Map)

On the map, landslides are classified as rockfalls, slides, and torrent flows (based on Varnes 1978). Slides include translational, rotational, complex, and shallow slides, and earth flows. Torrent flows include debris flows. In fact, we are dealing with quite different phenomena, which are controlled by different factors, and have different type of motion. Consequently the treatment applied to each one of them is specifically adapted.

As explained before, the analysis process includes the susceptibility and hazard analysis (Fig. 8).

Susceptibility Analysis

The first step is to obtain the susceptibility. It is done by crossing lithology with slope inclination according to Table 1. This is obtained through GIS analysis by crossing the geological map 1:25,000 with the slope map obtained from the digital terrain model 5 × 5 m (ICC) (Fig. 9). For

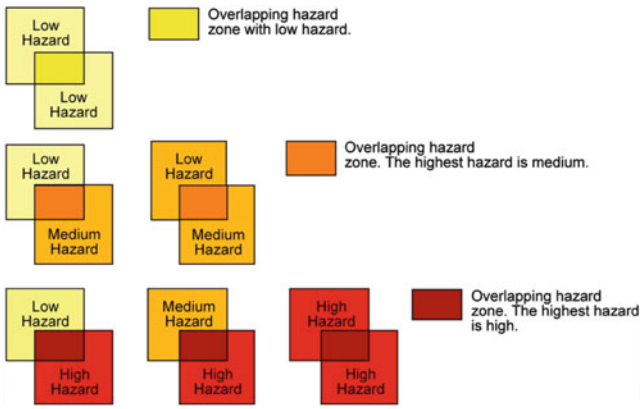

Fig. 5 Multi-hazard representation

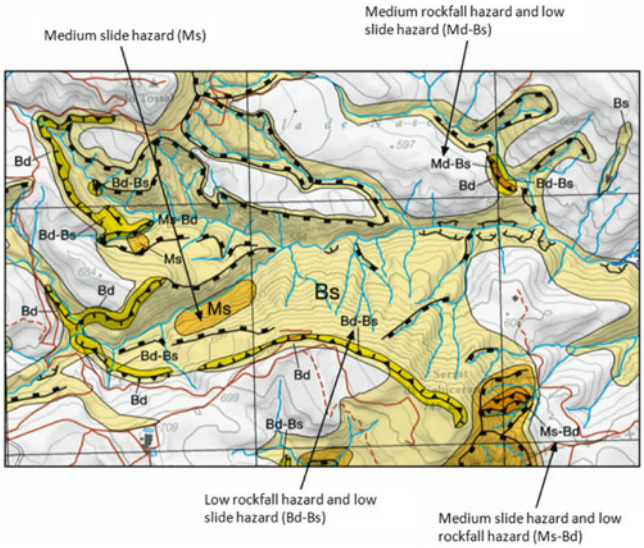

Fig. 6 Example of multi-hazard representation. This figure is part of the explanatory information of the map (original scale: 1:25,000)

such a purpose the geological map is automatically processed and converted into a superficial deposits map. From this map susceptible lithologies are identified, listed in Table 1. Combining it with their critical slope inclinations, a first approach to susceptibility to iniciation for slides is obtained. For rockfalls a simpler classification is used in order to detect rocky slopes (45–70°) and escarpments (>70°), for any kind of rock (bedrock or engineering soil) (Table 2).

This procedure identifies the terrain susceptible to develop the phenomena. To identify the terrain susceptible of being affected by the different phenomena, the inventory is essential. With the inventory, a first map that includes starting, track and runout susceptible terrain is drawn. Table 3 shows the activity and geomorphological indicators considered for the different types of phenomena.

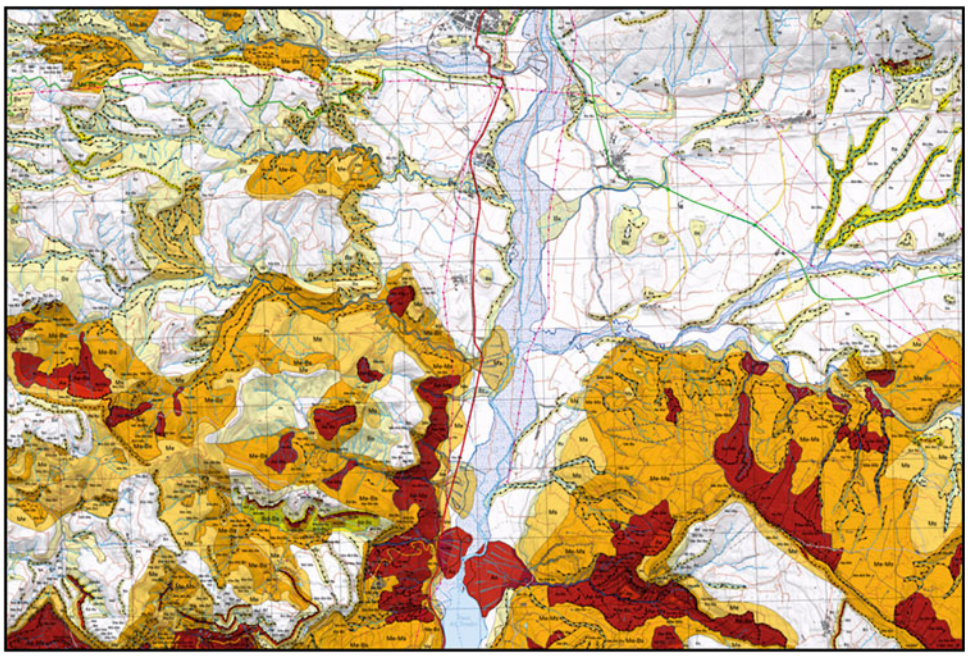

Fig. 7 Main map 1:25,000, which includes landslides, avalanches, sinking and flooding according to geomorphologic criteria

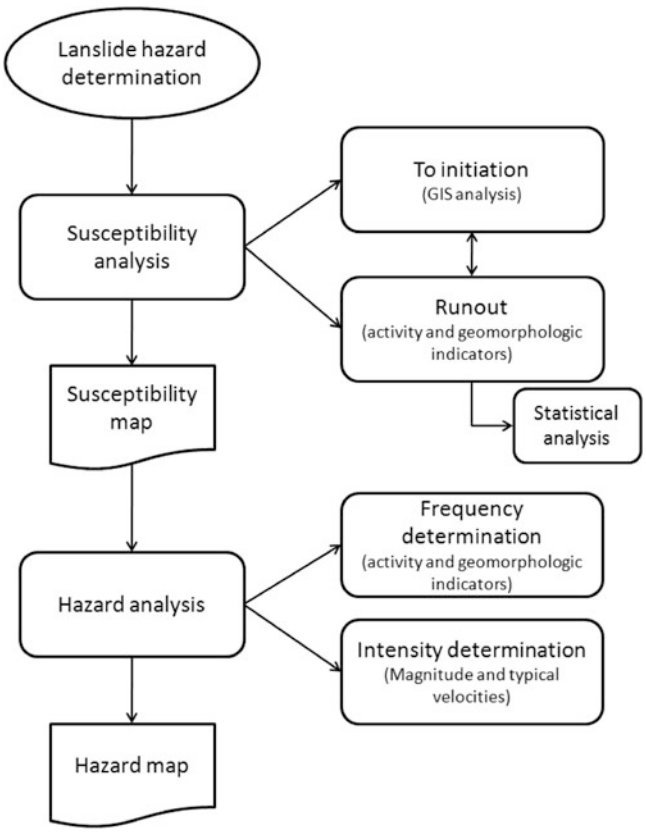

Fig. 8 Lanslide hazard determination process

To validate the susceptibility on the one hand and in order to improve the inventory during field work, on the other hand, the susceptibility map and the inventory map are compared, with a search for activity indicators in areas where susceptibility was identified. If evidence corroborates automatic susceptibility, it is confirmed. If no evidence is found, the expert validates or rejects it.

For rockfalls a further analysis is done in order to improve the susceptibility map. The event inventory is checked with the reach angles defined by Corominas (1996), shown in Table 5. This is done systematically by using the CONEFALL1.0 software (Quanterra 2011), which can be broadly applied to obtain maximum reach boundaries in function of observed or expected rockfall volumes. This procedure allows for another approach, by contrasting the map based on terrain indicators with the one based on the statistically obtained angles of reach (Table 4).

For debris flow, the availability of unstable material on the catchment slopes and its capacity to generate this kind of phenomena is evaluated. (Table 5).

Hazard Analysis

Hazard analysis is attained specifically for each phenomenon according to the hazard matrix by combining frequency/activity with intensity values (Fig. 3). Bearing in mind the scale of the map, these parameters are given as an order of

Table 1 Parameters used for obtaining slides and debris flow susceptibility to initiation

Lithologies	Slope angle	Susceptibility
Scree slopes, and uncohesive clastic units in general	> 30°	Moderately high
Superficial deposits and claystone units in general	> 25°	
Superficial deposits and plastic claystone units and slided materials	> 15°	Very high
Plastic claystone units and slided materials	>8°	Extremely high

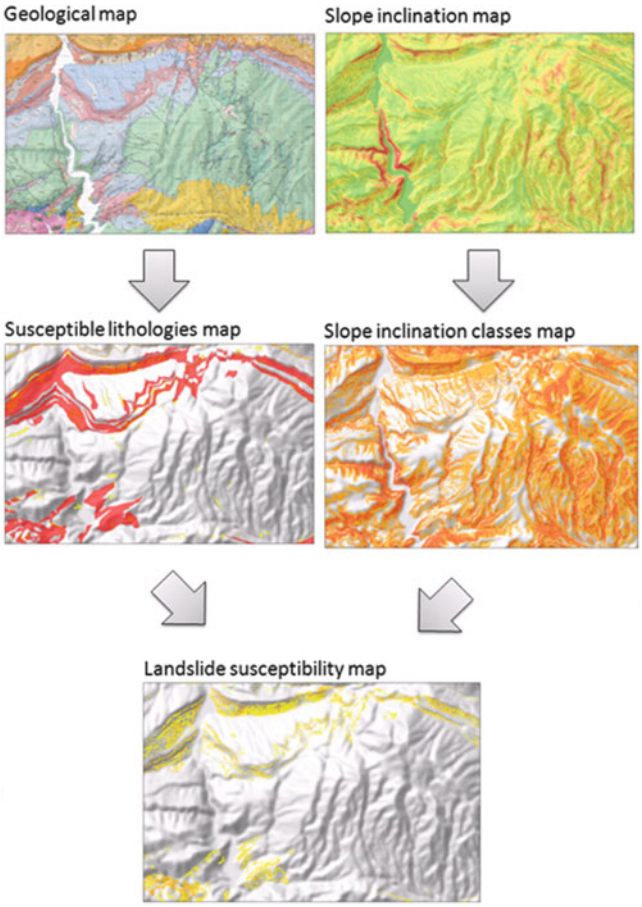

Fig. 9 Process to obtain lanslide susceptibility to initiation

magnitude in a logarithmic scale. Frequency is assigned to repetitive phenomena as rockfalls and debris flows. Activity is assigned to slides as non repetitive phenomena but with a long stabilization process (Table 6).

However, taking into account the scale of the work, it would be unlikely to have enough data to determine the return periods for a particular slope, so that an estimate of the frequency according to the abundance of indicators and their activity is performed. In the case of slides, it is generally difficult to establish frequency beyond 100 years. For this reason the frequency/activity of the movements must be considered taking into account the preservation of the phenomena and the abundance of activity evidence.

A practical criterion is shown in Table 7. In 1956 the first available photographic flight was made over Spain (Servicio Geográfico del Ejército 1956). This flight provided the first aerial images of the country and it is usually used as a starting point. Comparing these images with the present ones, it is possible to observe changes indicating recent landslide activity.

For rockfalls, frequency is obtained from the percentage of scars existing on the escarpment, the number of recent identifiable events, and the existence of blocks of rock at the foot of the escarpment.

Intensity is indirectly obtained through magnitude estimation, and is defined as a function of landslide volume and expected velocity, which is considered an intrinsic characteristic of each type of phenomenon (Cardinali et al. 2002). In Table 8, a classification of magnitudes for slides and debris flows is shown.

For rockfalls, the height of the escarpment is incorporated for obtaining magnitude (Table 9).

Once frequency and intensity are determined, hazard level can be obtained from the hazard matrix shown in Fig. 3.

Final Remarks

The target of the MPRG25M is to give an overview of the territory at 1:25,000 scale, with respect to geological hazards, identifying areas where it is advisable to carry out detailed studies in case of urban or infrastructure planning.

The plan has just started and has shown that some methodological limitations have to be reviewed. A line of applied research is working in parallel to the project in order to improve methodologies and quality of results (e.g. Abancó et al. 2009).

Geohazard information is dynamic. For this reason, a database is being implemented. It will incorporate all the information obtained for the elaboration of these maps, and information coming from the geohazard surveillance service of the IGC. In the future it will become the Geological Hazard Information System of Catalonia (SIRGC).

Table 2 Susceptibility to initiate rockfall. It combines slope angle and lithology

Lithology	Slope angle		
	> 70°	70–45°	45–35°
	(Escarpment)	(Rocky slope)	
Bedrock	High	Medium	
Engineering soils	High	High	
Non cohesive deposits/scree slopes	High	High	Low

Table 3 Activity and geomorphological indicators used for determining susceptibility to a given phenomenon

Indicators	Rockfalls	Slides	Torrent flows
Activity indicators	Scars of recent and old rockfalls	Slide scars	Erosion rate on unstable deposits in the catchment area
		Scarps	
		Undrained depressions	
		Marshy areas	
		Tilted trees	
Geomorphological indicators	Individual rockfall events	Badland areas	Torrent fan
	Individual blocks and deposits at the foot of the escarpment	Creep areas	Debris flow deposits
		Solifluction areas	Levees
	Escarpment	Rock slide deposit	Unstable deposits in the catchment area (tills, slides)
	Scree slopes	Mass slide deposit	

Table 4 Maximum angles of reach (Corominas 1996). Starting volumes are determined from photointerpretation and field observation

Rockfall volume (m^3)	Angle of reach value (absence of obstacles, in °)
1–10	48–40
10–100	40–33
100–1,000	33–26
>1,000	<26

Table 5 Susceptibility determination criteria for debris flows

Magnitude class	Criteria
Low	With little or no availability of material in the catchment and channel (surface covered by moveable material less than 5 %) or slope of the basin below the 10°
Medium	Availability of moveable material in the basin and channel (surface covered by moveable material between 5 % and 25 %) and slope of the basin between 10° and 20°
High	Abundant availability of moveable material in the basin and the channel or large landslides (surface covered by moveable material over 25 %) and slope of the basin higher than 20°

Table 6 Frequency/activity parameters (based on a synthesis from Mather et al. 2003)

F/A class	Frequency	Activity	Age	Preservation
High	<50 years	Historic. Active or reactivable	<100 years	Good
Medium	50–500 years	Dormant young. Inactive but reactivable	100–5,000 years	Medium
Low	>500 years	Dormant mature/old. Inactive	>5,000 years	Bad

Table 7 Activity based on photointerpretation by comparing recent and old aerial photographs

Activity	Activity indicators
Low	Without indicators
Medium	Activity indicators before 1956
High	Activity indicators after 1957

Table 8 Intensity parameters for slides and debris flows (slow to rapid moving landslides)

	Intensity		
Phenomena	High	Medium	Low
Slides and debris flows	>2,000 m^3	800–2,000 m^3	<800 m^3

Table 9 Rockfall magnitude for bedrock based on starting volumes and height of the escarpment (fast moving landslide)

Magnitude	Height of the escarpment (or height of the starting zone)		
Estimated starting volume	<10 m	10–100 m	>100 m
<1 m^3	Low	Medium	Medium
1–10 m^3	Medium	High	High
> 10 m^3	High	High	High

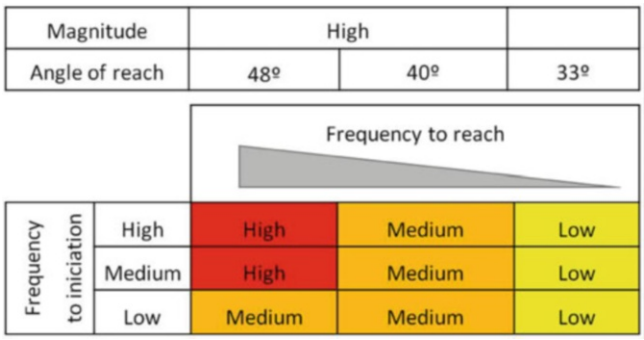

Fig. 10 Example of hazard zoning for expected rockfall of 10–100 m^3

Acknowledgments The authors would like to thank Ian Caldwell for the English reviewing.

References

Abancó C, Lantada N, Hürlimann M, Corominas J, Copons R (2009) Validación de mapas de susceptibilidad de deslizamientos elaborados mediante diferentes técnicas. Aplicación a la zona de Sant Salvador de Toló (Cataluña). In: Proceedings of the VII Simposio Nacional sobre Taludes y Laderas Inestables. Barcelona, 27–30 Oct 2009, pp 725–736

Altimir J, Copons R, Amigó J, Corominas J, Torrebadella J, Vilaplana JM (2001) Zonificació del territori segons el grau de perillositat d'esllavissades al Principat d'Andorra. Actes de les 1es Jornades del CRECIT. 13 I 14 de setembre de 2001, pp 119–132

Cardinali M, Reichenbach P, Guzzetti F, Ardizzone F, Antonini G, Galli M, Cacciano M, Castellani M, Salvati P (2002) A geomorpholgical approach to the estimation of landslide hazards and risks in Umbria, Central Italy. Nat Hazard Earth Syst Sci 2:57–72

Corominas J (1996) The angle of reach as a mobility index for small and large landslides. Can Geotech J 33:260–271

DGPAT (1985) Mountain Regions Hazard Map 1:50000. Generalitat de Catalunya, Barcelona

ICC (2003) Risk Prevention Map of Catalonia 1:50000. Generalitat de Catalunya, Barcelona

Mather E, Griffiths J, Stockes M (2003) Anatomy of a "fossil" landslide from the Pleistocene of SE Spain. Geomorphology 50:135–149

Quanterra (2011) CONEFALL1.0. Homepage. URL: http://www.quanterra.org/softs.HTM#soft01. Last accessed 19 June 2011

Servicio Geográfico del Ejército (1956) Vuelo Americano. Serie B. Madrid

Varnes J (1978) Slope movement types and processes. In: Schuster RL, Krizek RJ (eds) Landslides, analysis and control, Transportation Research Board Sp. Rep. No. 176. National Academic of Sciences, Washington, DC, pp 11–33

Zoning and Mapping Landslide Hazard in the Castelnuovo di Garfagnana Region (Tuscany, Italy)

Paolo Roberto Federici, Alberto Puccinelli, Giacomo D'Amato Avanzi, Francesco Falaschi, Roberto Giannecchini, Daria Marchetti, Alberto Pochini, Franco Rapetti, and Adriano Ribolini

Abstract

ISPRA and Tuscany Region Administration recently funded a project aimed at assessing and mapping landslide hazard of the area of the n. 250 "Castelnuovo di Garfagnana" map (1:50,000 scale). The area includes the upper Serchio River basin (Tuscany, Italy) and exhibits peculiar geological and geomorphological features and severe climatic conditions, which cause high landslide hazard. The project proceeded as follows:

- 1:10,000 geomorphological survey and landslide inventory map;
- Physical and mechanical properties of rocks (discontinuities, strength, rock mass classification) and soils (grain size, consistency);
- GIS oriented organization of the spatial distribution of the considered factors;
- GIS supported statistical analysis (spatial analysis, conditional and multivariate analyses, neural network technique);
- Landslide hazard map, where landslide hazard is subdivided into five classes based on instability probability;
- Final products: landslide hazard map at 1:50,000 scale, together with other related maps (landslide map, structural sketch, geotechnical sketch, isohyet map, etc.); explaining booklet; database.

Keywords

Landslide • Hazard • GIS • Statistical analysis • Map • Tuscany

Introduction

Landslide hazard and risk assessment, zonation and mapping are crucial items for protection and planning of either rural or urban areas and population. These are great challenges for applied research and are among the main topics of the International Consortium on Landslides and the International Programme on Landslides (Sassa 2004a, 2004b).

In that context this paper presents the main results of an experimental research project promoted by ISPRA (Italian Institute for Environmental Protection and Research) and Tuscany Region Administration: it aimed at assessing and zoning landslide hazard in the area covered by the sheet n. 250 « Castelnuovo di Garfagnana » of the Topographic Map of Italy at 1:50,000 scale. The study area (Fig. 1) is mainly part of North-Western Tuscany, while a minor part falls within South-Western Emilia-Romagna. This territory, nearly 600 km^2 wide, shows high landslide susceptibility because of its geological, morphological and climatic characteristics: thousands of landslides involve natural and man-made environments and often threaten properties and

P.R. Federici (✉) • A. Puccinelli • G.D.A. Avanzi • R. Giannecchini • D. Marchetti • A. Pochini • F. Rapetti • A. Ribolini
Dipartimento di Scienze della Terra, Università di Pisa, Via Santa Maria 53, Pisa 56126, Italy
e-mail: damato@dst.unipi.it

F. Falaschi
Autorità di Bacino del Fiume Serchio, Via Vittorio Veneto 1, Lucca 55100, Italy

C. Margottini et al. (eds.), *Landslide Science and Practice*, Vol. 1,
DOI 10.1007/978-3-642-31325-7_62,

human lives. Therefore it was selected for developing and testing the experimental method explained here.

The conceptual framework of landslide hazard and risk assessment constitutes a large and rather complex amount of knowledge about landslides, and is based on a few assumptions widely accepted by scientists (Guzzetti et al. 1999). It must also face problems and difficulties due to both conceptual and operative constraints.

Techniques aiming at defining landslide susceptibility are divided into two basic categories: direct and indirect methods. Direct approach is based on the ability of scientists in evaluating the potential slopes instability considering many instability factors and parameters, derived from geological and geomorphological maps or detected on site. Drawbacks concern the high subjectivity and uncertainty of such investigation. Indirect methods could be either semi-quantitative (heuristic or index method) or quantitative (statistical, probabilistic and physically-based methods) (Guzzetti et al. 1999). Among them, statistical methods are suitable for wide scale assessment projects (Carrara et al. 1991, 1992; Federici et al. 2007; Falaschi et al. 2009). Goodness of statistical methods relies on the ability of the model in estimating statistical weight and efficacy of the instability factors, in order to prevent errors and meaningless classification of the terrain units (Meijerink 1988; Carrara et al. 1995). Nevertheless, evaluations built up for one specific area cannot be easily inferred to very different test areas (Guzzetti et al. 1999).

Materials and Methods

The study area falls within the Northern Apennines, a fold and thrust chain mainly formed during the Upper Cretaceous–Upper Miocene. Since the upper Miocene tensional tectonics gave origin to tectonic depressions bounded by NW-SE trending normal faults (Fig. 2). Here many geological units crop out, belonging to Ligurian and Subligurian units, Tuscan Nappe and Apuan Alps metamorphic core. Pliocene and Quaternary deposits include fluvial-lacustrine sequences and slope, alluvial and glacial sediments (Puccinelli et al. 2010).

This region is placed between the Apuan Alps to SW and the Apennines main chain to NE and shows typical mountain landforms and steep slopes (Fig. 1). Its altitude varies between about 100 m and almost 2,000 m a.s.l. Rainfalls are remarkable and vary between 1,300 and more than 2,000 mm/year. Due to its geological, geomorphological and climatic features, high landslide susceptibility and frequency characterize this area and press to assess its hazard.

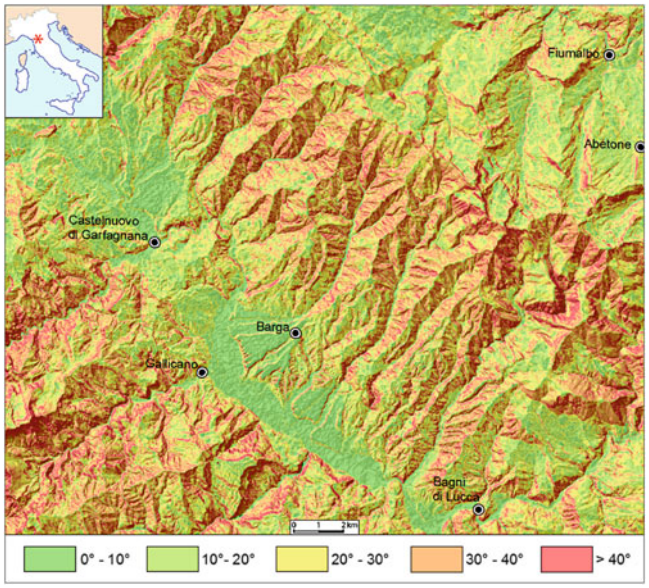

Fig. 1 Slope angle map and location of the study area (After Federici et al. 2011, modified)

A multidisciplinary approach was implemented: data coming from the investigation (geotechnical features, slope gradient, slope aspect, land cover, distance from streams, distance from tectonic elements) were converted into GIS-oriented layers and matched with the actual landslide distribution. Then two distinct statistical methods were applied in order to rank slope instability.

The study proceeded as follows:

- Inspection of available landslide inventories and maps of the study area (Nardi et al. 1986, 2000; D'Amato Avanzi et al. 2000, and references therein).
- Geomorphologic investigation, to realize a landslide inventory and know the relationship between geomorphological processes and slope instability;
- Geotechnical investigation, to analyse physical and mechanical properties of rocks and soils and link them to instability;
- Organization of the spatial distribution of the considered factors in different layers, their overlay and matching with landslide distribution, to link instability factors and landslide occurrence;
- GIS supported statistical analysis (spatial analysis, conditional and multivariate analysis), to supply hypothetical connections with quantitative response.

The landslide inventory considered 14,136 landslides, involving 90.9 km^2 (15.3 % of the whole area) and included information on morphometry, types of movement and activity, according to Cruden and Varnes (1996). The landslide sketch

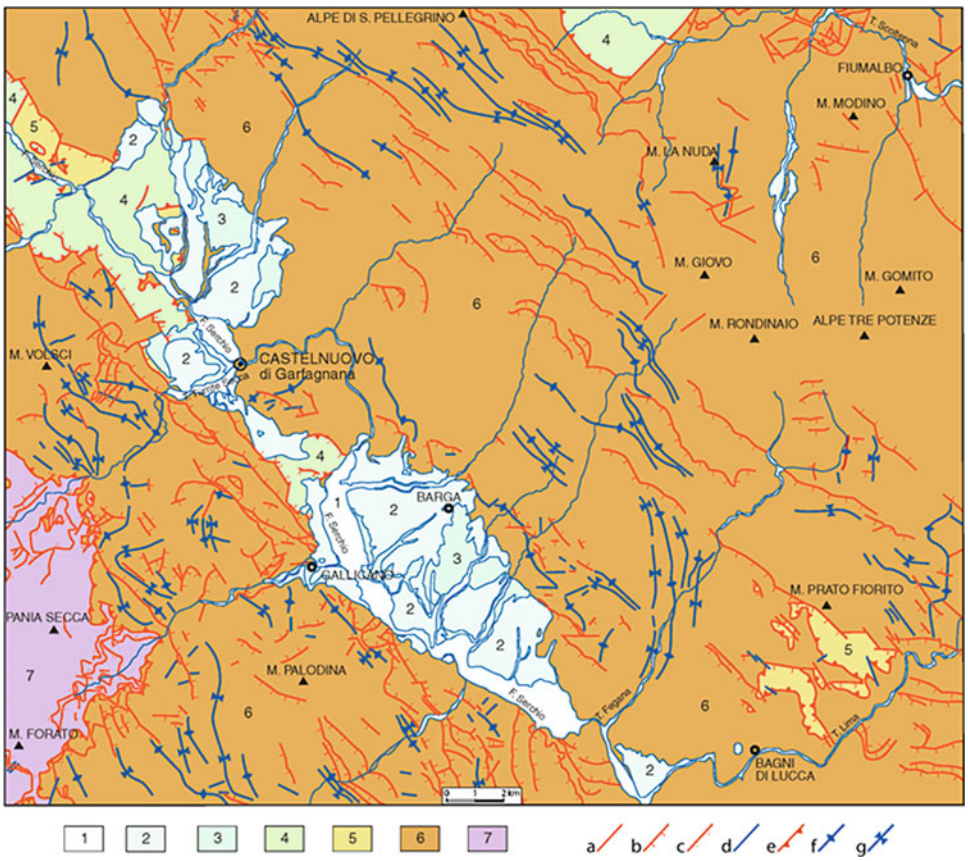

Fig. 2 Tectonic sketch of the study area. *1* Present alluvial sediments, *2* Ancient alluvial deposits, *3* Fluvial-lacustrine deposits, *4* Ligurian Unit, *5* Subligurian Unit, *6* Tuscan Nappe, *7* - Apuan Alps metamorphic core, *a* Fault, *b* Normal fault, *c* Reverse fault, *d* Transfer fault, *e* Thrust, *f* Anticline axis, *g* Syncline axis (After Federici et al. 2011, modified)

map shows the overall distribution of the landslides detected in the study area (Fig. 3). Most of the detected mass movements are translational and/or rotational landslides, which may evolve in flow and take nearly 83 % of the area investigated. The other types of movements are a minority.

Geotechnical investigations allowed to classify and map rock mass and soil characteristics and improved the statistical significance of the lithological factor. Several properties were investigated (ISRM 1978, 1981): strength, discontinuity spacing and conditions, Rock Mass Rating (Bieniawski 1989) for rocks; texture and consistency for soils. So, tens of geotechnical units were identified. Basing on their behaviour they were grouped into 33 units, a reasonably manageable number for the multivariate analysis. Thirteen basic units were also identified and mapped, basing on several different parameters: structure, weak rock/hard rock, strength for rocks; grain size, consistency, frictional or cohesive behaviour for soils. Table 1 and Fig. 4 list and depict features and spatial distribution of these basic units.

Landslide hazard assessing and mapping using statistical methods is based on a fundamental assumption: the presence of a set of factors believed in connection with slope instability and related to the geological, geomorphological, geotechnical and climatic conditions, to be processed using predicting model of landslide occurrence (Dietrich et al. 1995).

The past and present landslide distribution is the key parameter to predict landslide occurrence in the future (Varnes and IAEG 1984; Carrara et al. 1991; Hutchinson 1995); landslide frequency in each map unit, corresponding to landslide susceptibility (Morgan 1968) is powerful in ranking slope instability.

A probabilistic approach also needs selection of method and map unit type. At first Conditional Analysis was applied and 316 Unique Conditions map Units (UCU) were identified. The UCUs imply the classification of each slope instability factor into few significant classes, which are stored into a single map, or layer. By overlaying all layers, homogeneous domains (i.e. UCUs) are singled out (Hansen 1984). Number and size of the UCUs depend on the criteria used in classifying the input factors. Finally, landslide frequency in each UCU is computed, and instability is firstly classified applying a classificatory algorithm to the distribution of landslide frequency in each UCU. This technique, named Jenks' algorithm (Jenks 1989), identifies the most significant and natural break points of an ordered distribution of data and maximizes the differences between classes. Five instability classes, ranked from very low to very high, were stated.

Afterwards, multivariate regression analysis (Logit model) was performed. Regression analysis plays a central role in

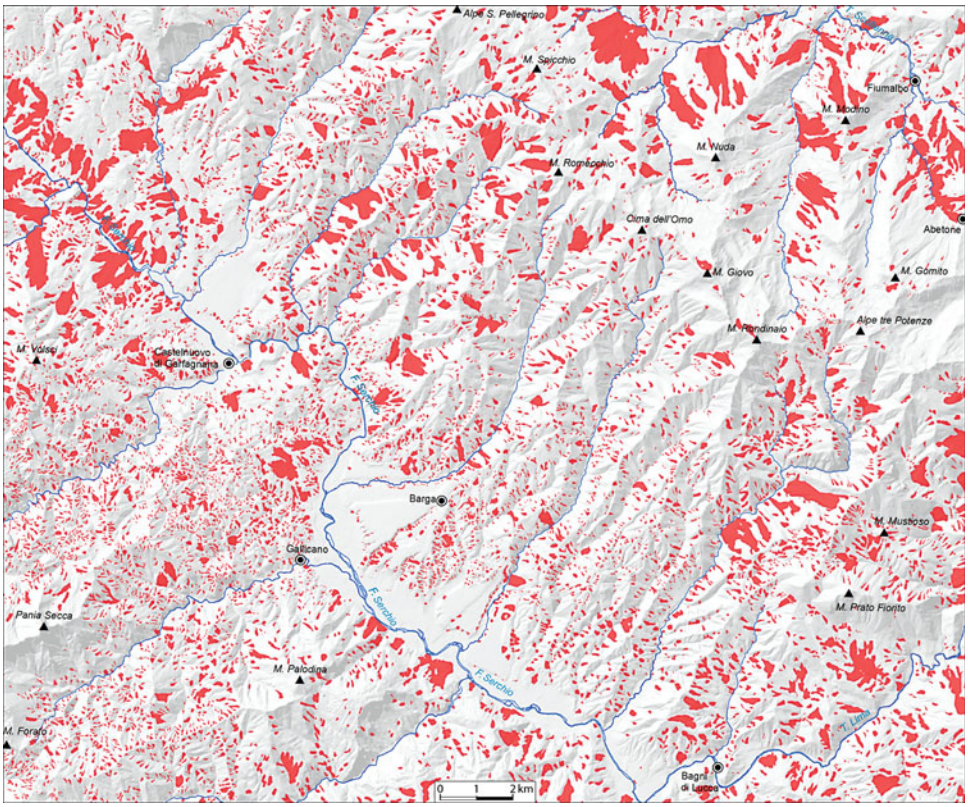

Fig. 3 Landslide map of the study area (in *red*: landslide areas; after Federici et al. 2011)

Table 1 Basic geotechnical units of the study area

Geotechnical unit	Remarks
1 Massive or thick bedded hard rocks	Massive structure, medium-high mass strength
2 Roughly bedded hard rocks	Mainly massive structure, medium-high mass strength
3 Stratified hard rocks	Bedded structure, very rare or absent pelitic, weak layers, medium-high mass strength
4 Hard rocks with pelitic interbeds	Mainly hard complex unit (weak rock, pelite < 25 %)
5 Hard rocks alternating with pelitic rocks	Complex unit (pelite from 25 % to 75 %)
6 Pelitic rocks with hard rock interbeds	Mainly pelitic complex unit (weak part < 25 %)
7 Highly deformed mainly pelitic rocks	Mainly weak, pelitic units
8 Grain-supported conglomerate and breccia	Mainly frictional behaviour
9 Matrix-supported sandy conglomerate and breccia	Mainly frictional behaviour
10 Very consistent and/or cemented sand	Mainly frictional behaviour
11 Consistent silt	Mainly cohesive behaviour
12 Gravel with boulders, cobbles and pebbles	Mainly frictional behaviour
13 Gravel with sand	Mainly frictional behaviour

statistics, being one of its most powerful and commonly used techniques. The standard linear regression models assume that the response variable is normal (or at least can be transformed into a normal one). Unfortunately, this case is not so frequent. A wide variety of models with a categorical response is a typical example, where the assumption of normality cannot be accepted as reasonable. Using the Generalized Linear Model, data mining was approached by mean of an extension of the General Linear Model, in order to include response variables that follow any probability distribution in the exponential family of distributions (McCullag and Nelder 1989).

Then GIS-supported map algebra drives the computation of the landslide index for each UCU. The 316 UCUs were divided into two groups: (1) unstable units and (2) stable units, discriminated by a threshold corresponding to the landslide density in the overall study area (about 15.8 %). This threshold falls within the landslide density range of the whole territory and can be a reasonable value, reflecting the geological and geomorphological setting of the study area.

This *a priori* definition of two distinct groups, and data codification by means of dummy variables, provides the dataset for advanced multivariate statistics through logistic

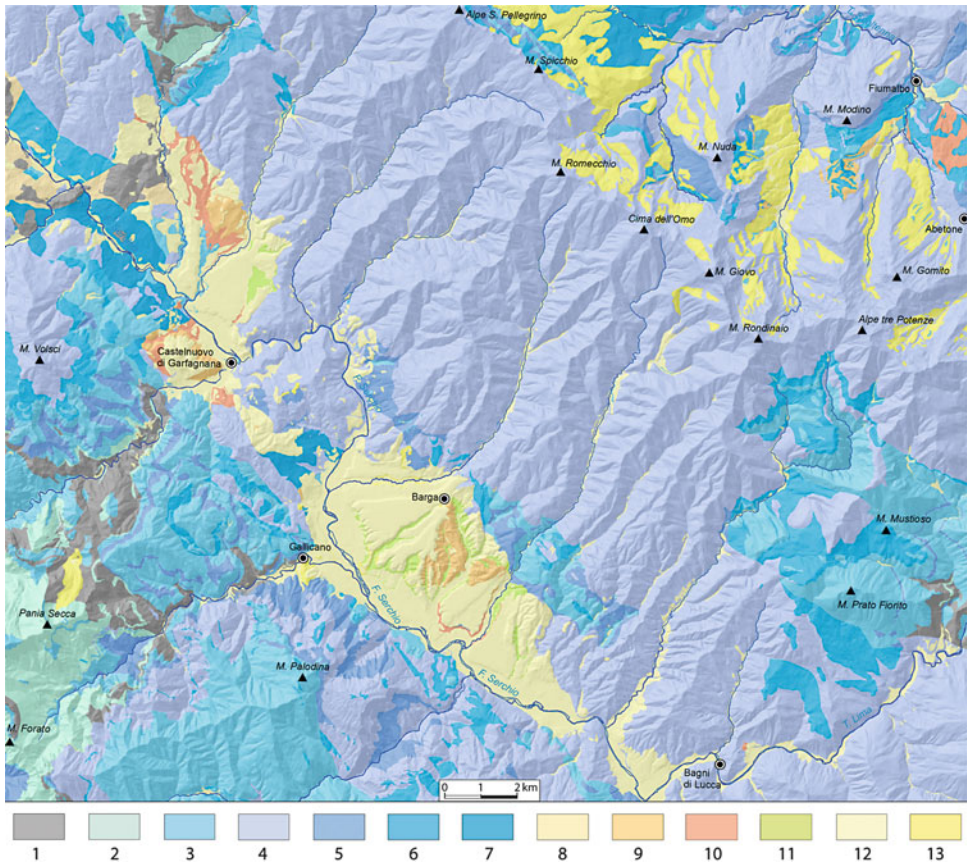

Fig. 4 Geotechnical sketch map of the study area (After Federici et al. 2011) (See Table 1 for legend and explanations)

regression. Logistic regression model was computed by using the Logit function (Piccolo 2000). Finally, the prediction power of the model was calculated and a likelihood-ratio test was applied, in order to calculate the effectiveness of the logistic regression analysis (McCullagh and Nelder 1989; Casella and Berger 1990).

Results

The procedure above resumed lead to subdivide the study area into five classes of landslide hazard (relative hazard or landslide susceptibility), based on their probability on instability (Table 2 and Fig. 5).

Among the variables entered into the Logistic Regression model, those reflecting the rock type and its geotechnical features are generally most effective in differentiating unstable and stable units. Conversely, land cover proved to be a rather poor predictor of landslide distribution, because more than 80 % of the investigated area is covered by wood. General comments can be made comparing the landslide hazard map (Fig. 5) with the geotechnical and landslide maps (Figs. 3 and 4).

Very low and low hazard areas prevail at the lower altitudes, mainly along and around the Serchio river course:

Table 2 Hazard classes, probability of instability (Pi), taken surface and % of the study area

Legend	Hazard	Pi	Km^2	%
	Very high	82 % ≤ Pi < 100	61.2	10.3
	High	61 % ≤ Pi < 82	108.7	18.3
	Intermediate	39 % ≤ Pi < 61	173.6	29.3
	Low	16 % ≤ Pi < 39	114.5	19.3
	Very low	0 % ≤ Pi < 16	134.9	22.8

alluvial deposits with mainly frictional behaviour crop out there and slope gradient is very low or null. Carbonate, massive or bedded strong rock formations underlie other very low or low hazard zones, in the western and eastern parts of the study area, where slope gradient is higher.

Intermediate hazard characterizes most of the study area, where medium-hard sandstone, interbedded by pelite, crops out and the slope gradient is medium to high. This sandstone

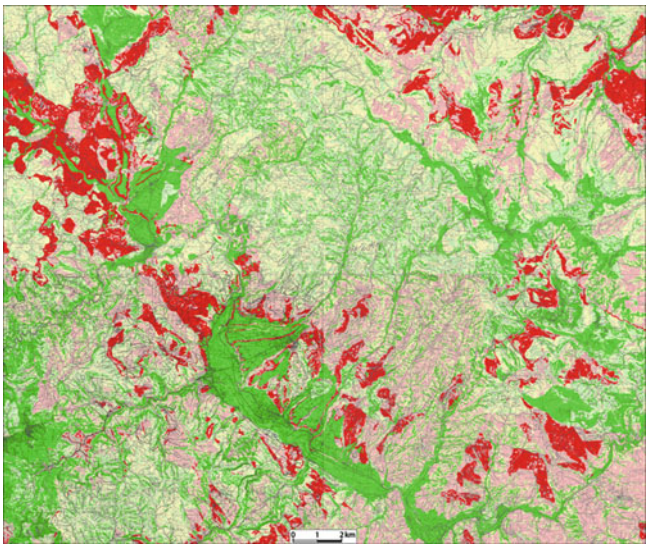

Fig. 5 Landslide hazard map (After Federici et al. 2011) (See Table 2 for legend and explanations)

is typical of a well-known rock formation, named Macigno Fm., which underlies most of the Northern Apennines ridge.

Very high and high hazard areas take 169.9 km^2 of the study area (28.6 % of the total, Table 2). They are mainly due to pelitic weak rocks and clay–sandy fluvial-lacustrine deposits, with cohesive or cohesive-frictional behaviour. High hazard zones cover wide areas along the Serchio river course and the eastern and north-eastern portion of the study area.

Discussion and Conclusion

Landslide hazard zonation and mapping are fundamental in planning land use and protect territory and population.

Results and products of the research project presented here can improve the current knowledge on these items. The statistical approach used conditional and multivariate regression analyses and GIS techniques to collect and process data from geological, geomorphological and geotechnical investigations. So, the instability factors were analysed and compared each other in relation to landslide occurrence and distribution.

The zonation of the land surface in different landslide hazard classes is the main outcome of this multidisciplinary approach. Comparison of the results with actual geomorphological and instability features showed a good fitting. However, benefits and drawbacks of this method are not fully clear. This model is still experimental and needs further investigations and checks before applying it to forecasting.

Acknowledgments ISPRA (Italian Institute for Environmental Protection and Research) and Tuscany Region Administration funded this research project, aimed at assessing and mapping landslide hazard of the area of the n. 250 « Castelnuovo di Garfagnana » map (1:50,000 scale). The Authors are grateful to the Reviewers for their useful suggestions.

References

Bieniawski ZT (1989) Engineering Rock Mass Classification. Wiley, New York, p 251

Carrara A, Cardinali M, Detti R, Guzzetti F, Pasqui V, Reichenbach P (1991) GIS tecniques and statistical models in evaluating landslide hazard. Earth Surf Process Landf 16:427–445

Carrara A, Cardinali M, Guzzetti F (1992) Uncertainty in assessing landslide hazard and risk. ITC J 2:172–183

Carrara A, Cardinali M, Guzzetti F, Reichenbach P (1995) GIS technology in mapping landslide hazard. In: Carrara A, Guzzetti F (eds) Geographical information systems in assessing natural hazards. Kluwer, Dordrecht, pp 135–175

Casella G, Berger L (1990) Statistical inference. Duxbury Press, Belmont, p 650

Cruden DM, Varnes DJ (1996) Landslides types and processes. In: Turner AK, Schustedr RL (eds) Landslides investigation and mitigation, Transport Research Board, Spec. Report 247. National Academic Press, Washington, DC, pp 36–75

D'Amato Avanzi G, Puccinelli A, Verani M (2000) Progress in methods in the studies on slope instability in North-Western Tuscany. Atti Soc Tosc Sci Nat Mem A 107:115–123

Dietrich EW, Reiss R, Hsu ML, Montgomery DR (1995) A process-based model for colluvial soil depth and shallow landsliding using digital elevation data. Hydrological Process 9:383–400

Falaschi F, Giacomelli F, Federici PR, Puccinelli A, Casarosa N, D'Amato Avanzi G, Pochini A, Ribolini A, Testi C (2009) Logistic regression vs. artificial neural networks: landslide susceptibility evaluation in a sample area of the Serchio River valley, Italy. Nat Hazards 50:551–569

Federici PR, Puccinelli A, Cantarelli E, Casarosa N, D'Amato Avanzi G, Falaschi F, Giannecchini R, Pochini A, Ribolini A, Bottai M, Salvati N, Testi C (2007) Multidisciplinary investigations in evaluating landslide susceptibility. An example in the Serchio River valley (Italy). Quat Int 171–172:52–63

Federici PR, Puccinelli A, N, D'Amato Avanzi G, Falaschi F, Ribolini A, Bottai M, Capitani M, Casarosa N, Giannecchini R, Marchetti D, Pochini A, Rapetti F, Salvati N, Testi C (2011) Carta della pericolosità geologica per instabilità dei versanti alla scala 1:50.000. Foglio 250 Castelnuovo di Garfagnana. http://www.isprambiente.gov.it/media/carg/tematici/250_Castelnuovo_pericolosita/Foglio.html. (In press)

Guzzetti F, Carrara A, Cardinali M, Reichenbach P (1999) Landslide hazard evaluation: a review of current techniques and their application in a multi-scale study, Central Italy. Geomorphology 31:181–216

Hansen A (1984) Landslide hazard analysis. In: Brunsden D, Prior DB (eds) Slope instability. Wiley, New York, pp 523–602

Hutchinson JN (1995) Landslide hazard assessment. In: Bell DH (ed) Landslides. Balkema, Rotterdam, pp 1805–1841

ISRM (1978) Suggested methods for the quantitative description of discontinuities in rock masses. Int J Rock Mech Min Sci Geomech Abstr 15:319–368

ISRM (1981) Rock characterization, testing and monitoring: suggested methods. Pergamon, New York, p 211

Jenks GF (1989) Geographic logic in line generalization. Cartographica 26(1):27–42

McCullagh P, Nelder JA (1989) Monographs on statistics and applied probability 37. Chapman & Hall, London, p 511

Meijerink AMJ (1988) Data acquisition and data capture through terrain mapping unit. ITC J 1:23–44

Morgan BW (1968) An introduction to Bayesian statistical decision processes. Prentice Hall, New York, p 116

Nardi R, Pochini A, Puccinelli A, D'Amato Avanzi G, Trivellini M (1986) Valutazione del rischio da frana in Garfagnana e nella Media Valle del Serchio (Lucca). Boll Soc Geol It 104:585–599

Nardi R, Puccinelli A, D'Amato Avanzi G (2000) Carta della franosita' del bacino del Fiume Serchio. Autorità' di Bacino del Fiume Serchio, Lucca. http://www.autorita.bacinoserchio.it/cartografie

Piccolo D (2000) Statistica. Il Mulino, Bologna, p 969

Puccinelli A, D'Amato Avanzi G, Perilli N (2010) Carta Geologica d'Italia alla scala 1:50.000. Foglio 250 Castelnuovo di Garfagnana. http://www.isprambiente.gov.it/media/carg/250_Castelnuovo/Foglio.html. In press

Sassa K (2004a) The international consortium on landslides. Landslides 1(1):91–94

Sassa K (2004b) The international programme on landslides. Landslides 1(1):95–99

Varnes DJ, IAEG Commission on Landslides (1984) Landslides Hazard Zonation – a review of principles and practice. UNESCO, Paris, pp 1–60

Landslide Hazard Zonation Using RS & GIS Techniques: A Case Study from North East India

Kuntala Bhusan, M. Somorjit Singh, and S. Sudhakar

Abstract

Remote Sensing (RS) and Geographic Information System (GIS) play a significant role in landslide investigation, in terms of evaluation and analysis of specific landslide event from local to regional scale. It greatly assists in identifying vulnerable zones of future landslide occurrences, which is very important to those who settle in unstable slopes. Generation of regional to large scale landslide hazard zonation map is of great importance for developmental planning in North Eastern Region (NER) of India which falls in the high and medium to high category of the Global Landslide Susceptibility map. In addition to this, rugged and highly undulating topography of the eight states of NE India require serious concern on development of Landslide Early Warning System to reduce landslide related risk. NESAC, being the nodal agency for Space Applications in NER has taken up initiative in the same direction.

Keywords

Remote Sensing • GIS • Landslide

Introduction

The physiography of India shows strikingly that the country can be divided into three well marked regions each having distinguishing characters of its own (Krishnan 1982). The first is the *Peninsula*, the second is the *Indo-Gangetic* alluvial plains and the third is the *Extra-Peninsula*. North Eastern Region (NER) of India is a part of Extra-Peninsula i.e. the mountainous region of the Mighty Himalayan Ranges and its extensions with folded and overthrust mountain chains and is of geologically recent origin. NER has an aerial extent of 2.33 sq.km, comprising difficult mountainous terrain of Sikkim and Arunachal Pradesh and vast alluvial plain of Brahmaputra and Barak valley of Assam. The region also has Patkai-Naga-Lusai range of Nagaland and Manipur extending up to Myanmar (Arakan-Yoma belt); alternate ridge and valley topography of Mizoram and Tripura as well as plateau region of Meghalaya. NER has a distinctive rocks of different geological ages form Archaean to Quaternary. The rock types varies from Archaean crystalline rocks of gneissic complex; quartzites with intercalated phyllites of Shillong Group of Proterozoic sediments, Precambrian to Early Paleozoic rocks of granite gneiss, migmatites, low grade schists, phyllites, quartzites, dolomite, graphite bearing quartz-biotite-sillimanite schist, massive vesicular basaltic rocks, siltstone, carbonaceous shale, and coal etc. of Middle to Late Paleozoic age; Cretaceous rocks of basalts, acid tuff; Tertiary rocks of calcareous shale, sandstone-limestone, fossiliferous limestone (Jaintia Group); dark grey splintery shale, thin sandstone (Disang Group); flaggy sandstone and subordinate shale, sandy shale, carbonaceous shale with interbedded hard sandstone, massive bedded sandstone and thick coal seam (Barail Group); alternations of sandstone and sandy shales, thin conglomerate, coarse ferruginous sandstone, siltstone, mudstone (Surma Group); bluish grey to greenish, coarse to gritty ferruginous sandstone, mottled clay, shale, conglomerate (Tipam Group); coarse, gritty,

K. Bhusan (✉) • M.S. Singh • S. Sudhakar
Department of Space, North Eastern Space Applications Centre (NESAC), Shillong, India
e-mail: kuntalabhusan@yahoo.com

C. Margottini et al. (eds.), *Landslide Science and Practice*, Vol. 1,
DOI 10.1007/978-3-642-31325-7_63,

poorly consolidated sandstone and conglomerate with coal pebbles (Dupitila Group); pebble beds, soft sandy clay, clay, conglomerate, grit, sandstone (Dihing Group); Sand, clay, pebble, gravel and boulder deposits of Quaternary and Recent deposits (Krishnan 1982). The unique combination of topography and varying geology which has undergone different stages of deformations made this region vulnerable to ranges of natural disasters. The results from GPS measurements carried out in NE India indicate that about 15–20 mm/year of convergence is being accommodated there (Mukul et al. 2010). The major disaster in this region is earthquake while deformation in active mountain belts coupled with heavy rainfall made hilly terrains of this region vulnerable to landslide and subsidence. Every year this region also experiences cloud burst/thunder storm/cyclone, flood/flash flood, etc. damaging lots of properties and life.

Landslide or slope failure is one of the major natural hazards in India, which causes loss of human lives and properties almost every year apart from disrupting communication links. Nearly 14 % of India's land area is landslide prone; out of which one fifth is located in the North Eastern region (Raju 2002) which has 8 % of Indian total geographic area and 4 % of total population. More than 50 % of the national highway located in this region is affected by recurrent landslide phenomenon especially during monsoon season. Majority of NER falls in the high and medium to high category of the Global Landslide Susceptibility Map with few hotspot areas along Arunachal Himalaya (Kirschbaum et al. 2009). This shows that a systematic study of landslide affected areas/events over the NER are valuable for reducing landslide related risk in this region. Recent advances in satellite remote sensing technology and increasing availability of high-resolution geospatial products have provided an unprecedented opportunity for such study. In this paper, a framework for developing a preliminary real-time prediction system to identify where rainfall-triggered landslides will occur is proposed by combining two necessary components: landslide hazard zonation map and a real-time ground-based sensor. First, a landslide hazard zonation map derived from a combination of surface characteristics using a GIS weighted linear combination approach. Second, a set up for Landslide Early Warning System aided by wireless support of instrumentation transmitting the data through INSAT Satellite similar to Automatic Weather Station (AWS).

Study Area

This paper exemplifies a case study from Mizoram state. The Landslide Hazard Zonation (LHZ) map was prepared along the national highway, 54 (NH 54) for total length of nearly 35 km. between Vairengte to Kolasib townships (Fig. 1). The area is covered between latitudes 24^0 15′ 0″N and 24^0 27′ 30″N and longitudes 92^0 37′ 30″E and 92^0 47′ 30″E. This is the only road connecting Mizoram state and its capital city Aizwal with rest of the India. Kolasib landslide (Fig. 2) present in the southern most part of the study area is one of the major landslides caused by steep slope and road cutting and subsequently it has become a constant trouble especially during rainy season.

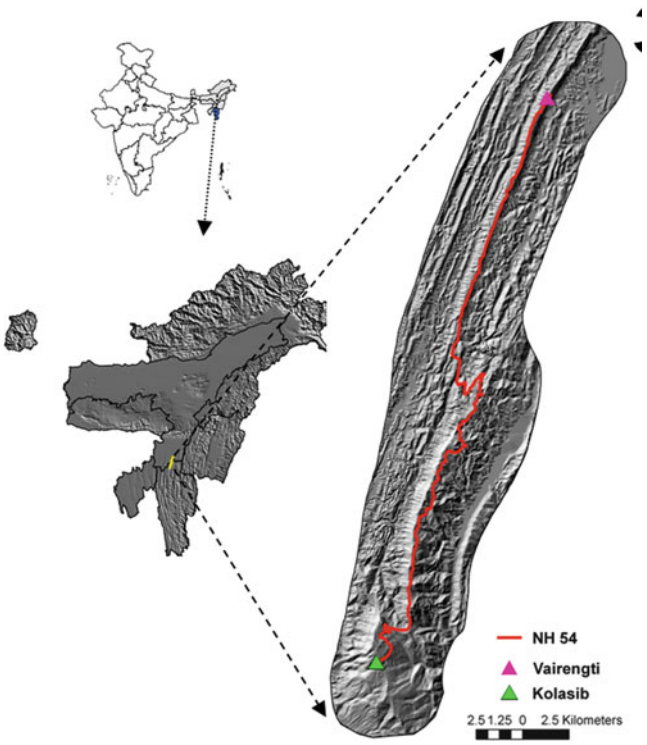

Fig. 1 Location map of the study area

However, apart from this, number of small scale landslide and slip surfaces made this highway highly susceptible to future slides

Methodology

The Landslide Hazard Zonation Mapping on 1:25,000 scale is initiated with preparation of detailed landslide inventory from ground surveys in conjunction with existing collateral data and consulting remotely sensed imageries. Remotely sensed data greatly aid in the investigations of landslides, on both local and regional scale. Although they do not replace fieldwork, interdisciplinary research strategies, and testing the reliability of landslide prediction models, it offer an additional tool from which we can extract information about causes of landslide and most importantly location of its occurrences. Landslide Hazard Zonation (LHZ) refers to the division of the land surface into homogenous areas or domains and their ranking according to different degrees of hazard due to mass movement (Varnes et al. 1984).

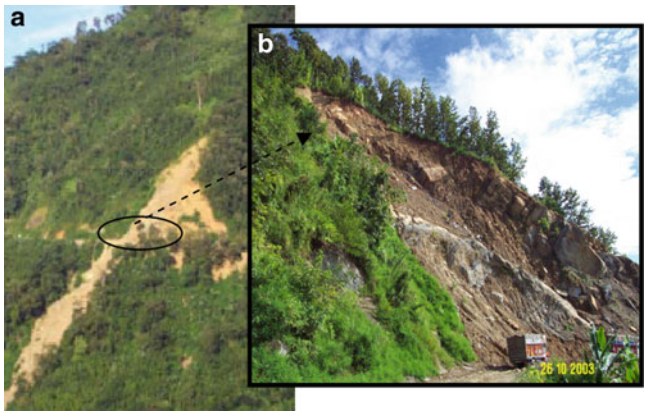

Fig. 2 Kolasib landslide; (**a**) As seen from opposite side of the road, (**b**) Close view of a portion of the slide

Universally, geological and terrain factors play an important role in controlling the slope stability and landslide occurrences (Varnes et al. 1984; Hansen 1984; Cruden 1991, 1993). It is therefore necessary to characterize these parameters for delineating the hazard-prone areas. Precision geo-coded merged FCCs of IRS 1D PAN (spatial resolution of 5.8 m) and LISS III (spatial resolution of 23.5 m) data products of January, 2000 to February, 2003 and Cartosat-1 data of 17th January 2007 (spatial resolution of 2.5 m) along with LISS IV MX data (spatial resolution of 5.8 m) of 20th February 2007, were used for generation of thematic maps. Thirteen thematic maps, namely Drainage Map, Lithological Map, Fault/Lineament Map, Geomorphological Map, Rock Weathering Map, Landslide Map, Land Use/Land Cover Map, Slope-Discontinuity Relation Map, Anthropogenic Factor Map, Soil Texture Map, Soil Depth Map, Slope Map, Slope Aspect Map were generated for the 5 km buffer zone on either side of the highway. Field survey and ground data collection were carried out to validate pre-field interpreted maps. Finally, Landslide hazard assessment and zonation is carried out in GIS environment using multi-layer data integration technique following Analytic Hierarchy Process (AHP) after Satty (1980). The study uses AHP to establish a hierarchical structure for all affecting geo-factors and acquires the weight of each factor by pair-wise comparison. The Hierarchical Structure is achieved by building a mutually independent hierarchical relationship considering the field criteria, and analyzing the elements/geo-factors that might affect the slope stability condition.

Results and Discussion

The Landslide Hazard Zonation Map thus prepared is divided in to five hazard classes, namely, 'Very low hazard, Low hazard, Moderate hazard', High hazard' and Very high' hazard (Fig. 3). The results were validated with respect to

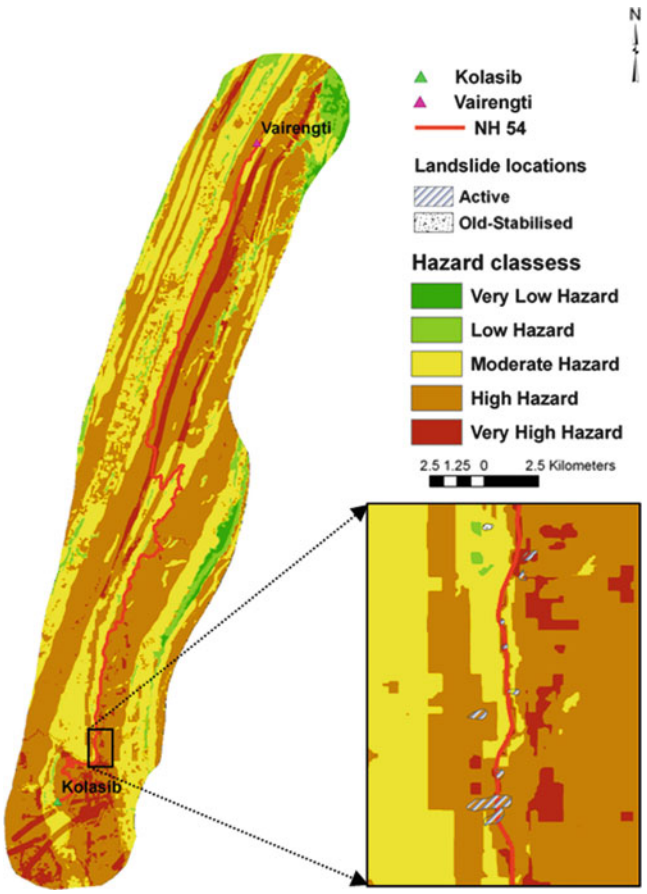

Fig. 3 Landslide Hazard Zonation Map

actual landslide occurrences, and approximately 65 % of existing landslides are distributed in 'Very high' and 'High hazard' classes covering about 50 % of the study area. The 'Very low hazard' class covering about 7 % of the area does not show any landslides as expected. 'Low' and 'Moderate hazard' classes cover about 43 % of the study area.

The study highlights that the slope failure problem is resulted due to interactions of different causes such as geological, structural, hydrological and seismological. Beside these, the quantity, duration and kind of precipitation have also been considered to be as direct mechanical cause. Inter bedded sandstone with shale of Barail Group of rock is the main lithological unit where the interplay of geological structures plays very significant role. In most of the cases shale layers after coming in contact with percolating water from precipitation acts as the sliding plane on which overlying material in this case mostly sandstone along with overburden slides. In highly fractured and jointed areas wedge and planar failure is predominant. Anthropogenic activities like road cutting, jhum cultivation, deforestation etc. are the main causes that have further accentuated instability of the slopes. Extensive deforestation/forest clearing mainly for jhum cultivation/plantation is seen throughout the

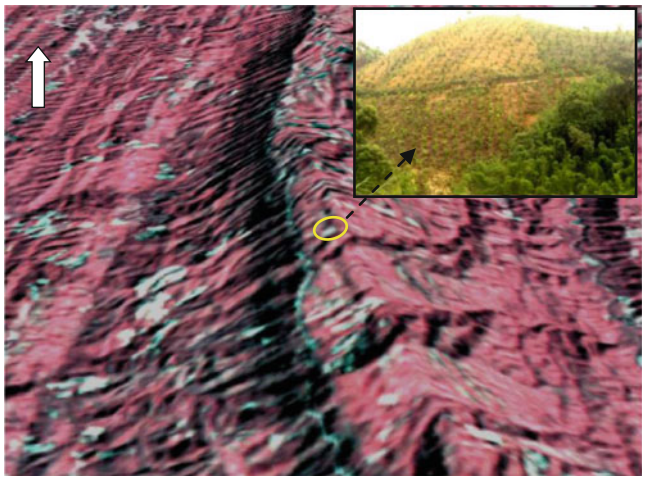

Fig. 4 View of forest cleared land

Fig. 5 Settlements in an old landslide area

study area, in fact the same is true for the whole State. Remotely sensed data is of great help in identifying those areas. One such example is shown in three dimensional perspectives in the Fig. 4.

The State of Mizoram has rugged and highly undulating topography dominated by N-S trending linear anticlinal ridges and synclinal valleys with steep slopes. With the increasing population scenario, rate of urbanization is also fast and many places it has been seen that people are residing in already hazardous areas (Fig. 5).

Conclusion

The Landslide Hazard Zonation map thus prepared can be used for developmental planning. However, only planning at developmental stage can not reduce the landslide related risk moreover a hill slope once safe can become vulnerable over the years. The eight states of North East India due to moderate to highly rugged terrain coupled with increasing anthropogenic activities hence, require serious concern on development of Landslide Early Warning System aided by wireless support of instrumentation transmitting the data through INSAT Satellite similar to Automatic Weather Station (AWS). In those scenarios, the Landslide Hazard Zonation map thus prepared would be an important input for site selection and identification of strategic landslide areas where installation of certain sensors are need of the hour. Since in most of the cases landslides in NER are triggered by rainfall, it was decided to install combination of few sensors, namely, moisture sensor, pore pressure sensor, strain gauge, tilt mete etc. to monitor changes in active landslide areas incorporated due to heavy rainfall. In this line North Eastern Space Application Centre has taken an initiative to generate Landslide Early Warning aided by wireless support of instrumentation and transmitting the data through INSAT Satellite. In addition determination of site specific rainfall threshold for landsliding and establishing their correlation with recorded sensor data would help in taking proper measure in advance to reduce the risk related to landslide in North Eastern Region of India, where landslides and related phenomena are inevitable.

References

Cruden DM (1991) A simple definition of a landslide. Bull Int Assoc Eng Geol 43:27–29

Cruden DM (1993) The Multilingual Landslide Glossary, Bitech Publishers, Richmond. British Columbia, for the UNESCO Working Party on World Landslide Inventory in 1993

Hansen A (1984) Landslide hazard analysis. In: Brunsden D, Prior DB (eds) Slope instability. Wiley, Christchurch, pp 523–602

Kirschbaum D, Adler R, Hong Y, Lerner-Lam A (2009) Evaluation of a preliminary satellite-based landslide hazard algorithm using global landslide inventories. Nat Hazards Earth Syst Sci 9:673–686

Krishnan MS (1982) Geology of India and Burma. CBS Publishers and Distributors, Delhi, p 536 (81-239-0012-0)

Mukul M, Jade S, Bhattacharyya AK, Kuntala B (2010) Crustal shortening in convergent orogens: insights from Global Positioning System (GPS) measurements in Northeast India. J Geol Soc India 75:302–312

Raju M (2002) Landslide hazard zonation for effective land management of mountainous terrain. "Arunachal Pradesh: Environmental Planning and Sustainable Development-Opportunities and Challenges" Hepaticas Occasional Publication No. 16, 439–443, G. B. Pant Institute of Himalayan Environment & Development, Almora

Satty TL (1980) Analytical hierarchy process. McGraw-Hill, New York, p 320 (096203178X)

Varnes DJ, International Association of Engineering Geology Commission on Landslides and Other Mass Movements (1984) Landslide hazard zonation: a review of principles and practice. Natural Hazards, vol 3, UNESCO, Paris, 6p

Landslide Processes and Susceptibility Mapping in NE Sicily, Italy

Salvatore Scudero and Giorgio De Guidi

Abstract

Many destructive debris flows hit several villages in the Peloritani Mountains area (Sicily, Italy) in October 2009. The collection of several types of spatial data, together with the landslides inventory, allowed the assessment of the landslide susceptibility by the application of two different bivariate techniques.

Furthermore, the susceptibility analysis allowed to state which classes within the different factors, have greater relevance in slope instability and afterwards if some of these can somehow be linked (with a short-medium term incidence) to some of the endogenic processes acting in the area (huge regional uplift, fault activity). Therefore we are able to propose a geomorphologic model of cyclic evolution of the relief in which the endogenic processes are directly linked to the superficial ones.

This work shows just some preliminary results of a greater study that involve the susceptibility analysis and its interpretation in a geodynamics perspective, for the whole southern Calabrian Arc.

Keywords

Landslide susceptibility • Debris flow • Tectonic uplift • Calabrian Arc • Peloritani Mountains

Introduction

On October 1, 2009, hundreds (about 550) of shallow landslides were triggered by an intense rainfall event and occurred over a ~30 km^2 area. The slope instabilities occurred mainly in the lower part of the 14 small catchments involved (Fig. 1). Landslides caused 35 fatalities, the total devastation of several villages in Messina province (Sicily, Italy) and severe damages to public heritage and local economy (Fig. 2).

The rainfall event had great intensity: 223 mm occurred in 7 h with a peak of 10.6 mm in 5 min (Maugeri and Motta 2010) but the colluvial slopes were already saturated and weighted by the precipitations of the previous weeks.

All the landslides took place within the patchy layer of loose, heterogeneous and often weathered material, with variable thickness, that covers the majority of the slopes (colluvium). Such deposit is characterised by a high content of the coarser portion (gravel content more than 50 %), whereas the clay content is not always present. Its friction angle can reach more than 35° allowing the material to remain, with normal conditions, onto the steep slopes of the catchments. The landslide events have been generally triggered by the detachment of small boulders from natural scarps, rocky cliffs, or ancient retaining walls used for terracing the slope for agricultural purposes, over a saturated portion of colluvium and originating its collapse. Another mechanism of generation of such flows is the sudden fluidification of the colluvial material due to superficial or subsuperficial water currents or temporary springs rising from the bedrock (Agnesi et al. 2009).

S. Scudero (✉) • G. De Guidi
Department of Geological Sciences, University of Catania, Corso Italia 55, Catania 95129, Italy
e-mail: scu.sal@libero.it

C. Margottini et al. (eds.), *Landslide Science and Practice*, Vol. 1,
DOI 10.1007/978-3-642-31325-7_64,

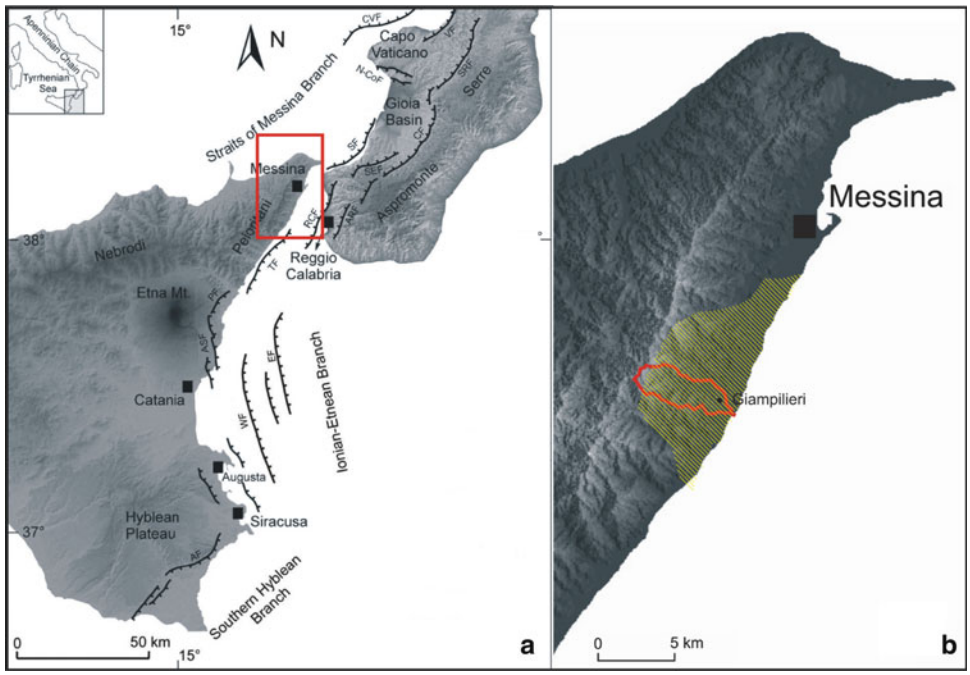

Fig. 1 (**a**) Location map of the study area and main tectonic outline, modified from Catalano et al. (2008); (**b**) in *red* the study area of Giampilieri basin, in *yellow* the area involved in the landslide events

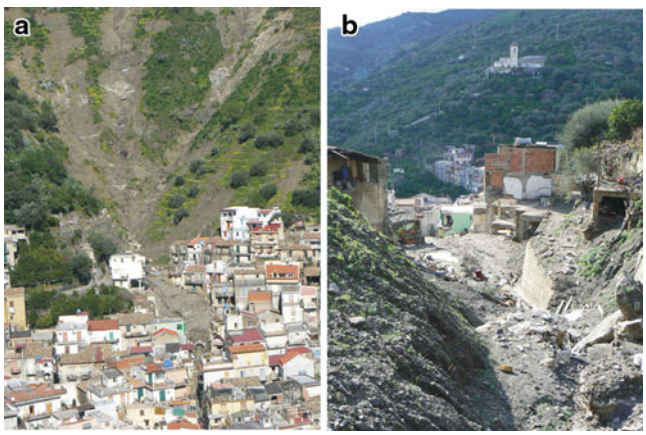

Fig. 2 Landslides in the village of Giampilieri; (**a**) front view and (**b**) downslope view

The flows usually developed downslope, even though lateral enlargements or upslope regressions have been observed. The material often canalized following the natural drainage, eroding and sometimes exhuming buried gullies. During the way down, the flows eroded the base or the lateral edge of their canal, gaining further material and increasing their volume, until they stopped in the zone of accumulation, usually located at the foot of the slopes.

The simultaneous occurrence of many landslides, usually triggered by an exceptional rainfall event or by an earthquake, gives the exclusive opportunity to study their distribution in relation to several environmental factors. This study aims to produce a landslide susceptibility map for debris flows for a representative area, through the combination of the inventory of the 2009 events with some causative factors, employing statistical methods that assign numerical weight values to each class of the considered causative factors. Moreover, we will try to understand how the very complicated geological heritage influences the present day processes and to explain our results within the tectonically active framework of the study area.

Spatial Data

Many factors can play somehow a role in landslide occurrence. Understanding which are determinants requires a good knowledge of the study area, of the phenomena and the assessment of the scale of analysis and of the methodology (van Westen et al. 2008; Cascini 2008). We considered six different factors (lithology, geomechanical classification, geomorphology, distance to stream, slope angle, aspect) and their spatial distribution for the area of the Giampilieri watershed (Figs. 1 and 3), at the 1:10,000 scale. The spatial layers have a 12× 12 m pixel size resolution.

The bedrock geology of the study area consists of three different types of metamorphic rocks. They include low-grade phyllar rocks that are tectonically covered by higher-grade mica schist and paragneiss. Because of their geological history these rocks are deeply fractured and weathered, therefore we performed a geomechanical characterization of the rock masses according to RMR proposed by Bieniawski (1979). Such subdivision provides more information concerning the rock masses differences and could be a more representative causative factor in describing landslide occurrence.

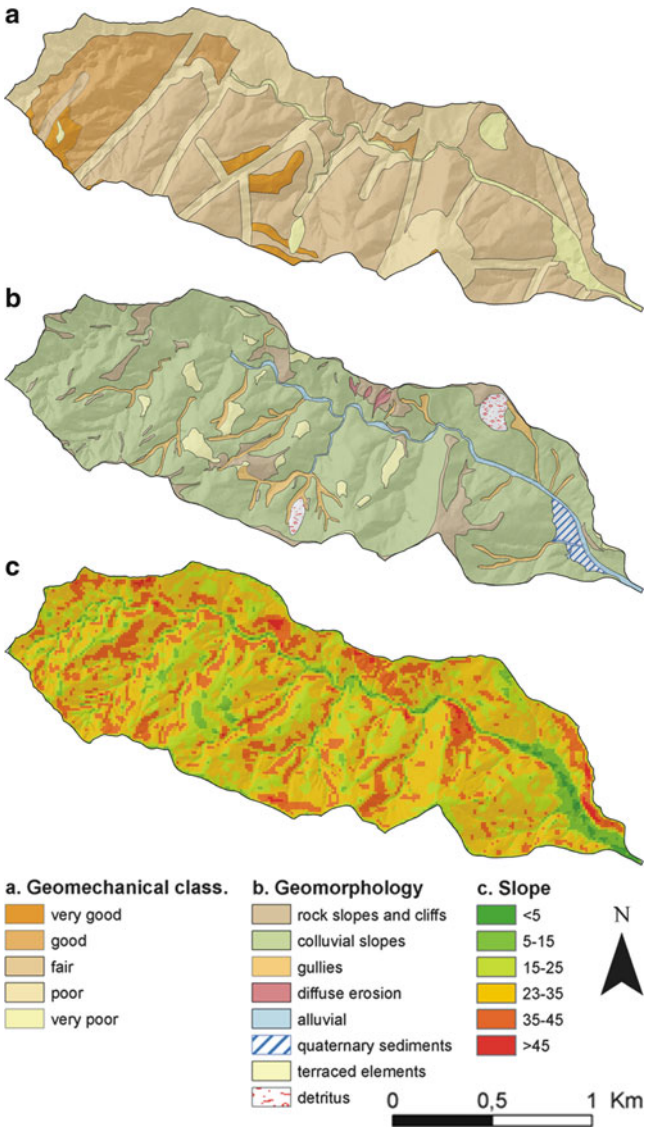

Fig. 3 Maps of three among six causative factors; (**a**) geomechanical classification of rock types; (**b**) geomorphological units; (**c**) slope map

The geomorphological map distinguishes terrain units according to the processes acting, the origin of the features and the materials involved.

Finally we generated a Digital Elevation Model (DEM) from a 1:10,000 map with 10 m contour intervals and derived three topographic features (1) slope is one of the most relevant factor in controlling landsliding; (2) aspect of the slope has influces on the hydrological process and thus also indirect influence on weathering, vegetation and root development; (3) distance from drainage network has been considered because the intense erosion of many stream segments.

The landslide inventory map by Regional Civil Defence (Basile 2010) was integrated with missing data. We considered as source areas of the shallow landslides a circle of 30 m in diameter around each initiation point (Salciarini et al. 2006). Such value is coherent with the scale of our analysis and with the spatial variability of the causative factor as observed in the field.

Susceptibility Analysis and Mapping

The susceptibility analysis was performed with the application of two different bivariate methods. Each of the layers discussed in the previous paragraph has been considered as an independent variable in causing landsliding. In the bivariate approach each independent variable is correlated with the dependent one (landslide map), and their relationships with the landslide occurrence are calculated through pairwise map crossing. The bivariate techniques assume that the independent variables are not inter-related and that they all concur with the same weight in landsliding. In particular, we performed landslide susceptibility analysis with the Statistical Index method (van Westen 1997) and with the Probability method (Süzen and Doyuran 2004).

In the Statistical Index method the weights of the classes of each factor are calculated as the natural logarithm of the ratio between the density of landslide in the considered class and the density of landslide in the whole map. Instead, the Probability method provides the weights of the classes as the frequency of observed landslide in the considered class divided by the frequency of non-observed landslide in the same class.

We present the numerical rating values for each class of the six causative factors (Table 1) for both methods. The calculated weights are summed together in order to map the landslide susceptibility index for the whole study area. The value of the susceptibility index ranges between 20.6 and 13.4 for the Statistical Index method and from 2.0 to 21.6 for the Probability method. Afterwards the landslide susceptibility index is classified in four different categories from low, medium, high and very high. The zonation follows the criterion of the natural breaks according to Jenks Algorithm (Ruff and Czurda 2008). This subdivision has been preferred to other classification systems because the distribution of the landslide index shows several jumps. The final susceptibility maps are shown in Fig. 4.

Discussion and Conclusion

Both the bivariate techniques provided comparable results regarding the calculation of the weights.

For the geology factor, the highest weight is given by the Plio-pleistocenic calcarenites. They outcrop in a very small part of the basin forming some cliffs just above the initiation points of some landslides. The weight is high for this reason but likely there is not a direct influence of this lithology on

Table 1 Calculated weights for the classes of the six causative factors

Instability factor/classes	% area covered by the class	Landslide density (%)	Weights with SIM 4	Weights with PM
Lithology				
Slope deposit	1.33	2.7	0.69	3.16
Present-day alluvial deposits	2.06	0.0	0.00	0.00
Recent alluvial deposits	1.24	0.0	0.00	0.00
Calcarenites	0.09	2.2	[a]1.00	[a]5.00
Aspromonte Unit (gneiss)	48.35	41.9	−0.14	0.04
Mela Unit (mica schist)	21.82	10.2	−0.76	0.04
Mandanici Unit (phyllar)	20.61	42.9	0.73	0.21
Marble	4.49	0.0	0.00	0.00
Geomechanical classification				
Very good	3.62	0.0	0.00	0.00
Good	11.57	0.4	−3.49	0.01
Fair	49.41	67.8	0.32	0.06
Poor	30.67	26.9	−0.13	0.06
Very poor	4.73	4.9	0.04	0.45
Geomorphology				
Rock slopes and cliffs	8.70	13.9	0.47	0.39
Colluvial slopes	78.17	78.1	0.00	0.03
Gullies	5.09	2.5	−0.72	0.20
Areas with diffuse erosion	0.33	0.3	−0.07	5.92
Alluvial	2.06	0.0	0.00	0.00
Quaternary sediments	1.24	0.0	0.00	0.00
Terraced elements	3.20	2.6	−0.22	0.52
Detritus	1.22	2.6	0.77	3.76
Slope angle (°)				
<5	5.11	2.5	−0.72	0.20
5–15	4.07	0.9	−1.55	0.11
15–25	19.03	14.9	−0.24	0.08
25–35	38.65	40.2	0.04	0.06
35–45	25.50	30.5	0.18	0.10
>45	7.65	11.0	0.37	0.39
Aspect				
Flat	5.03	2.5	−0.70	0.20
North	8.67	6.4	−0.30	0.18
Northeast	18.68	18.6	−0.01	0.11
East	18.28	12.3	−0.39	0.08
Southeast	13.11	9.7	−0.30	0.12
South	11.64	17.2	0.39	0.26
Southwest	5.93	11.4	0.65	0.68
West	2.16	4.2	0.66	1.89
Northwest	7.40	4.2	−0.56	0.16
North	9.09	13.5	0.39	0.34
Distance to stream				
<30	24.01	5.0	−1.58	0.02
30–150	60.05	69.0	0.14	0.04
>150	15.94	26.0	0.49	0.21

SIM Susceptibility index method, *PM* Probability method
[a]Arbitrarily assigned

instability. Relatively high weights also occurr where large body of detritus or loose deposit cover the slopes. The Mandanici Unit (phyllar) is sharply the most favourable for landsliding compared to the other metamorphic units of the Peloritani Mountains.

For the geomechanical characteristics of the rock types a clear trend is showed. Good rocks have no influence, while the poor ones favour landsliding.

For the geomorphological factor, the occurrence of large body of mobilized material and areas with gullies and strong

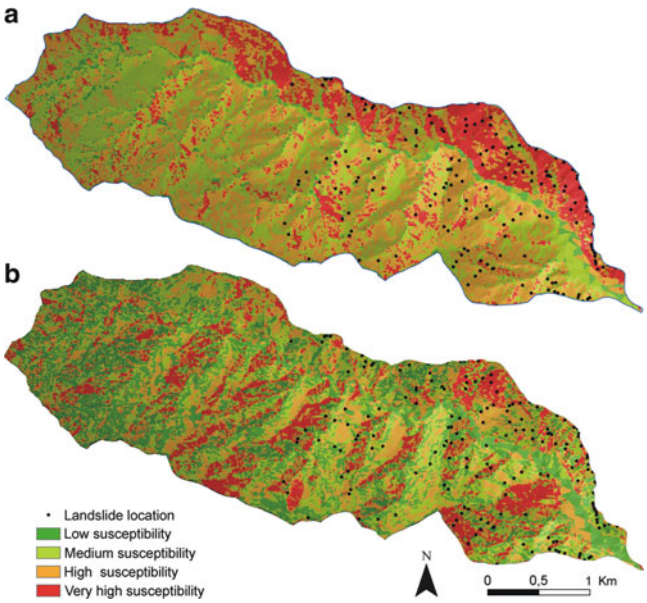

Fig. 4 Landslide susceptibility maps performed with the (**a**) statistical Index method and (**b**) the Probability method

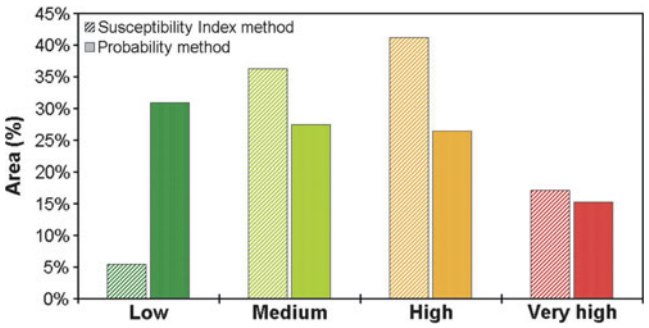

Fig. 5 Percentage of the area within the different landslide suscepitibility classes. Left columns correspond to Susceptibility Index method, right columns to Probability method

erosional evidences, have the highest influence. Rocky slopes and cliffs result to have influence because they can trigger shallow landslide through the fall of boulders.

Landslide occur when the slope angle is greater than 15°. The class with the highest incidence of landslide correspond to high slope angles (> 45°), while the frequency is lower for intermediate slope angles (25°–45°).

The last two factors considered are less significant. Three classes of the aspect factor have influence on landsliding, in particular, South to West facing slopes are the most favourable. Distances from drainage network greater than 150 m are the most important for landsliding.

Although the investigations we preformed are only preliminary and focused only in a small representative basin, we are able to speculate about some direct relationship between the general setting deriving from the active endogenic dynamics and the superficial phenomena of the relief evolution.

The area of the Calabrian Arc has a long and complex gelogical history. In fact, it has been involved in two orogenic cycles since late Palaeozoic time. More recently (Middle Pleistocene time) the entire Calabrian Arc underwent a strong tectonic uplift (Tortorici et al. 1995) with rates even greater than 1.0 mm/year and that was accompanied since 700 ka ago by the activity of a normal fault belt system (Fig. 1). For the last 125 ka the total tectonic uplift rate of the northeastern Ionian cost of Sicily has been estimated constant and it reaches its maximum value of 1.7 mm/y very close to the study area (Catalano and De Guidi 2003). Moreover the entire area is located at the footwall of an active normal fault (De Guidi et al. 2003).

Such active tectonics framework induce very intense erosional processes with the formation of a consequent drainage network and very steep slopes. The erosion is mainly concentrated along the stream incisions but also areas with large diffuse erosion occur on some slopes. The erosion is favoured by the geological conditions, in particular the metamorphic rock are very prone to the chemical weathering. Moreover the tectonic uplift, coupled with the strong erosion, allow the release of the lithostatic load originating a shallow and dense net of discontinuities on the rock masses. All these processes act together allowing the weathering and consequently the formation of a loose and heterogeneous level of material (colluvium). It covers most of the slopes and sometimes accumulates in very a thick deposit that cyclically reveals unstable under particular conditions (Dietrich et al. 1982).

The interaction of the geomorphological and tectonic processes sholud be further investigated by the application of more sophisticated methods for the analysis of the susceptibility (i.e. multivariate techniques) that allow to estimate the relative influence of the single causative factors.

In conclusion, the spatial distribution of the landslide susceptibility highlights how large portions of the study area (more than 15 % for both methods) is characterised by very high susceptibility (Fig. 5), testifying how the susceptibility analysis is of fundamental importance, not only for the comprehension of the geologic dynamics, but also for a good management of this fragile territory.

References

Agnesi V, Rasà R, Puglisi C, Gioè C, Privitera B, Cappadonia C, Conoscenti C, Pino P, Rotigliano E (2009) La franosità diffusa dell'1 ottobre 2009 nel territorio ionico-peloritano della Provincia di Messina: stato delle indagini e prime considerazioni sulle dinamiche geomorfiche attivate. Geologi di Sicilia 2009(4):23–30

Basile G (2010) Evento del 1 ottobre 2009, Carta dei dissesti. Dipartimento Regionale della Protezione Civile, Sicilia

Bieniawski ZT (1979) The geomechanics classification in rock engineering applications. In: Proceedings of the 4th international congress on rock mechanics, Montreux, 2–8 Sept 1979

Cascini L (2008) Applicability of landslide susceptibility and hazard zoning at different scales. Eng Geol 102:164–177

Catalano S, De Guidi G (2003) Late quaternary uplift of northeastern Sicily: relation with the active normal faulting deformation. J Geodyn 36:445–467

Catalano S, De Guidi G, Monaco C, Tortorici G, Tortorici L (2008) Active faulting and seismicity along the Siculo-Calabrian Rift Zone (southern Italy). Tectonophysics 453:177–192

De Guidi G, Catalano S, Monaco C, Tortorici L (2003) Morphological evidence of Holocene coseismic deformation in the Taormina region (NE Sicily). J Geodyn 36:193–211

Dietrich WE, Dunne T, Humphrey NF, Reid LM (1982) Construction of sediment budgets for drainage basins. In: Sediment Budgets and routing in forested drainage basins. Proceedings of the Symposium; 31 May–1 June 1982; Corvallis, Oregon. General Technical Report PNW-141. Portland, Oregon: Pacific Northwest Forest and Range Experiment Station, Forest Service, U.S. Department of Agriculture, pp 5–23

Maugeri M, Motta E (2010) Effects of heavy rainfalls on slope behavior: the1 Oct 2009 Disaster of Messina (Italy). Geotechnics/earthquake geotechnics towards global sustainability, Kyoto, 12–14 Jan 2010

Ruff M, Czurda K (2008) Landslide susceptibility analysis with a heuristic approach in the Eastern Alps (Vorarlberg, Austria). Geomorphology 94:314–324

Salciarini D, Godt JW, Savage WZ, Conversini P, Baum RL, Michael JA (2006) Modeling regional initiation of rainfall-induced shallow landslides in the eastern Umbria Region of central Italy. Landslides 3:181–194

Süzen ML, Doyuran V (2004) A comparison of the GIS based landslide susceptibility assessment methods: multivariate versus bivariate. Environ Geol 45:665–679

Tortorici L, Monaco C, Tansi C, Cocina O (1995) Recent and active tectonics in the Calabrian arc (Southern Italy). Tectonophysics 243:37–55

van Westen CJ (1997) Statistical landslide hazard analysis. In: Application guide, ILWIS 2.1 for Windows. ITC, Enschede, pp 73–84

van Westen CJ, Castellanos E, Kuriakose SL (2008) Spatial data for landslide susceptibility, hazard, and vulnerability assessment: An overview. Eng Geol 102:112–131

Regional and Local Approaches on Landslide Susceptibility Assessment in the Region Located Between the Buzau and the Slanicul Buzaului Valleys, Romania

Mihaela Constantin, Martin Bednarik, Marta-Cristina Jurchescu, Koji Ishida, and Kei Higuchi

Abstract

The paper presents the results of landslide susceptibility maps elaboration for the Sibiciu, Panatau and Saratel basins (Buzau Carpathians and Subcarpathians, Romania) and the assessment of landslide displacements using extensometers in Romania. The landslide susceptibility maps were elaborated using the bivariate statistical analysis and the index of entropy. Observations concerning landslide displacements using extensometers were focused on two test sites located in the Ivanetu Summit (the Colti church area) and the Buzau Subcarpathians (Maguricea landslide). The system measurement from Maguricea landslide using optical fiber is the first system installed on a test site in Europe. The studies were elaborated in cooperation with Comenius University, Bratislava, Slovakia and the Public Works Research Institute, Tsukuba, Japan.

Keywords

Landslides • Susceptibility • Extensometers • Optical fiber sensors • Romania

The Description of the Area

The Sibiciu, Panatau and the Saratel basins (Fig. 1) are located mainly in the Buzau Subcarpathians, the northern part of the Sibiciu basin and the north-western part of the Saratel basin being located in the Ivanetu Summit. The Sibiciu, Panatau and Saratel rivers are leftside tributaries of the Buzau River. The region is strongly affected by different geomorphological hazards (Badea et al. 2008; Constantin et al. 2005).

M. Constantin (✉) • M.-C. Jurchescu
Institute of Geography, Romanian Academy, Str. D. Racovita 12, Bucharest 023993, Romania
e-mail: mihaela.constantin@gmail.com

M. Bednarik
Faculty of Natural Sciences, Department of Engineering Geology, Comenius University, Mlynska Dolina, Bratislava 84215, Slovakia

K. Ishida
Public Works Research Institute, 1-6 Minamihara, Tsukuba, Ibaraki 3058516, Japan

K. Higuchi
Sakata Denki, 2-17-20 Yagisawa, Nishi-Tokyo, Tokyo 2020022, Japan

The Sibiciu basin (47.11 km^2) developed on two relief units: the northern part of the Ivanetu Summit and the Buzau Subcarpathians. The highest altitudes are in the northern part of the basin (Zboiu Peak, 1,114 m). In the western part, the area is bordered by some peaks, their altitudes decreasing from north to south (Oii Peak; Racadaului Peak; Dragan Peak). The slope gradients are 12–24° and 24–36°, and are related to lithology represented by Kliwa sandstones. Slope gradients with small values are at the contact with the hilly area. The drainage density has values of 3–4 km/km^2. The vegetation is represented mainly by forests and pastures.

The Panatau basin has an area of 24.00 km^2. The highest altitude reaches 820 m in Blidisel Peak and is located in the northern part of the area. The Panatau valley has an asymmetrical transversal profile with steep slopes (24°). High slope gradients are found in the northern part of the basin where the sands of Sarmatian age crop out. The relief energy has values of 150–250 m. The drainage density has values typical for mollasse deposits. These are of 5.7–5.9 km/km^2 in areas affected by ravines (Catanei valley and Fantanii valley). The average annual precipitation at Patarlagele is 635.8 mm. The vegetation is represented by

C. Margottini et al. (eds.), *Landslide Science and Practice*, Vol. 1,
DOI 10.1007/978-3-642-31325-7_65, © Springer-Verlag Berlin Heidelberg 2013

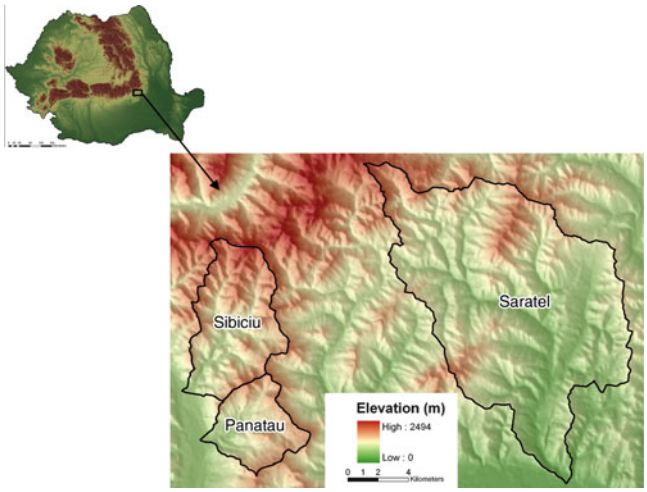

Fig. 1 The location of the Sibiciu, Panatau and Saratel basins

forests in the north-east and south-eastern parts. Orchards and pastures are less frequent, and arable terrains are only found around the Panatau and Plaisor settlements.

The Saratel basin has a surface of 189.45 km^2 and is developed mainly in the Buzau Subcarpathians. The north-western part is located in the Ivanetu Summit where the highest altitude from the basin (930.0 m) is found. The altitude values decrease from north to south and from west to east. Slope gradients with values of 24–45° are found at the contact with the mountain area represented by Kliwa sandstones. The slope aspect is mainly south, south-west and west oriented. The relief energy is different in the two relief units: in the hilly area it is 150–200 m while in the mountain area it is 200–250 m. The drainage density has average values of 1–3 km/km^2. The forests cover small areas in high hilly areas near the mountain unit. The pastures and the arable terrains cover large areas in the south-eastern parts of the basin. In all three basins, landslides have a strong effect on the slope morphology.

Landslides

From all processes affecting slopes in the basins, landslides are the most important.

The landslide types are as follows (Bălteanu 1983):

- Shallow landslides which affect the soil cover on a depth of 1.5 m;
- Medium-deep landslides with a depth of deluvium between 1.5 and 10 m and a volume of displaced material up to 10^5 m^3;
- Deep landslides, with the slip plane located at a depth over 10 m and a volume of displaced material $>10^5$ m^3.

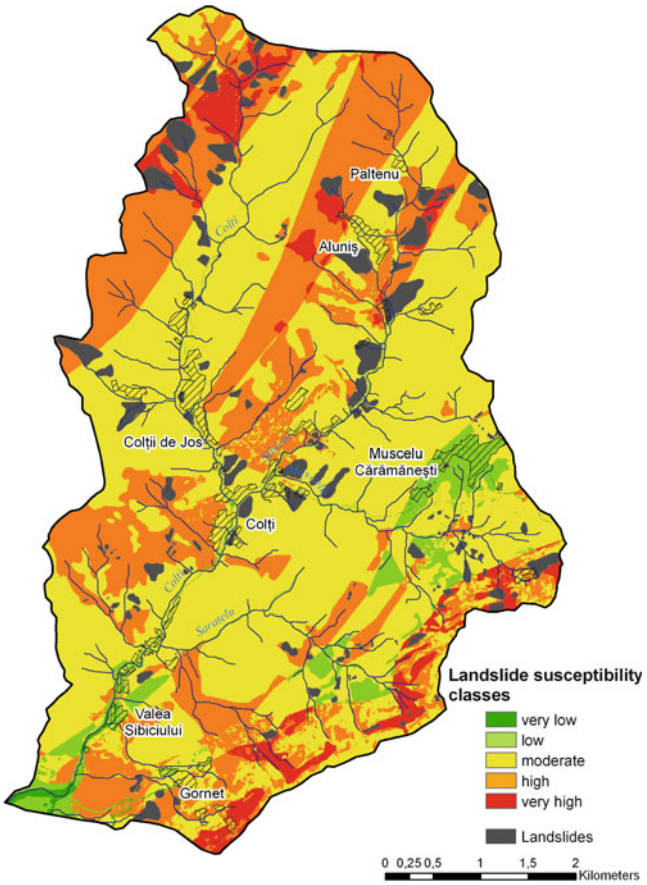

Fig. 2 The landslide susceptibility map of the Sibiciu basin

The Landslide Susceptibility Maps for the Sibiciu, Panatau and Saratel Basins

The landslide susceptibility maps were elaborated using the bivariate statistical analysis (Constantin et al. 2010a, b).

Both shallow and deep-seated landslides were mapped: 169 in the Sibiciu basin; 236 in the Panatau basin and 337 the Saratel basin.

The thematic maps were realized using the geologic map at the scale 1:200,000 and the Digital Elevation Model obtained by interpolating the points at a resolution of 20 m (Source: the National Geodetic Found). The landslide distribution map was compared with the following five thematic maps: geology, slope gradient, slope aspect, curvature and land use (derived from aerial photos with a 1:5,000 scale). For the calculation of the landslide probability the weight of each variable class was calculated using the entropy index (Costantin 2008; Constantin et al. 2010b).

The resulting landslide susceptibility maps, classified in five susceptibility classes, for the Sibiciu, Panatau and Saratel basins are presented in Figs. 2, 3, 4 and 5.

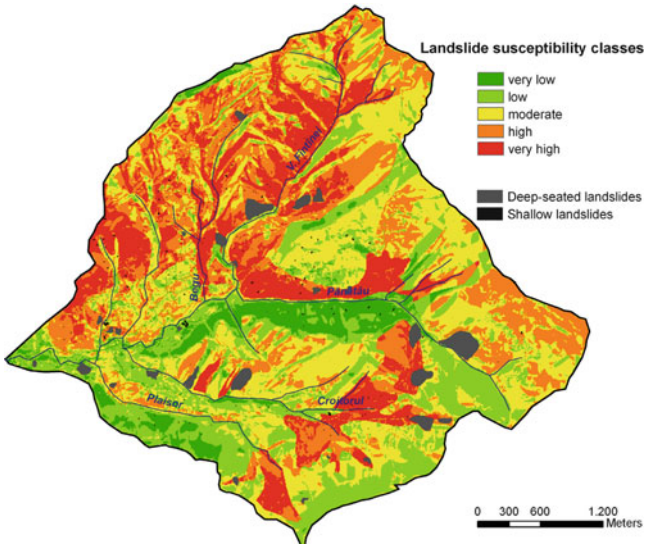

Fig. 3 The landslide susceptibility map of the Panatau basin

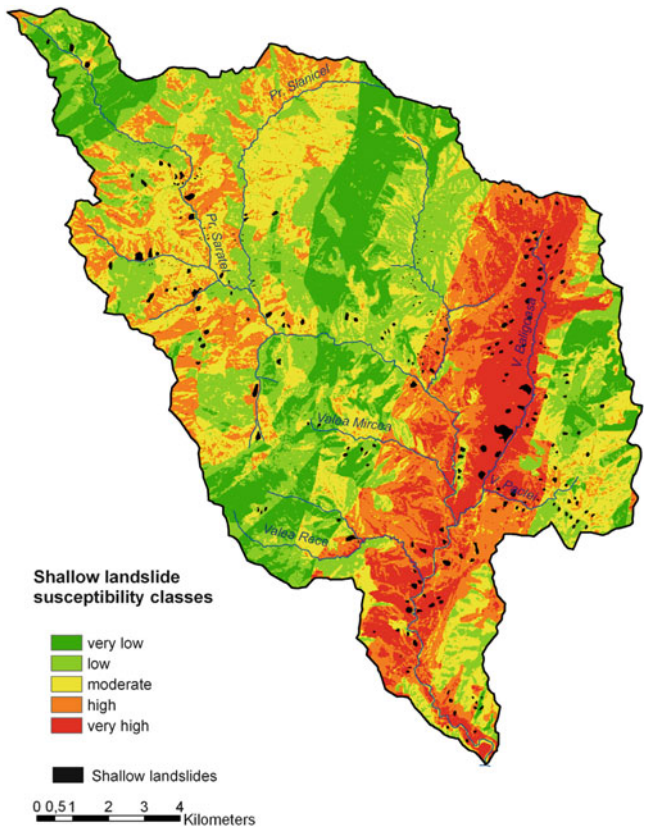

Fig. 4 The landslide susceptibility map of the Saratel basin for shallow landslides

The obtained success rates were low to moderate for the Sibiciu basin (58 %) and for the Panatau basin (69 %). The best result was obtained for the landslide susceptibility map of the Saratel basin where the statistical analysis was applied differentiated for deep landslides and shallow landslides (success rates of 94 % and 65 % respectively).

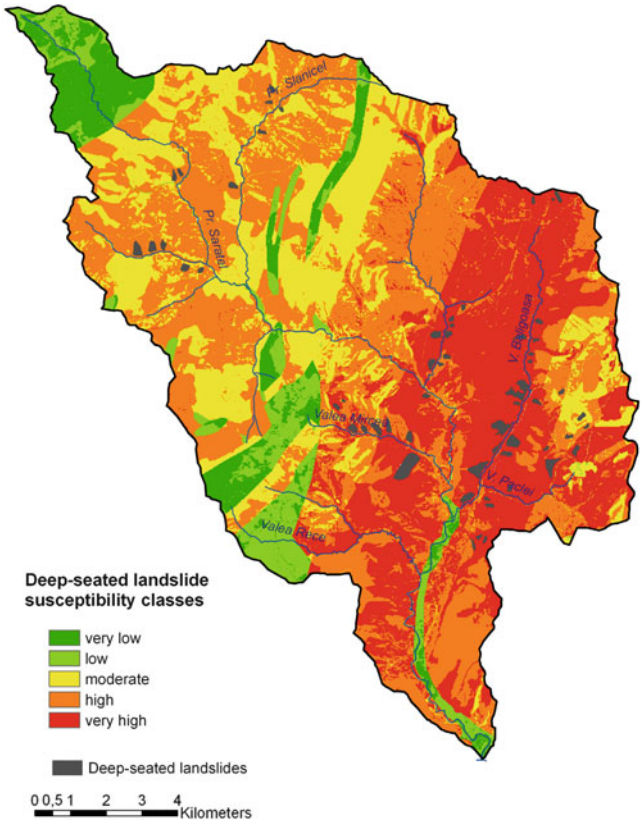

Fig. 5 The landslide susceptibility map of the Saratel basin for deep-seated landslides

Displacement Measurements on Case Studies

The Landslide from the Colti Church

Continuous displacement measurements were recorded using the digital extensometer set-up at the landslide scarp located at the entrance of the Colti church (Ivanetu Summit, Buzau Carpathians) (Fig. 6).

The displacement data were correlated with the climatic data obtained using the meteo station Irox X Pro in the period 05.11.2008–30.06.2010. The total value of extension displacements (the movement of the mobile pile) was −22.1 mm while those of compressions (movements at the landslide scarp) were +51.7 mm.

Considering these values, we can consider that the landslide is a slow type. Rapid episodes like the one from 27–30.06.2010 were also observed (4.6–6.4 mm/day).

The result of our study revealed that the displacements are extensions or compressions with values between −15.00 and +5.00 mm. Comparing the precipitation values with those of displacements we conclude that in the case of precipitation with values over 45 mm/day extension movements with values of 4–6.00 mm/day might occur. Precipitation with values of 20 mm/day can trigger compressions with values of 2–5 mm/day.

Fig. 6 The SRL-16 analog and digital extensometer placed across the landslide scarp which affects the entrance in the Colti church

Fig. 7 The conventional extensometer and optical fiber sensor set-up at the landslide scarp (Maguricea landslide)

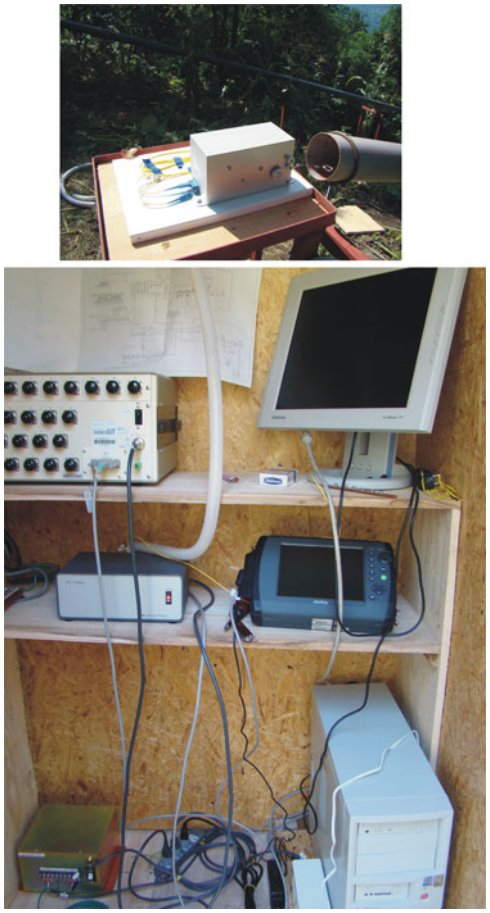

Fig. 8 The automatic and optical fiber measurement system installed at Maguricea landslide

The Landslide from Maguricea

Maguricea landslide is located in the Buzău Subcarpathians, Curvature Subcarpathians, Romania in the Măguricea village area. The landslide occurred in the source area of the Cuculesti Valley, a tributary of the Teghii Valley (one of the Buzău Valley tributaries). Maguricea landslide occurred after heavy rainfall (autumn of 1972), when a number of rotational slides occurred at the supply basin of the mudflow (Bălteanu 1983). The landslide scarp is 79.0 m long and landslide length is 220.0 m. The average width is 70.0 m. A height difference of 50 m between landslide scarp and toe was observed.

One conventional extensometer and one optical fiber sensor were placed along the main scarp of the landslide (Fig. 7).

This system measurement of displacements using optical fiber is the first system installed on a test site in Europe (Fig. 8).

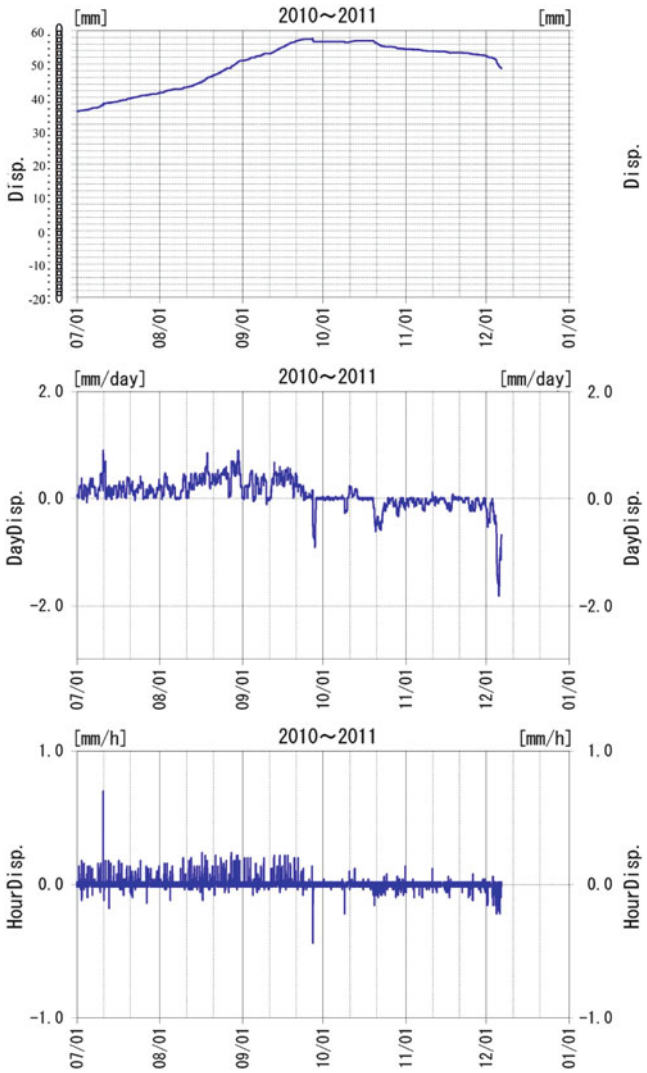

Fig. 9 The displacements values measured by means of conventional extensometer (06.09.2010–06.12.2010)

Displacement measurements using the automatic system are made continuously at the Maguricea landslide from September 2009. For the conventional extensometer using the Logmaster data-logger, daily displacements were up to +1 mm in the case of compressions and −2 mm in the case of extensions (Fig. 9).

The differences between the displacement values registered in the conventional extensometer and the values obtained using the optical fiber sensor were of 0.1–1 mm/day. The maximum displacement value per hour measured using the conventional extensometer was up to 0.25 mm/h while those measured using optical fiber sensors was up to 0.5 mm/h.

Conclusions

The Sibiciu, Panatau and Saratel basins are located in the Buzau Mountains and Buzau Subcarpathians (Romania) between the Buzău and Slănicul Buzăului valleys. Characterized by geological deposits consisting mainly of interbedded sandstones and clays in the mountain area and marls, clays and sands in the hilly area, the region is affected by many landslides of different depths and magnitudes. Both regional and local landslide studies were conducted in the region.

Landslide susceptibility maps using the bivariate statistical analysis and the index of entropy to assign weights to the conditioning factors (geology, slope, aspect, curvature and land use) involved in the landslide occurrence were elaborated for the basins mentioned above. The model validation was applied to all three basins. The success rate was calculated and five landslide susceptibility classes from very high to very low were delineated. Local studies were focused on two landslide sites: the Colţi Church landslide and the Măguricea landslide. The measured surface displacements using one digital extensometer were correlated with the characteristics of the rainstorm events that occurred during the monitoring period in order to establish local rainfall thresholds for the landslide initiation in the case of the Colţi Church landslide. In the case of the Măguricea landslide, a complex automatic and optical fiber (OTDR) system was set-up. This system is the first one with an optical fiber sensor installed on a test site in Europe. The data obtained by means of conventional extensometer indicate slow movements in the landslide scarp area and were compared with those obtained from optical fiber sensor (Higuchi et al. 2005, 2007). Until now, differences of 0.1–1 mm/day were registered between the two extensometer types. Future studies will focus on improving optical fiber systems, the important advantages being that they are not affected by thunderbolt and lightning-induced surge, offering the possibility to measure a large landslide area.

Acknowledgments The present study was supported by the Ministry of Education and Research through the grant in aid PNII-IDEI_367 (2007–2010) financed by The National University Research Council of Romania (CNCSIS). The cooperation with Landslide Research Team, Public Works Research Institute, Tsukuba, Japan and Department of Engineering Geology, Comenius University, Bratislava, Slovakia is fully appreciated.

References

Badea L, Niculescu Gh, Sandu M, Roata S, Micu M, Sima M, Jurchescu M (2008) Unitatile de relief ale Romaniei, vol III. In: Dealurile Pericarpatice. Ed. Ars Docendi, Bucuresti, 143p.

Bălteanu D (1983) Field experiment in geomorphology, (in Romanian). Romanian Academy Press, Bucharest, 157p

Constantin M (2008) The landslide susceptibility assessment in Romania. A review of regional approaches. In: Proceedings of the

international conference on management of landslide hazard in the Asia-Pacific region, satellite symposium of the first world landslide forum, Sendai, Japan, 11–15 Nov 2008, pp 510–518

Constantin M, Rotaru A, Nishimoto H, Yamakoshi T (2005) Geomorphological hazards in Romania. Some examples from the area situated at the contact between Buzău Carpathians and Buzău Subcarpathians. J Jpn Soc Eros Control Eng 58(1):59–62

Constantin M, Trandafir AC, Jurchescu MC, Ciupitu D (2010a) Morphology and environmental impact of the Colti-Alunis landslide (Curvature Carpathians), Romania. Environ Earth Sci 59(7):1569–1578

Constantin M, Bednarik M, Jurchescu MC, Vlaicu M (2010b) Landslide susceptibility assessment using the bivariate statistical analysis and the index of entropy in the Sibiciu Basin (Romania). Environ Earth Sci. doi:10.1007/s12665-010-0724-y

Higuchi K, Nomura Y, Asai K, Fujisawa K, Pasuto A, Marcato G, Fukuoka F, Iwao T (2005) Development of landslide displacement detection sensor using an optical fiber in the OTDR method. In: Proceedings of 44th conference of the Japan Landslide Society, Japan, pp 315–318

Higuchi K, Fujisawa K, Asai A, Pasuto A, Marcato G, Society for Study of Optical Fiber Sensors (2007) Application of new landslide monitoring technique using optical fiber sensor at Takisaka landslide, Japan. In: Proceedings of 1st North American landslide conference, Vail, Colorado, June 2007, pp 3–8

Landslide Susceptibility, Hazard and Risk Mapping in Mailuu-Suu, Kyrgyzstan

Almazbek Torgoev and Hans-Balder Havenith

Abstract

This paper presents the results of landslide susceptibility and landslide hazard mapping together with preliminary landslide risk studies on qualitative basis. The target area is situated in the south of Kyrgyzstan, Central Asia, in the valley of Mailuu-Suu River. There are several uranium waste tailings situated in the target area and there is the risk that landslide activity can result in an environment catastrophe through destruction of waste tailing and damming of river channel leading to flooding of radioactive material. For remediation measures and risk mitigation there is the need to have reliable estimates of landslide susceptibility and hazard in target area on local and regional scales.

Keywords

Kyrgyzstan • Mailuu-Suu River • Landslide susceptibility • Hazard • Risk

Introduction

Mailuu-Suu River valley is characterized by a combination of geological and tectonic settings favouring intense landslide activity in this area (Alioshin et al. 2000). Together with the hazardous environmental situation due to presence of radioactive tailings close to some active mass movements, landslide activity itself poses significant risk to society. During the last years significant efforts from responsible agencies, such as the Ministry of Emergency Situation Agency, were spent on environmental risk reduction measures. These efforts also take into account the possibility of a regional environmental catastrophe, caused by landslide failure, uranium waste tailing destruction and penetration of radioactive material to Mailuu-Suu River flowing to the densely populated Fergana Valley. But, the effectiveness of risk reduction measures strongly depends on results of landslide hazard and risk studies, because some measures, like the removal of radioactive material and its transportation to another site, demand reliable estimation of landslide hazard in any new place of radioactive material disposal.

Previous studies (Daneels 2004; Roessner et al. 2005; Havenith et al. 2006) showed the potential of GIS and Remote Sensing approaches to estimate landslide hazard in the south of Kyrgyzstan and in Mailuu-Suu River valley, in particular. Here, we present examples of landslide susceptibility, hazard and risk mapping using state-of-the-art GIS and Remote Sensing approaches in the target area counting up to 166 landslides in 2007 (Schlogel et al. 2010).

Mapping of Affecting Factors

Landslide susceptibility mapping was based on a series of relevant affecting factors: slope angle, land cover, lithological units and structural geology.

The slope angle map and classification of obtained results was derived from the Digital Elevation Model (DEM) constructed on the basis of ASTER satellite imagery

A. Torgoev (✉)
Scientific-Engineering Center GEOPRIBOR, Academia of Sciences of Kyrgyz Republic, Institute of Geomechanics and Development of Subsoil, Mederova street, 98, Bishkek 720035, Kyrgyzstan
e-mail: torgoeval@yahoo.com

H.-B. Havenith
Department of Geology, University of Liege, B-18, Liege 4000, Belgium

C. Margottini et al. (eds.), *Landslide Science and Practice*, Vol. 1,
DOI 10.1007/978-3-642-31325-7_66,

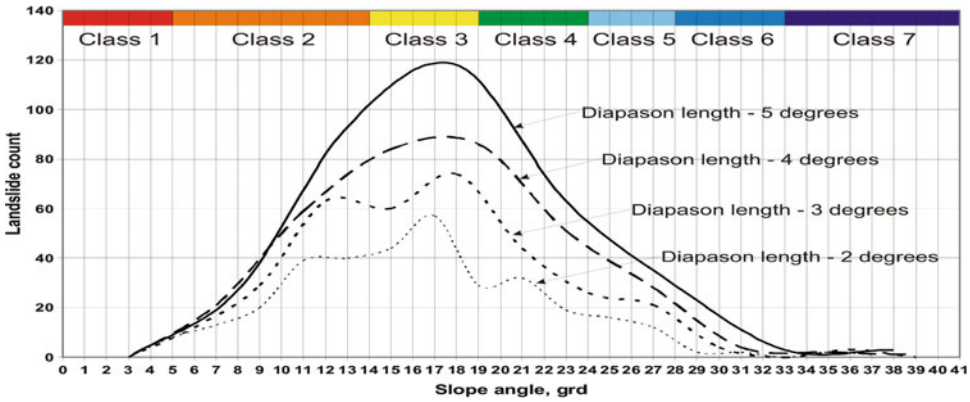

Fig. 1 Landslide area distribution within chosen classes of slope angle

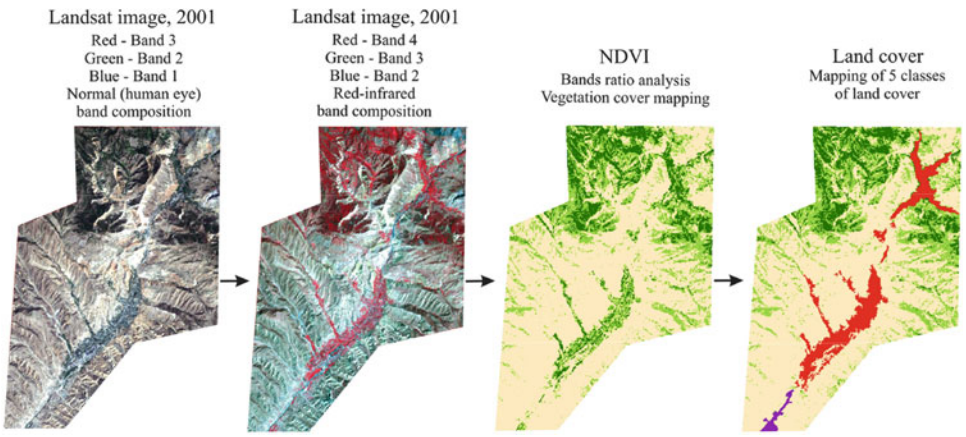

Fig. 2 Generalized scheme of land cover mapping

stereopairs. The final variant of slope angle map has seven classes of slope angles with class limits set using statistical analyses of the DEM with final resolution 30 × 30 m. The landslide area distribution within chosen classes of slope angle is presented in Fig. 1.

Land cover mapping was based on Landsat satellite imagery. The analyses of this imagery lead to the construction of a thematic map of land cover with five classes (rich vegetation, poor vegetation, bare surface, urbanized territory and rural areas). The generalized scheme of analyses for land cover mapping is presented in Fig. 2.

Mapping of lithological units was based on a digitized geological map (scale 1:50,000 from Soviet Geological Survey, 1956) of the target area incorporating available information on geotechnical properties of involved geological units. The final variant of lithological units map with resolution 30 × 30 m has six classes representing 21 geological units of the area presented in Table 1.

A structural geology map was constructed based on photogeological interpretation of aerial stereopairs with a scale 1:33,000. This approach allowed us to derive the strikes and dips of geological layers all over the target area. Later, the results of photointerpretation were combined with the results of morphological mapping (slope angle and slope exposition) in order to map four types of interconnection – conformable, intermediate, non-conformable and massive.

The results of affecting factors mapping contributed to more reliable estimates of landslide susceptibility, because they incorporated almost all factors affecting of landslide activity in the sub-regional scale. Figure 3 presents the results of mapping of all affecting factors with resolution 30 × 30 m.

Landslide Susceptibility Mapping

Landslide susceptibility mapping was completed using three different approaches wide spread in international practice:

- Discriminant Analyses (DA)
- Artificial Neural Network (ANN)
- Newmark Displacement (ND)

There is the difference between all three methods in data preparation and data postprocessing stages. DA and ANN approaches are statistical methods, while ND is physically based approach. There are also some differences concerning the mapping units used by each of these methods in our case: while ANN and ND were pixel-based approaches (30 × 30 m resolution in our study), DA we used as slope

Table 1 Description of geological units and their classification

Geological unit	Description	Class
Q IV	Gravel, sand	1
Q III–IV	Colluvium, deluvium, proluvium	1
Q III	Colluvium material of big grain size	1
Q I–II	Sand and material of middle grain size	1
Pr 2 ? Kb	Marble, schist, quarzite	4
P3 – N1 – ms1	Sandstone, gravelite, conglomerate	6
P3 – N1 – ms2	Sandstone, gravelite, conglomerate	6
P2–3	Clay, siltstone	2
P1–2	Limestone, clay, sandstone, gravelite, conglomerate	5
K2 t – Sn	Limestone, clay	5
K2s	Clay, sandstone, gravelite, limestone	3
K2 – Sn2	Clay, sandstone with limestone	3
K1n + al	Clay, lime-sandstone	3
K1hd	Conglomerate, gravelite, sandstone, basalt	4
J2	Sandstone, siltstone	6
J1ts2	Clay, siltstone	2
J1ts1	Clay, siltstone	2
C1v – s	Limestone	5
S1–2 asA	Effusive sillicates	4
S1–2 as_	Effusive sillicates	4
D 1–2 ab	Laves, silicates, siltstone	4

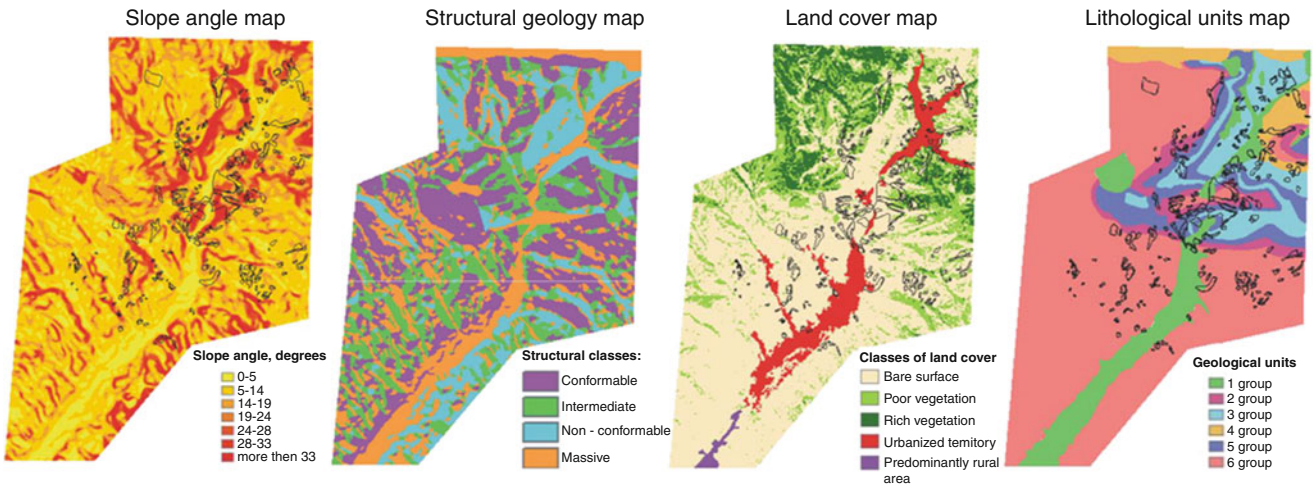

Fig. 3 Final results of affecting factor mapping

units based approach. But despite this difference there was a possibility to compare these approaches on a quantitative and qualitative basis. Figure 4 presents the results of landslide susceptibility mapping using the aforementioned approaches. Visual comparison of obtained results shows that there is a certain grade of similarity between them, but more detailed analyses reveals some differences. The quantitative evaluation of models based on statistical analyses of landslide density within certain classes of landslide susceptibility shows that ND mapping has the best performance of results. But, as it was mentioned above, all approaches have their own advantages and disadvantages – so, ND approach provides qualitative estimates, while the DA and ANN approaches give quantitative results showing spatial probability of landslide occurrence in certain places of the target area. For validation studies we used the latest available inventory (2007), while earlier inventories were used for construction of susceptibility models. Application

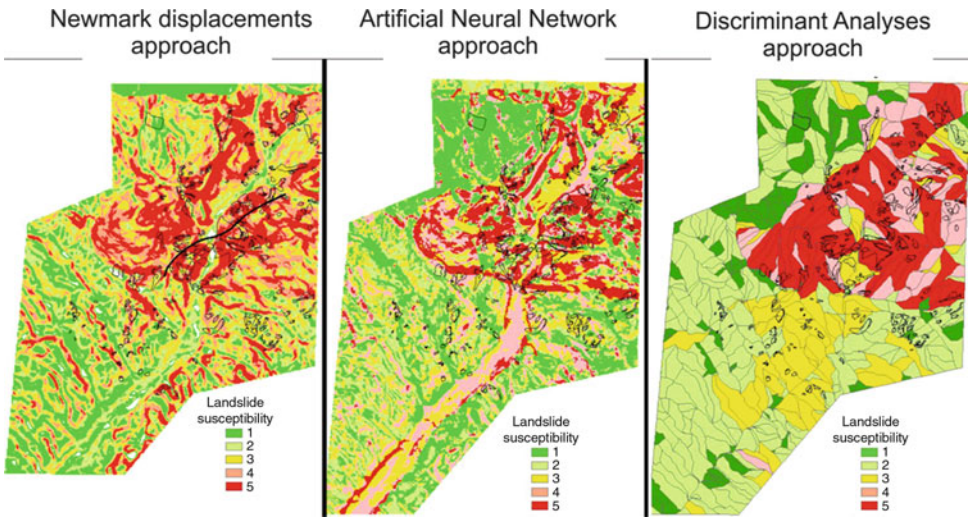

Fig. 4 The results of landslide susceptibility mapping using different approaches

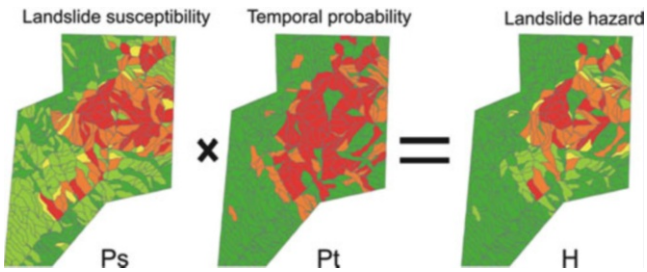

Fig. 5 Basic conception of landslide hazard estimation

of different methods of landslide susceptibility mapping provided us qualitative estimates of spatial probability of landslide occurrence, as well as quantitative ones giving probability of landslide occurrence in certain place of the target area.

Landslide Hazard Mapping

The basic conception of landslide hazard estimation is presented in Fig. 5. As it can be seen, landslide hazard (H) is expressed by multiplication of spatial probability of landslide occurrence, P_s (landslide susceptibility) and temporal probability of landslide occurrence, P_t. The last parameter, P_t, can be calculated for certain periods of time, called prognostic period, for example for 50 years using approach presented in Fig. 6. Here, we used four landslide inventories (1962, 1977, 1984 and 2003) with different time spans to calculate temporal probability of landslide occurrence for certain places.

Figure 7 presents the results of landslide hazard mapping using DA landslide susceptibility mapping and different prognostic periods. Logically, landslide hazard for longer prognostic periods will be higher than for shorter ones.

Landslide Risk Mapping

Landslide risk mapping in the target area was provided using the results of landslide hazard estimation and preliminary evaluation of vulnerability of targeted elements at risk (road network, urbanized territory, radioactive waste tailing). Vulnerability studies for the urbanized territory was based on information on construction type and land use. Road network vulnerability estimation was based on the level of importance and average density of vehicles on the road. Information on vulnerability of elements at risk was incorporated with information on landslide hazard mapping, which resulted in landslide risk mapping in the target area.

Figure 8 presents an example of preliminary landslide risk mapping for uranium waste tailing, urbanized territory and road network for the period of 50 years. However, accurate evaluations of landslide risk require more detailed vulnerability studies

Conclusions

The presented research on landslide susceptibility, hazard and risk mapping in the target area was done considering different kinds of input information (prognostic period, affecting factors, vulnerability studies). Obtained results on landslide susceptibility mapping have certain grade of similarity with the results of previous studies (Daneels 2004; Havenith et al. 2006; Braun 2010) while there was some difference because of principles of approaches used in the present activity. Future research perspectives will include dynamic modelling of slope stability and incorporation of obtained results into the calculations of landslide susceptibility and hazard in the target area.

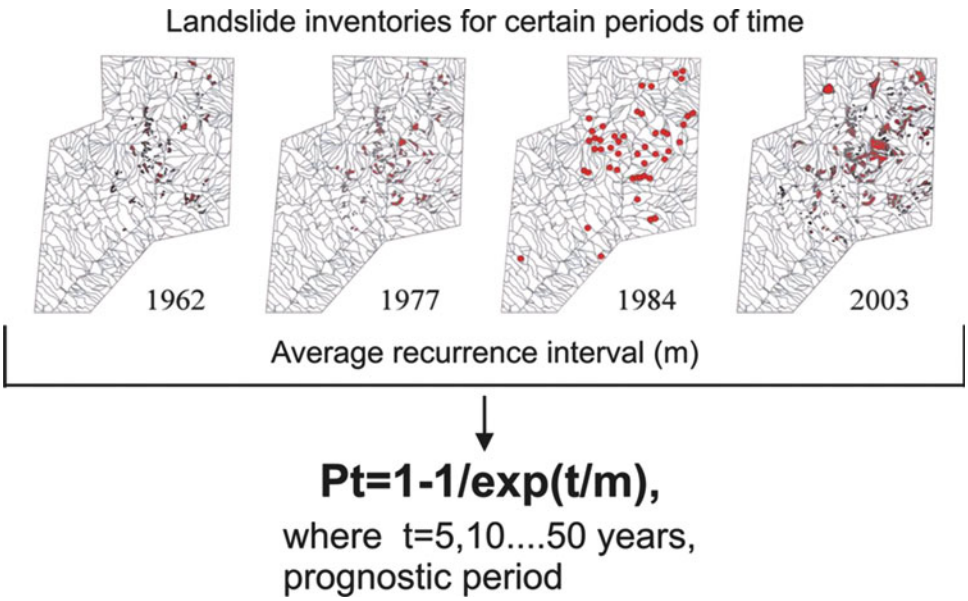

Fig. 6 Basic conception of temporal probability of landslide (P_t) occurrence calculation

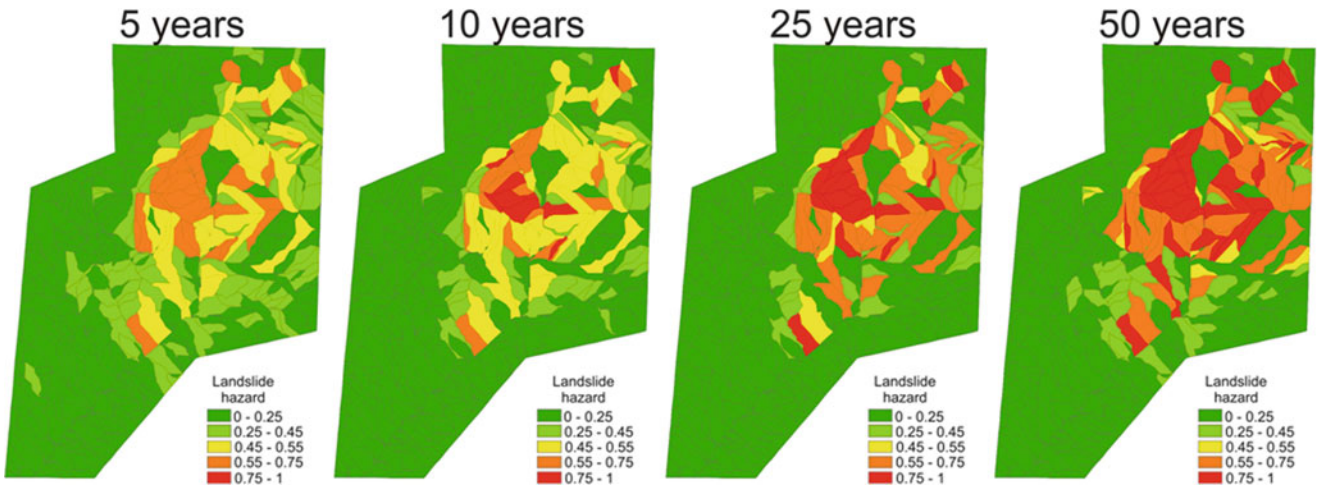

Fig. 7 The results of landslide hazard mapping using DA landslide susceptibility mapping

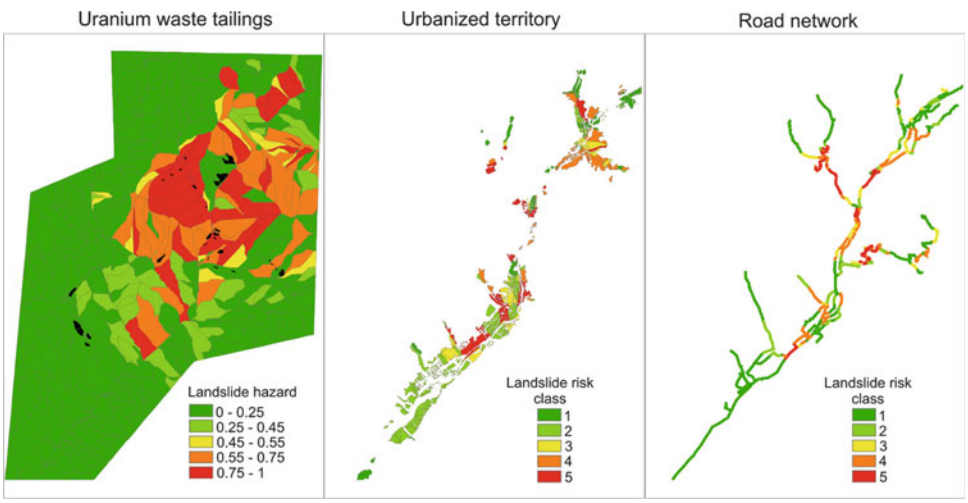

Fig. 8 The results of landslide risk mapping for uranium waste tailings (*black outlines*), urbanized territory and road network for the period of 50 years

The applied approaches can also be used in other areas with a high level of landslide hazard and risk. The present study provides both scientific results and practical outputs important for responsible agencies and society. It was shown that GIS and Remote Sensing are very useful tools for regional scale decision making in case of landslide prone areas. The advantage of utilized approaches is their low unit costs as well as their flexibility and effectiveness. Such kinds of studies can precede more localized studies and instrumental measurements giving important information for following more detailed investigations. The database created and utilized during these studies is very flexible with the possibility to make changes in a rapid way if needed. Despite disadvantages of these approaches, they are essential for complete assessment of landslide susceptibility, hazard and risk in the landslide-prone areas.

Acknowledgments This activity was provided within the frame of NATO SfP-983289 project "Prevention of Landslide Dam Disasters in the Tien Shan, Kyrgyz Republic" and with help of INTAS Young Scientists Fellowship 04-83-2914.

References

Alioshin YG, Torgoev IA, Losev VA (2000) Radiation ecology of Mailuu-Muu. ILIM, Bishkek, 96p

Braun A (2010) Investigation of landslide susceptibility in Maily-Say, Kyrgyzstan, with data mining methods. RWTH Aachen, Aachen, 131p

Daneels G (2004) Landslide susceptibility assessment in the Maily-Say Valley (Kyrgyzstan) by means of remote sensing techniques. University of Liege, Liege, 110p

Havenith H-B, Torgoev IA, Meleshko AV, Alioshin Yu G, Torgoev AD, Daneels G (2006) Landslides in the Mailuu-Suu valley, Kyrgyzstan: hazards and impacts. Landslides 3:137–147

Roessner S, Wetzel H-U, Kaufmann H, Sarnogoev A (2005) Potential of satellite remote sensing and GIS for landslide hazard assessment in southern Kyrgyzstan (Central Asia). Springer, London, 22p

Schlogel R, Torgoev I, De Marneffe C, Havenith H-B (2011) Evidence of a changing size-frequency distribution of landslides in the Kyrgyz Tien Shan, Central Asia. Earth Surf Process Landf 36 (12):1658–1669

MSUE Conditional Method Predictive Power, Milia Basin, Tuscany, Italy

Marco Capitani and Paolo Roberto Federici

Abstract

An attempt to assess the predictive power of the MSUE Conditional Method was made in landslide susceptibility zonation of the Milia Basin, Tuscany, Italy. A detailed geomorphological mapping, combined with aerial photographs analysis, enabled us to build two landslide inventories using a time scale. The landslides related to a period before 1975 were used to create the models, while those related to a period after 1975 were used to validate the models predictive power. Five time invariant factors maps were also developed in a GIS environment. Finally, the inventory landslides maps and the five landslide-related factor maps were processed using a model in a GIS environment. The procedure was applied separately to the most frequent landslides typologies and for each different combination of the five factors. The comparison between the distribution of landslides after 1975 and the predicted distribution derived from susceptibility models established the predictive power of each model.

Keywords

Landslide susceptibility • MSUE conditional method • Predictive power

Introduction

Over the last few decades, many researchers have produced landslide susceptibility maps using different methods of statistical analysis applied to Unique Condition Units (UCUs) (Carrara et al. 1995; Chung et al. 1995; Guzzetti et al. 1999; Irigaray et al. 1999; Clerici et al. 2002; Falaschi et al. 2008). However, no one has emphasized how the choice of representing the dependent variable (which is defined into the landslides inventory) can lead to the construction of models with un-definable predictive power.

Theoretically, since susceptibility assessment tries to identify under what conditions landslides are generated, the dependent variable should be represented in the landslides inventory as the area where landslides originated, i.e., the detachment zones (Nefeslioglu et al. 2008). Moreover, if the landslides are represented also with their accumulation zone, the environmental factors so acquired are erroneously considered to be prone to landsliding (Clerici et al. 2006, 2010; Magliuolo et al. 2008).

Due to the fact that the detachment zones are only partially visible, their definition into an inventory map is highly subjective. Moreover, without a geophysical prospecting, there is not the possibility to define how our representation differs from reality. This fact introduces unquantifiable errors in the dependent variable resolution that imply unquantifiable errors both in the definition of UCU type involved in landslides and in the definition of the UCU instability extension (independent variables). Therefore, this way of variable dependent representation makes uncertain the results of the predictive power validation for the models so built. In fact, the dependent variable is used both in the construction of models and in their validation (Chung and Fabbri 2003, 2008; Guzzetti et al. 2006, 2009; Rossi et al. 2010). Basically, if the "undefined" detachment zone is

M. Capitani (✉) • P.R. Federici
Dipartimento Di Scienze Della Terra, Università Di Pisa,
Via S. Maria 53, Pisa 56126, Italy
e-mail: capitani@dst.unipi.it

C. Margottini et al. (eds.), *Landslide Science and Practice*, Vol. 1,
DOI 10.1007/978-3-642-31325-7_67,

considered as way to correlate the UCUs to the events of instability the best predictive model, that is chosen from a validation process, could actually have a low predictive power for the future landslides occurrence. So, only a certain dependent variable should be used into landslides susceptibility analysis.

Among the systems of representation of the landslide inventory that do not introduce large margins of subjectivity and therefore unquantifiable errors, the Main Scarp Upper Edge method (MSUE) (Clerici 2002) is the only that could be better adapted to the purposes of the landslide susceptibility analysis.

On the other hand, among the methods of statistical analysis used to create landslide susceptibility maps, the conditional method appears to be one of the easiest to understand and to read for non-specialists.

Therefore, this study represents an attempt to assess the predictive capability of the MSUE Conditional Method and its advantages and limitations.

Study Area

The MSUEs Conditional Method was applied to the T. Milia basin, situated in the southern-central of Tuscany, Italy, about 100 km to S-SE of Pisa town (Fig. 1). The study area has an extension of 101 km^2 and elevation ranging from 39 to 913 m above sea level, with an average value of 336 m (standard deviation = 167.5 m). The basin is stretched out to SW direction and shows a prevalent hilly character. Hillslopes are generally not very steep. The highest value of the slope gradient is present in the eastern part of the Milia basin where the carbonatic formations outcrops.

Main Geological and Geomorphological Features

In the T. Milia basin the compressional events occurring before and during the collisional apenninic episode, originated the complex sheet stack where three allochthonous units are emplaced above the Tuscan Unit. The two uppermost of these units are derived from the Ligurian Domain and are, from top to bottom, the Palombini Shale Ophiolitic Unit and the Monteverdi-Lanciaia Ophiolitic Unit. Between these units and the Tuscany Unit there is the Argille and Calcari Unit that belong to the Sub-Ligurian Domain (Costantini et al. 1991). All the allochthonous units are characteristic of distal turbiditic and hemipelagic environments and are composed by altering siltitic, argillitic and fine arenitic formations and by argillitic with inter-bedded limestone formations. The ophiolitic units

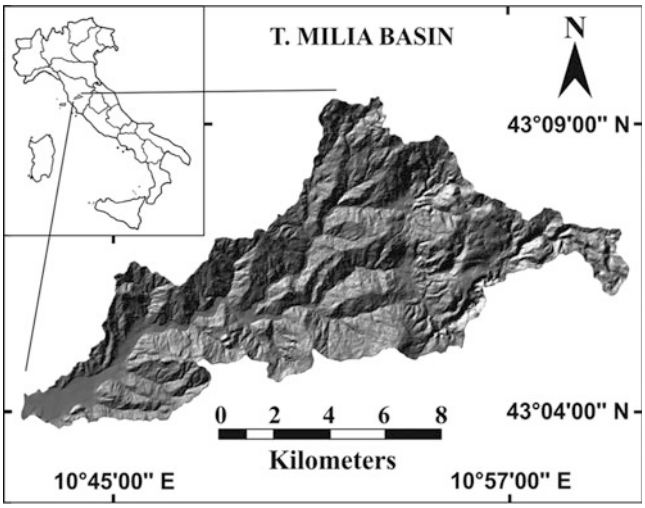

Fig. 1 Location of the study area and hillslope characters

also contain remains of the basalt, gabbros and serpentinites complex that are disseminate as blocks in their sediments.

The Tuscan Unit is represented prevalently by the Mesozoic carbonatic succession, associated to very few outcrops of the middle and upper turbiditic and hemipelagic sequence.

Ligurian units show a complex, pre-upper Oligocene deformation history related to subduction, accretion and later exhumation events. The deformation history includes almost two deformation phases of veining, folding and thrusting (Marroni et al. 2004). These deformative structures are successively superimposed by the deformative structures due to collisional and post collisional events. In the collisional event the Ligurian and Sub-Ligurian Units are overthrust the Tuscan Domain and have been deformed, with the units belonging to this later domain, by a kilometric folds that in the Milia basin have a WNW-ESE axial general direction.

Post collisional deformations are strictly related to the extensional tectonic, which began at the end of the Early Miocene and caused the collapse of a large part of the Apennines chain. This extensional event started with low and high angle normal faults as result of thinning of the upper crust. Then differential uplift, lowering and tilting phenomena occurred from the middle Pleistocene on (Bossio et al. 1993). The deposition of the Neogene-Quaternary successions has been largely controlled by vertical crustal movements. These successions are representative of coastal-marine and continental environments and are generally characterized by sandy clays and sandy conglomerates deposits.

The extensional phase conditioned the hydrographic evolution of the Milia basin. In particular, from the Pleistocene the tectonic evolution was followed by a rapid sinking of the

hydrographic network, with the development of considerable level difference. The lowering of the network base level is suggested by numerous erosive terraces that are located at different altitudes along the basin. The lateral erosion action of the T. Milia and of its main tributaries is still-active important morphogenetic process.

The morphology of the study area is also strongly conditioned by the numerous mass movements related to a prevalent rotational slide, translational slide and flow types (Cruden and Varnes 1996). Moreover, many phenomena of Deep-seated Gravitational Slope Deformation (DGSDs) are present and their evolution appears strictly related to the Pleistocenic tectonic evolution and the base level fluvial lowering. From a classification point of view, the type of movement of these DGSDs could be considered similar to Block-slide and Sackung (Zischinsky 1969; Sorriso-Valvo 1988; Dramis and Sorriso-Valvo 1994; Cruden and Varnes 1996). Most of these DGDSs are involved in landsliding processes.

Materials and Methods

MSUE-Conditional Method

The Conditional Method is based on Bayes Theorem (Morgan 1968) where the probability of the future occurrence of an event with determinate boundary conditions is determinate by the same type of events that occurred in the past with the same boundary conditions (conditional probability). In particular, for the landslide susceptibility (LS) assessment the conditional probability of landslide occurrence at specific UCU (boundary conditions) is assumed equivalent to the currently landslide density in that UCU (Carrara et al. 1995).

Considering the problems for the use of the detachment zones as dependent variables representation, the landslides have been identified by their MSUEs (Clerici 2002; Clerici et al. 2006, 2010). Furthermore, an upstream buffer of 10 m is used for each MSUEs, in order to consider the UCUs involved in the landslide process as potential representative of the boundary conditions existing before the landslides development (Clerici 2002; Süzen and Doyuran 2004a, b; Clerici et al. 2006, 2010; Nefeslioglu et al. 2008).

Therefore, in the method applied to the LS zonation of the Milia Basin the conditional probability of landslide occurrence for a given UCU is assumed as the ratio of the sum of the areas of each UCU that fall within the MSUEs buffer and the total area for each specific UCU.

Considering the different orders of magnitude between the areas of the UCU inside the MSUE buffer and the total of the specific UCU, the landslide density has been expressed in m^2/km^2.

Mapping of Landslides

The landslides map is the result of a detailed geological and geomorphological 2 year-field surveys. The landslides were mapped on a 1:10,000 Tuscany Region topographic map. This process has been carried out also with the aid of the aerial photographs of 1975 at the scale 1:13,000 (flight EIRA75). The use of aerial photographs of 1975 was necessary to dived the landslides into two temporal groups. The landslides occurred before the 1975 have been used to create the models, while the landslides occurred after the 1975 have been used to validate their predictive capability.

Following the division proposed by Keefer (1984), only 2,039 deep-seated ($\geq$3 m) landslides were considered. They occupy a surface of about 22.66 km^2, representing the 22.43 % of the whole study area.

In accord to Guzzetti et al. (1999), LS analysis should be carried out for different landslide types. For this reason, the landslides have been mapped into separate datasets on the base of their prevalent movement typology. Because in this study the MSUE is considered as the dependent variables, the landslides belonging to the complex typology have been classified on the base of their initial prevalent movement. So in the study area 2,039 landslides have been regrouped into three typologies: translational slide (1,577), flow type (155), and rotational type (307). Among these, 128 translational, 31 flow and 46 rotational have been occurred after the 1975.

For the correct mapping of the MSUEs into a ArcGIS (ESRI) feature-class the landslides occurred before the 1975 have been mapped directly over the orthophotos (at the scale 1:10,000), with the aid of the aerial photograph inspection. The orthophotos have been successively scanned, imported into ArcGIS, rectified, geo-referenced, assembled and digitized into a feature-class. For the landslides occurred after the 1975, a GPS (Garmin 60CSx) field survey was necessary to delimit their MSUEs, where almost 7 points for a single main scarp have been marked. Within these 7 points, the landslide main scarp-body contact are also taken. The MSUEs points have been successively imported into a ArcGIS and digitized as lines.

Instability Factors

In the LS assessment of the Milia Basin also old landslides have been introduced into the statistical analysis. This fact has made necessary to consider only time-invariant (or quasi-static) environmental factors that can be supposed to change over geomorphological time scale, as geological or morphometric characteristics (Clerici et al. 2010). In fact, if time-variant factors – i.e. human activity, land-use and climatic conditions – are introduced into LS analysis, the

resulting role of these factors can be completely misunderstood (Atkinsons and Massari 1998). Moreover, applying the Conditional Method to LS zonation, it is necessary to limit the number of factors that have to be introduced into the analysis, in order to limit the presence of small UCU of little statistical significance (Carrara et al. 1995). As consequence, only the following five time-invariant factors are considered.

Lithology

The lithology map has been derived from the geological field survey. The map was scanned, imported into ArcGIS, rectified, geo-referenced, assembled and digitized into a feature-class. The process of geologic map digitalization is resolved by the topologic method of ArcGIS. Even though this method is a very complex way to create a polygon feature class, it can resolve the problem of the sliver polygons.

For lithology, different classes have been extracted from the geological map on the basis of their lithological and structural analogies. Moreover, considering that in the study area many landslides have been occurred from the body of other landslides and from the DGSDs, it was also necessary to insert these elements into a specific class. On the whole, 11 different classes have been introduced into the analysis.

The extension of the lithological class and their relative MSUEs density for each landslide type are reported in Fig. 2.

Morphometric Factors DEM-Derived

Among the morphometric factors usually used in the LS assessment, slope angle and slope aspect are the most commons. While the slope angle is accepted as one of the most landslide-influencing factor, the importance of the slope aspect as landslide-controlling factor is nowadays still debated.

In the study area the slope angle and the slope aspect are derived from the 10 × 10 pixel resolution DEM, obtained by transforming a TIN in GRID. The TIN was generated by interpolation of digital contour lines and elevation points, extracted from a topographic map at scale 1:10,000 (Shape Files of the Region Tuscany, CTR). These morphometric factors, expressed in a raster form, have been reclassified and transformed in a vector format (polygonal feature class).

According to Clerici et al. (2010), in order to create classes statistically significant, i.e., classes with great areas, the reclassification of the slope angle has been made into six classes with similar areas (percentile criteria), while slope aspect has been reclassified into the eight classes corresponding to the classic angular sectors, 45° wide and clockwise from north (equal interval criteria). During the transformation of the factors maps from raster to vector format the classes so identified have been codified with a respective unique value. For all of these classes MSUEs density has been performed (Fig. 3).

Distance from Hydrographic and Tectonic Elements

Considering that the evolution of the Milia Valley is strictly connected to the neogenic tectonic activity and to the fluvial erosion phases, it was also necessary to consider these the matic elements as probable landslide-inducing factors. Distance from hydrographic and tectonic elements maps are derived in a vector format directly from the geological and geomorphological maps. The procedure consists of extracting the thematic linear elements and by buffering these in a relative polygonal feature class. The relative maps have been then reclassified in their attribute tables. The maps of the distance from hydrographic and tectonic elements have been made by four similar area classes. Their MSUEs density is reported in Fig. 3.

Procedure to LS Zonation

A preliminary univariate analysis was performed by crossed tabulation (contingency tables) to understand the possible relations between each factor (predictor variable) and the landslides occurrence. This analysis was made for each single landslide typology. Then, Cramer's V coefficient was derived from Chi^2 (χ^2) to tests the strength of factors-landslides association (Table 1). From this first analysis it was possible to ascertain how the selected factors have usually a high degree of association with the landslides inventories. Only the slope aspect shows a low Cramer's V to flow type. Among the factors, lithology and slope angle show the highest degree of association with the MSUEs distribution.

A conditional analysis was performed to evaluate the relationship between landslides and the factors considered simultaneously. Though the conditional method is conceptually very simple to understand, it is operationally very complicated because it needs to be applied many times for the same study area and for different landslide types. So a Model-Builder (scripts) in ArcGis (ESRI) has been created in which all geoprocessing steps have been automatized.

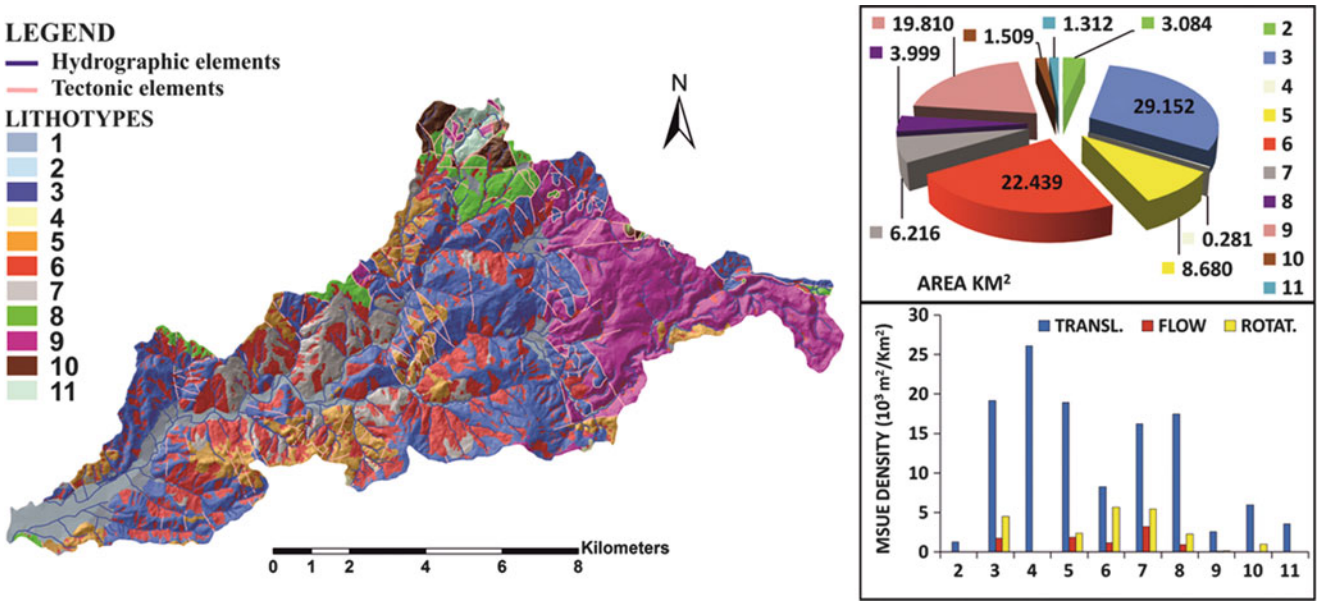

Fig. 2 Lithological class, their extension and MSUE density. *1* sandy gravelly complex, *2* sandly complex, *3* shale complex, *4* clayey marly complex, *5* sandy gravelly clayey complex, *6* landslide body, *7* DGSD, *8* marly limestone flysch complex, *9* carbonatic complex, *10* sandy turbiditic complex, *11* siliceous complex

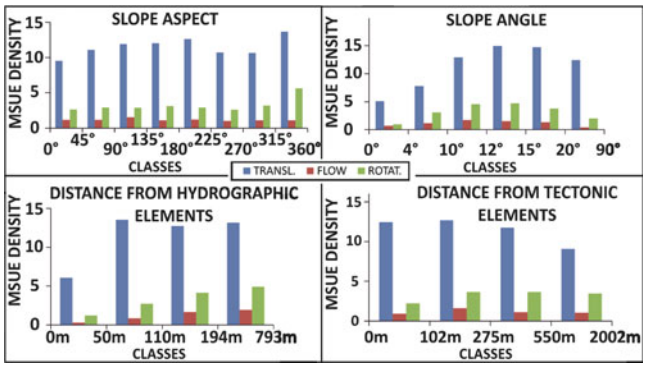

Fig. 3 Factors classes MSUE density (10^3 m^2/km^2)

In the Model-Builder, for each landslides type, all of the 31 possible factors combinations (UCUs feature class) are overlaid (intersect) with the buffer feature class of the MSUE belonging to pre-1975 landslides. For each UCU the ratio of the sum of the UCU area that fall within the MSUEs buffer and the total area for that UCU is calculated. Successively, the UCUs are grouped into five density classes (LS classes) on the basis of their ratio value. For the classes definition it is used a similar method already used by Clerici et al. (2010). The classes are defined on the base of the MSUEs mean density, computed by dividing the sum of the MSUEs buffer area and that of the study area. This value (Md) represents the middle point of the middle class. More precisely, the class interval on which LS maps are created is $Ci = (Md/5) \times 2$ and the susceptibility class intervals are: 0–Ci (Very Low), Ci–2Ci (Low), 2Ci–3Ci (Medium), 3Ci–4Ci (High) and 4Ci–5Ci (Very High).

For each of the three landslide type, 31 LS zonation have been built. A validation procedure has been performed into Model-Builder to choose the best-model. The validation procedure is based on the "see and wait" concept, that is the only rigorous way to evaluate the LS map reliability. In this method the distribution into the LS classes of pre-1975 MSUEs (training set) is compared with that of the post-1975 MSUEs (validation set). For each of the five susceptibility class the absolute value of the difference between the pre-1975 and post-1975 MSUEs percentage is computed. The sum of these latter values, Validation Error (VE), is reported for each LS Models. The VE assesses the predictive power of each model built and its value ranging from 0 (the best predictive power) to 200 (the worst predictive power).

In according with Clerici et al. (2010), a good validation is a necessary but not a sufficient prerequisite for assessing the model efficiency. A good model should have a great dispersion around the main density value to distinguish between significantly different landslides density distributions. Therefore, a MSUE mean deviation (MD) was computed for each model and the ratio VE/MD (Best Model Index, BMI) was utilized to choose the best LS model, that should have the highest MD/VE value (Clerici et al. 2010).

The best five models are presented in Table 2 for each landslides type. For translational type, the LS zonation map is displayed in Fig. 4.

Table 1 Univariate relations between MSUEs and Lithology (L), Slope (S), Aspect (A), Distance from tectonic elements (DF) and Distance from hydrographic elements (DI)

	Tranl.		Flow		Rotat.	
FC	$\chi 2$	V	χ^2	V	χ^2	V
L	5,885	0.31	665	0.18	1,482	0.22
S	1,179	0.18	175	0.10	563	0.15
A	153	0.11	10	0.05	276	0.13
DF	281	0.13	156	0.11	205	0.12
DI	884	0.17	377	0.14	639	0.16

Table 2 The five best models of LS obtained by MSUE Conditional Method, ordered from the highest to the lower BMI value

	Transl.			Flow				Rotat.			
FC	VE	MD	BMI	FC	VE	MD	BMI	FC	VE	MD	BMI
LS	3.4	8,575	2,522.1	LDI	12.3	1,025	83.3	SDF	19.5	1,644	84.3
LDIDF	5.6	9,042	1,614.6	LS	12.7	911	71.7	LSDF	28.2	2,255	80.0
LDF	5.5	8,083	1,469.6	LSDI	17.2	1,086	63.1	LADF	42.5	2,395	56.3
LSDI	7.3	10,145	1,389.8	ADI	12.9	643	49.8	LSA	50.2	2,224	44.3
LDI	9.1	8,781	964.9	ADIDF	19.9	878	44.1	LADIDF	72.0	3,150	43.7

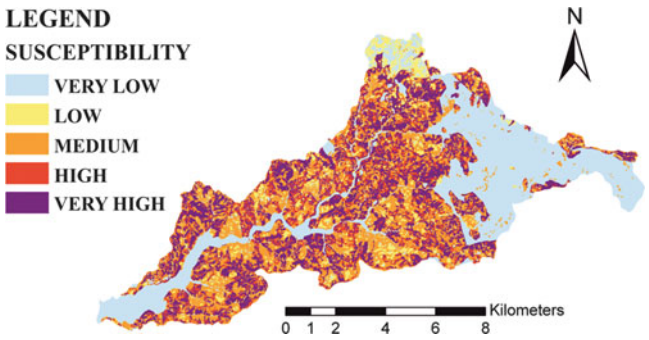

Fig. 4 LS zonation map for the translational best model

Discussion and Conclusions

The MSUE Conditional Method shows a good predictive power only for the translational landslides, where the combination of the Lithology-Slope angle (LS) factors represents the best model with a BMI = 2,522.1 (Table 2). For rotational and flow types the best model is represented by the Slope Angle-Distance from Tectonics elements (SDF) and Lithology-Distance from Hydrographics elements (LDI) factors combinations respectively. Considering the results of the univariate analysis, the Conditional Method seems to confirm the same important factors in the prediction of the translational and the flow landslides occurrence. For the rotational type, the conditional method reveals the landslide-influencing factors different to the factors that have a highest Cramer's V coefficient. This fact confirms that the conditional analysis has a greater capacity to extract the landslide-influencing factors than the univariate analysis.

For each landslide type the VE value tends generally to increase as the number of factors introduced into the analysis increases. The VE increasing is strictly related with the introduction of a large number of small UCUs that have a littler statistical significance (Clerici et al. 2010). Furthermore, the presence of small UCUs makes the choose of the MSUE as detachment zone representation more unsuitable. In fact, the UCUs individuated by the MSUEs are less representative than those belonging to the detachment zones as much as the UCUs are small.

The predictive power of the three best models moves from a 3.4 VE for the translational landslides to a 19.5 VE for the rotational landslides (Table 2). The VE value for flow and rotational types is not fully acceptable. This discrepancy can reflect the presence of landslides belonging to these later typologies with MSUEs buffer extension statistically more high than that of the translational type. In fact, MSUEs buffer of the translational landslides has a mean extension of 837.2 m^2 (standard deviation = 352.2 m^2) against those of the flow and rotational types that have mean of 995.3 and 1293.5 m^2 (standard deviation = 350,537 m^2) respectively. The lowering of the predictive power, connected to the increasing of the mean MSUEs extension, can be associated to the MSUEs degradation processes that involve the main scarps, causing a withdrawal effect. The MSUEs withdrawal implies the buffering of the UCUs that are not strictly connected to those present before the landslides occurrence and so a lowering of the predictive power of the MSUE Conditional Method. This problem is particularly accentuated for the MSUEs with greater original extension (i.e. large landslides), for the MSUEs originated in more degradable lithotypes and for the MSUEs related to the oldest landslides. Therefore, the introduction of the big and

old landslides into the MSUE Conditional Method can provide a LS models with a low predictive power. Even if the old landslides are not introduced into the statistical analysis, the MSUE Conditional Method applied for LS assessment in areas where very degradable lithotypes outcrop can also show a lower predictive power.

Acknowledgments The authors thank A. Clerici, S. Lorenzini, A. Ribolini and the anonymous referees for their valuable suggestions and constructive comments.

References

Atkinsons PM, Massari R (1998) Generalised linear modeling of susceptibility to landsliding in the central Apennines, Italy. Comput Geosci 24(4):373–385

Bossio A, Costantini A, Lazzarotto A, Liotta D, Mazzanti R, Mazzei R, Salvatorini G, Sandrelli F (1993) Rassegna sulle conoscenze sulla stratigrafia del Neoautoctono toscano. Mem Soc Geol Ital 49:17–98

Carrara A, Cardinali M, Guzzetti F, Reichenbach P (1995) GIS technology in mapping landslide hazard. In: Carrara A, Guzzetti F (eds) Geographical information systems in assessing natural hazards. Kluwer Academic, Dordrecht, pp 135–175

Chung CF, Fabbri AG (2003) Validation of spatial prediction models for landslide hazard mapping. Nat Hazards 30(3):451–472

Chung CJ, Fabbri AG (2008) Predicting landslides for risk analysis – spatial models tested by a cross-validation procedure. Geomorphology 94:438–452

Chung CF, Fabbri AG, Van Westen CJ (1995) Multivariate regression analysis for landslide hazard zonation. In: Carrara A, Guzzetti F (eds) Geographic information systems in assessing natural hazards. Kluwer, Dordrecht, pp 107–133

Clerici A (2002) A GRASS GIS based shell script for landslide susceptibility zonation. In: Ciolli M, Zatelli P (eds) Open source free software GIS-GRASS users conference, Trento. http://www.ing.unitn.it/*grass/conferences/GRASS2002/proceedings/proceedings/pdfs/Clerici_Aldo.pdf

Clerici A, Perego S, Tellini C, Vescovi P (2002) A procedure for landslide susceptibility zonation by the conditional analysis method. Geomorphology 48:349–364

Clerici A, Perego S, Tellini C, Vescovi P (2006) A GIS-based automated procedure for landslide susceptibility mapping by the conditional analysis method: the Baganza valley case study (Italian Northern Apennines). Environ Geol 50(7):941–961

Clerici A, Perego S, Tellini C, Vescovi P (2010) Landslide failure and runout susceptibility in the upper T. Ceno valley (Northern Apennines, Italy). Nat Hazards 52:1–29

Costantini A, Lazzarotto A, Maccantelli M, Sandrelli F (1991) Ligurian units in the Monti della Gherardesca area (Southern Tuscany). Boll Soc Geol Ital 110:849–855

Cruden DM, Varnes DJ (1996) Landslide types and processes. In: Turner AK, Schuster RL (eds) Landslides investigation and mitigation, special report 247. Transportation Research Board, National Research Council, Washington, DC, pp 36–75

Dramis F, Sorriso-Valvo M (1994) Deep seated slope deformations, related landslide and tectonics. Eng Geol 38:231–243

Falaschi F, Federici PR, Puccinelli A, D'Amato Avanzi G, Pochini A, Spagnolo M, Bottai M, Salvati N (2008) Statistical approach and GIS techniques in evaluating landslide susceptibility in a sample area of the Serchio River Basin (Italy). Ital J Eng Geol Environ Special issue 1:119–136

Guzzetti F, Carrara A, Cardinali M, Reichenbach P (1999) Landslide hazard evaluation: a review of current techniques and their application in a multi-scale study, Central Italy. Geomorphology 31:181–216

Guzzetti F, Reichenbach P, Ardizzone F, Cardinali M, Galli M (2006) Estimating the quality of landslide susceptibility models. Geomorphology 81:166–184

Guzzetti F, Reichenbach P, Ardizzone F, Cardinali M, Galli M (2009) Landslide hazard assessment, vulnerability estimation and risk evaluation: an example from the Collazzone Area (Central Umbria, Italy). Geogr Fis Dinam Quat 32:183–192

Irigaray C, Fernández T, El Hamdouni R, Chacón J (1999) Verification of landslide susceptibility mapping: a case study. Technical report. Earth Surf Process Landf 24:537–544

Keefer DK (1984) Landslides caused by earthquakes. Geol Soc Am Bull 95:406–421

Magliuolo P, Di Lisio A, Russo F, Zelano A (2008) Geomorphology and landslide susceptibility assessment using GIS and bivariate statistics: a case study in southern Italy. Nat Hazards 47:411–435

Marroni M, Meneghini F, Pandolfi L (2004) From accretion to exhumation in a fossil accretionary wedge: a case history from Gottero unit (Northern Apennines, Italy). Geodin Acta 17:41–53

Morgan BW (1968) An introduction to Bayesian statistical decision process. Prentice-Hall, New York, 116p

Nefeslioglu HA, Duman TY, Durmaz S (2008) Landslide susceptibility mapping for a part of tectonic Kelkit Valley (Eastern Black Sea region of Turkey). Geomorphology 94:401–418

Rossi M, Guzzetti F, Reichenbach P, Mondini AC, Peruccacci S (2010) Optimal landslide susceptibility zonation based on multiple forecasts. Geomorphology 114:129–142

Sorriso-Valvo M (1988) Studi sulle deformazioni gravitative profonde di versante in Italia. Mem Soc Geol Ital 41:877–888

Süzen ML, Doyuran V (2004a) Data-driven bivariate landslide susceptibility assessment using geographical information systems: a method and application to Asarsuyu catchment. Turkey Eng Geol 71(3):303–321

Süzen ML, Doyuran V (2004b) A comparison of the GIS-based landslide susceptibility assessment methods: multivariate versus bivariate. Environ Geol 45(5):665–679

Zischinsky U (1969) Uber Sackungen. Rock Mech 1:30–52

Debris Flow Risk Assessment in the Aguas Calientes Village (Cusco, Perù)

Claudio Puglisi, Luca Falconi, Azzurra Lentini, Gabriele Leoni, and Carlos Ramirez Prada

Abstract

In this paper a landslide risk assessment in the area of Aguas Calientes village (Machu Picchu, Cusco, Perù) is applied. A study carried out into a capacity building project (FORGEO) was focused on localising source areas and runout of debris flows triggered by heavy rainfall in the Alcamayo catchment and on assessing debris flow intensity. Starting from an inventory of several previous debris flows occurred in the area, an evaluation of the local predisposing parameters to these events was used as input for susceptibility and hazard GIS based analysis. Empirical formulas reported in the literature were adapted to the research area context to estimate the runout of potential events. An analysis of exposure of structures and infrastructures was also performed during the project and high residual risk conditions were found for the Aguas Calientes village. These results may aid local authorities involved in land use planning, management policies and landslide risk reduction.

Keywords

Debris flow • Susceptibility • Intensity • Risk map • Aguas Calientes • Peru

Introduction (Study Area, Geology, Geomorphology)

Aguas Calientes village (Machupicchu Pueblo, 1,600 inhabitants in 2002 and approximately 1,500 tourists daily) is located on a fan of mixed origin (alluvial and landslides deposits) and is regularly impacted by debris flows and floods that originate from the upstream creeks (Aguas Calientes and Alcamayo streams) and by floods of the Vilcanota (Urubamba) river. As a consequence of natural conditions and recent urban expansion, some of the structures and infrastructures of the village, particularly a new subdivision near the banks of Alcamayo creek, are subject to damage.

The study area consist of the catchment of the Alcamayo creek (about 3.7 km^2, near latitude 8544351° N and longitude 769213° E; maximum height: 3,950 m a.s.l.; minimum height: 2,080 m a.s.l.), which is a right-hand tributary of the Vilcanota river. The catchment of Alcamayo creek is dominated by steep slopes with an average angle of 42°. Almost 70 % of the area is characterised by slope angles between 30° and 56° (mean value +/−σ), and almost one third of the catchment is characterised by slope angles between 40° and 49°. Due the morphological features of the river basin, the time of concentration is on the order of minutes. The average annual rainfall registered in the Machu Picchu meteorological station (Registro pluviometrico de la estación de Machupicchu, SENAMHI) reaches 2,038.70 mm, with a maximum in February (333.31 mm) and a minimum in August (60.78 mm). It is remarkable that 70 % of this rainfall occurs during a 5-month period between December and April.

C. Puglisi (✉) • L. Falconi
ENEA – Italian National Agency for new technologies, energy and sustainable economic development, ENEA -Utpra-Prev Via Anguillarese, 301 – 00123, Italy
e-mail: claudio.puglisi@casaccia.enea.it

A. Lentini
GSF – Geology Without Borders, Italy

G. Leoni
Consultant Geologist, Italy

C.R. Prada
INC – National Institute of Cultural Heritage, Peru

C. Margottini et al. (eds.), *Landslide Science and Practice*, Vol. 1,
DOI 10.1007/978-3-642-31325-7_68,

According to the hydrological balance of this area, 67 % of the precipitation contributes to superficial runoff and only 18 % to infiltration (Carreño and Kalafatovich 2006). A subtropical-tropical humid forest with medium high vegetation completely covers the catchment with the exception of the little village area and the steeper slopes.

The territory of the Historic Sanctuary of Machu Picchu belongs to the Eastern Cordillera, a WNW-ESE chain characterized by metamorphic and igneous rocks. The area around Aguas Calientes village is primarily underlain by the Permian Machu Picchu batholith (246 ± 10 My), an intrusive body characterized by granite with lesser amounts of granodiorite, tonalite and several aplite, quartz-monzonite and andesite hypoabisal dikes (Carlotto et al. 1999, 2009).

Depositional formations produced by recent and present chemical and physical weathering outcrop above the Paleozoic bedrock. Quaternary fluvial terraces and alluvial cones amassed large volumes of deposits through mixed processes with catastrophic character as debris flows (Vilímek et al. 2007). Alluvial fans occur at the mouth of the tributary drainage (e.g., the fans of the Aguas Calientes creek and Aobamba river), where they form thick debris bodies. Terraces belonging to fluvial deposits mainly outcrop along the Vilcanota valley at different altitudes and less often along the bottom of the valleys of its tributaries. Considerable talus bodies lie at the foot of the steeper rock slopes, which are mainly composed of heterometric sediments with granite boulders in a sandy-clay matrix. A thick (1–5 m) colluvium mantle resulting from bedrock alteration processes is distributed throughout the slopes. Where the Alcamayo and Aguas Calientes creeks flow into the Vilcanota river, two overlapping fans composed of several generations of alluvial and debris flow deposits have been formed.

Discontinuities (joints and failure surfaces) are widespread structural features of the intrusive bodies, which are strictly bound by compression dynamics that have affected the whole Andean range since the Palaeocene age. Granite fracturing, which is due to many families of shear zones and joints, has strongly conditioned the geomorphological evolution of the area. The action of exogenous agents has therefore contributed to the development of a thick layer of fractured rocks with huge boulders immersed in a pervasive silty-sandy fine matrix. On top of the reliefs, where the matrix has been removed by weathering, piles of loose boulders known as "granite chaos" outcrop. All this loose and heterometric material is susceptible to be triggered by debris flow processes.

The morphological features of the area are linked to the regional uplift and characterised by steep and high-energy slopes. Deepening of the river bed causes erosion processes at the foot of the rocky slopes and of the recent debris deposits favouring landslide phenomena. At the foot of the slopes and in the narrow river bed lie loose blocks with volumes of more than 1,000 m^3 and heterometric debris produced by falls and debris flows (Figs. 1 and 2). Abundant local rainfall is the main triggering factor for debris flows due to rapid saturation of the shallow portions of the soil layer. Several debris flows

Fig. 1 Debris flow trigger and transit area in the study area

Fig. 2 Debris flow accumulation area in the study area

were documented near Aguas Calientes village over the last 50 years (Canuti et al. 2009; Carreño and Kalafatovich 2006; Vilímek et al. 2006).

Method

A detailed geomorphological survey of the Alcamayo creek catchment has been performed during a field work carried on in June 2009, with the aim of improving the knowledge on the geological features of the area (Fig. 2). Field observations were integrated with geomorphological analysis based on aerial photo-interpretation of two sets of stereoscopic aerial photographs (1991 and 2006, Servicio Aerofotogrametico Nacional) of the entire catchment.

The study approach is based on a landslide inventory, an analysis of past events and the identification, for each detected landslide, of predisposing parameters (Varnes 1984; Dietrich et al. 1995; Hutchinson 1995; Casagli et al. 2004; Abbattista et al. 2005; Leoni et al. 2009). The predisposing parameters detected in each censused landslide area were recorded in a data base, by landslide typology in question. Using descriptive statistical processing based on the frequency distribution of predisposing parameters surveyed, the most significant factors are extrapolated. By comparing the landslide inventory and the DEM derived maps, slope and aspect classes and the distance from the drainage net of the areas affected by previous landslides were identified. Each spatial data set of predisposing parameters, once it has been digitised, has been constituted an information layer. The GIS overlay of all the layers generated a subdivision of the area into Homogeneous Land Units (HLUs), each of which are characterised by the existence of one or more predisposing parameters (Casagli et al. 2004). In the susceptibility degree assessment of each HLU, two subsequent phases have been involved:

- Attribution of weighting to the predisposing parameters;
- Identification of a susceptibility function.

Through a heuristic approach, a weight for each parameter and an index for the different classes that comprise each parameter were assigned. Subsequently, the susceptibility of source areas has been assessed.

Once identified source areas with the greatest susceptibility value, transit and runout areas were identified on the basis of a detailed DEM (cell size 5 × 5) processed by aerial photos. Areas with different potentials to be affected by debris flow runout were distinguished and mapped.

On the basis of a past debris flow event (2004; Fig. 3) and of an empirical formula, runout distance and velocity of potential new events triggered in high susceptibility sample areas were estimated. By using the Rickenmann (1999) formula that describes theoretical relationship between travel distance and energy for debris flows of different size, the maximum runout of potential debris flows was estimated. By measuring the river bed deposited material and eroded banks features in two curves of the Alcamayo watercourse, the flow velocities of the 2004 event have been estimated using the Johnson and Rodine (1984) formula. Possible runout tracks of the potential debris flows were defined and different levels of runout susceptibility (spatial hazard) were attributed.

Applying a qualitative approach, structures and infrastructures were discriminated into different exposure classes. The classification has attributed a higher value on structures of collective importance and human lives. Overlap of runout susceptibility and exposure maps allowed to define a qualitative risk map of Aguas Calientes village.

Results

The censused debris flows show typical morphology with an initial, usually short, source area composed of an irregular or circular crown, followed by a ribbon shaped area ending in the talweg, into which the landslide body is channelled. The identified source areas are homogenously distributed throughout the catchment and located at altitudes between 3,060 m and 2,060 m a.s.l., where the soil cover thickness ranges from 0.5 m to more than 5 m. Failure surfaces may develop both within the soil cover layer and at the contact surface with the granite bedrock.

Slope angle, aspect and distance from the drainage net are the only predisposing parameters that were used in this study to determine the different susceptibility classes. These parameters and their values (slopes angle range, exposure range and distance from the river network) were detected in the past censused landslides.

Two general trends for the original slope gradient in the niche zone have been identified in the local debris flow family: “high angle phenomena” occurring in the steeper slopes (50–70°), where the soil is moderately thick, and “low angle phenomena” with thicker soil bodies lying on smoother slopes (25–55°). The landslide inventory showed distinct aspect trends: the high angle phenomena were largely present in slopes towards S and the low angle landslides definitely in slopes towards W.

The source areas of both the high-and low-angle debris flows are concave across the slope and many of them were found to contain a considerable amount of water. Since these areas are typically located along a drainage network, 15-m and 30-m buffer areas were used in the layers as predisposing parameters.

Two different maps show the susceptibility zonation concerning the source areas of both landslide typologies (Figs. 4 and 5). Low angle debris flows could occur along a wider part of the catchment than the high angle phenomena, whose higher susceptibility areas are concentrated along the

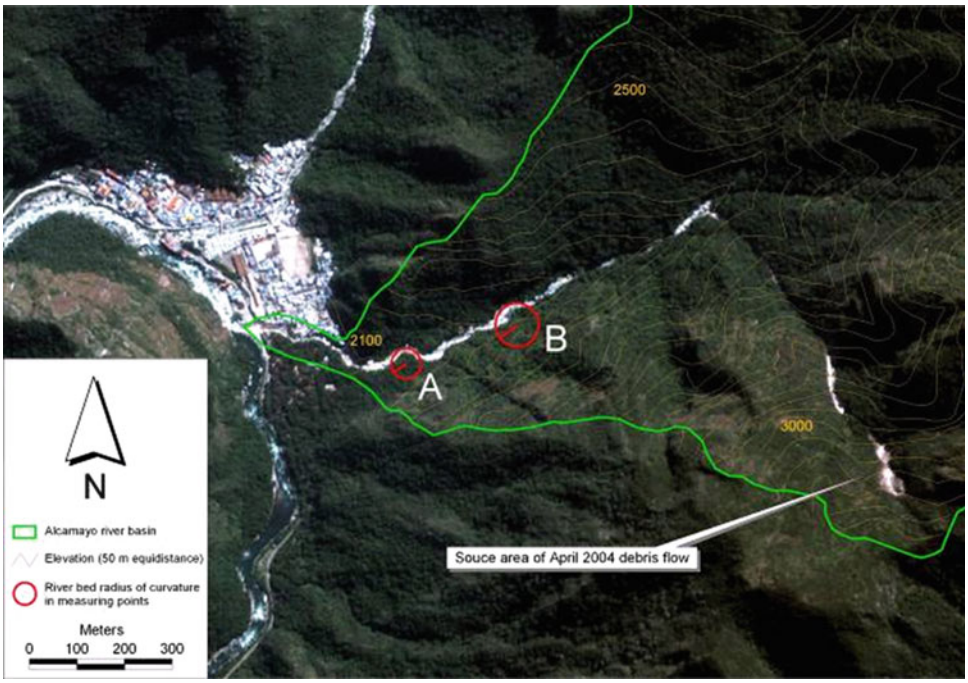

Fig. 3 Localization of the 2004 debris flow event and of the two curves of the Alcamayo watercourse where velocity has been estimated

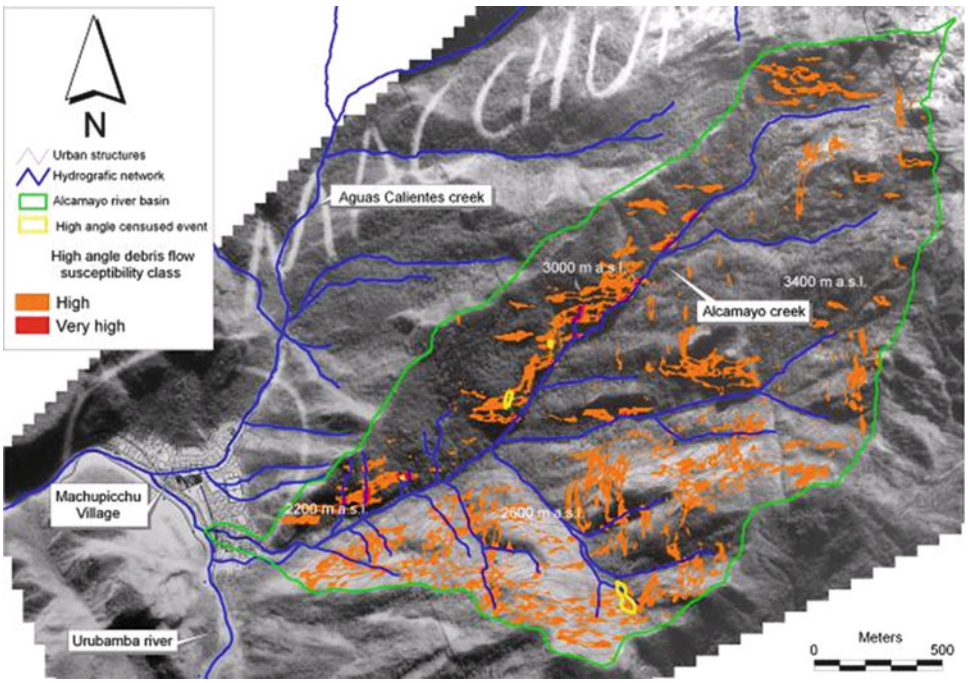

Fig. 4 Susceptibility map of the high angle debris flow (source area)

SE side. The source areas for both typologies could be triggered along several stretches of the drainage net.

Different empirical formulas were used to analyse the runout of the 2004 event (Corominas 1996; García-Ruiz et al. 2002; Crosta et al. 2003; Devoli et al. 2009). Assuming that a failure surface of 3 m in depth developed in the soil cover layer, the Rickenmann formula (1999) seemed to better approximate the real runout, with an underestimation of 11 %. This formula has been applied to three high susceptibility areas (Fig. 5), with a correction factor corresponding to the underestimation of the event occurred in 2004. Results underline that the potential debris flows could reach the village of Aguas Calientes in at least two cases of the three sample areas.

A detailed geomorphological model of the fan allowed to identify the topographically lower zones of the fan (mostly paleo drainage lines). The southern part of the alluvial fan is

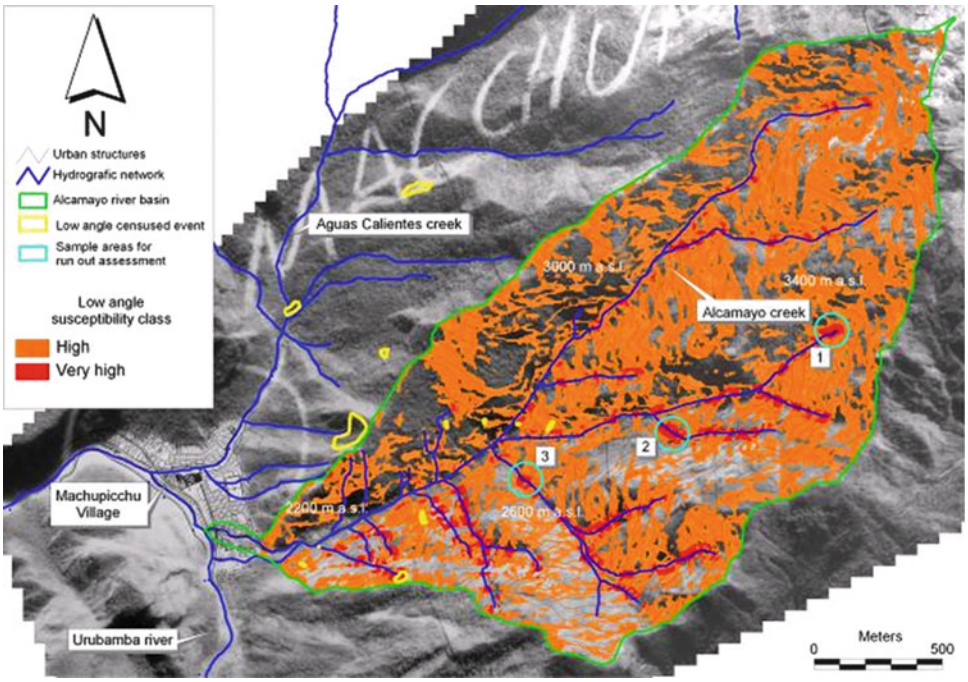

Fig. 5 Susceptibility map of the low angle debris flow (source area); the *light blue rings* indicate the three sample areas used for runout assessment of potential debris flows

characterised by four former drainage lines that have a direct morphological relationship with the current active river bed of the Alcamayo creek. These depressed areas may be used as channels by future debris flows. In fact, under the centrifugal force effect, where the stream makes slight curves immediately before the Alcamayo outlet to Vilcanota river, water and debris can overflow and overrun old sewer lines. These areas have been attributed the higher levels of runout susceptibility (spatial hazard) (Fig. 6). Damming effects due to a complete or partial obstruction of the rail bridges in this stretch may favour this process. Similar alluvial fan morphology is found along the Aguas Calientes creek (Vilímek et al. 2006).

In two curves of the last stretch of the Alcamayo watercourse, the flow velocities of the 2004 event have been estimated (Vb = 12 m/s; Va = 9.7 m/s). Assuming a decreasing linear trend of the velocity, its value should have been 5 m/s (Fig. 7) before stopping at the bottom of the catchment in the Vilcanota river, at the location of the first buildings in the village.

Assuming a density of 200 kg/m^3 for the debris material, 200–500.000 kJ of energy could be developed in this point by each of the three high susceptibility sample areas (Fig. 5). A single boulder of 150 m^3, like several were found along the slopes and in the river bed, that was dragged by a 5 m/s flow, could develop 5000 kJ of energy, which is the same magnitude of energy as a truck moving at 180 km/h.

An exposure map that included the location of the elements at risk and the attribution of a relative value index was developed (Fig. 8). All of the depressed zones of the fan were attributed an elevated risk level (Fig. 9). Inside these zones, part of the railway station is characterised as having the greatest risk.

Discussion

Debris flow susceptibility is widespread throughout the Alcamayo river basin, particularly for low angle phenomena (25–55°). Since this slope angle class is more frequent in the catchment and tends to involve larger volumes of debris material, this typology appears to be more dangerous than the high angle class (50–70°).

The triggering of areas with high and very high susceptibility values may allow to the displaced material to reach the village of Aguas Calientes and cause damage as in the April 2004 event. Nevertheless, smaller phenomena can dam the Alcamayo creek with serious repercussion to the village below.

Formulas used in runout assessment have been developed for contexts (Alps, Pyrenees, Central America) distinct from this study area. Although Rickenmann's (1999) formula fits the events in the Alcamayo catchment better than the other formulas, the observed margin of error suggests the need to revise this equation in order to provide a more reliable runout assessment tool for this area. The revisited relationship with the higher performance coefficients is:

$$L = 34(V \cdot \Delta)^{\frac{1}{4}}$$

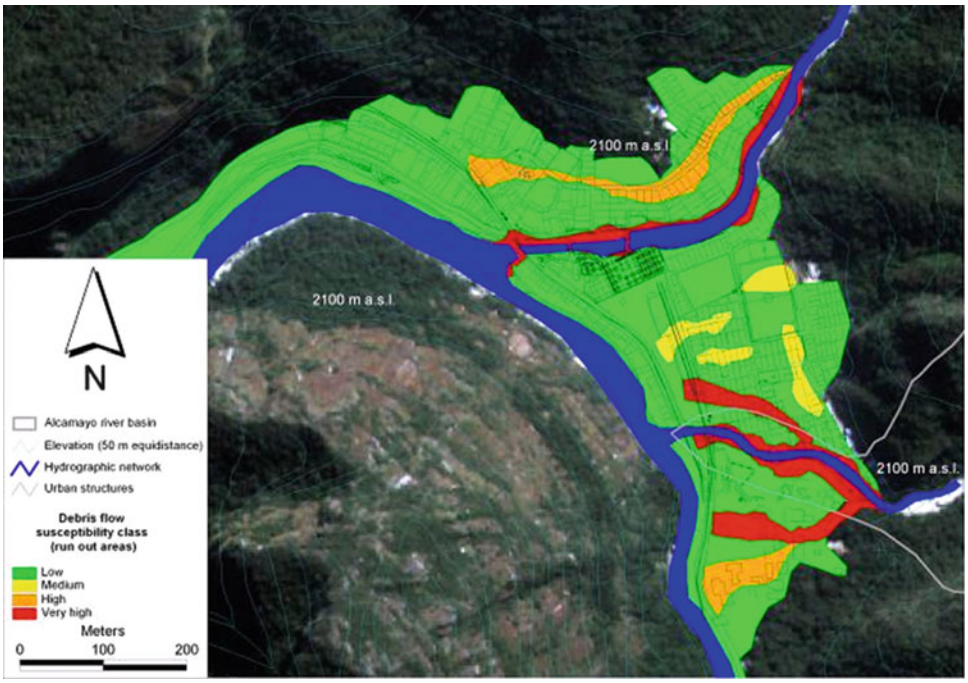

Fig. 6 Runout susceptibility (spatial hazard) in the Aguas Calientes village

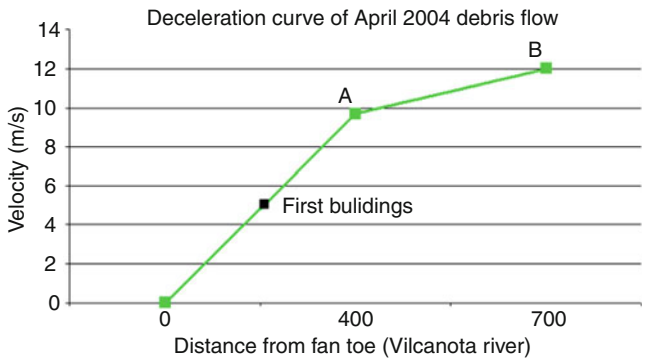

Fig. 7 Flow velocities of the 2004 event in the two measurement points (A and B), at the first Aguas Calientes buildings (estimated suggesting linear trend) and at the outlet in the Vilcanota river

Where:

- L = travel distance of the mass movement;
- V = total volume mobilized by the debris flow;
- Δ = elevation difference between the starting point and the lowest point of the deposition of the mass movement

The accuracy of this speed estimation is notoriously low even because of the time that elapses between the debris flow event and the field measurements. However, the calculated values seem to be comparable with the method proposed by Prochaska et al. (2008) that relates flow velocity to channel slope and flow depth.

According to the Ojeda-Moncayo et al. (2004) classification, the three potential debris flows and the 2004 event are in the 3rd class of magnitude (total rating = 20, Lm = III) based on 6 parameters (volume, velocity, runout, depth, affected area and deformation). Using the debris flow size classes proposed in Jakob (2005) and based on debris-flow volume, peak discharge and area inundated by debris, the examined events would be classified as a Size Class 3 or 4 (volume: 103/104 m^3; peak discharge: 400 m^2/s; inundated area: 103 m^2).

Major runout hazard in the Aguas Calientes village occurs where structures are placed in current or old river beds, where the fan is topographically lower. This study stresses the high debris flows risk in the new urbanisation areas of the village. In particular, buildings located in the morphological depression near the railroad station are in the higher risk areas (class 4). Comparison of the current hazard zone map (Carlotto and Cárdenas 2001) and the April 2004 Alcamayo debris flow accumulation map (Vilímek et al. 2006) shows good concordance between the "extremely high damage" areas and the "very high risk" zones. However, it also shows an underestimation of the potential overflow of the streams. The hazard evaluation of Aguas Calientes village used in the current plan for civil protection (Carlotto et al. 2007) does not take sufficiently into account the depressed areas between the Aguas Calientes and Alcamayo creeks.

Spatial susceptibility evaluation and intensity assessment of potential events are only two of the three factors that are used to evaluate landslide hazards. Thorough analysis of rainfall data constitutes an indispensable step for identifying the temporal occurrence of landslide phenomena and for determining the site-specific pluviometric thresholds.

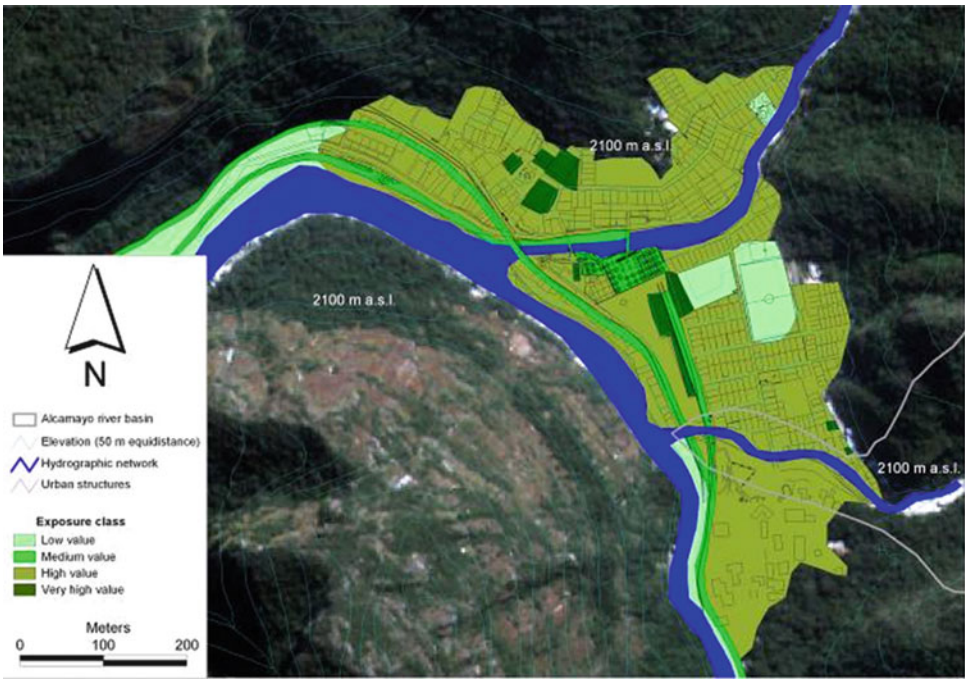

Fig. 8 Exposure map of Aguas Calientes village

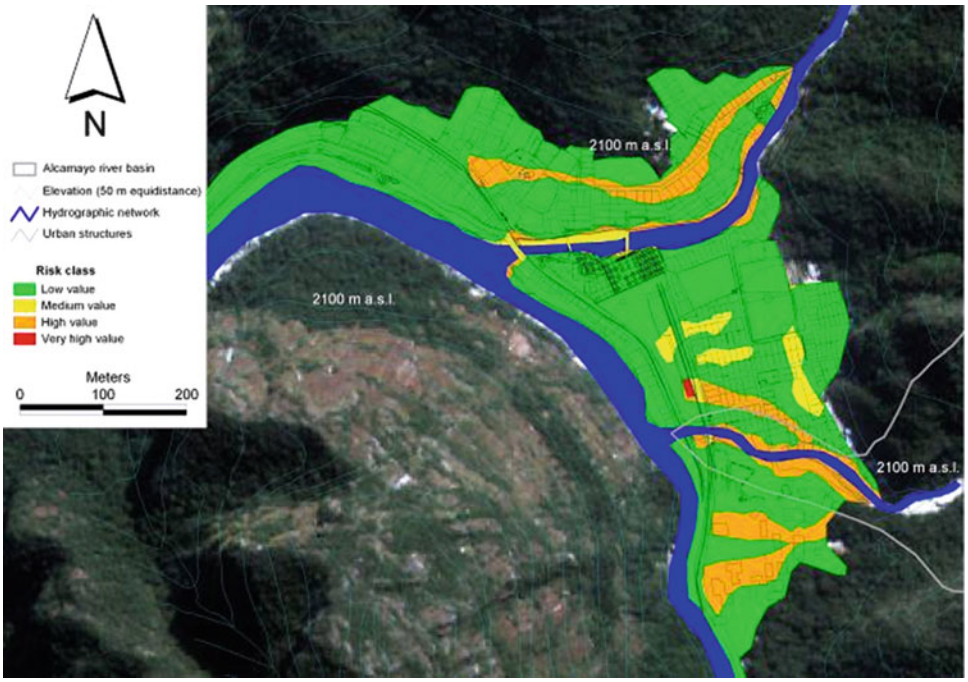

Fig. 9 Debris flow risk map of Aguas Calientes village

Conclusions

The debris flow hazard in the Alcamayo catchment and the residual risk for the village are seriously high. Especially the latter has been further worsened by the rapid urban development that has occurred over last few decades. The depressed zones of the fan present an elevated residual risk level and the railway station is characterised by the greatest risk for debris flow.

The results presented here may aid administrative authorities involved in natural risk management in the Machu Picchu area. Strengthened civil protection plans that account for the runout paths identified in this study are an indispensable short term measure that may be taken to improve the sureness of this area. In the medium and long term, partial structures and infrastructures relocation may be a sustainable solution to reduce the landslide risk for Aguas Calientes village.

References

Abbattista F, D'Agostino G, Delmonaco G, Di Filippo L, Falconi L, Leoni G, Margottini C, Puglisi C, Romano P, Spizzichino D (2005) La valutazione della suscettibilità da frana: applicazione alle colate rapide di Cervinara (AV). Geologia tecnica & ambientale, no 1/2005. ISSN 1722-0025

Canuti P, Margottini C, Casagli N, Delmonaco G, Falconi L, Fanti R, Ferretti A, Lollino G, Puglisi C, Spizzichino D, Tarchi D (2009) Monitoring, geomorphological evolution and slope stability of Inca Citadel of Machu Picchu: results from Italian INTERFRASI project. In: Sassa K, Canuti P (eds) Landslides – disaster risk reduction. Springer, Berlin, pp 249–258. ISBN 978-3-540-69966-8

Carlotto V, Cárdenas J (2001) Machu Picchu: a giant built on a fragile foundation. Geotimes 46:22–24

Carlotto V, Cárdenas J, Romero D, Valdivia W, Tintaya D (1999) Geologia de los cuadrangulos de Quillabamba y Machupicchu. Boletin N°127, Serie A: Carta Geologica Nacional. INGEMMET, Lima

Carlotto V, Cárdenas J, Fidel F (2007) La Geología en la Conservación de Machupicchu. Boletín INGEMMET, Serie I Patrimonio y Geoturismo 1, Lima, 305p

Carlotto V, Cárdenas J, Fidel L (2009) La geología, evolución geomorfológica y geodinámica externa de la ciudad inca de Machupicchu, Cusco-Perú. Revista de la Asociación Geológica Argentina 65(4):725–747

Carreño R, Kalafatovich S (2006) The Alcamayo and Cedrobamba catastrophic debris flow (January, March and April 2004) in Machupicchu area – Peru. Landslides 3(1):79–83

Casagli N, Catani F, Puglisi C, Delmonaco G, Ermini L, Margottini C (2004) An inventory-based approach to landslide susceptibility assessment and its application to the Virginio River Basin, Italy. Environ Eng Geosci X(3):203–216

Corominas J (1996) The angle of reach as a mobility index for small and large landslides. Can Geotech J 33:260–271

Crosta GB, Dal Negro P, Frattini P (2003) Soil slips and debris flows on terraced slopes. Nat Hazards Earth Syst Sci 3:31–42

Devoli G, De Blasio FV, Elverhøi A, Høeg K (2009) Statistical analysis of landslide events in Central America and their run-out distance. Geotech Geol Eng 27(1):23–42

Dietrich EW, Reiss R, Hsu ML, Montgomery DR (1995) A process-based model for colluvial soil depth and shallow landsliding using digital elevation data. Hydrol Process 9:383–400

García-Ruiz JM, Beguería S, Lorente A, Martí C (2002) Comparing debris flow relationships in the Alps and in the Pyrenees. Instituto Pirenaico de Ecología, Zaragoza

Hutchinson JN (1995) Keynote paper: landslide hazard assessment. In: Bell DH (ed) Landslides. Balkema, Rotterdam, pp 1805–1841

Jakob M (2005) A size classification for debris flows. Eng Geol 79(3–4):151–161

Johnson AM, Rodine JR (1984) Debris flow. In: Brusden D, Prior DB (eds) Slope stability. Wiley, Chichester, UK, pp 257–361

Leoni G, Barchiesi F, Catallo F, Dramis F, Fubelli G, Lucifora S, Mattei M, Pezzo G, Puglisi C (2009) GIS methodology to assess landslide susceptibility: application to a river catchment of Central Italy. J Maps 5:87–93

Ojeda-Moncayo J, Locat J, Couture R, Leroueil S (2004) The magnitude of landslides: an overview. In: Lacerda WA, Ehrlich M, Fontoura SAB, Sayao ASF (eds) Landslides, evaluation and stabilization. Balkema, Leiden/London/New York, pp 379–384

Prochaska AB, Santi PM, Higgins JD, Cannon SH (2008) A study of methods to estimate debris flow velocity. Landslides 5(4):431–444

Rickenmann D (1999) Empirical relationship for debris flow. Kluwer Academic, Dordrecht

Varnes DJ, IAEG Commission on Landslides (1984) Landslides hazard zonation – a review of principles and practice. UNESCO, Paris, 63p

Vilímek V, Klimeš J, Vlcko J, Carreño R (2006) Catastrophic debris flows near Machu Picchu village (Aguas Calientes), Peru. Environ Geol 50(7):1041–1052

Vilímek V, Zvelebil J, Klimeš J, Patzelt Z, Astete F, Kachlík V, Hartvich F (2007) Geomorphological research of large-scale slope instability at Machu Picchu, Peru. Geomorphology 89:241–257

Landslide Hazard Assessment on the Ugandan Footslopes of Mount Elgon: The Worst Is Yet to Come

Lieven Claessens, Mary G. Kitutu, Jean Poesen, and Jozef A. Deckers

Abstract

On the 1st of March 2010 a heavy rainfall event triggered a devastating landslide in the Bududa region on the footslopes of Mount Elgon in eastern Uganda, destroying life and property. Earlier studies published in 2006 and 2007 looked at characteristics and causal factors of older landslides in the area based on a landslide inventory and a detailed digital terrain analysis. In addition, a landslide hazard assessment was conducted with the LAPSUS-LS landslide model identifying susceptible landslide triggering sites and scenarios of landslide erosion and deposition quantities and pathways. This paper revisits the earlier studies and assesses how accurately the recent landslide was predicted. In addition a revised landslide scenario for the near future is elaborated based on the critical rainfall threshold that triggered the recent landslide.

Keywords

LAPSUS-LS • Landslide hazard • Uganda • Bududa

Introduction

Landslides occur frequently in the East African highlands with steep slopes, high weathering rates and slope material with a low shear strength or high clay content as the main causal factors (Glade and Crozier 2004). In addition, increasing population pressure, with slope disturbance, inconsiderate irrigation and deforestation as consequences and triggering factors like earthquakes and extreme rainfall events turn the East African highlands into an inherently susceptible region. There are however only limited studies assessing spatially explicit causal factors in detail and performing hazard assessments for disaster mitigation in the region (Claessens et al. 2007).

In Uganda, the south-western footslopes of the Mount Elgon volcano is the most vulnerable area for landslides. Mass movements associated with intense rainstorms are reported to have occurred periodically since the early twentieth century but the increase in fatalities and losses as a consequence of the enormous population growth draws attention to the phenomenon nowadays (Knapen et al. 2006). On the 1st of March 2010 heavy rains (52 mm on the 28th of February and 52 mm on the 1st of March) caused a landslide and associated debris flow to occur in the Bududa region, burying houses and killing hundreds of people.

This paper revisits earlier studies by Knapen et al. (2006) and Claessens et al. (2007) and places the recent landslide within their findings. Knapen et al. (2006) mapped 98 recent landslides (66 shallow and 32 deep rotational landslides) and by statistically comparing topographical characteristics from landslide sites with those from the whole study area, it was shown that landslides occur predominantly on steep concave slopes that are oriented to the main rainfall direction (north-east) and at a relatively large distance from the water divide.

L. Claessens (✉)
International Potato Center, Nairobi, Kenya

Wageningen University, Wageningen, The Netherlands
e-mail: l.claessens@cgiar.org

M.G. Kitutu
National Environmental Management Authority, Kampala, Uganda

J. Poesen • J.A. Deckers
Catholic University, Leuven, Belgium

C. Margottini et al. (eds.), *Landslide Science and Practice*, Vol. 1,
DOI 10.1007/978-3-642-31325-7_69,

A digital terrain analysis by Claessens et al. (2007) confirmed most of the causal topographic factors for shallow landsliding: in general, shallow landslides occur at a relatively large distance from the water divide, on the transition between steep concave and more gentle convex slope positions. This topographic position points to concentration of (sub)surface flow, often on a stagnating soil horizon, as the main hydrological triggering mechanism. In addition Claessens et al. (2007) grouped the recent shallow landslides in a specific landslide hazard class (critical rainfall values of 0.03–0.05 m day^{-1}) with the LAPSUS-LS landslide model (Claessens et al. 2005). By constructing a landslide hazard map and simulating future landslide scenarios with the model the study area was identified as inherently susceptible and volumes of soil redistribution were simulated to yield four times higher than currently observed.

Materials and Methods

Study Area

The 275 km^2 study area on the south-western footslopes of Mount Elgon is bounded by latitude 2° 49′–2° 55′N and longitude 34° 15′–34° 34′E (Fig. 1). Altitude ranges from 1,300 to 2,850 m.a.s.l. Because of this high altitude, precipitation values are high with an annual average of 1,800 mm. Two distinct wet seasons can be distinguished, separated by a pronounced dry period from December to February and by a period of dispersed, less intense rains from July to early August. The mean annual air temperature is about 23 °C (National Environment Management Authority 2001).

The dominant soil types in the study area are Acrisols, Ferralsols, Nitisols and Luvisols. On the western slopes, deep Nitisols occur whereas on the steep slopes in the east, shallow soils dominate (Breugelmans 2003; Kitutu et al. 2009). The average population density amounts to 952 persons km^{-2} (Uganda Bureau of Statistics 2004), with >1,300 persons km^{-2} in the densely populated western part. Due to land scarcity land parcels are small and even slopes steeper than 80 % are cultivated (Knapen et al. 2006). The main crops grown in the subsistence agricultural system are banana, yam, cassava and maize. Nowadays, forest constitutes 45 % of the study area, whereas before the large-scale deforestation starting in the 1930s, the forest was more extensive and most slopes in the east were under forest (Hamilton 1984).

LAPSUS-LS

The LAPSUS-LS landslide model was developed to assess spatially explicit shallow landslide hazard and to simulate the triggering of landslides (by scenario) and their subsequent movement, erosion and deposition down-slope. First the amount of rain that will trigger a landslide (the critical rainfall threshold, Q_{cr}) is calculated on a cell basis in a grid structure. This methodology is based on previous work by Montgomery and Dietrich (1994) and Pack et al. (2001), which combines a steady state hydrologic model with a deterministic infinite slope stability model to delineate areas prone to landsliding due to surface topographic effects on hydrologic response. The minimum steady state critical rainfall predicted to cause slope failure, Q_{cr} [m day^{-1}] can be defined as:

$$Q_{\mathrm{cr}} = T \sin\theta \left(\frac{\mathrm{b}}{\mathrm{a}}\right)\left(\frac{\rho_{\mathrm{s}}}{\rho_{\mathrm{w}}}\right)\left[1 - \frac{(\sin\theta - C)}{(\cos\theta \tan\phi)}\right]$$

where T is saturated soil transmissivity [m^2 day^{-1}], θ local slope angle [rad], a the upslope contributing drainage area [m^2], b the unit contour length (the grid resolution [m] is taken as the effective contour length as in Pack et al. (2001)), ρ_s wet soil bulk density [g cm^{-3}], ρ_w the density of water [g cm^{-3}], ϕ the effective angle of internal friction of the soil [rad] and C the combined soil and root cohesion term [−], made dimensionless relative to the perpendicular soil thickness (Pack et al. 2001). Parameters used are derived from a 10 × 10 m digital elevation model (DEM) and soil physical and hydrological data were obtained from the laboratory and literature (Table 1). For an assessment of the sensitivity of the LAPSUS-LS model to variability of soil physical and topographic parameters, the reader is referred to Claessens et al. (2005). After a landslide is triggered in a certain critical rainfall scenario (all sites with a Q_{cr} value lower than the set critical rainfall threshold fail), the downslope trajectory is calculated for both the erosional and depositional phases of the landslide. Sediment delivery to streams is also calculated by counting the amount of available sediment in the depositional phase crossing the user defined stream network. More details about the algorithms and parameters used in LAPSUS-LS can be found in Claessens et al. (2005, 2007).

Results and Discussion

A landslide hazard map for the study area was constructed by overlying the classified critical rainfall values calculated with LAPSUS-LS with the DEM (Fig. 2) Being relative measures of landslide susceptibility rather than physically interpretable absolute numbers, the Q_{cr} values were classified in six classes (Claessens et al. 2007):

1. Unconditionally unstable
2. Very high landslide hazard: $0.0 < Q_{cr} < 0.05$ m day^{-1}
3. High landslide hazard: $0.05 < Q_{cr} < 0.1$ m day^{-1}
4. Moderate landslide hazard: $0.1 < Q_{cr} < 0.2$ m day^{-1}

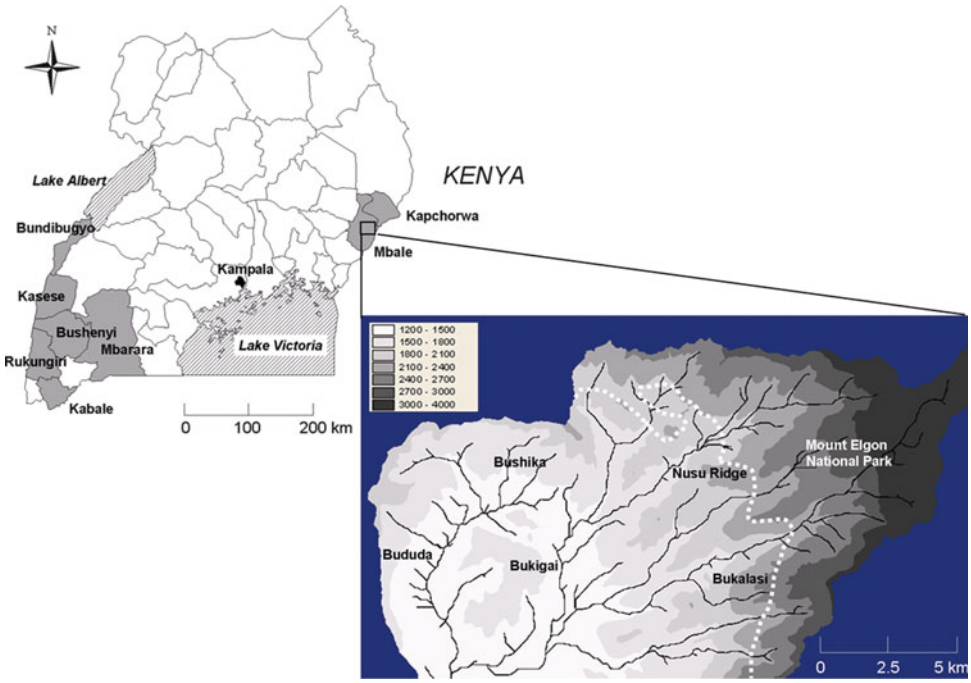

Fig. 1 Location of the study area in Uganda. *Grey coloured districts* are vulnerable to landslides. *Grey shades* in the detail of the study area reflect altitude according to the DEM (*legend top left*)

Table 1 Soil physical and hydrological properties of the study area used in the LAPSUS-LS model.

Zone	C [−]	ϕ [rad]	ρ_s [g cm^{-3}]	T [m^2 day^{-1}]
East	0.15	0.7	1.6	15
Central	0.47	0.5	1.5	17
West	0.35	0.4	1.6	17

5. Low landslide hazard: $0.2 < Q_{cr}$ m day^{-1}
6. Unconditionally stable

The older landslides from the inventory by Knapen et al. (2006) are depicted as dots in Fig. 2. The site where the recent landslide was triggered is marked with a star. From the map it is apparent that slopes in the eastern part of the study area are relatively more vulnerable to landsliding than the central and western parts but in general slopes of the study catchment should be regarded as inherently unstable. Most of the causes for mass movement are inherent characteristics of the study area, merely dictated by soil physical properties, conversion of forest into agricultural land use and topography with excessive rainfall and the resulting concentration of subsurface flow as the most important triggering mechanism.

The Q_{cr} value of the site where the recent landslide was triggered is 0.03 m day^{-1} and falls in the category of very high landslide hazard. An optimistic scenario of triggering landslides with a critical rainfall threshold value of 0.03 m day^{-1} or lower (meaning a higher landslide hazard than the recent landslides) was simulated. In this scenario all these sites are failing and enter the soil redistribution (landslide erosion and -deposition) and sediment yield algorithms of the LAPSUS-LS model. The results for this scenario, according to the LAPSUS-LS model, are a total estimated volume of 39.3 million m^3 of soil material displaced by shallow landslides in the 13,360 ha catchment. The fraction of this ending up in the stream network and contributing to the catchment sediment yield is estimated by the model to amount to 20.9 million m^3. This scenario indicates that the total volume of eroded material and sediment deposited caused by shallow landslides could be four times higher than the total volume observed in the Knapen et al. (2006) field survey (ca. 10 million m^3 soil material displaced, for both shallow and deep landslides). In addition, more than half of this soil material can reach the stream network, possibly damming rivers and causing fatalities and major damage to infrastructure or siltation and pollution of streams.

Conclusions

This paper revisited earlier studies of landslides on the eastern footslopes of Mount Elgon in Uganda in the context of a fatal landslide that occurred on the 1st of March 2010. The earlier studies assessed characteristics and causal factors of older landslides in the area based on a landslide inventory and a detailed digital terrain analysis. In addition, a landslide hazard assessment was conducted with the LAPSUS-LS landslide model identifying susceptible landslide triggering sites and scenarios of landslide erosion and deposition pathways as well as sediment delivery to streams. The location of the recent landslide was mapped on the landslide hazard map and had a critical rainfall value of 0.03 m day^{-1}. An optimistic scenario of triggering landslides with a critical rainfall value of 0.03 m

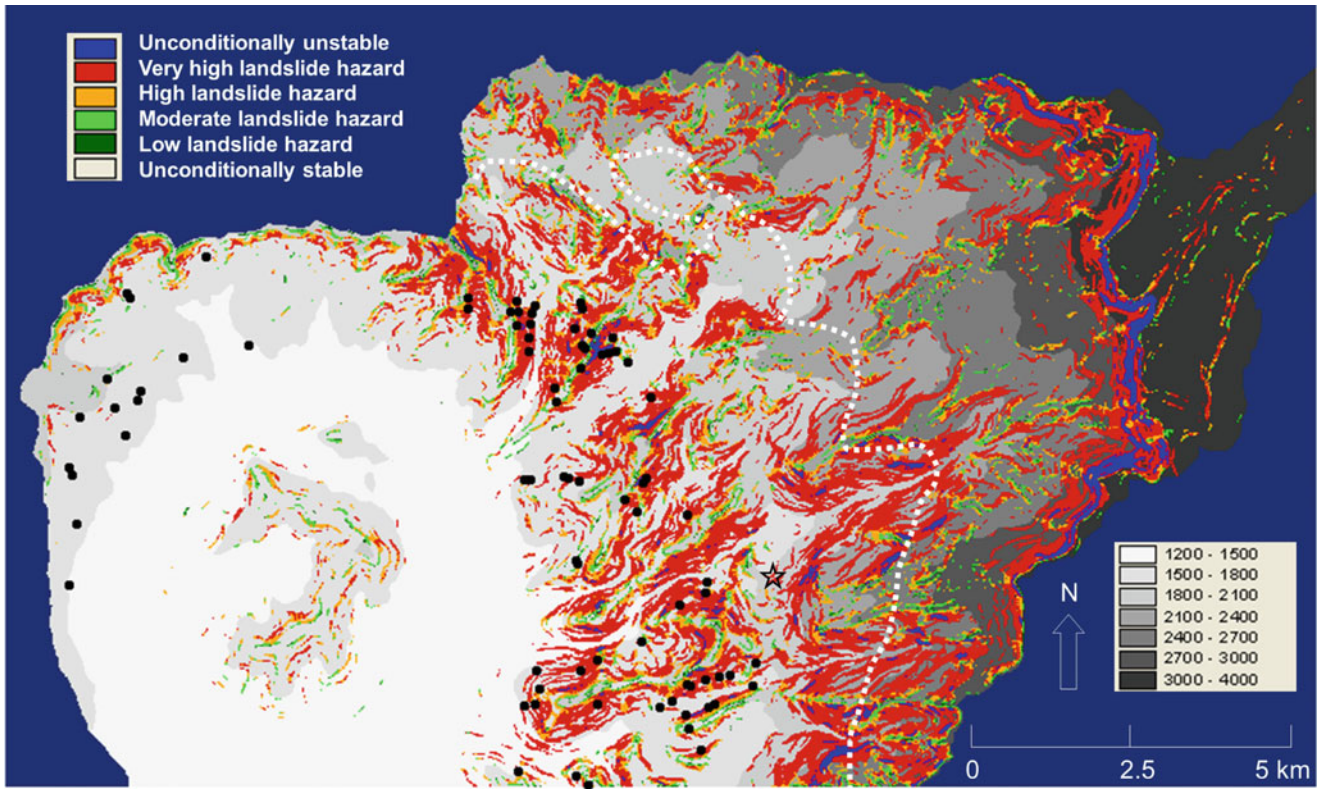

Fig. 2 Overlay of classified landslide hazards (*Qcr*, legend top left) calculated with LAPSUS-LS and the classified DEM (*greyshades*) for the study area. Observed landslides from the Knapen et al. (2006) survey are indicated as *black dots*. The recent landslide is marked by a *star*

day^{-1} or lower was simulated as being representative for what might happen in the near future. According to the model, the volume of soil material displaced could be four times higher than observed in the Knapen et al. (2006) field survey. In addition, more than half of this volume is predicted to end up in the stream network and so contribute to the catchment sediment yield. This soil material can cause damming of rivers causing major damage to life and property or siltation and pollution of streams.

Most of the causes for mass movement are inherent characteristics of the study area, merely dictated by soil physical and hydrological properties, topography and heavy rainfall events with concentration of (sub)surface flow as triggering mechanism. Therefore solutions for the landslide problem, other than resettling people, are difficult to find. As population pressure increases, not only the stability of the slopes will be reduced, but people will also be forced to cultivate even more unstable slopes. As pointed out by Knapen et al. (2006), the instability could partly be reduced by tempering the human impact (e.g. by avoiding excavation or terracing of slopes and construction of structures concentrating water to vulnerable zones). In addition, reforestation with deep-rooted trees could effectively reduce the shallow landslide hazard on certain landscape positions. Still, these measures can never completely prevent the occurrence of landslides and a long-term solution for the problem can only be found in developing and implementing policies that provide alternative livelihoods to inhabitants.

Acknowledgments Funding for the initial fieldwork was provided by the Belgian Technical Cooperation (BTC), the World Conservation Union (Mount Elgon Conservation Project) and the fund for Scientific Research Flanders. Farmers and officers of Manjiya and the Department of Geology at Makerere University (Uganda) provided information and logistic support. Financial support from the Katholieke Universiteit Leuven (Belgium) and the USAID Soil Management Collaborative Research Support Program (SM-CRSP) is gratefully acknowledged.

References

Breugelmans W (2003) The influence of soil, land use and deforestation on the occurrence of landslides in Mount Elgon area, Eastern Uganda. Unpublished M.Sc. thesis, Catholic University Leuven, Leuven

Claessens L, Heuvelink GBM, Schoorl JM, Veldkamp A (2005) DEM resolution effects on shallow landslide hazard and soil redistribution modelling. Earth Surf Process Landf 30(4):461–477

Claessens L, Knapen A, Kitutu MG, Poesen J, Deckers JA (2007) Modelling landslide hazard, soil redistribution and sediment yield

of landslides on the Ugandan footslopes of Mount Elgon. Geomorphology 90:23–35

Glade T, Crozier GM (2004) The nature of landslide hazard impact. In: Glade T, Anderson MG, Crozier GM (eds) Landslide hazard and risk. Wiley, Chichester, pp 43–74

Hamilton AC (1984) Deforestation in Uganda. Oxford University Press, Nairobi

Kitutu MG, Muwanga A, Poesen J, Deckers JA (2009) Influence of soil properties on landslide occurrences in Bududa district, Eastern Uganda. Afr J Agric Res 4(7):611–620

Knapen A, Kitutu MG, Poesen J, Breugelmans W, Deckers JA, Muwanga A (2006) Landslides in a densely populated county at the footslopes of Mount Elgon (Uganda): characteristics and causal factors. Geomorphology 73(1–2):149–165

Montgomery DR, Dietrich WE (1994) A physically-based model for the topographic control on shallow landsliding. Water Res Res 30(4):1153–1171

National Environment Management Authority (2001) State of the environment report for Uganda 2000/2001. National Environment Authority, Kampala

Pack RT, Tarboton DG, Goodwin CN (2001) Assessing terrain stability in a GIS using SINMAP. In: 15th annual GIS conference, Vancouver, BC

Uganda Bureau of Statistics (2004) The 2002 Uganda population and housing census. Uganda Bureau of Statistics, Entebbe

Geomorphology Hazard Assessment of Giampilieri and Briga River Basins After the Rainfall Event on the October 1, 2009 (Sicily, Italy)

Luca Falconi, Danilo Campolo, Gabriele Leoni, Silvia Lumaca, and Claudio Puglisi

Abstract

Mud and debris flows constitute a serious threat for several Italian regions as attested by recent several disasters attributable to such phenomena. The adoption of effective mitigation measures is complicated by the difficulty in predicting spatial and intensity features of future events.

This paper applies a practical application of debris/mud flows hazard assessment in the area of Messina province. The study was based on an inventory of several debris flows triggered by heavy rainfall occurred in the Giampilieri and Briga catchments after the event of October 1, 2009. Data elaboration was focused on mapping source areas and on assessing the runout of landslides and their intensity. An evaluation of the factors that make the area prone to these events was used as input for a GIS based hazard prediction model.

Keywords

Debris/mud flows • Landslide susceptibility • Hazard assessment • Intensity • Peloritani Mountains • Messina • Sicily

Introduction

Mud and debris flows are the most dramatic among landslides in terms of loss of life. In recent past there have been several disasters in Italy attributable to such phenomena (Piemonte 1994, Versilia 1996, Sarno, 1998, Cervinara 1999, Val d'Aosta e Valle Anzasca, 2000, Ischia 2006 e 2009, Messina 2007, 2009, e 2011) with over 300 victims.

The high risk of rapid flow is accompanied by the difficulty in the hazard assessment. In fact, source areas of these phenomena are rarely located two times in the same slope portion. Being primarily first generation phenomena, their spatial prediction is particularly problematic. This difficulty is closely related to the triggering causes of these landslides, consisting essentially of sporadic and sudden rainfall events. An increasing trend in precipitation and a decrease in their duration have been documented over the past 50 years in Italy (Ferrara and Farruggia 2007). This scenario leads to assume an increase of debris-mud rapid flows hazard in the next future.

It therefore seems necessary to improve knowledge tools aimed to assess the hazard of such phenomena. In this context, a geomorphological approach focused on the central issues of susceptibility and intensity prediction of the first generation phenomena has been tried by ENEA during the last decade and tested in about 15 sites at different scales. This paper describe the application of this methodology in the Ionian coast of Peloritani (Messina Province) affected by such events on October 1, 2009 (Fig. 1), in particular in the river basins of Giampilieri and Briga.

On the night of 1–2 October 2009 the Ionian coast and the Peloritani Mountains (Messina province, Sicily) were affected by a sudden downpour, accompanied by strong

L. Falconi (✉) • C. Puglisi
ENEA – Italian National Agency for new technologies, energy and sustainable economic development, Rome, Italy
e-mail: luca.falconi@casaccia.enea.it

D. Campolo • S. Lumaca
Consultant Geologist

G. Leoni
University of Roma Tre, Italy

C. Margottini et al. (eds.), *Landslide Science and Practice*, Vol. 1,
DOI 10.1007/978-3-642-31325-7_70,

Fig. 1 Panoramic view of a slope affected by a pervasive series of mud/debris flows in the Briga catchment

Fig. 2 Damages after the October 1, 2009 event in Briga village

winds and lightning. It is estimated that more than 200 mm of rain fell in 7 h (according to Sicilian Agrometeorological Informative Service – S.A.I.S). This meteoric event triggered about a thousand of debris/mud flows. The territory of Giampilieri Superiore, Briga Superiore and Scaletta Zanclea, small villages situated few kilometres southward from the city of Messina, was the most damaged area (Fig. 2).

Study Area

The Peloritani represent the southern termination of the Calabro-Peloritano Arc and are characterized by metamorphic units of pre-Alpine age. Involved in Hercynian and Alpine orogenic processes, these units are tectonically superimposed to sedimentary Maghrebidi units (Lentini et al. 2000; Vignaroli et al. 2007). The crystalline-schistose formations show different metamorphic degrees (phyllites, schists, marbles, gneisses) and are extensively covered by a thick layer of colluvium.

The Peloritani Mountains range stretches along the coast and is characterized by narrow and steep catchments of small size (5–10 km^2). These catchments have also high relief energy (up to 1,000 m drop in about 5 km) and time of concentration in the order of few minutes. The morphology of the Peloritani was influenced especially by metamorphic lithology, complex geostructural conditions related to the orogenic processes and recent tectonic uplift, active in the area since late Miocene. The steep slopes of the valley and the low permeability of the bedrock give the drainage network a remarkable ability to erosion and transport. The hydrological regime is markedly torrential, typical of the "fiumare", with little or no runoff in the spring and summer and high and sudden floods in autumn and winter months. These factors increase the energy of runoff waters, causing high stream capacity and transport of solid blocks, even decametric, during rainfall events. The huge rainfall events may cause rapid gravitational phenomena classified as rapid debris-mud flows, which affect the shallow natural or anthropic debris layer. These phenomena have led to the development of wide debris cones at the mouth of the streams and in the floodplains of the major tributaries, as well as extensive debris bands at the base of the slopes. These morphological and hydrological conditions have meant that the flows, triggered by heavy rainfall on October 1, 2009, have reached, in a few minutes and with great

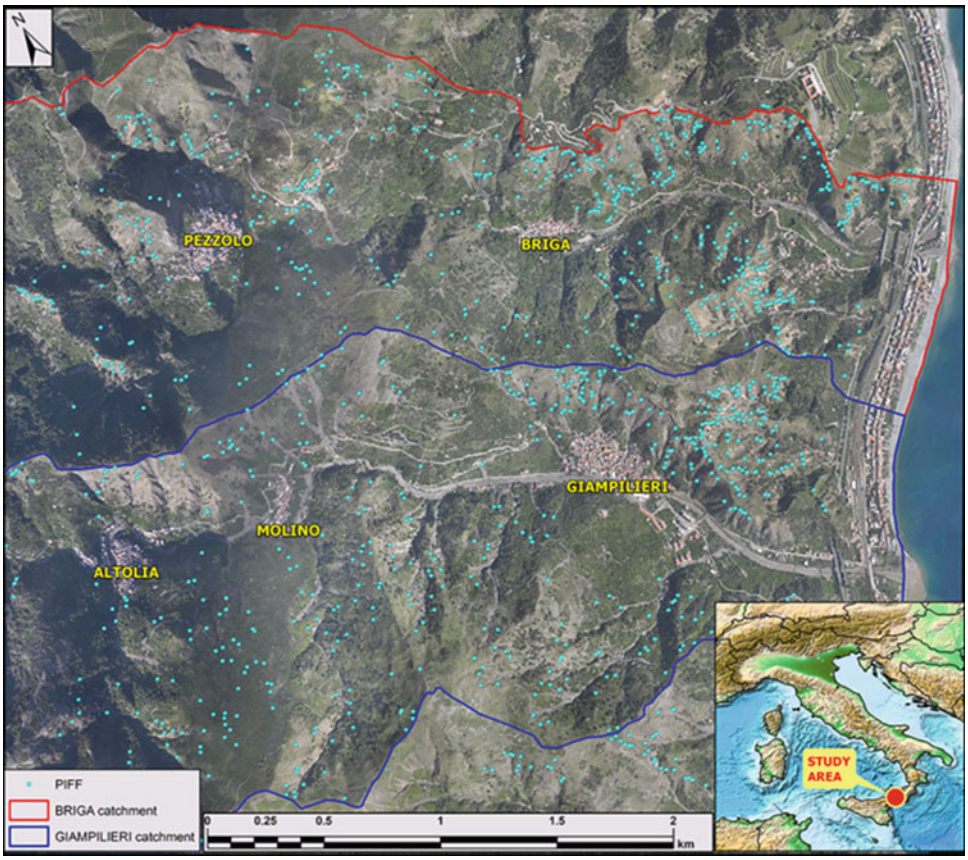

Fig. 3 Study area and landslides identification points (PIFF; *light blue dots*)

energy, the urban areas located along the Ionic coast, the main valley's bottom and fluvial-gravitational fans, causing heavy damage and casualties.

The two river basins of this study extend from the sea up to the watershed of the Peloritani. The catchment of the Giampilieri stream (maximum altitude 1,040 m a.s.l.) has an area of approximately 9.2 km^2 and a length of about 8.5 km. Inside there are the villages of Giampilieri Marina, Giampilieri Superiore, Altolia and Molino. The catchment of the Briga stream (maximum altitude 1,016 m a.s.l.) has an area of about 9.6 km^2 and a length of about 9 km. Inside there are the villages of Briga Marina, Briga Superiore and Pezzolo. (Fig. 3)

Methods

This study followed the Enea methodology as developed in several other case studies (Casagli et al. 2004; Abbattista et al. 2005; Puglisi et al. 2007; Leoni et al. 2009; Falconi et al. submitted). Localising source, transportation and runout areas of debris flows has been the first task of the study, followed by velocity and intensity assessment of the past events. Subsequently, source areas, runout, velocity and intensity of potential events have been investigated.

The first step of this study was an analysis of past events aimed to obtain a landslide census. An inventory map was produced through a detailed geomorphological and morphometric field survey (1:5,000–1:10,000) and an aerial photos analysis. More than 1,000 debris flows have been recognised in the Giampilieri and Briga basins and recorded in a data base. The inventory was focused on identifying discriminating parameters (necessary but not sufficient conditions like slope angle in the niche zone and lithology on which the rupture surface is imposed) and predisposing factors (factors affecting the slope instability like geomorphological, geological, lithological, hydrogeological and land use features). Through a statistical analysis, the variability range of the discriminating parameters and of the most significant predisposing factors were determined. Each parameter and each factor was mapped and implemented as a layer in a Geographic Information System. Using descriptive statistical processing based on the frequency distribution of the surveyed features, the most significant predisposing factors were extrapolated.

Consequently, a site-specific susceptibility function was identified and, through GIS overlapping of these weighted layers, the susceptibility map of the area was obtained.

An empirical formula to estimate the runout of potential events was obtained comparing volume and runout of past

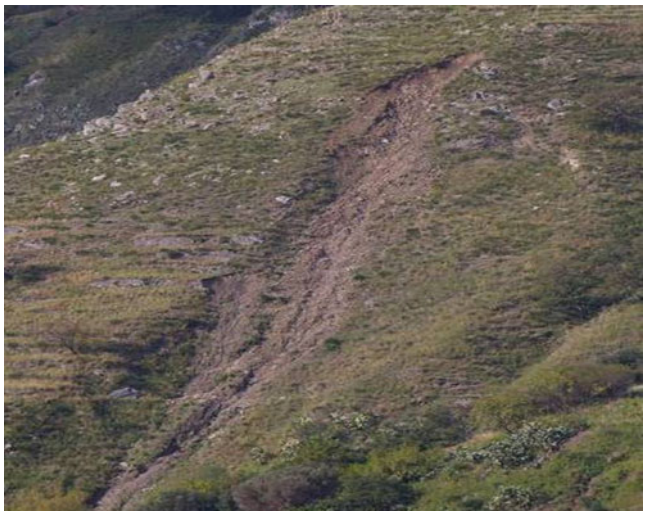

Fig. 4 Source area with punctual morphology

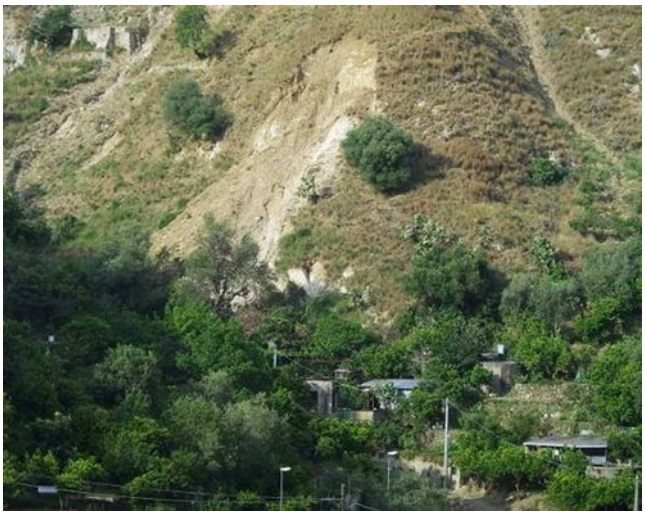

Fig. 5 Source area with curved morphology

events (Rickenmann 1999). Assigning a soil layer thickness to the higher susceptibility areas and consequently obtaining their volume, the runout distance of potential events was estimated. Velocity measurements with Johnson and Rodine (1984) method were carried out in different points of occurred landslides and in the same points was calculated the energy released. These results were then applied to some potential events. So it was possible to model the expected energy in each morphological part of potential debris/mud flows.

Results

Landslide Inventory and Susceptibility Map

All the surveyed phenomena are classified as debris and mud flows. For each event has been attributed some specific morphological elements: the Landslide Identification Point (PIFF), trigger areas, transport areas and the Landslide Foot Identification Point (PIP). Most of the landslides are located in the eastern part of the study area, including specifically the lower-middle portions of the Giampilieri and Briga catchments.

Landslides have been categorized according to the morphological characteristics of source areas in punctual, curved, rectangular and lobed (lobed-curved, rectangular-lobed, lobed-mixed; Figs. 4, 5, 6 and 7). The lobed types are characterized by contiguous source areas having deeply indented margins with lobes not entirely separate from each other.

The source areas have been divided into “channeled”, when bundled into a pre-existing drainage line, and “not channeled”. The latter typology spread on open slopes with ribbon-like or triangular morphologies, whose width increases away from the triggering area according to an angle of about 20°, as described in the literature for other Italian areas as Sarno and Cervinara (Guadagno and Perriello Zampelli 2000; Abbattista et al. 2005).

A field survey has been necessary to deepen landslides details and validate the preliminary inventory of the phenomena. A survey form, specifically developed for this type of phenomena, was used to gather information about a total of 124 landslides. Further than the morphological and morphometric elements, the form contains all the information about the discriminating parameters and predisposing factors. Some parameters have also been detected by analysis of aerial photographs and through a very detailed DEM.

The discriminating parameters for rapid flows are constituted by the presence of a soil layer covering the bedrock and by a specific angle of the original slope in the source area. The soil layer is approximately continuous in the study area, with the exception of urban areas, some rock outcrops and the source areas of the October 1, 2009 shallow landslides. The slope angle in the niches observed in the field survey ranges from 22° to 73°, but the most significant range of slopes, based on its relative frequency, is between 36° and 56°.

A heuristic approach was applied in order to quantify the different influence of each predisposing factor (Table 1) on the landslide susceptibility. A weight from 0 to 5 was assigned to each of these factors. Instead, an index increasing from 0 to 9 was assigned to each class of each predisposing factor. Once digitized, discriminating parameters and predisposing factors have been integrated through a GIS overlapping with the aim to produce

Fig. 6 Source area with rectangular morphology

Fig. 7 Source area with lobed morphology

Homogeneous Territorial Units (UTO). The following susceptibility function has been applied:

$$S = (Icop \times Ipend) \times \frac{\sum_{i=1}^{n} (i_n \times P_n)}{\sum_{i=1}^{n} P_n}$$

where:
S = Susceptibility
Icop = soil layer discriminating parameters index
Ipend = slope angle discriminating parameters index
i_n = index of the nth predisposing factors
P_n = weight of the nth predisposing factors

This function draws a susceptibility map initially divided into 9 levels. Then they are qualitatively grouped into five classes (Fig. 8), described in Table 2.

Table 1 Discriminating parameters and predisposing factors used in this study

Discriminating parameters	Predisposing factors
Presence of soil layer	Bedrock lithology
	Land cover
	Anthropic elements
Specific slope angle	Longitudinale slope curvature
	Slope aspect

Debris Flow Intensity

Intensity may be expressed in a relative scale, referring it to damage or loss levels, or in terms of characteristic variables of the phenomenon (e.g. speed, volume, energy). According to the methodology, the intensity is considered as equal or proportional to the kinetic energy developed by the landslide, since the ratings for speed and size may be partial.

Observing a series of channeled debris flows, Rickenmann (1999) estimated that the average runout of a debris flow depends on the volume that it mobilizes and on the height difference between the trigger point and stop point of the mobilized material.

All the quantities needed to evaluate the kinetic energy were calculated for both past and potential phenomena. These measures are: the mobilized volume in the source and transit areas, the propagation distance and the speed of flows.

The product of the maximum depth of the niche (which varies from 0.5 to 2.5 m) was calculated by the extension of the source area, obtained by photo-interpretation, in order to estimate the mobilized volume of each debris/mud flow. This product was then reduced by a correction form factor, experimentally obtained. Also the mobilized volumes along the transit areas were considered. The mean thickness of these zones varies from 0.3 to 1 m, as observed in the field survey. Once multiplied these values by the transit area extension, the product was summed to the source area volume.

The effective distance traveled from PIFF to PIP for each occurred phenomenon was measured using 3D photo-interpretation and GIS analysis, and the runout "site specific" laws have been generated, both for channeled and not channeled flows (Fig. 9):

- Channeled flows: $L = 6.147(V \cdot \Delta)^{0.3078}$
- Not channeled flows: $L = 3.266(V \cdot \Delta)^{0.3148}$

where:
L = travel distance of the mass movement;
V = total volume mobilized by the debris flows;
Δ = elevation difference between the starting point and the lowest point of the deposition of the mass movement

Adopting Johnson and Rodine (1984) approach, it is possible to estimate the average speed of a flow by the

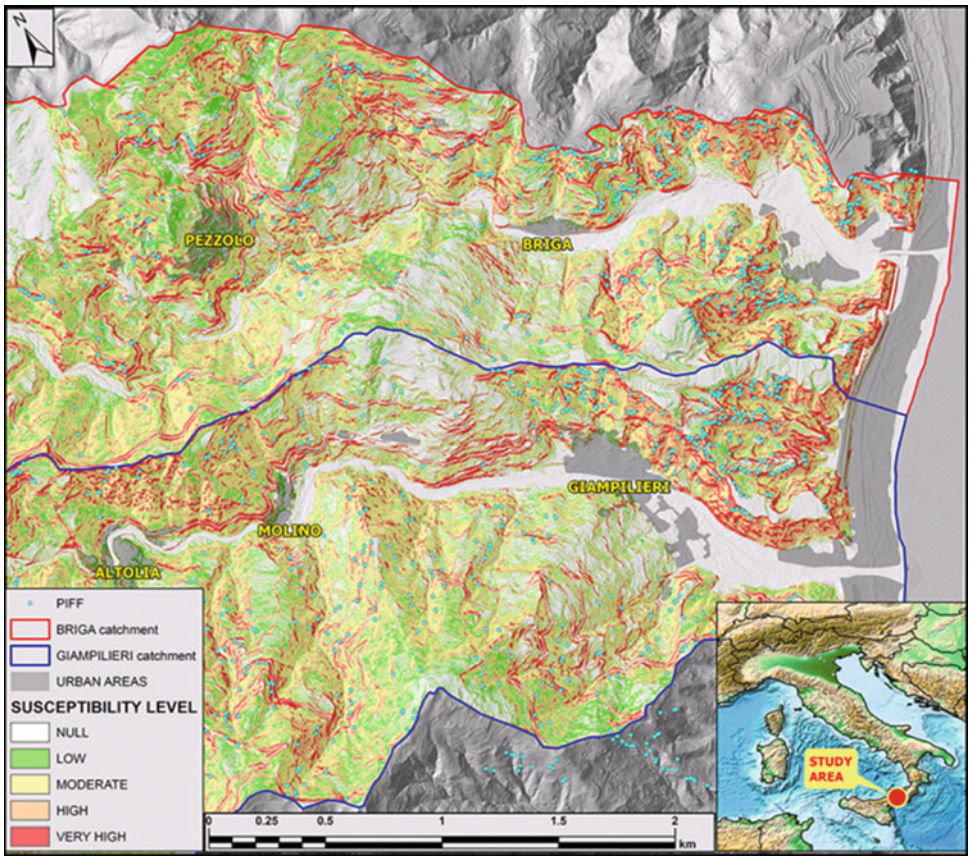

Fig. 8 Susceptibility map of the study area (in *red* the higher class areas)

Table 2 Conversion from levels to susceptibility classes

Level	Susceptibility
0	Null
1–3	Low
4	Moderate
5	High
6–9	Very high

measurement of the raising that occurs in the outer portion of a curve due to the centrifugal force. Some points were identified during the field survey in order to measure the speed achieved by mud and debris flows occurred in October 1, 2009. The identified measurement points were characterized by the presence of traces left by the passage of the debris flow like mud deposits or abrasions in the tree bark. The formula used to calculate the average speed is:

$$V = \sqrt{R \cdot g \cdot \cos i \cdot tgb}$$

where:
V = average speed,
R = radius of curvature of the stream axis,
g = acceleration of gravity,
i = slope angle of the stream in the measurement point,
b = angle of the fluid mixture surface in motion across the curve.

This formula was applied to different points of the debris flow paths and specific velocities were calculated, in order to outline the deceleration curves for different surveyed debris flows. Maximum speed values range between 8 and 16 m/s. Once obtained the runout distance and the debris flow velocities of past events, the energy developed by investigated rapid flows has been evaluated (Fig. 10).

Along the path traveled by the considered debris flow, at each point where speed was calculated, the value of developed kinetic energy was obtained.[1] Maximum developed energies were estimated in the order of thousands of kilojoule (Fig. 11).

Finally the volume, the distance of propagation and the velocity were estimated for some potential phenomena, identified by the susceptibility map to achieve an estimation

[1] The energy estimation ($E = 1/2MV^2$) was performed by calculating the product of mass (M), considered constant and equal to the product of volume by the average density (estimated at 2,000 kg/m^3), by speed (V) in the considered points.

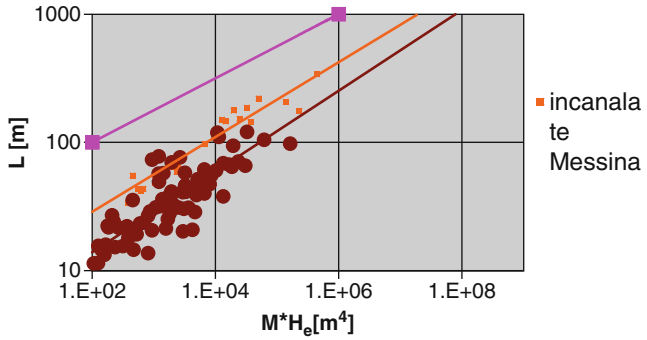

Fig. 9 Site specific equations about debris flows runout in comparison with Rickenmann formula (*orange*: channelled; *brown*: not channelled; *pink*: Rickenmann)

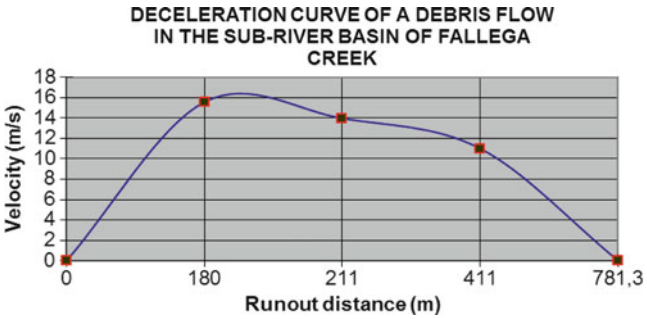

Fig. 10 Example of deceleration of a past debris flow

of the potential energy in different points along the path in which new phenomena could be developed (Fig. 12).

Conclusions

This study stresses the huge and complex problems in the Giampilieri and Briga river basins in reference to the geomorphological hazard. The debris flows susceptibility and their intensity in the area are very high. The proposed methodology constitutes a contribute to the development of the quantitative geomorphological approach in landslide investigation. Complementary to the definition of return times and rainfall thresholds, similar studies may lead to a full hazard assessment. This quantitative knowledge base of the debris-mud flow hazard constitutes a necessary step for subsequent phases of vulnerability assessment of exposed elements, and ultimately may play an important role in the definition of risk scenarios and effective mitigation measures. In this sense, the results presented here may be useful to administrative authorities involved in natural risk management.

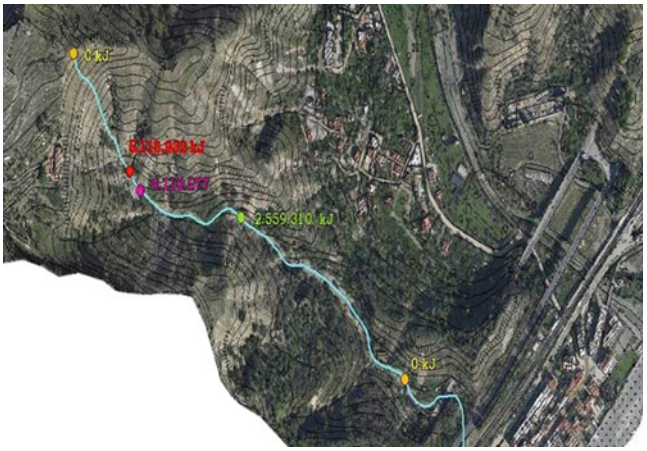

Fig. 11 Maximum developed energies in the Fallega creeks between Giampilieri Marina and Briga Marina

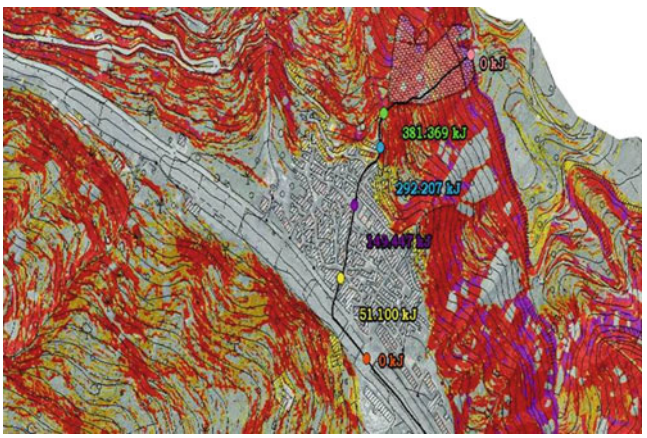

Fig. 12 Maximum energies of the potential debris flow in the Giampilieri village

References

Abbattista F, D'Agostino G, Delmonaco G, De Filippo L, Leoni G, Margottini C, Puglisi C, Romano P, Spizzichino D (2005) La valutazione della suscettibilità da frana: applicazione alle colate rapide di Cervinara (AV). Geologia Tecnica e Ambientale. 1 (Jan–Mar):25–40

Casagli N, Catani F, Puglisi C, Delmonaco G, Ermini L, Margottini C (2004) An inventory-based approach to landslide susceptibility assessment and its application to the Virginio River Basin, Italy. Geol Soc Am Assoc Eng Geol 10(3):203–216

Falconi L, Lentini A, Leoni G, Puglisi C, Prada CR (submitted) A geomorphological-based approach for debris flow risk assessment in the Alcamayo creek catchment (Aguas Calientes, Cusco, Perù). Landslides

Ferrara V, Farruggia A (2007) Clima: istruzioni per l'uso. I fenomeni, gli effetti, le strategie. Edizioni Ambiente, Milano

Guadagno FM, Perriello Zampelli S (2000) Triggering mechanisms of the landslides that invested Sarno, Quindici, Siano and Bracigliano (southern Italy) on May 5–6, 1998. In: Bromhead EM, Dixon J, Ibsen ML (eds) Proceedings of the 8th international symposium on

landslides, June, Cardiff. Publ 2. Thomas Telford, London, pp 671–676

Johnson AM, Rodine JR (1984) Debris flow. In: Brunsden D, Prior DB (eds) Slope Instability. Wiley, Chichester, U.K, pp 257–361

Lentini F, Catalano S, Carbone S (2000) Nota illustrativa della Carta geologica della Provincia di Messina (Sicilia Nord-Orientale). Scala 1:50,000. S.EL.CA, Firenze, 70p

Leoni G, Barchiesi F, Catallo F, Dramis F, Fubelli G, Lucifora S, Mattei M, Pezzo G, Puglisi C (2009) GIS methodology to assess landslide susceptibility: application to a river catchment of Central Italy. J Maps v2009, 87–93. 10.4113/jom.2009.1041

Puglisi C, Falconi L, Leoni L, Pino P, Rasà R, Tripodo A (2007) Analisi della Suscettibilità da frana in Sicilia (1:250,000): Relazioni con scenari climatici futuri. Workshop "Cambiamenti Climatici e Dissesto Idrogeologico: Scenari Futuri per un Programma Nazionale di Adattamento", Napoli, 9–10 July 2007

Rickenmann D (1999) Empirical relationships for debris flows. Nat Hazards 19:47–77

Vignaroli G, Faccenna C, Jolivet L, Piromallo C, Rossetti F (2007) Subduction polarity reversal at the junction between the Western Alps and the Northern Apennines, Italy. Tectonophysics 450:34–50

Factor Selection Procedures in a Google Earth™ Aided Landslide Susceptibility Model: Application to the Beiro River Basin (Spain)

D. Costanzo, E. Rotigliano, C. Irigaray, J.D. Jiménez-Perálvarez, and J. Chacón

Abstract

A procedure to select the controlling factors connected to the slope instability has been defined. It allowed to assess the landslide susceptibility in the Rio Beiro basin (about 10 km^2) over the north-eastern area of the city of Granada (Spain). Field and remote (Google Earth™) recognition techniques allowed to generate a landslide inventory consisting in 127 phenomena. Univariate tests, using both association coefficients and validation results of single parameter susceptibility models, allowed to select among 15 controlling factors the ones that resulted as good predictor variables; these have been combined for unique conditions analysis and susceptibility maps were finally prepared. In order to verify both the goodness of fit and the prediction skill of the susceptibility models, two different validation procedures were applied and compared. Both procedures are based on a random partition splitting of the landslide archive for producing a test and a training subset. The relative error, considered between the intersected target landslides by the different susceptibility classes, was used to estimate the predictive skill of the maps.

Keywords

Multivariate landslide susceptibility models • Conditional analysis • Controlling factor selection • Model validation • Google Earth™

Introduction

One of the key points in assessing landslide susceptibility by means of multivariate statistical models based on the conditional analysis is the selection of the controlling factors (i.e. the predictor variables). In fact, though we can generally accept that the greater the number of factors the higher the predictive performance, two basic considerations drive to the need of using a number of predictor variables as low as possible. First, each informative layer from which the spatial distribution of a possible controlling factor can be derived often requires both time and money costs. Second, increasing the number of factors is responsible for a higher number of combinations (or unique condition units: UCUs), consequently decreasing the mean number of cells for each UCU. This effect will be different for each specific UCU, depending on the spatial correlation between the factors, resulting in a decreasing of the predictive performance of the susceptibility model. Procedures and criteria for a priori taking a decision whether to include a factor in the definition of multivariate models are needed. Among the possible approaches, the statistical analysis of contingency tables produced by spatially crossing factors and landslides allows to compute some correlation or association indexes, capable to drive the decision (Fernàndez et al. 2003; Chacòn et al. 2006; Irigaray et al. 2007; Jiménez-Pelvàrez et al. 2009). However, to exhaustively define a factor selection procedure, verifications must also be performed. These

D. Costanzo (✉) • E. Rotigliano
Department of Earth and Sea Sciences, University of Palermo, Palermo, Italy
e-mail: dario.costanzo@unipa.it

C. Irigaray • J.D. Jiménez-Perálvarez • J. Chacón
Department of Civil Engineering. ETSICCP, University of Granada, Granada, Spain

C. Margottini et al. (eds.), *Landslide Science and Practice*, Vol. 1,
DOI 10.1007/978-3-642-31325-7_71,

verification will focus on relationship between the predictive performances, estimated for each factor models, and the multivariate model. In fact, together with the specific general association between factors and landslides, which is considered as a whole when a contingency table is produced, the results of the validation of susceptibility models are also controlled by the spatial stability of such geostatistical relationships, when splitting in training and test sub-sets UCUs or landslides. In the present paper results are presented of a research aimed at analyzing the relationships between a priori ranking of controlling factors and predictive performance of multivariate models prepared by variously singling out the ones to be combined.

Material and Methods

Setting of the Study Area

The area considered in the study (Fig. 1a) stretches NE of the city of Granada (Andalusia, Spain), coinciding with the basin of the Beiro river (10 km^2), which is a sub-basin of the Genil river, a subsidiary of the Guadalquivir river that flows through South of Spain to the Atlantic Ocean. Despite the nearness to the sea, the climate in the area is Mediterranean with continental influence, being characterized by marked temperature and rainfall short and long-period changes. According to the termo-pluviometric station of "Granada-Cartuja" (720 m above sea level) rainfall is mainly concentrated between October and April, while between May and September it is generally very low (particularly in July and August when it is less than 10 mm). Temperatures in winter are often below zero while in summer they are always above 30 °C. High diurnal temperature ranging is also recorded, reaching up to 15 °C. According to the De Martonne (1942) aridity index the area can be classified as a semi-arid climate.

The geological setting of the Beiro river basin (Fig. 1b, c) is characterized by the outcropping of post-orogenic deposits, which are aged from Pliocene to recent Quaternary, being tectonically limited to the North by Triassic dolomitic marbles which are very tectonized (Vera 2004). The post-orogenic deposits filled the deep valleys in the area, so that from North-East to South-West it is possible to follow the stratigraphic sequence. These units, from bottom to top, are: the terrains of the "Pinos-genil formation", that marks the transition to continental facies (mainly Pliocenic conglomerates and, in the higher part of the sequence, sandy layers); the Cenes-Jun sequence, made of lacustrine deposits of lutite, sand, silt and gravel; the "Alhambra conglomerates" sequence made mainly of conglomerates and sand. The sequence is closed by Quaternary alluvial deposits.

The landscape is generally marked by sub-planar areas, corresponding to a lower Pleistocene smoothing of the previous relief, which are deeply engraved by Upper Pleistocene to Holocene stream incision, and surrounded by steep reliefs. The geomorphological setting, together with the climatic conditions, is responsible for a wide diffusion of landslides, characterized by several movement typologies and variable area extensions (Chacón 1999; Chacón et al. 2001, 2007).

Landslides

An inventory of 127 slope movements has been produced for the Beiro river basin, which have been classified (Varnes 1978; Cruden and Varnes 1996; Dikau et al. 1996) as falls, translational slides, earth flows, debris flows, and flow slides. The inventory was obtained by using field survey, carried out between March and April 2010, and photo-interpretation (aerial photos in a scale of 1:33,000 taken between 1956 and 1957 by "*Ejército del Aire de España*" and European air force, and the ones taken in 1978, at scale of 1:18,000, by the Geographic Minerary Institute of Spain). During the field survey, rock and soil samples were collected and analyzed, in order to distinguish between debris and earth type material.

The landslide archive was also compared to the one obtained through the use of open source software or free images like Google Earth (GE) (Conoscenti et al. 2009; Costanzo et al. 2011) The latter were chosen because of the excellent spatial resolution (spatial resolution: 46–60 cm per pixel) of the images, as well as the easy access to updated cartography and of the possibility to dynamically manage the view angles for each slope (Fig. 2).

The final landslide archive was composed of:

Falls (28 cases, 3.8 % of the landslide area): these landslides mainly affect the over-consolidated silty and sandy quaternary terrains. The fall movements found in this area are not very frequent and cover areas of tens of square meters each. The areas affected by this kind of movement are usually the ones where the geostructural conditions form near vertical slopes. Weathering processes and high diurnal and seasonal temperature ranging are responsible for fractures enlargement inside over-consolidated soils. The triggering factors for fall movements are the undercutting at foot of escarpments and the intensive rainfall.

Translational slide (1 case, 18.7 % of the landslide area): this landslides generally affect conglomeratic deposits with sandy and silty intercalations (Alhambra Formation). A great Translational slide, whose landslide body has an extension of near 70,000 m^2, with a width of 420 and a length of 225 m, was recognizes in a south part of the basin. This is called the Beiro's translational slide, it is the only movement in the area to be considered diachronic (Chacón 2008a, b; Chacón et al. 2010) in dormant stage or active with low or extremely low velocities.

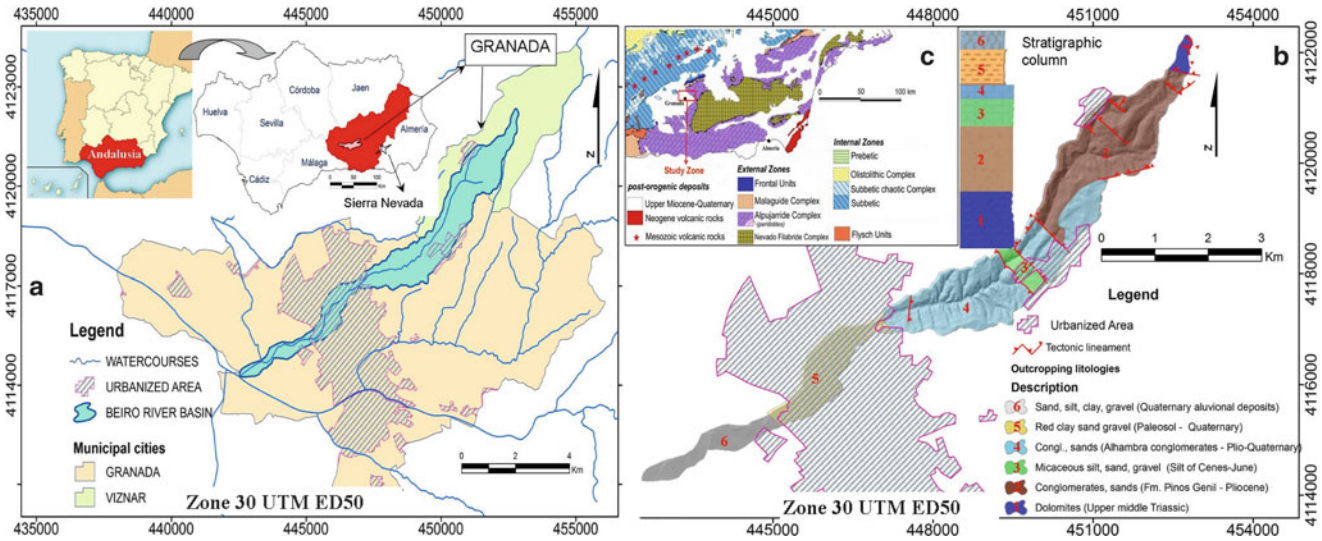

Fig. 1 (**a**) Geographical setting of the study zone; (**b**) Geological setting of the study zone, modified from Vera (ed.) (2004); (**c**) Structural scheme of study area. Coordinate Reference System UTM zone 30 European Datum 50

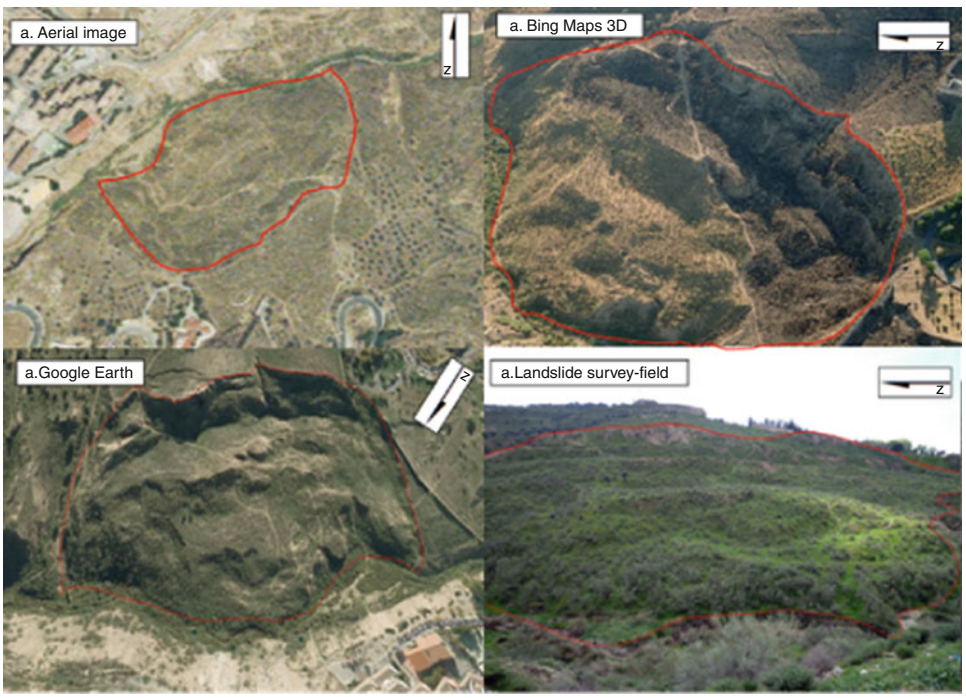

Fig. 2 Beiro translational slide view by different techniques

Earth flows (36 cases, 54.1 % of the landslide area): the terrains affected by earth flows are over-consolidated sands and silts, or conglomerates.

Debris flows: (57 cases, 12.7 % of the landslide area) these are the most common slope failures in the area but they only cover 0.5 % of the Beiro river basin. The debris flows involve terrains mainly consisting in surficial regolithic layers produced by intensive weathering and typically are triggered by rainfall, along with highly steep slopes.

Flow-slides (5 cases, 10.6 % of the landslide area): these landslides are complex movements that initiate with the collapsing and the flowing of saturated earth or debris volumes, the movement of the mass evolves downhill in a slide (Dikau et al. 1996). The terrains typically interested by flow-slides are carbonates, sandstones and

conglomerates. The slip surface is not easily defined for this type of landslide.

Susceptibility Modelling

In order to define the landslide susceptibility in the Beiro river basin, the matrix method in a GIS environment was applied (Irigaray et al. 1999, 2007; Jiménez-Pelvárez et al. 2009). In this approach, the susceptibility of each mapping unit is defined as a function of its conditioning factors, depending on the spatial relationships between factors and past landslides. This method requires that grid layers for a set of selected conditioning factors are derived and combined (overlapped) to obtain a single grid layer ("Management Unit Matrix"), in which for each combination of factors, the total area is calculated. A "Landslide Matrix" is then prepared from the inventory of diagnostic areas (e.g. rupture zones) of the mapped landslide, calculating the area affected by movements in each combination of factors. A "Landslide-Susceptibility Matrix" is finally obtained in which the value of each cell is determined by dividing those corresponding to the landslide matrix by those of the management unit matrix. The landslide-susceptibility matrix values correspond to the conditional probability of new landslides occurring in each cell given its specific geo-environmental conditions or factor combination. The susceptibility level of each combination is then obtained by intersecting the UCU layer and a layer of diagnostic areas (Rotigliano et al. 2011), that are derived from the landslide inventory. The density of diagnostic areas for each UCU gives the landslide susceptibility.

A very similar theoretical background has been used by different authors (Davis 1973; Carrara et al. 1995, 2006; Soeters and van Westen 1996; Guzzetti et al. 1999, 2006; Clerici et al. 2002; Chung and Fabbri 2003; Conoscenti et al. 2008).

According to largely adopted procedures (Fernández et al. 2003; Rotigliano et al. 2011), the area limited between the landslide crown and the toe of the failure surface ("rupture zone") has been used as the diagnostic area, as it better allows to single out physical-environmental conditions that are similar to those responsible for the past landslide activations.

Factor Selection

Slope stability is directly connected to the types of terrain, the presence of discontinuity surfaces, the morphology of the slopes (slope angle, aspect, curvature, land use, hydrogeological conditions, etc.), while the triggering of new landslides, is usually connected to internal and external conditions, such as intensive rainfall or earthquakes. The triggering factors can also be anthropologically induced by deforestation, intensive water erosion, landuse, drilling, etc. (Crozier 1984; Hansen 1984).

For this study we considered a set of 15 controlling factors which were derived from a DEM (topographic factors), a geologic and a land use maps (geo-environmental factors).

Topographic Factors

In describing and quantifying the environmental conditions, DEM is the most important data source as it directly influences the quality of the derived factors, (Burrough 1986). The DEM here used was derived by digitalizing the cartography (1:10,000) made by the Government of Andalusia, which was obtained from aerial photos in scale 1:20,000. The following variables were derived from the DEM:

Slope Aspect (ASPECT): reclassified in classes of 45°, it is measured in degrees from 0 (due north) to 360, (again due north, coming full circle) clockwise. Flat areas, having no downslope direction are given a value of −1. Elevation above sea level (ELEV) (Fernández et al. 2008): reclassified in equal classes from 650 m to 1,659 m above sea level.

Illumination (ILL): values ranging from 0 to 255, 0 represents the shadowed areas and 255 the brightest.

Plan Curvature (PLAN) (Ohlmacher 2007): reclassified in ½ standard deviation (from −17.2 to +16.4 rad^{-1}).

Profile Curvature (PROF): in ½ standard deviation, from −16.5 to +22.9 rad^{-1}, (Dikau 1989).

Slope angle (SLOPE): in six natural breaks intervals expressed in degrees (0–2°; 2–5°; 5–15°; 15–25°; 25–35°; > 35°).

Topographic wetness index (TWI): reclassified in standard deviation from 4.7 to 17.9 m (Rodhe and Seiber 1999; Zinko et al. 2005). The TWI represents the spatial distribution of surface saturation (Sharma et al. 2010).

Topographic roughness (ROUGH): is a measure of the texture of a surface. It is quantified by the vertical deviations of a real surface from its ideal form. Reclassified in five classes, from 1 to 1.9 by natural breaks (Hobson 1972).

Topographic position index (TPI): Compares the elevation of each cell in a DEM to the mean elevation of a specified neighbourhood around that cell (Weiss 2001; Zinko et al. 2005); it was reclassified in 10 natural breaks classes from −8.4 to 9.2.

Stream power index (SPI): Stream power is the time rate of energy expenditure and has been used as a measure of the erosive power. SPI is calculated as: $SPI = As \tan \beta$, where As is specific catchment area and $\tan \beta$ is the local slope (Sharma et al. 2010).

Geo-environmental

Starting from available thematic maps, geological, geomorphological, soil and land use factors were derived. Data have been validated and detailed for this research through field checks.

The following factors were derived:

Lithology (LITH): is one of the most important factors because of its influence on the geo-mechanical characteristics of terrains. The various litho-stratigraphic units outcropping in the area were grouped in six lithological classes (1. Alluvial; 2. Calcarenites, sands, marls and limestones; 3. Calcareous Marble; 4. Conglomerates, sands and limestone; 5. Phyllite, micaschist, sandstone; 6. Sand, silt, clay, gravel), which were defined on the basis of the prevailing rock composition (Clerici et al. 2006).

Distance of tectonic lineament (DIST): reclassified in (1) 0–200 m, (2) 200–400 m, and (3) $>$ 400 m, depending on the distance from faults or thrust faults.

Geomorphological units (GEOM): reclassified in (1) karst platform, (2) Floodplain, (3) Hills, and (4) Mountain chain.

Edafic units (EDAF): reclassified in (1) Calcareous cambisol, (2) Regosol, (3) Lithosol, (4) Luvisol, and (5) Fluvisol.

Land use (USE): this factor was classified in (1) Bush, (2) Permanent crops, (3) Shrubland, (4) Urban areas, (5) Extractive areas, and (6) River beds.

Before combining in a UCU layer the parameters, univariate geostatistical relationships between each variable and landslides were estimated, by analyzing the association coefficients of contingency tables. By cross tabulating a factor grid layer and a landslide vector layer, it is possible to derive contingency tables whose statistical correlation can be quantitatively estimated (Irigaray et al. 1999, 2007; Fernández et al. 1996, 2003; Chacón and Corominas 2003). By using statistical software packages like Unistat and IBM SPSS, the following correlation indexes were computed: linear and contingency correlation coefficient (R), Goodman e Kruskal's gamma (G-K) (Goodman and Kruskal 1954; Davis 1973).

The predictive role of each single factor concerning the assessment procedure was estimated, by validating susceptibility models based on single factor. The method requires (Chung and Fabbri 2003) the spatial random partition of the landslide inventory in a training subset, to classify the susceptibility levels of the UCUs and to produce a prediction image, and a test subset, considered as the unknown target pattern. The prediction image is then compared to the actual spatial distribution of the test rupture zones and success and prediction rate curves are produced. On the contrary in the only case of translational slide present in the study area where it is not possible to split the archive, the approach is based on the random division of the (UCU), identifying UCUs training domain, and a UCUs test domain to obtain the prediction rate curve. Some morphometric indexes of the validation curves were used to estimate the performance of the models. The quality of the susceptibility models was estimated by applying a procedure based on the quantitative analysis of the shape of the success and prediction rate curves, which exploited two morphometric indexes: ARPA, areas above randomly predicted area; and SHIFT, shift between prediction and success rate curves (Rotigliano et al. 2011). Since the diagonal trend attests for a non-effective prediction, a high performance produces high values of ARPA; a good fit of the model is testified by low SHIFT results. By drawing a theoretical validation curve respecting these threshold values, Rotigliano et al. (2011) indicate 0.12 as the lower limit of ARPA for an effective susceptibility model.

Model Suite

In light of the results of the procedure for evaluating the relevance of each factor, it was possible for each of the landslide typologies, to rank the controlling factors according to a predictivity scale.

Among the very high number of possible models which can be prepared for each landslide typology starting from the 15 factors, a suite of models is here discussed, which has been defined to the aim of highlighting the way in which the univariate performances of the single factors propagate when the latter are combined in multivariate models. Particularly starting from the single parameter best model, predictive performances were estimated both when progressively or randomly adding less performing factors.

The results of the multivariate models were submitted to validation by applying both the success and prediction rate curve method and the analysis of the degree of fit (Chung and Fabbri 2003; Remondo et al. 2003; Chacón et al. 2006; Irigaray et al. 2007).

Results

Factors

Table 1a–e show the results of the analysis of the contingency tables for each landslide typology, showing the factors listed according to a decreasing order of the G-K's absolute value. G-K has ranges from −1 to +1. We chose to use the G-K gamma because. When G-K is close to 1, we have high correlation (for positive values we have a direct correlation, for negative ones it is indirect or negative); instead, G-K values close to zero indicate no correlation. The predictor variables are classified as "effective" (EFF) or "not effective" (NEF) depending if the condition G-K

Table 1 Correlation between the source area of the landslide and the determining factors. **R:** linear and contingency correlation coefficient; **G-K:** Goodman e Kruskal's gamma; **ARPA**: areas above randomly predicted area; **SHIFT:** shift between prediction and success rate curves

Factor	R	G-K	ARPA	SHIFT
(A) Falls				
ROUGH	0.48	0.97	0.467	0.00
USE	0.47	0.96	0.453	0.00
SLOPE	0.42	0.95	0.450	0.02
EDAF	0.28	−0.68	0.376	0.01
SPI	0.20	0.48	0.248	0.05
TWI	0.20	−0.41	0.177	0.04
LITH	0.19	−0.41	0.022	−0.30
(B) Translational slides				
USE	0.54	−0.72	0.243	0.61
TWI	0.44	−0.63	0.172	0.08
SLOPE	0.44	−0.62	0.028	−0.18
DIST	0.43	0.55	0.112	0.08
ILL	0.42	0.54	0.291	−0.07
GEOM	0.31	0.48	−0.047	0.40
ROUGH	0.31	0.47	0.083	0.09
(C) Earth flows				
USE	0.54	−0.73	0.393	−0.11
SLOPE	0.43	0.67	0.266	0.03
LITH	0.52	−0.67	0.350	−0.02
ROUGH	0.16	0.67	0.254	0.01
TWI	0.36	−0.67	0.275	0.04
ELEV	0.27	0.67	0.378	−0.09
SPI	0.17	0.29	0.084	0.01
(D) Debris flows				
LITH	0.54	−0.92	0.327	0.05
SLOPE	0.45	0.90	0.368	0.03
ROUGH	0.45	0.90	0.417	−0.02
TPI	0.43	0.89	0.345	0.03
USE	0.43	−0.67	0.343	−0.10
(E) Flow slides				
ROUGH	0.55	0.83	0.384	−0.05
GEOM	0.49	0.83	0.256	0.07
SLOPE	0.42	0.81	0.494	−0.15
TWI	0.41	−0.80	0.371	0.08
USE	0.28	−0.60	0.401	−0.15

index > 0.5 and $R > 0.4$ applies or not (Fernández et al. 1996, 2003; Irigaray et al. 2007).

Regarding the factors, slope angle is among the more effective instability factors for all the five landslide typologies, having very high G-K values (G-K > 0.8) for falls, debris flows, and flow slides. Roughness, land use and topographic wetness index are also among the main causative factors. Roughness has high correlation (G-K > 0.8) for all the typologies, with the exception of earth flow (G-K $= 0.67$) and translational slides, for which it does not enter among the more predictive variables. Land use is a good predictor variable for all the typologies, with the exception of flow slides, while topographic wetness index is not among the effective variables both for debris flows and falls. Among the factors which are classified as EFF variables for only one landslide typology, geomorphologic units, for flow slides, topographic position index and lithology, for debris flows, are strongly (G-K > 0.8) effective. Finally, the distance from tectonic lineaments and illumination, for translational slides and elevation, for earth flows, show medium G-K values. All the other variables do not satisfy the condition and are in the following considered as not effective.

By looking at results from the "landslide typology point of view" the following results can highlighted: falls can be explained by three EFF variable, which produces very high G-K (> 0.95) and ARPA (> 0.45) values; five EFF variable have been observed for debris flows, giving high G-K (close to 0.9, except for use) and variably high ARPA values; four variables for flow slides produces G-K values close to 0.8, and medium-high ARPAs; medium G-K and very variably low ARPA values characterize the five explanatory variables for translational slides; the six EFF variable for earth flows, finally, are characterized both by medium G-K and ARPA values.

The relationships between G-K and ARPA can be summarized as follows. The validation of all the models prepared by using a single effective variable gives high ARPA values, well above the threshold of 0.12 (typically > 0.25). Translational slide represents an exception, since the models prepared for slope and dist do not fit the ARPA threshold limit; for this landslide typology, ARPA values quite above the 0.12 limit are among the NEF variables. Larger (> 0.3) ARPA values for NEF single parameter values are observed for falls (edaf, elev, aspect, tpi, geom), earth flows (geom, edaf), debris flows (twi, elev, geom, plan) and flow slides (use, lith). Five of the latter cases are represented by factors just below the limit of the EFF factors (edaf, for falls, geom, for earth flows, twi, for debris flows, use and lith, for flow slides). ARPA values close or larger than 0.4, seems to be strictly related with EFF variable or, in case of NEFs, with G-K greater than 0.45, with the very surprising exceptions of geom, for falls and debris flows.

Multivariate Models

According to the results of the contingency tables, for each landslide typology, the factors have been ranked from I (the best predictor) to XV (the least predictor), depending on the value of the association indexes (Table 2).

In order to verify both the correctness of the threshold values adopted in classifying the factors and the extent to which univariate correlation between each single factor and landslides propagates onto the predictive performances

Table 2 Summary of the results of the validation of the suite of susceptibility models, for best and best+1. FLL: falls; TSL: Translation slides; EFL: Earth flows; DFL: Debris flows; FSL: Flow slides

Summary					
Factor	FLL	TSL	EFL	DFL	FLS
ELEV	VIII	XI	VIII	VIII	XIV
SLOPE	**III**	**V**	**VI**	**II**	**III**
ASPECT	XIII	IX	XIII	XI	IX
TWI	VI	**II**	**V**	**I**	**IV**
PROF	XI	XIV	XIV	XV	XII
PLAN	XII	XV	XI	XIII	X
ROUGH	**I**	VII	**IV**	**III**	**I**
TPI	XIV	XIII	XV	IX	XI
SPI	V	X	VII	VII	VII
LITH	VII	**I**	**III**	VI	VI
USE	XV	**III**	**I**	**V**	V
DIST	IX	**IV**	IX	X	XIII
GEOM	**II**	VI	**II**	**IV**	**II**
EDAF	IV	XII	XII	XIV	XV
ILL	X	VIII	X	XII	VIII

of multivariate models, a large set of combinations of variables has been used to prepare susceptibility models. The factors have been combined to produce a suite of UCU layers, which have been then intersected with the landslide (rupture zone) archive, to derive the susceptibility grid layer. All the prepared models have been submitted to validation procedures. Particularly prediction and success rate curves were drawn, by randomly splitting the landslide archive in a training and a test balanced subsets. For the quantitative evaluation of the results of the validation, two morphometric parameters have been computed (ARPA and SHIFT).

Table 3 lists the results of the validation of the suite of susceptibility models which were prepared, whose validation graphs are showed in Fig. 3.

All the models are largely satisfactory, with ARPA values higher than 0.35 and very limited SHIFT (<0.05), with the exception of EFLBEST+1, which is characterized by low ARPA and high SHIFT, and FSLBEST+1, which associate high ARPA to a very high SHIFT. Generally, the best models gave ARPA values greater than the ones which were produced by one of the single combined variables or, when ARPA are similar to the ones resulted from a single factor model (e.g. debris flow and flow slides) a lowering of SHIFT is produced by combining EFF variables. Particularly, the susceptibility models for falls and debris flows, which are prepared by combining EFF variables characterized by high G-K and ARPA (Table 1a, d), confirmed to have a high predictive skill; coherently, the earth flow best model shows a quite (ARPA < 0.4) predictive skill, in accordance to the quite good performances of the single combined variables. Surprisingly, flow slides and translational slides best models produce results opposite to the expected ones. TSLBEST is in fact characterized by very high performance, in spite of the medium to low G-K and ARPA values (Table 1b); on the contrary, FSLBEST gives a results that is similar to the performance of the single combined factors (Table 1e). It seems that variables add in a congruent increasing and incongruent decreasing way, for translational slides and flow slide, respectively.

Finally, as regard to the best+1 models, it must be noticed that high ARPA (> 0.4) best models are less susceptible to decrease their performance when the best NEF variables are added.

Susceptibility Maps and Validation

Susceptibility maps for the five best models were prepared, in which six standard deviation reclassified susceptibility classes have been produced: from −1 standard deviations to more than 4, with a medium of 9.8 % of density. The relative error between intersected target landslides by the different susceptibility classes was used to estimate the predictive skill of the maps. The degree of fit was computed for each susceptibility class confirming a very good predictive performance of the five susceptibility models. Finally, a general landslide susceptibility map was produced by cumulating, for each of the five classes, the landslide area produced for the five typologies. Also in this case, fully satisfactory predictive results have been obtained (Fig. 3a, c and Fig. 4).

Discussion and Concluding Remarks

A procedure to select the best determining factors connected to landslide susceptibility has been defined. It allows the determining factors to be ranked according to their power of prediction, classifying them as “effective or non-effective” and the factors were ranked from I (the best predictor) to XV (the poorest predictor), depending on the value of the association indexes for each landslide typology and establish their best susceptibility model. The identification of the most determinant factors is an important step in a classification process. The susceptibility model complexity can be reduced and become easier to interpret and the reduction of the number of variables to locate and derive is an advantage during the deployment of the model. In some cases, the variable selection could improve the model accuracy. Theoretically, a manual selection of the most relevant factors, by an expert domain, could be considered the best approach, but because the number of probable descriptors is often large, it is not always actually possible. Therefore, the best variables must be selected automatically. The automatic process can be used as a preliminary approach in order to filter unnecessary attributes. This

Table 3 Summary of the results of the validation of the suite of susceptibility models, for best and best+1. FLL: falls; TSL: Translation slides; EFL: Earth flows; DFL: Debris flows; FSL: Flow slides

Model	Code	Combined fators	ARPA	Shift
FALLS_BEST	FLLBEST	ROUGH-USE-SLOPE	0.476	0.00
FALLS_BEST+1	FLLBEST+1	**BESTS**+EDAF	0.437	0.05
TRANSLATIONAL SLIDES_BEST	TSLBEST	LITH-TWI-USE-DIST-SLOPE	0.468	0.01
TRANSLATIONAL SLIDES_BEST+1	TSLBEST+1	**BESTS**+GEOM	0.432	0.05
EARTH FLOWS_BEST	EFLBEST	USE-GEOM-LITH-ROUGH-TWI-SLOPE	0.392	0.00
EARTH FLOWS_BEST+1	EFLBEST+1	**BESTS**+SPI	0.299	0.11
DEBRIS FLOWS_BEST	DFLBEST	TWI-SLOPE-ROUGH-GEOM-USE	0.438	0.03
DEBRIS FLOWS_BEST+1	DFLBEST+1	**BESTS**+LITH	0.437	0.04
FLOW SLIDES_BEST	FSLBEST	ROUGH-GEOM-SLOPE-TWI	0.379	0.04
FLOW SLIDES_BEST+1	FSLBEST+1	**BESTS**+USE	0.334	0.21

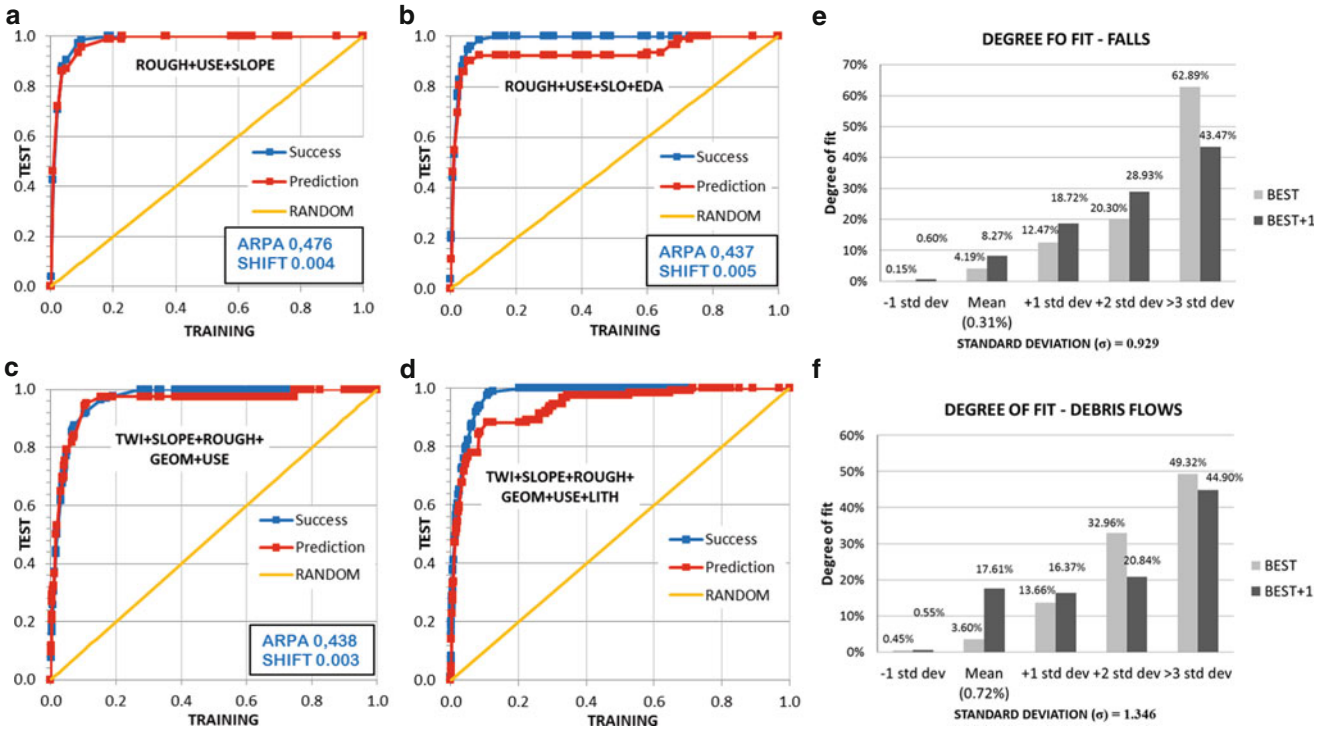

Fig. 3 Comparison of best and best+1 model. With validation curves Fall best model (**a**); fall best+1 model (**b**); debris flows best model (**c**); debris flows best+1 model (**d**). Degree of fit between susceptibility range and falls (**e**) or debris flows (**f**)

methodology has been applied to the Beiro River basin in the north-eastern area of the city of Granada (Spain), where slope angle is among the more effective instability factors for all the five landslide typologies studied. Roughness, land use and topographic wetness index are also among the main causative factors. Roughness has high correlation in all the typologies, with the exception of earth flow, for which it is not among the predictive variables. Land use is a good predictor variable for all the typologies, with the exception of flow slides, while topographic wetness index is not among the effective variables for debris flows or falls. Surprisingly, the lithology is not always present in the suite of the best models selected by the chosen statistical coefficients. The latter, in fact, is particularly determining for medium-large landslides, for instance earth flows, while is not of great significance for smaller landslides like falls and debris flows. This can be explained by considering that these movements affect equally the debris landslides and those over-consolidated terrains, that outcrop in the area, leading to a non significative statistic in the determining factors; the geological map used does not have the necessary resolution to allow appreciation of the spatial variations of the terrains with the same detail that the landslide archive does However the best susceptibility maps obtained following the GIS matrix method and the proposed procedure effectively explain the spatial distribution of slope movements.

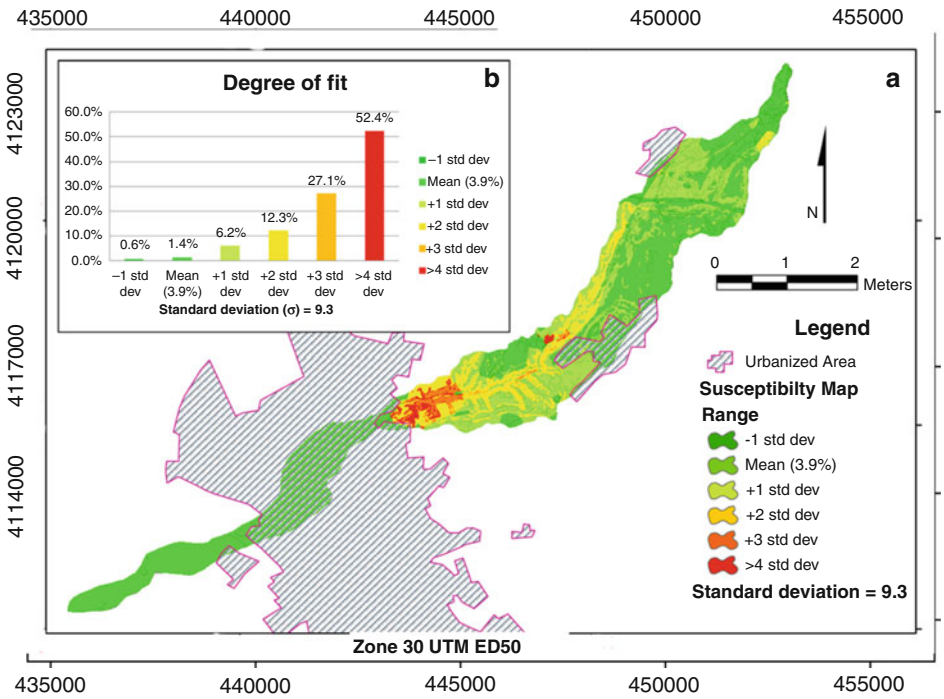

Fig. 4 Landslide susceptibility map (**a**) and validation (**b**). Coordinate Reference System UTM zone 30 European Datum 50

These maps provide valuable information on the stability conditions of broad regions, and are essential in the planning phase to ensure suitable corrective measures are taken. The option of organizing the controlling factors according to a statistical correlational coefficient could save both economical and time resources. This kind of statistical approach, however, requires excellent quality of the data input, regarding both the variables examined and the details and the resolution of the landslide archive, even though Google Earth™, was of excellent help in identifying the area subject to geomorphological instabilities.

The main limit is thus due to the scale of the maps available for an area, which is also the scale that the definitive map will have. The possibility of exploiting Google Earth™ images, here demonstrated by comparing a remote and a field coeval landslide dataset, also seems to offer the opportunity to implement multi-temporal landslide archives. This could be particularly helpful when facing the need to assess landslide and offers a new possibility where the object is to define the susceptibility conditions on a regional scale (thousands of square kilometers), without disclaim to stochastic quantitative and objective methods, thus avoiding approaching the problem only by heuristic qualitatively and subjective procedures.

Acknowledgments The findings and discussion of this research were carried out in accordance with the bilateral agreements between University of Palermo and University of Granada supporting an international Ph.D. programme.

This research was supported by project CGL2008-04854 funded by the Ministry of Science and Education of Spain, It was developed in the RNM121 Research Group funded by the Andalusian Research Plan.

References

Burrough PA (1986) Principles of geographical information systems for land resource assessment. Clarendon, Oxford, 194p

Carrara A, Cardinali M, Guzzetti F (1995) GIS technology in mapping landslide hazard. In: Carrara A, Guzzetti F (eds) Geographical information systems in assessing natural hazards. Kluwer Academic, Dordrecht, pp 135–175

Carrara A, Cardinali M, Detti R, Guzzetti F, Pasqui V, Reichenbach P (2006) GIS techniques and statistical models in evaluating landslide hazard. Earth Surf Process Landf 16:427–445

Chacón J (1999) Riesgos Naturales en el borde suroriental de la depresión de Granada. In: Rivas Carrera P y Gómez-Caminero García R (eds) Ciclos Naturales y Desarrollo Sostenido. Grupo Editorial Universitario, Granada, pp 71–134

Chacón J (2008a) Los conceptos actuales de susceptibilidad, peligrosidad y riesgo, en la prevención de movimientos de ladera, con ejemplos de aplicaciones prácticas. In: Lima RE, y Leite JC (eds) 44° Congresso Brasileiro de Geología. Publicaçao Especial. 30 Octubre 2008. "Desastres e riscos geológicos em Curitiba e litoral. Roteiro de Excursao Técnica. 43 páginas.

Chacón J (2008b) Movimientos de Ladera. In Master oficial Ingeniería Geológica Aplicada a la Obra Civil. Copicentro. ETS Ingenieros de Caminos, Canales y Puertos. 77 páginas

Chacón J, Corominas J (2003) Special issue on "landslides and GIS". Nat Hazards 30:281–295

Chacón J, El Hamdouni R, Arroyo JM, Irigaray C, and Fernández T (2001) Slope instability in the north-eastern sector of the Granada basin (Spain): events following recent rainfall (1995–1998). In Sanz C,

Peláez A, López Garrido AC (eds) La cuenca de Granada: Estructura, Tectónica Activa, Sismicidad, Geomorfología y dataciones existentes. CSIC – Universidad de Granada, pp 189–197

Chacón J, Irigaray C, Fernàndez T, El Hamdouni R (2006) Engineering geology maps: landslides and Geographical Information Systems (GIS). Bull Eng Geol Environ 65:341–411. doi:10.1007/s10064-006-0064-z

Chacón J, Irigaray C, Fernández T (2007) Movimientos de Ladera (pp. 45–82). In: Ferrer M (coord) Atlas de Riesgos Naturales en la Provincia de Granada. Diputación de Granada-Instituto Geológico y Minero de España (IGME). 190p

Chacón J, Irigaray Cm EL, Hamdouni R, Jiménez-Perálvarez JD (2010) Diachroneity of landslides. In: Williams et al (eds) Geologically active. Taylor & Francis, London, pp 999–1006. ISBN 978-0-415-60034-7

Chung CF, Fabbri A (2003) Validation of spatial prediction models for landslide hazard mapping. Nat Hazards 30:107–142

Clerici A, Perego S, Tellini C, Vescovi P (2002) A procedure for landslide susceptibility zonation by the conditional analysis method. Geomorphology 48:349–364

Clerici A, Perego S, Tellini C, Vescovi P (2006) A GIS automated procedure for landslide susceptibility mapping by the conditional analysis method: the Baganza valley case study (Italian northern Apennines). Environ Geol 50:941–961

Conoscenti C, Di Maggio C, Rotigliano E (2008) GIS analysis to assess landslide susceptibility in a fluvial basin of NW Sicily (Italy). Geomorphology 94:325–339

Conoscenti C, Costanzo D, Rotigliano E (2009) Extension of landslide susceptibility models: a test in the Platani river basin (southern Sicily). VII Forum Italiano di Scienze della Terra – Geoitalia 2009, Rimini, Italy, 9–11 Sept 2009. Epitome 03.0254, pp 68

Costanzo D, Cappadonia C, Conoscenti C, Rotigliano E (2011) Exporting a Google Earth aided earth-flow susceptibility model: a test in central Sicily. Nat Hazards 61(1):103–114. ISSN 0921-030X, DOI 10.1007/s11069-011-9870-0

Crozier MJ (1984) Field assessment of slope instability. In: Brunsden D, Prior DB (eds) Slope instability. Wiley, Chichester, pp 103–142

Cruden DM, Varnes DJ (1996) Landslide types and processes. In: Turner A, Schuster L (eds) Landslides: investigation and mitigation. TRB special report, vol 247. National Academy Press, Washington, DC, pp 36–75

Davis JC (1973) Statistics and data analysis in geology. Wiley, New York

De Martonne E (1942) Nouvelle carte mondiale de l'indice d'aridite´. Annales de Geographie 51:242–250

Dikau R (1989) The application of a digital relief model to landform analysis in geomorphology. In: Raper J (ed) Three dimensional applications of geographic information systems. Taylor & Francis, New York, p 55571

Dikau R, Brunsden D, Schrott L, Ibsen M (1996) Landslide recognition. Identification, movement and courses. Report No. 1 of the European Commission Environment Programme, Wiley, Chichester, 251p

Fernández T, Irigaray C, El Hamdouni R, Chacón J (1996) Inventory and analysis of landslides determinant factors in Los Guajares Mountains, Granada (Southern Spain). In: Senneset K (ed) Landslides. Proceedings of the international symposium on landslides, vol 3. Balkema, Rotterdam, pp 1891–1896

Fernández T, Irigaray C, El Hamdouni R, Chacón J (2003) Methodology for landslide susceptibility mapping by means of a GIS. Application to the Contraviesa area (Granada, Spain). Nat Hazards 30:297–308

Fernández T, Irigaray C, El Hamdouni R, Chacón J (2008) Correlation between natural slope angle and rock mass strength rating in the Betic Cordillera, Granada, Spain. Bull Eng Geol Environ 67(2):153–164. doi:10.1007/s10064-007-0118-x

Goodman LA, Kruskal WH (1954) Measures of association for cross classifications, part I. J Am Stat Assoc 49:732–764

Guzzetti F, Carrara A, Cardinali M, Reichenbach P (1999) Landslide hazard evaluation: a review of current techniques and their application in a multi-scale study, central Italy. Geomorphology 31:181–216

GuzzettI F, Reichenbach P, Ardizzone F, Cardinali M, Galli M (2006) Estimating the quality of landslide susceptibility models. Geomorphology 81:166–184

Hansen A (1984) Landslide hazard analysis. In: Brunsden D, Prior DB (eds) Slope instability. Wiley, New York, pp 523–602

Hobson RD (1972) Surface roughness in topography: quantitative approach. In: Chorley RJ (ed) Spatial analysis in geomorphology. Methuer, London, pp 221–244

Irigaray C, Fernàndez T, El Hamdouni R, Chacón J (1999) Verification of landslide susceptibility mapping: a case study. Earth Surf Process Landf 24:537–544

Irigaray C, Fernàndez T, El Hamdouni R, Chacòn J (2007) Evaluation and validation of landslide-susceptibility maps obtained by a GIS matrix method: examples from the Betic Cordillera (southern Spain). Nat Hazards 41:61–79

Jiménez-Pelvárez JD, Irigaray C, El Hamdouni R, Chacón J (2009) Building models for automatic landslide-susceptibility analysis, mapping and validation in ArcGIS. Nat Hazards 50:571–590

Ohlmacher GC (2007) Plan curvature and landslide probability in regions dominated by earth flows and earth slides. Eng Geol 91(2):117–134. doi:10.1016/j.enggeo.2007.01.005

Remondo J, Gonzalez A, Diaz de Teran JR, Cendrero A, Fabbri A, Chung CJ (2003) Validation of landslide susceptibility maps; examples and applications from a case study in northern Spain. Nat Hazards 30:437–449

Rodhe A, Seiber J (1999) Wetland occurrence in relation to topography: a test of topographic indices as moisture indicators. Agric Forest Meteorol 98–99:325–340

Rotigliano E, Agnesi V, Cappadonia C, Conoscenti C (2011) The role of the diagnostic areas in the assessment of landslide susceptibility models: a test in the Sicilian chain. Nat Hazards. doi:10.1007/s11069-010-9708-1

Sharma B, Sharma N, Sharma N (2010) Simulation of Different SPI Models. Int J Comput Appl 1(10):22–25.

Soeters R, van Westen CJ (1996) Slope instability recognition, analysis and zonation. In: Turner AK, Schuster R (eds) Landslides investigation and mitigation. Transportation Research Board special report, National Academy Press, Washington, DC, p 247

Varnes DJ (1978) Slope movements, type and processes. In: Schuster RL, Krizek RJ (eds) Landslides analysis and control. Washington Transportation Research Board special report 176. National Academy of Sciences, Washington, DC, pp 11–33

Vera JA (2004) Geología de España (*geology of Spain*). SGE-IGME, Madrid, 890p

Weiss A (2001) Topographic position and landforms analysis. Poster presentation, ESRI User Conference, San Diego

Zinko U, Seibert J, Dynesius M, Nilsson C (2005) Plant species numbers predicted by a topography-based groundwater flow index. Ecosystems 8(4):430–441

A Case Study on Landslide Hazard Mapping in Changunarayan VDC, Nepal

Bikas Chandra Bhattarai and Ananta Man Singh Pradhan

Abstract

An application of GIS for landslide hazard assessment using multivariate statistical analysis, mapping, and the evaluation of the hazard maps is presented. The study area is the Changunarayan VDC (8.19 km^2) located in the central region of Nepal and listed on the UNESCOs world heritage site in 1979 A.D., which is under pressure of high construction activities. Data used to construct the landslide hazard maps were obtained from published works, topographical and geological maps, satellite images and aerial photographs and other digital sources. To determine the factors and classes influencing land sliding, layers of topographic factors derived from a digital elevation model, geology, and landuse/land cover were analyzed and the results were used for hazard mapping. Hazard map of the study area shows 15.13 % area lies in the high hazard level, 53.87 % on moderate hazard level and 28.53 % in low hazard level.

Keywords

Changunarayan • Digital elevation model • Landslide hazard mapping

Introduction

Nepal is a mountainous, geologically young country that straddles the boundary between the Indian and Himalayan tectonic plates. The country is geologically young and still evolving. Landslides are very common occurrences in Nepal and are also one of the main natural hazards (Dikshit 1983). Many hill slopes in Nepal are situated on or adjacent to unstable slopes and old land-slides, which are reactivated from time to time (Howell 1999). In Nepal, on an average 260 people lost their lives every year and about 30,000 families are affected annually (UNDP, Nepal 2002).

Landslide is a natural process and its occurrence is controlled by the geologic, geomorphologic, hydrologic and climatic and vegetation conditions (Keshi Raj 1998). Anthropogenic activities may also reactivate pre-existing landslide or may also initiate entirely new landslides. Landslides have been identified as a source of hazard which results in environmental, social or economic loss such as human lives, houses, vehicles, passengers, cultivated land, community forests, and development infrastructures like electric power station, road, and irrigation cannel. Hazard is the probability of occurrence of a particularly damaging phenomenon whining a specified period of time and area because of a set of existing or predicted conditions (Deoja et al. 1991).

Hazard mapping is the process by which the probability of occurrence of any damaging phenomena can be predicted in any given area (Markus 1985). In order to conduct landslide hazard mapping, it is necessary to identify the elements at risk such as population, infrastructures, economic activities, environment etc. that are exposed to known hazard and that are likely to be adversely affected by the impact of the hazard (Pradhan 2003).

A landslide hazard map indicates the possibility of landslide occurring in a given area. A hazard map may be as

B.C. Bhattarai (✉)
Central Department of Environmental Science, Tribhuvan University, Kirtipur, Kathmandu, Nepal
e-mail: bikasbhattarai@gmail.com

A.M.S. Pradhan
Ministry of Energy, Government of Nepal, Kathmandu, Nepal

C. Margottini et al. (eds.), *Landslide Science and Practice*, Vol. 1,
DOI 10.1007/978-3-642-31325-7_72,

simple as a map which uses the location of old landslides to indicates potential instability, or as complex as a quantitative map incorporating probabilities based on variables such as rainfall thresholds, slope angle, soil type, and level of earthquake shaking (Varnes 1984). In hazard map, the area is divided into low, medium and high hazard zones. The low hazard zone is considered to be more stable whereas medium hazard zone may have possibility of landslide disaster. Very dangerous and active landslide area represents the high hazard zone. The sign of instabilities occur in the high hazard zone, which has high possibility of failure in the future (Ghimire 1993). So hazard mapping is an important tool in predicting the probability of occurrence of any damaging phenomena with in any given area. Thus, if the prediction is significant, the damage to lives property and ecosystem can be minimized to large extent. This study mainly focuses on the making hazard zonation mapping such that preliminary measures can be applied to before large type of hazard occurs.

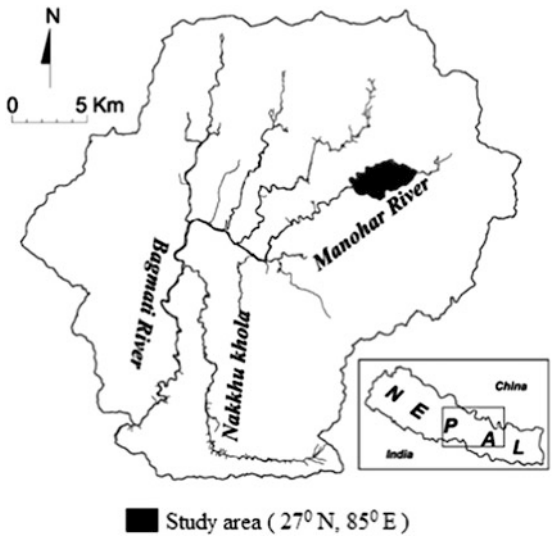

Fig. 1 Location of study area

Study Area

This study is conducted in the Changunarayan VDC of Bhaktapur District, Nepal. Changunarayan VDC is the place where the Changunarayan temple is located. It is the oldest monument in Kathmandu valley came in existence in third century situated 18 km east of Kathmandu and standing 1,541 m, above the sea level at 27° 42′ 36″ N latitude and 85° 25′ 46″ E longitudes (Figs. 1 and 2).

This monument is significant from artistic, religion, cultural, historical, and archaeological view point. This is one of the seven world heritage sites of Kathmandu valley; listed on the UNESCOs world heritage site in 1979. The temple is adorned by some of the best specimen of stone, wood, and metal-craft in the valley. The temple stands as the epitome of culture, religion, history and faith of the Kathmandu valley. It is one of important site to attract tourist by which Bhaktapur district can collect revenue. Due to various reasons the Changunarayan hill and the temple has not received due attention towards its conservation. In 1998 researchers found significant physical degradation in the temple.

Many of the buildings and monuments were dilapidated and in various stages of disrepair, with cracked and collapsing walls, leaking roofs, etc. Stairways and paths were also in the state of disrepair. Recently the indications of increased landslide hazard in the Changunarayan hill are getting more prominent. Land subsidence, cracks on the hills, minor landslides, bulged and twisted structures, cracked walls, and floors, can be seen in various locations in the Changunarayan hill. If these early warning signs are ignored for too long and timely precaution and preventative measures are not taken, then it can be too late to save the hill and a world heritage site.

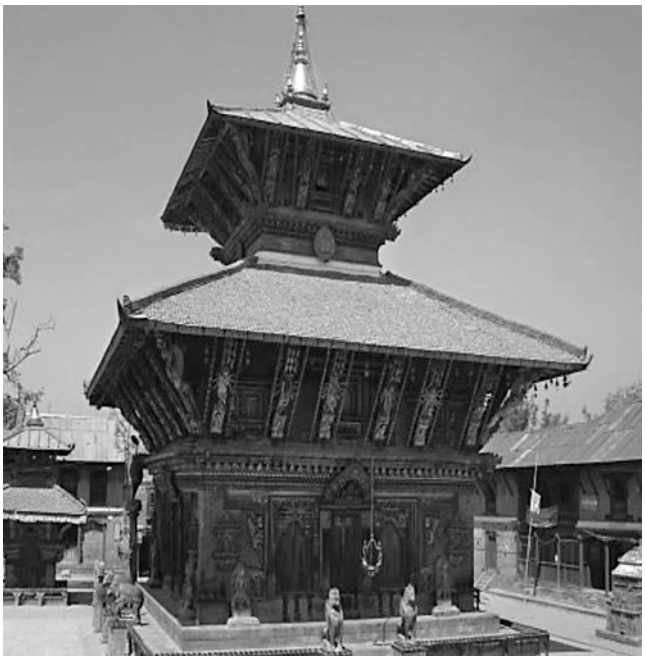

Fig. 2 Changunarayan Temple, a world heritage

Methodology

The preparation of hazard map is based on identifying various hazard components followed by a rating of these components and finally all rating values are augmented. For this, basic maps for the hazard mapping were prepared

which include landuse map, slope map, relief map, aspect map, landslide inventory map, etc. Landslide hazard mapping is based on the assumption that landslide occurs as a result of similar geological, geographic, and hydrological conditions that lead to past and present landslides (Ghimire 1993). A landslide hazard map refers to an arithmetic method of portraying the spatial variation in the susceptibility of slope failure, based on assessment of various landslides causative factors (Dhakal et al. 2000).

Data used to construct the landslide hazard maps were obtained from the published works, topographical and geological maps, satellite images, and aerial photographs and other digital sources. Map compilation was accomplished using ARC View GIS 3.2, ILWIS 3.4 and SINMAP. Landslide occurrence factors were obtained by employing the probability-frequency ratio model. Field observation for landslide inventory was carried out.

Frequency Ratio Model and Relationship Between Landslides and Landslide-Related Factors

In general, to predict landslides, it is necessary to assume that landslide occurrence is determined by landslide related factors, and that future landslides will occur under the same condition as past landslides (Pradhan 2003). Using this assumption, the relationship between landslides occurring in an area and the landslide related factors can be distinguished from the relationship between landslides not occurring in an area and the landslide related factors (Boots and Gettis 1988). In this study frequency ratio is used to represent the distinction quantitatively. The frequency ratio of the area where landslides occurred to the total study area, and also, is the ratio of the probabilities of a landslide occurrence to a non-occurrence for a given factors attribute (Upreti and Dhital 1991). Therefore, the grater the ratio above unity, the stronger the relationship between landslide occurrence and the given factors attribute, and the lower the ratio below unity, the lesser the relationship between landslide occurrence and the given factors attribute (Lee and Pradhan 2006). To calculate the frequency ratio, the ratio of landslide occurrence and non-occurrence was calculated for each range or type of factor, and the area ratio for each range or type of factor, to the total area was calculated. Finally the frequency ratio for each range or type of factor was calculated by dividing the landslide-occurrence ratio by the **area ratio**. The factors chosen such as slope, aspect, relief, internal relief, geology, landuse, precipitation, and vegetation index were evaluated using the frequency ratio model to determine the level of correlation between the location of the landslides in the study area and these factors. Probabilistic approaches are based on the observed relationship between each factor and the distribution of landslides (Arnoff 1989).

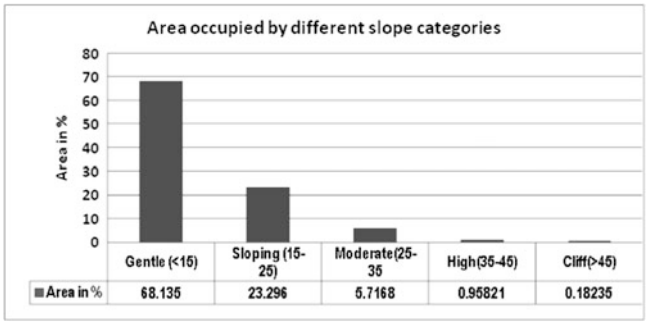

Fig. 3 Area occupied by different slopes

Landslide Hazard Rating Components

The influencing factors of hazard, for this particular study, as represented by the slope map, aspect map, geology map, relief map, and landuse map are archived to integrate the hazard level. The precipitation factor is not included in this study. Geology of the region has also a great deal of control over the process of mass wasting in the region, but because the study area is not large, the difference in geology does not look apparent. The components use for the landslide hazard mapping in this study is described below:

Slope

The natural slopes are primary factor to dictate the stability of the terrain. The slope condition includes the slope angle and the slope aspect. In general, the stability of the slope is the interplay of slope angle with, material properties such as permeability, friction angle, and cohesion of the material. The slope is divided into the range of: $<15°$, 15–25°, 25–35°, 35–45° and $>45°$. In the study area, most of the area is occupied by the gentle slope followed by the sloping (Fig. 3).

Aspect

The windward and leeward faces as well as northern and southern slope of a mountain differ in their climatic conditions. It is because of the difference in the amount of rainfall and sunshine received which in turn controls the diversity, density and the distribution of vegetation in the area. All these factors control the soil type, drainage type and a susceptibility to mass wasting over an area. An aspect map shows to which side a slope is directed. An aspect value of zero means that the slope is facing the north. The distribution of aspect of the mountain slope in the study area is shown in Fig. 4.

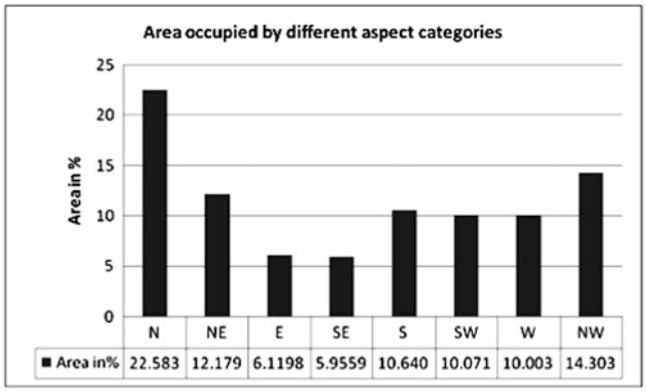

Fig. 4 Area occupied by different aspect

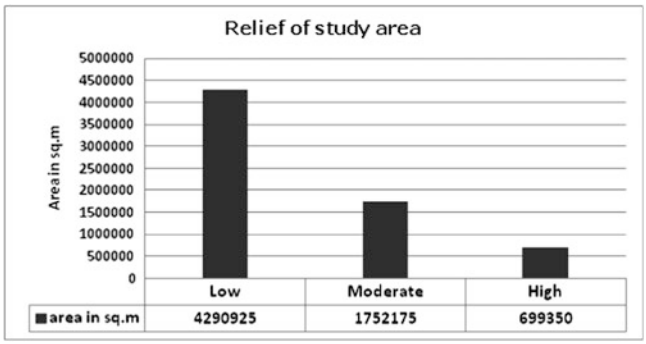

Fig. 5 Relief of study area

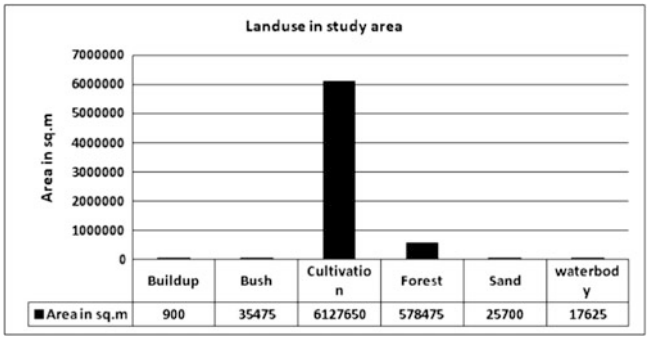

Fig. 6 Landuse in study area

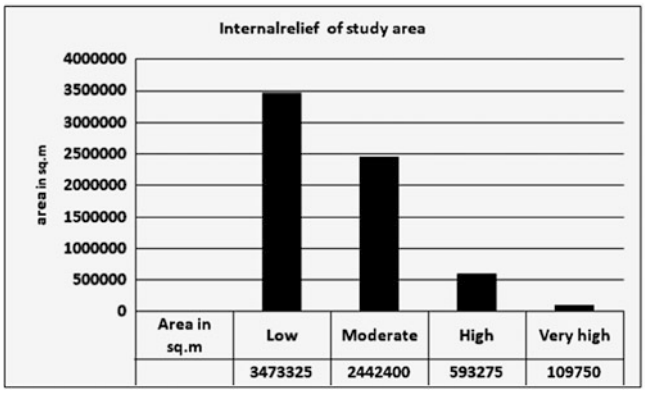

Fig. 7 Internal relief map of study area

Relief

The surface relief is the variation in height of land surface. Different reliefs have different climatic conditions. Another important aspect relating relief and landslide hazard is that construction activities like roads are preferentially built along the same relief. It is therefore that the landslide hazards in an area are observed more or less on the same relief. The distribution of land in the study area in various relief groups is shown in Fig. 5. The area covered by each group is given in table.

Landuse

The landuse has also significant role in the stability of soil slope. The land covered by forest regulates continuous water flow and an infiltration regularly whereas the cultivated land affect the soil slope stability due to saturation of covered soil.

The landuse pattern of the study area is categorized into barren land, cultivation, and forest. The distribution of different land use cover along with the area occupied is given in Fig. 6, in which must of the land is occupied by the cultivated land.

Internal Relief

Internal relief map shows the local relief that is the local difference in height within a unit area. It indicates the potential energy for erosion and a mass movement. Internal relief shows the major breaks in the slope of the study area. Four categories of internal relief in meter have been chosen for hazard evaluation (Fig. 7).

Analysis and Result

In the study area, the landslides have been taken as the indicator of slope instability process. The Universe Transverse Mercator (UTM) projection is used. The slope instability is an outcome of complex interaction among a large number of interrelated terrain factors (Yin and Yan 1988). Only some of the crucial terrain parameters: such as geology, internal relief, slope, aspect, landuse pattern has been used for the purpose of instability analysis. To evaluate

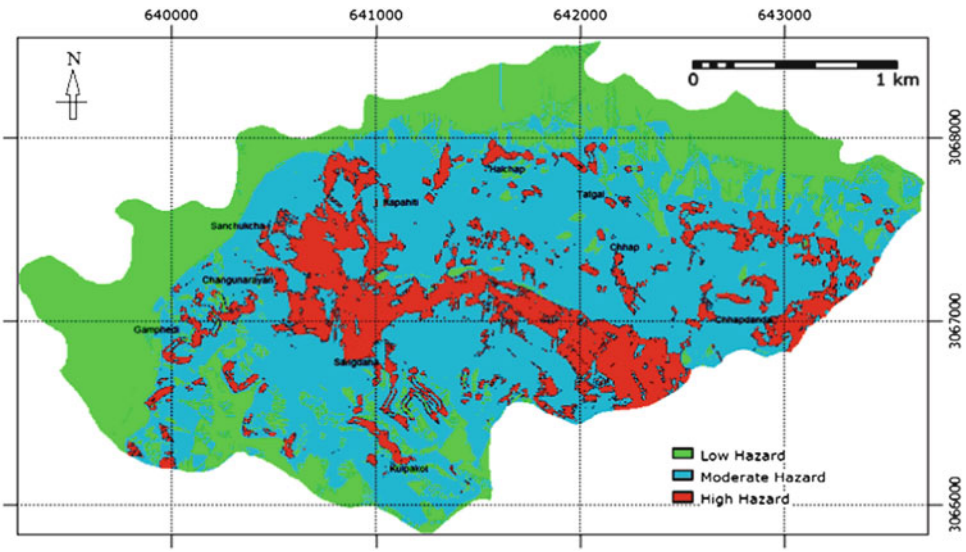

Fig. 8 Landslide hazard map

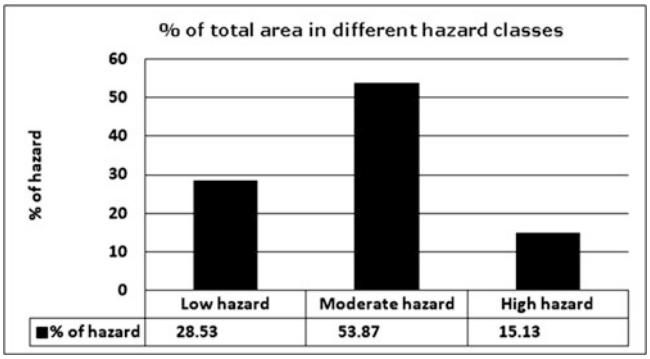

Fig. 9 Percentage of area in different hazard classes

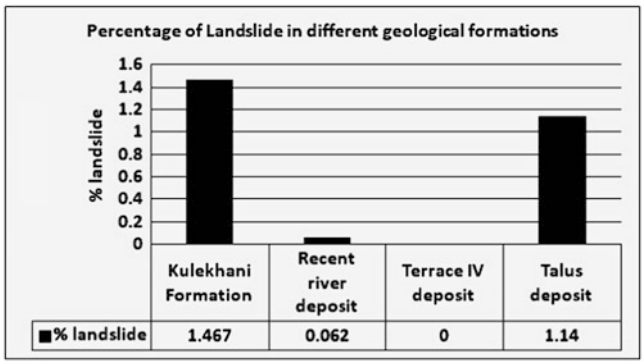

Fig. 10 percentage of landslides in different geological deposits

the contribution of each of factor towards landslides, distribution data layer were compared to various thematic data layers separately. The resulting total weight directly indicates the importance of total weights is positive the factor is favourable for landslide and if it is negative, it is unfavourable.

Based on the clustering of total weights, as well as concentration of instabilities, the area under study was divided into the low, moderate and high hazard categories. The landslide in different categories is divided in to low, moderate, and high class. Of the total landslides present in the study area about 15.13 % of the land slide is under the high hazard class (Figs. 8 and 9).

Geology plays an important role in the causes of landslide failure (Carson 1985). Figure 10 shows the relation between geological formation and landsides density along with their weight value. The high favourability of the Kulekhani formation may be probably due to the presence of thrust that make the zone seismically active and the presence weak geological formation.

The distribution of the different aspect categories in the area shows that the study area is found to be predominately facing North (N) (22.583 %) and North-West (NW) (14.303 %) (Fig. 11). The landslide distribution map was superimposed on the aspect map and area of landslide in each aspect was calculated. The percentage of landslide in different aspect categories are shown in Fig. 12. Slope facing south-west is found to be highest share of landslide occurrence, followed by north facing slope.

Figure 13 shows the distribution of the different relief categories in the area. The largest share of the study area falls in low relief zone (<1,800 m), followed by moderate zone (1,800–2,100 m). When the landslides distribution map was superimposed on the aspect map and the area of landslide in each relief categories calculated, it is clear to see that the most prominent of landslide falls in the low relief zone (52.997 %) followed by moderate zone (44.832 %) (Fig. 14).

The distribution of different landuse categories in the area is given in Fig. 15. The largest share of the study area is covered by cultivation (90.29 %) followed by the forest area

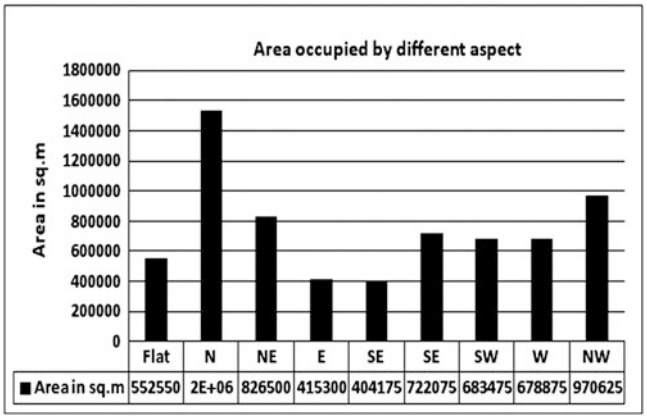

Fig. 11 Area occupied by different aspect categories

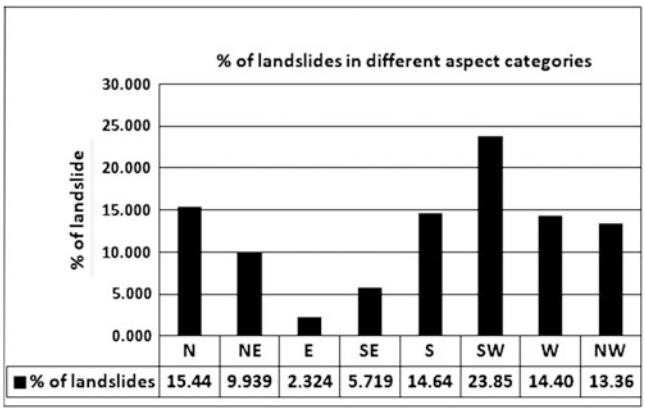

Fig. 12 Percentage of landslide in different aspect

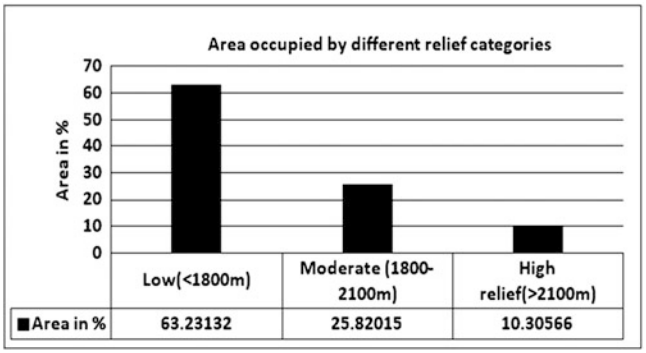

Fig. 13 Area occupied by different relief categories

(8.52 %) while the least is covered by buildup (0.013 %). The landslide map is superimposed on the landuse map and the area of landslide in different landuse group is calculated. The prominent occurrence of landslide is found on cultivation area (77.37 %) followed by forest region (8.52 %). Land under the forest is comparatively low as compared to the cultivation area. There is complete absence of landslide on the water, sand and bush area (Fig. 16).

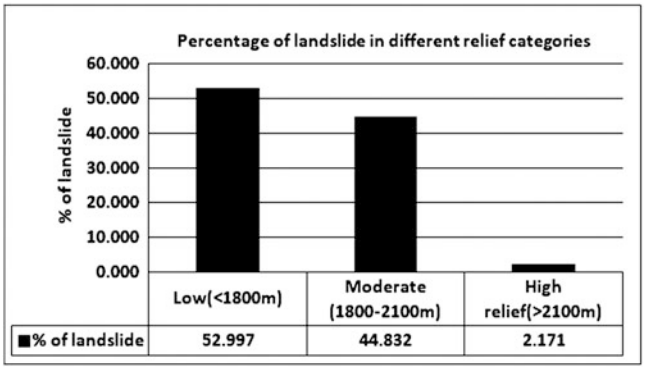

Fig. 14 Percentage landslide in different relief categories

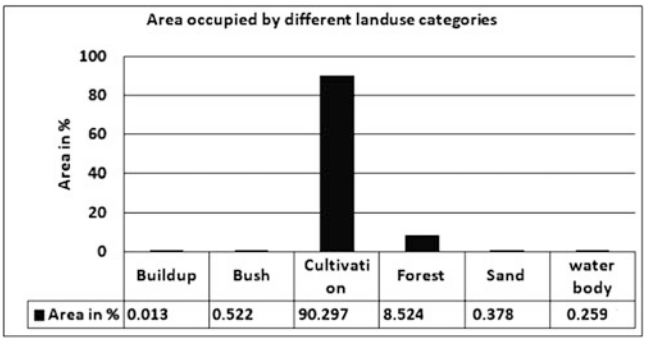

Fig. 15 Area occupied by different landuse categories

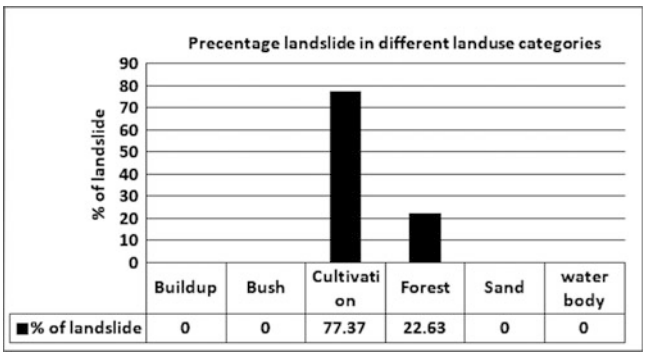

Fig. 16 Percentage landslide in different landuse categories

The distribution of different slope categories in the area is given in Fig. 17. Of the total study area, 68.135 % falls under the gentle (<15°), 23.296 % falls under sloping (15–25°), 5.71 % falls under the moderate (25–35°), 0.958 % falls under the high (35–45°) and cliff (>45°) does not contain any percentage.

The landslide distribution map was superimposed on the slope map and the areas of landslide in each slope categories were calculated. The percentages of landslide in different slope categories are shown in Fig. 18. Gentle slope type (<15°) has the dominant landslide occurrence (43.45 %)

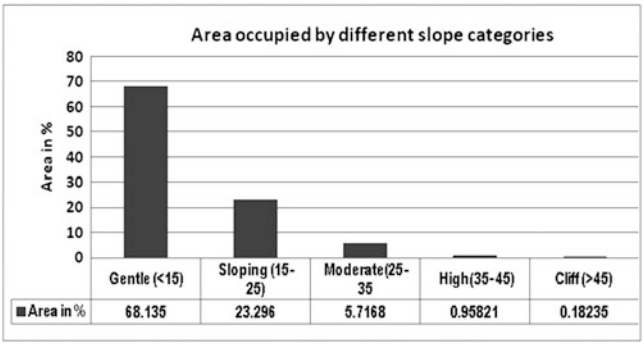

Fig. 17 Area occupied by different slope categories

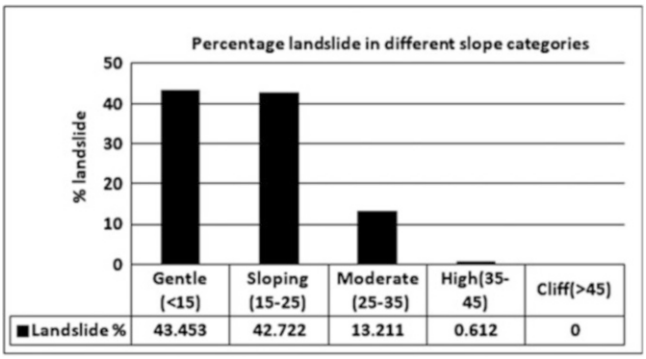

Fig. 18 Percentage landslide in different slope categories

which is the earthflow type and the sloping type (15°–25°) has 42.72 % followed by the moderate (25°–35°) having only 13.21 % and high slope have only 0.61 % of landslides.

Discussion

The hazard map generated has displayed degree of reliability as over whelming number of active and old landslides scars occur on high and very hazard zone. The hazard assessment shows that almost 53 % of the study area lies in the moderate hazard and 28 % of the area lies in the low hazard zone of hazard map prepared after detail investigation of the factor that might be responsible causes for the onset of landslide. This agrees with the fact that weak geological formations of the slope of the lesser Himalayas are greatly susceptible to landslide hazards. More over such weaker formation in our study area is disturbed by the construction of roads and buildings. Construction of roads and construction of buildings or other heavy structure through slopes makes it vulnerable to mass wasting phenomenon which in turn increase the driving force of slope area. From the field observation it indicates that the majority of the landslides in the area where the human interference is more.

From the hazard map of Changunarayan, the temple which is the world heritage site, is under the high hazard zone. The over exploitation of sand from the base of this hill slope i.e. from Manohara river is the other triggering cause for the occurrence of landslide on Changunarayan (Fig. 20). The study also revealed that the slope class 0–15° has the most occurrence of landslides. Human activity i.e. construction of building and other structure is relatively low in moderate and high slope area. And the other parameters like, landuse also showed the effects of human activity on the stability of land. From the landuse map analysis, 77.37 % of landslide observed in the cultivation area, have the highest percentage of landslide.

The study area is characterized by steep slope, steeper channel course and fragile geology. These factors have contributed to frequent slope movement and intense erosion processes during the heavy rainfall in monsoon.

This is obvious by widespread of landslide scars, gully development in the study area. The topographic and geomorphic features reflect the marginality and susceptibility of the environment in terms of productivity and human habitat. The growing population pressure has been pressurizing the marginal ecosystem of the area. The expansion of the cultivation land on the steep slope either encroaching the forest area or shrub or bushes is evident to this.

The instability of slope is shown by drunken trees, trees displaced from their normal vertical alignment. This is due to slow movement of the slope. Small sub ducted pits area found around the side of hill indicate the instability of the hill (Fig. 19).

Cause of Landslide in Changunarayan

There can be many factors responsible for the damages depicted in Changunarayan temple and Changunarayan hill. One of the factors can have greater bearing on the cause of these damages. At this point the exact reasons for these damages are not clear. The damages to the structure of the temple can be from poor workmanship, poor design, timely wear and tear and land subsidence. However, since damages to superstructures can be seen in several structures in the temple area, it is more likely that land movement is at least partly responsible for these damages. The damages to the Changunarayan hills, is in the form of land cracks and small landslides can be due to reduction in tree coverage, increase in developmental activities, unscientific agricultural practices, unmanaged grazing, accelerated sand mining from the base of the hill or natural causes like weak geological formations and intense rainfall. A detailed study is required to point out the exact reasons for these damages.

Fig. 19 A drunken tree at the study area

Fig. 20 Sand mining in Manohara River at the base of Changunarayan hill

Terraced farming is practiced at this part of the hill for growing rice, wheat, corn, potato and tomato. The farmers seem unaware of the amount of water requirement for various types of plants. Normally, to be on the safe side, a lot more water is used than is required for the plants. Flood irrigation is the preferred method of irrigation, especially during rice plantation; any excess water is not properly channelled out. Excessive water use raises water table, which can severely lower slope stability by increasing pore water pressure and decreasing effective stress of the soil over a potential slip surface which, in turn, reduces the shear resistance of the soil. High amount of water in soil reduces cohesion value of soil also. Excessive use of water in agricultural field is a recipe for triggering landslides.

The legal and illegal sand extraction from the river bed has considerably lowered the level of Manohara River which flows through the north and south part of Changunarayan hill. The lowering of bed level in Manohara River at the section of the river, shown in Fig. 20, clearly indicates the magnitude of the problem. The reduction in bed level accelerates the erosion of river bank in the west season. The river bank of Manohara River constitutes the base of Changunarayan hill.

Conclusion

The study focused mainly on the identification and classification of the hazardous zone as well as the identification of the causes of the slope instability that will help divert the preventive work to area of high susceptibility indicated as high hazard region on the hazard zonation map. So as to minimize the implication of natural hazards by methods such as bio-engineering technique or immediate mechanical intrusion can be applied. This paper also demonstrates that the instability in the structure of Changunarayan temple and surrounded area is due to the instability of the hill slope. Most of the temple area lies under the high hazard zone.

Acknowledgements The authors are grateful to Dr. Kedar Rijal, Head of Department of Central Department of Environmental Science, Tribhuvan University for providing research opportunity and Prashant Baral and Sonika Shahi for helping in writing this paper. Special thanks to District Development Committee of Bhaktapur for providing financial aid, and others not mentioned here specifically, are gratefully acknowledged.

References

Arnoff S (1989) Geographical information system: a management perspective. WDL Publications, Ottawa, Canada

Boots BN, Gettis A (1988) Analysis of the spatial distribution of drumlins: a two mosaic approach. J Glaciol 6:717–736

Carson,B (1985) Erosion and segmentation process in the Nepalese Himalaya. ICIMOD, occasional paper no. 1, ICIMOD, Kathmandu

Deoja B, Dhital MR, Thapa B, Wagner A (1991) Mountain risk engineering handbook. ICIMOD, Kathmandu, p 857

Dikshit AM (1983) Report on preliminary engineering geology investigation of landslide and subsidence in Kera Bari character area in the Siddhartha highway. Ministry of Industry, Department of mine and geology, Kathmandu

Dhakal AS, Amada T, Aniya M (2000) Landslide hazard mapping and its evaluation using GIs: an investigation of sampling schemes for a grid-cell based quantitative method. Photogramm Eng Rem Sens 66 (8):981–989

Ghimire KK (1993) Landslide of Likhi Khola area along with in study of landslide in Nepal during the period (1950–1969). Unpublished dissertation. Central Department of Geology, Tribhuvan University

Howell J (1999) Road side bio-engineering. Department of Road, Babar Mahal, Kathmandu, Nepal, Reference Manual 216p and Site Handbook 160p

Keshi Raj K (1998) Mass movement in lower base of Chandragiri range south of Kirtipur. Unpublished dissertation. Central Department of Geology, Tribhuvan University

Lee S, Pradhan B (2006) Probabilistic landslide hazard and risk mapping on Penang Island, Malaysia. Earth Sci 115(6):661–672

Markus J (1985) Mountain hazard mapping in Khumbu Himal. Mt Res Dev 6(1):29–40

Pradhan AMS (2003) Engineering geological investigation of Pharping-Kulekhani road alignment from chainage km 6 + 400 m 12 + 63. Unpublished dissertation. Central Department of Geology, Tribhuvan University, Kirtipur

UNDP (2002) Human Development Report. Working with partners in more than 160 countries, UNDP is the UN's global development network to help people build a better life. Working with partners in more than 160 countries, UNDP is the UN's global development network to help people build a better life

Upreti BN, Dhital MR (1991) Landslide studies and management in Nepal. ICIMOD, Katmandu, Nepal, p 87

Varnes DJ (1984) Landslide hazard zonation: a review of principle of and practices. Commission on landslides of the IAEG, Natural hazard no. 3, UNESCO

Yin KL, Yan TZ (1988) Statistical prediction model for slope instability of metamorphosed rocks. In: Bonnard C (ed) Proceedings of the 5th international symposium on landslides, vol 2, Lausanne. Balkema, Rotterdam, pp 1269–1272

Analyses of Landslide Hazard Evaluation Factors Using Polynomial Interpolation

Ilorad Jovanovski, Biljana Abolmasov, and Igor Peshevski

Abstract

This paper describes a method for analysis of various input parameters used in preparation of Landslide Hazard Zonation Maps. The method is based on the quantitative approach, which includes four Landslide Hazard Evaluation Factors grouped into four ranges of values. Since the various parameters are not equally important for estimation of Total Landslide Hazard Evaluation Factor (TLHEF), importance ratings are allocated to the different value ranges. Importance ratings for Lithological types (LT), Ground Water Level (GWL), Slope Angles (SA) and Soil Debris Cover (SDC) are defined using polynomial interpolation. With this procedure, each evaluation factor is related to the corresponding ratings using interpolation charts and equations. Based on the correlation between the adequate parameters and the rating, the Total Rating Hazard Evaluation Factor can be calculated.

Keywords

Landslide • Hazard evaluation • Risk • Zonation

Introduction

It is well known fact that the susceptibility of a given area to sliding can be determined using hazard zonation techniques. The best approach is when a landslide hazard map is prepared early in the planning study and developed in more detail as the study progresses. It can be used as a tool to help identify land areas best suited for development by examining the potential risk of sliding. Such maps are especially important in a process of urban planning of certain areas (Abolmasov and Stojkov 1994; Jovanovski et al. 2005).

I. Jovanovski (✉) • I. Peshevski
Faculty of Civil Engineering, University Ss Cyril and Methodius, Skopje, blvd. Partizanski odredi 24, Skopje 1000, Republic of Macedonia
e-mail: jovanovski@gf.ukim.edu.mk

B. Abolmasov
Faculty of Mining and Geology, University of Belgrade, Djusina 7, Belgrade, Serbia

There is a lot of assessment method and techniques in the practice which defines landslide hazard with a quantitative index as an output (Abolmasov and Stojkov 1995; Huma and Radulsecu 1978; Nefeslioglu et al. 2008; Varnes 1984).

In the present state of the art, the trend is to use GIS techniques and remote sensing methods in defining of landslide risks (Hazarika and Honda 2001; Milevski et al. 2009; Milevski et al. 2010).

According to author's opinion, all methods for map preparation can be classified as coverage and grid methods.

The coverage method is based on a selection of several parameters. For each parameter, a rating system can be defined, so that each parameter has several classes. This is followed by the creation of a coverage map for each parameter, and then creation of a map of intersection for all coverage maps. The result can be presented as a coverage map with attributes of total landslide hazard index.

The grid method usually uses more parameters than the coverage method does, since the map is handled as a grid rather than coverage. An array of ratings of each parameter is prepared for each grid cell on the map. Furthermore, the

C. Margottini et al. (eds.), *Landslide Science and Practice*, Vol. 1,
DOI 10.1007/978-3-642-31325-7_73,

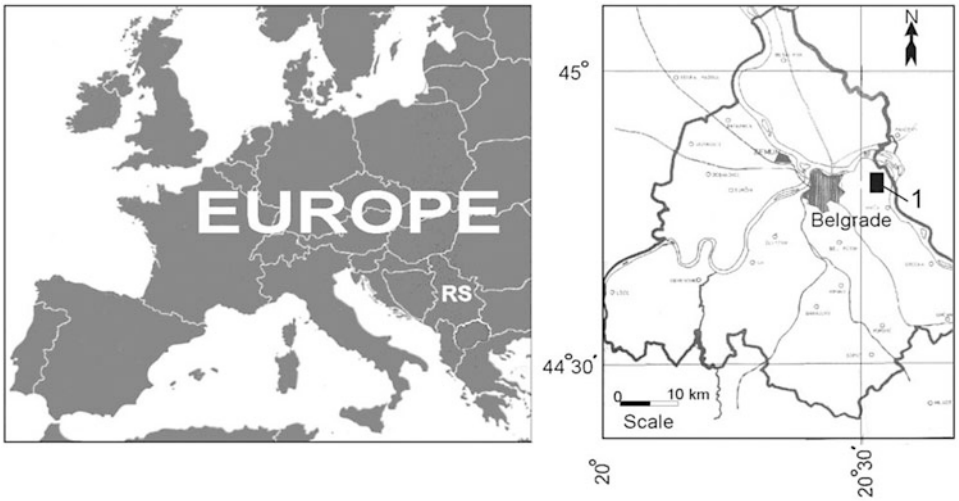

Fig. 1 Geographical position of the analyzed area: RS republic of Serbia; (1) area of presented LHZ map on a Figs. 4 and 5

elements of the array are used to calculate the landslide hazard index at the grid cell by predefined arithmetic calculations. Carrying out the calculation for each grid cell, we have a grid map having an index assigned to each grid cell.

However, it is clear that the degree of landslide hazard is considered relative since it represents the expectation of future landslide occurrence based on the conditions of particular area. Even with detailed investigation and monitoring, it is very difficult to predict landslide hazards in absolute terms.

In any case, it is necessary to prepare some calculations for each grid cell or representative areas. So, in a frame of this article, the basics of so-called polynomial interpolation method are presented. The main idea in developing of this method is to find a way to establish analytical correlations between any value of evaluation factor and its rating. The other goal is to remove impression that abrupt changes in rating occur between evaluation categories.

Authors believed that the given approach can help in a better and easier definition of Landslide Hazard Evaluation Factor and it can be useful for calculating of landslide hazard index at any grid cell or in representative areas for coverage maps by predefined arithmetic calculations.

Selection of Landslide Hazard Evaluation Factors

It is obvious that interpretation of the landslide occurrence requires an understanding of conditions and processes controlling landslides in the study area.

In the practice, known assessment procedures use few significant physical factors to estimate relative landslide hazard. Most of the methods usually take into account analyses of distribution of past landslides, type of bedrock, slope steepness and hydrologic factor (Varnes 1984; U.S. Geological Survey 1982). Some other methods use data about vegetation covering and field exposure of an area (Huma and Radulsecu 1978).

This approach uses 4 (four) Landslide Hazard Evaluation Factors (LHEF). The selection of these parameters is according to the detailed analyses of their influence on the stability of the terrain for the wider area of Belgrade, the capital of Republic of Serbia (Abolmasov and Stojkov 1995). Namely, for purposes of urban planning of Belgrade City, an extensive investigations were performed on an area of about 1,700 km^2. Maps at a scale 1:5,000 are used for engineering-geological mapping during the field campaign Latter, all geological, hydrogeological and data for surface processes were presented on the engineering-geological and landslide hazard zonation maps at a scale 1:20,000.

More precisely, the selected factors are related to the definition of the Lithological Type (LT), Ground Water Level (GWL), Slope Angles (SA) and Soil Debris Cover (SDC).

The geographic position of the investigated area is presented in Fig. 1.

It is important to mention that for regions with different geological, hydrological, vegetation cover conditions and regional seismicity, some other evaluation factors can be used, depending on their influence on the slope stability.

Definition of Ratings for Selected Landslide Hazard Evaluation Factors

Taking into consideration that the different parameters are not equally important for estimation of the Total Landslide Hazard Evaluation Factor (TLHEF), in this work, an approach has been used where the important ratings are related to the different values of individual evaluation factors. The ratings had been defined earlier (Abolmasov and Stojkov 1995), while here some minor changes have been done to the original values in order to insure smooth connection for analytical calculations.

Table 1 Maximal values for different evaluation factors

Classification parameter	Rating
SA	**3**
GWL	**3**
LT	**3**
SDC	**1**
Total (TLHEF)	**10**

Table 2 Range of values for Slope angle as evaluation factor

Slope angle (degrees)	Rating
0–5	0
5–10	1.5
10–15	2.3
15–20	2.8
20–25	2.9
>25	3

Table 3 Range of values for ground water level as evaluation factor

Ground water level (meters bellow surface)	Rating
<1	3
1–2	2.5
2–3	1.8
3–8	1
8–12	0.3
>12	0.1

Table 4 Range of values for soil debris cover as evaluation factor

Soil debris cover (thickness over bedrock in m)	Rating
<3	1
3–6	0.5
6–12	0.2
>12	0

Table 5 Range of values for Lithological type with arbitrary ratings

Lithological composition defined with Lithological type	Rating
1	**0**
2	**1.2**
3	**2**
4	**2.5**
5	**2.9**
6	**3**

The ratings have been determined using empirical approach, similar as in the recognized procedures for Rock Mass Classification methods (Bieniawski 1993) or as in the methods for defining of the Groundwater Vulnerability (Aller et al. 1987). A rating from 0 to 3 has been assigned for each evaluation factor. The maximal values for the used evaluation factors are presented in the Table 1, while the details for ratings for each class of evaluation factors are given in Tables 2, 3, 4, and 5.

It can be noted, that the presented numerical values for ratings can be speculative because they are defined according to the experience, but they are suitable for definition of relative landslide susceptibility of the analyzed area.

Analyzing the data from the Table 5, it can be seen that lithological composition of the bedrock is defined with adequate Lithological Type (LT). For this factor, it is necessary to find a way for connection with ratings. Arbitrary values were used from 1 to 6 as a basis for correlation with ratings for Lithological Types. So, the following types are differentiated:

1. Loose rocks with low shear strength and high deformability (clays and silts with high plasticity and with range of internal friction angle values of f = 10–15° and cohesion c = 0–10 kPa).
2. Loose detritial rocks or with a reduced degree of lithification, as clays with low plasticity, sandy clays, sandy silts (range of values for angle of friction f = 16–20° and cohesion c = 10–15 kPa).
3. Group of rocks with a reduced degree of lithification; soft rocks to hard soils as hard clays, compacted sands, and claylike gravels (range of values for internal friction angle of f = 21–25° and cohesion c = 15–30 kPa).
4. Group of rocks with a relatively reduced degree of lithification: marly clays, poorly cemented sandstones, marls, argillaceous shale, weathered schist's with range of values for angle of friction f = 26–35° and cohesion c = 30–50 kPa.
5. Group of consolidated rocks: soft to semi hard rocks (sandstones, calcareous marls, schist with favorable dip of foliation with range of values for angle of friction f = 36–45° and cohesion c = 50–100 kPa).
6. Hard magmatic, metamorphic or sedimentary rocks as granites, marbles, massive limestone and others, with range of values for angle of internal friction f >45° and cohesion c > 100 kPa.

The hydrogeological aspect is defined with Ground Water Level (GWL). The topography of the field is defined with a range of values of Slope Angles (SA), while the influence of disintegrated soil over bedrock with thickness of the Soil Debris Cover (SDC). Specific combinations of these factors are associated with differing degrees of landslide hazard. The sum of individual ratings gives a value for TLHEF.

All factors can be mapped, calculated, measured or assumed using different direct or indirect investigation methods.

The shear strength of each Lithological Type can be determined with laboratory testing, or using empirical approaches. For example, for Lithological Type 4, 5 and 6, the estimation of shear strength can be done using Hoek and Brown empirical strength criteria (Hoek and Brown 1997).

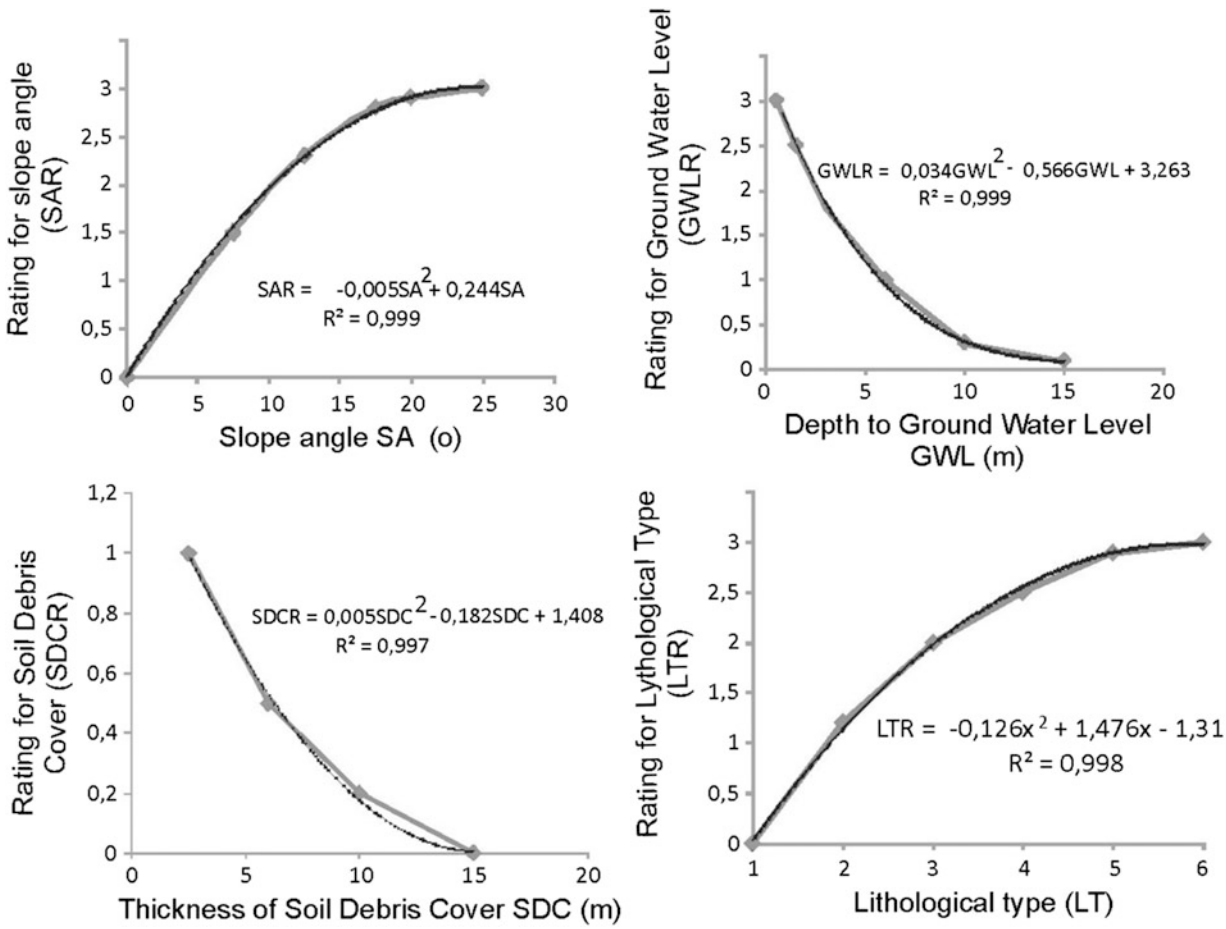

Fig. 2 Correlations between ratings for slope angle, ground water level, soil debris cover and lithological type and evaluation factor values using polynomial interpolation

If no data are available from direct investigation methods, the prognosis of Ground Water Level and Soil Debris Thickness can be done using data from detailed geological mapping, together with surface waters etc.

In this case, topographical maps at a scale 1:5,000 were the basis for geological mapping. Also, data from analyses of aerial photography, geophysical and drilling investigation techniques are used in a preparation of landslide hazard zonation maps.

It is important to note that some of these factors are periodic, thus determining various development stages for the landslide processes as well. The occurrence of a new stage of evolution presumes the influence of the preponderance either of the same factor or others.

Application of Polynomial Interpolation Method

The polynomial interpolation method, used for solving many problems in geotechnics, here applies for Landslide Hazard Zonation. Similar procedure with other classification parameters is presented by Bieniawski (1993) and Kuzelicki (1999).

The method is applied using the data from Tables 2, 3, 4 to 5. So, for all evaluation factors correlative curves are defined, with a main goal to have possibility to assign an adequate rating for all parameters. The established correlations between values for evaluation factors and ratings are presented with following equations:

$$SAR = -0.005SA^2 + 0{,}244SA \quad (1)$$

$$GWLR = 0{,}034GWL^2 - 0{,}566GWL + 3{,}263 \quad (2)$$

$$SDCR = 0{,}005SDC^2 - 0{,}182SDC + 1{,}408 \quad (3)$$

$$LTR = -0{,}126LT^2 + 1{,}476LT - 1{,}31 \quad (4)$$

where SAR, GWLR, SDCR and LTR are adequate calculate ratings for any value of indivudual parameters.

The determination coefficient for all cases has very high values ($R^2 = 0.998$ to $R^2 = 0.9999$) which indicates on very strong relation betweeen analysed parameters. Graphical

Table 6 Arbitrary values for Landslide Hazard Zonation Classes (LHZC) and connection with TLHEF

LHZ class	Value for TLHEF
0	**0**
1	**2.3**
2	**4.5**
3	**6.5**
4	**7.5**
5	**9**
6	**10**

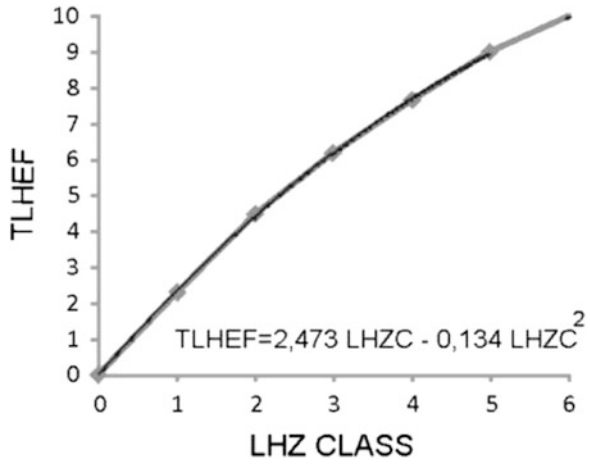

Fig. 3 Correlation between LHZC and TLHEF using polynomial interpolation

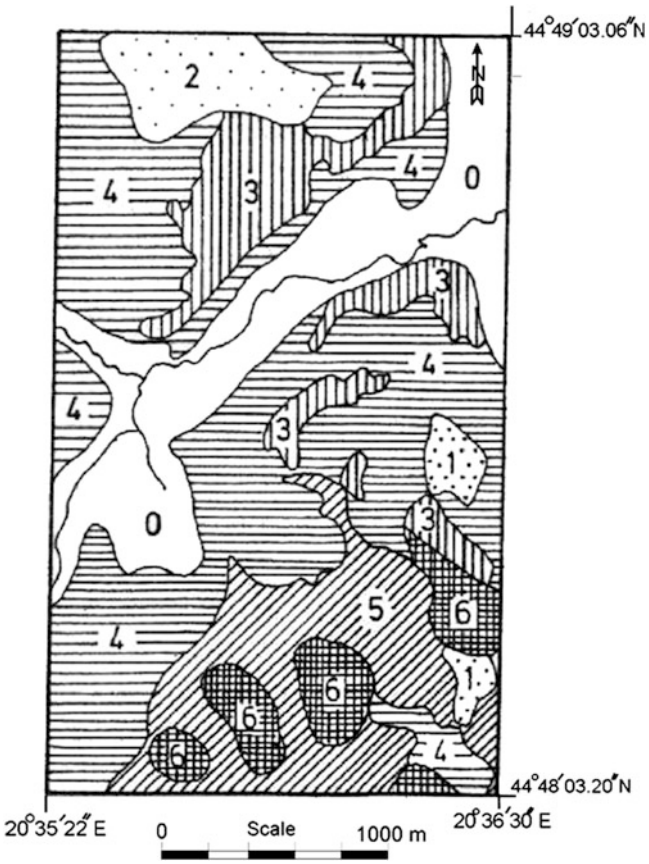

Fig. 4 Prepared LHZ map using classical coverage method, Abolmasov and Stojkov 1995

presentation of the defined polynoms in a form of interpolation charts is given in Fig. 2.

The numeration of Landslide Hazard Zonation Classes (LHZC) and adequate values for TLHEF is presented in Table 6.

The meaning of LHZ classes is according following categorization:

- Class 0 – Stable Zones;
- Class 1 – Zones with Very Low Hazard;
- Class 2 – Low Hazard;
- Class 3 – Middle Hazard;
- Class 4 – High Hazard;
- Class 5 – Very High Hazard;
- Class 6 is for Active landslides.

The defined interpolation chart for analytical connection between LHZC and TLHEF is presented in Fig. 3.

The established correlation is presented with the following equation:

$$TLHEF = 2{,}473LHZC - 0{,}134LHZC^2 \quad (5)$$

The presented equations can be used for different calculations necessary for a definition of the Landslide Hazard Zonation Classes and the Total Landslide Hazard Evaluation Factor.

Examples of LHZ Maps Using Classical Approach and Polynomial Interpolation Method

In order to demonstrate possible practical application of the presented analyses, one part of the whole analyzed area is presented in Figs. 4 and 5.

Consequently, the Fig. 4 gives an example of the prepared LHZ map with the classical coverage approach.

On the other hand, LHZ map prepared using calculations with polynomial approach and grid method is presented in the Fig. 5.

Both presentation give different view on LHZ map, evidently. Namely, the map in Fig. 4, gives better impression from a physical point of view. On the other hand, the map presented in Fig. 5 using grid method and defined correlations, is more practical for arithmetic and analytical calculations. Here, the isolines are main elements that

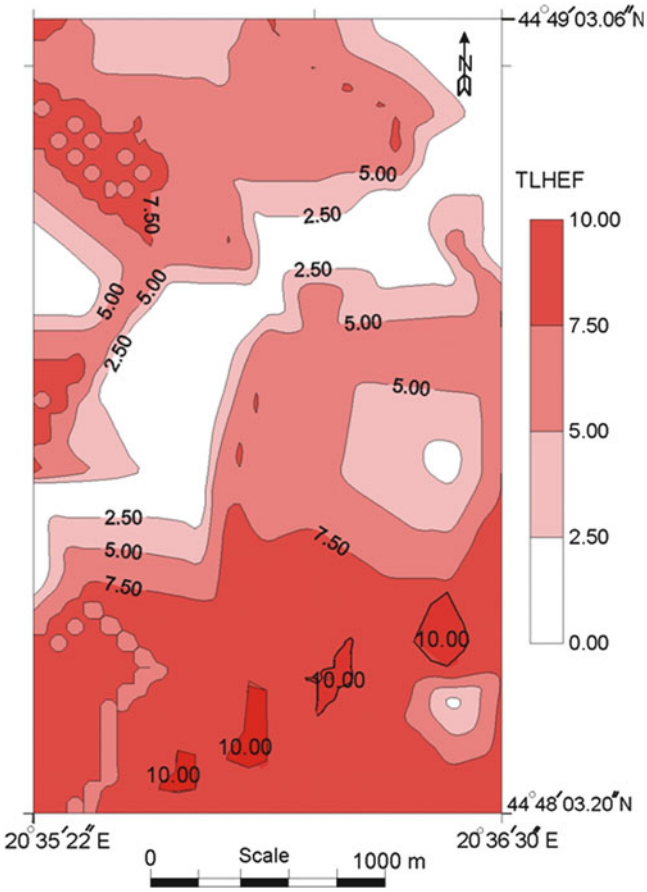

Fig. 5 Prepared LHZ map using grid method and polynomial interpolation

present the distribution of TLHEF in the investigated area. Using both methods in parallel in the practice can be suggested.

Conclusion

According to the analyses in this paper, the authors would like to emphasize that the method based on polynomial relations between the evaluation factors and the rating for parameters can be one of the possible approaches in the process of identification of potential risk of land sliding.

This approach can be used as a basis for preparation of LHZ maps with grid method.

The further development can be done in a sense to connect value of TLHEF with safety factor of slopes, as parameter which is used mostly in defining of stability of the terrain.

The philosophy of the methodology presumes dynamical, critical and evolutionary period due to the fact that this is an empirical approach based on certain level of experience. Therefore, it should be subjected to a critical review, and should be used in combination with other methods developed for this problem.

References

Abolmasov B, Stojkov K (1994) The influeunce on the landslide in urban planning in Belgrade City. In: Proceedings of VII IAEG Congress, vol III, Lisboa, pp 2161–2168

Abolmasov B, Stojkov K (1995) Jedan primer izrade karte mogucnosti pojave i razvoja klizanja. Drugi Simpozijum Istrazivanje i sanacija klizista, Donji Milanovac

Aller L, Bennett T, Lehr JH, Petty RJ, Hacket G (1987) DRASTIC – a standardized system for evaluating groundwater pollution potential using hydrogeological settings. US-EPA Report 600/2-87-035, Washington DC

Bieniawski ZT (1993) Classification of rock masses for engineering: the RMR System and future trends. In: Hudson JA (ed) Comprehensive rock engineering. Pergamnon Press, New York

Hazarika M, Honda K (2001) Estimation of landslide using remote sensing and GIS, its valuation and economic implication on agricultural products. In: Stott DE, Molnar RH, Steinhardt GC (eds) Sustaining the global farm, pp 1090–1093

Hoek E, Brown ET (1997) Practical estimates of rock mass strenght. Int J Rock Mech Min Sci Geomech Abstr 34(8):1165–1186

Huma I, Radulsecu D (1978) Automatic production of thematic maps of slope stability. Bull Int Assoc Eng Geol 17:95–100, Krefeld

Jovanovski M, Gjorgevski S, Dolenec JJ, Vckova K (2005) landslide in town Veles, from a natural hazrd to prevention. In: International symposium on latest natural disasters – new challenges for engineering geology, geotechnics and civil protection, Sofia, 5–8 Sept 2005

Kuzelicki R (1999) Primjena polinoma na ulazne parameter geomehanicke klasifikacije. Zbornik radova, Simpozijum Mehanika stijena i tuneli, Zagreb

Milevski I, Markoski B, Gorin S, Jovanovski M (2009) Application of remote sensing and GIS in detection of potential landslide areas. In: Proceedings of the international symposium geography and sustainable development, Ohrid, pp 453–463

Milevski I, Markoski B, Jovanovski M, Svemir G (2010) Landslide risk mapping by remote sensing and GIS in Gevgelija-Valandovo Basin. Geologica Balcanica, no. 39, Sofia, BAS, pp 255

Nefeslioglu HA, Duman TY, Durmaz S (2008) Landslide susceptibility mapping for a part of tectonic Kelkit Valley (Eastern Black Sea region of Turkey). Geomorphology 94(3–4):401–418

U.S. Geological Survey (1982) Goals and tasks of the landslide part of a ground-failure hazards reduction program. U.S. Geological Survey Circular 880. U.S. Geological Survey, Reston

Varnes D (1984) Landslide hazard zonation: a review of principles and practice. UNESCO Press, Paris

Landslide Susceptibility Mapping for Yadak-Tevil Watershed (Northeast Iran), Using AHP Method

Mohammad Ghafoori, Gholam Reza Lashkaripour, Naser Hafezi Moghaddas, and Safura Zamani

Abstract

Landslides form major natural hazards in hilly terrain in the area, and caused extensive damages to road, human dwellings and agricultural lands. There is still a great danger of further landslides in the region. Therefore, it is important to prepare a landslide susceptibility map of the region. In this study a landslide susceptibility map of Yadak-Tevil watershed was prepared using the Analytical Hierarchy Process (AHP) with the help of GIS. For this purpose, thematic layers including landslide inventory, lithology, distance from drainage, slope, slope aspect, and elevation were the main contributory factors to be considered for landslides susceptibility zonation. The landslide susceptibility map was classified into four different landslide susceptibility classes. The four landslide susceptibility classes are: low 16.13 % (33.50 km^2), moderate 33.34 % (69.38 km^2), high 33.00 % (68.68 km^2), and very high 17.53 % (36.48 km^2), respectively. Results of this study show that the AHP method is precise method for evaluation of landslide potential due to the use of binary comparison affecting factors and considering numerous factors for landslide evaluation at the same time in comparison to the other prevalent method.

Keywords

Landslide • Susceptibility • Watershed • Analytical Hierarchy Process

Introduction

Determining the extent of landslide hazard requires identifying those areas which could be affected by a damaging landslide and assessing the probability of the landslide occurring within some time period. Landslide hazard zonation has been actively pursued for the last two decades and various methodologies are still being refined. Several attempts (e.g.,Carrara 1983; Carrara et al. 1991; Chung and Leclerc 1994; Djamaluddin 1994; Chung and Fabbri 1995; Guzzetti et al. 1999; Zaitchik and van Es 2003; Lee and Pradhan 2007) have been made to estimate the degree of landslide susceptibility and provided some procedures for landslide prediction modeling and quantitative hazard zonation. Recently, there have been studies on landslide hazard evaluation using GIS, and many of these studies have applied different methods to analyze landslide and to create landslide susceptibility mapping. Lee and Pradhan 2007, have used logistic regression method to model landslide distribution. Lee et al. 2006 and Gupta et al. 2008 have shown better results from application of artificial neural network black box approach. Bivariate statistical approach was used by Yalcin (2008) to compare each individual factor and landslide distribution map to assign weighting value to the various parameter and finally to prepare a landslide hazard map. Analytical hierarchy process (AHP) was another procedure that was applied by Barredo et al. 2000, to deal with the paradoxical role of different factors in landslide occurrence.

Iran is heavily exposed to natural hazard such as earthquake, landslide, and floods. Landslide is one of the

M. Ghafoori (✉) • G.R. Lashkaripour • N.H. Moghaddas • S. Zamani
Department of Geology, Ferdowsi University of Mashhad, Mashhad, Iran
e-mail: ghafoori@um.ac.ir

C. Margottini et al. (eds.), *Landslide Science and Practice*, Vol. 1,
DOI 10.1007/978-3-642-31325-7_74,

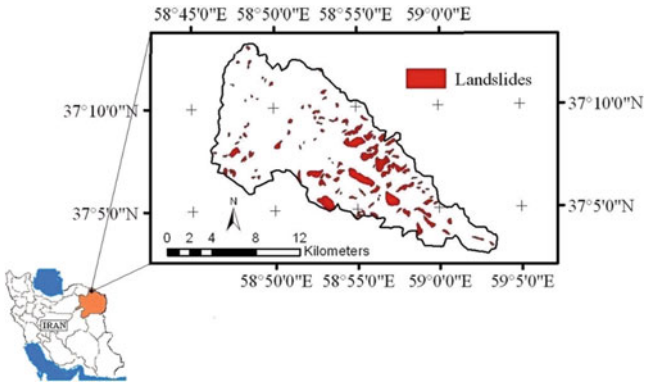

Fig. 1 A location map of the study area

most frequently occurring and devastating natural hazards in the mountainous region of Iran. They occur because of specific topographic and geological conditions (Lashkaripour and Ghafoori 2002). In hilly terrains of Iran, such as Yadak-Tevil watershed area in the Kopet-Dogh Basin, northeast of Iran, landslides are a major and widely spread natural hazards. In recent year, the population growth and the expansion of settlements over hazardous area have increased in the Kopet-Dogh Basin.

In this study, a landslide susceptibility map of the study area was prepared using AHP method with the help of the geographic information system. The study area occupies an area of about 208.1 km^2 and is located between N 37° 02′ to 37° 13′ and E 58° 46′ to 58° 03′ (Fig. 1).

Geology of the Study Area

Yadak-Tevil watershed area is located in a part of the Kopet-Dogh mountain physiographic province termed the Kopet-Dogh Basin. The Kopet-Dogh formed as an inter-continental basin in northeast of Iran and southwest of Turkmenistan (Berberian and King 1981), and contains more than 6,000 m thickness of Mesozoic and Cenozoic marine and fluvial sedimentary rocks. During the early Jurassic, an epicontinental sea transgressed (from NW to SE) across the study area and a thick series of siliclastic sediments was unconformably deposited over Triassic rocks in fluvial, deltatic and marine environments. The general stratigraphy of the Kopet-Dogh basin comprises 15 formations from mid Jurassic to Oligocene age (Fig. 2).

The watershed area is underlain by Quaternary deposits and rock units of Cretaceous age. A generalized geological map of the catchment site is shown in Fig. 3. This map shows the outcrops of the geological bedrock units and the various types of surficial deposits. They consist of the following stratigraphic formations.

Mouzdouran formation which refers to upper Jurassic time and it is mostly made of carbonate and dolomite stones.

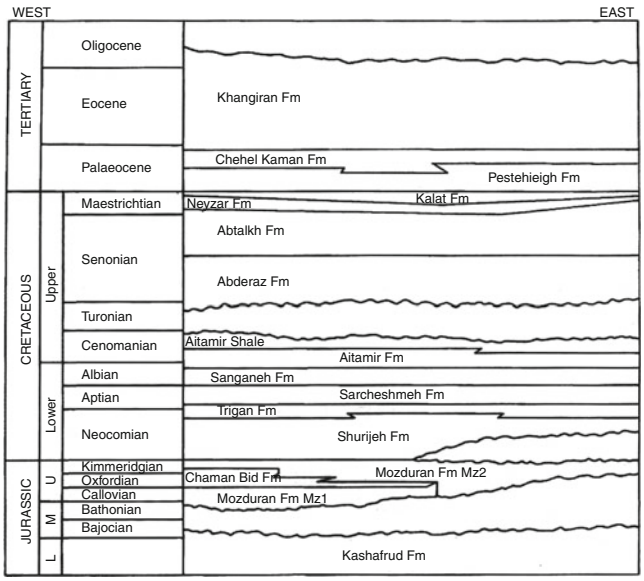

Fig. 2 General stratigraphy of the Kopet-Dogh basin (After Afshar-Harb 1979)

Shurijeh formation mainly consists of reddish brown shale, sandstone, and quartzite sandstone of Upper Jurassic and Lower Cretaceous age. The Tirgan formation, of early Cretaceous age, is mainly formed of oolitic and bioclastic limestone with subordinate layers of marl and calcareous shale that conformably overlies and underlies the Shurijeh and Sarcheshmeh formations, respectively. Rock falls are frequent in this region. The Sarcheshmeh formation consists of two members. The lower member is characterized by uniform light green-grey pencil type weathered marl. The upper member consists of alternating shale and thin layers limestone. This formation is moderately resistant to weathering, and form a distinct white-grey weathered unit between the ridge formed by the brown weathered Tirgan formation and slightly weathered dark grey to black Sanganeh formation. The Sanganeh formation is a uniformly weathered dark grey to black shale with few very thin, light brown weathered siltstone beds. Septarian and cone-in-cone concretions are present. This formation, with its dark color, is a distinct rock unit in the region and forms badland topography. Quaternary deposits are mainly represented by alluvial and debris flow materials. The alluvium is composed of clay, silt and rounded to sub-rounded coarse-grained materials, mixed with large angular rock blocks. These deposits fill synclinal valleys and flood plains. Part of the area is covered by terrace deposits exposed at varying elevations.

Rock fall, creep and soil slide are slide types that are recognized during site investigations in the area. Steep slope, joint, and abundant fissures in limestones of Tirgan formation which has covered a great part of the area, caused numerous rock falls in this area.

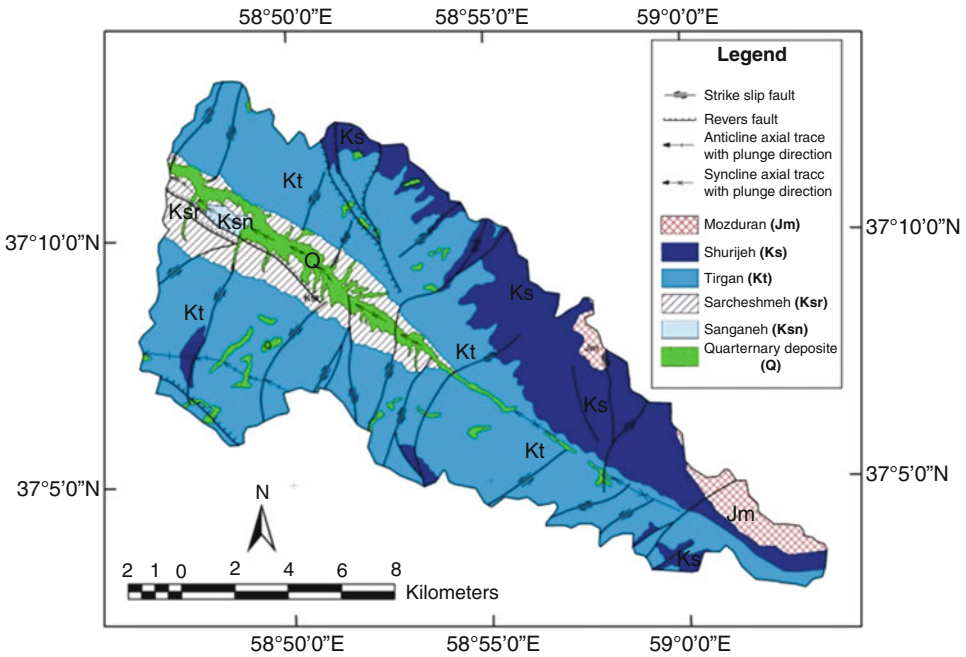

Fig. 3 Geology map of the study area

Rock falls were not considered in this paper. Therefore the study of creep and soil slide is only covered. Slide phenomenon is seen around the roads and in the alluvium. These alluviums contain a lot of clay and they are making more problems, especially in the parts which are cut by the road. The existing shale layers and marl of Sarcheshmeh formation underneath these alluviums are help to their slow movement.

Spatial Data Layers

In the present study, five factors namely, lithology, distance from drainage, slope, slope aspect, and elevation were considered to be the main contributory factors for landslides.

Thematic layers of the area, using topographic maps and published literature, were derived from the DEM with a 25 m cell size. The resultant grid of the study site has 759 rows and 1,034 columns. The total number of cells in the area is 332,974; the number of cells occupied by each category of all the factors was calculated to compute area density value in GIS. A digital elevation model (DEM) is the digital representation of a topographic surface with the elevation above a geodetic datum. The DEM of the study area was prepared from the contour information given in the topographic maps (in 1:25,000 scale) using ArcMap of ArcGIS 9.2 software. From this model, the maps showing slope and aspect were obtained. Lithology is a key parameter conditioning landslide occurrence because

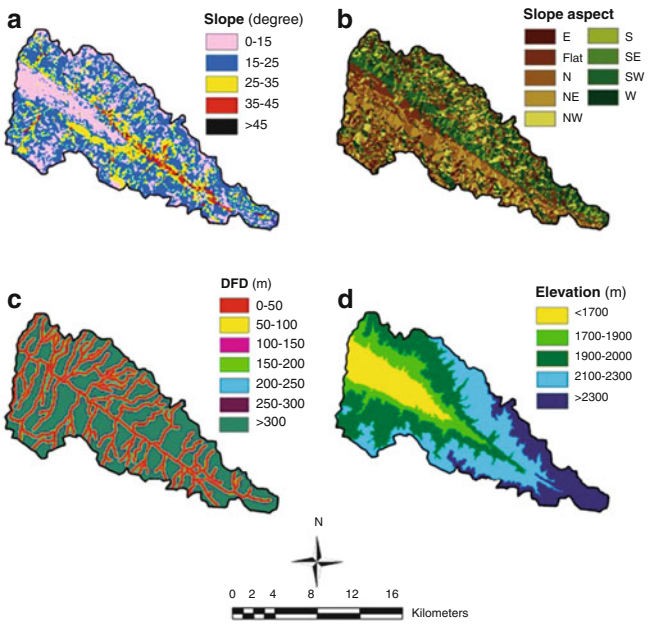

Fig. 4 The slope angle, slope aspect, distance from drainage and the elevation maps

different lithologic units have different sensitivities to active geomorphological processes such as landslides. The lithology layer has been derived through the digitization of the published geological maps (scale of 1:100,000) which display major rock groups and structural features. The slope angle, slope aspect, distance from drainage and the elevation maps are shown in Fig. 4.

Table 1 Pair-wise comparison matrix, factor weights and consistency ratio of the data layers

Factors	(1)	(2)	(3)	(4)	(5)	(6)	(7)	(8)	(9)	Weights
Lithology (formation)										
(1) Shurijeh	1	4	3	2	5	7				0.188
(2) Sanganeh		1	1/2	1/3	3	4				0.035
(3) Quaternary deposit			1	1	3	5				0.055
(4) Tirgan				1	3	7				0.068
(5) Sarcheshmeh					1	2				0019
(6) Mozduran						1				0.011
Slope angle (degree)										
(1) <15	1	1/3	1/4	1/5	1/2					0.018
(2) 15–25		1	1/2	1/3	2					0.048
(3) 25–35			1	1/2	2					0.072
(4) 35–45				1	3					0.118
(5) 45<					1					0.033
Slope aspect										
(1) NE	1	1	2	3	5	5	7	7	7	0.020
(2) SW		1	2	3	5	5	7	7	7	0.020
(3) N			1	2	3	5	7	7	7	0.014
(4) NW				1	3	2	5	5	5	0.009
(5) S					1	2	3	3	5	0.006
(6) SE						1	2	2	2	0.004
(7) E							1	1	1	0.002
(8) W								1	1	0.002
(9) Flat									1	0.002
DFD (m)										
(1) <50	1	2	2	3	3	3	8			0.065
(2) 50–100		1	1	2	3	3	8			0.045
(3) 100–150			1	1	2	3	8			0.038
(4) 150–200				1	1	2	7			0.028
(5) 200–250					1	1	7			0.022
(6) 250–300						1	6			0.018
(7) >300							1			0.005
Elevation (m)										
(1) <1,700	1	1/3	1/7	1/9	1/7					0.003
(2) 1,700–1,900		1	1/5	1/7	1/5					0.006
(3) 1,900–2,100			1	1/2	1					0.025
(4) 2,100–2,300				1	2					0.043
(5) >2,300					1					0.025

Analytical Hierarchy Process (AHP) for Landslide Susceptibility Mapping

The Analytical Hierarchy Process was developed at Wharton School of Business by Thomas Saaty 1980. The AHP overcomes the problems with arbitrary weights and scores approaches, by its ability to enable decision-makers to drive ratio scale properties or weights as opposed to arbitrary assign them (Yalcin 2007). Normally, the determination of the values of the parameters relative to each other is a situation that depends on the choices of the decision-maker. However, in this study, both the comparison of the parameters relative to each other and the determination of the decision alternatives, namely the effect values of the sub-criteria of the parameters (weight), were based on the comparison of landslide inventory maps constructed using aerial photos with the other data layers. Consequently the weight values were determined accurately for the real land data (Table 1). This is done by structuring complexity as a hierarchy and by deriving ratio scale measures through pairwise relative comparisons. AHP application for landslide susceptibility can be found in many applications (Chung and Leclerc 1994; Barredo et al. 2000; Ayalew et al. 2004; Komac 2006; Yalcin 2007). AHP is a multi-objective, multi-criteria decision-making approach which enables the user to arrive at a scale of preference drawn from a set of alternatives. AHP gained wide application in

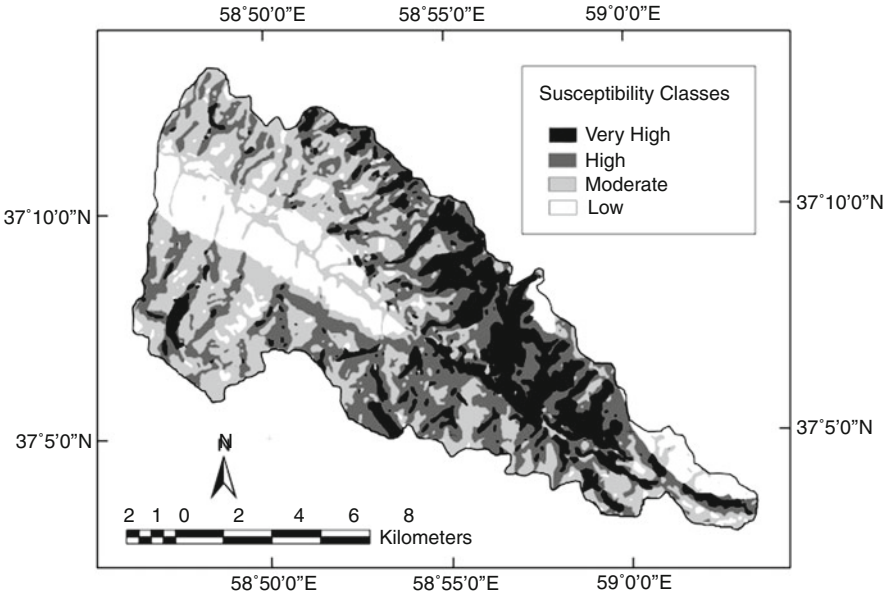

Fig. 5 Landslide susceptibility map of the study area

site selection, suitability analysis, regional planning, and landslide susceptibility analysis (Ayalew et al. 2005). In this study the AHP method was used for creating a map of landslide susceptibility zonation. In construction of a pairwise comparison matrix, each factor is rated against every other factor by assigning a relative dominant value between 1 and 9 to the intersecting cell (Table 1). These values are assigned by expert judgment to each pair of parameters yielding a square reciprocal matrix by rating rows relative to columns as shown in Table 1. When the factor on the vertical axis is more important than the factor on the horizontal axis, this value varies between 1 and 9. Conversely, the value varies between the reciprocals 1/2 and 1/9. In these techniques, firstly, the effects of each parameter to the susceptibility of landslides relative to each other were determined by dual evaluation in determining the preferences in the effects of the parameters to the landslide susceptibility maps. In this study, spatial databases were used, obtained as a result of the field, laboratory and office studies carried out to create landslide susceptibility maps. As a result of these analyses, the landslide susceptibility map was produced for the Yadak-Tavil region (Fig. 5). The landslide susceptibility map was classified into four different landslide susceptibility classes as shown in Fig. 5. The four landslide susceptibility classes are: low 16.13 % (33.50 km^2), moderate 33.34 % (69.38 km^2), high 33.00 % (68.68 km^2), and very high 17.53 % (36.48 km^2), respectively.

Discussion

This study includes method and application devoted to the construction of a landslide susceptibility map for Yadak-Tevil watershed, where landslides constitute an important natural hazard affecting not only the landscape but also human developments. The selection of a proper assessment method and the use of suitable parameters that affect landslide occurrence in the studied area are two important points that should be considered. When selecting the assessment method, existing data and their practibility to the method selected should be considered. However, the selection of the proper landslide-conditioning parameters plays an important role in a sensitive landslide susceptibility assessment.

In the study area using the weight values calculated by the pair wise matrix and assigning these weights to the relevant parameters, the weighted parameters were produced. By overlying these weighted parameters using a weighted linear combination method, the landslide susceptibility map was obtained. When examining this map, the southeastern part of the study area was revealed more prone to landslide occurrence. The reason for this is the presence of lithologies that are susceptible to landsliding due to their level of weathering, sensitive topography, and additional factors such as land use and land cover.

Conclusion

There are various possible causes for landsliding, with complex inter-relationships. Therefore, accurate landslide susceptibility mapping on a regional scale strongly depends on the selection of landslide causative factors, which can be quite different according to various researchers. In this study, the analytical hierarchy process (AHP) was used to develop landslide susceptibility map for the Yadak-Tevil watershed in Khorasan Razavi Province, in northeastern part of Iran. To achieve this objective, five landslide inducing factors were taken into consideration, which are the lithology, distance from drainage, slope, slope aspect, and elevation. The four

landslide susceptibility classes of the landslide susceptibility map of the AHP approach give 16.13 %, 33.34 %, 33.00 %, 17.53 %, for respectively low, moderate, high, and very high susceptibility. This study shows that when field conditions and characteristics are correctly determined by good expertise, the AHP's approach gives better results.

References

Afshar-Harb A (1979) The stratigraphy, tectonics and petroleum geology of the Kopet Dagh region, northern Iran. Unpublished Ph.D. thesis, Imperial College of Science and Technology, London

Ayalew L, Yamagishi H, Ugawa N (2004) Landslide susceptibility mapping using GIS-based weighted linear combination, the case in Tsugawa area of Agano River, Niigata prefecture, Japan. Landslides 1:73–81

Ayalew L, Yamagishi H, Marui H, Kanno T (2005) Landslides in Sado Island of Japan: Part II. GIS-based susceptibility mapping with comparisons of results from two methods and verifications. Eng Geol 81:432–445

Barredo JI, Benavides A, Hervas J, van Westen CJ (2000) Comparing heuristic landslide hazard assessment techniques using GIS in the Tirajana basin, Gran Canaria Island, Spain. Int J Appl Earth Obs Geoinf 2(1):9–23

Berberian M, King GCP (1981) Towards a palaeogeography and tectonic evolution of Iran. Can J Earth Sci 18:210–265

Carrara A (1983) A multivariate model for landslide hazard evaluation. Math Geol 15:403–442

Carrara A, Cardinalli M, Detti R, Guzetti F, Pasqui V, Reichenbach P (1991) GIS techniques and statistical models in evaluating landslide hazard. Earth Surf Proc Landf 16(5):427–445

Chung CF, Fabbri AG (1995) Multivariate regression analysis for landslide hazard zonation. In: Carrara A, Guzetti F (eds) Geographical information systems in assessing natural hazards. Kluwer Academic, Dordrecht, pp 107–142

Chung CF, Leclerc Y (1994) A quanititative technique for zoning landslide hazard. In: International association for mathematical geoloogy annual conference, Mont Tremblant, QC, pp 87–93

Djamaluddin R (1994) Application of remote sensing and GIS to mass movement hazard zonation in West Java, Indonesia. In: 10th thematic conference on geologic remote sensing, vol 1, pp 375–384

Gupta RP, Kanungo DP, Arora MK, Sarkar S (2008) Approaches for comparative evaluation of raster GIS-based landslide susceptibility zonation maps. Int J Appl Earth Obs Geoinf 10(3):330–341. doi:10.1016/j.jag.2008.01.003

Guzzetti F, Carrara A, Cardinali M, Reichenbach P (1999) Landslide hazard evaluation: a review of current techniques and their application in a multi-scale study, Central Italy. Geomorphology 31:181–216, Elsevier

Komac M (2006) A landslide susceptibility model using the analytical hierarchy process method and multivariate statistics in perialpine Slovenia. Geomorphology 74(1–4):17–28

Lashkaripour GR, Ghafoori M (2002) The engineering geology of the Tabarak Abad Dam. J Eng Geol 66:233–239

Lee S, Pradhan B (2007) Landslide hazard mapping at Selangor, Malaysia using frequency ratio and logistic regression models. Landslides 4:33–41

Lee S, Ryu JH, Lee MJ, Won JS (2006) The application of artificial neural networks to landslide susceptibility mapping at Janghung. Math Geol 38(2). doi:10.1007/s11004-005-9012-x

Saaty TL (1980) The analytical hierarchy process. McGraw Hill, NewYork

Yalcin A (2007) GIS-based landslide susceptibility mapping using analytical hierarchy process and bivariate statistics in Ardesen (Turkey). Catena 72(1):1–12

Yalcin A (2008) GIS-based landslide susceptibility mapping using analytical hierarchy process and bivariate statistics in Ardesen (Turkey): comparisons of results and confirmations. Catena 72:1–12

Zaitchik BF, van Es HM (2003) Applying a GIS slope-stability model to site-specific landslide prevention in Honduras. J Soil Water Conserv 58(1):45–53

Topographic Data and Numerical Debris-Flow Modeling

Jošt Sodnik, Tomaž Podobnikar, Urška Petje, and Matjaž Mikoš

Abstract

The digital elevation models (classical DEM 5 and DEM 12.5), publically available in Slovenia, have been evaluated as a basis to prepare numerical square grids 5 × 5 m for 2D modeling of possible debris flows on torrential fans, using the model Flo-2D. Also recently available LiDAR data in their original resolution have been used, as well as their decreased resolution to the one of the numerical grid (e.g. 5 × 5 m). From our numerical results it seems obvious that the use of more precise LiDAR data over classical DEMs for numerical debris-flow modeling is fully justified. Better quality of input topographic data assures higher accuracy of results and therefore also accuracy of hazard maps produced in such a way. The LiDAR data promises better representation of torrential channels on torrential fans (narrow, deep channels) and computed results (velocities, depths) are generally better estimated. Using more precise data also increases computational times compared to using classical DEMs.

Keywords

Debris flows • Hazard mapping • Numerical modeling • Roughness • Sensitivity analysis • Topography

Introduction

Debris flows are a disastrous type of landslides occurring occasionally in many places of the world, triggered mainly by earthquakes, heavy short-termed rainfalls, caused by typhoons, cyclones, and thunderstorms, and prolonged steady rainfall.

In some countries, debris-flow hazard assessment is regulated by national or local legislation. Different methods may be used, but there are some common bases for the procedures used. Debris-flow hazard assessment may be just in a written form (debris-flow scenarios, estimation of damages) or in a cartographic form (hazard maps with several hazard zones shown in different scales). In any case, source areas of future debris flows should be recognized, and a step towards that is a susceptibility map of debris flows. Such a map will help to estimate real debris flow hazard only if a realistic debris-flow scenario is assumed. Part of such a scenario is not only recognition

J. Sodnik (✉) • U. Petje
Vodnogospodarsko podjetje Kranj, Ulica Mirka Vadnova 5, Kranj 4000, Slovenia

Faculty of Civil and Geodetic Engineering, University of Ljubljana, Ljubljana, Slovenia
e-mail: jost.sodnik@vgp-kranj.si

T. Podobnikar
Scientific Research Centre of the Slovenian Academy of Sciences and Arts, Ljubljana, Slovenia

Faculty of Civil and Geodetic Engineering, University of Ljubljana, Ljubljana, Slovenia

M. Mikoš
Faculty of Civil and Geodetic Engineering, University of Ljubljana, Ljubljana, Slovenia

C. Margottini et al. (eds.), *Landslide Science and Practice*, Vol. 1,
DOI 10.1007/978-3-642-31325-7_75,

of a source area but also estimation of a debris-flow magnitude. In many cases such magnitudes can only be empirically determined on the basis of historical data available in the region. Why do we need an estimation of a debris-flow magnitude? This is in a way needed to estimate realistic run-outs and delineate safe areas from endangered ones.

If we want to separate endangered areas into several hazard zones according to chosen debris-flow parameter values (i.e. flow depths and flow velocities), we should step away from empiric run-out determination and use mathematical modeling to determine hazard areas. If we want to do that we need furthermore specific rheological characteristics of the debris material and a very good representation of the terrain (slope surface, torrential fan, and torrential channel).

In the last years, precise topographic data, such as LiDAR data, were made broadly available. In Slovenia, a systematic gathering of LiDAR data is still under way. Therefore, one may ask a question, what the benefits of this new technology are over classical digital elevation models (DEMs) developed in the recent past and that have found wide acceptance and numerous applications.

In the field of hydromorphological alpine hazards:

- Scheidl et al. (2008) used LiDAR data to estimate magnitudes of debris-flow events in Switzerland,
- Cavalli and Marchi (2008) used LiDAR technology to characterize surface morphology of a small alpine alluvial fan in Eastern Italian Alps,
- Conway et al. (2010) used LiDAR technology in NW Iceland to study very recent debris-flow events and to derive a simple empirical model that allows future debris-flow characteristics to be predicted without the need to determine the precise fluid dynamic flow parameters (viscosity, velocity), which are required to implement more complex models, to be used,
- Lopez Saez et al. (2011) combined aerial LiDAR data and tree-ring data to reconstruct debris-flow activity in abandoned channels in French Prealps, and
- Bull et al. (2010) applied differenced LiDAR data to a debris flow event to demonstrate potential of this technique as a precise and powerful tool for hazard mapping and assessment.

The classical DEMs, as well as the ones developed from LiDAR data can be used for a debris-flow post-event analysis. A well-defined topography is also needed when establishing debris-flow hazard maps. Further topography improvement can be achieved using other techniques (i.e. radar interferometry) and by different topographic data handling and integration by so-called data fusion.

Fig. 1 The ortophoto of the Koroška Bela torrential fan, used as a test area for 2D debris-flow numerical modeling

Materials and Methods

Test Area: The Koroška Bela Torrential Fan

The Koroška Bela torrential fan in NW Slovenia (Fig. 1) covers 1.02 km^2 with numerous houses and 2,200 residents (high damage potential). The torrential watershed area is 6.4 km^2 with average slope of 52 % and height difference of 570 m. In the headwaters there is an active landslide that might under unfavorable conditions turn into a debris flow. In 1789, a large debris flow on the fan ruined 40 houses and several mills (Jež et al. 2008).

Debris-Flow Model Description

We used for debris-flow modeling a commercial model Flo-2D that has been applied successfully several times in Slovenia for these purposes (Mikoš and Majes 2010), i.e. in Log pod Mangartom (Četina et al. 2006), in Koseč (Mikoš et al. 2006), for the official determination of the risk area due to potential debris flows in Log pod Mangartom (Mikoš et al. 2007), and for a potential debris flow in Kropa (Sodnik and Mikoš 2006, 2010).

Flo-2D (O'Brien 2011) is software for two-dimensional mathematical modeling of water movement and fast flowing slope processes including debris flows. This model is in the USA a software tool recommended by the Environmental

Protection Agency (EPA) for analysis of natural hazards that found wide usage in many countries. Modeling is based on physical laws of the flow and is useful under different geographical conditions – the specialties of each single treated problem are taken into account by selecting different model coefficients and, of course, by the input of topographic data. For the description of the area geometry the model uses the numeric grid made out of quadratic cells of selected size. Water flow respectively debris-flow modeling depends on the form of the computing model as well as on the roughness of each computing cell. A very important role when modeling movement of debris flows is also given to rheological parameters of a water-debris mixture that are into more detail described in continuation of this paper. The basic model equations in all directions (shown here are only equations for the x-direction) are the continuity equation:

$$\frac{\partial h}{\partial t} + \frac{\partial h V_x}{\partial x} = i \tag{1}$$

and the dynamic equation:

$$S_{fx} = S_{0x} - \frac{\partial h}{\partial x} - \frac{V_x}{\partial x}\frac{\partial V_x}{\partial x} - \frac{V_x}{g}\frac{\partial V_x}{\partial x} - \frac{1}{g}\frac{\partial V_x}{\partial t} \tag{2}$$

where h is flow depth [m], V_x is depth-averaged flow-velocity component in the *x-direction [m/s]*, S_{fx} is slope of energy line or simply the total friction slope [−], and S_{ox} is the channel (relief) slope [−]. Part of the equations are also pressure gradient i [−] and local flow accelerations.

The dynamic equation is used in such a way that we compute the depth-averaged flow velocity in each computing cell separately for eight directions (similarly as the directions in the sky are defined; a similar procedure named the D8 algorithm is used for modeling rock falls on slopes; Petje et al. 2005). The velocity in each direction is computed as one-dimensional quantity not-dependent on the other velocities. The stability of the computing numerical scheme is assured by selecting a correspondingly short computing step as a function of the selected computing cell size.

Other Parameters of the Model

Besides topography data and inflow hydrograph with volume concentration and rheological parameters we had to define other model parameters like: computational grid element size, control parameters of the model, manning roughness coefficient and inflow hydrograph position. For better comparison between different topographical data we left all other parameters similar for all the models. Defined values (settings) are: Control parameters (Surface detention 0.03, Percent change in flow depth 0.200, Dynamic wave stability coefficient 5.00), Manning roughness coefficient (forest 0.16, meadow 0.033, building area 0.2, and torrential channel 0.13), computational grid size (5 × 5 m), and inflow hydrograph was positioned on the peak of the fan.

Topographical Data Preparation

The digital elevation models are basically recorded as raster layers in 2.5D, with one attribute of elevation (Podobnikar 2005, 2009). The 3D DEM production requires much more complex structure and modelling, especially when using very detailed laser scanning-based (LiDAR) data. In our case the solution of the problem requires only 2.5D DEMs that are realised as raster data sets where each square cell contains an elevation value.

Quality of the DEMs has been considerably increased during the last years and consequently more advanced applications based on DEM-analysis are used, e.g., for enhanced morphometric analysis of floods or debris flows (Podobnikar 2009). The quality of any spatial analysis that is based on a DEM depends greatly on its geometrical and, especially, on morphological accuracy. However, due to its complexity, the primary challenge is to produce a high quality DEM according to well defined nominal ground (data model), ideally without errors and in an appropriate resolution. Many acquisition methods – especially contemporary ones through LiDAR or radar interferometry are relatively fast and can offer quality data sources.

Four DEMs were applied in our study: DEM 12.5, DEM 5, DEM 0.5 and DEM5 derived from DEM0.5 (Table 1). The first two are property of Surveying and Mapping Authority of the Republic of Slovenia (public available data) and the second two of the Flycom Company.

The DEM 12.5 was produced by appropriately fusion of various existing data sources of different quality, where their semantically and qualitatively best properties were exposed (Podobnikar 2005, 2010). The final DEM is overall of better quality than any of the used data sources. The method of weighted sum of sources with morphologic enhancement includes iterative repeated processes where the experiences and evaluations of the procedures and results acquired from previous steps provide a better starting-point for each of the subsequent steps. Such iterative process takes more time, however it was rationally finished within two loops. The principal steps for such DEM production are: (1) mosaicking selected data sources to produce a principal DEM, (2) weighted sum of secondary data sources, (3) (geo)morphologic enhancement, and (4) reference point consideration in the modeling. Different aspects of quality were continuously monitored trough the process. The final product was an optimised DEM that considered different properties of landform, geometrical and morphological accuracy, and wide range of users and applications. The DEM is somewhat universal for many different users' requirements.

Table 1 Characteristics of the DEMs used in this study

Name (produced)	Accuracy (RMSE)	Production method
DEM 12.5 (2001–2005)	3.8 m	Fusion of existing geodetic datasets of different type/quality
DEM 5 (2006–2007)	3.5 m	Resampling of DEM 12.5 + stereo photogrammetry and local adjusting with CAD-tools
DEM 0.5 (2009–2010)	5–10 cm[a]	Datasets of 12 blocks (leaves and snow); different approaches to filtering and interpolation
DEM 5 from DEM 0.5 (2010)	5–10 cm[a]	Resampling of DEM 0.5

[a]In channels gross errors >1 m

The DEM 5 was produced by simply resampling the DEM 12.5, and with further improving the geometrical accuracy on the areas where the previous RMSE was considerably significant (Podobnikar 2008). Aerial photographs and principles of stereo photogrammetry were applied. The areas with significant RMSE were locally adjusted using CAD-tools. The final DEM 5 is geometrically of higher quality than the DEM 12.5, but is quite inhomogeneous with low morphological accuracy (Sodnik et al. 2009). This DEM is unfortunately not very promising for any geomorphometric spatial analysis, i.e. for debris flow modeling, due to its spatial variability in quality.

The DEM 0.5 was captured as a fullwave point cloud in two different periods (2009-05-08 and 2010-04-11), when some snow cover was present in the high mountains and leaves were present on most trees in the lower parts of the study area. Both of these facts make difficulties for the DEM generation. Point density was inhomogeneous, and ranged from 1 to 10 points/m^2. The vertical angle of scanning was 0° to ±30° with laser scanner Litemapper LM 5600 (alias Riegl LMS-Q560). Orthophotos with a resolution of 0.5 m were acquired together with the scanning. The final DEM of 0.5 m resolution was produced with Terrasolid software. The result is not perfect. The problem was reconstruction of a surface of the bare ground on the areas with canopies with leaves and buildings, but especially on the areas with streams. The main problems for our debris flow simulation are the areas of streams and their surroundings. Most problematic are stream areas where alluvial plane is covered with canopies with leaves and buildings located just along the streams. Less important, but obvious errors occur due to rough mountain landscape. The produced DEM 0.5 needs further improvement by including more advanced filtering and possible combination and fusion of other data sources. An additional model for the debris flow simulation will be produced, i.e. a digital surface model (DSM) as combination of the DEM 0.5 and buildings (required is LOD 0).

All DEMs were resampled to resolution of 5 and 12.5 m using two interpolation approaches. In case of interpolation to lower resolution a bilinear interpolation was applied and in case of interpolation to higher resolution a spline interpolation with filtering was applied.

Table 2 Computational times on an average PC (3.0 GHz dual-core processor) for 15-min simulation time

Model name	DEM used	Computational time
BelaLF7	Classical DEM 12.5	1.9 h
BelaLF6	Classical DEM 5	2.8 h
BelaLF8	LiDAR DEM 0.5	32 h
BelaLF5	LiDAR DEM 5	26 h

Results and Discussion

Modeled Debris-Flow Event Scenario

There is only one written description of past events (the 1789 event), and there are no reliable debris flow magnitude estimations for Koroška Bela torrent. The 100-year peak discharge is 55 m^3/s. We chose a 15-min potential event with a peak discharge of 250 m^3/s and with volume concentration C_v of 0.42. The total magnitude of the potential debris flow event in the study is 155,500 m^3 (water + debris). The event scenario is defined with inflow hydrograph on the peak of the fan. When defining the debris flow scenario, besides peak discharge (inflow hydrograph) we have to define also rheological characteristics of the mixture. Since for a potential debris flow in the test region we do not have precise material rheological data from past debris flow events, we used parameter values gathered when calibrating Flo-2D model for other recent debris flow cases in Slovenia: critical shear stress 20Pa, and Bingham viscosity 19Pa.s for $C_v = 0.42$ (Četina et al. 2006). The goal of the studied models is to test the importance of topographic data used in the model. Apart from the accuracy of the results, also computational times of the Flo-2D models differ a lot with different data (Table 2).

The maximum flow depths of the studied models are shown in Fig. 2. In Fig. 2a the lack of morphologic accuracy of the classic DEM 5 is shown. In the upper part of the fan the torrential channel, 5–7 m wide on average, is poorly expressed. The flow overbanks and the depths all over the fan are practically the same. In the model with DEM 12.5 (Fig. 2b) the channel is more explicit but made wider than in nature due to the DEM resolution. The inundated areas of both models are generally the same. But comparison

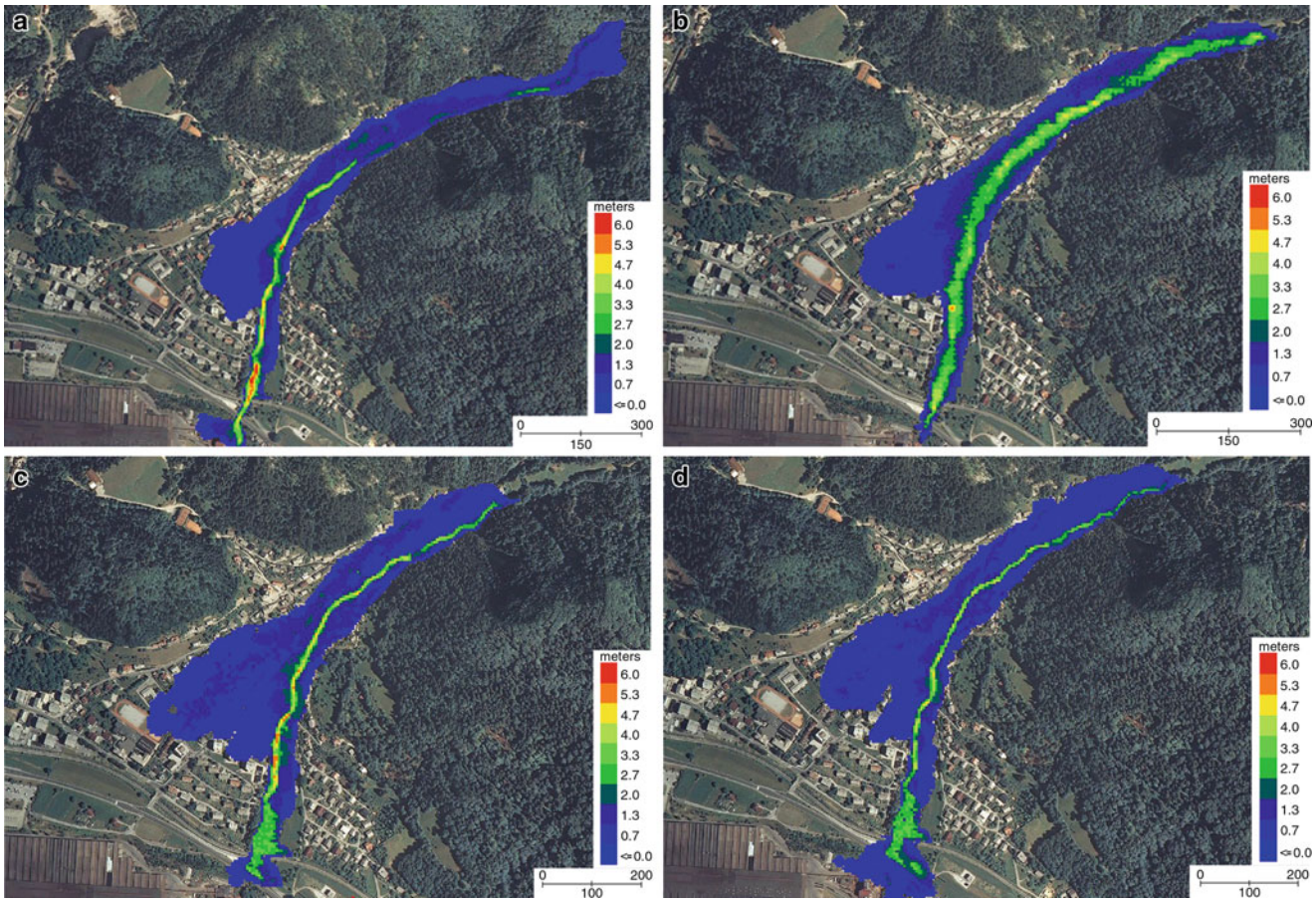

Fig. 2 Comparison of 2D modeling (maximum flow depths in m, uniform scale) using: (**a**) classical DEM 5; (**b**) classical DEM 12.5; (**c**) DEM 0.5 (original LiDAR data); (**d**) DEM 5 (re-sampled LiDAR data); on the Koroška Bela torrential fan

between Fig. 2a and b shows that despite of poor resolution the DEM 12.5 is morphologically more correct and more useful for preliminary hazard assessment. Using DEM 5 in our test area would derive a hazard map with an underestimation of the hazard in the upper part of the fan.

In Fig. 2c, d the comparison between the LiDAR-derived DEM 0.5 and DEM 5 is shown. In both cases the result is geomorphologically more correct (looking at the channel width, even though the channel is rather non-homogenous due to errors in zones covered with broad-leafed trees) than in case of the classic DEM 5 and DEM 12.5. Also the inundation areas are better represented when using LiDAR-derived DEMs. The modeled flow depths outside of the channel are more heterogeneous, because the surface is more agitated due to better topographical input data. In this case the hazard map in the inundated area is more precise. Intercomparison between the models with LiDAR derived DEMs (Fig. 2c, d) shows that the main difference is the modeled flow depth in the inundation areas outside of channel. The model with DEM 0.5 (grid cell height interpolation integrated in a Flo-2D) derives bigger differences in flow depths in the inundation area when compared to LiDAR derived DEM 5 (bilinear interpolation) which leads to more precise hazard mapping.

Conclusions

From our numerical results it seems obvious that the use of more precise LiDAR data for numerical debris-flow modeling is justified, even if using LiDAR derived DEM 5 instead of classical DEM 5. Better morphological quality of input topographic data assures higher accuracy of the results and therefore also of the resulting hazard maps. The LiDAR data promises better representation of torrential channels on torrential fans (narrow, deep channels) and computed results (velocities, depths) are generally better estimated and therefore delineation of a hazard area into corresponding zones is of higher accuracy for a selected debris-flow scenario. Nevertheless, LiDAR derived data can be potentially further improved, especially in morphological sense.

It also has to be noted that higher resolution topographic data means much longer computational times (not a real problem anymore). For delineation of hazard areas the magnitude of potential debris flow has to be estimated

with reasonable certainty, because magnitude, beside topographic data, is one of the most important input data for the model and hazard map preparation.

In 2011, a systematic gathering of LiDAR data in Slovenia is under way; it is rather questionable if the data density (5 m^{-2} on average) will serve all possible applications, including numerical debris-flow modeling.

Acknowledgments We worked within the EU research project PARAmount (www.paramount-project.eu), financially supported by the European Regional Development Fund (ERDF) and by the Research Agency of Slovenia (grant P2-0180 "Hydrotechnics, hydraulics, and geotechnics"). The digital elevation data were kindly provided by the Surveying and Mapping Authority of the Republic of Slovenia and the LiDAR data by the Flycom Company.

References

Bull JM, Miller H, Gravley DM, Costello D, Hikuroa DCH, Dix DK (2010) Assessing debris flows using LIDAR differencing: 18 May 2005 Matata event, New Zealand. Geomorphology 124(1–2):75–84

Cavalli M, Marchi L (2008) Characterisation of the surface morphology of an alpine alluvial fan using airborne LiDAR, Nat Hazards Earth Syst Sci 8(2):323–333. http://www.nat-hazards-earth-syst-sci.net/8/323/2008/

Četina M, Rajar R, Hojnik T, Zakrajšek M, Krzyk M, Mikoš M (2006) Case study: numerical simulations of debris flow below Stože, Slovenia. J Hydraul Eng 132(2):121–130

Conway SJ, Decaulne A, Balme MR, Murray JB, Towner MC (2010) A new approach to estimating hazard posed by debris flows in the Westfjords of Iceland. Geomorphology 114(4):556–572

Jež J, Mikoš M, Trajanova M, Kumelj Š, Budkovič T, Bavec M (2008) Vršaj Koroška Bela – Rezultat katastrofičnih pobočnih dogodkov = Koroška Bela alluvial fan – The result of the catastrophic slope events (Karavanke Mountains, NW Slovenia). Geologija 51(2):219–227

Lopez Saez J, Corona C, Stoffel M, Gotteland A, Berger F, Liébault F (2011) Debris-flow activity in abandoned channels of the Manival torrent reconstructed with LiDAR and tree-ring data. Nat Hazards Earth Syst Sci 11(5):1247–1257

Mikoš M, Majes B (2010) Mitigation of large landslides and debris flows in Slovenia, Europe. In: Werner ED, Friedman HP (eds) Landslides: causes, types and effects. Nova Science Publishers, New York, pp 105–131. ISBN 978-1-60741-258-8, eISBN 978-1-61470-186-6

Mikoš M, Majes B, Fazarinc R, Rajar R, Žagar D, Krzyk M, Hojnik T, Četina M (2006) Numerical simulation of debris flows triggered from the Strug rock fall source area, W Slovenia. Nat Hazards Earth Syst Sci 6(2):261–270

Mikoš M, Fazarinc R, Majes B (2007) Delineation of risk area in Log pod Mangartom due to debris flows from the Stože landslide. Acta Geogr Slov 47(2):171–198

O'Brien J (2011) FLO-2D Reference manual, version 2009. http://www.flo-2d.com/wp-content/uploads/FLO-2D-Reference-Manual-2009.pdf. 6 June 2011

Petje U, Mikoš M, Ribičič M (2005) Computer simulation of stone falls and rockfalls. Acta Geogr Slov 45(2):93–120. http://giam.zrc-sazu.si/zbornik/05_AGS_45-2_PetjeRibicicMikos.pdf

Podobnikar T (2005) Production of integrated digital terrain model from multiple datasets of different quality. Int J Geogr Inf Sci 19(1):69–89

Podobnikar T (2008) High-quality data for enhancement of the terrain model of Slovenia. Geod Vestn 52(4):834–853

Podobnikar T (2009) Methods for visual quality assessment of a digital terrain model. SAPIENS 2(2):15–24

Podobnikar T (2010) DEM production/updating based on environmental variables modeling and conflation of data sources. J Civil Eng Archit 4(11):33–44

Scheidl C, Rickenmann D, Chiari M (2008) The use of airborne LiDAR data for the analysis of debris flow events in Switzerland. Nat Hazards Earth Syst Sci 8:1113–1127

Sodnik J, Mikoš M (2006) Estimation of magnitudes of debris flows in selected torrential watersheds in Slovenia. Acta Geogr Slov 46(1):93–123. http://giam.zrc-sazu.si/zbornik/ags46-1-4-SodnikMikos_str-93-123.pdf

Sodnik J, Mikoš M (2010) Modeling of a debris flow from the Hrenovec torrential watershed above the village of Kropa. Acta Geogr Slov 50 (1):59–84. http://giam.zrc-sazu.si/sites/default/files/ags50103.pdf

Sodnik J, Petje U, Mikoš M (2009) Terrain topography and debris-flow modelling Geod Vestn 53(2):305–318. http://www.geodetski-vestnik.com/53/2/gv53-2_305-318.pdf

Comparing the Performance of Different Landslide Susceptibility Models in ROC Space

Miloš Marjanović

Abstract

This article addresses performance evaluation routine for comparison of results of several different landslide susceptibility models. The study area is located on the NW slopes of Fruška Gora Mountain (Serbia). Five modelling methods were considered: Stability Index, Analytical Hierarchy Process (AHP), Fuzzy sets, Conditional Probability, and Support Vector Machines (SVM). In this respective order they gave more accurate spatial prediction of landslides. The performance of their "probabilistic" prediction is estimated by Receiver Operating Characteristics (ROC). Evaluation in ROC space is discussed in both quantitative – Area Under Curve (AUC) value, and qualitative manner – ROC curve trends. Finally, the article summarizes the advantages of the proposed ROC-based performance comparison.

Keywords

ROC curve • AUC • Landslide susceptibility

Introduction

In recent years the interest in landslide susceptibility modelling looks at the constant increase (Gokceoglu and Sezer 2009), which improves the awareness on landslide-related hazard. Nevertheless, it also leads toward sublimation of knowledge on physical and statistical relations between the phenomenon itself and the conditioning factors that cause it. One of the explanations for such a trend is certainly the contemporary fusion of Geographic Information Science (GIS) and advanced computational techniques. In such context, numerous approaches have been introduced for handling the landslide susceptibility, ranging from heuristic, to statistic, stochastic, deterministic, and advanced approaches, such as fuzzy set and machine learning concepts (Chacón et al. 2006). They have shown different complexity, reliability and applicability, but generally all of them have found their purpose at some level of planning or engineering. All of them also showed a strict dependency on the quality of inputs, particularly on the quality of landslide inventories (Carrara and Pike 2008).

This paper attempts to outline several landslide susceptibility modelling approaches in order to compare their performance on a common study area, using nearly identical inputs, and performance measurement metric which has been proven as the most realistic for spatial model comparison (Frattini et al. 2010).

Study Area

The study area encompasses the NW slopes of the Fruška Gora Mountain (Serbia). The site (N 45°09′20″, E 19°32′34″ – N 45°12′25″, E 19°37′46″) spreads over approximately 100 km^2 of hilly landscape, with intriguing dynamics and abundance in landslides. As speculated in some previous investigations in this area (Marjanović 2010; Marjanović and Caha 2011), landsliding is chiefly governed by geological and

M. Marjanović (✉)
Department for Geoinformatics, Palacký University, Tř. Svobody 26, Olomouc 77146, Czech Republic
e-mail: milos.marjanovic01@upol.cz

C. Margottini et al. (eds.), *Landslide Science and Practice*, Vol. 1,
DOI 10.1007/978-3-642-31325-7_76,

morphological factors, while the dominant triggering mechanism appears to be excessive rainfall. Most severely affected are the northernmost outskirts of the area, facing the Danube River, where younger (post-Mesozoic) formations are hosting deep-seated rotational and translational slides.

Input Datasets

Landslide Inventory

The landslide inventory served for most[1] of the modelling approaches as a reference for estimating a relation between landslide occurrences and conditioning factors.[2]

The inventory (photogeological map at 1:50,000 scale) was compiled by combining different Remote Sensing techniques (including stereoscopy of 1:33,000 aerial footage, and satellite image processing/interpretation) and field investigation. The adopted resolution in inventory's raster format representation (Fig. 1a) is 30 m. Around 50 evidenced landslides cover approximately 10 % of the total area, giving the density of one occurrence per 10 km^2. Rotational, deep-seated slides (dormant and active) are most abundant. The dimension of the occurrences varies from bellow 30 m (under the adopted resolution), to about 1 km in length or width.

Conditioning Factors

Conditioning factors included different geological, geomorphometric, hydrological and environmental attributes, obtained from different resources, converted to raster grid format with 30 m cell resolution.

Geological data were assembled by compiling geological map 1:50,000, photogeological map 1:50,000, and field survey data. Appropriate segments of these data were digitized and simplified to form the following factors: *lithology*, *proximity to faults*, and *proximity to the hydrogeological boundary*.

A Digital Elevation Model (DEM) was created from contour maps at 1:25,000 scale, by calculating Triangulated Irregular Network (TIN) and converting it to 30 m cell raster. Given the model of terrain surface, various geomorphometric factors were calculated: *aspect*, *elevation*, *slope angle*, *slope length*, *profile curvature* and *plan curvature*. These were all generated as first and second order derivatives of DEM.

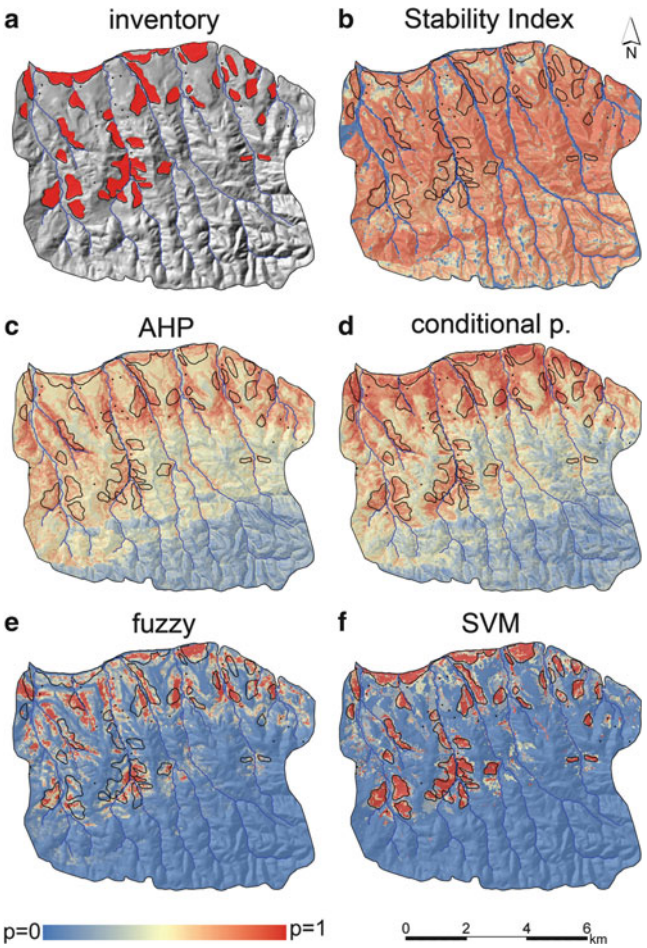

Fig. 1 (**a**) Landslide inventory of the study area, with landside occurrences in *red polygons* (contoured in *black* in all remaining images); Landslide susceptibility as probability *p* (0–1) of landslide occurrence: (**b**) Stability Index model, (**c**) Analytical Hierarchy Process model, (**d**) Conditional Probability model, (**e**) Fuzzy model, (**f**) Support Vector Machines model (note that the scale bars and north arrow apply for all figures equally)

Hydrological factors are represented by *Topographic Wetness Index* (*TWI*) as the second order derivate of DEM, and *proximity to stream* (calculated from the drainage pattern, automatically generated from DEM).

Land cover, was used to separate between deforested and cultivated areas (as suggested more convenient for landslide development) from vegetated areas. The attribute was created by K-means, semi-supervised classification over vegetation indices (using Landsat TM bands). Since the area of the interest is not particularly populated, urban influence was not considered.

Input dataset involved continual numeric, and categorical data. Most of the methodological approaches (excluding the Stability Index and SVM; see next section) required ranging (specifying class intervals or cut-offs) of continual data, prior to their implementation. In favour of chosen Natural Break cut-offs, chi-square-based feature selection proved

[1] For Stability Index model landslide inventory was used only to calibrate the classification of the result.

[2] Quintessential idea in landslide assessment revolves around the fact that a combination of terrain conditions that have caused landslides in the past might as well lead to new ones.

that all inputs had statistical dependence to referent landslide inventory (Marjanović and Caha 2011). Categorical data had to be additionally processed for the SVM model case, i.e. these were structured as binary-coded dummy variables, which gave them equal preferences in the eyes of the algorithm. Also, this model used only normalized continual data (while ranging was not necessary).

Landslide Susceptibility Models

Herein, several landslide susceptibility modelling methods are considered: Stability Index, Analytical Hierarchy Process (AHP), Conditional Probability, Fuzzy, and Support Vector Machines (SVM). Most of the models are addressed in detail in some earlier works, and only a brief retrospective will be presented here.

Stability Index Model

The Stability Index concept (Pack et al. 2001) accompanies ArcGIS/MW-SinMap© extension package. It represents a partially stochastic stability model for the infinite slope case in steady-state hydrologic conditions, which (among other assumptions) confine this approach mainly to shallow landslide scenario. The expectations of this model were not particularly high from the beginning, hence the domination of deep-seated landslides in the study area. Apart from the topographic data (for calculation of the upslope area and geometry of the slope), the model required geomechanical parameters such as cohesion c, bulk density γ, and internal friction angle φ of the material, but also an estimation of the soil-transmissivity-to-precipitation-recharge ratio T/q, to calculate the Stability Index (SI). In respect to the intervals of input parameters and under assumption of their uniform distribution, SI is calculated as a stochastic (probabilistic) measure of stability over the area. It follows the standardized, 6-level stability classification that is reciprocal to the probability of failure (closer the SI value to 1 greater the stability, and vice-versa). For the purpose of this research, SI needed to be inversed and normalized to portray the landslide occurrence probability.

One particular convenience of the model was exploited and it included regionalization of the input parameters. Since the lithological background is different within the area, it is suspected that these parameters should differ, too. Table 1 summarizes these parameters throughout delimited regions. Since there were no detailed investigations in this particular study area, the values of parameters were adopted from the literature standard (Bell 2007). The sensitivity of the model was also regarded (by slightly varying the inputs in a series of experiments, and calculating SI per each) so that the average inversed SI was generated using the average parameter intervals (Table 1). One can dispute the resulting model (Fig. 1b) as plausible since too many overestimations dominate the model. As mentioned before, this was expected up to some degree due to physical misconception of the model in respect to deep-seated landslide mechanism.

Table 1 Average parameters over different lithological domains (regions) of SI model

Parameter	Clayey/marly soils	Calcareous/ sandy soils	Solid bedrock domain
c [kPa]	0.1–0.5	0.1–0.3	0.3–0.6
γ [kg/m^3]	2,100.0	2,300.0	2,500.0
φ [°]	10.0–25.0	15.0–35.0	25.0–45.0
q/T [log]	500.0–1,000.0	4,000.0–5,000.0	6,000.0–7,000.0

Analytical Hierarchy Process Heuristic Model

Heuristic model offers the most straightforward but the most subjective solution, since it directly implements the expert's preference to control the importance of a conditioning factor. Analytical Hierarchy Process (AHP) was used herein to quantify that arbitrary judgement (Saaty 1980). AHP relies on the expert's reasoning of relations between the conditioning factors, i.e. on pair-wising their scoring preference. The final quantification takes place by normalizing and aggregating these scores.

Then they become readily applicable in the GIS environment, where each quantified score becomes the multiplier of the appropriate conditioning factor. In turn, the result can be generated as an additive model that sums scored factors, and if normalized (to 0–1), gives the scoring probability of landslide occurrence (Marjanović 2009). Visually, it could be inferred that the model tracked down some unstable zones, but yet tends to overestimate the probability of failure (Fig. 1c). The subjectivity of the model is substantial, and heavily depends on the expert's familiarity with the study area.

Conditional Probability Model

This statistical model uses the landslide inventory to estimate landslide frequency of each class interval in each conditioning factor. The scores or weights could be estimated (using the Weight of Evidence technique) and similarly as in the AHP model, used as a conditioning factor's multiplier in a GIS environment (Bonham-Carter 1994). The model proved to be sensitive to variation of ranges (class intervals) of conditioning factors, and therefore shows some subjectivity. Tendency of overestimation of high probabilities of landslide occurrence is also obvious (Fig. 1d). However, the actual occurrences are mapped very well (Marjanović 2010).

Table 2 Contingency table and ROC space coordinates

		Landslide inventory		
		True	False	ROC space coordinates
Model	Positive	tp (true positive)	fp (false positive)	$tp_{rate} = tp/(tp + fn)$
	Negative	fn (false negative)	tn (true negative)	$fp_{rate} = fp/(fp + tn)$

Fuzzy Set Model

Similarly as in the previous model, a function that relates the frequency of landslide occurrence to each class interval of each conditioning factor is used to generate fuzzy class memberships (Bonham-Carter 1994). Frequency Ratio and Cosine Amplitude membership functions were chosen for this task and obtained memberships were fed to the model. Fuzzy model included two-levelled Fuzzy Gamma (gamma = 0.5) operators. First level operated a Gamma combination over three conditioning factor groups: geological buffers, geomorphometric, and hydrological. The second level combined the results of the first level and the remaining categorical inputs (*lithology* and *land cover*), also by means of Gamma operation. The raw result (Marjanović and Caha 2011) was normalized (0–1) and revealed substantial correlation with the inventory map (Fig. 1e).

Support Vector Machines Model

Herein, the problem is structured as a classification task in order to separate landslide versus non-landslide instances throughout all conditioning factors (Marjanović et al. 2009). The basic SVM is defined as a binary, one-versus-one classifier, but it could be transformed to a one-versus-all case. In the scope of landslide susceptibility, this actually entails the modelling of the conditioning factors according to the binary classes of the landslide inventory. The model first performs the training of the algorithm over known. This is done within a specified portion of the terrain defined as training area, where the classifier learns how to rate the conditioning factors in order to obtain the given binary class. The classification rule that successfully separated training instances is applied to remaining, unclassified instances (of no landslide inventory coverage). The true advantage of SVM lies in its ability to generalize the classification rule (obtain optimal classification), from sparse data. The latter not only prevents the learning overfit, but enables a better sampling strategy (Burges 1998). The optimization requires only two SVM parameters to be optimized (penalty and kernel dimension), which can be seen as another advantage. The probability of landslide occurrence for this discrete classifier is calculated by measuring the frequency of hits, while slightly changing the training sample. The model nearly-perfectly corresponds to the inventory (Fig. 1f).

Method of Performance Evaluation

Receiver Operating Characteristics (ROC) represents an evaluation metric that depicts relative tradeoffs between benefits and costs, i.e. true positive rate (tp_{rate} or hit rate) and false positive rate (fp_{rate} or false alarm rate). These are the coordinates of a 2-D plot defined as ROC space. ROC curves, given their contingency table parameters (Table 2) at given probability threshold intervals, are simply the performance functions in that space (Fawcett 2006). It is important to highlight that the term probability can refer to any scoring scale. Accordingly, some models in this research represent actual probabilities while others represent just relative scoring scales, but their comparison is hence plausible in ROC space. This is particularly due to usage of ratios of contingency table elements ($tp - fp_{rate}$), indifferent to the actual class distribution. Other benefits that arise from within are that approach can handle of unbalanced classes (e.g. it is often that non-landslide instances predominate), and dealing with cost-sensitive (fp_{rate}-sensitive) models. The latter is not necessarily beneficial for landslide mapping, since the case is that false negatives are even less desirable than false positives (favouring of safety – conservativeness). The most common numeric parameter of evaluation in ROC space is Area Under Curve (AUC). The higher the AUC (within the 0–1 span) the better the performance and vice-versa. Additional characteristics of the ROC plot (e.g. random performance marker is the diagonal, conservative performance marker is lower left sector and liberal performance marker is upper right sector of the plot) allow descriptive evaluation, useful when choosing among the models with similar AUC.

Results

Final results of the research are depicted in a series of ROC plots in Fig. 2a–e.

The Stability Index (Fig. 2a) fails to discern landslide instances in the area as anticipated. Its performance (AUC = 0.54) is almost no different from random (AUC = 0.50) and the model might be entirely rejected.

The AUC of the AHP model (0.78) suggests a plausible result, which is not directly evident from the probability map (Fig. 1c). Thus ROC performance (Fig. 2b) rather goes in its

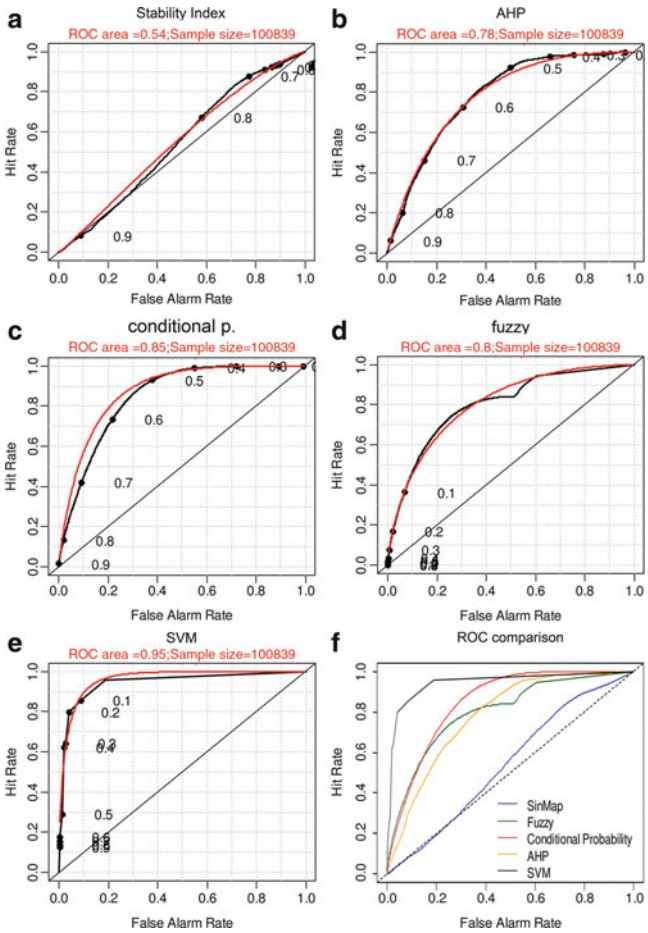

Fig. 2 Model performance in ROC space (**a**) Stability Index (steady-state infinite slope model), (**b**) Analytical Hierarchy Process, (**c**) Conditional Probability (Weight of Evidence scoring technique), (**d**) Fuzzy model (Gamma operator and Frequency Ratio/Cosine Amplitude for fuzzy membership estimation), (**e**) Support Vector Machines (with Gaussian kernel), (**f**) comparison of ROC curves

favour. However, the performance curve is moderately right-skewed, meaning that the model was not equally successful in discerning what is, and what is not a landslide. Such trend usually entails more liberal estimation than it suppose to. AHP tends to underestimate the landslides by claiming that there is low probability of occurrence on an actual landslide site, which is an important drawback of the model.

The Conditional Probability model (Fig. 2c) seems to map landslide/non-landslide instances very successfully (AUC = 0.85). In addition, the performance curve is nearly symmetrical in the ROC space, thus it exhibits no tendency of overestimation or underestimation. In fact, its performance is the highest (the closest to perfect classification) in the probability range of 0.6–0.55 (rather close to 0.5), which makes this model truly mediocre in terms of landslide susceptibility.

Fuzzy model (Fig. 2d) has a very similar performance to Conditional Probability and AHP models. However, its conservative preference is noticeable, since almost all ranges of relative probability thresholds fall down to the lower left section. It is this conservativeness that could credit slight advantage of this model over the previous ones, despite a bit smaller or nearly equal AUC performance (AUC = 0.8).

SVM model (Fig. 2e) responded extremely well (AUC = 0.95), outperforming all previous models. Its ROC curve is balanced (symmetrical) and yet probabilities are concentrated on the "safe" (conservative) side of the plot, i.e. it gives a high performance for 0.1 probability, similarly as Fuzzy model.

Conclusion

This work concludes a series of preceding landslide susceptibility investigations, which had resulted in several susceptibility models. For the purpose of their comparison in ROC space, most of the models had to be scored in probability-like scales, while the others already represented true probabilities. The comparison results came as expected, but some significant details are revealed. For instance, Fuzzy model was ranked lower than Conditional Probability on the AUC scale, but it has been also recognized as conservative, and therefore preferred. In pure visual or class-distribution-dependent metrics (such as accuracy, F-score, kappa index) it was impossible to obtain such straightforward comparison. Finally, all evidences strongly approve of SVM model for generating the landslide susceptibility map. It reached the highest performance (Fig. 2f), exhibited certain conservativeness and therefore, can be promoted as the model of choice for this case study.

Due to nature of the available landslide inventory (binary classes), models were limited to retrieve only landslide/non-landslide label. It would be interesting to observe the same models against multi-class inventory, as probability intervals would then turn more meaningful. Multi-class is also a challenging scenario from ROC analysis point-of-view (Fawcett 2006). Another direction is to try cost functions due to cost-sensitivity of the landslide susceptibility models (Frattini et al. 2010).

Acknowledgements This work was supported by the Czech Science Foundation (Grant No. 205/09/079).

References

Bell FG (2007) Engineering geology. Elsevier, Oxford, 581 p. ISBN_0750680776_

Bonham-Carter G (1994) Geographic information system for geosciences: modeling with GIS. Pergamon, New York, 398 p. ISBN_008042420_

Burges CJC (1998) A tutorial on support vector machines for pattern recognition. Data Min Knowl Disc 2(1):121–167

Carrara A, Pike R (2008) GIS technology and models for assessing landslide hazard and risk. Geomorphology 94:257–260

Chacón J, Irigaray C, Fernández T, el Hamdouni R (2006) Engineering geology maps: landslides and geographical information systems. Bull Eng Geol Environ 65:341–411

Fawcett T (2006) An introduction to ROC analysis. Pattern Recognit Lett 27:861–874

Frattini P, Crosta G, Carrara A (2010) Techniques for evaluating performance of landslide susceptibility models. Eng Geol 111:62–72

Gokceoglu C, Sezer E (2009) A statistical assessment on international landslide literature (1945–2008). Landslides 6:345–351

Marjanović M (2009) Landslide susceptibility modelling: a case study on Fruška gora mountain, Serbia. Geomorphol Slov Bohem 1:29–42

Marjanović M (2010) Regional scale landslide susceptibility analysis using different GIS-based approaches. In: Proceedings of IAEG conference, Auckland, New Zealand, 2–6 Sept 2010, pp 435–442

Marjanović M, Caha J (2011) Fuzzy approach to landslide susceptibility zonation. In: Proceedings of Dateso 2011 workshop, Písek, Czech Republic, 21–23 Apr 2011, pp 181–195

Marjanović M, Bajat B, Kovačević M, (2009) Landslide susceptibility assessment with machine learning algorithms. In: Proceedings of INCoS, Barcelona, Spain, 4–6 Nov 2009, pp 273–278

Pack RT, Tarboton DG, Goodwin CN (2001) Assessing terrain stability in a GIS using SINMAP. In: Proceedings of 15th annual GIS conference, Vancouver, BC, 19–22 Feb 2001

Saaty TL (1980) Analytical hierarchy process. McGraw-Hill, New York, 287 pp. ISBN_0070543712_

Case Event System for Landslide Susceptibility Analysis

Paraskevas Tsangaratos, Ioanna Ilia, and Dimitrios Rozos

Abstract

Landslides are considered as a geological disaster that has an unfavourable effect on lives and properties, generating both direct and indirect economic and human losses every year. Compared to other geological disasters, landslides are considerably smaller in scale, more dispersed, but more disastrous in many cases.

The presented methodology is based on a case–event system, which uses spatial analysis functions and artificial intelligence techniques, to evaluate potential instability problems concerning natural or artificial slopes. The methodology allows the user to examine new cases or areas of interest and compares them to previously recorded cases of instability problems that occur in the research area. The effectiveness of the methodology is evaluated in Kimi, Euboea, Greece, an area experienced substantial landslide events, where a well documented database of previous studies existed.

Keywords

Case event system • Landslide • Susceptibility analysis

Introduction

Landslides are generally thought to occur as a result of a localized process that affects a site that may not be very large in size. However, this localized process can occur with a high frequency over a region, influenced by variable factors interconnected to each other by complex relationships (VanWesten et al. 2006). This characteristic makes the evaluation of landslide susceptibility difficult.

At present, the study on the key techniques and methods for landslide susceptibility and hazard analysis is one of the hot research themes in the area of landslide study (Wang and Niu 2010). Landslide susceptibility zoning, involves the spatial distribution and rating of the terrain units according to their propensity to produce landslides (Fell et al. 2008). Susceptibility analysis provides information and knowledge, combining several factors that influence landslide occurrence (Ilia et al. 2010). As Varnes stated in 1984, this analysis requires a landslide inventory map that is based on three basic principles, that still remain active and fundamental: (a) the past and present are keys to the future, (b) the main factors that cause landsliding can be identified, (c) the degrees of hazard can be estimated. Nowadays, a forth statement have been added, (d) the risk derived from landslides may also be assessed and quantified (Chacón et al. 2006).

The methods for susceptibility and hazard analysis are qualitative or quantitative and for both approaches various techniques have been developed. Some of the methods are based on the site-specific experience of experts with the susceptibility determined directly in the field or by combining different index maps. Others perform statistical or probabilistic analysis while others follow deterministic approaches that involve the analysis of specific sites based on geo-engineering models (Soeters and Van Westen 1996; Aleotti and Chowdhury 1999; Fell et al. 2008). These

P. Tsangaratos (✉) • I. Ilia • D. Rozos
School of Mining and Metallurgical Engineering, Laboratory of Engineering Geology and Hydrogeology, National Technical University of Athens, Athens, Greece
e-mail: ptsag@metal.ntua.gr

C. Margottini et al. (eds.), *Landslide Science and Practice*, Vol. 1,
DOI 10.1007/978-3-642-31325-7_77,

methods of analysis often count problems, considering the assigning of weighting values, the data quality and quantity and the oversimplifications needed for the geological and geotechnical model. Recently, Data Mining Techniques have been introduced as efficient tools in susceptibility and hazard analysis (Flentje et al. 2007; Wang and Niu 2010). These techniques use the Knowledge based analysis, which refers to the science of computer modeling of a learning process (Quinlan 1993). Specifically, Data Mining is the process of analysing large amounts of data, in order to discover new meaningful patterns and rules, extracting useful information and knowledge (Berry and Broadbent 1995).

In this study, the susceptibility analysis is based on a Data Mining Technique, which implements a k-Nearest Neighbour algorithm, introduced in a case–event system. More specific, each case event (i.e. landslide event) is assumed to occupy a small unit area called unit cell and described by a set of spatial and non-spatial parameters. By implementing a distance function, the system evaluates the distance between each unit cell (affected or not affected by a landslide event) of the research area and the previous landslide events. This distance is expressed as a similarity index which corresponds to the probability of slope instability for each cell unit. The produced susceptibility map includes the classes of potential instability, based on the similarity index. The classes consider the parameters that contribute to the potential instability in the research area as well as the previously recorded cases of landslide instability. Each parameter and the similarity index, affect potential instability in a different way and therefore they obtain different weights defined by expert knowledge and data mining techniques. The effectiveness of the methodology is evaluated in Kimi, Euboea, Greece, an area experienced substantial landslide events, where a well documented and formulated database of previous cases existed (Ilia et al. 2008).

Methodology

Case-Event System (CES) is a system that evaluates past cases (known case B) in order to examine and characterize new cases (query case, Q). The specified system adopts an artificial intelligence technique, a method in which generalization beyond the training data is delayed until a query is made to the system (Mitchell 1997).

The case database contains all cases of unstable slopes throughout the research area, identified by field inspection and the study of previous technical reports. By applying the methodology, the probability of occurrence of unstable slopes was evaluated over the wider area, based on previously reported cases (Fig. 1).

Each case-event is generally represented as follows:

$$(\text{case event})\ \mathrm{I} = (\mathrm{a1(i)}, \mathrm{a2(i)}, \ldots, \mathrm{an(i)}; \mathrm{s}) \qquad (1)$$

where a1(i), a2(i),. . ., an(i) are the factors of each case-event and s is a Boolean variable in which the unstable case receives a value of 1, while the stable case receives a value of 0. In our study each case that forms the case library has an s value equal to 1, which means unstable conditions.The main purpose of the developed methodology was to evaluate the similarity between queried cases (Q) and known cases (B) of unstable slopes. The expressed similarity and final characterization, as unstable or stable, is based on the Nearest Neighbour algorithm, while the type of distance metric used by the system adopts the Davey-Wilson method (1990). It assumes that, concerning query cases that contained no data values, the similarity index is equal to 0. For query cases that are equal with known cases (B) of the constructed database, the class similarity is set to 1. In any other citation the value is calculated by the equation shown in Table 1.

In a graph of n-dimensions, plotting the n number of factors that characterize a case, when a new, unknown case is entered, the nearest-neighbour is the base case closest to the new one.

The similarity between a query case (Q) and a known case (B) are measured by calculating the distance in the feature space of the attributes that describes each case–event:

$$Similarity(Q, B) = \sum_{i=1}^{n} f(Q_i, B_i) \qquad (2)$$

Values of similarity close to 1 indicate unstable condition since the case library contains cases of reported instability, while values close to 0 indicate more stable conditions. However, the importance of each thematic factor may be different in the calculation and so a different weight should be assigned to address the contribution of each factor in calculating the similarity. In the present study a Rock Engineering System (RES) (Hudson 1992) was applied to calculate the weighting coefficient of each factor, through the development of an interaction matrix. The principal factors where placed in its main diagonal position together with the potential instability, while in all off-diagonal positions binary interactions between every pair of factors were placed. Values corresponded to no, weak, medium, strong and critical interaction ranging from 0 to 4 (Hudson 1992; Mazzoccola and Hudson 1996). The influence of each factor on the system (named cause, C) and the influence of the system on each factor (named effect, E) are presented in an external row and column, respectively.

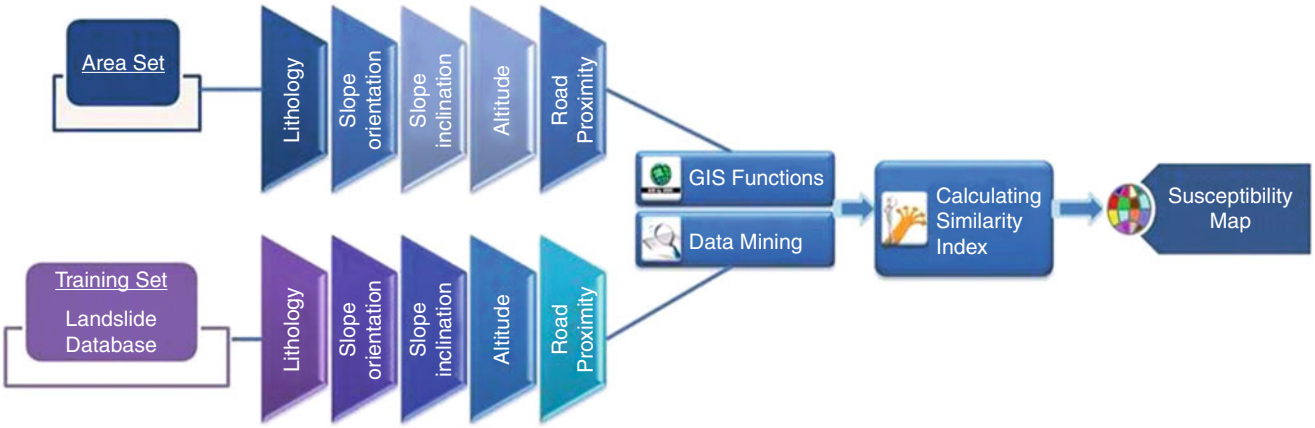

Fig. 1 Research flowchart

Table 1 Davey-Wilson method of calculating class similarity

Value of class	Similarity index
Known (B) or Query (Q) case = 0 or blank	0
Known (B) case = Query (Q) case	1
Known (B) case ≠ Query (Q) case ≠ 0 or blank	$1 - \frac{Abs(QueryCase - BaseCase)}{ClassRange}$

These C and E values are then transformed into a percentage corresponding to weighting coefficients for each factor (Rozos et al. 2006).

The final similarity index is then calculated by the equation:

$$Similarity(Q,B) = \sum_{i=1}^{n} f(Q_i, B_i) fW_i \quad (3)$$

where fWi = weighting coefficients

The necessary similarity index of each thematic factor is calculated with the use of a visual basic script code, embodied in a Graphical User Interface (GUI) application that was developed specifically for the present study. The GUI is capable in handling ASCII files and performs the needed distance calculations as described by the methodology. The output is an ASCII file that expresses the similarity of the research area, based on the landslide event database. After transforming the selected factors from grid format into ASCII format, the GUI produces a single text file that contains each unit cell of the research area, described by an identification number and values corresponding to each factor layer. The embodied algorithm calculates and assigns, in each cell, a value of similarity that the cell exhibits in relation with each known landslide event contained in the database. The value of overall similarity that corresponds to the probability that a unit cell has to be referred as a landslide event, could be calculated by taking into account k-nearest neighbours. The appropriate k number is essential for the final susceptibility map and could be found by producing different outcomes by trial and error procedures.

Case Study

Geological Characteristics

The Municipality of Kimi extends along the eastern-central coast of Euboea Island northeast of Attica prefecture covering an area of 167.6 km^2.

Regarding the relief, the south-eastern part of the municipality is hilly to mountainous with elevation ranging from 0 to 500 m, while its northern part is mountainous with cliffs and scarps along the coast of the sea and with elevation ranging from 500 to 1,000 m.

Three tectonic units (Katsikatsos et al. 1986), the 'Pelagonian Unit', the 'South Euboea Blueschist Belt' and 'Almyropotamos Unit' are present on Euboea Island. The study area extends mostly in "Kimi-Aliveri basin", which was formed in the Early Miocene. This basin was filled by conglomerates and marls of 500 m thick, with lignite intercalations, which was later intruded by volcanic rocks (Pe-Piper and Piper 1994). In the southern margin of this basin, conglomerates, with a thickness of 1,000 m, of late Miocene in age (Katsikatsos et al. 1981) were accumulated (Fig. 2).

More analytically, as presented by previous studies (Koumantakis et al. 2008; Ilia et al. 2008), the study area consists of quaternary deposits, upper horizons of neogene sediments, base conglomerates and flysch formations. Also, ultrabasic rocks consisting of peridotites, dounits and at places serpentine peridotites outcrop in the eastern part of

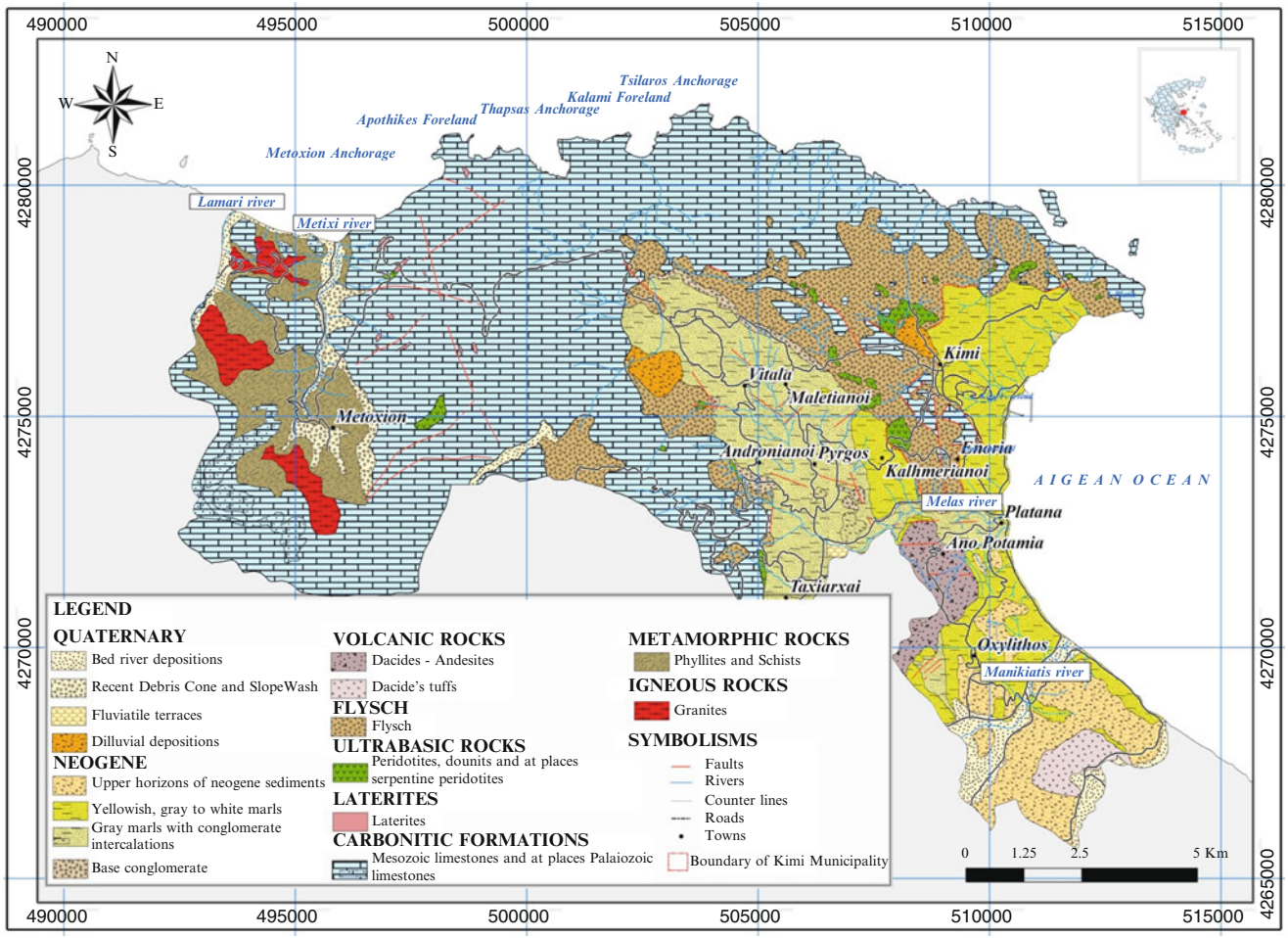

Fig. 2 Geological map of Kimi municipality

examined area, while Carbonate rocks are presented with Mesozoic, and Palaiozoic limestones. Finally, granites Carboniferous in age, are presented in the Western part of Kimi basin (Fig. 2).

Climatic Features

The analysis of the climatic features taken from the Kimi station of the Meteorological Service showed that the mean annual temperature for the period 1956–1990 is 16 °C, while January is the coldest month with an average monthly temperature of 8.6 °C. On the other hand, July is the warmer month, with an average monthly temperature of 24.9 °C. The average annual amount of rainfall is 1,071 mm, but in highland zones of the region, the annual amount of rainfall is expected to be higher. The wettest month is January with an average monthly value of 180.2 mm, followed by December with 173.9 mm and February with 164.7 mm. Concerning the seasonal distribution of rainfall, a rate of 48.5 % of the average total annual amount is attributed to the winter, followed by 27.4 % in autumn, 20.3 % during the spring and 6.8 % during the summer.

Landslide Distribution

Landslides are distributed in several locations in the Municipality of Kimi, mainly due to the thickness and the general geotechnical behaviour of the formations, but in most cases combined with human interventions.

Numerous landslides resulted in the destruction of the main coastal road network as well as in the collapsing of several structures, causing disastrous socio-economic implications and putting the locals at risk. With regard to the landslide type, the study area is affected by creep, rotational and translational slides, lateral spreads and rock falls. Most of them occurred on steep slopes after heavy rainfall or tectonic activity.

The 62 landslide event locations were identified from field surveys, technical reports and interpretation of aerial

photographs. Information of thematic factors was collected from various sources (topographic, geological, land cover maps etc.) and introduced into a spatial database using GIS technology. The above data sources have been used to generate various thematic data layers that have been resampled to 20 × 20 m grid size.

Generating Thematic Layers

As mentioned above, lithology, altitude, slope inclination, slope orientation and road network proximity are included in the model as causative factors responsible for landslide manifestation. The amount of precipitation and the tectonic activity have been excluded from the model, since the objective was to produce a landslide susceptibility map, regardless of any triggering factor. More specifically:

- Lithology is represented by the different lithologic complexes present in the study area, and is derived by grouping geological formations that are homogeneous from the lithological point of view. Landslide events mainly took place at the upper horizons of the neogene marls and flysh formations, which were mainly covered by a thick weathering mantle (Fig. 3a).
- The altitude of a site is a combined result of the tectonic activity and the erosion-weathering processes and is related to climatic conditions through an interactive influence. Altitude is indirectly contributing to the slope failure manifestation since it controls the degree and type of erosion (Dai and Lee 2002), and the degree of human intervention in some regions. In the study area the alltitude evidence layer was subdivided in 6 classes (Fig. 3b).
- The inclination of a slope along with the orientation plays a significant role in the concept of landslide manifestation as a causative factor (Rozos et al. 2008). The slope angle is easily relatable to the slope movement, because it is strongly linked to the forces involved. High slope angle sites are more susceptible to landslide phenomena. This parameter was subdivided in four classes (Fig. 3c).
- Slope orientation is associated with increased snow concentration, higher erosion and intense weathering since these features contribute to the cyclic alteration of dry and wet periods. Slope aspect in the study area was subdivided in four classes (Fig. 3d).
- Finally, it has been observed that many landslides occur close to the road network. The slope instability could be caused either by the uncontrolled or controlled blasting and widening of the roads, or by the loss of support due to removal of material from the lower portion of the slopes during road widening (Ilia et al. 2010). The distance to road was subdivided in four classes (Fig. 3e).

Results and Discussion

Figure 4, shows the interaction matrix developed during the study, in order to estimate the weight of each factor, the values of which are shown in Table 2. Lithology appeared to be the most interactive feature, while the altitude the least interactive. The outcome of the methodology was the production of a similarity index that expresses the susceptibility, scaled in range of [0, 1], where 1 equals unstable area.

As it can be seen in Table 3, for small k numbers the maximum similarity was found to be high (0.987), however the percentage of correctly classified cases was found to be low (82.26 %). When calculating the similarity index taking into account the whole set of landslide cases, the maximum similarity index was found to be 0.872 and the correctly classified cases reached 95 %. The appropriate number of k nearest neighbours for calculating the overall similarity is found by a trial and error procedure ($k = 15$) considering high values of both maximum similarity index and correctly classified cases.

As it can be seen (Fig. 5), the similarity index ranges between 0.934 and 0.364. The percentage of correctly classified cases pointed out the high accuracy of the method since almost all landslide events (88.71 %) where placed in the class that ranged from 0.87 to 0.934.

The main purpose of any susceptibility analysis is to highlight the distribution of potentially unstable slopes based on a detailed study of the factors responsible for landsliding (Ayalew et al. 2005). However, such a task is considered to be difficult since complex and mostly hidden relationships exist between spatial factors. The most crucial and fundamental assumption made during any susceptibility and hazard analysis, is that landslides will always occur in the same geological, geomorphological, hydrogeological and climatic conditions as in the past. As a consequence, the susceptibility map could actually express the similarity that a unit area has, estimated by combining the produced similarity results of the predictor features multiplied by a feature weighted distance function, with known areas of landsliding. However, this process presents several problems concerning the applied similarity metric technique, the selected factors, the constructed classes and also the determination of the weighted coefficients each factor has. The applied RES method was proved to be a useful tool for estimating each weighted coefficient, since it

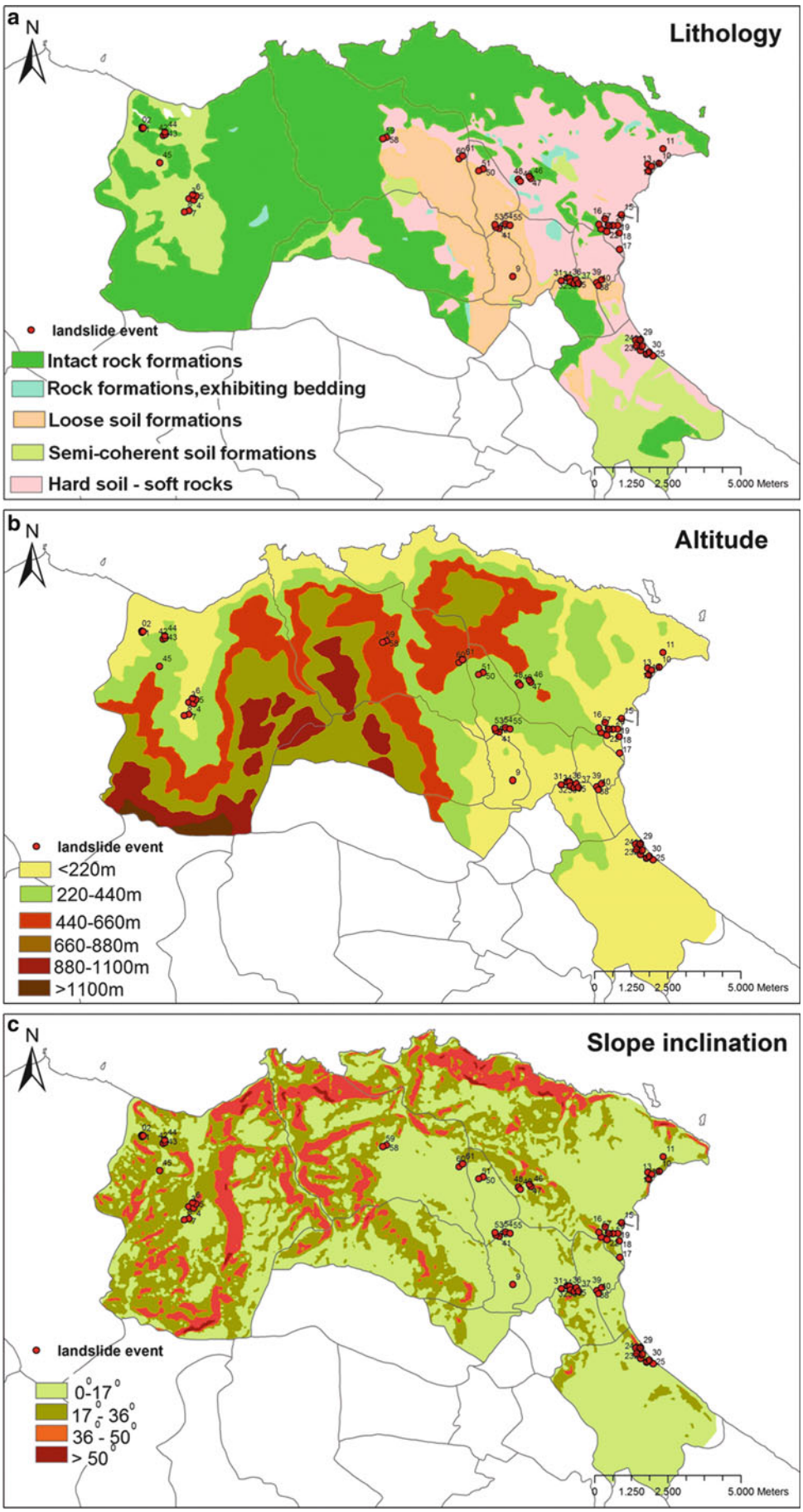

Fig. 3 (continued)

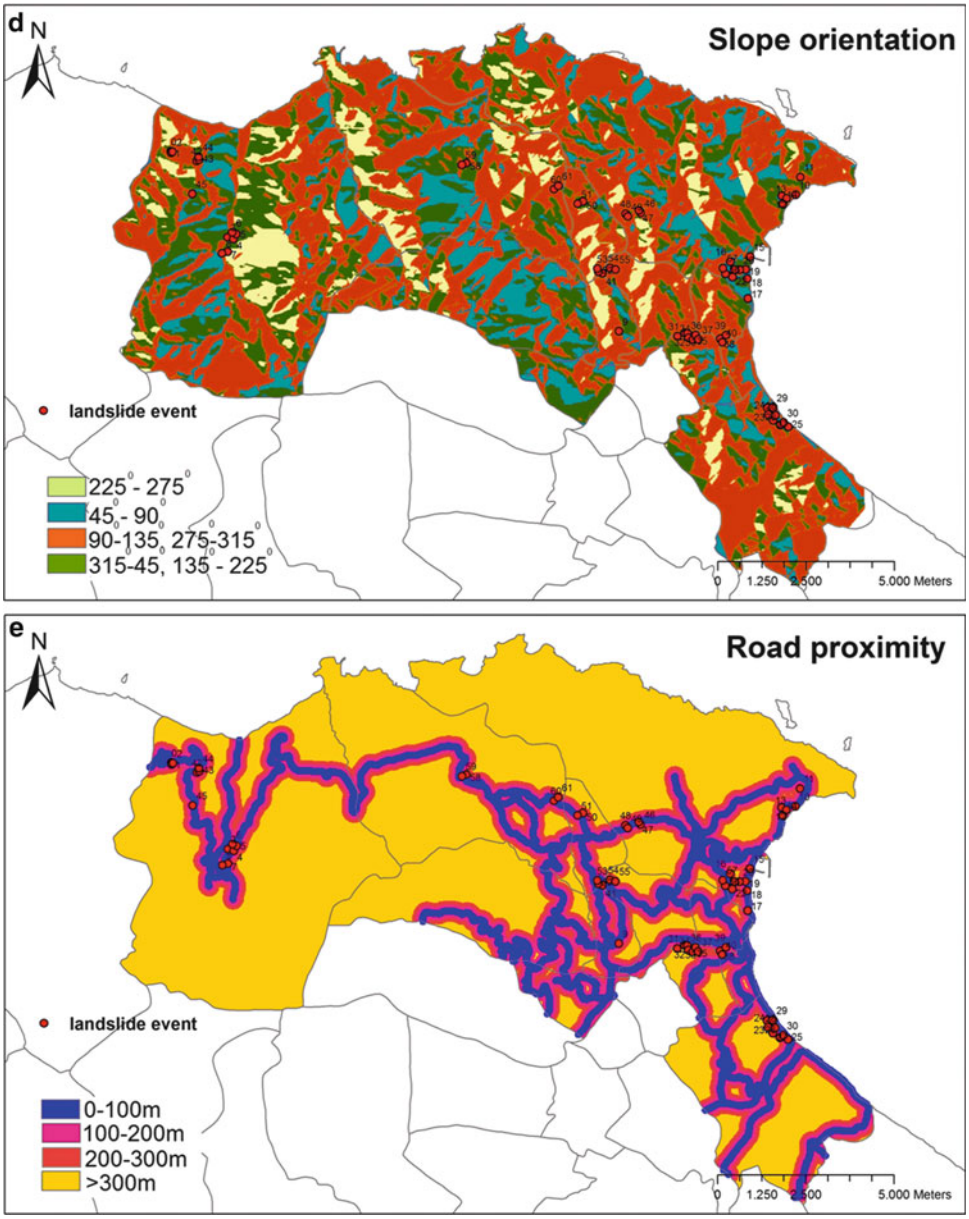

Fig. 3 Maps of the considered parameters: (**a**) lithology, (**b**) altitude, (**c**) slope inclination, (**d**) slope orientation, (**e**) road proximity

INTERACTION MATRIX							
f1	3	3	3	2	3	14	CAUSE
0	f2	1	1	0	4	6	
0	2	f3	2	0	3	7	
0	1	1	f4	0	3	5	
1	2	0	2	f5	1	6	
0	0	0	0	0	Pi	0	
1	8	5	8	2	14	38	
EFFECT							

Fig. 4 Interaction matrix. *f1* lithology, *f2* slope inclination, *f3* slope orientation, *f4* road network proximity, *f5* altitude, *Pi* potential instability

combines adaptability, objectivity, repeatability, efficiency and effectiveness (Mazzoccola and Hudson 1996; Benardos and Kaliampakos 2004).

Conclusions

In the present study, a Case Event System was developed in order to calculate the similarity of each unit area (20 × 20 m grid size) of the municipality of Kimi, Euboea, Greece with known landslide sites over the region. The calculation was performed by a visual basic script code that was capable in handling spatial factors, while the final susceptibility map was produced by a GIS application. The RES method was applied in order to combine expert knowledge with an artificial intelligence

Table 2 Weighting coefficients of each thematic layer. C and E are the cause and effect values listed in the interaction matrix

Thematic layer	C + E	Weighting coefficient
Lithology (f1)	15	0.242
Slope inclination (f2)	14	0.226
Slope orientation (f3)	12	0.193
Road network proximity (f4)	13	0.21
Altitude (f5)	8	0.129

Table 3 Trial and error results

k-nearest neighbours	Maximum similarity index	Correctly classified cases %
5	0.987	82.26
10	0.979	87.09
15	0.934	88.71
25	0.91	93.54
62 (whole set)	0.872	95.16

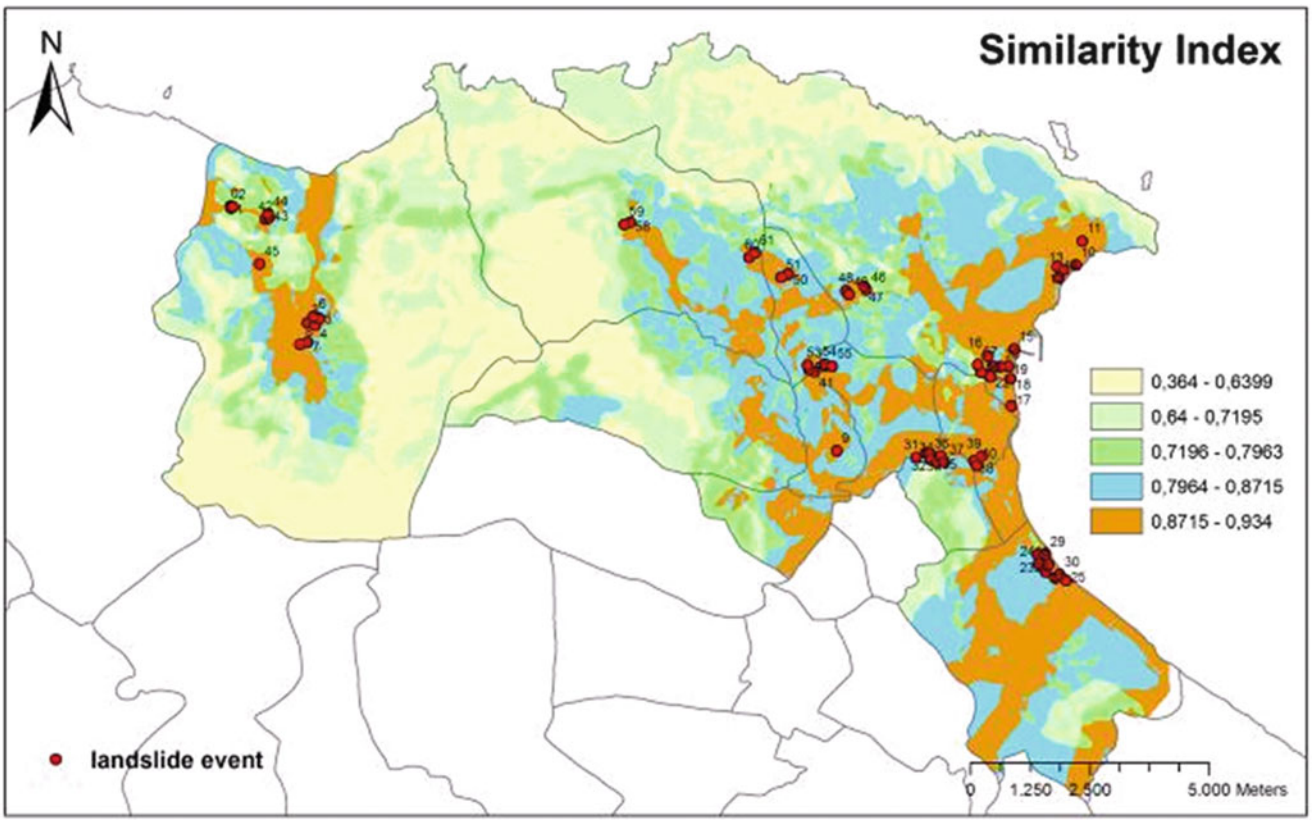

Fig. 5 Final similarity index

method and produce weighted coefficients for each controlling factor. The Data Mining approach is considered to be an efficient tool in handling spatial related problems. The outcome of the implementation is satisfactory, making the developed methodology a valuable tool for urban planning and development.

References

Aleotti P, Chowdhury R (1999) Landslide hazard assessment: summary review and new perspectives. Bull Eng Geol Environ 58:21–44

Ayalew L, Yamagishi H, Marui H, Kanno T (2005) Landslides in Sado Island of Japan: Part II. GIS-based susceptibility mapping with comparisons of results from two methods and verifications. Eng Geol 81:432–445

Benardos AG, Kaliampakos DC (2004) A methodology for assessing geotechnical hazards for TBM tunnelling—illustrated by Athens Metro, Greece. Int J Rock Mech Min Sci 41(4):987–999

Berry DC, Broadbent DE (1995) Implicit learning in the control of complex systems: a reconsideration of some of the earlier claims. In: Frensch PA, Funke J (eds) Complex problem solving: the European perspective. Lawrence Erlbaum Associates, Hillsdale, pp 131–150

Chacón J, Irigaray C, Fernández T, El Hamdouni R (2006) Engineering geology maps: landslides and geographical information systems. Bull Eng Geol Environ 65:341–411

Dai FC, Lee CF (2002) Landslide characteristics and slope instability modeling using GIS, Lantau Island, Hong Kong. Geomophology 42:213–238

Davey-Wilson IEG (1990) Knowledge representation using fact-segments. Microcomput Civil Eng 5(3):245–250

Fell R, Corominas J, Bonnard C, Cascini L, Leroi E, Savage W (2008) Guidelines for landslide susceptibility, hazard and risk zoning for land-use planning. Eng Geol 102:99–111

Flentje P, Stirling D, Chowdhury R (2007) Landslide susceptibility and hazard derived from a landslide inventory using data mining — an

Australian case study. In: Proceedings of the first North American landslide conference, Vail, Colorado, June 2007

Hudson JA (1992) Rock engineering systems. Theory and practice, Ellis Horwood series in civil engineering. Ellis Horwood, New York, 185 p

Ilia I, Koumantakis I, Rozos D, Markantonis K, Tsangaratos P (2008) Landslide phenomena in Kimi area, Evia Island, central Greece. Geophys Res Abstr 10, EGU2008-A-06831, 2008 SRef-ID: 1607-7962/gra/EGU2008-A-06831 EGU General Assembly 2008

Ilia I, Tsangaratos P, Koumantakis I, Rozos D (2010) Application of a Bayesian approach in GIS based model for evaluating landslide susceptibility. Case study Kimi area, Euboea, Greece. In: Proceedings of 12th international congress of the Geological Society of Greece (GSG), Patras, No. 3, May, pp 1590–1600

Katsikatsos G, De Bruijn H, Van der Meulen AJ (1981) The Neogene of the island of Euboea (Evia): a review. Geol Mijnb 60:509–516

Katsikatsos G, Migiros G, Triantaphyllis E, Mettos A (1986) Geological structure of internal Hellenides (E. Thessaly SW Macedonia, Euboea Attica Northern Cyclades and Lesvos). I.G.M.E., Geol Geophys Res (Special issue):191–212

Koumantakis I, Rozos D, Markantonis K, Ilia I, Tsagaratos P (2008) Landslide phenomena of Kimi municipality. Research Program founded by the Prefecture of Euboea Island

Mazzoccola DE, Hudson JA (1996) A comprehensive method of rock mass characterization for indicating natural slope instability. Q J Eng Geol 29:37–56

Mitchell T (1997) Machine learning. McGraw Hill, New York, 432 p

Pe-Piper G, Piper DJW (1994) Miocene magnesian andesites and dacites, Evia, Greece: adakites associated with subducting slab detachment and extension. Lithos 31:125–140

Quinlan JR (1993) C4.5: programs for machine learning. Morgan Kaufmann Publishers, San Mateo, 302 p

Rozos D, Tsagaratos P, Markantonis K, Skias S (2006) An application of Rock Engineering System (RES) method for ranking the instability potential of natural slopes in Achaia County, Greece. In: Proceedings of XIth international congress of the Society for Mathematical Geology, University of Liege, Belgium, S08-10

Rozos D, Pyrgiotis L, Skias S, Tsagaratos P (2008) An implementation of rock engineering system for ranking the instability potential of natural slopes in Greek territory: an application in Karditsa County. Landslides 5(3):261–270

Soeters R, Van Westen CJ (1996) Slope instability recognition, analysis and zonation. In: Turner AK, Schuster R (eds) Landslides investigation and mitigation. Transpotration Research Board special report. National Academy Press, Washington, DC, 247 p

VanWesten CJ, Van Asch TWJ, Soeters R (2006) Landslide hazard and risk zonation—why is still so difficult? Bull Eng Geol Environ 65:167–184

Varnes DJ (1984) Landslide hazard zonation: a review of principles and practice. UNESCO, Paris, 63 pp

Wang X, Niu R (2010) Landslide intelligent prediction using object-oriented method. Soil Dyn Earthq Eng 30:1478–1486

Jogyura Landslide: Impact of Main Boundary Thrust, a Case Study from Central Himalaya

Anita Pande

Abstract

The Himalayan mountain range, divided by deep and active thrusts, is a region of highly sensitive to tectonic stability. The Main Boundary Thrust (M.B.T.) defines the boundary of the Lesser Himalaya against Outer Himalaya. In this, an old landslide was reactivated during monsoon period in 1992 and the area is now experiencing frequent slides throughout the year affecting 50–60 ha of area. On an average 1–2 ha of land is being swept away every year in the area. The existence of Main Boundary Thrust (MBT), toe erosion by Nihal River, loading of slope crest (intensive settlement and agricultural processes and village path), regular and heavy water discharge in slided area, highly jointed rocks, low vegetation cover, high monsoonal precipitation and thin soil cover were found to be foremost causative factors. Major anthropogenic activity i.e. construction of 'cart-track' amid the critical slope had promoted vulnerability of the area. The land conservation measures adopted by Soil Conservation Department and Forest Department also proved futile. Rambans Plants (*agave americana*) and Chari hurbs (*Sorghum bicolor*) are being planted by the inhabitants for land conservation. Various recommendations are proposed.

Keywords

Main Boundary Thrust • Outer Himalaya • Lesser Himalayan • Tectonic instability • Monsoonal precipitation • Anthropogenic activities

Introduction

The term landslide refers to a rapid displacement of a mass of rock, residual soil or sediment adjoining a slope in which the centre of gravity of the moving mass advances in a downward and outward direction (Zaruba and Mencl 1969). The Himalayan mountain belt comprise of tectonically unstable younger geological formations subjected to severe seismic activity. The Central sector of Himalaya is geologically divided into Outer Himalaya (Siwalik), Lesser, Great and Tetheys Himalayas from South to North. The present study looks into the landslide scenario along Main Boundary Thrust that exists between the Outer and Lesser Himalaya. The Outer Himalaya comprises conglomerates, sandstones and clays of Tertiary age. The Upper beds of Outer Himalaya possess loosely aggregated conglomerates and soft earthy deposits while soft sandstones resting on hard sandstones may be seen below the upper beds. The existence of open folds and reverse faults near Main Boundary fault (MBF) speak of the structural complexity of Outer Himalaya. The paleontological characteristics have subdivided the Siwaliks into three divisions – Upper, Middle and Lower. The study area in the Central Himalaya is constituted of the two major tectonic units: (1) Siwalik belt: It comprises of sandstone and shale facies of molasse type of Cenozoic sediments. The belt is flanked to the south by the Ganga alluvium and delimited in the north by the Main Boundary Thrust. (2) The Lesser Himalaya: It comprises mainly metamorphic rocks (quartzite, slate, dolomite, gneiss, schist etc.) occasionally intruded by

A. Pande (✉)
Department of Geography, Kumaun University, Nainital, Uttarakhand, India
e-mail: anni_pan@rediffmail.com; anita.ku.ntl@gmail.com

C. Margottini et al. (eds.), *Landslide Science and Practice*, Vol. 1,
DOI 10.1007/978-3-642-31325-7_78,

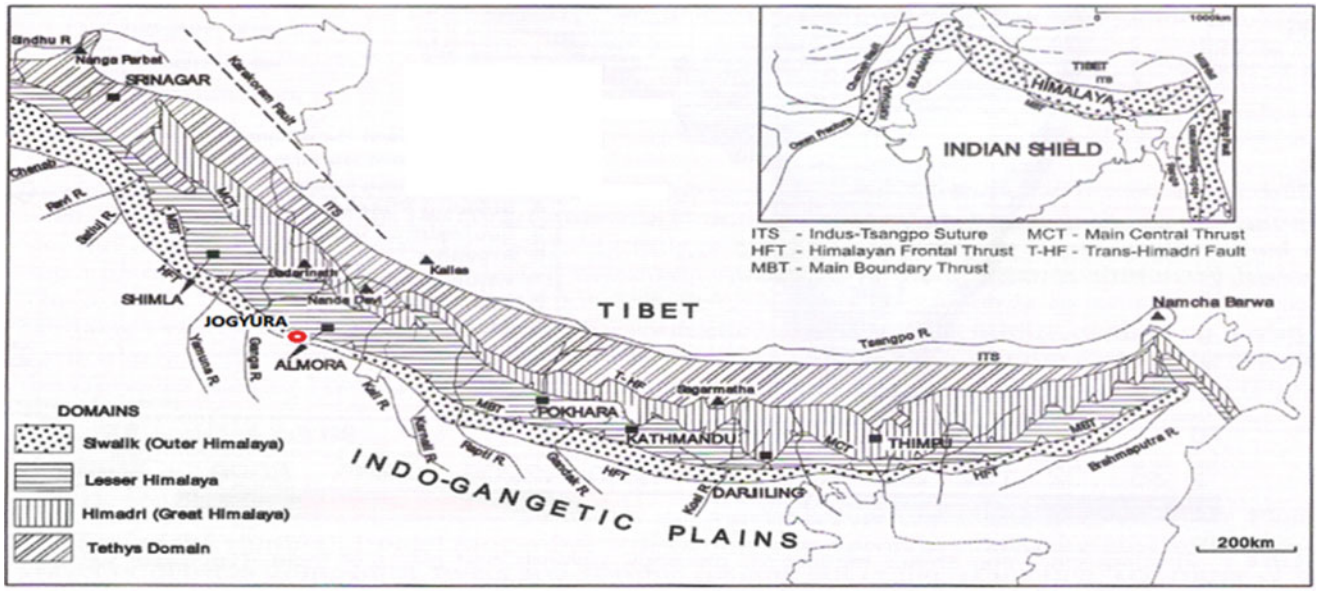

Fig. 1 Location of study site (map after Valdiya 1998)

granite rocks ranging from Precambrian to Mesozoic period (Fig. 1).

The Lesser Himalayan rocks rest upon the Siwalik molasse. The contact is very sharp and the rocks are strongly tectonized. This originally was known as Main Boundary Fault, a name introduced by Medlicot (1864). It was Middlemiss (1890) who defined it as the Main Boundary Thrust. According to the new concept (Valdiya 1980) the M.B.T. is the chain of four different thrusts which separate the sub-Himalayan Cenozoic sedimentary including the Siwalik from the Lesser Himalayan Pre-tertiary rock formation. This thrust dip 30° to 40° west of Jogindiya and runs in approximately WNW-ESE direction. The neotectonic activity along M.B.T. are represented by the recurrent landslides tilting of trees and cracks in houses. The upliftment of the terraces in the Nihal valley is suggestive of upliftment in sub-recent times.

Investigations have been done by several scholars in the identification of the problem of landsliding in Himalaya and other mountainous regions of the world, viz. Oldham (1880), Mehra and Natrajan (1966), Hukku et al. (1977), Nasmith and Mercer (1979), Cain and Mool (1982), Valdiya (1983, 1985, 1998), Kienholz et al. (1984), Valdiya et al. (1984), Bhandari and Gupta (1985), Jalal (1985), Bartarya and Valdiya (1989), Haigh et al. (1989),Joshi and Pant (1990), Bartarya (1996) Sharma (1996), Smith and Ellison (1999), Pande et al. (2002), Chen and Lee (2003), Rautela and Pande (2005), Sharma (2005), Fourniadis et al. (2007), Alexander (2008), Owen et al. (2008) and Starkel (2010).

In this study an attempt is made to carry out the information on the landsliding using only those variables which are readily measurable in the local environment. These are further classified as:

1. To discover a suite of easily measurable natural, geological, geomorphological and ecological indicators and anthropogenic (such as; construction of 'cart-track' settlement, faulty land use, deforestation and grazing) factors that together can be used to predict the occurrence of a high frequency of landslides along the existing M.B.T. zone
2. To differentiate between the main factor (that started the sliding process) and the subsidiary factors (which contributed to the sliding processes),
3. To differentiate between natural as well as those anthropogenic factors which are more dominant in landsliding processes under MBT. zone of Himalaya.
4. Finally to assess the impact of landslide process upon the physical and cultural landscape of the region.

Study Area

The Jogyura landslide (Fig. 1) is located in the latitude of 29° 21.524′ N and longitude of 79° 25. 826′ E and an elevation of 1,217 m (at the toe of landslide) and the latitude of 29° 21.682′ N and longitude of 79° 25.768′ E and an elevation of 1,399 m (at the crown of landslide). The latitude of 29° 21.596′ N and longitude of 79° 25.764′ E and an elevation of 1,312 m (at the middle of landslide). The orientation of landslide is NW-SE (150–330°).

The toe of this landslide is located along Nihal River. Numbers of landslides are active along river as this river is flowing along Nihal fault (neo-tectonically active) and the area falls under Main Boundary Thrust (MBT) Zone. During field investigation it has been observed that about ten

landslides are found under per kilometer stretch in up stream and down stream valley from Jogyura landslide.

Data Base and Methodology

The study is based on primary data collected through intensive field work. Landslide Analysis Questionnaire (Mehra and Natrajan: 1966) is used for the data base preparation. However, all information was not available so selected part of the questionnaire is used.

GPS, Brunton Compass, Meter Tape and Abney Level are used to locate landslides and their physical parameters (dip, strike, slope and morphology)

The study has been undertaken using standard geological and geomorphological field techniques. Geological data and field verification of rocks were obtained from Valdiya (1980). Geological and lithotectonic units that might influence the distribution of the landslides were mapped separately. In addition to this a large number of structural measurements such as, bedding and joint planes, thrusts and other minor faults were recorded.

In order to assess the hydrological conditions of the critical slopes, direct observations were made in the field of springs/seepage zones; perennial and non-perennial streams and also irrigation networks (e.g. storage tanks etc.) were also recorded. The condition of the local vegetation cover was evaluated and the percent of vegetal cover on the affected area was estimated with reference to the total landslide area.

Anthropogenic factor are the most important parameter that use to overstresses the fragile Himalayan terrain. These were assessed by direct observation as well as query of the present and past history of the landslide by inhabitants of the Jogyura locality.

Some variables could not be measured directly, viz. the total affected area of landslide and the existing debris produced by particular landslide (i.e. the volume of the landslide). For these purposes

$$\text{Area} = \text{Width} \times \text{Length}$$

Volume of the debris can not be measured in present case because all the slide debris is washed away by the Nihal stream due to its existence along the toe of the sliding hillock.

Many of the parameters detailed above are listed in Table 1.

Table 1 Characteristics of Jogyura landslide

Parameters	Site observations
Location (as observed using GPS)	Crown: Latitude 29° 21.682′ N
	Longitude 79° 25.768′ E
	Toe: Latitude 29° 21.524′ N
	Longitude 79° 25.82′ E
Date of occurrence	1992
Rock type	Dolomite,sandstone, slate
Nature of rock	Disintegrated rocks and soil
Interbeded rock	Slate
Weathering	Mechanical weathering
Length: toe to crown (m)	800
Average width of slide(m)	47
Height: toe to crown (m)	182
Orientation (°)	150–330° (NW-SE)
Area affected (m^2)	37,328
Nature: slope	Concave
Nature: succession	Primary
Damage caused	Loss of agricultural land

Physiography

Slope is an important contributing factor in the development and accentuation of landslides in the structurally complex and complicated area. The degree of slopes and their proximity to major planes of structurally weak zones are considerably responsible for the amount of runoff, mechanical breakdown, degree and extent of erosion, landslides, creep and depth of slope profile. The Nihal valley has steep slope more than 28° because they follow fault and valley sides show scarps and triangular facets.

There are steep scarps overlooking narrow and deep valleys. The highly elevated Siwalik Hills are steeply sloped and exhibit a youthful topography, whereas the northern part across the Main Boundary Thrust comprising the Lesser Himalayan rocks has comparatively mild and mature topography. In general, the topography of the area changes very rapidly from place to place due to activeness of eroding agencies. In general area is constituted of dolomite, shale and slates of the Krol formation. Since this area is in the vicinity of M.B.T. It has suffered repeated and extensive landslides in the recent past, as a result of which a large amount of debris has accumulated at the foot of Krol belt i.e. in the north of M.B.T. The material is poorly sorted and composed of large blocks of dolomites and other slates, marl fragments embedded in the sandy matrix (Fig. 2)

The river Nihal following the Nihal fault has cut through this material and deposited huge material in the valley forming the T1 terrace. Later on due to uplift, the river cut through the T1 terrace and deposited this material in the valley forming the T2 terrace and similarly formed the T3 terrace. Due to change in the gradient of the river flow it starts braiding near Dhapla thus depositing its load and in consequence the formation of Island bar took place.

The climate condition of the area varies with altitude. The area experiences about 170 cm per annum. The rainfall is maximum during August and September. The maximum temperature in Summer reaches up to 290 °C in June while

Fig. 2 View of Jogyura landslide

minimum 20–30 °C in January. December and January are the coldest months while May and June are the hottest months. The maximum humidity (75–80 %) is during August and September.

The vegetal cover of the area under investigation speaks off a combination of trees, shrubs, herbs and climbers. Present study site represent an old as well as active landslide area. This site was originally dominated by chir-pine (Pinus roxburghii) forest. After landslide many pioneer species started growing on damaged site.

Within landslide area many plant species were present, viz. *trees*: chir (*Pinus roxburghii*), alder (*Alnus nepalensis*) khinna (*Sapium insigne*) gethi (*Bohemeria regulosa*) jamun (*syzygium cuminii*); *shrubs*: dhaul (*Woodfordia fruticosa*), makoi (*Coriaria nepalensis*), Agave (*Agave americana*), Kilmora (*Berberis aristata*), Lantana (*Lantana camara*); *herbs*: Chara (*Lindernia nummularifolia),* Bedins (*Bedins biternata*); *climbers*: Tarur (*Dioscorea deltoidea*), Beduli (*Parthenocissus himalyana*). Most of the species growing in damaged soil were early successional capable of growing in harsh environment i.e. low moisture and nutrient. Outside the landslide area original vegetation was retained including 16 species Out of these 8 are trees, 4 species are shrubs, 2 species are climber and 2 species are grasses, viz. *trees*: Garura (*Olea Glandulifera*), Timil (*Ficus*), Bedu (*Ficus palmata*), Bhimal (*Grewia optiva*), Amla (*Emblica officinalis*), Kanl (*Flacourtia indica*), Khair (*Acacia catechu*), Meethi-neem (*Murraya koingii*); *shrubs*: Tusara (*Debrigesia longifolia*), Ghingaru (*Pyracantha crenulata*), Hisalu (*Rubus ellipticus*), Rambans (*Agave americana*); *herbs*: Ghunsmura, Chari(*Sorghum bicolor*); *climbers*: Ladari (*Parthenocissus semicordata*), Bilau.

It is observed that the pattern of recovery i.e. changes in vegetation composition following external perturbation in this degraded landslide area is influenced by the local climate, geographical and ecological conditions. It can be assessed by the presence of higher plants following disturbances.

Observations and Discussion

It is situated near the Jogyura locality. The crown part of the slide zone is under the influence of anthropogenic processes, viz. agriculture, settlement and footpath. In extreme down at toe part of the slide, the existence of fast flowing Nihal river is responsible for slope instability due to the lateral erosion. In this area Nihal river is following a fault. This fault is trending approximately NNW-SSE. This fault is younger in age to M.B.T., because it has caused considerable amount of horizontal shift along M.B.T. and Mangoli thrust. The other evidences are seen as:

1. Wide straight valley of Nihal river along the fault zone
2. Strongly sheared, crushed and shattered zone
3. Steep scarps on the sides of Valley of Nihal River
4. Triangular facets along the valley sides in continuation. In addition to the Nihal fault there are many other faults exist which are across the M.B.T.

Due to the presence of Main Boundary thrust this area is made up of highly crushed slaty material. A few boulders of dolomite are embedded within the slide material. In the free face of the slope sandstone beds are overlain by slate. This area appears to be made of fluvial deposits under the influence of the huge supply from the surrounding loose and fragile rocks. Due to thrusting and faulting rocks are very loose and having very low slope bearing capacity. As a result of above process, rock strength is decreasing. Further due to toe cutting (erosion) slope is increased resulting the frequent landslide occurrence. Monsoonal precipitation exaggerates slope failure processes. Those thrust and faults which are seismically active further deteriorates degradation processes.(Fig. 3)

Causes of Landslide

An overall evaluation of the pattern and nature of landslide occurrences in Himalaya (M.B.T. zone) reveals the following main features:

1. Almost all mass movements generally occur during and after monsoon (SW and NE monsoon) period indicating that main triggering mechanism is the over-saturation of overburden caused by heavy rains. There seems to be a relation between intensity of rainfall and slope failures.
2. High tectonic activity in the area, viz. existence of Main Boundary Thrust along with presence of faults exaggerates the vulnerability of critical slopes of Himalayan territory.
3. High relief, high dip of rocks, presence of high angle joints and the bedding and fracture cleavage exposed along slopes and road cuts.

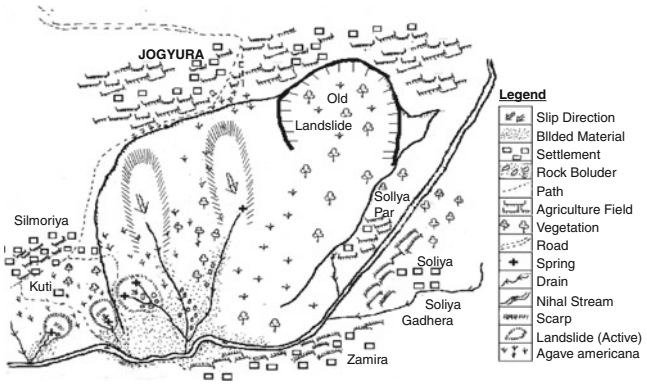

Fig. 3 Sketch of Jogyura landslide(not to the scale)

4. Rain water acts as lubricating agent and after percolating in the rocks reduces the shearing resistance and thus triggers down under the influence of gravity.
5. Loose/crushed rocks generated on account of intense thrusting.
6. Monsoonal precipitation provides huge amount of water to the loose material which is reducing slope bearing capacity.
7. Regular and intensive toe cutting by Nihal River.
8. Slided mass is falling in the river bed and being taken away by water. As a result of which slope is not getting time to stabilize.
9. From top to river bed there are three breaks along the slope where landsliding is taking place. It gives the impression of rotational landslide.
10. Presence of natural spring/seepage zone: Hard rocks are overlain by huge deposit of loose material. During rainy season it is absorbing water which comes out at thecontact zone as seepage or spring. In these areas sometime overlain mass falls down towards valley.

Mitigation Measures

There are rare chances to stop the sliding because the basic causative factor is found frail litho-structural (presence of M.B.T. along with fault) setting. However, the frequency can be minimizes through vegetative measures. In general the chief mitigatory measures to be adopted for such areas are:

1. *Drainage correction*: The most important triggering mechanism for mass movement is the water infiltration into the over burden during heavy rains and consequent increase in pore pressure within the overburden. When this happens in steep slopes the safety factor of the slope material gets considerably reduced causing it to move down. Hence the natural way of preventing this situation is by reducing infiltration and allowing excess water to move down without hindrance. As such, the first and foremost mitigation measure is drainage correction. This involves maintenance of natural drainage channels both micro and macro in vulnerable slopes.
2. *Proper land use measures*: The universal use of contour bounding for all types of terrain without consideration of the slope, overburden thickness and texture or drainage set-up needs to be controlled especially in the plateau edge regions. It is time to think about alternative and innovation, which are suitable for the terrain, to be set up. It need not be over-emphasized the governmental agencies have a lot to contribute in this field.
3. *Reforestation for the areas occupied by degraded Vegetation*: Leaving aside the 'critical zones' with settlement could be avoided altogether and which could be preferably used for permanent vegetation, the 'highly unstable zones' generally lie in the upper regions, which are occupied by highly degraded vegetation. These areas warrant immediate afforestion measures with suitable plant species. The afforestation programme should be properly planned so the little slope modification is done in the process. Bounding of any sort using boulders etc. has to be avoided. The selection of suitable plant species should be such that can with stand the existing stress condition in this terrain.
4. Creation of awareness among local population: the people of Jogyura, Silmoriya, Kuti, and Soliya villages have been suggested to shift themselves to some safe areas.
5. Jalal (1985) suggested three particular eco-development programmes, comprising afforestation, masonry work and agricultural diversification for immediate implementation along the M.B.T.

Conclusion

To conclude it can be stated that the present study supports the general phenomena of Himalayan Mountain system that basically the area is tectonically sensitive and fragile so vulnerable to landslide processes. Further monsoonal precipitation along with anthropogenic intervention is associating factors that contribute to exaggerate the landsliding process in Himalayan terrain.

The planning and implementation of development schemes in Himalayan terrain should take into account the existing instability of slopes. The parameters discussed should provide first hand information to planners so that precautions can be taken at an early stage.

Acknowledgement Prof. K. S. Valdiya, F.N.A. for coming up with his sincere guidance in understanding the geology of Himalaya. Prof. R. C. Joshi, Department of Geography, Kumaun University, Nainital is acknowledged for painstaking help during field work. Dr. Kiran Bargali, Department of Botany, Kumaun University, Nainital deserves my special thanks for brainstorming sessions in the identification of vegetal cover of the site in the tough Himalayan terrain. Sincere thanks are to Prof. P. D. Pant, Department of Geology for discussions relating to geological environment of the site under investigation.

References

Alexander DE (2008) A brief survey of GIS in mass-movement studies, with reflections on theory and methods. Geomorphology 94:261–267

Bartarya SK (1996) Landslide hazards: some case studies from the Satluj Valley, Himachal Pradesh. Himal Geol 17:193–207

Bartarya SK, Valdiya KS (1989) Landslides and erosion in the catchment of Gaula river, Kumaun Lesser Himalaya, India. Mt Res Dev 9(2):405–419

Bhandari RK, Gupta C (1985) In: Singh JS (ed) Environmental regeneration in Himalaya, concepts and strategies. Gyanodaya Prakashan, Nainital, 468 p. ISBN 10:8185097070, 13:978-8185097077

Cain N, Mool PK (1982) Landslides in Kolpu Khola drainage: middle mountains, Nepal. Mt Res Dev 2(2):157–173

Chen H, Lee CF (2003) A dynamic model for rainfall-induced landslides on natural slopes. Geomorphology 51:269–288

Fourniadis IG, Liu JG, Mason PJ (2007) Landslide hazard assessment in the Three Gorges area, China, using ASTER imagery: Wushan–Badong. Geomorphology 84:126–144

Haigh MJ, Rawat JS, Bartarya SK (1989) Environmental indicators of landslide activity along the Kilbury Road, Nainital, Kumaun Lesser Himalaya. Mt Res Dev 9:25–33

Hukku BM, Srivastava AK, Jaitly GN (1977) Measurement of slope movements in Nainital area. Eng Geol 4:557–467

Jalal DS (1985). In: Singh JS (ed) Environmental regeneration in Himalaya, concepts and strategies. Gyanodaya Prakashan, Nainital, 468 p. ISBN 10:8185097070, 13:978-8185097077

Joshi M, Pant PD (1990) Causes and remedial measures for rockfalls and landslides on Naina Peak, Nainital, Kumaun Himalaya, U.P., India. Mt Res Dev 10(4):343–346

Kienholz H, Schneider G, Bischel M, Grunder M, Mool P (1984) Mapping of mountain hazards and slope stability. Mt Res Dev 3:247–266

Medlicot HB (1864) On the geological structure and relationship of the southern portion of the Himalayan ranges between the rivers Ganges and Ravee. Mem Geol Surv Ind 3(2):1–212

Mehra SR, Natrajan TK (1966) Handbook on landslide analysis and correlation. Central Research Road Institute, New Delhi, 114 p

Middlemiss CS (1890) Geological sketch of Nainital with some remarks on natural conditions governing the mountain slopes. Rec Geol Surv India 21:213–234

Nasmith H, Mercer AG (1979) Design of dykes to protect against debris flows at port Alice, British Columbia. Can Geotech J 16:748–757

Oldham RD (1880) Note on the Nainital landslide 18th September 1880. Rec Geol Surv India 13:277–281

Owen LA, Kamp U, Khattak GA, Harp EL, Keefer DK, Bauer MA (2008) Landslides triggered by the 8 October 2005 Kashmir earthquake. Geomorphology 94:1–9

Pande A, Joshi RC, Jalal DS (2002) Selected landslide types in central Himalaya – their relation to geological structures and human activities. The Environmentalist 22(3):269–287

Rautela P, Pande RK (2005) Traditional inputs in disaster management: the case of Amparav, North India. Int J Environ Stud 62(5):505–515

Sharma VK (1996) Slope mass rating technique in landslide susceptibility evaluation in parts of Nainital area. J Eng Geol 25:287–295

Sharma VK (2005) Landslide catastrophes of holocene period in Northwest Himalaya, India. In: Proceedings of IGCP workshop-490 on environmental catastrophes of holocene period, Chennai, 17–19 Aug 2005, p 12

Smith A, Ellison RA (1999) Applied geological maps for planning and development. A review of examples from England and Wales. Q J Eng Geol Hydrogeol 32:S1–S44

Starkel L (2010) Ambotia landslide valley-evolution, relaxation, and prediction (Darjeeling, Himalaya). Studia Geomorphologica Carpatho – Balcanica Landform Evolution in the mountain areas, pp 113–133

Valdiya KS (1980) Geology of Kumaun Lesser Himalaya. The Himachal Times Press, Dehradun, 291 p

Valdiya KS (1983) Location of landslides and hazard zoning. Report on landslides in U.P. Hills. Directorate General of Mining (GM 366/84), Lucknow

Valdiya KS (1985). In: Singh JS (ed) Environmental regeneration in Himalaya, concepts and strategies. Gyanodaya Prakashan, Nainital, 468 p. ISBN 10:8185097070, 13:978-8185097077

Valdiya KS (1998) Dynamic Himalaya. Universities Press, Hyderabad, 178 p. ISBN 81 7371 0945

Valdiya KS, Joshi DD, Sanwal RS, Tondon SK (1984) Geomorphologic development across the active Main Boundary Thrust: an example from the Nainital Hills in Kumaun Himalaya. J Geol Soc India 25:761–774

Zaruba Q, Mencl V (1969) Landslides and their control. Elsevier, Prague, 206 p

GIS Analysis of Heavy-Rainfall Induced Shallow Landslides in Japan

Hiromitsu Yamagishi, Shoji Doshida, and Edgar Pimiento

Abstract

Heavy rainfall often triggers shallow landslides (slope failures) in Japan. In addition, the Geographical Survey Institute (GSI) now provides digital elevation data and digital geological maps from the Geological Survey of Japan are also available. Hence using GIS, we analysed the distribution of heavy-rainfall induced shallow landslides at six locations (Fig. 1) in relation to slope gradient.

Results showed that shallow landslides are concentrated on slopes with gradients between 25° and 30°, regardless of the difference in bedrock geology at the six locations. The former suggests that the occurrence of shallow landslides depend on slope gradient rather than bedrock geology.

Keywords

Heavy-rainfall • Shallow landslides • GIS analysis • Slope gradient

Introduction

Japanese Islands are composed mostly of fragile rocks because of young ages and fracturing due to tectonic deformation and faulting. Therefore, earthquakes and heavy rainfalls often trigger shallow landslides.

Here we describe the relation between the distribution of shallow landslides triggered by heavy rainfall and slope gradient, at six locations with different bedrock geology (Fig. 1). The events and their occurrence are Hamada (Jul, 1983), Hidaka (Aug, 2003), Izumozaki_Tochio (Jul, 2004), Nihama (Oct, 2004), Houfu (Jul, 2009) and Shobara (Jul, 2010).

H. Yamagishi (✉)
Center for Disaster Management Informatics Research, Ehime University, Bunkyocho 3, Matsuyama, Ehime, Japan
e-mail: hiroy@sci.ehime-u.ac.jp

S. Doshida
National Research Institute for Earth Science and Disaster prevention (NIED), Japan

E. Pimiento
Department of Public Works, Matsue, Shimane, Japan

Method

Using GIS (ArcView 9.3.1) we compared the distribution of shallow landslides (which were inventoried from aerial photographs taken just after their occurrence) in relation to 5° interval slope gradient data calculated from 10 m grid DEM (Geographical Survey Institute 2011) at six locations (Fig. 1).

We calculated the number of shallow landslides within slope gradient classes based on vector data (using the centroid of the source area of slope failures) and the landslide area density for the same slope gradient classes based on raster data (number of landslide cells/number of slope gradient class cells).

Results

Hamada (Shimane Prefecture)

In Hamada area, western Shimane Prefecture (Fig. 1), intensive rainfall between July 20th and 23rd, 1983, triggered numerous landslides and caused flooding. The total

C. Margottini et al. (eds.), *Landslide Science and Practice*, Vol. 1,
DOI 10.1007/978-3-642-31325-7_79,

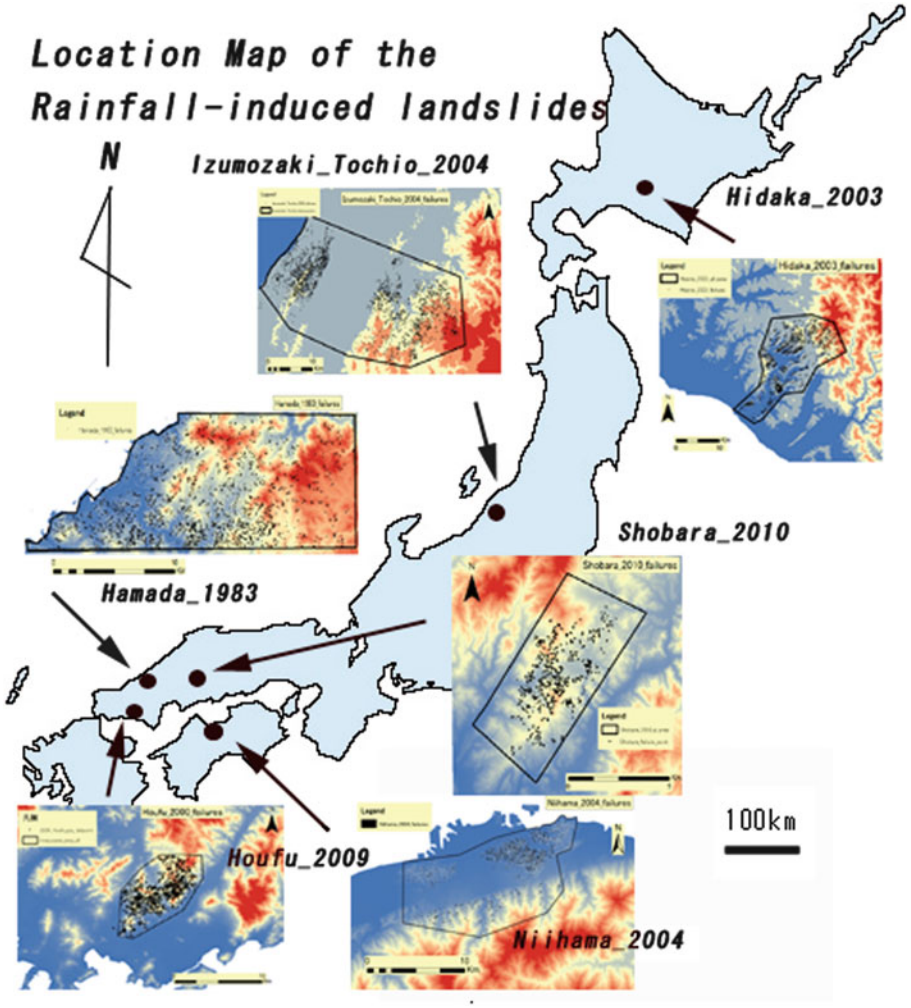

Fig. 1 Location map of the recent heavy rainfall-induced failure areas. *Small maps* indicate the GIS calculated area at each location

precipitation was 742 mm, and the maximum daily precipitation reached 372 mm/day. Most of the landslides were from colluvium and residual soil slope failures. A total 2,404 failures were recorded within 150 km^2. The highest number of failures occurred on 25–30^o slope gradient slopes (Fig. 2a). The highest landslide area density occurred on slopes with gradients between 35° and 40°, although the highest is at 65–75° exceptionally (Fig. 2b).

The area consists of hills and plains with elevations up to 400 m. The bedrocks of the area consist mainly of Paleozoic to Mesozoic metamorphic rock, granitic rocks and Paleozoic volcanic rocks.

Hidaka (Hokkadio)

In Hidaka area, Hokkaido (Fig. 1), in August 9th–10th, 2003, when the typhoon No. 10 was closing and landing at Hidaka Mountains. The typhoon brought more than 400 mm precipitation within the 2 days. At maximum, 50 mm/h was recorded. As the results, many failures were taking place along the Sarugawa and Appetsugawa tributaries(Civil Engineering Research Institute for Cold Region (CERI)). We were analyzing the failures of the polygonal area (Fig. 1). The total number was counted as 3,404 and the maximum number is located at 20° and 25° in slope gradient (Fig. 3a) and the maximum failure density increased toward 60–65° (Fig. 3b), but the highest is at 65–70° exceptionally.

The Hidaka area is composed of bedrocks of Paleogene mudstone and Miocene conglomerates and sandstone (Ishimaru et al. 2003; Ishimaru et al. 2004). However, this area is mostly covered by volcanic ash and pumice layers (up to 1 m thick).

Izumozaki-Tochio (Niigata Prefecture)

On July 13, 2004, heavy rainfalls due to strong activities of rain front, occurred in the Mid-Niigata Region, Japan. They were as much as 400 mm within 24 h, bringing about serious

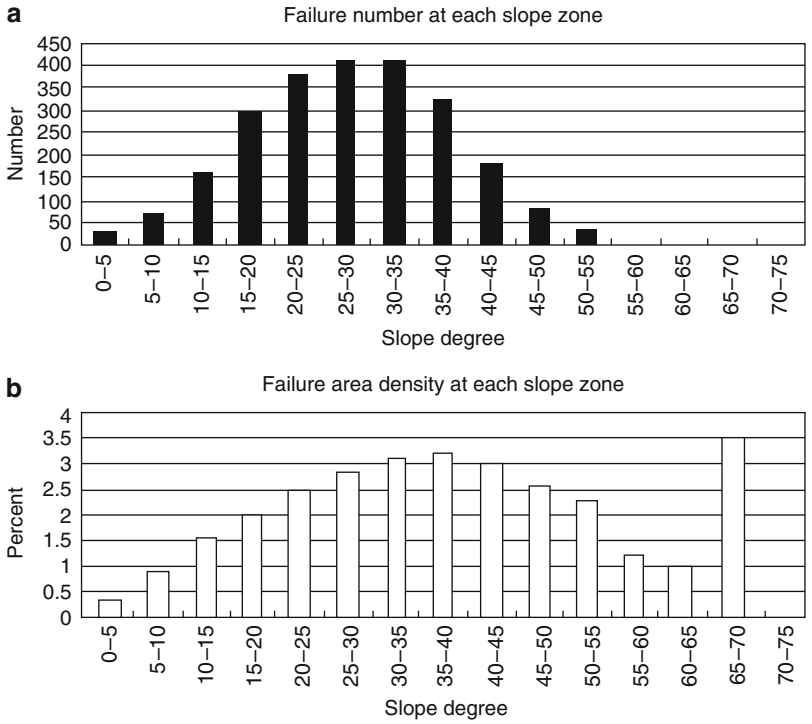

Fig. 2 (**a**) Graph showing the failure number at each slope gradient zone of the 1983 Hamada failures. (**b**) Graph showing the failure density (percent) at each slope gradient zone

flooding by breaking the river banks and shallow landslides (failures), killing 14 and 2 people, respectively. In the Izumozaki-Tochio area (Fig. 1), the heavy rainfalls triggered in particulary many failure which were inventoried by airphotographs by Asia Air Survey Co. Ltd. The airphotograph interpretation and field research revealed that two types of the landslides were recongized; one is shallow landslides (Iwahashi and Yamagishi 2010) and the other is deep landslide which is associated usually with mudflows (Yamagishi and Iwahashi 2007). We were analyzing the former type using GIS, which lead to that the total number is 3,095, and the maximum one is located from 25° to 30° in slope gradeint (Fig. 4a) and the failure density increases toward 45–50° at the most, but exceptionally, the maximum density is at 55–60° zone (Fig.4b).

The bedrock geology of the Izumozaki-Tochio area is mostly composed of Neogene mudstone and sandstones.

Niihama (Ehime Prefecture)

In 2004, total ten typhoons landed on Japanese Islands, and many places were affected by heavy winds and rains throughout Japan. According to the Meteorological Agency of Japan (MJA), Typhoon No. 21 took a way to southern island of Japan and reached the southwest Japan on September 27th, 2004, and passed Shikoku Island on September 29th–30th, where totally more than 400 mm precipitation was recorded. By the precipitation, Niihama area, Ehime Prefecture was damaged by many shallow lanslides (Matsuzawa and Chigira 2007). The total number is as much as 1,745. The results using GIS is that the maximum number is located from 25° to 30° (Fig. 5a) and the muximum of the failure density is at 40–50°, however, the highest peak is 55–60° exceptionally. (Fig. 5b)

The bedrock geology of the Niihama area consists of Cretaceous sandstone and mudstones (Matsuzawa and Chigira 2007).

Houfu (Yamaguchi Prefecture)

On July 21th to 22th, 2009, heavy rainfall attacked the Houfu area, Yamagichi Prefecture (Fig. 1). Total daily precipitation reached 275 mm on 21th, and the maximum hour precipitation was documented at 72.5 mm (MJA). Due to the precipitation many shallow landslides and debris flows occurred along the Sabagawa Tributaries, killing 14 persons and destroyed many houses and facilities.

In particular, the landslides and associated debris flows mostly took place in the areas of Cretaceous granites as pointed by Kanaori et al. (2009). The surface of the granites was deeply weathered into coarse-grained “Masa”. We analyzed all of the shallow landslides interpreted by

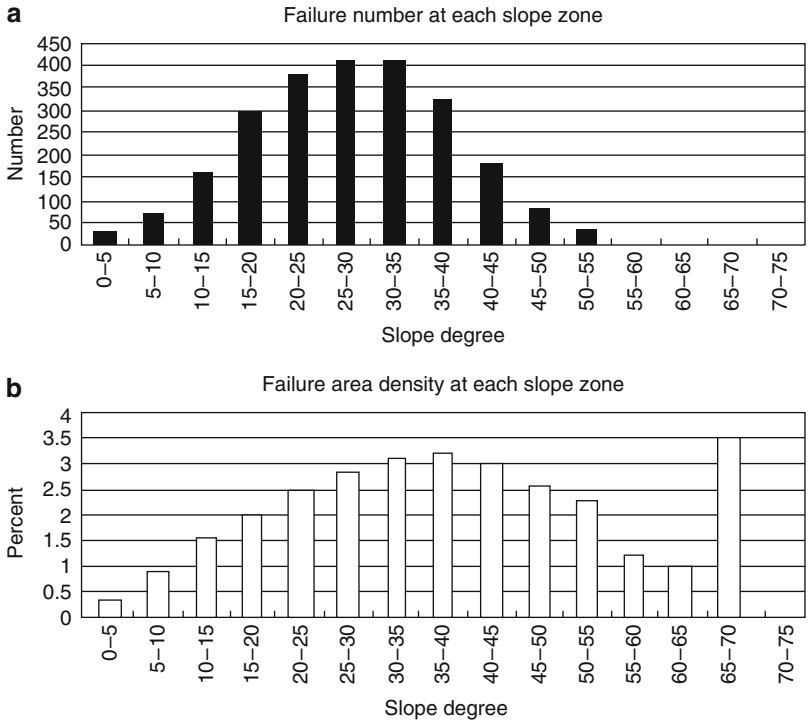

Fig. 3 (**a**) Graph showing the failure number at each slope gradient zone of the 2003 Hidaka failures. (**b**) Graph showing the failure density (percent) at each slope gradient zone

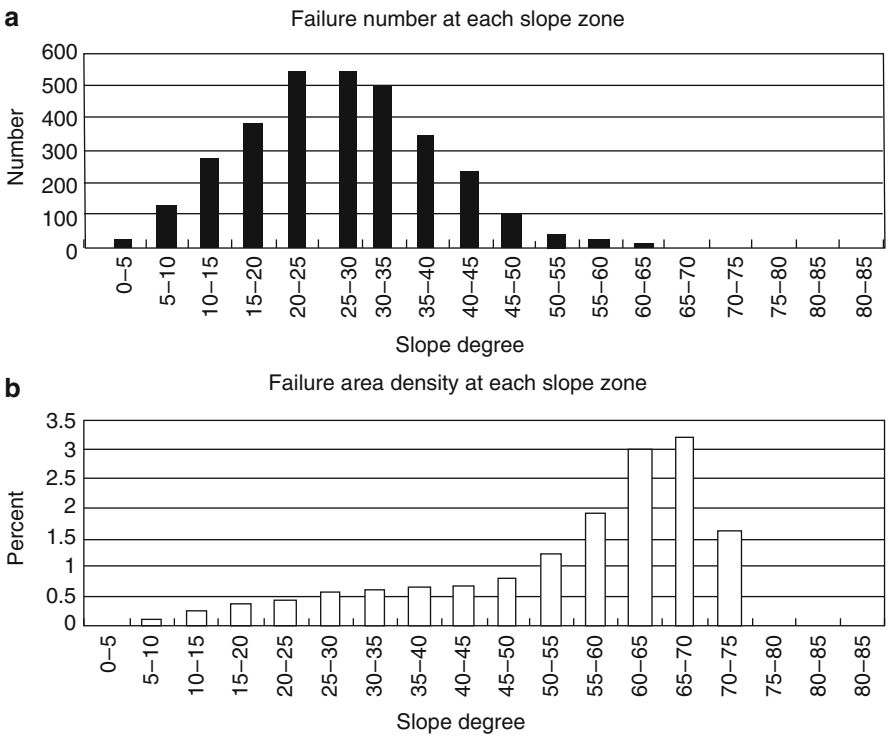

Fig. 4 (**a**) Graph showing the failure number at each slope gradient zone of the 2004 Izumozaki-Tochio failures. (**b**) Graph showing the failure density (percent) at each slope gradient zone

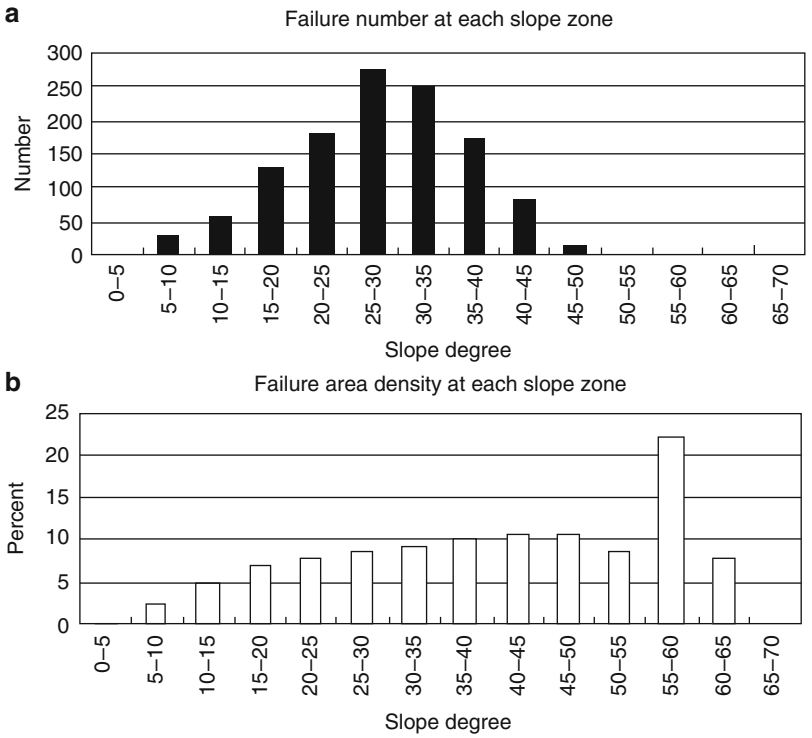

Fig. 5 (**a**) Graph showing the failure number at each slope gradient zone of the 2004 Niihama failures. (**b**) Graph showing the failure density (percent) at each slope gradient zone

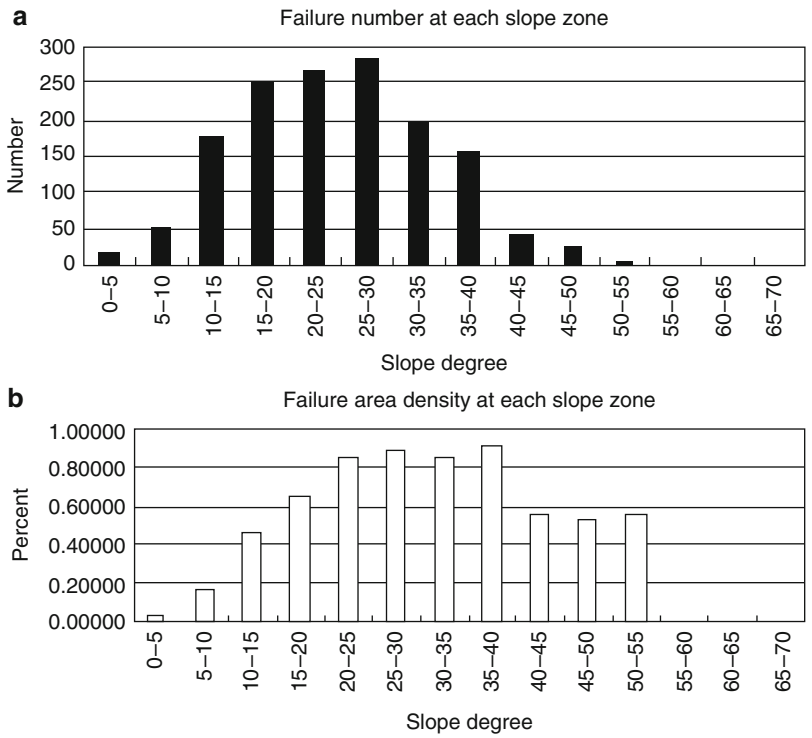

Fig. 6 (**a**) Graph showing the failure number at each slope gradient zone of the 2009 Houfu failures. (**b**) Graph showing the failure density (percent) at each slope gradient zone

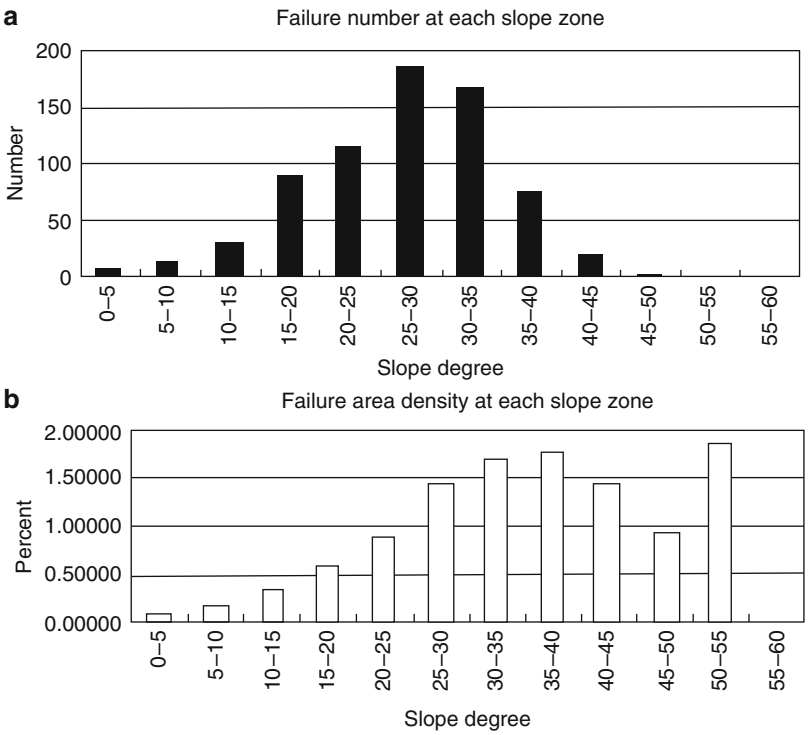

Fig. 7 (**a**) Graph showing the failure number at each slope gradient zone of the 2010 Shobara failures. (**b**) Graph showing the failure density (percent) at each slope gradient zone

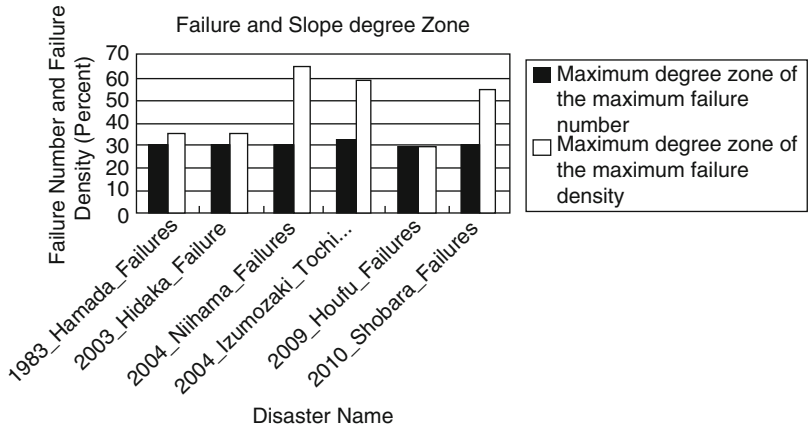

Fig. 8 Graph showing summary of the maximum gradient zones of the highest failure numbers and area density of the six locations

PASCO Corporation from the airphotographs which were taken just after the event. Using GIS the total number of the shallow landslides waws calculated to be 1,460, and the maximum is ranging from 25° to 30° in slope gradient (Fig. 6) and the density ranges from 35° to 40° (Fig. 6b).

Shobara (Hiroshima Prefecture)

On July 16th, 2010, heavy rainfall brought about many shallow landslides in the montainous area of Shobara, Hiroshia Prefecture (Fig. 1). On that day the daily precipitation reached 59 mm and total precipitation in July, was 416 mm. Such heavy rainfall triggered many shallow lanslides. We analyzed the landslides from the airphotographs by PASCO Corporation. Using GIS the total number was counted to be 700, and the maximum number is located at 25–30° in slope gradient (Fig. 7) and the maximum density at 35–40°, but the highest peak is appearing at 50–55° exceptionally.

The bedrock of the Shobara area is composed of Mesozoic rhyolitic and basalt (Geological Survey of Japan 2011).

Conclusion and Discussion

In this paper, we analysed using GIS (ARCVIEW9.3.1) the heavy rainfall-induced shallow landslides (failures) at six locations (Fig. 1) for clarifying the relation between the failure numbers and failure area density, and slope gradients (5° intervals) using 10m_DEM from Geographical Survey Institute (GSI). As the results, we have obtained that the maximum failure number occurred on slope gradient ranging from 25° to 30°, while the failure area density (number of landslide cells/number of slope gradient class cells) were located variably from 35° to 60° (Fig. 8)

Namely, such failure numbers are constant up to 30° in slope gradient, however the failure density show considerable variation, the reason of which is not clear at this time although the latter seems to be important than the former. Similar study on GIS analyses was done by Dai and Lee (2002). They revealed that the maximum number of the failures occurred on the slope zone of 35–40°, and fewer on the slope gradient zone of more than 40°. Namely, they showed that such shallow landslides due to heavy rainfall do not necessarily occur on steepest slopes likely to our results. In this time, we used 10m_DEM as topographic data, but If we use much more detailed scale DEM, such as 2m_ and 1m_DEM, another results may be obtained.

As we mentioned above, the bedrock geology of the six location is different; Hamada and Shobara area are composed of Mesozoic volcanic and sedimentary rocks, Hofu is of Mesozoic granite. Hidaka, Izumozaki-Tochio areas are of Cenozoic sedimentary rocks, and Niihama area is of Cretaceous sedimentary rocks. In addition, the bedrocks of Hidaka area are covered by volcanic ash up to one meter thick and Houfu area by thick deeply weathered materials called "Masa". The other areas are also more or less weathered on the surface.

In this paper we show only the relation to slope gradients, because we believe that such shallow landslides (failures) are mostly dependent on topography rather than bedrock geology. However, we have to investigate also relation to surficial geology as well as bedrock geology in the future.

Acknowledgments We are grateful to Aero Asahi Corporation Co. Ltd., Asia Air Survey Co. Ltd., PASCO Corporation, Ehime Prefecture, and Civil Engineering Research Institute for Cold Region (CERI), for providing useful digital data for GIS analyses. We also thank to Dr. Junko Iwahashi for useful suggestions. Finally, we appreciate the two peer reviewers for useful comments.

References

Dai FC, Lee CF (2002) Landslides characteristic and slope modelling using GIS, Lantau Island, Hong Kong. Geomorphology 42:213–228

Geographical Survey Institute (GSI) Kiban Chizu Joho http://fgd.gsi.go.jp/. (10 Feb 2011)

Geological Survey of Japan Integral Geological Map Database (Geo_DB: http://iggis.muse.aist.go.jp/seamless/en/top.htm. (10 Feb 2011)

Ishimaru S, Tajika J, Otsu S, Takami M (2003) Slope failures caused by Typhoon 10, 2003 in Hidaka, Hokkaido. J Jpn Lands Soc 40:339, 81–82 (in Japanese with English abstract)

Ishimaru S, Tajika J, Otsu S, Takami M (2004) Disaster caused by Typhoon 10, 2003, in Hidaka district, Hokkaido. Rep Geol Surv Hokkaido 75:61–70 (in Japanese with English abstract)

Iwahashi J, Yamagishi H (2010) A reinvestigation on spatial distribution of shallow landslides induced by the August 1961 and the July 2004 heavy-rainfalls in Izumozaki area, Niigata-GIS analyses using high resolution ortho images and a 2-m DEM. J Jpn Lands Soc 47:274–282 (in Japanese with English abstract)

Kanaori Y, Imaoka T, Okawa Y (2009) The heavy rain of July 2009 in Chugoku and Northern Kyushu districts: details of debris flows occurred along the River Tsurugi in Houfu City, Yamaguchi Prefecture, Japan. In: Proceedings of the Engineering Geology Society Chugoku-Shikoku Branch, pp 31–34 (in Japanese with English abstract)

Matsuzawa M, Chigira M (2007) Geological and geomorphological features of landslides caused by the 2004 heavy rainfalls in Niihama City, Eastern Ehime Prefecture. Chikei Trans J Jpn Geomorphol Union 28:286–287 (in Japanese with English abstract)

Yamagishi H, Iwahashi J (2007) Comparison between the two triggered landslides in Mid-Niigata, Japan-by July 13 heavy rainfall and October 23 intensive earthquakes in 2004. Landslides 4:387–397